UNIVERSIDAD DE CANTABRIA

E.T.S. DE INGENIEROS DE CAMINOS, CANALES Y PUERTOS

Departamento de Ciencias y Técnicas del Agua y del Medio Ambiente

---

TESIS DOCTORAL

DESARROLLO DE UNA METODOLOGÍA PARA DELIMITAR ZONAS DE MEZCLA DE VERTIDOS INDUSTRIALES EN ESTUARIOS

Presentada por: **D. JAVIER FRANCISCO BÁRCENA GÓMEZ**

Dirigida por: **D. ANDRÉS GARCÍA GÓMEZ**

D. CÉSAR ÁLVAREZ DÍAZ

Santander, agosto 2015

DEVELOPMENT OF A METHODOLOGY TO ALLOCATE MIXING ZONES OF INDUSTRIAL DISCHARGES IN ESTUARIES

Author: Mr. Javier F. Bárcena
Advisor: Dr. Andrés García
Advisor: Dr. César Álvarez

The following web-page addresses contain up to date information about this dissertation and related topics:
http://www.ihcantabria.com/en/personal-ih/item/568-javier-bárcena
https://www.researchgate.net/profile/Javier_Barcena
Text printed in Santander
First edition, November 2015

A Marta, Javi, Leo y mi familia, especialmente mis padres...

Agradecimientos

Quiero agradecer en primer lugar al Instituto de Hidráulica Ambiental de la Universidad de Cantabria y al Gobierno de España por haberme dado la oportunidad de realizar la Tesis doctoral mediante una beca para la Formación de Personal Investigador (BES-2010-032763).

En segundo lugar a mis directores de Tesis Andrés García Goméz y César Álvarez Díez por la confianza depositada en mí y por permitirme realizar este trabajo. Sin su ayuda y apoyo este estudio no podría haberse realizado. Me gustaría agradecer en concreto a Andrés García Gómez por su dedicación, paciencia y esfuerzo. Por sus revisiones y comentarios, con los que siempre he aprendido, y por inculcar en mí el sentido del rigor académico, sin el cual no podría tener una formación completa como investigador.

Quiero agradecer especialmente a Javier García Alba por toda su ayuda a lo largo de este trabajo. Como, por ejemplo, resolver todas las dudas que he tenido con toda clase de modelos numéricos, ayudarme con la implementación de códigos en distintos lenguajes de programación o enseñarme a tener una visión más "física" de los problemas. En mi fuero interno siempre serás el "tercer codirector de esta Tesis" porque sin tu inestimable ayuda nunca hubiera terminado.

Agradezco también a Sonia Castanedo, Raúl Medina, Araceli Puente y José Antonio Juanes por su apoyo, respaldo y motivación para ayudarme a empezar y terminar este proyecto.

Gracias también a todos los coautores de los artículos que forman parte de esta Tesis, además de los ya mencionados, y a todos los investigadores que han aportado conocimientos y datos imprescindibles a este estudio, especialmente a Aina García por toda su ayuda en temas de vulnerabilidad y Paula Camus por adentrarme en las técnicas de clasificación.

Agradecer también de manera especial a los revisores externos Giovanni Coco y Giovanni Besio por la lectura detallada de esta Tesis y por todas las recomendaciones y mejoras aportadas a la misma. Además, me gustaría agradecer al Gobierno de España y a Giovanni Besio que me dieran la oportunidad de realizar una estancia de investigación en el Dipartamento de Ingegneria Civile, Chimica e Ambientale de la Università degli Studi di Genova (EEBB-I-14-00521).

También agradecer a todo el personal del Instituto por, entre todos, generar y mantener un ambiente de trabajo excepcional permitiendo que seamos una "gran familia".

Finalmente, quiero dar las gracias a toda mi familia, por su apoyo, paciencia y ayuda. Ellos son las principales personas en mi vida y sin las cuales esta Tesis nunca hubiera sido posible. Agradecer en especial a mis padres por todas las oportunidades que me han brindado en la vida, por invertir en mi educación, por su apoyo incondicional y por haberme enseñado a ser la persona que soy, y, a mi hermana por su comprensión y cariño en todo momento.

Por último, quiero agradecer especialmente a Marta, mi pareja, compañera y mejor amiga. Gracias por todo, por tu apoyo, ayuda, paciencia, por animarme siempre, por creer en mí, y por estar siempre a mi lado, en los buenos y malos momentos. Gracias por dos hijos como dos soles, Javi y Leo, nuestro futuro... Por eso y mucho más quiero dedicaros especialmente este trabajo.

Muchas gracias,

JaviB

Agosto 2015

Contents

List of Figures

List of Tables

List of Symbols

$\overline{[X_{i,j}]}_{f-f}^{k}$ - Average concentration of a toxicant during the k-statistical year
$[X_{med}]$ - Mean concentration of the toxicant
α - Dimensionless factor that reflects the effect of particle shape (1.0 for spheres)
α_s - Entrainment coefficient
β_p - Spreading coefficient of the jet-plume
ΔM_f - Vortex entrainment ("forced" entrainment) due to the ambient cross-flow
ΔM_k - Increase in mass of a plume element due to turbulent entrainment
ΔM_s - Shear entrainment due to the relative velocity between a plume element and the ambient velocity in the direction of the jet axis
Δt - Time step
ΔU - Relative buoyant jet velocity in the direction of the buoyant jet axis
Δx - Grid cell length in x direction
Δy - Grid cell length in y direction
$\Delta \rho_S$ - Density increment due to salinity
$\Delta \rho_{SS}$ - Density increment due to total suspended sediment
$\Delta \rho_V(t)$ - Time series of the bottom minus the surface densities
$\frac{\partial \overline{u_i' u_j'}}{\partial x_j}$ - Fluctuations of the momentum due to the turbulent flow (Reynolds stresses)
$\frac{\partial \overline{u_i' C'}}{\partial x_i}$ - Fluctuations of the mass due to the turbulent flow
κ - Von Kármán constant
λ_d - First order decay process
$\max(X)$ - Maximum of the initial database
$\min(X)$ - Minimum value of the initial database
μ - Dynamical viscosity
μ_{3D} - Part of eddy viscosity due to turbulence model in vertical direction associate to tridimensional processes
μ_H - Horizontal eddy viscosity
μ_H^{back} - Background horizontal eddy viscosity
μ_{mol} - Molecular viscosity
μ_{SGS} - Subgrid scale horizontal eddy viscosity
μ_V - Vertical eddy viscosity
μ_V^{back} - Background vertical eddy viscosity
μ_{water} - Water viscosity
μ_t - Turbulent or eddy viscosity
Ω - Earth rotation speed
ω - Velocity in the σ-direction in the σ-coordinate system
$\overline{\rho_{env}}$ - Time averaged density
$\overline{\rho_{env}}(t)$ - Time series of the vertical mean-depth density
$\overline{C}$ - Mean substance concentration
$\overline{p}$ - Time averaged pressure

$\overline{R_i}$ - Average of the measurements
$\overline{u_i}$ - Velocity in average values
$\overline{u}$ - Average characteristic velocity
$\overline{u}(t)$ - Time series of the vertical mean-depth velocity
ϕ - Pipe diameter of the single-port
ϕ_k - Angle of the buoyant jet axis with the horizontal plane
ρ_{air} - Density of air
ρ_{eff} - Density of the discharged effluent
ρ_{env} - Density of the receiving water
ρ_k - Density of a plume element
ρ_{par} - Particle density
ρ_T - Density of pure water as a function of temperature
ρ_0 - Reference density of water
σ_ε - Calibration coefficient
σ_{mol} - Prandtl-Schmidt number for molecular mixing
σ_t - Turbulent Schmidt number
σ_k - Calibration coefficient
$\sqrt{G_{\xi\xi}}$ and $\sqrt{G_{\eta\eta}}$ - Coefficients used to transform curvilinear to rectangular coordinates
$\tau_{\xi\xi}$, $\tau_{\eta\eta}$ and $\tau_{\xi\eta}$ - Contributions of secondary flow to shear stress tensor
θ_k - Angle between the z-axis and the projection of the buoyant jet axis on the horizontal plane
υ - Kinematic viscosity
ε - Dissipation rate of turbulent kinetic energy
$\vec{\Omega}$ - Angular velocity of the earth
$\vec{a}$ - Acceleration
$\vec{F_{fr}}$ - External forces
$\vec{F}$ - Applied force
$\vec{g}$ - Gravitational force
ζ - Elevation of the free surface on the reference plane
$||$ - Euclidean distance
$|\overrightarrow{u_b}|$ - Magnitude of the bottom-layer horizontal velocity
$|\overrightarrow{u}|$ - Magnitude of the depth-averaged horizontal velocity
$|\tau_S|$ - Magnitude of the shear stress at free surface in the wind direction
$A_{estuary}$ - Total area of the estuary
A_i - Area of the i grid cell
b' - Width of the jet where concentration on the axis is reduced by a factor $1/e$
b - Width of the jet where the velocity on the axis is reduced by a factor $1/e$
b_k - Half-width or radius of a plume element
C - Total concentration of a toxic substance
c - Travel speed of a tidal wave in shallow waters (celerity)
$C^{'}$ - Concentration variations (e.g. salinity or temperature)
$C_{1\varepsilon}$ - Calibration coefficient
$C_{2\varepsilon}$ - Calibration coefficient
$C_{out}(t)$ - Time series of outflow concentration
C_{sd} - Saturation dissolved concentration of the chemical in water
C_0 - Initial concentration at t=0
C_d - Concentration of a toxic substance in dissolved form
C_m - Maximum concentration of the jet-plume
C_p - Concentration of a toxic substance in particulate form
C_s - Sediment concentration of a toxic substance

Ch - Chezy coefficient
d - Depth respect to a reference plane of the free surface
D_{3D} - Diffusion due to turbulence model in vertical direction
d_{eff} - Distance of the single-port to the bottom
D_H - Horizontal eddy diffusivity
D_H^{back} - Background horizontal eddy diffusivity
d_{par} - Particle diameter
D_{SGS} - Diffusion due to the subgrid scale turbulence model
D_V - Vertical eddy diffusivity
D_V^{back} - Background vertical eddy diffusivity
D_x - Horizontal eddy diffusivity in x direction
D_y - Horizontal eddy diffusivity in y direction
D_t - Turbulent or eddy diffusivity
dP - Duration of the flow pulses
E - Evaporation
E_c - Correction term due to plume curvature
E_f - Total projected area entrainment
E_p - Projection or cylinder term
E_w - Correction term due to the increase in plume width
f - Coriolis parameter (inertial frequency)
f_{dis} - Dissolved fraction
F_l - Local jet densimetric Froude number
f_{OC} - Weight fraction of the total organic carbon in the suspended solids
f_{par} - Particulate fraction
f_R - Reaction terms or "processes"
f_{vol} - Correction factor
F_{vol} - Volatilization flux
fP - Frequency of the flow pulses
g - Gravity acceleration
g'_o - Reduced gravitational acceleration
H - Total depth of the water column
$H(t)$ - Time series of the total depth of the water column
H_C - Sensible heatflux due to conduction
h_c - Thickness of the bottom boundary layer
h_k - Thickness of a plume element
H_L - Net longwave radiation flux from the atmosphere and the waterbody
H_{max} - Maximum depth in the study area
h_n) - Plume thickness at the end of the near-field
H_{net} - Net heatflux across the air/water interface
H_E - Latent heatflux due to evaporation
H_S - Shortwave solar radiation flux
He - Henry's constant
hP - Hydrologic flow pulses
$HVEL_k$ - Magnitude of the horizontal velocity of a plume element
K - Calibration constant
k - Kinetic energy
$k_{1/2}$ - Decay rate
K_{12} - Partition coefficient
K_{aw} - Air–water partition coefficient

K_{bio} - Biodegradation rate
K_{gas} - Transfer coefficient for the OMP for the gas film and
K_{liq} - Transfer coefficient for the OMP for the liquid film
K_{oc} - Organic carbon–water partition coefficient
K_{ow} - Octanol-water partition coefficient
K_{pho} - Photolysis rate
k_{vol} - Volatilization rate
K_p - Particle–water partition coefficient
k_r - Rate constant of the m_r-order
L - Mixing length
L_B - Length-scale of buoyancy
L_M - Length-scale of momentum
LS - Characteristic length scale
m - Mass of an object
M_η - Source or sink of momentum in η-direction
M_ξ - Source or sink of momentum in ξ-direction
M_k - Mass of a plume element
M_{mf} - Minimum M clusters for explaining the forcing variability
M_{mm} - Minimum M clusters for running numerical models
M_{of} - Optimal M clusters for explaining the forcing variability
M_{om} - Optimal M clusters for running numerical models
m_r - Order of reaction
$MAWV$ - Mean annual water volume
n - Manning coefficient
$Norm_{i,j}$ - Normalized data of the initial database
P - Precipitation
P_η - Gradient hydrostatic pressure in η-direction
P_ξ - Gradient hydrostatic pressure in ξ-direction
Q - Flow (entering or exiting)
Q_{eff} - Discharged effluent flow
Q_i - River flow of the day i
q_{in} - Local source per unit volume
q_{out} - Local sink per unit volume
r - Dimensionless roughness coefficient
R - Gas constant
R_i - i-field data of the measurements
r_s - Toxic solid-phase concentration
Ri - Richardson Number
Ri_L - Richardson layer number
S - Salinity
S_i - i-model data of the simulations
S_k - Salinity of a plume element
S_n - Minimum primary dilution
SO - Source and sink terms
SS - Concentration of total suspended sediment (suspended solids)
T - Temperature
t - Time
$t_{i,j}$ - Time duration at which a toxicant exceeds MAC-EQS
T_k - Temperature of a plume element

t_{total} - Total time duration
t_f - Flushing time
t_I - Integral time scale
TR_i - Astronomical tidal range of the day i
u - Flow velocity in the ξ-direction
u_{ch} - Characteristic velocity of the study area
u_{env} - Environmental current velocity
u_k, v_k, w_k - Velocity of a plume element
u_i' - turbulent fluctuations of velocity
U_m - Velocity of the centerline of a jet-plume
v - Flow velocity in the η-direction
V - Volume of the control volume considered
v_j^* - Centroids on the j step
V_k - Magnitude of the velocity of a plume element
V_{sed} - Sedimentation velocity
w - Vertical velocity of a plume element
W_{10} - Averaged wind speed at 10 m above free surface
W_{drag} - Wind drag coefficient
X^S - "Synthetic series"' of Q or TR
$X_{i,j}$ - Initial database
x_k, y_k, z_k - Location of a plume element
z - Vertical coordinate in the physical space

List of Acronyms

A - Academic Use
AA - Annual Average
AC - Acceptability of the "worst and dry case of dilution"
AC* - Acceptability of the "real case of dilution"
AD - Final Admissibility of the "worst and dry case of dilution"
AD* - Final Admissibility of the "real and dry case of dilution"
AEF - Acute Effects of the "worst case of dilution"
AEF* - Acute Effects of the "dry case of dilution"
AEF** - Acute Effects of the "real case of dilution"
AEM - Algebraic Eddy Model
AEM - Algebraic Eddy Viscosity Closure Model
AIZ - Allocated Impact Zones for Areas of Non-Compliance
ALG - Algebraic Closure Model
As - Arsenic
B - Business Use
BAT - Best Available Technology
BAT-EA - Best Available Technology-Economically Achievable
BO - Boussinesq Approximation
CB - Closed Boundary
CCC - Criterion Continuous Concentration
Cd - Cadmium
CE - Model Efficiency
CEF - Chronic Effects of the "worst case of dilution"
CEF* - Chronic Effects of the "dry case of dilution"
CEF** - Chronic Effects of the "real case of dilution"
CEV - Constant Eddy Viscosity
CFD - Computational Fluid Dynamic
CFL - Courant-Friedrichs-Levy Number
$CHCl_3$ - Chloroform or Trichloromethane
CIS - Common Implementation Strategy
CMC - Criterion Maximum Concentration
COPC - Chemical Of Potential Concern
CP - Conventional Pollutant
Cr - Chromium
CTR - Conservative tracer
Cu - Copper
CV - Critical Value
CWA - Clean Water Act
DEP - Department of Environmental Protection

DESA - Distributed Entrainment Sink Approach
DOC - Dissolved Organic Matter
EC - Ecology Model
EC - European Commission
ecdf - empirical cumulative distribution function
EDO - Effluent Discharge Objective
EFDC - Environmental Fluid Dynamics Code
ELCOM - Estuary, Lake and Coastal Ocean Model
ELV - Emission Limit Value
EPA - U.S. Environmental Protection Agency
EQG - Environmental Quality Guideline
EQS - Environmental Quality Standard
EQSD - Environmental Quality Standard Directive
ESE - Ecological Singular Element
EU - European Union
EV - Ecological Value
EVI - Estuarine Vulnerability Index
FDM - Finite Difference Method
FEM - Finite Element Method
FL - Flushing Lag
FT - Flushing Time
FVCOM - Finite Volume Coastal Ocean Model
FVM - Finite Volume Method
GG - Grid Generator
GIS - Geographical Information System
GOTM - General Ocean Turbulence Model
GUI - Graphical User Interface
H3D - Hidrodinámica 3D
HA - Harbor Agitation
Hg - Mercury
HM - Heavy Metal
HP - Hydromorphological Pressure
HY - Hydrostatic Assumption
IC - Initial Condition
ID - Industrial Discharge
IDZ - Initial Dilution Zone
IEA - Integrated Environmental Authorization
IPH - Instrucción de Plan Hidrológica
IPPCD - Integrated Pollution Prevention and Control Directive
KMA - K-means Algorithm
LDEQ - Louisiana Department of Environmental Quality
LFT - Local Flushing Time
MAC - Maximum Allowable Concentration
MAS - Maximum Allowable Mixing Zone Size of the "worst and dry case of dilution"
MAS* - Maximum Allowable Mixing Zone Size of the "real case of dilution"
MDA - Maximum-Dissimilarity Algorithm
ML - Mixing Length
MOE - Ministry of Environment
MOEE - Ministry of Environment and Energy

MT - Mud Transport
MZ - Mixing Zone
NA - Naturalness
Ni - Nickel
NPDES - National Toxicant Discharge Elimination System
NWQMS - Australia's National Water Quality Management Strategy
OB - Open Boundary
OMP - Organic Micropollutant
OS - Open Source
PA - Pathogens
PAE - Projected Area Entrainment
PAH - Polyaromatic Hydrocarbons
PAI - Proposed allowable increase
Pb - Lead
PBDE - Polybrominated Biphenylethers
PBT - Persistent, Bioaccumulative and Toxic
PC - Process Contribution
PCB - Polychlorinated Biphenyl
PCDD/PCDF - Dioxins and furans
PDE - Partial Differential Equation
Pe - Peclet Number
PML - Prandtl's Mixing Length Model
POC - Particulate Organic Matter
POM - Princeton Ocean Model
POP - Persistent Organic Toxicant
PPT - Pre and Post-processing Tools
R - Research Use
RI - Relative Increase
ROMS - Regional Ocean Modeling System
RT - Residence Time
RWQCB - Regional Water Quality Control Board
SC - State of Conservation
Se - Selenium
SGS - Subgrid Scale
SOM - Self-Organizing Maps
SS - Survey Station
SSS - Smagorinsky Subgrid Scale
ST - Sediment Transport Module
ST - Stratification
SU - Susceptibility
SW - Shallow Waters
SWRCB - State Water Resources Control Board
TCDD - Tetrachlorodibenzo-pdioxin
TEQ - Toxicity Equivalents
Tl - Thallium
TNRCC - Texas Natural Resources Conservation Commission
TR - Transport Module
TRLA - Texto Refundido de la Ley de Aguas
TSD - Technical Support Document for Water Quality-based Toxic Control

TZ - Tidal Zoning
UK - United Kingdom
URANS - Unsteady Reynolds Averaged Navier-Stokes
USA - United States of America
Va - Vanadium
W - Wave
WASP7 - Water Quality Analysis Simulation Program
WD - Well Documented
WDOE - Washington Department of Ecology
WFD - Water Framework Directive
WQ - Water Quality Module
WQO - Water Quality Objectives

Resumen

1. Introducción

En esta sección, se presentan las motivaciones que llevan al desarrollo de esta tesis y se muestra una visión general del problema que supone “la descarga de vertidos industriales en aguas estuarinas”.

La importancia de los estuarios es amplísima ya que albergan multitud de procesos biológicos y ecológicos y numerosas actividades humanas. A pesar de generar múltiples beneficios, los estuarios se ven constantemente amenazados por la presencia de numerosas presiones que limitan su potencial productivo. Por ello, las zonas estuarinas precisan de respuestas específicas y una gestión eficaz para mitigar los efectos de dichas presiones, especialmente, para la evaluación del impacto generado por vertidos industriales.

En este sentido, se ilustra la importancia global de los estuarios, la presencia de la actividad industrial en ellos y el marco legislativo establecido para el control de la calidad del agua. A continuación, se revisan los fundamentos del transporte y mezcla de aguas residuales y se muestra su interrelación con el modelado numérico. Dicha interacción es importante porque demuestra la posibilidad y conveniencia de utilizar modelos numéricos como herramientas que facilitan la implementación y aplicación de las normas vigentes de una forma más sencilla y económica, siempre y cuando se seleccione el modelo apropiado.

A continuación, se detalla el objetivo general así como los objetivos específicos que permitirán conseguir el objetivo general. Por último, se concluye con una serie de consideraciones que determinan el rango de aplicabilidad de la metodología desarrollada.

1.1. Motivación

Todos los seres vivos están inmersos en un fluido u otro, sea el aire de la atmósfera o el agua de un río, lago, estuario u océano; incluso los suelos están impregnados de humedad, sin la cual la vida sería imposible (Cushman-Roisin 2013).

A lo largo de la historia, las sociedades han prosperado o fracasado con base en su capacidad para controlar el abastecimiento de agua potable para su consumo, la producción de alimentos o la higiene y la descarga de este agua, una vez que se ha empleado, para la asimilación y transporte de residuos. Sin embargo, a medida que se fue incrementado la densidad de población, las aguas circundantes se forzaron a absorber más y más contaminación hasta llegar a agotar su capacidad asimilativa. Algunas de las civilizaciones más grandes del mundo, fundamentadas en el éxito para asegurar agua potable y de riego, se derrumbaron en parte debido a su incapacidad para escapar de los efectos generados por su propia contaminación del agua (Alley 2007).

Los estuarios son zonas de transición entre el mar, el río, la tierra y la atmósfera que determinan la presencia de diferentes gradientes de condiciones físico-químicas y, por tanto, también de las comunidades biológicas. Como consecuencia, los flujos de agua dulce y salina así como los sedimentos fluviales y marinos confluyen en estas zonas generando muchos nichos biológicos y una elevada diversidad biológica. Esta característica

hace que sean ecosistemas únicos de gran belleza, complejidad, variabilidad, dinamismo y con una biota altamente especializada. Debido a ello, los estuarios constituyen un entorno de gran interés para todas aquellas disciplinas que tienen que ver con la biología, la geología, la química, la física, la historia o la sociología por las características específicas de su condición de ecotono.

A lo largo de la historia de la humanidad, los estuarios han sido siempre una de las zonas más pobladas de la Tierra. Actualmente, alrededor del 60 % de la población mundial vive cerca de la costa y/o los estuarios, comprendiendo el 5.2 % de la superficie de la Tierra y tan sólo el 2 % del volumen de los océanos (Lindeboom 2002). En este sentido, son áreas de gran importancia socioeconómica ya que 22 de las 32 ciudades más grandes del mundo se localizan en estuarios (Valle-Levinson 2010).

Por lo tanto, la principales amenazas para la salud, la productividad y la biodiversidad del medio estuarino son producto de las actividades humanas (Halpern *et al.* 2008, Lotze *et al.* 2006, Recio *et al.* 2013). Las más importantes son el desarrollo urbano en las márgenes del estuario, los desechos y la escorrentía de las actividades urbanas, industriales y/o agrícolas, el aumento de la demanda para usos recreativos, el desarrollo de infraestructuras en estuarios, el desarrollo de actividades en la cuenca, el desmonte y/o relleno de terrenos estuarinos, la excavación y el dragado, la introducción de especies invasoras, la extracción excesiva de recursos pesqueros y, finalmente, los cambios climáticos a largo plazo como la subida del nivel medio del mar (Figura 1). Los impactos generados por las actividades antrópicas incluyen el cierre de las zonas de cultivo de moluscos, la degradación de playas, la destrucción de hábitats de vital importancia para mantener la salud de los ecosistemas y la localización de sitios contaminados.

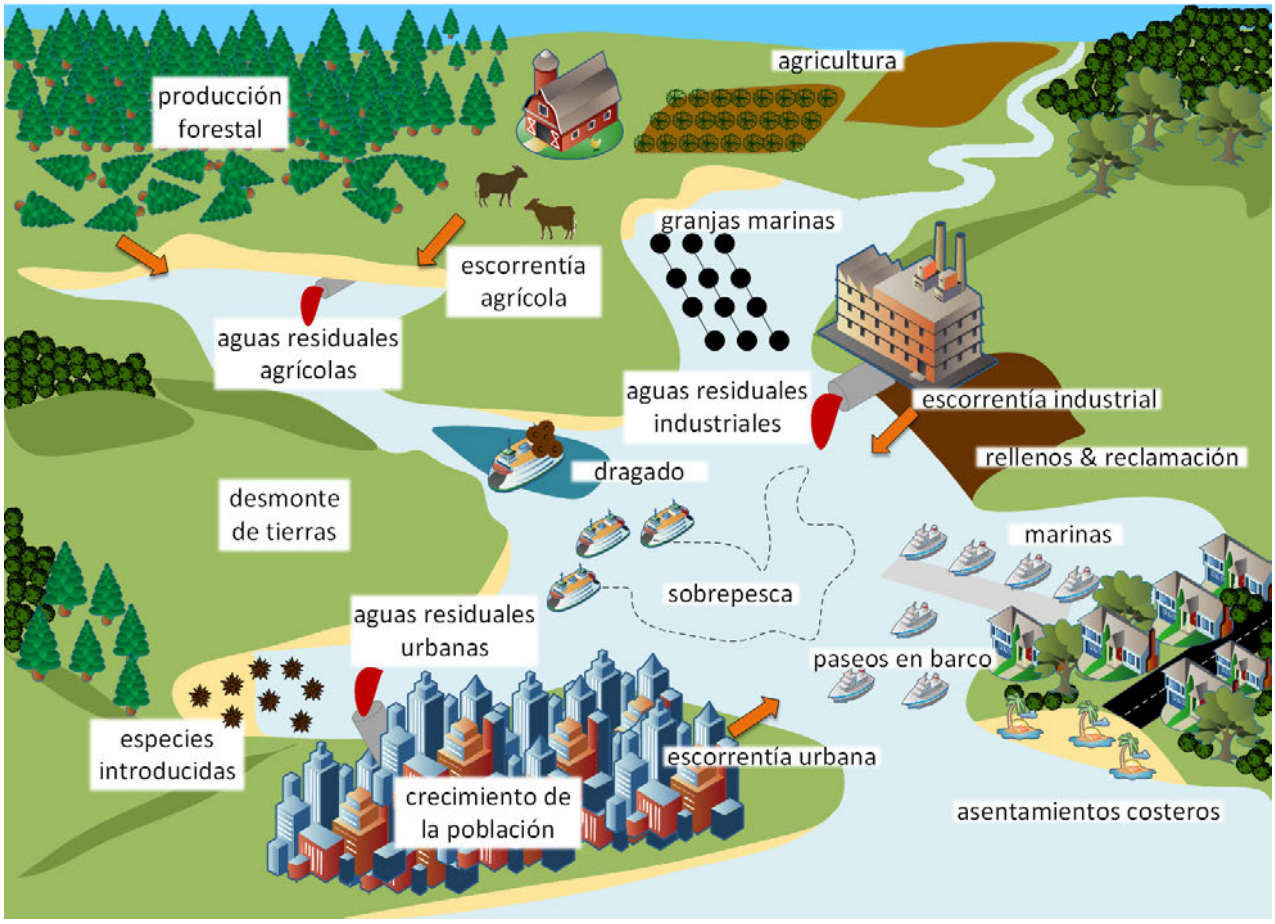

Figura 1: Diagrama de las principales actividades antrópicas que se desarrollan en y alrededor de los estuarios afectando a su salud, productividad y biodiversidad.

Aunque su conservación se ha convertido en una causa importante de preocupación, en la última década, se

ha constatado un declive significativo de los ecosistemas estuarinos en todo el mundo (Chainho *et al.* 2008, Foster *et al.* 2013, Ondiviela *et al.* 2015). Por ejemplo, el Millennium-Ecosystem-Assessment (2005) estimó que alrededor del 50 % del área original de los ecosistemas de marisma se han perdido o degradado. Las consecuencias de todos estos impactos están provocando que los estuarios sean incapaces de mantener la calidad de vida que la gente buscaba.

Una de las principales fuentes de contaminación de los estuarios procede de las aguas residuales industriales (Gómez *et al.* 2004, Roose & Brinkman 2005). Cualquier industria, en la que el agua se obtiene a partir de un sistema de tratamiento de agua industrial o entra en contacto con un proceso o producto, puede añadir contaminantes al agua. Los contaminantes se definen como sustancias en el medio ambiente que se encuentran por encima de las concentraciones de fondo esperadas. Cuando el agua resultante de un proceso industrial contiene contaminantes se clasifica como aguas residuales industriales.

La industria utiliza alrededor del 20 % global del agua dulce accesible generando una corriente de aguas residuales que fluye o se filtra en cualquier sistema acuático como pueden ser los estuarios. Alrededor de 300 millones de toneladas de compuestos sintéticos utilizados anualmente en productos industriales y de consumo encuentran parcialmente su camino en aguas superficiales (Schwarzenbach *et al.* 2006). La figura 2 ilustra la ubicación mundial de zonas industriales (puntos azules) y de zonas acuáticas donde estacionalmente se produce hipoxia (puntos rojos). Como puede verse en esta figura, las principales amenazas se correlacionan, generalmente, con zonas de alta densidad industrial y situadas en estuarios o áreas adyacentes.

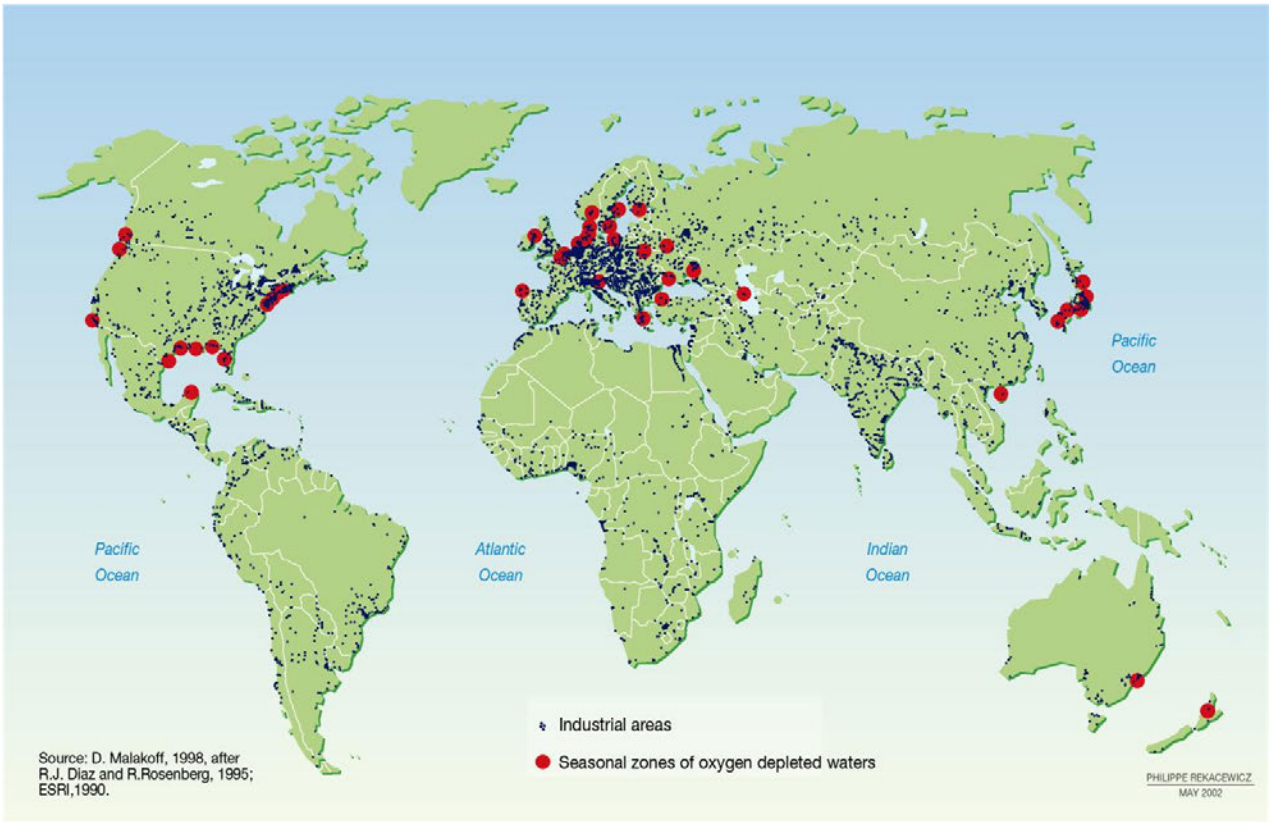

Figura 2: Localización mundial de zonas industriales (puntos azules) y de zonas acuáticas donde estacionalmente se produce hipoxia (puntos rojos). Fuente: http://www.unep.org/dewa/vitalwater/jpg/0320-oxygen-depleted-EN.jpg.

Por ejemplo, la industria es la mayor fuente de contaminación en los Estados Unidos, representando más de la mitad del volumen total de la contaminación del agua y conteniendo la mayoría de los contaminantes más letales. Aproximadamente en los Estados Unidos hay 50.000 autorizaciones de vertidos con permiso

para descargar durante 5 años (USEPA 2010). En su Inventario Nacional de Calidad del Agua, la Agencia de Protección Ambiental de Estados Unidos informó al Congreso en 1996 que aproximadamente el 40 % de los estuarios monitorizados estaban demasiado contaminados para proveer de usos básicos como el suministro de agua potable, la pesca o la natación (USEPA 1996). Por su parte, en Inglaterra y Gales hay más de 2.000 vertidos de aguas residuales descargando directamente a estuarios donde, muchos de ellos, se usan simultáneamente para actividades marisqueras (UKEA 2011c). Este número de vertidos de aguas residuales es probablemente similar en otros países y proporcional a su población.

Los tipos de contaminantes presentes en las aguas residuales industriales son muy heterogéneos reflejando la diversidad de la actividad industrial. Dichas aguas pueden incluir contaminantes físicos, químicos y/o biológicos. Todos ellos se pueden introducir en el medio de cualquier forma o cantidad y, además, no pueden ser cuantificados adecuadamente sin mediciones.

Cuando un contaminante puede producir, incluso a bajas concentraciones, una respuesta (efecto) adversa en un sistema biológico, dañando seriamente su estructura o funcionalidad o llegando a provocar su muerte, se la denomina como una sustancia tóxica o tóxico. Entre otros, los metales pesados y microcontaminantes orgánicos son dos grupos de sustancias tóxicas muy perjudiciales para los seres vivos. Se ha demostrado que ambos grupos, cuando son liberados en el medio ambiente, pueden viajar grandes distancias desde su fuente original. Adicionalmente, su exposición puede causar la interrupción de los sistemas endocrino, reproductivo e inmunológico, trastornos neurohormonales y cánceres (WHO 2003).

Las aguas residuales normalmente se descargan directamente en los estuarios como fuentes puntuales (Alley 2007). Una fuente puntual es una fuente de contaminación única e identificable tal como una tubería, un emisario o un desagüe. Por lo general, las aguas residuales industriales se descargan por tuberías circulares de boca única (Bárcena 2009). La figura 3 muestra algunos ejemplos de este tipo de mecanismo de descarga (Fuentes: [1], [2], [3], [4], [5], [6], [7], [8], [9]). Dichos vetidos se pueden medir o cuantificar así como evaluar de alguna manera su impacto sobre el medio ambiente circundante. Debido a ello, las fuentes puntuales son, en comparación con las fuentes de origen difuso, característicamente más fáciles de controlar, más fácilmente identificables y medibles y, generalmente, más tóxicas (Schwarzenbach *et al.* 2006).

En todo el mundo, hay multitud de ejemplos de estuarios sometidos a una contaminación industrial procedente de fuentes puntuales (véase la figura 4). En España, la Ría de Huelva, la Bahía de Pasajes, la Ría de Bilbao, el puerto de Tarragona, la Ría de Avilés o la Bahía de Cádiz son ejemplos de aguas de transición bajo dicha presión industrial. Al nivel regional de Cantabria, la Ría de Suances y la Bahía de Santander son las zonas que reciben la mayoría de los vertidos industriales.

Como se ha detallado, el aumento de la contaminación en todo el mundo con miles de compuestos químicos industriales y naturales es uno de los principales problemas ambientales a los que se enfrenta la humanidad. Aunque la mayoría de estos compuestos están presentes en concentraciones bajas, muchos de ellos plantean considerables problemas toxicológicos (Schwarzenbach *et al.* 2006). Por todo ello, existen graves impactos ambientales, económicos y sociales asociados con este tipo de contaminación.

Así, se acepta que no podemos seguir avanzando tecnológicamente, ignorando el deterioro ambiental que se produce cuando irresponsablemente se vierten los residuos de nuestra propia tecnología. De hecho, el

[1] http://greatlakesinform.org/sites/default/files/
[2] http://water.epa.gov/infrastructure/greeninfrastructure/
[3] http://www.seaweb.org/images/photos/
[4] http://coastecology.org/
[5] http://www.catawbariverkeeper.org/issues/coal-ash-1/
[6] http://cbf.typepad.com/
[7] http://blackwarriorriver.org/wp-content/uploads/
[8] http://toptenintheworld.com/
[9] https://lordfarmer.files.wordpress.com/

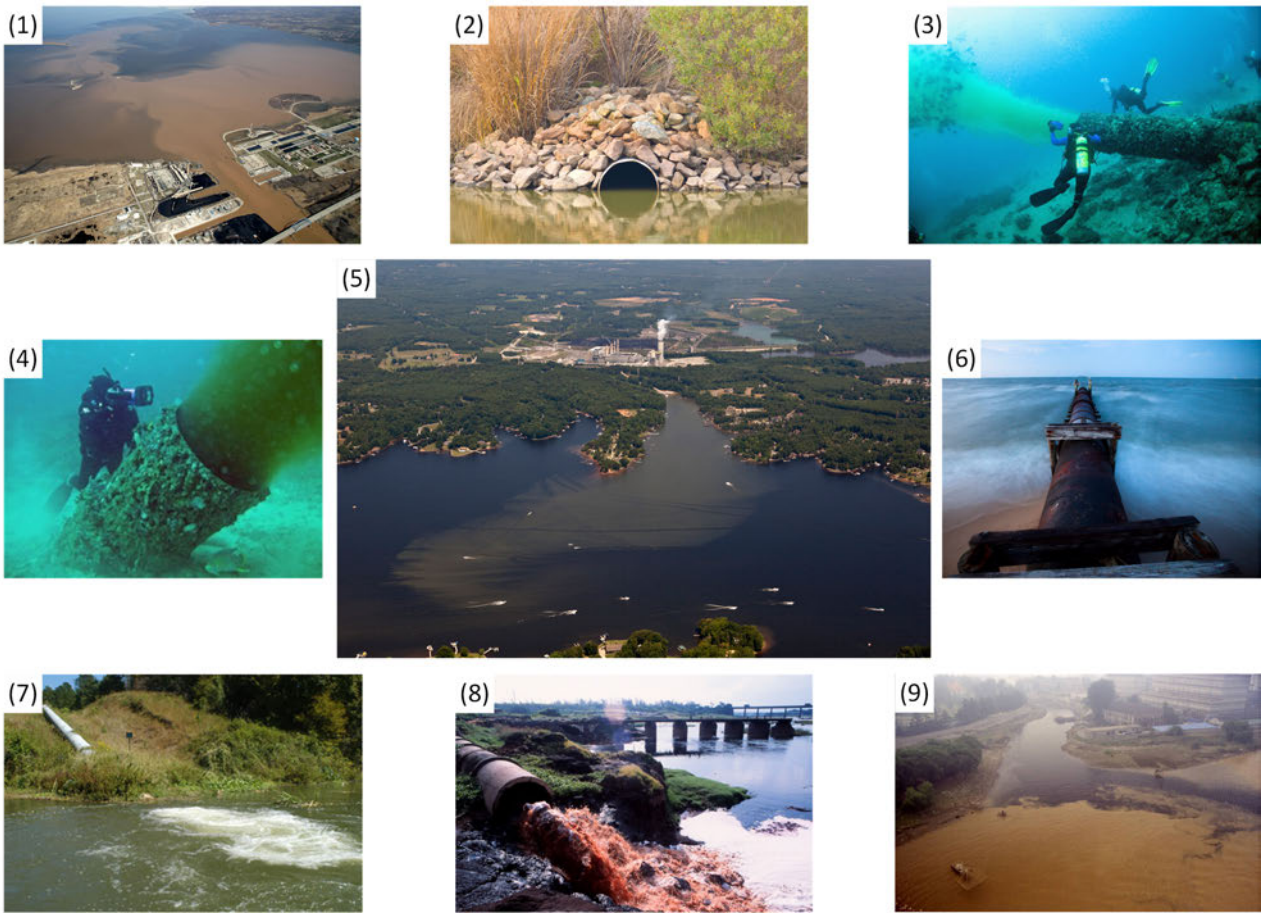

Figura 3: Composición de fotos con ejemplos de aguas residuales industriales descargadas a través de fuentes puntuales así como su impacto ambiental.

Figura 4: Mapamundi mostrando ejemplos de estuarios estresados por la actividad industrial. Fuente del mapa base: http://goto.arcgisonline.com/maps/World_Topo_Map.

crecimiento sostenible de nuestra civilización requiere que protejamos nuestro frágil medio ambiente como la única manera razonable y factible de coexistencia con la naturaleza en nuestro planeta (Alley 2007).

A pesar de emplear las tecnologías más nuevas y limpias, las industrias continúan, a menudo, emitiendo sustancias tóxicas sobre el medio ambiente acuático. Dichas sustancias tóxicas pueden envenenar cualquier tipo de vida salvaje y aumentar los riesgos para la salud humana por nadar en aguas contaminadas o comer pescado y mariscos contaminados. Además, también se producen pérdidas económicas por el cierre de areas marisqueras o la pérdida de turismo. En este sentido, las autorizaciones de vertidos pueden ayudar a disminuir todos estos problemas.

Por todo lo expuesto, una de las principales preocupaciones para las naciones del mundo ha sido y es la protección del medio ambiente con el fin de gestionar de forma sostenible la calidad del agua. Así, gran parte de la legislación promulgada para proporcionar protección al medio ambiente tiene como propósito el mantenimiento de la biodiversidad y los recursos naturales (AUS 2008, CCME 1999, EC 2000; 2008a;b, EU 2013, USA 1972; 1977; 1985). Para ello, dicha legislación obliga, en una primera fase, a asegurar el no deterioro de las condiciones ambientales actuales y, posteriormente, mejorar estas condiciones para corregir los abusos del pasado.

En lo referente a la legislación de vertidos tóxicos, el establecimiento de normas de calidad del agua (objetivos o estándares) es una de las partes más importantes. Generalmente, se pueden distinguir en la legislación dos enfoques: el enfoque basado en estándares de la calidad del medio ambiente (o EQS-based approach) y el enfoque basado en el valor límite de emisión (o ELV-based approach). Una combinación de ambos enfoques también es una posibilidad llamada enfoque combinado (Figura 5).

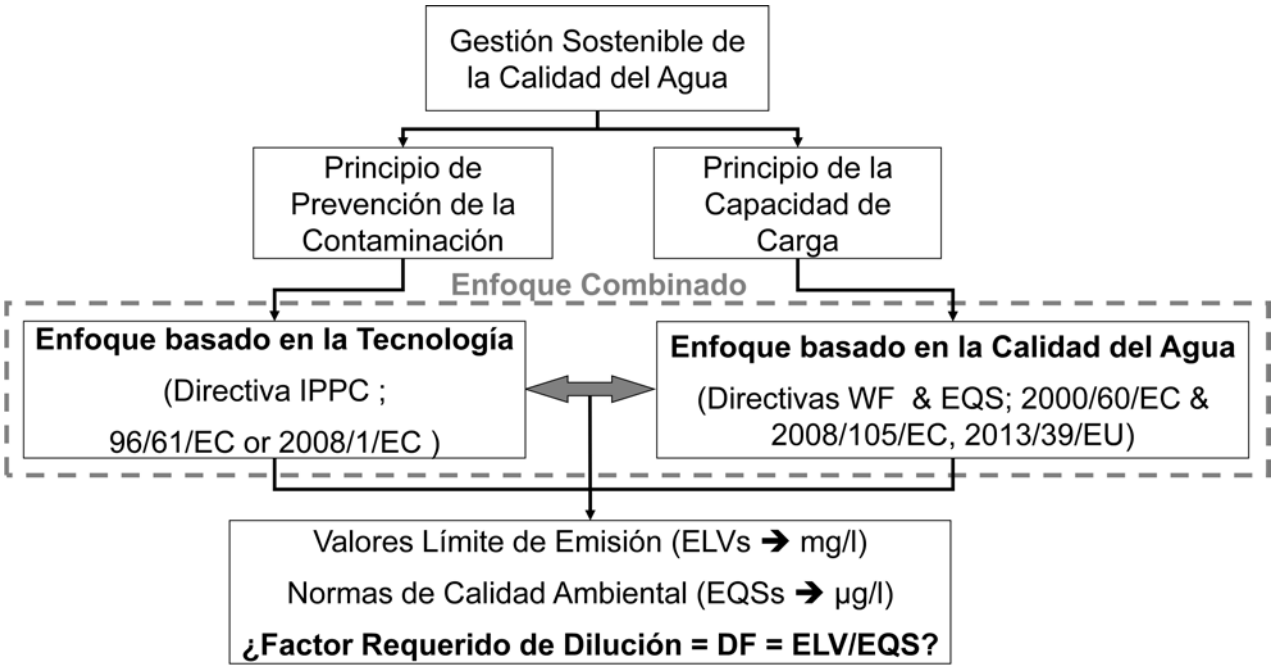

Figura 5: Relaciones entre los principios de prevención de la contaminación y de la capacidad de carga así como entre los enfoques relacionados con la gestión sostenible del agua basados en la tecnología y la calidad del agua.

El principio de prevención de la contaminación se basa en la idea de que cualquier forma de contaminación puede tener un impacto negativo sobre la calidad del agua y, por lo tanto, debería de ser evitado (Ragas *et al.* 1997). Dentro de este marco, las medidas orientadas al origen (también conocidos como valores límite de emisión) dependen de las posibilidades tecnológicas para reducir las emisiones y de sus consecuencias económicas y sociales (Figura 5). El método de establecer medidas orientadas al origen (ELVs) se denomina,

a menudo, como el enfoque basado en la tecnología.

El principio de la capacidad de carga se basa en la idea de que el medio ambiente puede asimilar determinadas cargas contaminantes sin producir efectos adversos, siempre y cuando no se exceda la capacidad de carga del sistema acuático (Ragas *et al.* 1997). En la mayoría de los casos, la capacidad de carga se establece con las normas de calidad ambiental (EQSs). Dichas EQSs se aplican con el fin de predecir la probabilidad de que se produzcan efectos adversos en el medio. Para ello, a partir de datos de redes de vigilancia o de resultados de modelos de calidad del agua, se calcula la evolución de la concentración con el fin de hacer predicciones sobre los efectos potenciales. Si la concentración ambiental es mayor que la EQS se espera que se produzca un efecto negativo por lo que será necesario realizar una evaluación de riesgos y se deberán tomar medidas orientadas a reducir la carga en origen o su efecto (Figura 5). El método de establecer medidas orientadas a reducir la carga en origen o su efecto basadas en EQS se denomina, generalmente, como el enfoque basado en la calidad del agua.

Ragas *et al.* (1997) y Ragas (2000) resumieron las ventajas y desventajas de los diferentes mecanismos de control en la autorización de vertidos a aguas superficiales, como son el enfoque basado en EQSs o el enfoque basado en ELVs. Las principales conclusiones fueron:

- EE.UU., Australia, Canadá y el Reino Unido tienen una larga tradición en la aplicación del enfoque basado en EQSs (ANZECC & ARMCANZ 2000, MOEE 1994b, SEPA 1998, USEPA 1991; 1994; 1996).
- La mayoría de los países europeos, como Alemania, Holanda, Bélgica, Austria, España o Portugal han utilizado un enfoque genérico basado en ELVs, consistente en aplicar sólo estos umbrales (Jirka *et al.* 2004).
- El ELV es un método directo y eficaz para limitar las cargas contaminantes de sustancias tóxicas porque limita la concentración de los tóxicos especificados en la descarga total del vertido. Este enfoque se prefiere desde el punto de vista administrativo debido a que el ELV se determina y monitorea fácilmente mediante el muestreo del tóxico al final de la tubería de descarga. Sin embargo, desde una perspectiva ecológica, un control de la calidad del agua basado sólo en ELVs no tiene sentido ya que no proporciona el efecto directo de cada descarga sobre la calidad de agua del medio receptor y, por lo tanto, se desconoce el efluente residual responsable de los daños sobre el medio.
- El EQS tiene la ventaja de tener en cuenta directamente las características y las respuestas de las propiedades físicas, químicas y biológicas del medio debido a la descarga del vertido tóxico y, por lo tanto, determina la responsabilidad directa de cada emisor. Sin embargo, el control de la calidad del agua basada sólo en valores de EQSs podría llevar a una situación en la que una industria podría utilizar la capacidad de asimilación del medio receptor para alcanzar los valores de concentración determinadas por la EQS, sin tener en cuenta la Mejor Tecnología Disponible (BAT).

El ratio de ELV/EQS describe el impacto de las sustancias tóxicas sobre el ecosistema, ya que los ELVs se han especificado para proteger al medio contra los efectos a corto plazo (efecto agudo), mientras que las EQSs se han establecido para prevenir al medio de los efectos a largo plazo (efecto crónico). Esta relación también expresa la dilución requerida en el punto de descarga mediante procesos físicos de mezcla, de desintegración biológica y/o transformaciones químicas para cumplir las EQSs. En este sentido, los regímenes de control de vertidos están normalmente diseñados para garantizar que las sustancias tóxicas en las aguas receptoras no excedan la EQS, no obstante, si el ELV es mayor que el valor de la EQS habrá una zona en las proximidades del punto de descarga donde se exceda la EQS.

Al utilizar el enfoque combinado, las limitaciones de ambos enfoques se compensan parcialmente mientras que la mayoría de las ventajas se mantienen. Al mismo tiempo, puede evitar las limitaciones de capacidad

técnica e institucional que conllevan la gestión completa del medio mediante un enfoque basado en normas de calidad ambiental.

La Unión Europea ha reconocido todas estas ventajas y ha decidido adoptar el enfoque combinado, dentro del marco establecido por la Directiva 2000/60/EC o Directiva Marco del Agua (WFD) (EC 2000), por la Directiva 2008/1/EC o Directiva para el Control y Prevención Integrado de la Contaminación (IPPCD) (EC 2008b) y las Directivas 2008/105/EC y 2013/39/EU o Directivas sobre las Normas de Calidad Ambiental (EQSDs) (EC 2008a, EU 2013), como un método para controlar la calidad del agua superficial (Figura 5). El llamado enfoque combinado se basa en un enfoque que requiere el establecimiento de ELVs basado en las BAT o el ajuste de ELVs adecuados a las EQSs. Por ejemplo, si una EQS requiere unas condiciones más estrictas para poder cumplirse, se establecerán en consecuencia controles de emisión más estrictos o se reducirá el ELV en la fuente. Como consecuencia de este enfoque, la calidad del agua en muchas aguas superficiales de toda Europa ha mejorado sustancialmente en los últimos años ayudada por la adopción de una filosofía que se fundamenta en la reducción, o en la medida de lo posible, la eliminación de la contaminación en el origen.

En el caso de la descarga de aguas residuales industriales, hay 45 sustancias o grupos de sustancias que figuran en la lista de sustancias prioritarias para las que se establecieron EQSs en la Directiva Marco del Agua (EC 2000) y, posteriormente, en las Directivas sobre las Normas de Calidad Ambiental (EC 2008a, EU 2013). La lista completa se encuentra en el anexo I, parte A, de la Directiva 2013/39/EU (EU 2013).

Sin embargo, si tenemos en cuenta los valores de las EQSs establecidas en la Directiva sobre Normas de Calidad Ambiental (EU 2013) y los ELVs establecidos para varias sustancias en otras Directivas, se puede fácilmente concluir que, por lo general, se requiere una dilución de algunos cientos o miles para poder cumplir con las EQSs (Gasperi *et al.* 2008, Ragas *et al.* 1997). Dichas sustancias son los principales responsables del desarrollo de esta tesis ya que sus EQSs se establecen generalmente en microgramos por litro mientras que sus ELVS se establecen en miligramos por litro por lo que habrá una zona donde no se puede cumplir con el enfoque combinado adoptado por Europa (Figura 5). Debido a esta problemática, aparece el concepto de **"zonas de mezcla"** (MZs) en la legislación de Europa, Australia, EE.UU. o Canadá, entre otros.

A escala europea, la Directiva 2008/105/EC (EC 2008a) permite a los Estados miembros admitir este tipo de zonas de excedencia en los cuerpos de agua siempre y cuando se cumplan una serie de criterios. En concreto, en su artículo 4 establece que:

1. Los Estados miembros podrán designar zonas de mezcla adyacentes a los puntos de vertido. Las concentraciones de una o más sustancias enumeradas en el anexo I, parte A, podrán superar las EQSs pertinentes dentro de dichas zonas de mezcla siempre que el resto de la masa de agua superficial siga cumpliendo dichas normas.

2. Los Estados miembros que designen zonas de mezcla incluirán en los planes hidrológicos de cuenca elaborados una descripción de:

   (a) los enfoques y los métodos aplicados para definir dichas zonas, y

   (b) las medidas adoptadas con vistas a reducir la extensión de zonas de mezcla en el futuro.

3. Los Estados miembros que designen zonas de mezcla se asegurarán de que la extensión de cada una de ellas:

   (a) esté limitada a las proximidades del punto de vertido;

   (b) sea proporcionada, atendiendo a las concentraciones de contaminantes en el punto de vertido y a las condiciones aplicables a las emisiones de contaminantes según la reglamentación previa, como autorizaciones o permisos, y en cualquier otra normativa comunitaria pertinente, de conformidad con el principio de aplicación de las mejores técnicas disponibles.

4. Las orientaciones técnicas para la identificación de las zonas de mezcla se adoptarán de conformidad con el procedimiento de reglamentación contemplado en el artículo 9, apartado 2.

Si las **"zonas de mezcla"** no se permitieran, las EQSs se convertirían en los ELVs pudiendo ocasionar que alguna tecnología quedara obsoleta, agregar un coste injustificado a la industria y dar lugar a impactos ambientales inadmisibles en medios no acuáticos (tratamiento y eliminación de residuos, consideraciones sobre el ciclo de vida de la tecnología, uso excesivo de energía, etc).

Desde el punto de vista de las características físicas de los procesos de mezcla, la WFD y las EQSDs no proporcionan ninguna información sobre la aplicación espacial de los valores de las EQSs. Además, ambas directivas no obligan a las autoridades responsables de cada nación a establecer dicha especificación. Por lo tanto, cabe esperar, en la práctica, una considerable incertidumbre así como interpretaciones o métodos de supervisión muy diferentes de las autoridades responsables de la gestión de la calidad del agua. De modo que el enfoque combinado está en peligro de ser pasado por alto o socavado en su aplicación práctica pese a ser un enfoque idóneo para el control ecológico integrado de la contaminación del agua.

Por todo lo anteriormente expuesto, el desarrollo de un método para asignar **"zonas de mezcla"** en estuarios es particularmente necesario y difícil debido a su alta complejidad y variabilidad natural, el escaso conocimiento existente acerca de su funcionamiento y la continua presión que vienen soportando debido a las actividades antropogénicas.

1.2. Descripción del problema: Las descargas industriales en aguas estuarinas

Los sistemas industriales liberan contaminantes de manera continua. Dicha contaminación no podría ser admisible en ausencia del transporte y dilución generado por las corrientes de aire y de agua. En suma, los movimientos de fluidos en el medio ambiente son vitales por lo que se tiene un fuerte incentivo para estudiarlos, en particular, los de aire en la atmósfera y los del agua en todas sus corrientes naturales desde los acuíferos subterráneos a los flujos superficiales de los ríos, lagos, estuarios y océanos (Cushman-Roisin 2013).

El estudio de estos flujos ha recibido considerable atención en los últimos años surgiendo varias disciplinas relacionadas como son la meteorología, la climatología, la hidrología, la hidráulica, la limnología o la oceanografía. Las preocupaciones en la ingeniería ambiental obligan a expertos en dichas disciplinas a considerar problemas que son esencialmente similares. Tales puntos comunes fomentan la multidisciplinariedad en un grado que aumenta en proporción a la relevancia de nuestros problemas ambientales (Cushman-Roisin 2013).

El transporte, mezcla y decaimiento de un efluente se separa habitualmente en tres regiones denominadas ***campo cercano***, ***campo intermedio*** y ***campo lejano*** en las que dominan diferentes mecanismos físicos y químicos (Figure 6):

1. En el ***campo cercano*** (también llamada región de dispersión activa o de dilución primaria), las características iniciales del chorro como son la cantidad de movimiento, la flotabilidad y la configuración del mecanismo de descarga (orientaciones y geometrías) influyen en la trayectoria y mezcla del efluente. La turbulencia inducida por el chorro/pluma mezcla el fluido ambiente con el efluente, dicho proceso se conoce como "entrainment" (Figura 6a,b). Aunque las condiciones ambientales afectan a la descarga una vez que el efluente sale de la tubería, éstas son de menor importancia hasta que se produzca cualquier interacción con algún contorno (superficie, fondo o laterales) o bien alcance una capa estratificada en la columna de agua (Fischer *et al.* 1979). Dicha interacción caracteriza la transición al campo intermedio.

2. El ***campo intermedio*** o zona de establecimiento del campo de contaminantes (Sanchez-Arcilla *et al.* 1998) se caracteriza por el impacto de la pluma turbulenta con los contornos y la transición de las

Procesos Dominantes	**Campo cercano**	**Campo intermedio**	**Campo lejano**
Forzamiento	flujos de cantidad de movimiento y flotabilidad	flujo de flotabilidad y resistencia de los contornos	marea, río, viento, movimientos barotrópicos/clínicos inducidos
Advección	velocidad inducida por el chorro	campo de velocidad ambiental	campo de velocidad ambiental
Mezcla	turbulencia inducida por fuerte cizalla	mezcla frontal en los bordes de la pluma	turbulencia inducida por el fondo y la cizalla, estratificación
Reacciones	conservativo	conservativo	no-conservativo
Variación Temporal	no-estacionario	no-estacionario	muy no-estacionario
Variación Espacial	no-uniforme	no-uniforme	muy no-uniforme

Tabla 1: Visión global de los procesos dominantes que gobiernan cada región de mezcla para descargas de boca única con flotabilidad positiva. Adaptado a partir de Bleninger (2006).

características verticalmente ascendentes de chorros/plumas a un movimiento horizontal generado por el colapso gravitacional de la nube contaminante. Las características iniciales del chorro se vuelven menos importantes. Generalmente, se forma una zona de aguas residuales inicialmente diluidas ya sea en la superficie o bajo la capa estratificada (véase en la figura 6a,b). En el campo intermedio, la condiciones verticales y horizontales de los contornos controlarán la trayectoria y la dilución a través de movimientos de esparcimiento por flotabilidad y la difusión pasiva debido a la mezcla interfacial entre el efluente y el fluido ambiente.

3. En el ***campo lejano*** (también llamado región de dispersión pasiva o de dilución secundaria), las condiciones ambientales controlan la trayectoria y la dilución de la pluma turbulenta a través de la dispersión pasiva inducida por la turbulencia ambiental y la advección pasiva generada por el campo de velocidades ambientales no uniforme y variable con el tiempo (Figura 6c). Además, la reducción de concentración en el campo lejano también está relacionada, de manera significativa, con los procesos de purificación naturales tales como reacciones de desintegración (volatilización, hidrólisis, fotólisis, ...). Finalmente, cabe resaltar que la mezcla vertical en masas de agua estratificados se reduce por lo que la dilución se debe principalmente a la mezcla horizontal por remolinos turbulentos (Fischer *et al.* 1979).

Aunque algunas cabeceras estuarinas se encuentran en áreas de agua dulce, los estuarios se consideran normalmente ambientes marinos. Un efluente de agua dulce vertido en agua salada, típico de aguas residuales industriales en estuarios, generalmente forma una pluma que emerge rápidamente y luego flota sobre la superficie alrededor del punto de descarga. En estos casos, la tasa inicial de mezcla depende de varios factores tales como la profundidad del agua y la turbulencia inducida por la descarga. Una vez en la superficie, la mezcla se limita a la capa superficial hasta que las densidades relativas de las dos masas de agua (efluente y medio receptor) permitan que la mezcla se extienda a lo largo de la columna de agua. En la tabla 1 y la figura 6, se proporciona una visión global de los procesos dominantes que gobiernan cada región de mezcla.

Por otra parte, el impacto ambiental se puede definir generalmente como el conjunto de los posibles efectos ambientales negativos que implican una modificación del entorno natural debido a las actividades humanas. Más específicamente, se puede entender como la perturbación inducida por el hombre que experimenta el medio (Gómez 2010). Para la evaluación de los diferentes efectos ambientales es necesario tener en cuenta la persistencia, duración y frecuencia de exposición a los tóxicos (Saouter *et al.* 2001, USEPA 1991). En lo referente a la delimitación de zonas de mezcla, el impacto ambiental es la superación de las EQSs correspondientes.

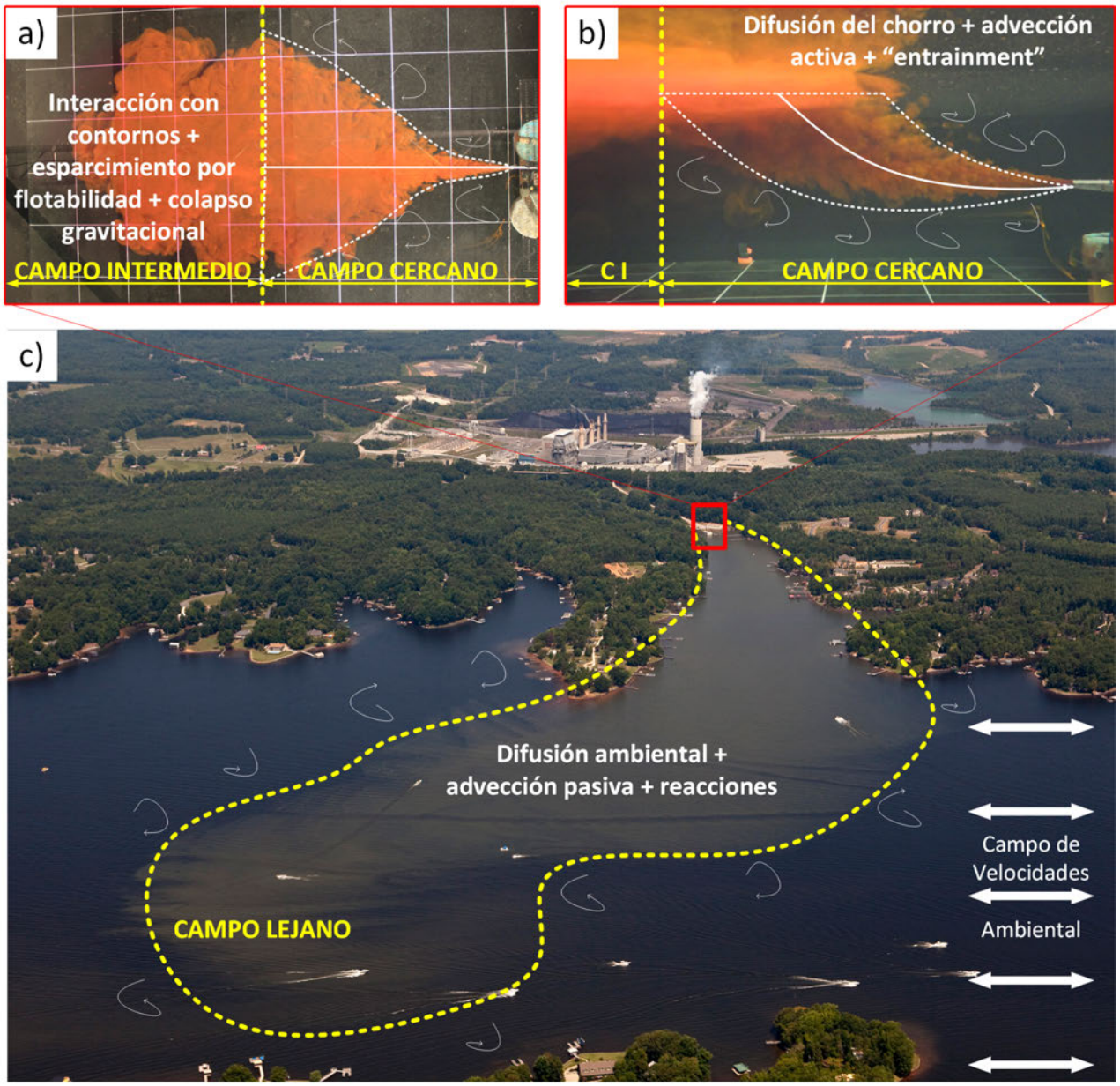

Figura 6: Vista esquemática de un emisario industrial operativo de boca única (c) fusionado con una imagen de un chorro con flotabilidad positiva en planta (a) y perfil (b). Fuentes: (a) y (b) de los experimentos VERTIZE (CTM2012-32538) y (c) http://www.catawbariverkeeper.org/issues/coal-ash-1.

Sin embargo, demostrar tal excedencia para vertidos en estuarios continua siendo una tarea complicada debido a que la calidad del agua depende de numerosas variables aleatorias. Principalmente, depende de las concentraciones de las sustancias presentes en el efluente y su reducción debido al proceso de dilución. Dicho proceso es hidrodinámicamente complejo ya que resulta de la combinación de fenómenos turbulentos inducidos tanto por la descarga como por el medio receptor de forma natural. Otras complicaciones surgen de la variabilidad de las condiciones ambientales en estuarios, incluyendo la estratificación por diferencias de densidad o los rápidos y amplios cambios de velocidad y dirección de las corrientes. Todo ello, puede causar grandes variaciones en la trayectoria y dilución de la pluma en el campo cercano mientras que, en el campo lejano, las concentraciones de la sustancia son enormemente variables debido al impacto intermitente de la pluma en cualquier lugar en particular, a la complejidad de la batimetría estuarina y al continuo y amplio cambio de valores de las variables ambientales (Roberts 1999a;b).

Todos estos factores hacen muy difícil de evaluar los procesos de dispersión de vertidos en estuarios para cuantificar su impacto ambiental y para predecir el riesgo para la salud humana o el riesgo ecológico al que la vida acuática puede estar expuesto, esto es, la delimitación de **"zonas de mezcla"**. No obstante, la introducción de todos estos factores disminuye la capacidad relativa de los datos de campo para investigar los efectos ambientales ya que las condiciones son más complejas. Una manera de abordar estos problemas es el uso del enorme potencial de los modelos numéricos (Moll & Radach 2003).

El modelado numérico puede obtener la evolución espacial y temporal de la concentración de una sustancia tóxica en un sistema acuático permitiendo el uso de criterios espaciales y temporales para la evaluación de sus efectos. Así, el modelado numérico permite la predicción de una respuesta continua en el espacio y el tiempo contra una perturbación a diferencia del uso de datos de campo que permite evaluar la respuesta sólo en lugares y tiempos discretos (Gómez 2010, Guérit *et al.* 2008, McIntyre & Wheather 2004, McIntyre *et al.* 2003, Severinsen *et al.* 1996).

Por todas estas razones, los modelos numéricos son muy valiosos para predecir los efectos sobre los componentes del ecosistema, siendo mucho más rápido y barato que los procedimientos físicos y/o experimentales, como la recolección de datos de campo o de modelado físico (Ruza *et al.* 2007, Westman 1985).

En el campo del análisis del riesgo ambiental, si los modelos numéricos son calibrados y validados adecuadamente se convierten en herramientas insustituibles para hacer frente a la complejidad de los sistemas estuarinos y para describir el impacto de un efluente residual en situaciones reales e hipotéticas (Giupponi *et al.* 1999, Yuan *et al.* 2006). Por todo ello, parece que los modelos numéricos son una herramienta adecuada para realizar estudios de delimitación de **"zonas de mezcla"**.

Por lo tanto, para evaluar zonas de mezcla se necesita predecir el impacto de los efluentes industriales en una amplia gama de condiciones ambientales. Dicha predicción plantea dificultades técnicas especiales ya que las descargas de efluentes a estuarios a menudo se encuentran en aguas relativamente poco profundas de 5-20 m de profundidad y no muy lejos (por ejemplo, 5-10 km) de medios receptores sensibles, tales como playas y/o zonas de pesca y marisqueo. Por ello, las decisiones para determinar apropiadamente las zonas de mezcla deben estar basadas en modelos que pueden abordar la evaluación del impacto en el campo cercano, intermedio y lejano (Choi & Lee 2007). En lugar de combinar los efectos de todas las regiones de mezcla en un sólo modelo, los modelos numéricos disponibles suelen concentrarse principalmente en el campo cercano o lejano debido a la disparidad de escalas temporales y espaciales que dominan cada región de mezcla (Figura 7). .

En las inmediaciones de la descarga (campo cercano), la trayectoria y mezcla del chorro con flotabilidad positiva puede predecirse correctamente por medio de un modelo integral de chorro donde se calcula el "entrainment" en función de las características de la fuente y de las condiciones ambientales (Figura 7). Mayoritariamente, estos modelos asumen que las características del medio receptor en el campo lejano (temperatura, velocidad, etc.) se conocen por lo que el efecto del campo cercano en el campo lejano no se tiene en cuenta

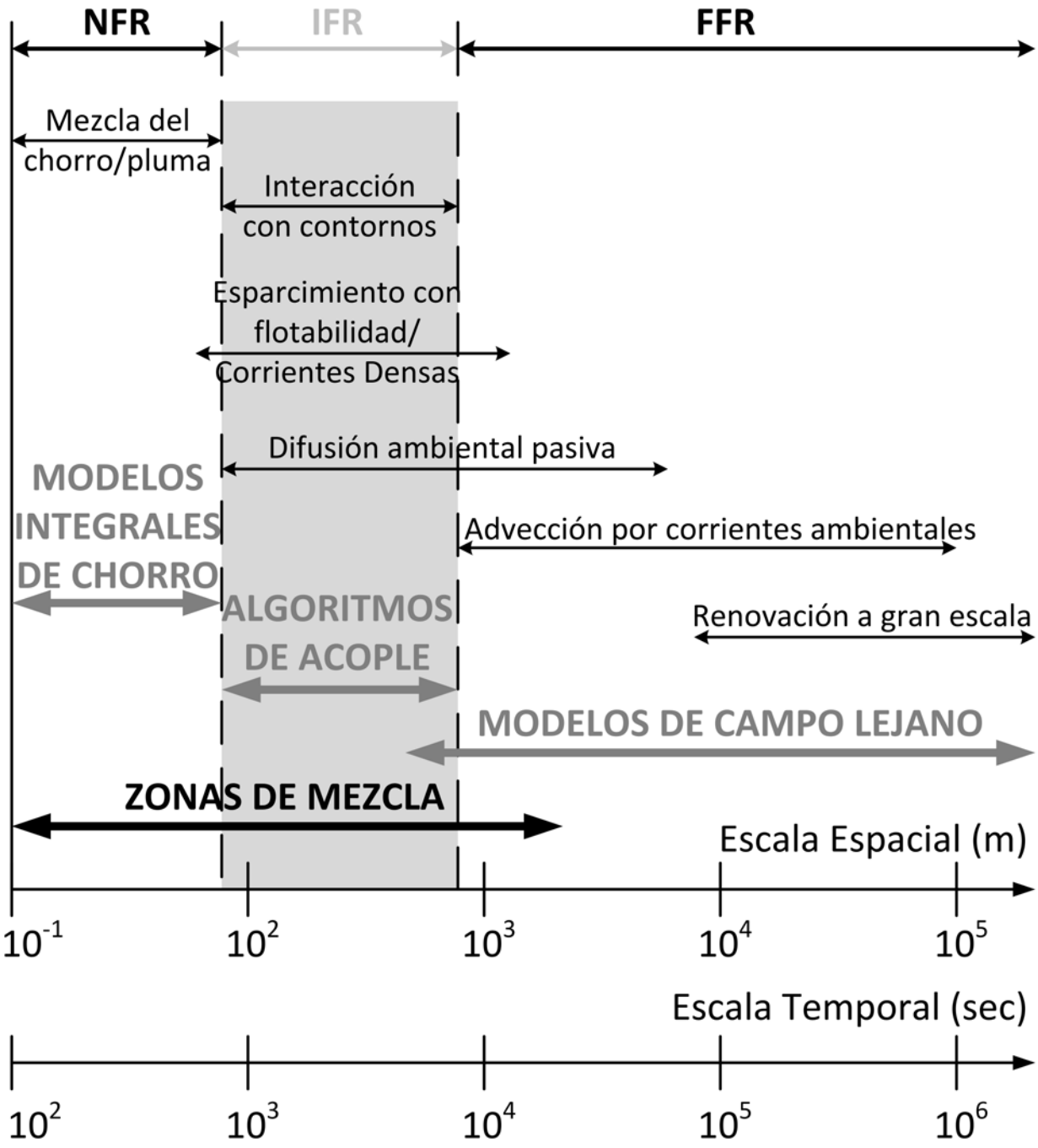

Figura 7: Escalas temporales y espaciales para los procesos de transporte y mezcla relacionados con la descarga de efluentes residuales a estuarios. NFR es la región del campo cercano, IFR es la región del campo intermedio y FFR es la región del campo lejano.

(Kaufman & Adams 1981).

Mientras tanto, en el campo lejano, el efluente se transporta de forma pasiva por las corrientes ambientales y se diluye por la difusión turbulenta en escalas de tiempo y longitud del orden de horas y kilómetros (Figura 7). En los estuarios, los modelos numéricos de transporte se tienen que emplear con el fin de predecir la distribución de tóxicos con condiciones más generales relativas a la circulación estuarina, el transporte de masa y las transformaciones. Estos modelos se basan en la ecuación de "advección-difusión-reacción" o ecuación de transporte (véase la ecuación (1)).

$$\frac{\partial C}{\partial t} + u\frac{\partial C}{\partial x} - D_x\frac{\partial C^2}{\partial x^2} + v\frac{\partial C}{\partial y} - D_y\frac{\partial C^2}{\partial y^2} + w\frac{\partial C}{\partial z} - D_V\frac{\partial C^2}{\partial z^2} = SO + f_R(C,t) \tag{1}$$

donde u, v y w son la velocidad del flujo en cada dirección, D_x, D_y y D_V son los coeficientes de dispersión para cada dirección, SO son los flujos adicionales de agua o masa y f_R son los términos de reacción o "procesos de transformación".

El campo de velocidades en estos modelos de transporte se puede calcular a partir de un modelo hidrodinámico independiente o se puede generar por medio de datos instrumentales. Los modelos de campo lejano tienden a simplificar los efectos del campo cercano al considerar el chorro simplemente como un flujo de masa en el punto de descarga. Dicho procedimiento descuenta muchas influencias del campo cercano en el campo lejano (Kaufman & Adams 1981).

En el caso de descargas por boca única, la magnitud del campo intermedio varía aproximadamente entre 1 hasta 100 m (Figura 7), dependiendo de las características de la descarga (Choi & Lee 2007). El gran tamaño de esta región es una de las principales razones por las que es necesario un enlace entre el modelado del campo cercano y lejano para llevar a cabo una adecuada evaluación del impacto ambiental para delimitar **"zonas de mezcla"**.

La forma más adecuada de resolver este problema es a través de la aplicación de modelos integrados. Dichos modelos constan de un modelo de campo cercano y un modelo de campo lejano que se conectan por medio de un algoritmo de acople. Los modelos de acoplamiento introducen cantidades de flujo (por ejemplo, impulso o masa) desde un modelo al otro y/o viceversa. En este sentido, sólo hay dos posibilidades para introducir cantidades de flujo en un modelo ya sea a través de las condiciones de contorno o mediante términos fuente.

Resumiendo todo lo expuesto, se requiere una aplicación de un modelo integrado para evaluar la delimitación de una **"zona de mezcla"** (Figura 8), incluyendo:

1. Un modelo hidrodinámico que proporciona la información dinámica para el modelo integral de chorro, el modelo de transporte de sedimentos y el modelo de campo lejano.

2. Un modelo integral de chorro que proporciona la información de dilución inicial alimentado por un modelo hidrodinámico.

3. Un modelo de transporte de sedimentos que proporciona la información de sedimentación al modelo de campo lejano alimentado por un modelo hidrodinámico.

4. Un algoritmo de acople que introduce las cantidades de flujo, calculadas con el modelo integral de chorro, en el modelo de campo lejano.

5. Un modelo de campo lejano que proporciona la evolución temporal y espacial de los tóxico/s estudiado/s en el estuario.

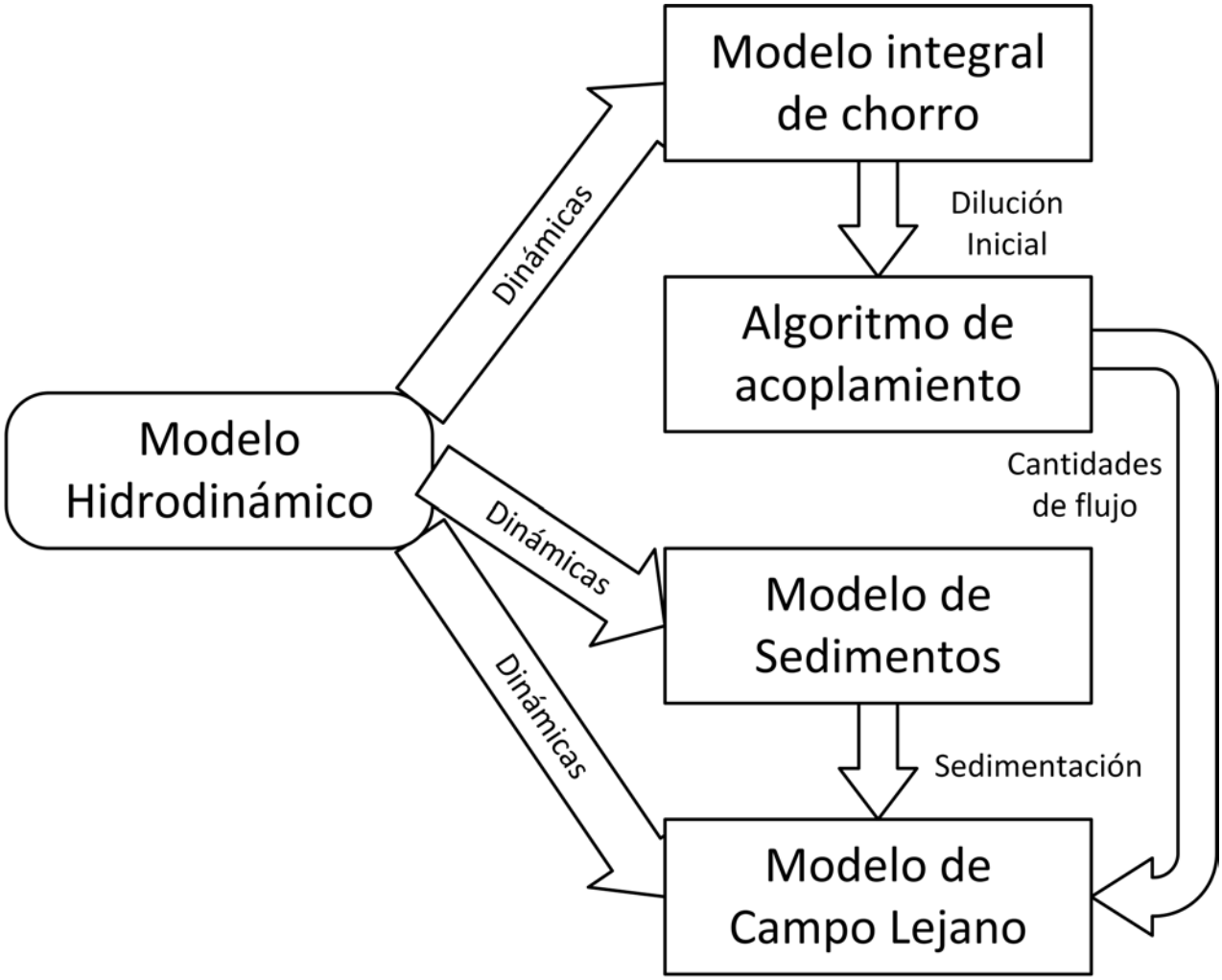

Figura 8: Configuración del modelo integrado requerido para la determinación de zonas de mezcla en medios estuarinos.

En las últimas décadas se han logrado avances significativos que han ayudado a los modelos matemáticos a convertirse en herramientas fiables para la gestión ambiental u otras aplicaciones de ingeniería dentro de todas las regiones de mezcla (campo cercano, intermedio y lejano). Entre estos modelos numéricos cabe destacar los siguientes:

- EFDC, ROMS, POM, MOHID, Delft3D-FLOW y TELEMAC-3D son programas de código abierto para docencia, investigación o uso comercial, motivando que se conviertan en las herramientas hidrodinámicas tridimensionales más utilizadas hoy en día.
- En la región de campo cercano, los modelos integrales como CORJET (sistema CORMIX), UM3 (paquete PLUMES VISUAL), JETLAG (sistema VISJET) y MOHIDJET (sistema MODHID) son los más difundidos internacionalmente.
- En la región del campo intermedio, un acople pasivo podría ser suficientemente preciso debido a que el flujo inducido por las descargas de aguas residuales, aunque es muy importante para la mezcla de campo cercano, no cambia las características de flujo del campo lejano. Además, las administraciones, consultoras e industrias generalmente utilizan diferentes modelos de modo que la introducción de cambios en este tipo de códigos (independientemente de si son comerciales o de código abierto) es costosa y requiere mucho tiempo, mientras que la aplicación de un acoplamiento pasivo entre modelos existentes proporciona una solución más fácil y barata.
- Por último, en la región del campo lejano, MOHID, D-Water Quality (Delft3D-FLOW) y WASP7 (EFDC) son sistemas integrados de modelado hidrodinámico y de calidad de aguas así como programas de código abierto para docencia, investigación o uso comercial. Estas características han conducido a que se conviertan en las herramientas más adecuadas para resolver la mezcla, el transporte y la reacción de aguas residuales en estuarios con el fin de determinar zonas de mezcla.

Por otro lado, la zonificación ambiental se ha convertido en la herramienta para identificar, distribuir, organizar y regular el medio ambiente de acuerdo con ciertos criterios y prioridades. Administrativamente, la zonificación ambiental se ha centrado en los usos del suelo a través de una serie de criterios, normas y planes que rigen las actividades del suelo para obtener una adecuada relación entre territorio, población, servicios e infraestructura. Su aplicación específica a los estuarios se ha llevado a cabo por medio de los planes de gestión, con el objetivo final de establecer los criterios para la protección de este espacio (Ondiviela *et al.* 2007). Para ello es necesario diseñar un procedimiento metodológico donde el medio estuarino se pueda clasificar en diferentes zonas a través del empleo de diferentes usos del estuario.

Como regla general, los enfoques metodológicos para asignar zonas de mezcla en cualquier sistema acuático se basan en dos criterios ambientales de calidad del agua: el criterio de toxicidad aguda debido a la máxima concentración (MAC-EQS) y el criterio de toxicidad crónica debido a la concentración media (AA-EQS). De acuerdo con estos valores, se pueden establecer dos tipos de zonas de mezcla de acuerdo con los mencionados criterios. Por último, si es necesaria una mayor protección de la calidad del agua del medio receptor se aplican límites más estrictos específicamente en cada caso.

A pesar de que todas las metodologías propuestas son buenas herramientas para empezar a hacer frente a los riesgos asociados a la descarga de aguas residuales, las métricas, fórmulas y cálculos que se describen en ellas están generalmente demasiado orientadas hacia otros sistemas acuáticos, especialmente hacia descargas fluviales. En el caso de vertidos estuarinos, la determinación de zonas de mezcla es un tanto ambigua porque carece de una explicación detallada de las tareas necesarias para llevar a cabo este tipo de trabajo.

Para ello, el método propuesto debe ser lo más general posible basándose en una metodología escalonada con un grupo de herramientas numéricas seleccionadas y/o desarrolladas. Además, un enfoque caso por caso es esencial para el uso racional de los recursos naturales de los estuarios debido a que cada zona de mezcla

debe adaptarse a las características físicas, químicas y biológicas del estuario y su particular comunidad de organismos.

Por todo lo anteriormente expuesto, se puede concluir que el desarrollo de una metodología para cumplir con todos estos imperativos es una tarea que aún no ha sido resuelta completamente. Por ejemplo, en Europa, la Autoridad Competente es responsable de la designación y desarrollo de zonas de mezcla bajo los mandatos de las Directivas 2008/105/EC y 2013/39/EU, debiéndose entregar una metodología o enfoque proporcionado para el cálculo del riesgo de tal manera que todos los factores relevantes se consideren con un nivel de detalle apropiado (EC 2008a, EU 2013). Si bien es cierto que un enfoque basado en un monitoreo uniforme podría permitir la determinación y administración eficiente de una gran proporción de casos, la complejidad inherente y variabilidad de las aguas estuarinas en toda Europa conduce a que, en algunos casos, no sean posibles soluciones simples. Por ello, se requiere la definición de criterios de aceptabilidad específicos para cada caso (EC 2010).

1.3. Objetivos generales y específicos

El objetivo del presente trabajo es proporcionar una metodología escalonada con un grupo de herramientas numéricas seleccionadas y/o desarrolladas con el fin de establecer dónde se requiere una zona de mezcla y determinar su tamaño y aceptabilidad con un nivel de detalle apropiado de acuerdo a su relevancia para cada vertido industrial descargado por boca única situado en un estuario. Esta propuesta puede ser aplicada tanto por los Estados miembros como las industrias a la hora de delimitar zonas de mezcla según lo establecido en la Directiva 2008/105/EC (EC 2008a) y la Directiva 2013/39/EU (EU 2013).

Teniendo en cuenta el objetivo general de esta tesis y la descripición del problema, con el fin de lograr este objetivo final, se determinan los siguientes objetivos específicos:

- Selección y descripción de las características de los modelos numéricos requeridos para el cálculo de la mezcla, el transporte y la reacción de sustancias conservativas y no conservativas en sistemas estuarinos. Dichos modelos numéricos deben ser capaces de caracterizar el flujo y las cargas tóxicas asociadas con vertidos puntuales continuos en diferentes condiciones hidrometeorológicas.

- Desarrollo de una herramienta matemática para el cálculo del campo intermedio, es decir, el acoplamiento del campo cercano y lejano. Para ello, se utilizará el campo de velocidades de un modelo de circulación estuarino como datos de entrada para un modelo integral de chorro con el fin de obtener las concentraciones de la sustancia en el campo cercano. A su vez, dichos resultados se emplearán como datos de entrada para un modelo de transporte en campo lejano con el fin de obtener las concentraciones de la sustancia en el campo lejano.

- Desarrollo de un método para determinar y seleccionar escenarios de modelado con base en los principales modos de variabilidad de los forzamientos estuarinos.

- Desarrollo de un procedimiento para determinar el periodo óptimo de estudio teniendo en cuenta una descripción adecuada de la variabilidad de los fenómenos hidrometeorológicos y ambientales relacionados con la evolución de tóxicos que minimize los costes computacionales.

- Desarrollo de una metodología para cuantificar la vulnerabilidad estuarina frente a descargas industriales puntuales teniendo en cuenta los patrones de estratificación estuarinos, las escalas temporales de transporte en estuarios y los usos del suelo.

- Definición de una métrica para determinar la extensión y la aceptabilidad de zonas de mezcla teniendo en cuenta los criterios de la Directiva 2008/105/EC (EC 2008a) y la Directiva 2013/39/EU (EU 2013).

1.4. Consideraciones finales

Finalmente, se han establecido una serie de consideraciones en este trabajo para las zonas de estudio y los vertidos de sustancias tóxicas.

En cuanto a las zonas de estudio, la propuesta se centra en estuarios donde la marea astronómica y los aportes fluviales son los forzamientos más importantes para entender el comportamiento medio de la hidrodinámica estuarina. Este tipo de estuarios se extienden por todo el mundo por lo que una metodología para entender su comportamiento podría ayudar a investigadores, técnicos y/o administradores a gestionar de manera más eficiente dichos estuarios. Entre otros, se podrían mencionar Suances (Bárcena *et al.* 2012b), Huelva (Sámano *et al.* 2012), Urdaibai (García *et al.* 2010a), Mandovi (Vijith & Shetye 2012), Mondego (Ascione-Kenov *et al.* 2012), Hudson (Warner *et al.* 2005), Alafia (Chen 2007), Tanshui (Liu *et al.* 2002), Columbia (Chawla *et al.* 2008), Yaquina (Frick *et al.* 2007), Ribble (Kashekipour *et al.* 2001), Haihe (Bai *et al.* 2003) o Humber (Edwards & Winn 2006).

En lo referente a vertidos de sustancias tóxicas, se ha asumido que las BAT están implementadas en toda la planta industrial. Esta tesis se centra en el estudio de descargas por boca única con flotabilidad positiva influenciadas por corrientes ambientales debido a que los vertidos industriales son generalmente de agua dulce (menos densa que las aguas salobres de estuarios). Por último, los vertidos hiperdensos y la escorrentía difusa no se han tenido en cuenta a la hora de desarrollar el método debido a su diferente naturaleza y comportamiento en el medio receptor.

En cuanto a los procesos físicos, químicos y biológicos, se han descartado ciertos procesos tales como cambios en el pH, el cálculo del coeficiente de partición en función de la salinidad, la determinación de algunas constantes específicas de cada área de estudio o la inclusión de procesos de mineralización, bioconcentración y/o resuspensión. Todos estos procesos permiten alcanzar una mayor precisión de los resultados. Sin embargo, también aumentan considerablemente todos los parámetros y coeficientes necesarios para realizar el modelado del transporte de sustancias tóxicas en aguas estuarinas. Como consecuencia de la inclusión de estos procesos se tiene que cuanto mayor es el nivel de complejidad de un modelo, mayor cantidad de información y mayores costos computacionales se requieren. Además, los datos necesarios para ejecutar y, posteriormente, calibrar el modelo son cada vez más específicos y escasos.

A pesar de que se han ignorado las últimas cuestiones para el desarrollo de la propuesta, se consideran futuros temas de investigación en escenarios específicos en los que la influencia de dichas cuestiones sea muy significativa para la determinación de zonas de mezcla.

2. Metodología general

En esta tesis se ha desarrollado una metodología escalonada (árbol de decisiones) que pueda ser adoptada por los Estados miembros y/o industrias a la hora de establecer zonas de mezcla (MZs) según lo establecido en la Directiva 2008/105/EC (EC 2008a) y la Directiva 2013/39/EU (EU 2013). Dicho método proporciona una solución a medida con un nivel de detalle adecuado para cada descarga en forma de diagramas de flujo. En la figura 9, se muestra una visión esquemática de la metodología desarrollada.

El árbol de decisiones se ha desarrollado mediante cinco pasos. En el Paso 1, se recopila la información necesaria del área de estudio y el vertido de sustancias tóxicas. El Paso 2 identifica la relevancia del vertido en el área de estudio. A continuación, el Paso 3 evalúa el efecto generado por el vertido y se delimita las MZs a partir de un cálculo simplificado, es decir, el escenario donde la dilución experimentada por la descarga es mínima ya que los principales forzamientos presentan magnitudes muy bajas. Después de esta etapa, el Paso 4 evalúa el efecto generado por el vertido y se delimita las MZs mediante un cálculo intermedio que considera el escenario en el que la dilución experimentada por la descarga está relacionada con el año más seco de

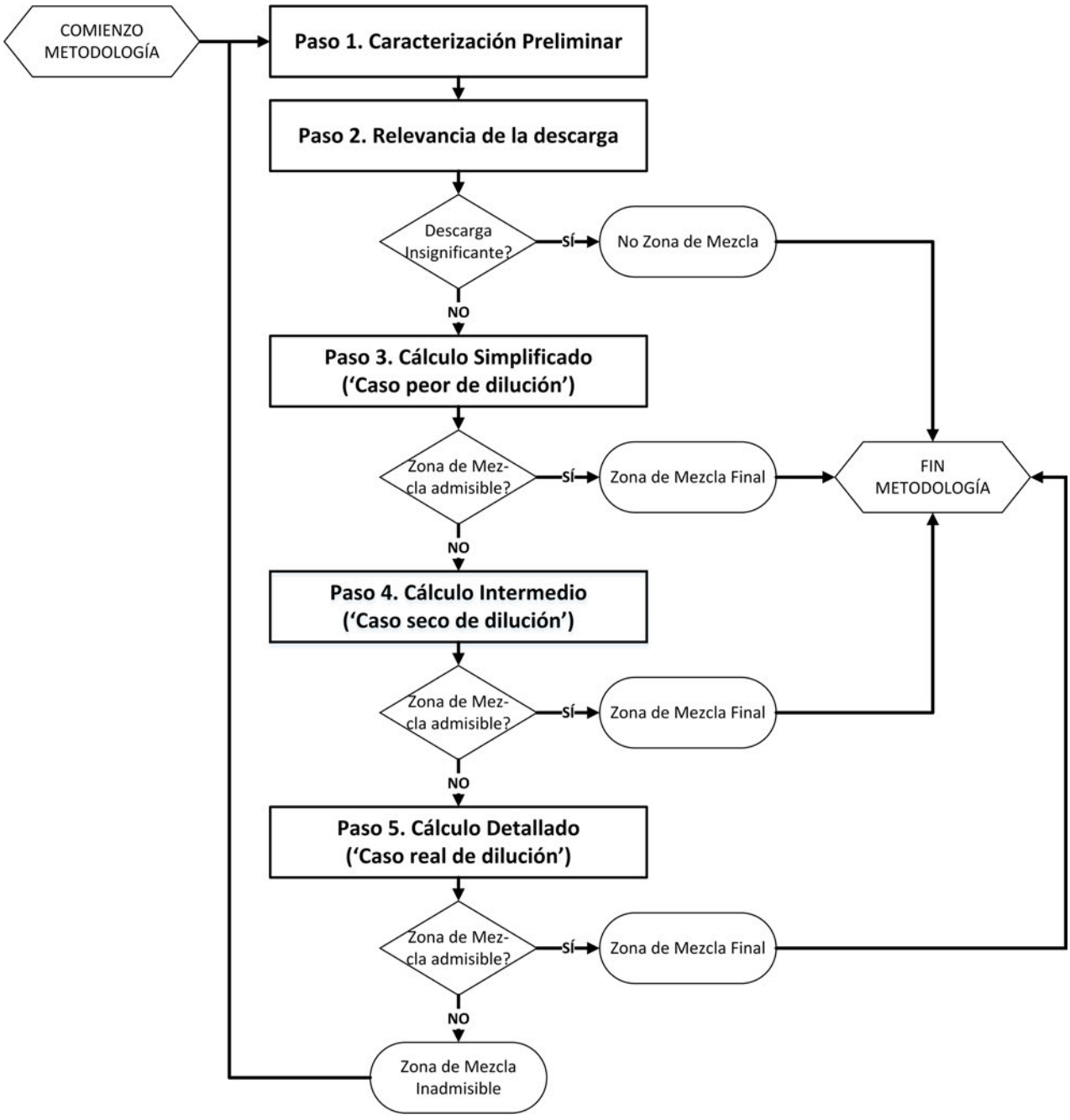

Figura 9: Visión esquemática de la metodología propuesta.

la serie de caudales fluviales. Finalmente, en el Paso 5, se "reevalúa" el efecto generado por la descarga y se "redelimita" la MZs mediante una selección de escenarios en los que la dilución experimentada por la descarga está sujeta a la variabilidad temporal de los principales forzamientos. Por otra parte, en el Paso 5, la admisibilidad de las MZs se evalúa a partir del concepto de vulnerabilidad y el porcentaje de área estuarina cubierto por las MZs.

La regla general del procedimiento de delimitación de MZs es que el grado de sofisticación y complejidad de los cálculos se elevará en cada paso de la metodología debido al aumento de la relevancia de la descarga. Los procedimientos más sencillos requieren menos datos y conocimientos pero también tienden a ser menos precisos. En cada etapa, el objetivo es identificar aquellos vertidos que no son motivo de preocupación y señalar las descargas que requieren medidas para poder reducir el tamaño de su MZ. De este modo, la filosofía del árbol de decisiones es la de aumentar los recursos utilizados cuando la entidad del vertido se incrementa (Figura 10).

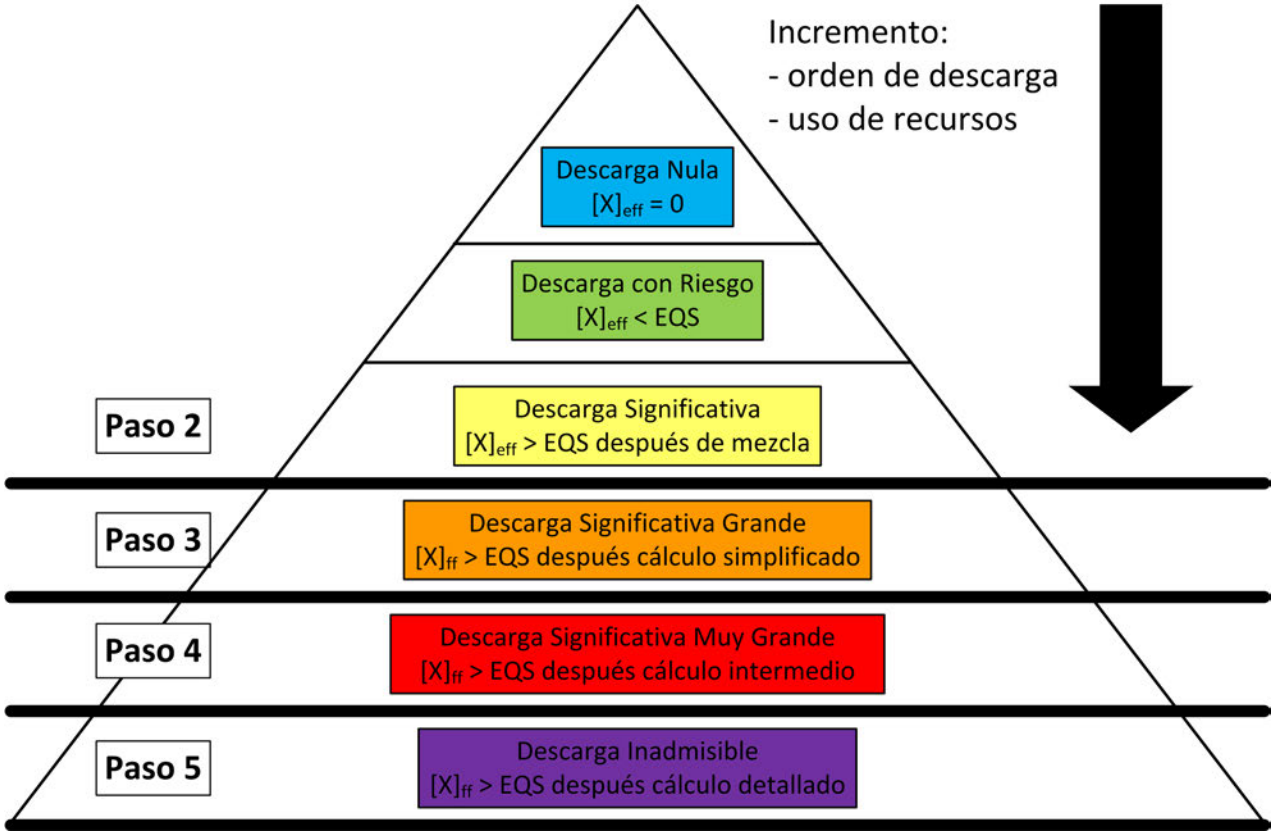

Figura 10: Filosofía del árbol de decisiones desarrollado en la propuesta metodológica.

Finalmente, cabe indicar que la metodología promueve un marco uniforme y con bases sólidas para tales determinaciones proporcionando soluciones que son: *eficientes* porque se utilizan los recursos sólo cuando son necesarios y proporcionales a las preocupaciones ambientales que se abordan; *robustas* porque conducen a decisiones sensatas y reproducibles que contribuyen al uso sostenible del medio ambiente estuarino; y *flexibles* porque satisfacen las necesidades de los estuarios de Europa.

2.1. Paso 1. Caracterización preliminar

Antes de comenzar el estudio del impacto generado por una descarga industrial sobre el medio ambiente estuarino, la caracterización preliminar del efluente/s y el área de estudio es una tarea esencial que determina todas

las decisiones adoptadas posteriormente en el árbol de decisiones desarrollado en este enfoque metodológico. Los principales aspectos de esta caracterización se muestran en la figura 11.

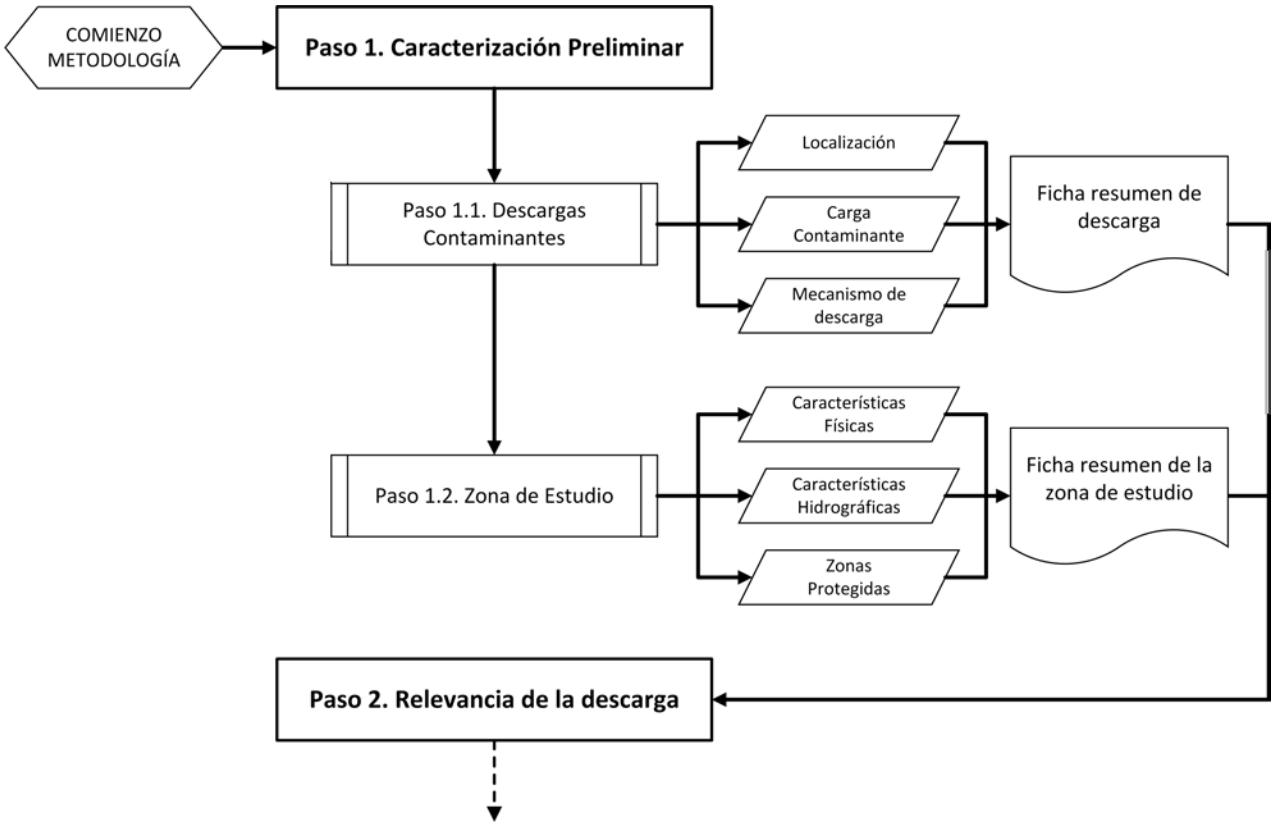

Figura 11: Diagrama de flujo desarrollado para el Paso 1. Caracterización preliminar.

2.1.1. Vertidos de sustancias tóxicas

La caracterización de los vertidos de sustancias tóxicas permite conocer los principales parámetros de la descarga, lo que facilitará la evaluación posterior de la mezcla o dilución experimentada por el efluente. Para obtener esta información, se ha elaborado una ficha resumen conteniendo tres tipos de datos de entrada (campos): localización, carga tóxica y mecanismo de descarga.

Una breve descripción de la información requerida se da a continuación (Figura 12):

- *Localización:* Este campo proporciona información sobre el nombre del sitio, el titular del vertido y las coordenadas geográficas del punto de descarga.
- *Carga contaminante:* En este campo, se especifican el caudal y la densidad del efluente, las sustancias tóxicas descargadas y su concentración. Además, se recogen las normas de calidad ambiental (EQS) establecidas en la Directiva 2013/39/UE para dichas sustancias (EU 2013).
- *Mecanismo de descarga:* Las principales características geométricas son el diámetro de la tubería, el ángulo con la línea de la costa medido a partir de la dirección norte y en sentido horario, la profundidad media del medio receptor y la profundidad en el punto de descarga.

Finalmente, cabe mencionar que el ángulo vertical de la tubería con un plano de referencia horizontal se considera nulo para todas las descargas ya que esta configuración es la más común.

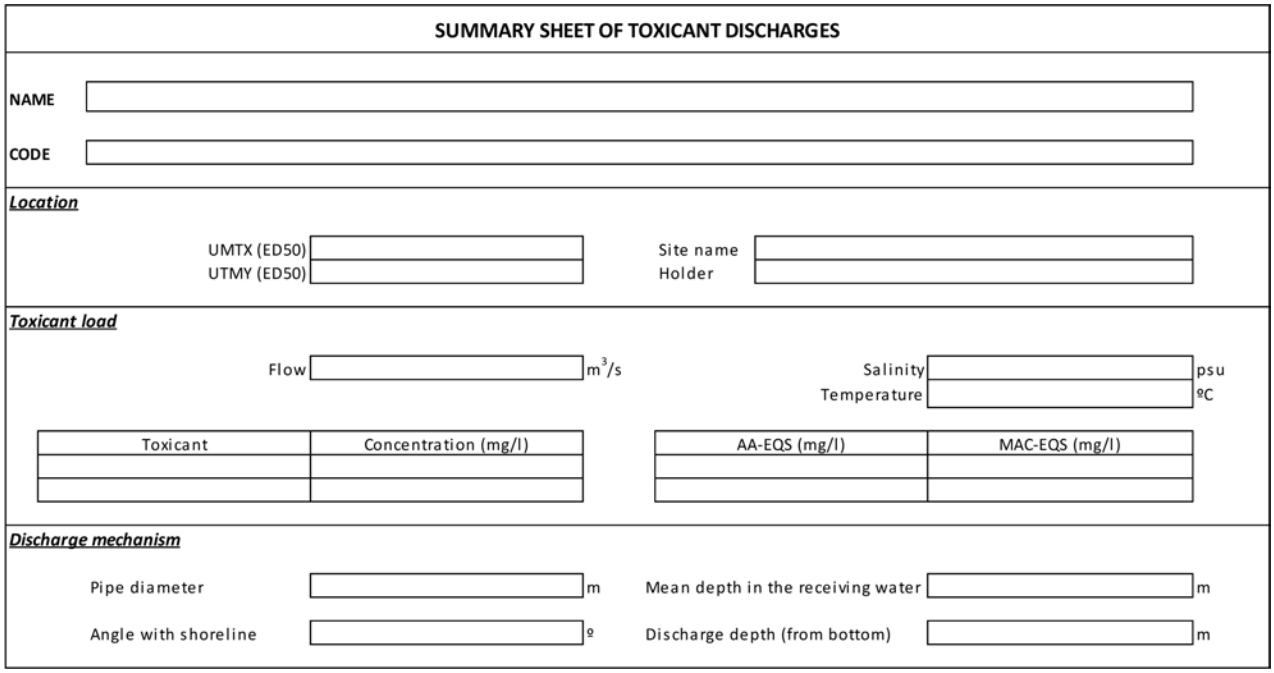

SUMMARY SHEET OF TOXICANT DISCHARGES

NAME

CODE

Location

UMTX (ED50)
UTMY (ED50)
Site name
Holder

Toxicant load

Flow m^3/s
Salinity psu
Temperature ºC

Toxicant	Concentration (mg/l)	AA-EQS (mg/l)	MAC-EQS (mg/l)

Discharge mechanism

Pipe diameter m
Mean depth in the receiving water m
Angle with shoreline º
Discharge depth (from bottom) m

Figura 12: Ficha resumen para caracterizar los vertidos de aguas residuales industriales descargados al medio estuarino.

2.1.2. Zona de estudio

La descripción del estuario se organizó también en tres campos: características físicas, características hidrográficas y zonas protegidas. En primer lugar, las características físicas representan las dimensiones del estuario. En segundo lugar, se describen las principales características hidrográficas del estuario y, en tercer lugar, se enumeran, si las hubiera, las zonas protegidas del mismo. Para facilitar esta tarea, una nueva ficha resumen se ha desarrollado con el fin de revisar y mostrar la información de partida disponible sobre la zona de estudio (Figura 13).

- *Características físicas:* Son el tipo geomorfológico de estuario, la batimetría, la superficie total de estuario, la superficie de zonas intermareales, la anchura máxima, mínima y media del estuario, la profundidad máxima, mínima y media del estuario y la longitud del canal principal.
- *Características hidrográficas:* Engloban a la serie temporal y la función de distribución de la marea astronómica y de los caudales fluviales, la carrera de marea y la salinidad máxima, mínima y media del estuario.
- *Zonas protegidas:* Estas zona se encuentran bajo protección especial gracias a alguna normativa específica para la protección de sus aguas superficiales o la conservación de los hábitats y especies que dependen directamente de esta agua. Los acuerdos internacionales, las directivas europeas y/o la legislación nacional y regional establecen diferentes categorías de zonas protegidas.

2.2. Paso 2. Relevancia de las descargas

Este módulo está diseñado para detectar los vertidos que no tienen un impacto significativo en el estuario, es decir, no se necesita evaluar las MZs, con el fin de evitar estudios detallados y costosos en descargas que son insignificantes. En la figura 14, se presenta el diagrama de flujo desarrollado para diferenciar la entidad de las descargas.

SUMMARY SHEET OF STUDY AREA

NAME

CODE

Physical features

	Geomorphological type	Source		Type		
	Bathymery	Source		Map		
	Estuarine total area	Source		Value		m^2
	Intertidal area	Source		Value		m^2
	Maximum, minimum and mean widths	Source		Value		m
	Maximum, minimum and mean depths	Source		Value		m
	Main channel length	Source		Value		m

Hydrographic features

	Tidal range distribution	Source		Value		m
	River flow distribution	Source		Value		m^3/s
	Maximum, minimum and mean salinities	Source		Value		psu

Protected areas

	General area	Source		Value		m^2
	Fish	Source		Value		m^2
	Shellfish	Source		Value		m^2
	Recreational use	Source		Value		m^2
	Vulnerable area	Source		Value		m^2
	Sensitivity area	Source		Value		m^2
	Protected habitat	Source		Value		m^2
	Birds	Source		Value		m^2
	Wetlands	Source		Value		m^2

Figura 13: Ficha resumen para caracterizar la información relativa al área de estudio.

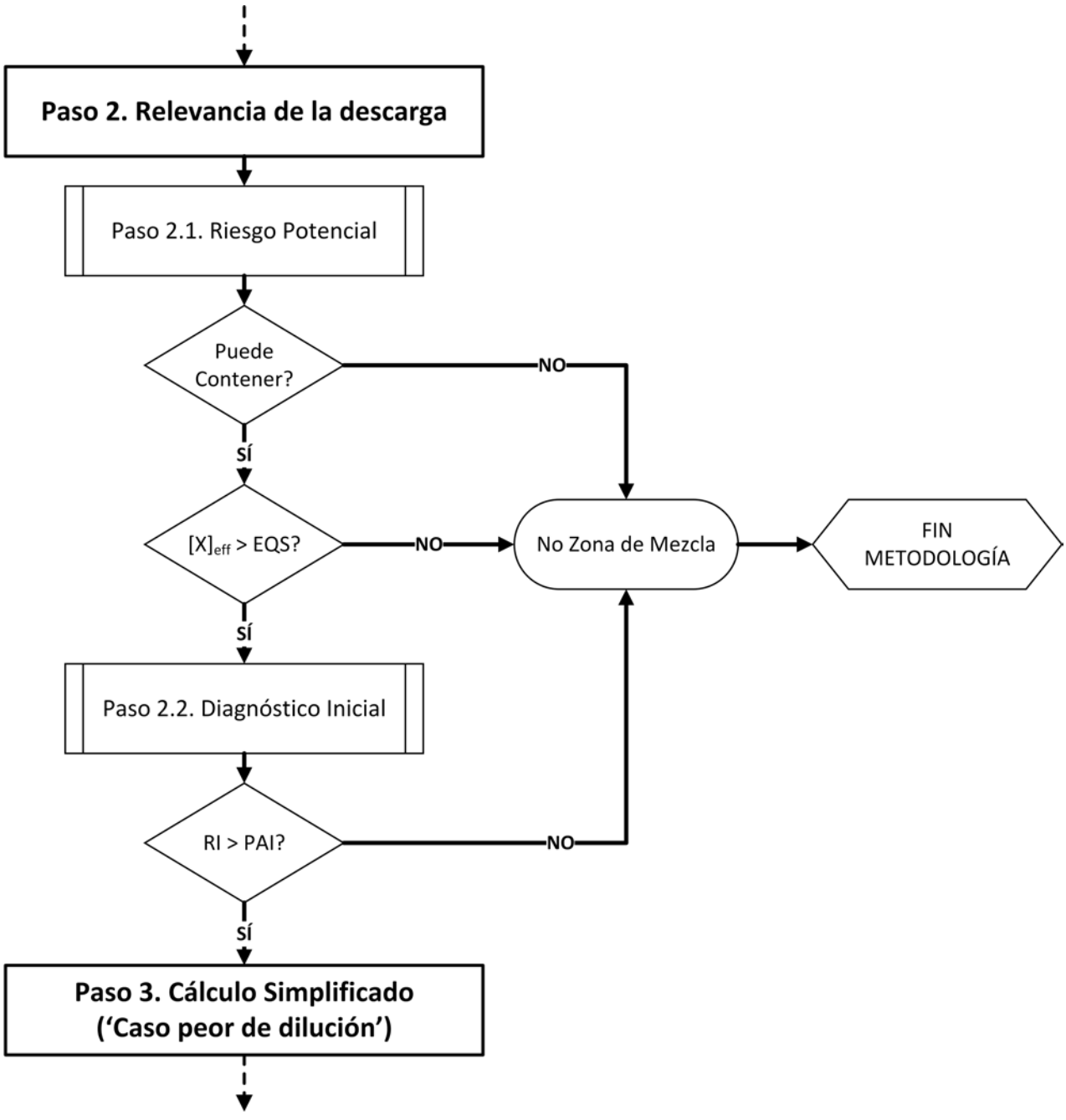

Figura 14: Diagrama de flujo desarrollado para el Paso 2. Relevancia de las descargas.

Tipos Río	Caudal (Q10) [m^3/s]	PAI después de mezcla como % EQS
Pequeño	Q $\leqslant$ 100	4.0
Medio	100 <Q $\leqslant$ 300	1.0
Grande	Q >300	0.5

Tabla 2: Propuesta de aumento autorizado (PAI) en la concentración tras mezcla completa para diferentes tipos de masas de agua. Fuente: EC (2010).

2.2.1. Riesgo potencial

Esta subsección identifica los vertidos con riesgo de sobrepasar los límites fijados en las Directivas EQS (EC 2008a, EU 2013), es decir, la AA-EQS y la MAC-EQS, en dos subetapas:

1. Se realiza una comprobación para ver si la descarga es susceptible de contener cualquier contaminante especificado en la Directiva EQS. En caso negativo, las MZs son insignificantes y el árbol de decisiones termina indicando que no hay MZs y clasificando la descarga como una descarga nula (Figura 10). Por el contrario, si existe un riesgo potencial de exceder la EQS es necesario abordar una siguiente verificación.

2. Se realiza una comprobación para ver si las sustancias tóxicas en cuestión superan las EQSs. Los umbrales de las EQSs se superan, si la concentración promedio del efluente es superior a la AA-EQS o la máxima concentración del efluente es superior a la MAC-EQS. Si ambas concentraciones son inferiores a las EQSs y ningún otro vertido libera las mismas sustancias tóxicas, las MZs son insignificantes. Una vez más, no hay MZs y el árbol de decisiones finaliza clasificando estos vertidos como descargas de riesgo (Figura 10). Por el contrario, si existe una evidencia de que se supera las EQS se pasa a la siguiente subetapa en el árbol de decisiones para determinar su relevancia.

2.2.2. Diagnóstico inicial

En este apartado, se realiza una estimación rápida del impacto generado por los posibles vertidos de riesgo mediante formulaciones sencillas (EC 2010). El objetivo es determinar la contribución del proceso (PC) de la descarga a la EQS tras la mezcla total (Ecuación (2)):

$$PC = \frac{[X_{med}]_{eff} Q_{eff}}{(Q_{river} + Q_{eff})} \tag{2}$$

Cuando se establece un máximo para estos contaminantes en la autorización de vertido, este es el valor que se puede utilizar en el cálculo. En caso contrario y si se dispone de datos suficientes de la calidad del agua del efluente, se debe emplear la concentración media ($[X_{med}]$). Además, se debe utilizar el caudal medio del efluente y el percentil 10 del caudal del río (caudal que no se supera durante el 10 % del tiempo).

Por último, se comprueba el aumento relativo (RI) del PC como un porcentaje de la EQS mediante la ecuación (3) con la propuesta de aumento autorizado (PAI) dado en la tabla 2 (EC 2010).

$$RI = \frac{PC}{EQS} \cdot 100\,\% \tag{3}$$

Si el aumento del PC es inferior a un porcentaje del valor de la EQS especificado en la tabla 2, entonces la descarga es insignificante. Sin embargo, antes de que finalmente se pueda aceptar el vertido, se debe comprobar que la ubicación del punto de descarga está fuera de cualquier zona protegida especificada en el Paso 1. Si,

por el contrario, la descarga se clasifica como significativa se continúa con la Etapa 3 del árbol de decisiones (Figura 10).

2.3. Paso 3. Cálculo simplificado (Caso peor de dilución)

Una vez que los vertidos significativos han sido detectados, se comienza a aplicar el Paso 3 del árbol de decisiones. En el cálculo simplificado, la mezcla física es el único mecanismo responsable de la dilución del tóxico en el campo cercano y lejano de modo que estas sustancias se consideran conservativas. Adicionalmente, los forzamientos hidrodinámicos se establecen a partir de un enfoque de precaución donde la dilución alcanzada es mínima.

El Paso 3 se compone por 6 subsecciones como se ilustra en la figura 15. A lo largo de los cálculos de este trabajo, se puede emplear cualquiera de los modelos hidrodinámicos, de campo cercano y de campo lejano mencionados.

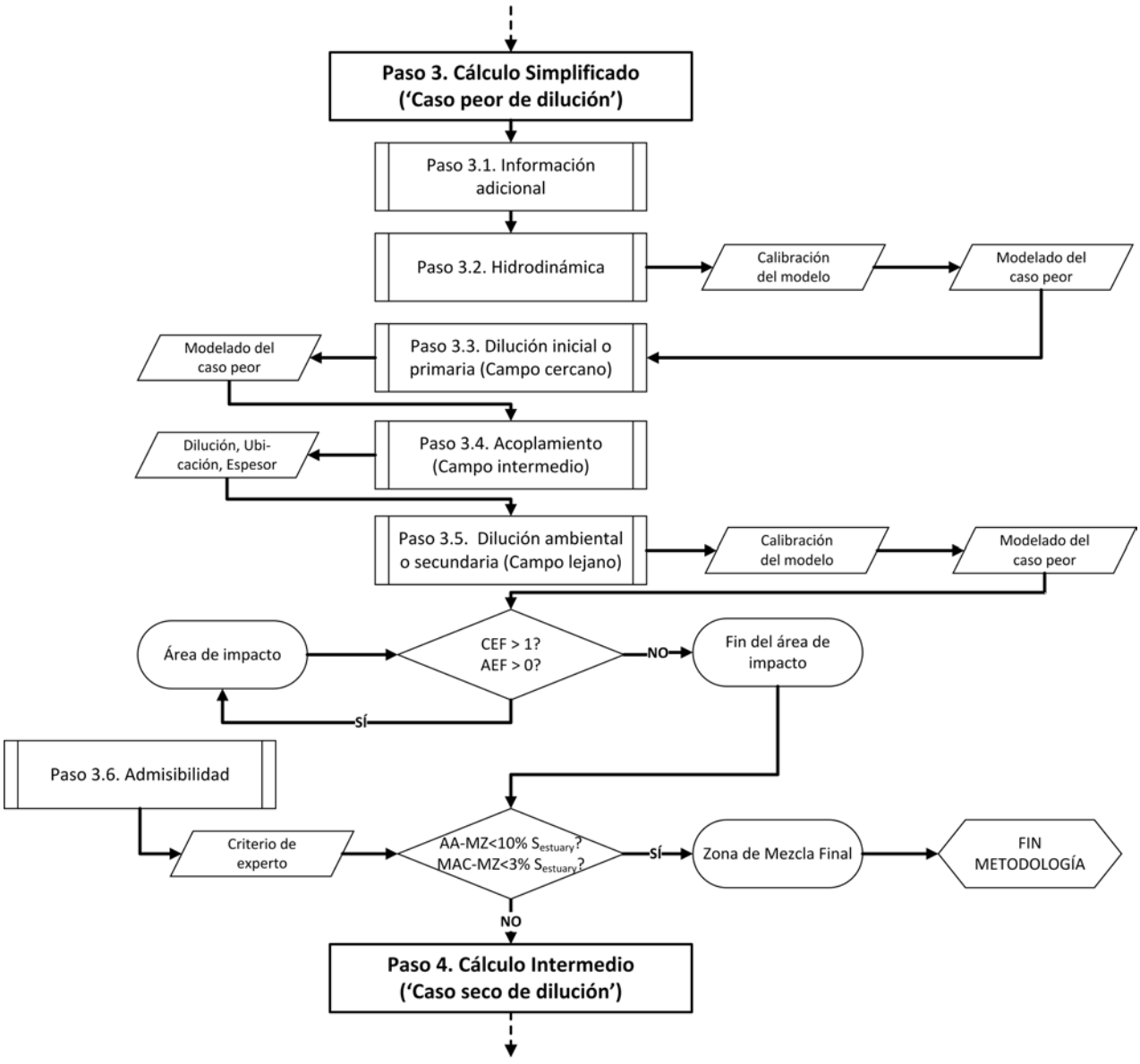

Figura 15: Diagrama de flujo desarrollado para el Paso 3. Cálculo simplificado (Caso peor de dilución).

2.3.1. Información adicional

Esta información está relacionada con las mediciones (datos de campo) necesarias para llevar a cabo la configuración de los modelos numéricos. Por lo tanto, los datos de muestreo como mínimo deben incluir:

- Mediciones de los niveles de agua en dos puntos del estuario cada 15 minutos durante 15 días.
- Mediciones de los caudales fluviales instantáneos en una sección no influenciada por la marea cada 24 horas durante 15 días.
- Perfiles verticales de corrientes instantáneas (velocidades y direcciones) y de salinidad en dos puntos del estuario en condiciones de marea muertas y vivas. En ambas condiciones de marea, las mediciones deben incluir dos valores para cada fase de marea (pleamar, vaciante, bajamar y llenante), es decir, dos ciclos de marea dentro del período de 15 días.

Además, se requieren datos de campo de temperatura y salinidad para definir los contornos abiertos. Por ello, las mediciones de ambas variables deben estar disponibles en un punto de muestreo para el río y, en otro, para la marea durante al menos un año con frecuencia estacional.

2.3.2. Hidrodinámica

2.3.2.1. Configuración del modelo

La configuración del modelo se requiere para definir la discretización del dominio del mismo, para proporcionar las condiciones de contorno e iniciales y, por último, para llevar a cabo la calibración/validación del modelo con el fin de seleccionar la mejor configuración de los parámetros de éste (Figura 16).

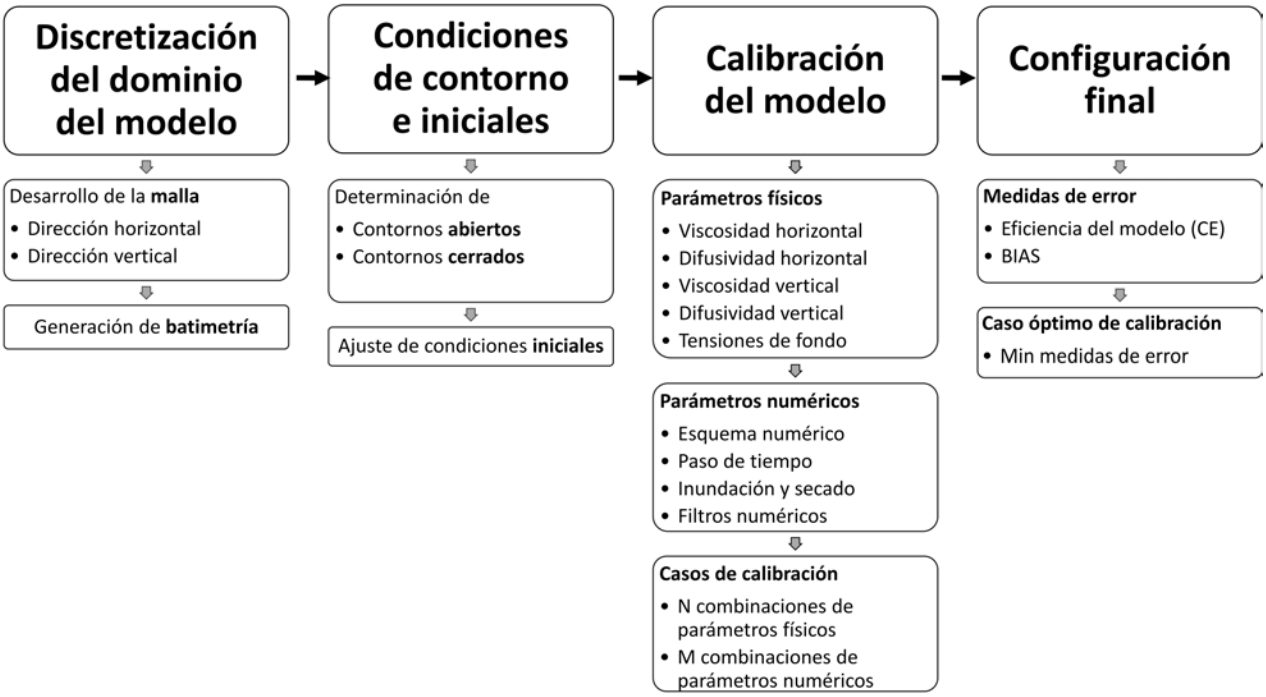

Figura 16: Esquema de los niveles involucrados para la configuración del modelo hidrodinámico.

La discretización del dominio del modelo consiste en la definición de cada nodo de la malla numérica en la dirección horizontal y vertical así como la generación de una batimetría.

Las condiciones de contorno se necesitan para definir los forzamientos del modelo. Éstos pueden ser datos del río más datos de marea (elevaciones y/o caudales) en el contorno exterior que representa el mar.

Las condiciones iniciales son valores de partida de las variables de una ecuación utilizados en el cálculo de soluciones numéricas. De este modo, se requieren datos iniciales para la profundidad del agua, la velocidad, la temperatura y la salinidad con el fin de inicializar el modelo.

El proceso de calibración determina los valores de los parámetros del modelo tanto físicos como numéricos con el fin de ajustar los resultados dados por el modelo numérico a datos medidos en el campo. Los parámetros físicos son la viscosidad y difusividad de remolino (horizontal y vertical) y las tensiones tangenciales (fondo, laterales y superficie). Los parámetros numéricos son una serie de características que aseguran la discretización correcta (esquemas numéricos) y la solución (paso de tiempo, filtros numéricos, ...) de las ecuaciones de gobierno del modelo hidrodinámico.

Los casos de calibración son todas las diferentes simulaciones realizadas por medio de N combinaciones de parámetros físicos y M combinaciones de parámetros numéricos con el fin de encontrar la mejor combinación. Los datos de calibración y validación consisten en niveles de agua, velocidades y direcciones de la corriente y salinidades en diferentes puntos situados a lo largo del dominio del modelo durante el período de interés.

La configuración final del modelo es la combinación de valores de los parámetros que mejor se adapten a los resultados obtenidos por el modelo y los datos medidos en el área de estudio. Se necesita un buen ajuste para demostrar que el modelo reproduce con precisión las características de advección y dispersión de la zona de estudio.

Con el fin de encontrar el caso óptimo de calibración, se calculan dos mediciones de error: el sesgo (BIAS) y la eficiencia del modelo (CE) para niveles de agua, velocidades de la corriente y salinidades.

En primer lugar, se calcula el BIAS mediante la ecuación (4).

$$BIAS = \sum_{i}^{N} \frac{S_i - R_i}{N} \tag{4}$$

donde R_i es el i-dato medido del muestreo, S_i es el i-dato modelado de la simulación e i es el valor i desde 1 hasta N medidas.

En segundo lugar, se calcula el error entre ambas series utilizando el coeficiente de eficiencia del modelo (CE) mostrado en la ecuación (5) y desarrollado por Nash & Sutcliffe (1970).

$$CE = 1 - \frac{\sum_{i}^{N}(R_i - S_i)^2}{\sum_{i}^{N}(R_i - \overline{R}_i)^2} \tag{5}$$

donde R_i es el i-dato medido del muestreo, S_i es el i-dato modelado de la simulación $\overline{R}_i$ es el promedio de las medidas e i es el valor i desde 1 hasta N medidas.

2.3.2.2. Modelado hidrodinámico del caso peor

El modelo hidrodinámico proporciona los campos de velocidades y de dispersión que se emplean para ejecutar los modelos de transporte en las regiones del campo cercano y lejano.

Con el fin de ejecutar el "caso peor de dilución", se propone que este escenario asuma unas condiciones constantes de forzado. A raíz de las propuestas formuladas por otras metodologías (Hansler & Fikslin 1995, Hansler *et al.* 1998, LDEQ 2010, USEPA 1991), se seleccionan los siguientes forzamientos:

- La amplitud de marea es constante e igual al valor que no se supera durante el 10 % del tiempo (A10).

- El caudal del río es constante e igual al valor que no se supera durante el 10 % del tiempo teniendo en cuenta el promedio de 7 días consecutivos (7Q10).

Este escenario de modelado se simula hasta llegar a una respuesta "cuasi-estacionaria", es decir, las variables hidrodinámicas muestran una señal modulada por las mareas y las descargas fluviales y, además, su magnitud no está variando entre dos períodos de marea. De esta forma, se minimiza el efecto de las condiciones iniciales en las simulaciones numéricas.

Una vez que se llega a esta situación, se registra horariamente un día de resultados del modelo hidrodinámico (24 datos). La figura 17 ilustra un ejemplo de la evolución de los niveles de agua (a), velocidades (b), salinidades (c) y temperaturas (d) en una celda arbitraria de la malla en la que se destaca la respuesta "cuasi-estacionaria".

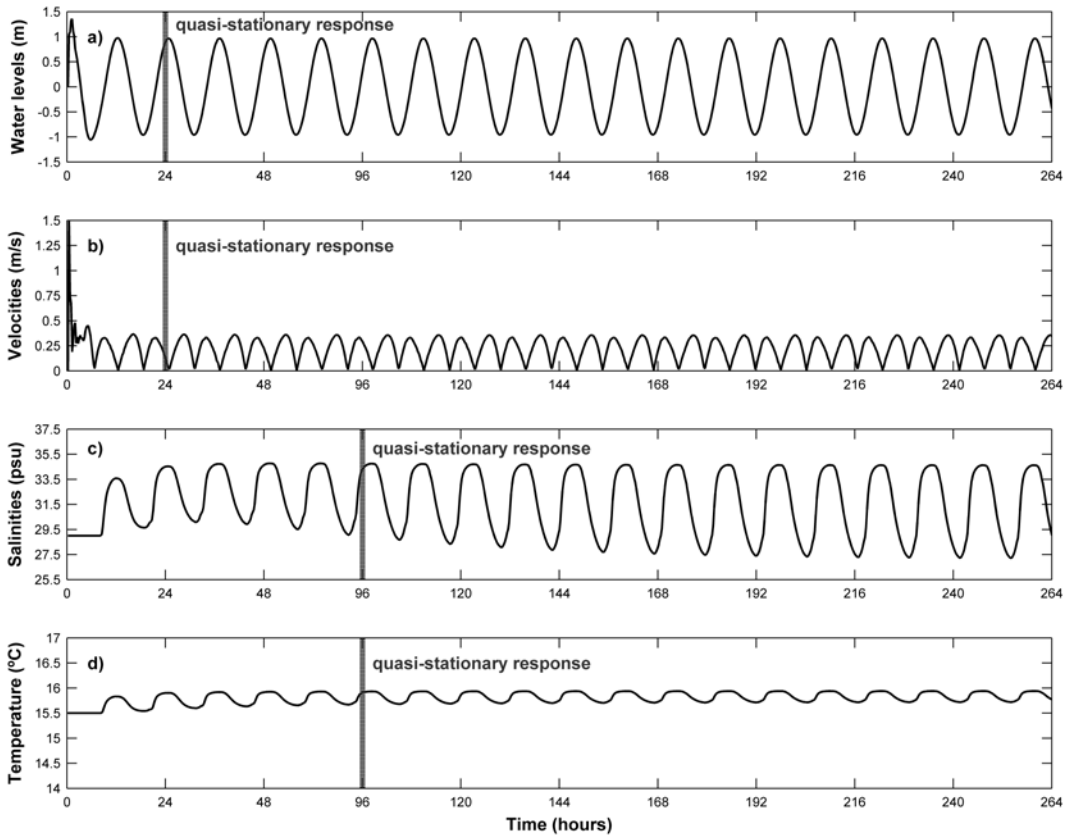

Figura 17: Ejemplo de la evolución de los niveles de agua (a), velocidades (b), salinidades (c) y temperaturas (d) así como la escala temporal de la respuesta "cuasi-estacionaria".

En cuanto a la escala temporal de la respuesta "cuasi-estacionaria", cabe destacar que ésta depende de la variable hidrodinámica estudiada. Así, los niveles de agua y velocidades reaccionan a los forzamientos lo suficientemente rápido como para que se pueda alcanzar el equilibrio en 1 o 2 ciclos de marea. Otras variables tales como la salinidad o la temperatura pueden necesitar de 4 a 12 o incluso más ciclos de marea para alcanzar el equilibrio debido a que la dispersión/difusión es un proceso más lento.

2.3.3. Dilución primaria o inicial (Campo cercano)

El comportamiento del chorro depende del caudal del efluente descargado (Q_{eff}), el diámetro de la tubería de boca única (ϕ), la distancia de la descarga al fondo (d_{eff}), la densidad del efluente vertido (ρ_{eff}), la densidad

del agua receptora (ρ_{env}), la profundidad total de la columna de agua (H) y la velocidad de la corriente ambiental (u_{env}).

Las primeras cuatro variables están asociadas con el mecanismo de descarga por lo que son independientes para cada descarga. El valor de estas variables se recoge en el Paso 1. Las variables restantes se relacionan con las condiciones ambientales que dependen de los forzamientos hidrodinámicos y la localización del punto de descarga. El valor de dichas variables se extrae del modelado hidrodinámico del "caso peor de dilución". Una vez que se han establecido las variables más importantes para el cálculo de la dilución inicial, diferentes formulaciones o modelos numéricos pueden utilizarse para calcular la evolución del efluente como UM3, CORJET, JETLAG o MOHIDJET.

Los cálculos de la dilución primaria se llevan a cabo para cada vertido clasificado como significativo en el Paso 2, teniendo en cuenta:

- Todas las sustancias se consideran trazadores conservativos. De acuerdo con Jirka (2004) y Jirka *et al.* (2004), esta hipótesis es correcta para la mayoría de aplicaciones ya que el tiempo de residencia en la zona del vertido es típicamente corto (segundos a horas). Por lo tanto, en estas áreas los procesos de degradación de tóxicos son generalmente insignificantes ya que las escalas temporales de estos procesos son del orden de días, meses o años, como sucede para los metales pesados, plaguicidas, compuestos orgánicos halogenados o hidrocarburos poliaromáticos.

- Las variables ambientales (ρ_{env}, H y u_{env}) se extraen horariamente del modelado hidrodinámico en cada celda donde se ubiquen los puntos de descarga considerados. Se asume un acople pasivo donde la salida del modelo hidrodinámico es la entrada para todo el tiempo de interés en el modelo de campo cercano.

- Los resultados más importantes obtenidos de estos modelos son la dilución primaria mínima (S_n), la localización (x, y, z) y el espesor (H_n) de la pluma al final del campo cercano.

2.3.4. Acople de la dilución primaria a la secundaria (Campo intermedio)

En este apartado, se describen las tareas requeridas para elaborar el acoplamiento entre los modelos de campo cercano y lejano. En esta metodología, se propone, desarrolla y programa el siguiente acoplamiento entre ambos modelos. Dicho acoplamiento se basa en Bleninger & Jirka (2004), Kim *et al.* (2002), Zhang & Adams (1999).

- Se asume un acoplamiento pasivo donde el flujo inducido por el vertido, aunque considerablemente importante para la mezcla en el campo cercano, no cambia las características de flujo del campo lejano, más allá de las regiones del campo cercano o intermedio. Debido a ello, el modelo de campo cercano calcula los valores específicos de flujo y concentración del tóxico de la descarga. Entonces, éstos se introducen como términos fuente en lugares específicos del modelo de campo lejano sin ninguna realimentación de los cálculos del campo lejano en el modelo de campo cercano. La cantidad de programación necesaria es mucho menor que para el acoplamiento activo debido a la clara separación de los cálculos.

- Se introduce tanto el caudal como la concentración diluida de la descarga. Dichos resultados se convertirán a concentración en cada una de las celdas de la malla que se ven afectadas por el chorro-pluma al final del campo cercano en cada paso de tiempo, que generalmente tendrá una frecuencia horaria. Con base en el espesor y la altura de atrape del chorro-pluma, se establecen las capas verticales del modelo de campo lejano donde se introduce la descarga (Figura 18). Por otro lado, las celdas horizontales de

la malla, dónde se introducen las concentraciones de tóxico, se identifican con la longitud, la anchura y dirección del chorro-pluma al final del campo cercano (Figura 19).

- Se necesita corregir la información del caudal para preservar la masa en el modelo de campo lejano cuando la introducción de la descarga se produzca en varias capas. Para resolver este problema, se considera que el caudal de descarga en cada capa es el ratio entre el caudal total y el número de capas cubierto por el campo intermedio ($Q_{capa} = Q_{total}/n^{o}{}_{capas}$).

- Dado que los modelos integrales de chorro no tienen en cuenta la interacción con los contornos, se considera que el campo cercano termina cuando el chorro-pluma toca cualquier contorno. En este impacto, la dilución primaria termina y las capas verticales afectadas se determinan por el espesor del chorro-pluma para la superficie libre o la capa estratificada. En el caso de impacto con paredes, dichas capas verticales afectadas van desde la altura de impacto hasta la superficie libre.

Esta metodología se puede ver gráficamente en las figuras 18 y 19. En dichas figuras se muestra la transferencia de los resultados del modelo de campo cercano al lejano teniendo en cuenta la información dada por el modelo hidrodinámico visto en perfil y en planta respectivamente.

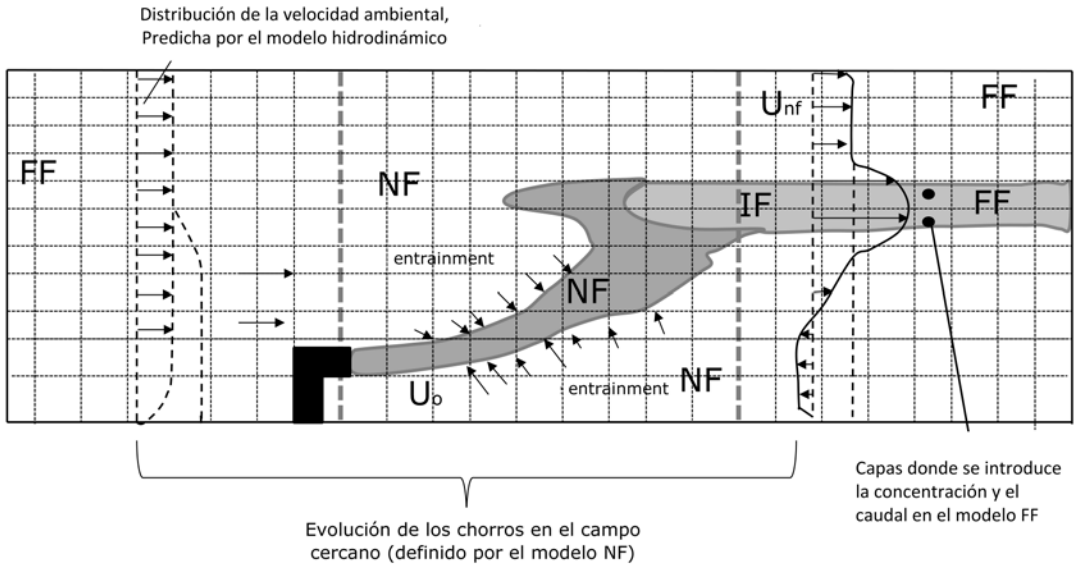

Figura 18: Croquis del acoplamiento entre el campo cercano y lejano utilizando información hidrodinámica en una vista de perfil.

2.3.5. Dilución secundaria o ambiental (Campo lejano)

En este apartado, se describen las tareas necesarias para llevar a cabo la simulación de vertidos significativos con modelos de campo lejano. Para realizar los cálculos, se utiliza un modelo de campo lejano tridimensional que resuelva la ecuación de advección-difusión. La variación local de la concentración por unidad de tiempo se considera que se origina como consecuencia de dos procesos de transporte: advección (debido a las corrientes hidrodinámicas existentes) y difusión (a través de los efectos de fenómenos turbulentos).

2.3.5.1. Configuración del modelo

La discretización del dominio del modelo es la misma que se utiliza para la configuración del modelo hidrodinámico, es decir, la malla del modelo de transporte tiene el mismo número de nodos (celdas) y capas.

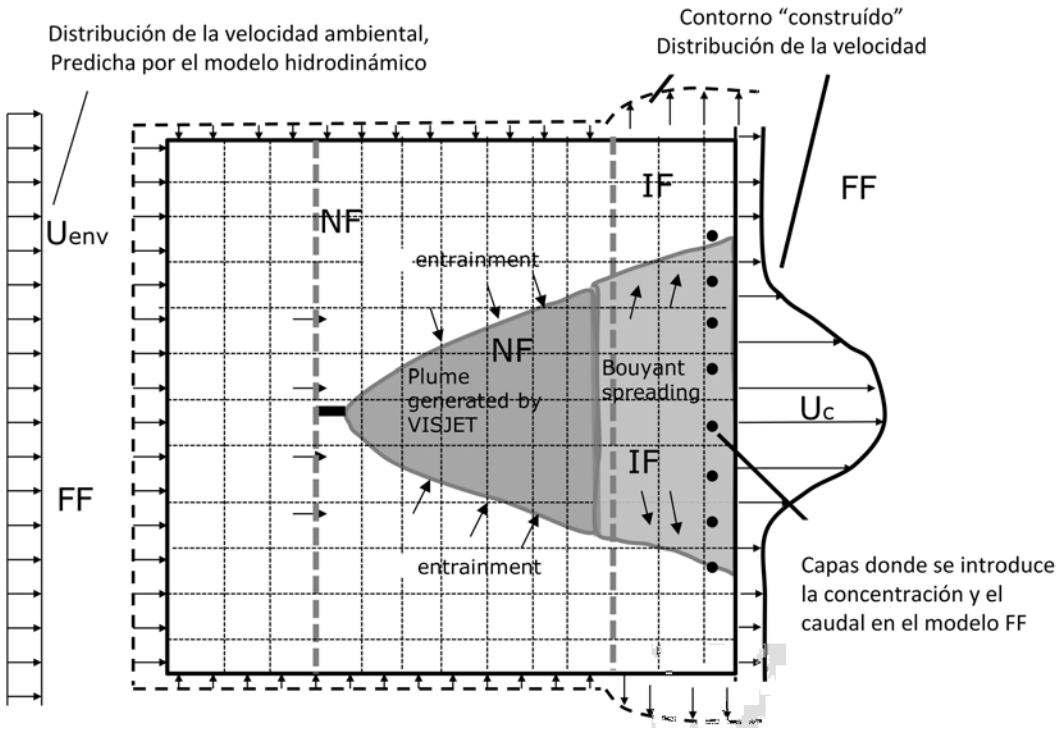

Figura 19: Croquis del acoplamiento entre el campo cercano y lejano utilizando información hidrodinámica en una vista en planta.

Debido a la escasez de datos disponibles de tóxicos, la idea para el modelo de campo lejano es que cuanto más lejos se sitúen los contornos de la zona de interés, menos afectarán los mismos a los resultados del modelo. De esta manera, se pueden establecer los contornos abiertos con una concentración nula.

Como se desconoce el campo de concentraciones del trazador conservativo en el área de estudio, se inicializa el modelo de transporte con un campo de concentraciones igual a cero. Por lo tanto, el sistema requiere un tiempo de respuesta con el fin de alcanzar un estado "cuasi-estacionario" para que los resultados obtenidos sean fiables. La figura 20 ilustra la inicialización y el estado "cuasi-estacionario" para la evolución de la concentración de una celda.

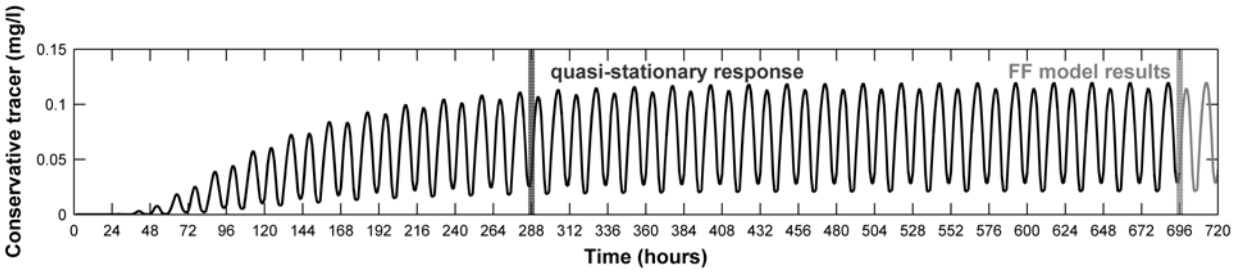

Figura 20: Ejemplo de la evolución de un trazador conservativo, el tiempo de respuesta "cuasi-estacionaria" y el período registrado para el transporte del "caso peor de dilución".

Debido a que las sustancias tóxicas se consideran conservativas en este escalón, los parámetros calibrados en el modelo hidrodinámico son los mismos que para el modelo de transporte y, en consecuencia, no se requiere realizar la calibración del modelo de campo lejano.

2.3.5.2. Modelado del transporte del caso peor

Con el fin de ejecutar el transporte del "caso peor de dilución", se emplean la simulación anterior del modelo hidrodinámico y los datos de dilución iniciales del acople. Dicho escenario de modelado se simula hasta llegar a una respuesta "cuasi-estacionaria" (Figura 20).

Una vez que se llega a esta situación, se registra horariamente un día (24 datos) de resultados del modelo de transporte (Figura 20). En cada paso de tiempo (hora) y celda de la malla, cabe destacar que la concentración registrada es la concentración máxima de todas las capas verticales tanto para este paso como todos los siguientes.

Esta respuesta "cuasi-estacionaria" depende de la ubicación, la concentración y caudal del vertido puntual, de la localización de la celda de la malla considerada respecto del punto de descarga y de la magnitud de los aportes fluviales y la marea. Por lo tanto, a fin de encontrar el tiempo máximo de la respuesta "cuasi-estacionaria" para el transporte, se debe llevar a cabo un análisis de sensibilidad con diferentes ubicaciones en todo el dominio del modelo. Dicha escala de tiempo indica la duración mínima de una simulación de campo lejano para garantizar que los resultados sean confiables.

2.3.5.3. Delimitación de las zonas de mezcla

Las Directivas EQS establecen que, para cada punto de control "representativo", la media aritmética de las observaciones no debe ser superior a la AA-EQS y la concentración de cada observación no supere la MAC-EQS.

Los efectos de la evolución de concentración de tóxico se determinan por la naturaleza de la exposición (Gómez *et al.* 2014b):

- *Efectos crónicos (CEF):* Los efectos crónicos de cada sustancia prioritaria en cada celda de la malla se calculan utilizando la ecuación (6).

$$CEF_{i,j} = \frac{[\overline{X_{i,j}}]_{ff}}{AA_{EQS}} \tag{6}$$

  donde $[\overline{X_{i,j}}]_{ff}$ es la concentración media de una sustancia tóxica durante el "caso peor de dilución". Las AA-EQS para el medio pelágico se recogen en la Directiva 2013/39/EU (EU 2013) en términos de concentración de agua ($\mu g/l$).

- *Efectos agudos (AEF):* Los efectos agudos de cada sustancia en cada celda de la malla se calculan mediante el porcentaje de tiempo con condiciones adversas.

$$AEF_{i,j} = \frac{t_{i,j}}{t_{total}} \times 100 \tag{7}$$

  donde $t_{i,j}$ es el tiempo con condiciones adversas, es decir, el tiempo que se supera la MAC-EQS y t_{total} es la duración total del "caso peor de dilución". De nuevo, las MAC-EQS para el medio pelágico se recogen en la Directiva 2013/39/EU (EU 2013) en términos de concentración de agua ($\mu g/l$).

Según lo establecido en las Directivas EQS y estos efectos, después de las simulaciones, se determinan dos MZs: la Zona de Mezcla para la Media Anual y Zona de Mezcla para la Concentración Máxima Permitida (en adelante AA-MZ y MAC-MZ, respectivamente). La AA-MZ indica dónde pueden ocurrir los efectos crónicos mientras que la MAC-MZ indica los efectos agudos.

1. La AA-MZ se calcula como una zona donde las concentraciones modeladas y promediadas en el tiempo exceden la AA-EQS, $CEF_{i,j} > 1$ (Figura 21).
2. La MAC-MZ se calcula como un zona donde las concentraciones modeladas exceden en algún momento la MAC-EQS, $AEF_{i,j} > 0$ (Figura 21).

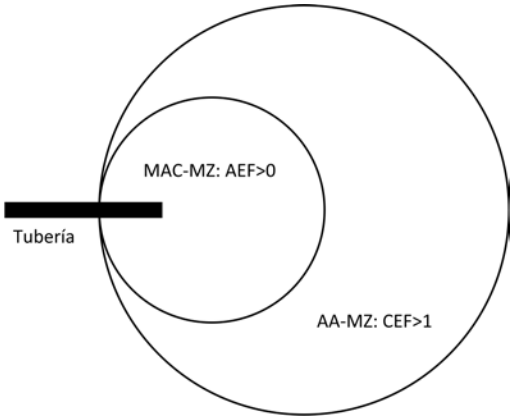

Figura 21: Diagrama de las dos partes delimitadas como zonas de mezcla (AA-MZ y MAC-MZ) en el cálculo simplificado.

2.3.6. Admisibilidad de las zonas de mezcla

Con el fin de definir la admisibilidad de una zona de mezcla, se ha desarrollado un método en tres niveles: Aceptabilidad (AC), Tamaño máximo permitido para MZs (MAS) y Admisibilidad final (AD).

2.3.6.1. Aceptabilidad (AC)

Para esta tarea, se comprueba si el punto de descarga se encuentra en una zona intermareal. Las zonas intermareales se definen como celdas de la malla donde la profundidad de la columna de agua (H) está por debajo del valor de la amplitud de la marea que no se supera durante el 95 % del tiempo ($A95$).

Si el punto de descarga se encuentra en una zona intermareal, las MZs no son aceptables. Si no lo están, se calcula el valor de AC como el porcentaje de área del estuario de cada celda (Ecuación (8)).

$$AC_i(H,A) = \begin{cases} \text{if } H_i < A95 & Non - Acceptable(\text{when discharge point}) \\ \text{if } H_i \geq A95 & \frac{A_i}{A_{estuary}} \cdot 100(\text{rest of grid cells}) \end{cases} \tag{8}$$

Respecto a la delimitación del estuario y su área superficial $A_{estuary}$, se han definido dos límites (el interior y exterior). El límite interior entre las aguas estuarinas y fluviales se localiza en el último punto donde se siente la influencia de la marea. El límite exterior del estuario se ha establecido con base en criterios fisiográficos, teniendo en cuenta la línea imaginaria que une los extremos de la bocana.

2.3.6.2. Tamaño maximo permitido para zonas de mezcla (MAS)

En el cálculo simplificado, el tamaño máximo permitido para MZs (MAS) ha sido definido mediante criterio de experto. Para ello, se realizó una encuesta a 20 expertos de todo el mundo pidiendo su opinión sobre el valor máximo que podría tener la extensión de una MZ en estuarios. Dicho criterio fue el valor medio y dice que el MAS no exceda el 10 % (AA-MAS) y 3 % (MAC-MAS) de la extensión total del estuario para la AA-MZ y la MAC-MZ, respectivamente (Figura 22).

2.3.6.3. Admisibilidad final (AD)

Por último, se evalúa la admisibilidad final de las MZs (AD) como la suma de todos los valores de AC cubiertos por AA-MZ y MAC-MZ (Ecuación (9)). Si la AD es mayor que MAS, la MZ es inadmisible mientras que si AD es igual o menor que MAS, la MZ es admisible.

$$AD(AC) = \sum_{i=1}^{n} AC_i \tag{9}$$

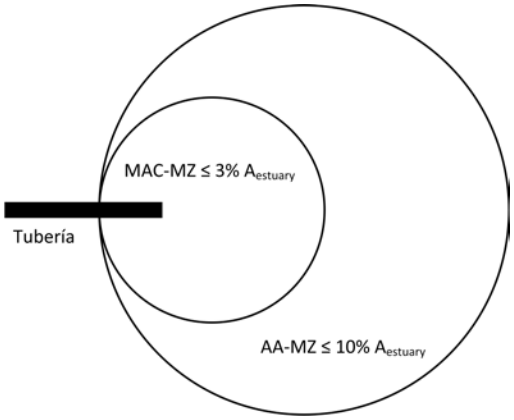

Figura 22: Diagrama del tamaño máximo permitido de una zona de mezcla para AA-MZ y MAC-MZ en el cálculo simplificado.

donde AC_i es la aceptabilidad de la celda i.

Si la extensión de la AA-MZ o MAC-MZ es inadmisible, la descarga se clasifica como significativa grande siendo necesario abordar el Paso 4 del árbol de decisiones (Figura 10).

2.4. Paso 4. Cálculo intermedio (Caso seco de dilución)

El cálculo intermedio propuesto se basa en la simulación continua del año más seco de la serie de caudal del río así como la marea astronómica asociada dicho año. Aunque este escenario del modelo continúa del lado de la seguridad, las variaciones de los forzamientos a lo largo del año conllevan a la modificación de la hidrodinámica. En consecuencia, se obtendrán diferencias en la evolución de la concentración de las sustancias tóxicas en todas las regiones (campo cercano, intermedio y lejano).

El Paso 4 está compuesto por 5 subsecciones como se ilustra en la figura 23.

2.4.1. Hidrodinámica

2.4.1.1. Configuración del modelo

En el "caso seco de dilución", la configuración del modelo hidrodinámico es la misma que en el "caso peor de dilución" por lo que no es necesario realizar tareas adicionales.

2.4.1.2. Selección de forzamientos

El cálculo intermedio propuesto se basa en la simulación continua del año más seco de la serie histórica del caudal del río. Para su selección, se calcula el volumen de agua anual media ($MAWV$) para cada i-año de la serie histórica por medio de la ecuación (10).

$$MAWV_i = \sum_{j=1}^{j} Q_j \times 86400 \tag{10}$$

donde Q_j is el caudal fluvial diario del j-día (m^3/s).

A continuación, se determina el escenario de modelado del "caso seco de dilución" que corresponde al año con el valor mínimo de $MAWV$. Por último, se extraen las series temporales del caudal del río y de niveles de marea astronómica asociadas a ese año para utilizarse como forzamientos del modelo hidrodinámico.

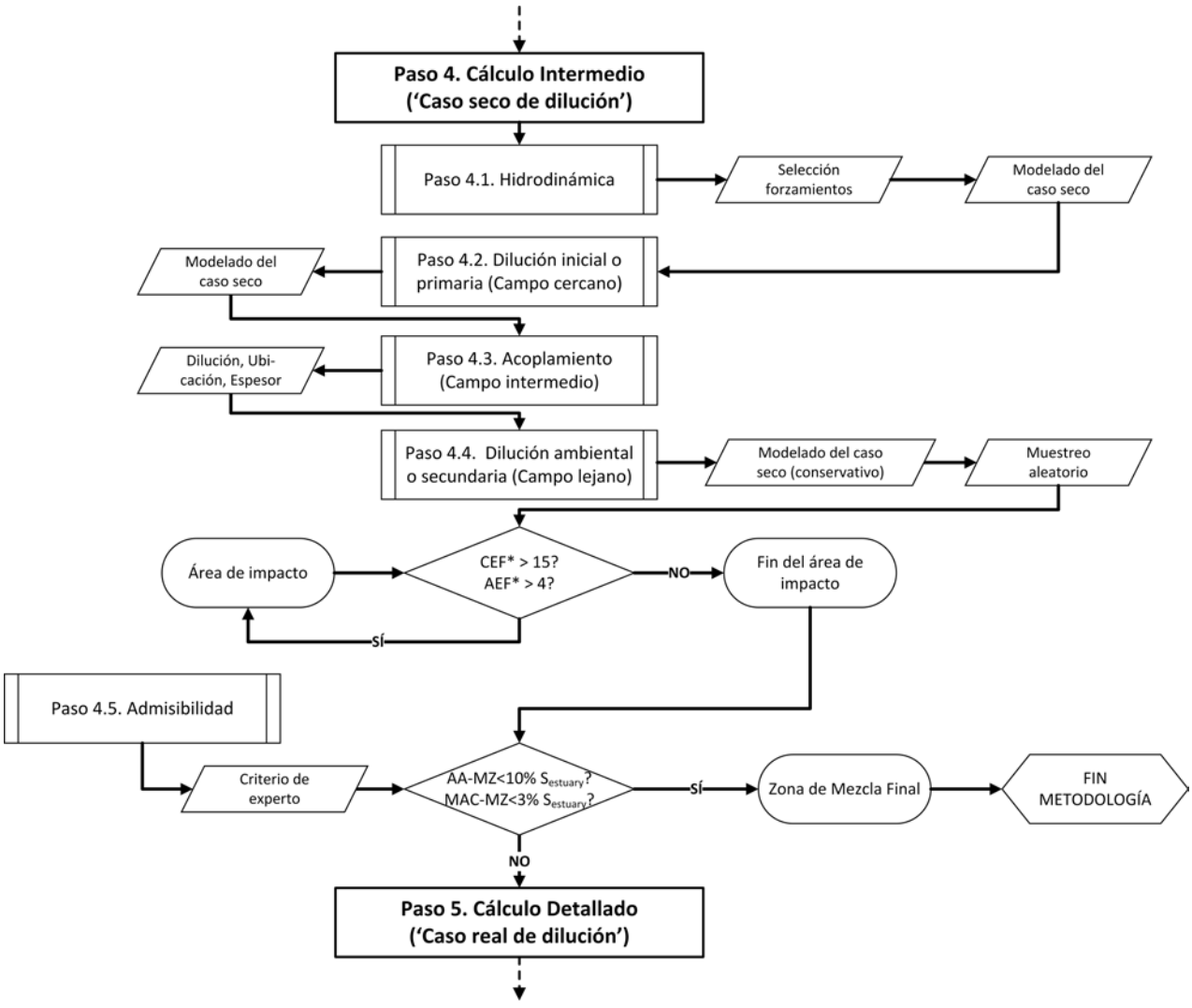

Figura 23: Diagrama de flujo desarrollado para el Paso 4. Cálculo intermedio (Caso seco de dilución).

2.4.1.3. Modelado hidrodinámico del caso seco

Una vez más, una cuestión importante al trabajar con modelos hidrodinámicos es el tiempo requerido para la estabilización de los resultados del modelo y la influencia de las condiciones iniciales en estos resultados como se muestra en la figura 17.

En este método, se propone llevar a cabo la simulación hidrodinámica asumiendo $X + 365$ días de caudal fluvial y de niveles de marea como forzamientos de modo que los primeros X días de simulación del modelo no se consideren. Una vez alcanzada la estabilización de modelo y evitada la influencia de las condiciones iniciales, se almacenan horariamente 365 días de resultados del modelo hidrodinámico.

2.4.2. Dilución primaria o inicial (Campo cercano)

Los cálculos de dilución primaria se realizan para cada descarga significativa grande, teniendo en cuenta los mismos supuestos que para el Paso 3.

2.4.3. Acople de la dilución primaria a la secundaria (Campo intermedio)

La metodología propuesta es la misma que para el Paso 3. Dicha metodología se puede observar gráficamente en las figuras 18 y 19 en una vista de perfil y de planta respectivamente.

2.4.4. Dilución secundaria o ambiental (Campo lejano): Enfoque conservativo

2.4.4.1. Configuración del modelo

En el enfoque conservativo, la configuración del modelo es la misma que en el Paso 3 por lo que no es necesario realizar tareas adicionales para calibrar el modelo de campo lejano.

2.4.4.2. Modelado del transporte del caso seco

En el "caso seco de dilución", los forzamientos no asumen condiciones fijas (un año real) por lo que se ha de abordar el posible efecto de la correlación serial en el tiempo en los resultados. Este problema sugiere que la condición inicial puede ser importante para capturar el "efecto de memoria" o, al menos, para minimizar su influencia en los resultados del modelo.

Al objeto de resolver estas cuestiones, se propone llevar a cabo una "presimulación" para obtener la adecuada condición inicial de concentración del tóxico y otra "simulación" para registrar la evolución de la concentración a lo largo del año seco.

En primer lugar, la "presimulación" se lleva a cabo con "condiciones hidrodinámicas cuasi-fijas". Para ello, se ejecuta el modelo de campo lejano con los resultados del primer día del modelo hidrodinámico en un bucle continuo hasta llegar a una respuesta "cuasi-estacionaria". Análogamente al "caso peor de simulación", la "presimulación" considera un caudal del río constante igual al del primer día y su marea asociada durante 24 horas (véase la figura 24).

El tiempo máximo de la respuesta "cuasi-estacionaria" para el transporte es la escala temporal del "caso peor de dilución". Por lo tanto, esta escala temporal indica la duración mínima de cualquier "presimulación" en el campo lejano para asegurar que las condiciones iniciales son fiables. Una vez alcanzada dicha respuesta, se registra el campo de concentración de la primera hora del año seco.

En segundo lugar, se ejecuta el escenario de modelado (365 días), con la condición inicial obtenida en la "presimulación". A continuación, se guardan horariamente 365 días de los resultados del modelo de transporte.

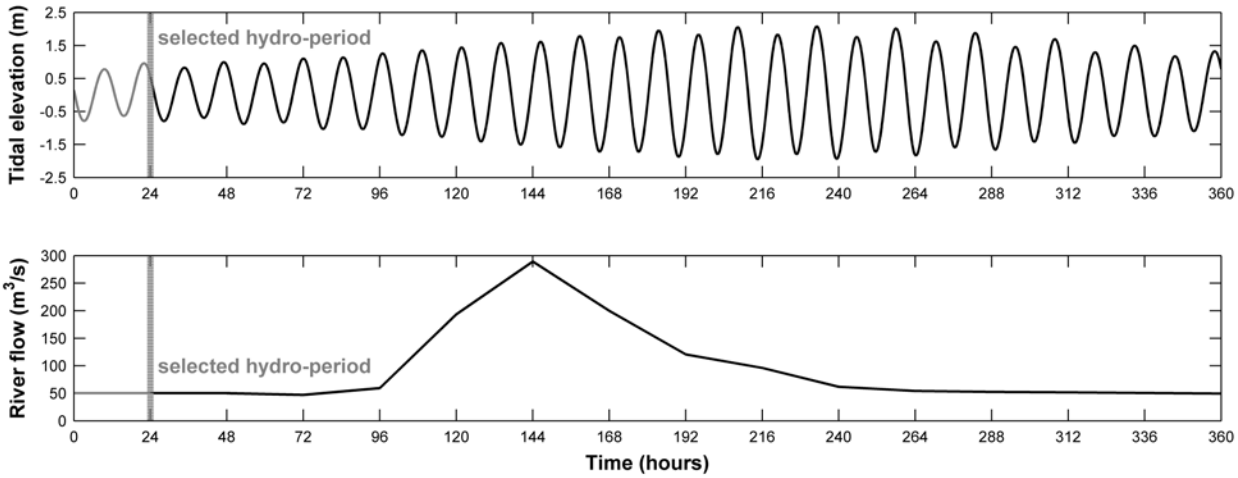

Figura 24: Ejemplo de forzamientos para las primeras 360 horas de un año seco e hidro-período seleccionado para el transporte de una "presimulación" en un "caso seco de dilución".

2.4.4.3. Delimitación de las zonas de mezcla

El problema en el "caso seco de dilución" se encuentra en cómo delimitar las zonas de mezcla teniendo en cuenta:

- La evaluación de ambas EQSs a partir de un año de resultados del modelo. Las Directivas EQS establecen que la media aritmética de las observaciones no debe exceder la AA-EQS y la concentración medida no debe superar la MAC-EQS con base en un cálculo anual a través de las medidas de los programas de vigilancia.
- La limitación de los programas de vigilancia para registrar datos (muestreos mensuales, bimensuales o estacionales) versus la predicción de la concentración, continua en el espacio y el tiempo, ofrecida por los modelos numéricos.
- La especificación temporal, que se puede permitir, de las superaciones de las EQS que continúa considerando aceptable el impacto sobre la masa de agua receptora.

A partir de estas consideraciones, surgen varios problemas cuando se delimitan zonas de mezcla:

- Uno de los aspectos más importantes de los programas de monitoreo es la frecuencia de muestreo a lo largo de un año en los puntos de control. En este sentido, las Directivas EQS (EC 2008a, EU 2013) no establecen una frecuencia mínima de muestreo, ni definen un valor máximo de muestras que deben tomarse, ni determinan el número óptimo de muestras.
- El alto grado de aleatoriedad que caracteriza a la evolución de la concentración en estuarios provoca que, en el momento del muestreo, la delimitación de MZs dependerá de dicha toma de muestras. De esta manera, la delimitación puede ser diferente en cada una de las tomas de muestras que se realicen.
- La delimitación de MZs se puede estimar a partir de los resultados del programa de vigilancia. Sin embargo, dicha delimitación es más eficaz si se lleva a cabo con base en los resultados del modelado de la calidad del agua ya que permite una visión continua de la evolución de las sustancias tóxicas. La primera idea es calcular la delimitación usando todos los datos proporcionados por el modelado. Por desgracia, esta idea podría llevar a delimitar una zona de mezcla con una alta probabilidad de incumplimiento de las normas de calidad ambiental debido a la diferencias entre modelado y los programas de seguimiento.

Después de simular el "caso seco de dilución", se propone de nuevo determinar dos MZs: la AA-MZ y la MAC-MZ. Para lograr esta delimitación, se sugiere un método que implica tres niveles: Especificación del número anual de muestras, Determinación del número óptimo de muestreos y Delimitación definitiva de las MZs (Figura 25).

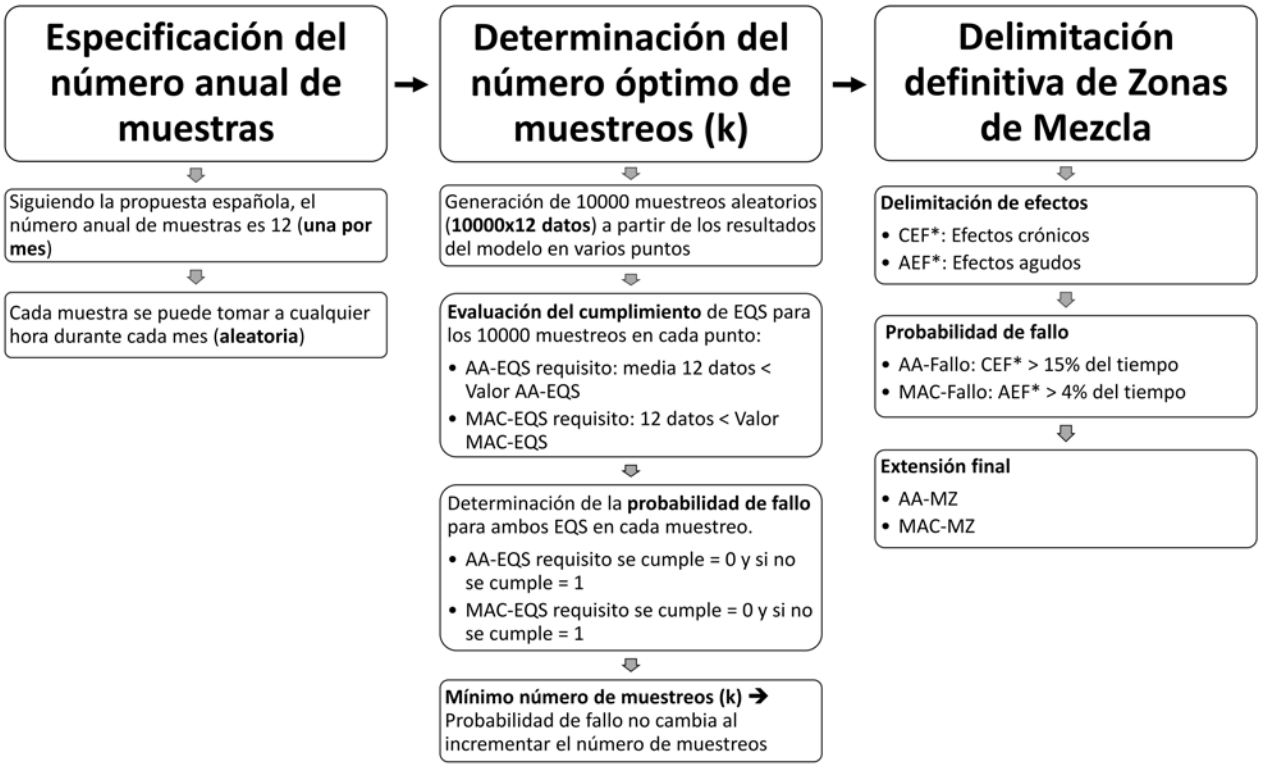

Figura 25: Metodología para delimitar zonas de mezcla en estuarios para el cálculo intermedio o "caso seco de dilución".

Especificación del número anual de muestras

En España se elaboró una propuesta donde el programa de vigilancia para las sustancias prioritarias y/o tóxicas debe ser un muestreo con, al menos, una frecuencia mensual (SPAIN 2014). Por lo tanto, en este método, se especifica que el número anual de muestras es de 12 (una por mes) siguiendo la propuesta española. En cuanto el período de muestreo, cada muestra se puede medir en cualquier momento durante cada mes (muestreo aleatorio).

Determinación del número óptimo de muestreos

En este segundo nivel, se investiga el número óptimo de muestreos ($k\times$ 12 datos) para asegurarse de que la delimitación de MZ es independiente del número. En primer lugar se generan 10.000 muestreos aleatorios (10.000×12 datos) a partir de los resultados del modelo en varios puntos a lo largo del dominio de cálculo, con especial atención a la zona de éstos puntos de descarga. Estos muestreos aleatorios se realizan siguiendo las especificaciones del primer nivel.

A continuación, se evalúa el cumplimiento de las EQSs para los 10000 muestreos en todos los puntos. Para cada muestreo, el requisito de la AA-EQS se cumple si el promedio de los 12 datos está por debajo de su valor mientras que el requisito de la MAC-EQS se cumple cuando todos los datos están por debajo de su valor.

Con el fin de encontrar el número óptimo de encuestas, iterativamente se promedian los resultados de los muestreos. En el primer paso, los resultados son la probabilidad de fallo del muestreo 1. En el segundo paso,

los resultados son la probabilidad media de los muestreos 1 y 2. Por último, en el paso 10000, los resultados son la probabilidad media de los muestreos 1 a 10000.

Por último, se grafica la probabilidad media de fallo versus el número de muestreos con el fin de investigar el número óptimo de muestreos (k). Este número es el número mínimo de muestreos que aseguran que el valor de la probabilidad no cambia debido a un aumento del número de muestreos. La figura 26 ilustra un ejemplo de la evolución de la probabilidad media de fallo con el aumento del número de muestreos para la AA-EQS (línea negra) y la MAC-EQS (línea gris) en una celda de la malla durante un "caso seco de dilución".

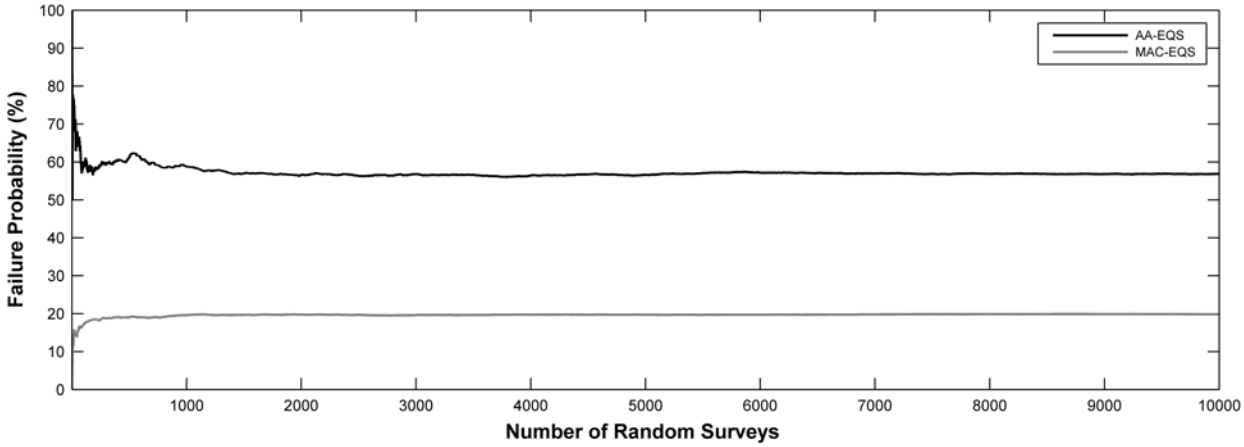

Figura 26: Ejemplo de la evolución de la probabilidad media de fallo con el aumento del número de muestreos para la AA-EQS (línea negra) y la MAC-EQS (línea gris) en una celda de la malla durante un "caso seco de dilución".

Delimitación definitiva de las MZs

En el cálculo intermedio, se obtienen k-muestreos de 12 datos con una probabilidad de ocurrencia igual a $1/k$. Por lo tanto, la delimitación de las MZs ha de considerar las probabilidades de los k-muestreos:

- *Efectos crónicos (CEF*):* Los efectos crónicos de cada tóxico en todas las celdas de la malla se computan utilizando la ecuación (11) para cada k-muestreo:

$$CEF*^{k}_{i,j} = \frac{[\overline{X_{i,j}}]^{k}_{ff}}{AA_{EQS}} \tag{11}$$

  donde $[\overline{X_{i,j}}]^{k}_{ff}$ es la concentración media de tóxico durante el k-muestreo (12 datos) en la celda i, j de la malla.

  A continuación, si $CEF*^{k}_{i,j} > 1$ entonces el k-muestreo no cumple la AA-EQS por lo que se marca el $CEF*^{k}_{i,j}$ de este k-muestreo con un uno. Por el contrario, si $CEF*^{k}_{i,j} \leq 1$ entonces se marca el $CEF*^{k}_{i,j}$ de este k-muestreo con un cero.

  Finalmente, el CEF* asociado a todos los muestreos se calcula por medio de la ecuación (12):

$$CEF^{*}_{i,j} = \sum_{h=1}^{k} CEF*^{k}_{i,j} \times \frac{100}{k} \tag{12}$$

- *Efectos agudos (AEF*):* Los efectos agudos de cada tóxico en todas las celdas de la malla se computan

utilizando la ecuación (13) para cada k-muestreo:

$$AEF*^{k}_{i,j} = \frac{fail^{k}_{i,j}}{12} \tag{13}$$

donde $fail^{k}_{i,j}$ es el número de datos en los que se excede la MAC-EQS durante el k-muestreo en la celda i, j de la malla.

A continuación, si $AEF*^{k}_{i,j} > 0$ entonces el k-muestreo no cumple la MAC-EQS por lo que se marca el $AEF*^{k}_{i,j}$ de este k-muestreo con un uno. Por el contrario, si $AEF*^{k}_{i,j} \leq 0$ entonces se marca el $AEF*^{k}_{i,j}$ de este k-muestreo con un cero.

Finalmente, el AEF* asociado a todos los muestreos se calcula por medio de la ecuación (14):

$$AEF^{*}_{i,j} = \sum_{h=1}^{k} AEF\ *^{k}_{i,j} \times \frac{100}{k} \tag{14}$$

En el cálculo intermedio hay una probabilidad de fallo de los requisitos de las EQSs. Por lo tanto, las variaciones temporales del sistema se pueden explicar por especificaciones temporal del cumplimiento de dichos requisitos.

En este trabajo, el valor de la especificación temporal se especifica como una probabilidad de fallo de la AA- y MAC-EQS debido a la naturaleza discreta del muestreo aleatorio y se basa en la opinión de expertos. Para ello, se realizó una encuesta a 20 expertos de todo el mundo pidiendo su opinión sobre el valor que podrían tener ambas probabilidades de fallo. El valor final fue el valor medio de todos los expertos, esto es, un $15\,\%$ para el AA-Fallo y un $4\,\%$ para el MAC-Fallo.

1. La AA-MZ se calcula como una zona donde se localizan los efectos crónicos, $CEF^{*}_{i,j} = 15$ (Figura 27).
2. La MAC-MZ se calcula como una zona donde se localizan los efectos agudos, $AEF^{*}_{i,j} = 4$ (Figura 27).

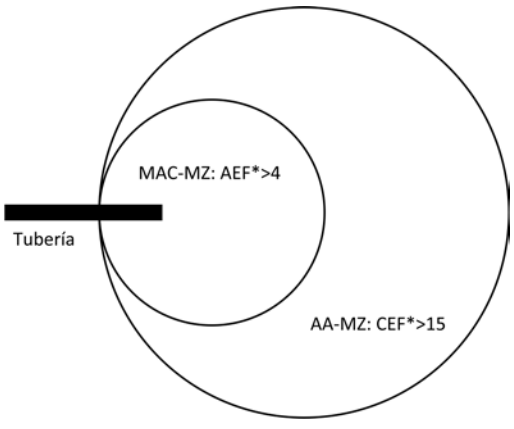

Figura 27: Diagrama de las dos partes delimitadas como zonas de mezcla (AA-MZ y MAC-MZ) en el cálculo intermedio.

2.4.5. Admisibilidad de las zonas de mezcla

En el "caso seco de dilución", se utiliza el mismo método de tres niveles propuesto en el "caso peor de dilución" para definir la admisibilidad de las MZs. En primer lugar, se evalúa la aceptabilidad. En segundo

lugar, se determina el tamaño máximo permitido de MZ (MAS). En tercer lugar, se calcula la admisibilidad final (AD).

La tarea final en el Paso 4 es determinar la delimitación de ambas MZs trazando un ábaco que relaciona la extensión de la zona de mezcla con la probabilidad de fallo de la misma. Para dibujar esta curva, se tiene en cuenta que la extensión no puede ser mayor que el 10 % y el 3 % del área estuarina para la AA-MZ y la MAC-MZ respectivamente. Además, la probabilidad de fallo no puede ser mayor del 15 % para el AA-Fallo y 4 % para el MAC-Fallo.

La figura 28 ilustra un ejemplo de un ábaco que muestra la evolución de la extensión de las MZs con la probabilidad de fallo. En dicha figura, la línea negra es la evolución de la AA-MZ y la línea gris de la MAC-MZ. Además, la línea gruesa negra representa la zona donde la AA-MZ es asignable porque ambos requisitos se cumplen simultáneamente mientras que la línea gris gruesa muestra la zona asignable para la MAC-MZ.

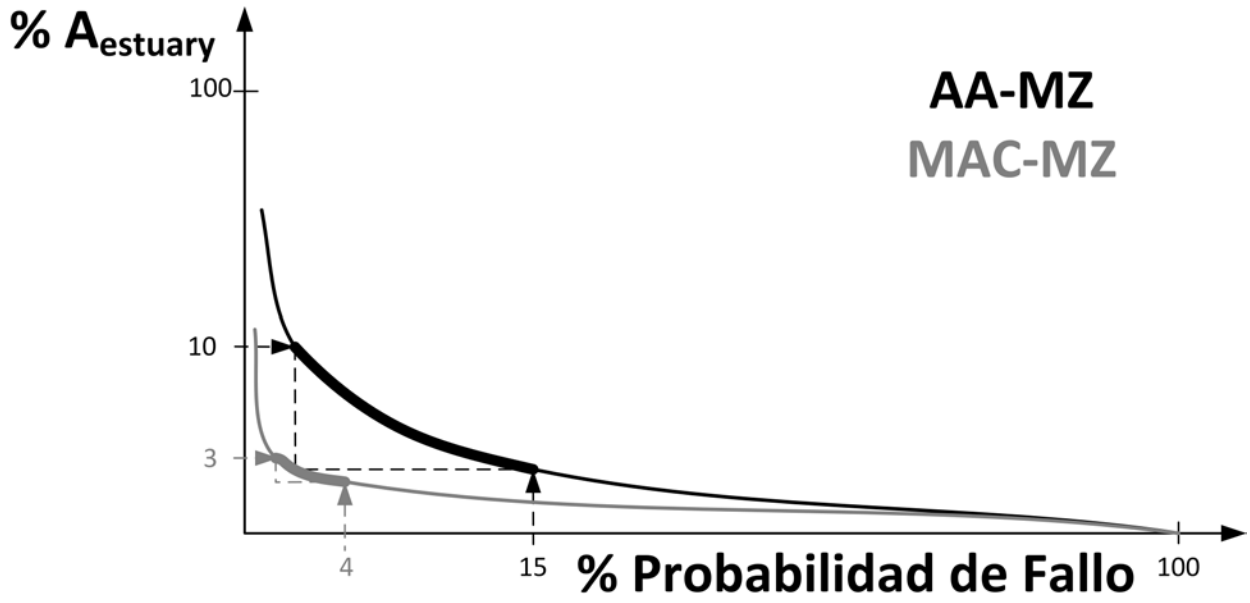

Figura 28: Ejemplo de un ábaco para la AA-MZ (línea negra) y la MAC-MZ (línea gris) en el cálculo intermedio.

Como se puede ver en la figura 28, podría haber un rango de MZs asignables. La delimitación definitiva se debe discutir y acordar entre el interesado y la autoridad competente debido a las implicaciones económicas, sociales y ecológicas de cualquier asignación:

1. Si la probabilidad de fallo se maximiza, la extensión se minimiza. Sin embargo, las autoridades competentes tienen que asumir que hay una alta probabilidad de incumplimiento de las normas de calidad del agua en un punto de control fuera de la zona de mezcla.

2. Si la extensión se maximiza, la probabilidad de fallo se minimiza. Sin embargo, las autoridades competentes tienen que asumir que hay un 10 % y 3 % del estuario, donde los efectos crónicos y agudos pueden aparecer respectivamente.

Si las MZs propuestas son admisibles, el procedimiento de delimitación finaliza. De lo contrario, la descarga se clasifica como significativa muy grande siendo necesario abordar el Paso 5 del árbol de decisiones (Figura 10).

2.5. Paso 5. Cálculo detallado (Caso real de dilución)

El cálculo detallado propuesto se basa en las variaciones espaciales y temporales de los forzamientos (marea y aportes fluviales) a lo largo de una serie temporal de largo plazo. Dichas variaciones conducen a modificaciones significativas de la hidrodinámica y, en consecuencia, también se esperan diferencias en la evolución de la concentración de las sustancias tóxicas en todas las regiones de mezcla.

En el calculo detallado, la evaluación tiene en cuenta, además de la dilución física, la química considerándose las sustancias tóxicas como no conservativas. Como consecuencia, se producirán, de nuevo, variaciones significativas en la evolución de la concentración de dichas sustancias.

El Paso 5 está compuesto por 5 subsecciones como se ilustra en la figura 29.

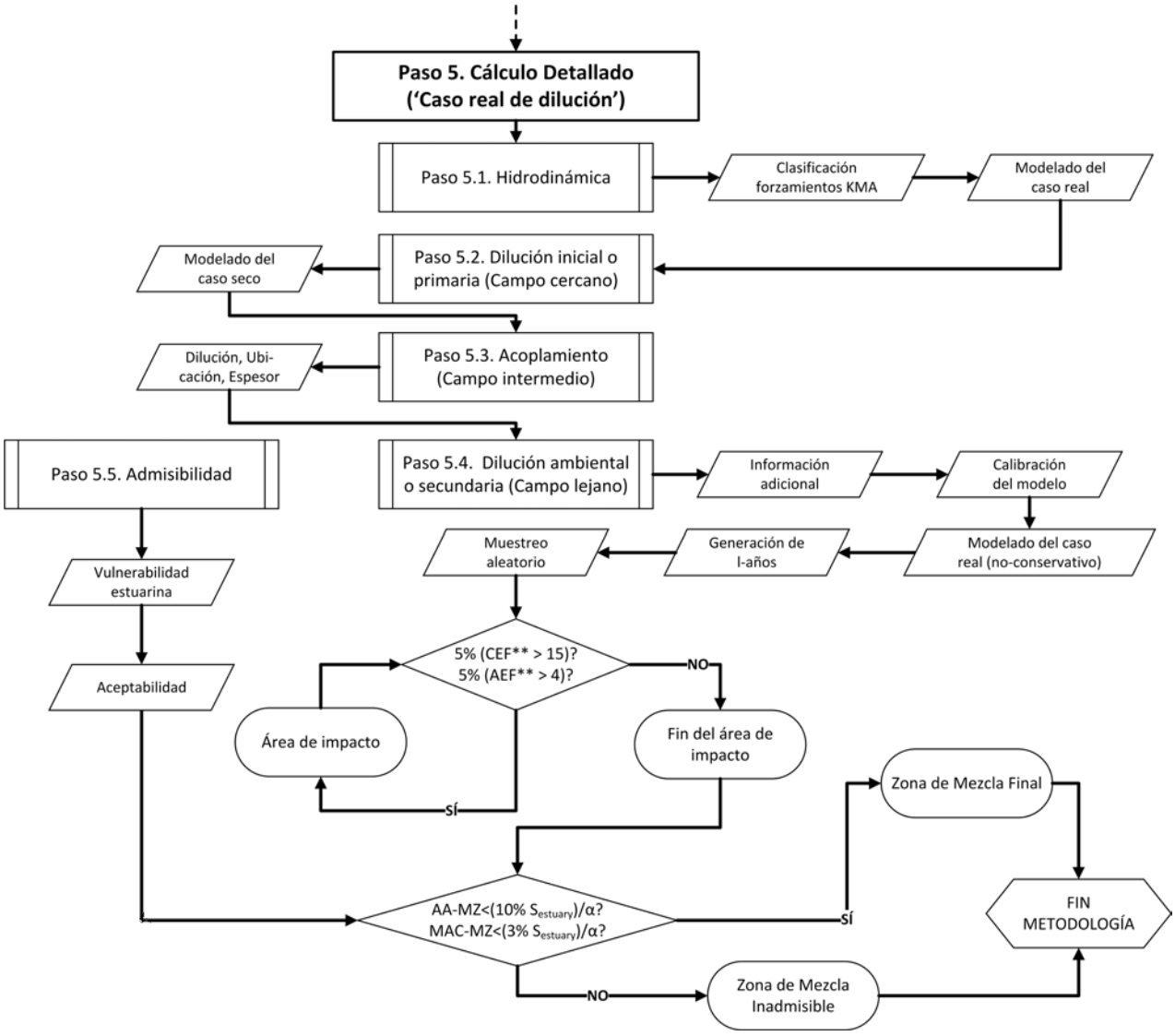

Figura 29: Diagrama de flujo desarrollado para el Paso 5. Cálculo detallado (Caso real de dilución).

2.5.1. Hidrodinámica

2.5.1.1. Configuración del modelo

En el "caso real de dilución", la configuración del modelo es la misma que en el "caso peor de dilución" por

lo que no es necesario realizar tareas adicionales.

2.5.1.2. Selección/Clasificación de forzamientos

En las últimas décadas, las series temporales a largo plazo de caudales del río y de la marea astronómica generados a partir de modelos numéricos han mejorado el conocimiento de la distribución temporal de estas dos variables (Andersen 1994, García *et al.* 2008, Pawlowicz *et al.* 2002, Singh & Woolhiser 2002). La complejidad y la variación temporal de la series de caudal del río (Q) y de la marea astronómica (A), sugieren que la minería de datos puede ser particularmente eficaz en la selección de forzamientos hidrodinámicos reales a partir de una serie temporal a largo plazo con el fin de simular los escenarios más probables que ocurren en el área de estudio.

Para ello, se desarrollan en este apartado herramientas metodológicas y numéricas para la selección de series de corto plazo (grupos) de forzamientos hidrodinámicos reales en estuarios gobernados por el río y la marea astronómica y la definición de escenarios de modelado con forzamientos reales para ejecutar modelos numéricos en estuarios. Este enfoque también podría ayudar a hacer frente a grandes volúmenes de datos con el fin de dar prioridad a los escenarios más frecuentes y significativos del comportamiento medio de la hidrodinámica en estuarios desde un punto de vista objetivo. Además, podría ayudar a reducir el coste computacional requerido por el modelado numérico convencional.

En este trabajo, se selecciona el algoritmo K-medias (KMA) como técnica de minería de datos ya que tiene la capacidad de clasificar series a largo plazo en un pequeño número de grupos identificando los modos principales de la variable estudiada y de reducir efectivamente la dimensionalidad del sistema. La metodología se divide en varios pasos: Obtención de los datos de los forzamientos hidrodinámicos, Reordenamiento de los datos de entrada para la agrupación, Aplicación del criterio de agrupamiento propuesto y Análisis de sensibilidad para los forzamientos y el modelado. En la figura 30 se muestra un esquema explicativo de la metodología.

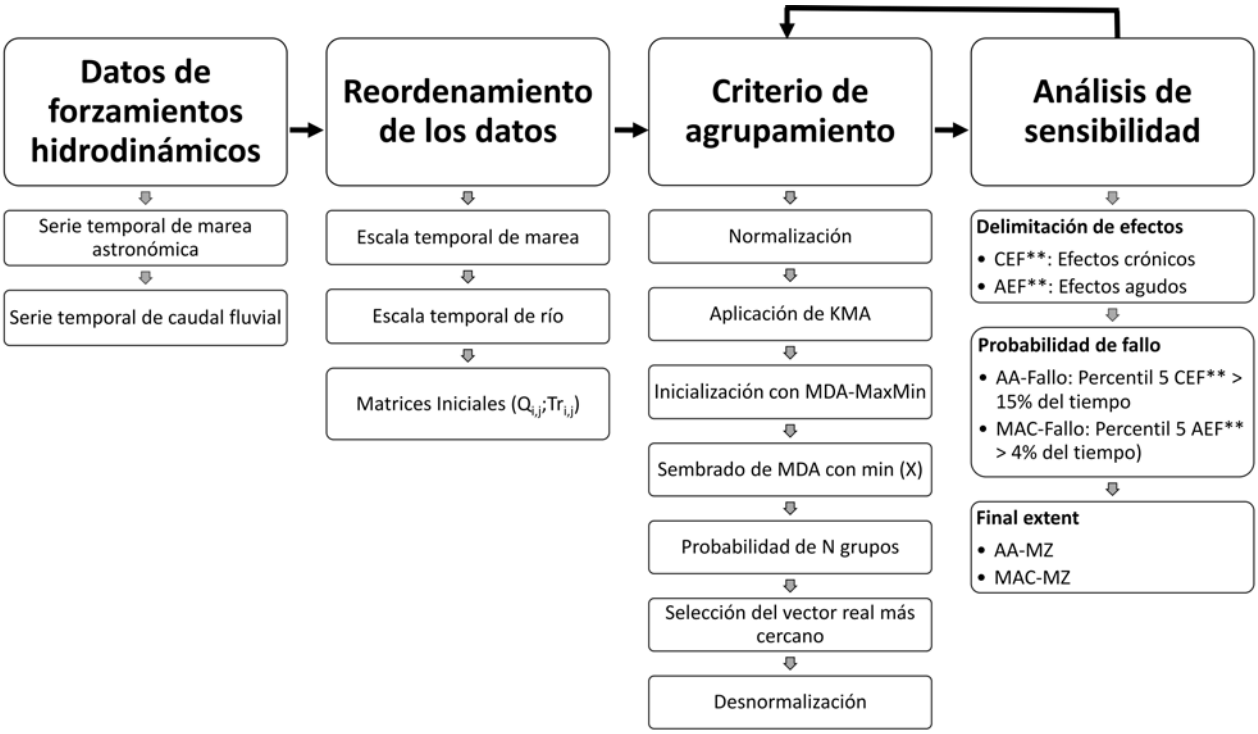

Figura 30: Metodología para seleccionar escenarios de forzamientos hidrodinámicos reales en estuarios gobernados por el río y la marea utilizando la técnica de agrupación K-medias.

Datos de los forzamientos hidrodinámicos

En primer lugar, se necesita disponer de la serie de caudal fluvial y la serie de la marea astronómica para un período a largo plazo (>30 años). Estas series temporales se puede obtener a partir de modelos numéricos o de datos instrumentales. En segundo lugar, se calcula la "serie diaria de caudal del río". Por último, a partir de la serie de la marea astronómica, se calcula la "la carrera de la marea astronómica" como la diferencia entre el valor máximo y mínimo de dicha serie durante 24 horas con el fin de calcular la "serie diaria de carrera de la marea".

Reordenamiento de los datos de entrada para la agrupación

Para la selección de series de corto plazo representativas (M grupos) a partir del registro a largo plazo de Q y A, se debe, en primer lugar, determinar el número de días utilizado para clasificar las bases de datos (n). Dicho número está ligado a las escalas temporales que rigen la señal de Q y A.

En el caso de A, los cambios de las mareas son el resultado neto de múltiples influencias que actúan sobre diferentes períodos. Las oscilaciones con períodos menores de 24 horas se llaman componentes armónicas (semidiurna, diurna o mareas mixtas). Por el contrario, los ciclos de días, meses o años se conocen como componentes de largos períodos (8 días, 2 semanas, 1 mes, 6 meses, ..., 18.6 años). Al objeto de determinar la escala de tiempo adecuada para la marea, se sugiere comprender la influencia de dichos ciclos en el área de estudio.

En el caso de Q, el clima local determina las escalas temporales, especialmente la distribución de las lluvias y la respuesta hidrológica de la cuenca a las precipitaciones. Para obtener la escala temporal del caudal del río, se propone estimar la duración de las avenidas (dP), con el índice propuesto por Richter *et al.* (1996), Richter *et al.* (1997) y Richter *et al.* (1998). Este índice ha sido aplicado por diferentes autores (Peñas *et al.* 2014, Snelder & Booker 2013) para clasificar las redes fluviales de acuerdo a la similitud de su régimen de caudales. Las avenidas (hP) se definen como aquellos eventos de caudal dentro de un año que superan el percentil 75 de todos los valores diarios. La frecuencia de las avenidas (fP) es el número de hP anuales. Por último, dP se calcula como la duración promedio de todos los hP anuales. Esta definición de avenidas se usa como escala de tiempo porque es mucho más corta que la duración de las condiciones de sequía. Si se clasifica con la escala temporal de las sequías, se podría fallar en la representación adecuada de las condiciones de avenidas.

Por último, según las escalas temporales de los forzamientos (Q y A), se reordena ambas series en secuencias de n días. De esta manera, se construye la matriz (base de datos) para el agrupamiento donde N es el numéro total de datos diarios de las series temporales.

Para Q, la primera fila de la matriz se conforma con los n primeros datos (días) de la serie temporal, la segunda fila se define desde el segundo día hasta el $n+1$ día y así sucesivamente hasta el final de la serie temporal $(N-n+1)$. La base de datos inicial está compuesta por una matriz de $(N-n+1)$ filas y n columnas, definida como $X = \{x_1, x_2, \ldots, x_{N-n+1}\}$ donde $x_i = \{Q_i, Q_{i+1}, Q_{i+2}, \ldots, Q_{i+n-2}, Q_{i+n-1}\}$ y, a su vez, Q_i es el caudal fluvial del día i.

Para A, la serie de marea astronómica se emplea para extraer la "serie diaria de carrera de marea". Esta transformación permite tener el mismo número de elementos para la agrupación de los forzamientos. La base de datos inicial se compone de una matriz de $(N-n+1) \times n$-dimensiones, definida como $X = \{x_1, x_2, \ldots, x_{N-n+1}\}$ donde $x_i = \{TR_i, TR_{i+1}, TR_{i+2}, \ldots, TR_{i+n-2}, TR_{i+n-1}\}$ y, a su vez, TR_i es la carrera de marea del día i.

Criterio de agrupamiento propuesto

En primer lugar, cabe señalar que Q y A se pueden considerar como dos eventos independientes y aleatorios. Esta característica permite la agrupación de los dos forzamientos de forma independiente y la obtención de la probabilidad conjunta como el producto de ambas probabilidades.

El procedimiento de agrupación comienza con la normalización de cada dato de la base de datos inicial $(X_{i,j})$. A continuación, se define el número de grupos (M) para la clasificación y se ejecuta el KMA. En este trabajo, los centroides iniciales son la selección dada por el MDA utilizando como semilla $\mathrm{mín}(X)$. Con respecto a la inicialización, se utiliza el $\mathrm{mín}(X)$ para garantizar que, al menos, un centroide se encuentre en esta zona espacial de la base de datos inicial. Después, se obtienen M grupos cada uno representado por un centroide con un valor de los n-días. Por último, el vector más cercano de los datos reales al M centroide se considera el M grupo y, para terminar, estos M grupos se desnormalizan.

Análisis de sensibilidad

Durante la aplicación de técnicas de minería de datos, el usuario selecciona el número de grupos. En esta sección, se presenta una estrategia para encontrar el número mínimo y óptimo de grupos para explicar la variabilidad de los forzamientos y ejecutar modelos numéricos con escenarios hidrodinámicos reales.

En primer lugar, se reconstruye la serie a largo plazo a partir de los M grupos para obtener la serie "sintética". Dicha reconstrucción se lleva a cabo mediante la búsqueda del grupo con mejor ajuste a la señal de Q y TR (serie "real") cada n-días a partir de los M grupos.

Respecto a la variabilidad de los forzamientos, se calcula el error entre la serie "sintética" y "real" de Q y TR utilizando el error CE (ecuación (5)). Si CE_f es menor que 0.5 la comparación se considera inaceptable, si la CE_f es mayor que 0.6 y menor que 0.8 la comparación es conveniente (buena) y si CE_f es mayor que 0.8 la comparación se considera excelente. Teniendo en cuenta estas cifras, se propone la realización de un análisis de sensibilidad, aumentando progresivamente el número de grupos, para encontrar el número necesario que explica la variabilidad de los forzamientos con una comparación conveniente (mínimo número de grupos, M_{mf}) y una comparación excelente (óptimo número de grupos, M_{of}).

En cuanto a la simulación de modelos numéricos, se quiere evaluar el funcionamiento a la hora de modelar la serie "sintética" en comparación con la serie "real". Para lograr esta tarea, se sugiere el uso de una formulación sencilla que proporcione los valores de una respuesta dependiente de Q y A ($WL = f(Q, TR) + \epsilon$). Para ser eficaz, la formulación (predictando) debe predecir una de las variables maestras utilizadas en el modelado hidrodinámico y de transporte en estuarios, como por ejemplo los niveles de agua, sobre una base de 12 o 24 horas con al menos una resolución temporal horaria en diferentes lugares del estuario. El predictando es un indicador de la calidad de la clasificación y proporciona una pista acerca de lo bien que se caracteriza la respuesta media del estuario.

Esta validación se debe realizar porque una comparación conveniente o excelente de la serie "sintética" frente a la serie "reales" para la variabilidad de los forzamientos no garantiza que la respuesta hidrodinámica, influenciada por ambas variables, sea conveniente (buena) o excelente. Finalmente, cabe mencionar que la validación de la serie "sintética" se podría hacer con una serie temporal a largo plazo de mediciones de un mareógrafo en lugar de la serie "real" calculada con la ecuación empírica.

Por tanto, se reconstruyen la serie "sintética" de WL teniendo en cuenta la secuencia de grupos de TR previamente determinada. A continuación, se calcula el CE con las series "sintética y real" de WL para analizar la capacidad de modelar de la serie "sintética". El procedimiento se inicia mediante la elección del número de grupos necesarios para llegar a un CE_f de 0.5 con las "series sintéticas" de Q y TR. Con los M grupos de Q y TR, se reconstruye la "serie sintética", se evalua la respuesta (WL) y se calcula CE_r de la respuesta. Este procedimiento se repite de manera iterativa, aumentando el número de grupos de Q y TR de acuerdo con un aumento de 0.01 en su valor de CE_f. Cuando la CE_r de la respuesta en cada ubicación sea mayor que 0.6, se alcanza el mínimo número de grupos para modelar M_{mm}. El procedimiento concluye cuando la media de CE_r de todas las ubicaciones es superior a 0.8, esto es, el número óptimo de grupos M_{om}.

El número final de escenarios de modelado (M) debe estar en una ventana que va desde M_{mm} hasta M_{om}. Estos M escenarios se deben seleccionar teniendo en cuenta los costes computacionales frente a la exactitud

de los resultados del modelo. Como base, se debe seleccionar M_{om}, sin embargo, dicho número de escenarios podría ser inaccesible debido a limitaciones computacionales. Como mínimo, se debe seleccionar M_{mm} para asegurar resultados válidos.

Además, cabe indicar que los datos que siempre se conocen cuando se realiza la clasificación son las series temporales de los forzamientos (Q y A). En un estudio particular, podría ocurrir que no existen fórmulas sencillas o datos medidos para validar la clasificación con las series "sintética y real".

En estas situaciones, se sugiere seleccionar el número final de grupos con base en CE_f y la duración de las simulaciones propuestas. Teniendo en cuenta estas cuestiones, el número final de grupos debe garantizar que la CE_f sea mayor de 0.7 y la duración de las simulaciones sea menor del $10\,\%$ de las series temporales de Q y A.

2.5.1.4. Modelado hidrodinámico del caso real

En este método, se propone llevar a cabo la simulación hidrodinámica para cada M escenario de modelado seleccionado. Estos M escenarios asumen $X + n$ días de caudales del río y de niveles de marea como forzamientos. Por lo tanto, los primeros X días de simulación del modelo no se tienen en cuenta porque representan la escala de tiempo de la respuesta "cuasi-estacionaria" calculada en el paso 3 (véase la figura 17).

Una vez alcanzada la estabilización de modelo y evitada la influencia de las condiciones iniciales, se registra horariamente n días de resultados del modelo hidrodinámico para los M escenarios de modelado.

2.5.2. Dilución primaria o inicial (Campo cercano)

Los cálculos de dilución primaria se realizan para cada descarga significativa grande teniendo en cuenta los mismos supuestos que para el Paso 3 y 4.

2.5.3. Acople de la dilución primaria a la secundaria (Campo intermedio)

La metodología propuesta es la misma que para el Paso 3 y 4. Dicha metodología se puede observar gráficamente en las figuras 18 y 19 en una vista de perfil y de planta respectivamente.

2.5.4. Dilución secundaria o ambiental (Campo lejano): Enfoque no conservativo

2.5.4.1. Modelo conceptual

El modelo de transporte de sustancias no conservativas debe incluir, al menos, el modelo conceptual (procesos e interacciones) descrito en este apartado (Figura 31). Dicho modelo es una adaptación del modelo desarrollado por Gómez (2010) para simular sustancias prioritarias/tóxicas (especialmente metales pesados y microcontaminantes orgánicos) donde las variaciones espaciales y temporales de la concentración de la materia en suspensión se incluyen en los cálculos.

El modelo conceptual propuesto considera los siguientes supuestos:

1. La concentración en el medio pelágico sólo se reduce por el proceso de volatilización que afecta a la fracción disuelta, el proceso de sedimentación que reduce la fracción particulada y los procesos de degradación que reducen la fracción total de tóxico (hidrólisis, fotólisis y biodegradación).

2. El equilibrio entre adsorción y desorción depende de la evolución de la fracción disuelta y particulada en función de la concentración de materia suspendida (orgánica e inorgánica).

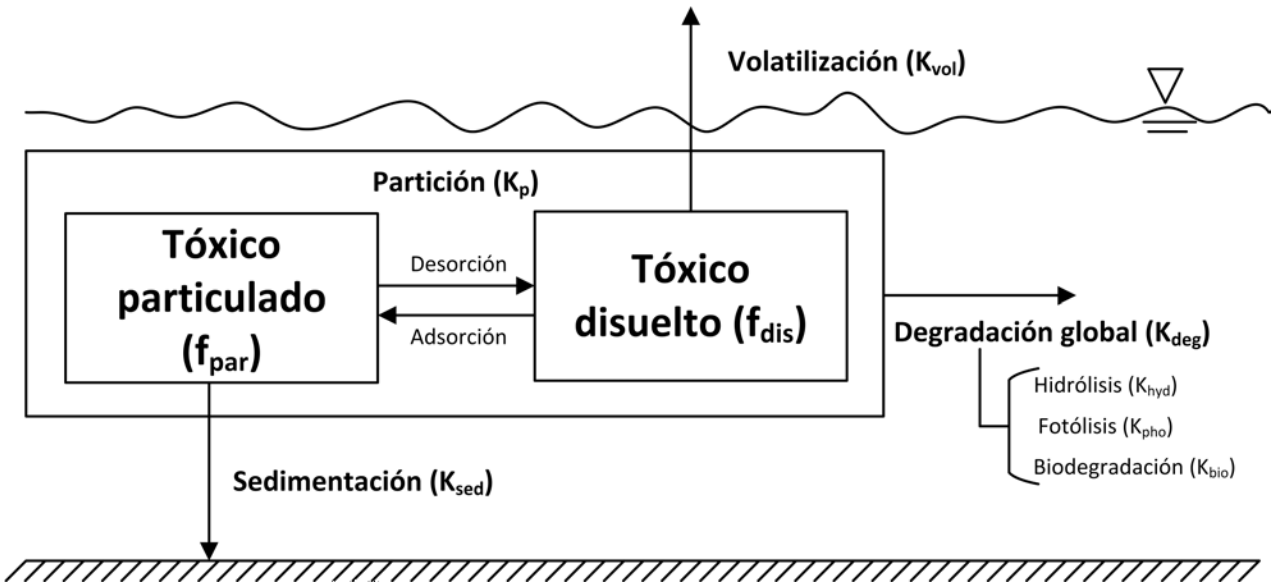

Figura 31: Modelo conceptual de transporte para sustancias no conservativas incluyendo los procesos mínimos requeridos para delimitar zonas de mezcla.

3. La materia inorgánica absorbe a los metales pesados (HM) y la materia orgánica a los microcontaminantes orgánicos (OMP).

4. Los metales pesados no se ven afectados por procesos de degradación.

5. La volatilización se ignora para metales pesados.

Dados estos supuestos, el balance de masa para cualquier OMP o HM se calcula de acuerdo a las ecuaciones (15) y (16), respectivamente:

$$\frac{dC_{OMP}}{dt} = -(K_{deg} + K_{vol} \cdot f_{dis} + K_{sed} \cdot f_{par}) \cdot C_{OMP} \tag{15}$$

$$\frac{dC_{HM}}{dt} = -(K_{sed} \cdot f_{par}) \cdot C_{HM} \tag{16}$$

Partición

La partición es el proceso en el cual una sustancia se distribuye entre las diversas especies disueltas y particuladas. La partición se determina en gran medida por el mecanismo de adsorción-desorción donde la sustancia se adhiere sobre la superficie de la materia en suspensión.

En el caso de HMs, se supone una relación lineal entre la concentración de la sustancia y la concentración de materia inorgánica en suspensión dependiente del coeficiente de partición (K_p). Dicho coeficiente es una propiedad inherente de cada HM al igual que el peso molecular.

Los OMPs se adsorben a la materia orgánica donde el coeficiente de partición es proporcional a la concentración de carbono orgánico en los sólidos en suspensión. Su cálculo se realiza usando la formulación de DiToro (1985).

Sedimentación

El proceso de sedimentación sólo afecta a la fracción particulada. Dicho proceso se considera como un flujo de masa a través del área de la interfaz agua-sedimento en el que la constante de sedimentación es proporcional

a la velocidad de sedimentación (Ecuación (17)).

$$K_{sed} = \frac{V_{sed}}{H} \tag{17}$$

donde H es la profundidad de la columna de agua y la velocidad de sedimentación (V_{sed}).

Volatilización

El transporte de OMPs a través de la interfaz agua-atmósfera se basa en la teoría de la doble película (Lewis & Whitman 1924). La transferencia de masa se determina por difusión molecular, siendo la velocidad de transferencia función del gradiente de concentración entre la interfase y los dos fluidos (líquido y gas). En este proceso, se supone que las concentraciones de OMP en la película de gas y en la película de líquido están en equilibrio de acuerdo a la ley de Henry con el fin de obtener la constante de volatilización (K_{vol}) como se muestra en la ecuación (18).

$$K_{vol} = [\frac{K_{gas} \cdot K_{liq} \cdot (\frac{He}{R \cdot T})}{\frac{He}{R \cdot T} \cdot K_{gas} + K_{liq}}] \cdot \frac{1}{H} \tag{18}$$

donde He es la constante de Henry, R es la constante de los gases, T es la temperatura, K_{liq} es el coeficiente de transferencia de OMP para la película líquida, K_{gas} es el coeficiente de transferencia de OMP para la película gaseosa y H es la profundidad de la columna de agua.

Degradación global

Se pueden distinguir tres tipos de procesos de degradación: fotólisis, hidrólisis y biodegradación. Para todos los procesos, la tasa de degradación es proporcional a la concentración de OMP y función de la temperatura. Los diversos procesos para la descomposición de OMPs se integran en un proceso global de degradación (Ecuación (19)). Para formular dicho proceso, se han utilizado cinéticas de primer orden dependientes de la temperatura.

$$K_{deg} = K_{pho} + K_{hyd} + K_{bio} \tag{19}$$

- La fotólisis (K_{pho}) es el proceso por el cual la radiación solar actúa sobre ciertas moléculas químicas alterando, degradando y/o descomponiendo su estructura. La tasa de fotólisis depende de la radiación solar.

- La hidrólisis (K_{hyd}) sucede cuando el OMP reacciona con el agua produciendo nuevos compuestos debido a la ruptura de enlaces. La tasa de hidrólisis depende del pH.

- Biodegradación (K_{bio}) se produce por la acción de bacterias. La tasa de biodegradación depende de la presencia de condiciones oxidantes o reductoras.

Para obtener la vida media del OMP (t_{mean}), la mayoría de estos procesos de degradación se estudiaron por medio de experimentos en el laboratorio. Dicho tiempo se define como el tiempo requerido para reducir la concentración inicial del OMP a la mitad debido al efecto del proceso específico de degradación estudiado.

Por último, la degradación global puede depender de la temperatura debido a la influencia que tiene sobre la velocidad de reacción (Ecuación (20)):

$$k_{Temp} = k^{20} \times k_T^{T-20} \tag{20}$$

donde k_{Temp} es la constante de velocidad a la temperatura T (d^{-1}), k^{20} es la constante de velocidad a la temperatura de referencia de 20 ºC (d^{-1}), k_T es el coeficiente de temperatura (-) y T es la temperatura ambiente del agua (ºC).

2.5.4.2. Información adicional

Esta información está relacionada con las mediciones (datos de campo) necesarios para llevar a cabo la configuración de modelo de transporte cuando se trata de sustancias no conservativas. Para la calibración del modelo, se requieren, como mínimo, medidas de los tóxicos en dos puntos del estuario durante 6 meses con frecuencia estacional. Además, se necesitan datos de campo o bases de datos de químicos para poder definir la condiciones de contorno así como las características de los procesos no conservativos:

- Mediciones de sólidos en suspensión durante un año con frecuencia estacional en 4 puntos del estuario, en 1 punto del contorno del río y en 1 punto del contorno de marea. Estas mediciones comprenden principalmente las características físicas de los sólidos en suspensión: concentración, forma, diámetro, densidad y peso de la fracción de carbono orgánico total.
- Densidad y viscosidad del agua en el dominio de cálculo (del modelo hidrodinámico).
- Coeficiente de partición octanol-agua.
- Coeficiente de transferencia de oxígeno disuelto.
- Peso molecular del oxígeno.
- Coeficiente de partición, constante de Henry, coeficiente de transferencia para la película líquida, coeficiente de transferencia para la película gaseosa, constante de velocidad de reacción de la fotólisis, constante de velocidad de reacción de la hidrólisis, constante de velocidad de reacción de la biodegradación, coeficiente de pérdida por temperatura y peso molecular del tóxico objeto de estudio.

2.5.4.3. Configuración del modelo

Se requiere configurar el modelo de transporte para definir la discretización del dominio del modelo, proporcionar condiciones de contorno e iniciales y, finalmente, llevar a cabo la calibración/validación del modelo (Figura 32).

La discretización del dominio del modelo es la misma que se utiliza para la configuración del modelo hidrodinámico y de transporte de sustancias conservativas.

Se pueden establecer contornos abiertos con con un valor constante, variable en el espacio, variable en el tiempo o variable en el espacio y el tiempo en función de las medidas disponibles para los tóxicos y sólidos en suspensión.

Como se desconoce el campo de concentraciones del tóxico en el área de estudio, se inicializa el modelo de transporte con un campo de concentraciones igual a cero para todas las sustancias modeladas. En cuanto a los sólidos en suspensión, la inicialización del modelo de transporte se establece con un valor constante o variable espacialmente y/o temporalmente en función de las medidas disponibles en el dominio del modelo.

El proceso de calibración determina los valores de los parámetros físicos, fisicoquímicos (OMP o HM) y numéricos del modelo con el fin de ajustar los resultados a datos medidos en el campo. Los parámetros físicos y numéricos son los mismos empleados en los Pasos 3 y 4. Los parámetros fisicoquímicos para metales pesados son la velocidad de sedimentación de la materia inorgánica, la tensión tangencial del fondo, la tensión tangencial crítica para la sedimentación, el coeficiente de partición y el tiempo medio de no equilibrio entre adsorción y desorción. En el caso de microcontaminantes orgánicos, los parámetros fisicoquímicos son la velocidad de sedimentación de la materia orgánica, la tensión tangencial del fondo, la tensión tangencial crítica

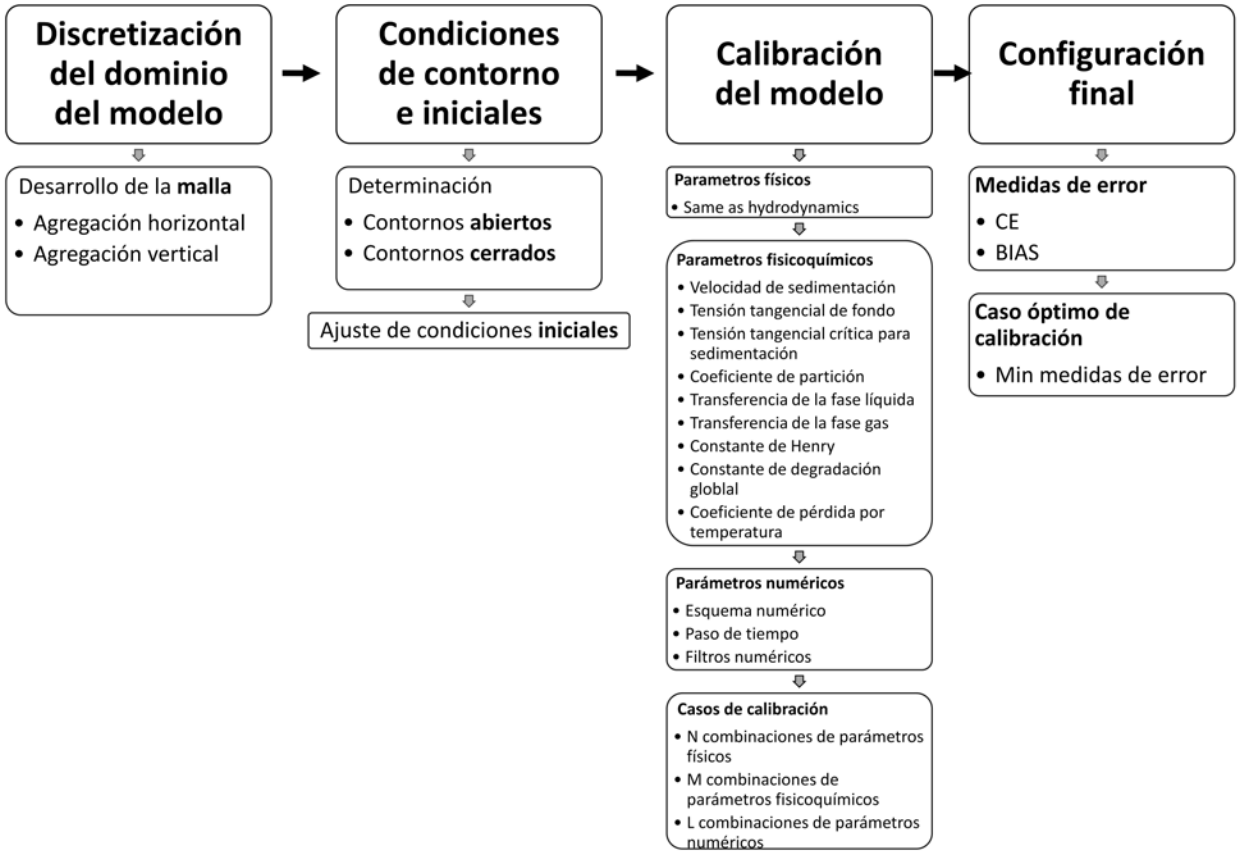

Figura 32: Esquema de los niveles involucrados para la configuración del modelo de transporte de sustancias no conservativas.

para la sedimentación, el coeficiente de transferencia de la fase líquida, el coeficiente de transferencia de la fase gas, la constante de Henry, la temperatura ambiente del agua, el coeficiente de pérdida por temperatura, la constante de velocidad de degradación global y el coeficiente de partición.

Los casos de calibración son todas las diferentes simulaciones realizadas por medio de N combinaciones de parámetros físicos, M combinaciones de parámetros fisicoquímicos y L combinaciones de parámetros numéricos. Con el fin de encontrar el caso óptimo de calibración, se calculan el sesgo (BIAS) y la eficiencia del modelo (CE). Para cada caso de calibración, se comparan los valores de los datos del modelo y los datos medidos en términos de concentraciones del tóxico. Se necesita un buen ajuste para demostrar que el modelo reproduce con precisión las características de advección, dispersión y reacción de la zona de estudio.

2.5.4.4. Modelado del transporte del caso real

Como se mencionó en el "caso seco de dilución", el tiempo necesario para la estabilización de los resultados del modelo de campo lejano y la influencia de las condiciones iniciales sobre estos resultados son muy relevantes en el "caso real de dilución". Para resolver estas cuestiones, se propone de nuevo realizar M "presimulaciones" para obtener la condición inicial adecuada de concentración de sustancia tóxica y de sólidos en suspensión. Para luego realizar otras M "simulaciones" donde se registra la evolución de la concentración para cada M escenario de modelado.

En primer lugar, la "presimulación" se lleva a cabo con un caudal del río constante e igual al primer día del escenario de modelado así como su marea asociada hasta alcanzar una respuesta "cuasi-estacionaria" para la hidrodinámica (véase la figura 24).

Por otra parte, la escala temporal del "caso peor de dilución" indica la duración mínima de cualquier "presimulación" para asegurar que los resultados de transporte son fiables. Una vez que se alcanza la respuesta "cuasi-estacionaria" para el trasnporte, se almacena la condición inicial para cada M "simulación" (ver figura 33).

Finalmente, se ejecuta cada M escenario de modelado (n días) con las condiciones iniciales obtenidas en las M "presimulaciones" donde se registra horariamente n días de los resultados del modelo de transporte.

2.5.4.5. Delimitación de las zonas de mezcla

Como se mencionó en el "caso seco de dilución", hay una falta de definición en la normativa sobre la manera de delimitar zonas de mezcla. Debido a esto, se propuso un método para delimitar MZs en el paso 4 siendo el punto de partida para la delimitación de MZs en el "caso real de dilución".

El problema en el "caso real de dilución" se encuentra en la forma de delimitar MZ teniendo en cuenta:

- La capacidad de los M escenarios de modelado para reconstruir adecuadamente la evolución de la concentración de sustancias tóxicas de "series reales" a partir de una combinación de estos M escenarios ("series sintéticas") con el fin de generar l-años basados en las series a largo plazo de los forzamientos o técnicas de Monte Carlo.

- La selección de un número de l-años representativos para realizar la delimitación que no influyan en los resultados y reflejen la variabilidad hidrodinámica. De esta manera, se evita la selección de sólo algunos años reales para el diseño como por ejemplo un año seco, un año húmedo y/o un año medio.

- La especificación temporal de los incumplimientos de EQSs permitidos si se considera aceptable el impacto sobre la masa de agua receptora.

Después de simular los M escenarios, se propone de nuevo determinar dos zonas de mezcla: la AA-MZ y la MAC-MZ. Para lograr esta delimitación, se propone un método que implica cuatro niveles: Validación de

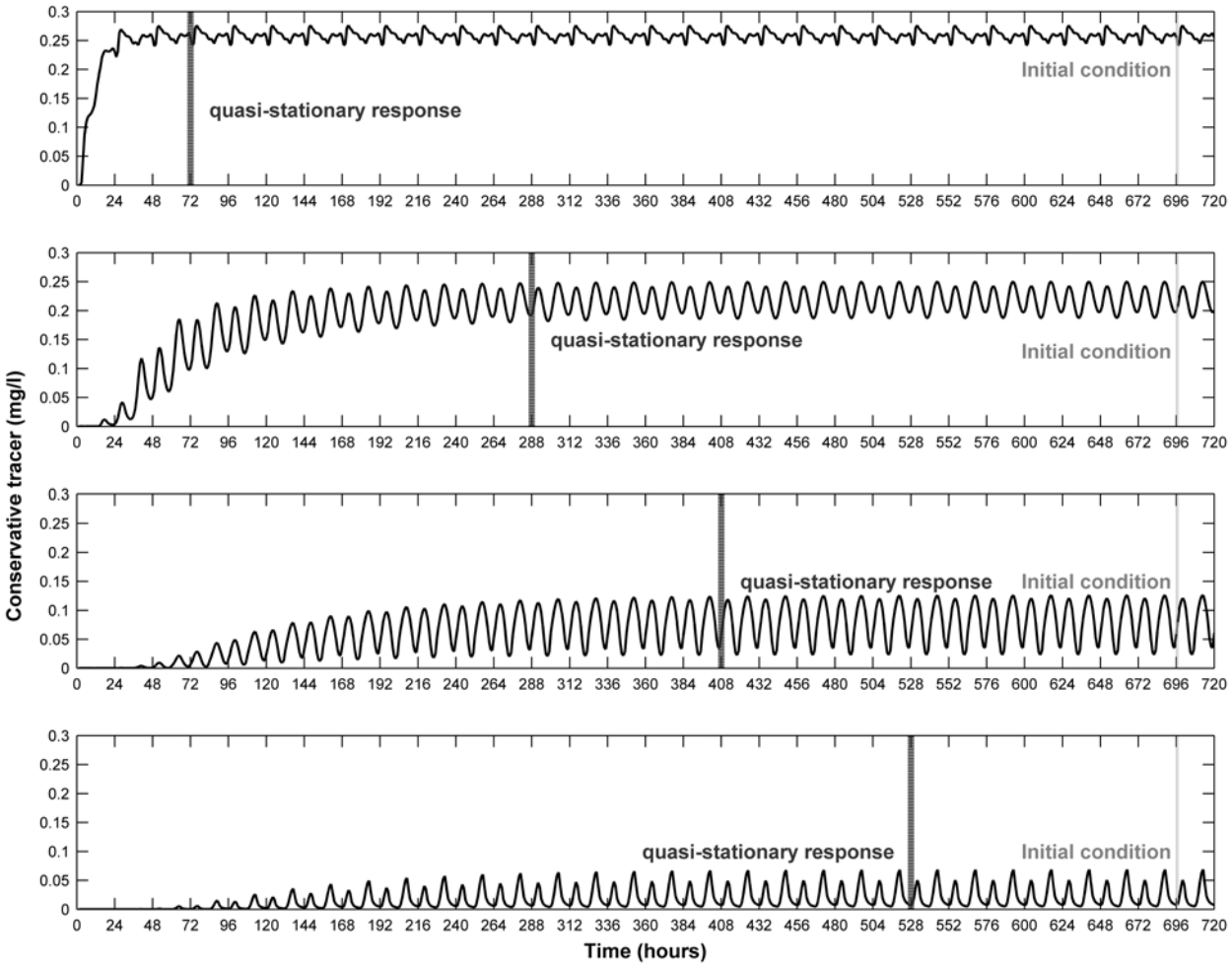

Figura 33: Ejemplo de la evolución de un tóxico, escala temporal de la respuesta "cuasi-estacionaria" para el trasporte y condición inicial para la "presimulación" del "caso real de dilución".

las series reconstruidas, Selección y generación de l-años reconstruidos, Muestreo aleatorio y Delimitación definitiva de MZs (Figura 34).

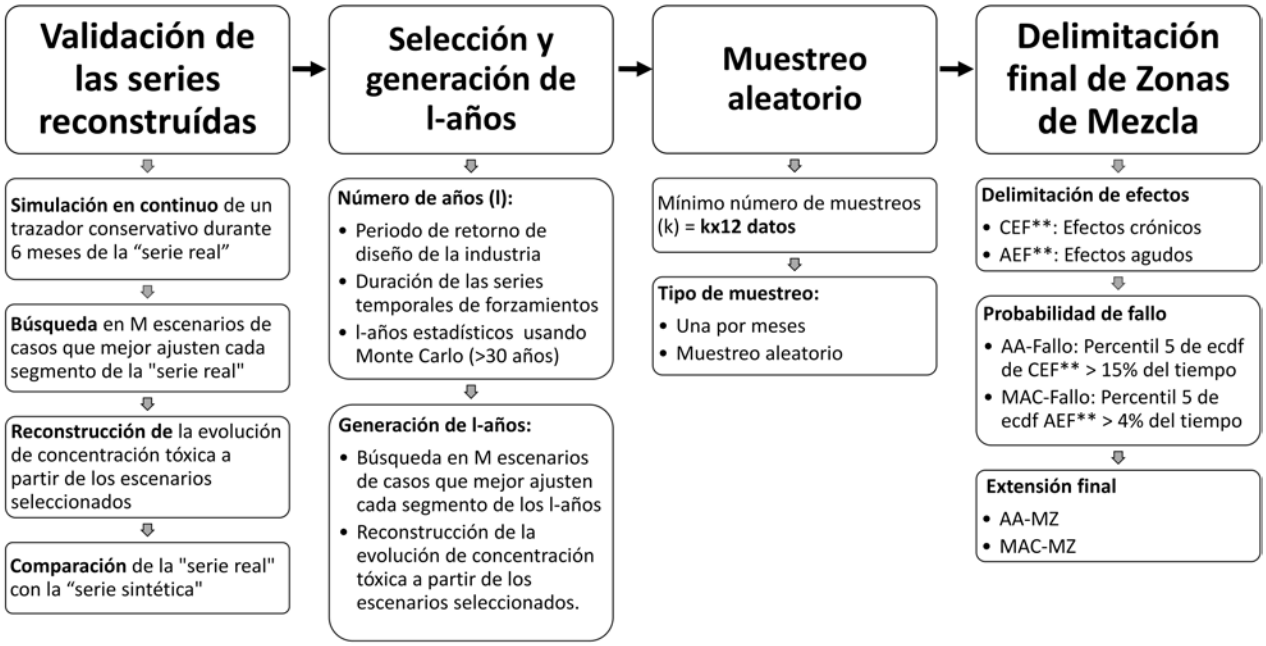

Figura 34: Metodología para delimitar zonas de mezcla en estuarios para el calcula detallado o "caso real de dilución".

Validación de las series reconstruidas

En el primer nivel, se valida la capacidad de los M escenarios de modelado para reconstruir adecuadamente "series reales", es decir, la reproducción de la evolución de la concentración de tóxico con base en la combinación de los M escenarios. Esta validación se efectúa en varios pasos:

1. Simulación continua de los trazadores no conservativos estudiados durante al menos 6 meses, teniendo en cuenta la serie de "real" del caudal fluvial y las elevaciones de marea.
2. Búsqueda en los M escenarios de modelado de cada escenario que mejor se adapte a cada segmento de n días de la serie "real".
3. Reconstrucción de la evolución de la concentración de tóxico a partir de los escenarios de modelado seleccionados ("serie sintética").
4. Comparación de la "serie real" y la "serie sintética" con el fin de validar y garantizar los resultados obtenidos a una resolución de tiempo diario (24 horas en promedio). Para ello, se utilizan como medidas de error el BIAS, el CE, la diferencia entre ambos promedios y el tiempo de superación de EQS. En cuanto a la comparación diaria, se propone dicha resolución porque la fase de marea no será la misma a lo largo de la evolución de la concentración de tóxico entre la "serie real" y la "serie sintética".

Después de esta validación, se puede generar cualquier "serie real" de concentración de tóxico con base en una secuencia de múltiples M resultados ("serie sintética") que mejor se adapten a la serie "real".

Selección y generación de l-años reconstruidos

En este segundo nivel, se propone la selección y generación de una serie de l-años representativos para llevar a cabo la delimitación. La consideración de una serie larga de años asegura una correcta caracterización de

la evolución de las sustancias tóxicas en el estuario con base en los fenómenos hidrometeorológicos. Esta selección de l-años podría establecerse atendiendo a los siguientes criterios:

1. La duración de las series temporales de caudal fluvial y nivel de marea utilizadas para clasificar.
2. El período de retorno de diseño de la instalación industrial. Dichos períodos suelen estar comprendidos entre 20 y 100 años.
3. La generación de l-años estadísticos mediante técnicas de Monte Carlo basados en la probabilidad de los M escenarios de modelado. Esta selección debe tener en cuenta la variabilidad de los forzamientos hidrodinámicos así como la independencia de los resultados.

En los dos primeros criterios, la selección del número de años es inmediata debido a que el período de retorno de diseño o la duración de las series temporales son datos conocidos.

En el tercer criterio, la generación de año estadísticos por Monte Carlo provoca que la probabilidad de ocurrencia de cualquier M escenario de modelado podría ser diferente a la probabilidad real de la selección con KMA. Estas diferencias se deben al hecho de que la duración de las series reconstruidas (un año) es menor que las series iniciales a largo plazo (por lo general más 30 años). Además, el número de eventos (x escenarios de modelado consecutivos) es también menor que los M escenarios de modelado. Por ello, se recomienda generar al menos 100 años como el número mínimo de años estadísticos (l) cuando se emplean técnicas de Monte Carlo.

Después de la selección de los l-años, se busca en los M escenarios de modelado los casos que mejor se adapten a cada segmento de n días para los l-años y se reconstruye la evolución de la concentración de tóxico a partir de los escenarios de modelado seleccionados para cada l-año.

Muestreo aleatorio

En el paso 4, se determinó el número óptimo de muestreos ($k\times12$ datos). En este tercer nivel, se calcula el muestreo aleatorio para los k-muestreos en cada l-año.

Delimitation final de MZs

En el cálculo detallado, también se generan l-años de evolución de la concentración de una sustancia tóxica. Por lo tanto, la delimitación de MZs calcula las probabilidades de los k-muestreos por cada l-año de la siguiente manera:

- *Efectos crónicos (CEF**):* Los efectos crónicos de cada sustancia tóxica en cada celda de la malla se calculan utilizando la ecuación (11) para cada l-año teniendo en cuenta cada k-muestreo. A continuación, si $CEF * *^{k}_{i,j} > 1$ entonces $CEF * *^{k}_{i,j} = 1$. Por en contrario, si $CEF * *^{k}_{i,j} \leq 1$ entonces $CEF * *^{k}_{i,j} = 0$. Luego, el CEF** asociado a todos los k-muestreos se computa por medio de la ecuación (12) para cada l-año. Finalmente, se obtiene un vector de l-CEF** valores en cada celda de la malla, es decir, la probabilidad de AA-Fallo de cada l-año. A partir de este vector, se calcula la función de distribución acumulada de CEF**.

- *Efectos agudos (AEF**):* Los efectos agudos de cada sustancia tóxica en cada celda de la malla se calculan utilizando la ecuación (13) para cada l-año teniendo en cuenta cada k-muestreo. A continuación, si $AEF * *^{k}_{i,j} > 0$ entonces $AEF * *^{k}_{i,j} = 1$. Por en contrario, si $AEF * *^{k}_{i,j} \leq 0$ entonces $AEF * *^{k}_{i,j} = 0$. Luego, el AEF** asociado a todos los k-muestreos se computa por medio de la ecuación (14) para cada l-año. Finalmente, se obtiene un vector de l-AEF** valores en cada celda de la malla, es decir, la probabilidad de MAC-Fallo de cada l-año. A partir de este vector, se calcula la función de distribución acumulada de AEF**.

Al igual que en el Paso 4, se asume una probabilidad de fallo mediante criterio de experto ($CEF^{**}_{i,j} > 15$ and $AEF^{**}_{i,j} > 4$). No obstante, en el Paso 5, se tiene la distribución de CEF** y AEF** para l-años en vez de un sólo año. Por ello, una nueva especificación temporal: número de años que una celda de la malla está por encima de una determinada probabilidad de fallo, se debe establecer con el fin de delimitar la extensión definitiva de MZs.

De acuerdo con Bárcena *et al.* (2012), se propone que una celda de la malla forme parte de la zona de mezcla definitiva en el cálculo detallado cuando la probabilidad de ocurrencia de las funciones de distribución acumuladas de CEF** y AEF** están por encima del percentil 5 (5 % de los l-años). Además, si el valor CEF** y AEF** del percentil 5 está por encima de $CEF^{**}_{i,j} > 15$ y $AEF^{**}_{i,j} > 4$ respectivamente, se considera que la celda de la malla también forma parte de la AA-MZ y MAC-MZ (Figura 35).

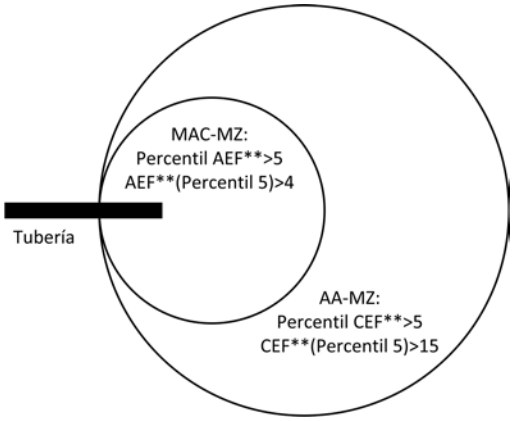

Figura 35: Diagrama de las dos partes delimitadas como zonas de mezcla (AA-MZ y MAC-MZ) en el cálculo detallado.

2.5.6. Admisibilidad de las zonas de mezcla

En primer lugar, se ha adaptado la metodología propuesta por Gómez *et al.* (2014b) para evaluar el riesgo ambiental de los procesos de dragado con el fin de estimar la vulnerabilidad en estuarios frente a los vertidos puntuales industriales (Figura 36).

A partir del concepto de vulnerabilidad y el porcentaje de área estuarina cubierto por las MZs, se define y determina la admisibilidad de las MZs en un método de cuatro niveles:

1. El Índice de Vulnerabilidad Estuarina (EVI) se calcula a nivel de celda de la malla mediante varios parámetros.
2. La Aceptabilidad (AC*) se calcula multiplicando los valores de EVI por el porcentaje de área de estuario cubierta por cada celda de la malla.
3. El Tamaño Máximo Permitido de MZ (MAS*) se calcula dividiendo el porcentaje máximo admisible del área estuarina que una MZ puede cubrir (criterio de expertos) por un factor de corrección (α) que depende del EVI medio que delimita el estuario.
4. La Admisibilidad de la MZ delimitada (AD*) se determina comparando la suma de todas las AC* cubiertas por la MZ delimitada con el MAS*.

La Vulnerabilidad en estuarios se refiere a las características de un ecosistema estuarino que describen su potencial de ser dañados. Por lo tanto, la vulnerabilidad se presenta como una combinación de cuatro parámetros: zonificación mareal (TZ), susceptibilidad (SU), estado de conservación (SC) y estratificación (ST).

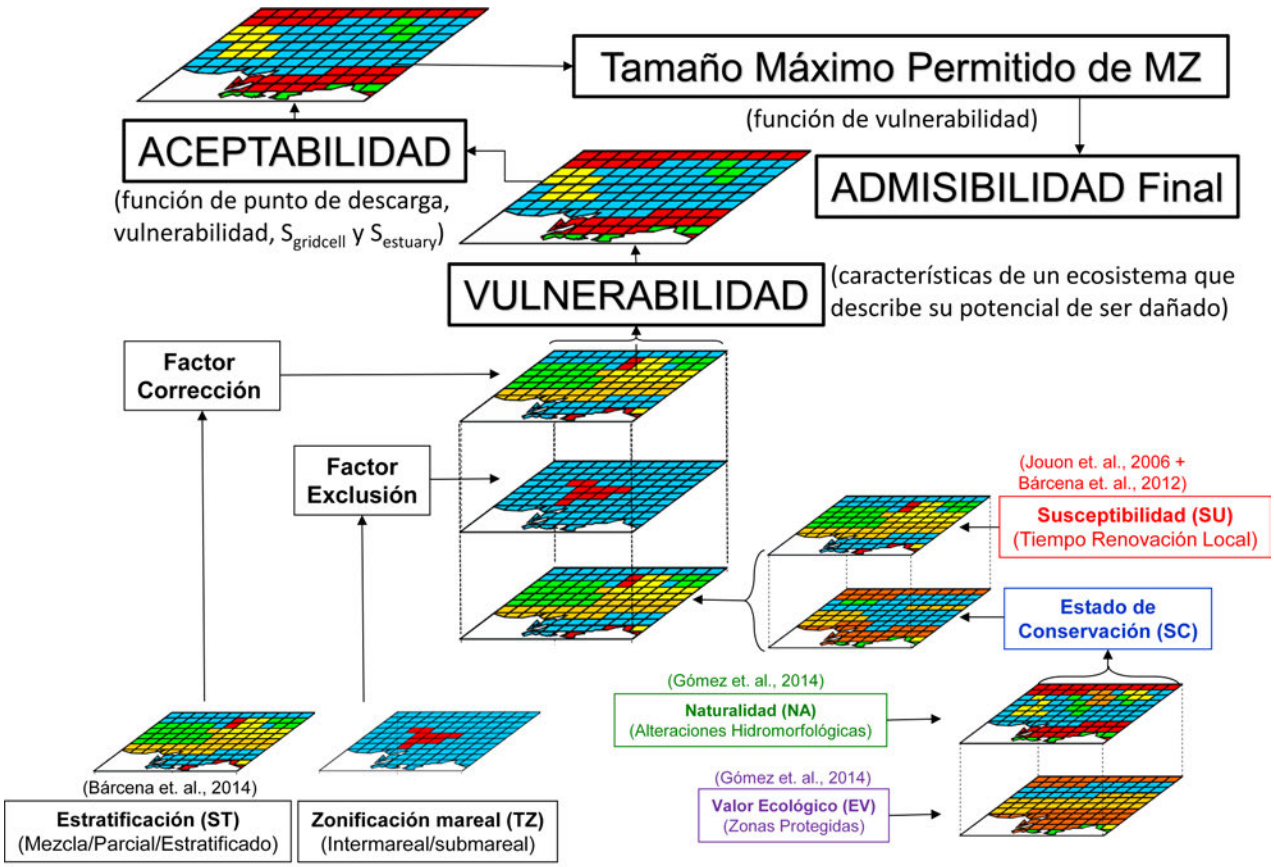

Figura 36: Vista esquemática de la metodología propuesta para cuantificar la vulnerabilidad del estuario y la admisibilidad de las zonas de mezcla.

2.5.6.1. Zonificación mareal (TZ)

TZ es la localización de zonas intermareales y submareales de acuerdo con el percentil 95 de la amplitud de la marea ($A95$) y la profundidad de cada celda de la malla (H). Este parámetro se ha diseñado con el fin de proteger las zonas de estuarios donde se producen procesos de inundación y secado.

2.5.6.2. Susceptibilidad (SU)

La susceptibilidad se relaciona con la capacidad de renovación del agua y se estima por medio de modelos numéricos. En este trabajo, se utiliza el concepto de tiempo de renovación local (Jouon *et al.* 2006) y la metodología propuesta por Bárcena *et al.* (2012b) para estimar dicha capacidad de renovación de acuerdo con las variaciones temporales de los principales forzamientos (río y marea) y las variaciones espaciales de la configuración estuarina (ver figura 37).

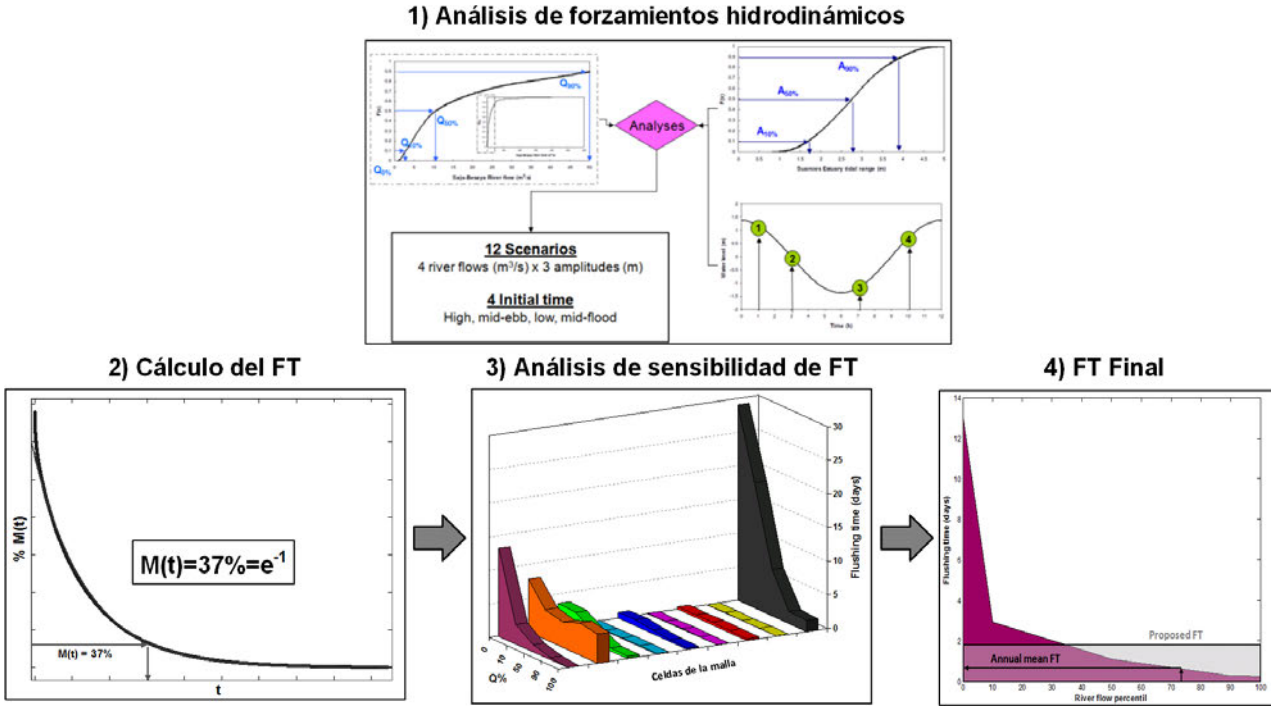

Figura 37: Vista esquemática de la metodología propuesta para calcular el tiempo de renovación en estuarios.

Análisis de los forzamientos hidrodinámicos

Para comprender la magnitud y la ocurrencia de estos forzamientos, la primera tarea es calcular la función empírica acumulada de distribución (ecdf) de la serie de caudal del río (m^3/s) y de la serie de carrera de la marea astronómica (m).

A partir de estas curvas, se seleccionan N caudales del río iguales a N percentiles, M carreras de marea iguales a M percentiles y, por último, L fases de marea que se corresponden con L situaciones de marea. Dicha selección se basa en los cambios de pendiente de cada curva ecdf (ver panel 1 de la figura 37).

Cálculo del tiempo de renovación

De entre todos los métodos existentes en la literatura, la metodología propuesta por Jouon *et al.* (2006) ha sido seleccionada para calcular la renovación del agua. Dicho método propone la aplicación de un modelo hidrodinámico tridimensional acoplado a un modelo de transporte tridimensional.

Si se considera que una cantidad conocida de una sustancia se inyecta en una masa de agua homogénea en el momento t_0 con una concentración inicial C_0, que no se añade más cantidad de esta sustancia después de

t_0, que el volumen de la masa de agua es constante y, por último, que los flujos en sus contornos son también constantes, la concentración de la sustancia dentro de la masa de agua a un tiempo t viene dada por la ecuación (21).

$$C(t-t_0) = C_0 e^{-Q/V*(t-t_0)} = C_0 e^{-(t-t_0)/t_f} \tag{21}$$

donde Q representa el caudal (entrando o saliendo), V es el volumen de control considerado, t es el tiempo ($t > t_0$) y t_f el el tiempo de renovación.

En esta tesis, se calcula el tiempo de renovación (FT) a escala local con el fin de poder definir un tiempo para cada celda de la malla denominado tiempo de renovación local (LFT). El método de cálculo es el siguiente:

1. Se lleva a cabo el modelado hidrodinámico de los escenarios propuestos.
2. Inicialmente, se impone una concentración C_0 de un trazador conservativo y no sedimentable en el área de interés con un valor distinto de cero (por ejemplo, $C_0 = 1$). En las celdas de la malla que se localizan fuera de la zona de interés, la concentración se mantiene en cero.
3. A continuación se calcula la evolución de esta concentración bajo la influencia de la hidrodinámica.
4. Cuando se alcanza un valor umbral de C_1 (establecido arbitrariamente como el $95\,\%$ de C_0) en una celda de la malla, se marca como t_1 y se considera que es el comienzo de la disminución exponencial de la concentración dentro de esta celda de la malla.
5. El LFT se define entonces como el tiempo (t_2) que se tarda en disminuir la concentración entre C_1 y $1/e * C_0$. Para ello, se utiliza una regresión exponencial como la ecuación (21).

El gradiente de la escala temporal de transporte dado por este método puede conducir a establecer una diferenciación espacial de las áreas dentro de estuarios, un resultado que es, al menos, muy interesante para definir la vulnerabilidad estuarina (ver panel 2 de la figura 37).

Análisis de sensibilidad del tiempo de renovación

El tercer nivel consiste en la realización de un multi-análisis de sensibilidad de los resultados LFT para entender la influencia de la profundidad, el tiempo inicial de simulación (fase de marea), el caudal del río y la carrera de la marea a lo largo de la ría.

Para analizar la tendencia descrita por el LFT debido a la profundidad (influencia de cada capa 3D en el tiempo de renovación), todos los resultados se representan gráficamente. Dependiendo de la variabilidad con la profundidad, se permite promediar los valores de LFT de todas las capas en cada escenario de modelado. En el caso de que la influencia de la profundidad sea significativa, la capa que muestra los valores máximos de LFT debe ser considerada.

Después, se grafica el LFT frente al tiempo inicial de simulación para entender esta influencia. Dependiendo de la variabilidad de la fase de la marea, se permite promediar los valores de LFT de todos los tiempos iniciales de simulación en cada escenario de modelado. En el caso de que la influencia de fase de marea sea significativa, la fase de marea que presenta los valores máximos de LFT debe ser considerada.

La siguiente tarea es llevar a cabo un análisis de sensibilidad de los forzamientos por medio del ajuste de los valores de LFT a superficies de respuesta en función de Q y A. La función de ajuste utilizada para generar dichas superficies tiene una forma cuadrática porque los principales procesos en un estuario son no lineales como se muestra en la ecuación (22).

$$LFT = aQ^2 + bA^2 + cQA + dA + eQ + f \tag{22}$$

donde a a f son los coeficientes del ajuste determinados por medio de un método basado en mínimos cuadrados. Adicionalmente, f representa el error en la respuesta.

Las superficies de respuesta explican las relaciones entre los forzamientos, las características geomorfológico y el LFT. A partir de estas consideraciones, se puede decidir promediar el forzamiento menos variable (Q o A) a lo largo de su eje. A modo de ejemplo, el panel 3 de la figura 37 muestra el valor del LFT para diferentes caudales fluviales en 9 celdas arbitrarias con la marea pomediada.

Tiempo de renovación final

Si se promedia el forzamiento de menor variabilidad, se sugiere integrar el área bajo la curva para cada celda de la malla con el fin de construir un rectángulo con el mismo área y, por lo tanto, proporcionar el tiempo de renovación final como la la altura de dicho rectángulo. Este cálculo permite preservar la influencia del forzamiento con mayor variabilidad en el valor final de LFT porque se pondera con la probabilidad de ocurrencia (ver panel 4 de la figura 37).

En el caso de que no se promedie porque ambos forzamientos son significativos, se sugiere integrar el volumen bajo la superficie para cada celda de la malla con el fin de construir un prisma con el mismo volumen y, así, proporcionar el tiempo de renovación final como la altura de dicho prisma. Este cálculo también permite preservar la influencia de ambos forzamientos ponderando la probabilidad de ocurrencia de los forzamientos en el valor final.

2.5.6.3. Estado de conservación (SC)

La naturalidad (NA) se define como la ausencia de modificaciones antropogénicas físicas. Se define una alteración por presiones hidromorfológicas (HP_{ij}), calculando la zona de protección alrededor de cada HP por medio de herramientas de análisis espacial en un sistema de información geográfico (GIS). La distancia de protección de un HP se muestra en la ecuación (23):

$$d = k_{HP} \cdot (\frac{L}{CV})^2 \tag{23}$$

donde k_{HP} es igual a 1 si el HP es continuo (dique, muelles) o k_{HP} igual a 0.5 si el HP es discontinuo (puente, pantalán), L es la longitud de la presión y CV es el valor crítico definido como la longitud de HP que se considera significante. CV es igual a 50 m para diques de encauzamiento, diques exentos o rompeolas secundarios. CV vale 100 m para canalizaciones, rompeolas principales, embarcaderos, muelles, dársenas, pantalanes o motas y 150 m para estructuras litorales tales como muros o bloques de cemento preformados.

La zonas de protección de todos los HP identificados se consideran áreas alteradas y presentan baja naturalidad (Gómez 2010).

El valor ecológico (EV) se describe como la capacidad de regeneración de un ecosistema para mantener las especies de flora y fauna. Dicho parámetro se cuantifica utilizando el indicador de Elementos Singulares Ecológicos (ESE_{ij}) definido por Gómez *et al.* (2014b).

ESE_{ij} se definen mediante el reconocimiento de las áreas protegidas regionales, nacionales e internacionales en la malla de cálculo con el uso de herramientas de localización en un GIS.

2.5.6.4. Estratificación (ST)

La circulación estuarina se rige por la estratificación de la densidad gobernada principalmente por la variación vertical de la salinidad. De acuerdo a la estratificación de la columna de agua o la estructura vertical de salinidad, los estuarios se pueden clasificar como estratificados, parcialmente estratificados/mezclados o mezclados verticalmente (Cameron & Pritchard 1963, Pritchard 1952).

En el contexto de la tesis, la estratificación puede afectar positiva o negativamente la mezcla de vertidos

industriales, dependiendo del tipo de estuario o, más localmente, el tipo de estratificación en la vecindad del punto de descarga. Si la descarga se encuentra en una zona bien mezclada, la circulación estuarina mejora la mezcla de las aguas residuales. Por el contrario, la estratificación inhibe la mezcla vertical reduciendo la dilución de las aguas residuales. Por lo tanto, una zona clasificada como mezclada es menos vulnerable que una zona clasificada como estratificada.

En este apartado, se presenta un método para localizar zonas mezcladas, parcialmente mezcladas/estratificadas y estratificadas en estuarios dividido en tres pasos: Selección y modelado de escenarios hidrodinámicos, Cálculo del número de Richardson y Zonificación definitiva de estratificación. La figura 38 muestra un esquema de la metodología propuesta donde los resultados se integran a nivel de celda de la malla para estimar temporal y espacialmente la estratificación en todo el dominio.

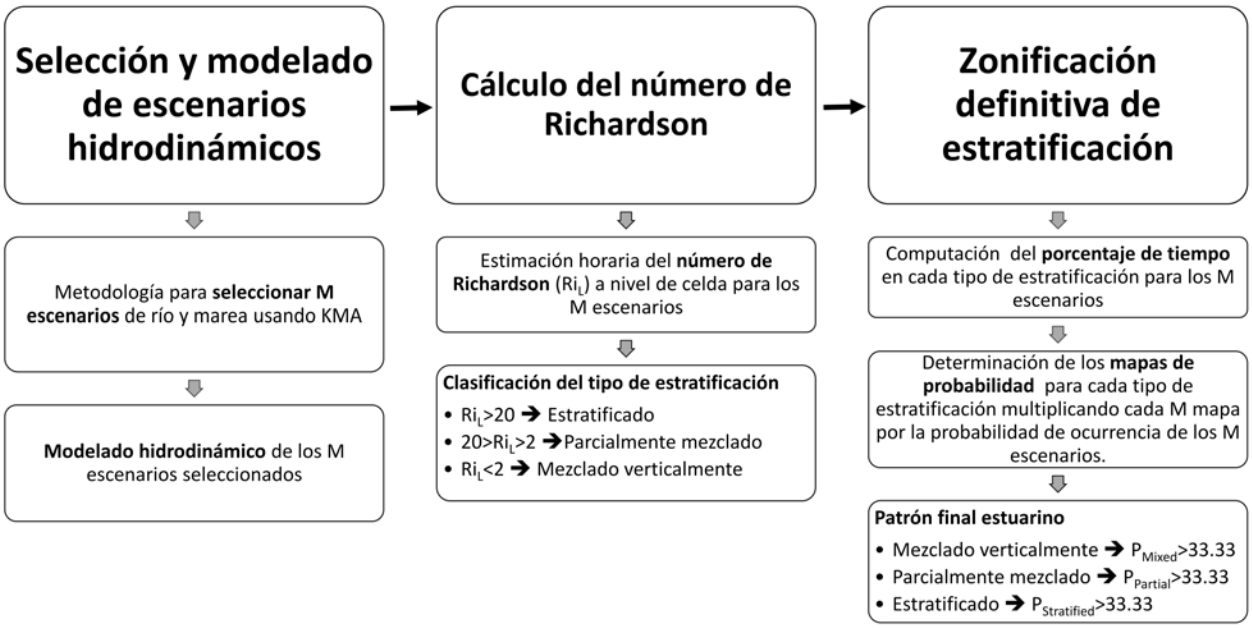

Figura 38: Vista esquemática de la metodología propuesta para estimar la estratificación en estuarios.

Selección y modelado de escenarios hidrodinámicos

En el primer nivel, se emplean los mismos escenarios de modelado seleccionados por medio de un algoritmo K-means. A partir de los resultados hidrodinámicos de los M escenarios de modelado, se calculará el número de Richardson a nivel de celda de la malla.

Cálculo del número de Richardson

La estratificación del estuario se analiza mediante el número de Richardson Ri_L dado por Bowden (1978) en la ecuación (24) para cada celda y paso de tiempo.

$$Ri_L(t) = \frac{g \cdot H(t) \cdot \Delta\rho_V(t)}{\overline{\rho_{env}}(t) \cdot (\overline{u})^2(t)} \tag{24}$$

donde g es la aceleración de la gravedad, $H(t)$ es la profundidad de la columna de agua, $\Delta\rho_V(t)$ es el gradiente de densidad entre el fondo y la superficie, $\overline{\rho_{env}}(t)$ es la densidad promediada en vertical y $\overline{u}(t)$ es la velocidad promediada en vertical.

La interpretación física del Ri_L fue dada por Dyer & New (1986):

1. Para $Ri_L > 20$, la turbulencia generada por el fondo no parece suficiente como para disminuir la estratificación, es decir, la columna de agua es muy estable presentando una mezcla vertical pequeña (tipo estratificado).

2. Para $20 > Ri_L > 2$, la mezcla es cada vez mayor debido a la turbulencia (tipo parcialmente estratificado/mezclado).

3. Para $Ri_L < 2$, se produce una mezcla totalmente desarrollada, esto es, la mezcla turbulenta hace que la columna de agua sea inestable (tipo mezclado verticalmente).

A partir de los resultados del modelo hidrodinámico, se cuantifica horariamente Ri_L para los M escenarios de modelado en cada celda de la malla. A continuación, se clasifica por hora el estado de estuario de acuerdo con el criterio propuesto por Dyer & New (1986).

Zonificación definitiva de estratificación

En este paso, se calcula el tiempo que cada celda de la malla está en cada estado de estratificación para cada M escenario. A continuación, se traduce dicha duración en el porcentaje de tiempo que una celda de la malla está mezclada, parcialmente mezclada/estratificada y estratificada para cada M escenario. De este modo se obtienen M mapas de probabilidad de ocurrencia para cada una de los tipos de estratificación ($M \times 3$).

Como se mencionó, los M escenarios de modelo tienen una probabilidad de ocurrencia. A partir de los $M \times 3$ mapas de probabilidad, se calculan 3 mapas de probabilidad para cada tipo de estratificación multiplicando cada M mapa por la probabilidad de ocurrencia del escenario M.

Por último, se integra toda la información en un único mapa que muestra el tipo de estratificación más probable a nivel de celda. Si la probabilidad de una celda para cualquier tipo de estratificación supera el 33.33 % del tiempo, entonces dicha celda de la cuadrícula se zonifica, definitivamente, con ese tipo de estratificación.

2.5.6.5. Índice de Vulnerabilidad Estuarina (EVI)

Una vez calculados todos los parámetros, en el primer nivel (ver en la figura 36) se integra toda la información por medio del llamado "Índice de Vulnerabilidad Estuarina" (EVI) cuya formulación matemática se detalla en la ecuación (25).

$$EVI(TZ) = \begin{cases} \text{if } TZ = 1 & 1 \\ \text{if } TZ = 0 & [a \cdot SU + b \cdot (c \cdot NA + d \cdot EV)] \cdot ST \end{cases} \tag{25}$$

Con el fin de ponderar la importancia de cada término (a, b, c, d) en la ecuación (25), se efectuó una encuesta a 20 expertos de todo el mundo preguntando su opinión acerca de los diferentes parámetros que intervienen en el índice. En primer lugar, se preguntó qué término debe tener más importancia para estimar la vulnerabilidad si a=SU o b=SC. El 85 % de los expertos contestó que SU (17 respuestas) mientras que el 15 % optó por SC (3 respuestas). Análogamente, se preguntó qué término debe tener más importancia para estimar el estado de conservación si c=NA o d=EV. En este case, NA obtuvo el 35 % de las respuestas (7) y el 65 % fue para el EV (13 respuestas).

A continuación, se presentan en la tabla 3 los criterios de evaluación, los umbrales y las métricas para cada parámetro de vulnerabilidad.

De acuerdo con los resultados de la encuesta y las métricas establecidas en la tabla 3, se asignan los valores de los coeficientes en la ecuación (26) y se cuantifica el valor del EVI a nivel de celda de la malla:

$$EVI_i(TZ_i) = \begin{cases} \text{if } TZ_i = 1 & 1 \\ \text{if } TZ_i = 0 & [0{,}85 \cdot SU_i + 0{,}15 \cdot (0{,}35 \cdot NA_i + 0{,}65 \cdot EV_i)] \cdot ST_i \end{cases} \tag{26}$$

Criterio	**Umbral (m)**	**TZ**
Intermareal	$H \leq A95$	1.0
Submareal	$H > A95$	0.0
Criterio	**Umbral (días)**	**SU**
Renovación total	0	0.0
Renovación	$0 < LFT_i < LFT_{max}$	$\frac{0{,}8 \cdot LFT_i}{LFT_{max}}$
Renovación mínima	LFT_{max}	0.8
Criterio	**Umbral (m)**	**NA**
Alterado por HP	$d = k_{HP} \cdot (\frac{L}{CV})^2$	0.0
No-alterado por HP	0	0.8
Criterio	**Umbral (-)**	**EV**
Ausencia de ESE	Otras zonas	0.0
Presencia de ESE	Zonas protegidas	0.8
Criterio	**Umbral (%)**	**ST**
Mezclado	$P_M > 33{,}33$	1.0000
Parcial	$P_P > 33{,}33$	1.1125
Estratificado	$P_E > 33{,}33$	1.2500

Tabla 3: Criterios de evaluación, umbrales y métricas para cada parámetro del Índice de Vulnerabilidad Estuarina (EVI).

En primer lugar, se utiliza como factor de exclusión el valor de TZ. Si TZ es igual a 1.0 entonces EVI es 1.0. De lo contrario, se calcula el EVI_i con la formulación propuesta. El valor de SU, NA y EV oscila entre 0.0 y 0.8 mientras que ST depende del tipo de estratificación actuando como un factor de corrección (1.0 para bien mezclado, 1.125 para parcialmente mezclado/estratificado y 1.25 para estratificado).

Por tanto, EVI oscila entre cero y uno. El cero representa las zonas estuarinas menos vulnerables a recibir descargas de aguas residuales mientras que las áreas con uno son las más vulnerables.

2.5.6.6. Aceptabilidad (AC*)

El siguiente nivel (ver en la figura 36) consiste en determinar la aceptabilidad (AC*) del estuario a nivel de celda. Para ello, si el punto de descarga se encuentra en una celda de la malla con un EVI igual a 1 no es aceptable. De lo contrario, se calcula el valor de AC* multiplicando el valor de EVI por el porcentaje de área estuarina cubierto por dicha celda (Ecuación (27)).

$$AC_i^*(EVI, A) = \begin{cases} \text{if } EVI_i = 1 & Inaceptable \\ \text{if } EVI_i \leq 1 & EVI_i \cdot \frac{A_i}{A_{estuary}} \cdot 100 \end{cases} \tag{27}$$

donde EVI_i es el Índice de Vulnerabilidad Estuarina para la i-celda, A_i es el área de la i-celda y $A_{estuary}$ es el área total del estuario siendo la misma que la del "caso peor de dilución".

EVI_i se puede entender como un factor de corrección de la superficie real de una celda de la malla en función de su vulnerabilidad. Si todas las celdas tuvieran $EVI_i = 1$ el AC* sería el mismo que el del "caso de peor de dilución". A la inversa, si todas las celdas tuvieran un $EVI_i = 0$ el AC * sería igual a cero, es decir, cualquier zona de mezcla sería admisible. Cabe mencionar que matemáticamente no es posible tener un $EVI_i = 0$ en todas las celdas del estuario debido a la formulación desarrollada.

2.5.6.7. Tamaño máximo permitido para zonas de mezcla (MAS*)

En el tercer nivel (ver en la figura 36), se calcula el tamaño máximo permitido de MZs corregido (MAS*) dividiendo el AA-MAS y MAC-MAS del "caso peor de dilución" entre un factor de corrección (α) que

depende del EVI promediado del estuario.

La ecuación (28) muestra el valor del MAS* mientras que la ecuación (29) la formulación para α.

$$MAS^* = \frac{MAS}{\alpha} \tag{28}$$

$$\alpha = \frac{1}{1 - \overline{EVI}_{estuary}} \tag{29}$$

donde $\overline{EVI}_{estuary}$ es el EVI promediado de todas las celdas cubiertas por el estuario.

α funciona como un factor de ponderación en el cálculo del MAS* en función del EVI promedio del estuario. Si $\overline{EVI}_{estuary} = 1$, el MAS* será infinito, esto es, no se admitirían zonas de mezcla. Como en el caso de AC*, no se puede tener esta situación debido a la formulación desarrollada. A la inversa, si $\overline{EVI}_{estuary} = 0$, el MAS* se convierte en el MAS, es decir, las zonas de mezcla se aceptan con el mismo porcentaje de superficie del estuario que en el "caso peor de dilución" (Figura 39).

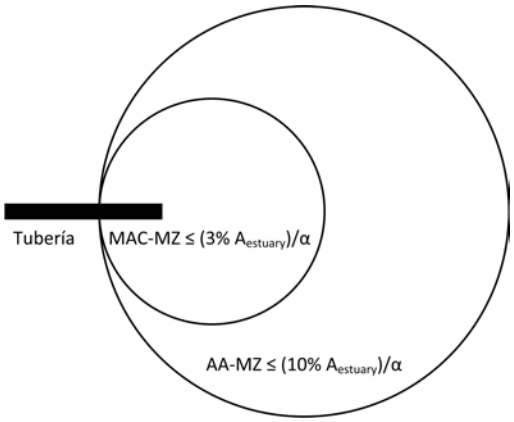

Figura 39: Diagrama del tamaño máximo permitido de la zona de mezcla para AA-MZ y MAC-MZ en el cálculo detallado.

2.5.6.8. Admisibilidad final (AD*)

En el cuarto nivel (ver en la figura 36), la admisibilidad final (AD*) se determina comparando la suma de todas las celdas de AC* cubiertos por la AA-MZ y la MAC-MZ previamente delimitadas con el AA-MAS* y el MAC-MAS* (Ecuación (30)). Si el AD* es mayor que el MAS* el tamaño de la MZ no es admisible mientras que si AD* es igual o menor que el MAS* la MZ es admisible.

$$AD^*(AC^*) = \begin{cases} \text{if } AD^* > MAS^* & \sum_{i=1}^{n} AC_i^* = No - Admisible \\ \text{if } AD^* \leq MAS^* & \sum_{i=1}^{n} AC_i^* = Admisible \end{cases} \tag{30}$$

donde AC_i^* es la aceptabilidad de la i-celda.

El EVI trabaja en la metodología de dos maneras como factor de ponderación multiplicativo en el cálculo de AC* a nivel de celda y como un factor de ponderación divisivo en el cálculo de MAS* a nivel de MZ.

De forma análoga al Paso 4, la tarea final en el Paso 5 es determinar la asignación de ambas MZs trazando un ábaco que relaciona la extensión de la zona de mezcla con la probabilidad de fallo de la misma. Para dibujar esta curva, se tiene en cuenta que la extensión no puede ser mayor que el $10\,\%/\alpha$ y $3\,\%/\alpha$ de área estuarina para el AA-MZ y para el MAC-MZ respectivamente. Además, el percentil 5 de la ecdf de la probabilidad de

fallo (AA y MAC) no puede ser mayor del $15\,\%$ para el AA-Fallo y $4\,\%$ para el MAC-Fallo, respectivamente.

La figura 40 ilustra un ejemplo de un ábaco que muestra la evolución de la extensión de las MZs con el percentil 5 de la ecdf de la probabilidad de fallo. En dicha figura, la línea negra es la evolución de la AA-MZ y la línea gris de la MAC-MZ. Además, la línea gruesa negra representa la zona donde la AA-MZ es asignable porque ambos requisitos se cumplen simultáneamente mientras que la línea gruesa gris corresponde a la zona de mezcla admisible para la MAC-MZ.

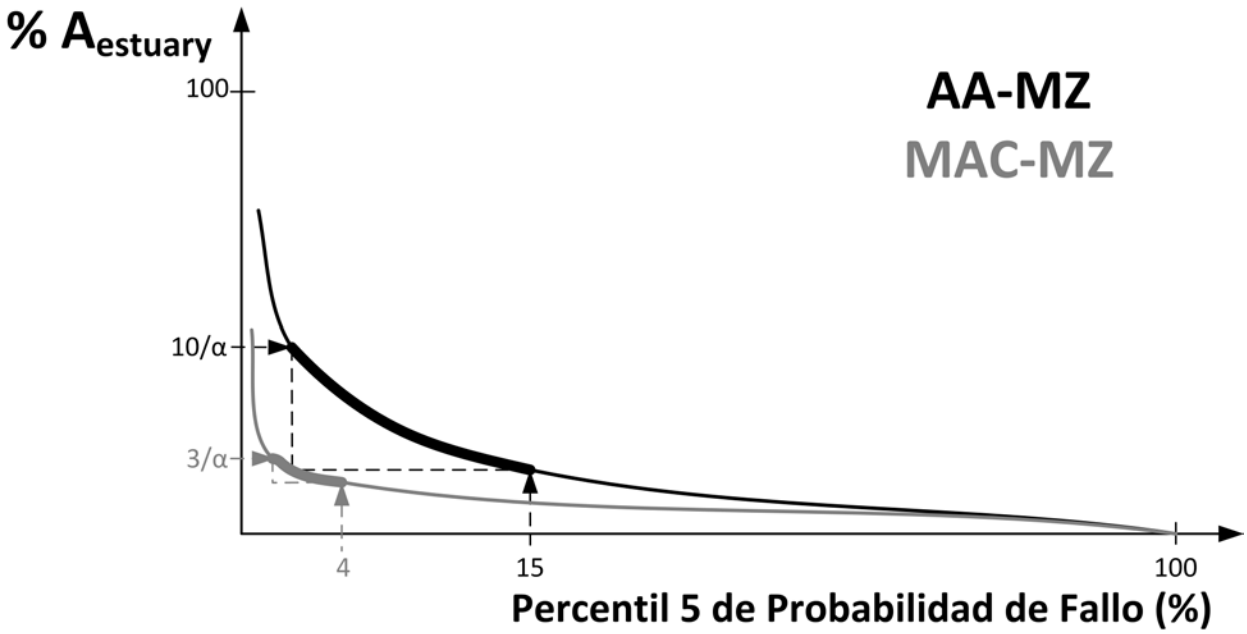

Figura 40: Ejemplo de un ábaco para la AA-MZ (línea negra) y la MAC-MZ (línea gris) en el cálculo detallado.

La delimitación final se debe discutir y acordar entre el interesado y la autoridad competente debido a las implicaciones económicas, sociales y ecológicas de cualquier delimitación como se ha mencionado en el Paso 4.

Después de todos los cálculos, si la descarga aún se clasifica como inadmisible, el árbol de decisiones recomienda reiniciar la metodología en el Paso 1 con el fin de continuar con el procedimiento de asignación (Figura 10) hasta alcanzar una zona de mezcla admisible. La manera de modificar las MZs es cambiando la localización del punto de descarga, reduciendo la carga tóxica (flujo o concentración) y/o ambas.

3. Resultados: Aplicación al Estuario de Suances

En esta sección, se presenta la aplicación al Estuario de Suances de la metodología desarrollada para delimitar zonas de mezcla de vertidos industriales. Este estuario, situado en la costa del mar Cantábrico (Norte de España), podría representar una valiosa oportunidad en términos de aplicabilidad del método a un caso real que requiere una gestión rápida y eficiente debido al alto grado de contaminación industrial.

Si bien la información disponible de los vertidos industriales y de la calidad del agua no es tan extensa y detallada como sería deseable. Dicha información es suficiente para establecer satisfactoriamente algunos casos de análisis y validación de los resultados generados por la metodología desarrollada en esta Tesis. Cabe destacar que la aplicación atraviesa por todos los Pasos de la metodología con el fin de facilitar su comprensión. Para ello, se analizó el transporte de dos sustancias tóxicas: cloroformo o triclorometano ($CHCl_3$) y el plomo

(Pb).

3.1. Paso 1. Caracterización preliminar

Se caracterizaron dos ejemplos de descargas de aguas residuales denominadas Descarga Industrial 1 (ID1) y Descarga Industrial 2 (ID2) con el fin de ilustrar la aplicación de la metodología propuesta en el estuario de Suances (en adelante, SE).

3.1.1. Vertidos de sustancias tóxicas

La ubicación de ID1 e ID2 se muestra en la figura 41. La profundidad media del agua receptora fue 2.87 m y el ángulo con la línea de la costa 163º para ID1 mientras que la profundidad media fue 6.28 m y el ángulo de 212º para ID2.

Las cargas reales de tóxico provinieron de la información contenida en permisos públicos para verter aguas residuales llamados Autorización Ambiental Integrada (IEA). En ambos vertidos, se consideró una descarga teórica constante y continua donde ID1 vierte cloroformo o triclorometano ($CHCl_3$) e ID2 plomo (Pb). De acuerdo con las IEA, ID1 descarga 0.02 mg/l con un caudal de efluente de 0.838 m^3/s mientras que, para ID2, 1 mg/l con un caudal de 0.004 m^3/s. Además, cabe mencionar que la salinidad y la temperatura se consideraron iguales para las dos descargas, siendo 0.5 psu y 15.2 ^oC respectivamente.

Por otra parte, teniendo en cuenta que las configuraciones más típicas de vertidos industriales en estuarios son a través de tuberías con boca única, se diseñaron dos mecanismos de descarga teóricos: ID1 presentó un diámetro de tubería de 0.85 m descargando a 1 m por encima del fondo. En el caso de ID2, se optó por un diámetro de tubería de 0.1 m descargando también a una altura de 1 m por encima del fondo.

Finalmente, se rellenaron las fichas resumen para ID1 e ID2 como se muestra en las figuras 42 y 43 respectivamente.

3.1.2. Zona de estudio

El Estuario de Suances (-4.0237/43.4007 ED50) es un estuario mesomareal ubicado en la costa norte española. Presenta una longitud aproximada de 7.5 km, con 150 m de anchura media y una superficie de 339.7 hectáreas donde los bajos intermareales ocupan el 76 % (Jiménez *et al.* 2012). Además, el 50 % de la ría está bordeada por diques (más de 13.000 m) que alteran drásticamente su naturalidad y condiciones de flujo (Romero *et al.* 2008).

En la figura 41, se mostró la batimetría de la zona de estudio obtenida de las cartas náuticas de la costa española disponibles en la base de datos BACO (González *et al.* 2007). Las zonas más elevadas son de 3.2 m (por encima del nivel medio del mar) que se corresponde con los páramos intermareales situados a lo largo de la ría de Suances. La profundidad del canal principal varía entre 1 y 8 m. En el mar costero adyacente, la mayor profundidad en el área de estudio es de 43 m (por debajo del nivel medio del mar), cerca de la esquina noroeste.

La entrada principal de agua dulce al sistema proviene de dos ríos similares drenando cuencas relativamente pequeñas, el Saja y el Besaya, que ocupan un área de 966.67 km^2 con un perímetro de 166.27 km. Durante el siglo pasado, las principales actividades industriales modificaron y modifican la cuenca hidrológica de los ríos extrayendo agua antes de la ría (2.25 m^3/s) y descargando aguas residuales al estuario (1.25 m^3/s) (Bárcena *et al.* 2012a).

Por un lado, se obtuvo la serie temporal del caudal fluvial proveniente de los ríos Saja y Besaya a partir

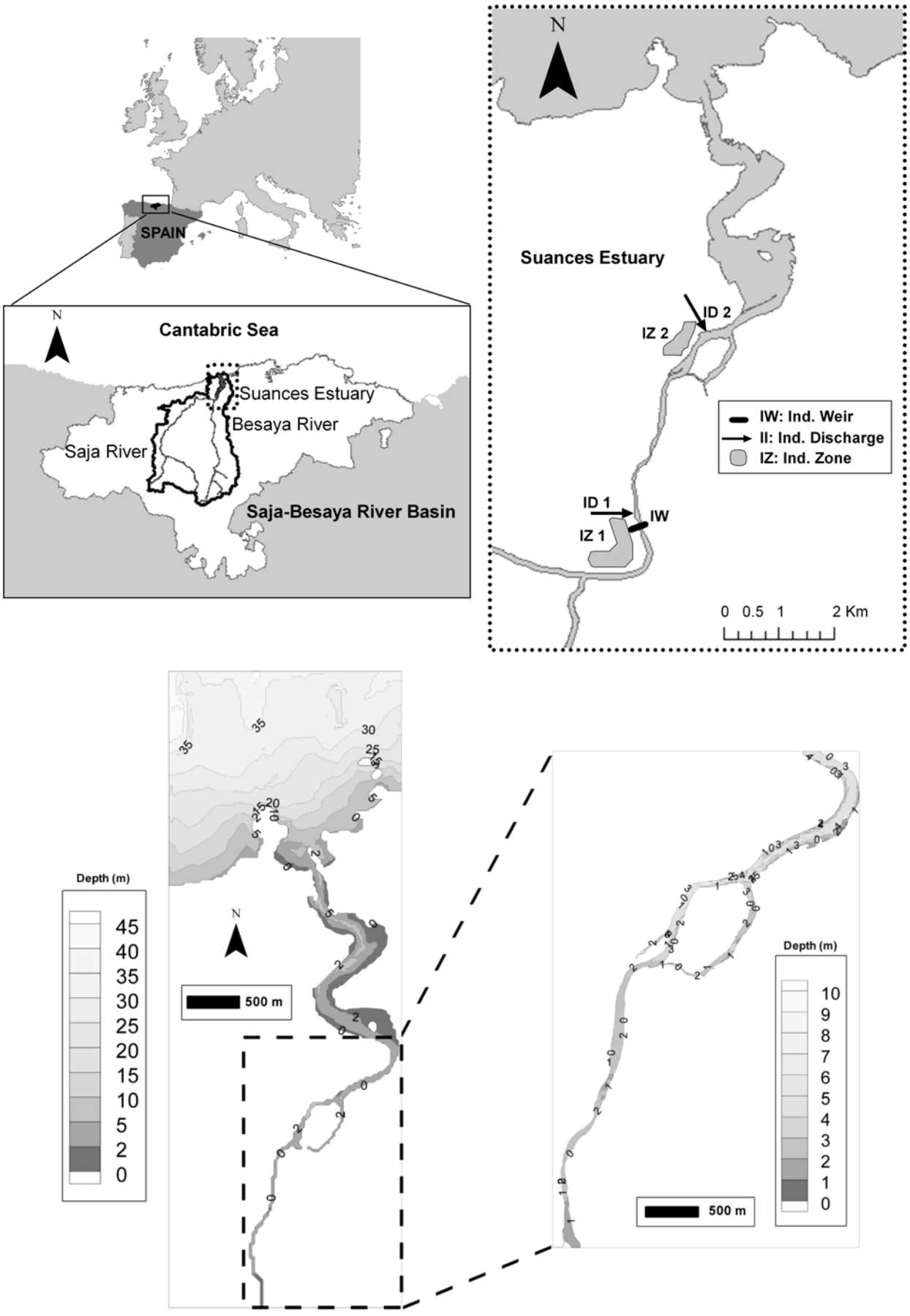

Figura 41: Localización, batimetría, cuenca fluvial y descargas seleccionadas (ID1 e ID2) en el Estuario de Suances.

SUMMARY SHEET OF TOXICANT DISCHARGES

NAME	Industrial Discharge 1
CODE	ID1

Location

UMTX (ED50)	415030.5	Site name	Hinojedo
UTMY (ED50)	4802252.0	Holder	Theoretical Factory 1

Toxicant load

Flow	0.83801	m^3/s	Salinity	0.05	psu
			Temperature	15.2	ºC

Pollutant	Concentration (mg/l)	AA-EQS (mg/l)	MAC-EQS (mg/l)
Trichloromethane ($CHCl_3$)	0.02	2.50E-03	Not applicable

Discharge mechanism

Pipe diameter	0.85	m	Mean depth in the receiving water	2.87	m
Angle with shoreline	163	º	Discharge depth (from bottom)	1.00	m

Figura 42: Ficha resumen para caracterizar ID1 en el Estuario de Suances.

SUMMARY SHEET OF TOXICANT DISCHARGES

NAME	Industrial Discharge 2
CODE	ID2

Location

UMTX (ED50)	416217.0	Site name	Hinojedo
UTMY (ED50)	4805564.4	Holder	Theoretical Factory 2

Toxicant load

Flow	0.00472	m^3/s	Salinity	0.05	psu
			Temperature	15.2	ºC

Pollutant	Concentration (mg/l)	AA-EQS (mg/l)	MAC-EQS (mg/l)
Lead (Pb)	1.00	1.30E-03	1.40E-02

Discharge mechanism

Pipe diameter	0.10	m	Mean depth in the receiving water	6.28	m
Angle with shoreline	212	º	Discharge depth (from bottom)	1.00	m

Figura 43: Ficha resumen para caracterizar ID2 en el Estuario de Suances.

de: “Estudio de Recursos Hídricos de las Cuencas de la Vertiente Norte de Cantabria Periodo 1970-2010”, realizado por IH Cantabria para el Gobierno de Cantabria (Figura 44a). Este trabajo se basa en un modelo hidrológico agregado desarrollado para la evaluación de recurso hídricos superficiales en cuencas escasamente intrumentalizadas por García *et al.* (2008). El caudal de agua dulce, en condiciones naturales, varía aproximadamente desde 1 hasta 600 m^3/s, con caudales medios anuales en el rango de 7-24 m^3/s (García *et al.* 2008) (Figura 45a).

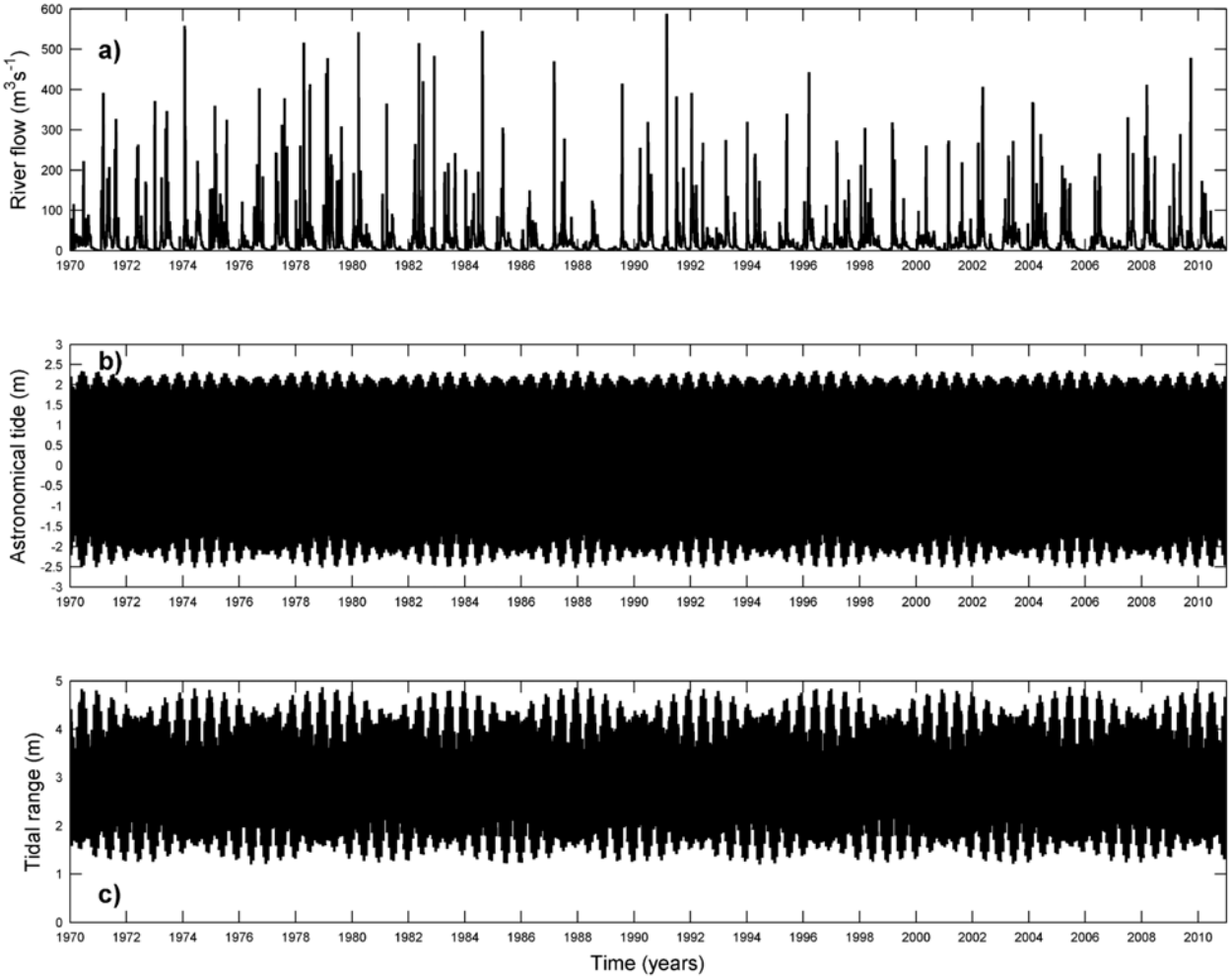

Figura 44: 40-años de series temporales de forzamientos desde 1970 hasta 2010 en el estuario de Suances. (a) Caudal del río, (b) marea astronómica y (c) carrera de marea astronómica.

Por otro lado, se seleccionó el modelo AG95.1 desarrollado por Andersen (1994) para obtener el nivel de la marea astronómica en el área de estudio desde 1970 hasta 2010 (Figura 44b). A partir de la serie de marea astronómica, se calculó el “período de carrera de marea astronómica” como la diferencia entre el valor máximo y el mínimo de la serie de la marea astronómica durante 24 h con el fin de calcular la “serie diaria de carrera de marea astronómica” (Figura 44c). El estuario de Suances presenta una señal de marea semidiurna con un ciclo típico de mareas vivas y muertas de aproximadamente 15 días. La carrera de marea varía aproximadamente entre 5 m durante mareas vivas equinocciales y 0.7 m cuando se producen mareas muertas solsticiales (Figura 45b).

Con respecto a las áreas protegidas, el estuario sólo presenta áreas de usos recreativos relacionados con aguas de baño y playas (Figura 46).

Por último, en la figura 47, se muestra la ficha resumen del estuario de Suances con la mencionada informa-

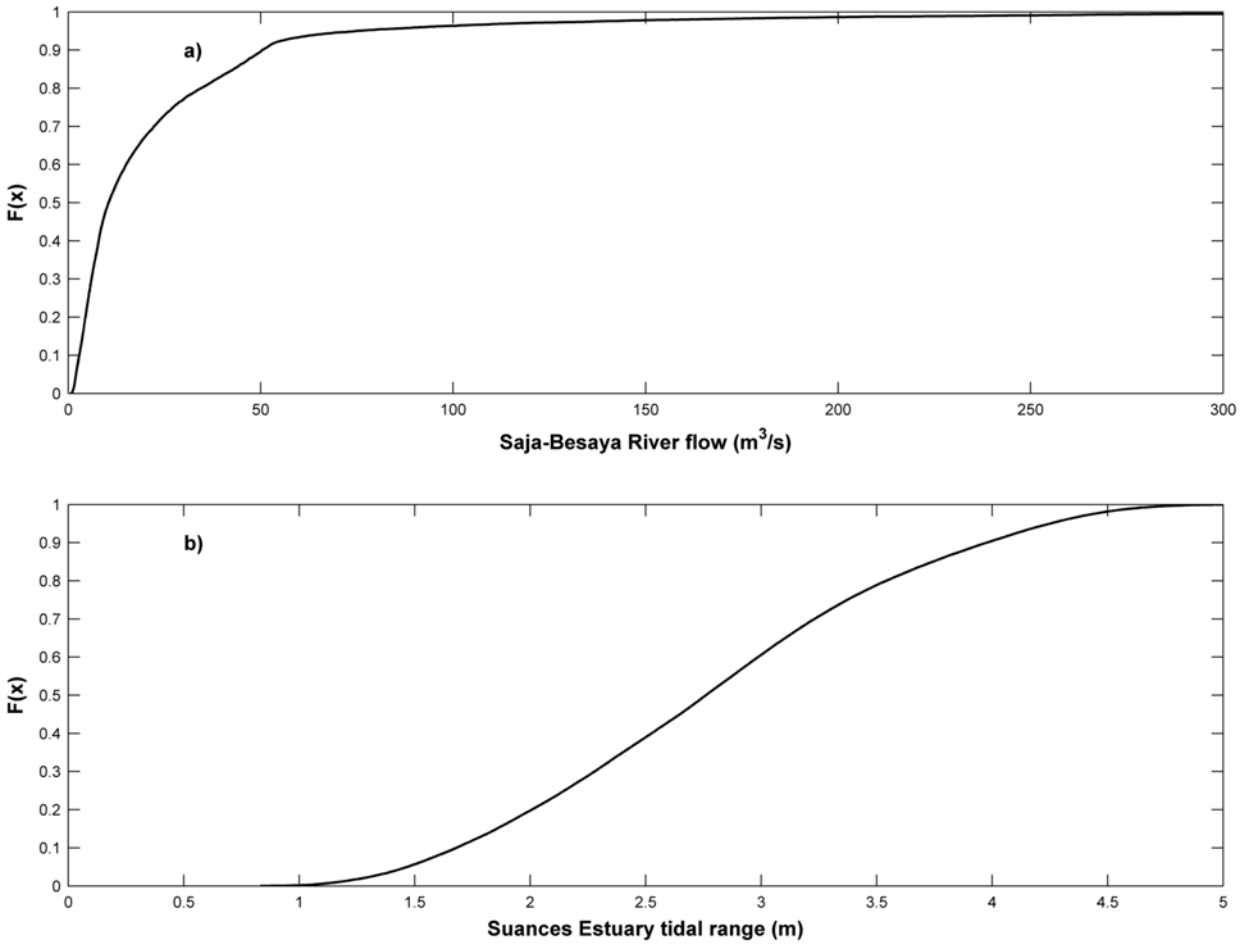

Figura 45: Función empírica de distribución acumulada del caudal fluvial (a) y de la carrera de marea (b) en el Estuario de Suances.

Figura 46: Localización de áreas protegidas (playas) en el Estuario de Suances.

ción.

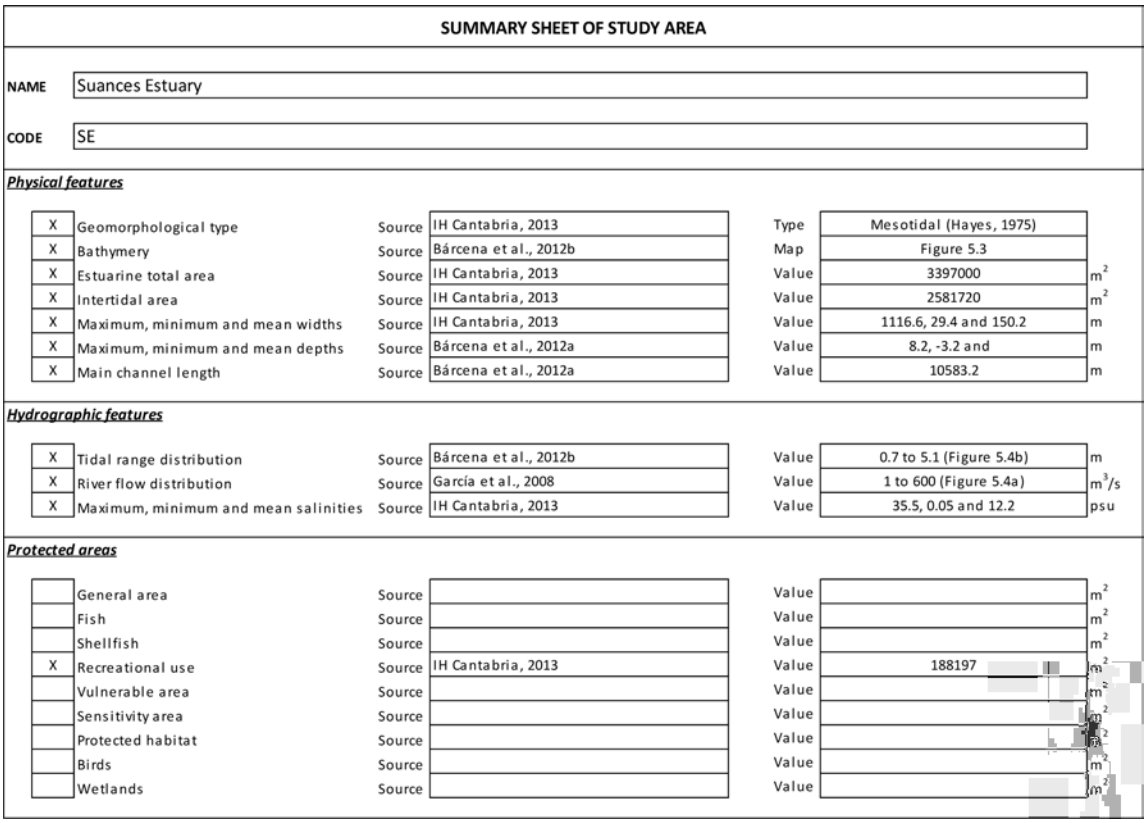

SUMMARY SHEET OF STUDY AREA

NAME	Suances Estuary					
CODE	SE					
Physical features						
X	Geomorphological type	Source	IH Cantabria, 2013	Type	Mesotidal (Hayes, 1975)	
X	Bathymery	Source	Bárcena et al., 2012b	Map	Figure 5.3	
X	Estuarine total area	Source	IH Cantabria, 2013	Value	3397000	m^2
X	Intertidal area	Source	IH Cantabria, 2013	Value	2581720	m^2
X	Maximum, minimum and mean widths	Source	IH Cantabria, 2013	Value	1116.6, 29.4 and 150.2	m
X	Maximum, minimum and mean depths	Source	Bárcena et al., 2012a	Value	8.2, -3.2 and	m
X	Main channel length	Source	Bárcena et al., 2012a	Value	10583.2	m
Hydrographic features						
X	Tidal range distribution	Source	Bárcena et al., 2012b	Value	0.7 to 5.1 (Figure 5.4b)	m
X	River flow distribution	Source	García et al., 2008	Value	1 to 600 (Figure 5.4a)	m^3/s
X	Maximum, minimum and mean salinities	Source	IH Cantabria, 2013	Value	35.5, 0.05 and 12.2	psu
Protected areas						
	General area	Source		Value		m^2
	Fish	Source		Value		m^2
	Shellfish	Source		Value		m^2
X	Recreational use	Source	IH Cantabria, 2013	Value	188197	m^2
	Vulnerable area	Source		Value		m^2
	Sensitivity area	Source		Value		m^2
	Protected habitat	Source		Value		m^2
	Birds	Source		Value		m^2
	Wetlands	Source		Value		m^2

Figura 47: Ficha resumen para caracterizar la información sobre el Estuario de Suances.

3.2. Paso 2. Relevancia de las descargas

3.2.1. Riesgo potencial

En este apartado, se identificaron los vertidos con riesgo de sobrepasar los límites fijados en las Directivas (EC 2008a, EU 2013) sobre normas de calidad ambiental, es decir, la AA-EQS y MAC-EQS.

1. ID1 e ID2 contienen una sustancia tóxica especificada en la Directiva EQS, Triclorometano ($CHCl_3$) y Plomo (Pb) respectivamente. Por lo tanto, existe un riesgo potencial de superar las EQSs.

2. Para ID1, la $[X_{med}]_{ID1}$=0.02 mg/l y la AA-EQS$_{CHCl3}$=2.5·10^{-3} mg/l $\Rightarrow$ $[X_{med}]_{ID1}$>AA-EQS$_{CHCl3}$. En el caso de ID2, la $[X_{med}]_{ID2}$=1.0 mg/l y la AA-EQS$_{Pb}$=1.3·10^{-3} mg/l $\Rightarrow$ $[X_{med}]_{ID2}$>AA-EQS$_{Pb}$. Por lo tanto, la concentración media de ambas sustancias en los efluentes ID1 e ID2 superan las AA-EQS.

3. Para ID1, la $[X_{max}]_{ID1}$=0.02 mg/l y la MAC-EQS$_{CHCl3}$=No aplicable $\Rightarrow$ No aplicable. En el caso de ID2, la $[X_{max}]_{ID2}$=1.0 mg/l y la MAC-EQS$_{Pb}$=1.4·10^{-2} mg/l $\Rightarrow$ $[X_{max}]_{ID2}$>MAC-EQS$_{Pb}$. Por lo tanto, la concentración máxima de Plomo en el efluente industrial ID2 supera la MAC-EQS.

Por todo ello, ambas descargas se clasificaron como vertidos con riesgo potencial.

3.2.2. Diagnóstico inicial

Primero, se determinó el caudal del río que no se excede durante el 10 % del tiempo (Q10) a partir de la distribución acumulada del caudal fluvial (Figura 45a), esto es, $Q10 = 3{,}6314 m^3/s$.

Segundo, se calculó el PC mediante la aplicación de la ecuación (3.1).

$$PC_{ID1} = \frac{[X_{med}]_{ID1} Q_{ID1}}{(Q_{river} + Q_{ID1})} = \frac{0{,}02 \cdot 0{,}83801}{(3{,}6314 + 0{,}83801)} = 0{,}003765 \tag{31}$$

$$PC_{ID2} = \frac{[X_{med}]_{ID2} Q_{ID2}}{(Q_{river} + Q_{ID2})} = \frac{1{,}0 \cdot 0{,}00472}{(3{,}6314 + 0{,}00472)} = 0{,}001298 \tag{32}$$

En tercer lugar, se estimó el RI del PC como un porcentaje de la AA-EQS por medio de la ecuación (3.2).

$$RI_{ID1} = \frac{PC_{ID1}}{AA_{CHCl3}} \cdot 100\,\% = \frac{0{,}003765}{2{,}5 \cdot 10^{-3}} \cdot 100\,\% = 150{,}60 \tag{33}$$

$$RI_{ID2} = \frac{PC_{ID2}}{AA_{Pb}} \cdot 100\,\% = \frac{0{,}001298}{1{,}3 \cdot 10^{-3}} \cdot 100\,\% = 99{,}84 \tag{34}$$

Por último, se comprobó el RI con la propuesta de aumento autorizado (PAI) dada en la tabla 3.2. La PAI para este río fue 4 de modo que **RI**$_{ID1}$**=150.60**$\gg$**PAI=4** y **RI**$_{ID2}$**=99.85**$\gg$**PAI=4**. En resumen, los dos vertidos de sustancias tóxicas se clasificaron como significativos por lo que es necesario abordar el Paso 3.

3.3. Paso 3. Cálculo simplificado (Caso peor de dilución)

3.3.1. Información adicional

La información se obtuvo de dos fuentes: una campaña de campo (CHN 1998) y la red de calidad del agua de la costa de Cantabria (IHCantabria 2012). En la figura 48, se muestra la ubicación de los datos de campo para ambas fuentes.

3.3.1.1. Campaña de campo hidrodinámica

La campaña se llevó a cabo en las dos últimas semanas de enero y la primera semana de febrero de 1998 y se centró en la recopilación de información sobre el comportamiento hidrodinámico de la ría. Los datos registrados en esta campaña de campo incluyen (ver figura 48):

- Mediciones del niveles de agua en dos puntos (TG1 y TG2) cada cinco minutos con un medidor de presión de marea (AANDERAA WLR-5).
- Mediciones de caudales instantáneos, temperaturas y salinidades en una sección, no influenciada por la marea, del río Saja-Besaya (FG1) cada dos horas con un medidor de flujo electromagnético (modelo FLOWMATE 2000) y una escala limnimétrica.
- Perfiles verticales de corrientes de velocidad instantáneas y direcciones en seis puntos (SS1 a SS6) medidos con un medidor de corriente portátil (BRAYSTORE 0008 MK3) en situaciones de mareas muertas entre el 24 y 25 de enero de 1998 y en situaciones de mareas vivas entre el 28 y 29 de enero de 1998. Para ambas situaciones, se efectuaron las medidas en pleamar, vaciante, bajamar y llenante.
- Perfiles verticales de salinidad y temperatura en seis puntos (SS1 a SS6) medidos con un dispositivo CTD en situaciones de mareas muertas entre el 24 y 25 de enero de 1998 y en situaciones de mareas

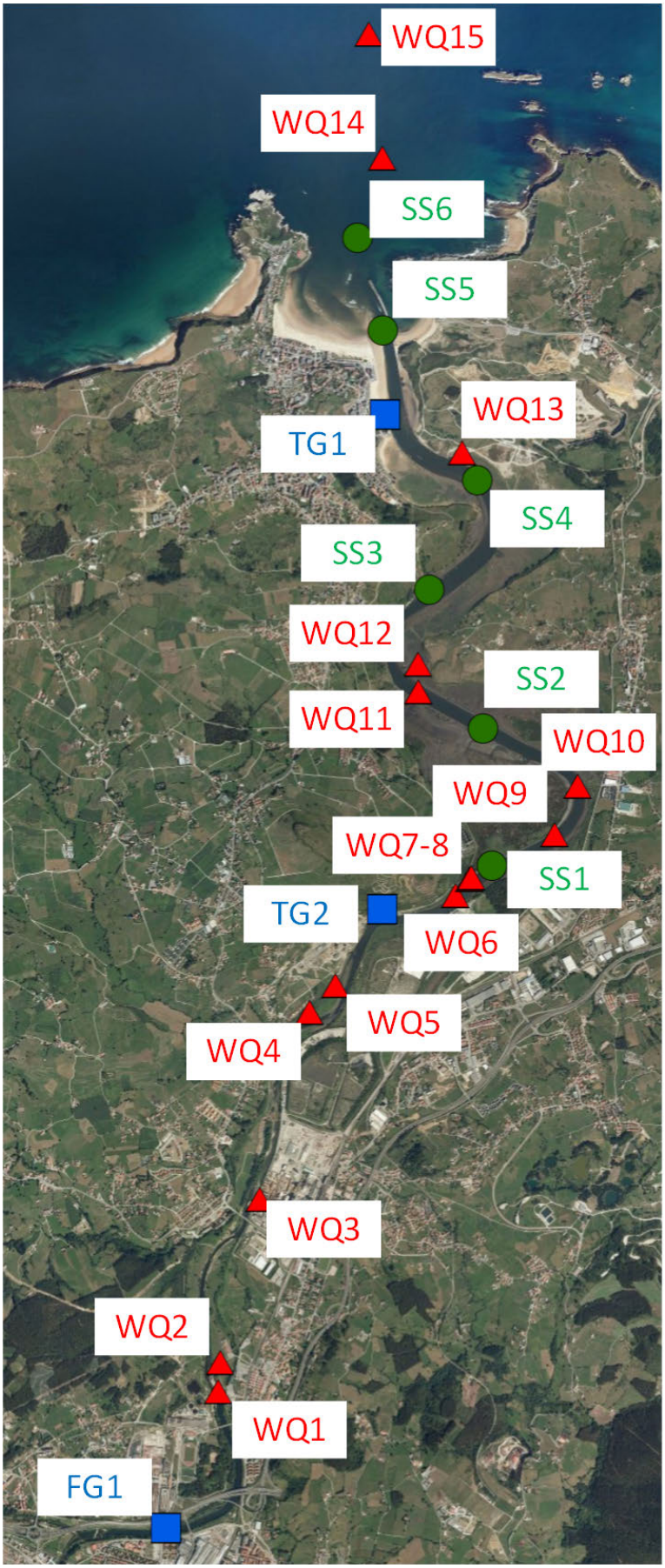

Figura 48: Localización de las estaciones de muestreo para la información adicional del Paso 3.

vivas entre el 28 y 29 de enero de 1998. De nuevo para ambas situaciones, se efectuaron las medidas en pleamar, vaciante, bajamar y llenante.

3.3.1.2. Red de Control de Calidad Litoral en Cantabria

En la Red de Calidad del Litoral de Cantabria, se realizan campañas de campo estacionales de agua, sedimentos y biota en los estuarios y la costa de Cantabria. Como se muestra en la figura 48, la red cuenta con 13 estaciones de muestreo (WQ1 a WQ13) situadas en SE y 2 más (WQ14 y WQ15) localizadas en la costa. Los datos seleccionados incluyeron mediciones de salinidad y temperaturas desde 2006 hasta 2013.

3.3.2. Hidrodinámica

Para modelar los niveles de agua, las corrientes y las salinidades por la acción de la marea y el río, se llevó a cabo la integración numérica de las ecuaciones de momentum, continuidad y transporte mediante la aplicación del modelo Delft3D-FLOW para el área de estudio.

3.3.2.1. Configuración del modelo

La malla tridimensional que cubre el estuario y su zona costera adyacente, se representó horizontalmente utilizando una discretización curvilínea (Figura 49). Dicha malla consta de en 93×800 celdas en las direcciones M y N respectivamente. La resolución espacial de las celdas varía entre 47 y 235 m en la zona costera adyacente y entre 4.3 y 30 m en el estuario. En cuanto a la discretización vertical, la malla se compone de 10 capas σ espaciadas igualmente a lo largo de la columna de agua.

En la figura 50, se muestra la batimetría utilizada para las simulaciones numéricas con un zoom de las áreas externas e internas del SE. Además, cabe resaltar que la alta resolución de la malla y batimetría permite la definición completa de los diques que bordean la canal principal (elipse roja).

En la figura 51, se muestran las condiciones de contorno e iniciales utilizadas. Los contornos cerrados se definen por la línea de costa, la batimetría y la superficie libre donde el flujo a través del contorno fue cero. El flujo difusivo vertical a través de la superficie libre y el fondo también se ajustó a cero excepto para el flujo de calor a través de la superficie libre. Por último, no se consideró la influencia de las tensiones tangenciales laterales (condición de libre deslizamiento).

En cuanto a los contornos abiertos, se definen cuatro contornos (superior, inferior y dos laterales):

- La condición de contorno superior se generó por medio de la base de datos Grenoble (Andersen 1994). Debido a que la variación vertical y temporal de la salinidad no fue significativa en SS6 durante el periodo de calibración, se estableció que el contorno fuera un perfil constante con una salinidad igual a la media de todas las mediciones, es decir, 35.6623 psu. En el caso de la temperatura del mar, la variación temporal fue significativa mientras que la vertical no lo fue en SS6. Por ello, se estableció la temperatura del mar como una serie temporal con perfil constante.

- La condición de contorno inferior se generó mediante la imposición de una condición de caudal con las mediciones disponibles para el río Saja-Besaya durante el periodo de calibración y validación (CHN 1998). Debido a que la variación vertical y temporal de la salinidad no fue significativa, se estableció un valor constante coincidente con la media de todos los datos disponibles, es decir, 0.286 psu. En el caso de la temperatura del río, la variación temporal fue significativa por lo que se estableció como una serie temporal con perfil constante.

- Las condiciones laterales se modelaron mediante la imposición de una condición de velocidad nula y los mismos valores de la condición superior en el caso de salinidad y temperatura.

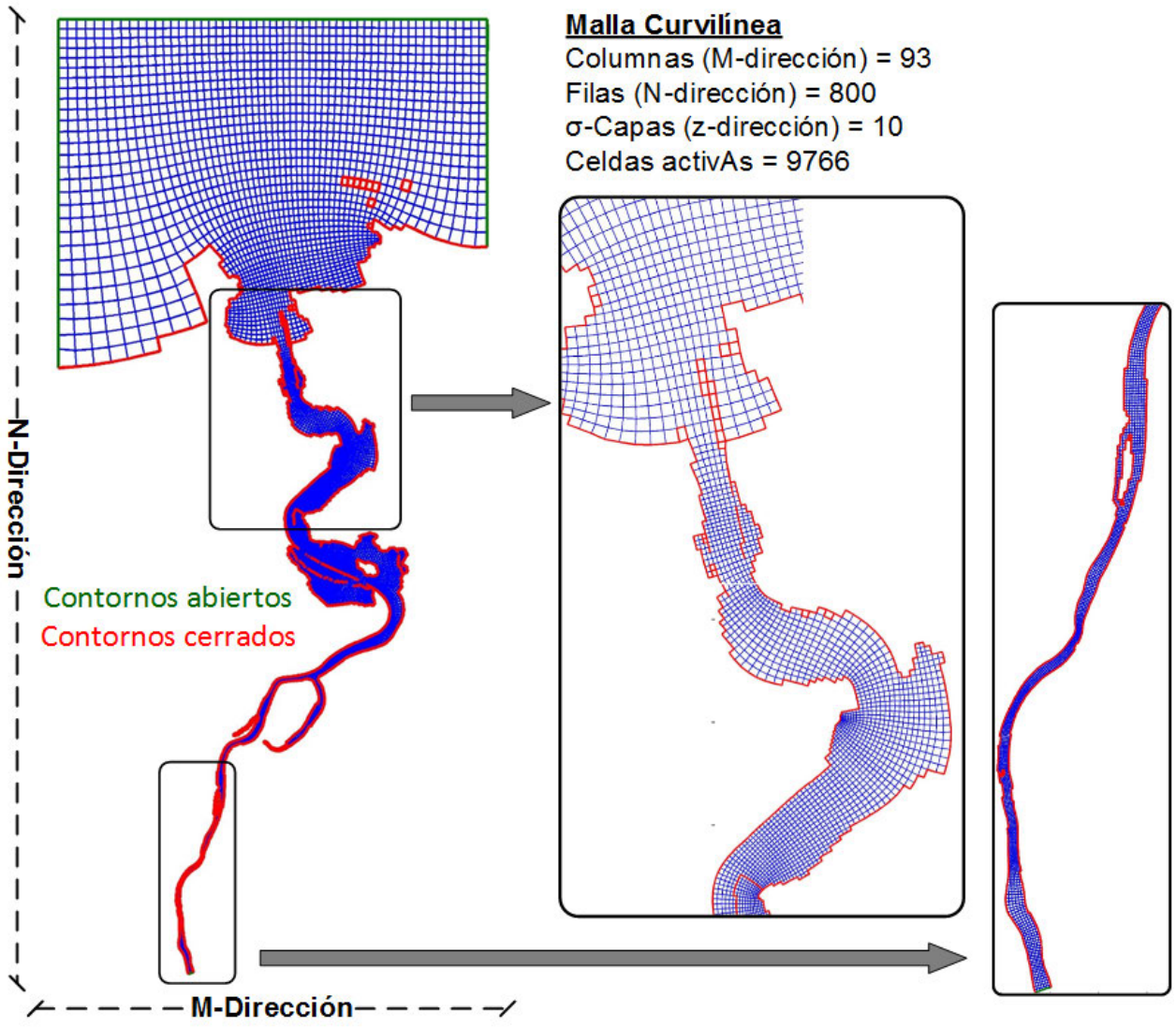

Figura 49: Malla para simulaciones numéricas y detalle del interior en el Estuario de Suances.

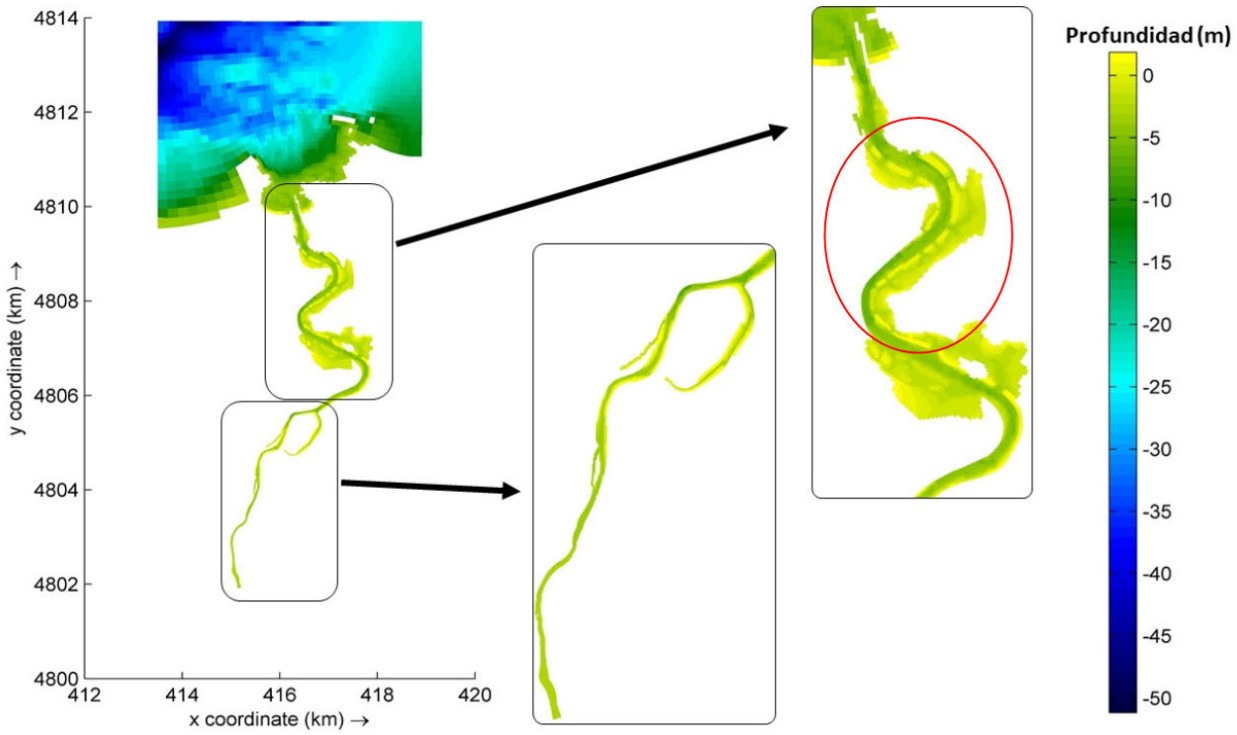

Figura 50: Batimetría utilizada en la malla con un zoom de las áreas externas e internas del Estuario de Suances.

Las condiciones iniciales se especificaron como mapas con valores constantes donde el nivel del agua fue de 1.225 m, la temperatura de 11 ^{o}C y la salinidad de 29 psu.

La combinación de parámetros físicos y numéricos generó multitud de casos de simulación para la calibración. La configuración final que se adoptó para el modelo fue el caso que mejor ajuste presentó entre los resultados del modelo y los datos medidos en el área de estudio. En este estudio, la calibración óptima fue la combinación de parámetros mostrada en la tabla 4.

Esta combinación de parámetros del modelo se utilizó para realizar las simulaciones hidrodinámicas requeridas por la metodología desarrollada en esta Tesis. Además, en la tabla 5, se muestra el valor de los errores promediados en profundidad (capa de superficie, intermedia y de fondo) en TG1, TG2 SS1, SS3 y SS5.

Como se puede observar en la tabla 5, el modelo calibrado muestra un nivel aceptable de rendimiento en

Parámetros físicos	**Valores calibrados**
Viscosidad de remolino horizontal	k=0.10
Difusividad de remolino horizontal	σ_t=0.7
Viscosidad de remolino vertical	$k-\varepsilon$
Difusividad de remolino vertical	σ_t=0.7
Fricción con el fondo	Iglesias & Carballo (2010)
Fricción en los laterales	Libre deslizamiento
Parámetros numéricos	**Valores calibrados**
Esquema numérico	Cyclic
Paso de tiempo	$\Delta t = 0{,}1$ min
Filtros numéricos	Mezcla vertical artificial
Inundación secado	Profundidad umbral$\leq$0.1 m

Tabla 4: Parámetros óptimos de calibración del modelo hidrodinámico para el Estuario de Suances.

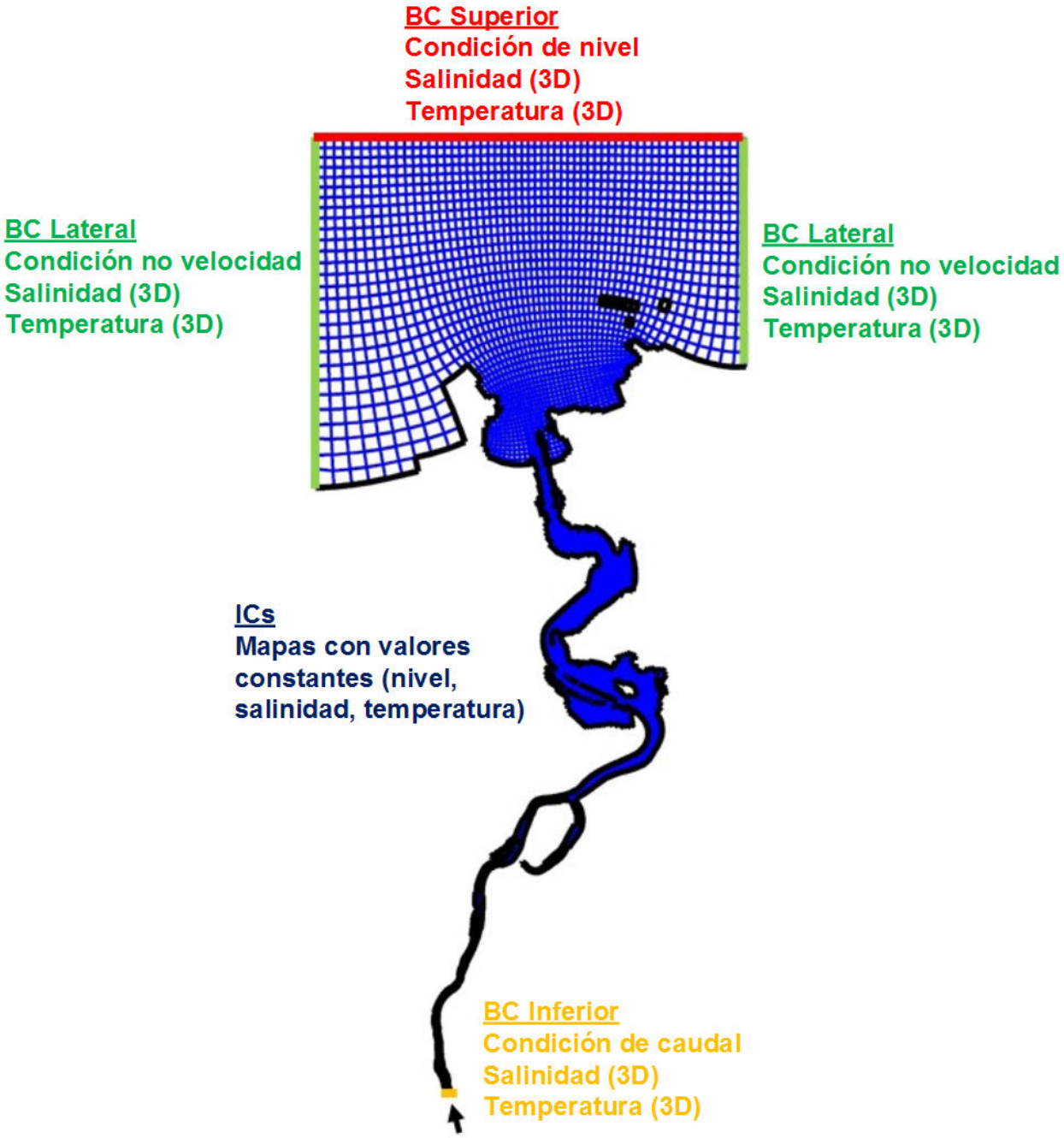

Figura 51: Vista esquemática de las condiciones de contorno e iniciales impuestas durante las simulaciones hidrodinámicas.

Variable	Estación	BIAS	CE	Rendimiento
Nivel de agua	TG1	0.015 m	0.994	Aceptable (excelente)
	TG2	0.077 m	0.987	Aceptable (excelente)
U Velocidad	SS1	-0.024 m/s	0.368	Aceptable (pobre)
	SS3	-0.058 m/s	0.566	Aceptable (conveniente)
	SS5	0.093 m/s	0.125	Aceptable (pobre)
V Velocidad	SS1	-0.073 m/s	0.099	Aceptable (pobre)
	SS3	-0.073 m/s	0.614	Aceptable (conveniente)
	SS5	-0.061 m/s	0.502	Aceptable (conveniente)
Salinidad	SS1	-1.269 psu	0.392	Aceptable (pobre)
	SS3	1.148 psu	0.476	Aceptable (pobre)
	SS5	1.382 psu	0.642	Aceptable (conveniente)

Tabla 5: Errores promediados en profundidad del caso calibración óptimo en el Estuario de Suances.

todas las estaciones y variables. Los niveles de agua se reprodujeron de manera excelente mientras que las velocidades y salinidades estuvieron entre pobre y convenientemente reproducidas.

3.3.2.2. Modelado hidrodinámico del caso peor

Siguiendo la metodología y considerando la ecdf de la marea astronómica y el caudal del río (ver en la figura 45), se asumieron condiciones fijas en el "caso peor de dilución":

- La amplitud de marea que no se excede durante el 10 % del tiempo (A10) es de 0.925 m.
- El caudal del río que no se excede durante el 10 % del tiempo, teniendo en cuenta el promedio de 7 días consecutivos (7Q10) es de 3.631m^3/s.

Como condiciones de contorno e iniciales se emplearon las mostradas en la figura 51.Los contornos cerrados fueron los mismos que los especificados para el proceso de calibración. En cuanto a los abiertos, se definieron cuatro contornos (superior, inferior y dos laterales):

- La condición de contorno superior fue una marea astronómica forzada por una componente M2 con una amplitud igual a A10. Debido a que la variación vertical y temporal de la salinidad y temperatura no fueron significativas en WQ15 a lo largo de los años, se estableció una condición constante siendo el promedio de todas las mediciones, es decir, 35.27 psu y 15.96 ^{o}C.
- La condición de contorno inferior fue el caudal del río igual a 7Q10. Debido a que la variación vertical y temporal de la salinidad y temperatura no fueron significativas en WQ1 a lo largo de los años, se estableció que el contorno fuera constante coicidiendo con el promedio de todos los datos disponibles, es decir, 0.238 psu y 15 ^{o}C.
- Las condiciones de contorno laterales fueron modeladas mediante la imposición de una condición de velocidad nula mientras que la salinidad y la temperatura se especificaron con los mismos valores del contorno superior.

Para iniciar la simulación del cálculo simplificado, se especificó un nivel de agua de 0 m, una temperatura de 15.5 °C y una salinidad de 29 psu en todas las celdas de la malla.

Este escenario de modelado se simuló hasta llegar a una respuesta "cuasi-estacionaria" para la hidrodinámica con el fin de evitar el efecto de las condiciones iniciales en la simulación numérica. Para el cálculo del tiempo de respuesta "cuasi-estacionaria" para la hidrodinámica, se seleccionaron dos puntos de control situados en

ambos puntos de descarga (ID1 e ID2) ya que se asume que la dilución inicial puede estimarse cuando se alcanza dicha respuesta en torno a los vertidos industriales.

En las figuras 52 y 53, se ilustra la evolución de niveles de agua (a), velocidades (b), salinidades (c) y temperaturas (d) en ID1 e ID2 respectivamente. En dichas figuras, cabe indicar que la respuesta "cuasi-estacionaria" para la hidrodinámica se resalta con una línea gris discontinua y el período guardado de resultados hidrodinámicos entre líneas rojas.

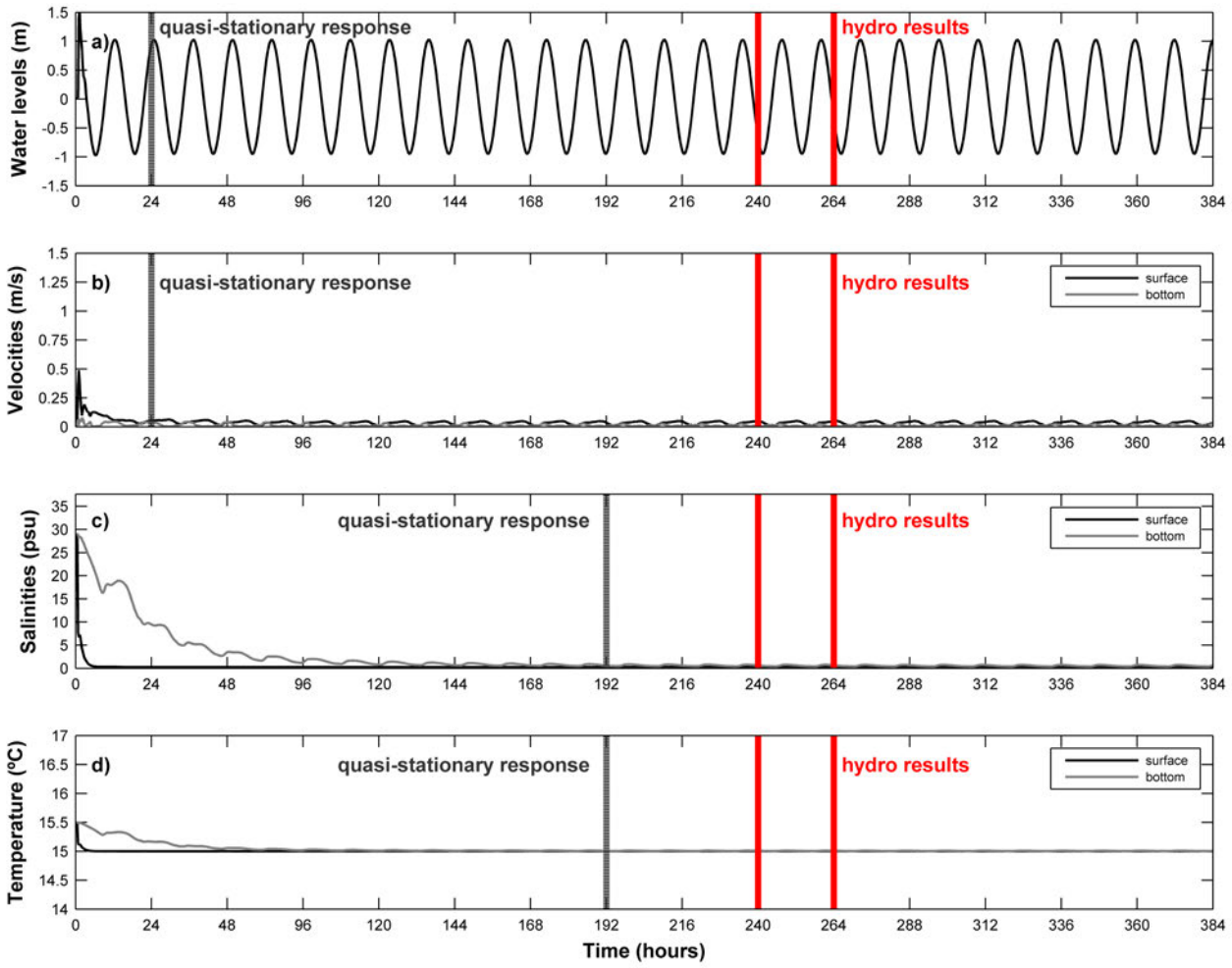

Figura 52: Evolución de niveles de agua (a), velocidades (b), salinidades (c) y temperaturas (d) en la superficie y el fondo para el punto descarga ID1. Además, el tiempo de la respuesta "cuasi-estacionaria" para cada variable se resalta con una línea gris discontinua y el período guardado de resultados hidrodinámicos entre líneas rojas.

De acuerdo con ambas figuras, la escala de tiempo más larga correspondió a la salinidad y la temperatura para ID2 y fue de 216 horas (9 días). Una vez que se llegó a esta situación en ID1 e ID2, se almacenó horariamente un día de resultados del modelo hidrodinámico (24 datos) en cada celda de la malla entre las horas 240-264 (ver líneas rojas en las figuras 52 and 53).

3.3.3. Dilución primaria o inicial (Campo cercano)

El comportamiento del elfuente descargado depende de Q_{eff}, ϕ, d_{eff}, ρ_{eff}, ρ_{env}, H y u_{env}. Las cuatro primeras variables están asociadas con el mecanismo de descarga siendo independientes para cada descarga (véase la tabla 6).

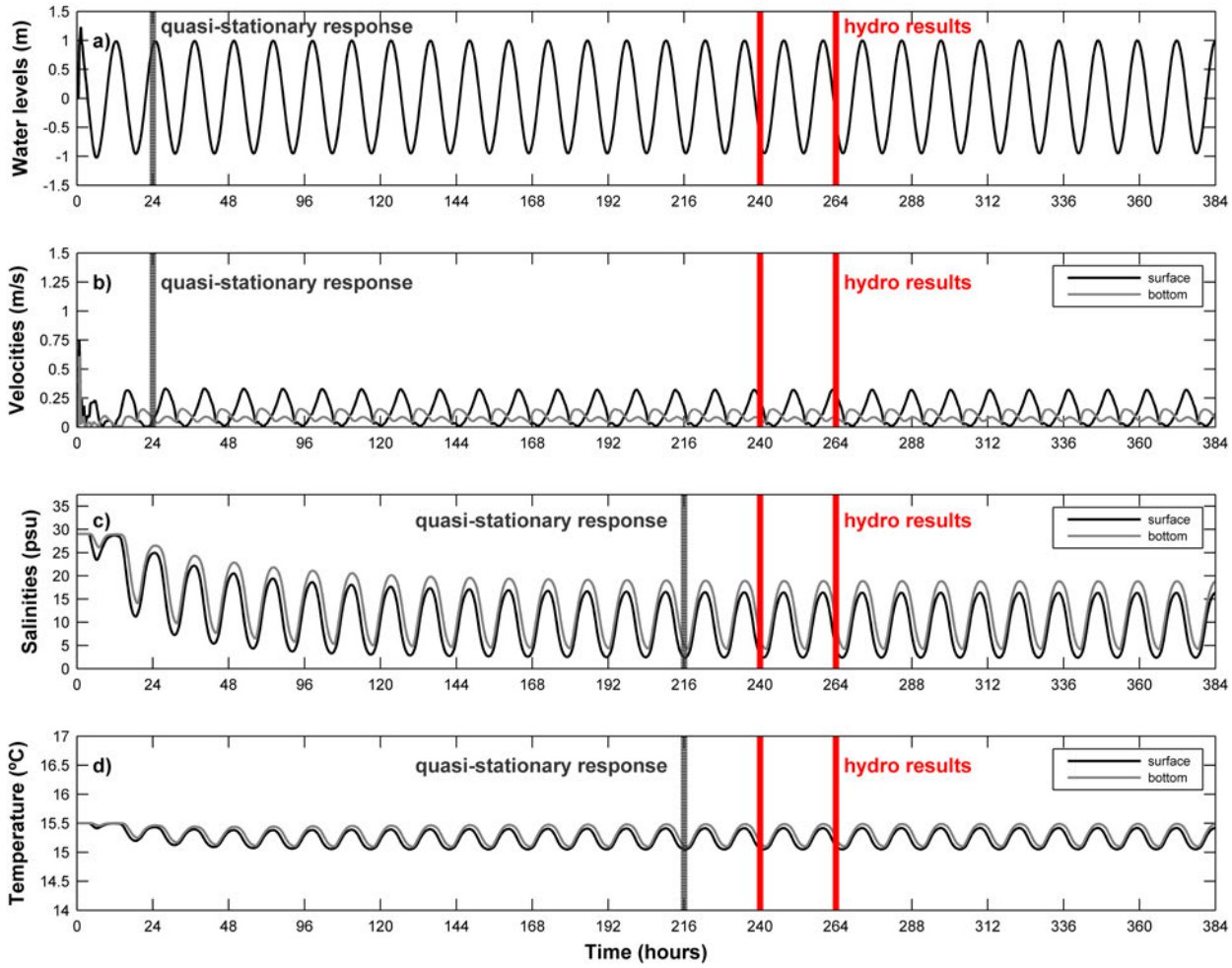

Figura 53: Evolución de niveles de agua (a), velocidades (b), salinidades (c) y temperaturas (d) en la superficie y el fondo para el punto descarga ID2. Además, el tiempo de la respuesta "cuasi-estacionaria" para cada variable se resalta con una línea gris discontinua y el período guardado de resultados hidrodinámicos entre líneas rojas.

Descarga industrial	Q_{eff} (m^3/s)	ϕ (m)	d_{eff} (m)	S_{eff} (psu)	$T_{eff})$ (°C)	ρ_{eff} (kg/m^3)
ID1	0.83801	0.85	1	0.05	15.2	999.11
ID2	0.00472	0.10	1	0.05	15.2	999.11

Tabla 6: Variables independientes del mecanismo de descarga para ID1 e ID2.

El resto de variables se relacionan con las condiciones ambientales que dependen de cambios hidrodinámicos y la ubicación del vertido. Los cálculos de dilución primaria se realizaron para cada descarga significativa (ID1 e ID2) empleando el modelo numérico JETLAG y teniendo en cuenta que:

- Todas las sustancias se consideran trazadores conservativos.
- Las variables ambientales (H, ρ_{env} and u_{env}) se extraen horariamente en cada ubicación de vertido a partir de los resultados de Delft3D-FLOW.
- Se asume un acople pasivo.

En las figuras 54 y 55, se muestra la profundidad total de agua (a), la magnitud de la velocidad ambiental (b), la dirección de la velocidad ambiental (c) y la densidad ambiental (d) para la capa superficial (línea azul) y la capa de fondo (línea verde) en ID1 durante el "caso peor de dilución". Además, en ambas figuras se ilustra la dilución inicial (e) del efluente (línea negra) y la concentración del efluente (f) al final del campo cercano (línea negra). Finalmente, en la figura 54 se indica la AA-EQS (línea magenta) del cloroformo ($CHCl_3$) mientras que en la figura 55 se indica la AA-EQS (línea magenta) y la MAC-EQS (línea roja) del plomo (Pb).

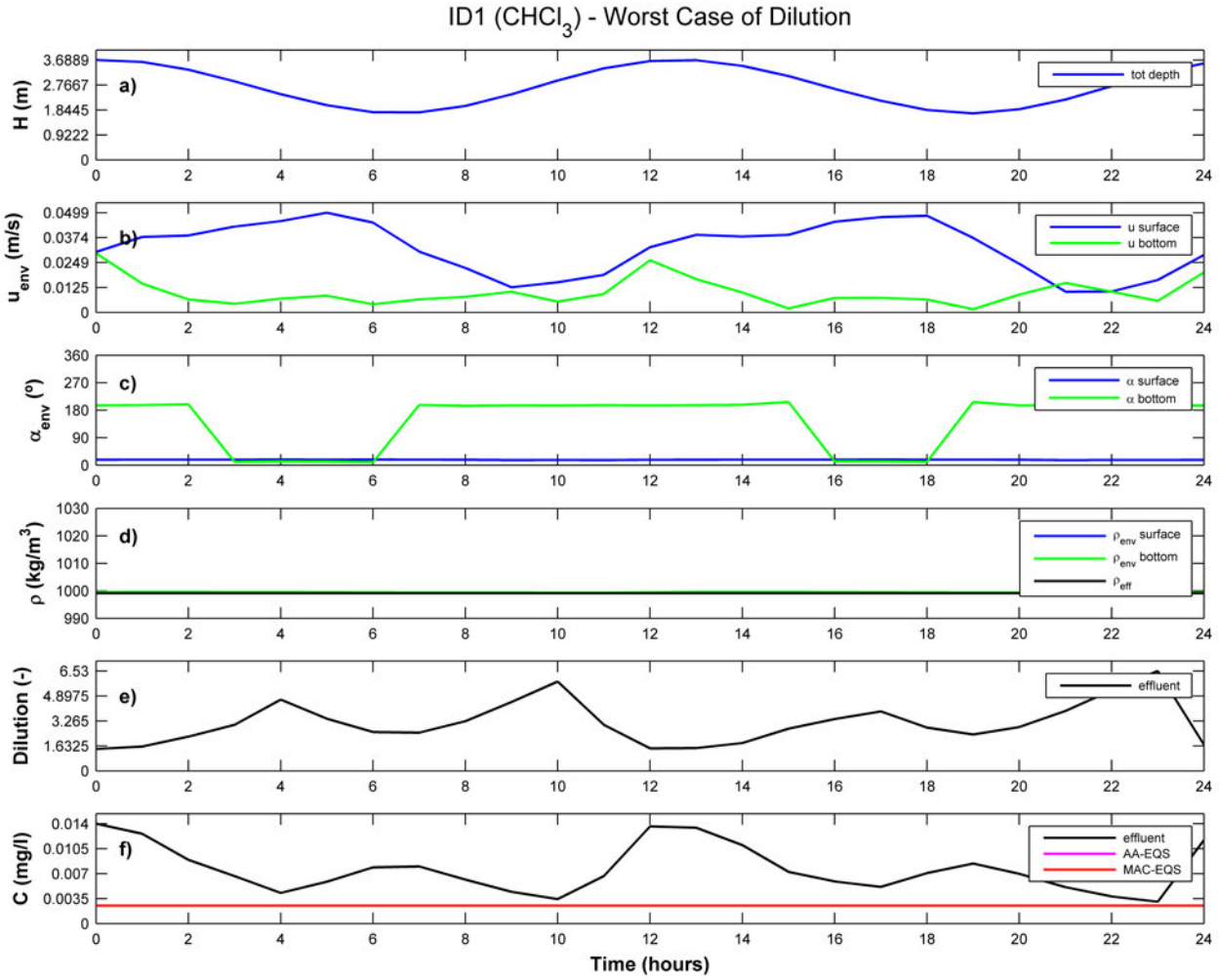

Figura 54: Evolución de la profundidad total de agua (a), la magnitud de la velocidad ambiental (b), la dirección de la velocidad ambiental (c) y la densidad ambiental (d) para la capa superficial (línea azul) y la capa de fondo (línea verde), la dilución inicial (e) del efluente (línea negra) y la concentración del efluente (f) al final del campo cercano (línea negra) en ID1 durante el "caso peor de dilución". Además se indica la AA-EQS (línea magenta) del cloroformo (f).

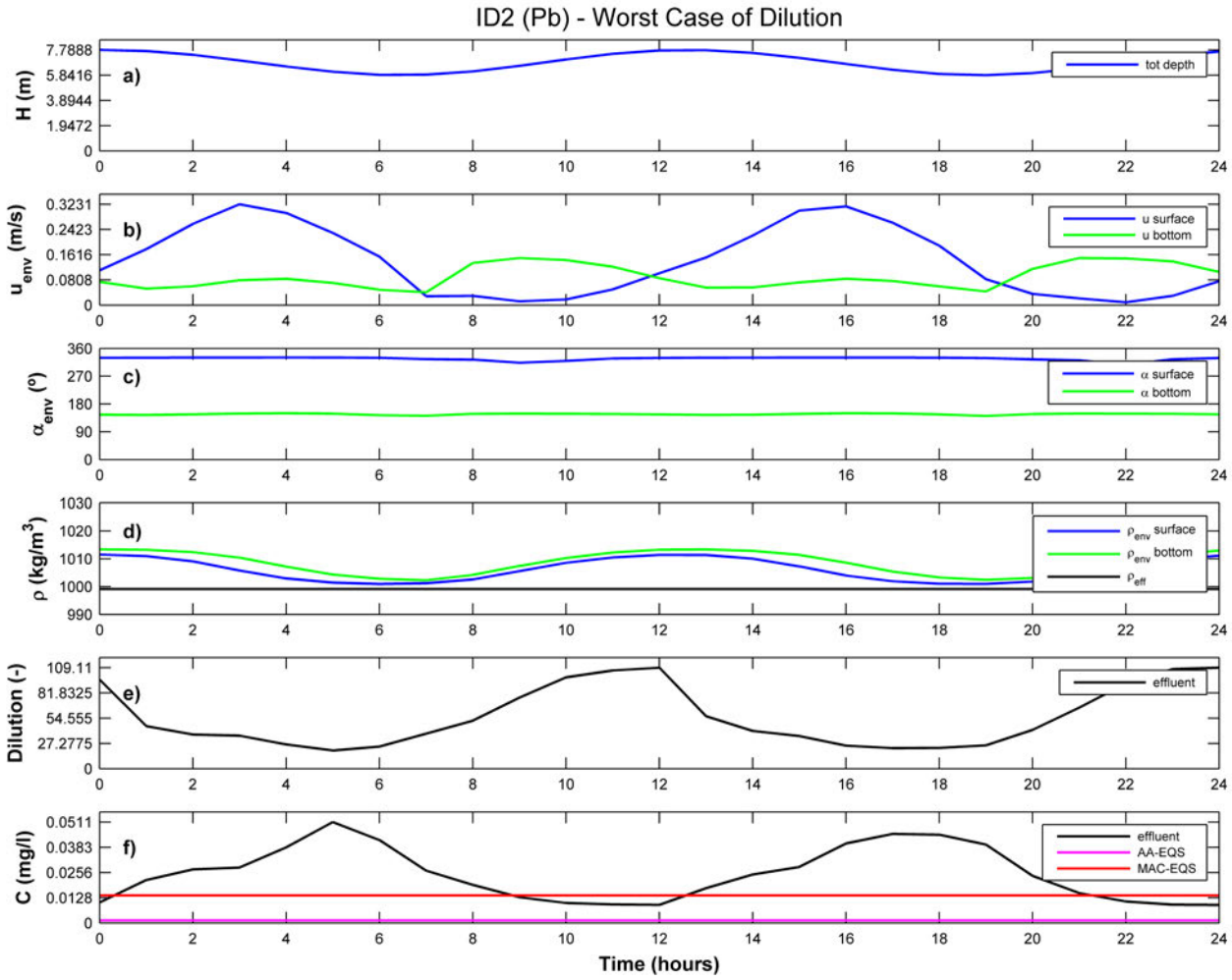

Figura 55: Evolución de la profundidad total de agua (a), la magnitud de la velocidad ambiental (b), la dirección de la velocidad ambiental (c) y la densidad ambiental (d) para la capa superficial (línea azul) y la capa de fondo (línea verde), la dilución inicial (e) del efluente (línea negra) y la concentración del efluente (f) al final del campo cercano (línea negra) en ID2 durante el "caso peor de dilución". Además se indica la AA-EQS (línea magenta) y la MAC-EQS (línea roja) del plomo (f).

La dilución en ID1 varió entre 1.63 y 6.53 y la dilución en ID2 entre 109.11 y 27.27 debido a los cambios en la profundidad total, la velocidad ambiental y la densidad ambiental. En cuanto a la concentración en ID1, la AA-EQS se superó durante todo el tiempo en el "caso peor de dilución" mientras que, en ID2, la AA-EQS se superó durante todo el tiempo en el "caso peor de dilución" y la MAC-EQS la mayoría del tiempo (Figuras 54 y 55).

3.3.4. Acople de la dilución primaria a la secundaria (Campo intermedio)

En este apartado, se llevó a cabo el acoplamiento entre el modelo de campo cercano (JETLAG) y el modelo de campo lejano (D-Water Quality). El método se describió gráficamente en las figuras 18 y 19 en perfil y planta, respectivamente.

Las figuras 56 y 57 presentan el porcentaje de tiempo que ID1 e ID2 estuvieron en diferentes celdas de la malla (panel izquierdo) y capas verticales (panel derecho) predichos por JETLAG durante el proceso de acoplamiento. En estas localizaciones, se introdujeron ID1 e ID2 como un término fuente de caudal y concentración diluida en el modelo de campo lejano.

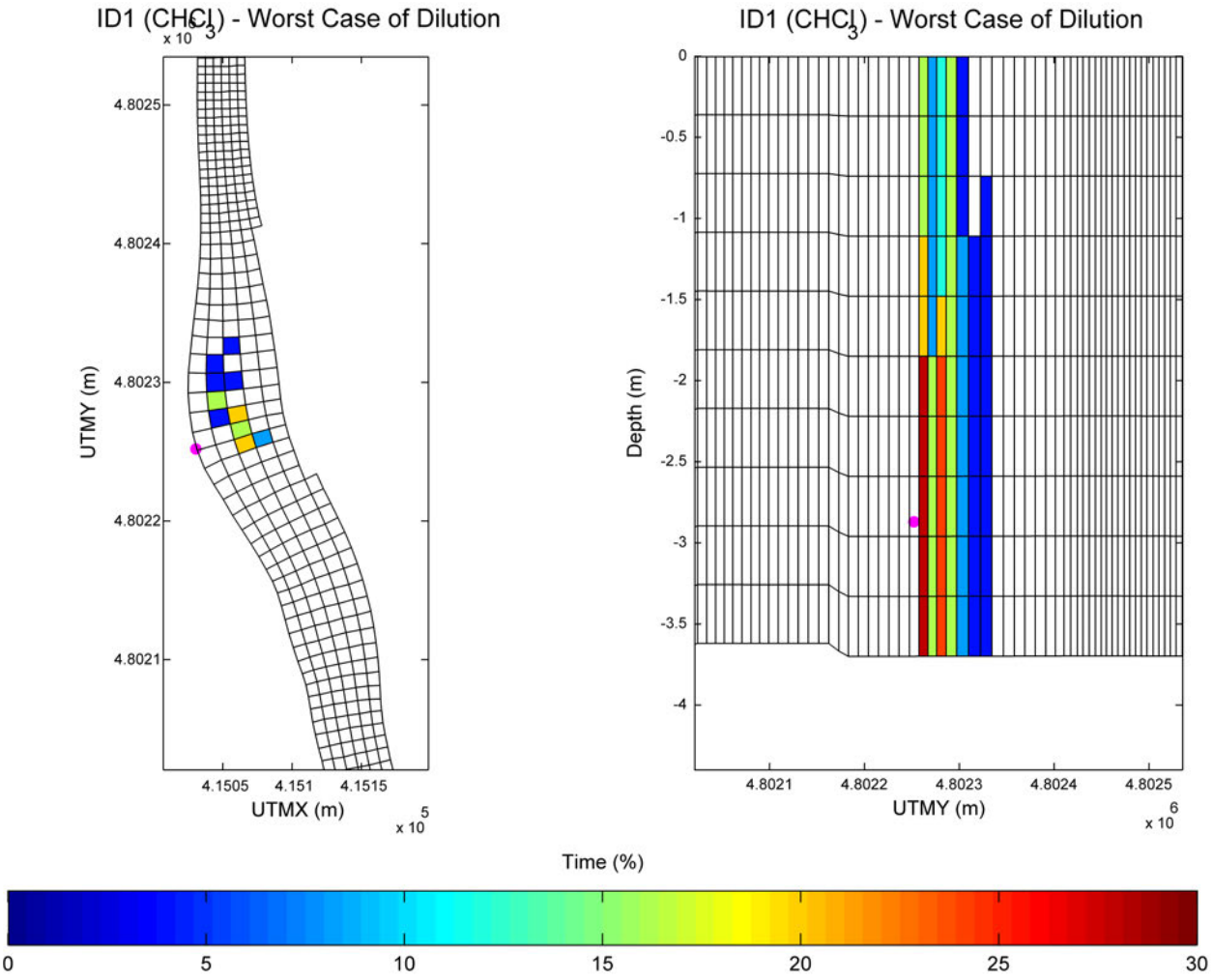

Figura 56: Vista esquemática de la distribución del tiempo de las celdas horizontales de la malla (panel izquierdo) y las capas verticales (panel derecho) cubiertos ID1 durante el acoplamiento entre la dilución primaria y secundaria en el cálculo simplificado.

Como se muestra en la figura 56, el efluente descargado por ID1 al final del campo cercano alcanzó varias

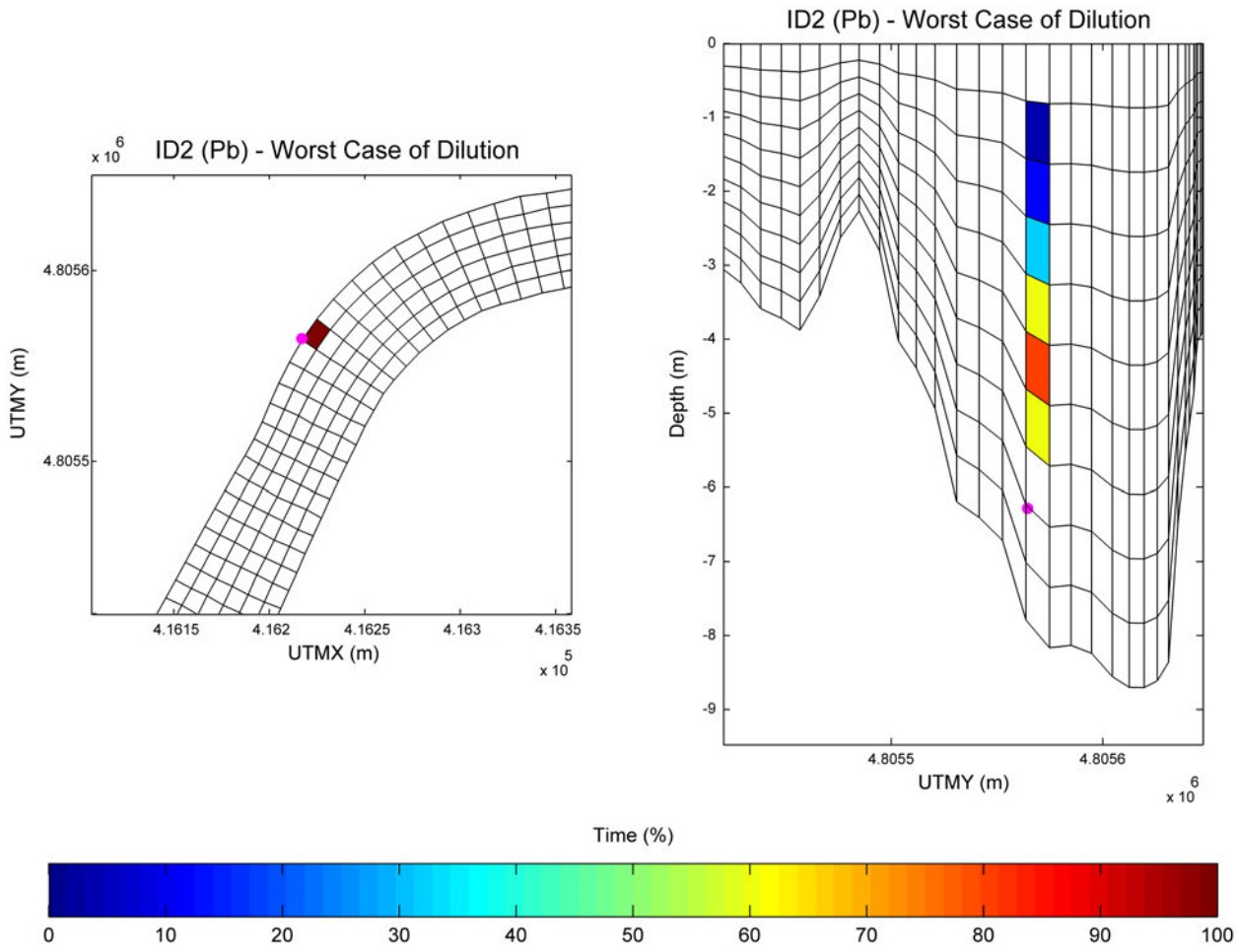

Figura 57: Vista esquemática de la distribución del tiempo de las celdas horizontales de la malla (panel izquierdo) y las capas verticales (panel derecho) cubiertos por ID2 durante el acoplamiento entre la dilución primaria y secundaria en el cálculo simplificado.

Parámetros físicos	**Valor Calibrado**
Todos los parámetros	Calibración hidrodinámica
Parámetros numéricos	**Valor Calibrado**
Esquema numérico	Esquema 15
Paso de tiempo	$\Delta t = 1$ min.
Filtros numéricos	No dispersión en intermareal No dispersión en OBs No valores negativos

Tabla 7: Parámetros óptimos de calibración del modelo de campo lejano (enfoque conservativo) para el Estuario de Suances.

celdas horizontales aguas abajo del punto de descarga, debido a la cercanía con el río y la magnitud del impulso inducido por ID1. En la dirección vertical, ID1 se ubicó la mayor parte del tiempo entre las capas 5 y 10. El resto del tiempo ID1 se mezcló completamente en la columna de agua.

Como se puede observar en la figura 56, ID2 siempre estuvo en la celda de la malla donde se realiza la descarga del efluente debido a que la flotabilidad y el caudal fueron relativamente pequeños. Respecto a la distribución vertical, ID2 estuvo la mayor parte del tiempo entre las capas 5 y 7, es decir, entre 3 y 5.5 m de profundidad indicando que la pluma ID2 se atrapa.

3.3.5. Dilución secundaria o ambiental (Campo lejano)

3.3.5.1. Configuración del modelo

La discretización del modelo fue la misma empleada para el modelo hidrodinámico. Como condiciones de contorno e iniciales se utilizaron mapas de los trazadores conservativos iguales a cero. Debido a que las sustancias tóxicas se consideraron conservativas en el Paso 3, los parámetros físicos para el modelo de transporte fueron los mismos que los calibrados en el modelo hidrodinámico y, en consecuencia, no fue necesaria llevar a cabo la calibración. Por ello, la calibración óptima fue la combinación de parámetros que se muestran en la tabla 7.

3.3.5.2. Modelado del transporte del caso peor

Con el fin de simular el transporte del "caso peor de dilución" con D-Water Quality, se utilizaron la simulación anterior del modelo hidrodinámico y los datos de dilución iniciales del acoplamiento. Como condiciones de contorno e iniciales se utilizaron las mismas que para la calibración del modelo de transporte.

Con el fin de encontrar la escala de tiempo máxima de la respuesta "cuasi-estacionaria" para el transporte, se realizó un análisis de sensibilidad con cuatro puntos diferentes a lo largo del dominio del modelo (WQ3, SS1, SS3 y SS5; véase la figura 48). Dicha escala de tiempo indica la duración mínima de una simulación de campo lejano para asegurar que los resultados sean fiables.

En las figuras 58 y 59, se muestra la inicialización, el estado "cuasi-estacionario" y los resultados del modelo de campo lejano para la evolución de la concentración de ID1 e ID2 en la capa de superficie (línea negra) y la capa de fondo (línea gris) para WQ3 (a), SS1 (b), SS3 (c) y SS5 (d), respectivamente.

De acuerdo con ambas figuras, la escala de tiempo mayor para alcanzar la respuesta "cuasi-estacionaria" se encontró en SS5 (d) para ID1 e ID2 siendo de 528 horas (22 días). Una vez que se llega a esta situación en ID1 e ID2, se almacenó horariamente un día de resultados del modelo de campo lejano (24 datos) en cada celda de la malla entre las horas 552-576 (ver líneas rojas en las figuras 58 y 59).

3.3.5.3. Delimitación de las zonas de mezcla

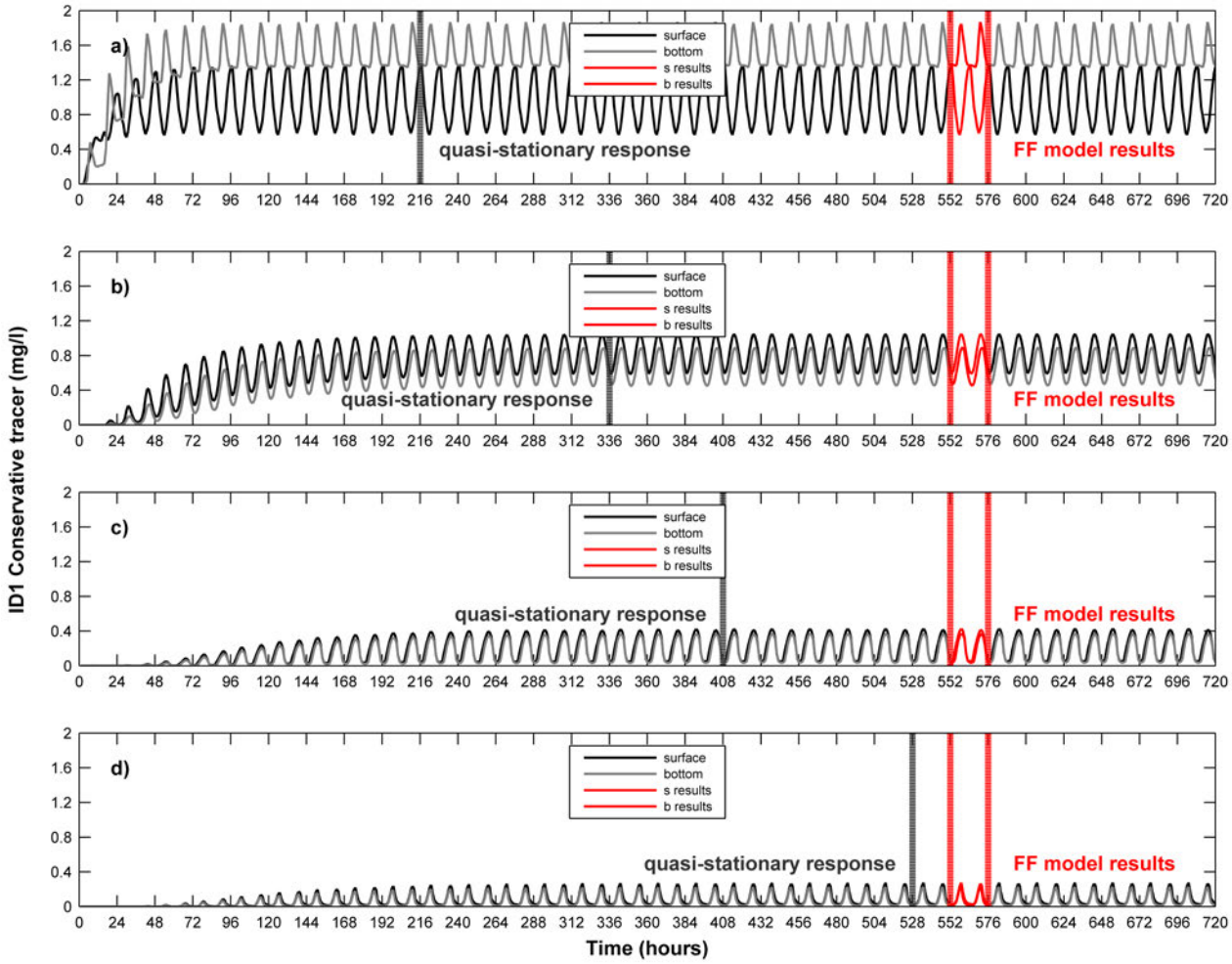

Figura 58: Evolución de la concentración ID1 en la capa superficial (línea negra) y la capa de fondo (línea gris), escala de tiempo de la respuesta "cuasi-estacionaria" y período registrado (línea roja) para el transporte del "caso peor de dilución" para WQ3 (a), SS1 (b), SS3 (c) y SS5 (d).

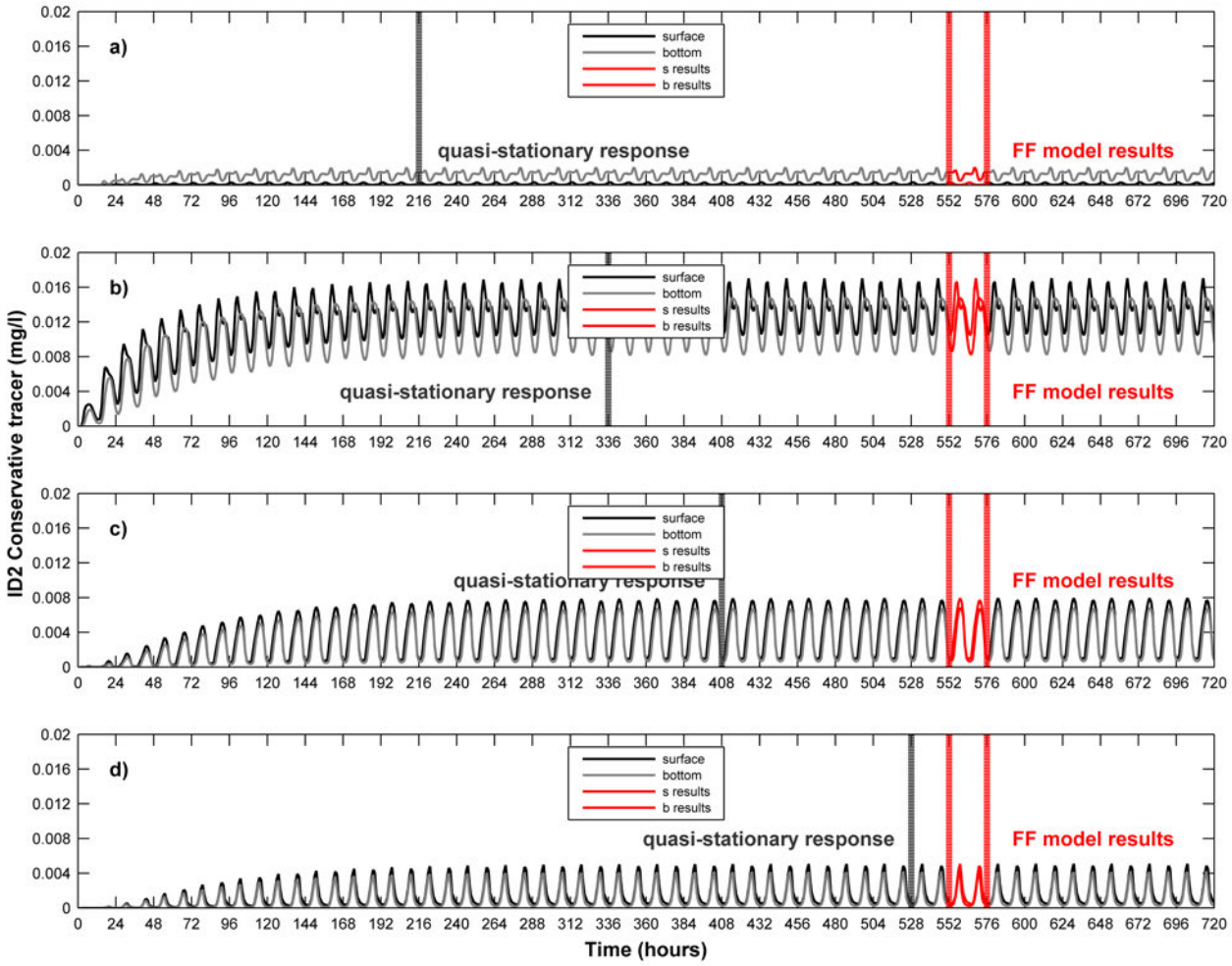

Figura 59: Evolución de la concentración ID2 en la capa superficial (línea negra) y la capa de fondo (línea gris), escala de tiempo de la respuesta "cuasi-estacionaria" y período registrado (línea roja) para el transporte del "caso peor de dilución" para WQ3 (a), SS1 (b), SS3 (c) y SS5 (d)

Nombre Tóxico	AA-MZ m^2	AA-AD AA-MAS	MAC-MZ m^2	MAC-AD MAC-MAS
ID1 ($CHCl_3$)	2557527.73	100.0>10	-	-
ID2 (Pb)	2533228.37	99.05>10	2510515.97	98.16>3

Tabla 8: Extensión de las zonas de mezcla delimitadas (AA-MZ and MAC-MZ) y admisibilidad final (AA-AD and MAC-AD) en el cálculo simplificado para ID1 e ID2.

Los efectos de la concentración del tóxico se determinaron mediante la ecuación (6) para el AA-MZ y la ecuación (7) para el MAC-MZ (Figura 21).

A continuación, se muestran en la figura 60 la AA-MZ y MAC-MZ delimitadas para el "caso peor de dilución" de ID1 (a-b) e ID2 (c-d). Cabe indicar que el cloroformo (ID1) no tiene un valor aplicable para MAC-EQS por lo que, en esta figura, la MAC-MZ es sólo un ejemplo de la extensión de la MAC-MZ considerando como umbral el mismo valor que para la AA-EQS.

3.3.6. Admisibilidad de las zonas de mezcla

Una vez que se delimitaron ambas MZs, se efectuó una comprobación para determinar si la aceptabilidad y la extensión de las delimitaciones fueron admisibles.

3.3.6.1. Aceptabilidad (AC)

Para esta tarea, se comprobó si el punto de descarga se ubicó en una zona intermareal (En SE, este valor es de $A95 < 2{,}138$ m). La profundidad de la columna de agua en ID1 e ID2 es de $H_{ID1} = 2{,}87$ m y $H_{ID2} = 6{,}28$ m respectivamente. Por tanto, ambos vertidos se ubican en zonas submareales por lo que son aceptables.

A continuación, se calculó el valor de AC como el porcentaje de cobertura de área estuarina por celda mediante la ecuación (8). Respecto al área superficial del estuario ($A_{estuary}$), el límite interior es un azud industrial que marca el final de la influencia de la marea en la cuenca del río. El límite exterior se estableció a partir de los espigones que canalizan la entrada de la ría (Figura 61). Teniendo en cuenta ambos límites y la resolución espacial de la malla, el $A_{estuary}$ es de 2557527 m^2.

3.3.6.2. Tamaño maximo permitido para zonas de mezcla (MAS)

En el cálculo simplificado, el MAS no puede exceder el 10 % y 3 % de la extensión global de la masa de agua para el AA-MZ y el MAC-MZ respectivamente (Figura 22).

3.3.6.3. Admisibilidad final (AD)

Por último, se evaluó la admisibilidad final de las MZs (AD) como la suma de todos los valores de AC cubiertos por las AA-MZ y MAC-MZ mediante la ecuación (11). En la tabla 8, se resume el área cubierta y la AD de la AA-MZ y MAC-MZ para ID1 e ID2.

Ambas descargas industriales presentaron un admisibilidad definitiva (AA-AD y MAC-AD) mayor que AA-MAS (10 %) y MAC-MAS (3 %). Por ello, la extensión de la AA-MZ o MAC-MZ resultó inadmisibles para ID1 e ID2 y, en consecuencia, ambos vertidos se clasificaron como significativos grandes siendo necesario avanzar al Paso 4 del árbol de decisiones con el fin de continuar con el procedimiento de asignación (Figura 10).

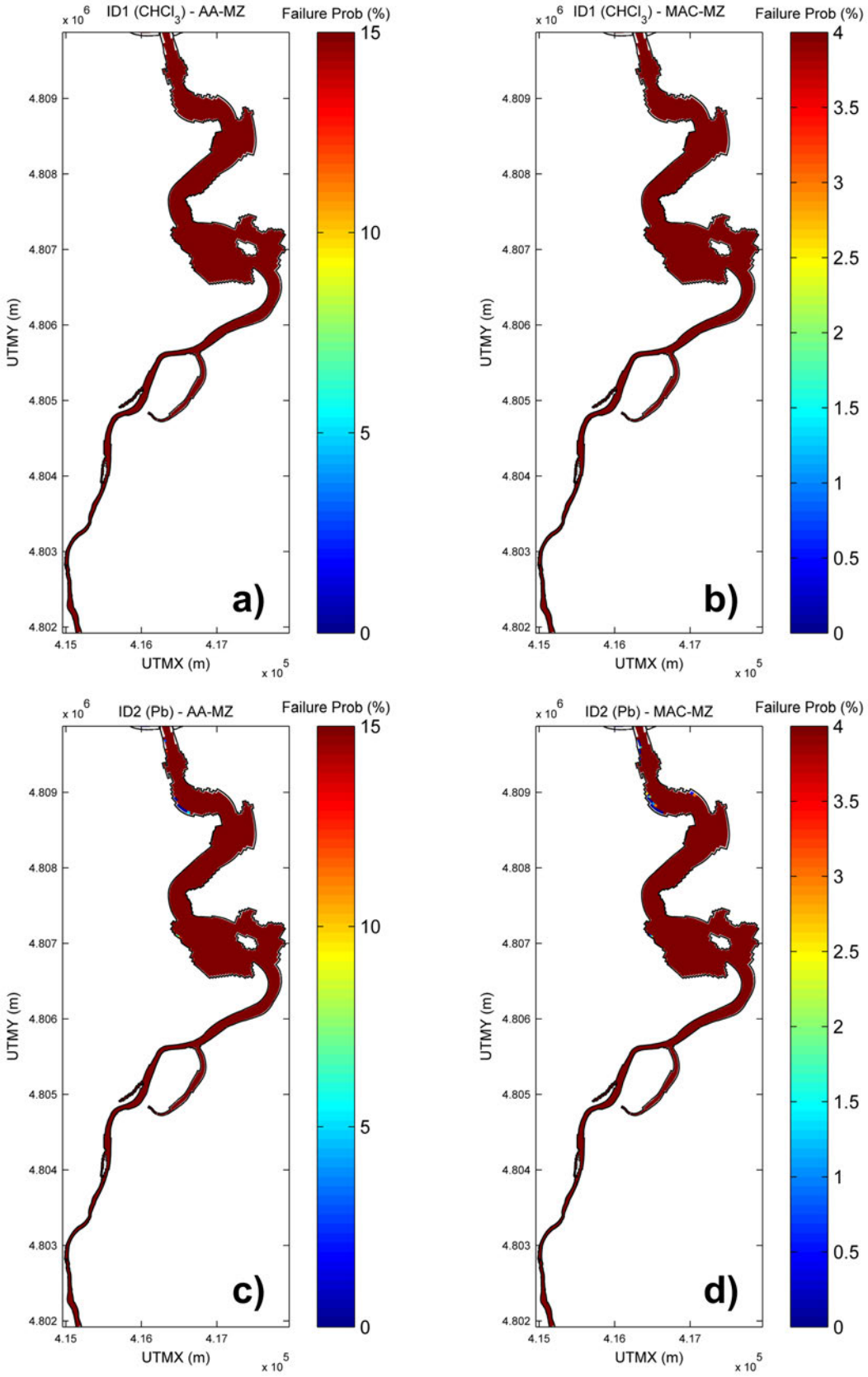

Figura 60: Zonas de mezcla delimitadas en el "caso peor de dilución". AA-MZ de ID1 (a), MAC-MZ de ID1 (b), AA-MZ de ID2 (c) y MAC-MZ de ID2 (d).

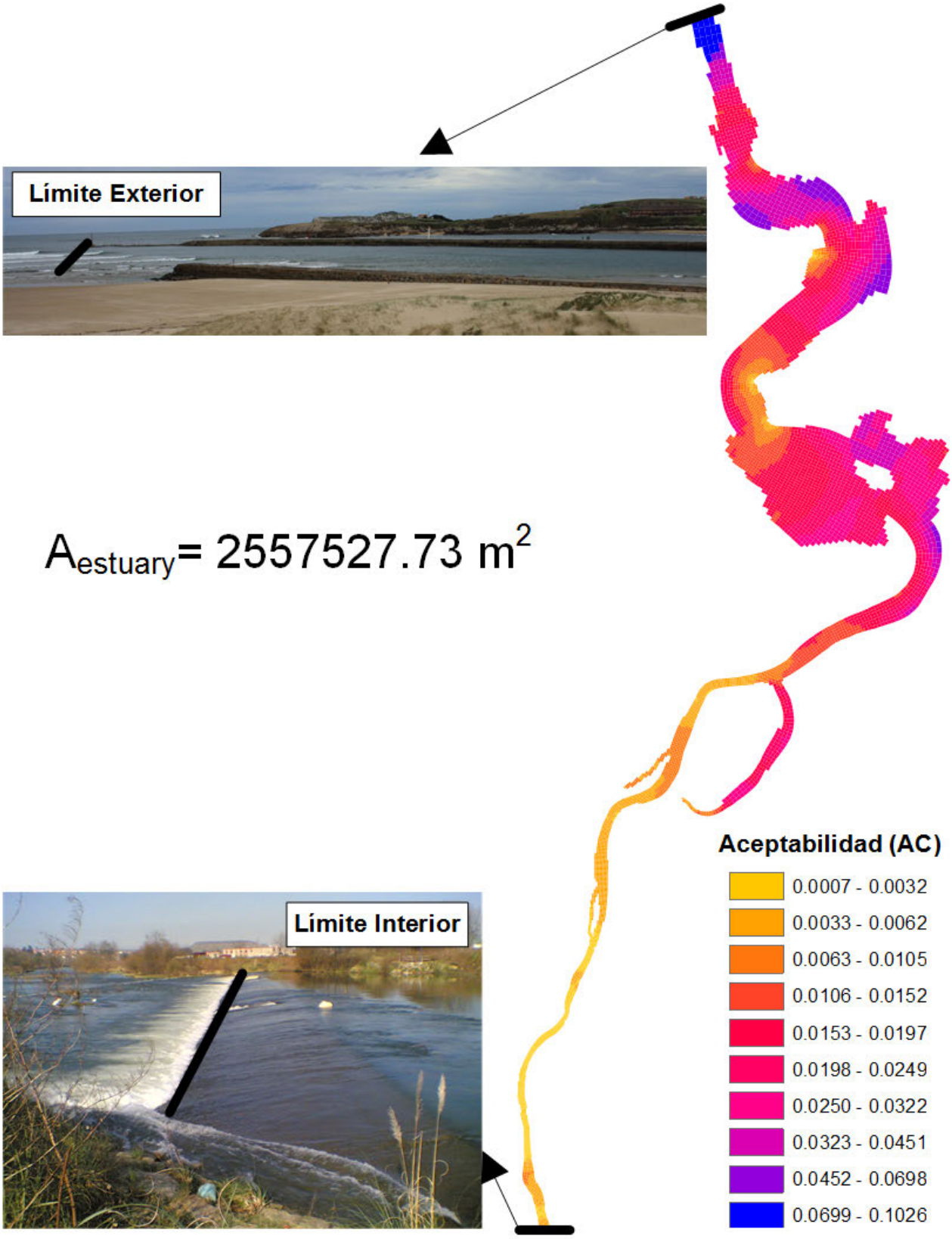

Figura 61: Límites exterior e interior considerados en el Estuario de Suances, valor de $A_{estuary}$ y aceptabilidad (AC) de las celdas de la malla.

3.4. Paso 4. Cálculo intermedio (Caso seco de dilución)

3.4.1. Hidrodinámica

3.4.1.1. Configuración del modelo

En el "caso seco de dilución", la configuración de modelo es la misma que en el "caso peor de dilución" por lo que no fue necesario realizar tareas adicionales.

3.4.1.2. Forcing selection

El cálculo intermedio se basa en la simulación continua del año más seco de la serie temporal de 40 años de caudal fluvial en el SE (Figura 44a). Para la selección de este año más seco, se calculó el volumen medio anual de agua ($MAWV$) para cada i-año por medio de la ecuación (10).

A continuación, se identificó al año 1989 como el valor mínimo de $MAWV$ extrayéndose para este año la serie temporal de caudal fluvial y de nivel de marea asociadas para utilizarlas como forzamientos del escenario de modelado hidrodinámico en el "caso seco de dilución" (ver figura 62).

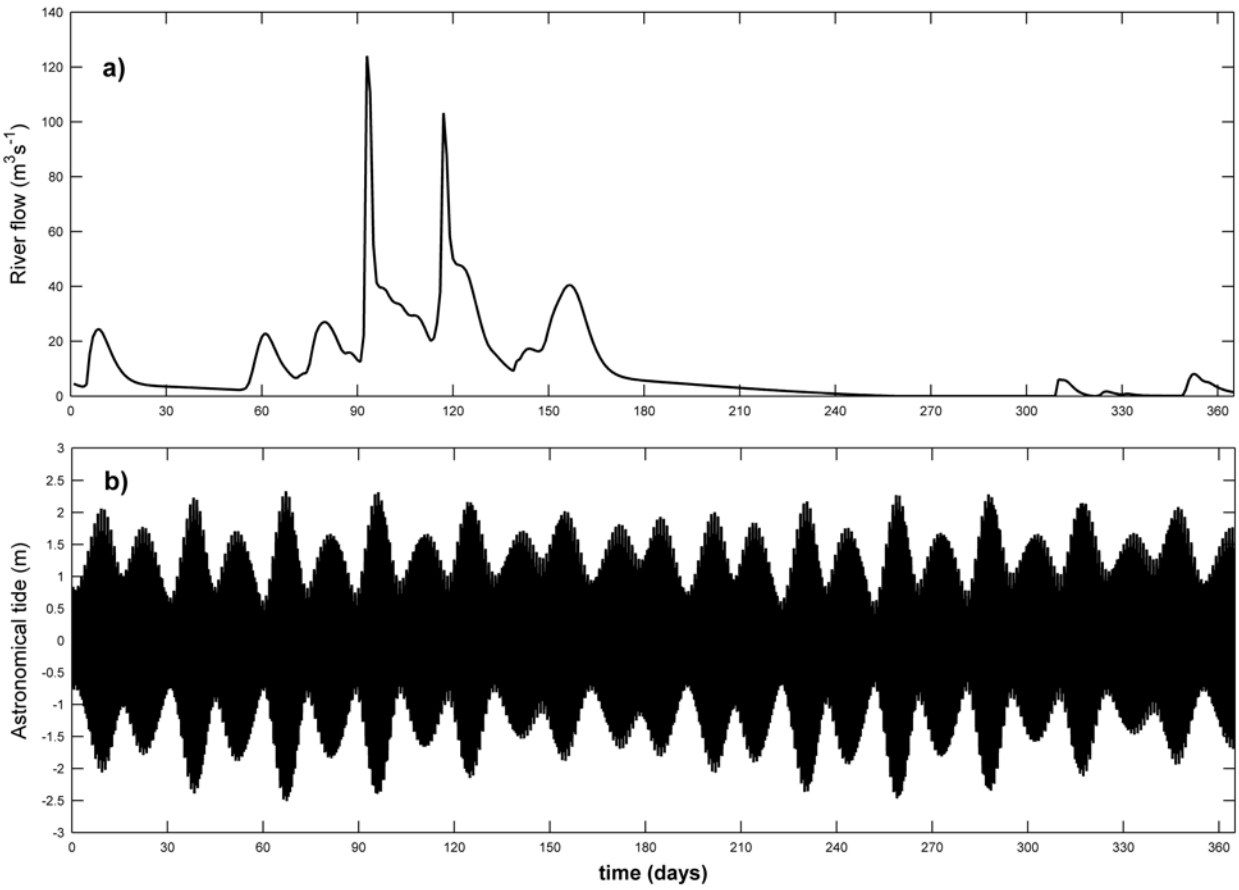

Figura 62: Año más seco de la serie de forzamientos (año 1989). Caudal del río (a) y onda de marea astronómica (b) en el estuario de Suances.

3.4.1.3. Modelado hidrodinámico del caso peor

De acuerdo con las figuras 52 y 53, la escala temporal de la respuesta "cuasi-estacionaria" para la hidrodinámica fue de 216 horas (9 días).

Por lo tanto, en el cálculo intermedio, se realizó la simulación hidrodinámica asumiendo 9+365 días de caudal

del río y de elevación de las mareas como forzamientos. Una vez que se alcanzó la estabilización de modelo y se evitó la influencia de las condiciones iniciales, se almacenó horariamente los 365 días de resultados del modelo hidrodinámico durante 1989.

3.4.2. Dilución primaria o inicial (Campo cercano)

En este apartado, se realizaron los cálculos de dilución primaria para cada descarga (ID1 e ID2) empleando el modelo integral de chorro JETLAG y los mismos supuestos que en el cálculo simplificado.

En las figuras 63 y 64, se muestra la profundidad total de agua (a), la magnitud de la velocidad ambiental (b), la dirección de la velocidad ambiental (c) y la densidad ambiental (d) para la capa superficial (línea azul) y la capa de fondo (línea verde) en ID1 durante el "caso peor de dilución". Además, en ambas figuras se presenta la dilución inicial (e) del efluente (línea negra) y la concentración del efluente (f) al final del campo cercano (línea negra). Finalmente, en la figura 63 se indica la AA-EQS (línea magenta) del cloroformo ($CHCl_3$) mientras que, en la figura 64 se indica la AA-EQS (línea magenta) y la MAC-EQS (línea roja) del plomo (Pb).

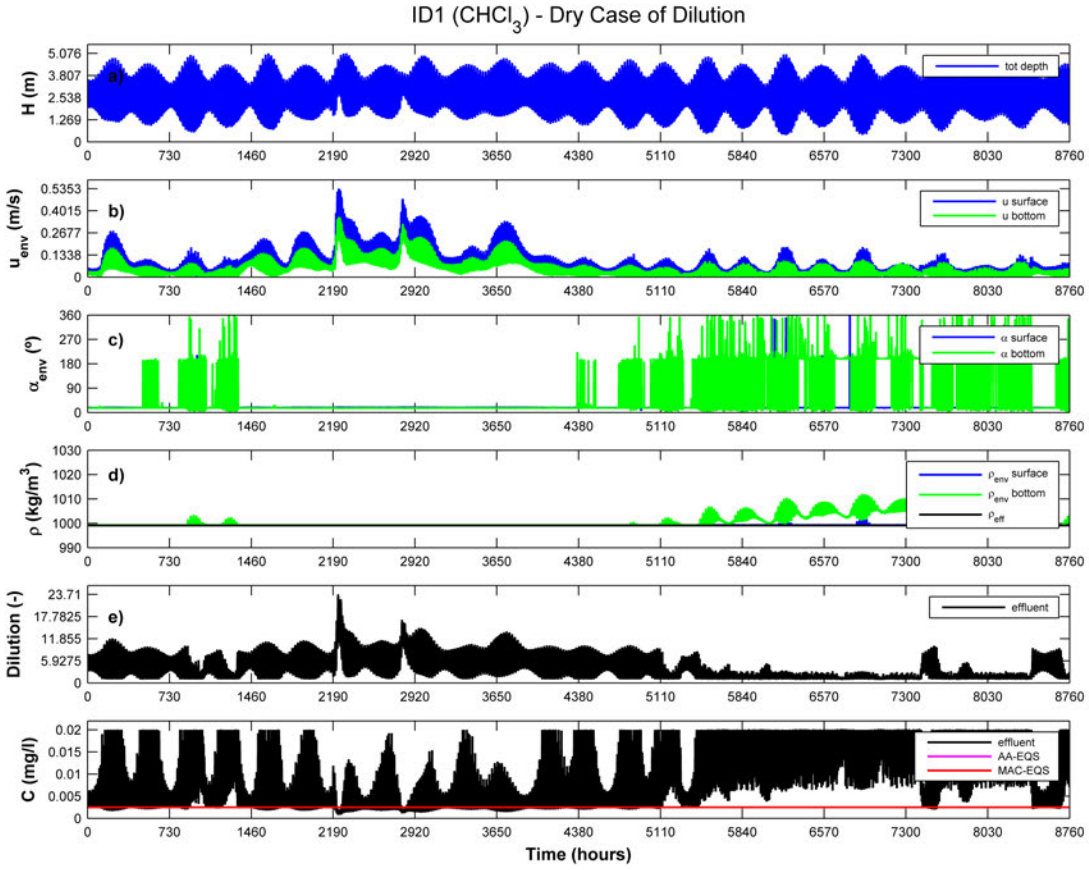

Figura 63: Evolución de la profundidad total de agua (a), la magnitud de la velocidad ambiental (b), la dirección de la velocidad ambiental (c) y la densidad ambiental (d) para la capa superficial (línea azul) y la capa de fondo (línea verde), la dilución inicial (e) del efluente (línea negra) y la concentración del efluente (f) al final del campo cercano (línea negra) en ID1 durante el "caso seco de dilución". Además se indica la AA-EQS (línea magenta) del cloroformo (f).

Como se muestra en las figuras 63 y 64, la dilución en ID1 varío entre 23.71 y 1.00 mientras que la dilución en ID2 entre 3356.78 y 4.13. De nuevo, las variaciones se debieron a los cambios en la profundidad total, la

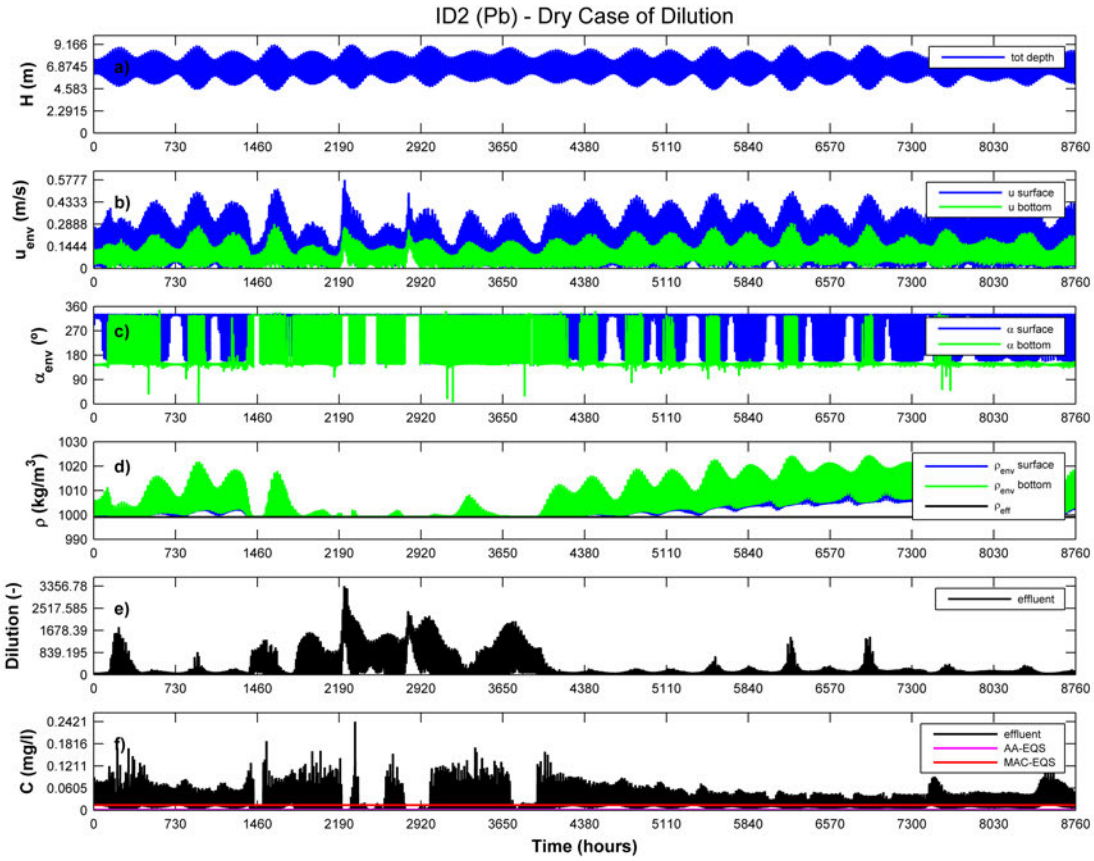

Figura 64: Evolución de la profundidad total de agua (a), la magnitud de la velocidad ambiental (b), la dirección de la velocidad ambiental (c) y la densidad ambiental (d) para la capa superficial (línea azul) y la capa de fondo (línea verde), la dilución inicial (e) del efluente (línea negra) y la concentración del efluente (f) al final del campo cercano (línea negra) en ID2 durante el "caso seco de dilución". Además se indica la AA-EQS (línea magenta) y la MAC-EQS (línea roja) del plomo (f).

velocidad ambiental y la densidad ambiental. Además, la dilución de ID1 e ID2 fue directamente proporcional a la serie temporal del caudal del río (ver figura 62a). En cuanto a la concentración en ID1 e ID2, las EQSs se superaron durante la mayor parte del tiempo en el "caso seco de dilución".

3.4.3. Acople de la dilución primaria a la secundaria (Campo intermedio)

Las figuras 65 y 66 presentan el porcentaje de tiempo que ID1 e ID2 estuvieron en diferentes celdas de la malla (panel izquierdo) y capas verticales (panel derecho) predichos por JETLAG al final del campo cercano. En estas localizaciones, se introdujeron ID1 e ID2 como un término fuente de caudal y concentración diluida en el modelo de campo lejano.

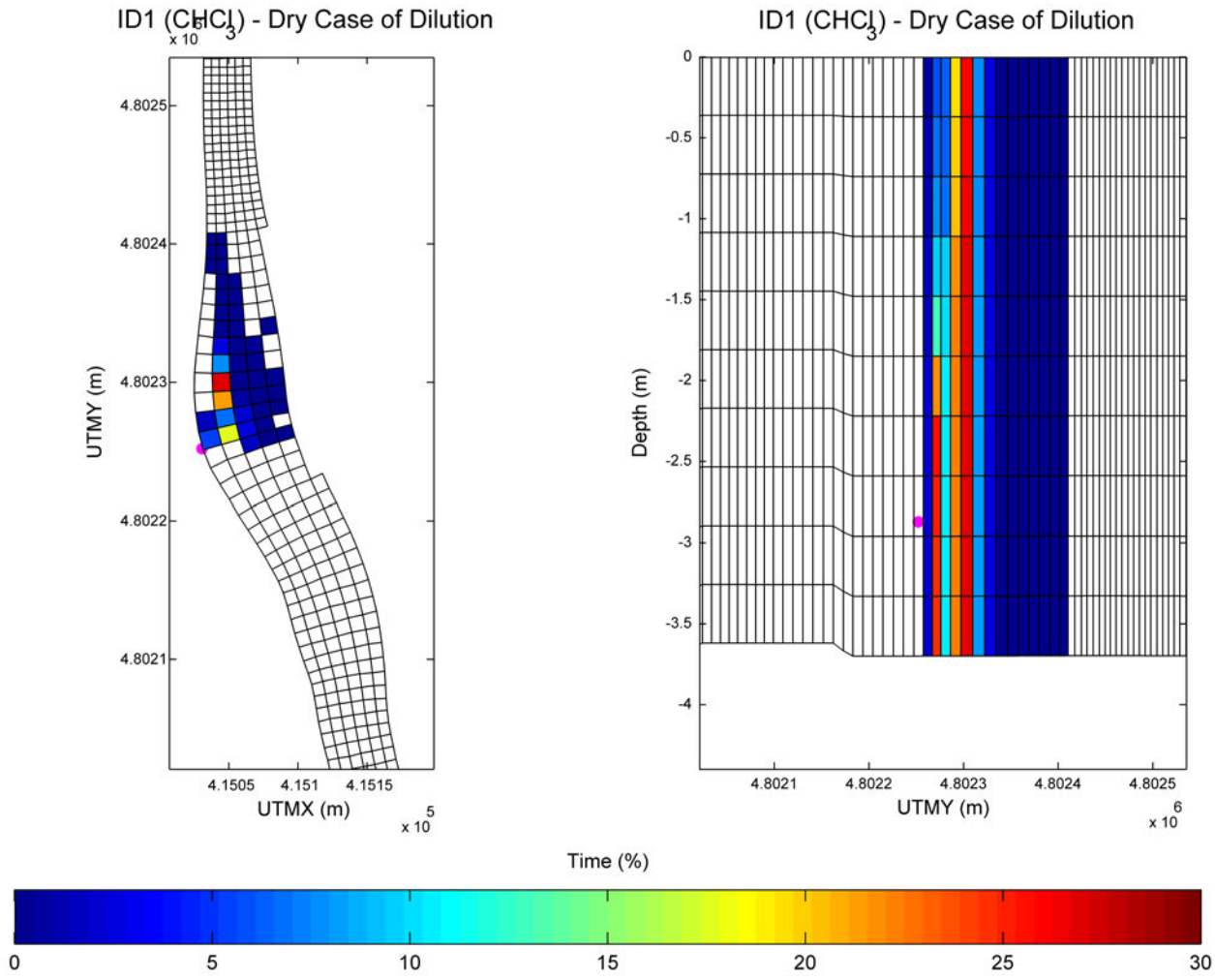

Figura 65: Vista esquemática de la distribución del tiempo de las celdas horizontales de la malla (panel izquierdo) y las capas verticales (panel derecho) cubiertos por ID1 durante el acoplamiento entre la dilución primaria y secundaria en el cálculo intermedio.

Como se muestra en la figura 65, el efluente descargado en ID1 se localizó en varias celdas horizontales aguas abajo del punto de descarga, debido a la cercanía con el río y la magnitud del impulso inducido por ID1. En la dirección vertical, ID1 se mezcló completamente en vertical la mayor parte del tiempo. El resto del tiempo ID1 se acopló principalmente entre las capas 5 y 10.

Como se puede observar en la figura 66, el efluente en ID2 estuvo siempre en la celda de la malla donde se encuentra la descarga debido a que la flotabilidad y el caudal fueron relativamente pequeños. Respecto a la

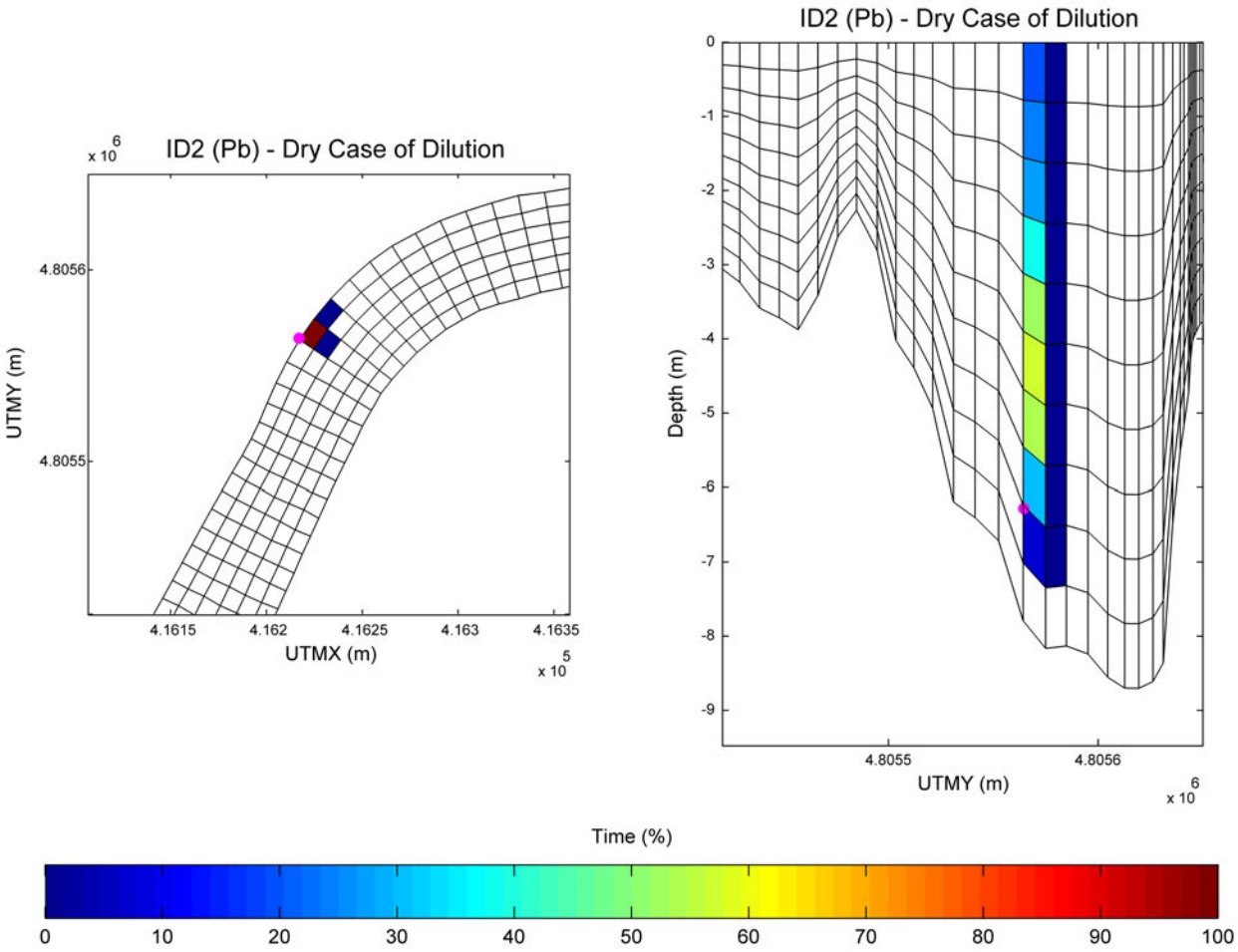

Figura 66: Vista esquemática de la distribución del tiempo de las celdas horizontales de la malla (panel izquierdo) y las capas verticales (panel derecho) cubiertos por ID2 durante el acoplamiento entre la dilución primaria y secundaria en el cálculo intermedio.

distribución vertical, ID2 estuvo la mayor parte del tiempo entre las capas 4 y 8, es decir, entre 2.5 y 6.5 m de profundidad indicando que la pluma ID2 se atrapa.

3.4.4. Dilución secundaria o ambiental (Campo lejano): Enfoque conservativo

3.4.4.1. Configuración del modelo

En el enfoque conservativo, la configuración del modelo fue igual que en el Paso 3 por lo que no fue necesario llevar a cabo tareas adicionales para calibrar el modelo de campo lejano.

3.4.4.2. Modelado del transporte del caso seco

Con el fin de estabilizar los resultados del modelo y disminuir la influencia de las condiciones iniciales, se realizó una "presimulación" para obtener la condición inicial adecuada de concentración de tóxico y otra "simulación" para registrar la evolución de la concentración a lo largo de 1989.

"Presimulación"

El tiempo máximo de la respuesta "cuasi-estacionaria" para el transporte se asocia a la escala temporal del "caso peor de dilución " e indica la duración mínima de cualquier "presimulación" en el campo lejano para asegurar que las condiciones iniciales son fiables. Dicho tiempo de respuesta fue de 528 horas o 22 días (véanse las figuras 58 y 59).

Los contornos abiertos y cerrados así como las condiciones iniciales fueron las mismas definidas en el "caso peor de dilución".

La "presimulación" se llevó a cabo utilizando un caudal constante de río igual al primer día de 1989 y su marea asociada durante 24 horas (véase la figura 67). A continuación, se ejecutó D-Water Quality para ID1 e ID2 con los resultados de Delft3D-FLOW del primer día en un bucle continuo durante 30 días.

Una vez que se alcanzó la respuesta 'cuasi-estacionaria para el transporte, se registró el mapa de la concentración de sustancia tóxica suponiendo un comportamiento conservativo que se correspondió con la primera hora de 1989. En las figuras 68 y 69, se presentan los mapas de la distribución espacial de cloroformo (ID1) y plomo (ID2) en la superficie (a) y el fondo (b) que constituyen la condición inicial para la "simulación" durante al año 1989.

"Simulación"

Los contornos abiertos y cerrados fueron los mismos definidos en el "caso peor de dilución" mientras que las condiciones iniciales fueron un mapa de concentración de tóxico para cada descarga obtenidas en la "presimulación" (ver figuras 68 y 69). Posteriormente, se ejecutó el escenario de modelado durante el año 1989 y se grabó horariamente 365 días de resultados del modelo de transporte, es decir, la evolución de la concentración de tóxico para ID1 (cloroformo) e ID2 (plomo) en el SE.

A modo de ejemplo, en las figuras 70 y 71 se muestra la evolución de las sustancias objeto de análisis en WQ3 (a), SS1 (b), SS3 (c) and SS5 (d) para ID1 e ID2 durante el "caso seco de dilución", respectivamente. En dichas figuras, la línea negra corresponde a la capa superficial y la línea gris a la de fondo.

3.4.4.3. Delimitación de las zonas de mezcla

En el cálculo intermedio se ejecutó un año (1989) bajo condiciones reales. Después de las simulaciones, se determinó la AA-MZ y MAC-MZ aplicando el método desarrollado (Figura 25).

Especificación del número anual de muestras

En este método, se adoptó la propuesta española (SPAIN 2014) y se especificó que el número anual de muestras fuera 12 (una por mes). En cuanto al período de muestreo, cada muestra se tomó en cualquier momento

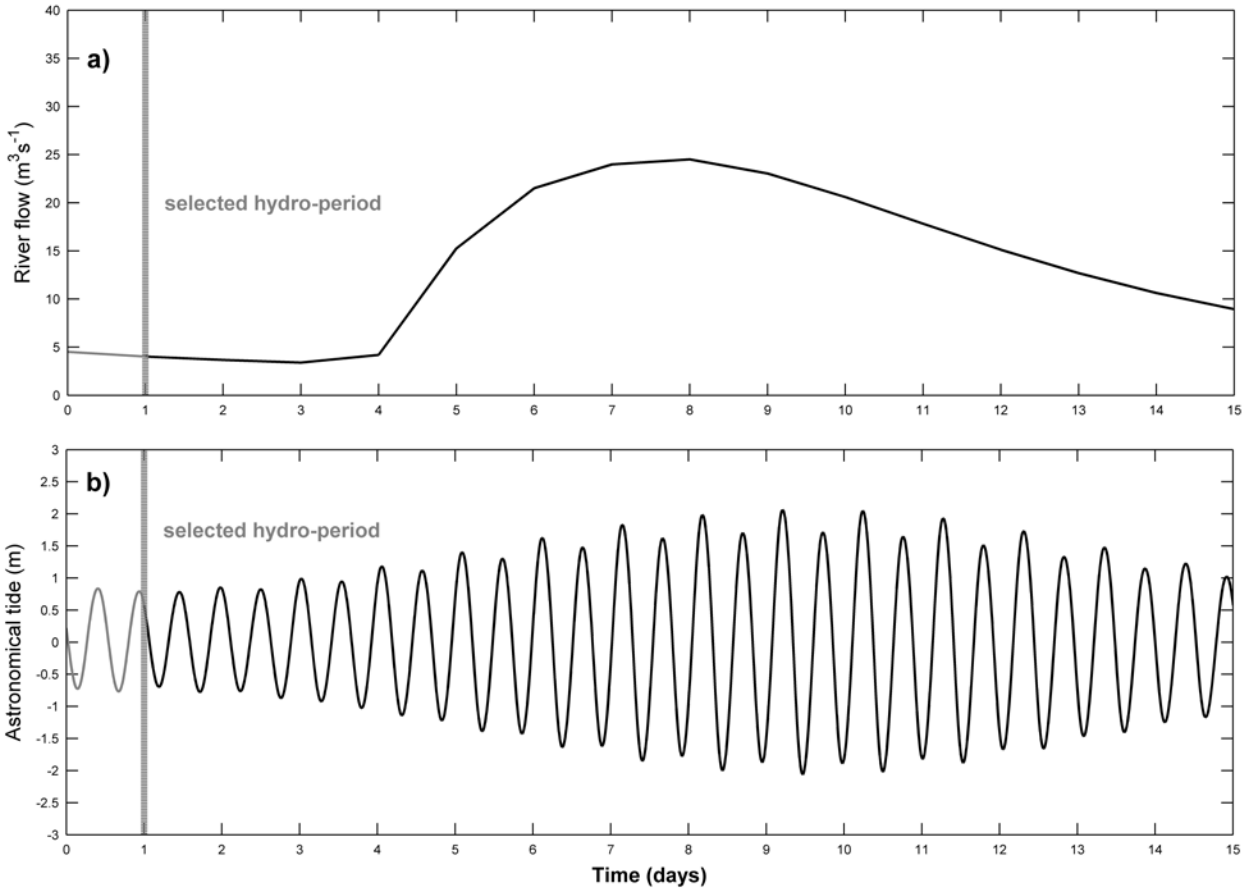

Figura 67: Forzamientos de las primeras 360 horas del año 1989 (año más seco) e hidro-período seleccionado para el transporte de la "presimulación" en el "caso seco de dilución".

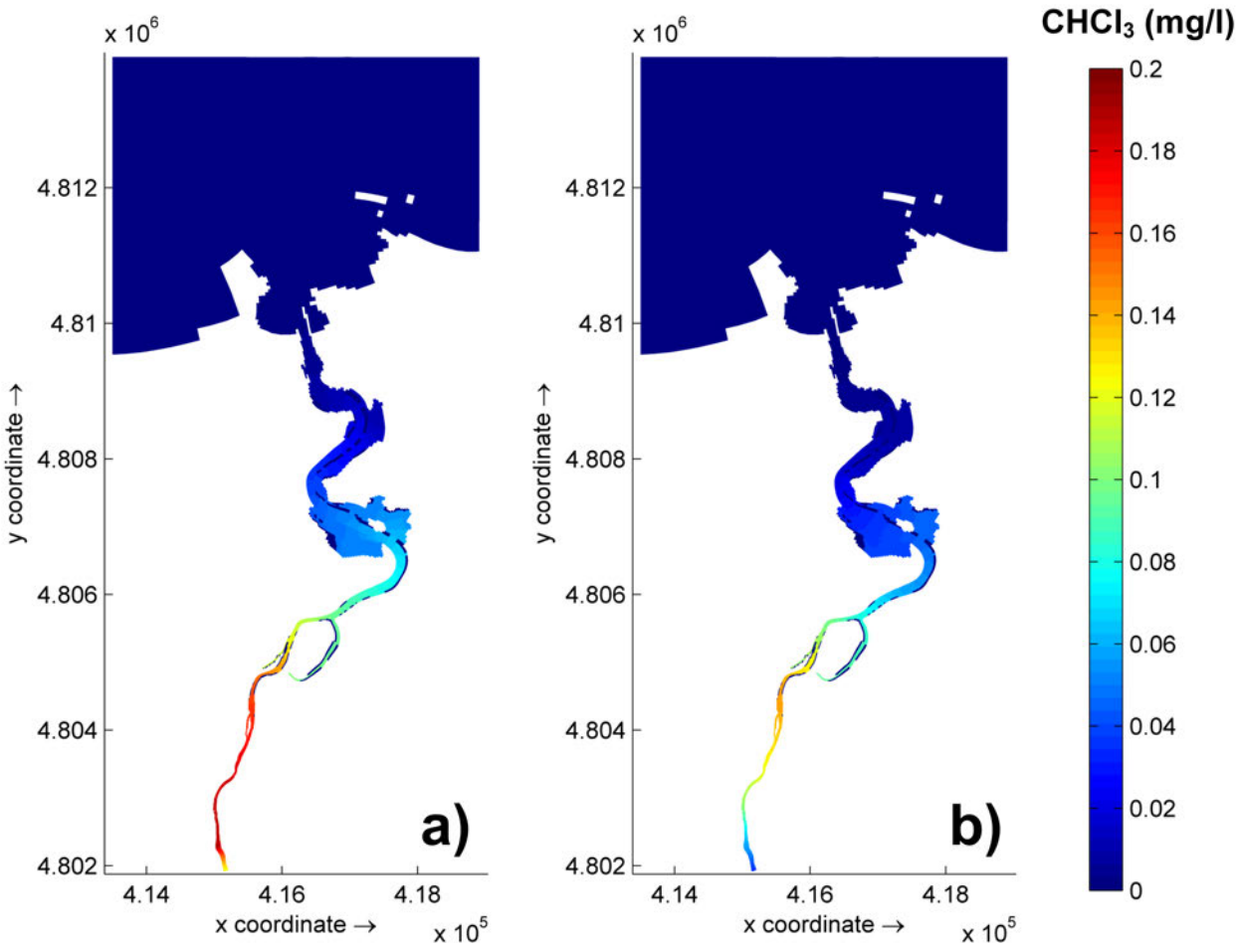

Figura 68: Mapa de la distribución espacial de cloroformo utilizado como condición inicial para la "simulación" durante el año 1989 ("caso seco de dilución" de ID1). Capa superficial (a) y capa de fondo (b).

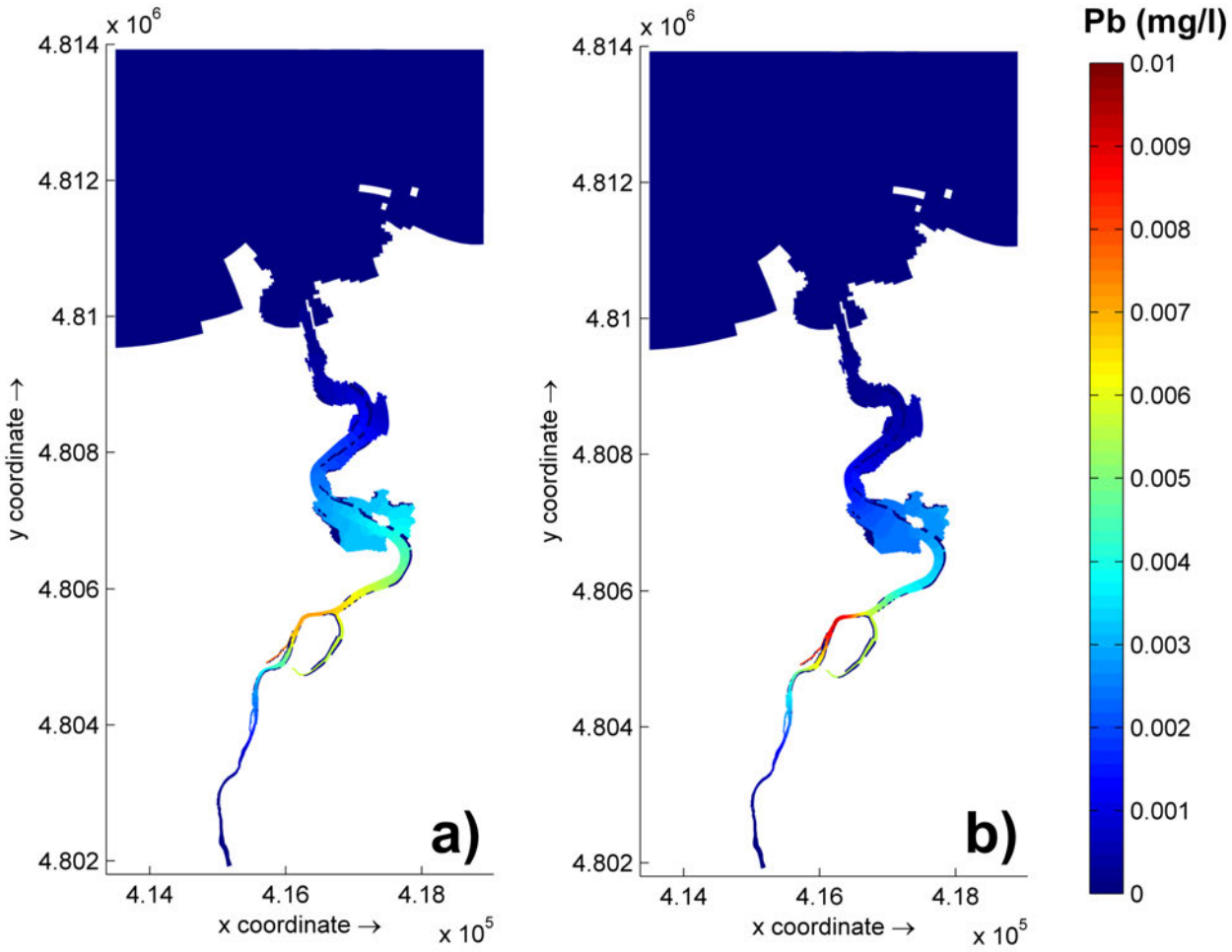

Figura 69: Mapa de la distribución espacial de plomo utilizado como condición inicial para la "simulación" durante el año 1989 ("caso seco de dilución" de ID2). Capa superficial (a) y capa de fondo (b).

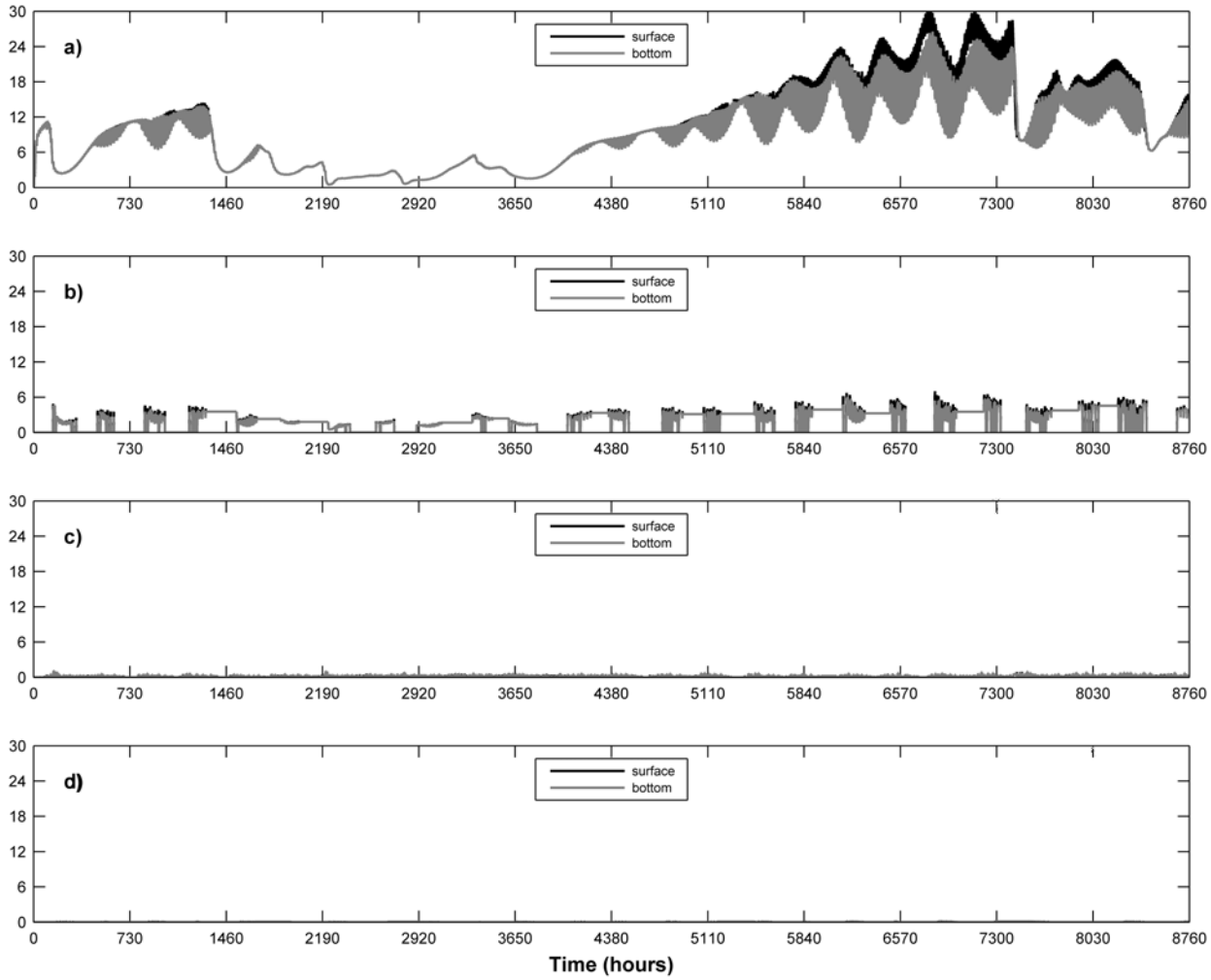

Figura 70: Evolución de la concentración de ID1 (cloroformo) en la superficie (línea negra) y el fondo (línea gris) para el transporte del "caso seco de dilución" en WQ3 (a), SS1 (b), SS3 (c) and SS5 (d).

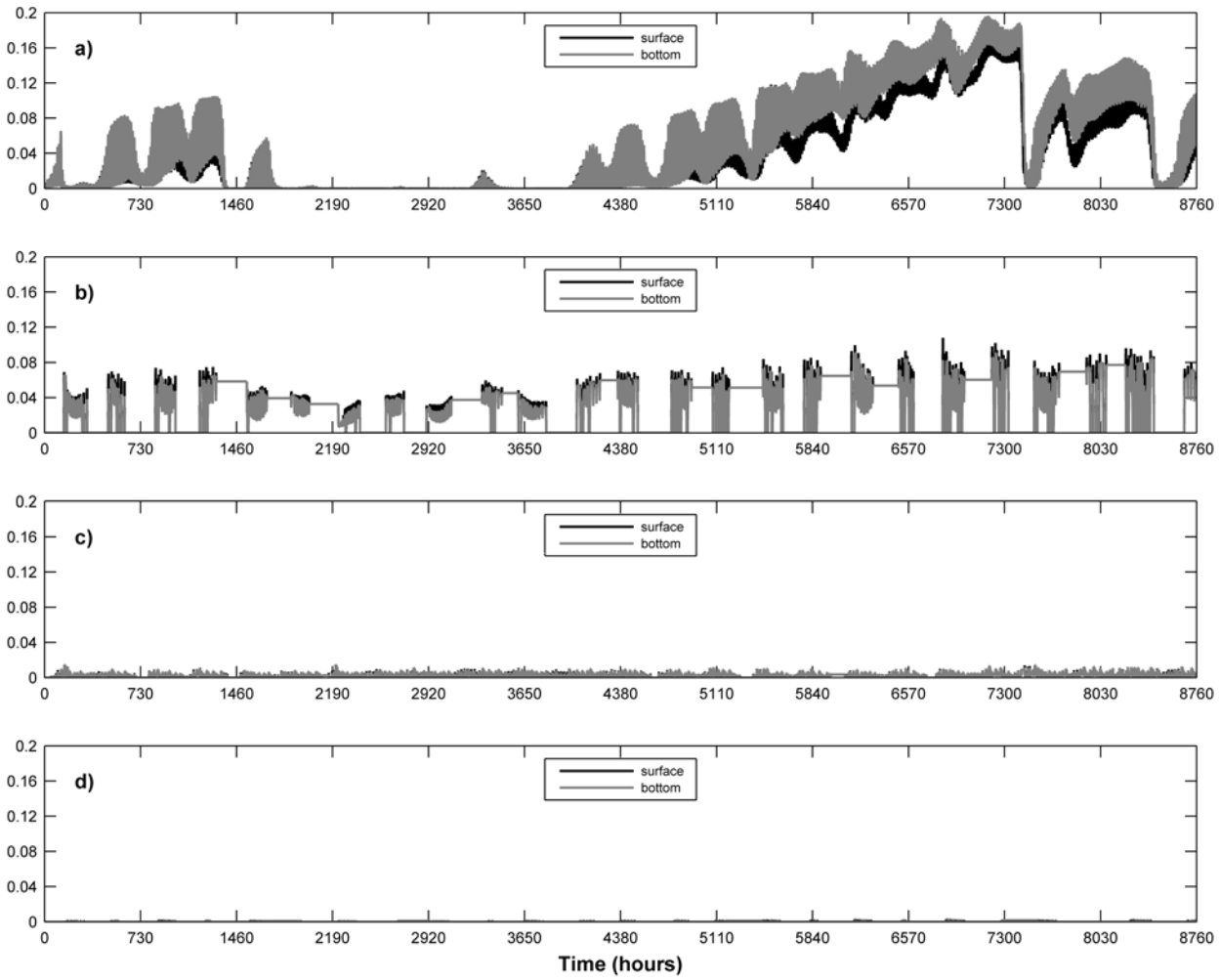

Figura 71: Evolución de la concentración de ID2 (plomo) en la superficie (línea negra) y el fondo (línea gris) para el transporte del "caso seco de dilución" en WQ3 (a), SS1 (b), SS3 (c) and SS5 (d).

Nombre Tóxico	AA-MZ m^2	AA-AD AA-MAS	MAC-MZ m^2	MAC-AD MAC-MAS
ID1 ($CHCl_3$)	2557527.73	100.0>10	-	-
ID2 (Pb)	2491395.12	97.41>10	2452000.71	95.87>3

Tabla 9: Extensión de las zonas de mezcla delimitadas (AA-MZ and MAC-MZ) y admisibilidad final (AA-AD and MAC-AD) en el cálculo intermedio para ID1 e ID2.

durante cada mes (muestreo aleatorio).

Determinación del número óptimo de muestreos

Primero se generaron 10000 muestreos aleatorios (10000×12 datos) a partir de los resultados del modelo en diferentes celdas de la malla con especial atención a la zona del punto de descarga.

A continuación, se evaluó el cumplimiento de las EQS para los 10000 muestreos en cada punto de control. Para cada muestreo, si el promedio de los datos es inferior al valor de la AA-EQS se cumple el requisito de la AA-EQS mientras que el cumplimiento para la MAC-EQS se produce cuando todas las muestras están por debajo del valor de la MAC-EQS. Después de estos cálculos, se determinó la probabilidad de fallo para ambas EQS en cada vertido y cada punto de control.

Por último, se representó gráficamente la evolución de la probabilidad de fallo promediada con el número de muestreos para la AA-EQS y la MAC-EQS con el fin de determinar el número óptimo de muestreos (k)que asegura la independencia de la probabilidad de fallo. En este estudio, el número óptimo se determinó a partir de la MAC-EQS en el caso de ID2 siendo de 1000 muestreos aproximadamente (ver figura 72).

Delimitación definitiva de las MZs

Los efectos crónicos de cada sustancia tóxica en cada celda de la malla se calcularon utilizando la ecuación (11) para cada muestreo. Si $CEF*^k_{i,j} > 1$ entonces $CEF*^k_{i,j} = 1$, por el contrario, si $CEF*^k_{i,j} \leq 1$ entonces $CEF*^k_{i,j} = 0$. Por último, se computó el CEF* asociado a los 1000-muestreos mediante la ecuación (12).

Los efectos agudos de cada sustancia tóxica en cada celda de la malla se calcularon utilizando la ecuación (13) para cada muestreo. Si $AEF*^k_{i,j} > 0$ entonces $CEF*^k_{i,j} = 1$, por el contrario, si $AEF*^k_{i,j} \leq 0$ entonces $AEF*^k_{i,j} = 0$. Por último, se computó el AEF* asociado a los 1000-muestreos mediante la ecuación (14).

De nuevo, se determinaron dos MZs: la AA-MZ ($CEF*_{i,j} > 15$) y la MAC-MZ ($AEF*_{i,j} > 4$). A continuación, en la figura 73 se muestran la AA-MZ y MAC-MZ delimitadas para el "caso seco de dilución" de ID1 (a-b) e ID2 (c-d). Al igual que en el cálculo simplificado cabe indicar que el cloroformo (ID1) no tiene un valor aplicable para MAC-EQS por lo que el mapa de la MAC-MZ es sólo un ejemplo.

3.4.5. Admisibilidad de las zonas de mezcla

En el "caso seco de dilución", se utilizó el mismo método de tres niveles propuesto para el "caso peor de dilución" (Figura 61). En la tabla 9, se resume el área y la AD de la AA-MZ y MAC-MZ teniendo en cuenta un AA-Fallo de 15 % y un MAC-Fallo de 4 % para ID1 e ID2.

Ambas descargas industriales presentaron un admisibilidad definitiva (AA-AD y MAC-AD) mayor que AA-MAS (10 %) y MAC-MAS (3 %). Por ello, la extensión de la AA-MZ o MAC-MZ no fueron admisibles para ID1 e ID2 y, en consecuencia, ambos vertidos se clasificaron como significativos muy grandes por lo que se sigue con la aplicación en el Paso 5 (Figura 10).

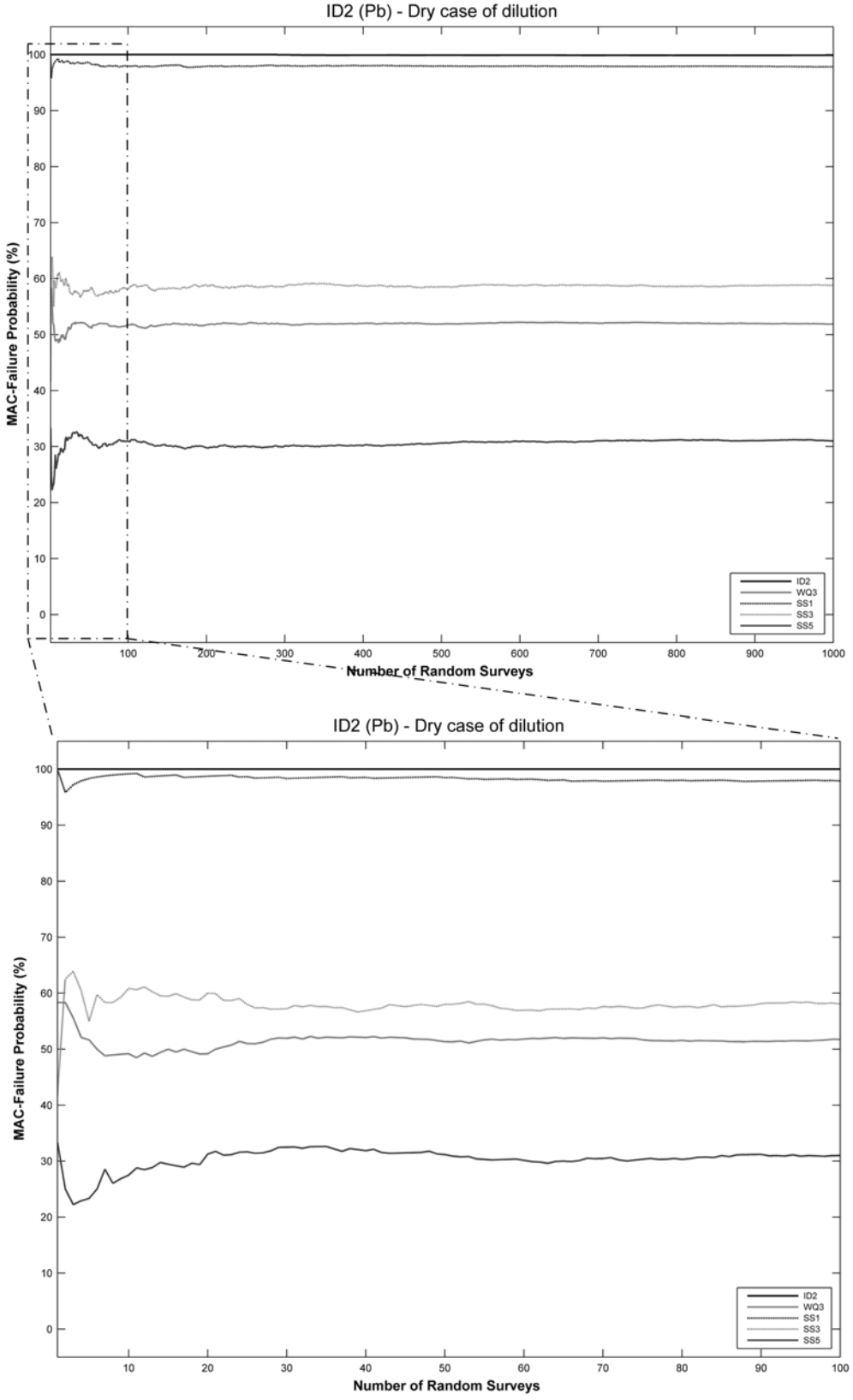

Figura 72: Evolución de la probabilidad de fallo promediada con el número de muestreos para la MAC-EQS de ID2 en ID2 (línea continua negra), WQ3 (línea continua gris clara), SS1 (línea punteada negra), SS3 (línea punteada gris clara) and SS5 (línea continua gris oscura) durante el "caso seco de dilución".

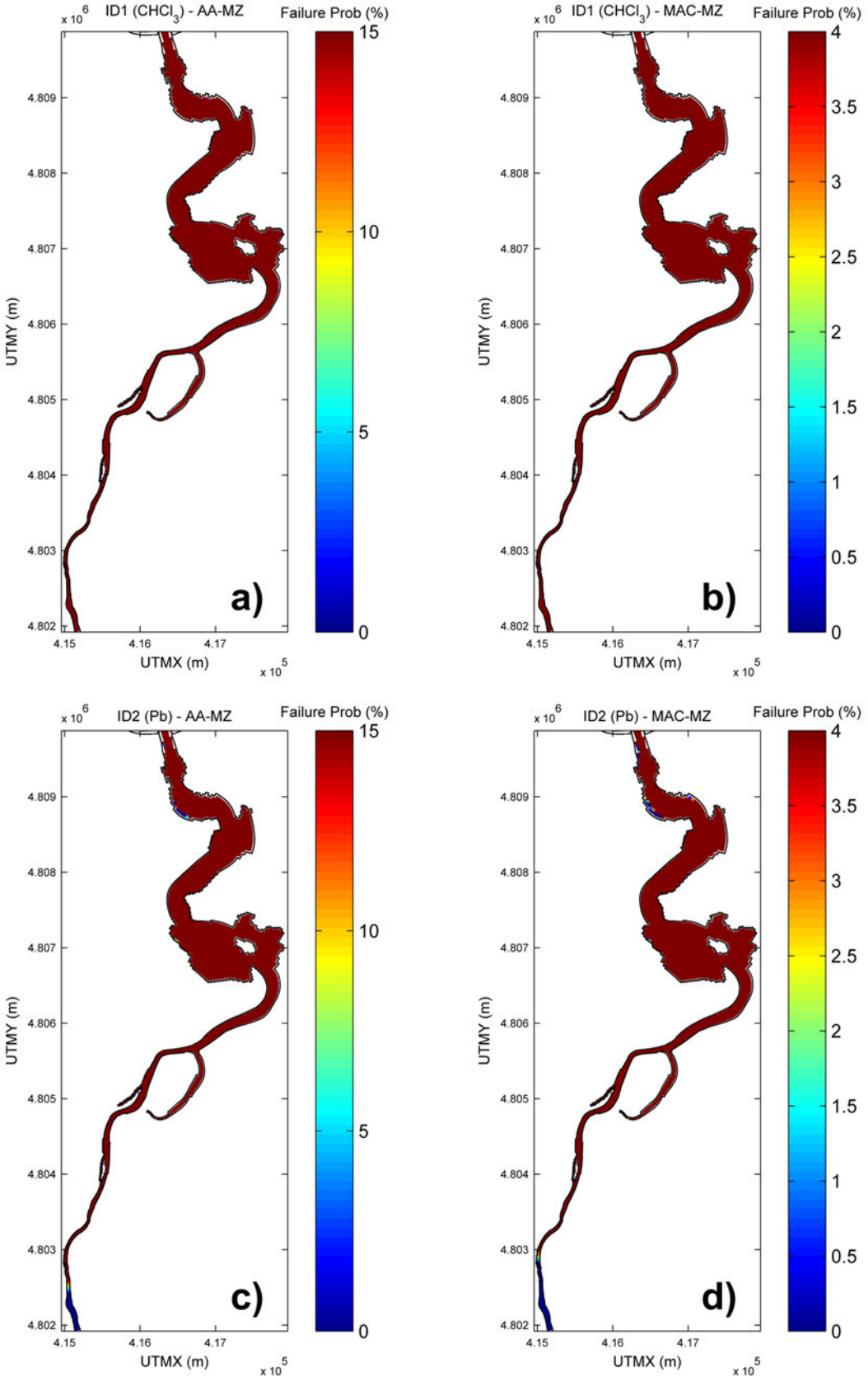

Figura 73: Zonas de mezcla delimitadas en el "caso seco de dilución". AA-MZ de ID1 (a), MAC-MZ de ID1 (b), AA-MZ de ID2 (c) y MAC-MZ de ID2 (d).

3.5. Paso 5. Cálculo detallado (Caso real de dilución)

3.5.1. Hidrodinámica

3.5.1.1. Configuración del modelo

En el "caso real de dilución", la configuración de modelo es la misma que en el "caso peor y seco de dilución" por lo que no fue necesario realizar tareas adicionales.

3.5.1.2. Selección/Clasificación de forzamientos

En este apartado, se aplicó la metodología propuesta para seleccionar escenarios de forzamientos reales en el SE (Figura 3.30).

Datos de los forzamientos hidrodinámicos

Los datos seleccionados fueron los 40-años de series temporales de caudal del río (Q) y de niveles de marea astronómica (A) recabados en el Paso 1 (ver figuras 44).

Reordenamiento de los datos de entrada para la agrupación

Para la selección de series temporales a corto plazo (grupos) a partir de los 40 años de registros de Q y A en el SE, se determinó, en primer lugar, el número de días de los grupos.

El SE presenta una señal de marea semidiurna con un ciclo típico de mareas vivas y muertas de aproximadamente unos 15 días. Además, la cuenca del río Saja-Besaya se encuentra en la costa norte española donde el mar Cantábrico determina el clima. Debido a ello, la señal de caudal de los ríos no presenta períodos secos o húmedos largos. Además, los dP de la cuenca del Saja-Besaya es 15.32 días teniendo en cuenta los 40 años de la serie de caudal diario en la cabecera del SE.

Ambos forzamientos presentan escalas temporales en el rango de quince días en el estuario de Suances, por lo tanto, los escenarios de forzamiento reales deben tener una longitud de 15 días también. De este modo, se reorganizó la serie a largo plazo de Q y A en secuencias de 15 días con el fin de construir la matriz (base de datos) que se utilizó para la agrupación.

Después de todos estos reordenamientos, la base de datos para la clasificación se compuso por dos matrices 14610$\times$15 elementos (carrera de marea diaria, TR, y caudal medio dario, Q). Dicha clasificación se realizó por separado ya que Q y A son eventos independientes.

Análisis de sensibilidad para variabilidad de forzamientos

Siguiendo los pasos metodológicos propuestos (figura 30), se realizó un análisis de sensibilidad para ambos forzamientos aumentando el número de grupos clasificados por el KMA con el fin de reconstruir las "series sintéticas" (series temporales a partir de la secuenciación de grupos que mejor se ajusta con cada segmento de 15 días de las serie temporal de cada forzamiento) para comparar con las "series reales" (series temporales de la bases de datos).

En la figura 74, se muestra el error de cada comparación utilizando el CE de los forzamientos (CE_f). En esta figura, la línea negra se corresponde con el error de la marea astronómica (A) y la línea negra con marcadores cuadrados al caudal del río (Q).

Con respecto a la marea astronómica, el número mínimo de grupos para explicar la variabilidad M_{mf} fue de 4 (CE$_f$=0.6149) y el número óptimo M_{of} fue de 12 (CE$_f$=0.8164). Cada grupo se compuso por 15 días por lo que 40-años de variabilidad de marea astronómica se podrían explicar convenientemente (bien) con sólo 60 días (0.1643 años) y de manera excelente con 180 días (0.4931 años).

Para el caudal del río, el M_{mf} fue de 7 (CE$_f$=0.6138) y el M_{of} fue de 35 (CE$_f$=0.8075). En este caso, los

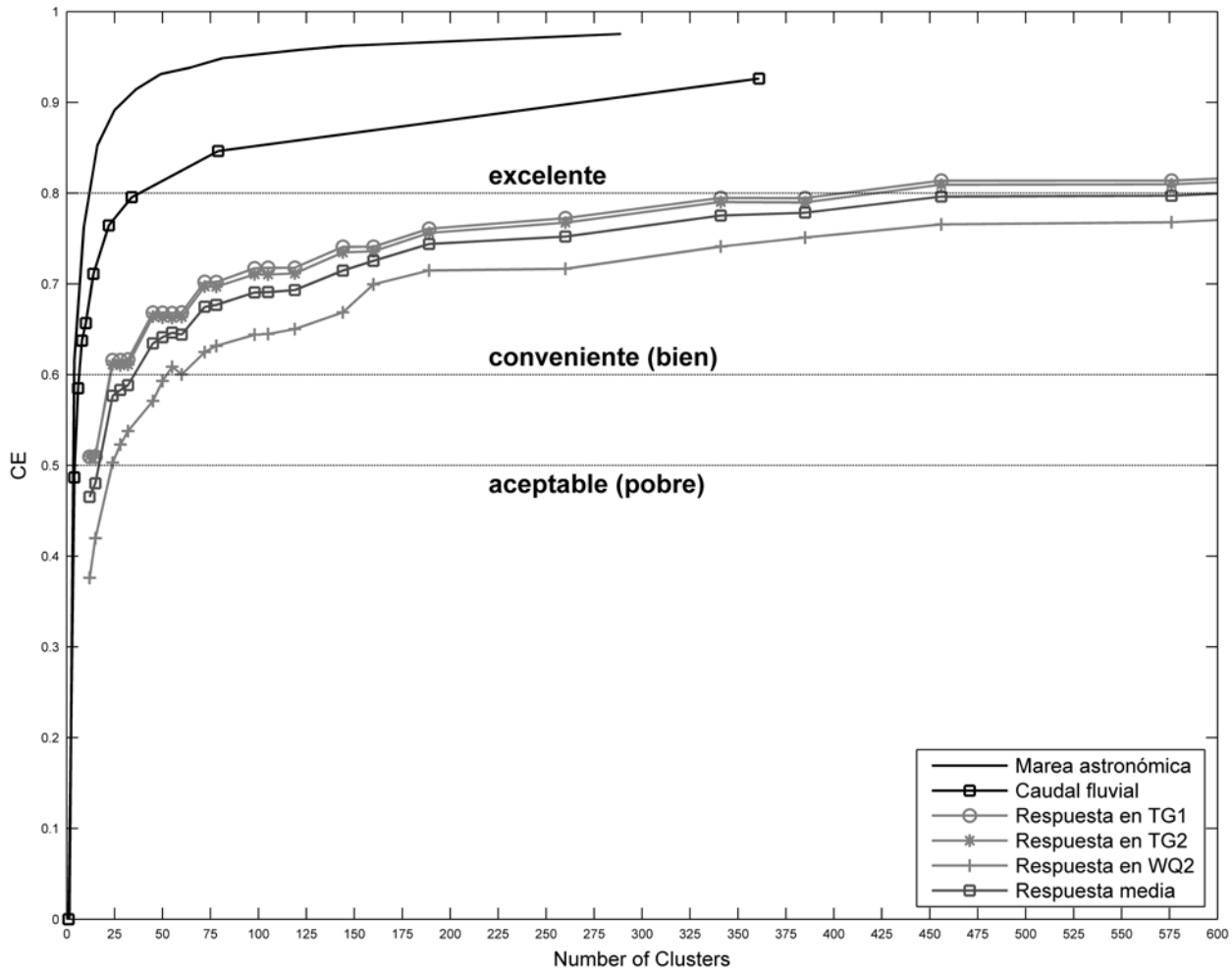

Figura 74: Análisis de sensibilidad para explicar la variabilidad de los forzamientos (marea y río) y para ejecutar modelos numéricos (Respuesta en TG1, TG2 y WQ2 y Respuesta media). La línea negra se corresponde con la marea astronómica, la línea negra con marcadores cuadrados al caudal del río, la línea gris clara con marcadores circulares a TG1 (estuario bajo), la línea gris clara con marcadores de asteriscos a TG2 (estuario medio), la línea gris clara con marcadores de cruces a WQ2 (estuario alto) y la línea gris oscura con marcadores cuadrados a la respuesta media de TG1, TG2 y WQ2.

40-años de variabilidad de caudal fluvial se podrían explicar convenientemente con sólo 105 días (0.2876 años) y excelentemente con 525 días (1.4383 años).

Análisis de sensibilidad para ejecución de modelos

La base de datos inicial y los grupos empleados fueron los mismos que se clasificaron en el análisis anterior. Además, se utilizó la formulación dada por Bárcena *et al.* (2012a) para determinar los niveles de agua (WL) con las "series sintéticas y reales" en TG1, TG2 y WQ2. Dicha formulación proporcionó los WL horariamente durante una onda de marea semidiurna con base en el caudal diario del río (Q) y la amplitud diaria de la marea astronómica ($TR/2$):

$$WL = aQ^2 + b(TR/2)^2 + cQ(TR/2) + d(TR/2) + eQ + f \tag{35}$$

donde a a f son los coeficientes de ajuste determinados por medio de un método basado en mínimos cuadrados.

En la tabla 10, se resumen dichos coeficientes ($a - f$) así como los de regression (R^2) en TG1, TG2 y WQ2.

Siguiendo los pasos metodológicos propuestos (figura 30), se efectuó un análisis de sensibilidad aumentando el número de grupos de Q y TR con un incremento de 0.01 en los valores de CE_f (comenzando en CE_f=0.5). Cuando el CE de la respuesta (CE_r) es mayor que 0.6 en TG1, TG2 y WQ2 se alcanza el mínimo número de grupos para simular M_{mm}. El procedimiento iterativo termina cuando el promedio de CE_r para TG1, TG2 y WQ2 es superior a 0.8 alcanzándose el número óptimo de grupos M_{om}.

En la figura 74, se muestra también el CE_r del nivel de agua en las tres ubicaciones para cada paso iterativo. En dicha figura, la línea continua gris clara corresponde a TG1 (estuario bajo), la línea de puntos y rayas gris clara a TG2 (estuario medio), la línea discontinua gris clara a WQ2 (estuario alto) y la línea continua gris oscura con marcadores de puntos a la respuesta media de los tres puntos de control.

El análisis realizado mestra que el número mínimo de grupos para poder ejecutar modelos numéricos se relacionó con la peor respuesta (WQ2) siendo igual a 5×11=55 grupos (CE_r=0.6149) y el número óptimo M_om fue igual a 12×48=576 (CE_r=0.8164). Por lo tanto, el modelado numérico de procesos hidrodinámicos y de transporte podría ser simulado convenientemente (bien) con sólo 825 días (2.2602 años) y excelentemente con 8640 días (23.6712 años).

Por último, el numero mínimo de grupos (M_{mm}) de carrera de marea (TR), nivel de marea (WL) y caudal del río (Q) se representan en las figuras 75, 76 y 77 respectivamente. En todas las figuras, el título de cada subgráfico muestra la frecuencia de aparición (f) del grupo en porcentaje ($\%$) para los 40 años. Adicionalmente, cabe indicar que los subgráficos se ordenaron en orden descendente de frecuencia, empezando en la esquina superior izquierda hacia la derecha. Por su parte, en las figuras 78, 79 y 80 se muestra el numéro óptimo de grupos (M_{om}) de carrera de marea (TR), nivel de marea (WL) y caudal del río (Q) respectivamente.

En cuanto a la clasificación de la marea, el KMA propuesto clasificó la señal de marea razonablemente. Dicho KMA diferenció grupos que comenzaron en mareas muertas, vivas o medias. También diferenció la magnitud de la TR y WL durante 15 días con grupos mostrando valores menores o mayores. Por ultimó, diferenció la evolución de las mareas con grupos comenzando con un aumento de la carrera y terminando con una disminución o viceversa. Además, la frecuencia de cada grupo fue bastante similar, por ejemplo, en el caso de los 5 grupos (M_{mm}, figuras 75 y 76,) los valores oscilaron entre 18.9 y 20.8 $\%$ mientras que para 12 grupos (M_{om}, figuras 78 y 79) entre 6.9 y 10.3 $\%$. Estas frecuencias ilustran la modulación continua y determinista de la señal de marea entre muertas y vivas.

En cuanto a la clasificación del río, el KMA propuesto clasificó la señal de caudal del río correctamente. Este KMA diferenció grupos con períodos secos, períodos cuasi-estacionarios y eventos de inundación. También

Hora	a	b	c	d	e	f	R^2
TG1							
1	-3.164E-02	5.299E-04	4.313E-07	9.368E-01	-2.695E-02	-9.099E-05	0.9898
2	-2.460E-02	4.634E-04	9.358E-07	5.835E-01	-1.686E-02	-3.821E-05	0.9905
3	-1.485E-02	4.007E-04	1.333E-06	8.402E-02	8.954E-03	1.004E-04	0.9959
4	5.859E-02	4.243E-04	1.696E-06	-5.858E-01	1.145E-01	2.114E-04	0.9571
5	1.314E-01	-5.555E-04	4.062E-06	-1.105E+00	1.904E-01	5.550E-04	0.9548
6	1.442E-01	-8.194E-04	4.125E-06	-1.291E+00	1.817E-01	9.099E-04	0.9901
7	1.201E-01	-1.108E-03	4.196E-06	-1.102E+00	9.829E-02	1.002E-03	0.9924
8	5.681E-02	-5.727E-04	3.060E-06	-6.275E-01	2.252E-02	5.053E-04	0.9904
9	1.639E-02	3.711E-04	9.036E-07	-8.854E-02	-1.003E-02	7.399E-05	0.9922
10	3.862E-03	6.749E-04	-2.166E-07	4.224E-01	-2.266E-02	5.084E-05	0.9906
11	-1.289E-02	7.567E-04	-5.494E-07	8.229E-01	-2.163E-02	3.756E-05	0.9898
12	-2.992E-02	6.642E-04	-1.320E-07	1.026E+00	-2.389E-02	-7.554E-05	0.9896
TG2							
1	-3.353E-02	1.572E-03	1.876E-06	9.570E-01	-2.591E-02	-4.260E-04	0.9901
2	-2.521E-02	1.567E-03	2.439E-06	6.311E-01	-1.852E-02	-2.674E-04	0.9926
3	-3.411E-02	1.792E-03	2.428E-06	1.861E-01	4.904E-03	-1.517E-05	0.9981
4	2.102E-02	1.986E-03	2.606E-06	-4.280E-01	1.094E-01	2.126E-04	0.9911
5	7.474E-02	1.408E-03	4.428E-06	-9.400E-01	2.053E-01	5.235E-04	0.9688
6	7.419E-02	1.388E-03	4.271E-06	-1.175E+00	2.137E-01	9.359E-04	0.9910
7	1.261E-01	1.027E-03	4.225E-06	-1.218E+00	1.799E-01	1.282E-03	0.9967
8	9.093E-02	-9.176E-06	5.802E-06	-7.434E-01	3.251E-02	1.150E-03	0.9952
9	2.684E-02	1.352E-03	2.425E-06	-1.735E-01	-3.372E-02	3.903E-04	0.9946
10	1.540E-03	2.158E-03	2.538E-07	3.351E-01	-3.797E-02	-8.491E-05	0.9937
11	-1.501E-03	2.068E-03	1.413E-07	7.215E-01	-1.167E-02	-2.096E-04	0.9900
12	-2.656E-02	1.758E-03	1.107E-06	9.888E-01	-1.411E-02	-4.268E-04	0.9894
WQ2							
1	-4.707E-03	6.891E-03	1.291E-06	9.499E-01	-1.967E-02	-1.147E-03	0.9949
2	1.473E-03	7.262E-03	8.179E-07	6.670E-01	-1.984E-02	-8.205E-04	0.9975
3	-2.419E-02	8.260E-03	-1.056E-06	2.707E-01	-4.288E-03	-3.552E-04	0.9995
4	-5.337E-02	9.944E-03	-4.583E-06	-1.916E-01	4.997E-02	1.438E-04	0.9996
5	-3.085E-02	1.148E-02	-7.416E-06	-7.168E-01	1.751E-01	4.171E-04	0.9956
6	-9.446E-02	1.339E-02	-1.185E-05	-9.381E-01	1.998E-01	7.866E-04	0.9965
7	-6.501E-02	1.440E-02	-1.471E-05	-1.089E+00	2.149E-01	1.093E-03	0.9964
8	2.730E-02	1.326E-02	-1.332E-05	-9.552E-01	1.371E-01	1.365E-03	0.9955
9	9.862E-03	1.021E-02	-7.051E-06	-3.049E-01	-3.482E-02	9.893E-04	0.9966
10	4.040E-03	8.227E-03	-1.891E-06	2.594E-01	-4.891E-02	-1.443E-04	0.9994
11	1.629E-02	7.570E-03	-3.942E-07	6.429E-01	-3.992E-03	-8.139E-04	0.9969
12	2.697E-03	6.956E-03	1.066E-06	9.337E-01	-5.889E-04	-1.193E-03	0.9942

Tabla 10: Coeficientes de las funciones de ajuste (a, b, c, d, e y f) para calcular niveles de agua (WL) y coeficientes de regresión (R^2) durante una onda de marea semidiurna en TG1, TG2 y WQ2.

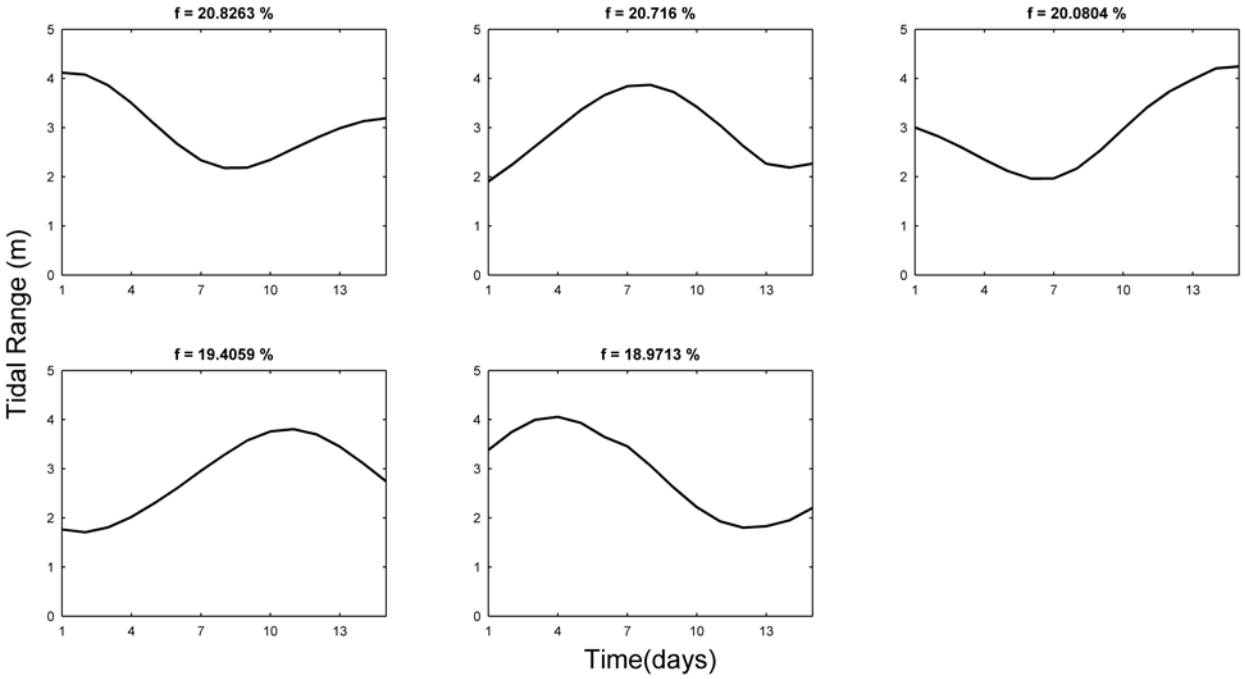

Figura 75: Número mínimo de grupos finales clasificados M_{mm} de carrera de marea donde f es la frecuencia del grupo en porcentaje.

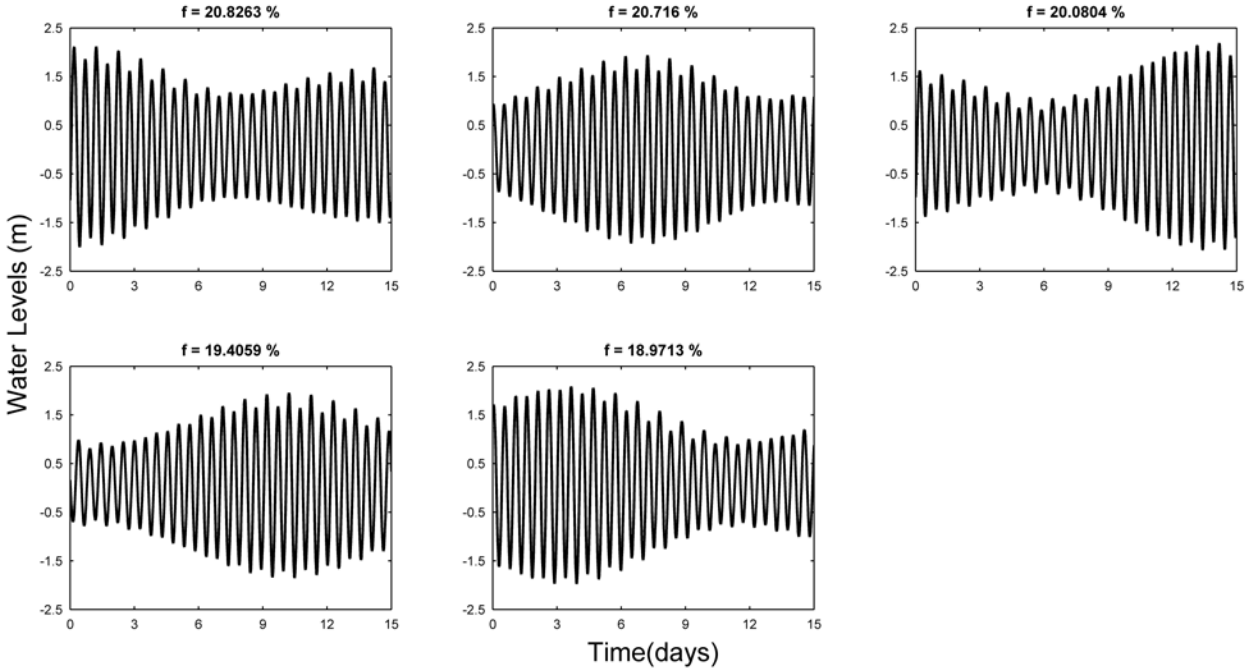

Figura 76: Número mínimo de grupos finales clasificados M_{mm} de nivel de marea donde f es la frecuencia del grupo en porcentaje.

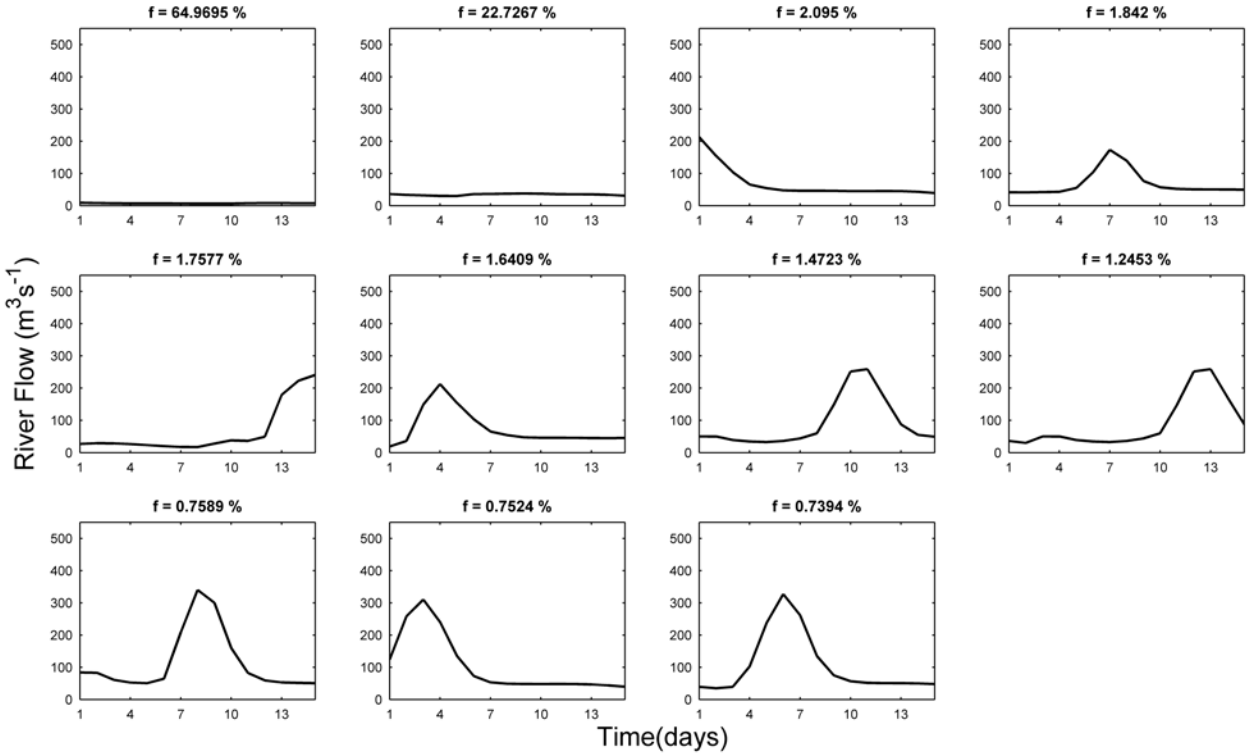

Figura 77: Número mínimo de grupos finales clasificados M_{mm} de caudal de río donde f es la frecuencia del grupo en porcentaje.

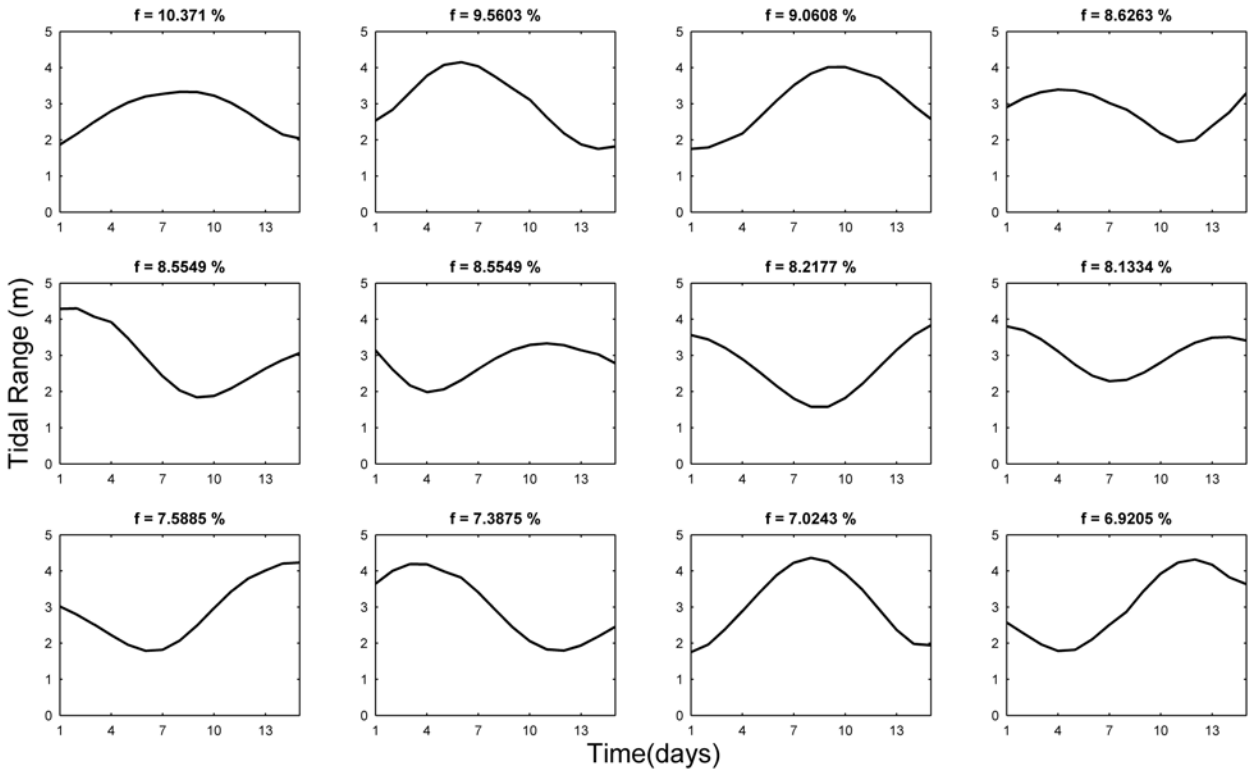

Figura 78: Número óptimo de grupos finales clasificados M_{om} de carrera de marea donde f es la frecuencia del grupo en porcentaje.

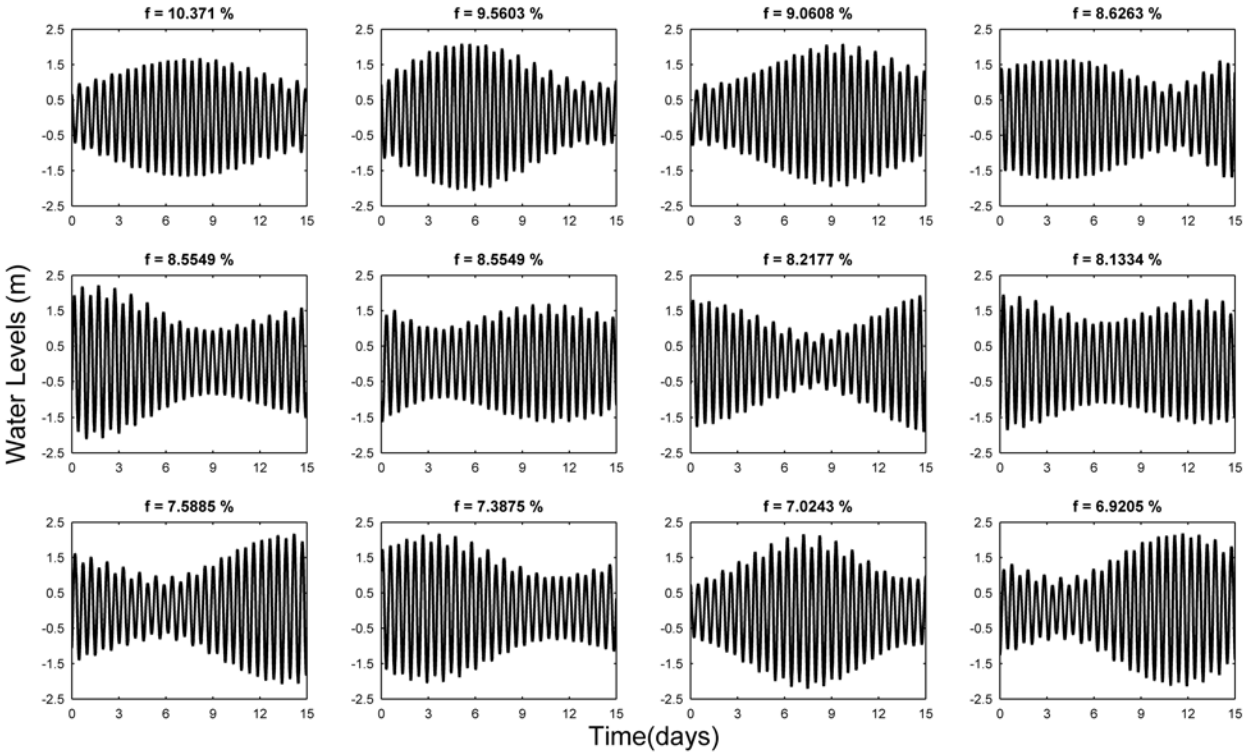

Figura 79: Número óptimo de grupos finales clasificados M_{om} de nivel de marea donde f es la frecuencia del grupo en porcentaje.

diferenció la magnitud del pico de los eventos de inundación con grupos mostrando valores en un amplio rango de caudales. Finalmente, diferenció la localización de dichos picos a lo largo de los 15 días con grupos presentando picos en cualquier día. A diferencia de la marea, la frecuencia de cada grupo fue muy diferente, en el caso de 11 grupos (M_{mm}, figure 77) los valores fluctuaron entre 64.9 y 0.7 $\%$ mientras que para los 48 grupos (M_{om}, figure 80) entre 41.4 y 0.01 $\%$. Los valores más altos de frecuencia se correspondieron con períodos secos (15 días de caudales muy bajos), los valores medios con períodos cuasi-estacionarios (15 días con caudales medios casi constantes) y los valores más bajos con eventos de inundación. Estas diferencias en las frecuencias indicaron que la señal de caudal del río presenta una variabilidad muy elevada, especialmente para los eventos de inundación. A partir de las figuras 77 y 80, se podría decir que a mayor número de grupos mejor se caracteriza las diferentes tipologías de las inundaciones.

Selección final de escenarios de modelado

El número definitivo (M) de escenarios de modelado debe estar en una ventana que abarca desde 55 hasta 576 grupos. En principio, se debe seleccionar M_{om} equivalentes a una simulación continua de 8640 días (23.6712 años), es decir, más de la mitad de los 40 años de la serie temporal (59.17 $\%$). Debido a ello, el número óptimo de simulaciones podría ser inaccesible por limitaciones computacionales (tiempo y tamaño). Por lo menos, se debe seleccionar M_{mm} para asegurar resultados válidos. Desde un punto de vista de coste computacional, dichos escenarios de modelado equivaldrían a una simulación continua de 825 días (2.2602 años) tan sólo 5.65 $\%$ de los 40 años de la serie temporal, no obstante, los resultados del modelo perderían precisión.

Teniendo en cuenta estas cuestiones, el número final de escenarios de modelado (M) se debe determinar por medio de un equilibrio entre el número de grupos, la exactitud de los resultados del modelo y los costes computacionales de estas simulaciones (véase también la figura 74). Por ello, el número final de grupos (M) debe garantizar que CE_f>0.7 y que el tiempo de simulación sea inferior al 10 $\%$ de los 40-años de serie temporal de río y marea. En el caso de SE, se seleccionaron 6(mareas)$\times$13(ríos)=78 escenarios de modelado

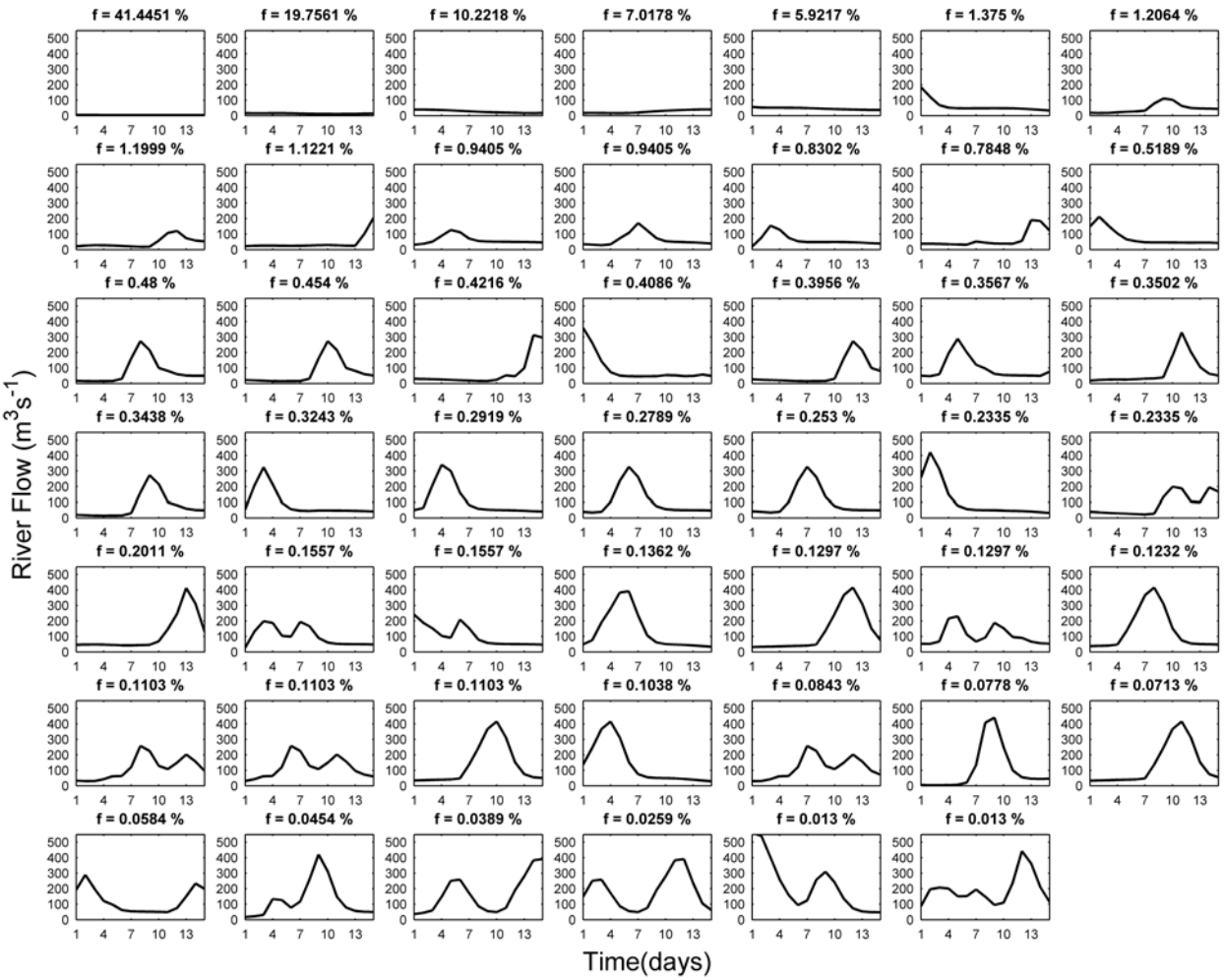

Figura 80: Número óptimo de grupos finales clasificados M_{om} de caudal de río donde f es la frecuencia del grupo en porcentaje.

correspondientes a CE_f=0.7 y CE_r=0.6747 siendo el tiempo de simulación igual a 3.2054 años (8.0135 % de 40 años).

En las figuras 81, 82 and 83 se mostraron los M grupos de TR, WL y Q respectivamente. En todas las figuras, el título de cada subgráfico indicó la frecuencia de aparición (f) del grupo en porcentaje (%) para los 40 años. Además, los subgráficos se ordenaron en orden descendente de frecuencia, empezando en la esquina superior izquierda hacia la derecha.

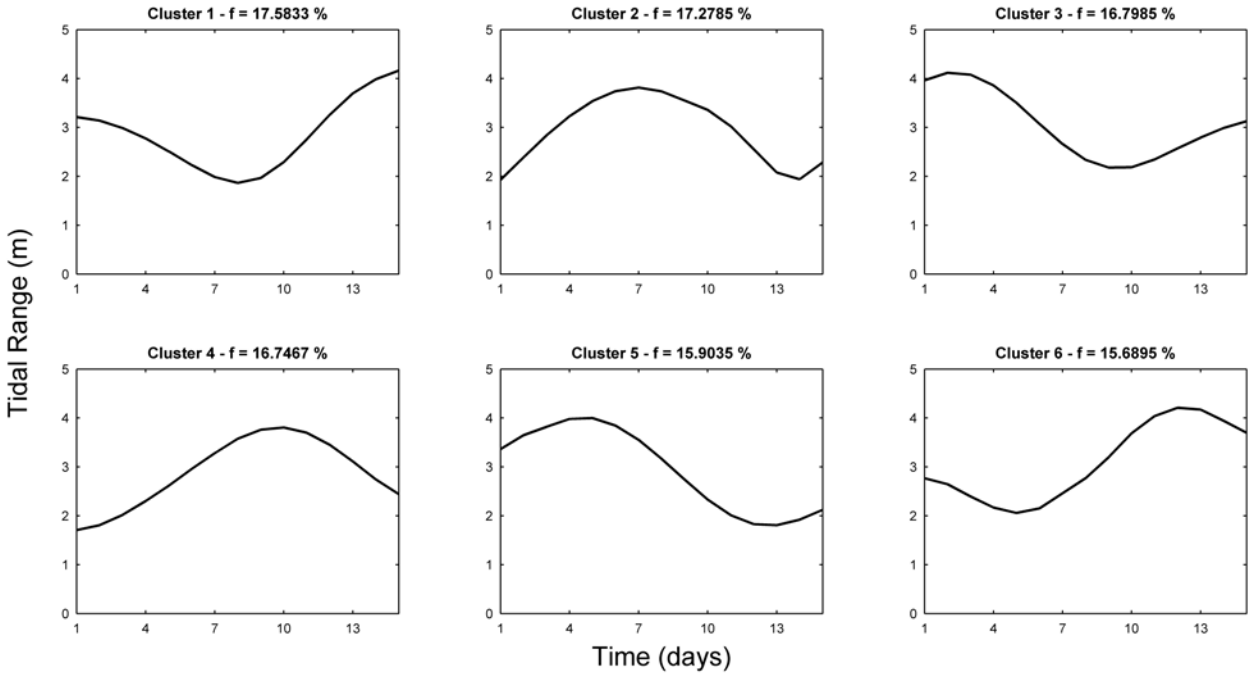

Figura 81: Grupos clasificados definitivos M para la carrera de marea donde f es la frecuencia del grupo en porcentaje.

Por último, las tablas 11 y 12 sintetizan la información de cada escenario de modelado presentando el nombre, el número de grupo de la marea y el río, la frecuencia de cada grupo de marea y río y la frecuencia final de cada escenario de modelado desde el grupo 1 hasta el 39 y del 40 al 78 respectivamente.

3.5.1.3. Modelado hidrodinámico del caso real

El tiempo necesario para estabilizar los resultados del modelo fue de 216 horas (9 días). Por lo tanto, en el cálculo detallado, se realizó la simulación hidrodinámica de los 78 escenarios de modelado asumiendo $9 + 15$ días de forzamientos. De este modo, los primeros 9 días de simulación no se tuvieron en cuenta y los 15 días siguientes de resultados del modelo hidrodinámico se registraron horariamente para cada escenario de modelo.

3.5.2. Dilución primaria o inicial (Campo cercano)

En este apartado, se realizaron los cálculos de dilución primaria para cada descarga (ID1 e ID2) empleando el modelo integral de chorro JETLAG y los mismos supuestos que en el cálculo simplificado e intermedio en cada uno de los 78 escenarios de modelado (15 días con un paso de tiempo horario). Debido al elevado número de casos, se ilustraron los resultados del caso 23 (ver figura 84) para ID1 e ID2 como ejemplo de dilución inicial.

De nuevo, en las figuras 85 y 86 se muestra la profundidad total de agua (a), la magnitud de la velocidad

Escenario Modelo	**Grupo Marea**	**Grupo Río**	**Frec (%) Marea**	**Frec (%) Río**	**Frec (%) Final**
Caso 1	1	1	17.5833	53.9564	9.4873
Caso 2	1	2	17.5833	23.5763	4.1455
Caso 3	1	3	17.5833	10.2348	1.7996
Caso 4	1	4	17.5833	2.2636	0.3980
Caso 5	1	5	17.5833	2.0690	0.3638
Caso 6	1	6	17.5833	1.2712	0.2235
Caso 7	1	7	17.5833	1.2583	0.2212
Caso 8	1	8	17.5833	1.1221	0.1973
Caso 9	1	9	17.5833	1.1026	0.1938
Caso 10	1	10	17.5833	0.8691	0.1528
Caso 11	1	11	17.5833	0.8107	0.1425
Caso 12	1	12	17.5833	0.7848	0.1380
Caso 13	1	13	17.5833	0.6810	0.1197
Caso 14	2	1	17.2785	53.9564	9.3228
Caso 15	2	2	17.2785	23.5763	4.0736
Caso 16	2	3	17.2785	10.2348	1.7684
Caso 17	2	4	17.2785	2.2636	0.3911
Caso 18	2	5	17.2785	2.0690	0.3575
Caso 19	2	6	17.2785	1.2712	0.2196
Caso 20	2	7	17.2785	1.2583	0.2174
Caso 21	2	8	17.2785	1.1221	0.1938
Caso 22	2	9	17.2785	1.1026	0.1904
Caso 23	**2**	**10**	**17.2785**	**0.8691**	**0.1501**
Caso 24	2	11	17.2785	0.8107	0.1401
Caso 25	2	12	17.2785	0.7848	0.1356
Caso 26	2	13	17.2785	0.6810	0.1176
Caso 27	3	1	16.7985	53.9564	9.0638
Caso 28	3	2	16.7985	23.5763	3.9604
Caso 29	3	3	16.7985	10.2348	1.7192
Caso 30	3	4	16.7985	2.2636	0.3802
Caso 31	3	5	16.7985	2.0690	0.3475
Caso 32	3	6	16.7985	1.2712	0.2135
Caso 33	3	7	16.7985	1.2583	0.2113
Caso 34	3	8	16.7985	1.1221	0.1885
Caso 35	3	9	16.7985	1.1026	0.1851
Caso 36	3	10	16.7985	0.8691	0.1459
Caso 37	3	11	16.7985	0.8107	0.1361
Caso 38	3	12	16.7985	0.7848	0.1318
Caso 39	3	13	16.7985	0.6810	0.1143

Tabla 11: Nombre y número de grupos de marea y río, frecuencia de los grupos de marea y río y frecuencia final para cada escenario final de modelado seleccionado M en el estuario de Suances. Cada fila muestra la configuración de cada escenario de modelado. Parte 1.

Escenario Modelo	Grupo Marea	Grupo Río	Frec (%) Marea	Frec (%) Río	Frec (%) Final
Caso 40	4	1	16.7467	53.9564	9.0359
Caso 41	4	2	16.7467	23.5763	3.9482
Caso 42	4	3	16.7467	10.2348	1.7139
Caso 43	4	4	16.7467	2.2636	0.3791
Caso 44	4	5	16.7467	2.0690	0.3465
Caso 45	4	6	16.7467	1.2712	0.2128
Caso 46	4	7	16.7467	1.2583	0.2106
Caso 47	4	8	16.7467	1.1221	0.1879
Caso 48	4	9	16.7467	1.1026	0.1845
Caso 49	4	10	16.7467	0.8691	0.1455
Caso 50	4	11	16.7467	0.8107	0.1357
Caso 51	4	12	16.7467	0.7848	0.1314
Caso 52	4	13	16.7467	0.6810	0.1140
Caso 53	5	1	15.9035	53.9564	8.5809
Caso 54	5	2	15.9035	23.5763	3.7494
Caso 55	5	3	15.9035	10.2348	1.6277
Caso 56	5	4	15.9035	2.2636	0.3599
Caso 57	5	5	15.9035	2.0690	0.3291
Caso 58	5	6	15.9035	1.2712	0.2021
Caso 59	5	7	15.9035	1.2583	0.2001
Caso 60	5	8	15.9035	1.1221	0.1784
Caso 61	5	9	15.9035	1.1026	0.1753
Caso 62	5	10	15.9035	0.8691	0.1382
Caso 63	5	11	15.9035	0.8107	0.1289
Caso 64	5	12	15.9035	0.7848	0.1248
Caso 65	5	13	15.9035	0.6810	0.1082
Caso 66	6	1	15.6895	53.9564	8.4654
Caso 67	6	2	15.6895	23.5763	3.6990
Caso 68	6	3	15.6895	10.2348	1.6057
Caso 69	6	4	15.6895	2.2636	0.3551
Caso 70	6	5	15.6895	2.0690	0.3246
Caso 71	6	6	15.6895	1.2712	0.1994
Caso 72	6	7	15.6895	1.2583	0.1973
Caso 73	6	8	15.6895	1.1221	0.1761
Caso 74	6	9	15.6895	1.1026	0.1729
Caso 75	6	10	15.6895	0.8691	0.1363
Caso 76	6	11	15.6895	0.8107	0.1271
Caso 77	6	12	15.6895	0.7848	0.1231
Caso 78	6	13	15.6895	0.6810	0.1068

Tabla 12: Nombre y número de grupos de marea y río, frecuencia de los grupos de marea y río y frecuencia final para cada escenario final de modelado seleccionado M en el estuario de Suances. Cada fila muestra la configuración de cada escenario de modelado. Parte 2.

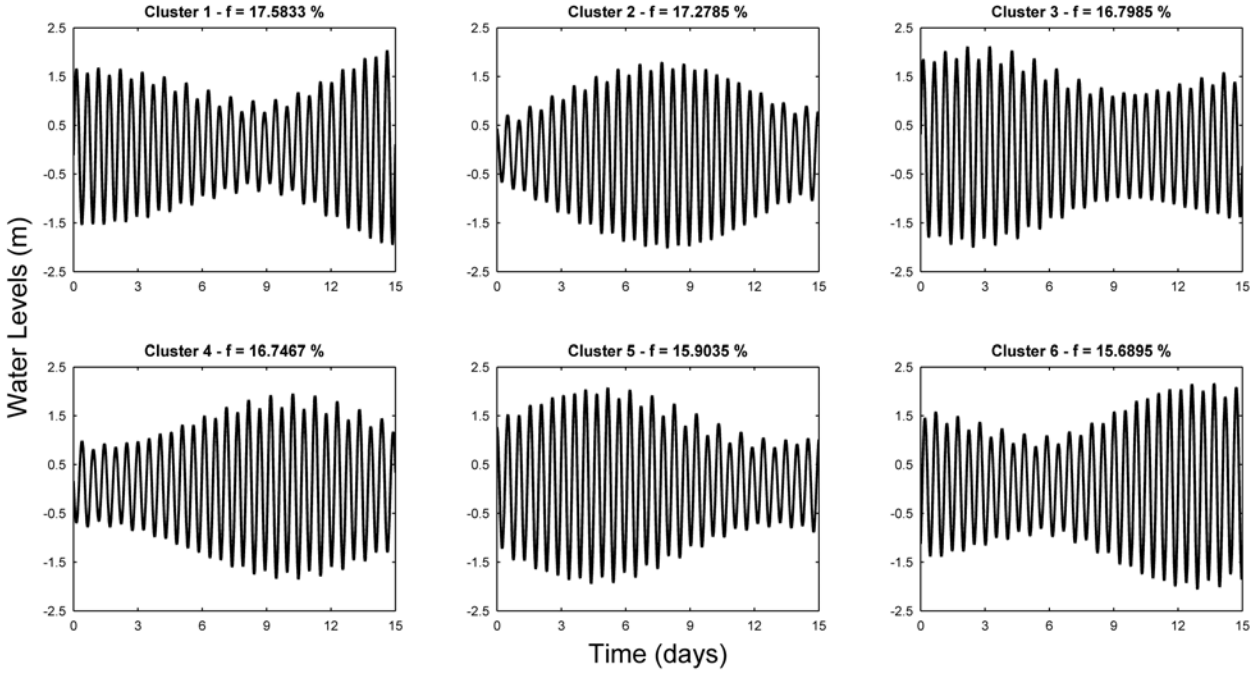

Figura 82: Grupos clasificados definitivos M para el nivel de marea donde f es la frecuencia del grupo en porcentaje.

ambiental (b), la dirección de la velocidad ambiental (c) y la densidad ambiental (d) para la capa superficial (línea azul) y la capa de fondo (línea verde) en ID1 e ID2 durante el "caso real 23 de dilución" respectivamente. Además, ambas figura presentan la dilución inicial (e) del efluente (línea negra) y la concentración del efluente (f) al final del campo cercano (línea negra). Finalmente, en la figura 85 se indica la AA-EQS (línea magenta) del cloroformo ($CHCl_3$) mientras que, en la figura 86 la AA-EQS (línea magenta) y la MAC-EQS (línea roja) del plomo (Pb).

Como se muestra en las figuras 85 y **??**, la dilución de la descarga ID1 osciló entre 47.89 y 2.69 mientras que la dilución de la descarga ID2 entre 6625.84 y 53.13 debido a los cambios en las condiciones ambientales. La dilución de ambas descargas fue directamente proporcional a la serie temporal del caudal del río (ver figura 84). En cuanto a la concentración en ID1 e ID2, la AA-EQS no se superó durante el evento de inundación mientras que, para el resto de la simulación, la AA-EQS se superó aproximadamente durante el 40 % y el 10 % del tiempo respectivamente. Por su parte, la MAC-EQS no se superó para ID2 durante las 360 horas del "caso real 23 de dilución" a excepción de unas horas.

3.5.3. Acople de la dilución primaria a la secundaria (Campo intermedio)

En este apartado, se llevó a cabo el acoplamiento entre el modelo de campo cercano (JETLAG) y el modelo de campo lejano (D-Water Quality) del mismo modo que para el Paso 3 y 4. Una vez que se recogió toda la información requerida, se aplicó el método a los vertidos ID1 e ID2 para el "caso real de dilución" (78 escenarios de modelado de 15 días con una resolución temporal horaria). De nuevo, como ejemplo del campo intermedio se ilustraron los resultados de caso 23 (ver figura 84) para ID1 e ID2.

Las figuras 87 y 88 presentan el porcentaje de tiempo que el final de campo cercano para los efluentes industriales ID1 e ID2 estuvieron en diferentes celdas de la malla (panel izquierdo) y capas verticales (panel derecho) para el "caso real 23 de dilución". En estas localizaciones, se introdujeron ID1 e ID2 como un término fuente de caudal y concentración diluida.

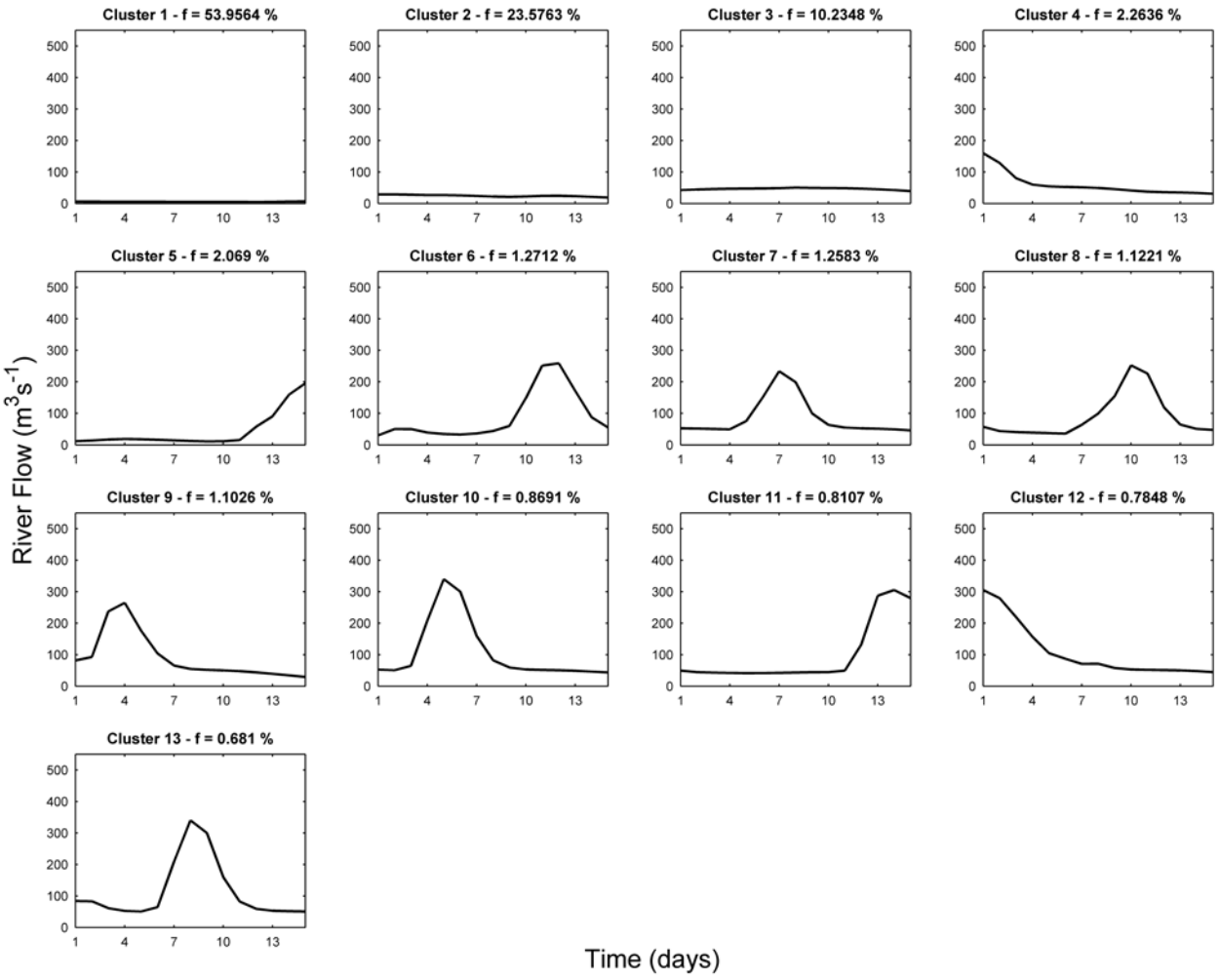

Figura 83: Grupos clasificados definitivos M para el caudal de río donde f es la frecuencia del grupo en porcentaje.

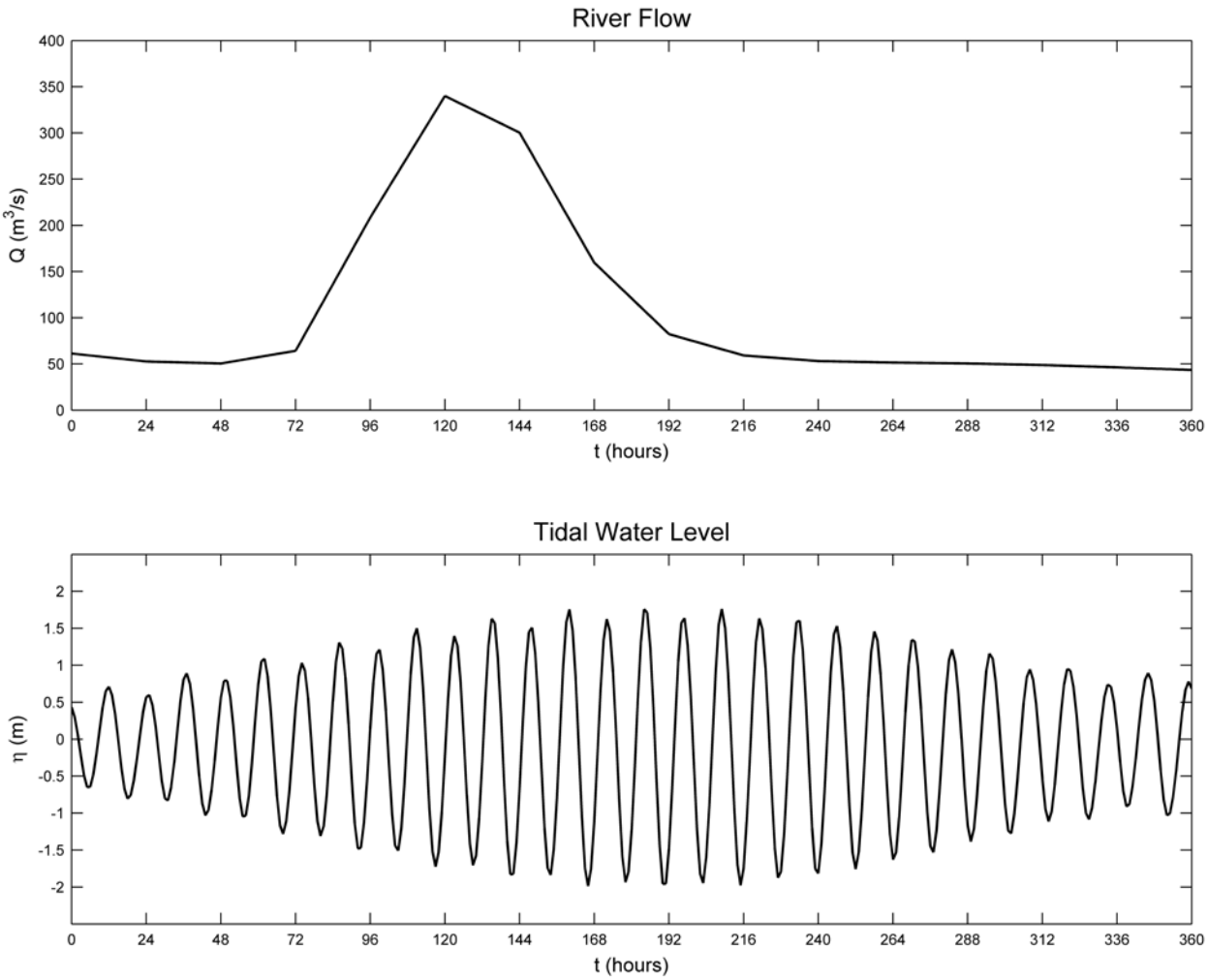

Figura 84: 15-días de serie temporal de forzamientos para el caso 23.

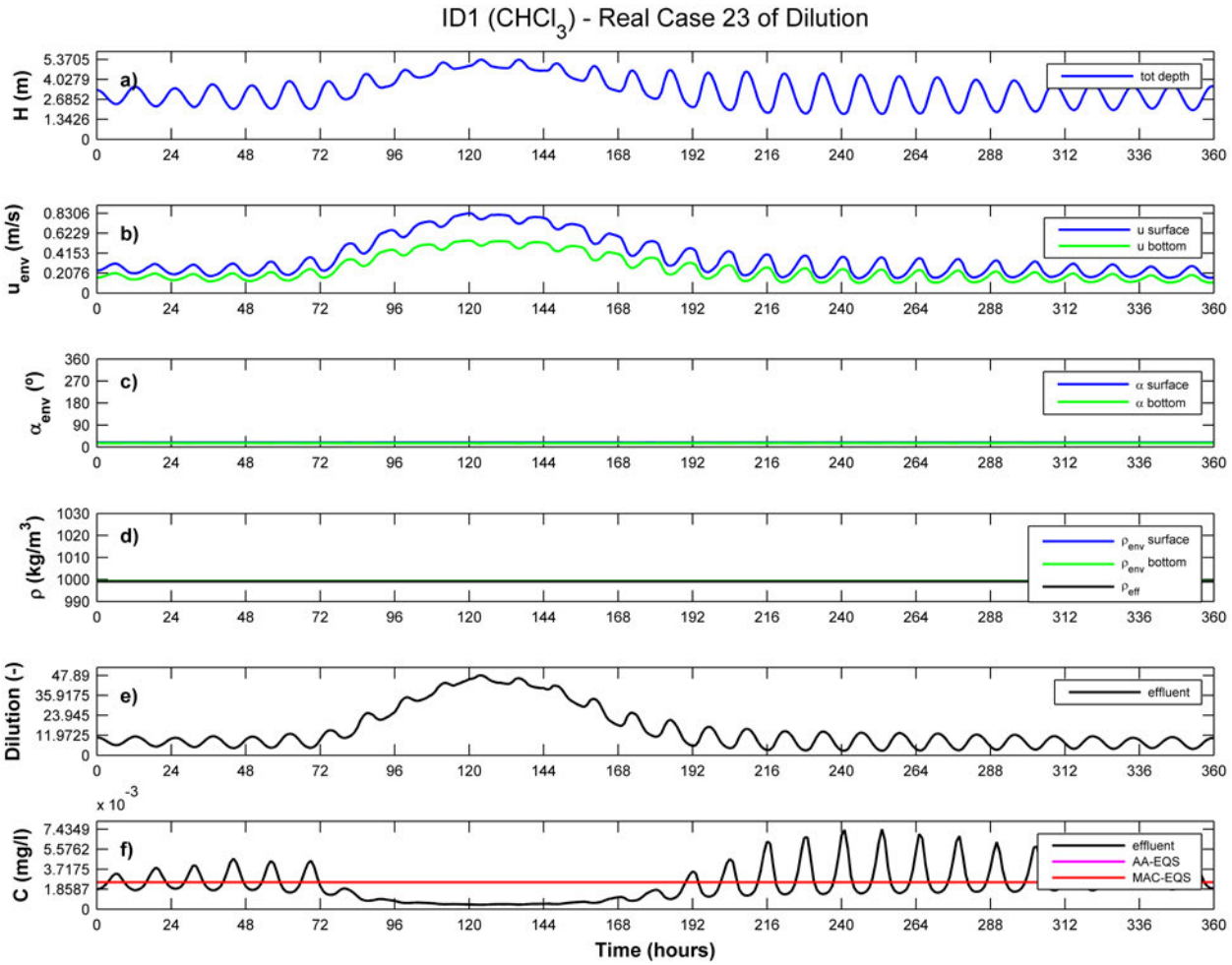

Figura 85: Evolución de la profundidad total de agua (a), la magnitud de la velocidad ambiental (b), la dirección de la velocidad ambiental (c) y la densidad ambiental (d) para la capa superficial (línea azul) y la capa de fondo (línea verde), la dilución inicial (e) del efluente (línea negra) y la concentración del efluente (f) al final del campo cercano (línea negra) en ID1 durante el "caso real 23 de dilución". Además se indica la AA-EQS (línea magenta) del cloroformo (f).

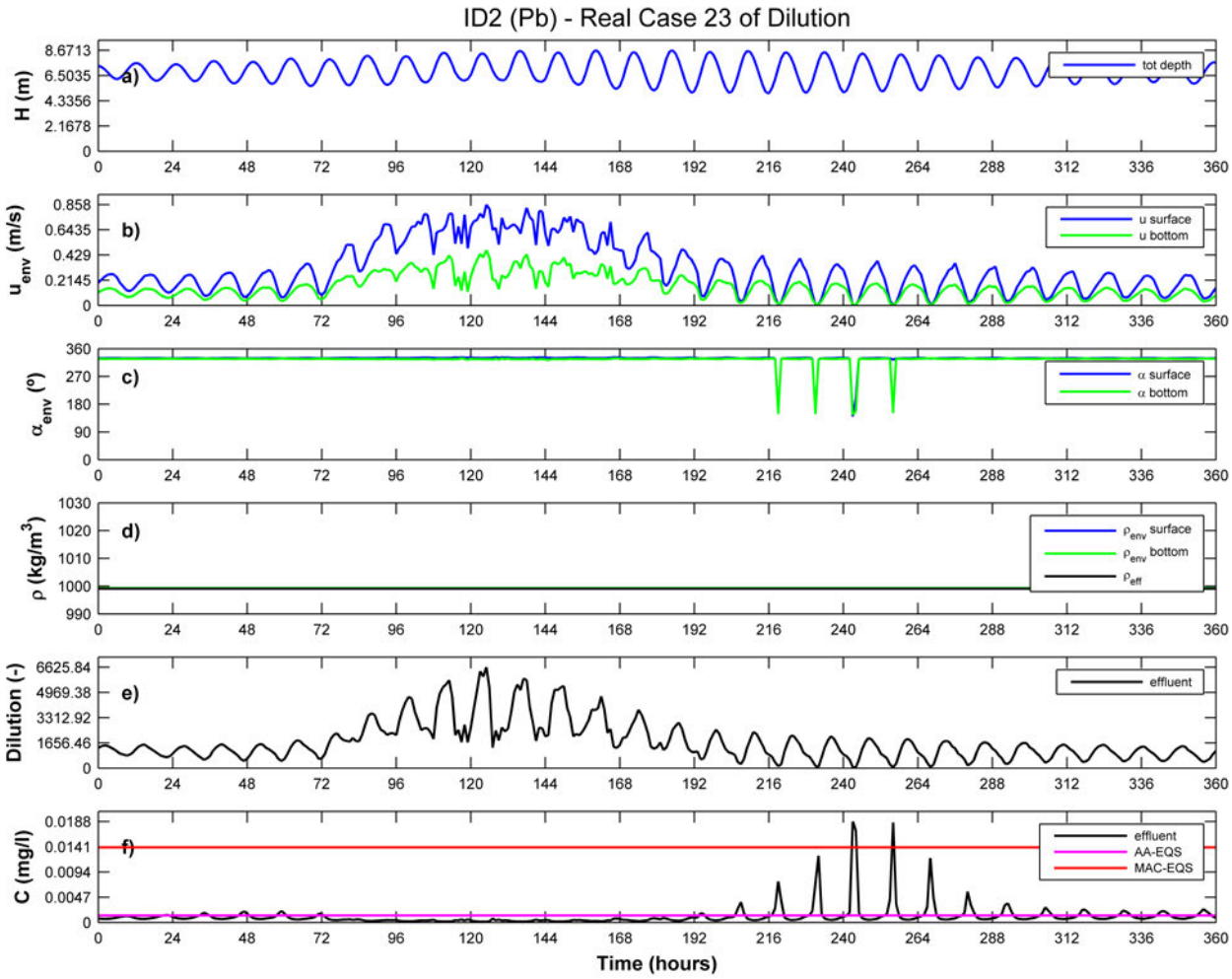

Figura 86: Evolución de la profundidad total de agua (a), la magnitud de la velocidad ambiental (b), la dirección de la velocidad ambiental (c) y la densidad ambiental (d) para la capa superficial (línea azul) y la capa de fondo (línea verde), la dilución inicial (e) del efluente (línea negra) y la concentración del efluente (f) al final del campo cercano (línea negra) en ID2 durante el "caso real 23 de dilución". Además se indica la AA-EQS (línea magenta) y la MAC-EQS (línea roja) del plomo (f).

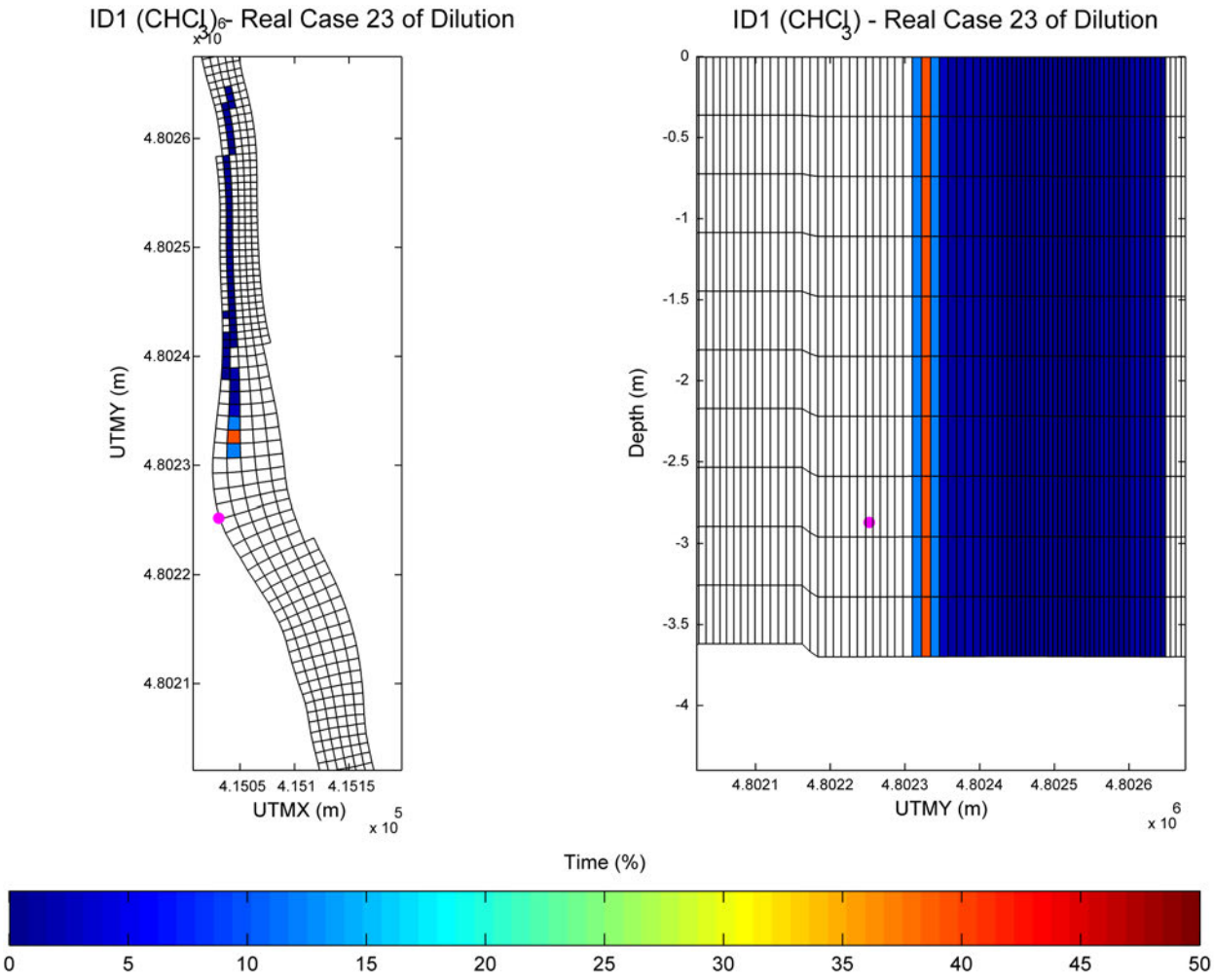

Figura 87: Vista esquemática de la distribución del tiempo de las celdas horizontales de la malla (panel izquierdo) y las capas verticales (panel derecho) cubiertos por ID1 durante el acoplamiento entre la dilución primaria y secundaria en el cálculo detallado (caso 23).

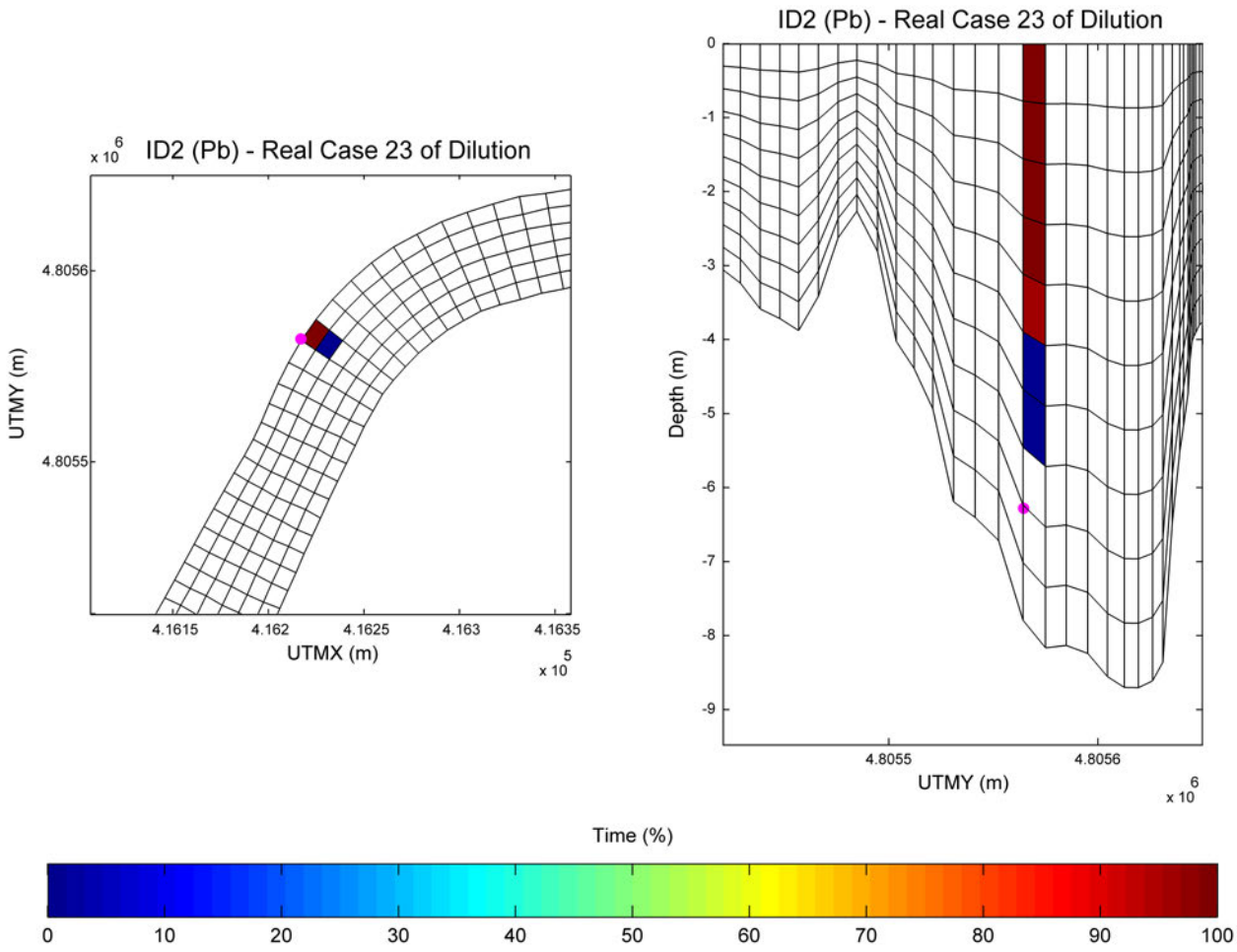

Figura 88: Vista esquemática de la distribución del tiempo de las celdas horizontales de la malla (panel izquierdo) y las capas verticales (panel derecho) cubiertos por ID2 durante el acoplamiento entre la dilución primaria y secundaria en el cálculo detallado (caso 23).

Fecha	Pb en WQ3	Pb en WQ6	$CHCl_3$ en WQ3	$CHCl_3$ en WQ6
23/06/2008	0.0050	0.0400	0.0004	0.0002
29/08/2008	-	0.0050	-	0.0003
12/11/2008	-	0.0010	-	0.0003

Tabla 13: Fecha y concentraciones de las medidas efectuadas durante la campaña de campo (IHCantabria 2008a).

Como se muestra en la figura 87, el acoplamiento ID1 se localizó en varias celdas horizontales aguas abajo del punto de descarga en este caso 23. En la dirección vertical, el vertido ID1 se mezcló completamente en vertical la mayor parte del tiempo. Como se puede observar en la figura 66, el final del campo cercano para ID2 se localizó en el punto de descarga debido a que la flotabilidad y el caudal fueron relativamente pequeños. Respecto a la distribución vertical, el vertido ID2 estuvo la mayor parte del tiempo entre las capas 1 y 5, es decir, entre 0 y 3.5 m de profundidad en el caso 23 ilustrando que la pluma emerge hasta alcanzar la superficie libre en el caso 23.

3.5.4. Dilución secundaria o ambiental (Campo lejano): Enfoque no conservativo

En esta sección, se describe la aplicación de la metodología para la simulación de los vertidos ID1 e ID2 suponiendo un comportamiento no conservativo de los tóxicos. Cabe recordar que el modelo de transporte no conservativo se basa en el modelo conceptual (procesos e interacciones) descrito en la figura 31.

3.5.4.1. Información adicional

Esta información se obtuvo a partir de dos fuentes: dos campañas de campo (CMA 2006-2007, IHCantabria 2008a) y la Red de Control de Calidad Litoral en Cantabria (IHCantabria 2012).

Campañas de campo

La Consejería de Medio Ambiente del Gobierno de Cantabria realizó una campaña de campo (CMA 2006-2007) en el contexto de los trabajos de inspección de los vertidos desde tierra al mar en Cantabria. La campaña se llevó a cabo durante 2006 y 2007 y se centró en la recogida de medidas de sustancias tóxicas contenidas en las descargas industriales de Cantabria. En esta tesis, se utilizaron las medidas disponibles de cloroformo y la concentración de carbono orgánico particulado para ID1 y de plomo así como la concentración de sólidos en suspensión para ID2 (ver figura 41).

El IH Cantabria efectúo otra campaña de campo (IHCantabria 2008a) durante el estudio del análisis preliminar para la detección de sustancias prioritarias en las aguas costeras de Cantabria. La campaña se llevó a cabo en tres fechas: 23/06/2008, 29/08/2008 y 12/11/2008 y en dos localizaciones WQ3 y WQ6 (ver figura 48). La tabla 13 sintetiza todas las medidas disponibles de $CHCl_3$ y Pb en el SE (mg/l).

Red de Control de Calidad Litoral en Cantabria

Los datos seleccionados de la Red de Control de Calidad Litoral en Cantabria incluyeron mediciones de sólidos en suspensión (SS) y de la fracción en peso de carbono orgánico total en los sólidos en suspensión (f_{OC}) desde el año 2006 hasta el 2013.

3.5.4.2. Configuración del modelo

En primer lugar, se ejecutó Delft3D-FLOW desde 01/06/2008 hasta 01/12/2008 (6 meses) con los parámetros calibrados, los caudales fluviales y los niveles de agua de este período.

A continuación, los contornos cerrados se especificaron con un flujo difusivo nulo. El flujo difusivo vertical de tóxico a través de la superficie libre y de fondo se determinaron con los procesos específicos, es decir, la volatilización ($CHCl_3$) y la sedimentación ($CHCl_3$ y Pb). Los contornos abiertos de ambas sustancias tóxicas

se ajustaron a cero (ver figura 89). El modelo utiliza la concentración de carbono orgánico particulado (POC) por lo que se asumió que POC=$SS \times f_{OC}$ (mg/l). Se definieron cuatro contornos abiertos para SS y POC (superior, inferior y dos laterales):

- En la condición de contorno superior, SS y POC (f_{OC}) se establecieron constantes e iguales al promedio de todas las mediciones disponibles en WQ15, es decir, 7.989 y 0.7787 (9.74 %) mg/l respectivamente.
- Las condiciones de contorno laterales fueron las mismas que las del contorno superior para todas las variables.
- La condición inferior se generó mediante una regresión a una función potencial que relaciona la concentración de sólidos en suspensión con el caudal del río (ecuación (36)).

$$SS(Q) = a_S \cdot Q^{b_S} \tag{36}$$

  donde a_S y b_S son valores empíricos específicos de cada río determinados por regresión.

  A partir de la ecuación (36), se ajustó una función potencial con la serie temporal del río y las medidas disponibles en WQ1 (IHCantabria 2012). La función potencial fue $SS = 0{,}0269 \cdot Q^{1{,}5773}$ y el coeficiente de regresión (R^2) de 0.8997.

  SS y POC (f_{OC}) se modelaron mediante la imposición de un perfil tridimensional utilizando las serie de caudales del río para el período de calibración y la función potencial entre Q y SS. Debido a que la variación temporal fue significativa, ambas variables se establecieron como una serie temporal diaria con un perfil constante de SS y POC (f_{OC}).

Las condiciones iniciales fueron mapas con valores constantes (Figura 89) de modo que se especificó una concentración igual a 0 mg/l para ambos tóxicos, una concentración de 8.886 mg/l para los sólidos en suspensión (utilizado en el modelo de Pb) y una concentración de 0.8662 (9.74 %) mg/l para el POC (utilizado en el modelo $CHCl_3$). Además, cabe indicar que los valores impuestos de SS y POC fueron el promedio de todos los datos disponibles durante el periodo de calibración en el dominio del modelo.

Como consecuencia de la inicialización con un campo nulo de concentraciones de tóxicos, la duración mínima de una simulación de campo lejano para asegurar que las condiciones iniciales no influencian los resultados del modelo es la escala de tiempo del "caso peor de dilución" siendo 528 horas (22 días).

Para llevar a cabo esta calibración, se utilizaron los datos de la campaña de campo (IHCantabria 2008a) en el período de 01/06/2008 a 01/12/2008 (6 meses). Los parámetros físicos se calibraron en el Paso 3 y los parámetros numéricos fueron los mismos empleados en el Paso 3 y 4. En el caso de los parámetros físico-químicos, la mayoría de ellos se obtuvieron a partir de estudios previos en la zona (Gómez 2010, Sámano *et al.* 2014) y bases de datos a excepción del coeficiente de pérdida por temperatura.

Debido a la escasez de datos de sustancias tóxicas (Tabla 13), en lugar de determinar medidas de error, se efectuó una calibración cualitativa. La configuración final del modelo fue la combinación de todos los parámetros mencionados en la tabla 14.

En las figuras 90 y 91 se presenta la comparación entre los datos observados en WQ3 (panel superior) y WQ6 (panel inferior) con los resultados del modelo de plomo y cloroformo, respectivamente. Como se puede observar, se obtuvo un buen ajuste entre las concentraciones pronosticadas por el modelo y los datos observados en ambas estaciones tanto para el plomo como el cloroformo.

3.5.4.3. Modelado del transporte del caso real

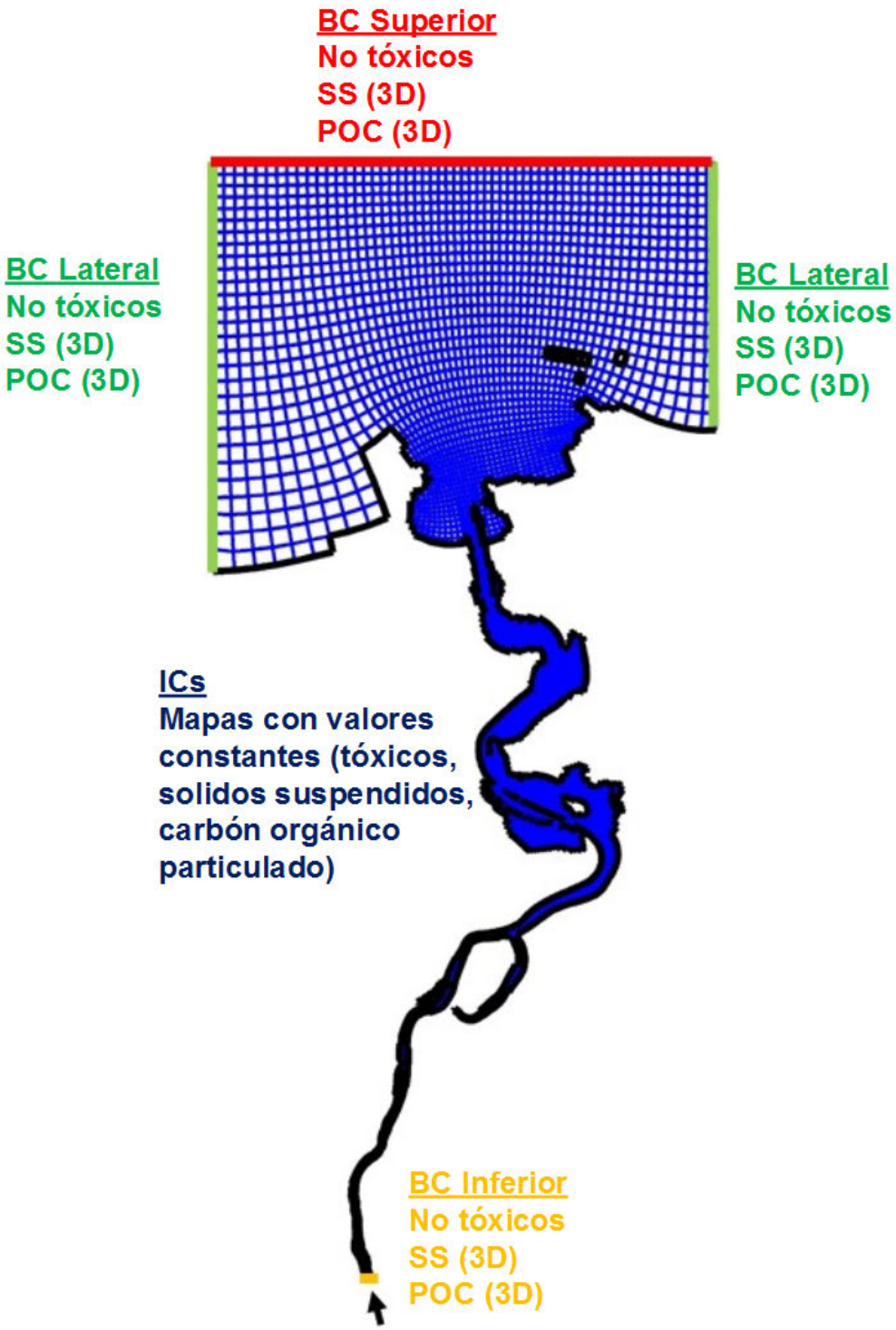

Figura 89: Vista esquemática de las condiciones de contorno e iniciales impuestas durante las simulaciones de transporte no conservativo.

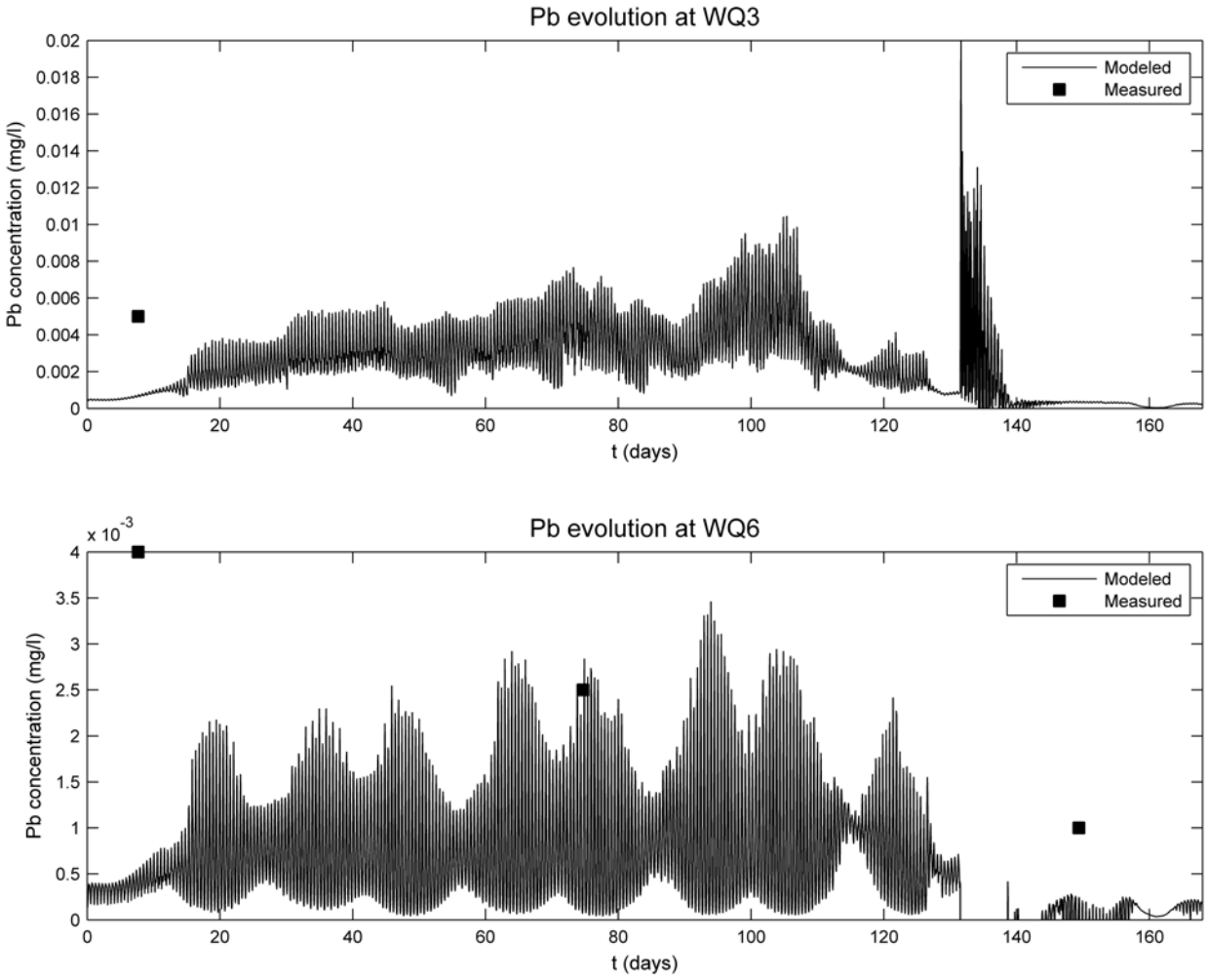

Figura 90: Comparación entre las concentraciones medidas y modeladas de plomo en los puntos de muestreo WQ3 (panel superior) y WQ6 (panel inferior).

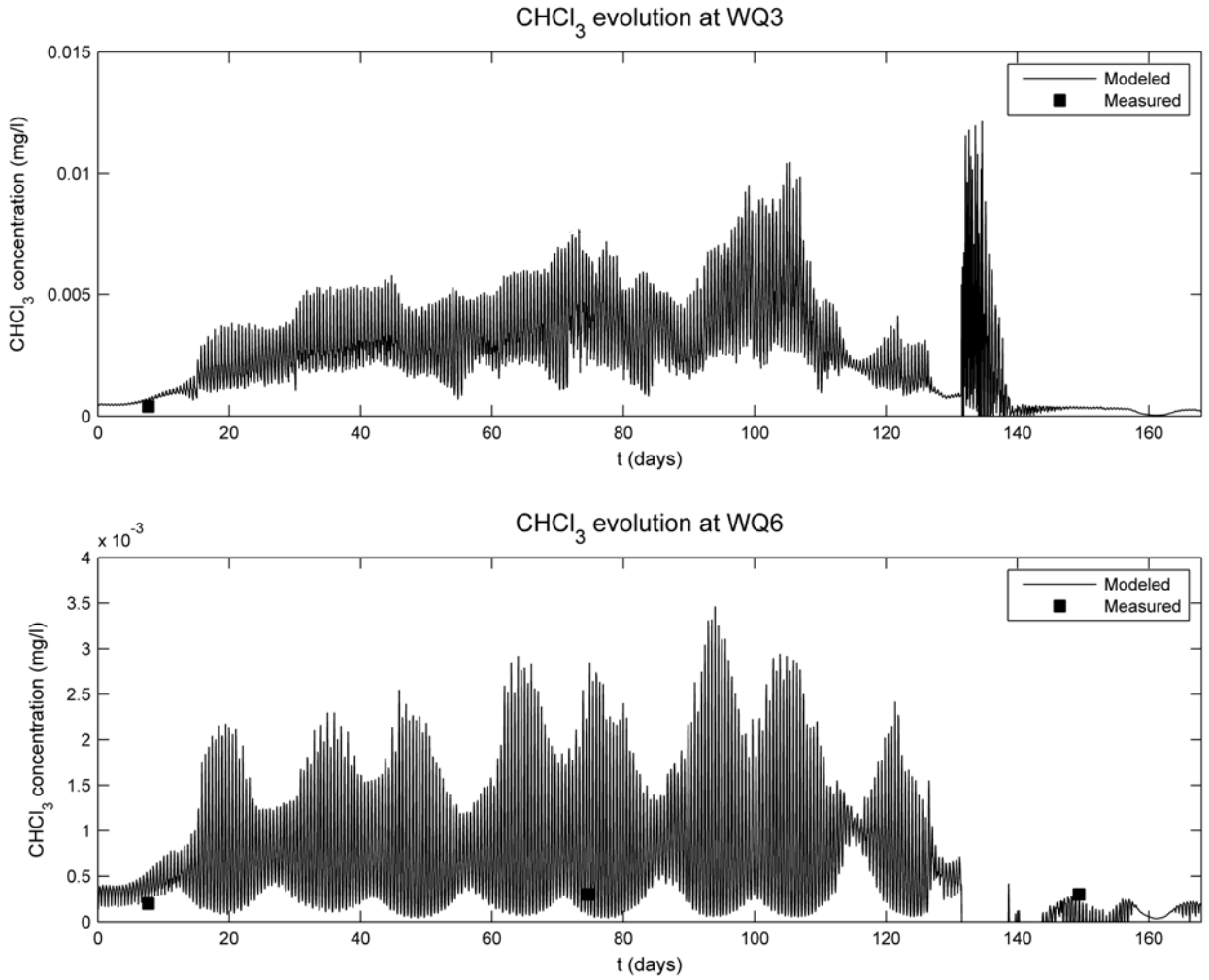

Figura 91: Comparación entre las concentraciones medidas y modeladas de cloroformo en los puntos de muestreo WQ3 (panel superior) y WQ6 (panel inferior).

Parámetros físicos	**Valores calibrados**
Todos los parámetros	Calibración hidrodinámica
Parámetros fisicoquímicos (Pb)	**Valores calibrados**
Velocidad de sedimentación de materia inorgánica	31.968 m/día
Tensiones tangenciales de fondo	Importado de hidrodinámica
Tensión tangencial crítica para sedimentación	0.0635 N/m^2
Coeficiente de partición	398 m^3/kg
Tiempo medio de adsorción y desorción	Cero
Parámetros fisicoquímicos ($CHCl_3$)	**Valores calibrados**
Velocidad de sedimentación de materia orgánica	31.968 m/día
Tensiones tangenciales de fondo	Importado de hidrodinámica
Tensión tangencial crítica para sedimentación	0.0635 N/m^2
Coeficiente de partición	18.52 l/kg
Coeficiente de transferencia para fase líquida	Mapa (espacial y temporal)
Coeficiente de transferencia para fase gas	Mapa (espacial y temporal)
Constante de Henry	3536.24 Pa/m^3/mol
Tasa constante de degradación global	0.008184 día^{-1}
Temperatura ambiente del agua	Importado de hidrodinámica
Coeficiente de pérdida por temperatura	1.07
Parámetros numéricos	**Valores calibrados**
Todos los parámetros	Calibración conservativo

Tabla 14: Parámetros óptimos de calibración del modelo de campo lejano de Pb y $CHCl_3$ (enfoque no conservativo) para el Estuario de Suances.

Con el fin de estabilizar los resultados del modelo y disminuir la influencia de las condiciones iniciales, se realizaron 78 "presimulaciones" para obtener la condición inicial adecuada de concentración de tóxico y otras 78 "simulaciones" para registrar la evolución de la concentración a lo largo de cada escenario de modelado.

"Presimulaciones"

Como se mencionó anteriormente, el tiempo de respuesta "cuasi-estacionaria" para el transporde del "caso peor de dilución" indica la duración mínima de cualquier "presimulación" siendo de 528 horas (22 días). Las condiciones de contorno e iniciales se muestran en la figura 89 donde los contornos cerrados fueron los mismos definidos en la calibración del modelo, los contornos abiertos para los tóxicos se ajustaron a cero y los contornos abiertos para SS y POC fueron nuevamente cuatro:

- En la condición de contorno superior, SS y POC (f_{OC}) se modelaron otra vez mediante la imposición de un perfil tridimensional constante e igual al promedio de todas las mediciones en WQ15, es decir, 8.978 and 0.6105 (6.80 %) mg/l respectivamente.
- Las condiciones de contorno laterales fueron las mismas que las del contorno superior para todas las variables.
- La condición inferior se generó mediante la función potencial ajustada $SS = 0{,}0269 \cdot Q^{1{,}5773}$. Por tanto, SS and POC (f_{OC}) se modelaron mediante una serie temporal diaria con un perfil constante de SS y POC (f_{OC}).

Para efectuar la simulación de los 78 escenarios de modelado, las condiciones iniciales fueron mapas con valores constantes (Figura 89) siendo el promedio de todas las medidas disponibles en el dominio del modelo. Así, se especificó una concentración igual a 0 mg/l para ambos tóxicos, una concentración de 11.013 mg/l

para los sólidos en suspensión (utilizado en el modelo de Pb) y una concentración de 0.7489 (6.80 %) mg/l para el POC (utilizado en el modelo $CHCl_3$).

Las 78 "presimulaciones" se llevaron a cabo utilizando un caudal constante de río igual al primer día de cada escenario de modelado y su marea asociada durante 24 horas. A continuación, se ejecutó D-Water Quality para ID1 e ID2 con los resultados de Delft3D-FLOW del primer día en un bucle continuo durante 30 días en cada escenario de modelado. Una vez que se alcanzó la respuesta 'cuasi-estacionaria, se registró el mapa de la concentración de las sustancias estudiadas coincidente con la primera hora de los 78 escenarios.

En la figura 92, se presentan los mapas de la distribución espacial de cloroformo y POC en la superficie (a-c) y el fondo (b-d) utilizados como condición inicial para la "simulación" del "caso real 23 de dilución" de ID1, respectivamente. Por otro lado, la figura 93 muestra los mapas de la distribución espacial de plomo y SS en la superficie (a-c) y el fondo (b-d) utilizados como condición inicial para la "simulación" del "caso real 23 de dilución" de ID2, respectivamente.

"Simulaciones"

Los contornos cerrados y abiertos fueron los mismos que en las "presimulaciones" mientras que las condiciiones inciales fueron dos mapas (10 capas) con la concentración obtenida en las 78 "presimulaciones". A continuación, se ejecutaron los 78 escenarios de modelado y se guardaron horariamente 15 días de resultados de transporte, esto es, la evolución de la concentración de tóxico para ID1 (cloroformo) e ID2 (plomo) en el SE.

A modo de ejemplo, en las figuras 94 y 95 se incluye la evolución de las sustancias modeladas en WQ3 (a), SS1 (b), SS3 (c) and SS5 (d) para ID1 (cloroformo) e ID2 (plomo) durante el "caso real 23 de dilución", respectivamente. En dichas figuras, la línea negra representa la capa superficial y la línea gris la de fondo.

3.5.4.4. Delimitación de las zonas de mezcla

En el cálculo detallado, se ejecutaron 78 escenarios en condiciones reales con una probabilidad de ocurrencia. Después de las "simulaciones", se determinó la AA-MZ y MAC-MZ aplicando el método desarrollado (Figura 34).

Validación de las series reconstruidas

En primer lugar, se realizó la simulación continua del tóxico teniendo en cuenta la "serie real" de caudales y elevaciones de marea a partir de 01/06/2008 hasta 01/12/2008 (período de calibración del enfoque no conservativo). Este período se eligió porque abarca diferentes grupos de marea y combina períodos secos y húmedos de caudales, es decir, dicho período fue un buen descriptor de la variabilidad ambiental de los forzamientos.

En segundo lugar, se buscaron entre los 78 escenarios los casos que mejor ajustaron a cada segmento (15 días) de la "serie real" en el período de 6 meses. En tercer lugar, se reconstruyó la evolución de las 10 capas de concentración del cloroformo y el plomo a partir de los escenarios de modelado seleccionados.

Por último, se comparó la "serie real" (datos proporcionados por el modelo de transporte) frente a la "serie sintética" (datos porpocionados por la secuenciación de grupos) con el fin de garantizar que los resultados obtenidos con "series sintéticas" son adecuados. Para ello, se calcularon como medidas de error para ID1 e ID2: el CE, el BIAS, la concentración media y el tiempo de superación de la MAC-EQS en ambas series.

Como ejemplo de la validación se ilustra en las figuras 96 y 97 la evolución de la concentración media diaria de cloroformo (ID1) y de plomo (ID2) para la "serie real" en color negro y la "serie sintética" en color gris durante el período de validación. En ambas figuras, los paneles (a, b y c) corresponden a la superficie, la capa media y el fondo en el punto de vertido ID1 e ID2, respectivamente. Mientras tanto, los paneles (d, c y e) representan la capa superficial, intermedia e inferior en SS5.

La tabla 15 resume las medidas de error para ID1 a tres profundidades en ID1, SS1 y TG1 mientras que, en

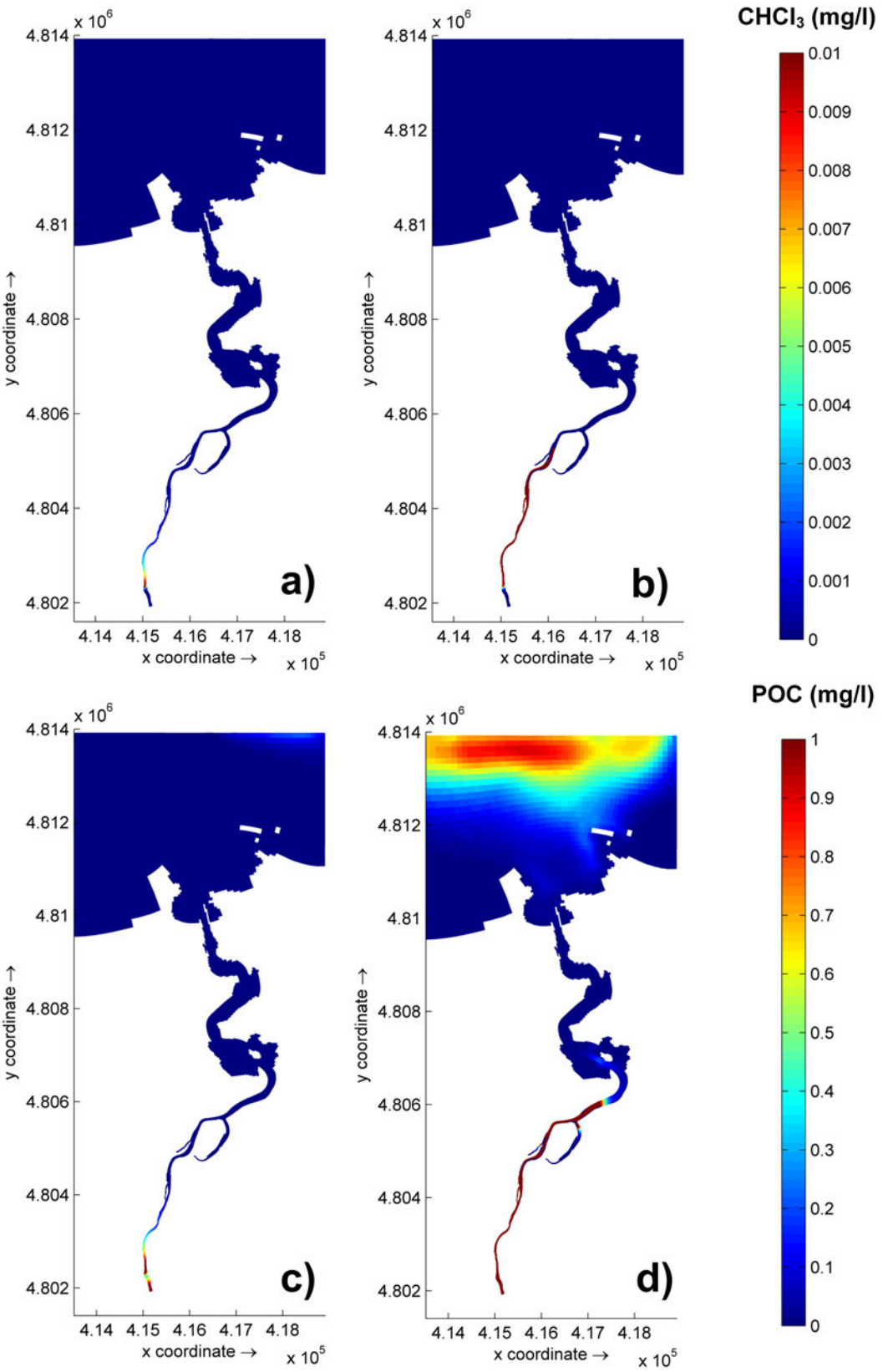

Figura 92: Mapa de la distribución espacial de cloroformo y POC utilizado como condición inicial para la "simulación" del "caso real 23 de dilución" de ID1. Capa superficial de $CHCl_3$ (a), capa de fondo de $CHCl_3$ (b), capa superficial de POC (c) y capa de fondo de POC (d).

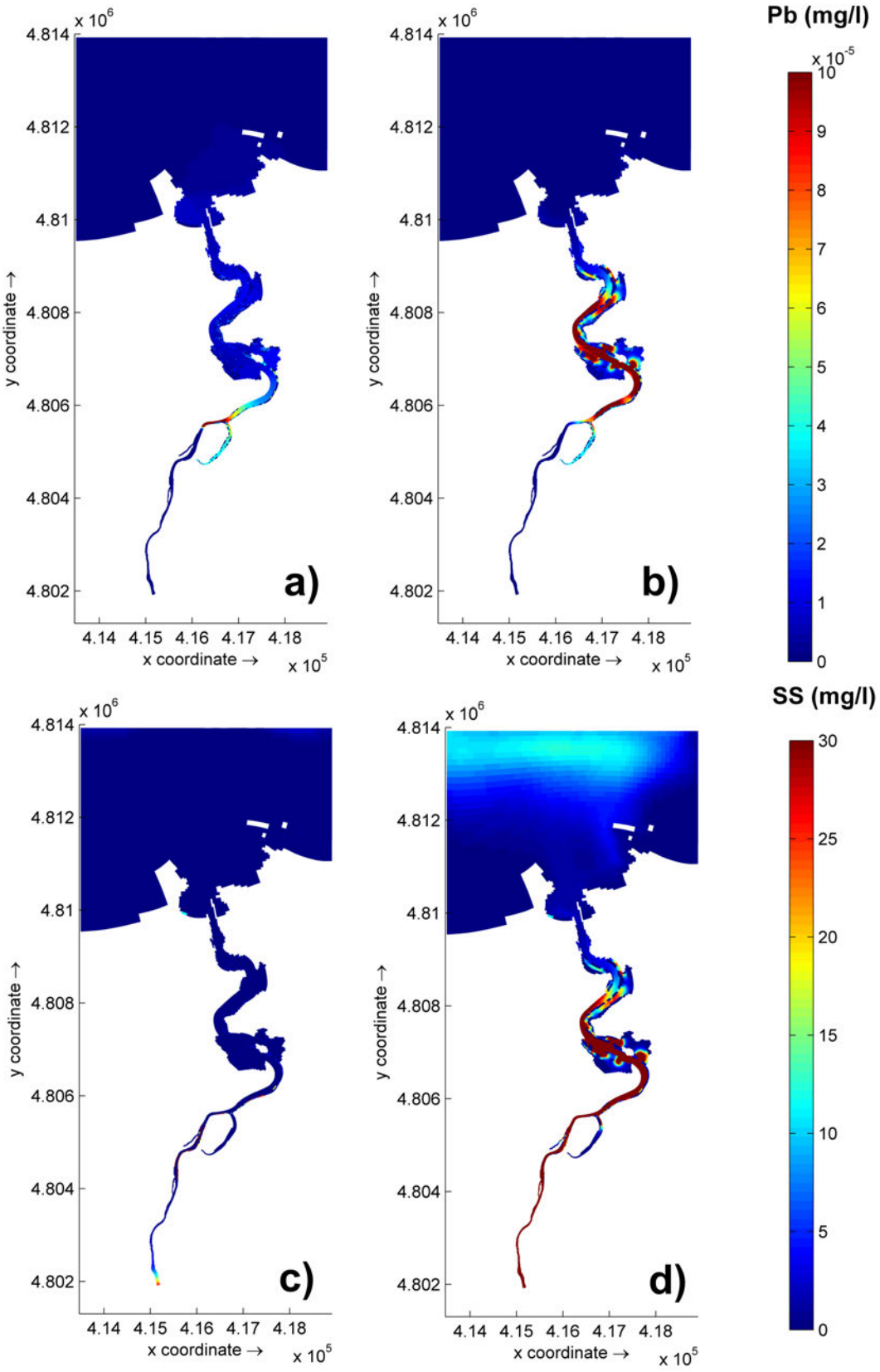

Figura 93: Mapa de la distribución espacial de cloroformo y sólidos en suspensión utilizado como condición inicial para la "simulación" del "caso real 23 de dilución" de ID2. Capa superficial de Pb (a), capa de fondo de Pb (b), capa superficial de SS (c) y capa de fondo de SS (d).

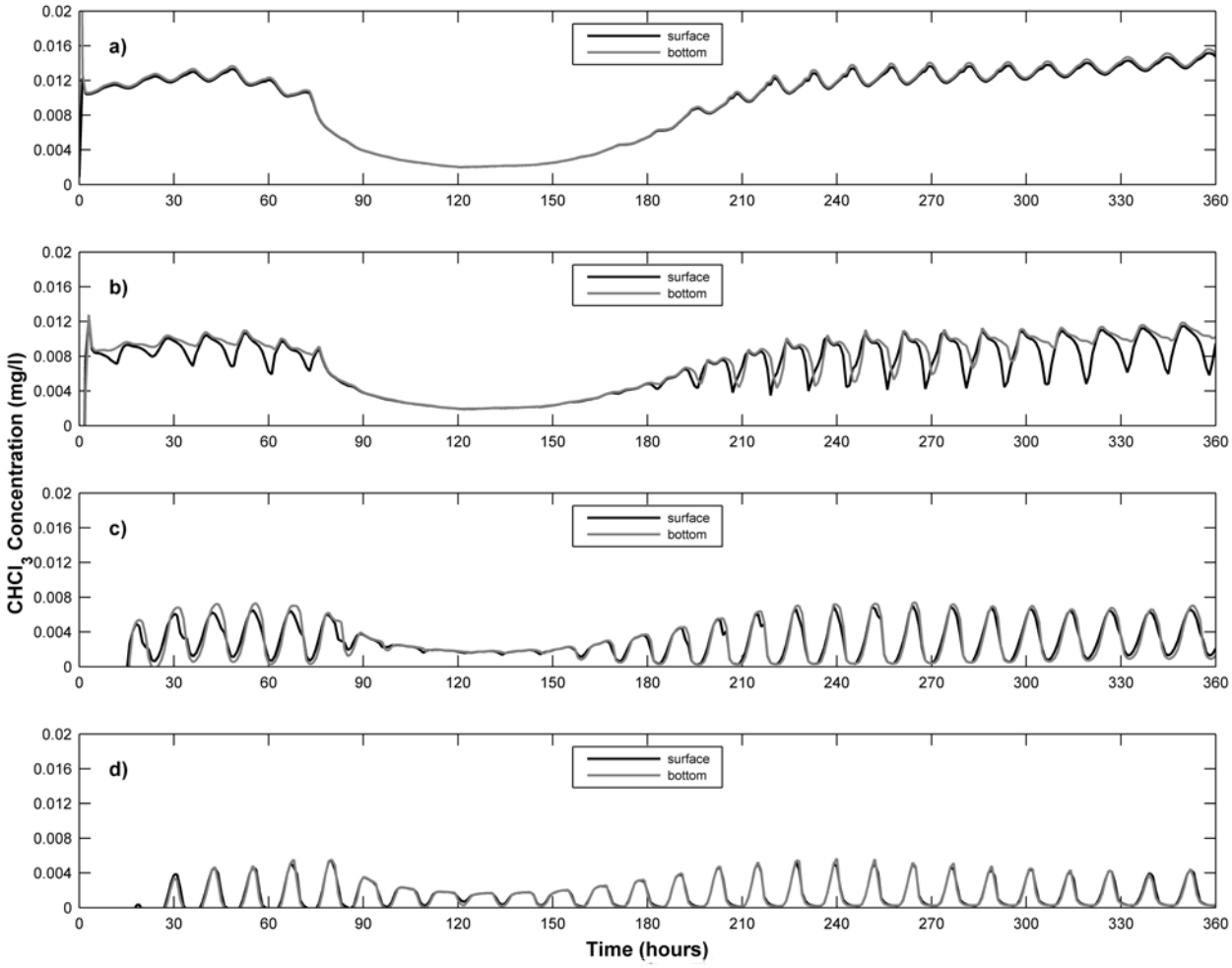

Figura 94: Evolución de la concentración de ID1 (cloroformo) en la superficie (línea negra) y el fondo (línea gris) para el transporte del "caso real 23 de dilución" en WQ3 (a), SS1 (b), SS3 (c) and SS5 (d).

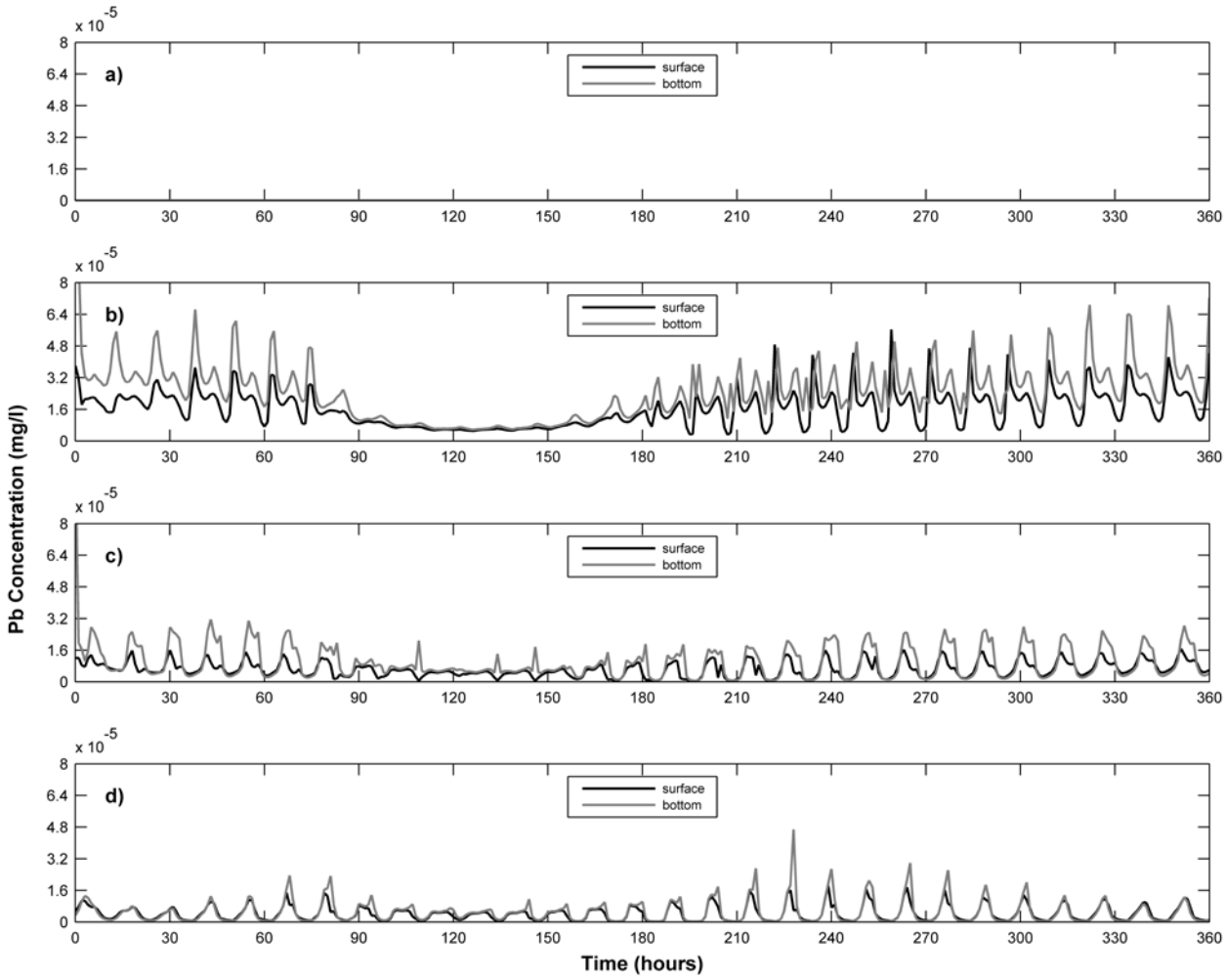

Figura 95: Evolución de la concentración de ID2 (plomo) en la superficie (línea negra) y el fondo (línea gris) para el transporte del "caso real 23 de dilución" en WQ3 (a), SS1 (b), SS3 (c) and SS5 (d).

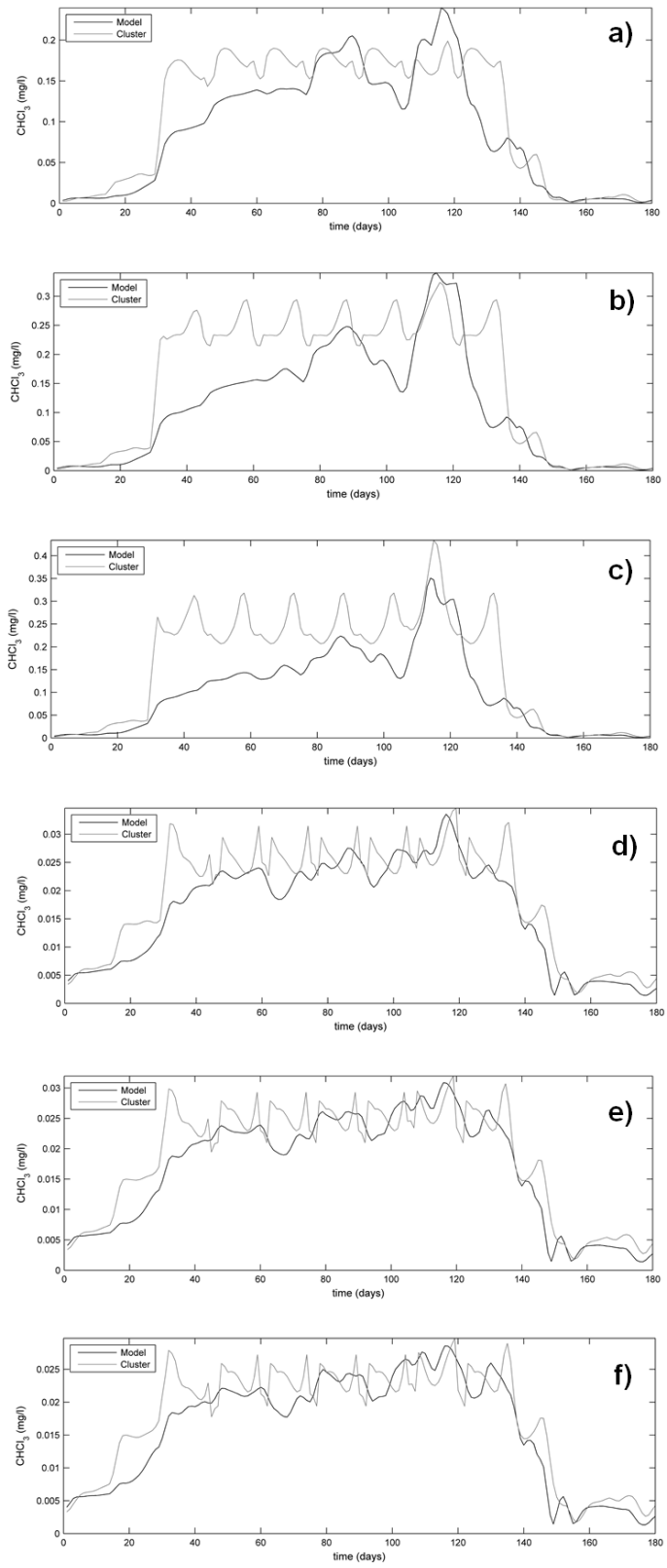

Figura 96: Evolución de la concentración de cloroformo de las "series reales" con modelo (líneas negras) y de las "series sintéticas" con grupos (líneas grises) para el transporte del período de validación (01/06/2008 a 01/12/2008) en el punto de vertido de ID1 (capa superficial (a), capa intermedia (b) y capa de fondo (c)) y en SS5 (capa superficial (d), capa intermedia (e) y capa de fondo (f)).

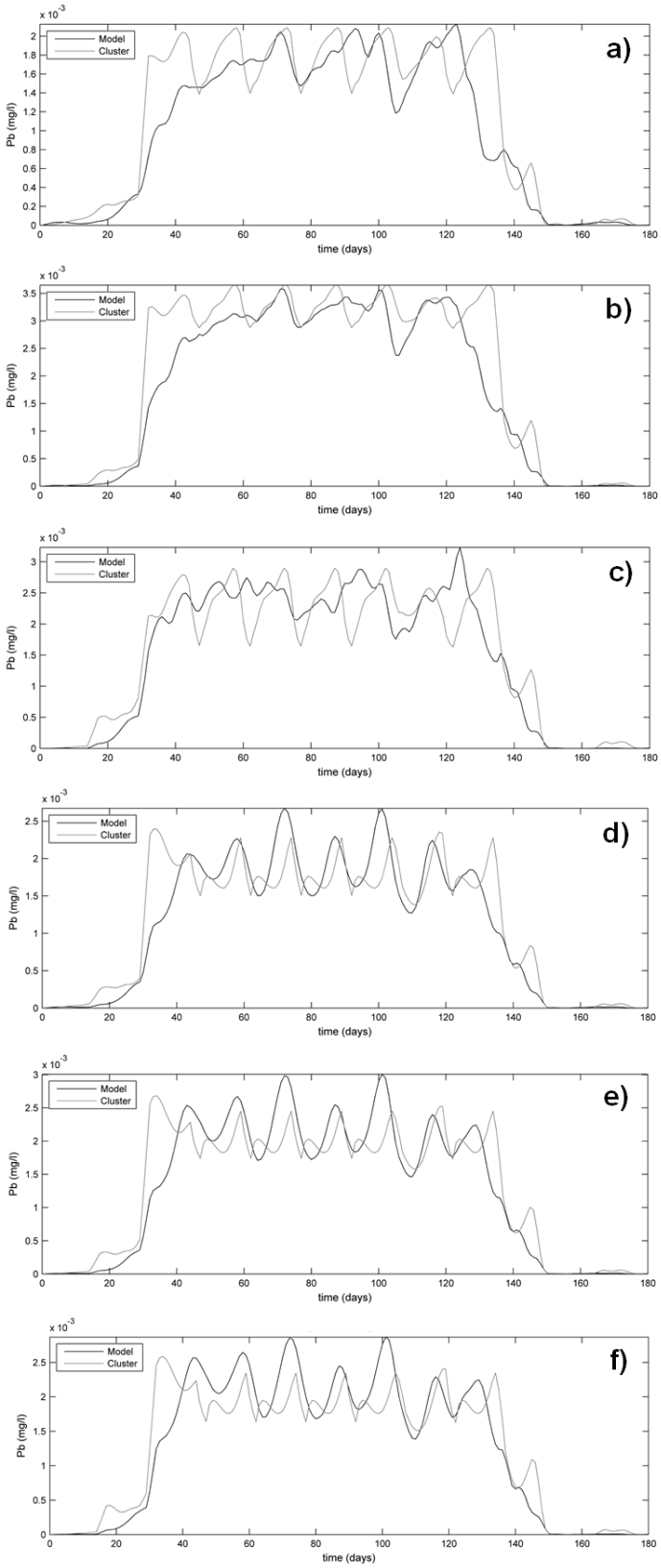

Figura 97: Evolución de la concentración de plomo de las "series reales" con modelo (líneas negras) y de las "series sintéticas" con grupos (líneas grises) para el transporte del período de validación (01/06/2008 a 01/12/2008) en el punto de vertido de ID2 (capa superficial (a), capa intermedia (b) y capa de fondo (c)) y en SS5 (capa superficial (d), capa intermedia (e) y capa de fondo (f)).

Estación	Profundidad	Modelo-Grupos Media (mg/l)	Modelo-Grupos MAC-duración (%)	BIAS (mg/l)	CE (-)
ID1	Superficie	0.0889 - 0.1081	96.11 - 95.56	-0.0192	0.7263 Aceptable (conveniente)
	Media	0.1098 - 0.1541	96.67 - 96.67	-0.0443	0.5742 Aceptable
	Fondo	0.1009 - 0.1573	96.67 - 96.67	-0.0564	0.5008 Aceptable (conveniente)
SS1	Superficie	0.0444-0.0591	98.33-99.44	-0.0147	0.6637 Acceptable (convenient)
	Media	0.0471-0.0645	98.33-99.44	-0.0175	0.6208 Acceptable (convenient)
	Fondo	0.0446-0.0592	98.33-99.44	-0.0146	0.6353 Acceptable (convenient)
SS5	Superficie	0.0164 - 0.0189	95.00 - 98.33	-0.0025	0.7934 Aceptable (conveniente)
	Media	0.0166 - 0.0186	95.00 - 98.33	-0.0019	0.8165 Aceptable (excelente)
	Fondo	0.0159 - 0.0175	95.00 - 98.33	-0.0016	0.8143 Aceptable (excelente)

Tabla 15: Medidas de error del período de validación (01/06/2008 a 01/12/2008) para cloroformo a tres profundidades en ID1, SS1 y TG1.

Estación	Profundidad	Modelo-Grupos Media (mg/l)	Modelo-Grupos MAC-duración (%)	BIAS (mg/l)	CE (-)
ID2	Superficie	0.0010-0.0011	0.0-0.0	-2.99e-04	0.7423 Aceptable (conveniente)
	Media	0.0017-0.0020	0.0-0.0	-5.64e-04	0.7969 Aceptable (conveniente)
	Fondo	0.0014-0.0015	0.0-0.0	-5.55e-05	0.7648 Aceptable (conveniente)
SS1	Superficie	0.0020-0.0021	0.0-0.0	-1.08e-04	0.6792 Aceptable (conveniente)
	Media	0.0021-0.0021	0.0-0.0	-3.02e-05	0.6070 Aceptable (conveniente)
	Fondo	0.0021-0.0021	0.0-0.0	-8.85e-06	0.5730 Aceptable
TG1	Superficie	0.0011-0.0011	0.0-0.0	8.54e-05	0.4352 Aceptable (pobre)
	Media	0.0013-0.0013	0.0-0.0	6.97e-05	0.5280 Aceptable
	Fondo	0.0013-0.0013	0.0-0.0	5.84e-05	0.6034 Aceptable (conveniente)

Tabla 16: Medidas de error del período de validación (01/06/2008 a 01/12/2008) para plomo a tres profundidades en ID2, SS1 y TG1.

la tabla 16 se sintetizan las mediciones de error para ID2 a tres profundidades en ID2, SS1 y SS5.

Estos datos confirman que los resultados son bastante precisos y razonables. Por ello, se puede generar cualquier "serie real" de concentración de sustancia tóxica ($CHCl_3$ y Pb) con base en una secuencia de los 78 resultados del modelo que mejor se ajustaron a cada segemento de 15 días de la "serie real" ("serie sintética").

Selección y generación de l-años reconstruidos

Se optó por la reconstrucción, en primer lugar, de 40 años de serie temporal y, en segundo lugar, de 100-años estadísticos basados en la probabilidad de ocurrencia de los 78 escenarios.

Muestreo aleatorio

En el Paso 4, se determinó el número óptimo de muestreos igual a 1000×12 datos para un año. Ahora, se calcularon dichos 1000-muestreos para los dos criterios de fallo (AA y MAC) en cada uno de los 40 años de series temporales (forzamientos reales) y de los 100-años estadísticos (Monte Carlo).

Delimitación final de MZs

Una vez se calcularon las medidas de concentración de tóxico en cada muestreo y año, los efectos crónicos de cada sustancia tóxica en cada celda de la malla se calcularon utilizando la ecuación (11) para cada uno de los 40 años o de los 100-años estadísticos, teniendo en cuenta cada uno de los 1000-muestreos. Posteriormente, se calculó el CEF** asociado a todos los 1000-muestreos mediante la ecuación (12) para cada uno de los 40

años o de los 100-años estadísticos. Por último, se obtuvo un vector con 40 o 100 valores de CEF** en cada celda de la malla, es decir, la probabilidad de AA-Fallo de cada uno de los 40 o 100 años. A partir de dicho vector, se calculó la ecdf de CEF** en cada celda de la malla para ambas reconstrucciones.

Como ejemplo de la ecdf de CEF**, la figura 98 muestra dicha distribución para el efluente industrial ID2 en el punto de vertido (línea negra), WQ3 (línea roja), SS1 (línea azul), SS3 (línea verde) y SS5 (línea magenta). Ambas figuras muestran la probabilidad de ocurrencia con base en 40 años (a) y 100 años (b) de tener una probabilidad de AA-Fallo específica para 1000-muestreos.

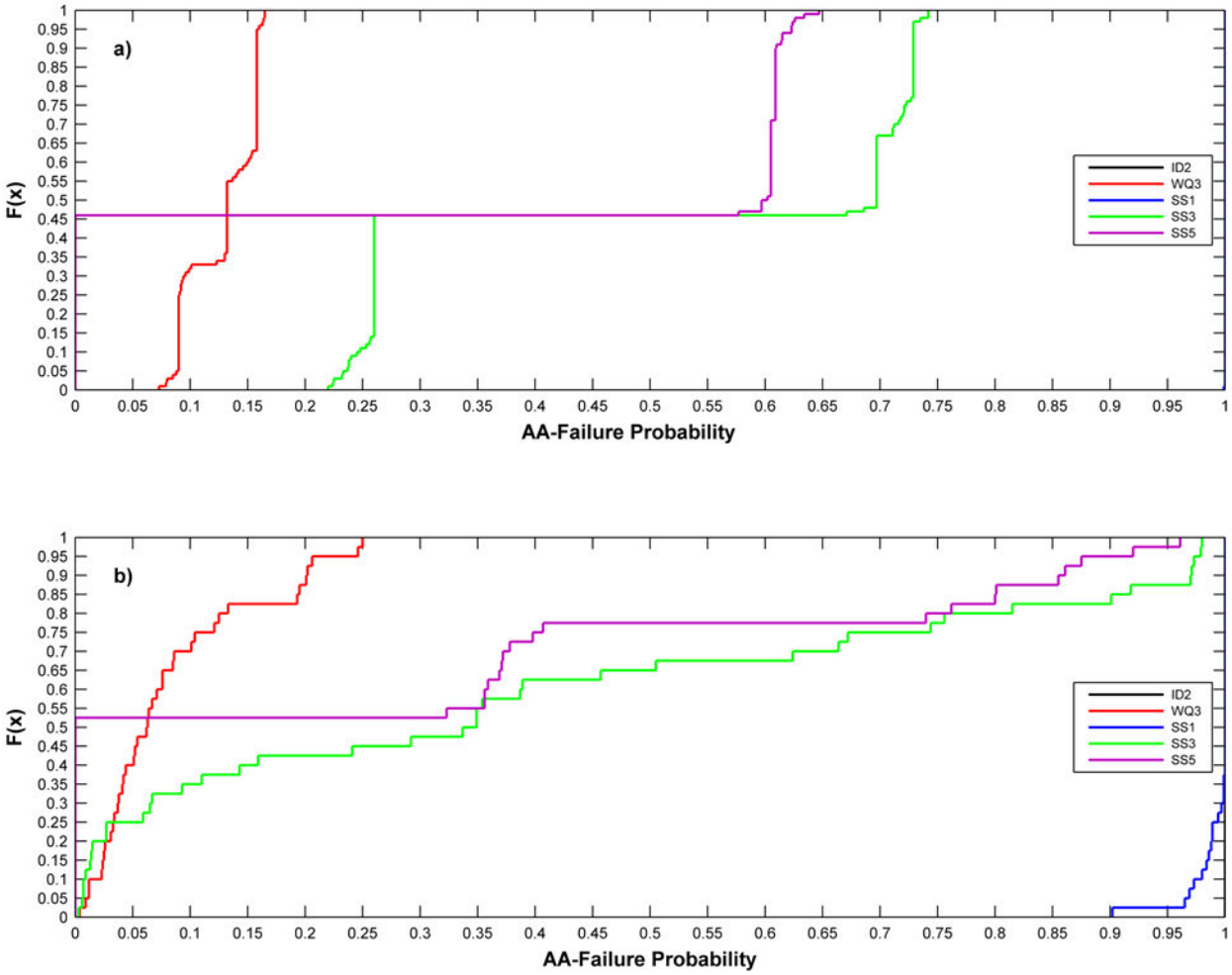

Figura 98: Función de distribución empírica acumulada de CEF** del vertido ID2 para 40-años (a) y 100-años (b) en ID2 (línea negra), WQ3 (línea roja), SS1 (línea azul), SS3 (línea verde) y SS5 (línea magenta)

Los efectos agudos de cada sustancia tóxica en cada celda de la malla se calcularon utilizando la ecuación (13) para ambas reconstrucciones en cada uno de los 1000-muestreos. Posteriormente, se calculó el AEF** asociado a dichos muestreos mediante la ecuación (14) para cada año reconstruido. Por último, se calculó la ecdf de AEF** en cada celda de la malla para ambas reconstrucciones a partir de los valores de AEF** calculados para cada año reconstruido.

Como ejemplo de la ecdf de AEF**, la figura 99 presenta dicha distribución para el efluente industrial ID2 en el punto de vertido (línea negra), WQ3 (línea roja), SS1 (línea azul), SS3 (línea verde) y SS5 (línea magenta). Ambas figuras muestran la probabilidad de ocurrencia con base en 40 años (a) y 100 años (b) de tener una probabilidad de MAC-Fallo específica para 1000-muestreos.

De nuevo, se delimitaron dos MZs (ver figura 35). Una celda de la malla del modelo pertenece a la AA-MZ

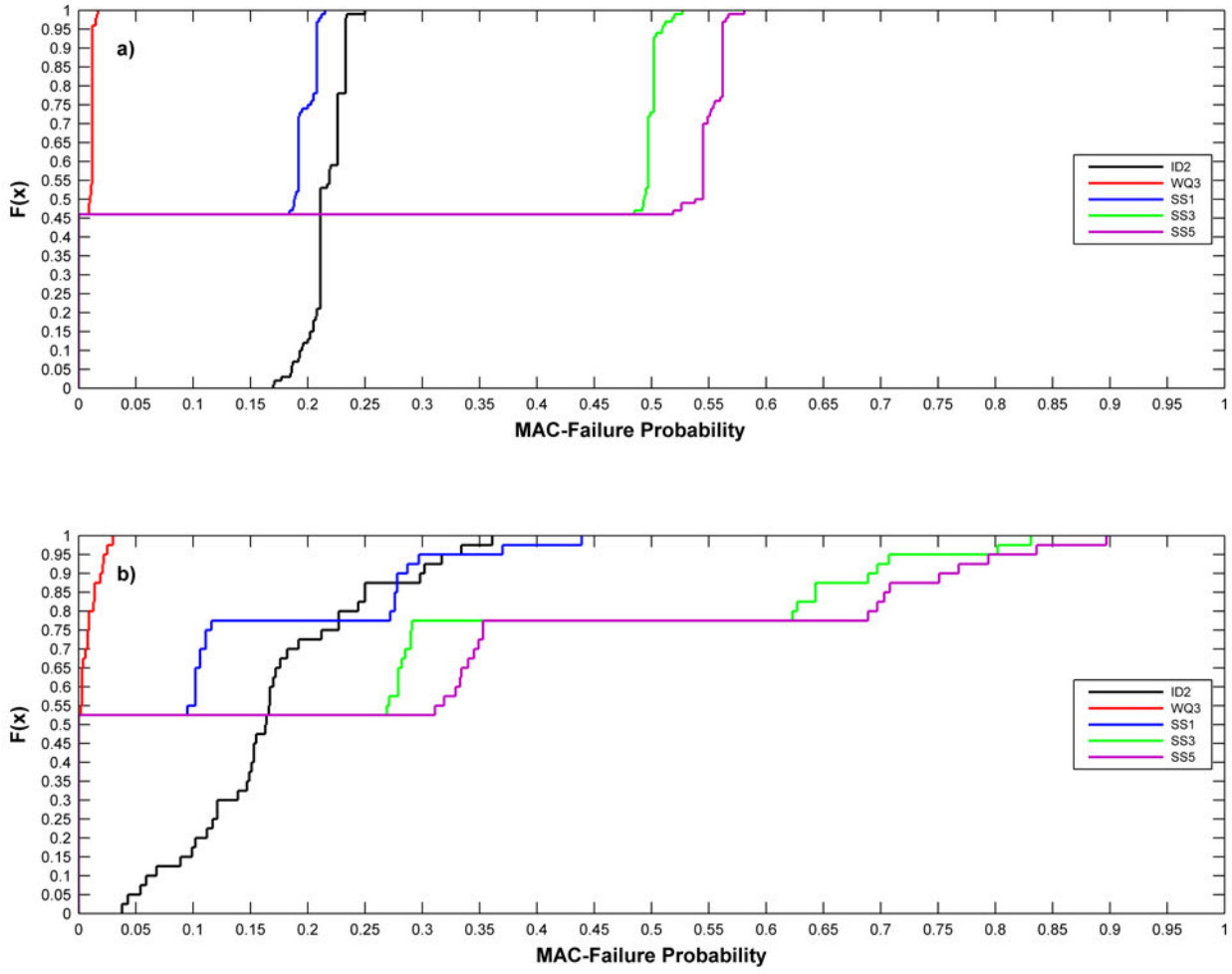

Figura 99: Función de distribución empírica acumulada de AEF** del vertido ID2 para 40-años (a) y 100-años (b) en ID2 (línea negra), WQ3 (línea roja), SS1 (línea azul), SS3 (línea verde) y SS5 (línea magenta)

cuando el valor de la ecdf de CEF** supera el percentil 5 o bien el valor del percentil 5 de la ecdf de CEF** sea mayor de 15 mientras que a la MAC-MZ cuando el valor de la ecdf de AEF** supera el percentil 5 o bien el valor del percentil 5 de la ecdf de AEF** fue mayor de 4.

Por último, la AA-MZ y MAC-MZ delimitadas del "caso real de dilución" para ID1 en el caso de 40 años (a-b) y el caso de 100-años estadísticos (c-d) se muestran en la figura 100. Mientras tanto en la figura 101 se presenta la AA-MZ y MAC-MZ delimitadas del "caso real de dilución" para ID2 en el caso de 40 años (a-b) y el caso de 100-años estadísticos (c-d).

3.5.5. Admisibilidad de las zonas de mezcla

A partir del concepto de vulnerabilidad y el porcentaje de área estuarina cubierto por las zonas de mezcla, se definió y determinó la admisibilidad de las MZs con base en un método de cuatro niveles (Figura 36). A continuación, se presenta la aplicación de la propuesta en el estuario de Suances con el fin de asignar zonas de mezcla en el Paso 5.

3.5.5.1. Zonificación mareal (TZ)

En este apartado se localizan las zonas intermareales y submareales con el percentil 95 de la amplitud de marea ($A95$=2.138 m) y la profundidad de cada celda de la malla (H). En la figura 102, se muestra la distribución de TZ en el SE donde las zonas submareales se colorearon en verde y las intermareales en rojo.

3.5.5.2. Susceptibilidad (SU)

La susceptibilidad se relacionó con la capacidad de renovación del agua y se estimó mediante modelos numéricos. Para ello, se desarrolló un enfoque metodológico dividido en cuatro niveles: Análisis de los forzamientos hidrodinámicos, Cálculo del tiempo de renovación, Análisis de sensibilidad del tiempo de renovación y Tiempo de renovación final (véase la figura 37).

Análisis de los forzamientos hidrodinámicos

Con base en los cambios de pendiente de cada curva ecdf (ver en la figura 45), se seleccionaron 5 caudales de río iguales a los percentiles $Q0 = 0{,}725, Q10 = 3{,}492, Q50 = 12{,}061, Q90 = 51{,}634, Q100 = 561{,}170$ m^3/s, 1 amplitud de marea igual al percentil $A50 = 1{,}468$ m y, por último, 4 fases de marea correspondientes a 4 niveles de marea iguales a $vaciante = 0, bajamar = -1{,}468, llenante = 0, pleamar = 1{,}468$ m. Resumiendo, se integró la variabilidad de los forzamientos en $5 \times 1 \times 4 = 20$ escenarios.

En cuanto a la marea astronómica, como indicó Bárcena *et al.* (2012b), las diferencias experimentadas por el FT debido a la amplitud de marea fueron insignificantes para casi cualquier caudal de río en el SE. Por ello, sólo se seleccionó una caso de marea correspondiente a la mediana de $A50$.

Cálculo del tiempo de renovación

De entre todos los métodos existentes en la literatura, la metodología propuesta por Jouon *et al.* (2006) ha sido seleccionada para calcular la renovación del agua. Dicho método propone la aplicación de un modelo hidrodinámico tridimensional (Delft3D-FLOW) acoplado a un modelo de transporte tridimensional (D-Water Quality). Después de 20 simulaciones con 10 capas, se obtuvieron $20 \times 10 = 200$ mapas con la distribución del tiempo de renovación local en el SE.

Análisis de sensibilidad del tiempo de renovación

El tercer nivel consistió en la realización de un análisis de sensibilidad múltiple de los resultados de LFT para entender la influencia de la profundidad (10 capas), el tiempo inicial de simulación (4 fases de marea) y las descargas de agua dulce (5 caudales fluviales) a lo largo de la ría.

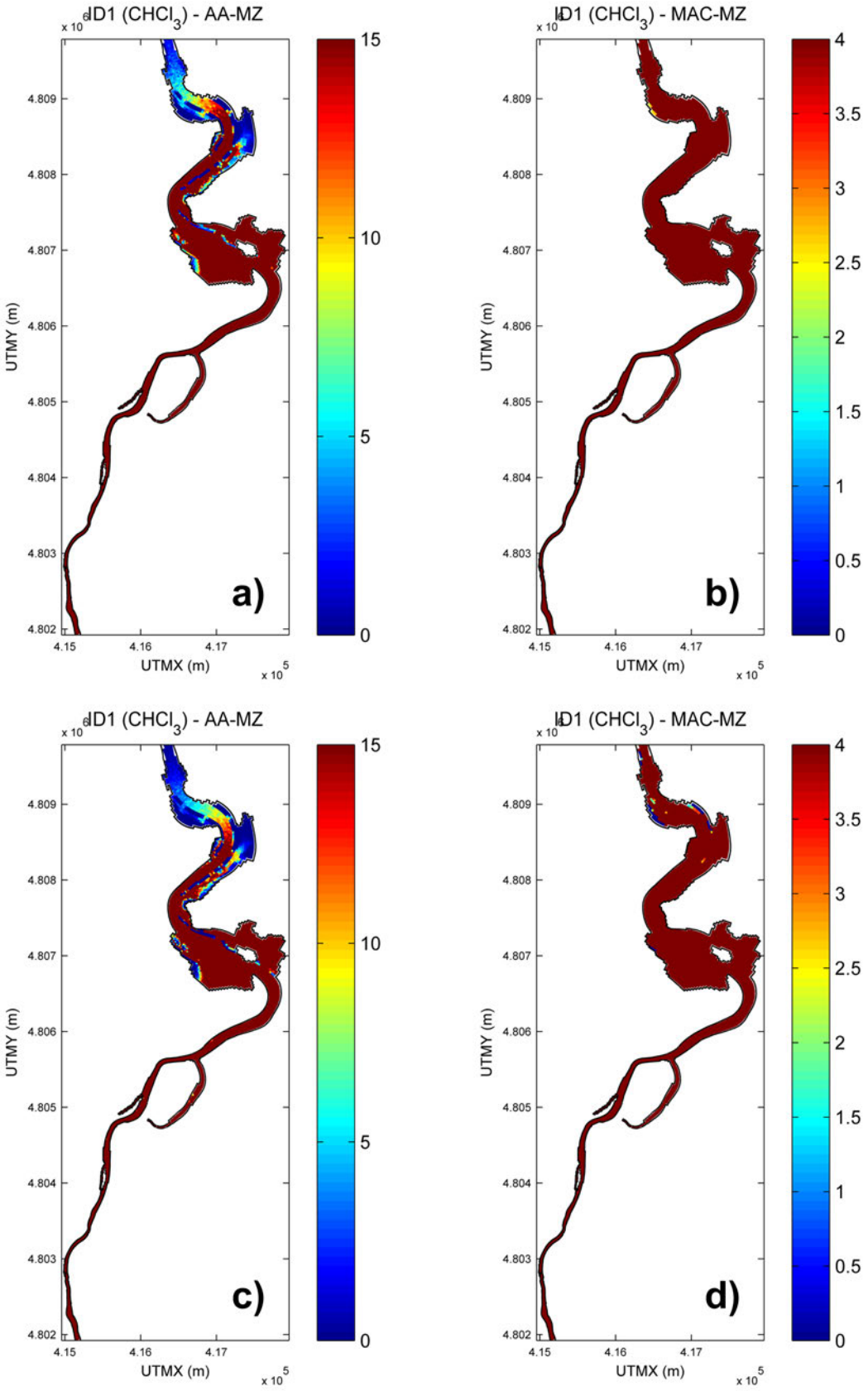

Figura 100: Zonas de mezcla delimitadas en el "caso real de dilución" para ID1. AA-MZ de 40 años (a), MAC-MZ de 40 años (b), AA-MZ de 100-años estadísticos (c) y MAC-MZ de 100-años estadísticos (d).

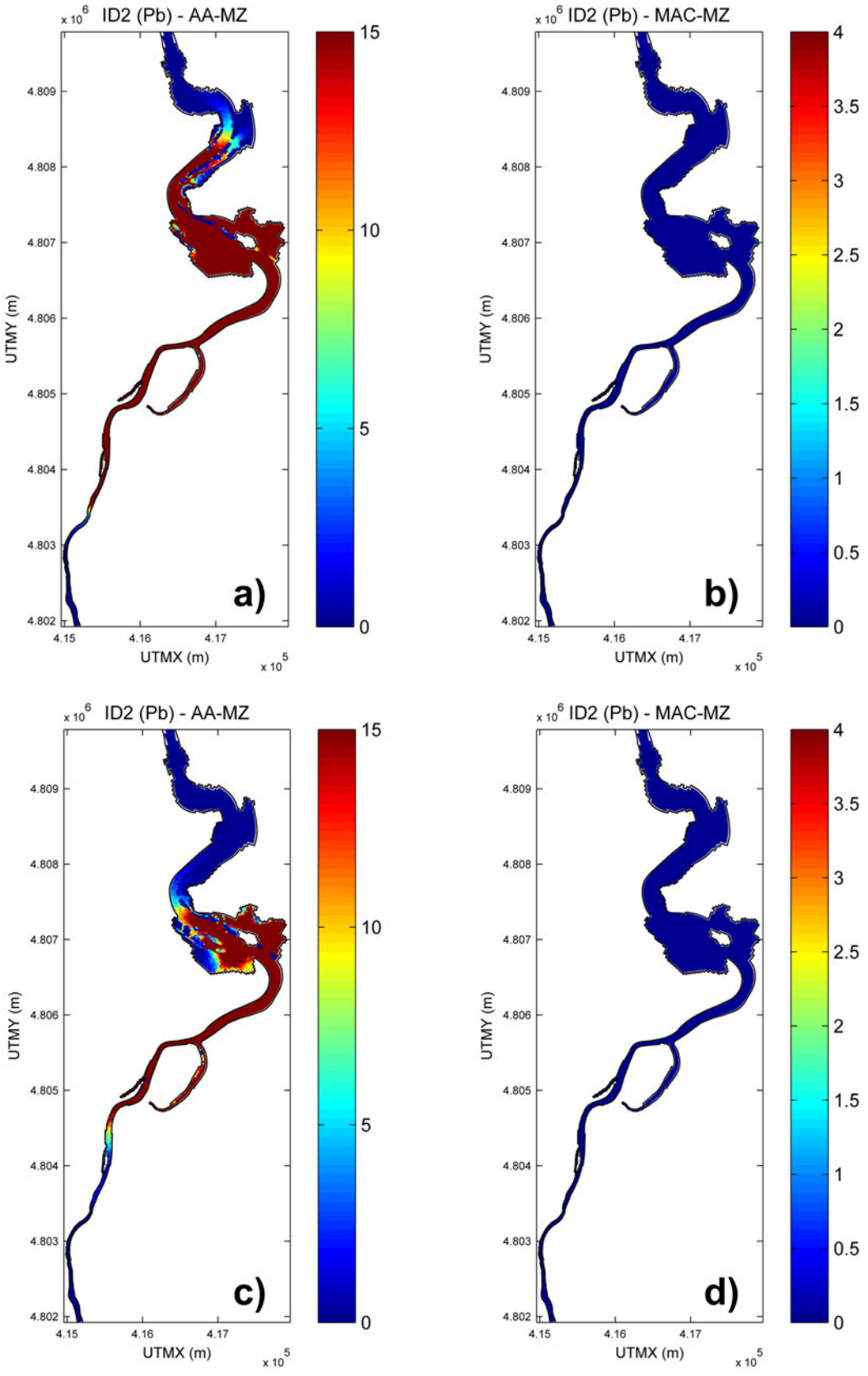

Figura 101: Zonas de mezcla delimitadas en el "caso real de dilución" para ID2. AA-MZ de 40 años (a), MAC-MZ de 40 años (b), AA-MZ de 100-años estadísticos (c) y MAC-MZ de 100-años estadísticos (d).

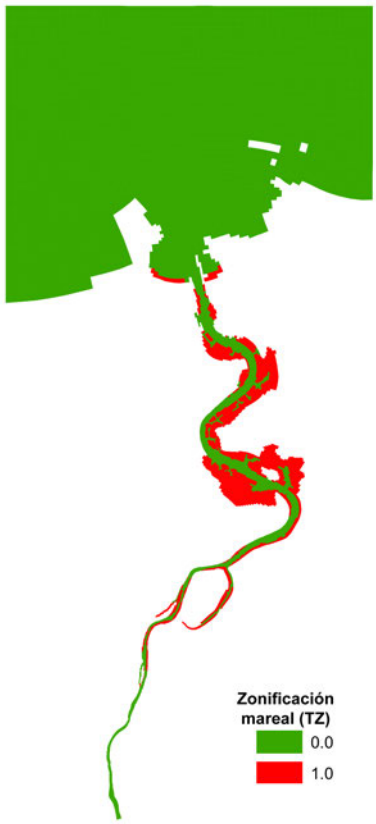

Figura 102: Zonificación mareal (TZ) de las celdas de la malla en el Estuario de Suances donde las zonas submareales se colorearon en verde y las intermareales en rojo.

Para analizar la tendencia descrita por el LFT debido a la profundidad, todos los resultados se representaron gráficamente y se analizaron. A pesar de las pequeñas diferencias experimentadas por el LFT debido a la profundidad, la variabilidad del LFT con la profundidad no fue significativa para todos los escenarios. Por lo tanto, se promediaron los valores de LFT de las 10 capas en cada celda de la malla para cada escenario de modelado reduciéndose la dimensionalidad de 200 mapas a 20 mapas.

Más tarde, se representaron y compararon los resultados de LFT en cada tiempo inicial de simulación para entender su influencia. Incluso cuando el caudal del río fue casi nulo, la variabilidad del LFT con la fase de marea no fue significativa. Esta tendencia fue similar en todos los escenarios así que, de nuevo, se promediaron los valores de LFT de las 4 fases en cada celda de la malla para cada escenario. En este momento, se redujo la dimensionalidad de 20 mapas a 5 mapas de LFT que describen la variabilidad de la renovación del agua en función del caudal del río.

Tiempo de renovación final

Finalmente, se integró el área bajo la curva para cada celda de la malla con el fin de construir un rectángulo con el mismo área y, por lo tanto, determinar el LFT final como la altura de dicho rectángulo. En la figura 103 se presenta , a modo de ejemplo, la evolución del LFT en función de los percentiles del caudal fluvial así como el LFT final para WQ3 (a), SS1 (b), SS3 (c) y SS5 (d).

En cuanto a los valores finales de LFT, el más alto sucede en SS1 (b) con 0.797 días (19.13 horas) ya que se trata de un punto menos energético debido a las distancias a los forzamientos (río en la cabecera y marea en la bocana). El más bajo con 0.126 días (3.02 horas) se encuentra en SS5 (d) por la proximidad a la bocana y su independencia con el río. En el caso de WQ3 (a), el LFT final es de 0.349 días (8.38 horas) e influenciado por la corriente del río: caudales bajos muestran valores altos mientras que caudales altos presentan valores

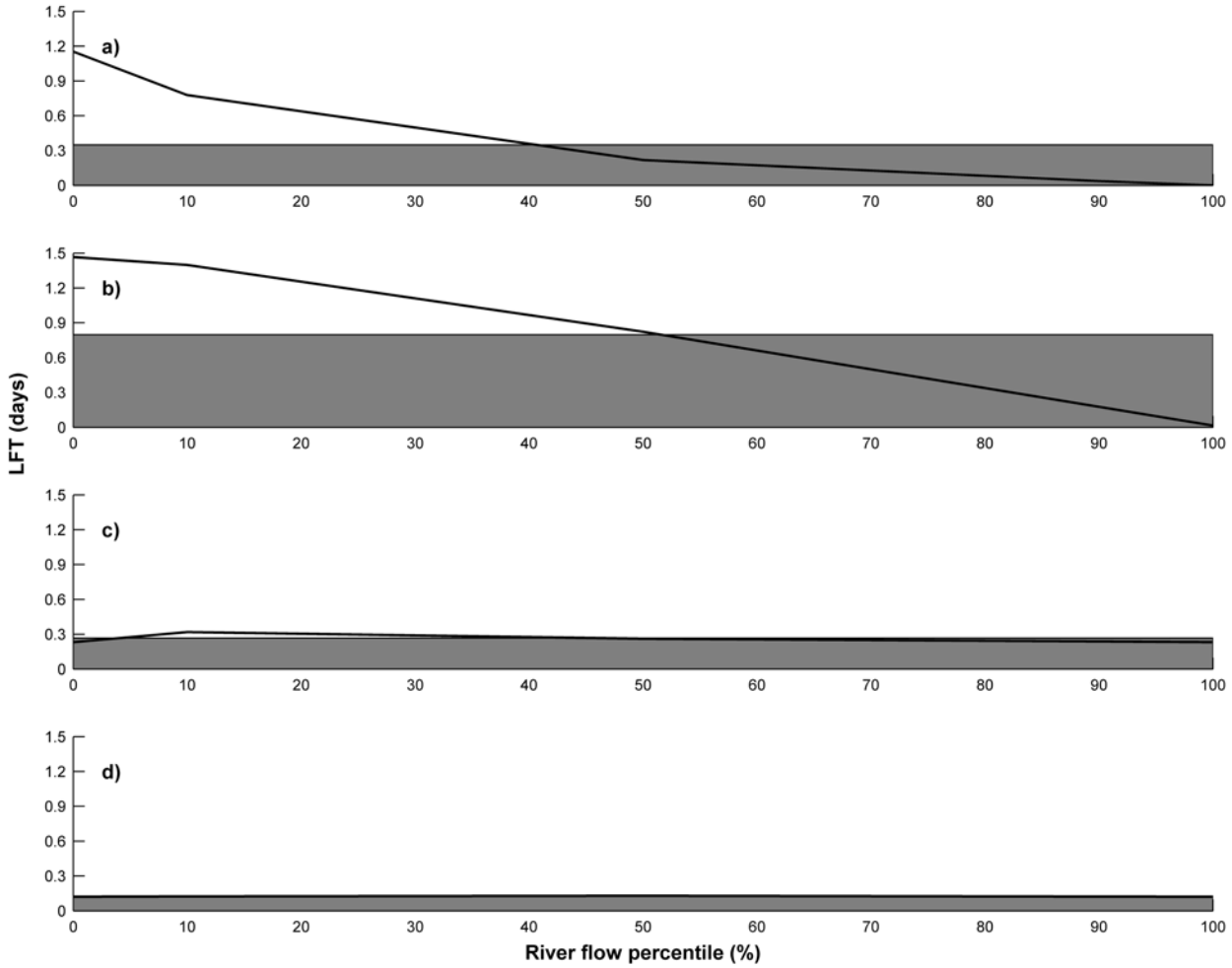

Figura 103: Evolución del tiempo de renovación local en función de los percentiles del caudal fluvial así como el tiempo final de renovación local para WQ3 (a), SS1 (b), SS3 (c) y SS5 (d).

bajos. El LFT final en SS3 (c) es de 0.267 días (6.41 horas), este valor es mayor que en SS5 debido a que la distancia a la bocana también es mayor.

Después de calcular el LFT final en cada celda de la malla, en la figura 104ba se presenta la distribución espacial final del LFT en el SE.

Por último, dicho mapa final de LFT fue traducido a términos de susceptibilidad mediante la expresión: $SU_{(}i) = \frac{0{,}8 \cdot LFT_i}{LFT_{max}}$. De esta forma, se normalizó el LFT por medio de su máximo en el SE, siendo de 0.949 días (22.78 horas). En la figura 104b, se muestra la distribución de la SU en el SE de acuerdo al LFT final donde SU bajas se asocian con el color azul (0.0 a 0.3), SU medias con verde (0.3 a 0.5), SU altas con amarillo (0.5 a 0.6), SU muy altas con naranja (0.6 a 0.7) y las SU más altas con rojo (0.7 a 0.8).

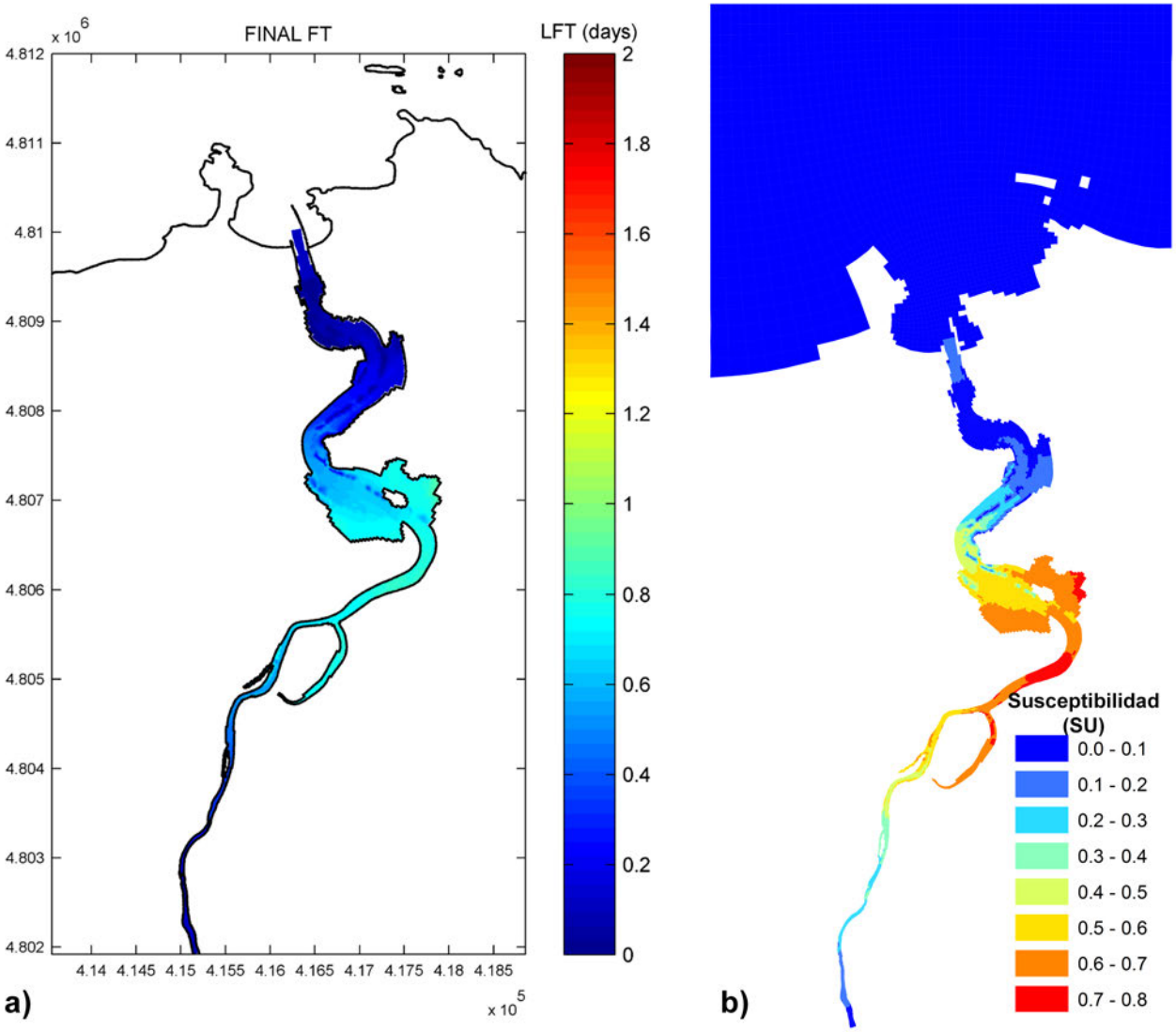

Figura 104: Panel a): Distribución espacial final del tiempo de renovación local teniendo en cuenta la influencia de la profundidad (10 capas), la magnitud de la marea (1 amplitud de marea), el tiempo inicial de simulación (4 fases de marea) y las descargas fluviales (5 caudales) a lo largo del estuario de Suances. Panel b): Distribución espacial de la susceptibilidad en el Estuario de Suances. La susceptibilidad baja se coloreó en azul (0.0-0.3, lo menos vulnerable), media en verde (0.3-0.5, vulnerable), alta en amarillo (0.5-0.6, más vulnerable), muy alta en naranja (0.6-0.7, mucho más vulnerable) y la más altas en rojo (0.7-0.8, lo más vulnerable).

3.5.5.3. Estado de conservación (SC)

Naturalidad (NA)

Cada distancia del buffer de un presión hidromorfológicas se calculó mediante la ecuación (23). En Suances, se tuvieron en cuenta 28 alteraciones hidrodinámicas: 1 puente y 27 diques. El puente se consideró discontinuo (k_{HP}=0.5) y el valor crítico CV fue de 50 m. Todos los diques se consideraron continuos (k_{HP}=1) y el valor crítico CV fue de 100 m. Por otra parte, se tomaron en cuenta 9 alteraciones morfológicas: todas ellas fueron protecciones de márgenes con $k_{HP} = 1$ y CV=100 m. Por último, cabe destacar que no se consideraron los rellenos porque se ubican fuera de la malla.

Como se muestra en la figura 105a, las áreas alteradas se ponderaron con 0 y se colorearon en amarillo (naturalidad y vulnerabilidad baja) mientras que las no alteradas se ponderaron con 0.8 y se colorearon en gris (naturalidad y vulnerabilidad alta).

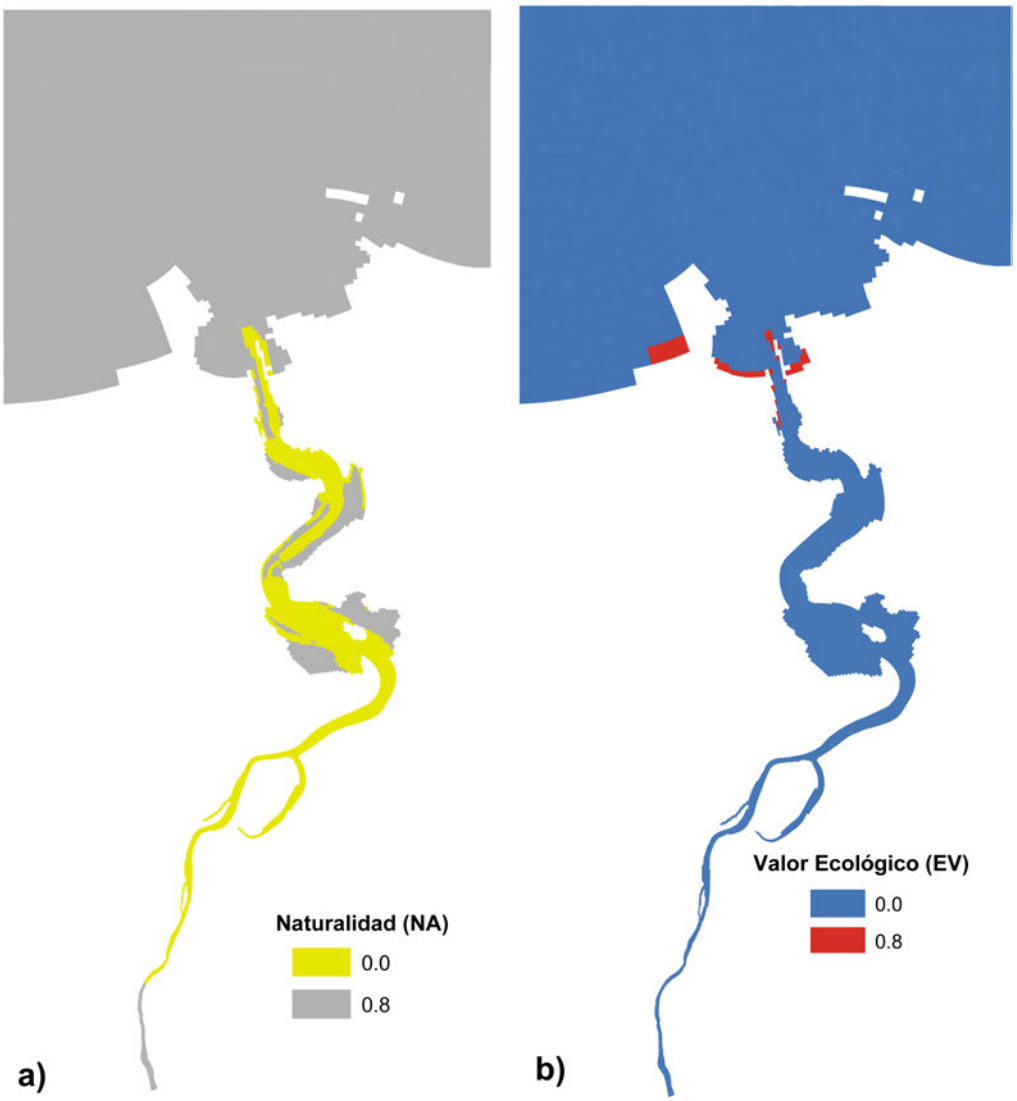

Figura 105: Panel a): Distribución espacial de la naturalidad en el Estuario de Suances. La naturalidad baja se colorea en amarillo (0, no vulnerable) y la alta en gris (0.8, vulnerable). Panel b): Distribución espacial del valor ecológico en el Estuario de Suances. El valor ecológico bajo se colorea en azul (0, no vulnerable) y el alto en gris (0.8, vulnerable).

Valor Ecológico (EV)

Los elementos ecológicos singulares se definieron mediante el reconocimiento de las áreas protegidas regionales, nacionales e internacionales. En Suances, las áreas protegidas se identificaron sólo con áreas de usos recreativos relacionados con aguas de baño y playas (ver figura 46).

Como se presenta en la figura 105b, dichas zonas se ponderaron con 0.8 y se colorearon en rojo (valor ecológico y vulnerabilidad alta) mientras que el resto de zonas tuvieron un 0 y color azul (valor ecológico y vulnerabilidad baja).

3.5.5.4. Estratificación (ST)

La metodología propuesta para el cálculo de la estratificación en estuarios se dividió en tres niveles: Selección y modelado de escenarios hidrodinámicos, Cálculo del número de Richardson y Zonificación definitiva de la estratificación (Figura 38).

Selección y modelado de escenarios hidrodinámicos

En este trabajo, se utilizaron los mismos 78 escenarios de modelado seleccionados previamente con el KMA. De este modo, se emplearon los resultados hidrodinámicos del cálculo detallado para computar horariamente el número de Richardson a nivel de celda en el SE.

Cálculo del número de Richardson

En segundo lugar, se cuantificó horariamente el Ri_L a partir de los resultados del modelo hidrodinámico mediante la ecuación (24) para los 78 escenarios en cada celda de la malla. A continuación, se clasificó horariamente el tipo de estuario en cada celda de acuerdo con el criterio dado por Dyer & New (1986).

Zonificación definitiva de estratificación

En este nivel, se delimita la ubicación de zonas mezcladas, parcialmente mezcladas/estratificadas y estratificadas en el estuario. Para ello, se calculó en primer lugar el porcentaje de tiempo que cada celda de la malla estuvo en cada tipo de estratificación para cada escenario (360 horas). Como ejemplo de los 78 mapas obtenidos, la figura 106 ilustró la distribución de la probabilidad de ocurrencia para cada tipo de estratificación en el "caso real 23 de dilución". En ella, se observó que el SE estuvo la mayor parte del tiempo completamente mezclado durante el "caso real 23 de dilución" debido a que el evento de inundación dulcificó el estuario.

A partir de los 78×3 mapas de probabilidad, se computaron 3 mapas de probabilidad para cada tipo de estratificación multiplicando cada mapa (78×3) por la probabilidad de ocurrencia de cada uno de los 78 escenarios (Figura 107).

Por último, se integró toda la información en un único mapa donde se muestra el tipo de estratificación más probable a nivel de celda. Dicho mapa clasificó cada celda de la malla en un tipo determinado de estratificación cuando la probabilidad de un tipo superó el 33.33 $\%$ del tiempo (Figura 108a).

De acuerdo con las figuras 107 y 108a, el SE estuvo completamente mezclado en la parte interior debido a la acción del río sobre la columna de agua. En la parte exterior, el estuario también estuvo mezclado debido a que la acción de las mareas generaron la suficiente turbulencia para mezclar verticalmente la columna de agua. Por otra parte, la sección intermedia de la ría se encontró parcialmente mezclada/estratificada en la canal principal o estratificada en zonas intermareales, debido a la combinación de forzamientos, el gradiente de profundidad entre el canal principal y las zonas intermareales y las diferencias de salinidad experimentadas por la columna de agua.

ST se puede entender como un factor de corrección dentro de la metodología. De este modo, la figura 108b presenta areas clasificadas como mezcladas verticalmente (1.000 en azul), parcialmente mezcladas/estratificadas (1.125 en amarilla) y estratificadas (1.250 en verde).

3.5.5.5. Índice de Vulnerabilidad Estuarina (EVI)

Una vez calculados todos los parámetros, se integró toda esta información por medio del llamado "Índice de Vulnerabilidad del Estuario" (ver en la figura 36). Teniendo en cuenta la métrica establecida para asignar valores a los parámetros de la tabla 3 y la ecuación (26), se cuantificó el valor del EVI en cada celda de la

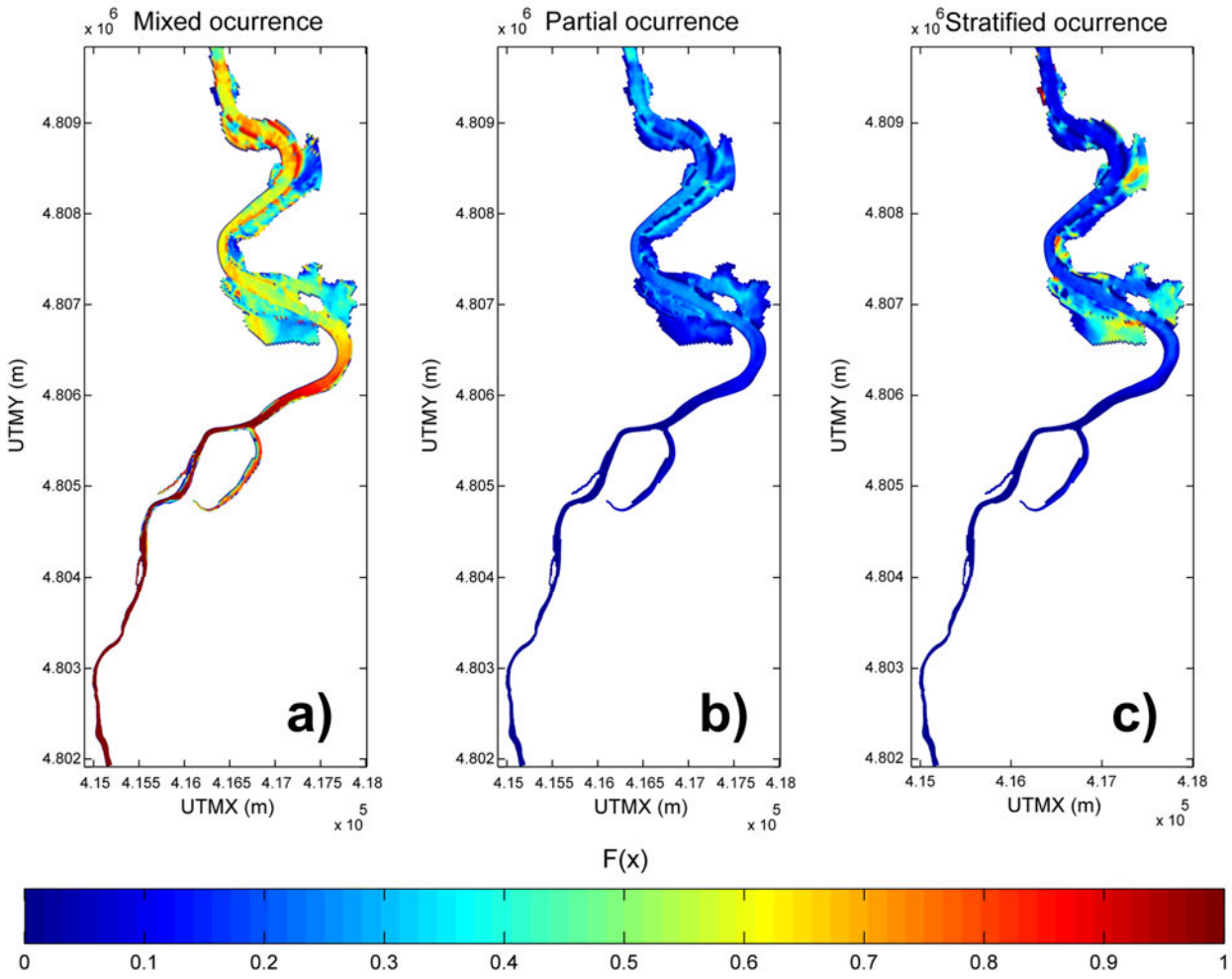

Figura 106: Distribución espacial de la probabilidad de ocurrencia para cada tipo de estratificación en el "caso real 23 de dilución". Mezclado verticalmente (a), parcialmente mezclado/estratificado (b) y estratificado (c).

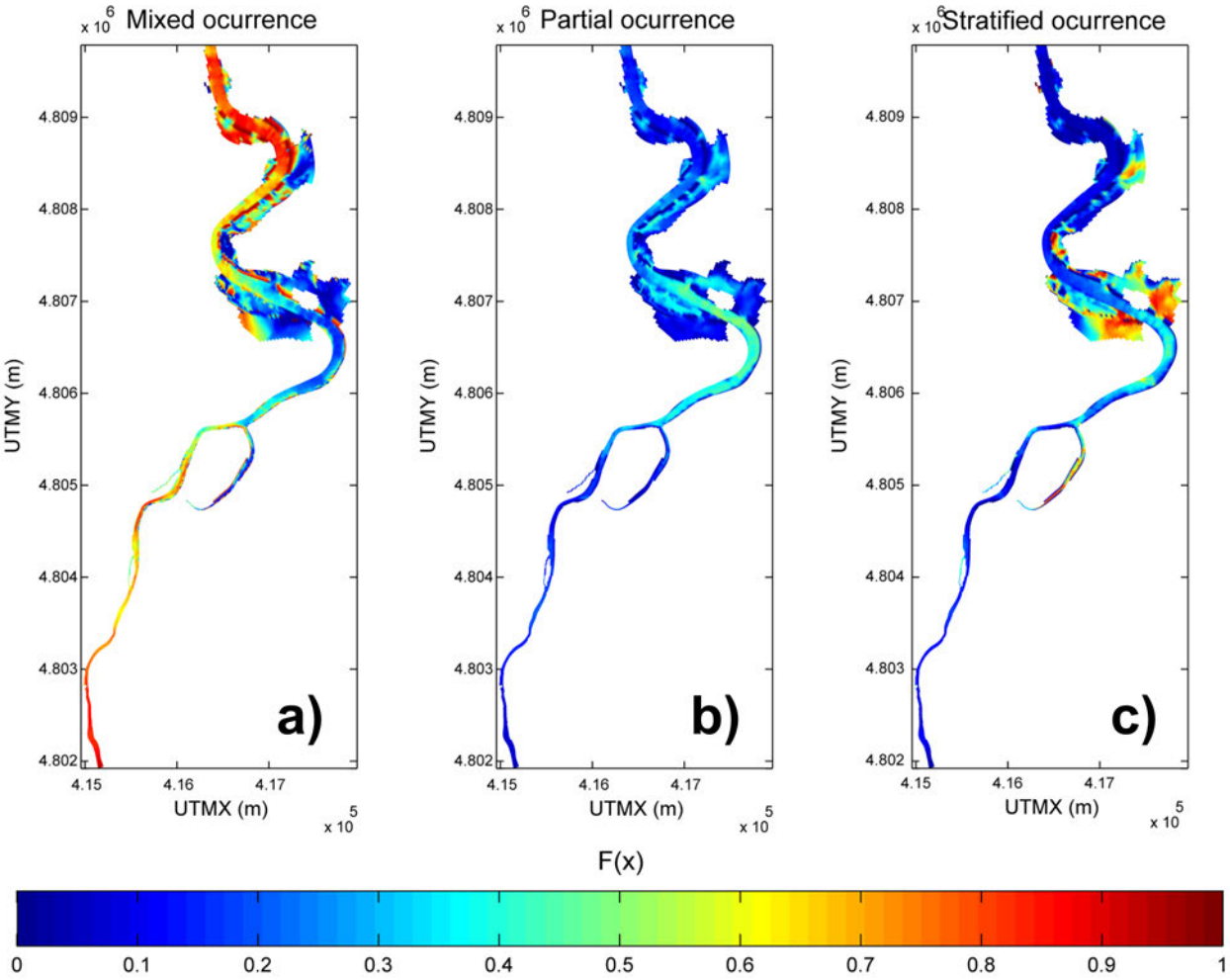

Figura 107: Distribución espacial de probabilidad de ocurrencia para cada tipo de estratificación en el Estuario de Suances. Mezclado verticalmente (a), parcialmente mezclado/estratificado (b) y estratificado (c).

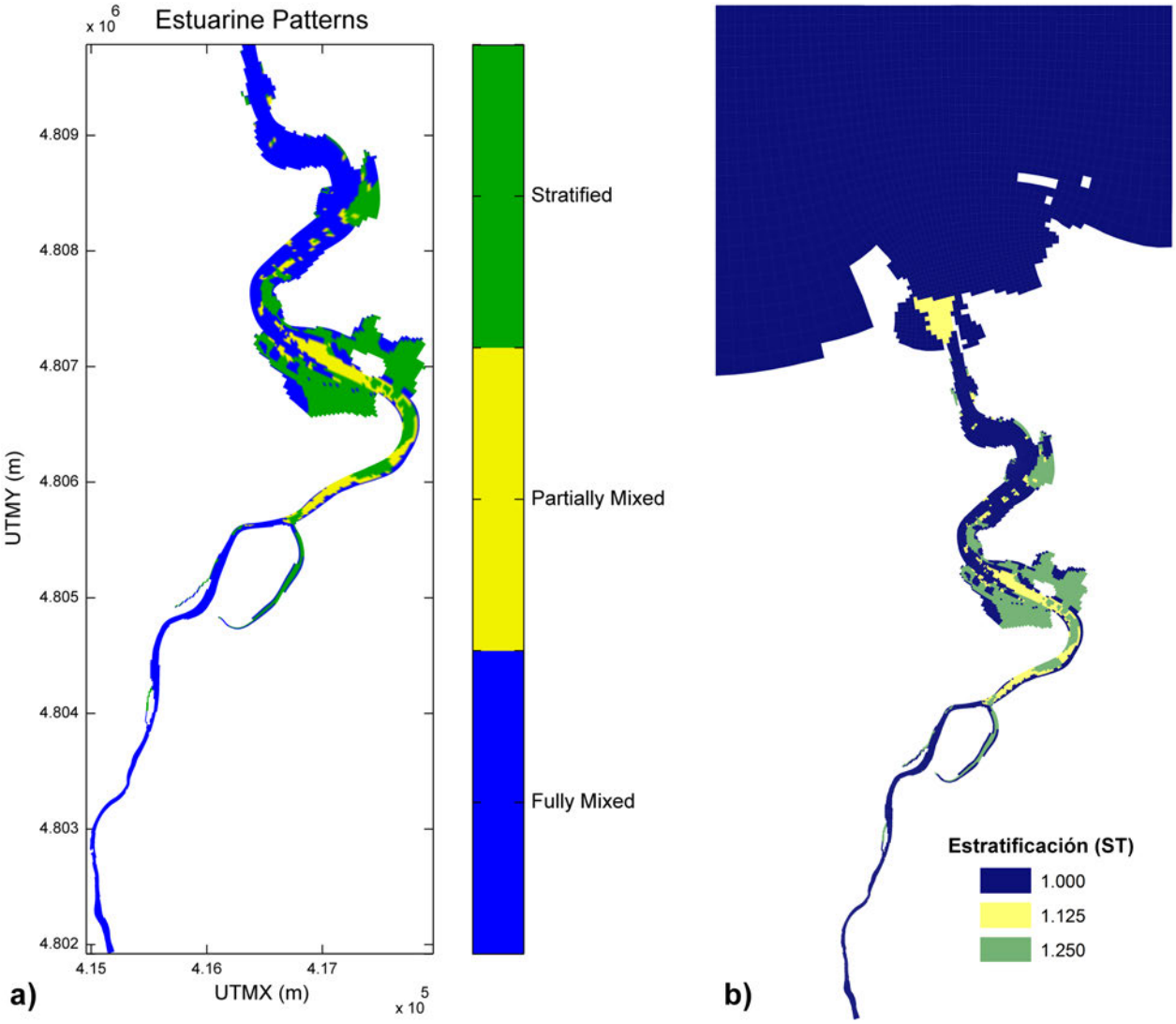

Figura 108: Panel a): Distribución espacial del tipo de estratificación más probable en el Estuario de Suances. Panel b): Distribución espacial de la estratificación en el Estuario de Suances. Mezclado verticalmente (1.000 en azul, menos vulnerable), parcialmente mezclado/estratificado (1.125 en amarillo, vulnerable) y estratificado (1.250 en verde, más vulnerable).

Número Años	Nombre Tóxico	AA-MZ m^2	AA-AD* AA-MAS*	MAC-MZ m^2	MAC-AD* MAC-MAS*
40	ID1 ($CHCl_3$)	1771132.96	51.13>3.85	-	-
100	ID1 ($CHCl_3$)	1631267.25	47.32>3.85	-	-
40	ID2 (Pb)	1519284.18	47.38>3.85	115.01	0.0024<1.15
100	ID2 (Pb)	933457.88	29.74>3.85	115.01	0.0024<1.15

Tabla 17: Extensión de las zonas de mezcla delimitadas (AA-MZ and MAC-MZ) y admisibilidad final (AA-AD* and MAC-AD*) en el cálculo detallado para ID1 e ID2.

malla. El EVI varió entre cero y uno siendo el cero zonas estuarinas menos vulnerables a recibir descargas mientras que las zonas con uno fueron las más vulnerables.

La figura 109a presenta la distribución espacial del EVI en el SE. En ella, EVIs bajos se colorearon en verde (0.0 a 0.4), medios en amarillo (0.4 a 0.6), altos en naranja (0.6 a 0.9) y los más altos en rojo (0.9 a 1.0).

3.5.5.6. Aceptabilidad (AC*)

El siguiente nivel determinó la aceptabilidad (AC*) del estuario por medio de la ecuación (27). El EVI se podría ver como un factor de corrección del área real de una celda de la malla en función de su vulnerabilidad. La figura 109b presenta la distribution espacial del AC* en el SE.

3.5.5.7. Tamaño máximo permitido para zonas de mezcla (MAS*)

En el tercer nivel, se computó el tamaño máximo permitido corregido para MZs (MAS*) para el cálculo detallado por medio de la división del AA-MAS y el MAC-MAS con un factor de corrección (α) (ver figura 36). Mediante la ecuación (28), se calculó el valor del MAS* mientras que la ecuación (29) mostró la formulación para α.

En Suances, $\overline{EVI}_{estuary}$ fue de 0.615 y se podría entender como un factor de corrección del MAS en función de la vulnerabilidad del estuario (Figura 39). Por tanto, $\alpha = \frac{1}{1-\overline{EVI}_{estuary}} = \frac{1}{1-0{,}615} = 2{,}597$.

Finalmente, los valores de ambos MAS* fueron de $AA^*_{MAS} = \frac{AA_{MAS}}{\alpha} = \frac{10}{2{,}597} = 3{,}85$ y $MAC^*_{MAS} = \frac{MAC_{MAS}}{\alpha} = \frac{3}{2{,}597} = 1{,}15$.

Debido a la vulnerabilidad del estuario frente a descargas de aguas residuales, los tamaños máximos permitidos para MZs en el "caso real de dilución" fueron de 3.85 y 1.15 para el AA-MAS* y MAC-MAS*, respectivamente.

3.5.5.8. Admisibilidad final (AD*)

En este nivel, se evaluó la admisibilidad (AD*) comparando la suma de todos los valores de AC* cubiertos por AA-MZ y MAC-MZ (Ecuación (30)) frente a los MAS* establecidos para las dos reconstrucciones consideradas.

En la tabla 17, se resume la extensión de la AA-MZ y la MAC-MZ así como el valor de la admisibilidad de AA-AD* y MAC-AD* para ID1 e ID2 en ambas reconstrucciones.

Como se puede observar en la tabla, no hubo AA-MZs admisibles ya que todas las descargas, independientemente de la reconstrucción, presentaron una AA-AD* mayor que el AA-MAS* (3.85 %). Respecto a la MAC-EQS, la descarga ID2 presentó una MAC-MZ admisible porque la MAC-AD* fue más pequeña que el MAC-MAS* (1.15 %). De hecho, todas las MAC-MZ delimitadas por debajo del 4 % de probabilidad de MAC-Fallo fueron admisibles porque también permanecieron por debajo del valor del MAC-MAS* (1.15 %).

Por tanto, la extensión de la AA-MZ no son admisibles para ID1 e ID2 y, en consecuencia, ambos vertidos fueron clasificados como inadmisibles finalizando el procedimiento de asignación (Figura 10).

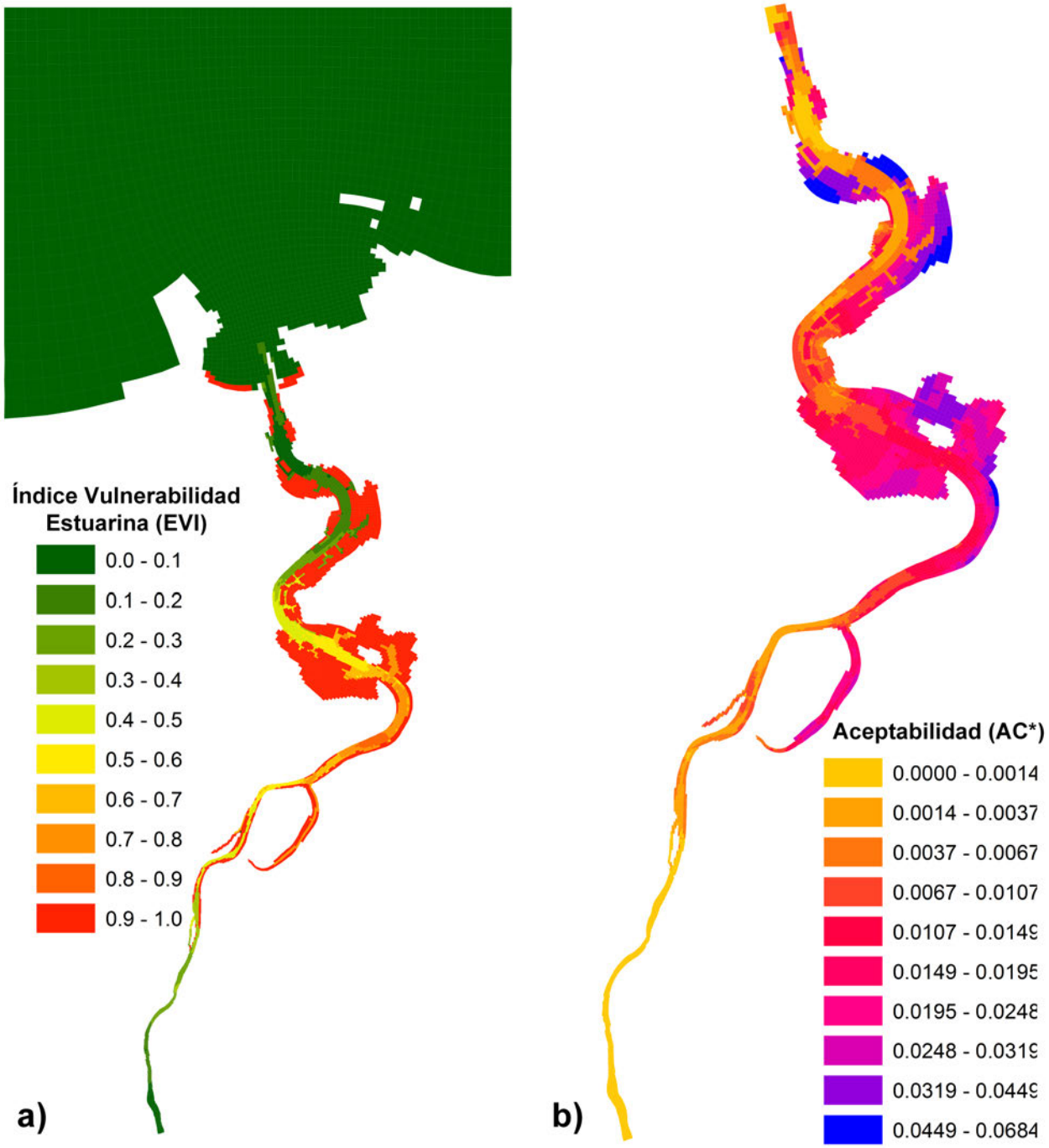

Figura 109: Panel a): Distribución espacial del Índice de Vulnerabilidad del Estuario en el Estuario de Suances. EVIs bajos en color verde (0.0-0.4, menos vulnerable), EVIs medios en color amarillo (0.4-0.6, vulnerable), EVIs altos en color naranja (0.6-0.9, más vulnerable) y EVIs más altos en color rojo (0.9-1.0, lo más vulnerable). Panel b): Distribución espacial de la aceptabilidad para el cálculo detallado en el Estuario de Suances.

Nombre Tóxico	Caso 0 C (mg/l)	Caso 1 C (mg/l)	Caso 2 C (mg/l)
ID1 ($CHCl_3$)	0.02	0.02/50=0.0004	0.02/100=0.0002
ID2 (Pb)	1.00	1.00/5=0.2	1/10=0.1

Tabla 18: Casos de revaluación de ID1 e ID2 mediante la reducción de la concentración de tóxico para delimitar MZs.

Número Años	Nombre Tóxico	AA-MZ m^2	AA-AD* AA-MAS*	MAC-MZ m^2	MAC-AD* MAC-MAS*
40	ID1 ($CHCl_3$)	1595842.23	47.13>3.85	-	-
100	ID1 ($CHCl_3$)	741056.16	19.62>3.85	-	-
40	ID2 (Pb)	1385980.74	44.45>3.85	115.01	0.0024<1.15
100	ID2 (Pb)	735870.42	23.11>3.85	0.00	0.00<1.15

Tabla 19: Extensión de las zonas de mezcla delimitadas (AA-MZ and MAC-MZ) y admisibilidad final (AA-AD* and MAC-AD*) en el cálculo detallado ("caso de reducción 1") para ID1 e ID2.

3.5.6. Revaluación de descargas inadmisibles

Después de efectuar el cálculo detallado, los efluentes industriales ID1 e ID2 continúan clasificándose como inadmisibles por lo que el árbol de decisiones recomienda reiniciar la metodología en el Paso 1 con el fin de continuar con el procedimiento de asignación hasta llegar a unas zonas de mezcla admisibles.

Como ejemplo de esta revaluación, se decidió reducir la concentración de ID1 e ID2 por diferentes factores como se señala en la tabla 18. En dicha tabla cabe señalar que el caso 0 se refiere a los vertidos sin ninguna reducción, es decir, el caso de estudio ilustrado en las secciones previas.

3.5.6.1. Caso de reducción 1

Delimitación de zonas de mezcla

Después de todas las simulaciones, se delimitaron la AA-MZ y MAC-MZ aplicando el método desarrollado para el "caso de reducción 1". De la misma manera que en el caso 0, se efectuaron dos reconstrucciones: 40-años de forzamientos y 100-años estadísticos generados por técnicas de Monte Carlo.

La AA-MZ y MAC-MZ delimitadas del "caso de reducción 1" para ID1 en el caso de 40 años (a-b) y el caso de 100-años estadísticos (c-d) se muestran en la figura 110. Como se mencionó anteriormente, el cloroformo (ID1) no tiene un valor aplicable de MAC-MZ por lo que en esta figura la MAC-MZ fue sólo un ejemplo de la extensión de la MAC-MZ considerando como umbral el valor de la AA-EQS. Mientras tanto en la figura 111 se indican la AA-MZ y MAC-MZ delimitadas del "caso de reducción 1" para ID2 en el caso de 40 años (a-b) y el caso de 100-años estadísticos (c-d).

Admisibilidad final (AD)*

Una vez delimitadas ambas MZs, se evaluó la admisibilidad final de dichas zonas (Ecuación (30)). En la tabla 19, se recoge la extensión de la AA-MZ y la MAC-MZ así como el valor de la admisibilidad de AA-AD* y MAC-AD* para ID1 e ID2 en ambas reconstrucciones.

Como se puede apreciar en la tabla 19, todas las descargas presentaron una AA-AD* mayor que el AA-MAS* (3.85 %) independientemente del numero de años empleado en la reconstrucción por lo que las AA-MZs no son admisibles. Además, la descarga del efluente ID2 presentó una MAC-MZ admisible porque la MAC-AD* fue más pequeña que el MAC-MAS* (1.15 %). De hecho, todas las MAC-MZ delimitadas por debajo del 4 % de probabilidad del MAC-Fallo fueron admisibles porque también permanecieron por debajo del valor del MAC-MAS* (1.15 %).

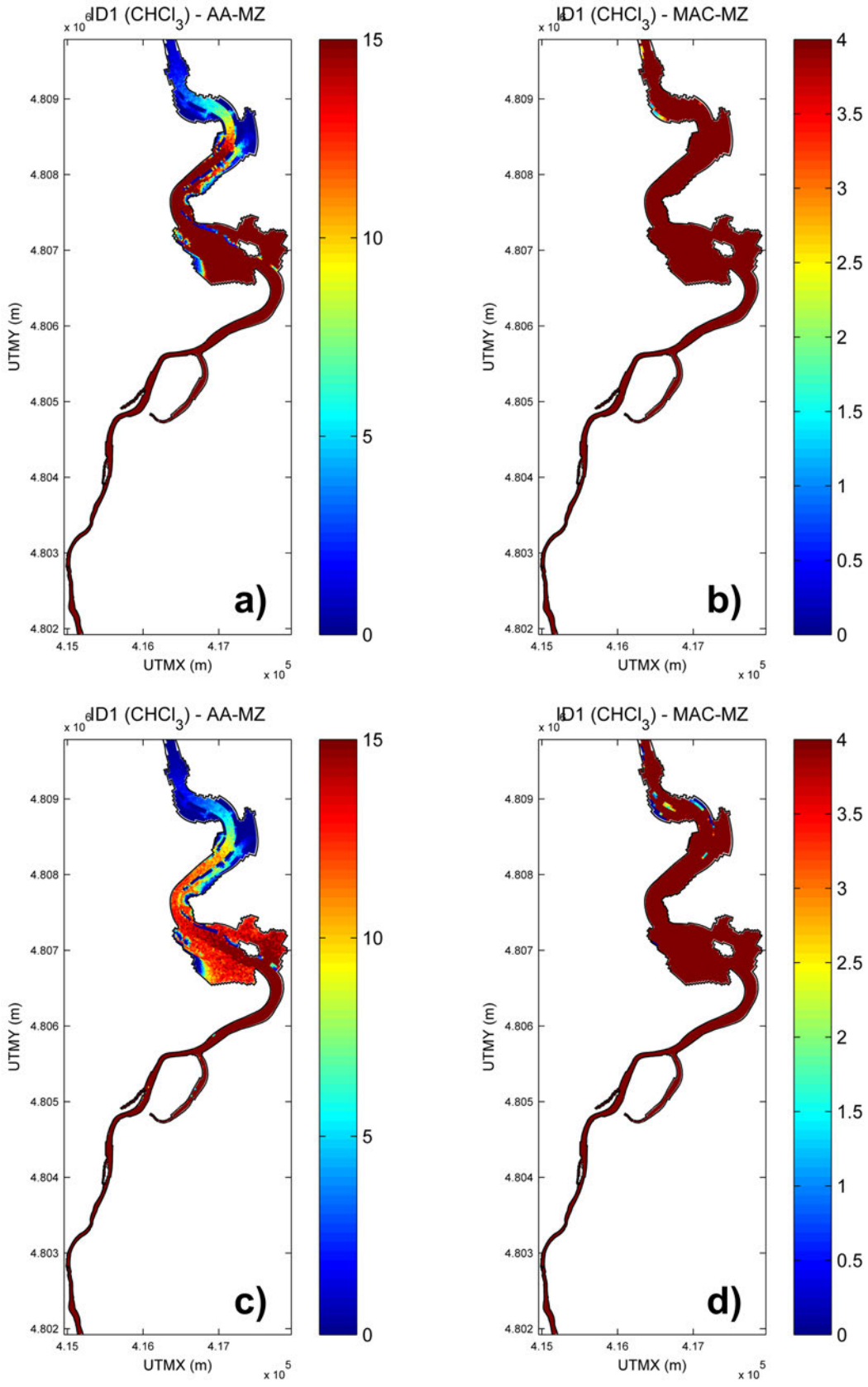

Figura 110: Zonas de mezcla delimitadas en el "caso de reducción 1" para ID1. AA-MZ de 40 años (a), MAC-MZ de 40 años (b), AA-MZ de 100-años estadísticos (c) y MAC-MZ de 100-años estadísticos (d).

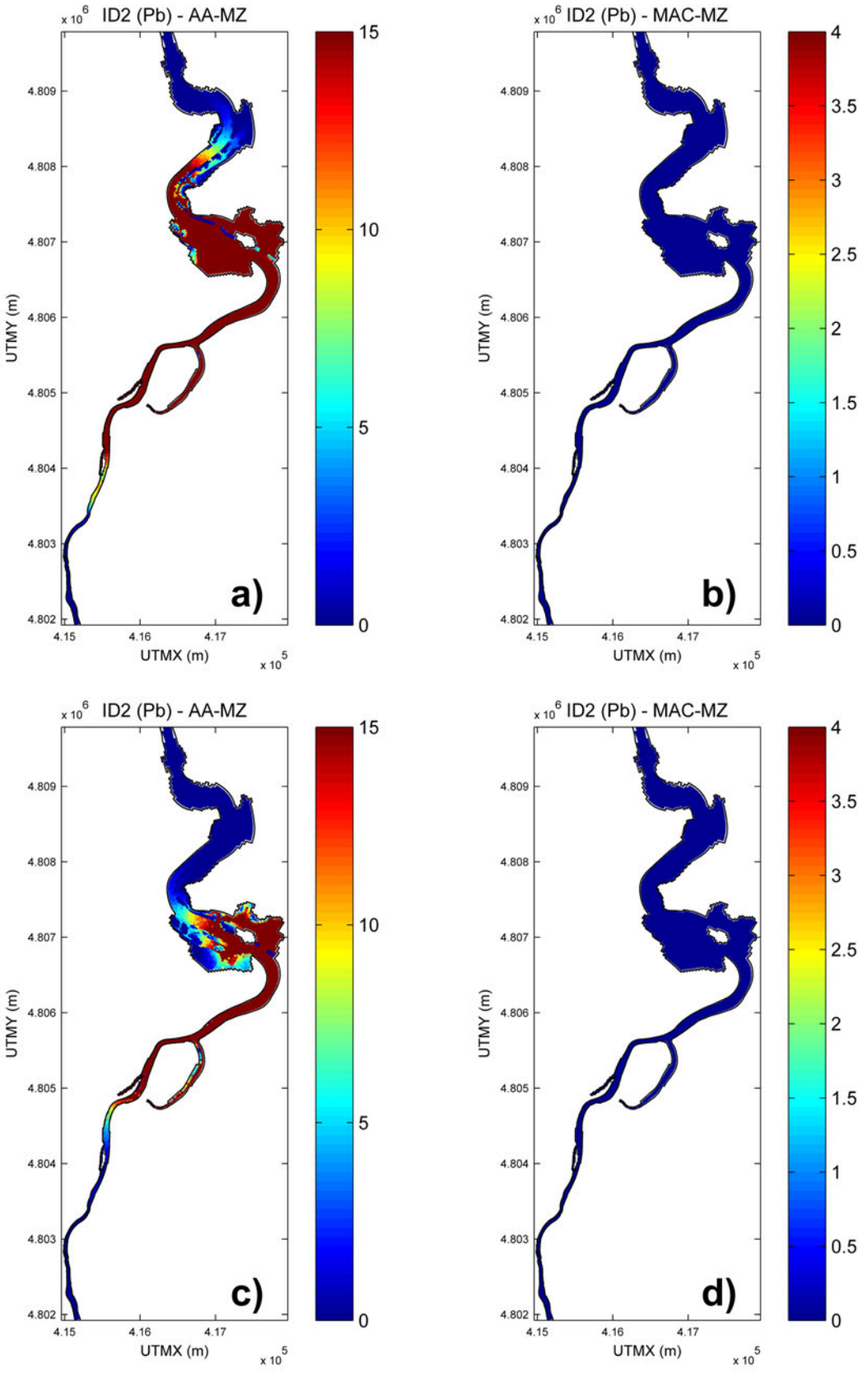

Figura 111: Zonas de mezcla delimitadas en el "caso de reducción 1" para ID2. AA-MZ de 40 años (a), MAC-MZ de 40 años (b), AA-MZ de 100-años estadísticos (c) y MAC-MZ de 100-años estadísticos (d).

Número Años	Nombre Tóxico	AA-MZ m^2	AA-AD* AA-MAS*	MAC-MZ m^2	MAC-AD* MAC-MAS*
40	ID1 ($CHCl_3$)	38420.27	0.174<3.85	-	-
100	ID1 ($CHCl_3$)	7302.25	0.027<3.85	-	-
40	ID2 (Pb)	0.00	0.00<3.85	0.00	0.00<1.15
100	ID2 (Pb)	0.00	0.00<3.85	0.00	0.00<1.15

Tabla 20: Extensión de las zonas de mezcla delimitadas (AA-MZ and MAC-MZ) y admisibilidad final (AA-AD* and MAC-AD*) en el cálculo detallado ("caso de reducción 2") para ID1 e ID2.

Por tanto, la extensión de la AA-MZ fue de nuevo inadmisible para ID1 e ID2 en el "caso de reducción 1" y, consecuentemente, ambos vertidos fueron clasificados como inadmisibles.

3.5.6.2. Caso de reducción 2

Delimitación de zonas de mezcla

Después de todas las simulaciones, se delimitaron la AA-MZ y MAC-MZ mediante la aplicación del método desarrollado para el "caso de reducción 2" de la misma manera que en el "caso de reducción 1".

La AA-MZ y MAC-MZ delimitadas del "caso de reducción 2" para los vertidos ID1 e ID2 en el caso de 40 años (a-b) y el caso de 100-años estadísticos (c-d) se muestran en las figuras 112 y 113 respectivamente.

Admisibilidad final (AD)*

Una vez delimitadas todas las MZs, se evaluó la admisibilidad final de dichas zonas (Ecuación (30)). En la tabla 20, se resume la extensión de la AA-MZ y la MAC-MZ así como el valor de la admisibilidad de AA-AD* y MAC-AD* para ID1 e ID2 en ambas reconstrucciones.

Como se puede apreciar en la tabla 20, el vertido ID2 no presentó MZs (0 m^2). En lo referente al vertido ID1, ambas reconstrucciones presentaron una admisibilidad final AA-AD* menor que el AA-MAS* (3.85 %). A continuación, se evaluó la asignación de dicha zona de mezcla mediante un ábaco (ver figura 114) que describe la evolución de la AA-AD* con el percentil 5 de la probabilidad de AA-Fallo para los 40-años (línea continua gris) y los 100-años (línea continua negra).

Todas las AA-MZ delimitadas por debajo del 15 % de probabilidad de AA-Fallo fueron admisibles porque estuvieron también por debajo del AA-MAS* (3.85 %). Dentro de estas AA-MZ admisibles, la delimitación definitiva debe ser discutida y acordada entre la industria y la autoridad competente debido a las implicaciones económicas, sociales y ecológicas de cualquier delimitación.

Por tanto, la extensión de cualquier MZ fue admisible para ID1 e ID2 en el "caso de reducción 2" y, consecuentemente, ambos vertidos fueron clasificados como admisibles (significativos muy grandes). Para finalizar, la figura 115 presenta la delimitación definitiva de la AA-MZ de la descarga industrial 1 (ID1) en el "caso de reducción 2" para los 40-años de reconstrucción (a) y los 100-años de reconstrucción (b) en el estuario de Suances. En esta figura, la probabilidad de AA-Fallo (%) se coloreó en amarillo claro para porcentajes entre 0 y 1, en amarillo oscuro de 1 a 2, en naranja claro desde 2 hasta 5, en naranja oscuro de 5 a 10, en rojo claro de 10 a 15 y en rojo oscuro desde 15 hasta 100.

Para concluir con la aplicación, cabe señalar que a la vista de los resultados obtenidos para 40 años y 100 años las zonas de mezcla delimitadas son menores en el caso de 100 años debido a que esta reconstrucción recoge una variabilidad mayor de los forzamientos hidrodinámicos.

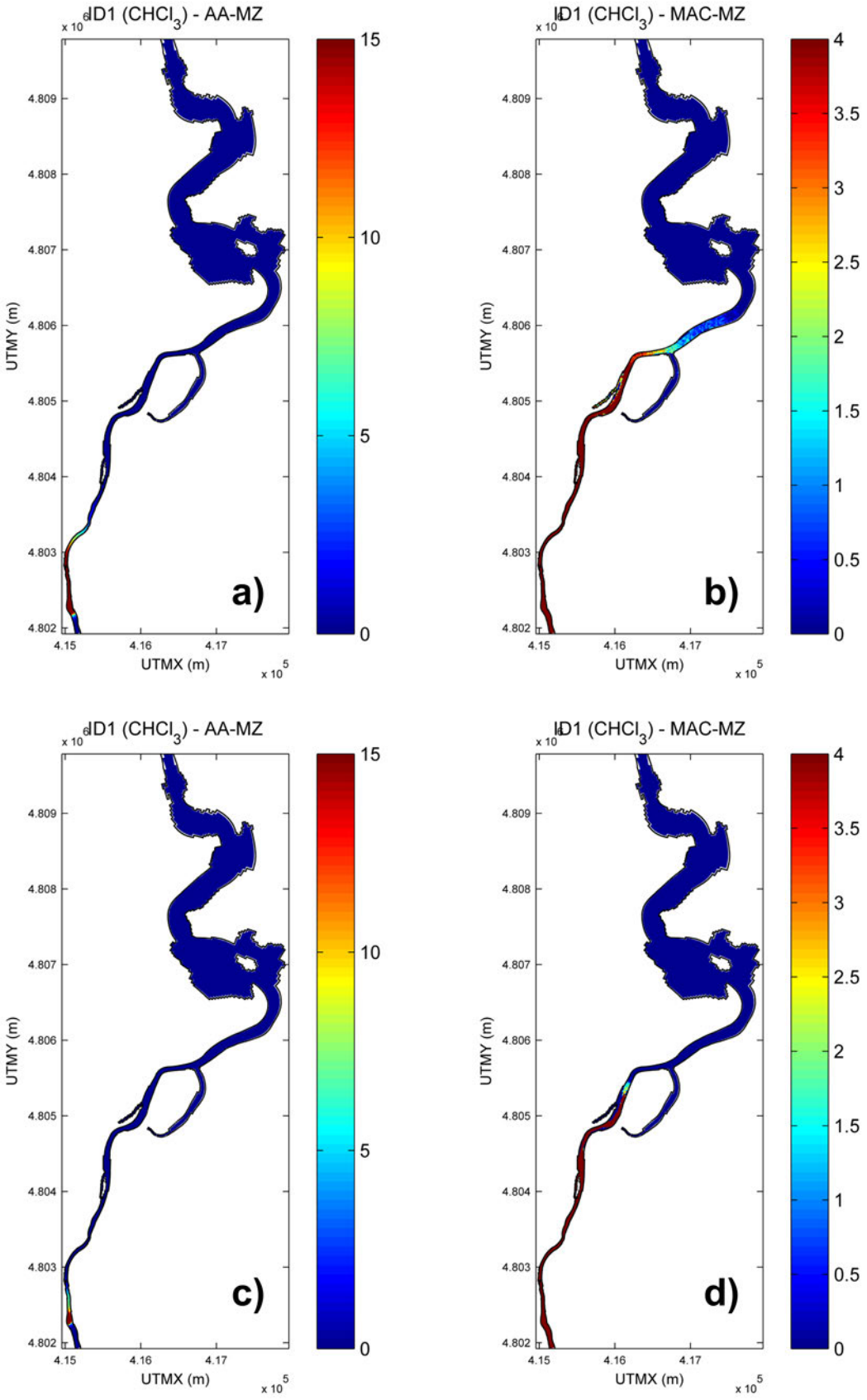

Figura 112: Zonas de mezcla delimitadas en el "caso de reducción 2" para ID1. AA-MZ de 40 años (a), MAC-MZ de 40 años (b), AA-MZ de 100-años estadísticos (c) y MAC-MZ de 100-años estadísticos (d).

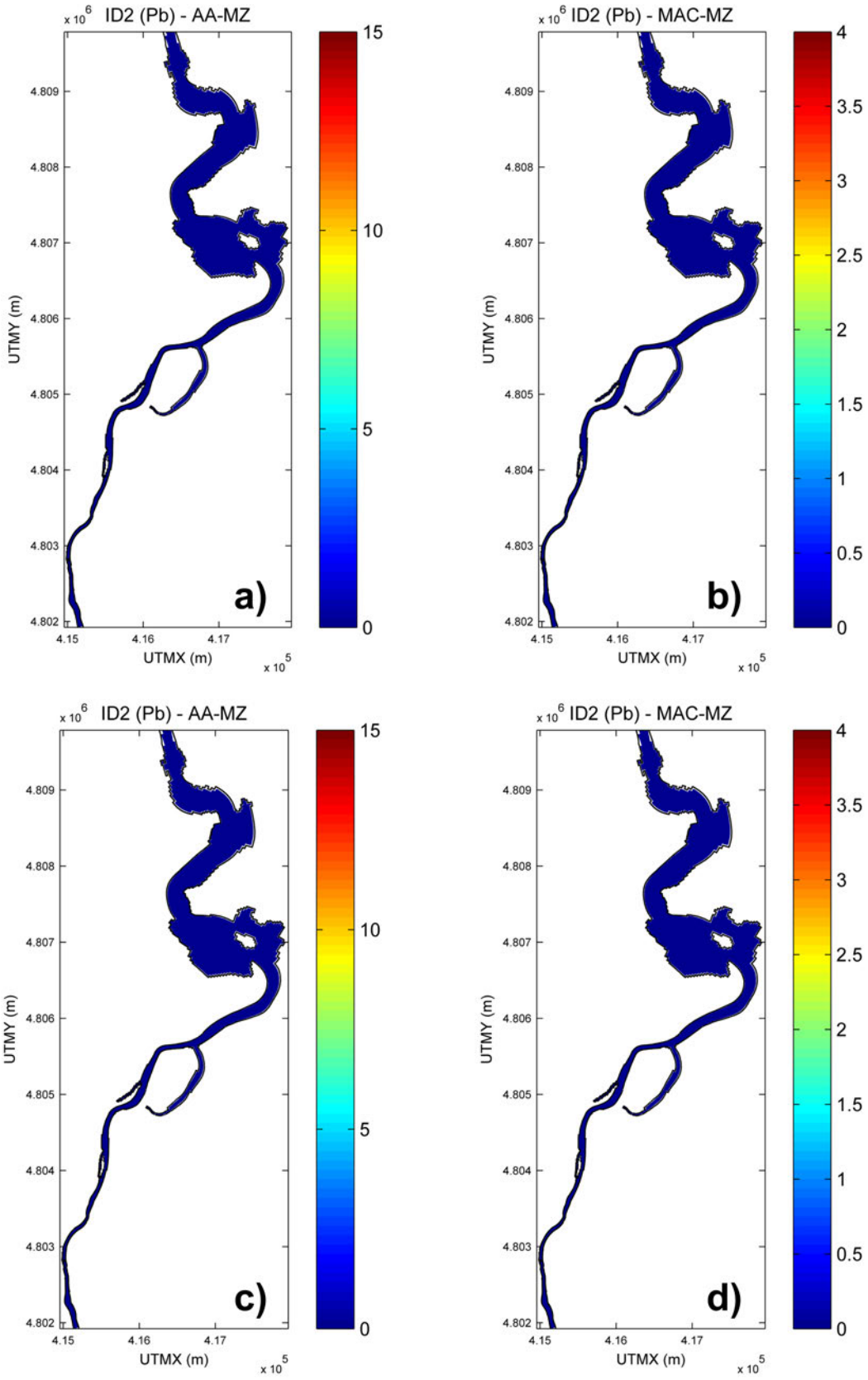

Figura 113: Zonas de mezcla delimitadas en el "caso de reducción 2" para ID2. AA-MZ de 40 años (a), MAC-MZ de 40 años (b), AA-MZ de 100-años estadísticos (c) y MAC-MZ de 100-años estadísticos (d).

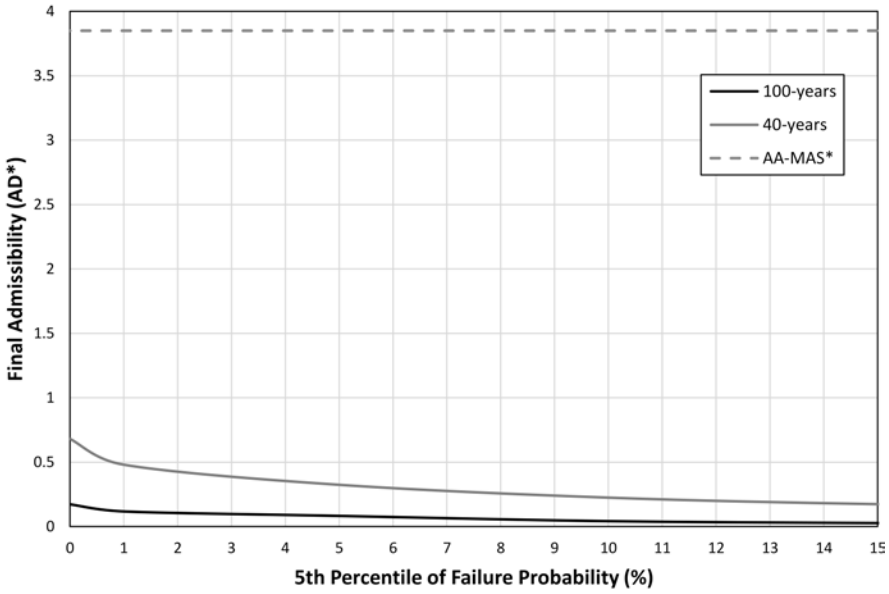

Figura 114: Ábaco de ID1 presentando la evolución de la admisibilidad final (AA-AD*) de zonas de mezcla (AA-MZ) con el percentil 5 de la probabilidad de AA-Fallo para los 40-años (línea continua gris) y los 100-años (línea continua negra) en el cálculo detallado del "caso de reducción 2". El valor del tamaño máximo permitido (AA-MAS*) en el estuario de Suances se representa con la línea discontinua gris.

4. Conclusiones y futuras líneas de investigación

4.1. Conclusiones

El término Zona de Mezcla, utilizado en las Directivas sobre normas de calidad de aguas, no tiene una relación directa con la clasificación en el campo cercano, intermedio o lejano. Por lo tanto, el mapa de isoconcentración admisible se puede encontrar en cualquiera de estas regiones en función de las características del efluente descargado, la advección, la mezcla y/o la degradación. Por esta razón, se necesita un enfoque de modelado zonal considerando la aplicación de diferentes modelos en regiones con propiedades hidrodinámicas distintas. Hoy en día, parece razonable abordar la delimitación de zonas de mezcla utilizando un modelo numérico integrado donde varios modelos de transporte para cada región de mezcla están alimentados por un modelo hidrodinámico.

En relación con estos modelos numéricos, en las últimas décadas, se ha hecho un progreso significativo en su desarrollo convirtiéndolos en herramientas fiables para la gestión ambiental y para aplicaciones de ingeniería dentro de todas las regiones de mezcla (campo cercano, intermedio y lejano).

Como regla general, los enfoques metodológicos para delimitar zonas de mezcla en cualquier sistema acuático se basan en dos criterios ambientales de calidad del agua: el criterio de toxicidad aguda de máxima concentración y el criterio de toxicidad crónica de concentración media. A pesar de que todas las metodologías propuestas son buenas herramientas para empezar a hacer frente a los riesgos asociados a la descarga de aguas residuales, las métricas, fórmulas y cálculos que se describen están generalmente demasiado orientados hacia otros sistemas acuáticos, especialmente las descargas fluviales. En el caso de vertidos estuarinos, la asignación de zonas de mezcla es un tanto ambigua porque carece de una explicación detallada de las tareas necesarias para llevar a cabo este tipo de trabajo.

Por todo ello, la delimitación de zonas de mezcla en estuarios necesita de una metodología que tenga en cuenta la variabilidad espacial y temporal de los procesos hidrodinámicos y de transporte, la vulnerabilidad de las aguas receptoras y los usos del suelo y del agua.

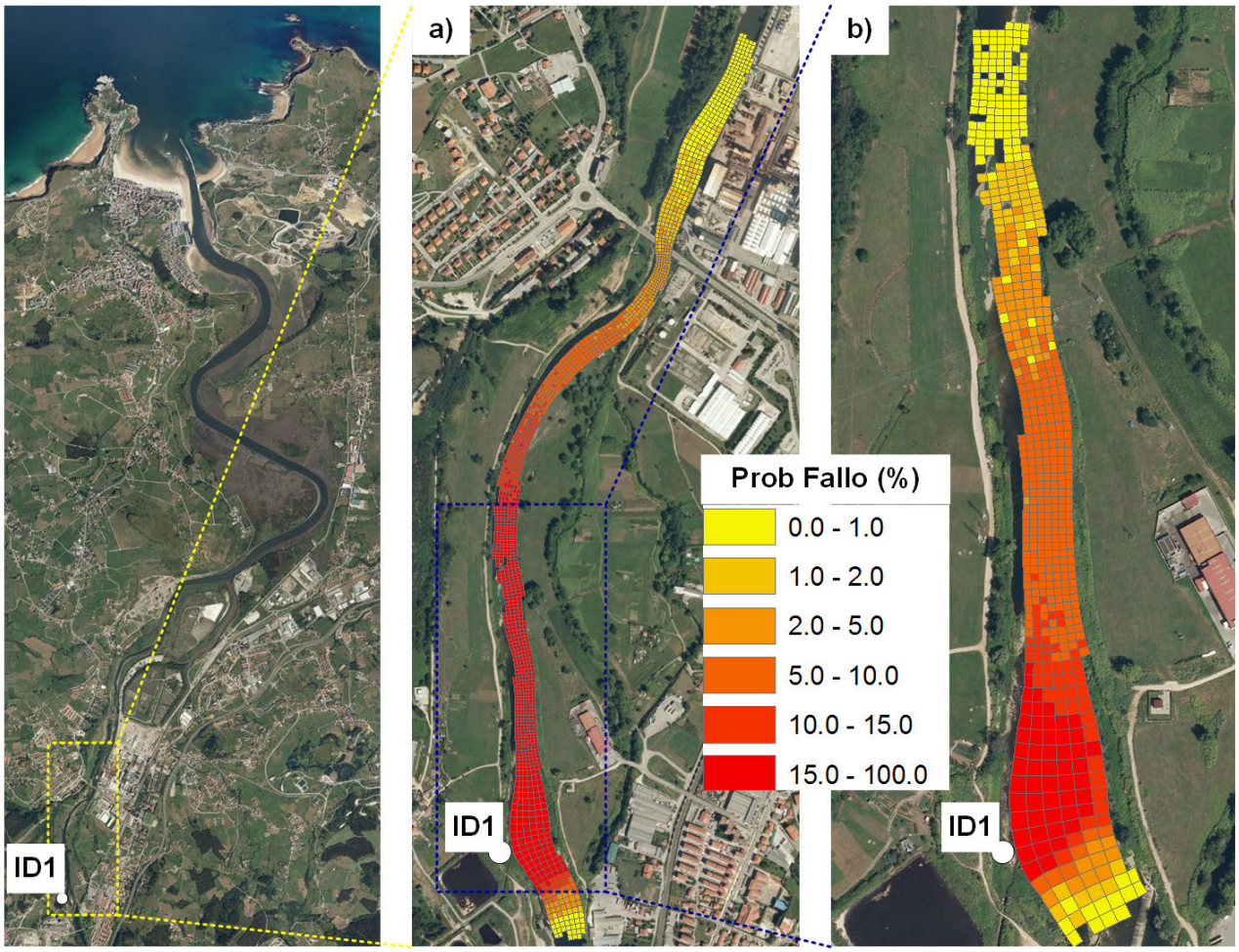

Figura 115: Delimitación definitiva de la AA-MZ en el "caso de reducción 2" para ID1 donde los porcentajes desde 0 hasta 1 se colorearon en amarillo claro, de 1 a 2 (amarillo oscuro), de 2 a 5 (naranja claro), de 5 a 10 (naranja oscuro), de 10 a 15 (rojo claro) y de 15 a 100 (rojo oscuro). AA-MZ de 40-años (a) y AA-MZ de 100-años (b).

Metodología general

La metodología escalonada propuesta proporciona una solución a medida con un nivel de detalle adecuado para la delimitación de zonas de mezcla de cada vertido en forma de diagramas de flujo esquemáticos. La regla general es que los costes del procedimiento de delimitación aumentarán con el nivel de sofisticación. En cada paso, el objetivo es identificar aquellos vertidos que no son motivo de preocupación y señalar las descargas que requieren medidas para reducir el tamaño de sus zonas de mezcla. La filosofía del árbol de decisiones es incrementar los recursos utilizados cuando aumenta el orden de la descarga.

Dicha metodología promueve un marco uniforme y sólido para tales delimitaciones con el fin de proporcionar soluciones que son: *eficientes* porque se emplean los recursos sólo cuando se necesitan, *robustas* porque conducen a decisiones reproducibles que contribuyen al uso sostenible del medio estuarino y *flexibles* porque satisfacen las necesidades de los estuarios de Europa.

Las figuras 116 y 117 ponen de relieve, en la metodología propuesta, las aportaciones realizadas por esta tesis con el fin de progresar en el conocimiento de las lagunas identificadas en color rojo.

En el Paso 1, se diseñaron dos fichas resumen con el fin de reunir la información referente a la caracterización preliminar de los efluente(s) y el área de estudio.

En el Paso 2, se implementó un método para detectar descargas que no tienen un impacto relevante en las aguas estuarinas con base en fórmulas sencillas.

En el Paso 3, se propuso un cálculo simplificado basado en la dilución física para el estudio de tóxicos en el campo cercano y lejano. Para ello, se consideraron las sustancias tóxicas como conservativos. En dicho cálculo:

- Se describieron y definieron los requisitos para configurar el modelo hidrodinámico. Para ello, se sugiere el uso de un modelo tridimensional que resuelva la ecuación de aguas someras mediante la discretización del área de estudio con una malla de celdas cuadradas o curvilíneas.
- Se establecieron los forzamientos hidrodinámicos del lado de la seguridad asumiendo condiciones fijas: una amplitud de marea constante e igual a A10 y un caudal del río constante e igual al 7Q10.
- Se asumió y desarrolló un enlace pasivo para el cálculo de la dilución inicial donde la salida del modelo hidrodinámico (variables ambientales) es la entrada para el modelo de campo cercano durante todo el tiempo de interés.
- Se supuso y desarrolló un acoplamiento pasivo donde el flujo inducido por la descarga, aunque considerablemente importante para la mezcla en el campo cercano, no cambia las características de flujo en el campo lejano. Las variables determinadas fueron la concentración diluida, la longitud, la anchura, el espesor y la altura de atrape del chorro-pluma.
- Dado que los modelos integrales de chorro no tienen en cuenta la interacción con los contornos, se desarrollo un algoritmo que determina el final de campo cercano cuando el chorro-pluma incide sobre cualquier contorno (superficie libre, capa estratificada o paredes).
- Se describieron y definieron los requisitos para configurar el modelo de transporte en el campo lejano (enfoque conservativo). Para ello, se sugiere el uso de un modelo tridimensional que resuelva la ecuación de advección-difusión mediante la discretización del área de estudio con una malla de celdas cuadradas o curvilíneas.
- La AA-MZ se definió como un área dentro del dominio del modelo donde las concentraciones modeladas, promediadas en el tiempo, exceden la AA-EQS. La MAC-MZ se definió como un área dentro del dominio del modelo donde las concentraciones modeladas exceden la MAC-EQS.

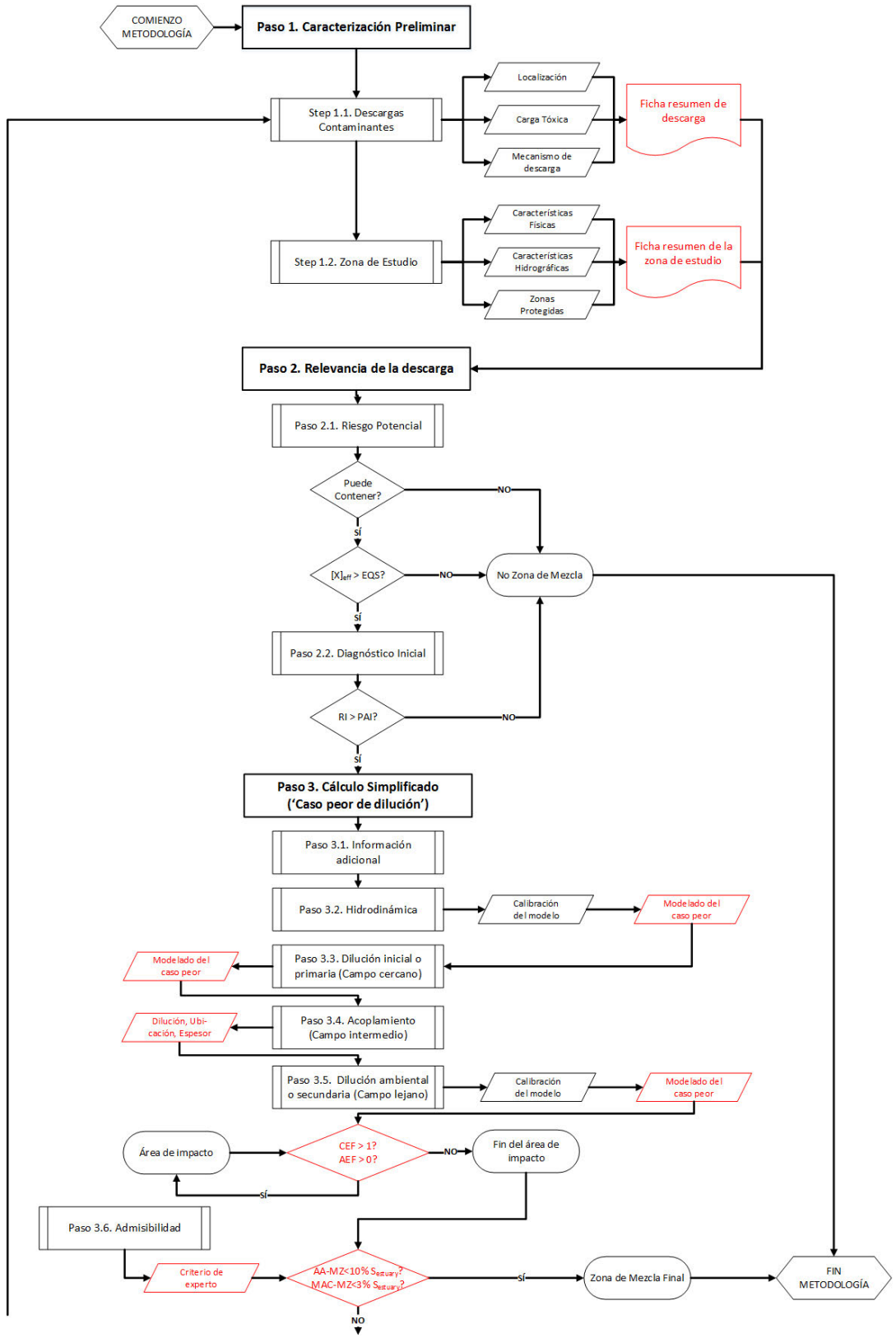

Figura 116: Vista completa de la metodología propuesta donde se destacan en color rojo las lagunas identificadas. Parte 1.

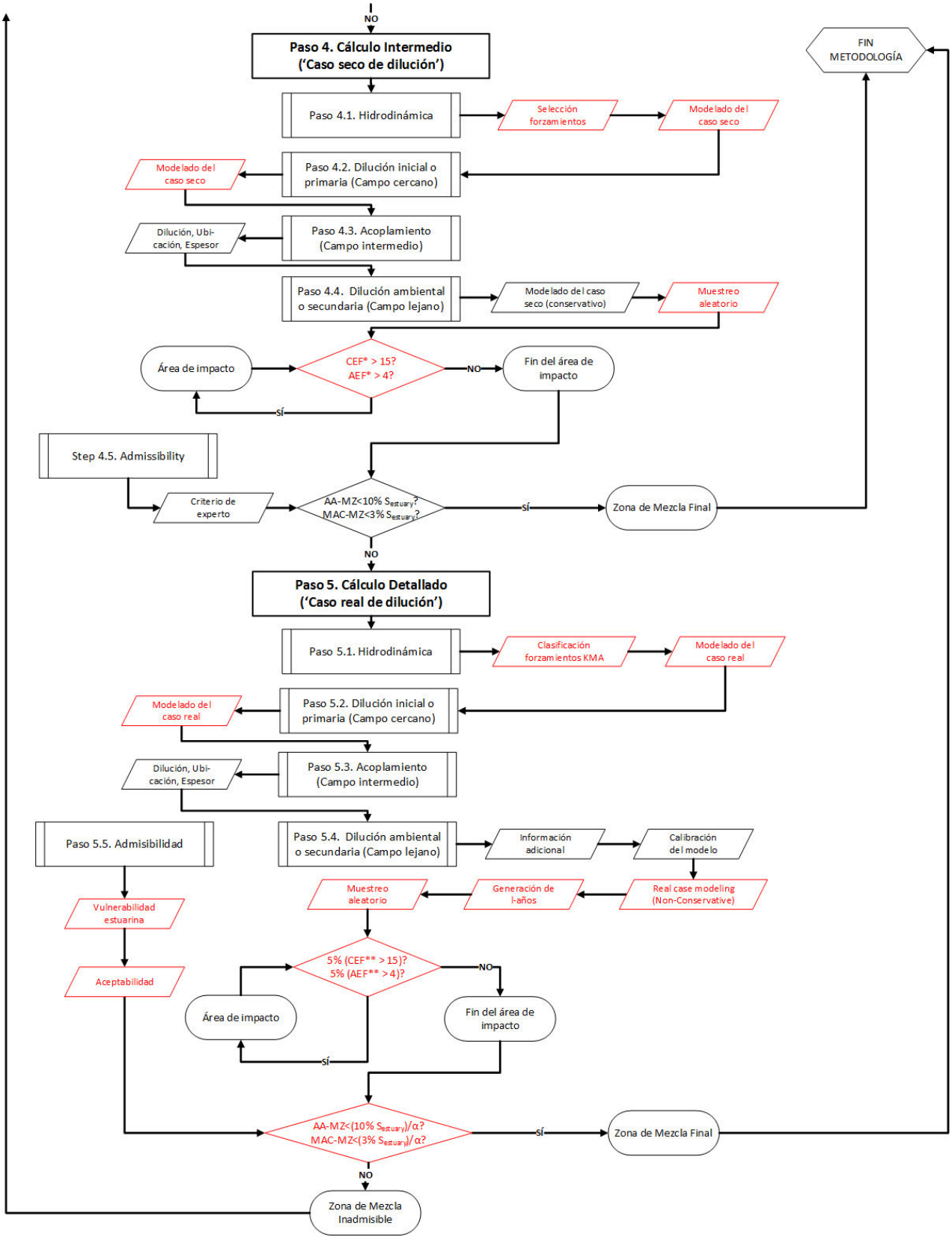

Figura 117: Vista completa de la metodología propuesta donde se destacan en color rojo las lagunas identificadas. Parte 2.

- Los criterios de admisibilidad se especificaron mediante criterio de expertos siendo para la AA-MZ que no supere el 10 % del área estuarina y para la MAC-MZ el 3 %.

En el Paso 4, se propuso un cálculo intermedio basado en la simulación continua de un año real donde:

- Se determinó el "caso seco de dilución" asumiendo un año real de forzamientos siendo el año más seco de la serie histórica a largo plazo del caudal fluvial y sus elevaciones de marea asociadas.
- Se propusieron dos simulaciones para modelar el transporte en el campo lejano: Una "presimulación" para obtener la condición inicial adecuada de concentración tóxica y otra "simulación" para registrar la evolución de concentración a lo largo del año más seco.
- Para lograr la delimitación de zonas de mezcla, se desarrolló un método en tres niveles: Especificación del número de muestras anual, Determinación del número óptimo de muestreos y Delimitación definitiva de las zonas de mezcla.
- En este Paso se asumió que la vida acuática está suficientemente protegida frente a la toxicidad crónica (AA-EQS) si la probabilidad de AA-Fallo de los muestreos es menor del 15 % y frente a la toxicidad aguda (MAC-EQS) si la probabilidad de MAC-Fallo de los muestreos es menor del 4 %.

Por último, en el Paso 5, se propuso un cálculo detallado basado en el análisis de las variaciones espaciales y temporales de los forzamientos (marea y ríos) y en un comportamietno no conservativo de los tóxicos.

- Se desarrolló una metodología capaz de seleccionar los escenarios hidrodinámicos más relevantes en un estuario con base en períodos de corto plazo teniendo en cuenta la evolución en el tiempo y la probabilidad de ocurrencia de los forzamientos. Dicha metodología se dividió en varias etapas: Obtención de los datos de forzamientos hidrodinámicos, Reordenamiento de los datos de entrada para la clasificación, Aplicación del criterio de agrupamiento propuesto y Análisis de sensibilidad para forzamientos y modelado.
- Se describió el modelo conceptual (procesos e interacciones) que, al menos, debe incluir el modelo de transporte de sustancias no conservativas.
- Se describieron y definieron los requisitos para configurar el modelo de transporte en el campo lejano (enfoque conservativo). Para ello, se sugiere el uso de un modelo tridimensional que resuelva la ecuación de advección-difusión-reacción mediante la discretización del área de estudio con una malla de celdas cuadradas o curvilíneas.
- Para obtener la delimitación de zonas de mezcla, se desarrolló un método en cuatro niveles: validación de la serie reconstruida, selección y generación de l-años, muestreo aleatorio y delimitación definitiva de las zonas de mezcla.
- En este Paso se asumió que la vida acuática está suficientemente protegida frente a la toxicidad crónica (AA-EQS) si el percentil 5 de la probabilidad de AA-Fallo de los muestreos es menor del 15 % y frente a la toxicidad aguda (MAC-EQS) si el percentil 5 de la probabilidad de MAC-Fallo de los muestreos es menor del 4 %.
- Con el fin de establecer los criterios de admisibilidad, se desarrolló una metodología basada en un enfoque holístico que considera simultáneamente los procesos físicos involucrados en los mecanismos de dispersión y de difusión, las características ecológicas de la masa de agua receptora y los aspectos sociales relacionados con los usos del agua (vulnerabilidad). Dicho método se estableció en cuatro niveles: Índice de Vulnerabilidad Estuarina (EVI), Aceptabilidad (AC*), Tamaño máximo permitido (MAS*) y Admisibilidad de la zona de mezcla delimitada (AD*).

- Para el cálculo del tiempo de renovación (FT), se desarrolló un enfoque metodológico basado en el uso de herramientas computacionales y dividido en cuatro niveles: Análisis de forzamientos hidrodinámicos, Cálculo del tiempo de renovación, Análisis de sensibilidad del tiempo de renovación y Tiempo de renovación definitivo.

- Se desarrolló un método para localizar las zonas mezcladas verticalmente, parcialmente mezcladas/estratificadas y estratificadas en estuarios basado en el uso de modelos hidrodinámicos y herramientas matemáticas para el cálculo de la estratificación y dividido en tres etapas: Selección y modelado de escenarios hidrodinámicos, Cálculo del número de Richardson y Zonificación final del tipo de estratificación.

Resultados: Aplicación al Estuario de Suances

La metodología escalonada propuesta se aplicó a la ría de Suances teniendo en cuenta dos descargas teóricas y pasando por todos los Pasos con el fin de ilustrarla. A continuación, se resumen las principales conclusiones:

- Se realizó una malla tridimensional utilizando un coordenadas horizontales curvilíneas (93$\times$800 celdas) y 10 σ-capas verticales que cubrieron el estuario de Suances y su zona costera adyacente.

- Tanto el modelo hidrodinámico como el de transporte (enfoque conservativo y no conservativo) se calibraron con un rendimiento aceptable para predecir todas las variables de interés en cualquier punto de la malla de cálculo.

- Para el modelado hidrodinámico, la escala temporal más larga de la respuesta "cuasi-estacionaria" se correspondió con la salinidad y la temperatura siendo igual a 216 horas (9 días). Para el modelado de transporte, la escala temporal más larga de la respuesta "cuasi-estacionaria" fue igual a 528 horas (22 días).

- Se identificó al año 1989 como el año más seco.

- El número óptimo de muestreos fue aproximadamente 1000.

- Las escalas temporales que regulan la señal del caudal fluvial se correlacionaron con la duración media de los eventos de inundación mientras que para las mareas astronómicas con los ciclos mareas muertas y vivas. En el estuario de Suances, ambos forzamientos presentan una escala temporal de unos 15 días. Por lo tanto, los escenarios de modelado se clasificaron con una longitud temporal de 15 días.

- Con base en la clasificación K-means, el número mínimo de simulaciones fue de M_{mm}=5$\times$11=55 y el óptimo de M_{om}=12$\times$48=576. A partir de este rango, el número final de grupos (M) fue de 6(mareas)$\times$13(ríos)=78 escenarios de modelado correspondiente a un tiempo de simulación de 3.205 años (8.013 $\%$ de 40 años). Dichos 78 escenarios asumieron $9 + 15$ días de caudal fluvial y nivel de marea como forzamientos.

- La dilución inicial en ID1 e ID2 computada en cada Paso fue directamente proporcional a la serie temporal del caudal del río. La concentración en ID1 e ID2 fue menor durante eventos de inundación mientras que, para el resto de situaciones, la concentración presentó un rango de variabilidad muy amplio.

- El final del campo cercano para el efluente industrial ID1 se localizó en varias celdas horizontales aguas abajo del punto de descarga. En la dirección vertical, ID1 se mezcló completamente en vertical la mayor parte del tiempo. Para el efluente industrial ID2, el vertido estuvo casi siempre en la celda de la malla donde se ubicó la tubería industrial. Respecto a la distribución vertical, ID2 estuvo la mayor parte del

tiempo entre las capas 4 y 8 (2.5 y 6.5 m) indicando que la pluma se atrapa mientras que, en el resto de situaciones, la pluma emergió hasta alcanzar la superficie libre.

- Los errores obtenidos para ambas descargas durante el período de validación del método de recosntrucción muestran que cualquier "serie real" de concentración de tóxico ($CHCl_3$ and Pb) se puede generar a partir de una secuencia que combina, cada 15 días, el resultado del modelo (78 escenarios) que mejor se ajusta a la "serie real" ("series sintéticas").
- Se efectuaron dos reconstrucciones: una de 40-años (longitud series temporales de forzamientos) y otra de 100-años estadísticos (técnicas de Monte Carlo).
- Se calculó el tiempo de renovación local (LFT) en 20 escenarios obteniéndose que el máximo tiempo fue de 0.949 días (22.78 horas).
- El estuario estuvo la mayor parte del tiempo completamente mezclado en la parte interior debido a la acción de río (agua dulce) llenó la columna de agua. En la parte exterior, el estuario también estuvo completamente mezclado debido a que la acción de las mareas (agua de mar) generó la suficiente turbulencia para mezclar la columna de agua. La sección intermedia estuvo parcialmente mezclada/estratificada en el canal principal y estratificada en zonas intermareales debido a la combinación de forzamientos, el gradiente de profundidad entre el canal principal y las zonas intermareales y las diferencias de salinidad experimentados por la columna de agua.
- Se computó el "Índice de Vulnerabilidad del Estuario" (EVI) siendo su promedio en Suances de 0.615. A partir de la vulnerabilidad, se determinaron los tamaños máximas permitidos para zonas de mezcla siendo el AA-MAS* igual a 3.85 y el MAC-MAS* igua a 1.15.
- Según los resultados obtenidos para 40 años y 100 años las zonas de mezcla delimitadas son menores en el caso de 100 años debido a que esta reconstrucción recoge una variabilidad mayor de los forzamientos hidrodinámicos.

4.2. Futuras líneas de investigación

Teniendo en cuenta los múltiples aspectos cubiertos por la delimitación de zonas de mezcla de vertidos industriales, las futuras líneas de investigación deben tener en cuenta diversos campos del conocimiento. A continuación, se resumen los principales aspectos que requieren mayor investigación.

Diferentes tipos de vertidos se podrían establecer considerando ***otros mecanismos de descarga*** (descargas superficiales o canales) y/o ***otras cargas de tóxico*** (caudal y concentración variables). Por lo tanto, se deben desarrollar herramientas numéricas para modelar otras configuraciones de descarga que pueden ser adecuadas en algunos casos como la descarga directa superficial, el derrame por un acantilado o canales. Para ello, se necesitan datos experimentales para calibrar, probar y validar dichas herramientas.

Otras investigaciones deben estar orientadas a la consideración de ***otros forzamientos hidrodinámicos***, por ejemplo, la velocidad y dirección del viento, el oleaje, la marea meteorológica o incluso la variabilidad espacial de forzamientos estuarinos cuando éstos sean significativos. Sin embargo, uno de los requisitos previos para aplicar el método es que el caudal del río y la marea se consideran eventos independientes. Si se introducen la marea meteorológica, el viento y/o el oleaje, se debe hacer un estudio preliminar de la correlación entre ellos porque la probabilidad conjunta, en este caso, puede no ser el producto de las probabilidades individuales de cada forzamiento. En estos casos, el método de clasificación se debe realizar combinando todas las variables correlacionadas en la misma matriz.

En cuanto a los procesos y modelos de dilución inicial, los modelos integrales de chorro fueron desarrollados para vertidos de aguas profundas por lo que no siempre son fiables cuando se aplican en aguas poco profundas.

En este campo, la ***inclusión de la concentración de fondo*** en el modelo de campo cercano podría ayudar a mejorar la precisión de los modelos integrales de chorro en un primer momento.

Por otro lado, los prometedores ***modelos CFD*** como FLUENT, OpenFOAM o Flow3D se han aplicado en casos relativamente sencillos o en regiones de extensión limitada como la región del campo cercano. Dichos modelos podrían abordar el transporte y mezcla en todas las regiones. Sin embargo, la elevada demanda de recursos computacionales de estos modelos provoca que no parezca factible su empleo hoy en día para la práctica común en todas las regiones de mezcla con multitud de casos hidrometeorológicos. No obstante, los modelos CFD podrían ser útiles para el análisis de casos especiales donde la experimentación física sea demasiado difícil o demasiado cara y los modelos integrales no se puedan aplicar.

Además, la combinación de datos experimentales de chorros con flotabilidad positiva de estudios de laboratorio (técnicas PIV-LIF) con una calibración adecuada de un modelo CFD podría ser una herramienta muy poderosa para mejorar los resultados de la dilución inicial y la definición del campo intermedio en el acoplamiento con modelos de campo lejano. Esta herramienta podría ser también capaz de extender los resultados experimentales con otras condiciones ambientales con el fin de cubrir un amplio rango de variabilidad. A continuación, los resultados del modelo CFD se podrían utilizar para construir un ábaco con la influencia de los parámetros clave en la dilución inicial para vertidos industriales. Finalmente, toda esta información se podría incluir en un sistema experto para predecir el comportamiento de cualquier descarga en el campo cercano.

Otros enfoques de acoplamiento se podrían desarrollar cuando el flujo de cualquier región sea dinámicamente importante. En este enfoque activo, además de la conservación de la masa del fluido y el tóxico ha de considerarse la conservación de cantidad de movimiento. En combinación con este acoplamiento activo, se debe realizar un acople dinámico donde el intercambio de datos entre el modelo de campo cercano y el del lejano se lleva a cabo en cada paso de tiempo, por lo tanto, ambos modelos se ejecutan en paralelo. Como consecuencia, se podría obtener un mayor grado de exactitud.

Los ***coeficientes de partición*** se tomaron a partir de bases de datos químicas. Sin embargo, dichos coeficientes están muy influenciados por el pH, la salinidad, la forma específica de la sustancia tóxica y la composición química de las dos fases (agua y sedimentos). Por lo tanto, una definición correcta de los coeficientes de partición se debe efectuar por medio de datos de campo y su análisis en un laboratorio sobre una base de caso por caso.

En la metodología propuesta, el ***modelo conceptual*** utilizado considera el número mínimo de procesos para el modelado de sustancias no conservativas para asegurar que los resultados sean fiables en la columna de agua. Estudios adicionales podrían incluir interacciones sedimento-agua tales como la difusión, la resuspensión y sedimentación y/o procesos específicos de sedimentos como la consolidación y el enterramiento. Por otra parte, otros ***bioprocesos*** se podrían también incluir con el fin de determinar la influencia de los factores bióticos como el biofilm (una película generada por microalgas y bacterias en la interfase agua-sedimento) en la distribución espacial y temporal de las concentraciones de sustancias tóxicas en agua y sedimentos.

La propuesta para la estimación de la renovación del agua basada en el ***tiempo de renovación local*** asumió condiciones fijas de los forzamientos. En este sentido, se podrían efectuar nuevos estudios con el fin de desarrollar un método basado en condiciones reales de los forzamientos. Por ejemplo, el método podría realizar la estimación del tiempo de renovación local comenzando en cada hora de la serie temporal de forzamientos con el fin de obtener la distribución espacial y temporal del tiempo de renovación local.

El uso del ***Índice de Vulnerabilidad del Estuario*** (EVI) en los criterios de admisibilidad considera el valor medio del estuario para determinar el tamaño máximo permitido de las zonas de mezcla (MAS). Este método se podría mejorar teniendo en cuenta el valor medio de EVI cubierto por cada zona de mezcla para poder delimitar con un criterio más flexible. Sin embargo, dicho enfoque se debe manejar cuidadosamente porque el MAS sería variable y específico para cada descarga.

La ***incertidumbre*** es una fuente inevitable de ruido en la gestión de la calidad del agua y debilitará la toma de decisiones adecuada. La incertidumbre se deriva de la información imperfecta, la variabilidad natural y la falta de conocimiento. La incertidumbre incluye la incertidumbre cuantitativa y la no cuantitativa o cualitativa. Un proceso sistemático de análisis de incertidumbre se puede desarrollar para ayudar en la gestión de la calidad del agua y refinar el proceso de toma de decisiones.

El método desarrollado se centra en descargas individuales pero se podría aplicar a ***descargas múltiples*** cuando dos efluentes están descargando la misma sustancia tóxicas. Sin embargo, los criterios de admisibilidad para descargas múltiples no se abordaron en la metodología. En zonas industrializadas, la descarga de múltiples efluentes puede generar que las zonas de mezcla se solapen o necesiten una evaluación adicional para determinar si el efecto acumulativo se puede considerar aceptable cuando no se crucen dichas zonas de mezcla. El enfoque inicial es el de considerar cada descarga puntual discretamente pero puede suceder que numerosas fuentes puntuales menores exijan la consideración colectiva. En consecuencia, la base para determinar la aceptabilidad de descargas combinadas debe considerar cada caso específicamente y tener en cuenta la carga diaria máxima total asimilada por el estuario, la posible no linealidad, la existencia de umbrales, la correlación entre las descargas o la posibilidad de efectos sinérgicos o antagónicos,

En esta tesis se explica cómo modelar metales pesados y microcontaminantes orgánicos mediante el modelado de plomo y cloroformo en el estuario de Suances. Próximos estudios en este estuario podrían incluir ***otros metales pesados*** como el mercurio, el cromo, el zinc o el arsénico y ***otros microcontaminantes orgánicos*** como PAHs, PCBs, dioxinas o furanos.

Finalmente, la metodología desarrollada o mejorada se podría ***implementar en otros estuarios*** con el fin de validar y reproducirla. De esta manera, se garantizará la idoneidad del método para delimitar zonas de mezcla en cualquier tipo de situación.

4.3. Contribuciones de la tesis

En este apartado, se agruparon todas las contribuciones realizadas por esta tesis en 4 categorías: artículos, conferencias, workshops y proyectos de I+D+i. A continuación, se enumeran las contribuciones llevadas a cabo en cada categoría.

Artículos

1. **Bárcena, J.F.**, García, A., García, J., Álvarez, C., and Revilla, J.A., 2012a. Surface analysis of free surface and velocity to changes in river flow and tidal amplitude on a shallow mesotidal estuary: An application in Suances Estuary (Northern Spain). Journal of Hydrology 420-421, 301-318.

2. **Bárcena, J.F.**, García, A., Gómez, A.G., Álvarez, C., Juanes, J.A., and Revilla, J.A., 2012b. Spatial and temporal flushing time approach in estuaries influenced by river and tide. An application in Suances Estuary (Northern Spain). Estuarine, Coastal and Shelf Science 112, 40-51.

3. Sámano, M.L., **Bárcena, J.F.**, García, A., Gómez, A.G., Álvarez, C., and Revilla, J.A., 2012. Flushing time as a descriptor for heavily modified water bodies classification and management: Application to Huelva Harbour. Journal of Environmental Management 107, 37-44.

4. López, I., Álvarez, C., Gil, J.L., García, A., **Bárcena, J.F.**, Revilla, J.A., 2013. A method for the source apportionment in bathing waters though the modeling of waste water discharges: Development of an indicator and application to an urban beach in Santander (Northern Spain). Ecological Indicators 24, 334-343.

5. Gómez, A.G., **Bárcena, J.F.**, Juanes, J.A., Ondiviela, B., and Sámano, M.L., 2014. Transport time scales as physical descriptors to characterize heavily modified water bodies near ports in coastal zones. Journal of Environmental Management 136, 76-84.

6. **Bárcena, J.F.**, Camus, P., García, A., and Álvarez, C., 2015. Selecting model scenarios of real hydrodynamic forcings on mesotidal and macrotidal estuaries influenced by river discharges using K-means clustering. Environmental Modeling and Software 68, 70-82.

7. **Bárcena, J.F.**, García, J., García, A., and Álvarez, C., 2015. Analysis of the stratification patterns in mesotidal and macrotidal estuaries influenced by river discharges using a 3D hydrodynamic model and K-means clustering. Estuarine, Coastal and Shelf Science (en revisión).

8. **Bárcena, J.F.**, Gómez, A.G., García, A., Álvarez, C., and Juanes, J.A., 2015. Estuarine vulnerability index: quantifying the vulnerability of mesotidal and macrotidal estuaries influenced by river discharges against point-source wastewaters. Ecological Indicators (en preparación).

Conferencias

1. Estuarine and Coastal Sciences Association 47 Symposium. **Javier F. Bárcena**, Andrés García, Aina García, César Álvarez, José A. Juanes, José A. Revilla, 2010. Influence of river flow and tide on water renewal in a narrow and shallow estuary. An application to the Suances Estuary (North of Spain). Comunicación Oral.

2. 9th International Symposium on Ecohydraulics. **Javier F. Bárcena**, Andrés García, César Álvarez, José A. Juanes, 2012. First-Order assessment to delimitate environmental risk zones due to wastewater discharges on estuaries. Comunicación Oral.

3. XVII Congreso de la Asociación Española de Limnología. **Javier F. Bárcena**, Aina G. Gómez, Andrés García, César Álvarez, José A. Juanes, 2014. Estuarine Vulnerability Index: Quantifying the acceptability of mixing zones generated by point discharges. An application to Suances estuary (N Spain). Comunicación Oral.

Workshops

1. Participante en el 2º CIS Mixing Zones Workshop (JRC Centre Ispra, Italy, 2010)

Proyectos I+D+i

Competitivos

1. VERTITOX: Desarrollo de procedimientos para el control operativo integrado de vertidos al medio litoral (urbano e industrial), mediante el uso de biomarcadores, bioensayos e indicadores del estado ecológico (018/RN08/02.1), 2008-2010.

2. QEST: Estudio de los aspectos clave para la determinación de caudales ecológicos en estuarios (CTM2009-10620), 2010-2012.

3. PORTONOVO: Water quality in harbours (2009-1/119), 2010-2012.

4. VULMA: Establecimiento de criterios para la valoración de la vulnerabilidad de las masas de agua sometidas a vertidos urbanos e industriales (CTM2009-11206), 2010-2012.

5. VERTIZE: Análisis de aspectos claves de la dispersión de vertidos industriales para la delimitación de zonas de mezcla ambiental de estuarios (CTM2012-32538), 2013-2015.

No Competitivos

1. Aplicación de la ROM 5.1. “Calidad de aguas litorales en áreas portuarias” en el Puerto de Santa Cruz de Tenerife, 2010-2011.
2. Impacto del nuevo canal de Bocachica en la renovación de agua, salinidad y turbidez de la bahía de Cartagena de Indias, Colombia, 2013.
3. Asistencia técnica para la aplicación de modelos matemáticos para sustitución de la existente EDAR Vuelta Ostrera, 2014-2015.

Be very careful about the beginning.
Then, be very careful about the end.
Then, be very careful about the middle.

Robert Fripp

1 Introduction

In this first chapter, the motivations to carry on the development of this thesis are presented and a schematic overview of the problem "industrial discharges into estuarine waters" is defined.

The importance of estuaries is highly significant because they host multitude of biological and ecological processes (biological niches, specialized biota,...) and numerous human activities (settlement, industry, agriculture, fishing, bathing,...). However, these areas, generating multiple benefits, are constantly threatened by the presence of numerous pressures that limit their productive potential. Therefore, estuarine areas require targeted strategies and effective management to mitigate the effects of such pressures, specially to asses the impact of industrial discharges.

In this sense, this chapter introduces the importance of estuaries, the presence of industrial activity and the established legislative framework in the water policy. Next, the transport and mixing of wastewaters is reviewed and their interrelationship with numerical modeling is presented. Such interaction is important since it demonstrates the possibility and desirability of using numerical models as tools that facilitate the implementation of the current regulations more easily and cheaply when the appropriate model is selected.

Next, the general aim, which will address adequately the underlying problem, is displayed. Lastly, we conclude with a brief description of the layout of this thesis in order to facilitate its following and reading.

1.1 Motivation

All living creatures are immersed in a fluid or another, be it the air of the atmosphere or the water of a river, lake, estuary or ocean; even, soils are permeated with moisture, without which life would be impossible. So, it is no exaggeration to say that life, including our own, is bathed in fluids. Most aquatic forms of life rely on the natural transport of water for their nutrients (Cushman-Roisin 2013).

Water is inextricably bound up with live and the availability of clean water is one of the most crucial factors in human development. Clean water is an essential natural resource. Throughout history, societies have thrived or failed on the basis of their ability to control the import of fresh water for drinking, food production and hygiene and the export of water once it has been employed for waste assimilation and transport. As population densities have increased, local waters have been called upon to absorb more and more pollution. Some of the

world's greatest civilizations, founded on successful efforts to secure clean water for drinking and irrigation, collapsed in part due to their inability to escape the downstream effects of their own pollution (Alley 2007).

Estuaries are transition zones between sea, river, land and atmosphere determining the presence of various gradients of physicochemical conditions and therefore also of biological communities. Consequently, they bring together fluxes of fresh and saline water, as well as fluvial and marine sediments, and contain many biological niches and high biological diversity. This feature makes them systems of great complexity, variability and dynamism, which is a unique ecosystem of great beauty and a specialized biota. Estuaries constitute an environment of great interest to those disciplines that deal with biology, geology, chemistry, physics, history or social issues by the specific features of their condition ecotone.

Throughout the history of humankind, estuaries have always been one of the most populated areas on Earth. Currently, about 60% of the world's population lives near the coast and estuaries comprising 5.2% of the Earth's surface, and only 2% of the volume of the oceans (Lindeboom 2002). Estuaries are areas of high socioeconomic importance, with 22 of the 32 largest cities in the world being located on them (Valle-Levinson 2010).

Thus, the major threats to the health, productivity and biodiversity of the estuarine environment result from human activities on land and further inland (Halpern *et al.* 2008, Lotze *et al.* 2006, Recio *et al.* 2013). The most important are estuary margin development (population growth and coastal settlement), wastes and run-off from urban, industrial and agricultural activities, increased demands for recreational uses (boating), development in estuaries (marine farms and marinas), catchment development (forestry and agriculture), land clearance and reclamation, excavation and dredging, introduction of invasive species, resource extraction (overfishing) and long term climate changes including sea-level rise (Figure 1.1). The impacts from land-based activities include closures of shellfish growing areas, degraded beaches, destroyed habitat of vital importance to maintain ecosystem health and contaminated sites.

Although their conservation has become a major cause of concern, in the last decade a significant decline of estuarine ecosystems have been reported worldwide (Chainho *et al.* 2008, Foster *et al.* 2013, Ondiviela *et al.* 2015). The Millennium-Ecosystem-Assessment (2005) estimated around the 50% of the original saltmarsh ecosystems are lost or degraded. The consequences of these impacts are causing that estuarine areas are unable to maintain the quality of life that people looked when they migrated first.

One of the main sources of pollution of estuaries could be considered coming from industrial wastewaters (Gómez *et al.* 2004, Roose & Brinkman 2005). Any industry, in which water obtained from an industrial water treatment system or a well comes in contact with a process or product can add pollutants to the water. Pollutants are defined as substances in the environment that occur above expected background concentrations. Then, the resulting water is classified as a wastewater. Industry use about 20% of the globally accessible runoff and generate a stream of wastewater, which flows or seeps into aquatic systems such estuaries. These wastewaters contain numerous chemical compounds in varying concentrations. About 300 million tons of synthetic compounds annually used in industrial and consumer products partially find their way into natural waters (Schwarzenbach *et al.* 2006). Figure 1.2 illustrates the worldwide location of industrial areas (blue dots) and seasonal zones of oxygen depleted waters (red dots). As it can be seen in this figure, the major threats are generally correlated to areas with high industrial density and located at estuarine areas.

For example, industry is the greatest source of pollution in the United States, accounting for more than half the volume of all water pollution and for the most deadly pollutants. There are approximately 50000 discharge permits with 5 years duration in the USA (USEPA 2010). In its National Water Quality Inventory, reported to Congress in 1996, the U.S. Environmental Protection Agency concluded that approximately 40% of the nation's surveyed estuaries were too polluted for such basic uses as drinking supply, fishing and swimming (USEPA 1996). In England and Wales, there are over 2000 wastewater outfalls discharging directly to estuaries, many of which are used for shellfish cultivation and harvesting (UKEA 2011c). This number of

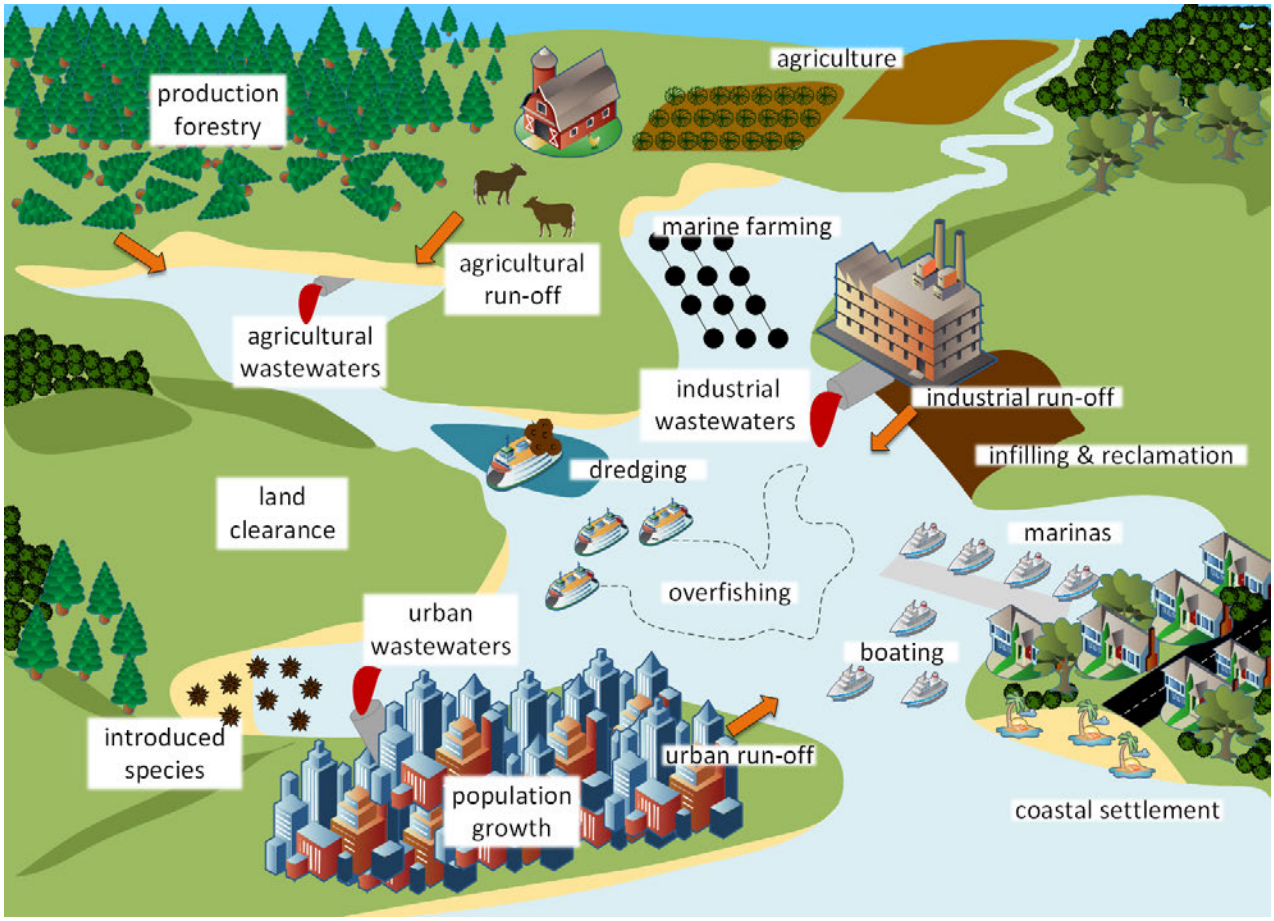

Figure 1.1: Diagram of the main human activities on land and further inland happening in and around estuaries that affect their health, productivity and biodiversity.

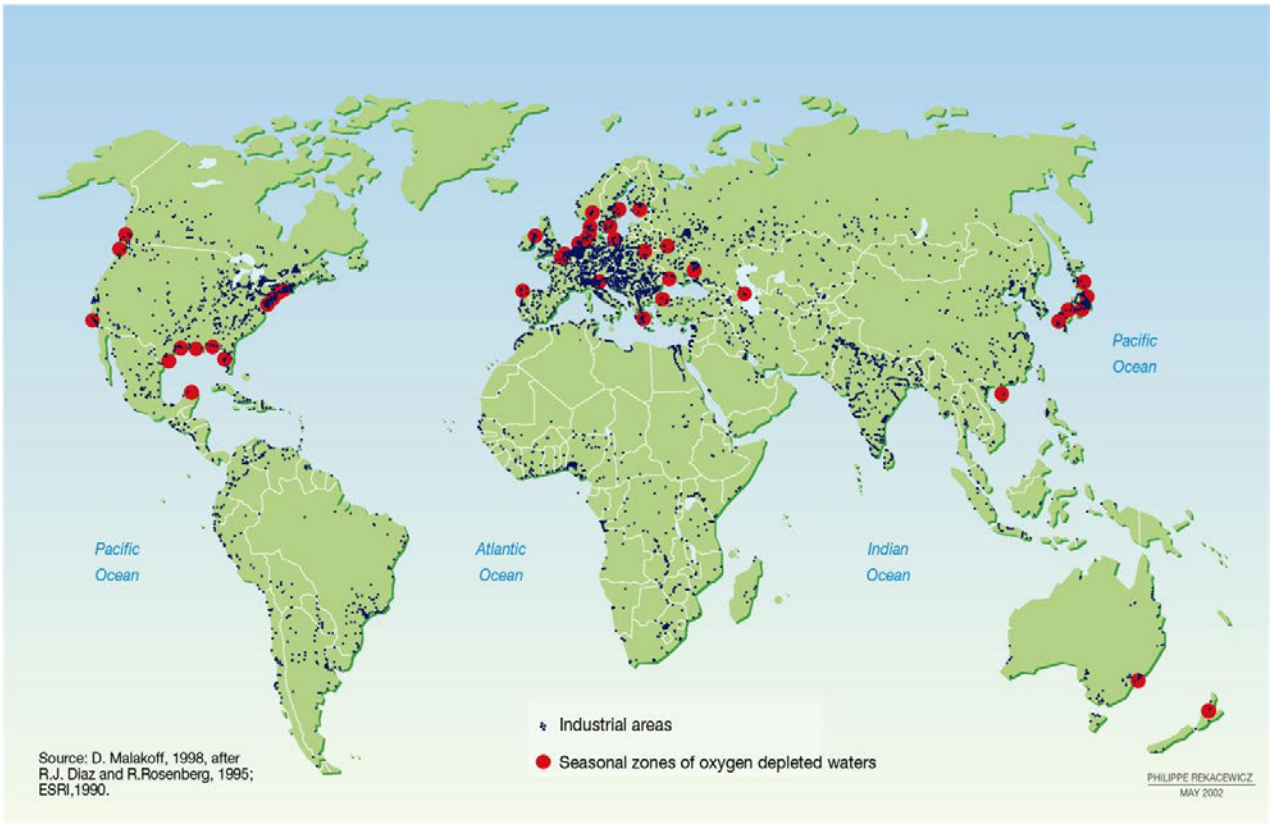

Figure 1.2: Worldwide location of industrial areas (blue dots) and seasonal zones of oxygen depleted waters (red dots). Source: http://www.unep.org/dewa/vitalwater/jpg/0320-oxygen-depleted-EN.jpg.

wastewater outfalls is probably similar in other countries and proportional to their population.

The types of pollutants present in industrial wastewaters are wide ranging reflecting the diversity of industrial activity. They may include physical pollutants such as temperature, salinity or oil; chemical pollutants like heavy metals (e.g. mercury, lead, copper, cadmium, zinc), organic micropollutants, pesticides, insecticides or detergent products; and/or biological pollutants such bacteria or viruses. All of them may be introduced in any form or quantity and cannot adequately be quantified without actual measuring and testing.

When a pollutant can produce, even at low concentrations, an adverse response (effect) in a biological system, seriously damaging its structure or function or resulting in death is called a toxic substance or toxicant. Among others, heavy metals and organic micropollutants are two groups of toxicants very harmful on living organisms. Both groups released to the environment have been shown to travel vast distances from their original source. Thus they can be found all over the world, including in areas where they have never been used and remote regions such as the middle of oceans and Antarctica. Their exposure can cause disruption of the endocrine, reproductive and immune systems, neurological disorders and cancers. Exposure to these toxicants can take place through diet, environmental exposure, or accidents (WHO 2003).

The wastewater will usally be discharged directly into estuaries as a point source (Alley 2007). A point source is a single, identifiable source of pollution, such as a pipe, an outfall or a drain. Typically, industrial wastewaters are discharged by single-port and round type systems (Bárcena 2009). Figure 1.3 shows some examples of this type of discharge mechanism (Sources: [1], [2], [3], [4], [5], [6], [7], [8], [9]). These sources can be measured or quantified, and their impact on the surrounding environment can be somehow evaluated. As such, point source toxicants are, compared to non-point source toxicants, characteristically easier to control, more readily identifiable and measurable, and generally more toxic (Schwarzenbach *et al.* 2006).

There are many examples of estuaries suffering industrial pollution coming from point sources around the globe (see figure 1.4). For instance, we can name in North America: Hudson Estuary, Duwamish Estuary, Chesapeake Bay, Narrangasett Bay, Columbia Estuary, Colorado Estuary or San Francisco Bay; in South America: Ría de la Plata, Bahía Blanca Estuary, Patos Lagoon or Paranagua Bay; in Europe: Falmouth Estuary, Severn Estuary, Humber Estuary, Rhine–Meuse–Scheldt Delta, Elbe Estuary, Tagus Estuary, Ría de Aveiro, Seine Estuary, Adour Estuary, Gironde Estuary or Dnieper-Bug Estuary; in Africa: Nile Delta, Lagos Lagoon, Rio-del-Rey Estuary, Congo Estuary, Durban Bay, Derwent Estuary, Mvoti Estuary, Richards Bay, Makoba Bay or Mombasa Estuary; in Asia: Trang Estuary, Pearl Estuary, Minjiang Estuary, Yangtze Estuary, Hooghly Estuary, Adyar Estuary, Gulf of Khambhat or Mekong Delta; in Oceania: Sydney Estuary, Southern Moreton Bay, Tamar Estuary, Port Philip Bay or Tamaki Estuary.

Regarding Spain, Ría de Huelva, Pasajes Bay, Ría de Bilbao, Tarragona Harbour, Ría de Avilés or Cádiz Bay are example of tidal waters under industrial pressure. Lastly, at the local scale of Cantabria, Suances Estuary and Santander Bay are receiving the majority of industrial discharges.

As it was itemized, the increasing worldwide contamination with thousands of industrial and natural chemical compounds is one of the key environmental problems facing humanity. Although most of these compounds are present at low concentrations, many of them raise considerable toxicological concerns (Schwarzenbach *et al.* 2006). There are hence serious environmental, economic and social impacts associated with these type

[1] http://greatlakesinform.org/sites/default/files/
[2] http://water.epa.gov/infrastructure/greeninfrastructure/
[3] http://www.seaweb.org/images/photos/
[4] http://coastecology.org/
[5] http://www.catawbariverkeeper.org/issues/coal-ash-1/
[6] http://cbf.typepad.com/
[7] http://blackwarriorriver.org/wp-content/uploads/
[8] http://toptenintheworld.com/
[9] https://lordfarmer.files.wordpress.com/

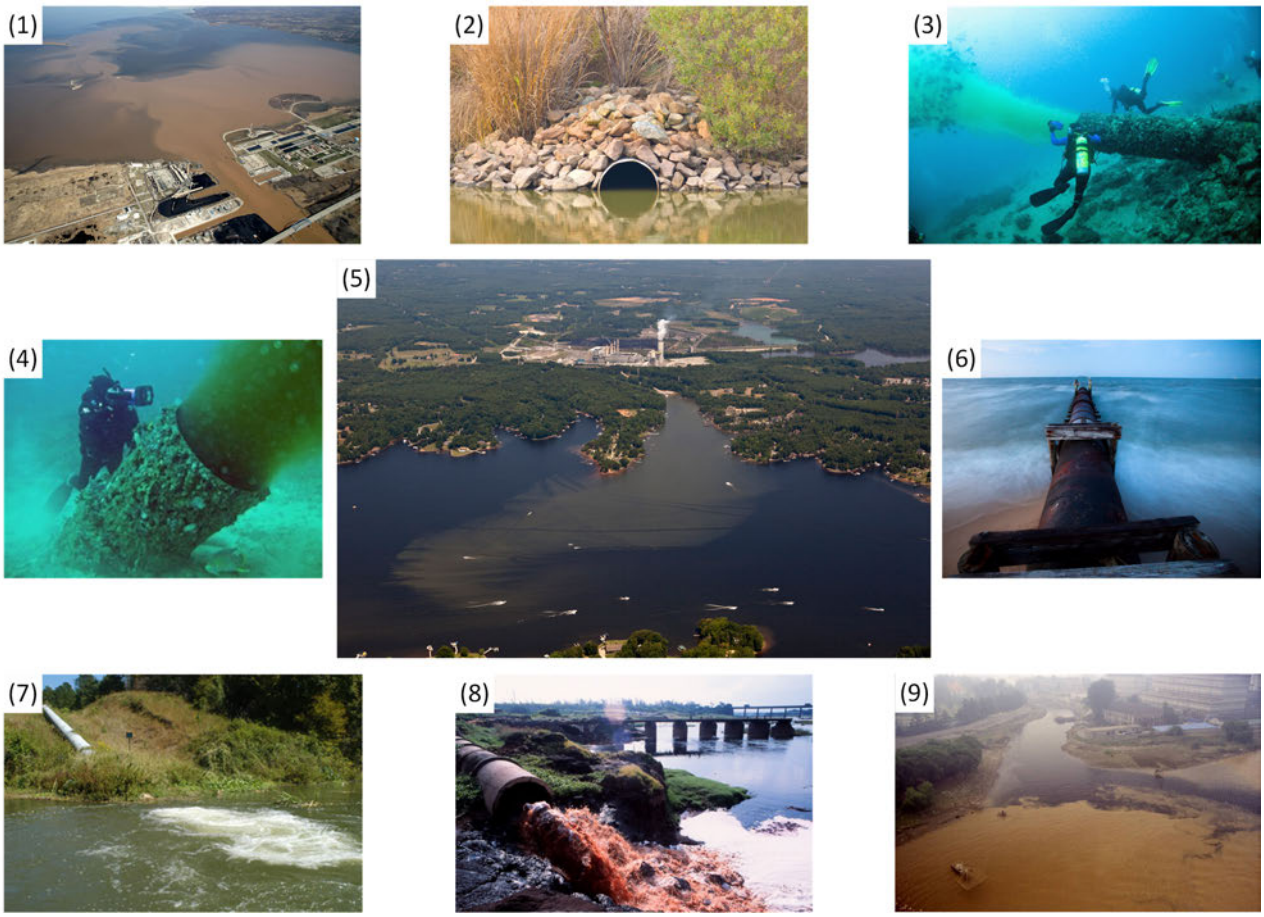

Figure 1.3: Composite of photos with examples of industrial wastewaters discharged by point sources and their environmental impact.

Figure 1.4: World map displaying examples of estuaries that are stressed by industrial activity. Source of basemap: http://goto.arcgisonline.com/maps/World_Topo_Map.

of pollution.

Consequently, it is accepted that humankind cannot continue to advance technologically while ignoring the environmental deterioration that occurs when we irresponsibly discharge the waste from our technology. Indeed, the sustainable growth of our civilization requires, as the only reasonable and feasible way to coexist on our planet with nature, that we protect our fragile environment (Alley 2007). Despite new and cleaner technologies, industries still often emit toxicants into the water environment. These toxicants can poison fish and wildlife and increase human health risks from swimming in polluted water and eating contaminated fish and shellfish. Economic losses also occur from closed shellfish beds and lost tourism. Permitting programs and continued technological improvements can help lessen these problems.

Therefore, environmental protection has been a major concern in the civilized nations of the world in order to sustainably manage the water quality. Much of the legislation promulgated to provide environmental protection has the purpose of maintaining the biodiversity and natural resources (AUS 2008, CCME 1999, EC 2000; 2008a;b, EU 2013, USA 1972; 1977; 1985). Moreover, these regulations establish the non-deterioration of present environmental conditions and the improvement of these conditions so that past abuse will be corrected.

Regarding the legislation of toxic discharges, an important part is a system of water quality norms (objectives or standards). Two approaches can generally be distinguished: the environmental quality standard-based approach (or EQS-based approach) and the emission limit value-based approach (or ELV-based approach). A combination of these two approaches is also a possibility named combine approach (Figure 1.5).

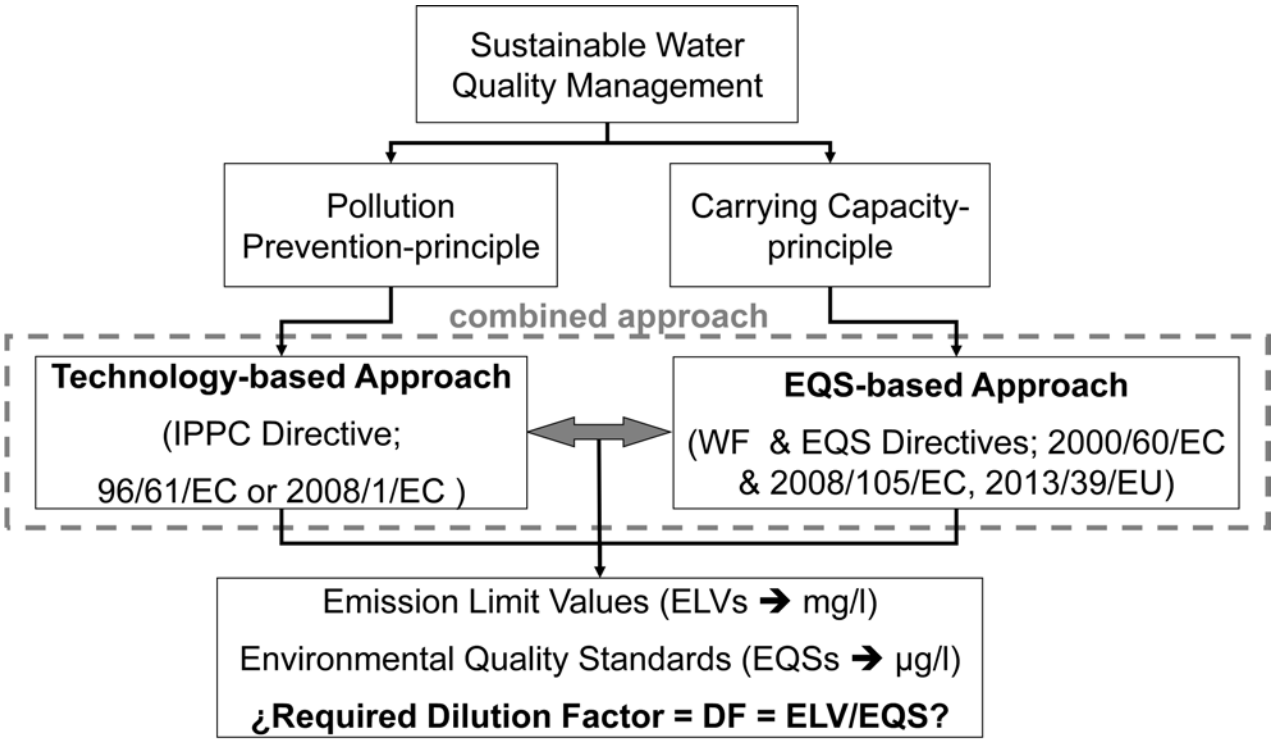

Figure 1.5: Relations between the pollution prevention and carrying capacity principles, and the related technology- and water quality-based approaches in sustainable water management.

The pollution prevention principle is based on the idea that any form of pollution may have an adverse impact on water quality, and should therefore be prevented (Ragas *et al.* 1997). Within this framework, source-oriented measures (also known as emission limit values) depend on the technological possibilities for emission reduction and their economic and social consequences (Figure 1.5). The method of establishing source-oriented measures (ELVs) is often referred to as the technology-based approach (also called ELV-based

approach).

The carrying capacity principle is based on the idea that the environment can cope with certain pollutant loads: as long as the carrying capacity of a water system is not exceeded, no adverse effects will follow (Ragas *et al.* 1997). In most cases, the carrying capacity is laid down in environmental quality standards (EQSs). EQSs are applied in order to predict the likelihood of adverse effects occurring. Monitoring data and water quality models are applied in order to make predictions about environmental concentrations. If the (predicted) environmental concentration is worse than the EQS is expected to be violated, a risk evaluation will be required and effect- and/or source-oriented measures should be taken (Figure 1.5). The method of establishing effect- and/or source-oriented measures based on EQSs is mainly referred to as the water quality-based approach (also called EQS-based approach).

Ragas *et al.* (1997) and Ragas (2000) have discussed the advantages and disadvantages of different control mechanisms in the authorization of discharges to surface waters such as the EQS-based approach or the ELV-based approach. The main conclusions were:

- USA, Australia, Canada and UK have a long tradition in applying the EQS-based approach (ANZECC & ARMCANZ 2000, MOEE 1994b, SEPA 1998, USEPA 1991; 1994; 1996).
- Most European countries, like Germany, Netherlands, Belgium, Austria, Spain or Portugal have been used a generic ELV-based approach, consisting in applying only these thresholds (Jirka *et al.* 2004).
- The ELV is a direct and effective method for limiting toxicant loads as restricts the concentration of specific toxicant in the total flow of the spill. This approach is preferred, from an administrative perspective, because the ELV is easily determined and monitored by sampling at the end of pipe. However, from an ecological perspective, a water quality control based only on the ELV is meaningless because it does not give the direct effect of each discharge on the water quality of the waterbody and therefore do not know the residual effluent liable for damages in the receiving environment. This usually occurred in estuarine industrial areas where the same toxicant could be discharged by several factories. Individually each factory meets the ELV, however, their cumulative effect could be an excessive pollution load exceeding the EQS.
- EQS have the advantage that consider the characteristics and responses directly physical, chemical and biological properties due to the discharge and therefore gives a direct responsibility to discharger. However, water quality control based only on EQS values might lead to a situation in which an industry could use assimilative capacity of the water body to achieve the concentration values determined by the EQS, without take into account the Best Available Technology (BAT).

The ratio ELV/EQS describes the impact of toxicants on the ecosystem, since the ELV are determined to protect against short-term effects (acute effect), while the EQS have been established to prevent long-term effects (chronic effect). This ratio also expresses the dilution necessary to be experienced at the point of discharge by physical processes of mixing, biological decay and chemical transformations. Discharge control regimes are normally designed to ensure that toxicants in the receiving water does not exceed the EQS, but if the ELV is greater than the EQS value there will be a zone of EQS exceedence in the vicinity of the point of discharge.

When using the combined approach, the constraints of both approaches are partly offset, while most of the key opportunities are maintained. Namely, the combined approach prevents avoidable pollution, as well as violations of EQSs through reflecting the requirements and sensitivity of the environment. At the same time, it avoids technical and institutional capacity constraints involved in a full EQS-based approach.

The European Union has recognized these advantages and has decided to adopt the combined approach in the framework laid down by Directive 2000/60/EC or the Water Framework Directive (WFD) (EC 2000),

Directive 2008/1/EC or the Integrated Pollution Prevention and Control Directive (IPPCD) (EC 2008b) and Directives 2008/105/EC and 2013/39/EU or Environmental Quality Standard Directives (EQSD) (EC 2008a, EU 2013) as a method for controlling surface water quality (Figure 1.5). The so called combined approach builds upon an approach that requires establishment of ELV based on BAT or setting of adequate ELV together with EQS. If an EQS requires stricter conditions to be met, more stringent emission controls shall be set accordingly. As a consequence, water quality in many surface waters across Europe has improved dramatically in recent years aided by the adoption of an underpinning philosophy to reduce, or where possible, eliminate pollution at source.

In the case of the discharge of industrial wastewaters, there are 45 substances or groups of substances on the list of priority substances for which EQS were set in WF Directive (EC 2000) and later on EQS Directives (EC 2008a, EU 2013). The list includes selected existing chemicals, plant protection products, biocides, metals and other groups like Polyaromatic Hydrocarbons (PAH), Polychlorinated Biphenyl (PCB) or Polybrominated Biphenylethers (PBDE). The complete list is given in Part A of Annex I of the Directive 2013/39/EU (EU 2013).

However, if we consider the EQS values set in the EQS Directive (EU 2013) and the ELV for several substances established in other Directives, it is feasible to conclude that, usually, it is required a dilution for EQS compliance of some hundreds or some thousands (Gasperi *et al.* 2008, Ragas *et al.* 1997). These chemical toxicants are the main responsible of the development of this thesis because its EQS are generally set in micrograms per litre meanwhile the ELV are set in miligrams per litre so there will be a zone where the combine approach can not meet the water policy specified in each country legislation (Figure 1.5). That is why the concept of **"mixing zones"** appears in the legislation of Europe, Australia, USA, Canada among others.

To avoid this issue, Directive 2008/105/EC (EC 2008a) allows Member States to permit such zones of exceedence in water bodies when a number of criteria are met. Specifically, its Article 4 states:

1. Member States may designate mixing zones adjacent to points of discharge. Concentrations of one or more substances listed in Part A of Annex I may exceed the relevant EQS within such mixing zones if they do not affect the compliance of the rest of the body of surface water with those standards.

2. Member States that designate mixing zones shall include in river basin management plans produced in accordance with Article 13 of Directive 2000/60/EC (EC 2000) a description of:

   (a) the approaches and methodologies applied to define such zones; and

   (b) measures taken with a view to reducing the extent of the mixing zones in the future.

3. Member States that designate mixing zones shall ensure that the extent of any such zone is:

   (a) restricted to the proximity of the point of discharge;

   (b) proportionate, having regard to the concentrations of toxicants at the point of discharge and to the conditions on emissions of toxicants contained in the prior regulations, such as authorizations and/or permits.

4. Technical guidelines for the identification of mixing zones shall be adopted in accordance with the regulatory procedure referred to in Article 9(2) of this Directive.

If **"mixing zones"** were not allowed EQS would be ELV which could rule out some technology, add unwarranted cost and lead to unwarranted environmental impacts in non-aquatic media (treatment and disposal, life cycle considerations, energy use, etc). However, the WFD and the EQS Directives do not provide any information on the spatial application of the EQS values. It also does not oblige the national authorities to

establish such specification. Therefore, it must be expected that considerable uncertainties and highly variable interpretations or monitoring methods will occur in the practice of water authorities, both as regards the continuing approval of existing discharges as well as the permitting of new ones. The combined approach that appears sensible for an integrated ecological water pollution control is in danger of being by-passed or undermined in its practical implementation.

This is why the development of a method to allocate **"mixing zones"** on estuaries is particularly necessary and difficult due to its high complexity and natural variability, the limited existing knowledge about their functioning and the continued pressure coming to bear because of anthropogenic activities.

1.2 Overview of the problem: Industrial discharges into estuarine waters

As it was aforementioned, our industrial systems, which release pollution on a continuing basis, would not be permissible in the absence of transport and dilution of nearly all emissions by natural air and water flows. In sum, natural fluid motions in the environment are vital, and we have a strong incentive to study the naturally occurring fluid flows, particularly those of air in the atmosphere and of water in all its streams, from underground aquifers to surface flows in rivers, lakes, estuaries and oceans (Cushman-Roisin 2013).

The study of these flows has received considerable attention over the years, and several distinct disciplines have emerged: meteorology, climatology, hydrology, hydraulics, limnology and oceanography. Whereas the particular objectives of each of these disciplines, such as weather forecasting in meteorology and design of water-resource projects in hydraulics, encourage disciplinary segregation, environmental concerns compel experts in those disciplines to consider problems that are essentially similar: the rise of a buoyant plume, the effect of turbulence on the dispersion of a dilute contaminant and the transfer of a substance between the fluid and a boundary. Such common points encourage multidisciplinarity to a degree that is increasing in proportion to the acuity of our environmental problems (Cushman-Roisin 2013).

The transport, mixing and decay of an effluent is generally separated into three regions called ***near-field***, ***intermediate-field*** and ***far-field*** in which different physical and chemical mechanisms dominate (Figure 1.6):

1. In the ***near-field*** (also called active dispersal region or primary dilution), the initial jet characteristics of momentum flux, buoyancy flux, and outfall configuration (orientations and geometries) influence the effluent trajectory and degree of mixing. Source induced turbulence entrains ambient fluid and dilutes the effluent (Figure 1.6a,b). Though ambient characteristics affect the discharge once the effluent left the outfall, they are still only of minor importance until any bottom or terminal layer interaction occurs (Fischer *et al.* 1979). This characterizes the transition to the intermediate field.

2. The ***intermediate-field*** or zone of wastefield establishment (Sanchez-Arcilla *et al.* 1998) is characterized by the impact of the turbulent plume with boundaries and the transition from the vertically rising plume/jet characteristics to a horizontal motion generated by the gravitational collapse of the toxicant cloud. Source characteristics become less important. Generally, a pool of initially diluted wastewater is formed either at the surface or at the level of submergence under stratification conditions (shown in figure 1.6a,b). Vertical and horizontal boundary conditions will control trajectory and dilution in the intermediate field through buoyant spreading motions and passive diffusion due to interfacial mixing.

3. After the wastefield establishment ambient conditions will control trajectory and dilution of the turbulent plume in the ***far-field*** (also called passive dispersal region or secondary dilution), through passive diffusion due to ambient turbulence, and passive advection by the often time-varying and non-uniform environmental velocity field (Figure 1.6c). Concentration reductions in the far-field are also related to natural dispersion but also significantly to natural purification processes such as decay reactions

(volatilization, hydrolysis, photolysis,...). Finally, vertical mixing in stratified water bodies is damped by buoyancy, so dilution is mainly due to horizontal mixing by turbulent eddies (Fischer *et al.* 1979).

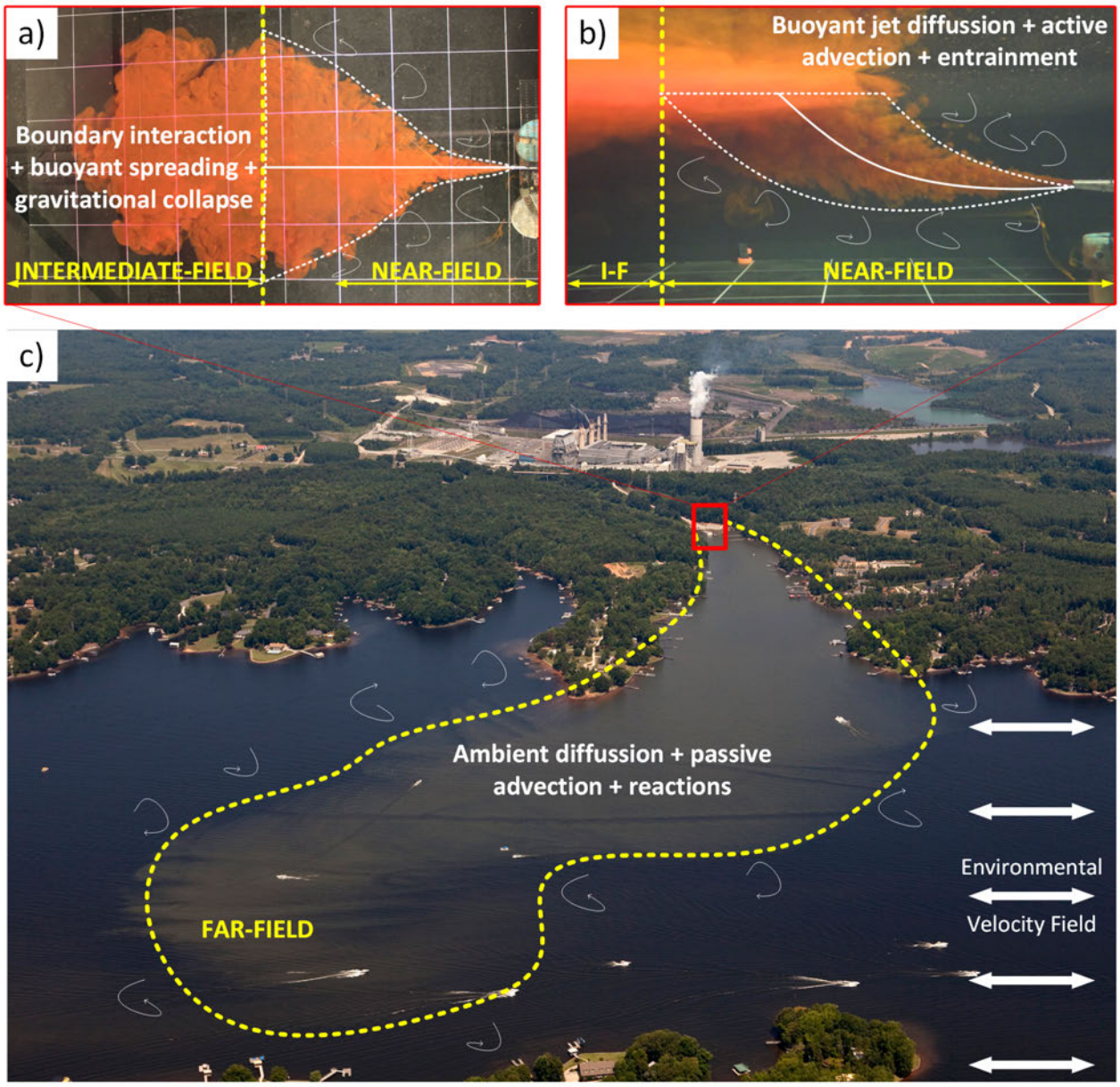

Figure 1.6: Schematic view of an operating industrial single-port outfall (c) merged with a laboratory picture of a buoyant jet in plan view (a) and side view (b). Sources: (a) and (b) from VERTIZE experiments (CTM2012-32538) and (c) http://www.catawbariverkeeper.org/issues/coal-ash-1.

Although certain heads of estuaries are located in freshwater areas, estuaries and coastal waters are usually considered to be marine environments. A freshwater effluent, typical from industrial wastewaters, discharged into salt water generally forms a plume that emerges rapidly and then floats on the surface around the discharge point. The initial mixing speed depends on several factors such as the water depth and the turbulence of the discharge. Once at the surface, the mix will be limited to the superficial layer until the relative densities of the two water masses allow it to spread throughout the water column. An overall picture of the dominant processes governing every mixing region is given in table 1.1 and figure 1.6.

The environmental impact can generally be defined as the set of potential negative environmental effects that entail a modification of the natural environment because of human activities. More specifically, can be under-

Dominant Processes	Near-field	Intermediate-field	Far-field
Forcing	momentum and buoyancy flux	buoyancy flux and boundary resistance	tide, river, wind, induced barotropic/clinic movements
Advection	buoyant jet induced velocity	ambient velocity field	ambient velocity field
Mixing	strong shear induced turbulence	frontal mixing at plume borders	bed and shear induced turbulence, stratification
Reactions	conservative	conservative	non-conservative
Temporal Variance	unsteady	unsteady	highly unsteady
Spatial Variance	non-uniform	non-uniform	highly non-uniform

Table 1.1: Overall picture of dominant processes for positive-buoyant single-port discharges. Adapted from Bleninger (2006).

stood as the human-induced disturbance experienced by the environment (Gómez 2010). For the evaluation of the different environmental effects is necessary to consider the persistence, duration and frequency to toxicants (Saouter *et al.* 2001, USEPA 1991). Regarding the allocation of mixing zones, environmental impact is the exceedence of the relevant EQS.

However, demonstrating such exceedence for estuarine discharges is still a hard task because water quality depends on several random variables (Figure 1.7). It depends on toxicant concentrations in the effluent and their reduction due to dilution. This dilution process is hydrodynamically complex as it results from turbulence that is both induced by the discharge and naturally present in the receiving water. Further complications arise from the variability of local estuarine conditions, including the density stratification. The speed and direction of estuarine currents usually vary widely and quickly. So this can cause wide variations in plume rise height and dilution in near-field. In far-field, toxicant concentrations are greatly variable due to the intermittent impact of the plume at any particular location, the complexity of the estuarine bathymetry and the wide and continuous range of environmental variables values (Roberts 1999a;b). All these factors make very difficult to model the dispersion processes of estuarine discharges, to quantify their environmental impact, and to predict the human health risk or the ecological risk to which aquatic life may be exposed, this is, allocating **mixing zones**.

The general problem that arises when trying to estimate the impact of various agents probabilistically is the inherent complexity of estuarine aquatic systems (Figure 1.7). Mixing of industrial discharges will take place longitudinally, transversely and vertically in the receiving water and may also be affected by seasonal, meteorological or other temporal changes. Thus, an appropriate level of consideration of the statistics (or probabilities) of frequency of possible EQS exceedence over space and time must be taken into account, in conjunction with spatial and temporal distribution of potential receptors, the variability of discharge and receiving water flow and the water quality of the discharges and the receiving water (EC 2010). However, the introduction of these factors decreases the relative ability to investigate the environmental effects from field data, since conditions are more complex. One way to tackle these issues is the use of the huge potential of numerical models (Moll & Radach 2003).

Numerical modeling can obtain the evolution of the concentration of a particular toxicant over time in different locations of the aquatic system, allowing the use of spatial and temporal criteria for the assessment of its effects. In addition, numerical modeling avoids the use of field data only at discrete locations and allows the prediction of a continuous response against a disturbance (Gómez 2010, Guérit *et al.* 2008, McIntyre & Wheather 2004, McIntyre *et al.* 2003, Severinsen *et al.* 1996). Numerical models represent environmental processes in a theoretical way by solving the governing equations of interested toxicants and by allowing the simulation and prediction of the environmental responses to different environmental conditions. Therefore, numerical models can estimate the effects of human pressures on the environment and study the possible solutions. For all these reasons, numerical models are invaluable for predicting effects on ecosystem compo-

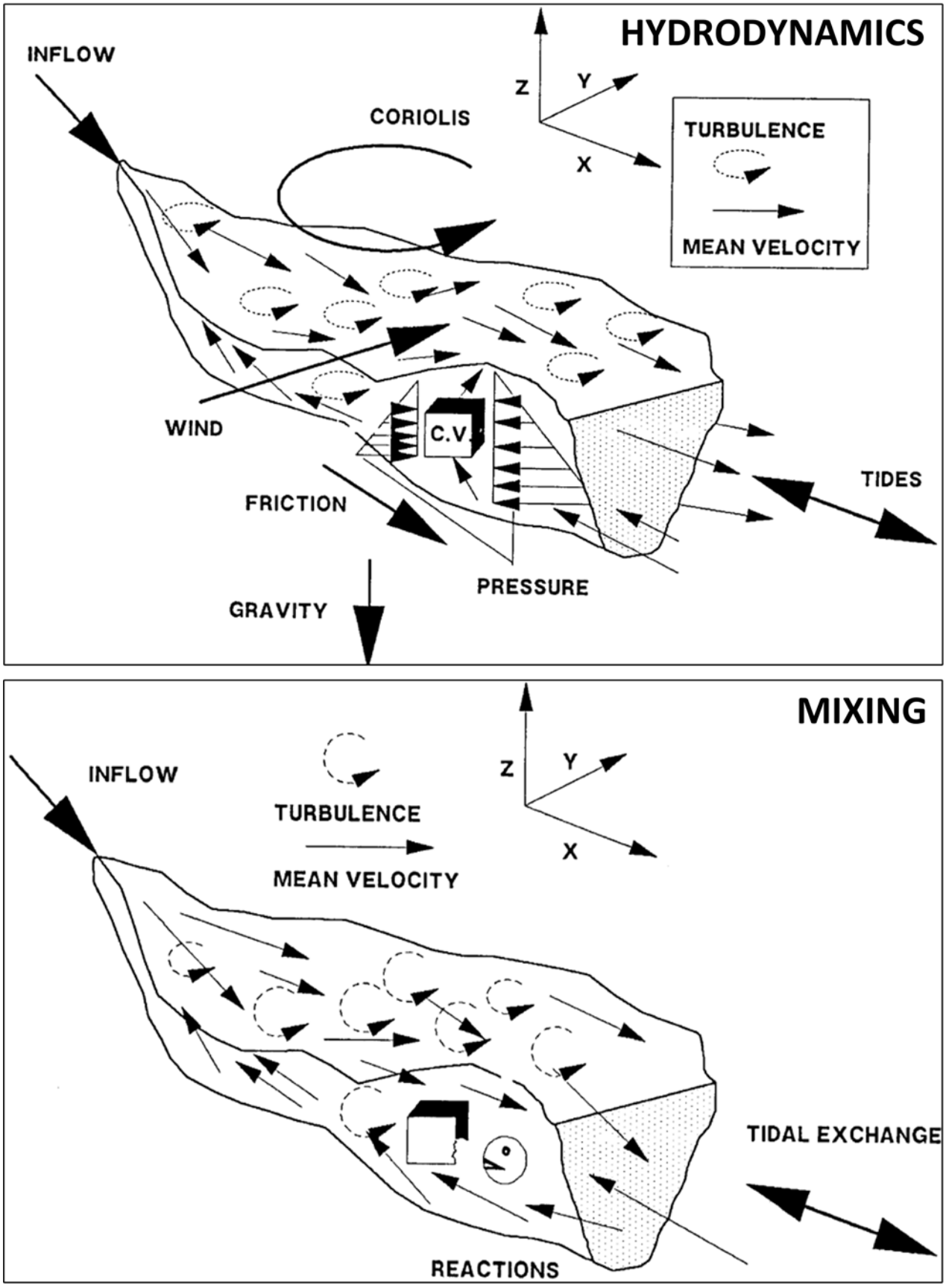

Figure 1.7: Hydrodynamic and mixing estuarine processes. Source: USEPA (1991).

nents, being much faster and cheaper than physical and experimental procedures such as collecting field data or physical modeling (Ruza *et al.* 2007, Westman 1985).

In the field of environmental risk analysis, if numerical models are properly calibrated and validated they are irreplaceable tools to deal with the complexity of estuarine systems and to describe the impact of a residual effluent in both real and hypothetical situations (Giupponi *et al.* 1999, Yuan *et al.* 2006). That is why numerical models are the right tool to conduct studies to allocate **mixing zones**.

Therefore, it is necessary to predict the impact of industrial effluents for a wide range of ambient conditions in mixing zone assessment. This prediction poses particular technical challenges. The effluent discharges are often located in relatively shallow waters of 5–20 m depth, not far (e.g., 5–10 km) from sensitive receivers such as beaches and/or fisheries. Management decisions on the appropriate mixing zones must be based on impact assessment models that can deal with the near-field, the intermediate-field and the far-field (Choi & Lee 2007). Instead of combining near- intermediate- and far-field effects in only one model, numerical models usually concentrate primarily on either the near- or the far-field due to the disparity of temporal and spatial scales in mixing regions (Figure 1.8). .

In the vicinity of the discharge (near-field), the buoyant jet trajectory and mixing can be well-predicted by a validated integral jet model that predicts the turbulent entrainment as a function of source characteristics, ambient velocity and stratification. Near-field models can resolve down to scales of the order of the jet diameter where typical time and length scales of the plume rise are in the order of minutes and meters, respectively (Figure 1.8). Near-field models generally assume that the far-field characteristics (receiving water temperature, velocity, etc.) are known with the consequence that the effect of the near-field on the far-field cannot be computed (Kaufman & Adams 1981).

Meanwhile, in the far-field, the effluent is passively transported by ambient currents and further diluted by turbulent diffusion where typical time and length scales are on the order of hours and kilometers (Figure 1.8). In tidal networks of complex topography and current structure, numerical transport models have to be employed in order to predict the far-field toxicant distribution under more general conditions regarding the estuarine circulation, mass transport and transformations. These models are based on the "advection-diffusion-reaction" equation or transport equation (see equation (1.1)).

$$\frac{\partial C}{\partial t} + u\frac{\partial C}{\partial x} - D_x\frac{\partial C^2}{\partial x^2} + v\frac{\partial C}{\partial y} - D_y\frac{\partial C^2}{\partial y^2} + w\frac{\partial C}{\partial z} - D_V\frac{\partial C^2}{\partial z^2} = SO + f_R(C,t) \tag{1.1}$$

where u, v and w are the flow velocity in every direction, D_x, D_y and D_V are the dispersion coefficients taken for every direction, SO are additional inflows of water or mass and f_R are the reaction terms or "processes".

The velocity field in these transport models may have to be calculated from a separate hydrodynamic model or generated by instrumental data. Far-field models tend to over simplify near-field effects by considering simply an influx of mass at the point of discharge. This procedure discounts many influences of the near-field on the far-field (Kaufman & Adams 1981).

However, the numerical prediction of intermediate flows has hitherto not been reported. In the case of single-port discharges, the scale of the intermediate-field ranges from about 1 m to the order of 100 m (Figure 1.8), depending on the discharge characteristics (Choi & Lee 2007). The large size of this region is a major reason why a link between near- and far-field modeling is necessary to carry out an adequate 3D environmental impact assessment in order to allocate **mixing zones** with similar spatial scales.

The most appropriate way to overcome these issues of the transport processes is via the application of integrated models consisting of a near-field model and a far-field model that are connected via a coupling algorithm. Coupling models means introducing flow quantities (e.g. momentum or mass) from one model into the other and viceversa. There are only two possibilities for introducing flow quantities into a model,

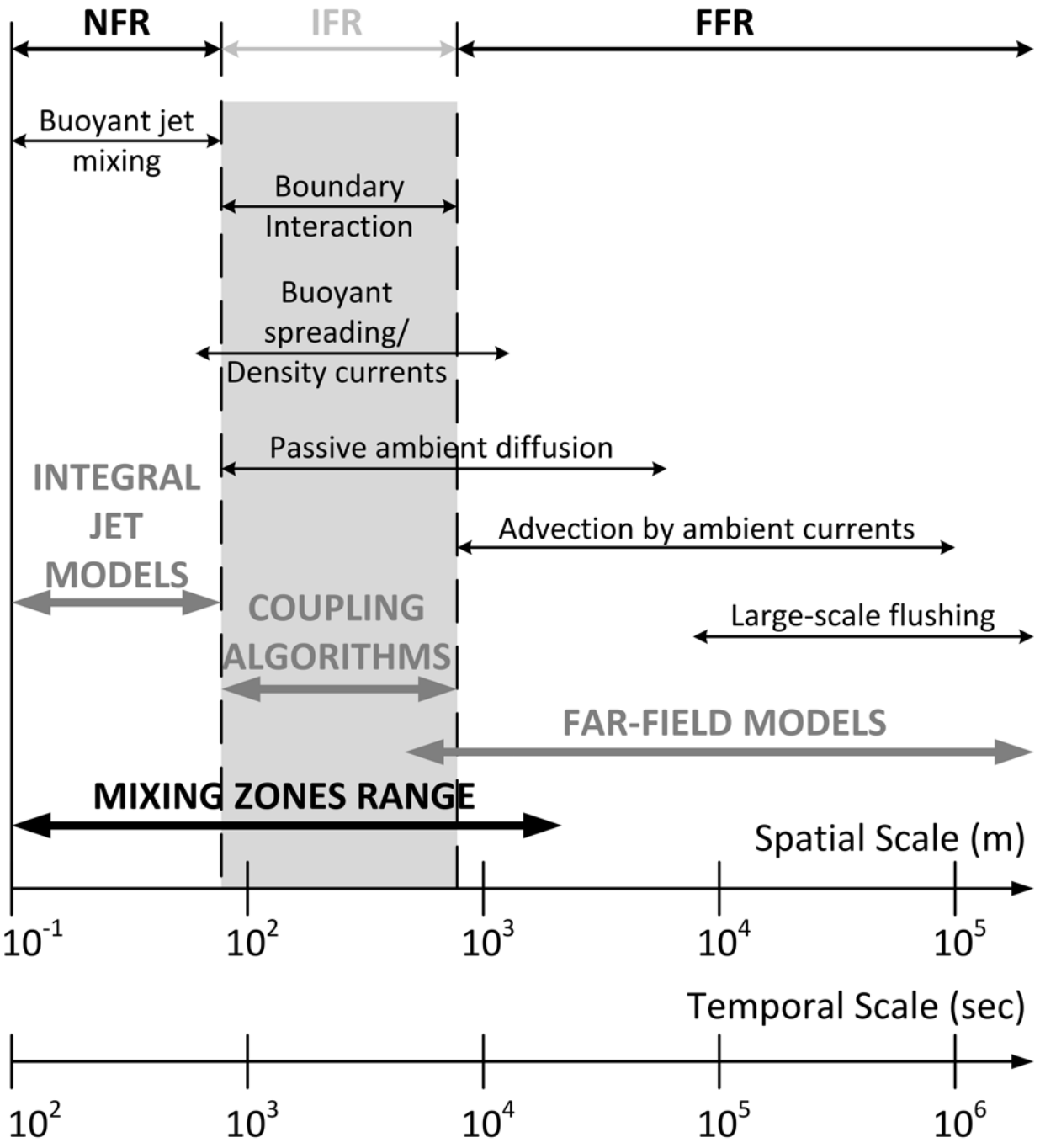

Figure 1.8: Temporal and spatial scales for transport and mixing processes related to estuarine wastewater discharges. NFR is near-field region, IFR is intermediate-field region and FFR is far-field region.

Model region	Type of Model	Application	Grid resolution
Near-field	Integral Jet Models	Local (scale of outfall)	No grid
Intermediate-field	Coupling Algorithms	Local (scale of outfall)	No grid
Far-field	Estuarine Circulation Models	Estuaries and Shelf areas	1-1000 m
Open boundaries	Ocean Circulation Models	Ocean wide	1-100 km

Table 1.2: Scales and resolutions of different modeling techniques for the discharge of industrial wastewaters into the estuarine environment in every mixing region.

either over the boundary conditions or via source terms.

Table 1.2 summarizes the type of model, application and grid resolution for the discharge of industrial wastewaters into the estuarine environment in every mixing region.

Summarizing, on one hand, the application of a integrated model is required to assess the allocation of a **mixing zone** (Figure 1.9), including:

1. A hydrodynamic model that provides the dynamic information for the integral jet model, the sediment transport model and the far-field model.

2. A integral jet model that provides the initial dilution information feeded by a hydrodynamic model.

3. A sediment transport model that provides the settling information for the far-field model feeded by a hydrodynamic model.

4. A coupling algorithm introducing flow quantities from the integral jet model into the far-field model.

5. A far-field model that provides the temporal and spatial evolution of the studied toxicant/s in the estuary.

On the other hand, environmental zoning has become the tool for identifying, distributing, organizing and regulating the environment in accordance with certain criteria and priorities. Administratively, environmental zoning has focused on land uses through a set of criteria, standards and plans governing the land activities to get a proper relationship between territory, population, services and infrastructure. Its specific application to estuaries has been carried out by means of management plans with the final aim of establishing the criteria for the protection of this space (Ondiviela *et al.* 2007). This requires to design a methodological procedure whereby the estuarine environment can be classified in different estuarine areas through the use of different land uses.

In this way, impact analyses of industrial wastewaters into estuarine waters might include the selection of the study cases, the size and acceptability of mixing zones based on an holistic approach and, finally, the allocation of mixing zones by means of an integrated model. That is why it can be concluded that the development of a methodology to meet all such imperatives is a task that has not yet been fully resolved.

For instance, in Europe, the Competent Authority is responsible for the designation and development of mixing zones under EQS Directives 2008/105/EC and 2013/39/EU, and will need to deliver a risk-based, proportionate approach such that all relevant factors are considered in appropriate detail (EC 2008a). While a uniform monitoring approach can be provided that should allow efficient determination and administration of a large proportion of cases, the inherent complexity and variability of receiving estuarine waters across Europe means that in some instances simple solutions are not possible and this necessitates the derivation of case-specific acceptability criteria (EC 2010).

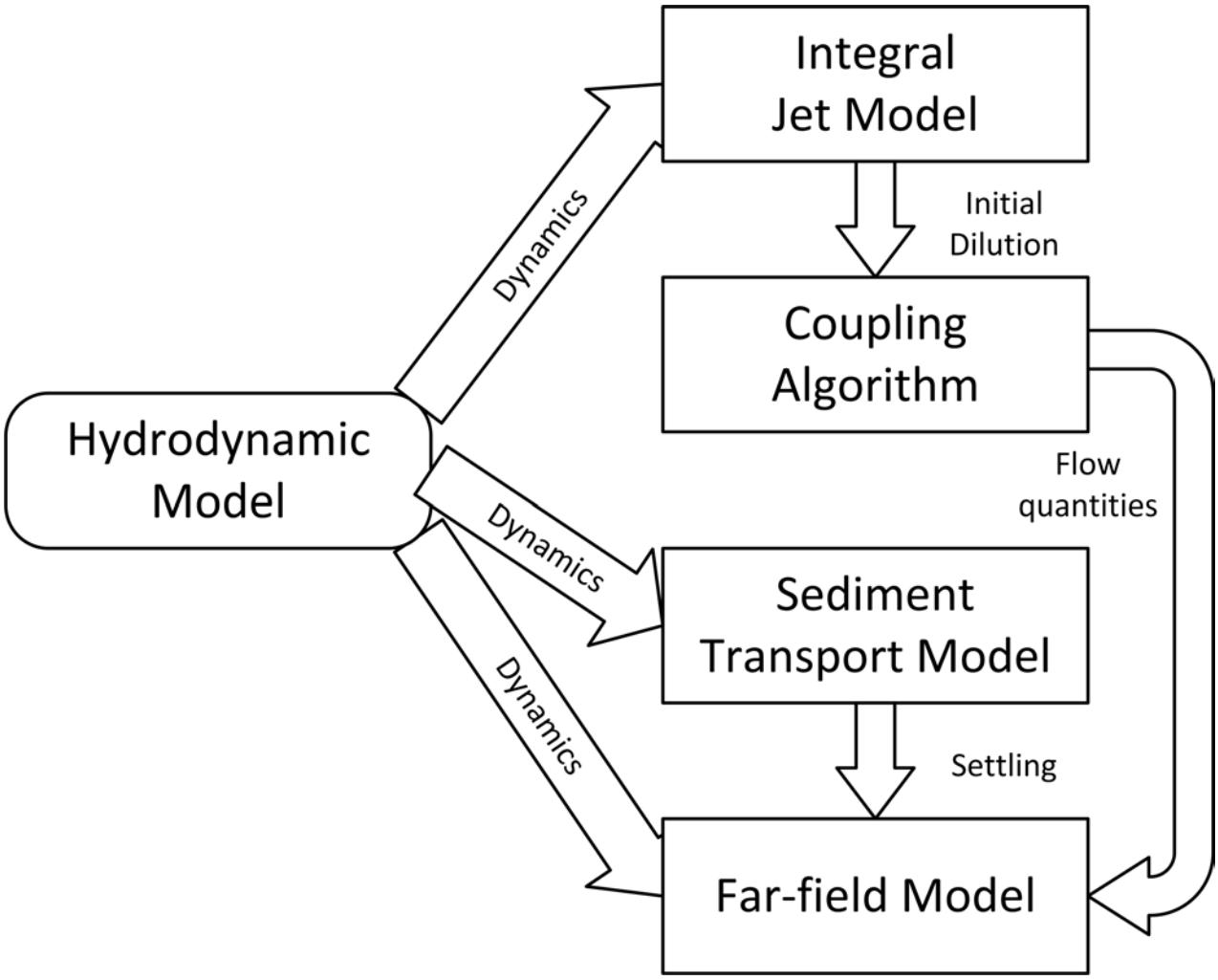

Figure 1.9: Configuration of the required integrated model for allocating mixing zones in estuarine environments.

1.3 General aim and layout

The main objective of the present study is to make a step forward in the assessment of mixing zones of single-port industrial discharges in estuaries by developing and implementing a stepped methodology according to the significance of the considered discharge. Thereby, this methodology establishes where a mixing zone is required and determines its size and acceptability for each point discharge based on numerical models and mathematical tools.

Thus, in this thesis a "Stepped Approach" has been developed to document the policy decision tree (methodology) that may be adopted by Member States and/or Industries when setting Mixing Zones under Directive 2008/105/EC (EC 2008a) and Directive 2013/39/EU (EU 2013).

The structure of the thesis is organized in six chapters as follows:

Chapter 1. Introduction. This chapter has introduced the reader in all other chapters of the thesis. Firstly, the motivations for research, explaining their importance and the reasons that led to the development of this thesis, are displayed. Secondly, the general aim of the thesis is presented and, finally, the organization of this thesis is explained.

Chapter 2. State of the Art. With the general aim in mind, a literature review is carried out in this chapter in order to evaluate the different methodological approaches used in daily practice around the globe, to state the contemporary issues in estuarine physics (hydrodynamics and mixing) and, finally, to gather the available numerical tools used to study estuarine hydrodynamics and mixing. This review highlights the strengths and deficiencies found in current approaches and allows the definition of the final objectives of the present work.

Chapter 3. Overall Methodology. In this chapter, the developed methodology, involving five steps, has been described. In Step 1, we collect the required information about the study area and the toxicant discharges. Step 2 identifies the significance of the discharge or discharges in the study zone. Next, Step 3 evaluates the effect generated by discharges and delimitates MZs from a simplified calculation that takes into account fixed conditions. Step 4 evaluates the effect generated by discharges and delimitates MZs during the driest year according to the river flow. Finally, in Step 5, we 'reevaluate' the effect generated by discharges and 'redelimitate' MZs according to a real case of dilution taking into account the variability of the environmental forcings.

Chapter 4. Numerical Tools. In this chapter, a review of the used numerical models and all the self-developed mathematical tools for integrating, transferring, communicating and plotting the required and obtained information along the overall methodology is presented.

Chapter 5. Results: Application to Suances Estuary. The implementation/application to Suances Estuary of the developed methodology in Chapter 3, using the proposed numerical tools described in Chapter 4, is presented.

Chapter 6. Conclusions and Future Research Topics. At the end of the document the conclusions of the present work are presented together with some proposals for future research topics that may complement the present study and the proposed methodology. Lastly, all the contributions made by this thesis were itemized.

A science is any discipline in which the fool of this generation can go beyond the point reached by the genius of the last generation.

Max Gluckman

2 State of the art

Two different features have been identified in the previous chapter as key aspects for the development of a methodology to allocate mixing zones in estuaries: the mixing, transport and reaction of wastewaters in estuaries and the existing methodological approaches. This chapter presents the state of knowledge in every one of the fields of interest. In order to clarify concepts and approaches, some historical definitions and classifications are also included at the beginning of this chapter.

In first place, the concept of estuaries and their classification are introduced. Secondly, an overview of the problem tackle in this thesis is given: the mixing, transport and reaction of wastewaters in estuaries. Moreover, a review of the models applied to study estuarine hydrodynamics and mixing, and the interaction with wastewaters is developed. Finally, mixing zones and the employed methodological approaches to allocate them in different countries around the globe are listed and reviewed.

2.1 Definitions and classifications of estuaries

Estuaries are more numerous and diverse than any other type of marine environment. Estuaries have the predominant characteristic of being sites of spatial and temporal continua, for example in environmental and biological variables. Because of this, any superimposed classification scheme is likely to be arbitrary and thus with a subjective element. In these cases, the desire for precise and unambiguous terms is even more important as there may be substantial legal and/or economic repercussions of poor definition (Elliot & McLusky 2002). Looking back to the relatively short history of estuarine research, there is not a definition and/or classification will ever satisfy all members of the estuarine community.

This section discusses definitions and classification of estuaries. It presents both the classical and more flexible definitions of estuaries. Then it shows a short review of separate estuarine classifications. Finally, a deeper review of classifications based on the vertical structure of salinity is presented due to its relationship with the expected behavior of wastewaters.

2.1.1 Definitions of estuaries

The most widely accepted definition of an estuary was proposed by Cameron & Pritchard (1963). Their definition says: *"An estuary is a semi-enclosed coastal body of water having a free connection with the open sea and within seawater is measurably diluted with freshwater derived from land drainage."*

Wolanski (2007) combines several definitions suggested by Cameron & Pritchard (1963), Day (1981), Kjerfve & Magill (1989), Perillo (1995) and Dalrymple *et al.* (1992) to lay out the next definition: *"An estuary is a semi-enclosed body of water connected to the sea as far as the tidal limit or the salt intrusion limit and receiving freshwater runoff, recognizing that freshwater inflow may not be perennial (i.e. it may occur only for part of the year) and that the connection to the sea may be closed for part of the year (e.g. by a sand bar) and that the tidal influence may be negligible."* The definition includes fjords, river mouths, deltas, rias, lagoons, tidal creeks, as well as the more classical estuaries.

Finally, it is worthy to mention that the WFD defines "transitional waters" as: *"bodies of surface water in the vicinity of river mouths which are partially saline in character as a result of their proximity to coastal waters but which are substantially influenced by freshwater flows."* (EC 2000). The problem for European Community legislators is that there is full range of brackish water habitats from tidal estuaries to closed brackish lagoons or seas present in the member states of the European Community. The term "transitional waters" is thus intended as a simple term that can encompass all these habitats and might be easily understood by legislators in all countries (McLusky & Elliott 2007).

2.1.2 Classifications of estuaries

From a geomorphologic point of view:

- The first known classification of estuaries is due to Pritchard (1952) who divided the estuaries in three groups: drowned rivers, fjords and bar-built estuaries. Later, Pritchard (1960) completed the classification by including a fourth category that contemplated those formed by tectonic processes.
- Next, Hayes (1975) in analyzing the morphology of sand deposits affiliated with estuaries recognized their different characteristics depending on tidal range. Hayes defined three types of estuaries: microtidal (tidal range <2 m), mesotidal (tidal range 2-4 m) and macrotidal (tidal range >4 m).
- Finally, Dalrymple *et al.* (1992) geomorphological classification, namely "evolutionary classification", is part of a complex model that combines the relative importance of river discharges, waves and tides with time. The result is a triangular prism that represents the different coastal environments associated to the three parameters.

On the basis of estuarine hydrodynamics:

- Hansen & Rattray (1966) managed to describe a continuum of estuaries and show how a given estuary may change over a season by plotting a stratification parameter versus a circulation parameter. The *stratification parameter,* $\partial S/So$ is the ratio of the surface to bottom difference in salinity ∂S divided by the average vertical or cross sectional salinity. The *circulation parameter,* u_s/u_f is the ratio of the net surface current to the mean cross sectional velocity.
- Later, Valle-Levinson (2008) proposed a classification of estuarine systems based on the lateral structure of density-driven exchange flows. Estuaries may be described in terms of whether the flows are vertically sheared or unidirectional in the deepest part of the cross-section. This exchange flows may

ultimately depend on the competition between Earth's rotation (Coriolis) and frictional effects, as characterized by the vertical Ekman number, which is a non-dimensional dynamical depth of the system. But the lateral structure of exchange flows may also depend on the Kelvin number, which is the ratio of the width of the estuary to the internal radius of deformation.

2.1.2.1 Classification on the basis of vertical structure of salinity

According to water column stratification or salinity vertical structure, estuaries can be classified as salt wedge, strongly stratified, weakly stratified or vertically mixed (Cameron & Pritchard 1963, Pritchard 1952). This classification considers the competition between buoyancy forcing from river discharge and mixing from tidal forcing (Figure 2.1).

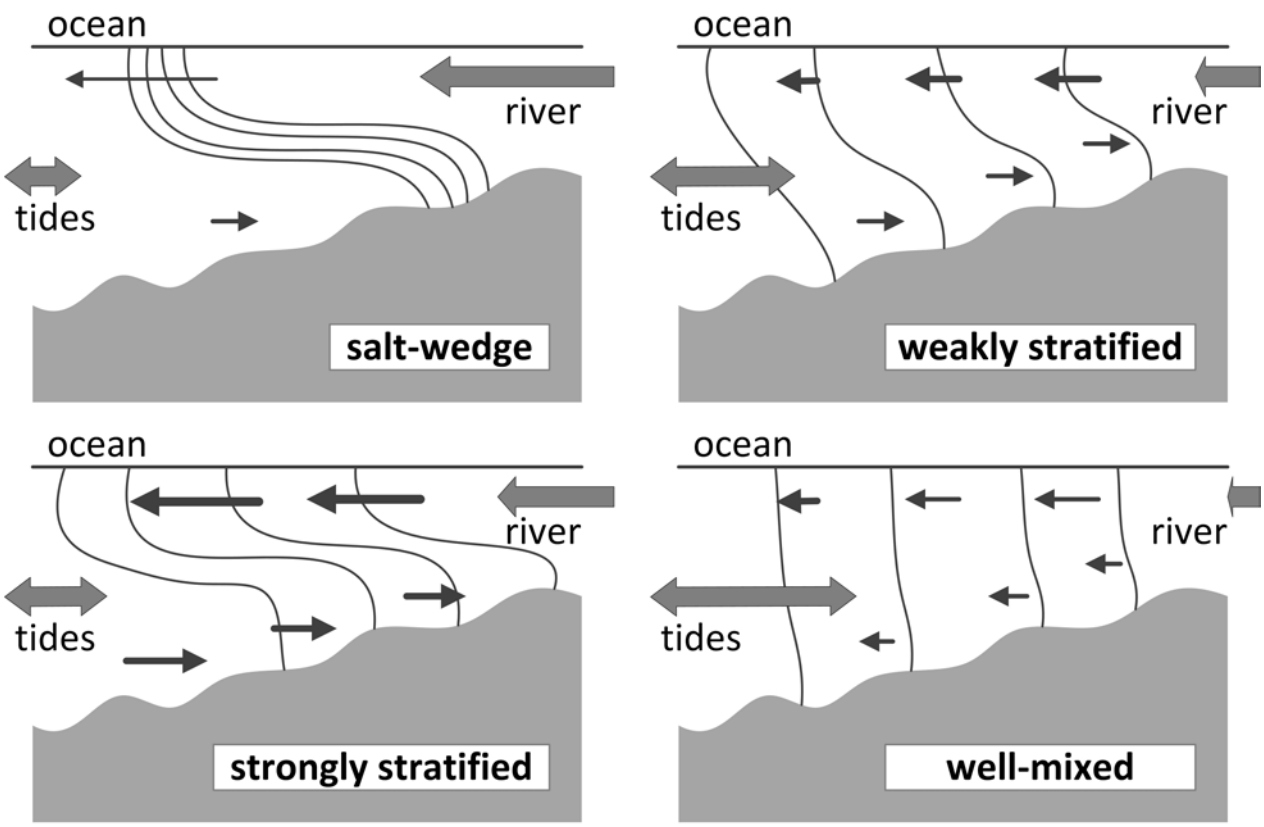

Figure 2.1: Classification of estuaries on the basis of vertical structure of salinity. Adapted from Valle-Levinson (2010)

- *Salt wedge*: Large river discharge and weak tidal forcing results in salt wedge estuaries. These systems are strongly stratified during flood tides, when the ocean water intrudes in a wedge shape.
- *Strongly stratified*: Moderate to large river discharge and weak to moderate tidal forcing result in strongly stratified estuaries. These estuaries have similar stratification to salt wedge estuaries, but the stratification remains strong throughout the tidal cycle as in fjords and other deep (typically >20 m deep) estuaries.
- *Weakly stratified*: Weakly stratified or partially mixed estuaries result from moderate to strong tidal forcing and weak to moderate river discharge.

- *Vertically mixed*: Strong tidal forcing and weak river discharge result in vertically mixed estuaries. Mean salinity profiles in mixed estuaries are practically uniform and mean flows are unidirectional with depth.

2.2 Mixing, transport and reaction of wastewaters in estuaries

As we mentioned in Chapter 1, the mixing of an effluent is generally separated into three regions called near-field, intermediate-field and far-field in which different physical, biological, geological and chemical mechanisms dominate.

In the following sections, a short review about the pollution of estuaries including the main sources and the type of pollutants is presented. Next, the basics and available models of estuarine hydrodynamics are displayed. Finally, the near and far-field are exposed as well as the available methods for the coupling between them (intermediate field) in order to give a full insight of the problem that is tackled in this thesis.

2.2.1 Pollution of estuaries

The present section describes a classification of pollutants based on their characteristics, and focuses on the two main types of substances whose transport can be relevant in estuaries regarding EQS Directives (EC 2008a, EU 2013), i.e., heavy metal pollution and organic micropollution coming from industrial discharges.

2.2.1.1 Classification of pollutants

Pollutants defining water quality are commonly categorised into three groups (Krenkel & Novotny 1980): chemical, physical and biological. A brief description of each type is given below.

Physical pollutants. These include colour, temperature, suspended solids and turbidity. The increase of temperature due to the discharge may affect physical, biological and chemical processes, possibly unbalancing the local ecosystem. The temperature rise increases metabolic activity in the nearby flora and fauna, decreases oxygen solubility in water and magnifies the toxic effects of cyanides. An excess of suspended solids in the water body may reduce the waste assimilation capacity, inhibit photosynthesis and retard the benthic activity and production due to the reduction in sunlight intensity.

Chemical pollutants. Broadly classified into organic and inorganic, where the former are defined as compounds containing a carbon atom. *Inorganic pollutants,* which include heavy metals, are generally the result of industrial waste discharges. Their major effects are changes in pH and severe toxicity if found in high concentrations. *Organic pollutants,* like organic pesticides, crude oils and hydrocarbons or nutrient substances can be dangerous due to the natural effect of the pollutant or in small concentrations may lead to eutrophication. They may additionally cause problems because of accumulation due to their non-biodegradability.

Biological pollutants. The effects of biological pollutants can be of two kinds: diseases, in which case the toxicant is called primary and increases in biological growths, caused by so-called secondary biological pollutants. *Primary biological pollutants* are mainly domestic and industrial wastewaters that include microbiological agents, such as bacteria, virus or protozoans, involved in waterborne diseases. *Secondary biological pollutants* are substances added to the water that may result in excessive growth of phytoplankton, macrophytes and fungi, leading to eutrophication.

As we commented in Chapter 1, there are 45 substances or groups of substances on the list of priority substances for which EQS were set in WF Directive (EC 2000) and, later, in EQS Directives (EC 2008a, EU 2013). The complete list is given in Part A of Annex I of the Directive 2013/39/EU (EU 2013).

In this thesis, we focus on the study of these chemical pollutants listed as priority substances, specially heavy metals and organic micropollutants. Both are considered toxicants due to they cause severe toxicity even at low concentrations. These groups of compounds are also classed as PBTs, this is, Persistent, Bioaccumulative and Toxic.

Figure 2.2 illustrates the key features and commonalities between exposure and effect assessment of these toxicants. Quantification of the pertinent processes that determine a compound's transport, fate, and effect in aquatic systems is a prerequisite for modeling the risks of chemicals, for designing mitigation strategies and for adapting manufacturing practices accordingly. Within this concept, toxicants interact with environmental and biological systems according to their intrinsic physicochemical properties and reactivities, yielding a characteristic pattern of environmental and internal exposure concentrations for each toxicant. Final exposure and effect assessment according to this concept will always be subject to uncertainty due to inherent variability and complexity of both environmental and biological systems (Schwarzenbach *et al.* 2006).

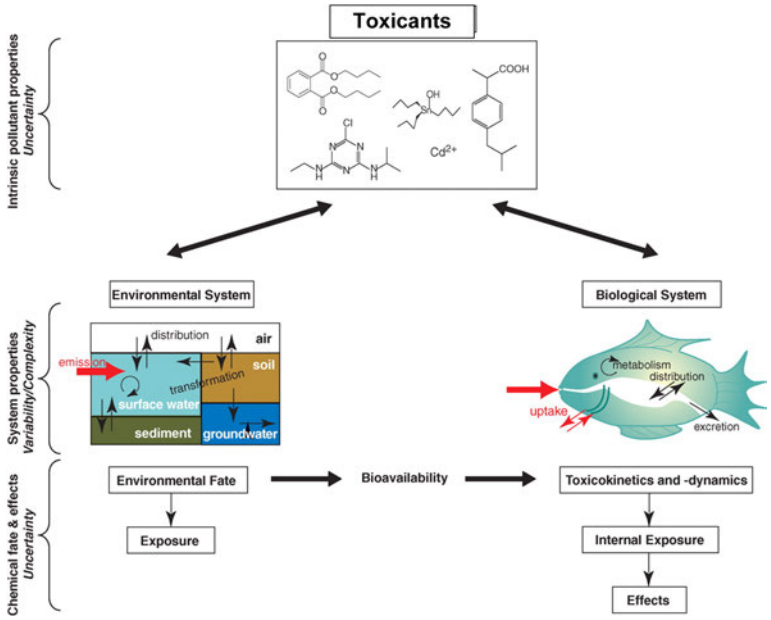

Figure 2.2: Consistent exposure and effect assessment is possible if processes in the environmental system and in the organisms (biological system) are treated with the same modeling structure and tools. Source: Schwarzenbach *et al.* (2006)

2.2.1.2 Heavy metal pollution

The term heavy metal (HM) refers to any metallic chemical element that has a relatively high density and is toxic or poisonous at low concentrations (Krenkel & Novotny 1980). Examples of heavy metals include, among many others (see figure 2.3), cadmium (Cd), copper (Cu), lead (Pb), mercury (Hg), nickel (Ni), chromium (Cr), arsenic (As), vanadium (Va), selenium (Se) or thallium (Tl).

Elevated levels of heavy metals in water systems can be attributed to both natural and anthropogenic sources. The most significant source of metals is weathering of rocks and volcanic activities. A large quantity of metals also suspends in the atmosphere from where they can reach the waters through dry deposition and precipitation. The anthropogenic sources of heavy metals include mainly domestic wastewaters and urban

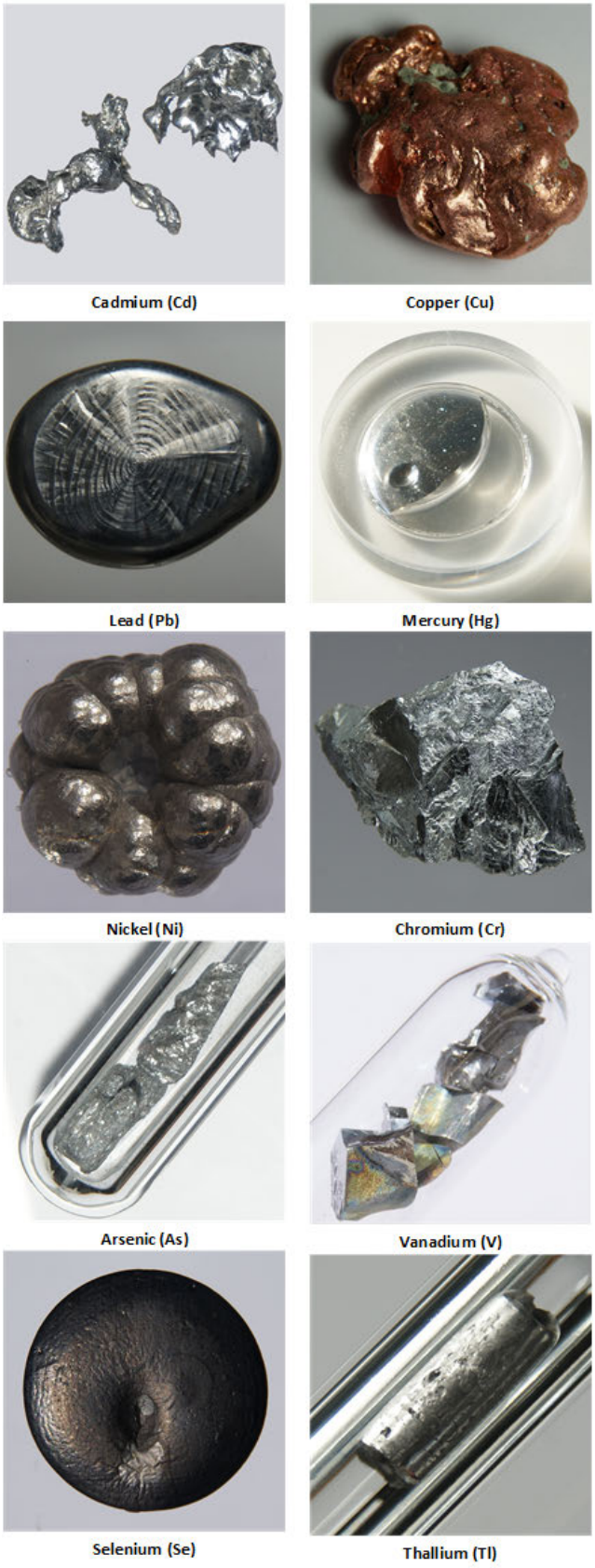

Figure 2.3: Images of heavy metals. Source: http://images-of-elements.com

runoff, industrial wastewaters, agricultural activities and mining activities (WHO 2007). To a small extent they enter our bodies via food, drinking water and air. As trace elements, some heavy metals (e.g. copper, selenium, zinc) are essential to maintain the metabolism of the human body.

HMs are bioaccumulative. It is calculated as the ratio of its concentration in the organism to the concentration in the medium to which this organism is exposed. Generally, fish are the preferred test organisms. As a consequence they are toxic at low concentrations, have neurological impacts and some are carcinogenic. They can also interfere with chemical processes by poisoning chemical catalysts and can impact on biochemical processes by interfering with enzyme action (WHO 2007).

HMs are conservative substances, i.e, they cannot be degraded or destroyed. Their fate in a water system is determined primarily by partitioning and by transport. The partitioning divides the total amount of a toxicant into a "dissolved" fraction and several "adsorbed" fractions.

2.2.1.3 **Organic micropollution**

The term "organic micropollutants", namely OMPs, is intended to include any organic compounds that may be found at microgram per litre concentrations or lower in water. There are a few natural sources of OMPs, but most OMPs are created by humans in industrial processes, either intentionally or as byproducts (WHO 2003). OMPs released to the environment have been shown to travel vast distances from their original source. Thus OMPs can be found all over the world, including in areas where they have never been used and remote regions such as the middle of oceans and Antarctica.

Some of the chemical characteristics of OMPs include low water solubility, high lipid solubility, semi-volatility and high molecular masses. This lipid solubility results in the ability to pass through biological phospholipid membranes and bioaccumulate in the fatty tissues of living organisms. Exposure to OMPs can cause disruption of the endocrine, reproductive and immune systems, neurobehavioral disorders and cancers. This exposure can take place through diet, environmental exposure or accidents (WHO 2003).

OMPs are frequently halogenated, usually with chlorine. The more chlorine groups a OMP has, the more resistant it is to being broken down over time (WHO 2003). The main categories of OMPs are (see figure 2.4):

- *Polycyclic Aromatic Hydrocarbons (PAHs)*: PAHs arise from incomplete combustion or pyrolysis of organic substances such as wood, carbon or mineral oil. Such combustion processes include food preparation in households and food shops, discharge of certain petroleum products, discharge of storm runoff with PAHs from car exhaust particles and road, and incomplete combustion processes in urban landfills.

- *Polychlorinated Biphenyls (PCBs)*: There are two main sources of PCBs. Directly manufactured PCBs (by chlorination of biphenyls), used as hydraulic liquids (hydraulic oils), emollients for synthetic materials, lubricants, impregnating agents for wood and paper, flame protective substances, carrier substances for insecticides and in transformers and condensers. The other main source of PCBs in the environment are combustion processes such as waste incineration plants or fossil fuel burning.

- *Dioxins and furans (PCDD/PCDF)*: The generic term "dioxins" represents a mixture of 219 different polychlorinated dibenzo-pdioxins and furans. The most well known and hazardous dioxin, is the tetrachlorodibenzo-pdioxin (TCDD). Dioxin concentrations are calculated as sum of the toxicity equivalents (TEQ) relevative to the most toxic dioxin TCDD.

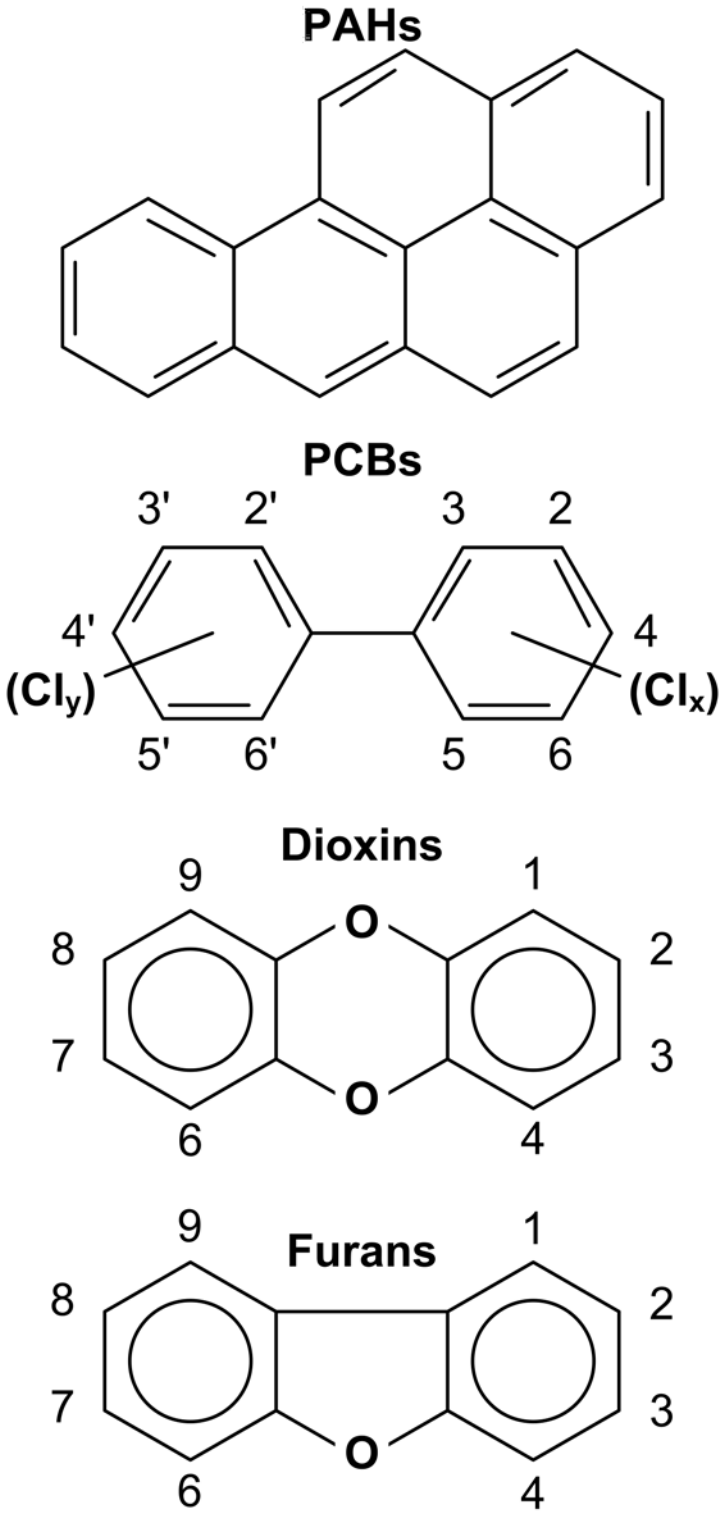

Figure 2.4: Generic chemical structure of PAHs, PCBs, PCDDs and PCDFs

2.2.2 Hydrodynamics

Hydrodynamics studies the motion of water and the forces acting on water. Water movements at different scales and of different types significantly affect the distribution of temperature, nutrients, dissolved oxygen, sediments, toxicants and algae.

Firstly, this section illustrates the basic processes in hydrodynamics of surface water systems. Secondly, the governing equations for 3D shallow water flows are presented. Finally, an overview of the available hydrodynamic models is shown.

2.2.2.1 Basics of hydrodynamics

The conservation laws that govern hydrodynamic processes include the conservation of mass, momentum and energy. These three conservation laws form the theoretical basis of hydrodynamics (Ji 2007).

Conservation of Mass

The law of conservation of mass states that mass can neither be produced nor destroyed. It is often expressed in a mass balance equation (also called continuity equation), which accounts for the flux of mass going into a defined area and the flux of mass leaving the defined area. For an incompressible fluid which is a very accurate description of surface waters in a defined area, the water flux in must equal the flux out (Equation (2.1)).

$$Mass(accumulation) = Mass(in) - Mass(out) + Source - Sink \tag{2.1}$$

The differential equation for the conservation of water mass can be further derived from equation (2.1) for incompressible flow under the cartesian coordinates, i.e., the continuity equation:

$$\frac{\partial u}{\partial x} + \frac{\partial v}{\partial y} + \frac{\partial w}{\partial z} = 0 \tag{2.2}$$

where u, v, and w are velocity components in x, y, and z directions, respectively. It means that the net rate of water mass flow across any closed surface is zero.

Conservation of Momentum

The conservation of momentum can be derived from Newton's second law:

$$\vec{F} = m \cdot \vec{a} \tag{2.3}$$

where $\vec{F}$ is the applied force, m is the mass of the object, and $\vec{a}$ is the acceleration of the object.

In addition to external forces, there are three forces important to hydrodynamics: gravitational force, force from water pressure gradient and viscous force. Gravitational force is due to the gravitational attraction of the earth. Water pressure gradient is caused by pressure gradient in a waterbody. Viscous force is due to water viscosity and turbulent mixing.

A Newtonian fluid is the one where the stress is linearly proportional to the rate of deformation. Most common fluids are Newtonian, such as water, air, and gasoline. When considering the rotation of earth and external forces, equation (2.4) is obtained:

$$\frac{\vec{dv}}{dt} = \frac{\partial \vec{v}}{\partial t} + \nabla \cdot (\rho_{env} \vec{v} \vec{v}) = \vec{g} - \frac{1}{\rho_{env}} \nabla p + \upsilon \nabla^2 \vec{v} - 2\vec{\Omega} \times \vec{v} + \vec{F_{fr}} \tag{2.4}$$

where $\vec{v}$ is the water velocity, $\vec{\Omega}$ is the angular velocity of the earth, $\vec{F_{fr}}$ are the external forces, and $\upsilon = \frac{\mu}{\rho_{env}}$ is the kinematic viscosity.

Equation (2.4) is the Navier–Stokes equation, valid for incompressible Newtonian flows. The meanings of each term in equation (2.4) are:

1. The acceleration term, $\frac{\vec{dv}}{dt}$, is composed of the local rate of change due to time variation ($\frac{\partial \vec{v}}{\partial t}$), plus the rate of change due to advection of the flow [$\nabla \cdot (\rho_{env}\vec{v}\vec{v})$]. This term is the acceleration, $\vec{a} = \vec{F}/m$, given in equation (2.3). The terms on the right-hand side of equation (2.4) are all the forces that cause this acceleration.
2. The gravitational force, $\vec{g}$, acts toward the center of the earth.
3. The pressure gradient term, $-\frac{1}{\rho_{env}}\nabla p$, represents the effects of spatial variation of water pressure. The two contributing factors to pressure gradients are water surface level slopes (the barotropic component) and changes in density (the baroclinic component).
4. The viscous term, $\upsilon\nabla^2\vec{v}$, includes the effects of water viscosity. This term can also be modified to represent turbulent mixing.
5. The Coriolis force term, $-2\vec{\Omega} \times \vec{v}$, represents the effect of earth rotation on water movement. It is significant only when large waterbodies are studied.
6. The external force term, $\vec{F_{fr}}$, is often used to include wind forces.

There are no analytical solutions to the Navier–Stokes equation. It is also too complex to be solved numerically for large domains over long periods of time. Further simplifications to the Navier–Stokes equation are needed in hydrodynamic models and will be described later in Section 2.2.2.2.

Conservation of Energy

The conservation of energy can be derived from Thermodynamic's first law. When heat flows to/or from a system, the system gains or loses an amount of energy equal to the heat transferred. The heat exchanges between the atmosphere and water columns are largely transferred by radiative processes and turbulent heat transfers (Ji 2007). The four heatflux components are the following:

1. The *solar radiation* is the short wave radiation from the sun that reaches the water surface.
2. The magnitude of *longwave radiation* is proportional to the fourth power of the absolute temperature and is determined by the Stephan–Boltzmann law.
3. The *latent heat* is the heat transfer due to water evaporation. The latent heat due to evaporation is the major heat loss for a waterbody.
4. *Sensible heat* exchange (or conduction) is the heatflux transferred between water and the atmosphere due to a temperature difference between the two.

The net heatflux can be described by equation (2.5):

$$H_{net} = H_S + H_L + H_E + H_C \tag{2.5}$$

where H_{net} is the net heatflux across the air/water interface, H_S is the shortwave solar radiation flux, H_L is the net longwave radiation flux from the atmosphere and the waterbody, H_E is the latent heatflux due to evaporation and, H_C is the sensible heatflux due to conduction.

Water density

Water density is a basic parameter in hydrodynamic and water quality studies. Accurate hydrodynamic calculations require accurate water densities. The density (ρ_{env}) is largely determined by three parameters: temperature (T), salinity (S) and concentration of total suspended sediment (SS). The relationship between the four variables, ρ_{env}, T, S, and SS, can be written as:

$$\rho_{env} = f(T, S, SS) = \rho_T + \Delta\rho_S + \Delta\rho_{SS} \tag{2.6}$$

where ρ_T is the density of pure water as a function of temperature (kg/m^3), $\Delta\rho_S$ is the density increment due to salinity (kg/m^3), $\Delta\rho_{SS}$ is the density increment due to total suspended sediment (kg/m^3). The actual form of function f is established empirically.

A variety of empirical equations have been proposed to describe the density of pure water as a function of temperature (Gill 1982, UNESCO 1981).

External forcing

Estuaries are subjected to forcing over a broad range of periods, ranging from hourly to seasonal variations. The primary factors controlling estuarine hydrodynamic processes are external forcing including tides, atmospheric forcing and external sources (figure 2.5).

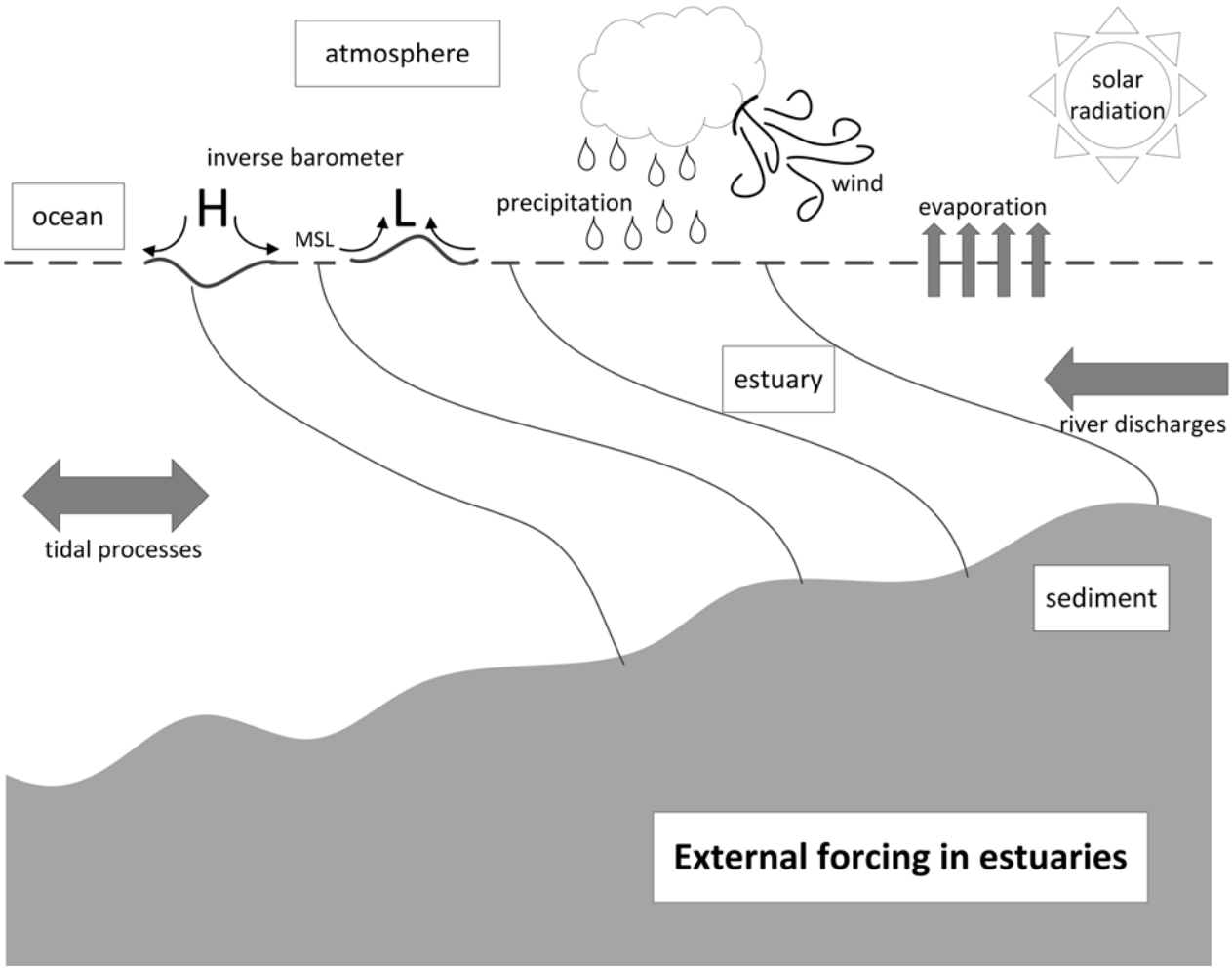

Figure 2.5: Primary external forcing in estuaries including tidal processes, atmospheric forcing (solar radiation, wind, precipitation, evaporation, inverse barometer) and river discharges.

Tidal Symbol	Generating force	Period
M_2	Moon	12.421
S_2	Sun	12.000
O_1	Moon	25.819
K_1	Moon, Sun	23.935
N_2	Moon	12.659
P_1	Sun	24.067
K_2	Moon, Sun	11.967

Table 2.1: Major tidal constituents and periods

Tidal processes

As Defant (1958) stated: *"Tides are the heartbeat of the ocean, a pulse that can be felt all over the world"*.

Tides are the alternate rising and falling of water levels resulting from the gravitational attraction between the earth, sun and moon. Tidal elevations control the tidal velocity and therefore control the transport of substances in the estuary. Tidal currents change speed and direction regularly and are among the strongest in the world's ocean. At high tide at the estuary mouth, the slope of the water surface forces water to rush into an estuary. At low tide, the reversal slope flushes water out of the estuary.

Tides can be represented as the sum of tidal constituents. Each constituent is a harmonic oscillation and has its amplitude, period and phase. There are hundreds of tidal constituents but most of them have very small amplitudes and therefore are neglected in tidal analysis. Table 2.1 lists the major tidal constituents and their periods. The subscripts of the tidal symbols in table 2.1 indicate the approximate number of cycles per 24 h. Diurnal constituents have a subscript of 1 while constituents with subscripts of 2 are semidiurnal.

Spring tides are exceptionally high tides that occur approximately every 2 weeks during new and full moons when the earth, sun and moon are in alignment and the lunar tide is in phase with the solar tide. Neap tides are exceptionally low tides that occur approximately every 2 weeks during the moon's first and third quarters, when the earth, sun and moon are at right angles to each other and the lunar tide is out of phase with the solar tide. This envelope of the spring-to-neap cycle occurs with a period of $\sim$ 14.77 days (Figure 2.6).

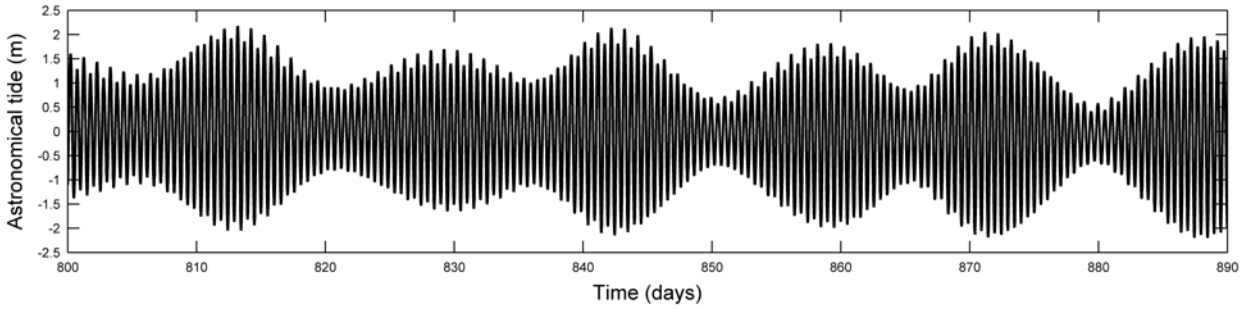

Figure 2.6: Example of 90-days of time series of the astronomical tidal wave.

Major factors that influence the propagation and amplitude of tides include: bottom friction, water depth, shoreline and Coriolis force. Interactions of tidal flows with these factors may result in a residual current that could play a significant role in the transport of toxicants. The residual current is generally obtained by averaging tidal velocities over tidal periods. An averaging time of 25 hours is often used to remove the semidiurnal tide (M_2 tide).

The rise or fall of tidal elevation propagates along an estuary in the form of a long-wave. The phase relation between the tidal elevation and the tidal current varies with water depth. The travel speed of a tidal wave in

shallow waters is given by $c = \sqrt{gH}$, which means that the deeper the water, the faster the wave speed.

Atmospheric forcing

Major atmospheric forcings include wind, air temperature, solar radiation, atmospheric pressure and precipitation. Besides, the atmospheric humidity, cloud cover and atmospheric pressure can also affect an estuary (Ji 2007).

Wind is usually a major source of energy in some estuaries. Wind driven currents are a major mechanism in the transport and distribution of floating toxicants, such as spilled oil. If the distance over which the wind blows and the wind duration are sufficient, wind driven surface currents can approach a velocity equal to 2–4% of the wind speed. But, given the lengths of open water found in most estuaries, it is likely that the resulting current velocity will be less than this magnitude (Ji 2007).

Air temperature affects surface waters via heatflux and evaporation exchange between the air and the water. The temperature differences between the air and the water strongly influence the exchange of heatflux and moisture between the two.

Solar radiation is often the most important heatflux component that acts as a heat source to a waterbody. Solar radiation is penetrative, distributing its heat through a significant range of the water column. The amount of solar radiation that enters the waterbody depends on: the altitude of the sun, which varies daily as well as seasonally for a fixed location on the earth, the dampening effect of scattering and absorption in the atmosphere due to cloud cover and the reflection from the water surface.

Precipitation is usually treated as an input of freshwater to a waterbody. For estuaries with relatively small surface water areas the direct precipitation can be insignificant, comparing to inflows from tributaries and runoffs.

Atmospheric pressure affects sea level through the "inverse barometer effect" that low atmospheric pressure causes the sea level to be higher than normal ($\sim$1 cm/millibar).

External sources

The main external source in estuaries is the freshwater inflows coming from tributaries. If a river discharges into an estuary connected to a nearly tideless sea, such as the Sea of Japan or the Mediterranean, the freshwater overrides the saltwater and flows as a nearly undiluted layer into the sea. If there is some tide the wedge moves back and forth. The more the wedge motion, the more kinetic energy is available to break down the interface and turbulently mix the fresh and saline layers.

The river may be thought as a source of deficit of potential energy or a source of buoyancy and the tide as a source of kinetic energy to overcome the deficit (Fischer *et al.* 1979).

Estuarine Variability and Complexity

Estuarine variability and complexity arises because two dynamic systems, rivers and coastal oceans, meet in a confined geologic space. Change in estuaries occurs on a continuum of space and timescales. The most distinctive feature of estuaries is the variability produced by the mixing of salt water from the ocean with fresh water from the land (Valle-Levinson 2010).

The timescales of variability associated with potentially important estuarine processes range from seconds to decades (see figure 2.7). Tidal forces dominate the short time scales of estuarine variability (hours to days) when the freshwater flow is low, and winds contribute small amounts of variance. At intermediate timescales, days to fortnights, estuarine variability must include both tidal, freshwater flow and wind effects. Over the longer periods such as months, seasons, and years, the primary cause of estuarine variability is related to changes in the discharge of the major source of freshwater.

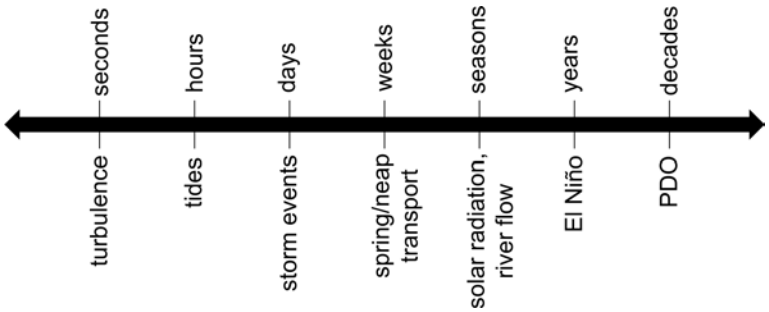

Figure 2.7: Schematic describing the range of time scales of variability characterizing processes influencing estuaries.

Valle-Levinson (2010) described the estuarine variability as:

- *Intratidal variability* that occurs at tidal frequencies of 12–25 hours or on even shorter time scales. The diurnal (daily) and semidiurnal (twice-daily) astronomical tides and their "overtides" (circulation driven by non-linear processes and occurring at sums or multiples of the basic astronomical frequencies) are the most obvious examples. Also in this category are variations in scalar properties (e.g., salinity, temperature and density) driven directly by tidal currents, the effects of a daily sea breeze, internal waves and variations in currents and scalar properties driven by tidal variations in vertical mixing and the along-channel density gradient.

- *Subtidal variability* that occurs at frequencies of <1 cycle/day. In this category are low-frequency tidal motions with periods of 13–15 days and at 27–31 days, variability related to weather systems (typical periods 3–10 days), the response to rapid changes in river flow, e.g., floods related to severe storms and rapid snow-melt events and changes in the mean circulation related to the annual river flow cycle and the balance of evaporation versus precipitation and inflow.

Summarizing, it is likely that an estuary will describe and ellipse of variability in consecutive tidal cycles from spring to neap tides, or from month to month, or dry to wet seasons, or from year to year, or from one location to another inside the same estuary.

Transport timescales

Timescales for different processes can be compared by calculating timescale ratios to determine which process is fastest and therefore most important. If the timescales for two processes are similar in magnitude, then they are approximately equally fast and thus roughly equally important.

Transport timescales such as "residence time", "flushing time" and "age" are often invoked to help explain variability of biological or chemical constituents in tidal and non-tidal aquatic ecosystems.

Flushing time is a bulk or integrative parameter describing the general exchange characteristics of a waterbody without identifying detailed underlying physical processes or their spatial distribution. Flushing time t_f may be estimated most simply as V/q, where V is the basin volume and q is the total volumetric flow rate of water in or out of the estuary (Monsen *et al.* 2002, Sheldon & Alber 2006).

Flushing time may also be calculated empirically with an exponential fit to a time series of outflow concentration $C_{out}(t)$ for a constituent mass that was instantaneously introduced to the system with initial concentration C_0 (Monsen *et al.* 2002):

$$C_{out} = C_0 \exp(-\frac{q}{V}t) = C_0 \exp(-\frac{t}{t_f}) \tag{2.7}$$

This approach assumes instantaneous and complete mixing within the basin and, given its exponential form, implicitly assumes the introduced mass is never completely flushed. With this approach, at time $t = t_f$ only 63% $(1-e^{-1})$ of the initial mass has been flushed.

Residence time is the time taken by a water parcel somewhere within the estuary to leave it. Thus, residence time is location-specific since for any arbitrary start time water parcels at different locations will require different lengths of time to leave the estuary, depending on their proximity to openings and the local hydrodynamics (Sheldon & Alber 2002, Takeoka 1984, Zimmerman 1978).

The *age of a fluid element* within an estuary is the time that has elapsed since the element entered the embayment (Bolin & Rodhe 1973, Zimmerman 1978). Thus, within a real natural waterbody, age is spatially heterogeneous (Banas & Hickey 2005, Monsen *et al.* 2002).

Clearly, longer transport times provide more time for chemical or biological processes to act on a water parcel amplifying the effects of biogeochemical transformations and modifying the net downstream transport of pollutants (Bárcena *et al.* 2012b, Gómez *et al.* 2014a, Lucas *et al.* 2009, Monsen *et al.* 2007, Sámano *et al.* 2012, Søballe & Bachmann 1984).

2.2.2.2 Governing equations for 3D shallow water flows

As discussed previously in this Chapter, conservation of mass (Equation (2.2)), momentum (Equation (2.4)) and energy (Equation (2.5)) provide the fundamental principles needed to develop hydrodynamic and mixing models. Even with advanced computers, these conservation equations are too complex to be solved numerically for large domains over long periods of time (Bleninger 2006). Therefore, further simplifications are needed to solve estuarine hydrodynamics:

- *Single-phase flow*: This thesis will not cover multi-phase flows (e.g. air-water or particle-water), thus only describe the liquid phase.
- *Incompressible fluids*: Waste discharges occur in hydrodynamic regimes where fluids can be considered as incompressible. This means that the density ρ_{env} is constant along a streamline. This approximation is valid for velocities and pressures occurring in environmental flows, provided that the Mach number is below 0.3 (Ferziger & Perić 2002).
- *Newtonian fluids*: Water, even when heated and with typical seawater or wastewater properties, is a Newtonian fluid. Therefore, approximations for the viscous terms of the momentum equation can be used.
- *Boussinesq approximation*: Density variations (ρ') in natural flows are generally small compared to the average density (ρ_{env}), thus $\rho'/\rho_{env} \ll 1$.

Besides the general simplifications regarding water, this section discusses the approximations that are widely used in the studies of estuaries: spatial and temporal simplifications, model domain discretization, open and closed boundaries, 3D shallow water equations and turbulence closure.

Spatial and temporal simplifications

Spatial scales: Effect of earth rotation

For very large scales, forcing due to earth rotation (Coriolis force) may have significant influence on the flow and transport characteristics. The Rossby number allows distinguishing between flows where rotation is

important or not (Equation (2.8)). If the Rossby number is of the order of one, rotation has to be considered.

$$Ro = \frac{\Omega L}{2\pi \overline{u}} \tag{2.8}$$

where $\Omega = 7.29 \cdot 10^{-05}$ (s^{-1}) is the earth rotation speed, L is the characteristic length scale and $\overline{u}$ is the average characteristic velocity.

Spatial scales: Shallow water approximation or hydrostatic assumption

If the water depth (H) is much smaller than the characteristic horizontal length scale (L) then $H/L \ll 1$. Vertical accelerations are dominated by gravitational accelerations and other contributions of accelerations can be neglected. This results in the so-called hydrostatic assumption reducing the governing equations significantly, i.e. the vertical components, thus leaving only the term $\partial p/\partial z = -\rho_{env} g$.

Spatial scales: Spatial averaging (2 or 3 dimensions)

Far-field flows in receiving waters are characterized by two-dimensional (depth-averaged) or three-dimensional unsteady flow and transport phenomena resulting from tidal and meteorological forcing, including the effect of density differences due to a non-uniform temperature and salinity distribution (density-driven flow).

A depth-averaged approach (2D) is thus only appropriate, if the fluid is vertically homogeneous. Three-dimensional modeling is of particular interest in transport problems where the horizontal flow field shows significant variation in the vertical direction.

Temporal scales: Simplification of turbulent fluctuations

Regarding the small-scale temporal variations, it is still very difficult to resolve up to the turbulence scales (Kolmogorov scale) and very often, there is no need for, because only temporal averaged values are needed. Therefore techniques to decompose the velocity in average values $\overline{u_i}$ and turbulent fluctuations u_i' are used.

The flow is hereby assumed stationary over the integral time scale (t_I) and the "Reynolds Averaged" equations are obtained by substituting the Reynolds decomposition $u_i(t) = u_i + u_i'(t)$ and averaging over t_I.

3D shallow water equations

Regarding estuarine hydrodynamics, implementing the previous simplifications over the general hydrodynamic equations derived from the conservation laws (Equations (2.2), (2.4) and (2.5)) result in the URANS (unsteady Reynolds Averaged Navier-Stokes) equations for 3D shallow flows (Rodi 1993):

Continuity equation

$$\frac{\partial \overline{u_i}}{\partial x_i} = 0 \tag{2.9}$$

Momentum equation

$$\frac{\partial \overline{u_i}}{\partial t} + \overline{u_j}\frac{\partial \overline{u_i}}{\partial x_j} + 2\Omega_i \times \overline{u_i} = -\frac{1}{\overline{\rho_{env}}}\frac{\partial \overline{p}}{\partial x_i} - \overline{\rho_{env}} g_z + \upsilon \frac{\partial^2 \overline{u_i}}{\partial x_j^2} + \frac{\partial \overline{u_i' u_j'}}{\partial x_j} + \frac{F_{i,e}}{\overline{\rho_{env}}} \tag{2.10}$$

where $\overline{\rho_{env}}$ is the time averaged density and $\overline{p}$ is the time averaged pressure. The term $\frac{\partial \overline{u_i' u_j'}}{\partial x_j}$ is defined as additional stress term called Reynolds stress.

Transport equation

$$\frac{\partial \overline{C}}{\partial t} + \overline{u_i}\frac{\partial \overline{C}}{\partial x_i} + \frac{\partial \overline{u_i' C'}}{\partial x_i} = D_m \frac{\partial^2 \overline{C}}{\partial x_i^2} + k\overline{C} \tag{2.11}$$

where $\overline{C}$ is the mean substance concentration and C' is the concentration variations.

As we can see, the implementation of the previous simplifications (especially the "Reynolds Averaged") produces two new terms. The term $\frac{\partial \overline{u_i' u_j'}}{\partial x_j}$ in the momentum equation (2.10) and the term $\frac{\partial \overline{u_i' C'}}{\partial x_i}$ in the transport equation (2.11) represent the fluctuations of the momentum and mass due to the turbulent flow respectively.

Turbulence closure

The resulting simplified equations still need further approximations for the turbulence closure because of the new unknowns before being solved numerically. The objectives of these approximations is to discretize the modeled equations on a grid of adequate size, so that the processing time will not be too large. This is a way to decrease the number of degrees of freedom. Thus, the idea is not to use a theory to provide an instantaneous turbulent solution but to provide a mean numerical solution on a rough grid, using a model.

The important point is the non-linearity of Navier–Stokes equations: the averaged equations are not closed and are expressed using small-scale instantaneous fluctuations, through the Reynolds tensor. The introduction of a model is then necessary to close the equations and provide, through an appropriate hypothesis, a "closure" expressing the Reynold's stress tensor using averaged quantities. There is no standard closure and the choice of the turbulence closure is strongly oriented to the application. There is a trade-off between the complexity of the turbulence closure and the computational cost.

Joseph Boussinesq was the first practitioner introducing the concept of eddy viscosity. In 1887 Boussinesq proposed relating the turbulence stresses to the mean flow to close the system of equations. Boussinesq observed that the increment of turbulence increased the deformation of the fluid. He proposed that the Reynold's stress could be linked to this deformation in a way similar to that manifested by viscous stress according to the principle of Newton viscosity:

$$\tau_{ij} = \mu\left(\frac{\partial u_i}{\partial x_j} + \frac{\partial u_j}{\partial x_i}\right) \tag{2.12}$$

where μ is the dynamical viscosity which is an intrinsic property of the fluids.

By analogy, in the case of the Reynolds stresses, Boussinesq proposes the following expression:

$$\tau_{ij} = -\rho_{env}\overline{u_i' u_j'} = \mu_t\left(\frac{\partial \overline{u_i}}{\partial x_j} + \frac{\partial \overline{u_j}}{\partial x_i}\right) \tag{2.13}$$

where μ_t is the so-called turbulent or eddy viscosity which is a property of the flow instead of the fluid because it varies spatially.

Similarly, in the transport equation is adopted the following expression:

$$-\rho_{env}\overline{u_i' \phi_i'} = D_t \frac{\partial \overline{\phi_i}}{\partial x_i} \tag{2.14}$$

where ϕ_i is the scalar being transported such as temperature, salinity or a substance.

The value of the turbulent or eddy diffusivity D_t is calculated by the turbulent or eddy viscosity and turbulent Schmidt number σ_t, which takes values generally between 0.7 and 1 (García-Alba 2011).

$$D_t = \frac{\mu_t}{\sigma_t} \tag{2.15}$$

For the modeling of estuarine hydrodynamics, a classical turbulence closure based on eddy-viscosity principles is applicable. The eddy-viscosity links Reynolds-stresses to the gradients of the mean flow.

An overview of four existing approaches are described to determine eddy viscosity and diffusivity in estuaries. The turbulence closure models differ in their prescription of the turbulent kinetic energy (k), the dissipation rate of turbulent kinetic energy (ε) and/or the mixing length (L) (Deltares 2014d).

1. Constant coefficients.
2. Zero-equation models such as the Algebraic Eddy viscosity closure Model (AEM).
3. One-equation models such as the $k-L$ turbulence closure model.
4. Two-equations model such as the $k-\varepsilon$ turbulence closure model.

The first turbulence closure model is the simplest closure based on a constant value which has to be calibrated and validated against field data.

The other three turbulence closure models are based on the so-called eddy viscosity concept of Kolmogorov (1942) and Prandtl (1945). The eddy viscosity is related to a characteristic length scale and velocity scale (Equation (2.16)).

$$\mu_t = c'_\mu L\sqrt{k} \tag{2.16}$$

where c'_μ is a constant determined by calibration, L is the mixing length, and k is the turbulent kinetic energy.

In zero equation models, as the name designates, we have not partial differential equation (PDE) that describes the transport of the turbulent stresses and fluxes. A simple algebraic relation is used to close the problem. For example, the algebraic eddy viscosity model (AEM) which uses analytical (algebraic) formulas to determine k and L. The turbulent kinetic energy k depends on the (friction) velocities or velocity gradients and for the mixing length L, the following function of the depth is taken (Bachmetev 1932):

$$L = \kappa(z+d)\sqrt{1-\frac{z+d}{H}} \tag{2.17}$$

where κ is the Von Kármán constant ($\kappa \approx 0.41$). For a homogeneous flow this leads to a logarithmic velocity profile.

In one-equation models, a PDE is derived for the turbulent kinetic energy and the unknowns (turbulent viscosity and diffusion coefficient) are expressed as a function of the turbulent kinetic energy. For example, the $k-L$ model (Uittenbogaard *et al.* 1992) involves one transport equation for k (Equation (2.18)) and the mixing length L is prescribed analytically with the same formulation used as for the AEM turbulence model.

$$\rho_{env}\frac{\partial k}{\partial t} + \rho_{env}\overline{u_j}\frac{\partial k}{\partial x_j} = \tau_{ij}\frac{\partial \overline{u_i}}{\partial x_j} - \rho_{env}\varepsilon + \frac{\partial}{\partial x_j}[(\mu + \frac{\mu_t}{\sigma_k})\frac{\partial k}{\partial x_j}] \tag{2.18}$$

where the local and convective variations are displayed in the left hand of the PDE. The right hand contains the production rate of turbulent kinetic energy k, its destruction rate and its transport by diffusion. The parameter σ_k is a calibration coefficient which usually equates to 1.00.

In the two-equation models, two PDEs are developed: one for the turbulent kinetic energy and one for the turbulent dissipation rate. For example, the $k-\varepsilon$ model (Launder & Spalding 1972). From k and ε the mixing length L and viscosity are determined. The mixing length is a property of the flow. The PDE for the turbulent kinetic energy is already given by equation (2.18). Now instead of modeling ε, an independent PDE for its transport is included:

$$\rho_{env}\frac{\partial \varepsilon}{\partial t} + \rho_{env}\overline{u_j}\frac{\partial \varepsilon}{\partial x_j} = C_{1\varepsilon}\frac{\varepsilon}{k}\tau_{ij}\frac{\partial \overline{u_i}}{\partial x_j} - C_{2\varepsilon}\rho_{env}\frac{\varepsilon^2}{k} + \frac{\partial}{\partial x_j}[(\mu + \frac{\mu_t}{\sigma_\varepsilon})\frac{\partial \varepsilon}{\partial x_j}] \tag{2.19}$$

where the first member contains the local and convective variations of ε. The second member represents the production rate of turbulent kinetic dissipation ε, its destruction rate and its transport by diffusion. The parameters $C_{1\varepsilon}$, $C_{2\varepsilon}$ and σ_ε are calibration coefficients which usually equates to 1.44, 1.92 and 1.00, respectively.

2.2.2.3 **Hydrodynamic available models**

Ocean circulation modeling began in 1960s at the Geophysical Fluid Dynamics Laboratory in New Jersey where ocean circulation models were developed for use with atmospheric models to study the influence of the oceans on climate. The models were far simpler and computers were far slower relative to today, so that months of computational time were needed to simulate a few years of real time. Consequently, grid resolutions were between two to five degrees latitude/longitude (very coarse). Many of these earlier models were related to the MOM (modular ocean model) series (TetraTech 2000).

During 1970s and 1980s a number of ocean circulation models were developed, including finite difference models that used curvilinear coordinates and a fewer number of finite element models. Gradually grid resolution began to decrease to about 1/10 degree, equivalent to about 10 km of distance. This allowed predictions to be made of more detailed features of the oceans' circulations, such as the meandering Gulf Stream (TetraTech 2000).

In 1990s, more efforts were focused on retaining the free surface features in models without incurring the tremendous computational costs of doing so. Los Alamos National Laboratory was one of the developers of the new techniques that began to take advantage of parallel processing machines (POP series model).

However most of these models are set up for large domains (order of hundreds of kilometers), where near coastal features are not as important, thus not resolved in detail. Conversely, estuarine discharge modeling especially needs to know about near coastal flow features for domains of the order of kilometers (estuarine domain), with high resolution in the discharge region (order of meters) (Davies *et al.* 1997). Additionally, effects on stratified waters, non-uniform velocity profiles, and baroclinic processes require a three dimensional flow representation.

Having in mind all these features about estuarine discharge modeling, in 2000s three-dimensional codes were refined to characterize barotropic and baroclinic estuarine circulation (Castanedo 2000). There are several estuarine circulation models in use today. Most cited models are:

- POM - Princeton Ocean Model from Princeton University (Blumberg & Mellor 1987).
- EFDC - Environmental Fluid Dynamics Code from Virginia Institute of Marine Science and School of Marine Science of The College of William and Mary (Hamrick 1992).
- MIKE3 from Danish Hydraulics Institute (Jacobsen & Rasmussen 1997).
- H3D - Hidrodinámica 3D from Universidad de Cantabria (Castanedo 2000).
- MOHID from Technical University of Lisbon (Miranda *et al.* 2000).
- TELEMAC3D from Electricité de France and Wallingford (Hervouet & Bates 2000).
- ELCOM - Estuary, Lake and Coastal Ocean Model from University of Western Australia (Hodges 2000).
- Delft3D-FLOW from Delft Hydraulics and Deltares (DelftHydraulics 2001).
- FVCOM - Finite Volume Coastal Ocean Model (Chen *et al.* 2003).

Name	Numerical Features	Turbulence Closure	Extensions/ Applications	Comments
POM	FDM,BO, HY	CEV,ML	None	OS(A,R,B)
EFDC	FDM,BO, HY	CEV,ML	GG,ST,TR	OS(A,R,B), PPT,WD
MIKE3	FVM,BO, HY	CEV,k-ε, SSS, mixed SSS/k-ε	EC,MT,ST, TR,WQ	non-OS, GUI,PPT,WD
H3D	FDM,BO, HY	CEV,AEM	TR,WQ,	OS(A,R)
MOHID	FVM,BO, HY	CEV,AEM, GOTM	EC,GG,MT, ST,TR,WQ	OS(A,R,B), GUI,PPT,WD
TELEMAC 3D	FEM,SW, non-HY	ML	HA,MT,ST, TR,W	OS(A,R,B), PPT,WD
ELCOM	FDM,BO, HY	CEV, mixed layer	WQ	non-OS, GUI,PPT,WD
Delft3D -FLOW	FVM,SW, BO,HY	CEV,AEM, k-L,k-ε	EC,GG,MT, ST,TR,W,	OS(A,R,B), GUI,PPT,WD, WQ
FVCOM	FVM,BO, HY	MY,GOTM	MT,ST,TR, WQ	OS(A,R), PPT,WD
ADCIRC	FEM,SW, BO,HY	CEV,AEM, ML	ST,TR,W	OS(A,R), PPT,WD
ROMS	FDM,BO, HY	CEV,ML, k-ε,k-w	EC,ST,MT, TR,W,WQ	OS(A,R,B), PPT,WD

Table 2.2: Examples of hydrodynamic circulation models

- ADCIRC from University of North Carolina and University of Notre Dame (Luettich & Westerink 2004).
- ROMS - Regional Ocean Modeling System from Rutgers University (Haidvogel *et al.* 2008).

Among these models, only EFDC, ROMS, POM, MOHID, Delft3D-FLOW and TELEMAC-3D are open source for academic, research or business, what motivated that they become three-dimensional hydrodynamic tools most widely used today. These models use curvilinear orthogonal horizontal coordinates, a horizontal numerical staggered "Arakawa-C" grid, and a vertical staggered grid with either a sigma or a more general s-coordinate system. Most models assume the vertical pressure distribution to be hydrostatic. The models are either finite element, finite difference, or finite volume, of which finite difference is the most common.

Although the basics of these models are similar, there are considerable differences in numerics and parameterizations. Main characteristics of these models are listed in table 2.2. From this review, it can be concluded that these models are appropriated for solving estuarine hydrodynamics and using their results as an input to study the estuarine mixing, transport and decay of wastewaters within the near- and far-field region.

2.2.3 Primary or initial dilution (Near-Field)

In environmental fluids, it is not a rare occurrence to see one fluid intruding into another. Common examples are wastewater discharges from pipes into rivers, lakes or estuaries and plumes exiting from industrial smokestacks. In every case, a fluid with some momentum and/or buoyancy exits from a relatively narrow

A = Academic Use	HY = Hydrostatic Assumption
B = Business Use	ML = Mixing Length
AEM = Algebraic Eddy Model	MT = Mud Transport
BO = Boussinesq Approximation	OS = Open Source
EC = Ecology Model	PPT = Pre and Post-processing Tools
CEV = Constant Eddy Viscosity	R = Research Use
FEM = Finite Element Method	SSS = Smagorinsky Subgrid Scale
FDM = Finite Difference Method	ST = Sediment Transport Module
FVM = Finite Volume Method	SW = Shallow Waters
GG = Grid Generator	TR = Transport Module
GOTM = General Ocean Turbulence Model	W = Wave
GUI = Graphical User Interface	WD = Well Documented
HA = Harbor Agitation	WQ = Water Quality Module

orifice and intrudes into a larger body of fluid with different characteristics. These flows can be characterized as partly turbulent because they create situations where the turbulence level is much higher in the vicinity of the intrusion than in the surrounding fluid (Cushman-Roisin 2013).

The near-field region is the initial mixing zone located in the vicinity of the discharge point. The mixing phenomena occurs at small scales (spatial and temporal variations in the order of meters and minutes). The analytical study of the initial dilution has not been able to give generalizable solutions in practice, except in very simple situations. Therefore, the study of the initial dilution has necessitated the use of laboratory or "in situ" testing which are subsequently used for the development of various mathematical tools and models (Roberts 1979).

2.2.3.1 **Basics of near-field mixing**

The physics of effluent mixing and dilution involve the principles of conservation of mass, momentum, and energy. Several key questions can be asked to determine how the discharge will interact with the receiving water in the near-field:

- What is the effluent discharge rate compared to the receiving water flow? (conservation of mass)
- What is the velocity of the effluent discharge compared to that of the receiving water? (conservation of momentum)
- What angle (if any) exists between the discharge direction and the receiving water flow? (conservation of momentum)
- What is the density difference between the discharge and the receiving water? (conservation of energy)

It is helpful to categorize the various types of intrusion according to whether they inject momentum, buoyancy or both in the ambient fluid (Kundu & Cohen 1990):

- If the dominant force is only Momentum then it is called Jet (Figure 2.8).
- If the dominant force is only Buoyancy then it is called Plume (Figure 2.9).
- If the dominant force are both Momentum and Buoyancy then it is called Buoyant Jet or Forced plume (Figure 2.10).

Jets

The first theoretical studies of round jets were made by Albertson *et al.* (1950), who found that linearly spreads on the receiving environment. This fact has been confirmed by Papanicolau & List (1988). Morton *et al.* (1956) introduced the idea that fluid momentum, vorticity and scalars in a jet are spread by turbulent entrainment rather than turbulent diffusion. They hypothesised that non-turbulent, irrotational fluid from outside the jet was entrained into the turbulent jet. This viewpoint was quickly incorporated into the already existing jet-integral methods. Keffer & Baines (1963) included a cross flowing ambient current in their experimental studies of the pure jet. Scorer (1959) introduced dimensional analysis and the use of length scales to separate regions of strong and weak deflections.

In the study of turbulent jets, two different zones are classical and usually distinguished: the zone of flow establishment (ZFE) or jet development and the zone of established flow (ZEF) or fully developed jet (see in figure 2.8).

1. The ZFE extends from the discharge point until water entrained at the edges of the jet affects the centerline velocity. The velocity profile has a top-hat distribution initially in the central part but attains a Gaussian shape at the end of the ZFE. This central part is not disturbed by the flow of the receiving environment. Outside of the central part called the diffusion zone, the velocity decreases to match the velocity of the flow of the receiving environment. A strong mixing between the two fluids is produced in this zone (Kundu & Cohen 1990).

2. The ZEF extends from where the water entrained at the edges of the jet affects the centerline velocity and to infinity. When the top-hat distribution has disappeared by the lateral diffusion, the ZEF begins and the mixing takes place in the entire section of the jet. In the ZEF, the velocity and concentration profile has a Gaussian shape.

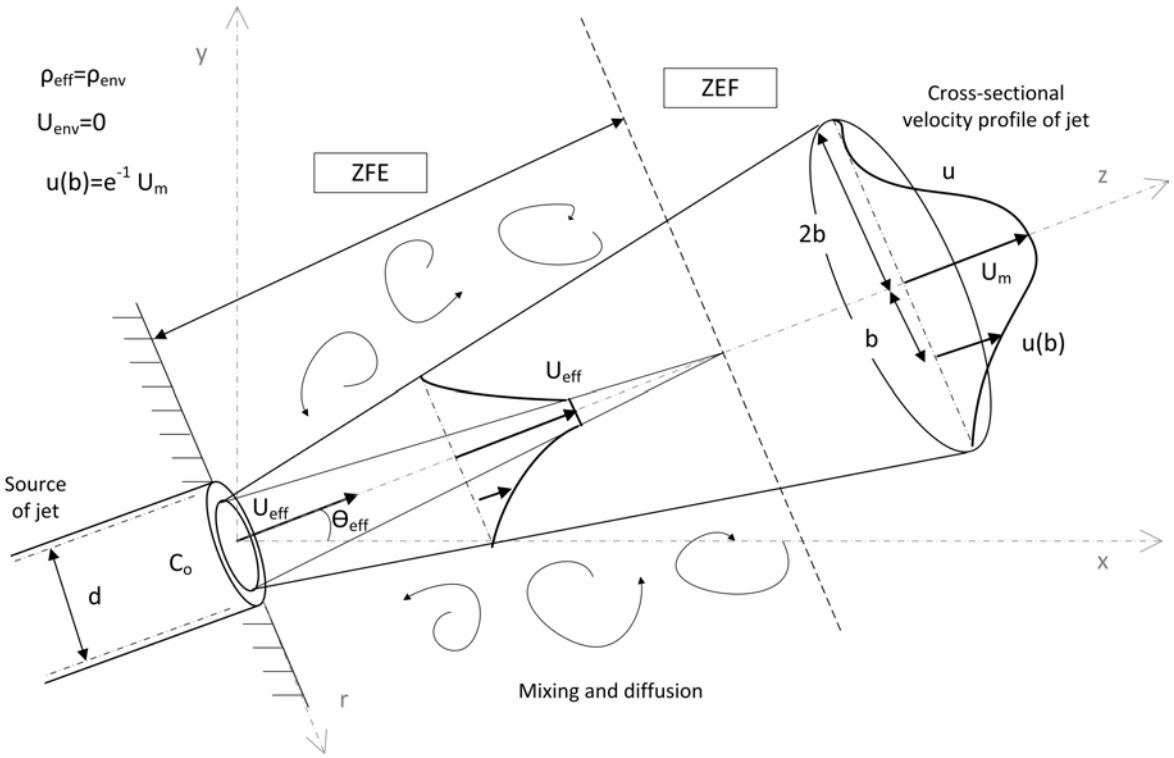

Figure 2.8: Scheme of a pure jet. Adapted from Kikkert (2006) and García-Alba (2011).

Plumes

The first studies of plumes were conducted by Rouse *et al.* (1952), who studied the heat convection in linear and point sources. Plumes have been extensively studied within the field of environmental hydraulics engineering because of their application to the study of urban wastewaters discharge into the marine environment (Cederwall 1968, Jirka *et al.* 1975). In the case of thermal plumes, most studies are based on measurements of the trajectories and the dilution in a central plane of symmetry (Csanady 1965, Fischer *et al.* 1979) from which asymptotic relations to describe their movement have been generated.

Detailed measurements of the cross sections and the deflection of the plume have been made by Knudsen (1988) and Chen & Lee (2002). It is remarkable that these theoretical studies of jets and plumes have been conducted in order to evaluate the behavior with open boundaries (trajectory and mixing with the receiving environment), regardless of the variations experimented by the discharge when interacting with closed boundaries such as free surface, bottom or side walls.

Buoyancy force per unit mass of fluid is known as reduced gravitational acceleration ($g'_o = \frac{(\rho_{env}-\rho_{eff})}{\rho_{eff}}g$). Thus, if buoyancy in a plume is produced by the discharge of a fluid with density (ρ_{eff}) and flow (Q_{eff}) in a medium with density ($\rho_{env} > \rho_{eff}$), buoyancy flux associated with that discharge would:

$$F_o = (\rho_{env} - \rho_{eff})gQ_{eff} \tag{2.20}$$

In the case of round plumes, cross sections at any height can be described in terms of velocity or concentration through Gaussian profiles (Figure 2.9).

Buoyant Jets or Forced Plumes

Most plume experiments have a significant initial momentum flux and these experiments are better described as buoyant jet flows. The flow travels firstly through a region where the initial momentum flux dominates and the behaviour of the flow is jet-like. In the region where the flow is driven by the buoyancy force, the buoyancy-generated momentum flux dominates and the behaviour is plume-like (see Figure 2.10).

On one hand, if the discharge is located in the jet-like region, its properties can be defined in terms of a length-scale of momentum (L_M):

$$L_M = \frac{(Q_{eff}w_o)^{1/2}}{u_{env}} \tag{2.21}$$

where Q_{eff} is the jet flow, w_o is the vertical velocity and u_{env} is the ambient velocity

On the other hand, if the discharge is located in the plume-like region, its properties can be defined in terms of a length-scale of buoyancy (L_B):

$$L_B = \frac{(\rho_{env} - \rho_{eff})gQ_{eff}}{u_{env}} \tag{2.22}$$

where ρ_{env} is the density os the ambient water, ρ_{eff} is the density of the discharged water, Q_{eff} is the plume flow and u_{env} is the ambient velocity.

As the buoyancy-generated momentum flux and the entrained ambient momentum flux act in perpendicular directions, the initial momentum flux determines whether a two-dimensional or a three-dimensional trajectory flow is created. In this cases, the use of integral models is required to track the path described by this type of discharge as well as its dilution, specially when stratification or geometric influences become dominant (Kikkert 2006).

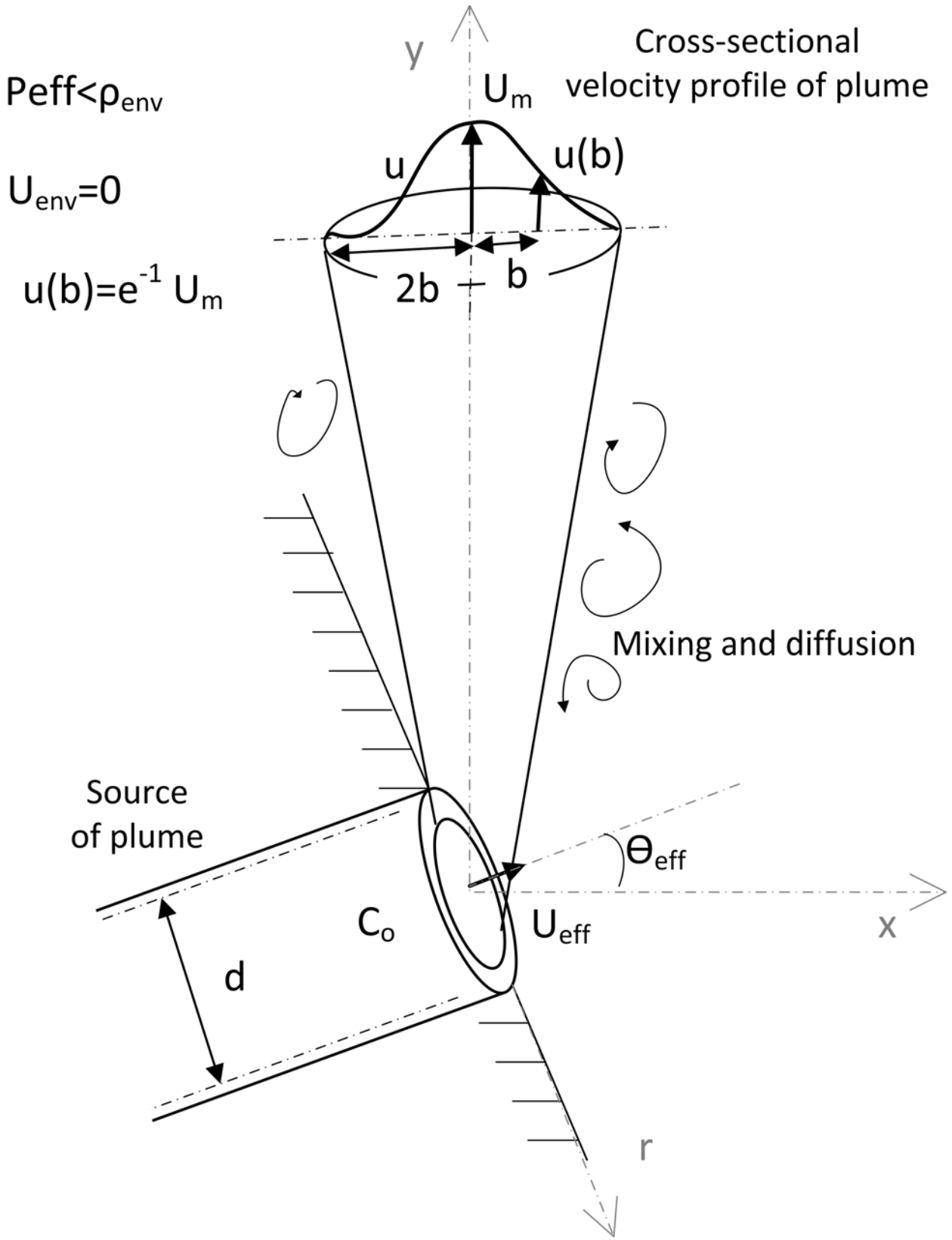

Figure 2.9: Scheme of a pure plume. Adapted from Kikkert (2006) and García-Alba (2011).

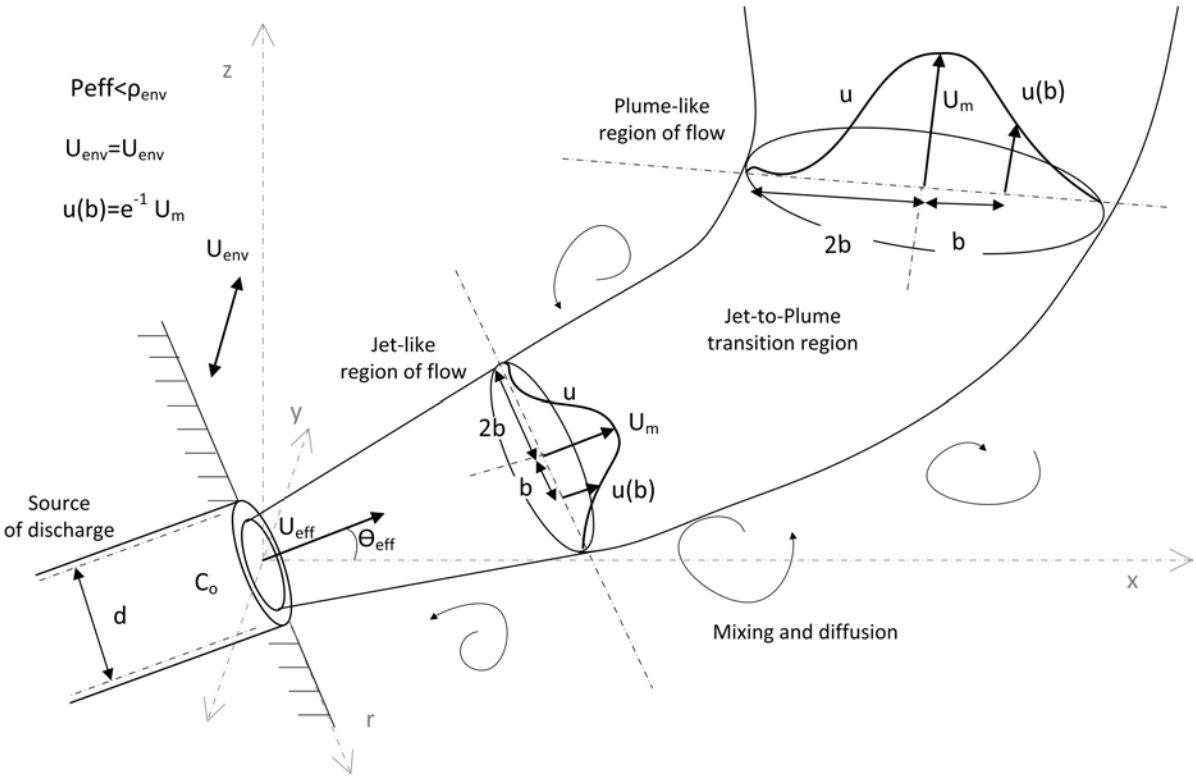

Figure 2.10: Scheme of a buoyant jet or forced plume. Adapted from Kikkert (2006) and García-Alba (2011).

2.2.3.2 Near-field available models

The considerable research activity in this area over the past 50 years has resulted in a number of different models to mathematically describe the trajectory and dilution of buoyant jets. Most models are now able to predict the behaviour of a buoyant jet with a three-dimensional flow trajectory. The different models can generally be split into two different categories: length-scale models and integral models.

- *Length-scale models* are based on the length-scale approach (Pun 1998). The first step in this approach is to determine the different flow regions. These flow regions are determined by the relative magnitude of the independent parameters of the flow. The independent parameters are the initial flow rate, the initial excess momentum flux, the initial density deficit flux and the ambient velocity.
- *Integral models* use hydrodynamic equations governing the conservation of mass and momentum, and of other quantities as toxicant mass, density deficit, temperature and/or salinity. This set of equations are solved stepwise along the general curved jet trajectory. The solution yields values of the trajectory position itself and of the centerline concentrations of these quantities, while the actual cross-sectional distribution is fixed a priori (mostly as a Gaussian distribution) in these models (Frick *et al.* 2001, Jirka 2004, Lee & Cheung 1990).

For buoyant jet flows, it is convenient to apply the integral models (Bleninger 2006, Kikkert 2006). A large number of buoyant jet integral models can be found in the literature with many variations. The most widespread internationally are CORJET (CORMIX system), UM3 (VISUAL PLUMES package), JETLAG (VISJET system) and MOHIDJET (MODHID system) which are briefly reviewed in the following paragraphs.

All the aforementioned models have advantages and disadvantages and can be used in a complementary way. For example, JETLAG and MOHIDJET have a dynamic interface that may be useful in the analysis. UM3

and JETLAG have the possibility of considering time series of effluent and environment characteristics. Other aspect is that CORJET and UM3 are recognized by the competent authorities of the USA and other countries having a very wide range of applications. Some models are free for download via Internet such as UM3 and MOHIDJET while JETLAG and CORJET are commercial tools.

CORJET (CORMIX system)

The CORMIX system (Doneker & Jirka 1990, Jirka *et al.* 1996) addresses the full range of discharge geometries and ambient conditions and predicts flow configurations.

At the heart of CORMIX is the integral jet model CORJET (Jirka 2004; 2006). Proximity effects due to the presence of a horizontal bottom boundary near the level of the discharge are included in CORJET. These are related to a "leakage factor" that measures the combined affect of port height and spacing in allowing the ambient flow to pass through the single-port in order to provide sufficient entrainment flow for the mixing.

The model has been validated intensively and the range of applicability of the integral model has been carefully evaluated where a number of spatial limitations have been proposed beyond which the integral model necessarily becomes invalid.

UM3 (VISUAL PLUMES package)

Visual Plumes (Frick *et al.* 2001) is a Windows-based program for predicting the dispersive and other physical processes affecting surface water effluents: plumes and jets.

UM3 is a Lagrangian initial dilution plume model based on the UM model described in some detail in Baumgartner *et al.* (1994), also known as PLUMES. The Lagrangian formulation offers comparative simplicity that is useful in developing the projected area entrainment (PAE) hypothesis. The PAE hypothesis is a statement of forced entrainment, the rate at which mass is incorporated into the plume in the presence of current. In addition to PAE, the traditional Taylor entrainment hypothesis (Morton *et al.* 1956) is also used.

UM3 has been modified for three dimensions. This change is possible by using vector math and by generalizing the PAE hypothesis (Frick 1984). The modification adds a term to the PAE hypothesis which represents the entrainment entering the plume element from the side represented by a vector pointing at right angles to the plane formed by the instantaneous direction of motion of the plume element and the gravitational acceleration vector.

JETLAG (VISJET system)

VISJET (Cheung *et al.* 2000) is a general predictive, PC-based, flow visualization tool to portray clearly the evolution and interaction of buoyant jets discharged at different angles to the ambient tidal current. It combines an extensively validated Lagrangian jet mixing model (JETLAG) with computer graphics techniques to trace the path and mixing characteristics of arbitrarily inclined jets in three-dimensional space, in a uniform or density-stratified crossflow.

The Lagrangian model JETLAG (Lee & Cheung 1990, Lee & Chu 2003) predicts the mixing of buoyant jets with three-dimensional trajectories. The model tracks the evolution of the average properties of a "plume element" at each step by conservation of horizontal and vertical momentum, conservation of mass accounting for entrainment, and conservation of tracer mass/heat. Details of the theory and computation can be found in Lee & Cheung (1990) and Lee & Chu (2003).

Over the past decade, supported by turbulence model computations and detailed laboratory LIF measurements, the entrainment computation has been significantly revised. First, based on a validated theory and experiments of a coflow jet (Chu *et al.* 1999), a general shear entrainment hypothesis is developed (Lee *et al.* 2000). Second, a general method of modeling the transition from the near to the far field has been proposed

(Lee *et al.* 2000, Lee & Chu 2003).

MOHIDJET (MOHID system)

The MOHIDJET integral model aims to simulate the initial dilution associated to outfalls jets. The model is used as an initial condition of the MOHID system Lagrangian tracers module. The MOHIDJET is a very helpful tool to simulate the impact of outfalls integrating the near-field (MOHIDJET) with the far-field (MOHID).

A Lagrangian approach was used in the MOHIDJET similar to the one use in the JETLAG model (Lee & Cheung 1990). Basically the trajectory and volume variation of a tracer with a cylindrical geometry is simulated . However, for the entrainment parametrization was used the work of Jirka (1999). This author is one of the main contributors to the development of CORJET.

2.2.4 Intermediate-Field: Coupling Near and Far-Field

The intermediate field is characterized by the impact of the turbulent plume with boundaries and the transition from the vertically rising plume/jet characteristics to a horizontal motion generated by the gravitational collapse of the toxicant cloud (Sanchez-Arcilla *et al.* 1998).

Instead of combining near- and far-field effects, models usually concentrate primarily on either the near- or the far-field. Near-field models typically assume that the far-field characteristics are known with the consequence that the effect of the near-field on the far-field cannot be computed. Far-field models, on the other hand, tend to over simplify near-field effects by considering simply an influx of mass at the point of discharge. This procedure discounts many influences of the near-field on the far-field (Kaufman & Adams 1981).

Because of the difficulty in the near- far-field coupling, certain aspects of interest, such as ***mixing zones***, are difficult to assess. In the following sections, an overview of the basics of intermediate-field mixing as well as the use of coupling approaches to model the complete dilution of a wastewater throughout the mixing fields (near-, intermediate- and far-region) are given.

2.2.4.1 Basics of intermediate-field mixing

At intermediate distances from the point of discharge the buoyant jet is still being affected by the initial buoyancy and momentum but it is also being influenced by the ambient flow. These phenomena have been observed and documented in laboratory studies (Lee & Cheung 1986, Roberts 1979, Wallace & Wright 1984).

However, the numerical prediction of such flows has hitherto not been reported. In the case of single-port discharges, the scale of the intermediate-field ranges from about 1 m to the order of 100 m, depending on the discharge characteristics. The large size of this region is a major reason why a link between near- and far-field modeling is necessary to carry out an adequate 3D environmental impact assessment (Choi & Lee 2007).

According to Jirka *et al.* (1996), the intermediate-field starts at the end of the buoyant jet regime (region (1) in Figure 2.11a) and is classified according to three main processes: the boundary interaction, where the vertical boundaries inhibit any vertical motion (region (2) in Figure 2.11a), the buoyant spreading, where the wastefield establishes horizontally (part of region (3) in Figure 2.11a) and the near-field instability (Figure 2.11b). Once these processes are of minor order compared to far-field transport and dispersion processes, the far-field is attained (region (4) in Figure 2.11a).

A brief description of the main processes is given below:

- *Near-field instability* is defined as the situation when discharge induced motions considerably influence

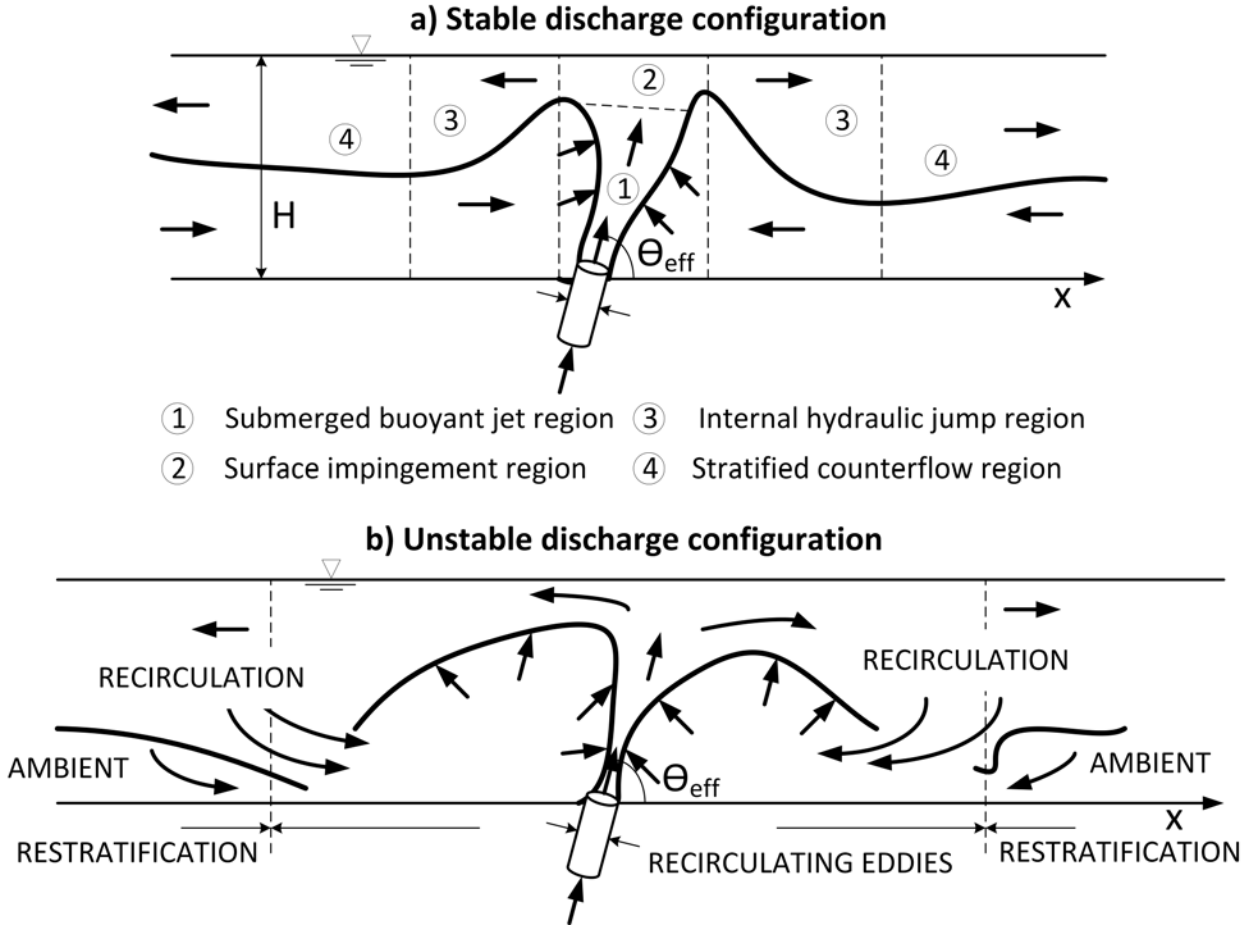

Figure 2.11: Submerged buoyant slot jet discharging into stagnant water of finite depth. a) Deep water discharge with stable discharge configuration, b) shallow water discharge with unstable recirculation zone. Adapted from Jirka *et al.* (1996).

the ambient motions in the near-field region (Jirka 2006). Large recirculation zones or vertically mixed currents that laterally entrain ambient water are typical examples for an unstable near-field (Figure 2.11b).

- *Boundary interactions* have strong implications on wastewater discharge assessments because location and concentration of plumes when hitting either the surface or the shoreline are important project criteria. Boundary interaction processes are classified into interaction with vertical boundaries (surface, bed, or pycnocline) and horizontal boundaries (shoreline). Additional mixing is referred to this impact and spreading motions, where so-called upstream spreading may extend considerably. Shallow conditions may furthermore lead to local recirculation.

- *Buoyant spreading processes* are related to the plume collapse after boundary or pycnocline interaction. These motions are no longer buoyant jet and concentration distributions change according to transport motions and spreading motions. Transport motions carry the substances away from the source with ambient velocities. Spreading motions spread the waste-field in the horizontal as illustrated in figure 2.12.

Only few lab and field studies examined these processes in more detail (Akar & Jirka 1994; 1995). Although these works generally confirm negligible scales of intermediate-field effects for discharges into reasonable strong turbulent current fields, they clearly show their importance in either stagnant or shallow waters, where boundary interactions, large spreading processes and/or instabilities occur such as it could be the case of estuarine waters.

2.2.4.2 **Coupling approaches: Near- far-field transition**

Lately promising Computational Fluid Dynamic (CFD) models (FLUENT, Open-FOAM, Flow3D,...) might deal with all the mixing regions (Tang *et al.* 2008). However, even if the increasing computational speed and memory of modern computers is considered, they do not appear feasible for present-day engineering practice considering all mixing regions. Nonetheless, CFD models are helpful for the analysis of special cases, where either experiments are too difficult or too expensive and integral models do not apply. Examples are described in Law *et al.* (2002), García-Alba *et al.* (2009) and García-Alba *et al.* (2010).

Coupling models means introducing flow quantities (e.g. momentum or mass) from one model into the other and viceversa. There are only two possibilities for introducing flow quantities into a model, either over the boundary conditions or via source terms. The former may only be specified at model boundaries and have direct effect on the whole flow. The latter only modify the existing flow by adding quantities. Both concepts are schematized in figure 2.13.

The most appropriate way to overcome these issues of the transport processes is via the application of integrated models consisting of a near-field model and a far-field model that are connected via a coupling algorithm. Basically, there exist two main methods of coupling (Bleninger 2006):

- *Passive coupling* assumes that the source-induced flow, though considerably important for near-field mixing, does not change the flow characteristics of the far-field, beyond the near-field or intermediate-field region. Thus, specific values of the discharge are determined by the near-field model. Then, these are introduced at specific locations of the far-field model as values or source terms without any feedback of the far-field computations to the near-field model.

- *Active coupling.* If considerable large effluent flows have to be considered, the ambient flow will be strongly disturbed and modified by the discharge induced flows, causing changes in the flow and concentration fields even beyond the near-field and intermediate-field regions. A coupling of all flow quan-

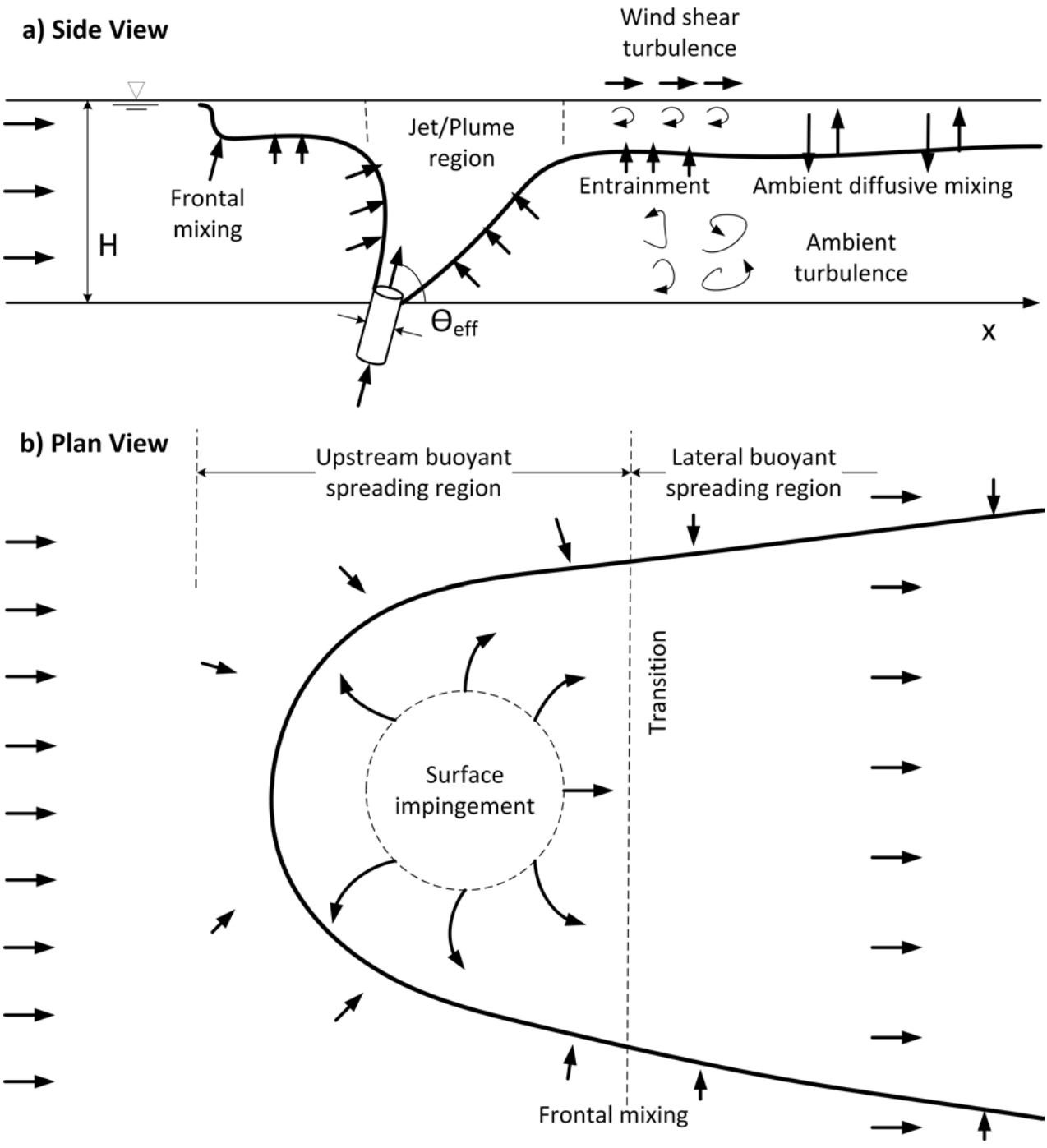

Figure 2.12: Buoyant spreading processes after near-field region (upstream and lateral spreading), superimposed on the transport by ambient currents. Adapted from Jirka & Akar (1991).

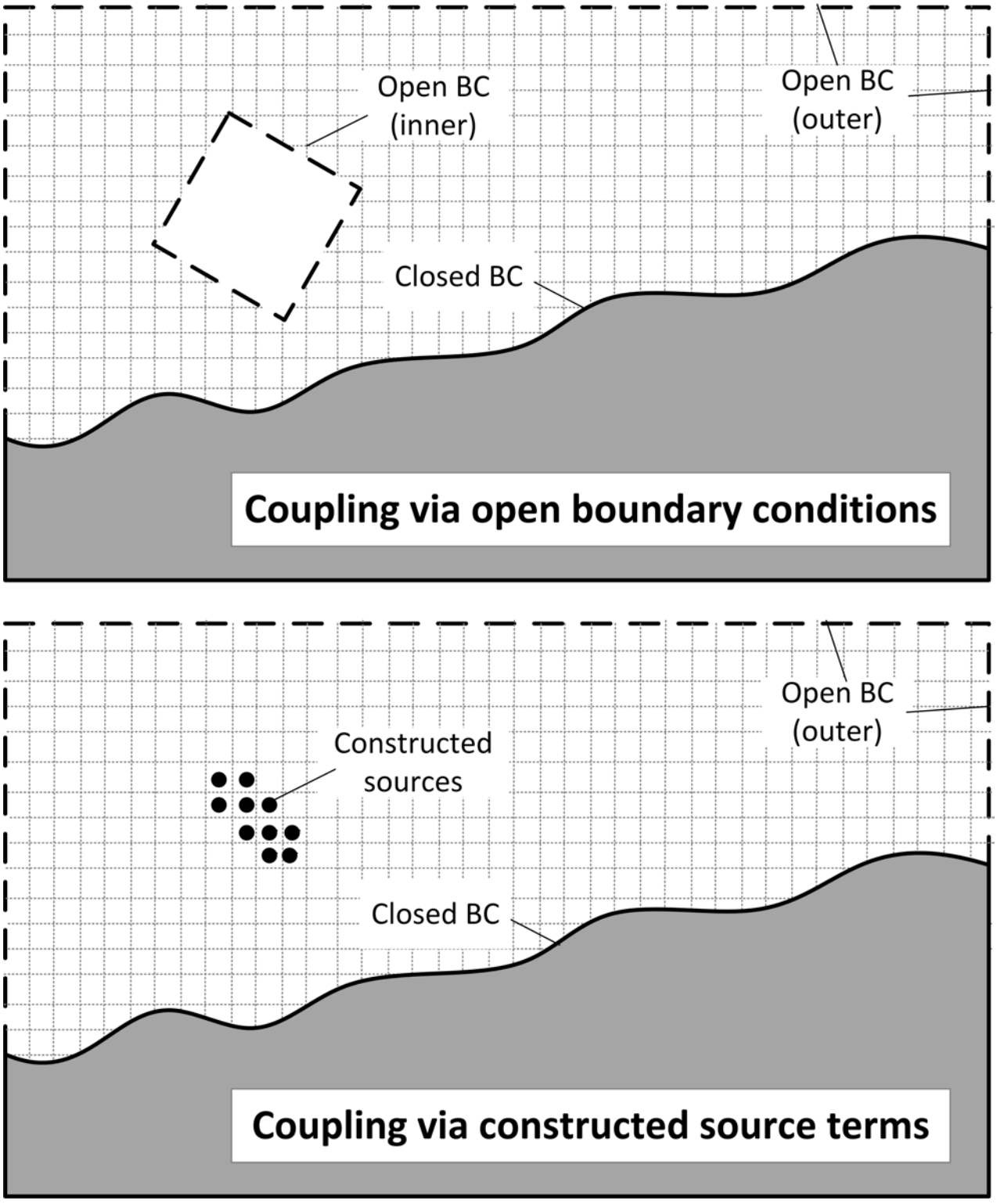

Figure 2.13: Schematization of coupling approaches for zone models, either using open boundary conditions or source definitions for the near-field representation in the far-field domain.

tities has to be accomplished. Momentum conservation principles have to be considered in addition to fluid and substance mass conservation for that linkage.

Regarding model execution, two approaches are possible (Bleninger 2006):

- A *static (offline)* linkage generates the output for one model for the entire time of interest. This output is then specified as boundary or source condition for the other model in a subsequent simulation. This is simple from the viewpoint of computation and data management but, obviously, there is a limited feedback between the two separate simulations.
- A *dynamic (online or realtime)* linkage exchanges data after every time-step, thus, both models run in parallel. A much higher degree of accuracy can be attained in this fashion. This coupling is only necessary if flow quantities from either region are dynamically important (active coupling).

The *"passive and static"* couplings are usually sufficient for relatively small discharges, whose near-field characteristics do not alter significantly the far-field characteristics. There are a significant number of researchers that apply this kind of coupled approaches.

Dimou & Adams (1993) developed a 3D finite element Eulerian-Lagrangian far field model and coupled it with a particle tracking model near the source using an initial dilution model for simulating passive toxicant transport and applied it to the Boston outfall.

Zhang & Adams (1999) employed the 3D far-field model ECOMsi and the near-field model RSB, suggesting four possible coupling techniques to introduce loadings to a far-field model using the trap height predicted by a near-field model:

1. Introduce the discharge flow rate and pollution load as source terms at the discharge point.
2. Introduce source flow at discharge point and release the pollution load at the trap height predicted by the near-field model.
3. Introduce both the diluted flow (including entrainment) and the pollution load at the predicted trap height.
4. Introduce the pollution load at the predicted trap height.

Suh (2001) linked the near-field model CORMIX3 to the 2D harmonic finite element hydrodynamic model TEA and the Eulerian–Lagrangian far-field transport model ELA. The near-field and the far-field models were coupled using the Gaussian puff algorithm incorporated into the far-field transport model. The integrated model was applied in Chonsu Bay (Korea) and calculations showed a very good agreement with field data.

Five years later, Suh (2006) presented a coupling approach based on a random walk particle tracking method near the source and a gradient-diffusion model in the far field. Their results strongly advocated the use of an Eulerian–Lagrangian approach (a random walk model in the near-field and a gradient-diffusion model in the far field).

Kim *et al.* (2002) coupled a jet integral near-field model with a particle tracking far-field model to simulate the mixing of a single buoyant jet discharge. Far-field was simulated by particles introduced at the equilibrium rise height or the end of the computed initial mixing zone.

Bleninger & Jirka (2004) proposed an algorithm to couple the near-field CORMIX model and the far-field Delft3D-WAQ model that is similar to method (3) of Zhang & Adams (1999), whereby the discharge flow rate and pollution load at the terminal height computed by CORMIX were introduced into the far-field model. Additionally, Delft3D-FLOW provided the hydrodynamic predictions.

On the other hand, discharges whose large flow rates may affect significantly the flow field in the far-field and vice versa requires an *"active and dynamic"* coupling that permits the interaction of the near-field and far-field. There are very few "active" integrated models published in the literature.

Choi & Lee (2007) presented the distributed entrainment sink approach (DESA), in which the near-field is modelled by the Lagrangian plume model JETLAG, while the far-field is simulated by the environmental fluid dynamics code (EFDC). In DESA, the coupling is achieved via the introduction of the discharge flow rate and pollution load derived by the near-field model as source terms in the continuity and scalar transport equations of the far-field model. With the computed flow and solute mass distributions in the far-field, the near-field plume model could then be driven by the updated ambient conditions to generate the new source and sink terms for the next time step.

Maderich *et al.* (2008) applied DESA combining the near-field model JETLAG with the far-field model THREETOX that was extended to account for the heat fluxes between water and atmosphere and between water and bottom sediments, for wetting and drying and for processes describing the effects of ship traffic on the dispersion of the discharged heat in stagnant canals.

Stamou & Nikiforakis (2013) presented an integrated model consisting of the near-field model CORJET and the far-field model FLOW-3DL, which are interconnected via an "active" coupling algorithm that is similar to DESA. The key difference between the proposed method and DESA is that the hydrodynamic and water quality information of the jet derived by the near-field model enter into the far-field model as actual velocities and concentrations, respectively, rather than flow rates and pollution loads of DESA. Thus, providing more information to the far-field including the orientation of the jet and the horizontal distribution of flow rates at the water surface.

2.2.5 Secondary or ambient dilution (Far-Field)

The far-field is defined as that region of the buoyant jet which is largely independent of the initial characteristics of the discharge. Therefore, far-field processes are mainly related to the description of natural estuarine flows that is why hydrodynamics is so important.

Once these processes are known, waste-field characteristics, as a result from the near-field region, are coupled with these flows either at the surface level or trapped within density stratification and transported and dispersed by ambient currents and turbulence.

2.2.5.1 Basics of far-field mixing

The existing turbulence in the ambient environment is the dominating mixing mechanism at sufficiently large distances from the discharge point. It is reasonable to always assume that the plume's motion in the ambient receiving water is turbulent. Spreading takes place much faster in turbulent flow than in laminar flow.

Far-field begins with gravitational collapse (also referred to as buoyant spreading). This is characterized by lateral spreading of the plume along the layer boundary while it is being advected by the ambient current. In general, the passively diffusing flow grows in width and in thickness until it interacts with the channel bottom and/or banks as illustrated in figure 2.14.

Following gravitational collapse, the remainder of far-field mixing is best explained by either the theory of turbulent diffusion or shear flow dispersion:

- *Turbulent diffusion* employs the turbulent mixing equation of Brooks (1960), wherein the coefficient describing the rate of spread of the plume increases with the size of the plume. The best known facet of

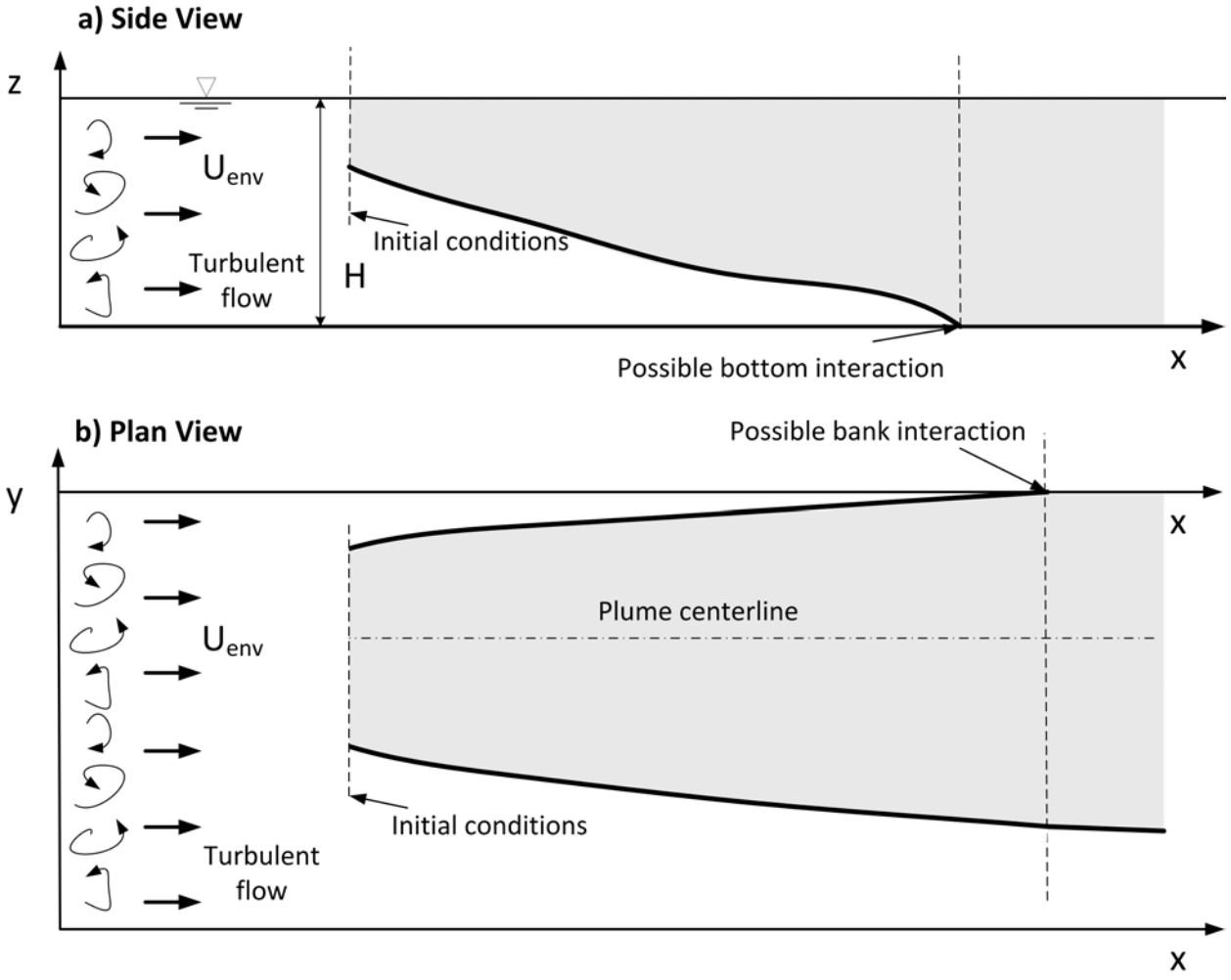

Figure 2.14: Passive ambient diffusion process with advection in the far-field. Adapted from Jirka *et al.* (1996).

this theory is the celebrated "4/3 Power Law", which says that the diffusion coefficient is proportional to the 4/3 power of the size of the plume. However, the Law only applies in homogeneous turbulence far from any boundaries.

- *Shear flow dispersion* employs the longitudinal dispersion equation of Taylor (1954) by the method of Fischer *et al.* (1979). The theory common to all shear flow is that spreading in the direction of flow is caused primarily by the velocity profile in the cross section. The mechanism Taylor analyzed is often referred to as the "shear effect". It gives a reasonably accurate estimate of the rate of longitudinal dispersion in rivers and a partial estimate of longitudinal dispersion in estuaries.

Finally, in tidal networks of complex topography and current structure, numerical transport models have to be employed in order to predict the far-field toxicant distribution under more general conditions regarding the estuarine circulation, mass transport and transformations. These models are based on the "advection-diffusion-reaction" equation or transport equation (see equation (2.23)).

$$\frac{\partial C}{\partial t} + u\frac{\partial C}{\partial x} - D_x\frac{\partial C^2}{\partial x^2} + v\frac{\partial C}{\partial y} - D_y\frac{\partial C^2}{\partial y^2} + w\frac{\partial C}{\partial z} - D_V\frac{\partial C^2}{\partial z^2} = SO + f_R(C,t) \tag{2.23}$$

where u, v and w are the flow velocity in every direction, D_x, D_y and D_V are the dispersion coefficients taken for every direction, SO are additional inflows of water or mass and f_R are the reaction terms or "processes".

The velocity field in these transport models may have to be calculated from a separate hydrodynamic model or generated by instrumental data.

Regarding the transport equation, there are two ways for concentration within the control volume to change over time (first term in left hand of the equation (2.23)):

- *Conservative behavior:* The net transport of concentration into or out of the control volume through the control volume faces due to advective (second, fourth and sixth terms of the left hand of the equation (2.23)), diffusive components (third, fifth and seventh terms of the left hand of the equation (2.23)) and/or external sources or sinks for concentration outside the control volume like wastewater discharges (first term of the right hand of the equation (2.23)).
- *Non-conservative behavior:* Internal sources or sinks for concentration within the control volume (i.e., "reactions"). The processes may be chemical such as decay or transformation to another chemical form (second term of the right hand of the equation (2.23)).

In the case of conservative behavior the advection, diffusion and turbulent mixing determine the fate and transport of toxic substances. A substance is assumed to be conservative when the rate of reaction is very low or zero.

When the non-conservative behavior becomes relevant, there are two additional key factors that determine the fate and transport of toxic substances: their reactivity and their mass-transfer processes. Next, we made a brief description of the most relevant additional processes governing the non-conservative behavior of toxic substances: sediment transport, equilibrium partitioning, mass-transfer processes and transformation processes (see figure 2.15).

Sediment transport

Sediment consists of particles of all sizes that are derived from rocks or biological materials. Sediment can either be suspended in a water column or settle and accumulate on the bottom of a waterbody. Sediment transport is simply the process of eroding sediment from one place, carrying it in the flow, and depositing it in another place. The four basic sediment processes are (Ji 2007):

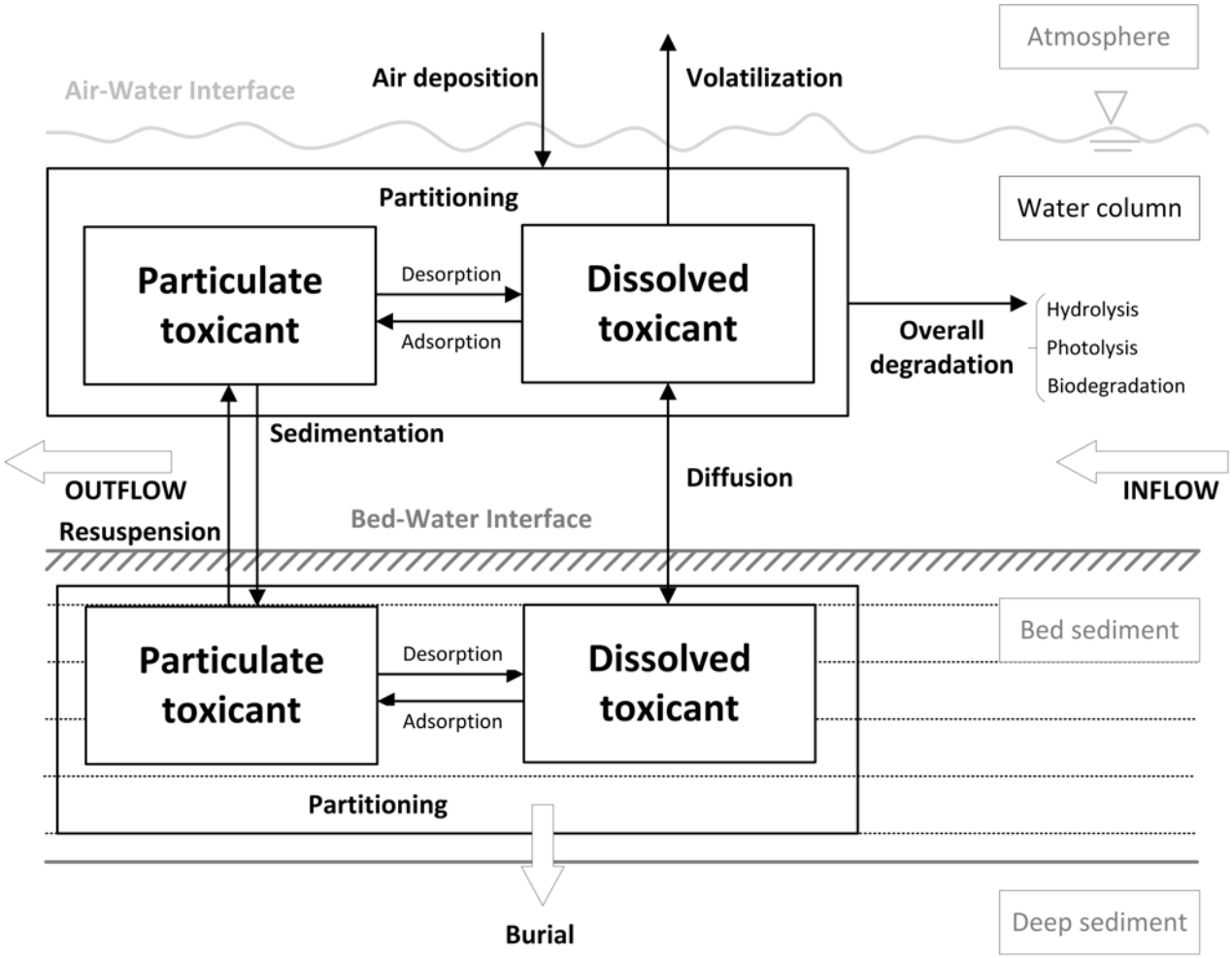

Figure 2.15: Fate and transport processes for a toxicant displaying a non-conservative behavior.

- *Resuspension of the sediment bed:* The terms "erosion" and "resuspension" are often used synonymously. Sediment resuspension is controlled primarily by bottom shear stress. Site-specific bed properties are also a primary factor in determining erosion rates and scour depths. Sediment on the bed will be eroded and transported when the bottom shear stress exceeds a critical value.

- *Transport of sediment in the forms of suspended load and bed load:* Sediment is moved as suspended load and/or bed load. Suspended load is the portion of the sediment load that is transported in suspension in the water column. The suspended load includes sediments resuspended from the bed and the wash load brought from upstream. Bed load is comprised of particles that move on or near the bed by saltation, rolling or sliding in the bed layer.

- *Settling of suspended sediment and deposition on the bed:* Settling velocity is the most fundamental property governing the motion of the sediment particles in water. It is defined as the terminal velocity at which a single particle falls through water. Settling velocity depends principally on the size, shape, and density of the particle and the viscosity and density of the water.

- *Consolidation and compaction of the sediment bed:* The rearrangement of the particles gives the bed increased shear strength and resistance to resuspension, primarily due to consolidation and armoring. Consolidation occurs over time and increases the cohesion between individual particles and flocs and their resistance to erosion. Armoring of the surface layer also increases with time.

Sediments from watersheds are carried into estuaries by rivers and runoffs and tend to accumulate there. As rivers approach the sea, their mouths broaden and currents slow down, reducing estuarine flushing and trapping sediment and toxicants. The high sediment concentration within this area provides a major site for physical, chemical, and biological reactions between dissolved and particulate materials. As a result, the area acts as a filter for removal of dissolved and suspended materials. In general, moderately stratified estuaries have the strongest estuarine circulation patterns and are the most effective filters trapping suspended materials. The trapping efficiency drops off quickly as freshwater flows increase (Fischer *et al.* 1979).

Equilibrium Partitioning

Non-conservative substances differ from conservative substances in that they are divided or "partitioned" into particulate and dissolved forms. The primary reason for solid-liquid partitioning is to produce a more mechanistically accurate characterization of the toxicant mass balance. In particular it is known that several key mechanisms act selectively on one or the other of the two forms (Chapra 1997).

When a small amount of a chemical is added to two immiscible phases and then shaken, the phases will eventually separate and the chemical will partition between the two phases according to its solubility in each phase. The concentration ratio at equilibrium is the partition coefficient (K_{12}):

$$\frac{C_1}{C_2} = K_{12} \tag{2.24}$$

In the laboratory, K_{12} is determined from the slope of C_1 versus C_2 over a range of concentrations. Partition coefficients can be measured for essentially any two-phase system. In water systems, the air–water, the octanol-water and the particle–water partitioning are the most important (Hodgson 2003).

- *Air–Water:* Air–water partition coefficients K_{aw} are essentially Henry's law constants (He):

$$K_{aw} = He = \frac{C_{air}}{C_{water}} \tag{2.25}$$

Chemicals with high Henry's law constants have a tendency to escape from water to air and typically have high vapor pressures, low aqueous solubilities, and low boiling points. Chemicals with low Henry's law constants tend to have high water solubility and/or very low vapor pressure.

- *Octanol-Water:* For many decades chemists have been measuring the octanol–water partition coefficient (K_{ow}) as a descriptor of hydrophobicity. Strong correlations exist between K_{ow} and many biochemical and toxicological properties. K_{ow} is generally expressed as $\log K_{ow}$ because K_{ow} values range from less than one (alcohols) to over one billion (larger alkanes and alkyl benzenes).

- *Particle-Water:* Many chemicals preferentially associate with soil and sediment particles rather than the aqueous phase. The particle–water partition coefficient (K_p) describing this phenomenon is displayed by equation (2.26).

$$K_p = \frac{C_p}{C_d} \tag{2.26}$$

  where C_p is the concentration of chemical in the soil or sediment (mg/kg) and C_d is the concentration in water (mg/l). In this form, K_p has units of l/kg or reciprocal density. Dimensionless partition coefficients are sometimes used where K_p is multiplied by the particle density (in kg/l). If the toxicant is a heavy metal, K_p depends on the metal properties.

  If the toxicant is an organic chemical, such as organic micropollutants, a plot of K_p versus the mass fraction of organic carbon in the soil (f_{OC}, g/g) is linear with a near-zero intercept yielding the simple relationship (Equation (2.27)).

$$K_p = f_{OC} K_{oc} \tag{2.27}$$

  where K_{oc} is the organic carbon–water partition coefficient (l/kg). Studies with many chemicals and many sediment/soil systems have demonstrated the utility of this equation when the fraction of organic carbon is about 0.5% or greater.

The dissolved phase is transported with water flows and the particulate phase is often attached to and transported with sediments (or particulate organic carbons). It is primarily the ones in the dissolved phase that cause harm to the environment. Compared with conventional pollutants, such as nitrogen and phosphorus, the toxic substances can be considered harmful at very low concentrations, such as in a few micrograms per milliliter (μg/l).

Mass-transfer processes

In the water column and the sediment bed, interchange between the dissolved and particulate toxicant occurs via sorption/desorption processes.

Sorption and Desorption

Sorption is the transfer of a substance from the aqueous to the solid phase. Desorption is the process by which substances are released from the particles back into water.

Sorption represents the interaction of a contaminant with a solid and can be further divided into adsorption and absorption. Adsorption is the process by which substances adhere to the surface of particles, while absorption is the process by which substances actually penetrate into the structure of the particles. Thus, sorption may be either absorption or adsorption, or a combination of the two.

Because of the preference for toxic substances to sorb to sediment, an accurate description of sediment concentration is important to the study of toxic substances. A change in the sediment mass balance will ultimately affect the overall toxic mass balance (Chapra 1997).

Sorption–desorption processes are usually fast relative to other environmental processes, such as the time

step of model integration or the time scales for decay. For this reason, the sorptive interaction between the dissolved and particulate components can be treated as instantaneous equilibrium.

Volatilization and Air deposition

Volatilization represents a chemical substance entering the atmosphere by evaporation from water. Volatilization is a reversible transfer, in which the dissolved concentration in water attempts to equilibrate with the gas phase concentration in the overlying atmosphere. Equilibrium occurs when the partial pressure exerted by the chemical in water equals to the partial pressure of the chemical in the atmosphere.

Henry's law states that, at a given temperature, the solubility of a gas is proportional to the pressure of the gas directly above the water. Volatilization is often treated similarly to surface oxygen exchange, where the volatilization flux is proportional to the difference between the chemical concentration in water and the saturation concentration, as:

$$F_{vol} = k_{vol}(C_d - C_{sd}) \tag{2.28}$$

where F_{vol} is the volatilization flux, k_{vol} is the transfer rate, C_d is the dissolved concentration of the chemical in water and C_{sd} is the saturation dissolved concentration of the chemical in water. Equation (2.28) indicates that the chemical enters the water (air deposition) when the chemical in the water is unsaturated ($C_d < C_{sd}$) and the chemical leaves the water (volatilization) when the chemical in the water is oversaturated ($C_d > C_{sd}$).

The saturation dissolved concentration is dependent on the atmospheric partial pressure and Henry's law constant for the chemical. The transfer rate (k_{vol}) depends on the properties of the chemical, as well as the characteristics of the waterbody and the atmosphere.

For many chemicals (with oxygen as a noticeable exception), the partial pressure in the atmosphere is negligible and the saturation dissolved concentration (C_{sd}) is much smaller than the dissolved concentration (C_d). In this case, equation (2.28) reduces to equation (2.29).

$$F_{vol} = f_{vol} k_{vol} C_d \tag{2.29}$$

where f_{vol} is a correction factor.

Transformation processes

The fate and decay of a toxicant represent the gradual decrease in the amount of a substance in an environmental system due to transformation processes. These processes are generally irreversible reactions that involve continuous exchange among chemical states.

If no degradation reactions occurred in Nature, every single contaminant discharged in the past would still be polluting the environment. Fortunately, natural purification processes dilute, transport, remove and degrade contaminants (Ji 2007).

This section summarizes the transformation processes and their mathematical formulations. For all these processes, the reaction kinetics can be described like a single reactant which is generally expressed as:

$$f_R(c,t) = \frac{dC}{dt} = -k_r C^{m_r} \tag{2.30}$$

where m_r is the order of reaction and k_r is the rate constant of the m_r-order reaction. In natural waters, the commonly used forms of equation 2.30 are with m_r=0 and 1.

- *Zero-Order Reactions:* A zero-order reaction (m_r=0) represents irreversible degradation of a reactant

that is independent of the reactant concentration. The solution to equation (2.30) is:

$$C = C_0 - k_r t \tag{2.31}$$

where C_0 is the initial concentration at t=0. In this case, a plot of concentration versus time should yield a straight line with a slope of k_r, as shown in the left panel of figure 2.16. Zero-order reactions have their reaction rates determined by some factor other than the concentration of the reacting materials. Hydrolysis products from anaerobic sediment is an example of zero-order reactions (Schnoor 1996).

- *First-Order Reactions:* First-order reactions (m_r=1) have their reaction rates proportional to the concentration of the reactant. For first-order reactions, the solution to equation (2.30) is:

$$C = C_0 e^{-k_r t} \tag{2.32}$$

Equation (2.32) indicates that for first-order reactions, reactant concentration decreases exponentially with time. In this case, a plot of logarithm concentration versus time should yield a straight line with a slope of k_r, as shown in the right panel of figure 2.16. Most of the reactions found in the environment can be conveniently expressed by a first-order approximation without much error. Examples of first-order reactions include biochemical oxygen demand in surface waters, death and respiration rates for bacteria and production reaction of algae (Thomann & Mueller 1987). Noted that, although most kinetic formulations are parameterized by first-order reactions, derivation of the reaction rate constant k_r might require a significant amount of data.

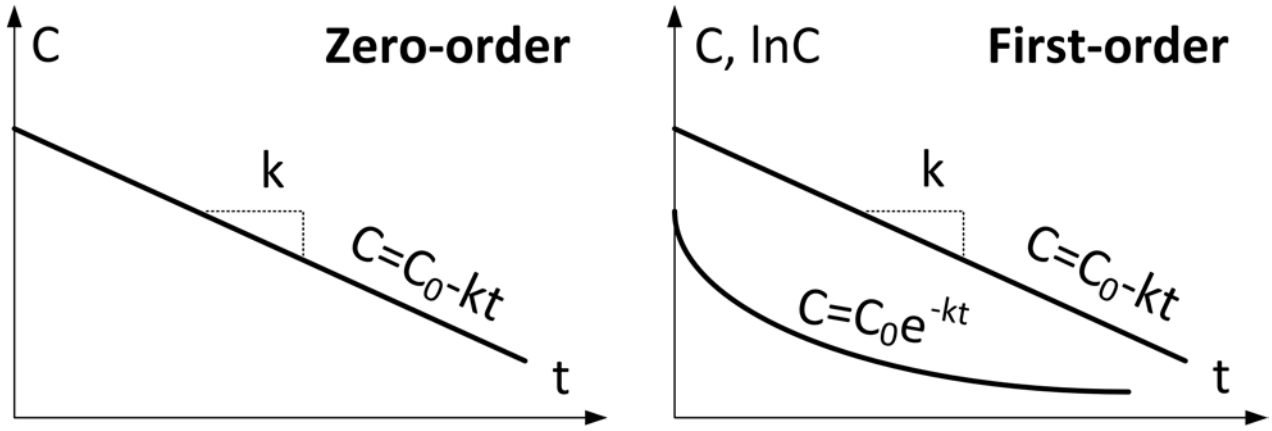

Figure 2.16: Concentration versus time for zero-order reaction (left panel). Concentration and logarithm concentration versus time for first-order reaction (right panel).

In the next paragraphs, a short description of transformation processes, determining the fate and transport of toxic substances in estuarine systems systems, is displayed.

Photolysis

Photolysis (photodegradation) is the transformation of a compound that results directly from the adsorption of light energy. Compounds that absorb sunlight may gain sufficient energy to initiate a chemical reaction. Some of these photochemical reactions result in the decomposition or transformation of a substance.

In this decay process, solar energy acts on certain chemical molecules in such a way as to alter the molecular structure. The chemical then degrades or is decomposed by this change in molecular structure (Delos *et al.* 1984, Mills *et al.* 1982).

The estimation of the rate of photolysis is through the approximate first-order reaction

$$\frac{dC_d}{dt} = -K_{pho}C_d \tag{2.33}$$

where K_{pho} is the overall photolysis rate (s^{-1}).

Hydrolysis

Hydrolysis is the reaction of a chemical with water, in which splitting of a molecular bond occurs in the chemical and there is a formation of a new bond with either the hydrogen (H^+) component or the hydroxyl (OH^-) component of a water molecule.

In general, hydrolysis depends on the molar concentrations of $[H^+]$ and $[OH^-]$, or water mediators. Since hydrolysis can also be mediated by enzymes (enzymatic hydrolysis), in natural waters hydrolysis may also be a biochemical degradation process (Chapra 1997).

Biodegradation

Biodegradation (biolysis) is the breakdown of a compound by enzyme-mediated transformation, primarily due to bacteria, and to a lesser extent, fungi. The presence of usually large numbers of such biological processors in natural waters usually means that the rates of biodegradation are one of the more important loss processes of chemicals in aquatic systems.

Even though the biodegradation process is largely mediated by bacteria, the growth kinetics of the bacteria is complicated and is not well understood. As a result, toxic models often assume constant decay rates rather than modeling the bacteria activity directly. The first-order decay rate is commonly used (Thomann & Mueller 1987).

$$\frac{dC_d}{dt} = -K_{bio}C_d \tag{2.34}$$

where K_{bio} is the biodegradation rate and C_d is the dissolved contaminant concentration.

In summary, to assess the effects of a toxic substance (toxicant), the mixing, transport and reaction of the toxicant in the environment should be determined, including the following:

- *Hydrodynamic processes*, such as advection and dispersion of the dissolved and particulate toxicants in the water column.
- *Sediment processes*, such as sediment transport in the water column, settling and resuspension of particulate toxicants due to sediment movement.
- *Mass-transfer processes*, such as the sorption and desorption of the particulate toxicants with the suspended sediment or the bed sediment and/or the volatilization and air deposition of toxicants with the atmosphere.
- *Transformation processes*, such as photolysis, hydrolysis and/or biodegradation.
- *External sources*, such as point sources from wastewaters of industrial plants and/or non-point sources from runoffs.

Therefore, an estuarine toxicant model should include at least the following (see figure 2.17):

1. A hydrodynamic and sediment model that provides the transport (advection and dispersion) and settling information.

2. Sorption–desorption interaction between dissolved and particulate toxicants in all the matrixes (air, water and sediment).
3. Transport, mixing and decay of the toxicants in the water column.
4. External loadings to the system.

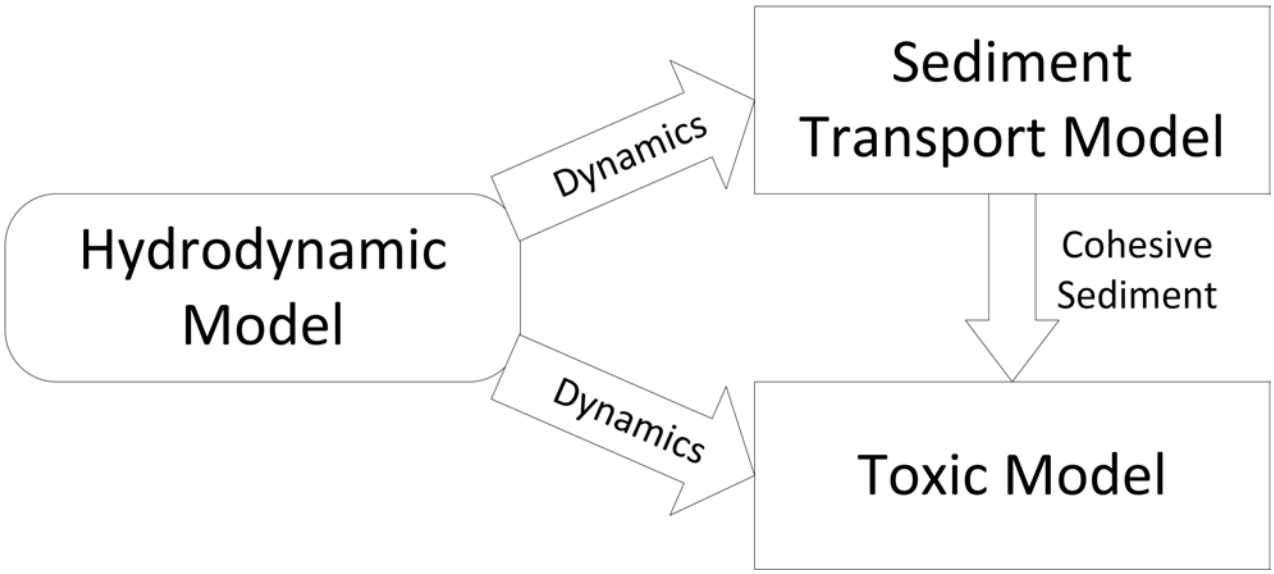

Figure 2.17: Structure of a typical estuarine toxic model. Adapted from: Ji *et al.* (2002).

2.2.5.2 Far-field available models

Water-quality modeling has evolved appreciably since its innovation in the early years of the twentieth century. As depicted in figure 2.18, this evolution can be broken into five major phases. These phases relate both to societal concerns and to computational capabilities that were available during each of the periods (Chapra 1997). The seminal work in the field was the model developed by Streeter & Phelps (1925).

In 1960s digital computers became widely available. This led to major advances in both the models and the ways in which they could be applied (Deininger 1965, Ravelle *et al.* 1967, Thomann & Sobel 1964).

During 1970s, societal awareness moved beyond dissolved oxygen and urban point sources to a more general concern for the environment. The principal water-quality problem addressed during this period was eutrophication (Canale & Vogel 1974, Chen 1970, DiToro 1969).

In 1980s and 1990s, the major modeling advance has been to recognize the prominent role of solid matter in the transport and fate of toxicants (Chapra & Reckhow 1983, O'Connor 1988, Thomann & DiToro 1983).

Finally, in 2000s, another shift is occurring in the development and application of water quality models due to:

- A strong and growing recognition that environmental protection is critical to the maintenance of a high quality of life.
- Developing countries around the world are beginning to recognize that environmental protection must be coupled with economic development.
- Computer hardware and software have undergone a new revolution. In particular, graphical user interfaces and decision support systems facilitate the generation and visualization of model outputs. Further,

1925-1960 (Streeter-Phelps)

Problems: untreated and primary effluent
Pollutants: BOD/DO
Systems: streams/estuaries (1D)
Kinetics: linear, feed-forward
Solutions: analytical

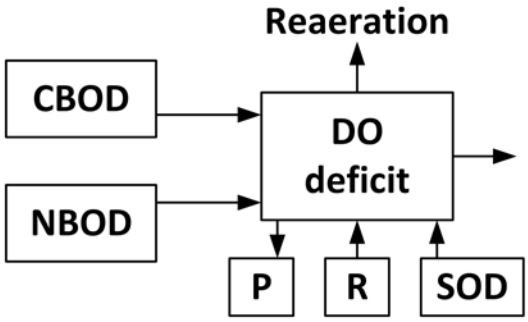

1960-1970 (computerization)

Problems: primary and secondary effluent
Pollutants: BOD/DO
Systems: streams/estuaries (2D)
Kinetics: linear, feed-forward
Solutions: analytical and numerical

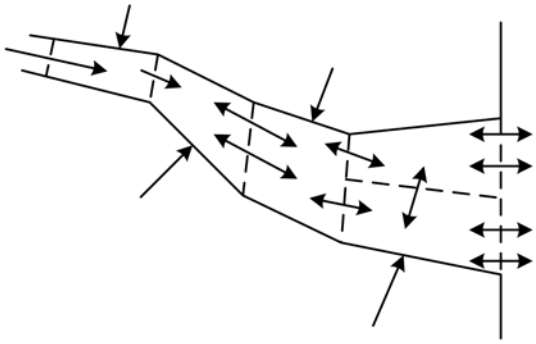

1970-1977 (biology)

Problems: eutrophication
Pollutants: nutrients
Systems: lakes/streams/estuaries (1D/2D/3D)
Kinetics: non-linear, feed-back
Solutions: numerical

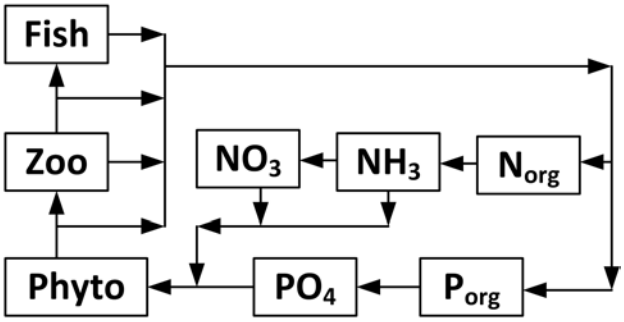

1977-2000 (toxics)

Problems: toxics
Pollutants: organics, metals
Systems: sediment-water interactions/ food-chain interactions (lakes/streams/estuaries)
Kinetics: linear, equilibrium
Solutions: numerical and analytical

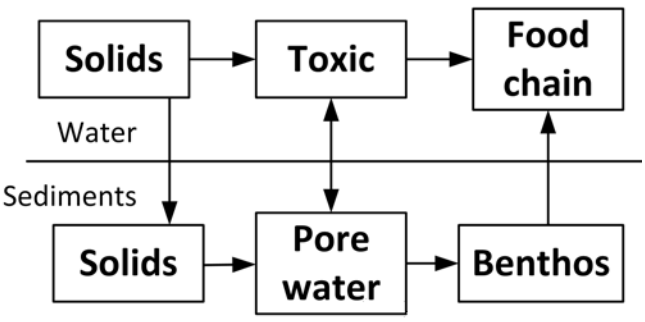

2000-present (integration)

Problems: all
Pollutants: BOD/DO/nutrients/sediments/organics/metals
Systems: all (lakes/streams/estuaries)
Kinetics: linear, non-linear, equilibrium
Solutions: numerical

Figure 2.18: Five periods in the development of water-quality modeling. Adapted from Chapra (1997).

clustering, parallelization and numerical methods are removing computational constraints that limited the scope of earlier models. Today two- and three-dimensional models with highly mechanistic kinetics can be simulated at reasonable cost.

- Mechanistic characterizations of sediment-water interactions and hydrodynamics have advanced to the point that they can be effectively integrated into water-quality-modeling frameworks.

Summarizing, in the past decades, significant progress has been made in numerical model development, data collection and computer software and hardware. These developments have helped mathematical models to become reliable tools for environmental management and engineering applications.

Toxic modeling often requires adjustment of the partition coefficient and the decay rate. For different toxicants, the values of these parameters vary significantly and are often temperature dependent. These parameters should be estimated, whenever possible, based on measured data taken from the site studied, since they are generally site specific and vary dramatically from toxicant to toxicant. In the event that measured data are not available for parameter estimation, values from literature reviews should be used as references. There are many publications on this topic, such as Thomann & Mueller (1987) and Chapra (1997).

There are a large number of water quality models that are in use today. In this review, only far-field models already coupled to the hydrodynamic models of subsection Hydrodynamics are cited:

- MIKE3 from Danish Hydraulics Institute (Jacobsen & Rasmussen 1997).
- IH-Dregde (H3D) from Universidad de Cantabria (García-Alba *et al.* 2014).
- MOHID from Technical University of Lisbon (Miranda *et al.* 2000).
- CAEDYM (ELCOM) - Estuary, Lake and Coastal Ocean Model from University of Western Australia (Hipsey *et al.* 2007).
- D-Water Quality from Delft Hydraulics, Deltares and HR Wallingford (Deltares 2014c).
- FVCOM - Finite Volume Coastal Ocean Model from Massachusetts Institute of Technology (Chen *et al.* 2003).
- WASP7 (EFCD) - Water Quality Analysis Simulation Program from USEPA (Ambrose & Wool 1988, Ambrose *et al.* 1988, DiToro *et al.* 1983).

The models are either finite element, finite difference, or finite volume, of which finite volume is the most common because preserves the mass. Although the basics of the models are similar, there are considerable differences in numerics and parameterizations. Some commonly used water quality models are listed in Table 2.3, indicating its characteristics.

Among this models, MOHID, D-Water Quality and WASP7 are integrated water-quality-modeling frameworks and open source for academic, research or business. These characteristics motivated that they become three-dimensional water quality tools most widely used today.

2.2.6 Numerical methods

All the equations listed on the hydrodynamic and far-field models cannot be solved analytically. Numerical solution methods divide the problem scales (temporal and spatial) into discrete elements, thus reducing the

Name	Discreti-zation/	Modelled Substances	Comments
MIKE3	FVM	CTR,ST,EC, CP,OMP,HM	non-OS, GUI,PPT,WD
IHDregde (H3D)	FDM	CTR,ST,PA, OMP,HM	OS(A,R)
MOHID	FVM	CTR,ST,EC, CP,HM,PA	OS(A,R,B), GUI,PPT,WD
CAEDYM (ELCOM)	FDM	CTR,ST,EC, CP,PA	non-OS, GUI,PPT,WD
D-Water Quality	FVM	CTR,ST,EC,PA, CP,OMP,HM	OS(A,R,B), GUI,PPT,WD
FVCOM	FVM	CTR,ST,PA, EC,CP	OS(A,R), PPT,WD
WASP7 (EFDC)	FDM	CTR,ST,PA,EC CP,OMP,HM	OS(A,R,B), PPT,WD

Table 2.3: Examples of water quality models

A = Academic Use	OMP = Organic Micro-Toxicants
B = Business Use	HM = Heavy Metals
CP = Conventional Toxicant	OS = Open Source
CTR = Conservative tracer	PA = Pathogens
EC = Ecology Model	PPT = Pre and Post-processing Tools
FEM = Finite Element Method	R = Research Use
FDM = Finite Difference Method	ST = Sediment Transport
FVM = Finite Volume Method	WD = Well Documented
GUI = Graphical User Interface	

differential equations to algebraic equations, which can be solved. Unfortunately, discretization for a numerical model creates truncation errors whose detailed form and behavior differ from one coordinate system to another (Bleninger 2006).

Although all codes are based on general fluid mechanical principles, they are generally not applicable for all problems. The correct model choice or correct choice of the numerical scheme in a modeling system is a major task for applications. Model results and unfortunately computational efforts generally vary considerably if different schemes are used.

2.2.6.1 Spatial discretization methods

Spatial discretization consist on the definition of each node of the model grid in the horizontal and vertical direction and the generation of a bathymetry, i.e., the determination of depths at each node of the model grid according to the available data of the study area.

Finite Differences

Differential equations are discretized over the numerical grid, built up from a series of nodes, and derivatives become difference equations that are functions of the values around surrounding nodes. This method is the easiest to implement and so far the most widely used method.

In the horizontal direction, two coordinate systems are typically used: cartesian coordinates (x, y) and curvilinear coordinates (ξ, η) as illustrated in figure 2.19.

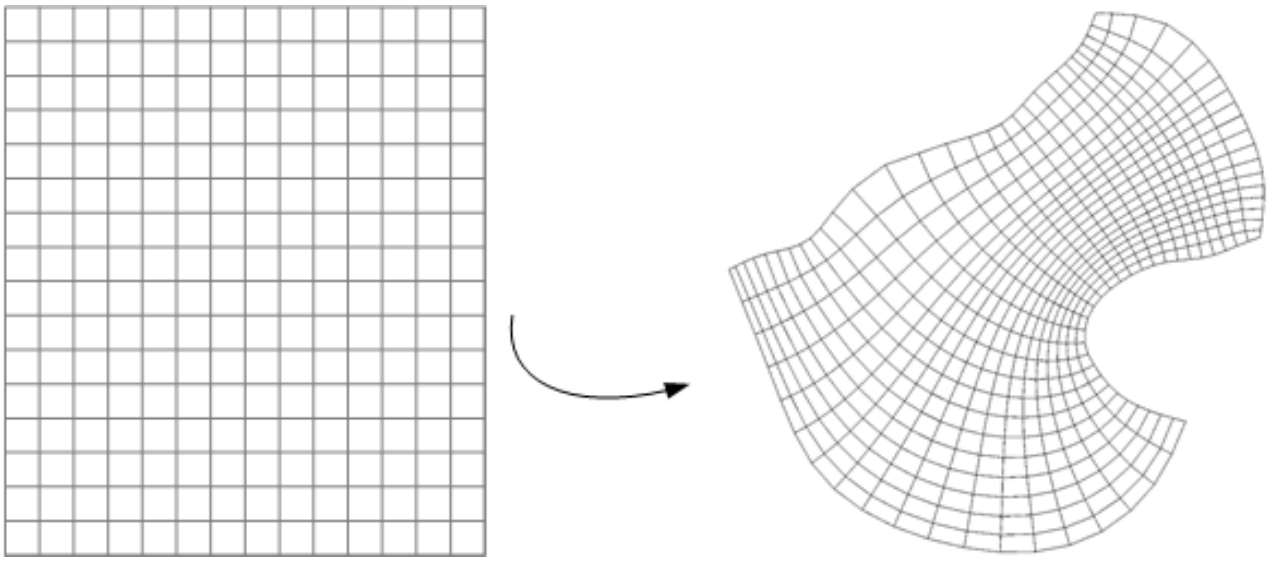

Figure 2.19: Example of mesh grids with rectangular and curvilinear coordinates.

In the vertical direction, two sets of different mesh discretization can be used: σ-coordinate system (σ-model) and Z-cartesian-coordinate system (Z-model) as shown in Figure 2.20.

The σ mesh was introduced by Phillips (1957) for atmospheric models, consisting of a group of layers contained by two σ levels. Since σ mesh grid is a boundary between the bottom and the free surface in motion, a smooth representation of the topography is obtained. The number of σ-layers in the model domain is constant regardless of the local depth of the water. The distribution of the relative thickness of each layer is not uniform. This allows higher resolution in areas of interest near the surface (important in stratified flows) and near the bottom (sediment transport).

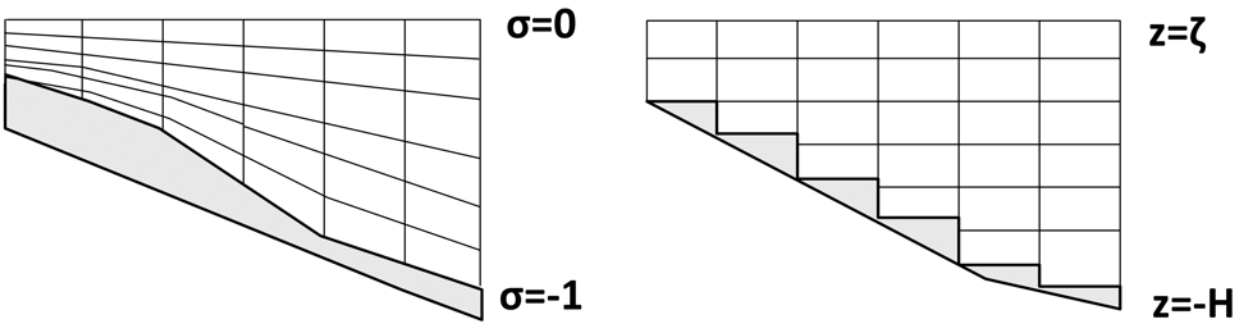

Figure 2.20: Example of mesh grids with σ and Z-cartesian coordinates.

The σ-coordinate system is defined in equation (2.35):

$$\sigma = \frac{z - \zeta}{d + \zeta} \tag{2.35}$$

where z is the vertical coordinate in the physical space, ζ is the elevation of the free surface on the reference plane (z = 0), d is the depth below the reference plane, and H is the total depth ($H = d + \zeta$).

Finite Volumes

Finite volumes are a generalization of finite-differences and built up from a group of grid cells. Thus, the same discretization and mesh grids are used. Fluxes through cells are tracked and the differential equations are integrated over the grid cell volume. Grid cells can be of different shapes and unstructured orientation and therefore apply to complex geometries, similar to finite element methods.

Finite Elements

This method is based on a group of elements comprised of two or more grid points (Figure 2.21). Basis functions are chosen to describe the variation of an unknown over the element and coefficients of the basis functions are found by substituting the basis functions as solutions into the governing equations. Unstructured finite elements give better simulation of complex geometries.

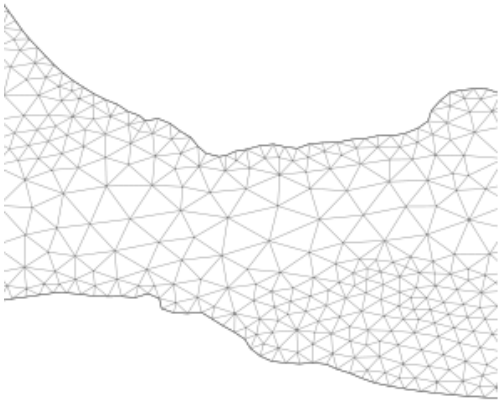

Figure 2.21: Example of mesh grid with finite elements.

However mass conservation may be limited, because these equations are not solved themselves, but rather a weighted residual version. This may not be an issue in ocean circulation applications, such as water temperature predictions, but could be important in the simulation of toxicants, such as heavy metals or organic

micropollutants. In addition, computational time for finite element models may be longer, due to high-order interpolation schemes (Bleninger 2006).

2.2.6.2 Temporal discretization methods

Explicit schemes

These schemes are easiest to solve because the unknowns are written as functions of known quantities. However, stability problems arise once the pathway of a fluid particle over one time step Δt is larger than the grid resolution Δx defined as the Courant-Fiedrichs-Lewy criterion (Courant *et al.* 1928):

$$CFL = \frac{u\Delta t}{\Delta x} \leq 1 \tag{2.36}$$

Additionally, in transport models, stability problems may give rise to non-physical spurious oscillations in the solution in the vertical direction. Therefore, the Peclet criterion must be also fulfilled.

$$Pe = \frac{u\Delta x}{D} \leq 2 \tag{2.37}$$

These rather strong restrictions have the consequence that either high resolutions are needed or models have to be tuned to overcome stability problems.

Implicit schemes

Implicit schemes are computationally more demanding, because equations for the unknowns are functions of other unknown quantities. These equations must be solved using matrix algebra. Implicit schemes are generally considered more accurate and do not demand a time step limitation as explicit schemes. Generally, time steps in this scheme are one order higher than implicit schemes.

2.2.6.3 Simplifications regarding boundaries

Regardless of their simplifications and numerical methods, the solution of the governing equations on any hydrodynamic or transport model requires the definition of boundary and initial conditions at all boundaries (open and closed).

Open boundaries

The world oceans, coastal waters and estuaries are all connected and, in theory, behave as parts of one system. However, it is often unpractical (and unnecessary) to simulate the entire system when dealing with a localized estuary. A common practice is to enclose the region of interest with an artificial boundary and to conduct modeling studies within this limited domain. When a limited domain is established, conditions for the sides of the domain not bounded by land need to be specified, namely open boundaries (OBs).

To minimize the impact of errors originating from the OB, the general rule is that the farther away the OB is from the area of interest, the less the OB errors will affect the model results. In designing the model domain, therefore, the open boundaries should be delineated at a sufficient distance away from the interior, so that the OB errors do not influence the solution within the interior domain.

Since there are no general laws to prescribe OBs, extrapolation, approximation, and/or assumption must be used in order to obtain boundary conditions. A variety of OBs have been proposed in the literature (Palma & Matano 1998; 2000). Examples of the boundary conditions are:

1. *Radiation Boundary Conditions:* The most widely used OB are derived from the radiation equation of Sommerfeld (1949), which provides a simple and stable extrapolation of the interior solution. The Sommerfeld radiation condition suggests that the interior disturbances approaching the boundary should propagate through it in a wave-like way.

2. *Clamped (or Specified) Boundary Conditions:* OBs can be clamped (or specified) in a number of ways. Time series of observed data can be used. The boundaries can also be set to constants, climatological values, or be interpolated from monthly mean values.

3. *Sponge Boundary Conditions:* The idea is to absorb outward propagating waves and disturbances so that they cannot reflect back into the model domain. In a numerical model, an additional set of grid points is used outside the area of interest to implement the sponge boundary condition.

4. *Nested Grids:* Values at the grid points from a model with a much larger domain are used as OBs in the smaller nested model.

Closed boundaries

Closed boundaries (CBs) are defined by the known shoreline where the flow through the boundary is set to zero for water, sediments and toxicants. The vertical diffusive flux of water through the free surface and bed is set to zero. For toxicants, the vertical diffusive flux through the free surface and bed is set with the specific processes acting on them, i.e. volatilization and sedimentation. In the case of suspended solids, the volatilization rate is zero so sedimentation is the only process acting on them.

Shear stresses act on all CBs. However, for the far-field region often only the bed shear is important, whereas the influence of the lateral shear stresses along the lateral boundaries may be neglected. Latter approximation applies generally for shallow flows, where a so-called free slip boundary condition is set at all lateral boundaries.

Common wall functions relate the bed shear stress to the current just above the bed and universal velocity distributions at the wall are used (i.e. the Newton-Taylor approach):

$$\tau_b = \rho_{env} r \overline{u} |\overline{u}| \tag{2.38}$$

where r is a dimensionless roughness coefficient.

Regarding wind-shear at the free surface a formulation analogous to bed-shear is

$$\tau_w = \rho_{air} W_{drag} \overline{W_{10}} |\overline{W_{10}}| \tag{2.39}$$

where W_{10} is the wind velocity in 10 meters height above the surface, ρ_{air} is the density of air, W_{drag} is the wind drag coefficient.

Initial conditions

The initial conditions (ICs) are starting values of the parameters of the shallow water equations (2.9) and (2.10) and/or the transport equation (2.23) which are used in calculating numerical solutions. Therefore, ICs are a prescription of the state of a dynamical system at some specified time. In many contexts, ICs are considered as boundary conditions in the dimension of time.

2.3 Methodological approaches to allocate mixing zones

Environmental protection has, for at least the last 50 years, been a major concern in the civilized nations of the world. As stewards of our environment, we are responsible for the protection of the environment, for our own sakes and for the benefit of generations to follow. It is accepted that humankind cannot continue to advance technologically while ignoring the environmental deterioration that occurs when we irresponsibly discharge the waste from our technology. Indeed, the sustainable growth of our civilization requires, as the only reasonable and feasible way to coexist on our planet with nature, that we protect our fragile environment (Alley 2007).

Much of the legislation promulgated to provide environmental protection has the purpose of not only non-deterioration of present environmental conditions, but the improvement of these conditions so that past abuse is corrected (AUS 2008, CCME 1999, EC 2000; 2008a;b, EU 2013, USA 1972; 1977; 1985).

Fetterolf (1973) discussed several concepts of the mixing zone (MZ) and considers that there is no uniform approach to the designation of zones to accommodate liquid waste discharges into an aquatic receiving system without interference with other beneficial uses. This leads to confusion and indecision among dischargers and enforcement agencies, and universally adaptable guidelines would initiate understanding and progress. Finally, he concluded that a case-by-case approach is essential to wise use of natural resources, because each mixing zone should be tailored to the physical, chemical, and biological characteristics of the ecosystem and its particular community of organisms.

In this section, a review of the regulations and the proposed methodologies to allocate MZs in different areas around the globe such as USA, Canada, Australia or Europe is displayed.

2.3.1 United States of America

The Clean Water Act (CWA) is the primary federal law in the United States governing water pollution (USA 1972). It established the goals of eliminating releases of high amounts of toxic substances into water, ensuring that surface waters would meet standards necessary for human sports and recreation by 1983, and eliminating additional water pollution by 1985. The principal body of law in effect is based on the Federal Water Pollution Control Amendments of 1972 which was a significant expansion of the Federal Water Pollution Control Act of 1948 (USA 1948). Major amendments were enacted in the Clean Water Act of 1977 (USA 1977) and the Water Quality Act of 1987 (USA 1985).

In USA, wastewater discharges to surface water are regulated through the National Toxicant Discharge Elimination System (NPDES) permit program. NPDES permits are issued and enforced either by the U.S. Environmental Protection Agency (EPA) or by state agencies under authority delegated by EPA. NPDES permits generally include technology-based effluent limitations and more stringent limits are applied on a case-by-case basis if necessary to protect receiving water quality.

Water-quality-based NPDES permit limits are set so that the fully diluted effluent will not exceed ambient water quality criteria. However, EPA and many states recognize that a receiving water can be protected without requiring an effluent to meet water quality criteria at the point of discharge. Water-quality-based permits often include MZ allowances to account for the dilution that takes place around an outfall. A MZ may be established by computing a dilution factor or it may be delineated as a spatial area with fixed boundaries.

Two numerical values are specified by EPA in the aquatic life criterion for each toxicant. The acute criterion maximum concentration (CMC) is a value which cannot be exceeded in ambient waters for a 1-hour averaging period more than once every 3 years. The criterion continuous concentration (CCC), or the chronic toxicity criterion, represents a 4-day average concentration which may not be exceeded more than once every 3 years.

Two types of MZs may be established, corresponding to the two-number aquatic life criteria (CMC and CCC). This concept is illustrated in figure 2.22. In the zone immediately surrounding the outfall, neither the CMC nor the CCC is met. The CMC must be met at the edge of this first MZ and throughout the next MZ. The CCC is met at the edge of the second, or "chronic," MZ.

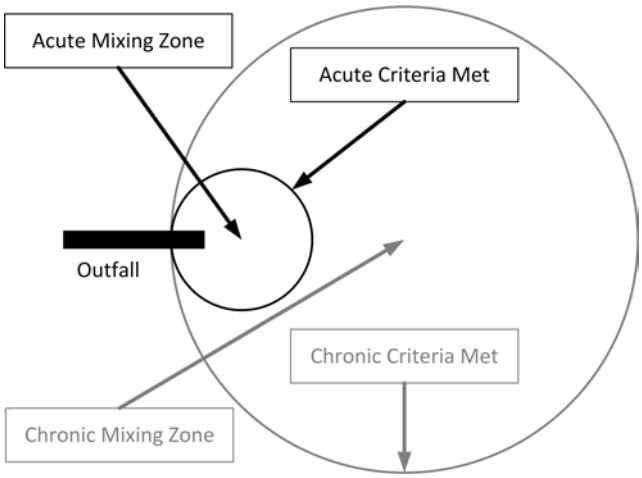

Figure 2.22: Diagram of the Two Parts of the Mixing Zone in USA.

2.3.1.1 Technical and Policy Guidance Documents

EPA has established its position on the role of MZs with a series of guidance and policy documents issued over the last 25 years. Underlying the EPA guidance and policy documents is the assumption that, for purposes of effluent mixing and dilution, it may be appropriate to allow ambient toxicant concentrations to exceed water quality criteria in small areas near a discharge. State regulatory agencies can decide to allow or deny a MZ on a site-specific basis. For a MZ to be permitted, the burden is on the discharger to show that state water quality standards are satisfied, including any MZ requirements (USEPA 1991).

A brief overview of the technical and policy guidance documents is included:

1. *Technical Support Document for Water Quality-based Toxics Control* (USEPA 1991). The TSD document provides guidance to States and EPA Regions for the water quality-based control of toxicants. It includes recommendations for controlling point source discharges of toxicants. The TSD recommends that MZs be designed to avoid lethality to aquatic organisms and to ensure that the designated use of the waterbody as a whole is protected. The TSD also recommends that states have a definitive statement in their standards on whether or not MZs are allowed and describe the procedures for defining MZs consistent with CWA goals.

2. *Water Quality Standards Handbook: Second Edition* (USEPA 1994). The handbook's overview of the water quality standards program provides a brief discussion of MZs, including: How states have the discretion to use MZs in their water quality standards, subject to EPA approval. How state water quality standards describe methods for determining location, size, shape, and other factors of MZs. How states should give careful consideration to the appropriateness of a MZ depending on the toxicants in the discharge.

3. *Allocated Impact Zones for Areas of Non-Compliance* (USEPA 1995). The AIZ document presents an impact allocation procedure. This procedure is an attempt to assess cumulative impacts and addresses the potential limitations of state water quality standards MZ policies. The procedure described in the AIZ document can be used to determine the environmentally acceptable size of MZs.

4. *Technical Guidance Manual for Performing Waste Load Allocations, Book III: Estuaries* (USEPA 1992). First, the book provides technical information and policy guidance for preparing estuarine waste load allocations. Second, it provides a guide to monitoring and model calibration and testing. Next, it describes the initial mixing of wastewater in estuarine and coastal environments and MZ requirements. Finally, it summarizes several historical case studies, with critical review by experts.

5. *U.S. EPA NPDES Permit Writer's Manual* (USEPA 1996; 2010). The manual provides guidance for writing and issuing legally defensible and enforceable NPDES permits to dischargers, including technical and legal issues that should be considered in permitting decisions. The document outlines the minimum requirements that all state and regional NPDES permit programs share. If a MZ is being considered, permit writers consider site-specific characteristics of a given discharge in addition to the condition of the receiving water to determine the dilution that will occur from the point source and to determine the impact that a discharge will have on the receiving water.

2.3.1.2 State-Specific Methodology

States may, at their discretion, include in their state water quality standards their own methodology to allocate MZ after EPA review and approval.

As a consequence, MZ implementation differs widely across the United States. Some states have very prescriptive policies and procedures for establishing MZs and calculating dilution factors. Others allow substantial flexibility, offering dischargers an opportunity for technical input and negotiation. States fall into two categories with regard to the overall process of establishing MZs (API 1998):

1. A state sets the dimensions of the MZ and calculates dilution factors for the discharger. In most cases, a discharger not satisfied with the results of the dilution estimate may conduct a more thorough MZ study and submit the results to the state for consideration. States that fit this general description include California, Illinois, Indiana, Louisiana, Minnesota, New Jersey, Oklahoma, Pennsylvania and Utah.

2. A state requires the discharger to submit a MZ study which establishes the dilution factor. These states typically describe the spatial extent of the MZ in the NPDES permit. The burden of gathering any additional information required for the study is on the discharger. Through a special review group, the state will consider the study submitted by the discharger and either accept the results or return comments. States included in this category are Alaska, Florida, Ohio, Texas, and Washington.

It is significant to mention that in tidal water bodies and estuaries the spatial definitions of MZ are not established in all States. Examples include establishing boundaries for the MZ based on distance from the point discharge such as Louisiana (<100 ft), New Jersey (<100 m), Texas (<200ft) or Washington (<300 ft+depth downstream and <100 ft upstream) or allowing mixing within a fraction of the receiving water area such as Alaska (<10% surface area).

Next, a review of the methodologies implemented to allow MZs is displayed in some states which have estuarine waters: Alaska, California, Florida, Louisiana, New Jersey, Texas and Washington.

Alaska (DEC 2006)

EPA has not delegated Alaska the authority to administer NPDES permits. All major NPDES permits in Alaska have MZs. State law requires that the MZs be as small as practicable, meaning that they are not an arbitrary size, as in some states. Instead, they are determined by performing an analysis to find the smallest MZ that allows the discharger to meet ambient water quality criteria as long as no historical maximum effluent concentration is exceeded.

Reviewers will generally accept any MZ model that is widely used, including the EPA-supported CORMIX and PLUMES. Under some complicated circumstances, field testing is required to calibrate the model. Detail required in the MZ submittal is a function of site-specific complexity.

Sediments and benthic organisms are considered in NPDES permitting by requiring a risk analysis which addresses bioaccumulation. In some cases, this may be the controlling parameter for a MZ allowance. Not all permits require a risk analysis, but it is being more frequently required, especially if there is any likelihood of sediment impacts. MZs are not automatically given to dischargers in Alaska.

California (Commins *et al.* 2010, SWRCB 2000)

California has been delegated authority by EPA to administer the NPDES permit program. Permits are issued and enforced by nine Regional Water Quality Control Boards (RWQCBs), each of which reports to the State Water Resources Control Board (SWRCB).

Statewide, California only allows MZs and dilution factors for ocean and estuarine discharges. Water-quality-based effluent limits for dischargers to inland waters, enclosed bays, and estuaries are determined regionally using whatever dilution factors may be provided in the nine separate Basin Plans adopted by the various RWQCBs. For example, the Basin Plan for San Francisco Bay allows permittees with discharges to deep water an arbitrary 10:1 dilution factor for both acute and chronic water-quality-based effluent limits. Background water quality is also taken into consideration and may limit the dilution credit.

For estuarine discharges, the request to calculate a dilution factor usually comes from a RWQCB at the time of NPDES permit renewal. Dilution estimates are made by SWRCB staff using the PLUMES model and input data provided by the permittee. The selected dilution factor will correspond to the lowest average near-field dilution within any single month of the year. Therefore, the MZ is bounded by the point at which the plume either surfaces or far-field processes dominate mixing. Dilution provided by the ambient currents cannot be considered in sizing a MZ.

Dischargers are required to characterize the point discharge and the area of the MZ in order to provide input to PLUMES. This involves surveying the discharge location to determine its depth with respect to the mean lower low water tidal elevation and sampling the receiving water at several depths to determine its density profile. Other information required of the discharger includes average and peak wastewater flow rates. Background water quality data are usually not requested from the discharger.

Once the dilution factor is finalized, it is used to calculate revised NPDES permit limits. The discharger may submit an independent estimate of available dilution for consideration by the RWQCB, but the state will generally rely on its own modeling analysis.

Florida (API 1998)

The Florida Department of Environmental Protection (DEP) is delegated NPDES permitting authority and has the responsibility of establishing all MZs. MZ requests are evaluated based on the ability of the applicant to provide DEP with reasonable assurance that conditions are met. The rule is supplemented with written policies to establish flow conditions for determination of available dilution. Typically, only dischargers greater than 3785 m^3 (1 million gallons) per day are required to perform MZ studies.

For new discharges, the state usually negotiates a technology-based permit through the first round or until the effluent is better characterized. A water-quality-based permit can be negotiated after discharge data have been collected. Most dischargers in Florida now have water-quality-based permits.

Simple desktop calculations could be acceptable if the applicant can demonstrate compliance with DEP rules. Under such conditions, the review could be completed by the permit writer within hours. In more complex situations involving multiple parameters, dischargers, or complex hydrodynamic conditions, DEP could re-

quire that a formal plan of study be developed and implemented using more sophisticated computer modeling techniques. Such complex studies could take months to review.

DEP accepts a variety of MZ models. The model selected for a particular case is controlled by site-specific issues and complexity. Models typically used include CORMIX and PLUMES. Proprietary models, even if based on other approved models, require peer review and documentation prior to state acceptance.

Receiving water characteristics play an important role in determining the degree of information required to establish MZs. If circumstances warrant, DEP can require the applicant to provide reasonable assurances that the discharge is not affecting benthic organisms, sediments, or otherwise contributing to violations of state surface water quality criteria. For all industrial wastewater dischargers, the burden of providing reasonable assurance is on the applicant. This evidence is based on existing data, data collected by the discharger, or state approved assumptions regarding toxicant fate and transport.

For tidally influenced bodies, the discharger must collect 2 weeks of velocity data over a neap tide cycle. The lowest 10^{th} percentile velocity is used in the dilution model.

Louisiana (LDEQ 2010)

The Louisiana Department of Environmental Quality (LDEQ) administers all NPDES permits in the state. The permit writer estimates dilution assuming complete mixing between the effluent and the receiving environment. Any further modeling of special conditions is done in a LDEQ modeling group. MZ studies submitted by dischargers are reviewed by this special modeling group.

In Louisiana, all dischargers begin with a technology-based permit. When a water-quality-based permit is in development, the state will compare effluent characteristics to water quality criteria. The initial estimate is based on a complete-mix dilution calculation using a percentage of the 7Q10, which can range from 3.3 percent to 100 percent depending on the receiving water conditions and whether acute or chronic conditions are being analyzed. After calculating dilution, the resulting ambient concentration is compared to water quality criteria following the guidelines of the Implementation Plan.

Louisiana only allows the jet momentum equation and CORMIX for dilution calculations. The jet momentum equation can only be used if the discharge centerline velocity is greater than 0.5 ft/s, the jet diameter is less than the receiving water depth, the discharge is neither strongly positively nor negatively buoyant, and there is no boundary interaction.

New Jersey (Hansler & Fikslin 1995, Hansler *et al.* 1998)

New Jersey has adopted USEPA (1991) guidance for evaluating MZs. A different process is followed in the development of MZs for existing and new dischargers. Some treatment plant expansions may be viewed as new discharges if significant flow increases result.

Existing dischargers going from a technology-based to a water-quality-based NPDES permit may elect to take default values for acute (10:1) and chronic (20:1) dilution factors. Alternatively, the discharger may perform a complete-mix dilution estimate using 1Q10 for acute and 7Q10 for chronic critical design flows. Typically, a 1-month review time is required for a complete mix dilution estimate.

New dischargers will be required to do instream studies for background water quality and flow (if necessary). Simple calculations will be used to develop water-quality-based limits. In lieu of calculations, a MZ study can be done to show better dilution.

New Jersey has settled on CORMIX for estimating dilution in complex situations. There is some PLUMES modeling done but it has the perception of being outdated. Regulations allow DEP to reduce dilution when MZs overlap. At that time, dye studies may become necessary.

For tidally influenced and ocean discharges, the MZ size is limited to a 100-meter radius for aquatic life criteria. Average tide conditions are used for chronic discharge dilution estimates and neap conditions are used for acute.

The burden of supplying data for the dilution estimate is placed on the dischargers. However, DEP will accept published values from previous studies. DEP uses USEPA (1991) guidance in determining data requirements. Dischargers collecting data for the MZ study need to submit a monitoring plan which is reviewed by DEP.

Texas (TNRCC 2003)

Texas has not been delegated NPDES permitting authority. EPA reviews the Texas MZ implementation plan and issues NPDES permits. However, decisions on MZs in specific permits are made by the Texas Natural Resources Conservation Commission (TNRCC). TNRCC (2003) is the main source of policy and guidance for the review of MZ studies.

The discharger submits the MZ study following TNRCC. Texas only allow CORMIX applications in tidal waters. The state requires a field study plan be submitted for review prior to begin the work.

The parameters for the study are rigidly defined by TNRCC:

- For bays and estuaries greater than 400 ft wide, the MZ is in a 200 ft radius from the discharge. The jet momentum equation (USEPA 1991) is used to estimate dilution for discharges greater than 37850 m^3 (10 million gallons) per day, and for smaller discharges dilution is assumed to be 8 percent.
- For narrow tidal rivers less than 400 feet wide, the MZ is half the width or 100 feet if little data are available. The minimum assumed dilution for this condition is 8 percent.
- For all the above cases, the zone of initial dilution for compliance with acute aquatic life criteria cannot be more than 25 percent of the total MZ.

Texas provides default data for input to the MZ study. The permittee is also allowed to submit site-specific data. Background contaminant concentrations are not taken into consideration unless there is a known problem. Under these circumstances, data are gathered jointly by TNRCC and EPA.

Washington (WDOE 2003)

In Washington, the state may make an initial estimate of dilution at the acute and chronic MZ boundaries. However, the Washington Department of Ecology (WDOE) typically requires the discharger to submit a MZ study demonstrating the dilution at these locations. The EPA PLUMES model is preferred. Review of the MZ report can take several months with WDOE submitting comments back to the discharger. The WDOE Permit Writer's Manual (WDOE 2003) provides detailed directions on how to structure this MZ report.

Typically, more detail is required in the MZ study if the discharge is to estuarine or ocean waters. Dye studies may be performed instead of desktop modeling studies and, in some cases, are preferred. Before performing a dye study, the discharger is encouraged to submit a study plan to WDOE for review. The burden of supplying data for the dilution estimate is typically on the discharger. Such data include effluent concentration and flow, background water quality, ambient density, and ambient current magnitude and direction.

For tidally influenced water bodies, the state requires the discharger to determine a velocity frequency distribution. Acute dilution is evaluated with the 10 percent low velocity, and chronic dilution is measured with the 50 percent velocity. The state may also require the discharger to test the 90 percent velocity to determine if it is the critical condition for acute dilution. Density measurements in the discharge are typically required for summer time, when ambient density stratification is strongest.

2.3.2 Canada

In Canada, each level of government has competence to protect the environment. The legislative authority for implementation of Canadian Environmental Quality Guidelines (EQGs) and other environmental assessment tools lies primarily with each provincial or territorial jurisdiction, with the exception of federal lands.

Canadian EQGs are used by federal, provincial, and territorial governments to achieve the highest levels of environmental quality across Canadian jurisdictions. Provincial and territorial governments may use EQGs in developing point-source licenses and permits for discharges, while at the federal level, the guidelines support various legislative acts, such as the Canadian Environmental Protection Act (CCME 1999). In addition, Canadian EQGs have been widely endorsed internationally by the United Nations and the World Health Organization.

CCME (1999) is the primary element of the legislative framework for protecting the Canadian environment and human health. A key aspect is the prevention and management of risks posed by toxic and other harmful substances. EQGs, so derived, have a number of important applications in Canada, including but not limited to assessing and managing contaminated sites and supporting the licensing and permitting of effluent discharges.

During the course of licensing or permitting wastewater discharges, responsible authorities may establish an initial dilution zone (IDZ which is also referred to as the MZ) in the vicinity of existing or proposed outfall. Although the definition of an IDZ differs among jurisdictions, the following definition is generally applicable (CCME 2003): *"An initial dilution zone is the area contiguous with a point source (effluent) where the effluent mixes with ambient water and where concentrations of some substances may not comply with water quality guidelines or objectives"*.

The concept of the IDZ is based on the understanding that it is often possible to allow somewhat elevated concentrations of chemicals of potential concern (COPCs) to occur within relatively small areas of a receiving water body, without significantly affecting the integrity of the water body as a whole. Such IDZs are typically established when wastewater discharges are known or predicted to contain elevated levels of COPCs and responsible authorities wish to limit the geographic area that could potentially be affected by the discharge. Importantly, establishment of an IDZ enables the regulated interest to utilize the dilution capacity of the receiving water system such that it is not necessary to achieve the water quality objectives at the end of pipe.

2.3.2.1 Technical and Policy Guidance Documents

Although the administrative tools available to support water resources management are similar across Canada, the approaches that have been used within the various jurisdictions differ depending on the management goals that have been established.

Many jurisdictions have applied a technology-based approach to manage releases of liquid effluents. This approach limits on the releases of COPCs are frequently established for point source effluent discharges based on the best available technology-economically achievable (BAT-EA).

A second approach is commonly referred to as the use-protection approach (water-quality-based in USA). Application of this approach involves the establishment of discharge limits for substances of concern based on an understanding of the assimilative capacity of the water body under consideration.

The third approach is referred to as the non-degradation approach. Using the non-degradation approach, discharge limits are established based on the natural background levels of substances of concern at the site. However, technological limitations and costs are likely to preclude the implementation of this option under most circumstances.

In Canada, licensing and permitting activities have largely relied on technology-based approaches to estab-

lish effluent limits for wastewater discharges. Because point source effluent discharges have the potential to significantly alter water quality conditions in receiving water systems and adversely affect one or more designated water uses, transitioning toward a use-protection approach is likely to improve the management of liquid effluents ("combine approach"). Water quality objectives (WQOs) provide the science-based tools needed to support such a transition.

The use-protection approach offers a scientifically-defensible basis for establishing effluent quality criteria for the protection of existing and/or future uses of aquatic ecosystems. Implementation of this approach involves several steps, including (CCME 2003):

- Identification of the physical, chemical, and/or biological variables of concern with respect to an existing or proposed wastewater discharge.
- Establishment of ambient WQOs for the receiving water system under consideration.
- Determination of the areal extent of the IDZ for wastewater discharge (note: IDZs must be established in accordance with the guidance provided by the responsible authority).
- Development of use-protection-based effluent quality limits that ensure that the ambient WQOs will be met at the edge of the IDZ (i.e., using dispersion modeling and/or other appropriate techniques).

Because authorization of IDZs has the potential to adversely affect existing and/or potential water uses, many jurisdictions have established a set of guiding principles to ensure that important water management interests are considered in the process. The following guiding principles are intended to identify some of the factors in the establishment of IDZs (CCME 2003):

- The dimensions of an IDZ should be restricted to avoid adverse effects on the designated uses of the receiving water system.
- The IDZ should not impinge on critical fish or wildlife habitats.
- Conditions outside the IDZ should be sufficient to support all of the designated uses of the receiving water system.
- Wastewaters that are discharged to the receiving water system must not be acutely toxic to aquatic organisms.
- Conditions within the IDZ should not cause acute or short-term chronic toxicity to aquatic organisms.
- Conditions within an IDZ should not result in bioconcentration of COPCs to levels that are harmful to the organism, aquatic-dependent wildlife or human health.
- A zone of passage for migrating aquatic organisms must be maintained.
- MZs for adjacent wastewater discharges should not overlap with each other.
- MZs should not unduly attract aquatic life or wildlife, thereby causing increased exposure to COPCs.
- MZs should not be used as an alternative to reasonable and practical pollution prevention, including wastewater treatment.
- Accumulation of toxic substances in water or sediment to toxic levels should not occur in the MZ.
- Adverse effects on the aesthetic qualities of the receiving water system (e.g., odour, colour, scum, oil, floating debris) should be avoided.

2.3.2.2 State-Specific Methodology

The administrative tools available to support water resources management are similar across Canada but the approaches that have been used within the various jurisdictions differ depending on the management goals that have been established. Certain jurisdictions in Canada have published guidance on the establishment of IDZs.

It is significant to mention that in tidal water bodies and estuaries the spatial definitions of MZ are again not established in all jurisdictions. Examples include establishing boundaries for the MZ based on distance from the point discharge such as Quebec (<300 m).

Next, a review of the methodologies implemented to allow IDZs is displayed in some jurisdictions which have estuarine waters: British Columbia, Yukon, Ontario and Quebec.

British Columbia and Yukon (BCMOE 2013)

In British Columbia and Yukon, the Ministry of Environment (MOE) regulates the discharge of industrial wastes under the Environmental Management Act through the use of permits, authorizations and regulations. While a formal mechanism has not been established, the WQOs are often used in the permitting and licensing processes in the region.

The extent of the IDZ is defined on a site-specific basis, with due regard to water uses, aquatic life, and other waste discharges. The existing guidance (BCMOE 2013) indicates that an IDZ may extend up to 100 m downstream from a discharge and may not encompass an area greater than 25-50% of the stream width (extending from the bed to the surface). IDZs are essential to allow for the initial mixing between effluents and the receiving water.

Within an IDZ, water quality may exceed WQOs and sub-lethal effects on aquatic life may occur, but effluent quality and dilution in the IDZ should be such that acutely toxic conditions do not occur. IDZs should not impinge on any sensitive area requiring protection. Outside of the IDZ, water quality should be suitable for all designated water uses, and should protect aquatic life from sub-lethal effects, as a minimum.

Information on permitted discharges is available from the Environmental Protection Division of the MOE. Each permit and authorization should be described in terms of the operation or process, and the permit requirements. Monitoring data should be discussed in terms of loadings, dilution available in the IDZ and with complete mixing. A discussion of substances which may have an environmental impact due to the nature of the discharge, but for which no data are available should also be included.

Ontario (MOEE 1994a;b)

The relevant legislative authority for the control of point source discharges in the Province of Ontario is found in the Environmental Protection Act and the Ontario Water Resources Act. Discharge specifications are contained in Certificates of Approval, Control Orders and other Ministry of Environment and Energy (MOEE) requirements and directions.

For the development of effluent requirements, the publications MOEE (1994a;b) are the primary documents used to provide interpretation of the legislation. Surface water quality management is addressed under a series of Surface Water Management Policies and the Provincial Water Quality Objectives.

In establishing effluent requirements for discharges to surface waters, the process outlined below should be followed (MOEE 1994a):

1. Appropriate site-specific receiving water assessments will be conducted to determine the effluent requirements based on the waste assimilative capacity of the receiver.

2. The site-specific effluent requirements will be compared to the federal or provincial regulations or guidelines for effluent discharges and the most stringent requirement will be applied.
3. The effluent requirements derived from the above procedures, expressed as both waste loadings and/or concentrations, will be incorporated into a Certificate of Approval.
4. For existing discharges in areas with water quality worse than the Provincial Water Quality Objectives, the Ministry may develop a pollution control program with each discharger that would meet the effluent requirement determined from the above procedures.

Through the incorporation of receiving-water quality based limits into legally enforceable control documents like a Certificate of Approval, the guidelines for water quality management become enforced.

The size of MZs are considered on a case-by-case basis depending on the local water quality conditions and water use, along with the contaminants of concern in the discharge. The derivation frequently involves the use of site-specific models to determine the extent of MZs. The impact of a point source discharge can be minimized by optimizing the design and location of the point discharge. Factors affecting the dilution efficiency of the discharge are considered in determining this impact.

Quebec (MDDEP 2007)

In Quebec, wastewaters discharged into aquatic environments are not regulated on a large scale. Discharge standards stipulated in the regulations are usually based on the performance of typical wastewater treatment technology. They constitute a basic level of protection without considering the location of discharges. The standards determined by the technological-approach can thus occasionally be insufficient to permit compliance with environmental water quality criteria. Consequently, different measures, such as more restrictive discharge limits or the method for determining effluent discharge objectives (EDOs), can be taken to ensure adequate environmental protection.

The method for determining EDOs is specific to each contamination source. It is based on surface water quality criteria, hydrodynamic conditions and the uses supported by the aquatic environment. The calculation of EDOs constitutes the application of surface water quality criteria to point-source discharges of wastewater into waterbodies.

In the presence of a discharge, water quality criteria based on chronic exposure may be exceeded locally without compromising the chemical integrity of the environment. An impact zone adjoining a discharge point, called the MZ, is usually tolerated. Water quality criteria can be exceeded in the MZ as long as there is no acute toxicity for aquatic organisms and no use is affected. The allocation of a MZ rests on the principle that a small zone of degradation can exist without harming the sustainability of the ecosystem as a whole. To satisfy the previous statement, MZs are defined for each discharge based on the physical limits, the hydrodynamics of the natural environment and best professional judgment. For the same discharge, several MZs may be delineated as a function of the targeted contaminants and designated uses as illustrated in figure 2.23.

Discharge dilution in estuaries and coastal waters is determined with the help of a hydrodynamic model or tracer studies, if desired. When the available data permit, the dispersal analysis in a large number of conditions will identify the critical mixing conditions (seasonal conditions). Once this period is defined, the determination of the dilution factor must take into account the average exposure level of organisms over a complete tidal cycle. To this end, computer simulations are performed at the slacks of high and low tide, as well as when the tide rises and falls. If the current reverses, the redirecting of the plume must be taken into account when evaluating the dilution factor. The results of different tests are then analyzed in a manner that represents the average dilutions of a tidal cycle.

The critical conditions in estuaries and coastal waters are often associated with periods of slower currents and low winds. Ideally, local or regional currents will have been studied, and modeling will be done in low wind

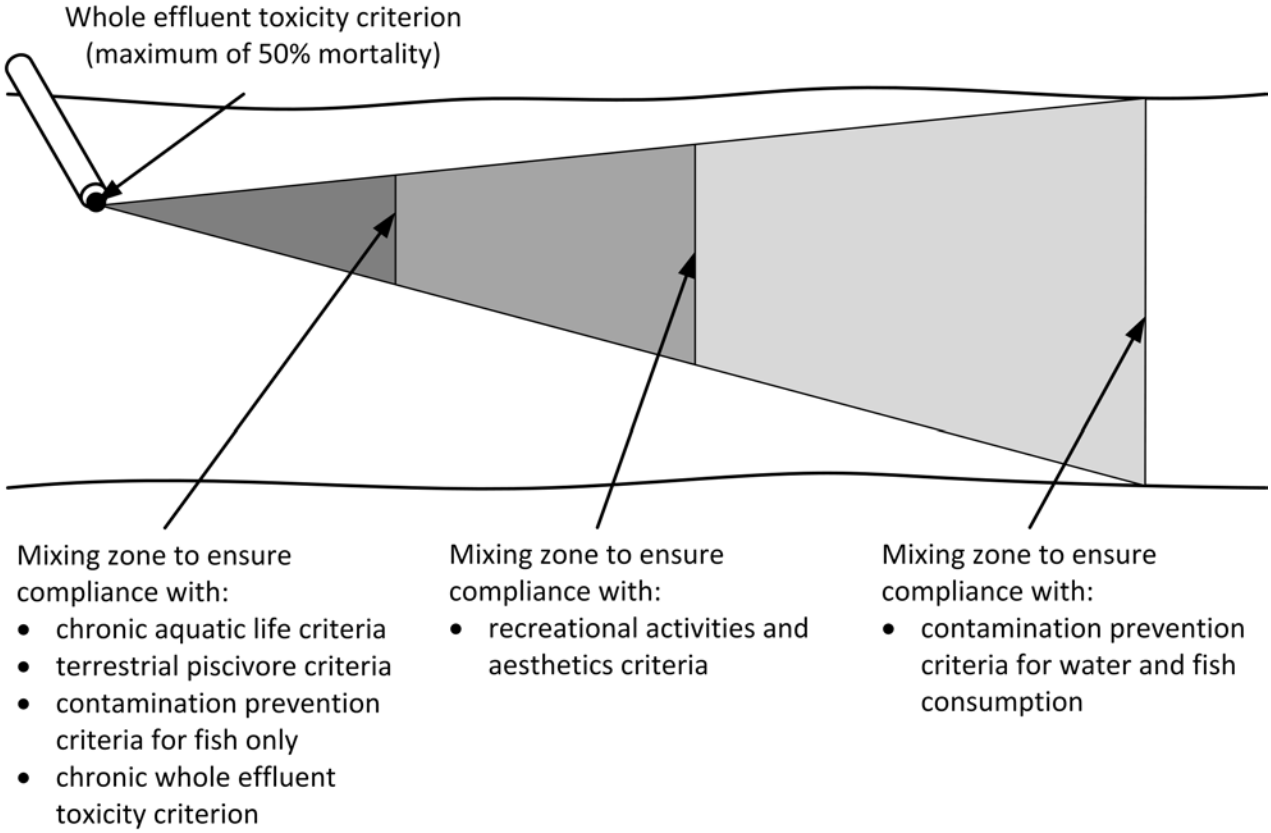

Figure 2.23: Examples of different possible MZs for the same discharge in Quebec. Adapted from MDDEP (2007).

conditions. In this type of environment, the MZ is delineated for all toxicants by a maximum radius of 300 m from the discharge point or a maximum dilution of 1 in 100.

2.3.3 Australia and New Zealand

In Australia and New Zealand, it is the responsibility of local stakeholders or regional governments to agree on the level of protection to be applied to water bodies. State or Territory and/or local jurisdictions are encouraged to use the national water quality guidelines to formulate their own regional guidelines or specific water quality objectives. Each State or Territory uses its own water planning and environmental policy tools to establish a framework that is compatible and consistent with the agreed national guidelines.

Effective discharge controls that consider both the concentration and the total mass of contaminants, combined with in situ dilution and waste treatment, should ensure that the area of a MZ is limited and the values of the waterbody as a whole are not jeopardised.

2.3.3.1 Technical and Policy Guidance Documents

The main document to allocate MZs in these countries is the Australian and New Zealand Guidelines for Fresh and Marine Water Quality (the Water Quality Guidelines) and its objective is to provide an authoritative guide for setting water quality objectives required to sustain current, or likely future, environmental values (uses) for natural and semi-natural water resources in Australia and New Zealand (ANZECC & ARMCANZ 2000). The guidelines are not mandatory.

The Water Quality Guidelines have been prepared as part of Australia's National Water Quality Management Strategy (NWQMS) and relate to New Zealand's National Agenda for Sustainable Water Management. They provide government and the general community with a sound set of tools for assessing and managing ambient water quality in natural and semi-natural water resources.

The vast range of environments, ecosystem types and food production systems in Australia and New Zealand require a critically discerning approach to setting water quality objectives. The NWQMS aims to achieve sustainable use of water resources by protecting and improving their quality while maintaining economic and social development. A three-tiered approach at national, State or Territory, and regional or catchment levels is required.

MZs are often defined as explicit areas around effluent discharges where the management goals of the ambient waters do not need to be achieved and hence the designated environmental values may not be protected. In this context MZs are sometimes termed exclusion zones.

2.3.3.2 State-Specific Methodology

As we mentioned, the administrative tools available to support water resources management are similar across Australia and New Zealand, the approaches that have been used within the various states differ depending on the management goals that have been established. Certain states in Australia and New Zealand have published guidance on the establishment of MZs.

It is significant to mention that in tidal water bodies and estuaries the spatial definitions of MZ are anew not established in all States. Examples include establishing boundaries for the MZ based on distance from the point discharge such as Queensland (<300m).

Next, a review of the methodologies implemented to allow MZs is displayed in some states which have estuarine waters: Queensland, Tasmania and Victoria.

Queensland (DEHP 2012)

The Queensland Environmental Protection Policy for Water requires appropriate consultation with the community before environmental values and water quality objectives for a water are decided. In Queensland, a MZ is a permitted zone of impact and is primarily for managing soluble toxicants where concentrations in the release are above National Water Quality Objectives.

The document *"Technical guideline - Wastewater release to Queensland waters"* (DEHP 2012) provides a risk-based assessment approach to licensing releases of wastewater to surface water. Decisions made by the administering authority in relation to wastewater release should be consistent with this approach and based on the latest scientific and technical knowledge, but also allow for flexibility for assessment on a case-by-case basis.

The information requirements for assessing wastewater releases are the following:

1. *Description of the proposed activity:* Definition of the industry type and size (estimated production, current and ultimate). Identification of the potential contaminants of concern. Assessment of the characteristics including the concentrations, volume, loads and potential variability. Location and configuration of the proposed release. Confirming best practicable measures have been used to avoid or minimize wastewater release. Identification of the activity risk (based on size, location etc).

2. *Description of the receiving environment:* Identification of water bodies potentially affected. Providing all relevant information on the receiving environment based on desktop and field studies (e.g. current, background water quality condition). Identification of all relevant environmental values (EVs) and water quality objectives (WQOs). Ensuring other sources and loads of relevant contaminants in the catchment (including future discharge). Ensuring all government planning requirements applying to these water bodies have been considered (e.g. RAMSAR wetlands).

3. *Prediction of outcomes or impacts of the proposed wastewater release:* Assessing whether contaminants are potentially toxic at end-of-pipe. If so, consideration of an initial mixing zone and the acceptability of the size. Prediction of the available assimilative capacity and sustainable load of the receiving environment, if required. Justification for the choice and application of all predictive methods/models used in the assessment, including model inputs, uncertainty and simulation results. Consideration of other potential impacts (other than direct impacts on water quality).

4. *Setting circumstances, limits and monitoring conditions:*. Specifying any circumstances related to the approved wastewater release (e.g. limitations or timing issues). Derivation of end-of-pipe limits from approved release loads and characteristics. Inclusion of a receiving environment monitoring program requirement. Inclusion of reporting requirements and management actions where limits/triggers/objectives for the approved activity are not achieved.

Compliance with reference criteria should be met within 300 m. Approval of zones with exceeded water ambient quality objectives greater than this size may be granted in specific cases where social and economic considerations support the discharge of residual wastewater and there are no other feasible alternatives. Regardless, localized environmental harm should not occur.

Tasmania (DPIPWE 1997)

Local communities and other stakeholders have a key role in identifying the water quality values for regional wetlands and waterways as part of the State Policy on Water Quality Management (DPIPWE 1997). Information provided on these values assists the Board of Environmental Management and Pollution Control and local councils to finalise Protected Environmental Values for surface waters. These values are reflected in management plans for the regions and in local council planning schemes.

MZs must be set in accordance with the following principles (DPIPWE 1997) but there are not methodological documents:

- The location and size of the MZ must be clearly defined in a permit or other legally enforceable instrument of approval.
- The MZ must be as small as practical and either alone or in combination with other MZs, should not occupy a significant proportion of the receiving waters designated for any given protected environmental value.
- The presence of the MZ, either alone or in combination with other MZs, should not detract from the values and uses of the surrounding waters.
- MZs should not generally be designated in waters which receive significant and regular use for primary contact recreation; or are recognised as of significant value as spawning or nursery areas; or are close to areas used for aquaculture; or are close to drinking water supply intakes; or are of outstanding ecological or scientific importance.
- MZs must not create a significant barrier to the migration of fish or other aquatic organisms.
- MZs designated in rivers, streams and estuaries should be set having regard to the effects of the MZ under low flow conditions (7Q10).

Where a MZ has been designated, the operator shall be responsible for monitoring their effluent(s) for toxicants, and the receiving waters, including baseline monitoring. These responsibilities shall be reflected in the conditions attached to the permit. Moreover, the emission limits should be set at levels which are unlikely to cause chronic or sub-lethal toxicity to living organisms present in the local ecosystem at the dilution expected at the boundary of the MZ.

Victoria (EPA 2003)

According to Victoria State Environment Protection Policies, a MZ is an area of a waterway or waterbody where the receiving water environment is detrimentally affected by a waste discharge. It is an area with explicitly defined boundaries where specified environmental quality objectives may be exceeded and consequently some beneficial uses may not be protected in the MZ (EPA 2003).

MZs are good examples of approaches aimed at assisting managers of wastewater discharges to reduce their impact on the environment in a progressive and affordable manner. These approaches recognise that it may take some time to improve the management of wastewater and that this can be costly. These provisions enable this expenditure to be incurred on a progressive basis, which gives businesses time to plan for these costs in budgets and pricing mechanisms.

In 2010 the EPA Victoria published the "Guidance for the determination and assessment of Mixing Zones" (EPA 2010). The purpose of these guidelines is to assist those in industry who are involved with MZs and to provide a clear and objective approach to the determination and assessment of MZs. They explain how MZs fit into the current legislative framework and places them in the context of the need for continuous improvement, and provide guidance on the process for determining, assessing, monitoring and reporting MZs.

Finally, these guidelines remark that every discharge to the environment presents a unique set of circumstances in terms of discharge characteristics and the nature of the waterway into which it discharges. Therefore, there is no one method that can be used for establishing the extent of all MZs. Each MZ should be analysed on a case-by-case basis.

Irrespective of the exact methods, this will involve identifying the beneficial uses and local values of the receiving waters, characterisation of the effluent and receiving water, determining the dilution and dispersion of the effluent, and assessing the impact of the effluent discharge to beneficial uses and local values.

2.3.4 Europe

European water pollution control began in 1970s with the First Environmental Action Programme (1973) followed by a first wave of legislation. In the field of ELV-legislation, the so-called Dangerous Substances Directive (i.e. Council directive 76/464/EEC) and several daughter directives on various individual substances were adopted. This directive is concerned with pollution by certain dangerous substances being discharged into the aquatic environment from point sources. A second wave of EU ELV-legislation includes the Urban Waste Water Treatment Directive (1991), the Nitrates Directive (1991) and the Plant Protection Products Directive (1991).

In the context of the European Water Framework Directive (EC 2000), the full implementation of existing EU ELV-legislation has to be provided. As it was mentioned, the WFD also contains a "combined approach" in which the source-oriented measures of the EQS-based approach are additional to those of the technology-based approach. Since 1999, such a combined approach was already adopted for new industrial facilities covered by IPPC directive. For existing discharges, the IPPC directive will come into effect in 2007 (EC 2008b;c, EU 2010). The "end-of-pipe" specification for the ELV is clear and unequivocal in the WFD: *"The emission limit values for substances should normally apply at the point where the emissions leave the installation, dilution being disregarded when determining them"*.

Finally, the EQS Directives (EC 2008a, EU 2013) establish that a "mixing zone" is: *"a zone adjacent to points of discharge, where concentrations of one or more toxicants may exceed the relevant EQS if they do not affect the compliance of the rest of the body of surface water with those standards"*. These zones must be restricted to the proximity of the point of discharge and proportionate.

2.3.4.1 Technical and Policy Guidance Documents

In order to clarify and establish MZs, the European Commission on December 2010, published a document entitled "*Technical Guidelines for the identification of MZs pursuant to Article 4 (4) of the Directive 2008/105/EC*" which creates the basis for determining which discharges may designate MZs and the methodology for calculating preliminary those areas (EC 2010).

It should be underlined that according to Article 4 of Directive 2008/105/EC, there is no obligation for Member States to designate MZs (EC 2008a). If they decide to do so, it is expected that they will follow these guidelines (EC 2010). However, a guideline, by definition, is not legally binding. Where Member States designate MZs, a description of the approaches and methodologies applied to define MZs and measures taken with a view to reducing the extent of the MZs in the future must be included in River Basin Management Plans. The precautionary principle should be considered as a guiding rule.

In the guidelines (EC 2010), a "Tiered Approach" has been developed that may be adopted by Member States when setting MZs under EQS Directives (EC 2008a, EU 2013). The tiered approach may be summarized as follows:

- *Tier 0. Contaminant of Concern present:* Tier 0 is a high-level filter designed to identify the presence of discharges with the potential to cause EQS exceedence for Contaminant of Concern. Any effluent discharges that do not contain concentrations above EQS need not be further considered and will not therefore require the determination of a MZ.

- *Tier 1. Initial Screening:* Tier 1 is designed to establish whether the discharges identified in Tier 0 require further attention, and remove from further consideration those discharges that are trivial using simple tests. A set of precautionary filters allow the determination of acceptability of MZs associated with small discharges.
- *Tier 2. Simple approximation:* The purpose of Tier 2 assessment is to eliminate those discharges that are clearly either acceptable or unacceptable on the basis of a simple case-specific assessment, using an initial indicative assessment of the size of the extent of EQS exceedence.
- *Tier 3. Detailed assessment:* Tier 3 provides a more detailed assessment, often involving the use of computer-based modeling techniques, to consider the individual circumstances for the discharge (or groups of discharges). In this tier, the approach is focused on detailed considerations of the spatial and temporal variation of EQS exceedence.
- *Tier 4. Investigative Study and Validation of the models:* If after assessment there is still uncertainty it may be appropriate to conduct investigative studies to validate the outputs, refine the approach taken or to characterise the actual impacts occurring within extents of EQS exceedence.

2.3.4.2 State-Specific Methodology

As we mentioned, the administrative tools available to support water resources management are being similar across Europe since the promulgation of new Directives (EC 2000; 2008a;b;c, EU 2010; 2013). However the used approaches differ depending on the established management goals by the various Member States. Certain Member States in Europe have published their guidelines on the establishment of MZs.

It is significant to mention that in tidal water bodies and estuaries the spatial definitions of MZ are not establish in all Member States. Examples include establishing boundaries for the MZ based on distance from the point discharge such as Netherlands (<150 m).

Next, a review of the methodologies implemented to allow MZs is displayed in some Member States which have estuarine waters: United Kingdom, Netherlands and Spain.

United Kingdom (UKEA 2011a;b;c)

In UK, the Environmental Protection Act mainly regulates the discharge permits. MZs are permitted under the EQS Directive. In April 2010 Environment Agency launched H1 Environmental Risk Assessment in modular format to meet the requirements of the Environmental Permitting Regulations. This resulted in an overview document supported by 11 technical annexes, called A to K.

In order to conduct the allocation of MZs, the H1 Environmental Risk Assessment – Overview guide (UKEA 2011c), Annex D - Basic Surface Water Discharges (UKEA 2011a) and Annex E - Complex Surface Water Discharges (UKEA 2011b) are required. These guides help stakeholder to quantify the impacts of substances and effluent released to surface water, which includes rivers, estuaries, coastal waters, lakes and canals. One of the key issues is the location of MZs in relation to the designations and other uses.

To quantify the impact of discharges into surface waters, they use one basic approach called chemical specific analysis with five stages:

1. *Calculation of the Process Contribution for either an emission to estuary water.* The first step is to calculate the concentration of each effluent constituent in a surface water after dilution and to carry out a simple screening assessment to identify insignificant releases.
2. *Screening out insignificant releases.* The second step is to screen out insignificant releases emitted in such small quantities that they are unlikely to cause a significant impact on the receiving water.

3. *Undertake detailed modeling*. If a release has not been screened out as insignificant (based on the Process Contribution being less than 4% of the EQS), then it may still be acceptable. The guidelines can help stakeholders decide whether to carry out more sophisticated modeling to give a more accurate assessment.

4. *Assessment of the acceptability of any MZs*. For estuarine waters, if the EQS is achieved after Initial Dilution then the discharge is likely to be acceptable. If the Process Contribution is greater than the EQS, then the acceptability is dependent on the size and location of the MZ. It should be provided details of the location and extent of the MZ in relation to conservation and other features and explain whether you think your releases are acceptable.

5. *Summary of the risks to water*. The final step is required when stakeholders are undertaking a BAT assessment and are comparing a number of different options. For each option, the procedure involves summing the impacts from all the substances, leading to an "Environmental Quotient".

Netherlands (DCIWM 2000, Kleissen 2012, Konterman *et al.* 2003, RIZA 2001)

In the Netherlands, a combined technology- and EQO-based approach for the evaluation of emissions is advocated. The Dutch Commission for Integrated Water Management published detailed guidelines for the implementation of the EQO-based approach (DCIWM 2000). Separate sets of guidelines have been published for the assessment of discharges and for the prioritization of substances and sources (DCIWM 2000).

The method for prioritization is used by Water Authorities when drafting Water Management Plans. Priority substances and sources are identified by monitoring programmes and by estimating emission loads with models. Environmental permitting procedures under the Netherlands Pollution of Surface Waters Act must take account of the applicable management plan but it is apparent from Dutch jurisprudence that it is not enough simply to refer to it. Specific reasons must be stated for measures to reduce emissions of priority substances and sources (Konterman *et al.* 2003).

The combined technology- and EQO-based approach used in the Netherlands involves the application of BAT to reduce emissions and taking additional measures if EQSs are not being achieved. In line with the European IPPC Directive (EC 2008b), the Dutch Implementation Order for State Waters lays down that applications for permits must be accompanied by details of significant emissions and the environmental impacts of those emissions (RIZA 2001).

Until 2007 discharges to surface waters in the Netherlands were assessed with a digital tool developed specifically for river systems. In 2007, Rijkswaterstaat indicated that they needed a general tool to help them assess discharges into all types of surface waters. In the same period the EU had introduced the concept of MZs.

In this context, a new tool was developed for Rijkswaterstaat between 2007 and 2012. The tool also took into account the concept of MZ operational, allowing it to comply with the EU Technical Guidelines for the Identification of MZs (EC 2010). The main challenge of this development was to ensure that the tool was applicable to most surface water types, while being based on sound science, easy to use and providing a first quick but reliable assessment of the acceptability of a discharge. Given the variety of surface water characteristics and the complexity of the processes that govern the spreading of effluent, it was decided to implement a decision tree based on a number of different calculation techniques. The application is linked to a database that contains the key surface-water data needed for the calculations (Kleissen 2012).

Depending on the characteristics of the receiving water and effluent discharge, the decision tree selects the most appropriate technique for calculating the toxicant concentration at a predefined distance from the discharge point. The tool will then check whether the resulting concentration meets the applicable water quality criteria. The tool has been developed to generate concentrations that are overestimated rather than underestimated. The implemented web-based tool is not only meant for use by Rijkswaterstaat but is publicly available

for use by industry and any other organisation both in the Netherlands and elsewhere (Kleissen 2012).

Finally, the maximum volume of the acceptable mixing zone for chemical substances corresponds with a radius of 150 m for estuarine waters.

Spain (CEDEX & IHCantabria 2008, SPAIN 2011)

In Spain, EQS Directive (EC 2008a) was transposed to "*Real Decreto 60/2011, de 21 de enero, sobre las normas de calidad ambiental en el ámbito de la política de aguas*" (SPAIN 2011). Wastewaters discharged into aquatic environments are not regulated on a large scale. Discharge standards stipulated in the regulations are usually based on the performance of typical wastewater treatment technology. They constitute a basic level of protection without considering the location of discharges. Regarding MZs, there are not new requirements in the transposition and no guidance documents of the Spanish government.

Additionally, it is worthy to mention that a technical report was conducted by CEDEX and IH Cantabria on December 2008 (CEDEX & IHCantabria 2008), providing a methodological approach to allocate MZs of urban wastewaters discharged by submarine outfall into coastal waters.

According to the proposals adopted in other countries as well as in the Directive 2008/105/EC (EC 2008a), CEDEX & IHCantabria (2008) determines that MZs should be established by the next principles:

- The MZ should be a well delimited area around a discharge point, defined with regulatory objectives, taking into account the EQSs established for the receiving environment.
- The MZ aims to ensure the preservation of ecosystem integrity of the coastal water mass in which it is located.
- The MZ should be as small as possible, established by the combined approach and assuming the adoption of BATs and compliance with the ELVs.
- Establishing a MZ does not exempt compliance with legislation uses, such as bathing waters or shellfish;
- The MZ can be defined for both conservative and non-conservative toxicants (organic and microbiological) and especially for those who require further dilution to meet quality objectives.
- The defined MZ should not overlap with areas that have been recognized other human or natural uses as priorities.
- The defined MZ will be incorporated into the design of operational control programs as well as monitoring programs for the management of water bodies.
- The MZ should be conveniently validated using numerical modeling and considering the temporal and spatial variations of the near- and far-field scales.

Taking into account these principles, the developed methodology to delimitate MZs comprises three stages (CEDEX & IHCantabria 2008):

1. *Preliminary allocation of MZ.* In the first stage, the criteria and procedures to delimitate the MZ as an area are defined. To establish criteria for delimitation of the MZ a holistic approach is used. This approach considers simultaneously hydrodynamics and mixing processes, ecological aspects of the environmental value and social aspects reflected by the interaction of the MZ with areas recognized with other uses.

2. *Verification of compliance with the EQSs in the MZ.* Once defined regulatory MZ, the buoyant jet evolution into the receiving waters must be studied in order to determine the degree of compliance with the EQS on the edge of the MZ.

3. *Proposal end of the MZ.* After verifying compliance with the EQSs, the acceptance of MZ is determined depending of its size. A non-acceptable MZ should consider other options alternative point discharges or diffuser section configurations.

2.4 Concluding remarks

With the general aim in mind, a literature review was carried out in order to know the state of the art of two main topics: the mixing, transport and reaction of wastewaters in estuaries and the methodological approaches to allocate mixing zones used in daily practice.

This review highlights the strengths and deficiencies found in the calculation of the evolution of toxic substances in estuaries and in the current approaches. Additionally, the review will allow defining the specific objectives of the present study.

2.4.1 Mixing, transport and reaction of wastewaters in estuaries

The term "mixing zone", which is used in the EQS Directives, does not have a direct relationship with the classification in near-, intermediate- or far-field. Therefore, the admissible iso-concentration map may be found in any of these regions depending on the outflow characteristics, the rate of advection and the rate of mixing. Due to these different temporal and spatial scales only CFD models such as FLUENT or Open-FOAM might deal with all the mixing regions. However, even if the increasing computational speed and memory of modern computers is considered, they do not appear feasible for present-day engineering practice.

For that reason a zonal modeling approach is necessary. This approach considers the application of zone models in regions with distinct hydrodynamic properties. It is then possible to simplify the governing equations by dropping unimportant terms. As an example, in the near-field region it is often possible to distinguish specific buoyant jet zones for which integral models apply. These only calculate near-field substance concentrations with explicitly calculating the flow field by means of a estuarine circulation model (hydrodynamic model).

On the other hand, in the far-field region, it is often possible to neglect vertical accelerations and employ the hydrostatic assumption and calculate the far-field flow field using a transport model and taking into account the near-field processes by means of a coupling algorithm (intermediate-field).

Thus, zone models have a considerable advantage in the mathematical treatment, improved accuracy and detail in the solution. Nowadays, it seems reasonable to deal with the allocation of Mixing Zones using several numerical models for every mixing region fed by a hydrodynamic model.

Regarding these models, it can be concluded that the available models and approaches are appropriated for solving the transport, mixing and reaction of toxic substances discharged by industrial wastewaters in estuarine systems within all the mixing regions (near-, intermediate- and far-field).

In the field of hydrodynamics, for over a 50 years researchers have developed ocean circulation models. For estuarine hydrodynamics since 1990s, the models present high resolution in the discharge region (order of meters) and large number of physical processes.

Among these models, EFDC, ROMS, POM, MOHID, Delft3D-FLOW and TELEMAC-3D are open source for academic, research or business, what motivated that they become three-dimensional hydrodynamic tools most widely used today.

In the near-field region, for over a 50 years researchers have investigated the behaviour of the buoyant jet discharge in ambient flow. The observations and quantitative results from early experimental research led to the formulation of empirical and analytical solutions. These solutions formed the basis of the mathematical models that are used today to predict the behaviour of these flows, specially integral models.

Among these integral models, CORJET (CORMIX system), UM3 (VISUAL PLUMES package), JETLAG (VISJET system) and MOHIDJET (MODHID system) are most widespread internationally. The characteristics of ease of use, ability to develop sensitivity analysis, data availability, data requirements, the time required to obtain results, the cost and the possibility of use in mixing zone allocations are elements to value when choosing an integral jet model.

In the intermediate-field region, no specific intermediate-field model has been found, though either near-field or far-field models include intermediate field processes partly. For over a 20 years researchers have investigated the most appropriate way to overcome these issues of the transport processes via the application of integrated models consisting of a near-field model and a far-field model that are connected via a coupling algorithm. Basically, there exist two main methods: passive offline coupling and active online coupling.

In the case of single-port discharges into estuarine waters, the scale of the intermediate-field ranges from about 1 m to the order of 100 m, depending on the discharge characteristics. The large size of this region is a major reason why a link between near- and far-field modeling is necessary to carry out an adequate 3D environmental impact assessment.

Therefore, a offline passive coupling approach might be sufficiently accurate because the source-induced flow by wastewater discharges, though considerably important for near-field mixing, does not change the flow characteristics of the far-field. Additionally, regulators, consultants and water companies generally use different models so changes in such codes (regardless if commercial or open-source) are generally costly and time-consuming, whereas the application of an onset coupling approach between existing models provides a cheaper and easier solution.

In the far-field region, water-quality modeling has evolved appreciably since its innovation in the early years of the twentieth century related to societal concerns and to computational capabilities that were available. This leads to significant progress in the considered physical, chemical and biological processes as well in computer software and hardware. Having in mind all these features about water quality modeling, in the 2000s three-dimensional codes were refined. Consequently, there are a large number of water quality models that are in use today.

Among these models, only MOHID, D-Water Quality (Delft3D-FLOW) and WASP7 (EFDC) are integrated hydrodynamic-water-quality-modeling frameworks and open source for academic, research or business. These characteristics motivated that they become the most appropriate tools in order to solve the mixing, transport and reaction of wastewaters in estuaries for allocating mixing zones.

2.4.2 **Methodological approaches to allocate mixing zones**

As a general rule, methodological approaches to allocate MZs in any aquatic system are based on two ambient water quality criteria: the acute criterion of maximum concentration and the chronic toxicity criterion of average concentration. According to these values, two types of MZs may be established, corresponding to the two-number aquatic life criteria (Figure 2.22). Finally, more stringent limits are applied on a case-by-case basis if necessary to protect receiving water quality.

Therefore, for mixing zone assessment it is necessary to predict the impact of point-source discharges for a wide range of discharge and ambient conditions. This prediction poses particular technical challenges. Management decisions on the appropriate degree of treatment must be based on impact assessment models

that can deal with both the near-field and intermediate/far-field. However, the term mixing zone does not have a direct relationship with the classification in near-, intermediate- or far-field so the admissible iso-concentration map may be found in any of these regions.

Furthermore, because authorization of MZs has the potential to adversely affect existing and/or potential water uses, many approaches have established a set of guiding principles to ensure that important water management interests are considered in the process:

- The dimensions of a MZ should be restricted to avoid adverse effects on the designated uses of the receiving water system.
- MZs should not impinge on critical fish or wildlife habitats.
- Conditions outside the MZs should be sufficient to support all of the designated uses of the receiving water system.
- Conditions within an MZ should not result in bioconcentration of toxicants to levels that are harmful to the organism, aquatic-dependent wildlife or human health.
- MZs for adjacent wastewater discharges should not overlap with each other.
- MZs should not unduly attract aquatic life or wildlife.
- MZs should not be used as an alternative to reasonable and practical pollution prevention, including wastewater treatment.
- Accumulation of toxic substances in water or sediment to toxic levels should not occur in the MZ.
- Adverse effects on the aesthetic qualities of the receiving water system (e.g., odour, colour, scum, oil, floating debris) should be avoided.

Nevertheless, the administrative tools available to support water resources management are being similar across the World since the promulgation of environmental regulations, MZ approaches greatly differ depending on the management goals and MZ implementations differ widely from one country to another. It should be underlined that, normally, there is no obligation to designate MZs by any competent authority. If they decide to do so, environmental regulations specify that a description of the approaches and methodologies applied to define MZs must be included.

To quantify the impact of discharges into surface waters, most methodological approaches are based on stepped or tiered methods with different stages. These stages may be summarized and combined in the following steps:

1. Characterization of the receiving environment and the point-source discharge.
2. Calculation of the toxicant contribution of the discharge to estuarine water.
3. Screening out insignificant releases.
4. Undertake simplified modeling.
5. Assessment of the acceptability of MZs.
6. Undertake detailed modeling.
7. Assessment of the acceptability of MZs.

8. Summary of the allocated MZs.

The assessment of the acceptability of MZs refers to the maximum allowable dimensions of a MZ. From a theoretical viewpoint, the maximum dimensions of a MZ should be based on scientific studies that relate MZ dimensions to the occurrence of adverse impacts. Unfortunately, scientific data on MZ dimensions and adverse impacts are extremely scarce. For this reason, MZ regulations are often based on normative assumptions concerning the occurrence of adverse impacts. Therefore, MZs are usually established by computing a dilution factor or it may be delineated as a spatial area with fixed boundaries.

Regarding estuaries, transitional waters or tidal water bodies, all methodologies follow the previous principles, stepped approaches and maximum sizes. Moreover, these methods remarks that the allocation of Mixing Zones on estuaries is particularly difficult due to its high complexity and natural variability, the limited existing knowledge about their functioning and the continued pressure coming to bear because of anthropogenic activities. Thus, this allocation should be done in a site-specific basis.

Despite all the proposed methodologies are good tools to start addressing the associated risks to the discharge of wastewaters, the metrics, formulations and calculations displayed on them are generally too oriented towards other aquatic systems, specially riverine discharges. In regard to estuarine discharges, the allocation of MZs is somewhat ambiguous because it lacks a detailed explanation of the tasks required to carry out such work. There are few methodologies where all the necessary steps to carry on the MZ allocation in estuaries considering the complex geometry, the natural variability and the different hydrometeorological conditions are well-established.

Summarizing, there are numerous methods, guidelines, documents and approaches to allocate MZs. However, most of them do not tackle adequately the problem when dealing with estuaries, transitional waters or tidal water bodies. Additionally, a case-by-case approach is essential to wise use of natural resources of estuaries, because each MZ should be tailored to the physical, chemical, and biological characteristics of the estuary and its particular community of organisms.

2.5 Specific aims and final considerations

The aim of the present study is to provide a stepped methodology with a group of selected and/or developed numerical tools in order to establish where a mixing zone is required and determines its size and acceptability with an appropriate level of detail for each single-port industrial discharge located in a estuary according to its significance. This proposal may be adopted by Member States and/or Industries when setting Mixing Zones under Directive 2008/105/EC (EC 2008a) and Directive 2013/39/EU (EU 2013).

Bearing in mind the general aim of this thesis and the concluding remarks of the literature review, in order to achieve this final objective, the following specific objectives are determined:

- Establishment and description of the characteristics of the required numerical models to calculate the mixing, transport and reaction of conservative and non-conservative substances (toxicants) in estuarine systems. These numerical models should be able to characterize the flow and toxicant loads associated with continuous point-sources in different hydrometeorlogical conditions.
- Development of a mathematical tool for the calculation of the intermediate-field, this is, the coupling between the near- and far-field. For this task, the flow field of a estuarine circulation model will be used as input of an integral jet model in order to obtain the primary diluted concentrations in the near-field (Offline passive initial dilution). Next, these results of an integral jet model will be used as input of a far-field model in order to obtain the secondary diluted concentrations in the far-field (Offline passive coupling in the intermediate-field).

- Development of a method to determine and select model scenarios based on the major modes of estuarine forcing variability.
- Development of a procedure to determine the optimal period of study taking into account an adequate description of the variability of hydrometeorlogical and environmental phenomena related to the evolution of toxicants and minimizing the computational costs.
- Development of a methodology to quantify the estuarine vulnerability to point-source industrial discharges, taking into account the stratification patterns, the transport timescales and the human uses in estuaries.
- Definition of a metric in order to establish the extent and acceptability of mixing zones considering the criteria of Directive 2008/105/EC (EC 2008a) and Directive 2013/39/EU (EU 2013).

In this thesis, a number of considerations for study areas, toxicant discharges and estuarine processes are established.

Regarding *study areas*, we are focused on estuaries where the astronomical tide and river discharges are the most important forcings to understand the mean behavior of the estuarine hydrodynamics. These type of estuaries are worldwide spreading so a methodology to understand their mean behavior could help researchers, technicians and/or regulators to manage them more efficiently. Among others, Suances (Bárcena *et al.* 2012b), Huelva (Sámano *et al.* 2012), Urdaibai (García *et al.* 2010a), Mandovi (Vijith & Shetye 2012), Mondego (Ascione-Kenov *et al.* 2012), Hudson (Warner *et al.* 2005), Alafia (Chen 2007), Tanshui (Liu *et al.* 2002), Columbia (Chawla *et al.* 2008), Yaquina (Frick *et al.* 2007), Ribble (Kashekipour *et al.* 2001), Haihe (Bai *et al.* 2003) or Humber (Edwards & Winn 2006) could be mentioned as suitable locations.

Regarding *toxicant discharges*, it is assumed that BAT are totally implemented on the industrial facility before any consideration is given to the designation of mixing zones. This thesis is only focused on round single-port pipes with positive buoyancy influenced by ambient currents because the industrial discharges are generally freshwater (less dense than brackish waters of estuaries). Finally, hyperdense discharges and diffuse runoff were discarded when developing the method due to their different nature and behavior in the receiving environment.

Regarding *physical, chemical and biological processes*, we neglected some processes such as changes in pH, calculation of the partitioning as a function of salinity, consideration of dredging and sand transport, inclusion of mineralization, bioconcentration and/or sediment processes. All of these processes allow greater accuracy of results. However, they also dramatically increases all the required parameters related to the transport and fate of toxicants in estuarine waters. Consequently, the greater the level of complexity of a model, the greater amount of information and the higher computational costs are required. Moreover, data collecting is becoming more specific and more scarce.

Nevertheless, we have ignored the latter issues for the development of our proposal, they are taking into account as future research topics in specific scenarios when the influence of these factors are highly significant.

An approximate answer to the right problem is worth a good deal more than an exact answer to an approximate problem.

John Tukey

3

Overall methodology

By "approaches" or "methodological approaches", we mean what kinds of problem solving tools to use, either on the various parts (steps) or on the whole problem. Problem solving is a process in which we perceive and resolve a gap between a present situation and a desired goal, with the path to the goal blocked by known or unknown obstacles. In general, the situation is one not previously encountered, or where at least a specific solution from past experiences is not known. In contrast, decision making is a selection process where one of two or more possible solutions is chosen to reach a desired goal.

The steps in both problem solving and decision making are quite similar. In fact, the terms are sometimes used interchangeably. Most researchers describe the problem-solving/decision-making process as beginning with the perception of a gap and ending with the implementation and evaluation of a solution to fill that gap. Each phase of the process includes specific steps to be completed before moving to the next phase (Huitt 1992). Most methodologies of problem solving and decision making include at least four phases:

1. An Input phase in which a problem is perceived and an attempt is made to understand the situation or problem
2. A Processing phase in which alternatives are generated and evaluated and a solution is selected
3. An Output phase which includes planning for and implementing the solution
4. A Review phase in which the solution is evaluated and modifications are made, if necessary

As described in the previous section, a method to allocate Mixing Zones on estuaries is particularly necessary and difficult. To achieve this task, the methodology is based on the use of mathematical tools and numerical models for the calculation of concentrations of toxicant substances in estuarine waters. Using these models, suitably calibrated and validated, allows the detailed description of the spatial and temporal evolution of these concentrations and, therefore, allocating MZs.

Thus, in this thesis a "Stepped Approach" has been developed to document the policy decision tree (methodology) that may be adopted by Member States and/or Industries when setting Mixing Zones under Directive 2008/105/EC (EC 2008a) and Directive 2013/39/EU (EU 2013). It provides a tailored solution with an appropriate level of detail in the form of flow diagrams. An schematic view of the methodology is displayed in figure 3.1.

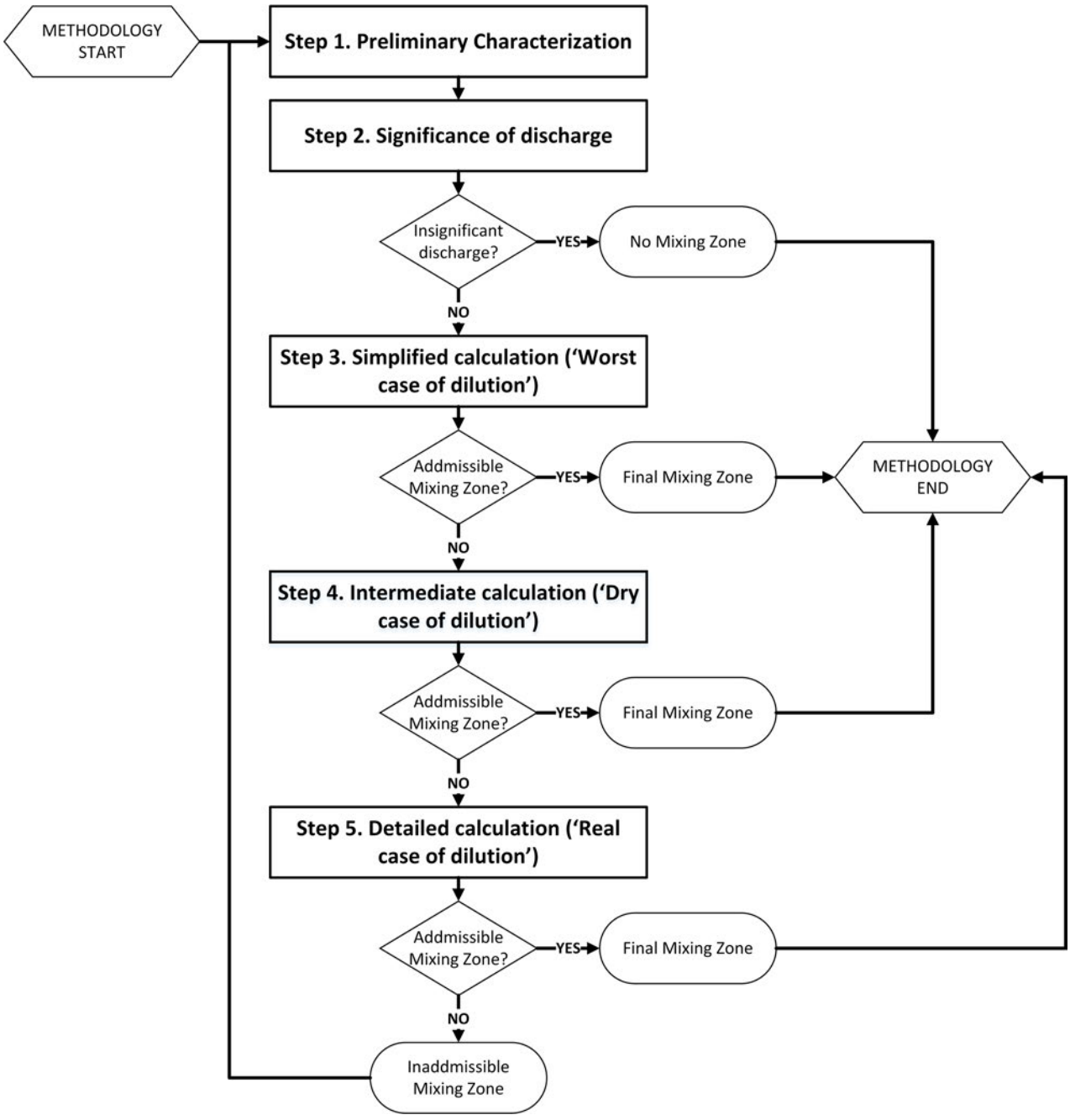

Figure 3.1: Schematic view of the proposed methodology.

The decision tree has been proposed involving five steps. In Step 1, we collect the required information about the study area and the toxicant discharges. Step 2 identifies the significance of the discharge. Next, Step 3 evaluates the effect generated by the discharge and delimitates the MZs from a simplified calculation where the dilution experimented by the discharge is minimum because of the main forcings display low magnitudes. After this step, Step 4 evaluates the effect generated by the discharge and delimitates the MZs from a intermediated calculation where the dilution experimented by the discharge is related to the driest year of the river flow series. Finally, in Step 5, we 'reevaluate' the effect generated by the discharge and 'redelimitate' the MZs where the dilution experimented by the discharge is subject to the temporal variability of the main forcings. Furthermore, in Step 5, the admissibility of the MZs is assessed from the concept of vulnerability and the percentage of estuarine area covered by the MZs.

The general rule of the MZs allocation procedure is that the level of sophistication and complexity of the calculations will rise at each Step of the methodology due to the relevance of the discharge. Simpler procedures require less data and expertise, but they also tend to be less accurate. At each step the aim is to identify those discharges that do not give cause for concern, and also to highlight discharges that require action to reduce the size of the MZ. The philosophy of the decision tree is to increase the resource uses when the order of the discharge increases (Figure 3.2).

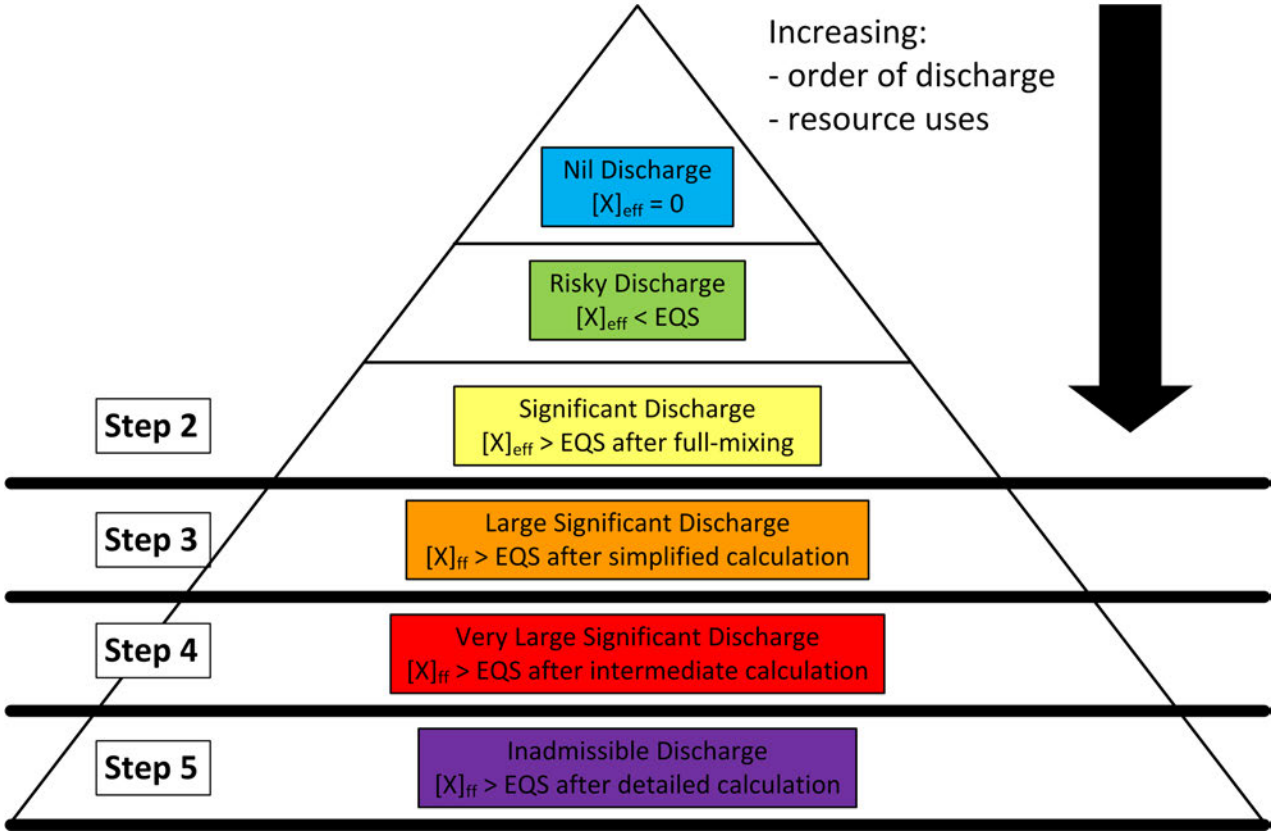

Figure 3.2: Philosophy of the decision tree developed in the methodological approach.

The methodology promotes a uniform and soundly-based framework for such determinations to provide solutions which are: *Efficient* because resources are used only when necessary and then are commensurate with the environmental concerns being addressed; *Robust* for leading to sound reproducible decisions contributing to sustainable use of the estuarine environment; and *Flexible* to meet the needs of Europe's estuarine environments.

3.1 Step 1. Preliminary characterization

Before we start the study of the impact generated by a discharge, the preliminary characterization of the effluent(s) and the study area is a primary and essential task that determines all decisions taken later in the decision tree. The main aspects of this characterization are shown in figure 3.3.

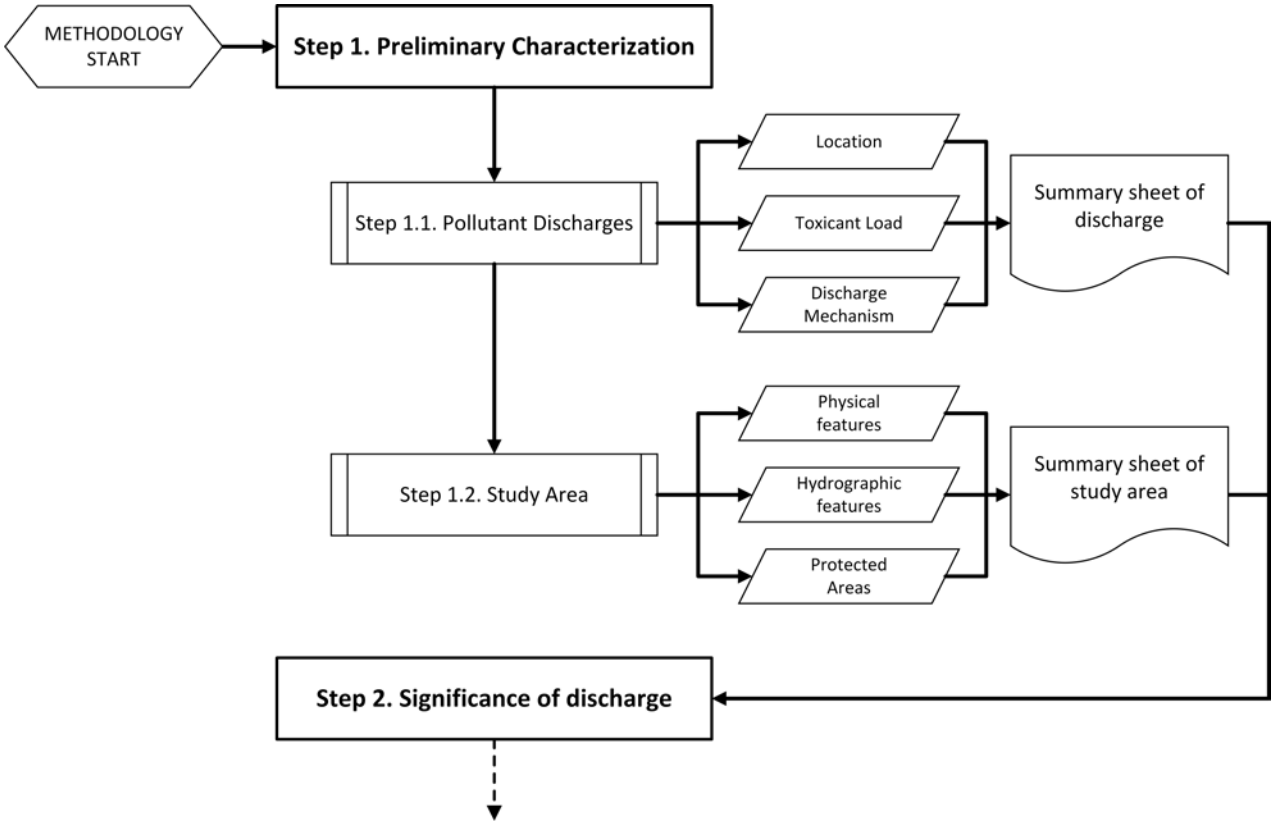

Figure 3.3: Developed flowchart of the Step 1. Preliminary characterization.

3.1.1 Toxicant discharges

Characterization of toxicant discharges allows to know the main discharge parameters which will facilitate the subsequent evaluation of the mixing or dilution experienced by the effluent. Moreover, the acquisition of this information provides a first understanding of the processes that will affect the behavior and dilution of the discharge on the receiving environment. In order to gather this information, we have elaborated a summary sheet which requires three types of input data: location, toxicant load and discharge mechanism. This sheet must be completed with the collection of information available for each field set (Figure 3.4).

A brief description of the required information is given below:

- *Location:* This field gives information about the site name, the stakeholder, and the geographical coordinates of the point source.
- *Toxicant load:* In this field, the effluent flow and density, the discharged substances and their concentration are specified. Furthermore, the environmental quality standards (AA-EQS and MAC-EQS) set in the Directive 2013/39/UE at European level for these substances are displayed (EU 2013).
- *Discharge mechanism:* For a single-port discharge, the main geometrical characteristics are the pipe

SUMMARY SHEET OF TOXICANT DISCHARGES

NAME

CODE

Location

UMTX (ED50)
UTMY (ED50)

Site name
Holder

Toxicant load

Flow m^3/s

Salinity psu
Temperature ºC

Toxicant	Concentration (mg/l)	AA-EQS (mg/l)	MAC-EQS (mg/l)

Discharge mechanism

Pipe diameter m

Angle with shoreline º

Mean depth in the receiving water m

Discharge depth (from bottom) m

Figure 3.4: Summary sheet to characterize the industrial wastewaters discharged to the estuarine environment.

diameter, the angle with the shoreline starting at north and counting in the clockwise direction (Figure 3.5), the mean depth in the receiving water and the depth of the point discharge.

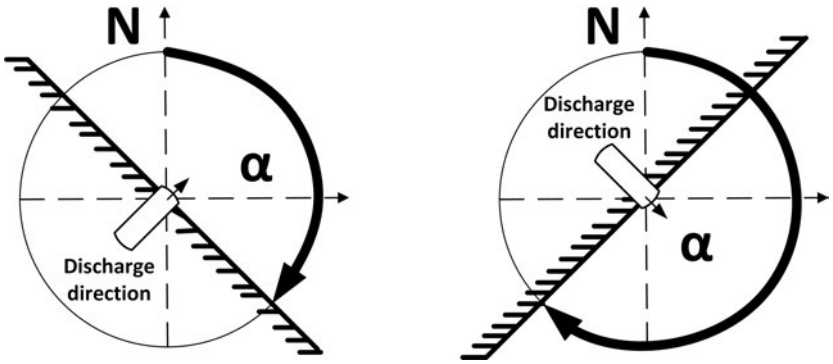

Figure 3.5: Scheme of how to measure the angle with the shoreline

Finally, it is worthy to mention that the vertical angle of the pipe with a horizontal reference plane is considered zero for all discharges. In these type of discharges, this configuration is the most common unlike for hyperdense discharges.

3.1.2 Study area

On the other hand, characterization of receiving waters is a crucial task to understand the toxicant dispersion. The estuary description is here organised in terms of physical features, hydrographic features and protected areas. Firstly, the physical features represent the dimensions of an estuary. Secondly, the main hydrographic features of the estuary are described and, thirdly, the protected areas of the estuary (if any) are enumerated. To facilitate this task, a new summary sheet has been developed in order to review and show the starting available information about the study area (Figure 3.6).

SUMMARY SHEET OF STUDY AREA

NAME

CODE

Physical features

	Geomorphological type	Source		Type		
	Bathymery	Source		Map		
	Estuarine total area	Source		Value		m^2
	Intertidal area	Source		Value		m^2
	Maximum, minimum and mean widths	Source		Value		m
	Maximum, minimum and mean depths	Source		Value		m
	Main channel length	Source		Value		m

Hydrographic features

	Tidal range distribution	Source		Value		m
	River flow distribution	Source		Value		m^3/s
	Maximum, minimum and mean salinities	Source		Value		psu

Protected areas

	General area	Source		Value		m^2
	Fish	Source		Value		m^2
	Shellfish	Source		Value		m^2
	Recreational use	Source		Value		m^2
	Vulnerable area	Source		Value		m^2
	Sensitivity area	Source		Value		m^2
	Protected habitat	Source		Value		m^2
	Birds	Source		Value		m^2
	Wetlands	Source		Value		m^2

Figure 3.6: Summary sheet to characterize the information about the study area.

Protected Area	International Regulations	Spanish Regulations
General area	Dir/2000/60/EC	TRLA, IPH
Fish	Dir/2006/44/EC	IPH
Shellfish	Dir/2006/113/EC	RD 571/199
Recreational use	Dir/2006/7/EC	RD1341/2007, RD1471/1989, IPH
Vulnerable area	Dir/91/676/EEC	RD261/1996, IPH
Sensitivity area	Dir/91/271/EEC	RDL 11/1995, RD509/1996, IPH
Protected habitat	Dir/92/43/EEC	Ley 42/2007, RD1997/1995, IPH
Birds	Dir/2009/147/EC	IPH
Wetlands	Ramsar	RD435/2004, IPH

Table 3.1: Summary of the legal basis for the designation of protected areas. TRLA is "Texto Refundido de la Ley de Aguas. IPH is "Instrucción de Plan Hidrológica".

- *Physical features:* They are the geomorphological type, the bathymetry, the estuarine total area, the intertidal area, the maximum, minimum and average widths, the maximum, minimum and average depth and the main channel length.
- *Hydrographic features:* The hydrographic characteristics are the tidal range series and distribution, the freshwater flow series and distribution, and the maximum, minimum and average salinities.
- *Protected Areas:* These areas are under special protection due to a special rule for protection of surface water, or conservation of habitats and species directly dependent on water. International agreements, European Directives and/or national and regional legislation establish a number of different categories of protected areas. Table 3.1 summarizes the legal basis for the designation of protected areas.

Note that, in this subsection, we propose to perform a compilation of information that may be helpful at Step 2 of the decision tree. Therefore, in subsequent steps, the need for additional information in order to continue making decisions is determined because it can be an expensive and time-consuming task.

3.2 Step 2. Significance of discharge

The calculation to delimitate areas of environmental risk is a very complex and often specific task for each discharge. This module is designed to detect those discharges that have not significant impact in order to prevent detailed and expensive studies. In the figure 3.7, the flowchart developed to differentiate the entity of discharges are presented.

3.2.1 Potential Risk

This subsection identifies discharges with the potential to exceed the thresholds set in the EQS Directive (EC 2008a, EU 2013), i.e, the AA-EQS and the MAC-EQS, in two substeps:

1. A check is made to see if the discharge is liable to contain any contaminant specified in the EQS Directive. In negative case, the MZs are negligible and the decision tree finishes indicating that there are not MZs and classifying the discharge as a nil discharge (Figure 3.2). On the contrary, there is a potential risk of exceeding the EQS so the discharge moves to the next substep in the decision tree.
2. A check is made to see if the concerned toxicants exceed the EQS. EQS thresholds are surpassed, if the averaged concentration of the effluent is greater than AA-EQS or the maximum concentration of the

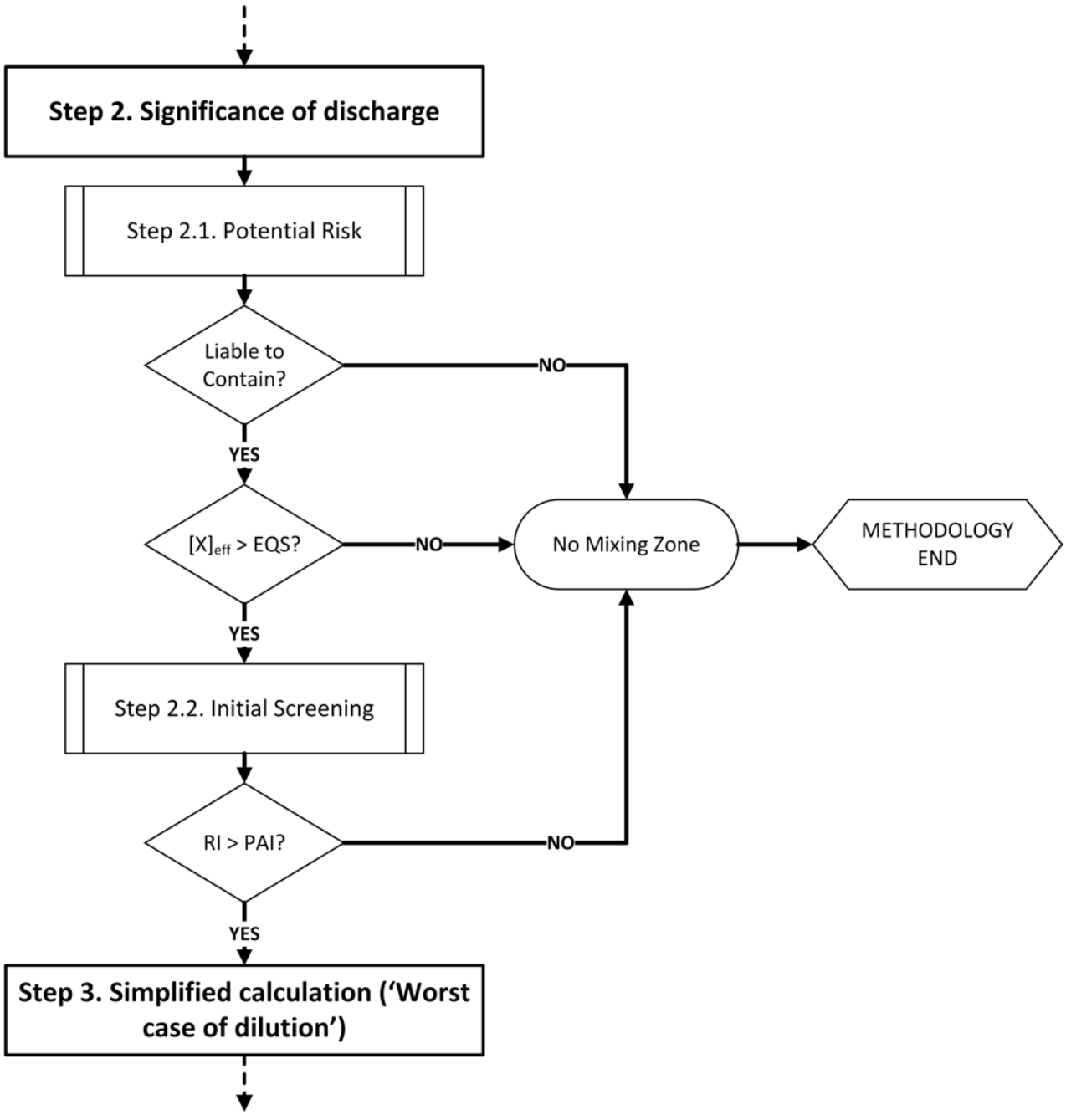

Figure 3.7: Developed Flowchart of the Step 2. Significance of discharge.

Water types	Net flow (Q10-flow) [m3/s]	PAI after complete mixing as % EQS
Small	$Q \leqslant 100$	4.0
Medium	$100 < Q \leqslant 300$	1.0
Large	$Q > 300$	0.5

Table 3.2: Proposed allowable increase (PAI) in concentration after complete mixing for different water types. Source: EC (2010).

effluent is greater than MAC-EQS. If both concentrations are smaller than EQSs and no other discharge is releasing the same toxicants, the MZs are negligible. Again, there are not MZs and the decision tree finalizes. We classify these discharges as risky discharges (Figure 3.2). On the contrary, there is an evidence of exceeding the EQS so the discharge moves to the next substep in the decision tree to determine its significance.

3.2.2 Initial Screening

In this subsection, a rapid estimate of the impact generated by the risky discharges is carried out using simple formulations (EC 2010). Initial screening test ignores the additional mixing afforded by the tidal exchange and the background concentration, but offers a preliminary assessment of significance. The objective is to determine the process contribution (PC) of the discharge to the EQS after full mixing, this is defined in equation (3.1):

$$PC = \frac{[X_{med}]_{eff} \cdot Q_{eff}}{(Q_{river} + Q_{eff})} \tag{3.1}$$

This test is only applied to the AA-EQS using the mean concentration ($[X_{med}]$), the mean effluent flow (Q_{eff}) and the river flow not exceeded during 10% of the time (Q_{river}).

The relative increase (RI) of the PC as a percentage of the EQS (equation (3.2)) needs to be checked with the proposed allowable increase (PAI) given in table 3.2 (EC 2010).

$$RI = \frac{PC}{EQS} \cdot 100\% \tag{3.2}$$

If the increase in PC is less than a percentage of EQS value in table 3.2 then the discharge is insignificant. However, before it can finally be accepted, a check should be made to determine if the location of the point discharge is the likelihood of an adverse impact on any protected area specified in Step 1. On the contrary, the discharge is classified as significant moving to the Step 3 of the decision tree in order to continue with the allocation procedure (Figure 3.2).

3.3 Step 3. Simplified calculation (Worst case of dilution)

Once the significant discharges has been detected, we start to apply the Step 3 of the decision tree. The proposed simplified calculation is based on the analysis of the "worst case of dilution". In this case, physical dilution is the only mechanism responsible for the toxicant decay in the near- and the far-field so toxicants are considered conservative tracers and hydrodynamics forcings are established from a precautionary approach where the achieved dilution is minimum.

Step 3 is composed by 6 subsections as illustrated in figure 3.8. Along the calculations of this work, it can be employed any hydrodynamic, near-field and far-field models suggested on Chapter 2.

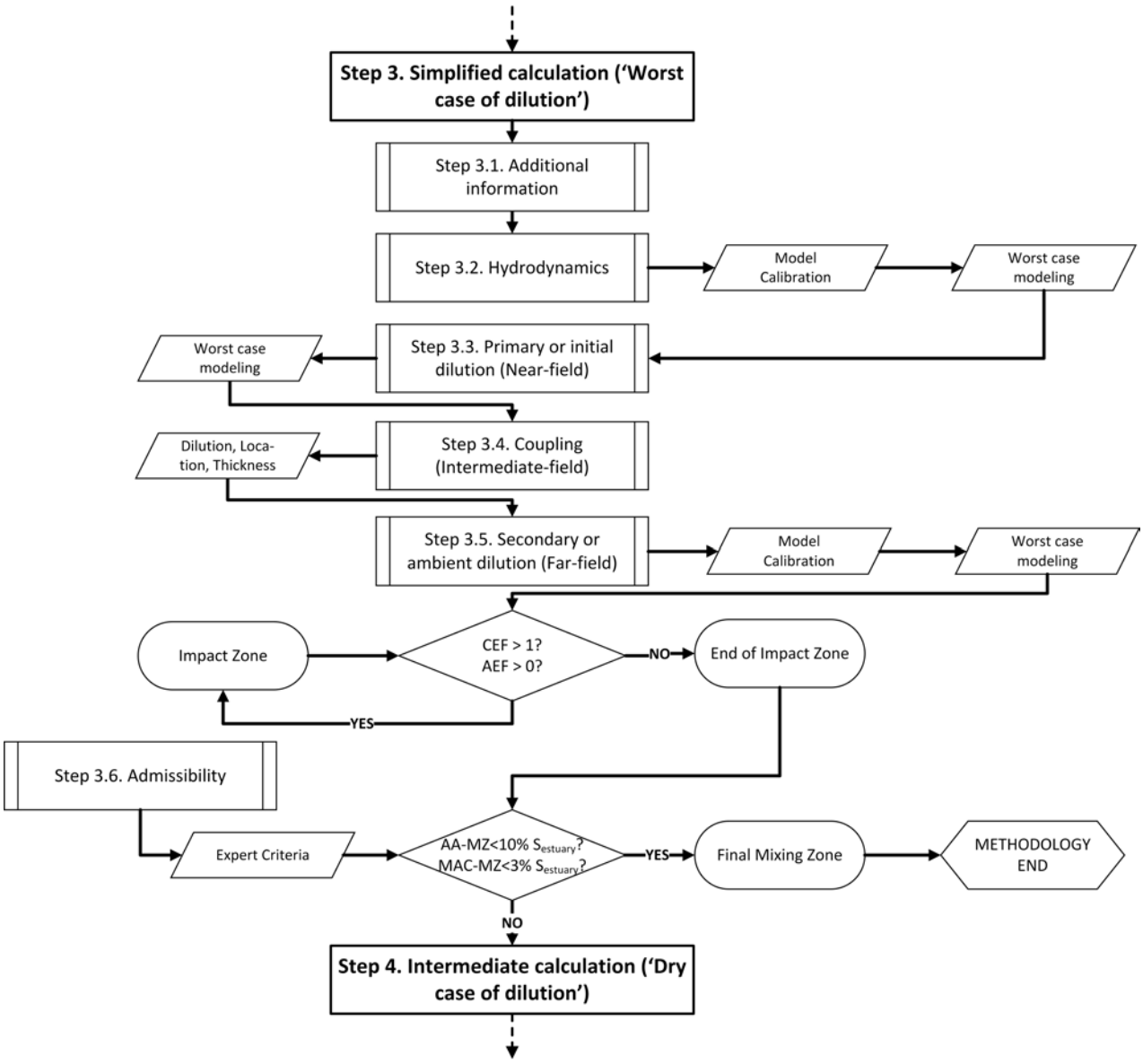

Figure 3.8: Developed flowchart of the Step 3. Simplified calculation (Worst case of dilution).

First, the additional required information for the simplified calculation is compiled in 3.3.1. Additional information. In 3.3.2. Hydrodynamics, the requirements for setting up the model and the specification of the model scenario are described. Next subsection, 3.3.3. Primary or initial dilution (Near-field) explains the approach used for the simulation of the "worst case of dilution" with a initial dilution model. In 3.3.4. Coupling (Intermediate-field), the procedure developed to integrate the outputs of the initial dilution model into the far-field model are explained. In the subsection 3.3.5. Secondary or ambient dilution (Far-field), the required tasks to conduct the simulation of the significant discharges with far-field models taking into account, as inputs, the results of the hydrodynamic model and the coupling are described. Finally, after model runs, the extent and acceptability of the MZs are delimitated according to the admissibility criteria defined in the subsection 3.3.6. Admissibility.

3.3.1 **Additional information**

In this subsection, the additional information to carry on the required tasks of Step 3 is gathered. This information is related to measurements (field data) necessary to conduct the model setup of numerical models. Thus, the survey data should include at least:

- Measurements of tidal water levels at two points across the estuary every 15 minutes during 15 days.
- Measurements of instantaneous river flows in a section non-influenced by the tide every 24 hours during 15 days.
- Vertical profiles of instantaneous current (speeds and directions) at two points across the estuary on neap and spring tidal conditions. For both spring and neap tidal conditions, the measurements should include two values at high, ebb, low and flood tidal phases, i.e., two tidal cycles (within the 15 days period).
- Salinity profiles at two points across the estuary on neap and spring tidal conditions. For both spring and neap tidal conditions, the measurements should include two values at high, ebb, low and flood tidal phases, i.e., two tidal cycles (within the 15 days period).

Moreover, field data of temperature and salinity are required to define open boundaries. Therefore, measurements of both variables should be available at one point in the open-river boundary and one point in the open-sea boundary during one year with seasonal frequency.

3.3.2 **Hydrodynamics**

Spatial and temporal evolution of any substance present in the water column in the estuarine environment is subject to know the velocity field at each point of the interest area. For modeling water levels, currents and salinities, the numerical integration of the equations of momentum, continuity and transport is performed using numerical methods that need to generate a grid that covers the area of interest and containing the depths at each point. The forcing is the different physical phenomena responsible for generating the movement of water.

The hydrodynamic model must be calibrated to demonstrate its validity for the representation of the phenomena being analyzed using available information gathered in the previous subsection. At least the hydrodynamic model must include tidal forcing, Coriolis force, density driven flows (pressure gradient terms in the momentum equations), an advection-diffusion solver to compute density gradients, coupled source and sink term formulations and space and time varying wind fields and atmospheric pressure.

3.3.2.1 Model setup

Model setup is required to define the model domain discretization, to provide boundary and initial conditions and, finally, to carry on the model calibration/validation in order to select the best configuration of model parameters (Figure 3.9).

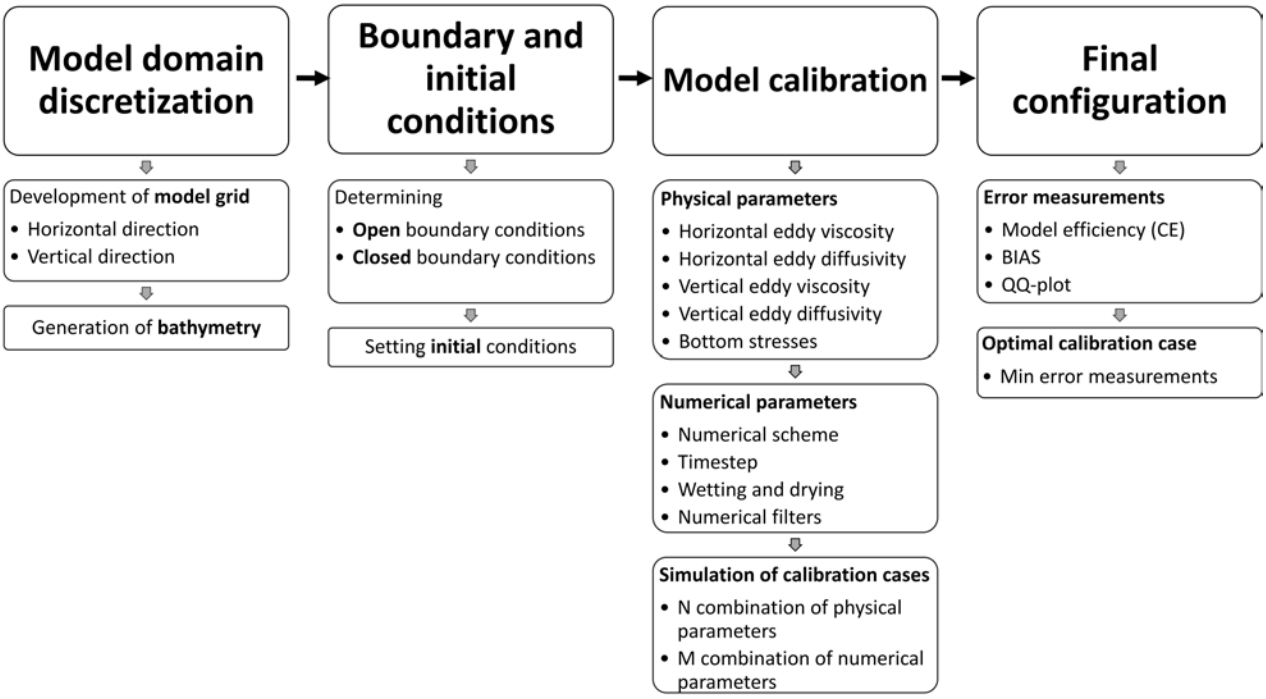

Figure 3.9: Scheme of involved tiers of the hydrodynamic model setup.

Model domain discretization

Model domain discretization consist on the definition of each node of the model grid in the horizontal and vertical direction and the generation of a bathymetry, i.e., the determination of depths at each node of the model grid according to the available data of the study area.

In the horizontal direction, Castanedo (2000) and García (2004) suggested the use of orthogonal rectangular coordinates when the model domain has simple geometry and curvilinear coordinates when the geometry is complex.

Regarding the vertical direction, the σ-coordinate system seems to be the most adequate because the bottom boundary and free surface are represented smoothly, the water column is divided into the same number of layers independent of the water depth and the vertical resolution increases automatically in shallow areas. However, for steep bottom slopes combined with vertical stratification, σ-transformed grids introduce numerical problems for the accurate approximation of horizontal gradients both in the baroclinic pressure term and in the horizontal diffusion term (Figure 3.10). Due to truncation errors, artificial vertical mixing and artificial flow may occur (Castanedo 2000, García 2004). Near steep bottom slopes or near tidal flats where the total depth becomes very small, truncations errors in the approximation of the horizontal diffusive fluxes in σ-coordinates are likely to become very large.

This is why both authors (Castanedo 2000, García 2004) suggested the use of σ-coordinate system with a σ-correction based on horizontal gradients of Z-coordinate system in shallow waters and estuaries. In this σ-correction, the horizontal diffusive fluxes and baroclinic pressure gradients are approximated in Z-coordinates by defining rectangular finite volumes around the the σ-coordinate grid points.

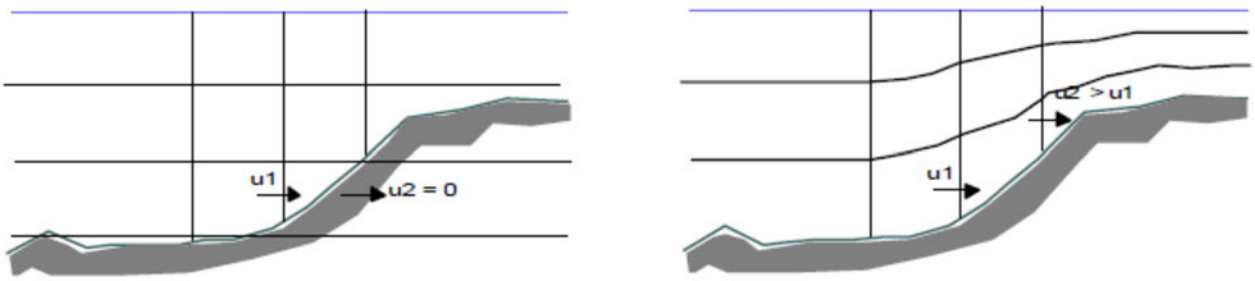

Figure 3.10: Problem of the σ-coordinate system in the bottom. Source: Castanedo (2000).

Boundary and initial conditions

Open and closed boundary conditions

In order to minimize the impact of errors originating from the open boundaries (OBs), the general rule is that the farther away the OB is from the area of interest, the less these OBs errors will affect the model results. In designing the model domain, therefore, OBs should be delineated at a sufficient distance away from the interior, so that these errors does not influence the solution within the region of interest. Since there are no general laws to prescribe them, extrapolation, approximation, and/or assumption must be used in order to obtain boundary conditions. A variety of OBs have been proposed in the literature (see Chapter 2).

Closed boundaries (CBs) are defined by the known shoreline, the bathymetry and the free water surface. The flow through these boundaries is set to zero. The vertical diffusive flux through the free surface and bed is also set to zero except for the heat flux through the free surface. Shear stresses act on all CBs. However, the influence of the lateral shear stresses along the lateral boundaries may be neglected.

Initial conditions

The initial conditions (IC) are starting values of the parameters of an equation which are used in calculating numerical solutions.

In order to run the hydrodynamic model, it is necessary to prescribe boundary and initial conditions taking into account the main forcings responsible of the water movements and the physical properties such as temperature and salinity.

Model calibration

The calibration process determines the values of physical and numerical model parameters in order to adjust the results given by the numerical model. Model calibration will focus on adjusting water levels, current speeds and salinities in order to simulate adequately hydrodynamics and transport of conservative tracers.

Physical parameters

Physical parameters are the eddy viscosity and diffusivity (horizontal and vertical) and the boundary stresses (bottom, lateral and surface). Next, we will explain how to evaluate these parameters in the hydrodynamic model according to different formulations and coefficients.

- *Horizontal eddy viscosity* (μ_H): The eddy viscosity is used to describe turbulence. The value of this coefficient depends on the grid cell dimensions and it can be estimated from equation (3.3) (Fischer *et al.* 1979):

$$\mu_H = K \Delta x u_{ch} \tag{3.3}$$

  where K is a calibration constant, Δx is the grid cell size (m) and u_{ch} is a characteristic velocity of the study area. K ranges between 0.05 and 0.15 and is the calibration parameter to obtain μ_H.

- *Horizontal eddy diffusivity* (D_H): The transport modeling of conservative tracers and heat is conducted by means of the 3D advection-diffusion equation where DH is the horizontal eddy diffusivity. D_H is calculated with the equation (3.4).

$$D_H = \frac{\mu H}{\sigma_t} \tag{3.4}$$

  where σ_t is the turbulent Schmidt number, ranging from 0.7 to 1 and it is the calibration parameter to obtain D_H.

- *Vertical eddy viscosity* (μ_V): Turbulence closure models account for the vertical eddy viscosity based on the eddy viscosity concept. As it was mentioned in Chapter 2, there are a great variety of turbulence closure models such as non-equations models where μ_V is a constant value, zero equation models where μ_V is calculated by means of an algebraic formulation, one equation models where μ_V is calculated by means of one transport differential equation and an algebraic formulation and two equation models where μ_V is calculated solving a system of two transport differential equations.

  Unfortunately, there are not guidelines to help in the selection of the turbulence closure model. This is why μ_V should be determined by a calibration process of trial and error. The best fitting between model data and field data gives the suitable model in a specific-case basis.

- *Vertical eddy diffusivity* (D_V): Similarly as D_H is calculated based on μ_V and σ_t by means of the equation (3.5).

$$D_V = \frac{\mu V}{\sigma_t} \tag{3.5}$$

  where σ_t is the turbulent Schmidt number, ranging from 0.7 to 1 being the calibration parameter to obtain the D_V.

- *Bottom stresses*: For 2D flows, bottom stresses are obtained from equation (3.6):

$$\overrightarrow{\tau_b} = \frac{\rho_{env} g \overrightarrow{u} |\overrightarrow{u}|}{Ch^2} \tag{3.6}$$

  where $|\overrightarrow{u}|$ is the magnitude of the depth-averaged horizontal velocity and Ch is the Chezy coefficient, i.e., bottom roughness. In the case of 3D flows, bottom stresses are obtained from equation (3.7):

$$\overrightarrow{\tau_{b3D}} = \frac{\rho_{env} g \overrightarrow{u_b} |\overrightarrow{u_b}|}{Ch^2} \tag{3.7}$$

  where $|\overrightarrow{u_b}|$ is the magnitude of the bottom-layer horizontal velocity.

  Bottom roughness can be introduced directly as Chezy coefficient or through formulations such as Manning or White-Colebrook.

  Independently of bottom roughness, rugosity can also be introduced as a constant value or spatially varying depending on the depth of grid cells (Cheng *et al.* 1993, Dias & Lopes 2006, Dias *et al.* 2009, Iglesias & Carballo 2010).

- *Lateral stresses*: In estuarine hydrodynamic simulations, the tangential shear stress for all lateral boundaries or vertical walls can be safely neglected (free-slip condition).

Numerical parameters

Numerical parameters are those features that ensure the correct discretization (numerical schemes) and solving (timestep, numerical filters,...) of the governing equations of the hydrodynamic and transport (conservative approach) models.

- *Numerical scheme:* Important features of numerical schemes are accuracy (determined by the order of the scheme), robustness (stability and positivity) and efficiency. Solution of the shallow water and transport equations with computers requires the use of discrete segments in space with finite mesh sizes Δx, Δy and Δz and with a finite time-step Δt.

  Various options for discretizing the partial differential equations in terms of Δx, Δy, Δz and Δt are possible. These options are called numerical discretization schemes. For example, for the space discretization central discretization or upwind discretizations may be applied. For the time integration, explicit, semi-implicit or implicit methods may be chosen. Having the numerical discretization different strategies, any of these can be followed to solve the discretized systems of equations.

- *Timestep:* To ensure the hydrodynamic model stability and accuracy, the Courant-Friedrichs-Levy number (CFL) is used (Equation (3.8)).

$$\Delta t \leq \frac{\Delta x CFL}{\sqrt{gH_{max}}} \tag{3.8}$$

  where Δt is the timestep, Δx is the grid cell length and H_{max} is the maximum depth in the study area.

  Moreover, to ensure the transport model (conservative tracers) stability and accuracy, the Peclet number (Pe) is used (Equation (3.9)).

$$\Delta t \leq \frac{Pe}{\frac{D_x}{\Delta^2 x} + \frac{D_y}{\Delta^2 y}} \tag{3.9}$$

  where Δt is the timestep, Δx is the grid cell length in x direction, Δy is the grid cell length in y direction, D_x is the eddy diffusivity in x direction and D_y is the eddy diffusivity in y direction.

- *Numerical filters:* Filters are available as a method to inhibit artificial mixing both vertically and horizontally. The numerical scheme for the vertical advection of heat and salt (central differences) may introduce small vertical oscillations. This computational noise may enhance the turbulent mixing.

  We advice to activate the vertical filters when the studied estuary may display significant stratification.

- *Wetting and drying processes:* Since there are tidal flats in estuaries, the effects of the moving boundary on the water exchange must be taken into account (Shi & Zhang 2011). Generally, a wet-dry point treatment is the implemented method. This method introduces an additional bottom boundary layer and redefines the total water depth (Hd) as $Hd = H + hc$ where H is real total depth and hc is the thickness of the bottom boundary layer. If H is larger than hc, the point is treated as a wet point and its velocity and elevation are computed from the finite difference equations. Otherwise it remains a dry point where water velocity is equal to zero.

  We recommend to have into account the wetting and drying processes when tidal flats are an important feature in the study estuary.

Simulation-calibration cases

Simulation-calibration cases are all the different model simulations performed by means of N combinations of physical parameters and M combinations of numerical parameters in order to find the best combination of model parameters. Table 5.2 synthesizes the calibration parameters, suggests the best option for estuarine modeling and gives the optimal value ranges of each parameter.

As it can seen from table 5.2, there are a huge range of possibilities to combine model parameters so model calibration is one of the tasks more time-consuming in the methodology. At the same time, model calibration is essential to achieve accurate hydrodynamic and transport results.

Final configuration

Physical parameters	**Suggestions**	**Value ranges**
Horizontal eddy viscosity	Equation (3.3)	k=0.05 to 0.15
Horizontal eddy diffusivity	Equation (3.4)	σ_t=0.7 to 1
Vertical eddy viscosity	Best fitting	Any turbulence model
Vertical eddy diffusivity	Equation (3.5)	σ_t=0.7 to 1
Bottom stresses	Manning	Constant value or Spatially varying
Lateral stresses	Free-slip condition	No roughness
Numerical parameters	**Suggestions**	**Value ranges**
Numerical scheme	Second order accuracy	Any numerical scheme
Timestep	Equations (3.8) and (3.9)	CFL<1 and Pe<0.5
Numerical filters	Activated	Vertical artificial mixing
Wetting and drying	Activated	threshold depth$\leq$0.1 m

Table 3.3: Overall picture of hydrodynamic model calibration parameters.

The final configuration of the model is the combination of values of model parameters that best match the results obtained by the model and the data measured in the study area.

Error measurements

In order to find the optimal calibration case, two error measurements are calculated: the BIAS and the model efficiency (CE). For each simulation-calibration case, we compare the values of the model data and the survey data in terms of water levels, current velocities and salinities.

First, BIAS is calculated by means of equation (3.10) and is defined as the difference, at the same date, between model results and real values.

$$BIAS = \sum_{i}^{N} \frac{S_i - R_i}{N} \tag{3.10}$$

where R_i is the i-field data of the measurements, S_i is the i-model data of the simulations and i is the i^{th} value from 1 to N measurements.

BIAS is the systematic error resulting in deviation in estimates of model simulations and leading to an under-estimation or an overestimation of results. A study with a small BIAS is said to have a high accuracy.

Second, the error between both series using the Model efficiency (CE), displayed in equation (3.11) and developed by Nash & Sutcliffe (1970) is calculated. CE was employed for two major reasons: (1) it is very commonly used in river and estuary model applications (Drewry *et al.* 2009, García *et al.* 2008, García-Alba *et al.* 2014, Krishna-Prasad *et al.* 2011, Moriasi *et al.* 2007, Sevat & Dezetter 1991, Usaquén *et al.* 2012, Wagner *et al.* 2011), and (2) Sevat & Dezetter (1991) also found CE to be the best objective function for reflecting the overall fit of a model output.

$$CE = 1 - \frac{\sum_i^N (R_i - S_i)^2}{\sum_i^N (R_i - \overline{R}_i)^2} \tag{3.11}$$

where R_i is the i-field data of the measurements, S_i is the i-model data of the simulations, $\overline{R}_i$ is the average of the measurements and i is the i^{th} value from 1 to N measurements.

CE is a normalized statistic that determines the relative magnitude of the residual variance ("noise") compared to the measured data variance ("information"). CE indicates how well the plot of observed versus simulated data fits the 1:1 line (Nash & Sutcliffe 1970). CE ranges between $-\inf$ and 1.0 (1 inclusive), with CE equals 1

being the optimal value. Values between 0.0 and 1.0 are generally viewed as acceptable levels of performance whereas values <0.0 indicates that the mean observed value is a better predictor than the simulated value, which indicates unacceptable performance.

If the CE is lower than 0.5 the comparison is considered poor, if the CE is higher than 0.6 and lower than 0.8 the comparison is convenient (good) and if the CE is higher than 0.8 the comparison is considered excellent.

Optimal calibration case

From error measurements of every simulation-calibration case, the optimal calibration case is the case simultaneously displaying the minimum BIAS and the maximum CE. Therefore, this combination of model parameters will be used along the rest of the methodology for conducting hydrodynamic simulations.

Finally, it is worthy to mention that the described calibration methodology has been encoded using the mathematical software MATLAB (see more information on Chapter 4).

3.3.2.2 Hydrodynamic worst case modeling

The hydrodynamic model predicts the surface elevation, current velocity, salinity and temperature fields across the model grid. Moreover, it provides the flow and dispersion data that can be used to run the transport models in the near- and far-field regions. Although hydrodynamic models can be quite time-consuming, once run the output files can be used to model scenarios for different wastewater locations and conditions.

In order to run the "worst case of dilution", we propose that this scenario assumes fixed conditions of the forcing. Following the proposals made by other methodologies (Hansler & Fikslin 1995, Hansler *et al.* 1998, LDEQ 2010, USEPA 1991), we select the following forcings:

- Tidal amplitude is constant and equal to the A10, i.e., forcing value that is not exceeded during the 10% of the time.
- River flow is constant and equal to the 7Q10, i.e., forcing value that is not exceeded during the 10% of the time, taking into account the average of 7 consecutive days.

The value of A10 and 7Q10 will be extracted from the analysis of the astronomical tide and river flow series.

This model scenario is simulated until reach a "quasi-stationary" response for hydrodynamics, i.e., hydrodynamic variables display a modulated signal because of tides and river discharges and their magnitudes are not varying with the tidal period. Thus, the effect of the initial conditions are minimized on the numerical simulations.

Once it is reached this situation, we record hourly one day of hydrodynamic model results (24 data). Figure 3.11 illustrates an example of the evolution of water levels (a), velocities (b), salinities (c) and temperatures (d) in a arbitrary grid cell where the "quasi-stationary" response is highlighted respectively.

Regarding the timescales of the "quasi-stationary" response, it should be underlined that this timescale depends on the studied hydrodynamic variable. Water levels and velocities react to the tidal forcing sufficiently fast, thus these variables may reach equilibrium in 1-2 tidal cycles. Quantities such as salinity, temperature may need 4-12 or even more tidal cycles to reach equilibrium because dispersion/diffusion is a slower process.

3.3.3 Primary or initial dilution (Near-field)

In this subsection, the required tasks to carry out the simulation of buoyant jets with initial dilution models taking into account, as inputs, the results of the hydrodynamic model are described.

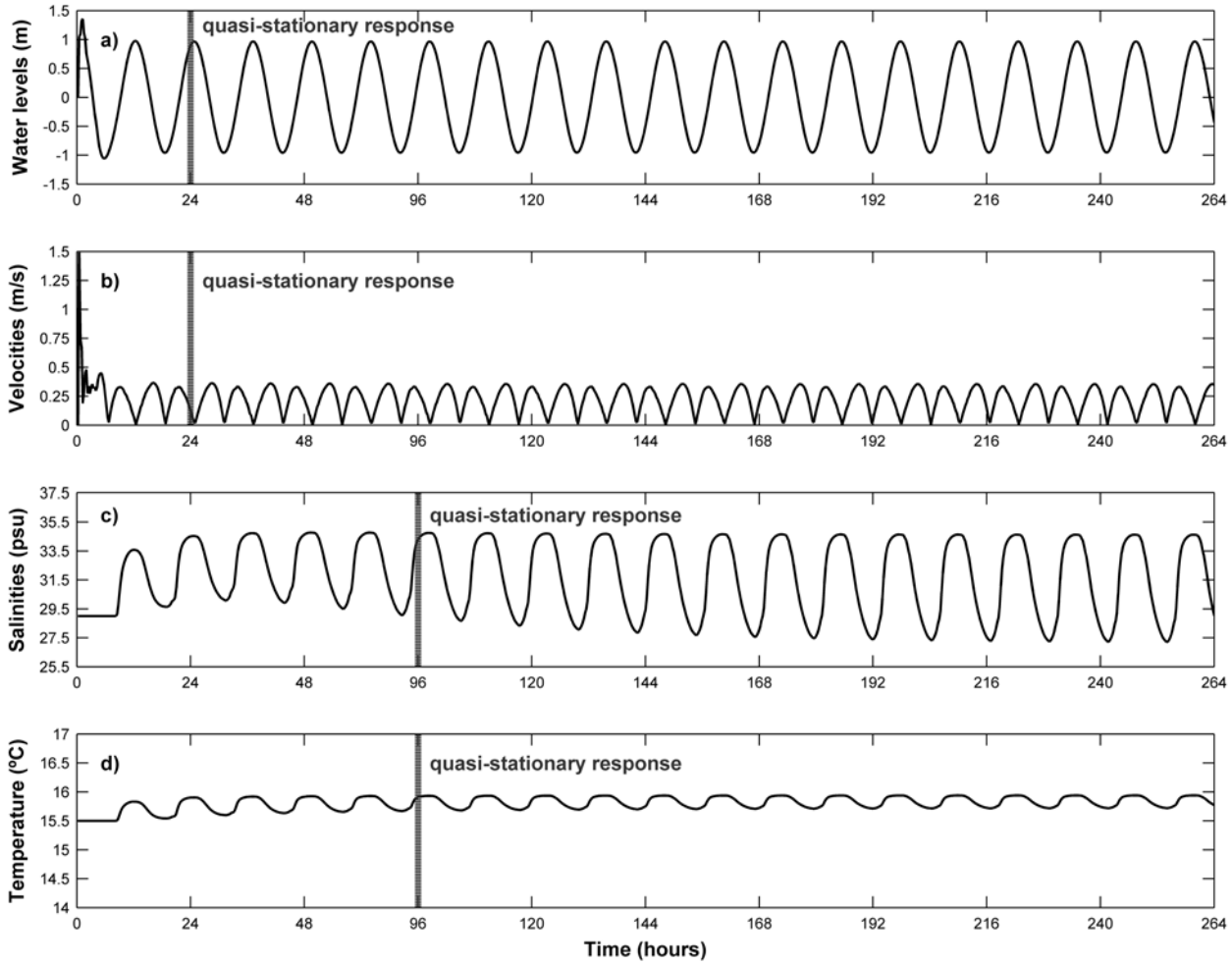

Figure 3.11: Example of the evolution of water levels (a), velocities (b), salinities (c) and temperatures (d), and timescales of the "quasi-stationary" response for hydrodynamics.

The buoyant jet behavior depends on the discharged effluent flow (Q_{eff}), the pipe diameter of the single-port (ϕ), the distance of the single-port to the bottom (d_{eff}), the density of the discharged effluent (ρ_{eff}), the density of the receiving water (ρ_{env}), the total depth of the water column (H) and the environmental current velocity (u_{env}). Additionally, it is worthy to mention that the behaviour of the primary dilution is essentially 3D because of the movements experimented by the buoyant jet.

The first four variables are attached to the discharge mechanism, they are independent for every discharge and the value of each variable is collected in the Step 1. The remaining variables are related to the environmental conditions, they are dependent of the hydrodynamic changes and the single-port location. The value of each variable is extracted from the hydrodynamic modeling of the "worst case of dilution".

Once the most important variables for the calculation of initial dilution have been set, different formulations or numerical models can be used to calculate the evolution of the effluent such as UM3, CORJET, JETLAG or MOHIDJET.

The primary dilution computations are conducted for every discharge classified as significant in Step 2, taking into account:

- All substances are considered conservative tracers. According to Jirka (2004) and Jirka *et al.* (2004), this hypothesis is correct for most applications since the residence time in the discharge areas are typically short (seconds to hours). Therefore, in these areas the processes of toxicant degradation are generally negligible since the time scales of these processes are of the order of days, months or years.
- Environmental variables (ρ_{env}, H and u_{env}) are hourly extracted at every single-port location from the 3D hydrodynamic modeling results. We assume an offline linkage where the output for hydrodynamic model is the input for the entire time of interest in the near-field model.
- The most important results obtained from the use of these initial models are the minimum primary dilution (S_n), the location (x, y, z) and the plume thickness (h_n) at the end of the near-field. These variables will be used for coupling the primary and secondary dilution in the intermediate-field in the next subsection.

Finally, it should be mentioned that a script was developed for reading all these results and graphing in a three-dimensional space each "plume element" as a sequential series of cylinders until reach the end of the near-field. Figure 3.12 displays an example of this graphical representation of the near-field in a 3D view. The described computation methodology has been encoded using the mathematical softwares PYTHON and MATLAB (see more information on Chapter 4).

3.3.4 Coupling primary and secondary dilution (Intermediate-field)

In this subsection, the required tasks to perform the coupling between the near-field model and the far-field models are described. For the study of the effluent dispersion, i.e., the analysis of what has been called the far-field, it is necessary to know the jet-plume concentrations at the end of the near-field when jet-plume velocities are predominantly horizontal and its movement is conditioned by the advection-dispersion dynamics.

As it was mentioned in Chapter 2, coupling models introduce flow quantities (e.g. momentum or mass) from one model into the other and vice-versa. In this methodology, we propose, develop and programme the following coupling between both models. The coupling is based on Bleninger & Jirka (2004), Kim *et al.* (2002), Zhang & Adams (1999).

- We assume a passive coupling where the source-induced flow, though considerably important for near-field mixing, does not change the flow characteristics of the far-field, beyond the near-field or

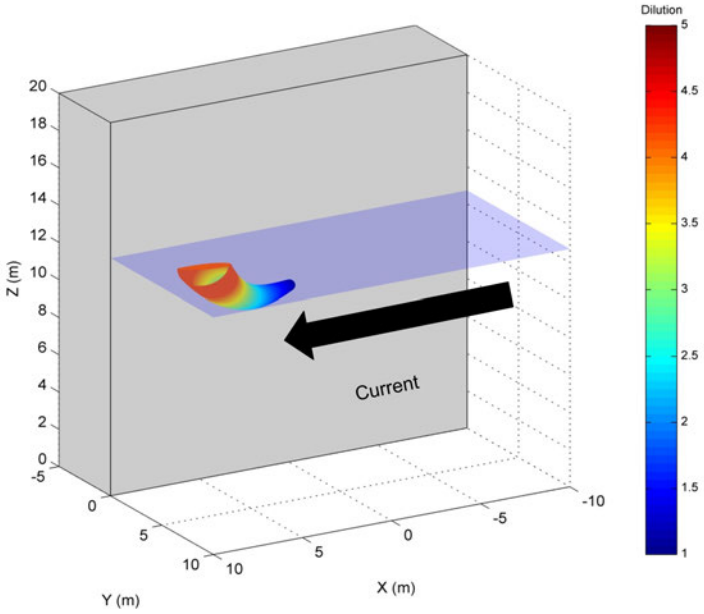

Figure 3.12: Example of a 3D buoyant jet graphic.

intermediate-field region. Thus, specific values of flow rates and toxicant concentration values of the discharge are determined by the near-field model. Then, these are introduced at specific locations of the far-field model without any feedback of the far-field computations to the near-field model.

- We generate an offline linkage where the output for near-field model is the input for the entire time of interest in the far-field model. This output is then specified as boundary or source condition for the other model in a subsequent simulation. This is simple from the viewpoint of computation and data management, but obviously, there is a limited feedback between the two separate simulations. The amount of programming necessary is much less than for online coupling due to the clear separation of computations.

- We introduce both the flow and the diluted concentration of the discharge at the predicted trap height. At each time step, the primary dilution will become concentration in each of the grid cells that are affected at the end of the near-field with a hourly frequency. Based on the thickness and the trap height of the jet-plume, the vertical layers of the far-field model, where will be introduced the discharge, are established (Figure 3.14). Furthermore, the horizontal grid cells where will be introduced toxicant concentrations are identified with the length, width and direction of the jet-plume at the end of the near-field (Figure 3.15).

- It is necessary to correct the flow information to preserve the mass in the far-field model when introducing the discharge in several layers. To solve this issue, we consider that the discharge flow on each layer is the ratio between the total flow and the number of layers covered by the intermediate-field ($Q_{layer} = Q_{total}/n^{o}{}_{layers}$).

- Because integral jet models do not take into account the interaction with boundaries, we consider that the near-field ends when the jet-plume touches any boundary (free surface, stratified layer or lateral boundaries). At this location, the primary dilution finishes and the affected vertical layers are determined by the thickness of the jet-plume in the case of the free surface and stratified layer. In the case of lateral boundaries or walls, these affected vertical layers goes from the impact height to the free surface (Figure 3.13).

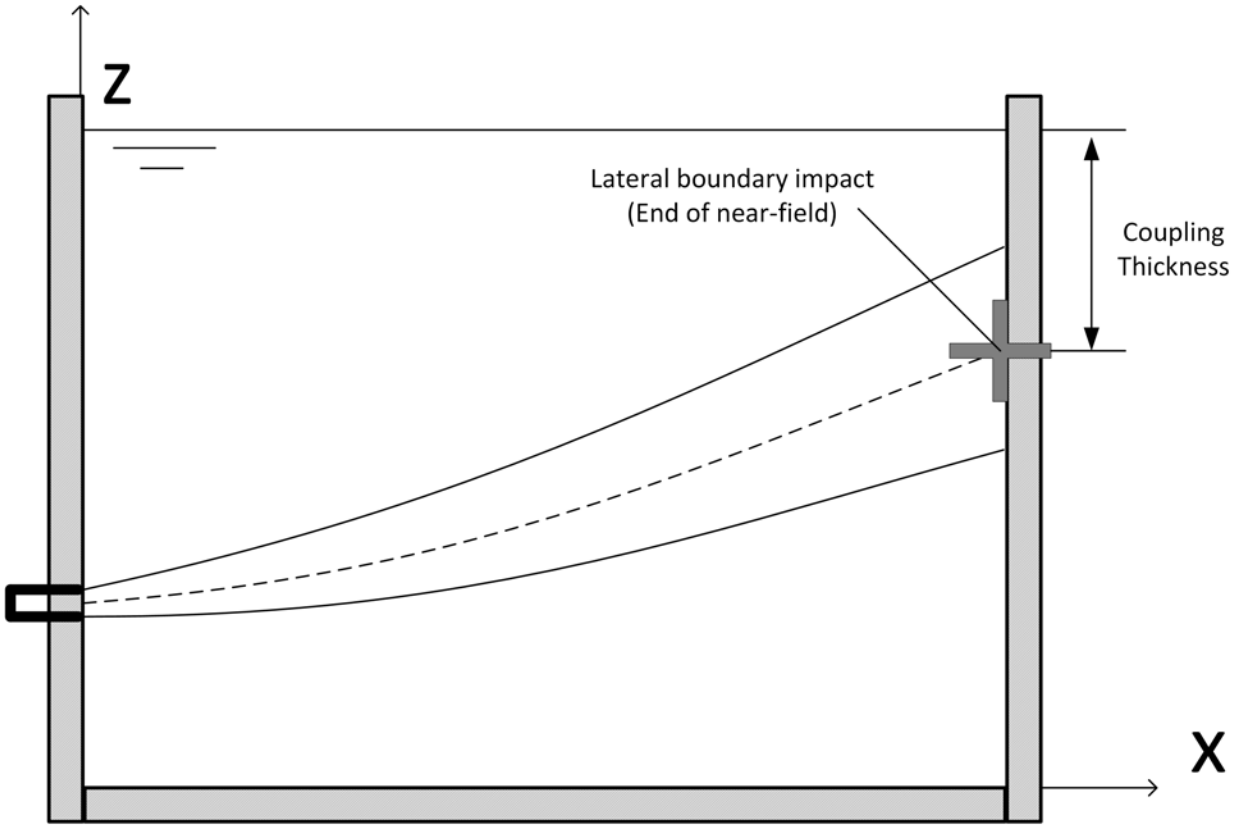

Figure 3.13: Sketch of the coupling boundary interaction in a side view.

This methodology can be seen graphically in figures 3.14 and 3.15, in which the transfer of near-field model results to the far-field model, taking into account the information given by the hydrodynamic model, is shown in a side view and plan view, respectively.

Additionally, it is significant to mention that the described coupling algorithm has been encoded using the mathematical softwares PYTHON and MATLAB (see more information on Chapter 4).

3.3.5 Secondary or ambient dilution (Far-field)

In this subsection, the required tasks to conduct the simulation of the significant discharges with far-field models are described. This simulation takes into account, as inputs, the results of the hydrodynamic model and the previous coupling (intermediate-field). We suggest the use of a 3D far-field model, involving the solution of the advection-diffusion equation, dividing the study area into square or curvilinear grids. The local variation of the concentration in the time unit is considered to originate as a consequence of two transport processes: advection (due to the existing hydrodynamic currents) and diffusion (through the effects of turbulent phenomena).

3.3.5.1 Model setup

The same way as for the hydrodynamic model (Figure 3.9), the first task for modeling the advection and dispersion of toxicants is setting up the transport model. This is required to define the model domain discretization, to provide boundary and initial conditions and, finally, to carry on the model calibration/validation.

Model domain discretization

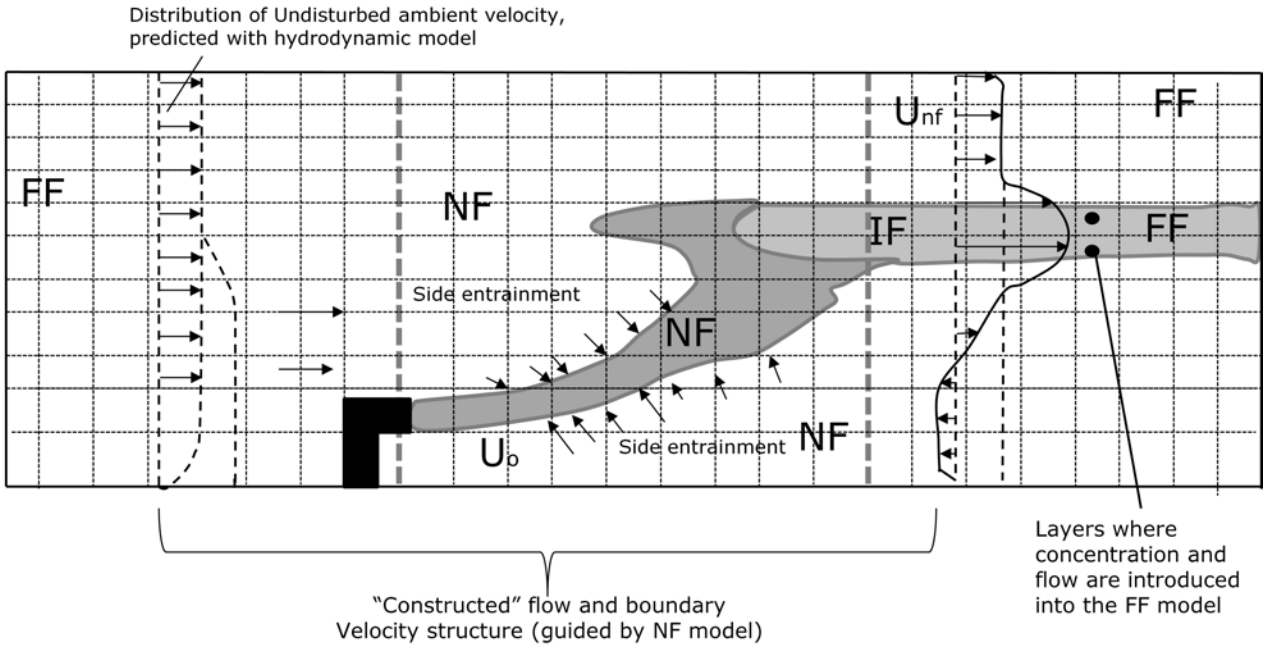

Figure 3.14: Sketch of the coupling using hydrodynamic information between near- and far-field in a side view.

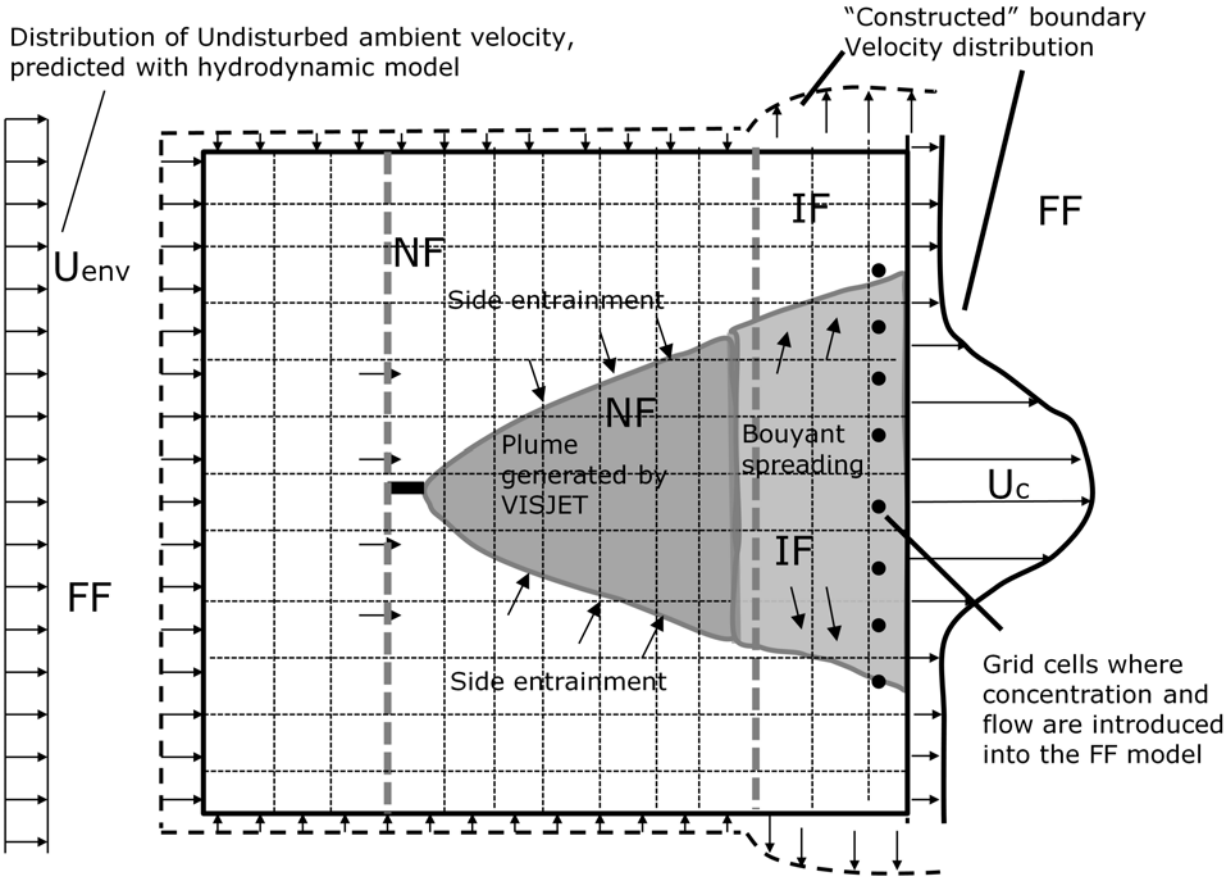

Figure 3.15: Sketch of the coupling using hydrodynamic information between near- and far-field in a plan view.

The model domain discretization is the same that it was used for the hydrodynamic model setup, i.e., the transport model grid has the same number of nodes (grid cells) and layers. No horizontal and/or vertical aggregation was used.

Boundary and initial conditions

Open and closed boundary conditions

In designing the model domain, OBs should be delineated at a sufficient distance away from the interior so the errors do not influence the solution within the interior domain. In this way, OBs can be set as a clamped (or specified) boundary condition with a constant value set to zero.

CBs are set to zero. The vertical diffusive flux through the free surface and bed is also set to zero.

Initial conditions

In order to run the transport model, it is necessary to prescribe ICs taking into account the main sources responsible of the evolution of a toxicant in the water column (industrial discharges). Due to the field of conservative tracer in the study area is unknown, the initialization of the transport model sets to zero all the modelled conservative tracers.

Therefore, the system requires a response time in order to achieve a "quasi-stationary" state where the obtained results are reliable. Figure 3.16 illustrates the initialization and the "quasi-stationary" state for the concentration evolution of a grid cell. This state is reached because the methodology assumes fixed conditions of forcings and constant flow and concentration of discharges.

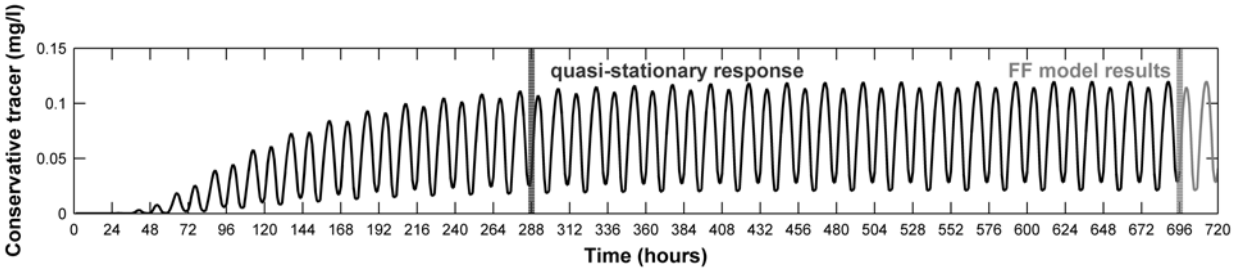

Figure 3.16: Example of the evolution of a conservative tracer, timescale of the "quasi-stationary" response and recorded period for the transport of a "worst case of dilution".

Model calibration

Due to the toxicants are considered conservative in this Step, the physical parameters calibrated in the hydrodynamic model are the same for the transport model and, consequently, calibration is not necessary to conduct.

Physical parameters

Physical parameters are the horizontal and vertical eddy diffusivity when all substances are considered conservative tracers.

Numerical parameters

In the case of far-field models, it should be underlined that the finite volume method (FVM) is the best computational method to solve the "advection-diffusion-(reaction)" equation because it is mass-conserving by definition.

Physical parameters	**Suggestions**	**Value ranges**
All parameters	Same hydrodynamic model	Hydrodynamic calibration
Numerical parameters	**Suggestions**	**Value ranges**
Numerical scheme	Best fitting	Any Scheme (FVM)
Timestep	Equation (3.9)	Pe<0.5
Numerical filters	Activated Activated Activated	No dispersion over tidal flats No dispersion over OB No negative values

Table 3.4: Overall picture of far-field model calibration parameters for conservative approach.

- *Numerical scheme:* Important features of numerical schemes are accuracy (determined by the order of the scheme), robustness (stability and positivity) and efficiency. Solution of the transport equation with computers requires the use of discrete segments in space with finite mesh sizes Δx, Δy and Δz and with a finite time-step Δt.

  Several numerical discretization schemes are available in transport models and any of these can be followed to solve the discretized systems of equations.

- *Timestep:* To ensure the transport model stability and accuracy, the Peclet number is used (Equation (3.9)).

- *Numerical filters:* The numerical scheme could enhance the dispersion in some situations. Thus, it is recommended that if the flow rate is zero, no dispersion is required for calculations with tidal flats or no dispersion over open boundaries in situations where the boundaries are far away from the area of interest.

  Moreover, the different numerical schemes do not guarantee positive solutions and consequently negative concentrations may occur. In case of negative concentrations, an iterative filter procedure based on local diffusion followed by a vertical filter should be started in order to remove the negative values.

Simulation-calibration cases

Simulation-calibration cases are all the different model simulations performed by means of N combinations of physical parameters and M combinations of numerical parameters in order to find the best combination of model parameters. Table 3.4 synthesizes the calibration parameters, suggests the best option for estuarine modeling and gives the optimal value ranges of each parameter.

As it can seen from table 3.4, there are a less range of possibilities to combine model parameters than in a hydrodynamic model when the latter is previously calibrated.

Final configuration

The final configuration of the model is the combination of physical and numerical parameters that best match the results obtained by the model and the data measured in the study area.

Error measurements

In order to find the optimal calibration case, two error measurements are anew calculated: the BIAS and the CE. For each simulation-calibration case, we compare the values of the model data and the survey data in terms of concentrations.

Firstly, BIAS is calculated by means of equation (3.10) and, secondly, the error between both series using the CE is calculated by equation (3.11).

Optimal calibration case

From error measurements of each simulation-calibration case, the optimal calibration case is the case simultaneously displaying the minimum BIAS and the maximum CE. Therefore, this combination of model parameters will be used along the rest of the methodology for conducting far-field simulations.

3.3.5.2 Transport worst case modeling

In order to run the transport of the "worst case of dilution", the previous simulation of the hydrodynamic model and the initial dilution data from the coupling approach are used. Thus, we propose that this scenario assumes fixed conditions.

As it was aforementioned, this model scenario is simulated until reach a "quasi-stationary" response for the transport (Figure 3.16). Once it is reached this situation, we record hourly one day (24 data) of transport model results (Figure 3.16). At each time step (hour) and grid cell, it should be underlined that the recorded concentration is the maximum concentration of all the vertical layers.

The "quasi-stationary" response for transport depends on the location, concentration and flow of the point discharge, the location of the considered grid cell respect to the point discharge and the magnitude of the river and tides. Therefore, in order to find the maximum timescale of the "quasi-stationary" response for transport, it should be conducted a sensitivity analysis with different locations across the model domain. This timescale indicates the minimum duration of a far-field simulation to ensure that results are trustable.

Figure 3.17 displays an example of the initialization, the "quasi-stationary" state and the far-field model results for the concentration evolution of four grid cells located across the model domain.

3.3.5.3 Delimitation of mixing zones

EQS Directives state that for each "representative" monitoring point the arithmetic mean of observations should not exceed the AA-EQS and the measured concentration does not exceed the MAC-EQS. However, in accordance with Directive 2000/60/EC (EC 2000), EC Member States may introduce statistical methods, such as a percentile calculation, to ensure an acceptable level of confidence and precision for determining compliance with the MAC-EQS. While the term "representative" is not defined, the implication is that a water body is compliant with the EQS only if all representative monitoring points are compliant.

Monitoring programmes of toxicants substances are typically limited to "spot" samples at monthly frequency. For example, Spain has drafted a proposal (SPAIN 2014) where the monitoring programme for priority substances (EC 2008a, EU 2013) must be sampled at monthly frequency. Thus, information on actual distributions will necessarily be limited and the results will only approximate the actual annual average for comparison with an AA-EQS value. The best solution is to undertake continuous monitoring but this may not be technically and economically feasible. In contrast, modeling may offer a continuous concentration prediction over space and time subject to a number of simplifying assumptions.

Bearing in mind these issues, the effects of the toxicant concentration evolution is determined by the nature of the exposure (Gómez *et al.* 2014b):

- *Chronic effects (CEF):* Pelagic community can be affected by long-term exposures of any priority substances present in the water column. Chronic effects of each priority substance in every grid cell are computed using the equation (3.12):

$$CEF_{i,j} = \frac{[\overline{X_{i,j}}]_{ff}}{AA_{EQS}} \tag{3.12}$$

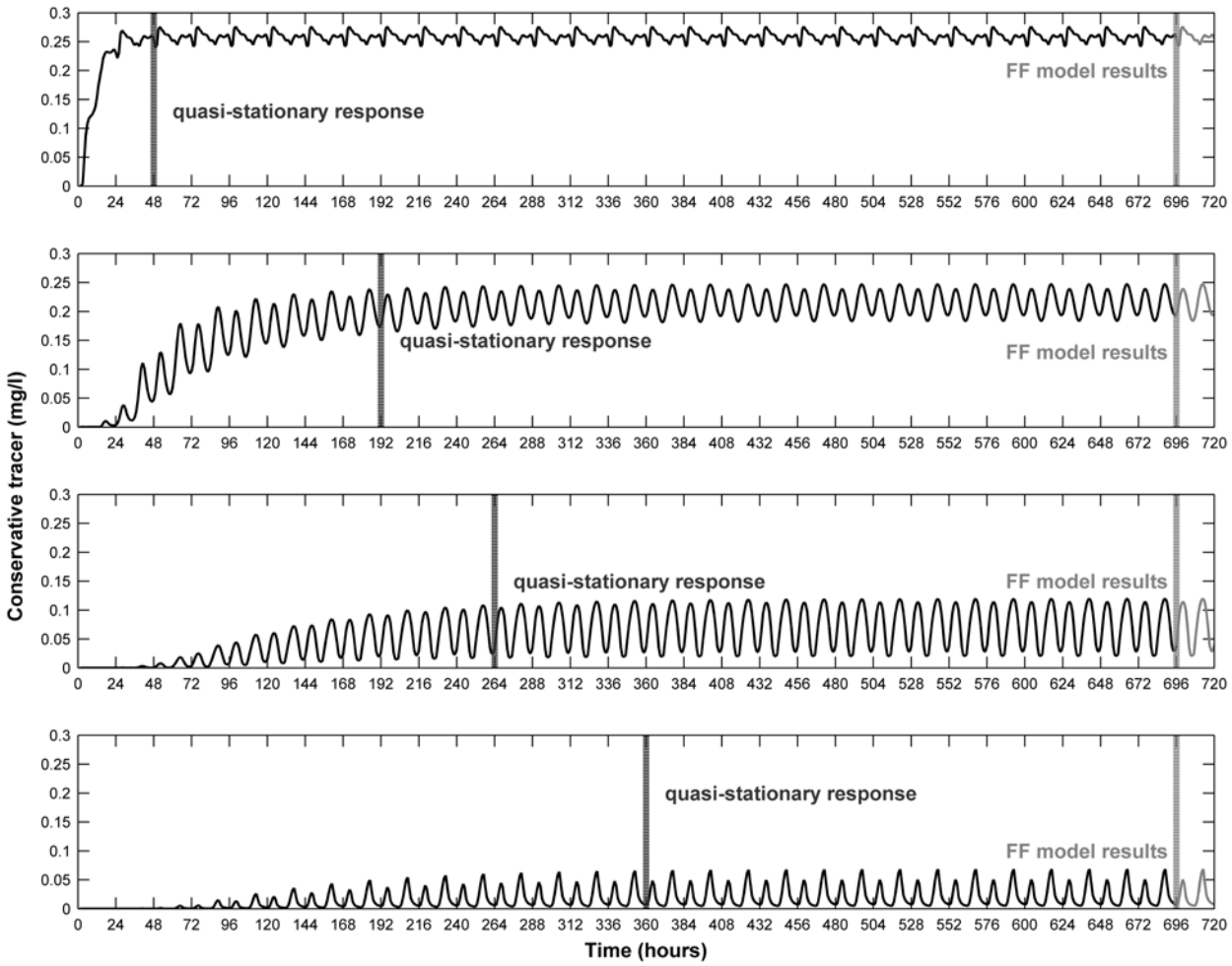

Figure 3.17: Example of the evolution of a conservative tracer, timescale of the "quasi-stationary" response for transport and recorded period for the transport of a "worst case of dilution" in four grid cells located across a model domain.

where $[\overline{X_{i,j}}]_{f-f}$ is the average concentration of a priority substance during the "worst case of dilution". AA-EQS for pelagic community are collected in the Directive 2013/39/EU (EU 2013) in terms of water concentration ($\mu g/l$).

- *Acute effects (AEF):* All priority substances present in the water column have the potential to affect the pelagic community in a short space of time. Acute effects of each priority substance in every grid cell are computed by the percentage of time in adverse conditions:

$$AEF_{i,j} = \frac{t_{i,j}}{t_{total}} \times 100 \tag{3.13}$$

where $t_{i,j}$ is the time in adverse conditions, i.e, the time during MAC-EQS is exceeded and t_{total} is the time duration of the "worst case dilution". MAC-EQS for pelagic community are also collected in the Directive 2013/39/EU (EU 2013) in terms of water concentration ($\mu g/l$).

According to EQS Directives statements and these effects, two MZs are determined: the Annual Average-Mixing Zone and the Maximum Allowable Concentration-Mixing Zone (henceforth AA-MZ and MAC-MZ respectively). The AA-MZ indicates where chronic effects might happen meanwhile the the MAC-MZ indicates the acute effects. Both zones are similar to those defined by many USA states (Figure 2.22) or Canada jurisdictions (Figure 2.23). The AA-MZ is calculated as an area where the time-averaged modeled concentrations are exceeding the AA-EQS, i.e, $CEF_{i,j} > 1$ (Figure 3.18). The MAC-MZ is calculated as an area where the modeled concentrations are exceeding the MAC-EQS, i.e, $AEF_{i,j} > 0$ (Figure 3.18).

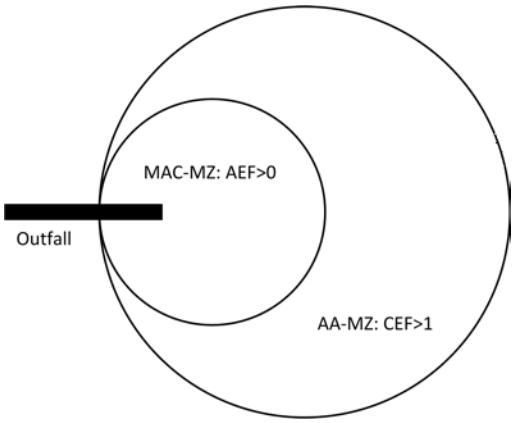

Figure 3.18: Diagram of the two delimitated parts of Mixing Zones (AA-MZ and MAC-MZ) in the simplified calculation.

3.3.6 Admissibility of Mixing Zones

Once both MZs are delimited, a check should be made to determine if the acceptability and extent of the MZs is admissible. The WF Directive (EC 2000) sets obligations on the results (i.e. the environmental objectives), not the means of achievement. The obligation on the results means that the effort to achieve the environmental standards may vary greatly from one place to another. This is why case by case assessment will be necessary in estuarine waters.

As it was mentioned in Chapter 2, there are some approaches that apply a MZ with an extent only a small distance beyond the initial dilution zone. In other approaches, the maximum extent of the acceptable MZ is proportionate to the width of the water body and limited to a chosen fixed maximum value. Furthermore, the MZ must not reach any protected area for other uses.

In order to define de admissibility of a MZ, we developed a three-tiered method. Firstly, we evaluate the acceptability (AC) as the percentage of estuarine area cover per cell. Secondly, the maximum allowable MZ size (MAS) is determined by expert criteria. Thirdly, the final admissibility (AD) is computed by summing all the AC values covered by the delimitated MZs and comparing these values with the MASs.

3.3.6.1 Acceptability (AC)

First tier is determining the acceptability (AC). For this task, we check if the discharge point is located at an intertidal zone. Intertidal zones are defined as the grid cells where the depth of the water column (H) are below the value of tidal amplitude that is not exceeded during the 95% of the time ($A95$).

If the point discharge is located in an intertidal area, MZs are non-acceptable. Therefore, as a principle, a point discharge cannot be located at intertidal areas. Otherwise, the value of AC as the percentage of estuarine area cover per cell is computed (Equation (3.14)).

$$AC_i(H, A) = \begin{cases} \text{if } H_i < A95 & Non - Acceptable \text{ (when discharge point)} \\ \text{if } H_i \geq A95 & \frac{A_i}{A_{estuary}} \cdot 100 \text{ (rest of grid cells)} \end{cases} \tag{3.14}$$

Regarding $A_{estuary}$, we defined two boundaries: the inner and outer. The inner boundary between estuarine and river waters are located in the innermost point where the influence of the tide is felt. The outer limit of the estuary has been established based on physiographic criteria, considering the line connecting the ends of the mouth. These ends can be artificial, natural, rocky or sandy. Thus, in some cases sandy spits are the boundary between transitional and coastal waters while in other cases the breakwaters that channel the entrance to the estuary are the limit.

3.3.6.2 Maximum allowable MZ size (MAS)

According to EQS Directives (EC 2008a, EU 2013), the acceptance of the proposal MZs shall ensure that the extent is restricted to the proximity of the point of discharge, is proportionate (having regard to the concentrations at the point of discharge and to conditions in prior regulations), do not compromise the attainment of "good chemical or ecological status" for the relevant water body under WF Directive (EC 2000) and EQS Directives and is consistent with requirements adopted for other point source discharges under other Community legislation such as IPPC Directive (EC 2008b).

Thus, a MZ should generally not plug an estuary. In the simplified calculation, the maximum allowable MZ size (MAS) has been defined by expert criteria. We performed a survey to 20 experts around the globe asking their opinion about the maximum value might have the extent of a MZ in estuaries.

This criteria was the average value of all the experts and reads that the MAS does not exceed 10% and 3% of water body extent overall for the AA-MZ and the MAC-MZ, respectively (Figure 3.19). Both values were named AA-MAS and MAC-MAS where MAS is the maximum percentage of the estuarine area that a MZ might cover.

3.3.6.3 Final admissibility (AD)

Lastly, we evaluate the final admissibility of the MZs (AD) as the sum of all the AC values covered by AA-MZ and MAC-MZ (Equation (3.17)). If the AD is greater than MAS the MZ size is not admissible meanwhile if AD is equal or lower than MAS the MZ size is admissible.

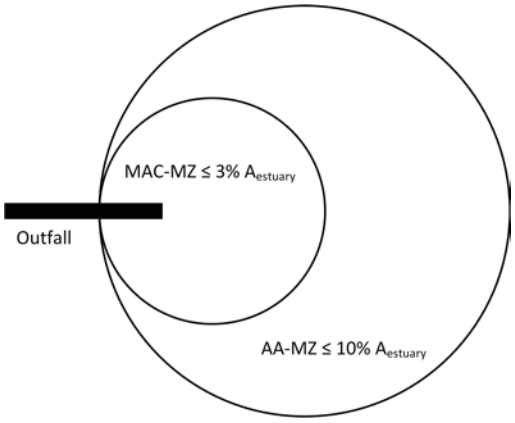

Figure 3.19: Diagram of the maximum allowable MZ size for AA-MZ and MAC-MZ in the simplified calculation.

$$AD(AC) = \sum_{i=1}^{n} AC_i \tag{3.15}$$

where AC_i is the acceptability of the i grid cell.

If the extent of the AA-MZ or MAC-MZ is inadmissible, the discharge is classified as large significant moving to the Step 4 of the decision tree in order to continue with the allocation procedure (Figure 3.2).

3.4 Step 4. Intermediate calculation (Dry case of dilution)

Once the large significant discharges has been detected, we start to apply the Step 4 of the decision tree. The proposed intermediate calculation is based on the continuous simulation of one real year of forcings. Although this model scenario still being a precautionary approach, the forcing variations through the year might led to modifications of the hydrodynamics quantities. Consequently, differences in the concentration of the toxicants in all mixing regions are expected.

Step 4 is composed by 5 subsections as illustrated in figure 3.20.

In 3.4.1. Hydrodynamics, the requirements for setting up the model and the specification and simulation of the model scenario are described. Next, subsection, 3.4.2. Primary or initial dilution (Near-field) explains the approach used for the simulation of the "dry case of dilution" with a initial dilution model. In 3.4.3. Coupling (Intermediate-field), the procedure developed to integrate the outputs of the initial dilution model into the far-field model are explained. The subsection 3.4.4. Secondary or ambient dilution (Far-field): Conservative approach describe the required tasks to conduct the simulation of the significant discharges with far-field models taking into account, as inputs, the results of the hydrodynamic model and the coupling (intermediate-field). Finally, the extent and the acceptability of the MZs are delimitated in the subsection 3.4.5. Admissibility, according to the admissibility criteria developed in Step 3.

3.4.1 Hydrodynamics

For the "wort case of dilution", the occurrence probability of the forcing is very low, consequently, results are too cautious because toxicant concentrations may be smaller during long periods of time. When MZs are inadmissible in Step 3, i.e., the discharge is classified as large significant (Figure 3.2), the decision tree must continue evaluating the discharge from a more real approach rather than a precautionary approach.

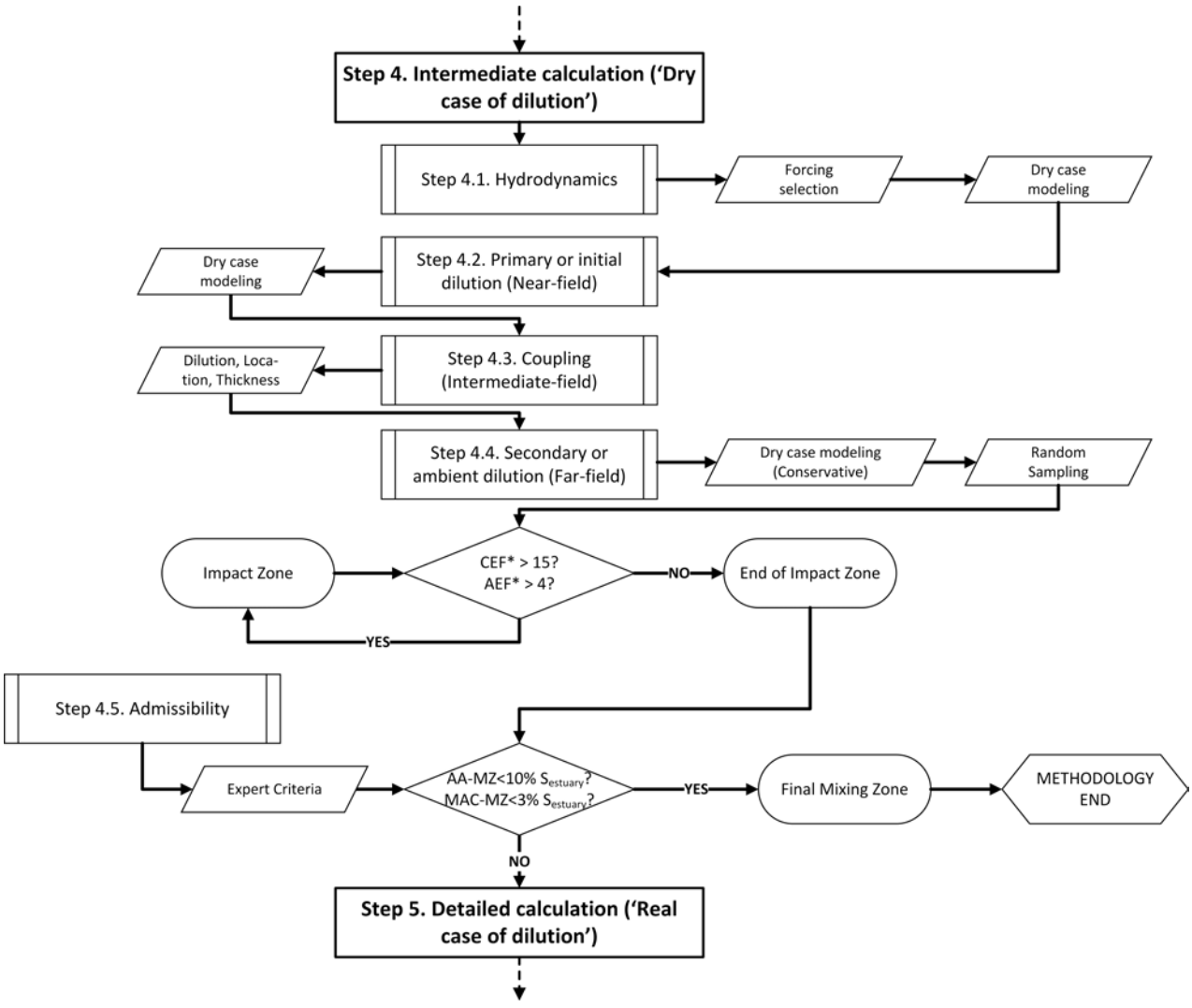

Figure 3.20: Developed flowchart of the Step 4. Intermediate calculation (Dry case of dilution).

3.4.1.1 Model setup

In the "dry case of dilution", model setup is the same as in the "worst case of dilution" so it is not necessary to conduct additional tasks.

3.4.1.2 Forcing selection

The proposed intermediate calculation is based on the continuous simulation of the driest year of the time series of river flow. In order to select this year, the mean annual water volume ($MAWV$) is computed for each i-year of the series by equation (3.16).

$$MAWV_i = \sum_{j=1}^{j} Q_j \times 86400 \tag{3.16}$$

where Q_j is the daily j-river flow (m^3/s).

Next, the model scenario of the "dry case of dilution" is the year with the minimum value of $MAWV$. Finally, the time series of river flow and their associated tidal elevations for this driest year are extracted from time series and used as forcings of the hydrodynamic model.

3.4.1.3 Hydrodynamic dry case modeling

The hydrodynamic model predicts the surface elevation, current velocity, temperature and salinity fields across the model grid during one year of simulation.

Again, an important issue is the time required for stabilizing the model results and the influence of initial conditions on these results as it was shown in figure 3.11. It should be underlined that this timescale is smaller than in the "worst case of dilution" because the magnitude of forcings is bigger. Therefore, if we would like to run simulations with the "dry case of dilution", we suggest running the model starting several days before the time of interest, i.e, the timescale of the "worst case of dilution" for hydrodynamics. In this way, the model is always capable of absorbing the influence of the initial condition.

In this method, we propose to carry on the hydrodynamic simulation assuming $X + 365$ days of river flow and tidal elevation as forcings. Note that 365 is the driest year selected by the minimum $MAWV$ and X is the same timescale calculated in Step 3 (see figure 3.11).

Once the model stabilization is reached and the influence of initial conditions avoided, we record hourly 365 days of hydrodynamic model results.

3.4.2 Primary or initial dilution (Near-field)

As it was mentioned, the primary dilution depends on the discharged effluent flow, the pipe diameter of the single-port, the distance of the single-port to the bottom, the density of the discharged effluent, the density of the receiving water, the total depth of the water column and the environmental current velocity. The first four variables are attached to the discharge mechanism and they are specific for every discharge.

The remaining variables are related to the environmental conditions, they are dependent of the hydrodynamic changes and the single-port location. The value of each variable is extracted hourly from the hydrodynamic modeling of the "dry case of dilution".

Once all variables have been set, different numerical models can be used to calculate the evolution of the

effluent such as UM3, CORJET, JETLAG or MOHIDJET.

The primary dilution computations are conducted for every large significant discharge, taking into account the same assumptions as for the Step 3.

3.4.3 Coupling primary and secondary dilution (Intermediate-field)

The same way as for the simplified calculation, in this subsection, the modeling results of the primary or initial dilution will be coupled to the transport model.

The proposed methodology is the same as for the Step 3. It can be seen graphically in figures 3.14 and 3.15, in which the transfer of near-field model results to the far-field model is shown in a side view and plan view, respectively.

3.4.4 Secondary or ambient dilution (Far-field): Conservative approach

In this subsection, the required tasks to conduct the simulation of the large significant discharges with far-field models taking into account, as inputs, the results of the hydrodynamic model and the coupling during the dry year are described.

3.4.4.1 Model setup

In the conservative approach, model setup is the same as in the Step 3 so it is not necessary to conduct additional tasks for calibrating the far-field model.

3.4.4.2 Transport dry case modeling

The hydrodynamic simulation provides the ambient flow and dispersion data that can be used to run the 3D transport models in the far-field while the coupling approach provides the way to introduce the discharge.

Any toxicant concentration may need several tidal cycles to reach equilibrium because dispersion/diffusion is a slower process. Moreover, the fact that discharges are continuous indicates that the time required to reach equilibrium will be higher because the system needs and additional time to reach the background concentration of toxicant due to the discharge.

In the “worst case of dilution”, the model scenario is simulated until reach a “quasi-stationary” response (Figure 3.16) because the forcings assume fixed conditions. However, in the “dry case of dilution”, forcings do not assume fixed conditions (one year of dry conditions) so the effect of serial correlation in time should be handled, e.g., the state at time “t” is a function of “t-1”. Therefore, if there is any “memory” within the system, there will be some serial correlation effect that may not be captured. This issue suggests that the initial condition may be very important to capture the “memory effect” or, at least, to minimize its influence on the model results.

In order to accomplish these issues, we propose to perform one “presimulation” to obtain the adequate initial condition of toxicant concentration and other “simulation” to record the concentration evolution along the dry year.

Firstly, the “presimulation” is carried out under ’quasi-fixed hydrodynamic conditions’. We run the far-field model with the hydrodynamic model results of the first day in a continuous loop until reach a “quasi-stationary” response. In this way, the “presimulation” is using a constant river flow of the first day of the

driest year and its associated tide during 24 hours (see Figure 3.21).

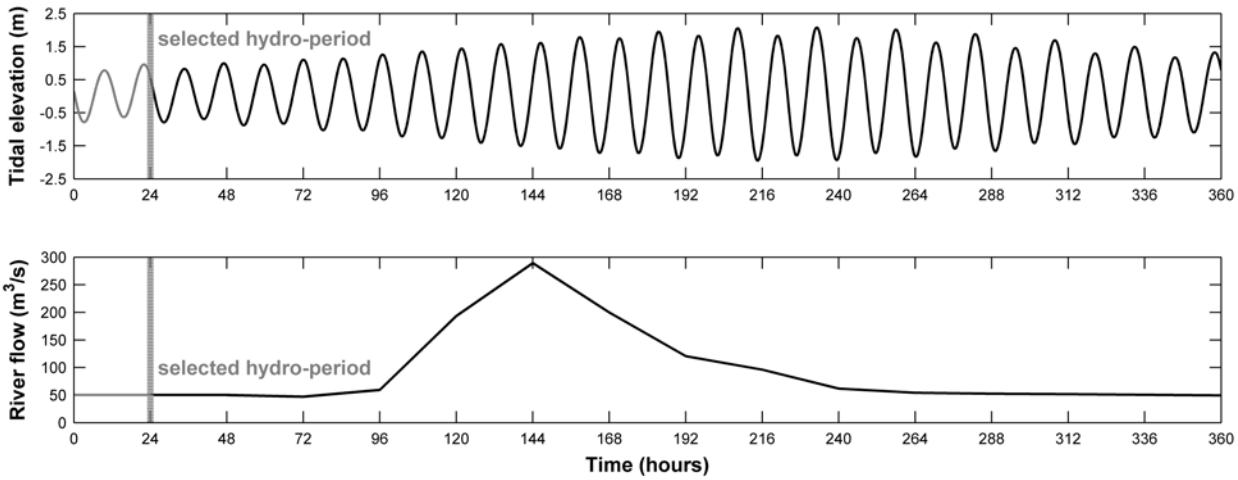

Figure 3.21: Example of the forcing of the first 360 hours of a year and selected hydro-period for the transport of a "presimulation" in a "dry case of dilution".

As in the "worst case of dilution", this "quasi-stationary" response depends on the location, concentration and flow of the point discharge, the location of the considered grid cell respect to the point discharge and the magnitude of the river and tide. Therefore, the maximum timescale of the "quasi-stationary" response for transport is the timescale of the "worst case of dilution". Thus, this timescale indicates the minimum duration of any far-field "presimulation" to ensure that initial conditions are trustable.

Once it is reached the "quasi-stationary" response, we record the concentration field of the first time step that corresponds to the first hour of the driest year, i.e, the initial condition for the "simulation" of the "dry case of dilution". Figure 3.22 displays an example of the initialization, the "quasi-stationary" state and the recorded far-field model results for the concentration evolution of four grid cells located across the model domain in a "dry case of dilution".

Secondly, we run the model scenario (365 days) with the initial condition obtained in the "presimulation". Next, we hourly record 365 days of transport model results, i.e., the concentration evolution of the considered conservative tracers. Figure 3.23 displays an example of the the far-field model results for the concentration evolution of four grid cells located across the model domain in a "dry case of dilution".

3.4.4.3 **Delimitation of mixing zones**

Unlike the simplified calculation where one model scenario is only run under fixed conditions, in the intermediated calculation we run one year under real conditions. The problem in the "dry case of dilution" lies on how to delimitate mixing zones taking into account:

- The evaluation of both EQS from one year of model results by means of the EQS statements: the arithmetic mean of observations should not exceed the AA-EQS and the measured concentration does not exceed the MAC-EQS in an annual basis calculation from monitoring programmes.

- The limitation of monitoring programmes to "spot" samples at monthly, bimonthly or seasonally frequency versus the continuous concentration over space and time subject to a number of simplifying assumptions offered by numerical models.

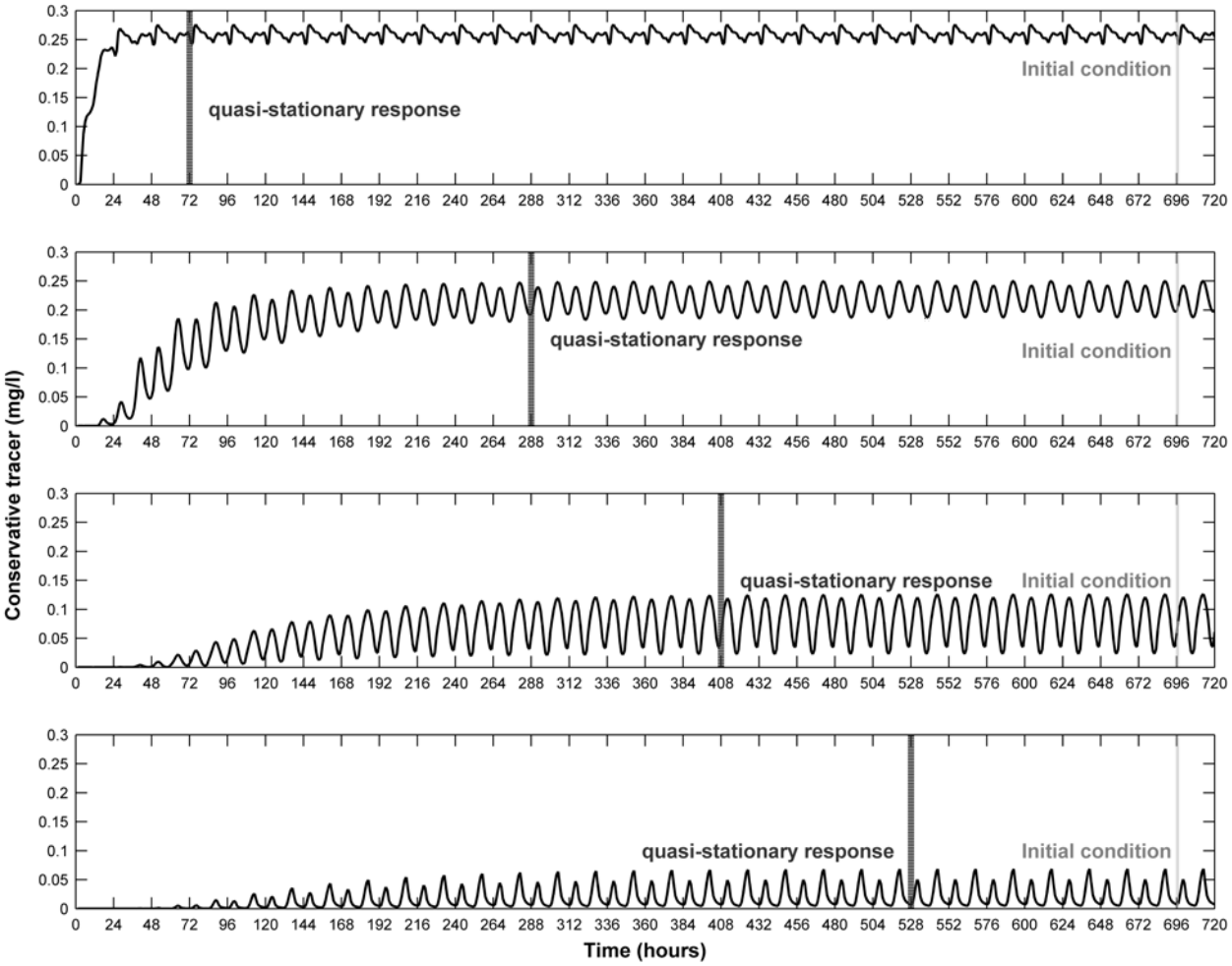

Figure 3.22: Example of the evolution of a conservative tracer, timescale of the "quasi-stationary" response and recorded period for the transport of a "presimulation" from a "dry case of dilution" in four grid cells located across a model domain.

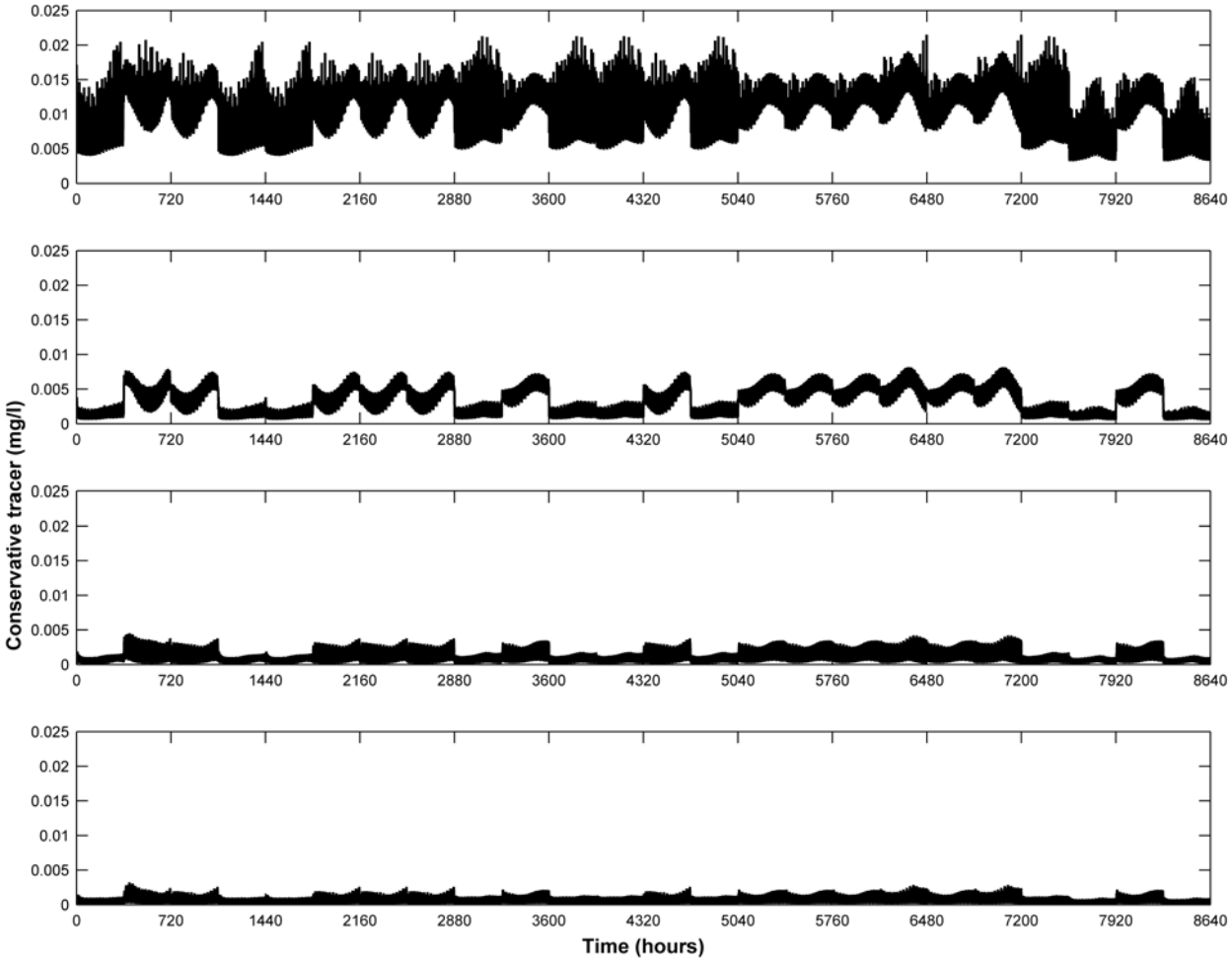

Figure 3.23: Example of the evolution of a conservative tracer for the transport of a “dry case of dilution” in four grid cells located across a model domain.

- The temporal specification of EQS excursions that can be allowed if the impact on the receiving water body is considered acceptable. As WF Directive states, EC Member States may introduce statistical methods, such as a percentile calculation, to ensure an acceptable level of confidence and precision for determining compliance with the EQS.

From these considerations, several issues arise when delimitating mixing zones:

- One of the most important aspects in monitoring programmes is the frequency of sampling along one year in the control points. So far, the definition of this parameter is frequently established under consideration of technical and economic aspects rather than the result of a specific interest in improving the statistical definition of the sample conditioning. In this sense, EQS Directives (EC 2008a, EU 2013) did not establish a minimum sampling frequency, define a maximum value of samples to be taken or determine the optimal number of samples.

- Even if the number of samples is determined and the metric to evaluate the EQS is given, the high degree of randomness that characterizes the evolution of toxicant concentration in estuaries at the time of sampling causes that the delimitation of MZs will depend on the sampling. In this way, the delimitation of MZs can be different depending on the conducted sampling.

- The delimitation of MZs can be estimated from results of the monitoring programme. However, it is more effective if carried out based on the results of water quality modeling, allowing a continuous view of the evolution of toxicants. The first idea would be calculating the delimitation based on all data provided by the modeling process. Unfortunately, this idea might lead to delimitate a MZ with a high probability of non-compliance of the EQS outside the MZ in the monitoring programmes. Thus, information on actual distributions will necessarily be limited in monitoring programmes and the results will only approximate the actual annual average or the EQS excursions calculated by model results for comparison with AA-EQS and MAC-EQS.

According to these considerations and issues, the method to delimitate MZ should specify the annual number of samples, take into account the continuous concentration prediction over space and time offered by numerical models, determine the minimum required number of surveys to ensure that the delimitation of MZ is independent of the conducted sampling along the one year of model results, and, finally, delimitate MZs allowing a temporal specification of EQS excursions.

After model simulations, we propose again to determine two MZs: the AA-MZ and MAC-MZ. To achieve this delimitation, we suggest a method involving three tiers: Specification of the annual number of samples, determination of the optimal number of surveys and final delimitation of MZs (Figure 3.24).

Specification of the annual number of samples

EQS Directives (EC 2008a, EU 2013) did not specify the annual number of samples. However, Spain has drafted a proposal (SPAIN 2014) where the monitoring programme for priority substances must be sample at monthly frequency. Therefore, in this method, we follow the Spanish proposal and specify that the annual number of samples is 12 (one per month). Regarding the sampling period, each sample can be measured at any time during every month (random sampling).

Determination of the optimal number of surveys

In this second tier, we investigate the optimal number of surveys ($k \times 12$ data) to ensure that the delimitation of MZ is independent of the number of surveys along the one year of model results. We firstly suggest generating 10000 random samplings (10000×12 data) from model results in several points along the model domain with

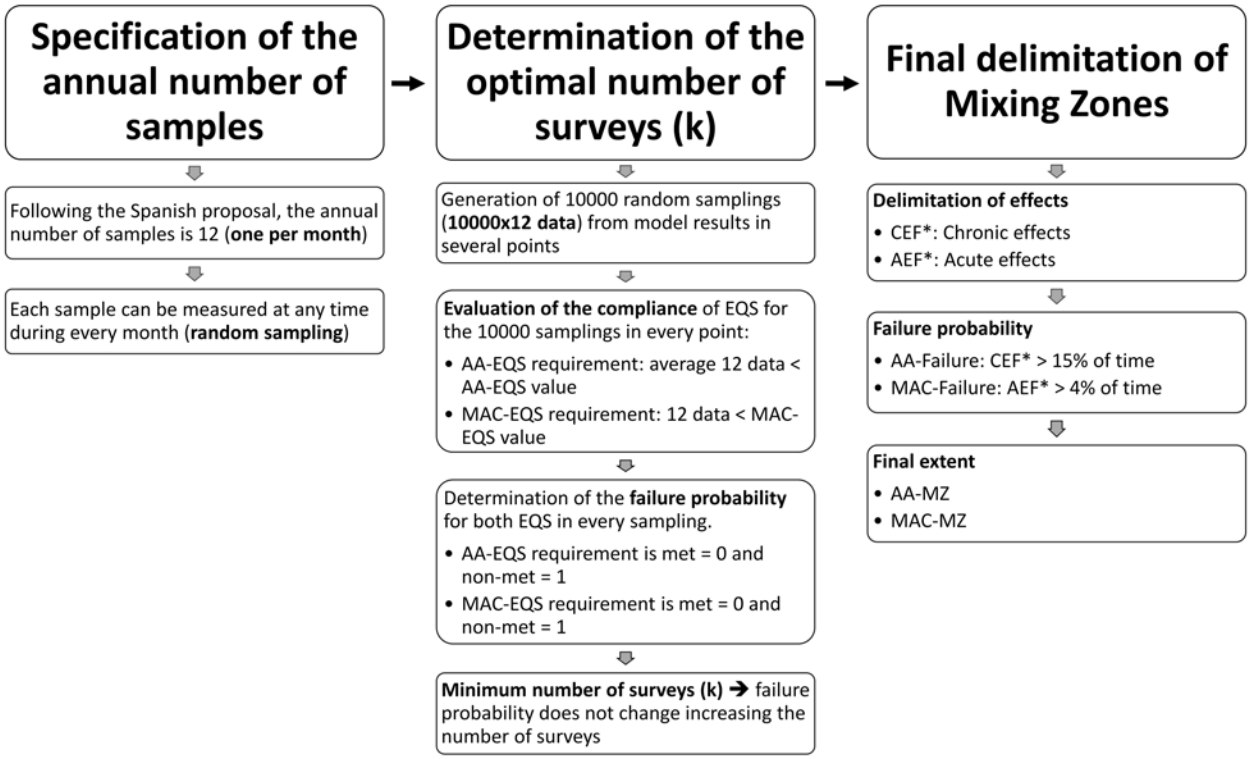

Figure 3.24: Methodology to delimitate mixing zones on estuaries in the intermediate calculation or "dry case of dilution".

special attention to the area of the point discharge. These random samplings are performed following the statements made in the first tier.

Next, we evaluate the compliance of EQS for the 10000 samplings in every point. For each sampling, AA-EQS requirement is met if the average of the 12 data is below the AA-EQS meanwhile MAC-EQS requirement is met when all data are below the MAC-EQS and is not met when one data is above the MAC-EQS. After these calculations, we determine the probability of failure for both EQS. Regarding AA-EQS for each survey, if the requirement is met then we flag this survey with a one. On the contrary, we flag this survey with a zero. In the case of MAC-EQS, if the requirement is met then we also flag this survey with a one. On the contrary, we flag this survey with a zero too.

In order to find the optimal number of surveys, we iteratively average the results of the surveys starting with 1 until 10000. In the first step, results are the probability of failure of the survey 1. In the second step, results are the mean probability of the survey 1 and 2. In the third step, results are the mean probability of the survey 1, 2 and 3. Lastly, in the 10000 step, results are the mean probability of the survey 1 to 10000.

Finally, we plot the mean probability of failure versus the number of surveys in order to investigate the optimal number of surveys (k). This number is the minimum number of surveys that ensure the independency on the probability of failure, i.e., the value of the probability does not change due to an increase of the number of surveys. Figure 3.25 illustrates an example of the evolution of the mean probability of failure with the increase of the number of surveys for the AA-EQS (black line) and the MAC-EQS (grey line) in one grid cell during a "dry case of dilution".

As it can be seen from figure 3.25, the AA-Failure probability starts with a non-compliance (100 %). Nevertheless, when increasing the number of surveys, the AA-Failure decreases in a oscillating way until reach a stationary response. At this point, the AA-Failure probability is not anymore influenced by the number of random samplings. In the case of the MAC-EQS, the MAC-Failure probability starts with a compliance (0 %).

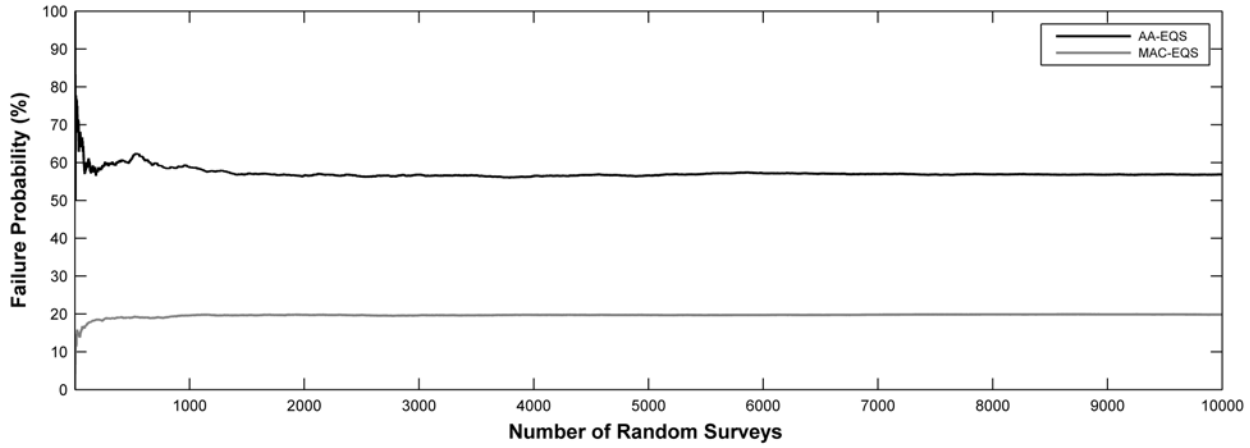

Figure 3.25: Example of the evolution of the mean probability of failure with the increase of the number of surveys for the AA-EQS (black line) and the MAC-EQS (grey line) in one grid cells during a "dry case of dilution".

After the first survey, when increasing the number of surveys, the MAC-Failure increases in a oscillating way until reach a stationary response. Anew, at this point, the MAC-Failure probability is not anymore influenced by the number of random samplings.

Final delimitation of MZs

Once the measures of toxicant concentration are calculated for the k-surveys, their effects are determined for every k-survey by the nature of the exposure (Gómez *et al.* 2014b). Unlike the Step 3 where we have one model scenario with 24 data, in the intermediate calculation, we obtain k-surveys of 12 data that have an occurrence probability equals $1/k$. Therefore, the delimitation of MZs has to take into account the probabilities of the k-surveys:

- *Chronic effects (CEF*):* Chronic effects of each toxicant in every grid cell are computed using the equation (3.17) for each k-survey:

$$CEF*_{i,j}^{k} = \frac{[\overline{X_{i,j}}]_{f-f}^{k}}{AA_{EQS}} \tag{3.17}$$

  where $[\overline{X_{i,j}}]_{f-f}^{k}$ is the average concentration of a toxicant during the k-survey (12 data) in the i,j grid cell.

  Next, if $CEF*_{i,j}^{k} > 1$ then the k-survey is not meeting the AA-EQS so we flag the $CEF*_{i,j}^{k}$ of this k-survey with a one. On the contrary, if $CEF*_{i,j}^{k} \leq 1$ then we flag the $CEF*_{i,j}^{k}$ of this k-survey with a zero.

  Finally, the CEF* associated to all the k-surveys is computed by the equation (3.18):

$$CEF_{i,j}^{*} = \sum_{h=1}^{k} CEF*_{i,j}^{k} \times \frac{100}{k} \tag{3.18}$$

- *Acute effects (AEF*):* Acute effects of each toxicant in every grid cell are computed by the fraction of data in adverse conditions using the equation (3.19) for each k-survey:

$$AEF*_{i,j}^{k} = \frac{fail_{i,j}^{k}}{12} \tag{3.19}$$

  where $fail_{i,j}^{k}$ is the number of data at which it exceeds MAC-EQS during the k-survey in the i,j grid

cell.

Next, if $AEF*^{k}_{i,j} > 0$ then the k-survey is not meeting the MAC-EQS so we flag the $AEF*^{k}_{i,j}$ of this k-survey with a one. On the contrary, if $AEF*^{k}_{i,j} \leq 0$ then we flag the $AEF*^{k}_{i,j}$ of this k-survey with a zero.

Finally, the AEF* associated to all the k-surveys is computed by the equation (3.20):

$$AEF^{*}_{i,j} = \sum_{h=1}^{k} AEF*^{k}_{i,j} \times \frac{100}{k} \tag{3.20}$$

Anew, two MZs are determined: the AA-MZ and the MAC-MZ. However, in the intermediate calculation there are a failure probability of the EQS requirements. Thus, temporal variations can be accounted for by temporal specification of the EQS. The basic idea underlying temporal specification is comparable to that of MZ regulation: "temporal EQS excursions can be allowed if it does not harm aquatic life, human health or other functions, in an unacceptable way". These temporal specification of EQSs should ideally be based on scientific studies that relate temporal variations in concentration levels to the occurrence of adverse impacts, but these data are scarce. In practice, temporal specification of EQSs is often based on assumptions or expert criteria.

In this work, the value of the temporal specification of EQS was translated into the AA-Failure probability and the MAC-Failure probability due to the discrete nature of the random sampling and based on expert judgement. We performed a survey to 20 experts around the globe asking their opinion about the value might have the AA- and MAC-Failure probability. The final value was the average value of all the experts being 15% for the AA-Failure and 4% for the MAC-Failure.

The AA-MZ is calculated as an area where the chronic effects are located, i.e., $CEF^{*}_{i,j} = 15$ (Figure 3.26). The MAC-MZ is calculated as an area where the acute effects are located, i.e., $AEF^{*}_{i,j} = 4$ (Figure 3.26).

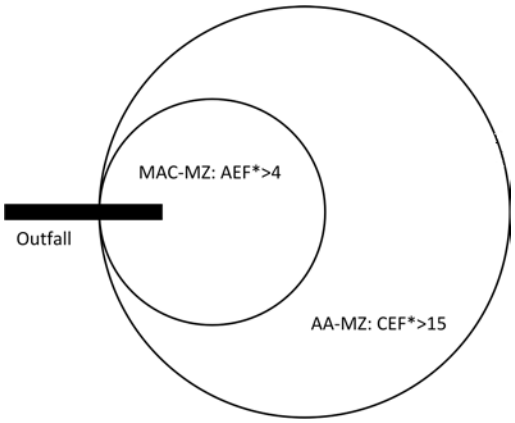

Figure 3.26: Diagram of the two delimitated parts of Mixing Zones (AA-MZ and MAC-MZ) in the intermediate calculation.

Finally, the admissibility of the proposed MZs is checked with the admissibility criteria of the next subsection. If the proposed MZs are admissible, the allocation procedure finalizes. Otherwise, the discharge is classified as very large significant moving to the Step 5 of the decision tree in order to continue with the allocation procedure (Figure 3.2).

3.4.5 Admissibility of Mixing Zones

In the "dry case of dilution", we use the same three-tiered method proposed for the "worst case of dilution" to define the admissibility of MZs.

In this method, firstly, we evaluate the acceptability (AC) as the percentage of estuarine area cover per cell. Secondly, the maximum allowable MZ size (MAS) is determined by expert criteria (see figure 3.19). Thirdly, the final admissibility (AD) is computed by summing all the AC values covered by the delimitated MZs and comparing these values with the MASs.

The final task in Step 4 is determining the allocation of both MZs by plotting an abacus that relates the extent and the failure probability of MZs. To graph this curves, we take into consideration that the extent of MZs cannot be larger than 10% and 3% of the estuarine area for the AA-MZ and for the MAC-MZ respectively. Moreover, the failure probability cannot be higher than 15% for the AA-Failure and 4% for the MAC-Failure.

Figure 3.27 illustrates an example of an abacus displaying the evolution of the extent of MZs with the probability of failure. Note that the black line is the evolution of the AA-MZ and the grey line for the MAC-MZ. In addition, the thick black line is representing the zone where the AA-MZ is allocatable because of both requirements are simultaneously fulfilled while the thick grey line is for the MAC-MZ.

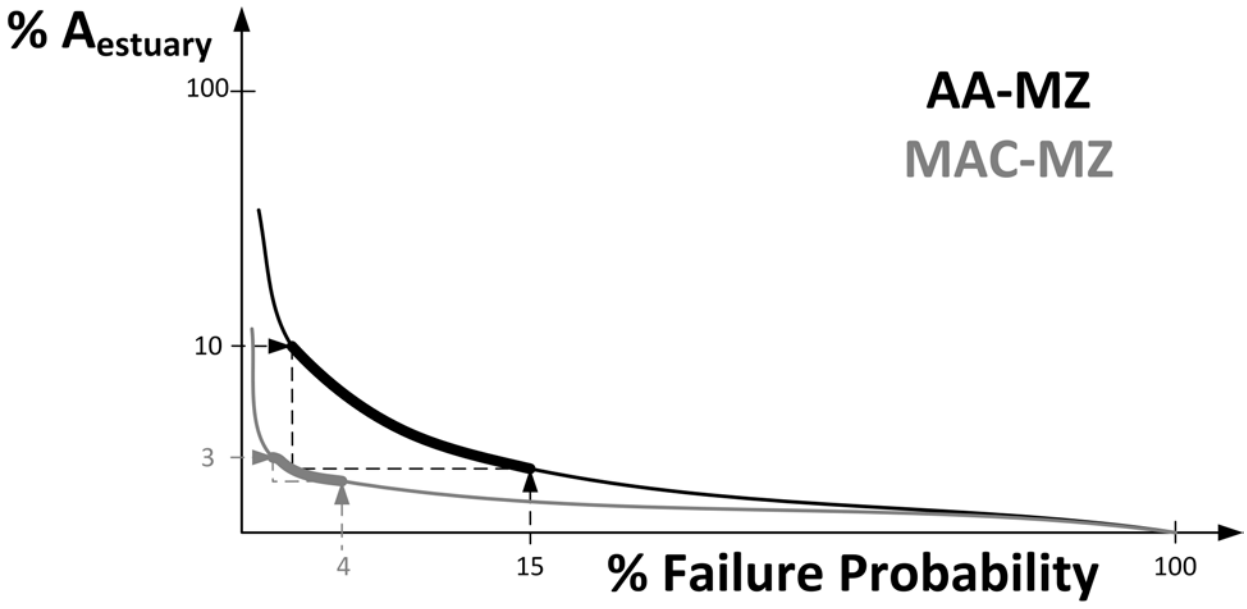

Figure 3.27: Example of an abacus of the AA-MZ (black line) and MAC-MZ (grey line) in the intermediate calculation.

As it can be seen in figure 3.27, there could be a range of allocatable MZs. The final allocation should be discussed and agreed between the stakeholder and the competent authority due to the economical, social and ecological implications of any allocation:

1. If the failure probability is maximized then the MZ extent is minimized. However, competent authorities have to assume that there are a 15% probability of non-compliance of the EQS in a control point outside the MZ.
2. If the extent of the MZ is maximized then the failure probability is minimized. However, competent authorities have to assume that there are a 10% and 3% of the estuary where chronic and acute effects might appear respectively.

3.5 Step 5. Detailed calculation (Real case of dilution)

Once the very large significant discharges has been detected, we start to apply the Step 5 of the decision tree. The proposed detailed calculation is based on the analysis of the "real case of dilution", i.e., the spatial and temporal variability of the forcing (tide and rivers) are considered. These variations lead to new significant modifications of the hydrodynamics quantities and, consequently, big differences in the concentration evolution of the toxicants in all regions are also expected.

Furthermore, physical and chemical dilution are now responsible for the toxicant decay in the far-field so toxicant are considered non-conservative. As a consequence, significant variations on the concentration evolution of toxicants are again expected.

Step 5 is composed by 5 subsections as illustrated in figure 3.28.

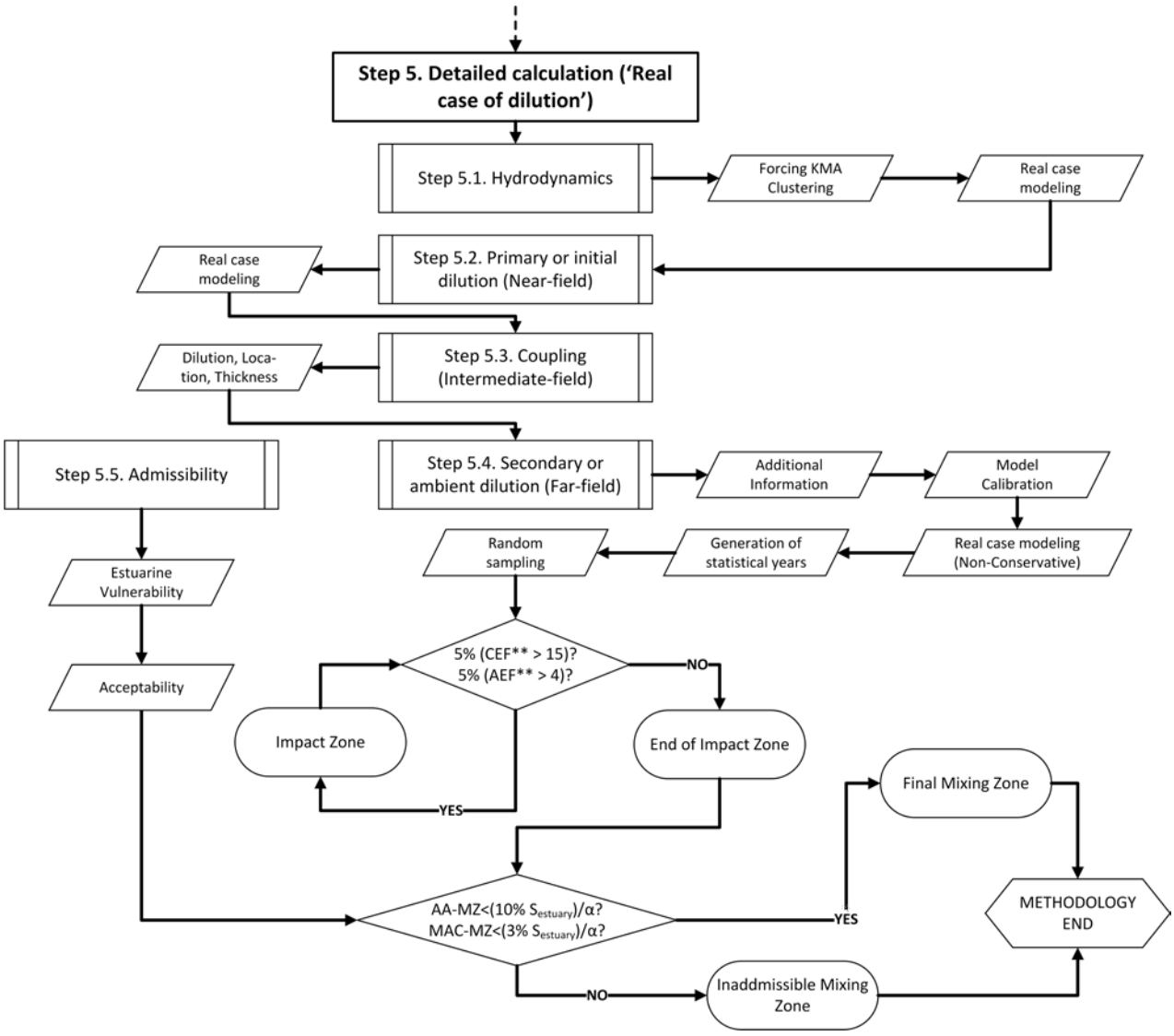

Figure 3.28: Developed flowchart of the Step 5. Detailed calculation (Real case of dilution).

In 3.5.1. Hydrodynamics, the requirements for setting up the model and the specification and simulation of the model scenarios are described. Next, subsection, 3.5.2. Primary or initial dilution (Near-field) explains the approach used for the simulation of the "real case of dilution" with a initial dilution model. In 3.5.3. Coupling (Intermediate-field), the developed procedure to integrate the outputs of the initial dilution model

into the far-field model are explained. In subsection 3.5.4 Secondary or ambient dilution (Far-field): Non-Conservative approach, the additional required information for the non-conservative approach is collected. Moreover, the subsection 3.5.4. describes the required tasks to conduct the simulation of the very large significant discharges with far-field models taking into account, as inputs, the results of the hydrodynamic model and the coupling. Finally, the extent and acceptability of the MZs are delimitated according to the admissibility criteria developed in the subsection 3.5.5 Admissibility.

3.5.1 Hydrodynamics

When the discharge is classified as very large significant in Step 4 (Figure 3.2), the decision tree must also continue evaluating the discharge from a more real approach rather than a precautionary approach like the intermediate calculation.

3.5.1.1 Model setup

In the "real case of dilution", model setup is the same as in the "worst case of dilution" so it is not necessary to conduct additional tasks.

3.5.1.2 Forcing selection/classification

As it was aforementioned in Chapter 2, tidal-river estuaries are mainly governed by tidal action and river inflows whereas other forcing such as wind, waves, evaporation or precipitation are negligible most of the time. Thus, an accurate classification of these two forcings, taking into account their environmental variability, is of high value to researchers as a source of information and a selection of the most representative scenarios for modeling hydrodynamic and transport processes.

In the last decades, long-term time series of river flow and astronomical tide from numerical models have been improving the knowledge of the temporal distribution of these two variables (Andersen 1994, García *et al.* 2008, Pawlowicz *et al.* 2002, Singh & Woolhiser 2002). These databases are especially important at locations where instrumental data are not available. In addition, they present the advantage of having an adequate spatial and temporal resolution without the problems of instrumental gauges such as missing data or sparse locations.

Typically, from these databases, the scientific community has performed their numerical simulations based on two different approaches in order to target the mean behavior of the system.

Firstly, the simulation of several scenarios using constant conditions in the hydrodynamic forcing (García *et al.* 2010b, Gómez *et al.* 2014a, Iglesias & Carballo 2010, Jouon *et al.* 2006). This constant conditions are extracted from the calculation of the empirical cumulative function (ecdf). The ecdf allows obtaining different return value quantiles for modeling. This approach is very useful to obtain quick and preliminary results about the estuarine functioning, nevertheless, as Grifoll *et al.* (2014) pointed, the study of realistic simulations suggests that response to real forcing cannot be deduced from the combination of simple idealized scenarios.

Secondly, the simulation of a few scenarios using the most frequent or extreme real hydrodynamic forcings of the study site during short-medium (<1 month - <1 year) term periods (Canu *et al.* 2012, Cucco *et al.* 2009, Harcourt-Baldwin & Diedericks 2006, Sousa *et al.* 2014). Generally, in this approach, the selection of scenarios is conducted by means of an expert judgment without a rigorous methodology that takes into account all the forcing variability. Hence, this approach could lead to an improper characterization of the estuary because the approach misses in giving the full picture of the estuarine mean functioning. It is feasible

that some significant scenarios could be discarded with this approach. In addition, the relative short period of time cannot represent the climate variability.

Thus, Grifoll *et al.* (2014) suggest the implementation of operational systems with increasing-resolution nested models with the objective of providing an accurate time evolution response of the involved processes. Unfortunately, these approaches applied to estuaries in a three-dimensional framework could be unmanageable because of the generation of large data set of results. Even if parallel computation is implemented on the simulations, the computational cost with high-resolution mesh grids may also be too expensive for 30 year time scales. Therefore, a methodology able to select the most relevant hydrodynamic scenarios in an estuary to perform high-resolution numerical modeling of short-term periods, taking into account the time evolution and the occurrence probability of the forcings in order to obtain realistic responses of the estuarine mean behavior, is highly demanded. From the proposed methodology, researchers could implement the hindcast of the estuarine hydrodynamics and/or the future prediction based on the selected scenarios.

The complexity and temporal variation of the river flow (Q) and the astronomical tide (A) series, suggest data mining methods may be particularly effective in selecting real hydrodynamic forcings from a long-term time series in order to simulate the most probable scenarios occurring in the study area.

Data mining consists of producing a particular enumeration of patterns or models over the data for the basic goals of prediction or description (Fayyad *et al.* 1996). A wide variety of methods are developed depending on the final purpose. It can be obtaining a compact description of the data (summarization), modeling the dependencies between variables (dependency modeling), mapping the data into several predefined classes (classification), identifying a set of categories (clustering) or fitting a function to a real-value prediction variable (regression). Data mining methods share the characteristic of a certain degree of search autonomy. The most popular are decision trees and rules, nonlinear regression and classification methods, example-based methods, probabilistic graphic dependency models or relational learning models.

Several statistical methods have been developed in the field of data mining to efficiently deal with huge amounts of information (see Camus *et al.* (2011b), Cofiño *et al.* (2003) for some applications in meteorology and oceanography respectively). Regarding hydrodynamics, self-organizing maps have been applied to identify surface outflows from radar records (Mau *et al.* 2007) or prototype hydrodynamic states from historical coastal ocean model outputs (Williams *et al.* 2014). Finally, Galván (2014) has applied K-means to classify clusters of river flow from long-term series. These techniques extract features from the data providing a more compact and manageable representation of some of the important properties contained in the data.

Because data mining techniques are designed to handle large amounts of data from a variety of different variables, the influence of the temporal sequence affecting Q and A evolution and distribution can be taken into account as inputs into the algorithm. This increase of information requires different data mining, in particular clustering and/or selection techniques, to deal with such amounts of information and to provide an easier analysis and description of the river flow (Q) and the astronomical tide (A) patterns.

Standard methods in data mining include clustering techniques in order to obtain a set of reference vectors representing the data such as Self-organizing maps (SOM), K-means algorithm (KMA) or Maximum dissimilarity algorithm (MDA). In figure 3.29, the distribution of the KMA centroids (left panel), the SOM centroids (middle panel) and the MDA subset (right panel) are represented with blue points over a data sample (red points). The effect of the topology preserving projection in the SOM algorithm can be observed in the distribution of the SOM centroids. KMA distributes the clusters over the data covering a large area, but there are none on the edge of the data domain. MDA begins by selecting one data on the edge of the data space and continues extending over the data domain until M vectors belong to the subset.

Regarding data on the edge of the data space, these scenarios have a very low occurrence so they are not representative of the mean behaviour of the system. Depending on the objectives, these scenarios can be discarded as in the case of allocating MZs.

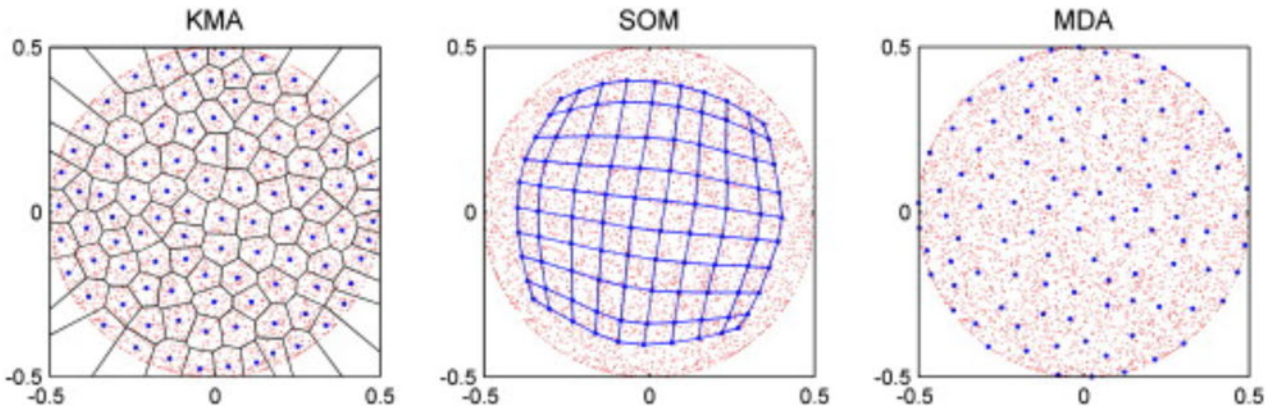

Figure 3.29: Distribution of the classified or selected data in a circle domain. Source: Camus *et al.* (2011b).

The objectives of this work are to develop the methodology and numerical tools for selecting short-time series (clusters) of real hydrodynamic forcings and defining model scenarios to run numerical models on estuaries driven by the river and the astronomical tide. This approach also could help the modeling community to deal with big data in order to prioritize the most frequent and significant scenarios of the mean behavior of the estuarine hydrodynamics from an objective point of view. Furthermore, it could help to reduce the required computational cost of the conventional numerical modeling.

The KMA was selected because it has the ability to classify long-term series in small number of groups identifying the major modes of the studied variable and reduces effectively the dimension of the system. In the following subsections, we describe the KMA and present the proposed methodology.

K-means algorithm (KMA)

In order to generalize the algorithm to be valid for any parameters, in this section we use a notation for n-dimensional data. The KMA clustering technique divides the high-dimensional data space into a number of clusters, each one defined by a prototype and formed by the data for which the prototype is the nearest (Hastie *et al.* 2001).

Given a database of n-dimensional vectors $X = \{x_1, x_2, \ldots, x_N\}$, where N is the total amount of data and n is the dimension of each data $x_k = \{x_{1k}, x_{2k}, \ldots, x_{nk}\}$, KMA is applied to obtain M groups defined by a prototype or centroid $v_k = \{v_{1k}, v_{2k}, \ldots, v_{nk}\}$, of the same dimension of the original data, being $k = 1, \ldots, M$.

Typically, the classification procedure starts with a random initialization of the centroids $\{v_1^0, \ldots, v_M^0\}$. Even for the same number of clusters, this procedure leads to a different classification for each running of the KMA algorithm. In order to avoid this issue, the initialization of the centroids in the proposed KMA starts with a dissimilarity-based sample selection because it has been suggested as an effective method, involving the identification of a subset comprising the M most dissimilar samples in a database containing N samples (Snarey *et al.* 1997). One subclass of these selection algorithms the MDA has been considered in order to initialize the KMA. The selected subset by this algorithm is fairly distributed across the space with some points selected in the outline of the data space (Camus *et al.* 2011a). In summary, we carry out this initialization in the KMA because the MDA explores very well all the data contained in the database and provides always the same centroids for a fixed number of clusters.

On each iteration r of the KMA, the nearest data to each centroid are identified and the centroid is redefined as the mean of the corresponding data. For example, on the $(r+1)$ step, each data vector x_i is assigned to the j^{th} group, where $j = min\{\|x_i - v_j^r\|_{j=1,\ldots,M}\}$, $\|\|$ defines the Euclidean distance and v_j^r are the centroids on the r step.

The centroid is updated as in equation (3.21):

$$v_j^{(r+1)} = \sum x_i \in C_j \frac{x_i}{n_j} \tag{3.21}$$

where n_j is the number of elements in the j^{th} group and C_j is the subset of data included in group j.

The KMA iteratively moves the centroids minimizing the overall within-cluster distance until it converges and data belonging to every group are stabilized (more details in Hastie *et al.* 2001). Last, the nearest vector (minimum of the Euclidean distance) of real data to the M centroid is considered the M cluster ($v_j^* j = 1, \ldots, M$) in order to allocate the real series of Q and A instead of the fictitious series given by the KMA centroids.

The proposed KMA has been implemented in MATLAB (see Chapter 4 for more information).

Methodology to select scenarios of river and tide

The methodology has been divided into several steps: Obtainment of the hydrodynamic forcing data, Rearrangement of the input data for clustering, Application of the proposed clustering approach and Sensitivity analyses for the forcing and modeling. An explanatory sketch of the methodology is shown in figure 3.30.

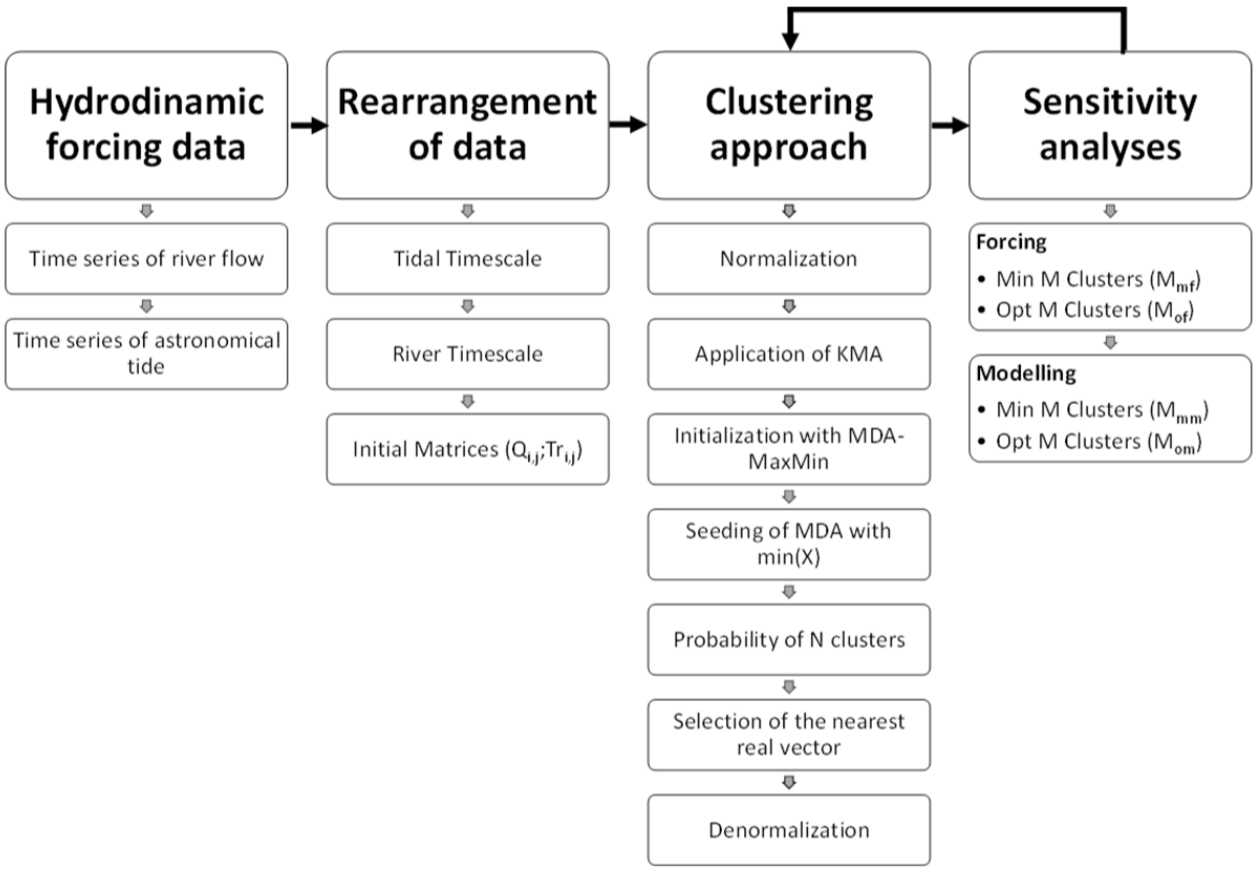

Figure 3.30: Methodology to select scenarios of real hydrodynamic forcings on estuaries driven by river and tide using K-means clustering.

Hydrodynamic forcing data

First, we need to acquire the river flow series and the astronomical tide series for a long-term period (>30 years). These time series could be obtained from numerical models (reanalyses) or from instrumental data (measurements).

Second, from the river flow series, we calculated the "daily river flow series" as the mean of the river flow for 24 hours.

Finally, from the astronomical tidal series, we calculated the "astronomic tidal range" as the difference between the minimum and the maximum value of the astronomical tide series for 24 hours in order to calculate the "daily tidal range series". This assumption is acceptable because of the experimented difference for 1 day on the tidal range is negligible in tidal-river estuaries governed by any harmonic constituents (semi-diurnal, diurnal or mixed).

Data rearrangement for clustering

In order to select representative short-time series (M clusters) from the long-term record of Q and A, we should firstly determine the hydrodynamic conditions with a temporal length representative of the time evolution of the estuarine forcings and its transient response, i.e., the number of days to classify databases. This length is attached to the timescales governing the Q and A signal.

In the case of A, the tidal changes are the net result of multiple influences that act over varying periods. Oscillations with periods of less than 24 hours are called harmonic constituents (semi-diurnal, diurnal or mixed tides). Conversely, cycles of days, months or years are referred to as long period constituents (8 days, 2 weeks, 1 month, 6 months,..., 18.6 years). We suggest understanding the tidal cycles using the harmonic and long constituents in the study area in order to identify the adequate timescale of the tide.

In the case of Q, the time scales at a local scale are determined by the local climate, especially the rainfall distribution, and the hydrological response to rainfall of the basin. To obtain the timescale of river flow, we propose estimating the duration of the flow pulses (dP) using the index proposed by Richter *et al.* (1996), Richter *et al.* (1997) and Richter *et al.* (1998). This index has been applied by different authors (Peñas *et al.* 2014, Snelder & Booker 2013) to classify river networks according to the similarity of their flow regime. Hydrologic pulses (hP) are defined as those flow events within a year in exceeding the 75^{th} percentile of all daily values. Frequency of the flow pulses (fP) is the number of annual hP. Finally, dP is calculated as the mean duration of all the annual hP. This definition is used because this time scale is much shorter than the duration of "low" flow conditions. If we classify with such time scale, we could fail in adequately represent the "high" flow conditions. We understand the "low" flow duration as the sequential repetition of these scenarios with high frequency and low flows.

Finally, according to the timescales of both forcings, we rearrange the long-term series of Q and A in sequences of n days. In this way, the matrix (database) to be clustered is built.

For Q, the first row of the matrix is composed by the n first data (days) of the time series, the second row is defined from the second day until the $n+1$ (day) and so on until the end of the time series $(N-n+1)$. The initial database is composed by a matrix of $(N-n+1)$ rows and n columns, defined as $X = \{x_1, x_2, \ldots, x_{N-n+1}\}$ where $x_i = \{Q_i, Q_{i+1}, Q_{i+2}, \ldots, Q_{i+n-2}, Q_{i+n-1}\}$ where Q_i is the river flow of the day i.

For A, the astronomical tide series was used to extract the daily tidal range series. This transformation allowed having the same number of elements for clustering both forcings. The initial database is composed by a matrix of $(N-n+1) \times n$-dimensions, defined as $X = \{x_1, x_2, \ldots, x_{N-n+1}\}$ where $x_i = \{TR_i, TR_{i+1}, TR_{i+2}, \ldots, TR_{i+n-2}, TR_{i+n-1}\}$ where TR_i is the astronomical tidal range of the day i.

Clustering approach

Firstly, it is important to point that Q and A can be considered two independent events. For example, extreme events of river flows could be happen during neap or tide periods at any tidal phase. Therefore, the river flow signal is not correlated to the tidal signal and vice-versa. This characteristic allows clustering the two forcings independently and obtaining the joint probability as the product of both probabilities.

The clustering procedure starts normalizing each data of the initial database $(X_{i,j})$ as follows in equation (3.22):

$$Norm_(i,j) = \frac{X_{i,j} - \min(X)}{\max(X) - \min(X)} \tag{3.22}$$

where $Norm_{i,j}$ is each normalized data of the initial database, $\min(X)$ is the minimum value of the initial matrix and $\max(X)$ is the maximum.

Next, the user defines the number of clusters (M) for the classification and run the KMA. In this work, the initial centroids are the output given by the MDA-MaxMin using, as seed of the MDA, the minimum value of the initial database $(\min(X))$. Regarding the seeding, we used the $\min(X)$ to ensure that, at least, one centroid is located in this spatial zone of the initial database.

Finally, M groups or clusters were obtained and represented by a centroid. The occurrence probability of each M cluster is calculated. The nearest vector of real data to the M centroid is considered the M cluster and, to finish, these M clusters are denormalized. Figure 3.31, 3.32 and 3.33 shows an example of the final classified clusters for tidal range, water levels and river flow, respectively.

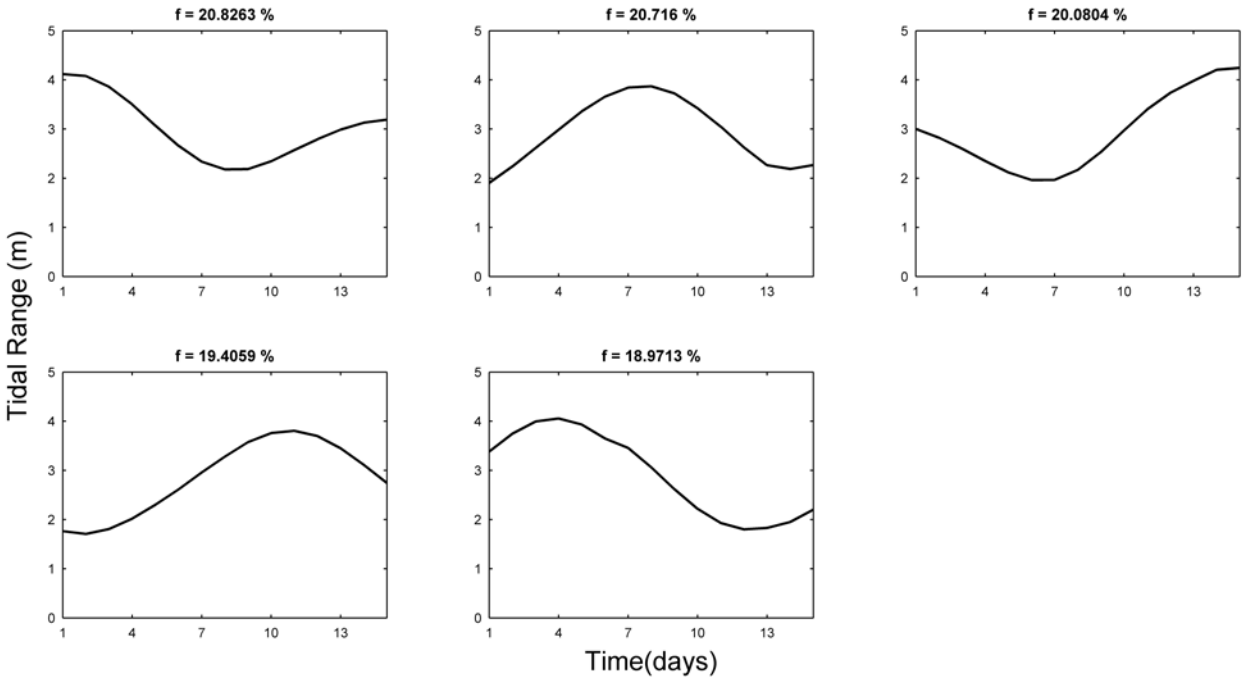

Figure 3.31: Example of final classified clusters for tidal range where f is the frequency of the cluster in percentage (%).

Sensitivity analyses

During the application of data mining techniques, the selection of the number of clusters is user-defined. In this section, we present a strategy to find the minimum and optimal number of clusters for: (a) explaining the forcing variability. i.e., the M clusters (sequences of n-days) are representative of the original long-term series of the forcings and (b) running numerical models with real hydrodynamic scenarios, i.e., the M clusters (sequences of n-days) are representative of the transient response of the estuary.

First, we reconstruct the long-term series from the M clusters to obtain the "synthetic series". This reconstruction is carried out by finding, every n-days, the cluster with the minimum of the Euclidean distance (best match) to the signal of Q and TR (long term-series or "real series") for those n-days (time step) from the M clusters. Mathematically, "synthetic series" are defined as $X^S = x_1^S, x_2^S, \ldots, x_{(N-n+1)}^S$ where $x_i^S = v_j^*$

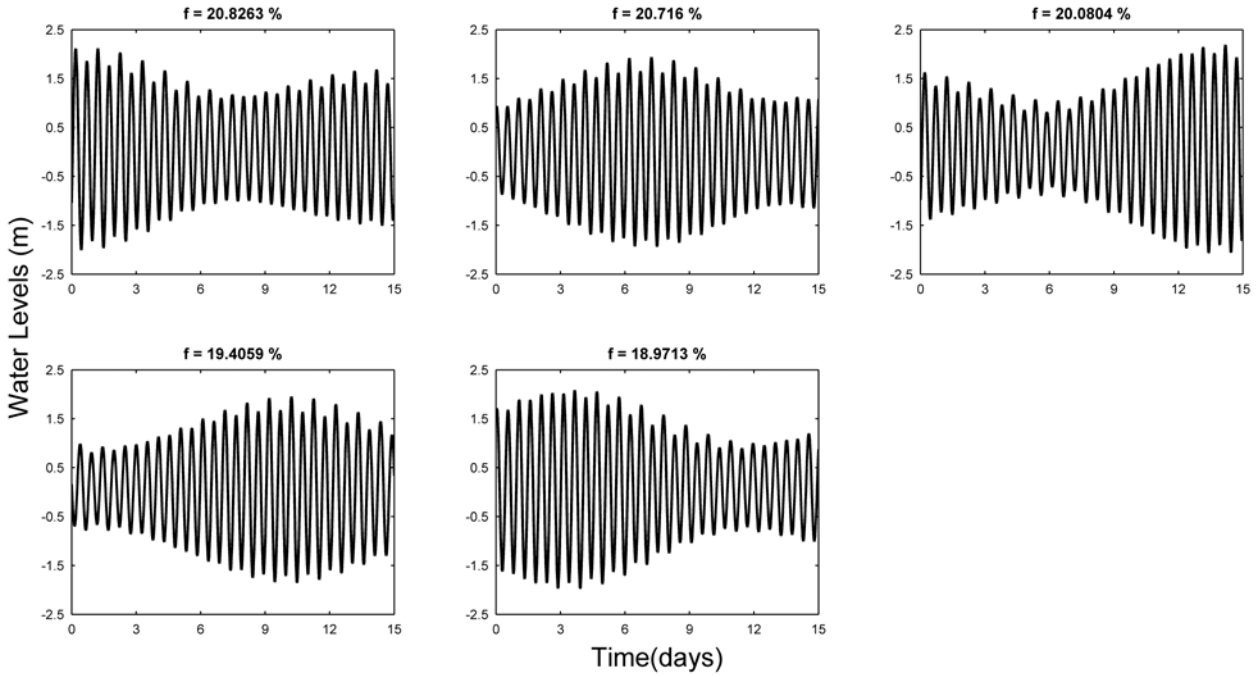

Figure 3.32: Example of final classified clusters for water levels attached to tidal range where f is the frequency of the cluster in percentage (%).

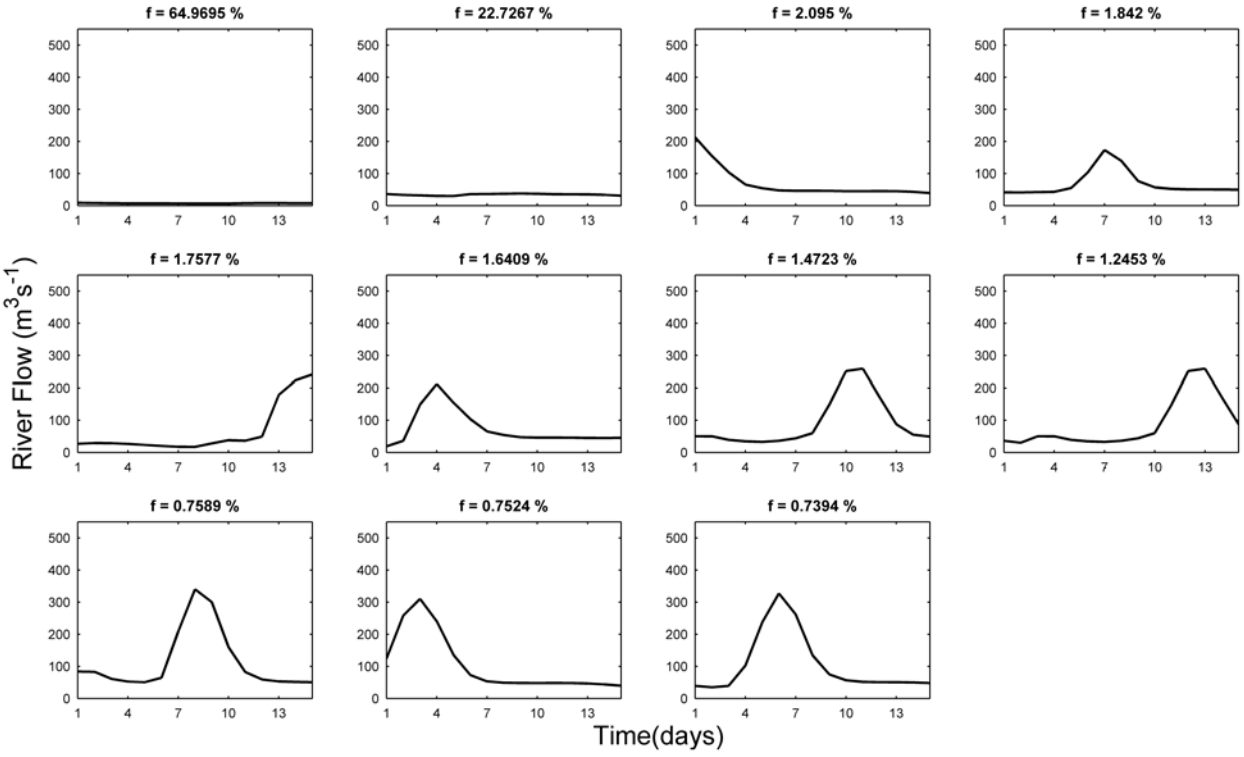

Figure 3.33: Example of final classified clusters for river flow where f is the frequency of the cluster in percentage (%).

where $j = \min |x_i - v_j^*|, j = 1, \ldots, M$. $||$ defines the Euclidean distance, X^S is the "synthetic series"' of Q or TR, and v_j^* are the centroids on the i step (n-days).

Second, we reconstruct the water levels (WL) series taking into account the previous sequence of clusters from TR.

On the one hand (case a), we calculate the error between both series using the CE, displayed in equation (3.11) and developed by Nash & Sutcliffe (1970).

If the CE_f is lower than 0.5 the comparison is considered unacceptable, if the CE_f is higher than 0.6 and lower than 0.8 the comparison is convenient (good) and if the CE_f is higher than 0.8 the comparison is considered excellent. Bearing in mind these numbers, we propose conducting a sensitivity analysis, increasing progressively the number of clusters, to find the number necessary to reach a convenient (good) comparison and an excellent comparison, namely minimum M clusters (M_{mf}) and optimal M clusters (M_{of}) for explaining the forcing variability respectively.

On the other hand (case b), we want evaluating the performance of the "synthetic series" for running numerical models against the performance of the "real series". To achieve this task, we suggest the use of a simple formulation that provides the values of a response dependent on the classified variables in the estuary. To be effective, the formulation (predictand) should predict one of the master variables used on estuarine hydrodynamic and transport modeling such as water levels on a 12 or 24 hours basis at different locations with at least a hourly time resolution. The predictand is a quality indicator of the classification and provides a hint about how well the mean response of the estuary is characterized.

In addition, the formulation (predictand) should give a quick response from the "synthetic" and "real series". This validation should be done because a convenient (good) or excellent comparison of the "synthetic" and "real series" (case a) does not ensure that the response, influenced by both variables, is convenient (good) or excellent. Therefore, we should ensure that the selected number of clusters is also adequately for numerical modeling.

The simple formulation to determine the water levels (WL) with the "synthetic" and "real series" in different locations along the study area should be correlated to the two loading variables, e.g., river flow (Q) and astronomic tidal range (TR) such that $WL = f(Q, TR) + \epsilon$ where ϵ represents any measurement error or random errors on the response (e.g. measurement, background noise, the effect of other variables, among others).

It is worthy to mention that the validation of the "synthetic series" could be done with a long-term series of measurements from a tidal gauge instead of the long-term series of the empirical equation applied to the "real series".

Next, we calculate the CE of both WL series to analyze the capacity of the "synthetic series" to be used on numerical modeling.

We propose performing a new sensitivity analysis to find the namely minimum M clusters (M_{mm}) and optimal M clusters (M_{om}) for running numerical models. The procedure starts by choosing the number of clusters necessary for reaching a CE_f of 0.5 in Q and A. With the M clusters of Q and the M clusters of TR, we reconstruct the "synthetic series", evaluate the response by means of the selected formulation and calculate the CE_r of the response at each location. This procedure is iteratively repeated, increasing the number of clusters of Q and A according to an increase of 0.01 on their CE_f values. When the CE_r of the response at each location is higher than 0.6, the M_{mm} is reached. The procedure finish when the average of the CE_r at every location is higher than 0.8 being the M_{om}.

Final selection of classified clusters

The proposed methodology provides a minimum (M_{mm}) and optimal (M_{om}) number of simulations necessary

to take into account the variability of the hydrodynamic forcings on estuaries driven by the river and the tide. Consequently, the final number of M model scenarios must be in a window spanning from M_{mm} to M_{om}. This M model scenarios should be selected taking into account the computational costs against the accuracy of the model results, i.e, the simulation time and size versus the obtained CE. At first, it should be selected M_{om}. However, these number of model scenarios might be unaffordable due to computational constraints. At least, it must be selected M_{mm} to ensure valid results.

Furthermore, it is important to point that the known data when performing the classification by KMA are always the forcing time series. In a particular study, it could happen that there are not simple formulations or empirical data to validate the classification with the "synthetic" and "real series". In these situations, we suggest selecting the final number of clusters based on the CE_f and the time duration of the proposed simulations. Bearing in mind these issues, the final number of clusters must ensure that the CE_f>0.7 and the time duration is less than 10 $\%$ of the long-term time series of river an tide.

3.5.1.3 **Hydrodynamic real case modeling**

The same way as for the simplified and intermediate calculation, the hydrodynamic model predicts the surface elevation, current velocity, temperature and salinity fields across the model grid.

Again, an important issue when running hydrodynamic models is the time required for stabilizing the model results and the influence of initial conditions on these results as it was shown in figure 3.11. Therefore, if we would like to run simulations with the "real case of dilution", we suggest running the model starting several days before the time of interest, i.e, the timescale of the "worst case of dilution".

In this method, we propose to carry on the hydrodynamic simulation for each M model scenario selected by the proposed clustering approach. These M model scenarios assume $X + n$ days of river flow and tidal elevation as forcings. Note that X is representing the same timescale calculated in Step 3 (see figure 3.11).

Once the model stabilization is reached and the influence of initial conditions avoided, we record hourly n days of hydrodynamic model results for each M model scenario.

3.5.2 **Primary or initial dilution (Near-field)**

Environmental conditions are dependent of the hydrodynamic changes and the single-port location. The value of each variable is extracted hourly from the hydrodynamic modeling of the "real case of dilution" (M model scenarios).

Once the most important variables for the calculation of initial dilution have been set, different numerical models can be used to calculate the evolution of the effluent such as UM3, CORJET, JETLAG or MOHIDJET.

The primary dilution computations are conducted for every large significant discharge, taking into account the same assumptions as for the Step 3.

3.5.3 **Coupling primary and secondary dilution (Intermediate-field)**

The same way as for the simplified and intermediate calculation, the modeling results of the primary or initial dilution will be coupled to the transport model.

The proposed methodology is the same as for the Step 3. It can be seen graphically in figures 3.14 and 3.15, in which the transfer of near-field model results to the far-field model is shown in a side view and plan view, respectively.

3.5.4 Secondary or ambient dilution (Far-field): Non-Conservative approach

In the detailed calculation, the assessment tends towards the "Non-conservative approach". Thus, improving confidence in the uncertainty ranges for some of the factors may be important such as the reaction terms of non-conservative behaviour. These variations could lead to significant modifications in the concentration evolution of the toxicants in the far-field and, consequently, reducing the extent of MZs.

As it was mentioned, in this thesis, we pay attention in the study of chemical toxicants listed by the EQS Directive (EC 2008a, EU 2013) as priority substances discharged by industrial facilities.

3.5.4.1 Conceptual Model

In a water system, the non-conservative substances are found in the dissolved fraction (f_{dis}) and the particulate fraction (f_{par}). These substances are subject to various processes through complex interactions between different fractions and matrixes (water, air and sediment).

In this context, as many toxicants can be adsorbed on inorganic matter (heavy metals) or organic matter (organic micropollutants), an appropriated modeling of the concentration distributions of non-conservative substances in estuarine waters should tackle not only the toxicant transport analysis but also the suspended solids or organic matter one.

The transport model for non-conservative substances must include, at least, the conceptual model (processes and interactions) described on this subsection. The proposal is an adaptation of the developed model by Gómez (2010) and it includes the spatial and temporal variations of suspended matter concentration. This readapted conceptual model considers the following assumptions (Figure 3.34).

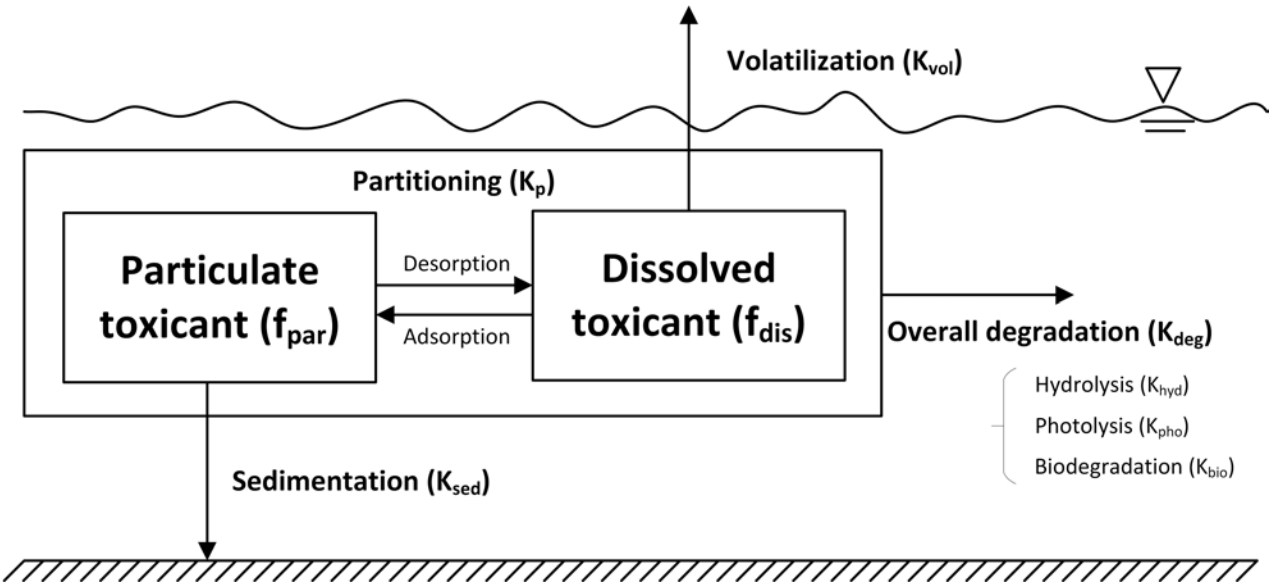

Figure 3.34: Conceptual transport model for non-conservative substances including the minimum required processes to allocate mixing zones.

1. The concentration in the pelagic environment is only reduced by the volatilization process, affecting the dissolved fraction, sedimentation processes that reduce the particulate fraction, and degradation processes which reduce the total fraction.

2. The equilibrium between adsorption and desorption depends on the evolution of the dissolved fraction

and the particulate fraction as a function of inorganic or organic matter concentration (Carrer *et al.* 2005).

3. Heavy metals (HM) adsorb to inorganic matter components and organic micropollutants (OMP) to organic matter components.

4. Heavy metals are not affected by degradation processes.

5. Volatilization is ignored for heavy metals.

Given these assumptions, the mass balance for any OMP or HM is calculated according to equations (3.23) and (3.24) respectively:

$$\frac{dC_{OMP}}{dt} = -(K_{deg} + K_{vol} \cdot f_{dis} + K_{sed} \cdot f_{par}) \cdot C_{OMP} \tag{3.23}$$

$$\frac{dC_{HM}}{dt} = -(K_{sed} \cdot f_{par}) \cdot C_{HM} \tag{3.24}$$

Partitioning

Partitioning is the process in which a substance is distributed among various dissolved and adsorbed species. Partitioning is determined largely by the process of adsorption-desorption mechanism. The substance is adhered onto the surface of suspended matter.

Generally, a linear relation between the concentration in the particulate phase and the concentration of the material in suspension is assumed (Chapra 1997, Thomann & Mueller 1987). The result of these assumptions are the equations for the calculation of the dissolved fraction (Equation (3.25)) and the particulate fraction (Equation (3.26)) in terms of the partition coefficient (K_p) and the concentration of suspended solids in the medium (SS).

$$f_{dis} = \frac{1}{1 + K_p \cdot SS} \tag{3.25}$$

$$f_{par} = \frac{K_p \cdot SS}{1 + K_p \cdot SS} \tag{3.26}$$

In the case of HMs, a linear relationship between the concentration is assumed. K_p is a inherent property of each HM such as the molecular weight.

OMPs adsorb to organic matter components, that is particulate organic matter (POC), dissolved organic matter (DOC) and phytoplankton. It is also important to note that the partition coefficient of OMPs is proportional to the concentration of organic carbon in suspended solids. According to DiToro (1985), the formulation considers the reversibility of the process by a factor of exchangeable distribution of organic carbon that is approximately the octanol-water partition coefficient (K_{ow}) displayed in equation (3.27).

$$K_p = \frac{2 \cdot f_{OC} \cdot K_{ow}}{1 + \frac{(SS \cdot f_{OC} \cdot K_{ow})}{1.4}} \tag{3.27}$$

where f_{OC} is the is the weight fraction of the total organic carbon in the suspended solids, usually ranging from 0.001 to 0.1.

Sedimentation/Settling

The sedimentation process affects only the particulate fraction. This process is considered as a mass flux through the area of water-sediment interface. The sedimentation constant is proportional to the sedimentation velocity (Equation (3.28)).

$$K_{sed} = \frac{V_{sed}}{H} \tag{3.28}$$

where H is the depth of the water column.

In this work, the sedimentation velocity is considered spatially and temporally constant (Equation (3.29)).

$$V_{sed} = \alpha \cdot \frac{g}{18} \cdot (\frac{\rho_{par} - \rho_{env}}{\mu_{water}}) \cdot d_{par}^2 \tag{3.29}$$

where α is a dimensionless factor that reflects the effect of particle shape (1.0 for spheres), g is the gravity acceleration, ρ_{par} is the particle density, ρ_{env} is the water density, μ_{water} is the water viscosity and d_{par} is the particle diameter.

Volatilization

Only the free dissolved OMP is available for volatilization. Transport of OMPs across the water-atmosphere interface (volatilization) is based on the double film theory (Lewis & Whitman 1924). The mass transfer is determined by molecular diffusion, being the transfer rate a function of the concentration gradient at the interface and at the two fluids (liquid and gas). Equilibrium is assumed between the concentrations of the OMP in the gas film and the liquid film according to Henry's Law in order to obtain the volatilization constant (K_{vol}) as shown in equation (3.30).

$$K_{vol} = [\frac{K_{gas} \cdot K_{liq} \cdot (\frac{He}{R \cdot T})}{\frac{He}{R \cdot T} \cdot K_{gas} + K_{liq}}] \cdot \frac{1}{H} \tag{3.30}$$

where He is the Henry's constant, R is the gas constant, T is the temperature, K_{liq} is the transfer coefficient for the OMP for the liquid film, K_{gas} is the transfer coefficient for the OMP for the gas film and H is the depth of the water column.

To calculate K_{liq} and K_{gas}, the approximation of Mackay & Yeun (1983) has been used. This approximation relates K_{liq} with the oxygen dissolved transport (Equation (3.31)) and K_{gas} with the water vapor transport (Equation (3.32)). Moreover, equation (3.31) considers O'Connor (1985) proposal which relates the K_{liq} with the transfer coefficient of dissolved oxygen ($D_{liq_{O2}}$), the mean velocity of the flow and the wind (U and U_w) and the depth of the water column (H). On the other hand, equation (3.32) assumes Mills *et al.* (1982) work, where K_{gas} has been considered to be proportional to wind speed (U_w). Finally, we took into account (Schwarzenbach *et al.* 1993) studies, which relates transfer coefficients to the molecular weight of the OMP (M_{OMP}), water (M_{water}) and dissolved oxygen (M_{O2}).

$$K_{liq} = [(D_{liq_{O2}} \cdot \frac{U}{H})^{0.5} + \frac{1}{86400} \cdot (0.728 \cdot U_w^{0.5} - 0.317 \cdot U_w + 0.0372 \cdot U_w^2)] \cdot (\frac{M_{O2}}{M_{OMP}})^{0.25} \tag{3.31}$$

$$K_{gas} = \frac{168}{86400} \cdot U_w \cdot (\frac{M_{water}}{M_{OMP}})^{0.25} \tag{3.32}$$

Overall degradation

Three types of degradation processes can be distinguished: photolysis, hydrolysis and biodegradation. For all processes the degradation rate is proportional to the OMP concentration and a function of temperature. The various processes for decomposition of OMPs are integrated in one overall degradation process (Equation (3.33)). First order temperature dependent kinetics have been used to formulate this process.

$$K_{deg} = K_{pho} + K_{hyd} + K_{bio} \tag{3.33}$$

- Photolysis (K_{pho}) is the process by which the solar radiation acting on certain chemical molecules, altering its structure, degrading and decomposing. The photolysis rate is also dependent on solar radiation.
- Hydrolysis (K_{hyd}) occurs when the OMP reacts with the water and new compounds are produced by breaking bonds. The hydrolysis rate is dependent on the pH.
- Biodegradation (K_{bio}) is produced by the action of bacteria. The biodegradation constants are dependent on the presence of oxidising or reducing conditions.

Most of these degradation processes were studied by experiments in the laboratory to give the half-life of the OMP (t_{mean}). This time is defined as the time required to reduce the initial OMP concentration to half due to the effect of the degradation process under study. Degradation processes are considered as an exponential decay in order to calculate the rate constants of the different processes (Equation (3.34)).

$$K_i = \frac{\ln 2}{t_{mean_i}} \tag{3.34}$$

Finally, the overall degradation might be influenced by the temperature dependency of reaction rates (Equation (3.35)):

$$k_{Temp} = k^{20} \times k_T^{T-20} \tag{3.35}$$

where k_{Temp} is the rate constant at temperature T (d^{-1}), k^{20} is the rate constant at reference temperature 20 ^oC (d^{-1}), k_T is the temperature coefficient (-), T is the ambient water temperature (^oC).

The temperature coefficient usually ranges between 1.01 and 1.10. With a value of 1.04 the reaction rate at 10 ^oC is 68 % of the rate at 20 ^oC. A value of 1.07 results in a doubling or halving of a reaction rate every 10 degrees increase or decrease respectively.

3.5.4.2 Additional information

These information is related to measurements (field data) necessary to conduct the model setup of transport model with non-conservative substances. In this context, we need to collect information about the studied toxicant(s), suspended solids in the water column and the additional processes included by the non-conservative approach.

For model calibration, measurements of toxicants at two points across the estuary during 6 months are requested. Moreover, field data or chemical databases are required to define open boundaries and the characteristics of active processes:

- Measurements of suspended solids at 4 points across the estuary, 1 point at the open-river boundary and 1 point at the open-sea boundary during one year with a seasonal frequency. These measurements encompass the physical characteristics of suspended solids: concentration, shape, diameter, density and weight fraction of the total organic carbon.
- Water density and viscosity (from hydrodynamic model).
- Octanol-water partition coefficient.
- Transfer coefficient of dissolved oxygen.
- Molecular weight of oxygen.
- Partition coefficient, Henry's constant, transfer coefficient for the liquid film, transfer coefficient for the gas film, photolysis constant rate, hydrolysis constant rate, biodegradation, temperature coefficient loss and molecular weight. Note that all of these coefficients are referred to the studied toxicant.

3.5.4.3 **Model setup**

Model setup of the transport model (non-conservative approach) is required to define the model domain discretization, provide boundary and initial conditions and, finally, carry out the model calibration/validation (Figure 3.35).

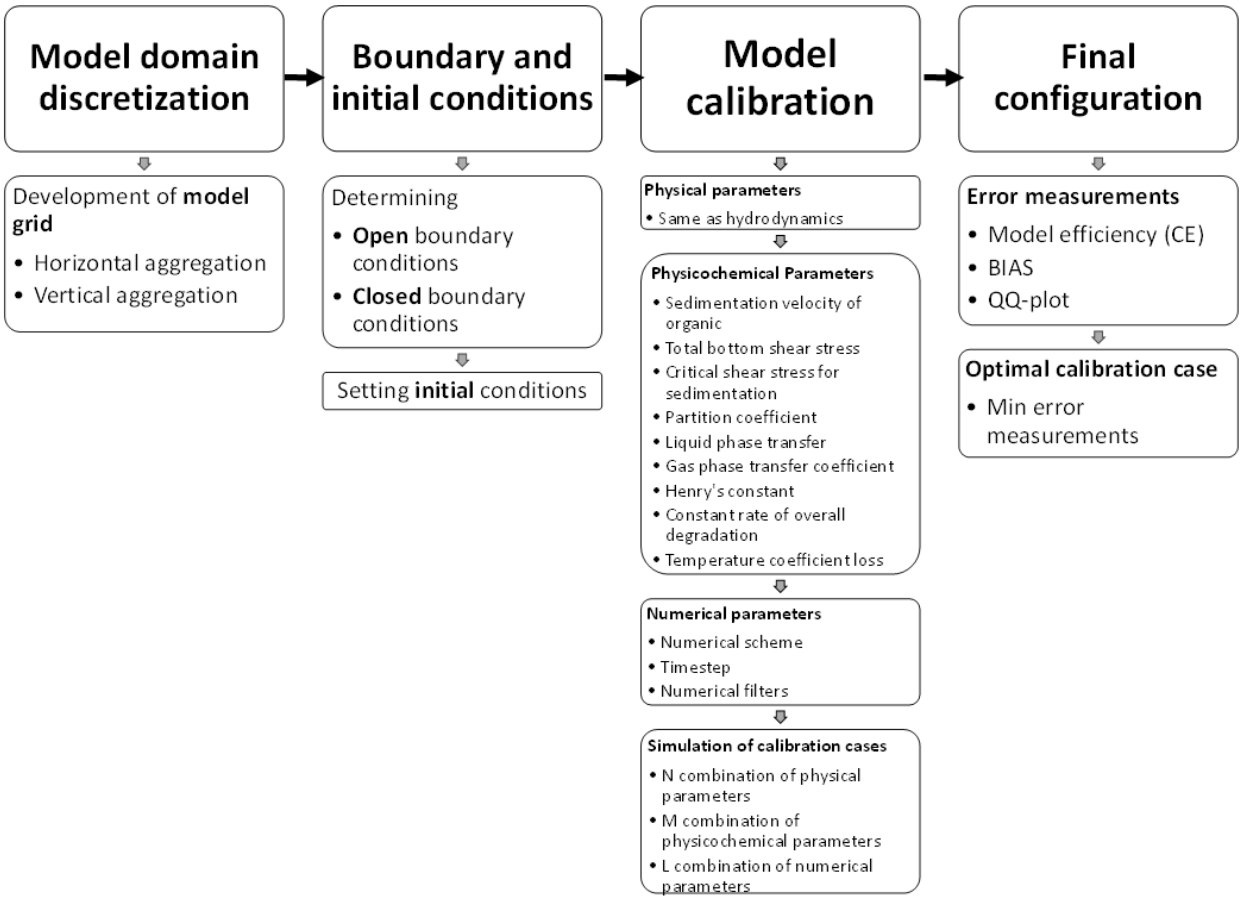

Figure 3.35: Scheme of the involved tiers of the far-field model setup for non-conservative substances.

Model domain discretization

The model domain discretization is the same that it was used for the hydrodynamic and transport (conservative) model setup, i.e., the transport (no conservative) model grid has the same number of nodes (grid cells) and layers. No horizontal and/or vertical aggregation was used.

Boundary and initial conditions

Open and closed boundary conditions

In designing the model domain, OBs should be delineated at a sufficient distance away from the estuary, so that the OB errors do not influence the solution within the interior domain. In this way, OB can be set as clamped (or specified) boundary condition with a constant, spatially variable or temporally variable value depending on the available measures for toxicants and suspended solids (inorganic and organic).

CBs are is set to zero. The vertical diffusive flux of toxicant through the free surface and bed is set with the specific processes acting on them, i.e. volatilization and sedimentation. In the case of suspended solids, the volatilization rate is zero so sedimentation is the only process acting on them.

Initial conditions

In order to run the transport model, it is necessary to prescribe ICs taking into account the industrial discharges.

Due to the field of non-conservative tracer in the study area is unknown, the initialization of the transport model sets to zero during the model calibration. As a consequence, the timescale of the "quasi-stationary" response of the "worst case of dilution" should be considered because this timescale indicates the minimum duration of any far-field simulation to ensure that initial conditions are not influencing the model results.

Regarding suspended solids, the initialization of the transport model sets to a constant, spatially variable or temporally variable value depending on the available measures in the model domain.

Model calibration

The calibration process determines the values of physical parameters, physicochemical parameters (HM and OMP) and numerical parameters in order to adjust the results given by the numerical model.

Physical parameters

Physical parameters are the same used for the transport model of conservative substances and, consequently, calibration is not necessary.

Physicochemical parameters for heavy metals

Physicochemical parameters for heavy metals are the sedimentation velocity of inorganic matter, the total bottom shear stress, the critical shear stress for sedimentation, the partition coefficient and the half-time of non-equilibrium adsorption and desorption.

Physicochemical parameters for organic micropollutants

Physicochemical parameters for organic micropollutants are the sedimentation velocity of organic matter, the total bottom shear stress, the critical shear stress for sedimentation, the liquid phase transfer coefficient, the gas phase transfer coefficient, the Henry's constant, the ambient water temperature, the temperature coefficient loss, the constant rate of overall degradation and the partition coefficient.

Numerical parameters

Numerical parameters are the same employed in Step 3 and 4.

Simulation-calibration cases

Physical parameters	**Suggestions**	**Value ranges**
All parameters	Same hydrodynamic model	Hydrodynamic calibration
Physicochemical parameters (HM)	**Suggestions**	**Value ranges**
Sedimentation velocity of inorganic matter	Equation (3.29)	Field data
Total bottom shear stress	Imported from hydrodynamics	-
Critical shear stress for sedimentation	Lab experiments	Field data
Partition coefficient	Specific of each HM	Chemical databases
Half-time of adsorption and desorption	Instantaneous equilibrium	Zero
Physicochemical parameters (OMP)	**Suggestions**	**Value ranges**
Sedimentation velocity of organic matter	Equation (3.29)	Field data
Total bottom shear stress	Imported from hydrodynamics	-
Critical shear stress for sedimentation	Lab experiments	Field data
Partition coefficient	Equation (3.27)	Field data
Liquid phase transfer coefficient	Equation (3.31)	Field data
Gas phase transfer coefficient	Equation (3.32)	Field data
Henry's constant	Specific of each OMP	Chemical databases
Constant rate of overall degradation	Equation (3.33)	Chemical databases
Ambient water temperature	Imported from hydrodynamics	-
Temperature coefficient loss	Equation (3.35)	1.01 to 1.10
Numerical parameters	**Suggestions**	**Value ranges**
All parameters	Same conservative model	Conservative calibration

Table 3.5: Overall picture of far-field model calibration parameters for non-conservative approach.

Simulation-calibration cases are all the different model simulations performed by means of N combinations of physical parameters, M combinations of physicochemical parameters and L combinations of numerical parameters in order to find the best combination of model parameters. Table 5.16 synthesizes the calibration parameters, suggests the best option for estuarine modeling and gives the optimal value ranges of each parameter.

As it can be seen from table 5.16, if hydrodynamic and transport (conservative) model are previously calibrated, the transport (non-conservative) model calibration is related to the specification of physicochemical parameters for the studied toxicant.

Final configuration

The final configuration of the model is the combination of all mentioned parameters that best match the results obtained by the model and the data measured in the study area.

Error measurements

In order to find the optimal calibration case, two error measurements are calculated: the BIAS and the CE. For each simulation-calibration case, we compare the values of the model data and the survey data in terms of concentrations.

Firstly, BIAS is calculated by means of equation (3.10) and, secondly, the error between both series using the CE is calculated by equation (3.11).

Optimal calibration case

From error measurements of each simulation-calibration case, the optimal calibration case is the case simultaneously displaying the minimum BIAS and the maximum CE. Therefore, this combination of model parameters will be used along the rest of the methodology for conducting far-field simulations of non-conservative substances.

3.5.4.4 **Transport real case modeling**

In order to run the transport of the "real case of dilution" for each M model scenario, the previous simulation of the hydrodynamic model and the initial dilution data from the coupling approach are used.

We propose to perform M "presimulations" to obtain the adequate initial condition of toxicant concentration and suspended solids. Then, M "simulations" to record the concentration evolution for each M model scenario is suggested.

Firstly, M "presimulations" are carried out under "quasi-fixed hydrodynamic conditions". We run the far-field model with model results (hydrodynamics and coupling) of the first day in a continuous loop until reach a "quasi-stationary" response (see Figure 3.21). The timescale of the "worst case of dilution" indicates the minimum duration of any far-field "presimulation" to ensure that initial conditions are trustable.

Once it is reached the "quasi-stationary" response, we record the concentration field of the first time step that corresponds to the first hour of each M model scenario, i.e, the initial condition for each M model scenario in the study area (see figure 3.22).

Secondly, we run each M model scenario (n days) with the initial conditions obtained in the M "presimulations". Next, we hourly record n days of transport model results for the M "simulations". Figure 3.36 displays an example of the the far-field model results for the concentration evolution of four grid cells located across the model domain in a "real case of dilution".

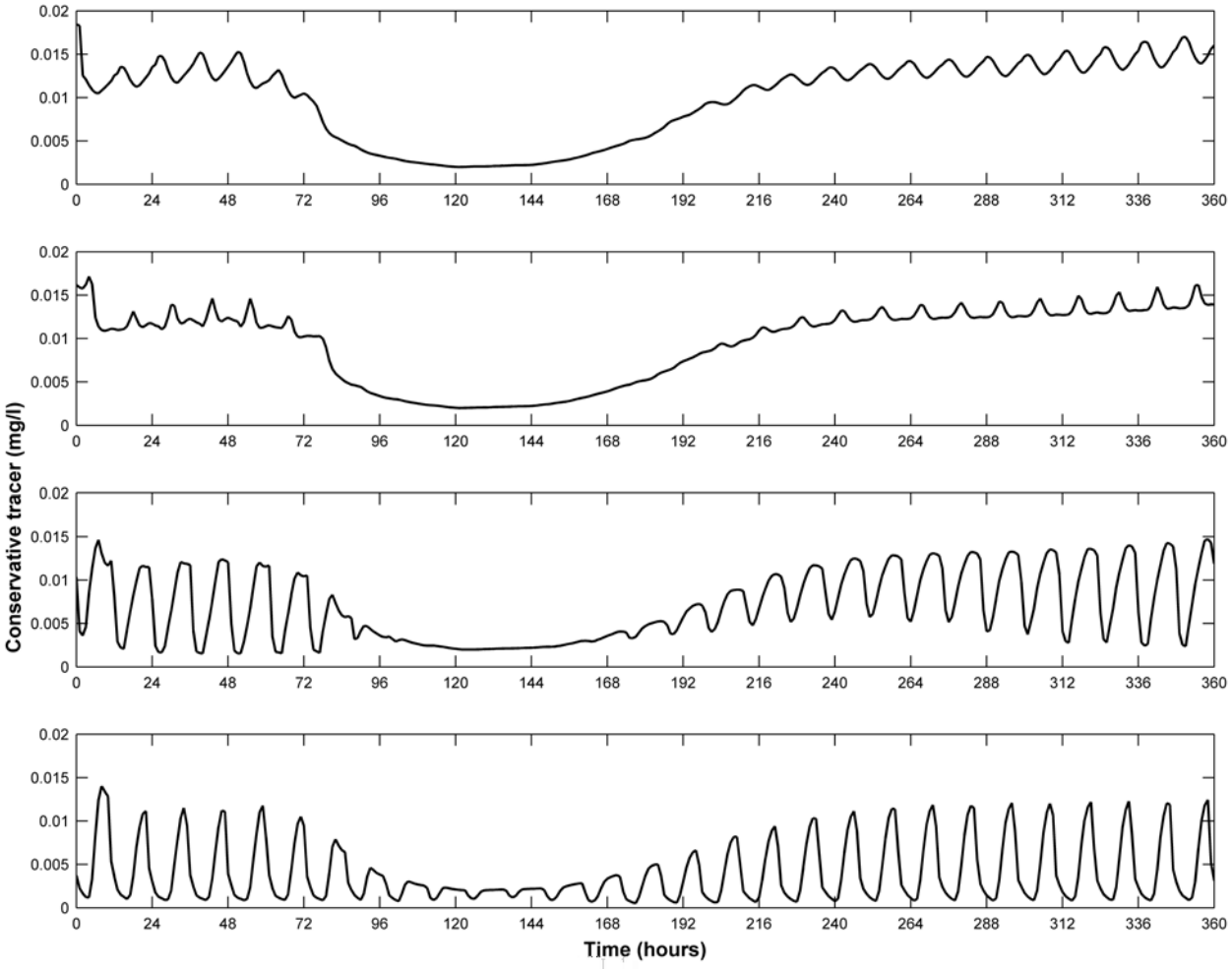

Figure 3.36: Example of the evolution of a non-conservative toxicant for the transport of a "real case of dilution" at four grid cells located across a model domain.

3.5.4.5 Delimitation of mixing zones

In the detailed calculation, we run M model scenarios under real conditions. These M model scenarios have and occurrence probability, this is the product of the probability of the M river flow group and the M tidal group.

There are a lack of definition in regulations in how to delimitate mixing zones. Among other issues, there is not specified a methodology to conduct monitoring programmes, to calculate the EQS compliance based on discrete or continuous data or to allow a temporal EQS excursion. Because of these, a method to delimitate MZ was proposed in Step 4 that is the starting point for the delimitation of MZ in the "real case of dilution".

The problem in the "real case of dilution" lies on how to delimitate MZ taking into account:

- The capability of the M model scenarios to adequately reconstruct the evolution of toxicant concentration of "real series" from a combination of this M model scenarios ("synthetic series").
- The selection of a number of l-representative years to carry out the delimitation that do not influence the results and reflect the forcing variability. In this way, we avoid the selection of only few real years for designing, i.e., what year is the most representative of the estuary? A dry year, a wet year, a mean year, all of them, etc.
- The temporal specification of EQS excursions that can be allowed if the impact on the receiving water body is considered acceptable.

According to these considerations and issues, the method to delimitate MZ should specify all the requirements of the methodology of the intermediate calculation (see figure 3.24) plus the validation of the M model scenarios to adequately reconstruct "real series" and the selection of a number of l-representative years.

After model simulations, two MZs are anew proposed: the AA-MZ and MAC-MZ. To achieve this delimitation, we propose a method involving four tiers: Validation of the reconstructed series, Selection and generation of l-years, Random sampling and Final delimitation of MZs (Figure 3.37).

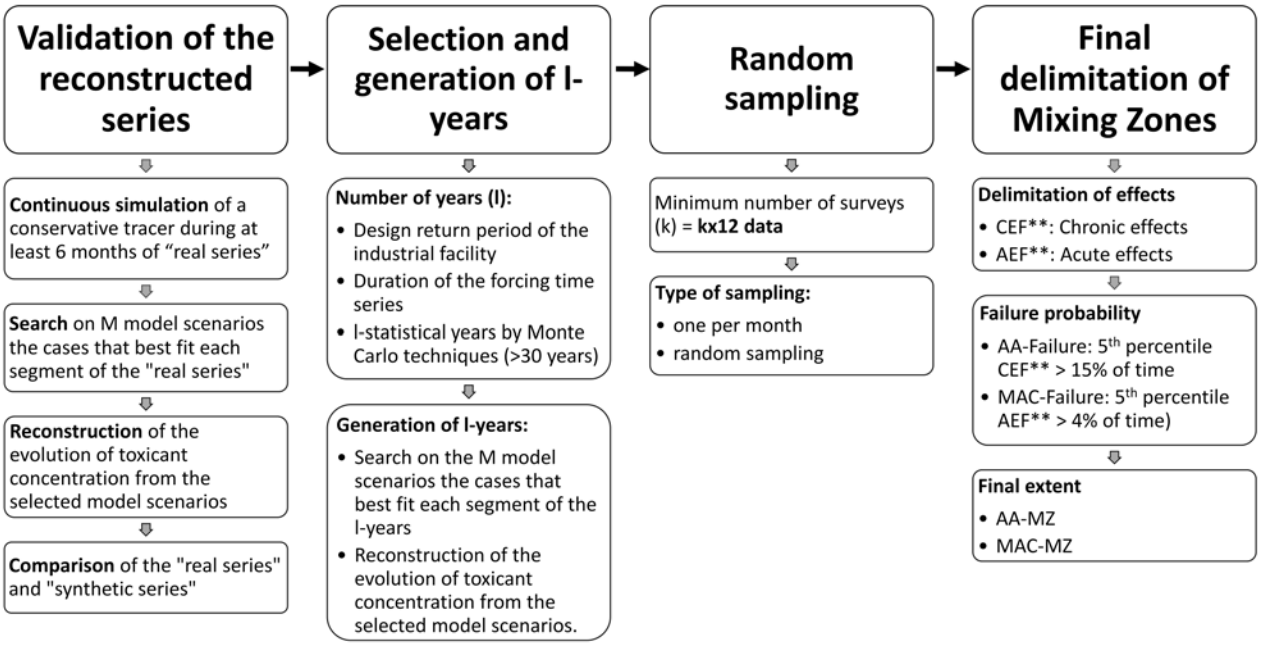

Figure 3.37: Methodology to delimitate mixing zones on estuaries in the detailed calculation or "real case of dilution".

Validation of the reconstructed series

The first tier is validate the ability of the M model scenarios to adequately reconstruct "real series", i.e, the evolution of toxicant concentration based on the combination of the M model scenarios. This validation is conducted in several steps:

1. Continuous simulation of the non-conservative toxicants taking into account the "real series" of river flow and tidal elevations during at least 6 months (Figure 3.38a, 3.38b and 3.38c). Regarding the

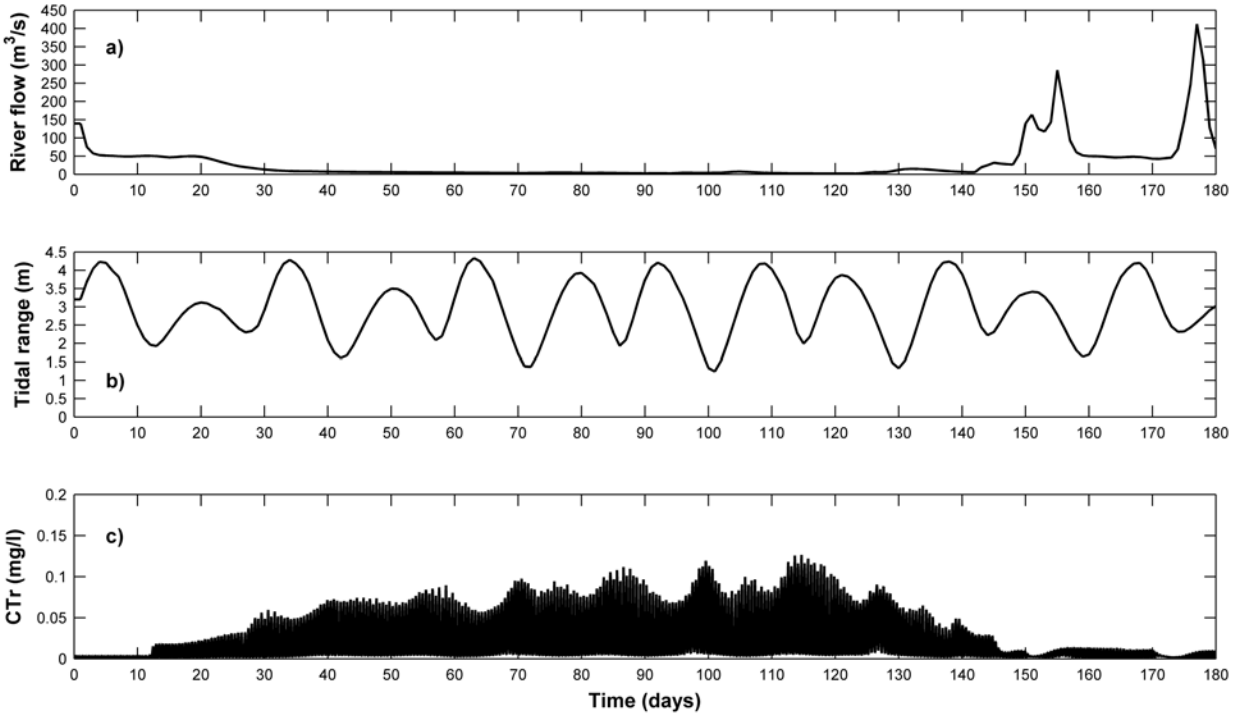

Figure 3.38: Example of 6-months of forcing time series and the evolution of concentration. The daily river flow series (a), the daily tidal range series (b) and the hourly evolution of concentration (c) are displayed.

stability of model results and the influence of initial conditions, we conduct again one "presimulation" under "quasi-fixed hydrodynamic conditions" for the 24 first hours of the "real series" until reach a "quasi-stationary" response (see Figure 3.21). Next, we record the concentration field of the first time step that corresponds to the first hour and, finally, we run all the simulation with the initial conditions obtained in the "presimulation" and recording, hourly, n days of transport model results (see Figure 3.22).

2. Search on the M model scenarios the cases that best fit each segment of the "real series" during at least 6 months.

3. Reconstruction of the evolution of toxicant concentration from the selected model scenarios (Figure 3.39).

4. Comparison of the "real series" and "synthetic series" in order to validate the obtained results with "synthetic series" (Figure 3.39) at daily time resolution (24-hours averaged). For this substep, CE, BIAS, the difference between both averages and the time exceeding a threshold (EQS) are used as error measurements.

   Regarding this daily comparison, we propose this resolution because the tidal phase will be not the same along the evolution of toxicant concentration of the "real series" and "synthetic series". Meantime the

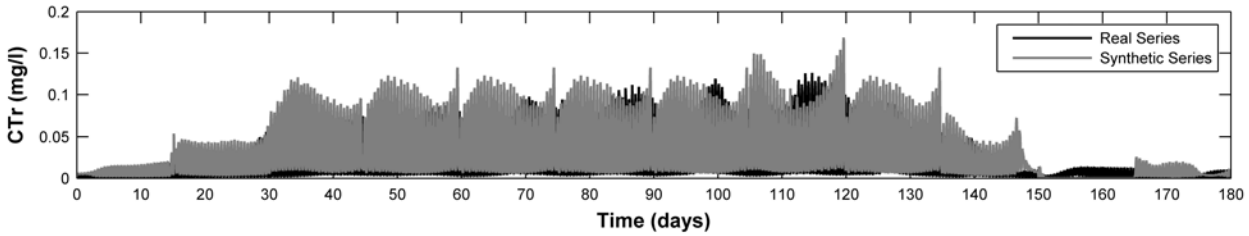

Figure 3.39: Example of 6-months of the evolution of concentration for the "real series" (black color) and the "synthetic series" (grey color).

"real series" are a continuous evolution, the "synthetic series" are made by the combination of M model scenarios (n days). As a consequence, there will be a lag between both series because they do not necessarily start at the same tidal phase, there will also be a gap in the union of 2 model scenarios because the end of one model scenario could be slightly different to the start of the next one and, anew, this new scenario could be out of phase related to the "real series".

We think that the daily tidal range is a good descriptor of the signal because it is the evolving curve. This curve retains all the important information of the semi-diurnal signal filtering considerably the lag differences will be experimented due to the reconstruction of the "synthetic series".

After this validation, if results are fairly reasonable we can generate any "real series" of toxicant concentration based on a sequence of multiple M model results ("synthetic series") that best fits the "real series".

Selection and generation of l-years

In this second tier, the selection and generation of a number of l-representative years to carry on the delimitation is presented. The consideration of a long sequence of years ensures a proper characterization of the evolution of toxicants in the estuary based on the hydrometeorological phenomena. This selection of l-years could be established attending to the following approaches:

1. The design return period of the industrial facility. These return periods are usually between 20 and 100 years.
2. The duration of the forcing time series used to classify M model scenarios. From these time series, we suggest reconstruct all these years based on the M model results that best fits them.
3. The generation of l-statistical years by Monte Carlo techniques based on the probability of the M model scenarios. This selection must take into account the variability of the hydrodynamic forcings and the independence of the results.

In the two first approaches, the selection of the number of years is immediate due to the design return period or the duration of the time series are known data.

In the third approach, the generation of statistical years by Monte Carlo sets that the occurrence probability of any M model scenario could be different to the actual M probability from KMA selection. These differences are due to the fact that the time duration of a single year is less than the initial long-term series used for the selection (usually plus 30 years). In addition, the number of events (x consecutive model scenarios) are also fewer than all the M model scenarios.

For instance, there will not be some M model scenarios in a single year due to a very low occurrence probabilities (less than one per year) so it might be required many years to reproduce the occurrence probabilities

displayed by the KMA selection. This is why we recommend to generate at least 100 years as the minimum number of statistical years (l) when employing Monte Carlo techniques and the occurrence probability of each M model scenario.

After the selection of l-years, we reconstruct the evolution of toxicant concentration from the selected sequences of M model scenarios. It is worth to mention that the values of the reconstruction are the maximum concentration of all the layers at each time step.

Random sampling

In the Step 4, the optimal number of surveys ($k\times12$ data) to ensure that the delimitation of MZ is independent of the number of surveys along one year of model results was determined. Now, the random sampling is calculated for the k-surveys in every l-statistical year.

Final delimitation of MZs

Once the measures of toxicant concentration are calculated, in the fourth tier, their effects are determined for each l-year by the nature of the exposure. Besides the k-surveys, in the detailed calculation, we also generate l-years of evolution of toxicant concentration. Therefore, the delimitation of MZs has to compute the probabilities of the k-surveys for every l-years as follows:

- *Chronic effects (CEF**):* Chronic effects of each toxicant in every grid cell are computed using the equation (3.17) for each l-year taking into account every k-surveys. Next, if $CEF**^k_{i,j} > 1$ then $CEF**^k_{i,j} = 1$. On the contrary, if $CEF**^k_{i,j} \leq 1$ then $CEF**^k_{i,j} = 0$.

  Then, the CEF** associated to all the k-surveys is computed by the equation (3.18) for every l-year. Finally, we obtain an array of l-CEF** values in every grid cell of the mesh grid, i.e., the AA-failure probability of every l-year. From this array, the ecdf of CEF** is calculated.

- *Acute effects (AEF**):* Acute effects of each toxicant in every grid cell are computed by the fraction of data in adverse conditions using the equation (3.19) for each l-year taking into account every k-surveys. Next, if $AEF**^k_{i,j} > 0$ then $AEF**^k_{i,j} = 1$. On the contrary, if $AEF**^k_{i,j} \leq 0$ then $AEF**^k_{i,j} = 0$.

  Then, the AEF** associated to all the k-surveys is computed by the equation (3.20) for every l-year. Finally, we obtain an array of l-AEF** values in every grid cell of the mesh grid, i.e., the MAC-failure probability of every l-year. From this array, the ecdf of AEF** is calculated.

Again, two MZs are determined: the AA-MZ and the MAC-MZ. Furthermore, as in Step 4, a failure probability is assumed by expert criteria ($CEF^{**}_{i,j} > 15$ and $AEF^{**}_{i,j} > 4$).

Besides the failure probability for one year of model sampling, in Step 5, we have the distribution of CEF** and AEF** for l-years. This is why a new temporal specification, number of years that a grid cell is above the failure probability, should be established in order to delimitate the final extent of MZs. For instance, if the new temporal specification is set to zero the delimitation is reduced to the intermediate calculation or "dry case of dilution". On the contrary, if the new temporal specification is set to 100 any MZ can be delimitated. Therefore, this temporal specification have also to bear in mind the trade-off between the extent of MZs versus the percentage of years allowed to surpass the failure probability.

Regarding the percentage of failure years, Bárcena *et al.* (2012) investigated its influence in the final extent of MZs by analyzing the evolution of toxicant concentration in three real years (2003-medium, 1993-wet and 2000-dry) taking into account three temporal specifications (10%, 5%, and 1% of the time). After mathematical calculations, we concluded that the 5% (5^{th} percentile) was the most suitable temporal specification because it balances the extent of MZs with the allowance of failure. According to this proceeding, we decided

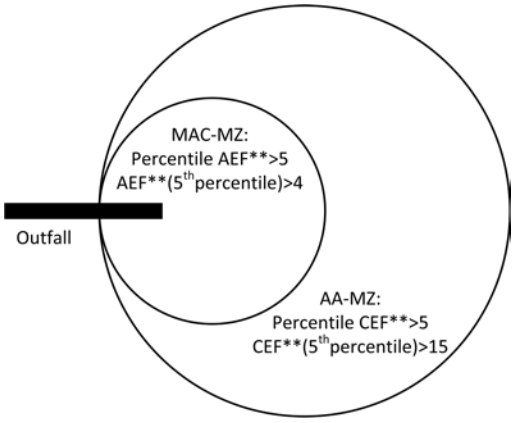

Figure 3.40: Diagram of the two delimitated parts of Mixing Zones (AA-MZ and MAC-MZ) in the detailed calculation.

that a grid cell is part of the delimitated MZs when the 5^{th} percentile of the ecdf of CEF** and AEF** are above 15 and 4, respectively (Figure 3.40).

Lastly, the admissibility of the proposed MZs is checked with the admissibility criteria developed in the Section 3.5.5. If the proposed MZs are admissible, the allocation procedure finalizes. On the contrary, the discharge is classified as inadmissible.

3.5.5 Admissibility of Mixing Zones

As we mentioned throughout this thesis, State Members may designate approaches and methodologies to define MZs (EC 2008a, EU 2013).

The methodology proposed herein is based on a holistic approach, which considers simultaneously the physical processes involved in dispersion and diffusion mechanisms, the ecological features of the receiving water body and the social aspects related with the water body uses. This approach provides the acceptability criteria of the size of MZs and location of point discharges in order to guarantee an effective decision-making process. We adapt the methodology proposed by Gómez *et al.* (2014b) to assess the environmental risk of dredging processes in order to estimate the vulnerability of industrial point discharges in estuaries (Figure 3.41).

From the concept of vulnerability and the percentage of estuarine area covered by MZs, we define and determine the admissibility of MZs in a four-tiered method:

1. Estuarine Vulnerability Index (EVI) is calculated at grid cell level by means of several parameters.
2. Acceptability (AC*) is estimated by multiplying EVI values with the percentage of estuarine area cover per grid cell.
3. Maximum allowable size (MAS*) is computed by dividing the maximum admissible percentage of estuarine area that a MZ can cover (expert criteria) with a correction factor (α) which depends on the average EVI of the estuary.
4. Admissibility of the delimitated MZ (AD*) is determined by comparing the sum of all AC* grid cells covered by the delimitated MZ with the MAS*.

Estuarine Vulnerability is referred to characteristics of an estuarine ecosystem that describes its potential to be harmed. Thus, vulnerability is presented as a combination of four parameters, namely tidal zoning (TZ), susceptibility (SU), state of conservation (SC) and stratification (ST).

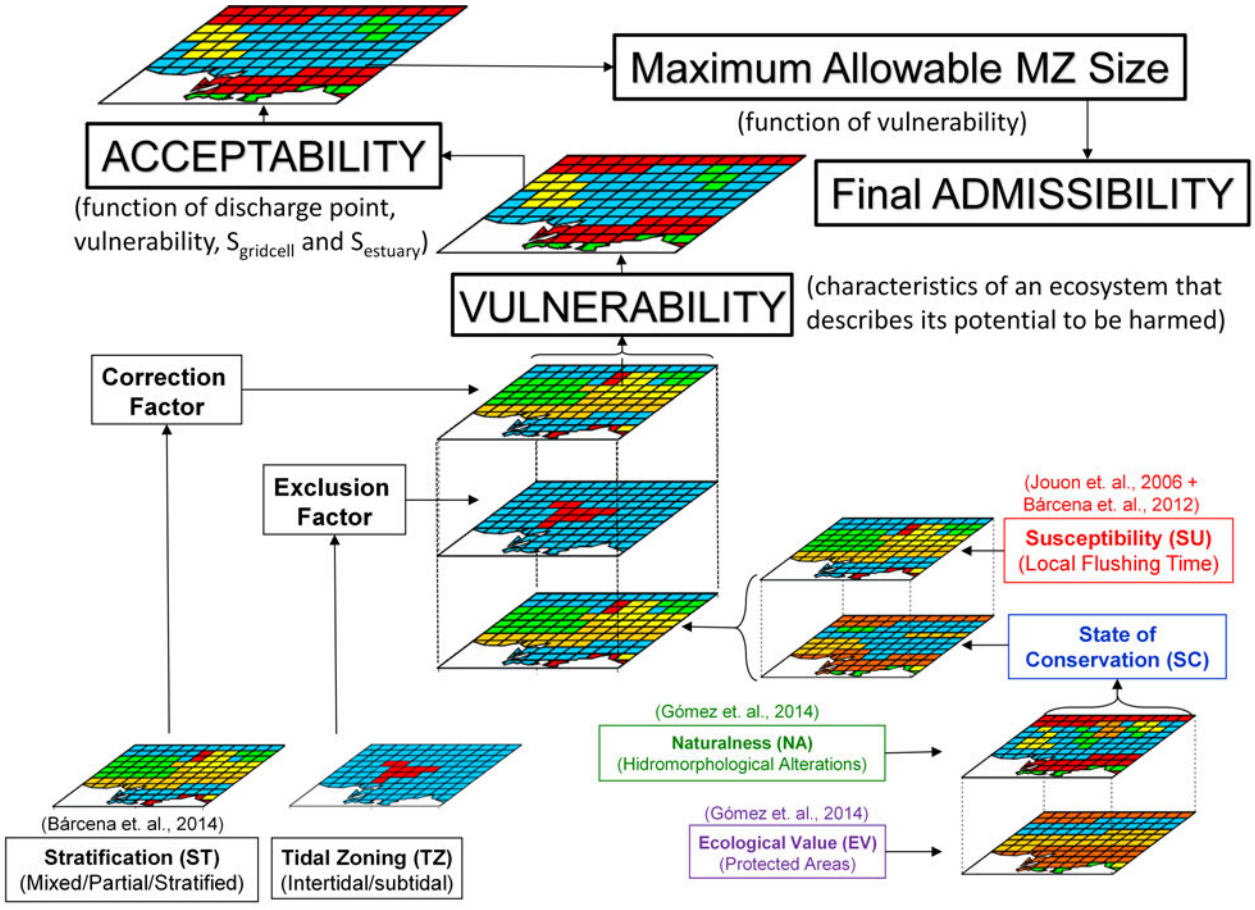

Figure 3.41: Schematic view of the proposed methodology to quantify the estuarine vulnerability and the admissibility of mixing zones.

Additionally, it is worthy to mention that all parameter calculations are carried out on the study area through the same mesh grid. TZ, SU and ST are computed using numerical models. SC is obtained using Geographical Information Systems (GIS). All results are integrated at grid cell level to estimate spatially the vulnerability and admissibility on the whole domain by means of a index namely Estuarine Vulnerability Index (EVI).

3.5.5.1 **Tidal zoning (TZ)**

TZ is the location of the intertidal and subtidal zones according to the percentile 95^{th} of the tidal amplitude ($A95$) and the depth of each grid cell (H). This parameter was designed in order to protect estuarine areas where drying and wetting processes occur.

Tidal flats are highly productive areas and although biological diversity may be relatively low, tidal flats support a high biomass of micro- and infaunal organisms, support fish and shellfish stocks and play an important role in nutrient chemistry. Collectively these intertidal habitats are of great importance to large numbers of invertebrates and fish, supporting complex estuarine food webs and providing resting and feeding areas to large numbers indigenous and migratory birds. Tidal flats provide enormous water carrying capacity, protecting areas of estuaries from storm surge, storm water runoff and/or waves (Galván *et al.* 2010).

Therefore, as a principle, a point discharge cannot be located at intertidal areas. TZ can bee seen as an exclusion factor inside the methodology.

3.5.5.2 **Susceptibility (SU)**

Susceptibility is related to the flushing capacity and is estimated by means of numerical models. Numerical simulations are a suitable tool to tackle the estimation of water renewal because they can account with realistic coastal geometry and bottom topography, as well as different physical factors.

Water renewal of estuarine ecosystems is a measure of its self-purification capacity. In general, the renewal time of an estuary is the average time that the dissolved or suspended matter resides in the system before it is transported to the open sea.

Determining the distribution of renewal time is an effective technique for diagnosing the fluid behaviour within a wide range of flow systems (Levenspiel 1972). In particular, the application to natural systems such as bays and estuaries is used to characterize the distribution of the renewal time of a toxicant discharge and the transport capacity of these loads (Abdelrhman 2005, Huang 2007, Jouon *et al.* 2006, Monsen *et al.* 2002, Sámano *et al.* 2012).

When selecting the indicator that determine the transport timescales, there is a certain ambiguity in scientific nomenclature. The term “residence or renewal time” is used interchangeably to refer to computational methods that differ in their theoretical formulations. Regarding this descriptor, there are different concepts such as the residence time and the flushing time (henceforth RT and FT).

RT is considered a local measure with spatial variation, whereas FT is considered a measure of the system level and a unique value for the entire water body (Choi & Lee 2004). Consequently, RT is defined as the period of time required for a water parcel, initially located at the point considered, to leave the domain (Soulsby & Tetzlaff 2008, Takeoka 1984), implying that the definition deals with moving individual pieces for a spatially varying situation (Zimmerman 1978). On the other hand, the estuarine FT considers the average amount of time that fresh water spends in the system (Alber & Sheldon 1999), that is, the rate at which river freshwater is flushed out of an estuary (Huang 2007).

Because of the geometry of estuaries is complex, the vertical flow structure might present a three-dimensional character and the circulation patterns might vary significantly between seasons, an indicator of residence or

renewal time that takes into account these aspects in its theoretical formulation is required. In this work, we use the local flushing time concept (Jouon *et al.* 2006) and the methodology proposed by Bárcena *et al.* (2012b) in order to estimate this flushing capacity according to the temporal variations of the main forcing (river and tide) and the spatial variations of the estuarine configuration.

Therefore, we suggest a methodological approach based on the use of computational tools for the calculation of flushing time (FT) divided into four tiers: Hydrodynamic forcing analysis, FT calculation, FT sensitivity analysis and Final FT. Figure 3.42 shows an outline of the methodology followed by this study. The calculation methodology described has been encoded using the mathematical software MATLAB (see more information on Chapter 4).

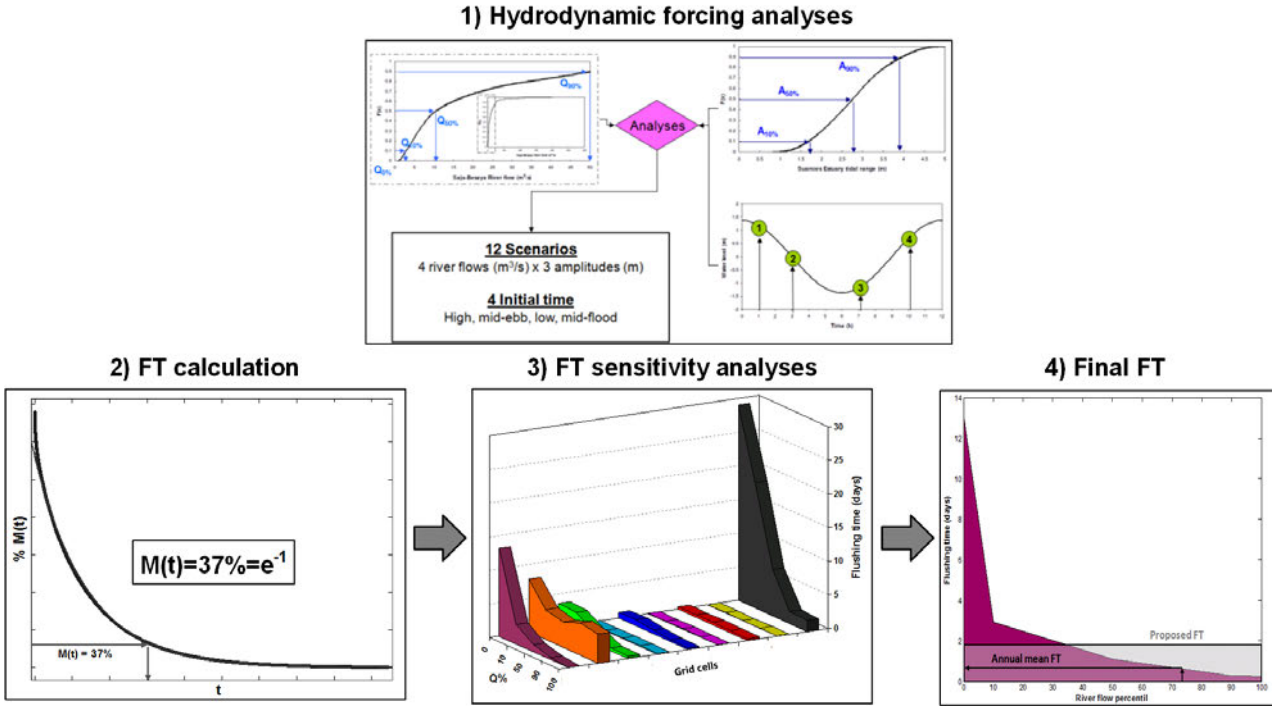

Figure 3.42: Schematic view of the proposed methodology to calculate flushing time in estuaries.

Hydrodynamic forcing analyses

In this approach, we consider hydrodynamic changes to be determined by river inflows and the astronomical tides. In order to understand the magnitude and the occurrence of these forcing, the first task is to calculate the empirical distribution functions (ecdf) of the river flow series (m^3/s) and the astronomical tidal range series (m).

From these curves, we select N river flows equal to N percentiles, M tidal ranges equal to M percentiles and, finally, L tidal phases corresponding to L tidal situations. This selection is based on the breaking points of each ecdf curve. Summarizing, we integrate the forcing variability and seasonality in $N \times M \times L$ scenarios.

Flushing time calculation

Among all the existing methods in the literature, the proposed methodology by Jouon *et al.* (2006) has been selected to compute water renewal. This method proposes the application of a three-dimensional hydrodynamic model coupled to a three-dimensional transport model.

The method generates two local parameters for every grid cell, the "flushing lag" (FL) relating to the time required for water coming from outside the control volume to reach the mesh in significant quantity, and the

"local flushing time" (LFT) which defines the time span required, after the FL, for water from inside the control volume (grid cell) to occupy approximately 37% ($1/e \approx 0.367$) of the grid cell's volume. If one considers that a known quantity of a substance is injected in a homogenous water mass at time t_0 at an initial concentration C_0, no further amount of this substance is added after t_0 and the volume of the water mass and fluxes at its boundaries are constant: the concentration of the substance within the water mass at time t is given by the equation (3.36).

$$C(t - t_0) = C_0 e^{-Q/V*(t-t_0)} = C_0 e^{-(t-t_0)/t_f} \tag{3.36}$$

where Q represents the flow (entering or exiting), V is the volume of the control volume considered, t is the time ($t > t_0$) and t_f is the flushing time.

The computation method is as follows:

1. Hydrodynamic modeling is carried out for the proposed scenarios.
2. Initially, a concentration C_0 of a conservative, non-settling tracer is imposed on the area of interest, and given a non-zero value (e.g. $C_0 = 1$). On the grid cells outside the area of interest, concentration is held at zero (see Figure 3.43a).

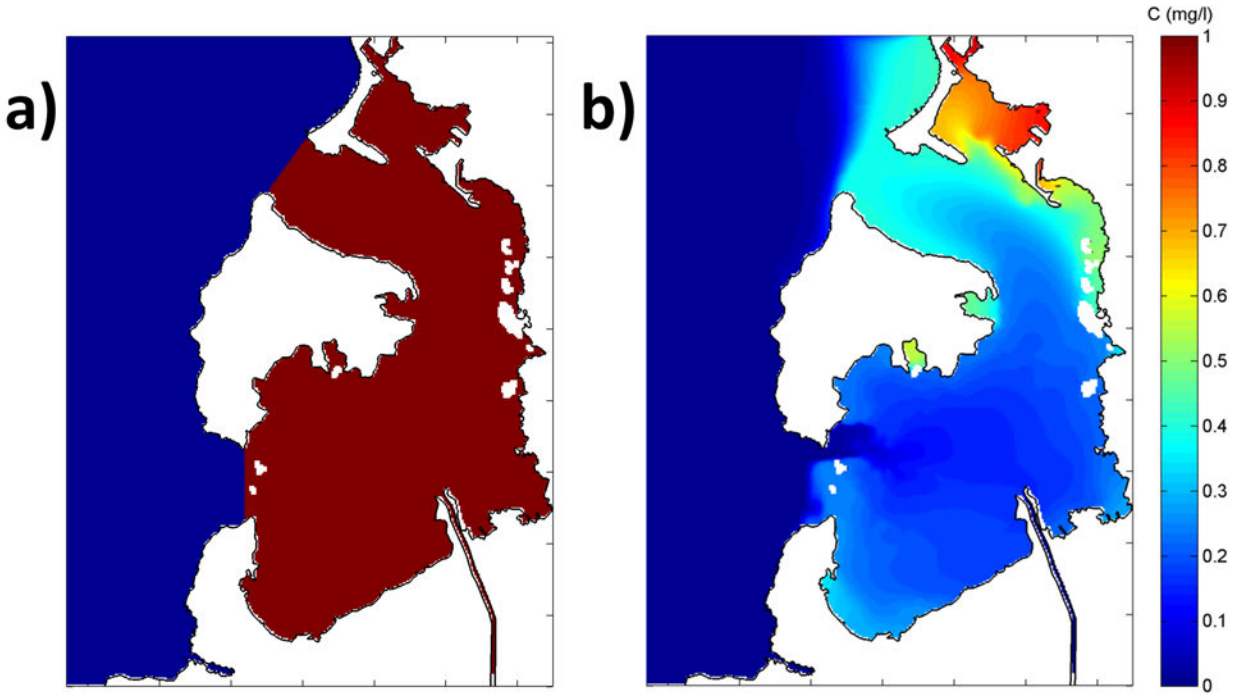

Figure 3.43: Panel a). Example of the initial mesh grid with the study domain (C_0=1, in red color) and the rest of grid cells (C_0=0, in blue color). Panel b). Example of the concentration evolution for a particular instant of simulation

3. The evolution of this concentration under the influence of the hydrodynamics is then calculated. This evolution shows the progression of a front by the transport equation. Figure 3.43b shows an example of the concentration distribution for a particular instant of simulation.
4. The moment when concentration within one grid mesh reaches a threshold value C_1 (arbitrarily set as 95% of C_0) is named t_1 and is considered to be the beginning of exponential decrease in concentration within this grid mesh. t_1 is called the FL (Figure 3.44).

5. LFT is then defined as the decrease in concentration between C_1 and $1/e*C_0$ (t_2), using an exponential regression of the same type as equation (3.36) that correlates best with the actual concentration decrease within the grid element (Figure 3.44).

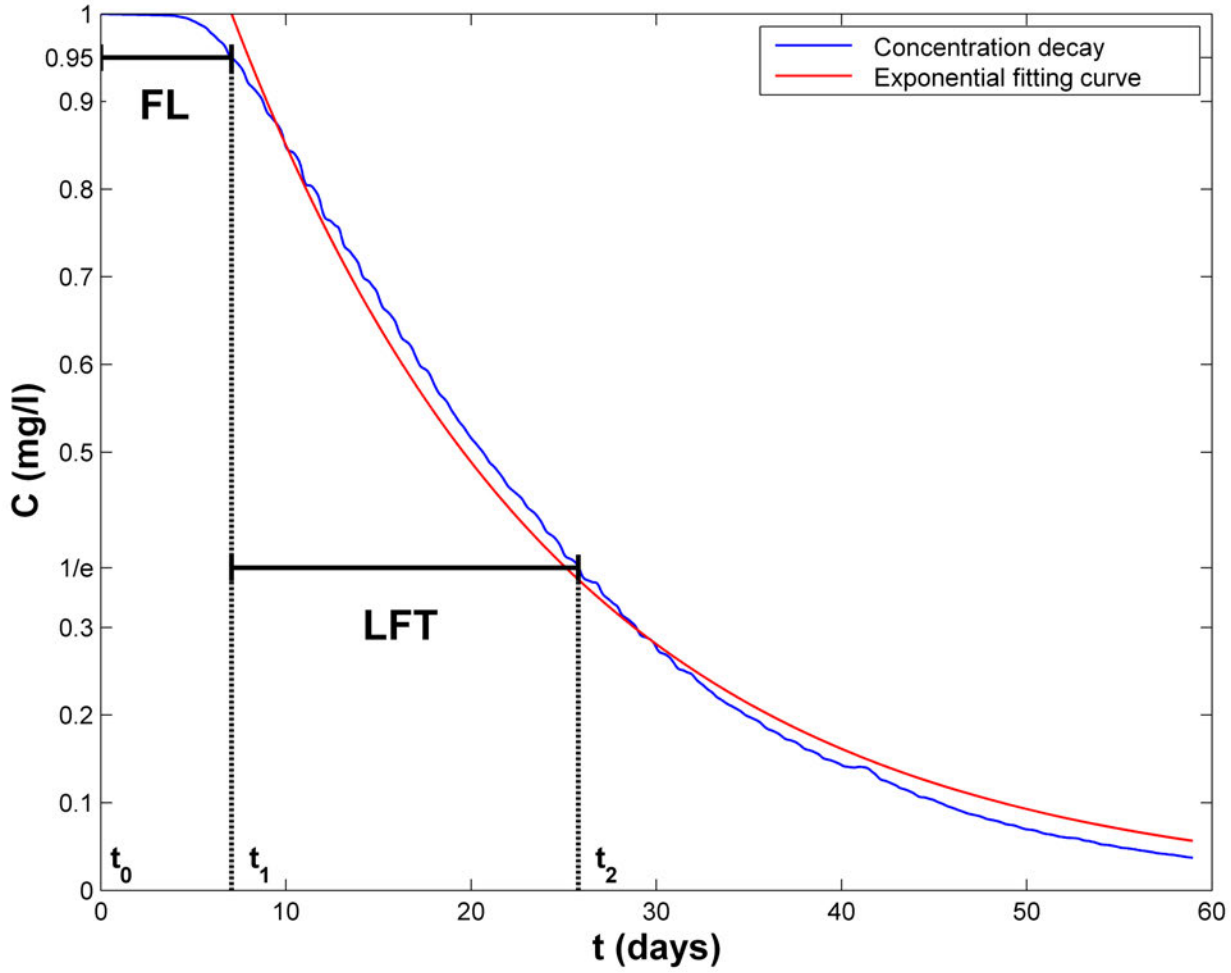

Figure 3.44: Example of concentration decay in a grid cell (blue line) and its exponential fitting curve (red line). Definition and calculation of FL and LFT are also indicated in black segments.

The accuracy of the numerical solving of advection terms, relating to the conservation of the front, and the accuracy of the turbulence model are important for the computation. Finer grid resolution also leads to a better representation of the evolution of the front, especially near to the coastline. Introducing such a transport timescale brings out the spatial variability of the hydrodynamics in a domain where currents are highly irregular, which is the case for estuaries. The transport timescale gradient given by this method can lead to establish a spatial differentiation of areas within estuaries, a result which is at least very interesting for defining the estuarine vulnerability.

The FL relates to the minimum age of the water masses at the studied point (Bolin & Rodhe 1973, Deleersnijder *et al.* 1998, Shen & Haas 2004, Takeoka 1984), in the sense that it indicates the time required for a water particle coming from outside the estuary to reach this point. The minimum age corresponds to the length of time required for water from outside the domain to begin to reach the grid mesh considered.

Flushing time sensitivity analyses

The third tier consist on performing a multi-sensitivity analysis of the LFT results to tailor the influence of

the depth, the initial simulation time (tidal phase), the river flow and the tidal range along the estuary.

To analyze the trend described by the LFT because of the depth, all the results are plotted. Depending on the variability with the depth, it is allowed averaging vertically the values of LFT on each model scenario, grid cell and tidal phase. In the case that depth influences significantly LFT, the layer displaying the maximum values of LFT should be considered.

Later, the initial simulation time for each grid cell are graphed to understand this influence. Depending on the variability of the tidal phase, it is allowed averaging the values of LFT on each model scenario and grid cell. In the case that tidal phase influences significantly LFT, the tidal phase displaying the maximum values of LFT should be considered.

The next task is to carry out a forcing sensitivity analysis by means of surface response plots. Herein, the response surface refers to a three-dimensional surface showing a response variable (LFT, days) as a function of two loading variables, e.g., river flow (Q, m^3/s) and astronomic tidal amplitude (A, m) such that $LFT = f(Q, A) + \varepsilon$ where ε represents any measurement error or random errors on the response.

The approximating function used to generate the response surface takes a quadratic form because this form is very adaptable and the main processes on an estuary are non-linear (equation (3.37)).

$$LFT = aQ^2 + bA^2 + cQA + dA + eQ + f \tag{3.37}$$

where a to f are the fitting coefficients to be determined by means of a method based on Least Square. Note that coefficient f represents the error on the response.

If the true response surface is flat, the second degree terms drop out in ordinary least square regressions. If the response surface is curved, the squared terms are significant. If multiplicative interactions between Q and A area important, that shows up in the cross product term.

Response surfaces explain the relationships between the forcing, the geomorphological features and the LFT. From these considerations, we can decide to average the lower variable forcing (Q or A) along its axis (x or y axis, respectively). Now, LFT is a function of the main forcing showing its influence. On the contrary, if the two forcings are significant we can not simplifying the function.

Final Flushing time

If the lower variable forcing is averaged, we suggest integrating the resulting area under the curve for each grid cell in order to build a rectangle with the same area and, thereby, providing a unique LFT value as the height of the rectangle.

In the case that forcing is not averaged because both are significant, we suggest integrating the resulting volume under the surface for each grid cell in order to build a prism with the same volume and, thereby, providing a unique LFT value as the height of the prism.

Finally, the LFT in estuaries is evaluated, as a unique value, taking into account the two most important issues to determine this physical attribute: the major forcing and the model domain.

Note that the LFT calculated with the annual mean forcing values might be not adequately representing the LFT. The annual mean approach miscalculates the LFT because LFT values are not attached to the occurrence probability of the forcing. The occurrence probability of the annual mean value could be very low and, consequently, it not explains all the forcing variability. The difference between both methods could be very significant depending on the forcing distribution.

3.5.5.3 State of conservation (SC)

SC is determined as a combination of naturalness (NA) and ecological value (EV) by means of GIS techniques (Gómez *et al.* 2014b).

Naturalness (NA) is defined as the absence of physical anthropogenic modifications. We define an alteration by hydromorphological pressures (HP_{ij}), computing buffer areas around each HP using buffer tools in GIS. Buffer distance of a HP is shown in equation (3.38).

$$d = k_{HP} \cdot (\frac{L}{CV})^2 \tag{3.38}$$

where k_{HP} equals 1 if the HP is continuous (dike, wharf), k_{HP} equals 0.5 if the HP is discontinuous (bridge, jetty); L is the length of the pressure; and CV is the critical value, defined as the length at the HP that is considered significant. CV equals 50 m for channeling dikes, detached breakwaters and breakwaters. CV is 100 m for canalizations, main breakwater, piers, quays, wharfs, jetties, margin protection and 150 m for shoreline structures such as wall, pre-formed concrete blocks, sheet piles.

Buffer areas of all identified HP are considered altered areas and present low naturalness (Gómez 2010).

Ecological value (EV) is described as the building capacity to support species of flora and fauna. This parameter is quantified using the indicator Ecological singular elements (ESE_{ij}) defined by Gómez *et al.* (2014b).

ESE_{ij} are defined by recognizing regional, national and international protected areas (see table 3.1) in the mesh grid by means of location tools in GIS.

3.5.5.4 Stratification (ST)

Estuary circulation is governed by density stratification mainly driven by salt concentration. Estuarine stratification is related to the vertical variation of salinity. It inhibits vertical mixing and plays a fundamental role in the salt balance.

According to water column stratification or salinity vertical structure, estuaries can be classified as salt wedge, partially stratified/mixed or vertically mixed (Cameron & Pritchard 1963, Pritchard 1952). This classification considers the competition between buoyancy forcing from river discharge and mixing from tidal forcing (Chapter 2).

In the thesis context, stratification could affect positively or negatively the mixing of industrial discharges depending on the type of estuary or, more locally, the type of stratification in the vicinity of the point discharge. If the discharge is located in a vertical mixed area, the estuarine circulation enhances the mixing of wastewaters. On the contrary, stratification inhibits the vertical mixing reducing the dilution of wastewaters. Therefore, an area classified as vertical mixed is less vulnerable than an area classified as salt wedge.

In this subsection, we suggest a methodological approach based on the use of hydrodynamic models and mathematical tools for the calculation of the ST divided into three steps: Selection and modeling of hydrodynamic scenarios, Calculation of the Richardson number and Final zoning of stratification.

Figure 3.45 shows an outline of the proposed methodology. Additionally, it is worthy to mention that all calculations are carried out on the study area through the same mesh grid used with the numerical models. All results are integrated at grid cell level to estimate temporal and spatially the stratification on the whole domain.

Selection and modeling of hydrodynamic scenarios

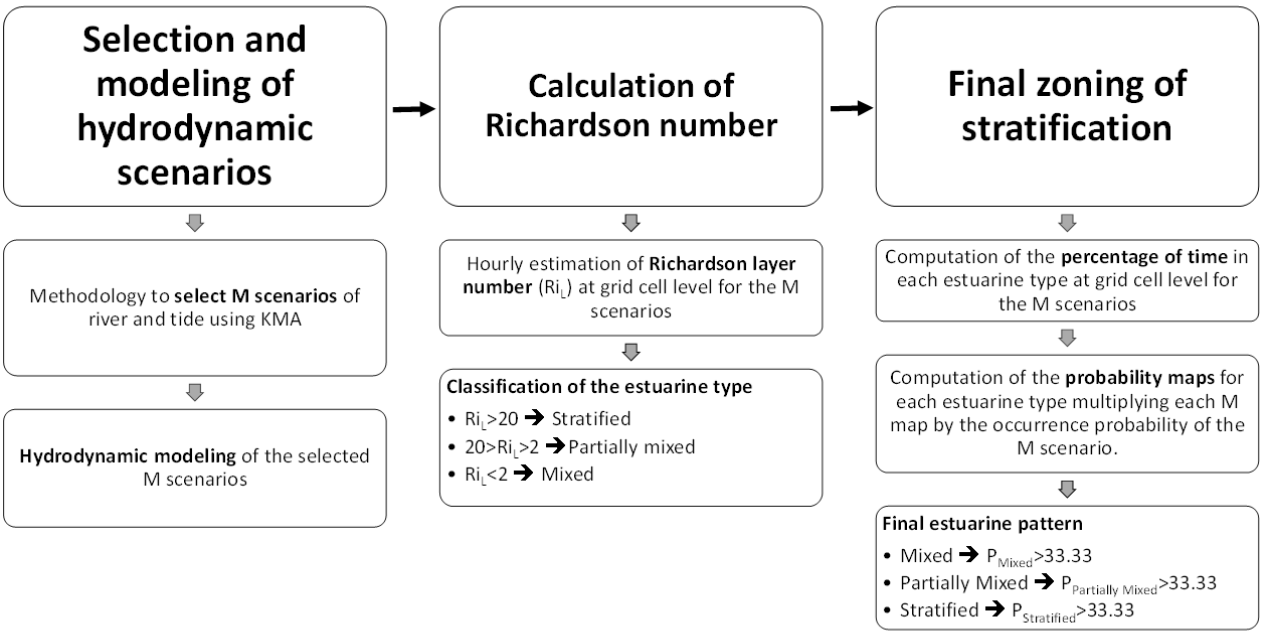

Figure 3.45: Schematic view of the proposed methodology to estimate the estuarine stratification.

We use the same model scenarios selected in the subsection of Hydrodynamics in Step 5. In that selection, we classified M model scenarios having into account the forcing variability using a K-means algorithm. This classification and the hydrodynamic results from the detailed calculation are used to compute the Richardson number at grid cell level.

Calculation of Richardson number

The main forcing mechanisms for the circulation and mixing processes and the stability characteristics of the estuary are analyzed by the classical Richardson layer number Ri_L given by Bowden (1978) in equation (3.39).

$$Ri_L(t) = \frac{g \cdot H(t) \cdot \Delta\rho_V(t)}{\overline{\rho_{env}}(t) \cdot (\overline{u})^2(t)} \tag{3.39}$$

where g is the gravity acceleration, $H(t)$ is the depth of the water column, $\Delta\rho_V(t)$ is the bottom minus the surface densities, $\overline{\rho_{env}}(t)$ vertical mean-depth density and $\overline{u}(t)$ is the vertical mean-depth velocity.

The physical interpretation of the Ri_L was given by Dyer & New (1986). These authors proposed a simplified mixing criterion for estuaries based on the Ri_L. This criterion is used to illustrate that mixing occurs preferentially in the shallow parts of the estuarine cross-section, and increases towards spring tides. Additionally, the Ri_L proportionates a valuable information about the intermittency of estuarine mixing in time and in space.

1. For $Ri_L > 20$, bottom-generated turbulence appears ineffective in decreasing the stratification, i.e, the water column is highly stable with low vertical mixing (Stratified type).
2. For $20 > Ri_L > 2$, mixing is increasingly active due to the turbulence (Partially stratified/mixed type).
3. For $Ri_L < 2$, fully developed mixing occurs, i.e., the turbulent mixing makes the water column unstable (Vertically mixed type).

From the results of the hydrodynamic model, we quantify hourly the Ri_L for all the M model scenarios for every grid cell. Next, we classify hourly the stratification type according to the criterion given by Dyer & New (1986) at grid cell level.

If the grid cell displays a $Ri_L > 20$ is classified as stratified, for values between $20 > Ri_L > 2$ is classified as partially mixed/stratified and for values of Ri_L below 2 is classified as vertically mixed.

Final zoning of stratification

In this step, the location of the mixed, partially mixed/stratified and stratified areas in the estuary is computed. To achieve this task, we calculate the time that each grid cell is in every stratification type for each model scenario, i.e., the time duration of mixed, partially mixed/stratified and stratified behaviour at grid cell level.

Next, we translate this time duration into occurrence probability dividing by the total duration of each M model scenario, i.e, the percentage of time that a grid cell is mixed, partially mixed/stratified and stratified for each M model scenario.

As it was mentioned, the M model scenarios have an occurrence probability. From the M probability maps, we compute three probability maps for each stratification type multiplying every M map by the occurrence probability of the M model scenario.

Last, we integrate all the information in a unique map showing the most probable stratification type at grid cell level. This map classify every grid cell into a stratification type according to the occurrence probability. If the probability of any stratification type surpasses 33.33% of the time then this grid cell is finally zoned with that stratification type.

ST can be seen as a correction factor inside the methodology. The calculation methodology described has been encoded using the mathematical software MATLAB (see more information on Chapter 4).

3.5.5.5 Estuarine Vulnerability Index (EVI)

Once all parameters are calculated, the first tier (see in Figure 3.41) is the integration of this information by means of the so called "Estuarine Vulnerability Index" (EVI) which its mathematical formulation detailed in equation (3.40).

$$EVI(TZ) = \begin{cases} \text{if } TZ = 1 & 1 \\ \text{if } TZ = 0 & [a \cdot SU + b \cdot (c \cdot NA + d \cdot EV)] \cdot ST \end{cases} \tag{3.40}$$

where TZ is the tidal zoning, SU is the susceptibility, NA is the naturalness, EV is the ecological value and ST is the stratification.

In order to weigh the importance of each term (a, b, c, d) in equation (3.40), we conducted a survey asking to 20 experts around the globe their opinion about the different parameters involved in the index. This survey presented the next questions and results:

1. Select which term should have more importance to estimate the vulnerability (a=SU and b=SC)? SU obtained 17 responses (85%) and SC 3 responses (15%).

2. Select which term should have more importance to estimate the state of conservation (c=NA and d=EV)? NA had 7 responses (35%) and EV 13 responses (65%)

Next, assessment criteria, thresholds and metrics for each vulnerability parameter are presented in Table 3.6.

Criteria	**Threshold (m)**	**Tidal Zoning (TZ)**
Intertidal	$H \leq A95$	1.0
Subtidal	$H > A95$	0.0
Criteria	**Threshold (days)**	**Susceptibility (SU)**
Full Renewal	0	0.0
Renewal	$0 < LFT_i < LFT_{max}$	$\frac{0.8 \cdot LFT_i}{LFT_{max}}$
Minimum Renewal	LFT_{max}	0.8
Criteria	**Threshold (m)**	**Naturalness (NA)**
Altered by HP	$d = k_{HP} \cdot (\frac{L}{CV})^2$	0.0
Non-altered by HP	0	0.8
Criteria	**Threshold (-)**	**Ecological Value (EV)**
Absence of ESE	Other areas	0.0
Presence of ESE	Protected areas	0.8
Criteria	**Threshold (%)**	**Stratification (ST)**
Mixed	$P_{Mixed} > 33.33$	1.0000
Partially Mixed	$P_{PartiallyMixed} > 33.33$	1.1125
Stratified	$P_{Stratified} > 33.33$	1.2500

Table 3.6: Assessment criteria, thresholds and metrics for each vulnerability parameter of the Estuarine Vulnerability Index (EVI)

According to the results of the survey and the metrics established by table 3.6, we assign the coefficient values into the equation (3.41) and quantify the value of EVI at grid cell level:

$$EVI_i(TZ_i) = \begin{cases} \text{if } TZ_i = 1 & 1 \\ \text{if } TZ_i = 0 & [0.85 \cdot SU_i + 0.15 \cdot (0.35 \cdot NA_i + 0.65 \cdot EV_i)] \cdot ST_i \end{cases} \tag{3.41}$$

First, we apply the Exclusion Factor using the TZ as threshold. If the TZ equals 1 then the EVI is 1. Otherwise, we calculate the EVI_i with the proposed formulation. The value of SU, NA and EV ranges between 0.0 and 0.8 meanwhile for the ST depends on the stratification type working as a Correction Factor (1.0 for well-mixed, 1.125 for partial stratified and 1.25 for stratified).

Finally, EVI_i is calculated ranging between 0 and 1. Zero is referred to the estuarine areas less vulnerable to receive wastewater discharges meanwhile the areas with one are the most vulnerable.

3.5.5.6 **Acceptability (AC*)**

Next tier (see in Figure 3.41) is determining the acceptability (AC*) of the estuary. If the discharge point is located in a grid cell with EVI equals 1 is non-acceptable. Otherwise, we compute the value of AC* by multiplying the EVI value with the percentage of estuarine area cover per grid cell (Equation (3.42)).

$$AC_i^*(EVI, A) = \begin{cases} \text{if } EVI_i = 1 & Non - Acceptable \\ \text{if } EVI_i \leq 1 & EVI_i \cdot \frac{A_i}{A_{estuary}} \cdot 100 \end{cases} \tag{3.42}$$

where EVI_i is the Estuarine Vulnerability Index of the i grid cell, A_i is the area of the i grid cell, $A_{estuary}$ is the total area of the estuary. Regarding $A_{estuary}$, we defined two boundaries exactly the same as for the "worst and dry case of dilution".

EVI works as a multiplicative weighing factor in the calculation of AC* as a function of estuarine vulnerability at grid cell level. If all the grid cells have $EVI_i = 1$, the estuary is the most vulnerable and the AC* is the

same as for the "worst case of dilution". Inversely, if all the grid cells have $EVI_i = 0$, the estuary is the less vulnerable and the AC* equals zero, i.e., all mixing zones are acceptable.

EVI_i can be seen as a correcting factor of the real area of a grid cell depending on its vulnerability. It is worthy to mention that it is mathematically not possible having all grid cells with $EVI_i = 0$ because of the developed formulation. Thus, we will always have AC* values.

3.5.5.7 **Maximum allowable MZ size (MAS*)**

The third tier (see in Figure 3.41) is computing the maximum allowable corrected MZ size (MAS*) by dividing the maximum admissible percentage of estuarine area that a MZ can cover in the "worst case of dilution" (AA-MAS and MAC-MAS) with a correction factor (α) which depends on the average EVI of the estuary. As it was mentioned in Step 3, the AA-MAS does not exceed 10% and the MAC-MAS 3% of water body extent overall (Figure 3.19).

Equation (3.43) displays the value of MAS* meanwhile equation (3.44) the formulation for α.

$$MAS^* = \frac{MAS}{\alpha} \tag{3.43}$$

$$\alpha = \frac{1}{1 - \overline{EVI}_{estuary}} \tag{3.44}$$

where $\overline{EVI}_{estuary}$ is the average EVI of all the grid cells covered by the estuary.

α works as a divisive weighing factor in the calculation of MAS* as a function of the average EVI of the estuary. If $\overline{EVI}_{estuary} = 1$, the estuary is highly vulnerable and the MAS* will be infinite, i.e, no MZ are allowable. As in the case of AC*, it is not possible having this situation because of the developed formulation. Inversely, if $\overline{EVI}_{estuary} = 0$, the estuary is lowly vulnerable and the MAS* equals the MAS, i.e., MZs are acceptable with the same percentage of estuarine area than in the "worst case of dilution".

Therefore, $\overline{EVI}_{estuary}$ can be seen as a correcting factor of the maximum admissible percentage of estuarine area that a MZ can cover in the "worst case of dilution" (MAS) depending on the estuarine vulnerability (Figure 3.46).

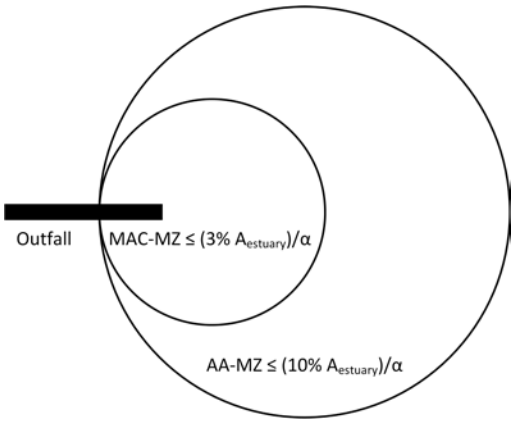

Figure 3.46: Diagram of the maximum allowable MZ size for AA-MZ and MAC-MZ in the detailed calculation.

3.5.5.8 **Final admissibility (AD*)**

In the fourth tier (see in Figure 3.41), we evaluate the AD* as the sum of all the AC* values covered by AA-MZ and MAC-MZ (Equation (3.45)). If the AD is greater than MAS* the MZ size is not admissible meanwhile if AD* is equal or lower than MAS* the MZ size is admissible.

$$AD^*(AC^*) = \begin{cases} \text{if } AD^* > MAS^* & \sum_{i=1}^{n} AC_i^* = Non - Admissible \\ \text{if } AD^* \leq MAS^* & \sum_{i=1}^{n} AC_i^* = Admissible \end{cases} \tag{3.45}$$

where AC_i^* is the acceptability of the i grid cell.

The difference between the admissibility of the "real case of dilution" and the "worst and dry cases of dilution" is the inclusion of EVI into the calculations of AC* and MAS*.

Analogously to Step 4, the final task in Step 5 is determining the allocation of both MZs by plotting an abacus that relates the extent and the failure probability of MZs. To draw this curves, we take into consideration that the extent of MZs cannot be larger than $10\%/\alpha$ and $3\%/\alpha$ for the AA-MZ and the MAC-MZ respectively. Moreover, the 5^{th} percentile of the ecdf of the failure probability cannot be higher than 15% for the AA-Failure and 4% for the MAC-Failure.

Figure 3.47 illustrates an example of an abacus displaying the evolution of the extent of MZs with 5^{th} percentile of the ecdf of the failure probability. Note that black line is the evolution of the AA-MZ and grey line for the MAC-MZ. In addition, the thick black line is representing the zone where the AA-MZ is allocatable because of both requirements are simultaneously fulfilled while the thick grey line is for the MAC-MZ.

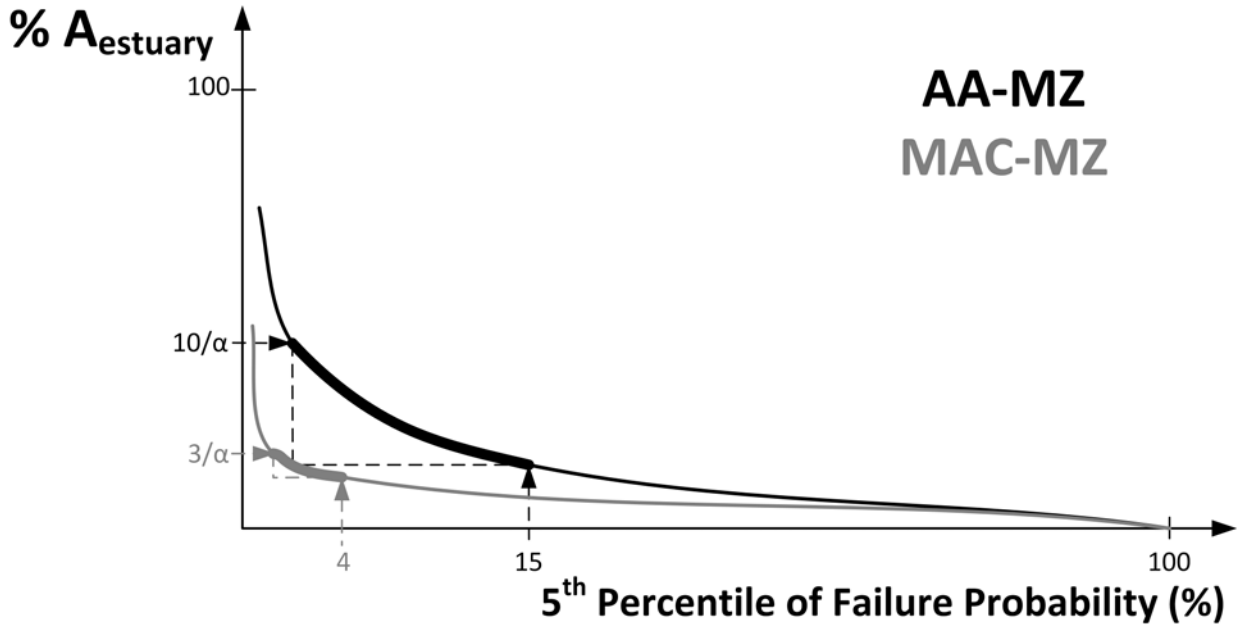

Figure 3.47: Example of an abacus of the AA-MZ (black line) and MAC-MZ (grey line) in the detailed calculation.

As it can be seen in figure 3.47, there could be a range of allocatable MZs. The final allocation should be discussed and agreed between the stakeholder and the competent authority due to the economical, social and ecological implications of any allocation as it was aforementioned in Step 4.

After all the calculations, if the discharge is still classified as inadmissible, the decision tree recommends to restart with the methodology at Step 1 in order to continue with the allocation procedure (Figure 3.2) until

reach an admissible MZ. The way to modify MZs is changing the location of the point discharge, reducing the toxicant load (flow or concentration) and/or both.

3.6 Conclusions

The proposed stepped methodology provided a tailored solution with an appropriate level of detail in the form of schematic flow diagrams. The general rule was that the costs of the MZs allocation procedure will rise with the level of sophistication. Simpler procedures require less data and expertise, but they also tend to be less accurate. At each Step the aim was to identify those discharges that do not give cause for concern, and also to highlight discharges that require action to reduce the size of the MZ. The philosophy of the decision tree was to increase the resource uses when the order of the discharge increases.

The methodology promoted a uniform and soundly-based framework for such determinations to provide solutions which are: *Efficient* because resources were used only when necessary and then were commensurate with the environmental concerns being addressed; *Robust* for leading to sound reproducible decisions contributing to sustainable use of the estuarine environment; and *Flexible* to meet the needs of Europe's estuarine environments.

Step 1. Preliminary characterization

Two summary sheets were elaborated in order to gather the preliminary characterization of the effluent and the study area.

Step 2. Significance of discharge

A method to detect those discharges that have not significant impact on the estuarine waters was implemented based on simple formulations. In these discharges, there was not need to evaluate the MZs in order to prevent detailed and expensive studies in discharges that are insignificance.

Step 3. Simplified calculation (Worst case of dilution)

A simplified calculation was proposed and based on the physical dilution and hydrodynamic forcings from a precautionary approach.

- The requirements for setting up the model were described and defined. These include the definition of the grid and bathymetry according to the study area, the prescription of boundary and initial conditions and the calibration and validation of the hydrodynamic model by the combination of physical and numerical parameters.
- The "worst case of dilution" was proposed assuming fixed conditions of the forcing: Tidal amplitude was constant and equal to the A10 and river flow was constant and equal to the 7Q10.
- An offline linkage was assumed where the output for hydrodynamic model is the input for the entire time of interest in the near-field model.
- An offline linkage was anew assumed where the source-induced flow, though considerably important for near-field mixing, does not change the flow characteristics of the far-field. The determined variables were the diluted concentration, the length, the width, the thickness and the trapped height of the buoyant jet.
- Because integral jet models did not take into account the interaction with boundaries, an algorithm was developed to specify the end of near-field when the jet-plume touches any boundary (free surface, stratified layer or lateral boundaries, i.e., walls).

- The requirements for setting up the conservative model were described and defined. The use of a 3D far-field model, involving the solution of the transport equation dividing the study area into square or curvilinear grids was suggested.
- The AA-MZ was defined as an area within the model domain where the time-averaged modeled concentrations are exceeding the AA-EQS. The minimum allowed MAC-MZ was defined as an area, within the model domain, where the modeled concentrations are not exceeding the MAC-EQS.
- The admissibility criteria was the average value of a survey to 20 experts around the globe asking their opinion about the maximum value might have the extent of a MZ in estuaries. The criteria reads that the AA-MZ does not exceed 10% of water body extent overall and the MAC-MZ does not exceed 3%.

Step 4. Intermediate calculation (Dry case of dilution)

A intermediate calculation was proposed and based on the continuous simulation of one year. Although this model scenario still being a precautionary approach (conservative tracers), the forcing variations through the year might led to modifications of the hydrodynamics quantities.

- The "dry case of dilution" was proposed assuming the driest year of the long-term time series of river flow and its associated tidal elevations.
- One "presimulation" to obtain the adequate initial condition of toxicant concentration and other "simulation" to record the concentration evolution along the dry year were proposed.
- To achieve this delimitation, a method was suggested involving three tiers: specification of the annual number of samples, determination of the optimal number of surveys and final delimitation of MZs.
- In this Step was assumed that aquatic life was sufficiently protected if the AA-EQS for chronic toxicity was maintained during at least 85% of the AA-Failure probability and the MAC-EQS for acute toxicity is maintained during at least 96% of the MAC-Failure probability.

Step 5. Detailed calculation (Real case of dilution)

A detailed calculation was proposed and based on the analysis of the spatial and temporal variations of the forcing (tide an rivers) throughout a long-term series. These variations led to new significant modifications of the hydrodynamics quantities. Furthermore, the physical and chemical dilution were the mechanisms responsible for the toxicant decay in the far-field so toxicants were considered non-conservative tracers in this region.

- A methodology able to select the most relevant hydrodynamic scenarios in an estuary to perform high-resolution numerical modeling of short-term periods, taking into account the time evolution and the occurrence probability of the forcings in order to obtain realistic responses of the estuarine mean behavior, was developed. This methodology was divided into several steps: Obtainment of the hydrodynamic forcing data, Rearrangement of the input data for clustering, Application of the proposed clustering approach and Sensitivity analyses for the forcing and modeling.
- The conceptual model (processes and interactions) that, at least, the transport model for non-conservative substances must include, was described.
- Model setup for the transport model was explained by defining the model domain discretization, providing boundary and initial conditions and calibrating and validating the model by the combination of physical, physicochemical and numerical parameters.

- To achieve this delimitation, a method was suggested involving four tiers: Validation of the reconstructed series, Selection and generation of l-years, Random sampling and Final delimitation of MZs.
- In this Step was assumed that aquatic life was sufficiently protected if the AA-EQS for chronic toxicity was maintained during at least 85% of the 5^{th} percentile of AA-Failure probability and the MAC-EQS for acute toxicity is maintained during at least 96% of the 5^{th} percentile of MAC-Failure probability.
- In order to establish the admissibility criteria, a methodology was developed and based on a holistic approach, which considers simultaneously the physical processes involved in dispersion and diffusion mechanisms, the ecological features of the receiving water body and the social aspects related with the water body uses. The admissibility of MZs was determined in a four-tiered method: Estuarine Vulnerability Index (EVI), Acceptability (AC*), Maximum allowable size (MAS*) and Admissibility of the delimitated MZ (AD*).
- A methodological approach was developed, based on the use of computational tools for the calculation of flushing time (FT) and divided into four tiers: Hydrodynamic forcing analysis, FT calculation, FT sensitivity analysis and Final FT.
- A method for locating the mixed, partially mixed/stratified and stratified areas in the estuary was also developed, based on the use of hydrodynamic models and mathematical tools for the calculation of the stratification and divided into three steps: Selection and modeling of hydrodynamic scenarios, Calculation of the Richardson number and Final zoning of stratification.

All models are wrong. Some are useful.

George E.P. Box

4

Numerical tools

The impact of a discharge on any water body is dependent on discharge quality and quantity and prevailing physical and chemical conditions of the receiving waters.

Depending on the characteristics of the receiving environment and the relevance of the discharge, the sophistication of the models and the cost of the project will vary according to the decisions made during the expert system decision. Next, a series of standard models are described in this thesis, based on the review of the state of the art (Chapter 2) for the calculation along the several Steps of the developed methodology (Chapter 3).

We use Delft3D-FLOW for simulation of hydrodynamics, VISJET for simulation of near-field (primary dilution) and D-Water Quality for simulation of far-field (secondary dilution).

Additionally, we developed and programmed a series of mathematical tools for pre- and post-processing the inputs and outputs of Delft3D-FLOW, VISJET and D-Water Quality, for performing a passive and continuous initial dilution in VISJET using Delft3D-FLOW results, for conducting a passive and continuous coupling between VISJET and D-Water Quality, for selecting model scenarios using K-means algorithms, for delimitating the AA-MZ and MAC-MZ, for estimating the flushing time, for determining the stratification patterns in estuaries, and for assessing the admissibility of MZs.

Nevertheless, these calculations can be conducted with any numerical model if they meet the following points:

- *Justification of the model:* To demonstrate that the model used is suitable for this study, this should include examples of previous applications in similar circumstances.
- *Technical description of model:* History of the model, development history, published articles, details of the conversion of the model into a software package and details of the experience and training of the model users.
- *Data collection:* Any model is only as good as the source data, the data required for the model must be clearly defined. The data collection and measurement techniques should be quoted, including expected errors and relevant quality assurance.
- *Calibration:* It is important that the model is calibrated against a full data set which is representative of the range of conditions to be modelled. The model coefficients to be calibrated and the procedures used to optimize the calibration must be stated clearly.

- *Validation:* Data sets independent of those used for calibration must be employed for validation tests. Every effort should be made to validate the model across the range of conditions for which it will be run. Validation tests and analysis of model errors must be undertaken for the key variables required from the modeling study.
- *Quality assurance:* To demonstrate that the model has been subject to an evaluation procedure establishing its suitability for the relevant tasks.
- *Reporting:* Clear description of the model including the underlying principles and implicit or explicit assumptions. Also a clear summary of the numerical output, the likely errors, bias, sensitivity and their implications for the objectives of the study and the conclusions.

These points list the key areas which any modeling studies for any estuary should cover. The points are equally applicable to a simple study of the environmental impact of a septic tank discharge or to the design and location of a large industrial facility, except that the scope and depth of the study will vary as it was pointed along Chapter 3.

The next sections of this Chapter include a short description of the selected models and a review of all the developed mathematical tools.

4.1 Hydrodynamics (DELFT3D-FLOW)

Delft3D-FLOW consists in a numerical model based on finite differences that solves the unsteady shallow water equations in two (depth-averaged) or three dimensions (hydrostatic assumption). These equations are derived from the three-dimensional Navier-Stockes equations for incompressible free surface flow (Deltares 2014d). In the assumptions of the model, the effect of variable density is exclusively considered in the horizontal pressure gradient term (Boussinesq assumptions). In this approach the vertical momentum equation is reduced to the hydrostatic pressure relation. Vertical accelerations are assumed to be small compared to the gravitational acceleration and are not taken into account. It aims to model flow phenomena of which the horizontal length and time scales are significantly larger than the vertical scales (Lesser *et al.* 2004).

Delft3D-FLOW has been applied to numerous studies confirming its capacity to simulate hydrodynamics in estuarine systems. Iglesias & Carballo (2010) implemented and applied Delft3D-FLOW to understand how high winds affect the circulation of an estuary called the Ría de Muros on the northwestern coast of the Iberian Peninsula. García-Alba *et al.* (2014) applied Delft3D-FLOW to derive the hydrodynamics forcing conditions in the Port of Marin (NW Spain) for coupling to a transport model (IH-Dredge) which simulates dredging processes effects. Zhou *et al.* (2014) used Delft3D-FLOW to investigate the initiation and long-term evolution of tidal networks by comparing controlled laboratory experiments and their associated scaling laws with outputs from a numerical model. Jiménez *et al.* (2014) used Delft3D-FLOW to scale properties of tidal networks from long-term numerical simulations in an idealized basin.

Mathematical formulations including in Delft3D-FLOW model are based on a large number of physical processes: tidal forcing at the open boundaries, time varying sources and sinks (e.g. river discharges), vertical exchange of momentum due to internal waves, transport of salt heat and other conservative constituents, horizontal density gradients in the pressure (baroclinic effects), water with variable density (equation of state), free surface gradient (barotropic effects), turbulence induced mass and momentum fluxes (turbulence closure models), space varying shear-stress at the bottom, space and time varying wind shear-stress at the water surface, the effect of the Earth's rotation (Coriolis force), effect of secondary flow on depth-averaged momentum equations, space and time varying atmospheric pressure on the water surface, drying and flooding of tidal flats, evaporation and precipitation, heat exchange through the free surface, lateral shear-stress at wall, influence of waves on the bed shear-stress (2D and 3D), wind driven flows including tropical cyclone winds and

flow through hydraulic structures. Due to the multitude of processes involved, DELFT3D-FLOW is suitable for predicting the flow in shallow seas, coastal areas, estuaries, lagoons, rivers, and lakes.

Further coupling to transport modeling allows for considerations of mixing, diffusion and decay processes in direct relation to far-field processes.

4.1.1 Model formulation (for σ-grid)

Delft3D-FLOW is based on a system of three equations: the continuity equation, the horizontal equations of motion and the transport equations for conservative constituents.

Continuity equation

$$\frac{\partial \zeta}{\partial t} + \frac{1}{\sqrt{G_{\xi\xi}}\sqrt{G_{\eta\eta}}}\frac{\partial[(d+\zeta)u\sqrt{G_{\eta\eta}}]}{\partial \xi} + \frac{1}{\sqrt{G_{\xi\xi}}\sqrt{G_{\eta\eta}}}\frac{\partial[(d+\zeta)u\sqrt{G_{\xi\xi}}]}{\partial \eta} + \frac{\partial \omega}{\partial \sigma} = H(q_{in} - q_{out}) + P + E \quad (4.1)$$

where ζ is the free surface elevation (m), t is the time (s), d is the depth respect to a reference plane of the free surface (m), u is the flow velocity in the ξ-direction (m/s), v is the flow velocity in the η-direction (m/s), ω is the velocity in the σ-direction in the σ-coordinate system (m/s), H is the total water depth (m), i.e., $H = d+\zeta$, q_{in} is the local source per unit volume (1/s), q_{out} is the local sink per unit volume (1/s), $\sqrt{G_{\xi\xi}}$ and $\sqrt{G_{\eta\eta}}$ are the coefficients used to transform curvilinear to rectangular coordinates (m), P is the precipitation (m/s) and E is the evaporation (m/s).

Momentum equations in horizontal direction

The momentum equations in ξ- and η-direction are given respectively by:

$$\frac{\partial u}{\partial t} + \frac{u}{\sqrt{G_{\xi\xi}}}\frac{\partial u}{\partial \xi} + \frac{v}{\sqrt{G_{\eta\eta}}}\frac{\partial v}{\partial \eta} + \frac{\omega}{d+\zeta}\frac{\partial u}{\partial \sigma} - \frac{v^2}{\sqrt{G_{\xi\xi}}\sqrt{G_{\eta\eta}}}\frac{\partial \sqrt{G_{\eta\eta}}}{\partial \xi} + \frac{uv}{\sqrt{G_{\xi\xi}}\sqrt{G_{\eta\eta}}}\frac{\partial \sqrt{G_{\xi\xi}}}{\partial \eta} - fv = -\frac{1}{\rho_{env}\sqrt{G_{\xi\xi}}}P_\xi + \frac{1}{\sqrt{G_{\xi\xi}}}\frac{\partial \tau_{\xi\xi}}{\partial \xi} + \frac{1}{\sqrt{G_{\eta\eta}}}\frac{\partial \tau_{\xi\eta}}{\partial \eta} + \frac{1}{(d+\zeta)^2}\frac{\partial}{\partial \sigma}(\mu_V \frac{\partial u}{\partial \sigma}) + M_\xi \quad (4.2)$$

$$\frac{\partial v}{\partial t} + \frac{u}{\sqrt{G_{\xi\xi}}}\frac{\partial v}{\partial \xi} + \frac{v}{\sqrt{G_{\eta\eta}}}\frac{\partial v}{\partial \eta} + \frac{\omega}{d+\zeta}\frac{\partial v}{\partial \sigma} - \frac{uv}{\sqrt{G_{\xi\xi}}\sqrt{G_{\eta\eta}}}\frac{\partial \sqrt{G_{\eta\eta}}}{\partial \xi} + \frac{u^2}{\sqrt{G_{\xi\xi}}\sqrt{G_{\eta\eta}}}\frac{\partial \sqrt{G_{\xi\xi}}}{\partial \eta} + fu = -\frac{1}{\rho_{env}\sqrt{G_{\eta\eta}}}P_\eta + \frac{1}{\sqrt{G_{\xi\xi}}}\frac{\partial \tau_{\eta\xi}}{\partial \xi} + \frac{1}{\sqrt{G_{\eta\eta}}}\frac{\partial \tau_{\eta\eta}}{\partial \eta} + \frac{1}{(d+\zeta)^2}\frac{\partial}{\partial \sigma}(\mu_V \frac{\partial v}{\partial \sigma}) + M_\eta \quad (4.3)$$

where P_ξ is the gradient hydrostatic pressure in ξ-direction (kg/m^{2}s^2), P_η is the gradient hydrostatic pressure in η-direction (kg/m^{2}s^2), $\tau_{\xi\xi}$, $\tau_{\eta\eta}$ and $\tau_{\xi\eta}$ are the contributions secondary flow to shear stress tensor (kg/ms^2), M_ξ source or sink of momentum in ξ-direction (m/s^2), M_ξ source or sink of momentum in η-direction (m/s^2), f Coriolis parameter (inertial frequency) (1/s) and μ_V vertical eddy viscosity (m^2/s).

Vertical velocities

Vertical velocities in the three dimensional models are computed from the continuity equation. The vertical velocity ω is relative to the moving σ-plane and is defined at the iso σ-surfaces; for this reason it can be considered as linked to up- or downwelling motions. Computations of the physical vertical velocities w are not considered in the model equations since they are only required for the post-processing step. These velocities can be expressed in the horizontal velocities, water depths, water levels and vertical ω-velocity (Deltares 2014d) according to:

$$w = \omega + \frac{1}{\sqrt{G_{\xi\xi}}\sqrt{G_{\eta\eta}}}[u\sqrt{G_{\eta\eta}}(\sigma\frac{\partial H}{\partial \xi} + \frac{\partial \zeta}{\partial \xi}) + v\sqrt{G_{\xi\xi}}(\sigma\frac{\partial H}{\partial \eta} + \frac{\partial \zeta}{\partial \eta})] + (\sigma\frac{\partial H}{\partial t} + \frac{\partial \zeta}{\partial t}) \tag{4.4}$$

The vertical momentum equation is reduced to a hydrostatic pressure equation, in accordance with the shallow water hypothesis:

$$\frac{\partial P}{\partial \sigma} = -g\rho_{env}H \tag{4.5}$$

Equation of state

In water with a non-uniform density, the local density is associated to the values of temperature and salinity by the equation of state. The UNESCO formulation is used (UNESCO 1981):

$$\rho_{env} = \rho_0 + A \cdot S + B \cdot S^{3/2} + C \cdot S^2 \tag{4.6}$$

where:

$$\rho_0 = 999.8 + 6.7 \cdot 10^{-2}T - 9.0 \cdot 10^{-3}T^2 + 1.0 \cdot 10^{-4}T^3 - 1.1 \cdot 10^{-6}T^4 + 6.5 \cdot 10^{-9}T^5 \tag{4.7}$$

$$A = 8.2 \cdot 10^{-1} - 4.0 \cdot 10^{-3}T + 7.6 \cdot 10^{-5}T^2 - 8.2 \cdot 10^{-7}T^3 - 5.3 \cdot 10^{-9}T^4 \tag{4.8}$$

$$B = -5.7 \cdot 10^{-3} + 1.0 \cdot 10^{-4}T - 1.6 \cdot 10^{-6}T^2 \tag{4.9}$$

$$C = 4.8 \cdot 10^{-4} \tag{4.10}$$

in which S is the salinity (ppt) and T is the water temperature (^{o}C).

The UNESCO expression is valid in the salinity and temperature ranges $0.5 < S < 43$ ppt and $0 < T < 40$ ^{o}C respectively.

Reynold's stresses

The Reynolds stress components are computed using the eddy viscosity concept (Rodi 1984) and are defined according to the following expressions:

$$\tau_{\xi\xi} = \frac{2\mu_H}{\sqrt{G_{\xi\xi}}}(\frac{\partial u}{\partial \xi} + \frac{\partial u}{\partial \sigma}\frac{\partial \sigma}{\partial \xi}) \tag{4.11}$$

$$\tau_{\xi\eta} = \tau_{\eta\xi} = \mu_H[\frac{1}{\sqrt{G_{\eta\eta}}}(\frac{\partial u}{\partial \eta} + \frac{\partial u}{\partial \sigma}\frac{\partial \sigma}{\partial \eta}) + \frac{1}{\sqrt{G_{\xi\xi}}}(\frac{\partial v}{\partial \xi} + \frac{\partial v}{\partial \sigma}\frac{\partial \sigma}{\partial \xi})] \tag{4.12}$$

$$\tau_{\eta\eta} = \frac{2\mu_H}{\sqrt{G_{\eta\eta}}}(\frac{\partial v}{\partial \eta} + \frac{\partial v}{\partial \sigma}\frac{\partial \sigma}{\partial \eta}) \tag{4.13}$$

where μ_H is the horizontal eddy viscosity defined by equation (4.14):

$$\mu_H = \mu_{SGS} + \mu_V + \mu_H^{back} \tag{4.14}$$

in which μ_{SGS} is the sub-grid scale (SGS) horizontal eddy viscosity (m^2/s), referred to processes that take place in a spatial scale smaller than grid cell dimensions, μ_H^{back} is the background horizontal eddy viscosity (ξ- and η-direction) (m^2/s) chosen by the user and referred to the turbulence linked to water characteristics.

The vertical eddy viscosity μ_V is defined by by equation (4.15):

$$\mu_V = \mu_{mol} + \max(\mu_{3D}, \mu_V^{back}) \tag{4.15}$$

where μ_{mol} is the kinematic viscosity (molecular) coefficient (m^2/s), μ_{3D} is the part of eddy viscosity due to turbulence model in vertical direction associate to tridimensional processes (m^2/s) and μ_V^{back} the background vertical eddy viscosity for momentum equations (m^2/s) chosen by the user and referred to the turbulence linked to water characteristics.

In Delft3D-FLOW, four turbulence closure models are provided to compute the vertical turbulent eddy viscosity μ_V and the vertical turbulent eddy diffusion D_V values:

- *Constant coefficient*, based on a constant value of the vertical and horizontal eddy viscosity.
- *Algebraic Eddy viscosity closure Model (AEM)*, a combination between the Algebraic Closure Model (ALG) and the Prandtl's Mixing Length model (PML).
- $k - L$ *turbulence closure model*, in which the mixing length L is computed by an analytic approach and the turbulent kinetic energy k is obtained resolving a transport equation.
- $k - \varepsilon$ *turbulence closure model*, based on the transport equations for the turbulent kinetic energy k and for the energy dissipation ε.

Each of the turbulence closure models allows calculating the part of eddy viscosity due to turbulence model in vertical direction μ_{3D}.

With the aim to solve the system of equations governing Delft3D-FLOW, a number of boundary conditions must be defined. For 2D depth-averaged flow the shear-stress at the bed induced by a turbulent flow is assumed to be given by a quadratic friction law (Deltares 2014d):

$$\vec{\tau_b} = \frac{g\rho_{env}\,\vec{u}\,|\vec{u}|}{Ch^2} \tag{4.16}$$

where $|\vec{u}|$ is the magnitude of the depth-averaged horizontal velocity vector (m/s), ρ_{env} is the density of ambient water (kg/m^3) and Ch is the Chezy coefficient (m$^{1/2}$/s).

For 3D models the bed shear stress is calculate using a quadratic formulation:

$$\vec{\tau_{b3D}} = \frac{g\rho_{env}\vec{u_b}|\vec{u_b}|}{Ch^2} \tag{4.17}$$

where $|\vec{u_b}|$ represents the magnitude of the horizontal velocity in the first layer above the bed (m/s).

The magnitude of the shear stress at free surface in the wind direction $|\tau_S|$ can be computed, using:

$$|\tau_S| = \rho_{air} W_{drag} W_{10}^2 \tag{4.18}$$

where ρ_{air} is the density of air (kg/m^3), W_{drag} is the wind drag coefficient (-) and W_{10} is the averaged wind speed at 10 m above free surface (m/s).

Transport equation

In the Delft3D-FLOW, the transport of dissolved substances and heat is taken into account using an advection-diffusion equation in three dimensions. The transport equation is formulated in a conservative form in orthogonal curvilinear coordinates in the horizontal direction and σ-coordinates in the vertical direction (Deltares 2014d):

$$\frac{\partial(d+\zeta)C}{\partial t}+\frac{1}{\sqrt{G_{\xi\xi}}\sqrt{G_{\eta\eta}}}\{\frac{\partial[\sqrt{G_{\eta\eta}}(d+\zeta)uC]}{\partial\xi}+\frac{\partial[\sqrt{G_{\xi\xi}}(d+\zeta)vC]}{\partial\eta}\}+\frac{\partial wC}{\partial\sigma}=$$
$$\frac{d+\zeta}{\sqrt{G_{\xi\xi}}\sqrt{G_{\eta\eta}}}\{\frac{\partial}{\partial\xi}(D_H\frac{\sqrt{G_{\eta\eta}}}{\sqrt{G_{\xi\xi}}}\frac{\partial C}{\partial\xi})+\frac{\partial}{\partial\eta}(D_H\frac{\sqrt{G_{\xi\xi}}}{\sqrt{G_{\eta\eta}}}\frac{\partial C}{\partial\eta})\}+$$
$$+\frac{1}{d+\zeta}\frac{\partial}{\partial\sigma}(D_V\frac{\partial C}{\partial\sigma}-\lambda_d(d+\zeta)C+S \quad (4.19)$$

where D_H is the horizontal diffusion coefficient (m^2/s), D_V is the vertical diffusion coefficient (m^2/s), λ_d is the first order decay process (1/s) and SO represent the source and sink terms per unit area due to discharge q_{in} or withdrawal q_{out} of water and/or the exchange of heat through the free surface H_{net}:

$$S=(d+\zeta)(q_{in}C_{in}-q_{out}C)+H_{net} \quad (4.20)$$

D_H and D_V are calculated using the equations (4.21) and (4.22):

$$D_H=D_{SGS}+D_V+D_H^{back} \quad (4.21)$$

$$D_V=\frac{\mu_{mol}}{\sigma_{mol}}+\max(D_{3D},D_V^{back}) \quad (4.22)$$

where D_{SGS} is the diffusion due to the sub-grid scale turbulence model (m^2/s), D_H^{back} is the background horizontal eddy diffusivity (ξ- and η-direction) (m^2/s), D_V^{back} is the background vertical eddy diffusivity (ξ- and η-direction) (m^2/s), σ_{mol} is the Prandtl-Schmidt number for molecular mixing (-) and D_{3D} is the diffusion due to turbulence model in vertical direction (m^2/s), related to the turbulence eddy viscosity.

More details of the theory and computation of Delft3D-FLOW can be found in Deltares (2014d).

4.2 Transport - Near field (JETLAG)

For discharges into estuaries, water quality objectives simply cannot be achieved if the effect of a tidal current (which is present for most of the time) and the primary dilution are not taken into account. In order to carry out satisfactory risk assessment, the model must give reliable predictions over a wide range of conditions (jet orientation, ambient current and stratification). On the other hand, few models can treat satisfactorily jets with three-dimensional trajectories, such as oblique buoyant jets.

VISJET (Cheung *et al.* 2000) is a general predictive, PC-based, flow visualization tool to portray clearly the evolution and interaction of the buoyant jets discharged at different angles to the ambient tidal current. It com-

bines an extensively validated Lagrangian jet mixing model (JETLAG) with computer graphics techniques to trace the path and mixing characteristics of a arbitrarily inclined jet in three-dimensional space, in a uniform or density-stratified crossflow.

IHCantabria (2008b) used JETLAG to design the environmental characteristics of the single-port outfall of a power plant located at the Musel harbor (Asturias). IHCantabria (2010) employed JETLAG to study the effect of the single-port outfall of a power plant located at Mogán (Canarias) by coupling JETLAG with a two-dimensional hydrodynamic circulation model. Xu *et al.* (2011) determine the trajectory of the sewage plume in Hong Kong's waters by means of the coupling of the JETLAG with a three-dimensional hydrodynamic shallow water circulation model. IHCantabria (2014a) successfully used JETLAG to simulate the effects of a thermal single-port discharge of a cooling system into the Santander Bay by means of the coupling of the JETLAG with Delft3D-FLOW.

The Lagrangian model JETLAG (Lee & Cheung 1990, Lee & Chu 2003) predicts the mixing of buoyant jets with three-dimensional trajectories. The unknown buoyant jet trajectory is viewed as a sequential series of "plume-elements" which increase in mass as a result of shear entrainment (due to the jet discharge) and vortex entrainment (due to the cross-flow) while rising by buoyant acceleration and being sheared over by the cross-flow. Each "plume element", which can be thought of as a section of a bent cone, is characterized by its location, average velocity, toxicant concentration, temperature and salinity, width, and thickness.

The model tracks the evolution of the average properties of a plume element at each step by conservation of horizontal and vertical momentum, conservation of mass accounting for entrainment, and conservation of tracer mass/heat. The turbulent entrainment of the ambient fluid into the plume element is calculated at each time step.

Figure 4.1 shows a round buoyant jet directed into a uniform horizontal cross flow of velocity (u_{env}). The ambient current is assumed to flow along the x-axis. The major parameters governing the flow are the jet volume flux, the kinematic momentum flux, and the specific buoyancy flux. The objective is to predict the unknown plume geometry and the characteristic dilution and velocity in the jet cross-section.

The evolution of a single plume element is then equivalent to a solution of the properties along the unknown jet trajectory in the three-dimensional steady flow. By defining the thickness of a plume element as proportional to the local jet velocity, the Lagrangian method is similar to a time integration along the jet trajectory.

4.2.1 Model formulation

At the k^{th} time step, a plume element located at (x_k, y_k, z_k) with velocity (u_k, v_k, w_k) where (u, v) is the horizontal velocity, and w is the vertical velocity is considered. $V_k = \sqrt{u_k^2 + v_k^2 + w_k^2}$ is the magnitude of the velocity and $HVEL_k = \sqrt{u_k^2 + v_k^2}$ is the magnitude of the horizontal velocity. The temperature, salinity and density are denoted by T_k, S_k and ρ_k. The buoyant jet axis makes an angle of ϕ_k with the horizontal plane and θ_k is the angle between the z-axis and the projection of the buoyant jet axis on the horizontal plane. The half-width or radius of the plume element is b_k. h_k is the thickness/length, defined as proportional to the magnitude of the local jet velocity, $h_k \propto V_k$ (Figure 4.1).

The mass of the plume element is then given by $M_k = \rho_k \pi b_k^2 h_k$. Given the increase in mass due to turbulent entrainment, ΔM_k, the plume element characteristics at the next time step are obtained by applying conservation of mass, horizontal and vertical momentum, energy, and tracer mass to the discrete element.

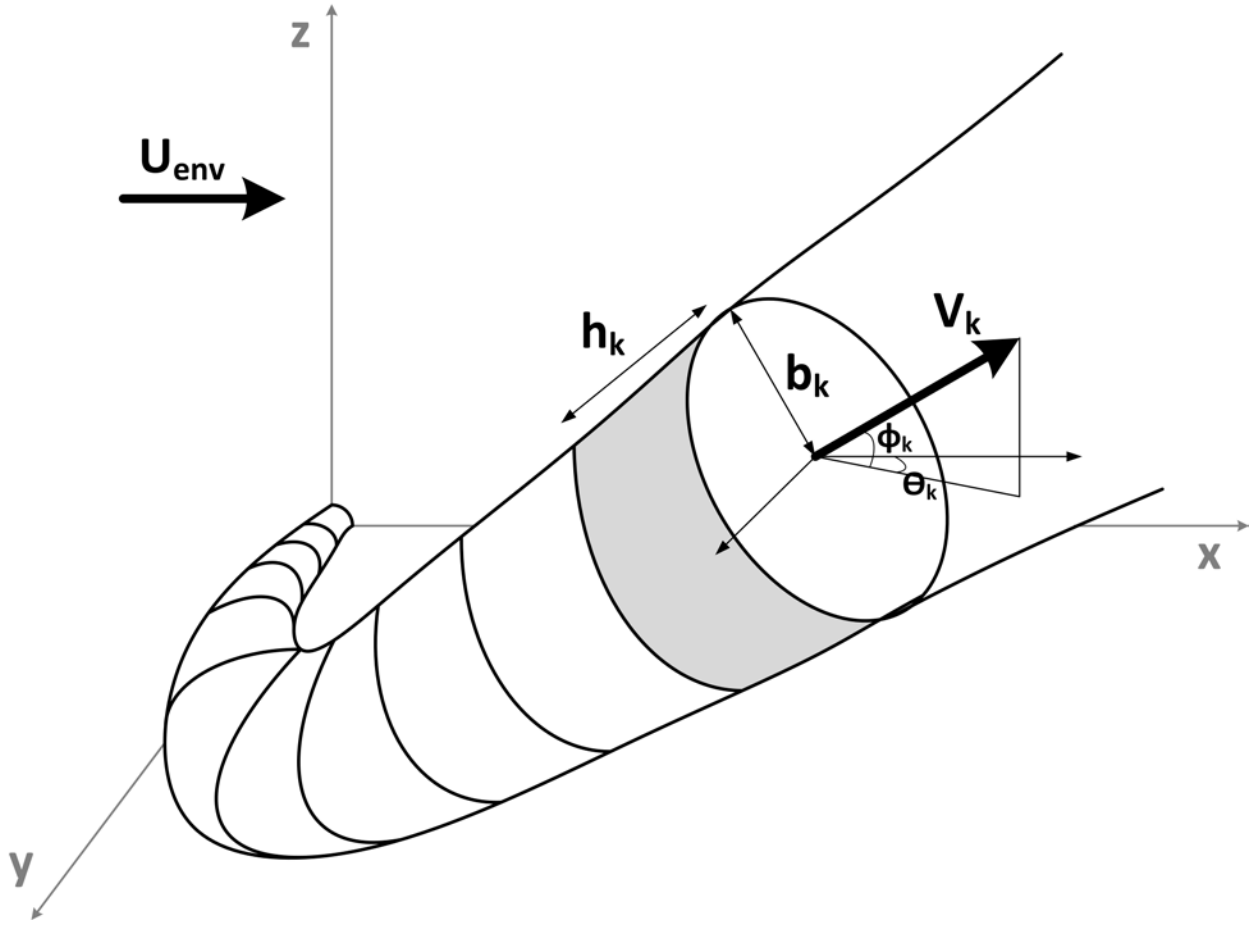

Figure 4.1: General Lagrangian model for buoyant jet with three-dimensional trajectories and schematic diagram of jet trajectory traced out by Lagrangian plume elements. Adapted from Lee & Chu (2003).

Mass

$$M_{k+1} = M_k + \Delta M_k \tag{4.23}$$
$$M_{k+1} = \rho_{k+1}\pi b_{k+1}^2 h_{k+1} \tag{4.24}$$

Concentration and density

$$S_{k+1} = \frac{M_k S_k + \Delta M_k S_a}{M_{k+1}} \tag{4.25}$$
$$T_{k+1} = \frac{M_k T_k + \Delta M_k T_a}{M_{k+1}} \tag{4.26}$$
$$\rho_{k+1} = \rho(S_{k+1}, T_{k+1}) \tag{4.27}$$
$$C_{k+1} = \frac{M_k C_k + \Delta M_k C_a}{M_{k+1}} \tag{4.28}$$

Horizontal momentum

$$u_{k+1} = \frac{M_k u_k + \Delta M_k u_{env}}{M_{k+1}} \tag{4.29}$$
$$v_{k+1} = \frac{M_k v_k}{M_{k+1}} \tag{4.30}$$

Vertical momentum

$$w_{k+1} = \frac{M_k w_k + M_{k+1}(\frac{\Delta\rho}{\rho_{env}})_{k+1} g \Delta t}{M_{k+1}} \tag{4.31}$$
$$HVEL_{k+1} = (u_{k+1}^2 + v_{k+1}^2)^{1/2} \tag{4.32}$$
$$V_{k+1} = (u_{k+1}^2 + v_{k+1}^2 + w_{k+1}^2)^{1/2} \tag{4.33}$$

Thickness/radius

$$h_{k+1} = \frac{V_{k+1}}{V_{k+}} h_k \tag{4.34}$$
$$b_{k+1} = (\frac{M_{k+1}}{\rho_{k+1}\pi h_{k+1}})^{1/2} \tag{4.35}$$

Jet orientation

$$\sin\phi_{k+1} = (\frac{w}{V})_{k+1} \tag{4.36}$$
$$\cos\phi_{k+1} = (\frac{HVEL}{V})_{k+1} \tag{4.37}$$
$$\sin\theta_{k+1} = (\frac{v}{HVEL})_{k+1} \tag{4.38}$$
$$\cos\theta_{k+1} = (\frac{u}{HVEL})_{k+1} \tag{4.39}$$

Location

$$x_{k+1} = x_k + u_{k+1}\Delta t \tag{4.40}$$
$$y_{k+1} = y_k + v_{k+1}\Delta t \tag{4.41}$$
$$w_{k+1} = w_k + w_{k+1}\Delta t \tag{4.42}$$
$$\Delta s_{k+1} = V_{k+1}\Delta t \tag{4.43}$$

Initial condition

$$(u, v, w)_0 = (V_0 \cos\phi_0 \cos\theta_0, V_0 \cos\phi_0 \sin\theta_0, V_0 \sin\phi_0) \tag{4.44}$$
$$(b, h)_0 = (0.5D, 0.5D) \tag{4.45}$$
$$(S, T, \rho, C)_0 = (S_0, T_0, \rho_{eff}, C_0) \tag{4.46}$$
$$\Delta t_0 = 0.1 \cdot \frac{h_0}{V_0} \tag{4.47}$$

In these equations, pressure drag is tacitly neglected and all of the entrained ambient flow is assumed to have the environmental velocity (u_{env}). The initial location of the plume element is set at the discharge location. By the nature of the formulation, there is no distinction between the zone of flow establishment (the potential core) and the zone of established flow of the buoyant jet. Only the average properties in the jet cross-section are represented. In effect, the model postulates a top-hat profile for both the velocity and the concentration.

4.2.2 Shear and vortex entrainment

The increase in mass of the plume element at each step (ΔM) is computed as a function of two components: the shear entrainment due to the relative velocity between the plume element and the ambient velocity in the direction of the jet axis (ΔM_s) and the vortex entrainment ("forced" entrainment) due to the ambient cross-flow (ΔM_f).

Shear entrainment

In JETLAG, the shear entrainment at each time step k is computed as:

$$\Delta M_s = 2\pi\alpha_s b_k h_k \Delta U \Delta t \tag{4.48}$$

$$\alpha_s = \sqrt{2}(0.057 + 0.554 \sin\phi_k / F_l^2)(\frac{2V_k}{\Delta U + V_k}) \tag{4.49}$$

where V_k is the jet velocity, $\Delta U = |V_k - u_{env}\cos\phi_k \cos\theta_k|$ is the relative buoyant jet velocity in the direction of the buoyant jet axis, and b_k, h_k are the radius and thickness of the plume element (Figure 4.1). α_s and F_l are the entrainment coefficient and the local jet densimetric Froude number respectively.

Projected area entrainment (PAE)

The vortex entrainment due to the cross-flow is modelled using the Projected Area Entrainment (PAE) hypothesis (Cheung & Lee 1996, Frick 1984, Lee & Cheung 1990). JETLAG assumes that all the ambient flow on the windward side of the plume is entrained into the plume element. The vortex entrainment of the ambient flow into an arbitrarily inclined plume element and the incremental increase in mass at each time step, ΔM_f, are formulated in the following PAE expression (Lee & Cheung 1990):

$$\Delta M_f = \rho_{env} u_{env} [2 b_k h_k \sqrt{1 - \cos^2 \phi_k \cos^2 \theta_k} + \pi b_k \Delta b_k \cos \phi_k \cos \theta_k + \frac{\pi b_k^2}{2} \Delta(\cos \phi_k \cos \theta_k)] \Delta t = \rho_{env} u_{env} (A_p + A_w + A_c) \Delta t \quad (4.50)$$

An initial estimate of ΔM_f can be obtained as:

$$\Delta M_f = \rho_{env} u_{env} b_k h_k [2 \sqrt{\sin^2 \phi_k + \sin^2 \theta_k - (\sin \phi_k \sin \theta_k)^2} + \pi \frac{\Delta b_k}{\Delta s_k} \cos \phi_k \cos \theta_k + \frac{\pi \Delta b_k}{2} \frac{(\cos \phi_k \cos \theta_k - \cos \phi_{k-1} \cos \theta_{k-1})}{\Delta s_k}] \Delta t \quad (4.51)$$

An improved estimate $(\Delta M_f)_k$ can then be obtained from equations (4.50) and (4.51), and the procedure repeated until convergence is achieved. The time step Δt can be fixed or variable. It is chosen via a "predict-correct" procedure to attain a prescribed fractional change in mass (typically of the order of 1%) at each time step. It should be emphasized that the ambient density ρ_{env} takes on local values, thus ambient stratification can be readily handled.

In equations (4.50) and (4.51), there are three contributing terms to the projected area. Firstly, the entrainment due to the projected plume area normal to the cross flow, i.e, the projection or cylinder term E_p. Secondly, a correction term due to the increase in plume width E_w. Thirdly, a correction term due to plume curvature E_c. The total projected area entrainment is $E_f = E_p + E_w + E_c$. Figure 4.2 illustrates the meaning of the respective projected area terms pictorially for a current flowing from the left.

Total entrainment

The total entrainment can be obtained from a maximum hypothesis, $\Delta M = \max(\Delta M_s, \Delta M_f)$. Alternatively an additive hypothesis, $\Delta M = \Delta M_s + \Delta M_f$ can be used. A general modeling framework is implemented in JETLAG to handle the transition from the shear entrainment regime to the vortex entrainment regime. More details of the theory and computation of JETLAG can be found in Lee & Cheung (1990) and Lee & Chu (2003).

4.3 Transport - Far field (D-Water Quality)

D-Water Quality, formerly Delft3D-WAQ, is the model providing the secondary dilution. That includes advection, diffusion and decay processes in direct relation to far-field processes.

Ballegooyen *et al.* (2004) successfully used Delft3D-WAQ model in order to determine the water quality of the Kromme and Palmiet estuaries in South Africa. Gils *et al.* (2008) used Delft3D-WAQ in the Pearl River Delta in order to provide a tool for the Environmental Protection Department of the Hong Kong Special Administrative Region and the Guangdong Environmental Protection Bureau to support their joint water quality management, one of the considered substances was copper. Brown *et al.* (2014) used Delft3D-FLOW and D-Water Quality to simulate freshwater and dissolved organic carbon transport over a 3-week period, following intense precipitation that led to high river discharge into the brackish Neuse River Estuary from Hurricane Irene on August 2011. IHCantabria (2014b) used Delft3D-FLOW and D-Water Quality to simulate wastewaters coming from a submarine outfall located at Xagó (Asturias) in order to analyze the industrial and

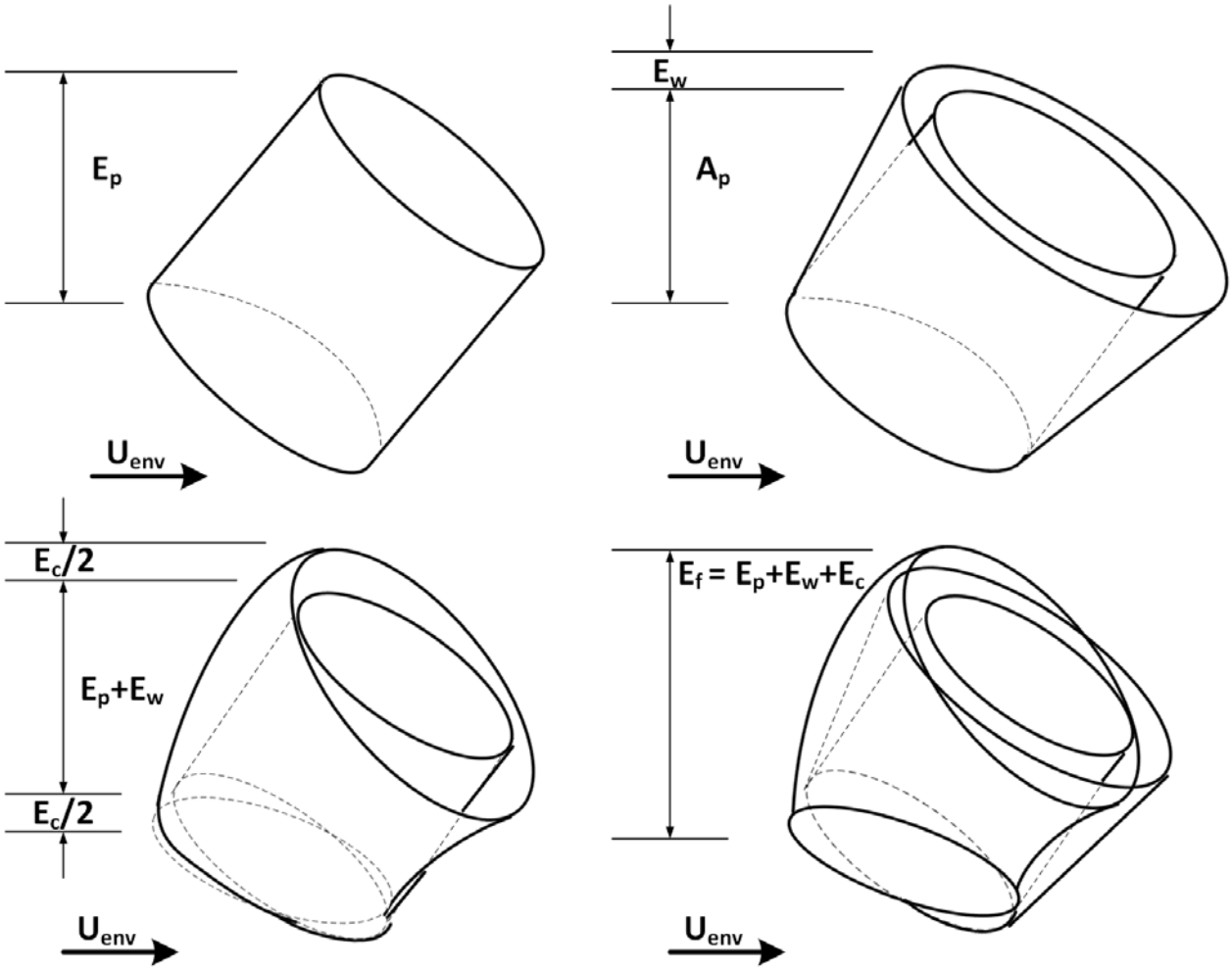

Figure 4.2: Illustration of the three contributions of the PAE: projected area term E_p, increase in area due to plume growth E_w and correction in area due to plume curvature E_c and the sum of all three terms E_f. Adapted from Lee & Chu (2003).

sewage waters, among the considered substances were cadmium and mercury.

D-Water Quality administrates the mass balance of selected state variables, such as heavy metals or organic micropollutants. A water quality model is in fact not more than a mass balance for the toxicants or state variables necessary to describe the problem at hand. D-Water Quality uses the finite volume method which is a computational method to solve the "advection-diffusion-reaction" equation. This method is mass-conserving by definition. By combining computational cells in one, two or three dimensions each water system can be represented and substances can be transported o decayed through computational cells and hence through the water system (Deltares 2014c).

4.3.1 Model formulation

Advection-diffusion-reaction equation

D-Water Quality solves the equations for transport and physical, (bio)chemical and biological processes. In this section we introduce the mathematical "advection-diffusion-reaction equation" that forms the basis of D-Water Quality:

$$\frac{\partial C}{\partial t} + u\frac{\partial C}{\partial x} - D_x\frac{\partial C^2}{\partial x^2} + v\frac{\partial C}{\partial y} - D_y\frac{\partial C^2}{\partial y^2} + w\frac{\partial C}{\partial z} - D_V\frac{\partial C^2}{\partial z^2} = SO + f_R(C,t) \tag{4.52}$$

where D_x, D_y and D_V are the dispersion coefficients taken for every direction. SO and f_R are the additional terms so-called source terms.

Discharges (S) are additional inflows of water or mass that were not present in the hydrodynamic module (Delft3D-FLOW). They are usually used for small rivers, discharges of industries, sewage treatment plants, small waste load outfalls, etc. Reaction terms or "processes" (f_R) are only considered if they can be written in the form of a partial differential equation:

$$(\frac{\partial \overline{C_i}}{\partial t})_R = f_R(\overline{C_1}, t) \tag{4.53}$$

where C_i is the concentration at a given location for substance "i", f_R is any functional prescription and t is the time.

Changes by transport include both advective and dispersive transport, that is the transport by flowing water and the transport as a result of concentration differences respectively. The flow of water and dispersion coefficients are derived from the Delft3D-FLOW. Dispersion, as defined here, differs from the physical concept of molecular diffusion as it stands for all transport that is not described by the advective transport.

Changes by processes include physical processes such as reaeration and settling, chemical processes such as adsorption and denitrification and/or biological processes such as primary production and predation on phytoplankton. Water quality processes convert one substance to another.

Changes by sources include the addition of mass by waste loads and the extraction of mass by intakes. Mass entering over the model boundaries can be considered a source as well.

Numerical discretization

As the model makes use of discrete computational elements and discrete time steps, equation (4.52) can not be applied directly. Therefore, solution of the "advection-diffusion-reaction" equation with computers requires the use of discrete segments in space with finite mesh sizes x, y and z and with a finite time step t. Various

options for discretizing the partial differential equations in terms of x, y, z and t are possible. These options are called numerical discretization schemes (see Chapter 2).

In D-Water Quality, for the space integration, central discretizations or (first or higher order) upwind discretizations may be applied. For the time integration, explicit, semi-implicit or implicit methods may be chosen. Having the numerical discretization, different strategies can be followed to solve the discretized systems of equations. These strategies are known as "solution methods" and can be divided in iterative solvers or direct solvers. More than 20 different integration schemes are available in D-Water Quality. For detailed information about the numerical discretizations and applied iterative solution methods in D-Water Quality, readers are referred to the D-Water Quality user manual (Deltares 2014c).

4.3.2 Implemented water quality processes

In D-Water Quality the constituents of a water system are divided in functional groups (Figure 4.3). A functional group includes one or more substances that display similar physical and/or chemical behavior in a water system. To get a complete description of the water system to simulate, the separate descriptions of the functional groups has to be combined. Within the functional group descriptions links to other functional groups are indicated.

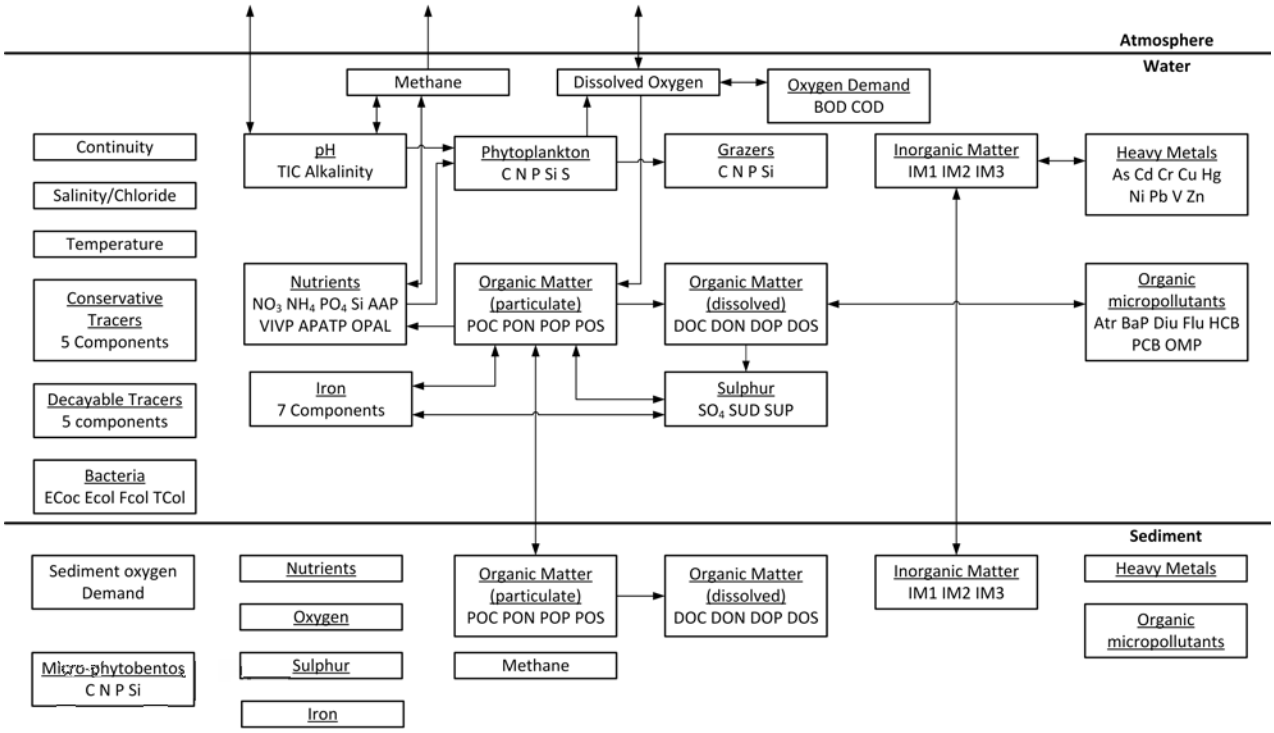

Figure 4.3: General overview of substances included in D-Water Quality. Substances are organised in functional groups indicated by a grey header, except for some substances that form a group of their own. Major links between substances are indicated by arrows; note that many links are omitted.

The functional groups include in D-Water Quality are:

1. Salinity, chloride and tracers
2. Water temperature and temperature dependency of rates
3. Coliform bacteria

4. Dissolved oxygen and biochemical oxygen demand (BOD)
5. Suspended sediment and sedimentation
6. Nutrients, detrital organic matter and electron-acceptors
7. Primary producers: phytoplankton
8. Primary consumption
9. Heavy metals and organic micro-toxicants
10. Sediment modeling

In this thesis, we will use the functional groups 1, 2, 5 and 9 for modeling the impact of discharging industrial wastewaters into estuarine waters. The next paragraphs review the main aspects of these functional groups.

Salinity, chloride and tracers

Salinity, chloride and tracers are special substances in D-Water Quality as they are not subject to water quality processes. These substances allow distinguishing between the effect of transport and processes for other substances, as they can isolate the effect of transport. Conservative tracers (conservative meaning "not subject to decay") have a wider range of application as they can be assigned at choice to sources of water. D-Water Quality allows specifying up to five conservative tracers.

Next to conservative tracers, D-Water Quality has five decayable tracers as well. Decayable tracers are subject to first order decay ($C(t) = C_0 e^{-kt}$).

Water temperature and temperature dependency of rates

The water temperature determines the rate at which water quality processes take place. As such, it is important that the water temperature is correct in the simulation. The temperature dependency of reaction rates has a uniform exponential equation (4.54):

$$k_{Temp} = k^{20} \times k_T^{T-20} \tag{4.54}$$

where k_{Temp} is the rate constant at temperature T (d^{-1}), k^{20} is rate constant at reference temperature 20 ^{o}C (d^{-1}), k_T is the temperature coefficient (-) and T is the ambient water temperature (^{o}C).

D-Water Quality allows calculating the ambient water temperature as a function of the ambient air temperature. The more elaborate temperature modeling through solar radiation, cloudiness, evaporation, etc. is implemented in Delft3D-FLOW (Deltares 2014d). Note that if the water temperature was included in the Delft3D-FLOW simulation, it is an option to include this in D-Water Quality as a forcing function.

Suspended sediment and sedimentation

Sediment is particulate material, formed by the physical and chemical desintegration of rocks from the earth's crust (inorganic) and by various biological processes (organic). The sediment carried by natural waters contains a mixture of inorganic and organic components. They can be classified according to the various grain sizes into Gravel (>2 mm), Sand (0.06 mm-2 mm), Silt (0.004 mm-0.06 mm), Clay (<0.004 mm) and Organic particles (up to several μm).

Considering the large adsorbing capacities, the fine fraction is characterised as cohesive sediment. Since flocculation and adsorbing capacities are of minor importance for larger particles, they are classified as non-cohesive sediment. In principal all particulate components are subject to settling.

Modeling framework

The mass balances for particulate (suspended) matter in the water column (c_w) is given in equation (4.55).

$$\frac{\Delta c_w}{\Delta t} = loads + transport - settling \tag{4.55}$$

Settling/sedimentation is proportional to a first order settling velocity (m/d). Settling occurs when the actual shear stress is lower than the user-defined critical shear stress for sedimentation. The actual shear stress is a function of flow velocity and waves from Delft3D-FLOW. Each particulate fraction has its own critical shear stress for sedimentation. For detailed information about the implemented mathematical formulations in D-Water Quality, readers are referred to the D-Water Quality user manual (Deltares 2014c).

Heavy metals and organic micropollutants

Two types of toxicants can be modelled with D-Water Quality heavy metals and organic micropollutants. Because the fate of most toxicants is largely determined by the adsorption to particulate matter, suspended inorganic and organic matter has to be included in the model in most cases. It may be necessary to include dissolved organic matter as well (Deltares 2014b).

Modeling framework

The mass balance equation (4.56) read for water:

$$\frac{\Delta C_{wT}}{\Delta t} = loads + transport - settling - losses \tag{4.56}$$

where C_{wT} is the total concentration of a toxicant in water (g/m^3) and t is the time (day).

Whereas D-Water Quality simulates total concentration (mass in fact), the particulate and dissolved fractions are needed for this purpose. The rates of transport processes that affect only the particulate or only the dissolved parts of a toxicant are corrected with these fractions. They are also used to produce output on the magnitude of the particulate and dissolved concentrations.

For detailed information about the implemented mathematical formulations in D-Water Quality of the processes affecting toxicants, readers are referred to the D-Water Quality user manual (Deltares 2014c) and the additional D-Water Quality technical reference manual "Processes Library Description: Detailed description of Processes" (Deltares 2014a).

Heavy metals

The fate of heavy metals in a water system is determined primarily by partitioning and by transport. The partitioning divides the total amount of a toxicant into a "dissolved" fraction and several "adsorbed" fractions. Adsorbed fractions of a metal are influenced by settling.

In the D-Water Quality the following assumptions for heavy metals has been made:

- Heavy metals can adsorb to particulate inorganic matter (up to three fractions).
- The adsorption to particulate matter and dissolved matter is described by means of equilibrium or kinetic partitioning, on the basis of partitioning coefficients.
- Volatilization is ignored for all heavy metals.
- Some metals, mercury in particular, are subject to methylation by microbes. Organic mercury species are important from a bioaccumulation point of view, but little important in terms of chemical speciation.

Quantification of the processes concerned is still difficult so formulations for these processes have not been implemented.

For detailed information about the implemented mathematical formulations in D-Water Quality of the processes affecting heavy metals, readers are referred to the D-Water Quality user manual (Deltares 2014c) and the additional D-Water Quality technical reference manual "Processes Library Description: Detailed description of Processes" (Deltares 2014a).

Organic micropollutants

The short term fate of organic micropollutants in a water system is determined primarily by partitioning and by transport. Organic micropollutants are also influenced by additional processes such as volatilization and degradation.

The presence of a micropollutant in a water system is described by the total concentration (sum of dissolved and particulate concentrations), the total particulate concentration and the total dissolved concentration. The particulate and dissolved concentrations are derived from the total concentration and the respective fractions. The latter are calculated from partitioning formulations.

In the D-Water Quality the following assumptions for organic micropollutants has been made:

- Organic substances adsorb to particulate, dissolved detrital organic matter (up to five fractions) and phytoplankton biomass (sum of the biomass of various algae species).
- The adsorption to particulate matter is described by means of equilibrium or kinetic partitioning, on the basis of a partitioning coefficient. Adsorption to dissolved organic matter (DOC) is described indirectly, by means of the partitioning coefficient for particulate organic carbon and an efficiency factor.
- All organic micropollutant is available for partitioning
- Transport of organic micropollutants across the water-atmosphere interface (e.g. volatilization) is based on the double film theory. Equilibrium is assumed between the concentrations of the micropollutant in the gas film and the liquid film according to Henry's Law. Only the free dissolved micropollutant is available for volatilization.
- Three types of degradation processes can be distinguished: photolysis, hydrolysis and biodegradation. For all processes the degradation rate is proportional to the micropollutant concentration, and a function of temperature. The formulations for the individual degradation processes have not yet been made operational in standard D-Water Quality.
- The various processes for decomposition of organic micropollutants are integrated in one overall degradation process. First order temperature dependent kinetics have been used to formulate this process. Different degradation rate constants can be provided to water and sediment compartments.
- By means of an option parameter the various dissolved fractions or the total concentration can be subjected to degradation.

For detailed information about the implemented mathematical formulations in D-Water Quality of the processes affecting organic micropollutants, readers are referred to the D-Water Quality user manual (Deltares 2014c) and the additional D-Water Quality technical reference manual "Processes Library Description: Detailed description of Processes" (Deltares 2014a).

4.4 Self-developed math tools

In this section, a review of all the self-developed mathematical tools for integrating, transferring, communicating and plotting the required and obtained information along the overall methodology is presented. These mathematical tools were coded using two programming languages: MATLAB and PYTHON and a GIS software: ArcGIS 10.1. MATLAB software was used for calculations of any type. PYTHON software was employed to run dynamically models and to modify and format ASCII files. ArcGIS was used to integrate all the results in a geodatabase and calculate spatial operations such as buffers. The following subsections display an schematic view and a brief description of the developed tools.

4.4.1 Hydrodynamic calibration

The calibration process provides the combination of values of calibration parameters to obtain the best match between the results obtained by the model and the data measured in the study area. Hydrodynamic calibration will focus on adjusting water levels, current speeds and salinities in order to simulate adequately hydrodynamics and transport of conservative tracers.

Figure 4.4 shows the schematic view of the hydrodynamic calibration. Note that light grey box represent the used tool (Delft3D-FLOW) and dark grey boxes are the developed tools (EXTRACTOR, GENERA and CALIBRA). This developed tools were coded using MATLAB software.

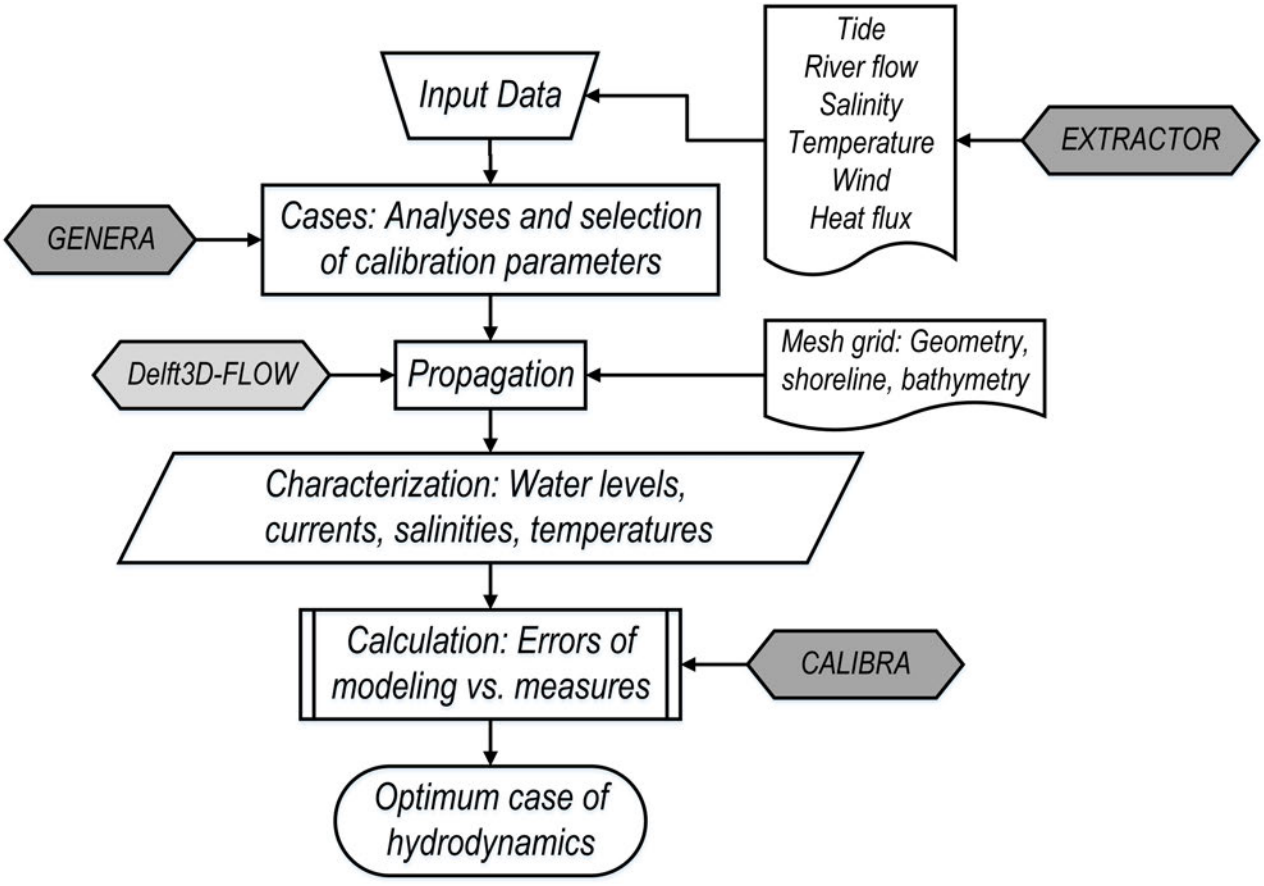

Figure 4.4: Schematic view of the hydrodynamic calibration. Light grey and dark grey boxes represent the used and developed tools respectively.

EXTRACTOR

This tool extracts the information about forcing data (water level, river flow, salinity, temperature, wind, heat flux,...) coming from different databases (TOPEX, Seawind HR, COADS05, WOA2009,...) and fits input files with the required formats of Delft3D-FLOW time series.

GENERA

This tool evaluates viscosity, diffusivity and rugosity values for each grid cell on the model domain for generating different map files.

Horizontal viscosity (μ_H) and diffusivity (D_H) are calculated with equations (3.3) and (3.4) respectively.

Rugosity is calculated by using the Manning coefficient (n) in two ways. First, we vary the value of n on each calibration case assuming a constant value in all the mesh grid. Second, we vary the value of n according to the depth of grid cells as suggested by Dias & Lopes (2006) and Iglesias & Carballo (2010).

CALIBRA

This tool calculates and plots errors between the model outputs and field measurements for water levels, current velocities and salinities. To achieve this task, the MATLAB script reads the model results and field measures. Next, it calculates a series of errors such as BIAS and Model efficiency (CE). Finally, it graphs the comparison between model and field data and generates the table of errors.

4.4.2 Offline passive initial dilution

The offline passive initial dilution characterizes the main variables (dilutions, distances, thickness and radius) of the toxicant evolution in the near-field. This process has into account the hydrodynamic model outputs as input data for the near-field model and it also works continuously during the simulation time of the hydrodynamic model.

Among the different initial dilution strategies, we decided to implement an offline and passive initial dilution. Passive initial dilution assumes that the source-induced flow, though considerably important for near-field mixing, does not change the flow characteristics of hydrodynamics. Offline linkage reads the output of the hydrodynamic model for the entire time of interest. This output is then specified as environmental conditions for the near-field model in a subsequent simulation.

Figure 4.5 shows the schematic view of the offline passive initial dilution. Note that light grey box represent the used tool (VISJET) and dark grey boxes are the developed tools (ENV-DATA, LANZA-VISJET and PAINT-JET). LANZA-VISJET was coded with PYTHON meanwhile ENV-DATA and PAINT-JET were programmed in MATLAB.

ENV-DATA

This tool extracts the information about the environmental data from Delt3D-FLOW outputs (water levels, currents, salinities, temperatures) and it also collects the required information of the studied discharge (concentration, temperature, salinity, pipe diameter, discharge angle with the horizontal and discharge depth).

LANZA-VISJET

This tool performs two tasks. Firstly, LANZA-VISJET fits all the input data with the required format of the JETLAG input files. Secondly, the tool runs all JETLAG simulations during the entire time of interest at each time step. It is worthy to mention that this script allows running the JETLAG model in a continuous mode without the use of the VISJET Graphical User Interface.

PAINT-JET

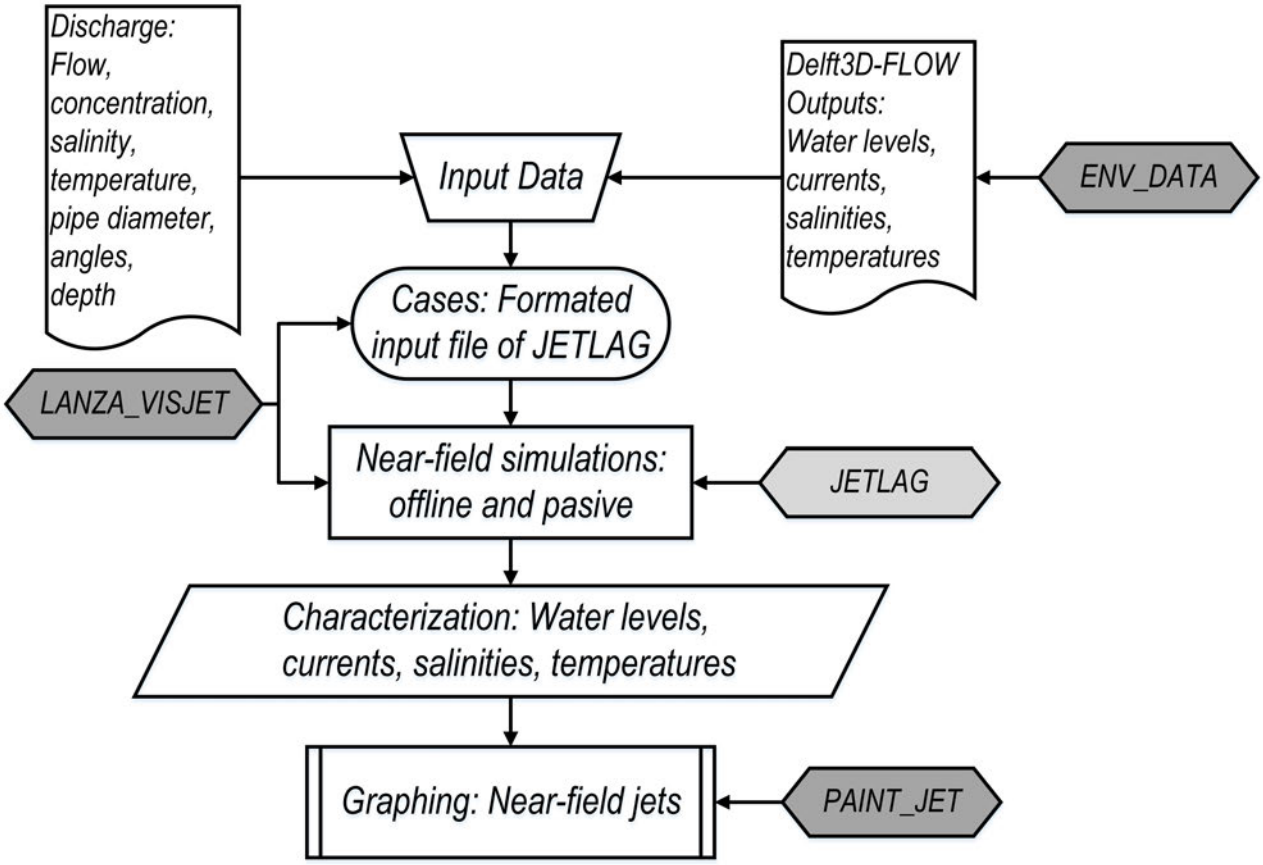

Figure 4.5: Schematic view of the offline passive dynamic initial dilution. Light grey and dark grey boxes represent the used and developed tools respectively.

JETLAG considers the unknown buoyant jet trajectory as a sequential series of "plume-elements". Once it has been characterized dilutions, distances, thickness and radius of each "plume element" along the near-field region, PINTA-JET reads all these results and graphs in a three-dimensional space each "plume element" as a sequential series of cylinders until reach the end of the near-field.

The center, height, radius and concentration of each cylinder is obtained from the distances, thickness, radius and dilutions of "each plume-element".

4.4.3 Offline passive coupling (intermediate-field)

The offline passive coupling transforms the near-field model outputs to obtain the required variables (dilutions, grid cells, layers) of the far-field discharge file, i.e., the tool calculates the toxicant loads at the end of the near-field (intermediate-field) to be read by the far-field model.

Among the different coupling strategies, we also decided to implement an offline and passive coupling. Passive coupling assumes that the initial dilution does not change the flow characteristics of the far-field and viceversa, i.e., the possible accumulation and interaction of toxicant concentration in the vicinity of the near- and intermediate field regions with the far-field region due to the release of a continuous discharge is neglected. Offline linkage generates the output of the intermediate-field for the entire time of interest. This output is then specified as boundary or source condition for the far-field model in a subsequent simulation.

Figure 4.6 shows the schematic view of the offline passive coupling. Note that dark grey boxes represent the developed tools (DILUTION, ACOPLA and VERTIDO). DILUTION and ACOPLA were programmed in MATLAB meanwhile VERTIDO was coded with PYTHON.

DILUTION

This tool performs two tasks. Firstly, it extracts the information about the intermediate-field from JETLAG outputs (dilutions, distances, thickness and radius). We assumed that the intermediate-field is the end of the near-field (last data of the JETLAG results). Secondly, the tool graphs the values of the intermediate-field.

ACOPLA

ACOPLA determines the final characteristics of the intermediate-field in terms of the used mesh grid by the far-field: concentration, flow, grid cell, layers. It also corrects these values when the jet interacts with the mesh grid boundaries.

Regarding boundary corrections, JETLAG calculates the buoyant jet trajectories without taking into account any boundary. These kind of approach could be reasonable when the discharge is released in ocean waters far away from the shoreline. However, in the case of estuaries, boundaries have a very significant impact and they cannot be neglected.

To avoid this issue, we assumed that the near-field ends if the jet collides with any boundary. In this situation, we also assumed that the dilution ends at that "plume element" where the collision is produced. From this point, we assumed that the buoyant jet does not experimented further entrainment, i.e., there are not more dilution. Additionally, we also assumed that the number of layers covered by the intermediate-field starts in the layer where the buoyant jet collides with the boundary and finishes at the free surface (Figure 3.13).

Furthermore, it is necessary to correct the flow information to preserve the mass in the far-field model when introducing the discharge in several layers. To solve this issue, we considered that the discharge flow on each layer is the ratio between the total flow and the number of layers covered by the intermediate-field ($Q_{layer} = Q_{total}/n^{o}{}_{layers}$).

After boundary and flow corrections, ACOPLA creates an output file where the concentration, location, num-

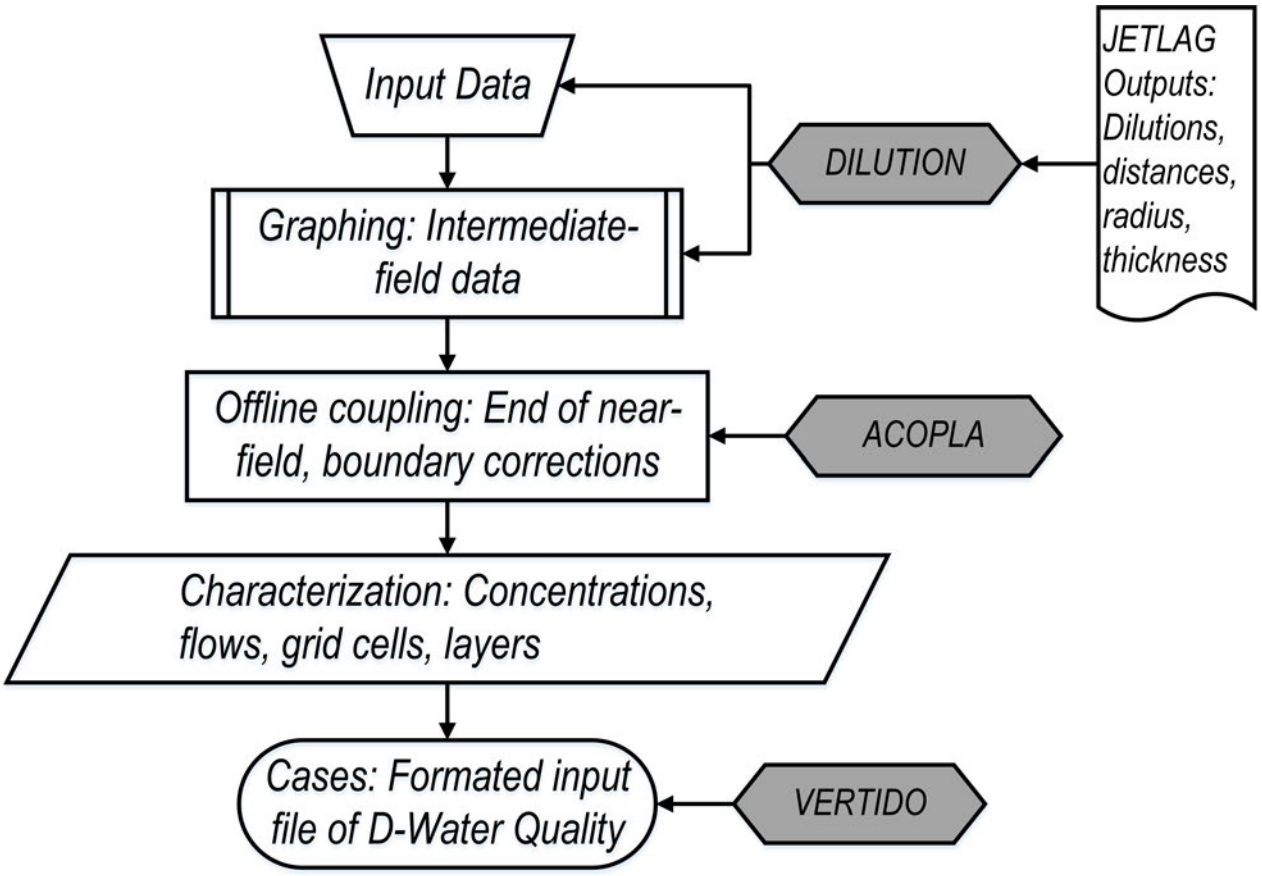

Figure 4.6: Schematic view of the offline passive coupling (intermediate-field). Dark grey boxes represent the developed tools respectively.

ber of layers and flow is specified for the entire time of interest.

VERTIDO

This tool generates the discharge file with the required format by D-Water Quality for the entire time of interest.

4.4.4 Far-field calibration

The calibration process provides the combination of values of calibration parameters to obtain the best match between the results obtained by the model and the data measured in the study area. Far-field calibration will focus on adjusting toxicant concentrations in order to simulate adequately the transport of non-conservative toxicants.

Figure 4.7 shows the schematic view of the far-field calibration process. Note that light grey box represent the used tool (D-Water Quality) and dark grey boxes are the developed tools (GENERA2, CALIBRA2). CALIBRA2 is very similar to the tool used in the hydrodynamic calibration. GENERA2 is very similar to GENERA. Both tools were also programmed in MATLAB.

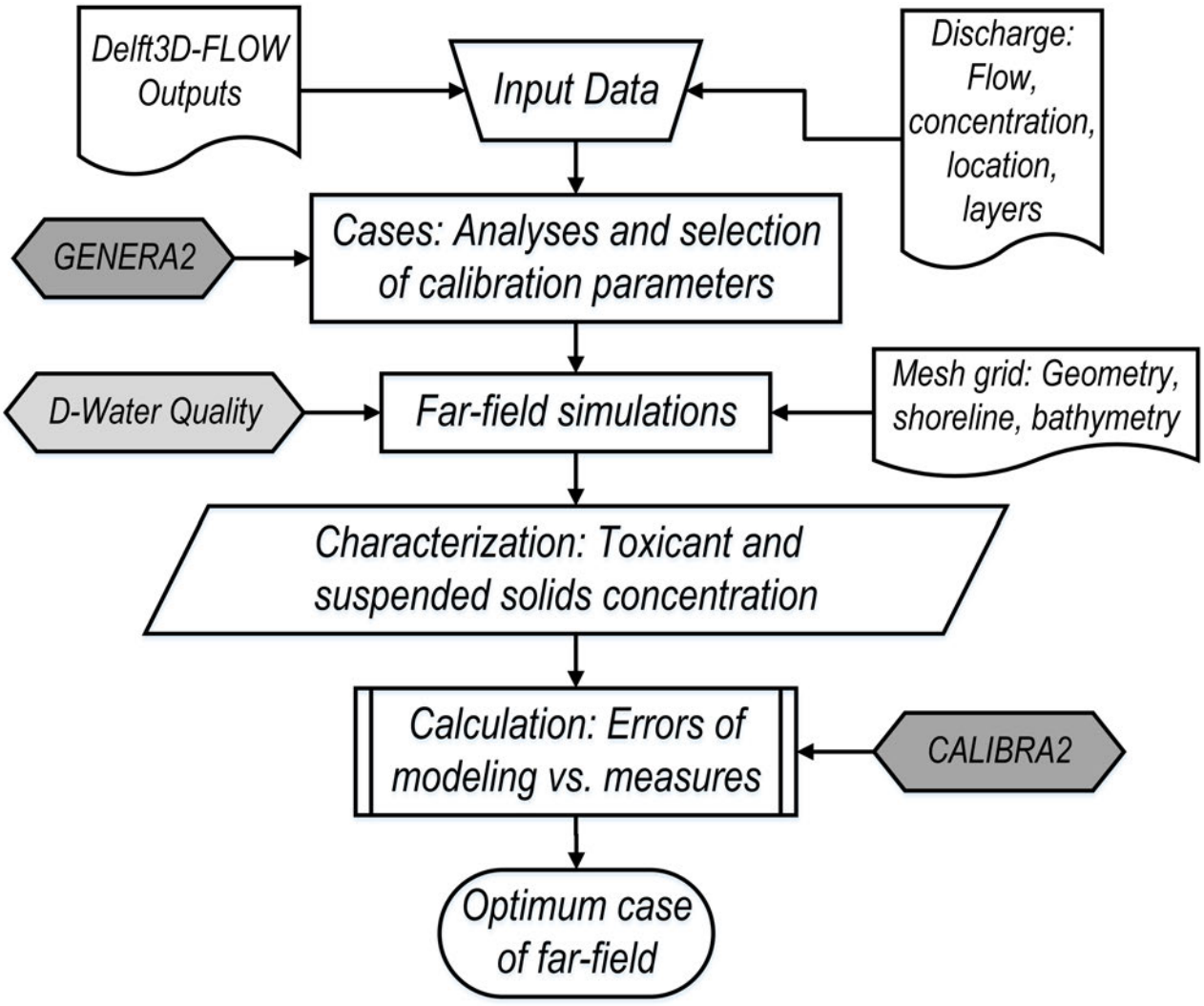

Figure 4.7: Schematic view of the far-field calibration process. Light grey and dark grey boxes represent the used and developed tools respectively.

GENERA2

This tool evaluates the sedimentation velocity (V_{sed}) according to equation (3.29), the liquid phase exchange coefficient (K_l) according to equation (3.31) and the gas phase exchange coefficient (K_g) according to equation (3.32). It also proportionates a temperature coefficient loss that varies on each calibration case.

CALIBRA2

This tool calculates and plots errors between the model outputs and field measurements for toxicant concentration in the same way as it was illustrated for hydrodynamics.

4.4.5 Selecting hydrodynamic forcings (model scenarios)

The selection of hydrodynamic forcings provides a combination of short-time series (clusters) of real hydrodynamic forcings on estuaries, optimizes the minimum number of clusters to identify the forcing variability and defines a simulation strategy to run numerical models on estuaries driven by the river and the tide. Figure 4.8 shows the schematic view of the selection of hydrodynamic forcings (model scenarios). Note that dark grey boxes represent the developed tools (KMA-FORZA and OPTIMIZA). Both tools were coded with MATLAB software.

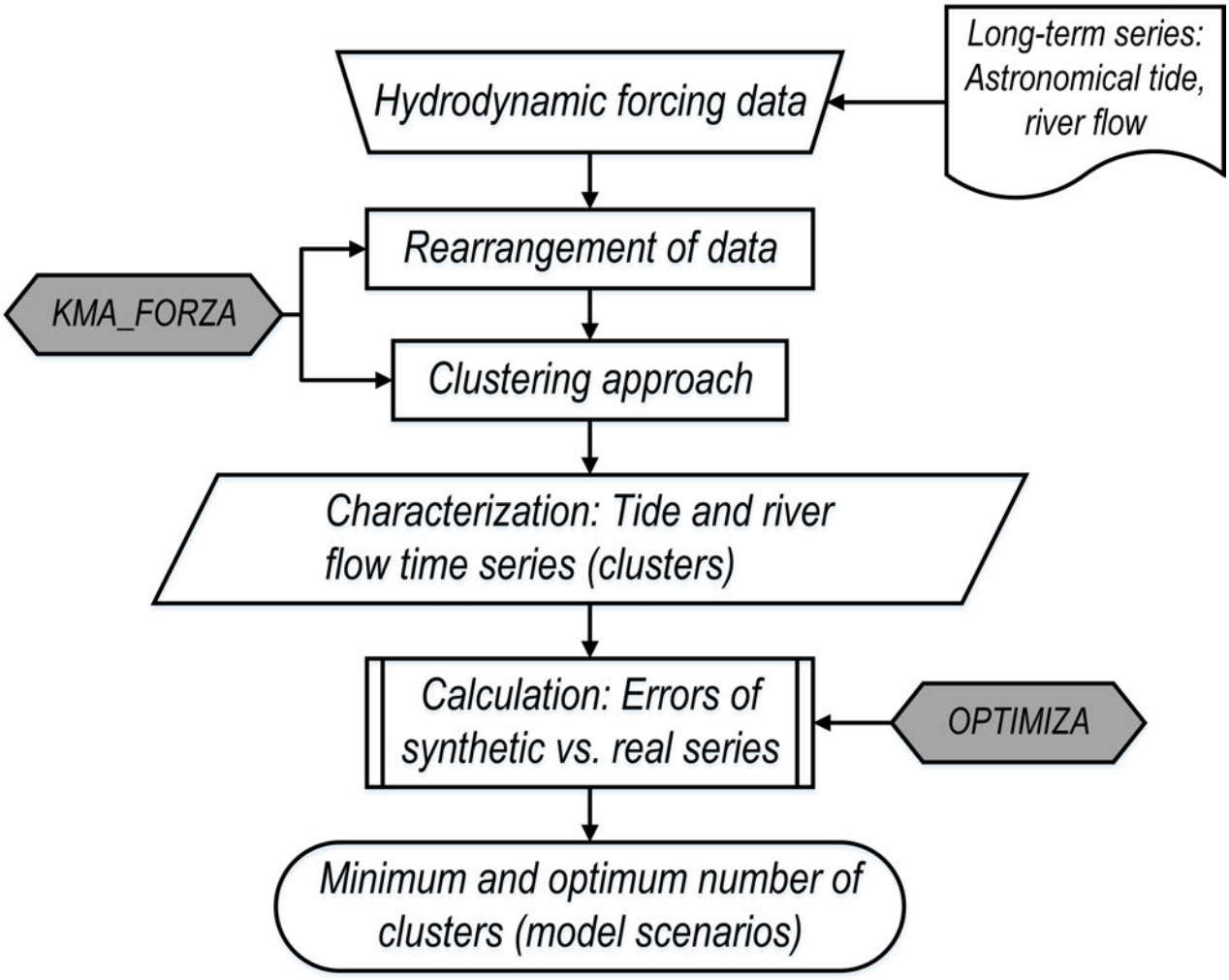

Figure 4.8: Schematic view of the selection of hydrodynamic forcings (model scenarios). Dark grey boxes represent the developed tools.

The methodology for selecting hydrodynamic forcings has been divided into several steps and is explained in the Chapter 3. An explanatory sketch of the methodology is shown in figure 3.30

KMA-FORZA

This tool carries out the rearrangement of the input data for clustering and applies the proposed clustering approach using a KMA-algorithm.

Firstly, it determines the hydrodynamic conditions with a number of days to classify the databases. This number is attached to the timescales governing the Q and A signal. Secondly, the tool rearranges the Q and A series in two matrices according to the timescales. Thirdly, the tools applies the KMA to obtain M groups or clusters representing n-days of river flow and astronomical tidal elevations. Finally, KMA-FORZA calculates the occurrence probability of each M cluster.

OPTIMIZA

During the application of data mining techniques, the selection of the number of clusters is user-defined. OPTIMIZA conducts a series of calculations in order to find the minimum and optimal number of clusters for:

- explaining the forcing variability. The M clusters (sequences of n-days) are representative of the original long-term series of the forcings.
- running numerical models with real hydrodynamic scenarios. the M clusters are representative of the transient response of the estuary.

Firstly, it reconstructs the long-term series from the M clusters to obtain the "synthetic series". This reconstruction is carried out by finding, every n-days, the closest cluster to the signal of Q and A for those n-days from the M clusters. Secondly, it calculates the error between both series using the model efficiency (CE).

On the other hand, OPTIMIZA determines water levels (WL) with the "synthetic and real series" in different locations along the study area using a simple formulation correlated to the two loading variables, e.g., river flow (Q) and astronomic tidal range (TR). It calculates the CE of both WL series to analyze the capacity of the "synthetic series" to be used on numerical modeling. Finally, it provides a minimum and optimal number of clusters necessary to take into account the variability of the hydrodynamic forcings on estuaries driven by the river and the tide.

4.4.6 Delimitating the AA-MZ and MAC-MZ

The delimitation of the AA-MZ and MAC-MZ determines the extent of both mixing zones in the study area according to the obtained values of a random sampling in the evolution of toxicant concentration for k-statistical years, the values of the AA-EQS and MAC-EQS and the failure probability for the AA-MZ and MAC-MZ. Figure 4.9 shows the schematic view of the delimitation of the AA-MZ and MAC-MZ. Note that dark grey boxes represent the developed tools (RECONSTRUCT, SAMPLEA, PROB-MZ and DELIMITA-MZ). All of them were coded with MATLAB.

RECONSTRUCT

This tool reconstructs time series of toxicant concentration at hourly level for l-years from the evolution of toxicant concentrations (model scenarios) based on the best match between each segment (n-days) of the year and the model scenarios.

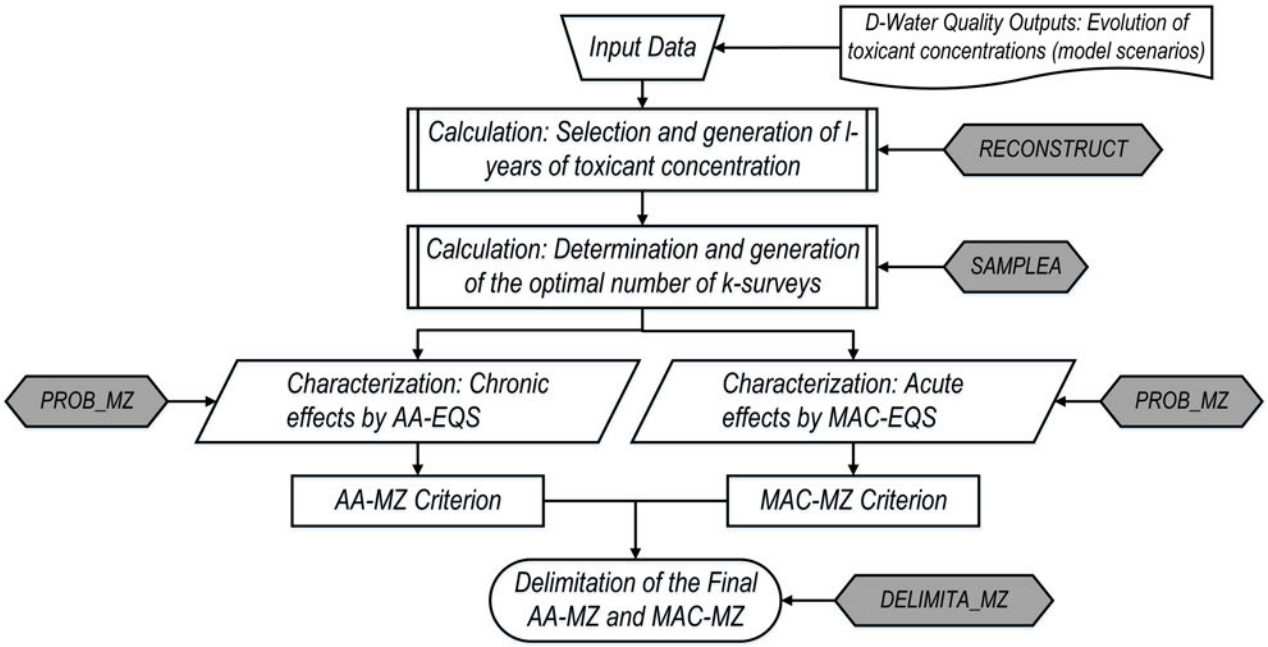

Figure 4.9: Schematic view of the delimitation of the AA-MZ and MAC-MZ. Dark grey boxes represent the developed tools.

To ensure the validity of the proposed l-years, these time series were generated using the real forcing time series or a Monte Carlo method. This Monte Carlo method is based on random selection of model scenarios (time series of n-days) depending on the occurrence probability of each model scenario.

SAMPLEA

As it was mentioned, numerical models provides continuous information about the variable of interest during the simulation time, in this case toxicant concentrations. However, water quality regulations are generally referred to discrete information (few samples during the period of interest) because they were promulgated more based on monitoring and pollution control than on outfall designing. Consequently, it is necessary to define a method for meeting the model information and the sampling information because the application of the AA- and MAC-EQS to these time series could give significant differences. Continuous information (numerical model) contains inherently all the variability of the time series. On the contrary, discrete information (sampling data) only represents a small part of the variability.

Bearing in mind these issues, SAMPLEA carries out a random sampling of k-surveys for one year. Each k-survey considers 12 samples where each sample corresponds to one month, i.e., one random sample within a month. This random sample can be located at any hourly position along the month and this position can be repeated on other months. Additionally, all the positions are available for a new survey (bootstrap method).

PROB-MZ

PROB-MZ characterizes the AA- and MAC-failure probability, i.e., the probability of not meeting the AA- and MAC-EQS on each k-survey for every l-year. Regarding AA-EQS application, one survey (12 samples) is meeting the requirements if the average is below the AA-EQS threshold. In the case of the MAC-EQS, if none sample is above the MAC-EQS threshold.

Taking into account the way to apply AA- and MAC-EQS, PROB-MZ assigns a value of 0 (if the requirements are met) and 1 (if the requirements are not met) for both EQS on each k-survey. Next, it calculates the AA- and MAC-failure probability for every l-year based on the previous assignment as follows $Prob_{EQS-year} = \sum_{i=1}^{k}(assignment)_i/k$. Finally, the tool evaluates the empirical cumulative distribution function of the AA-

and MAC-failure probability taking into account the probabilities of every l-year.

DELIMITA-MZ

This tool delimitates the AA- and MAC-MZ at grid cell level based on the AA-criterion (5_{th} percentile of ecdf of AA-failure probability equals 15%) and the MAC-criterion (5_{th} percentile of ecdf of MAC-failure probability equals 4%). If AA-criterion >15% the grid cell belongs to the AA-MZ and if MAC-criterion >4% to the MAC-MZ.

4.4.7 Estimating the local flushing time

The estimation of the LFT gives the distribution of the water renewal at grid cell level in the study area.

Figure 4.10 shows the schematic view of the estimation of the local flushing time. Note that light grey box represent the used tool (Delt3D-FLOW) and dark grey boxes are the developed tools (RENOVA and FINAL-LFT). Both were coded in MATLAB.

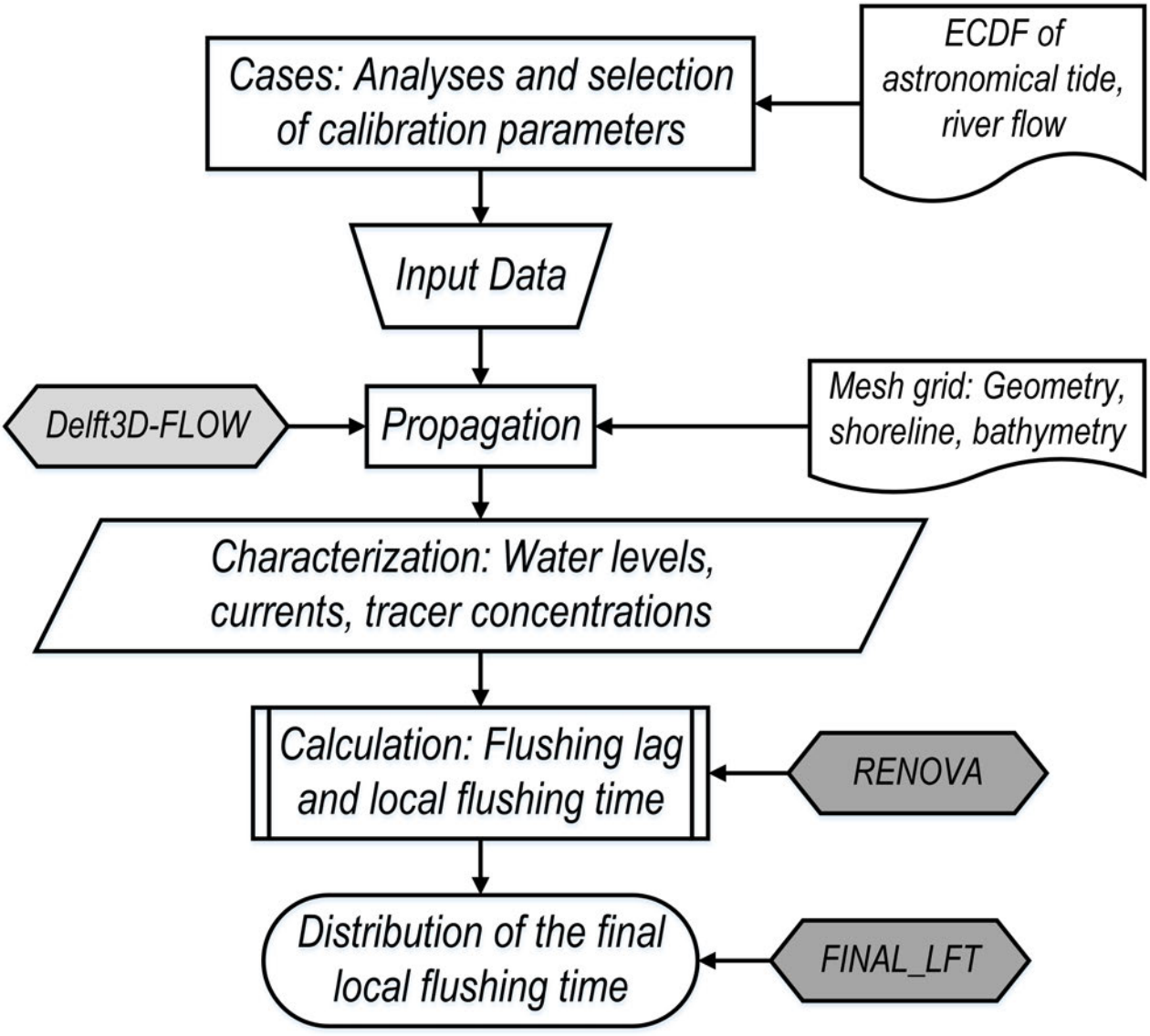

Figure 4.10: Schematic view of the estimation of the local flushing time. Light grey and dark grey boxes represent the used and developed tools respectively.

RENOVA

Firstly, the tool extracts the information about the tracer concentration from Delt3D-FLOW outputs. Secondly, the tool determines the flushing lag when the tracer concentration decays to a 95% of the initial concentration. Thirdly, it fits each tracer evolution to an exponential curve (Equation (3.37)). Finally, it calculates the LFT values.

FINAL-LFT

FINAL-FT evaluates the distribution of the LFT in estuaries as a unique value from a series of simulation cases taking into account the influence of the major forcing on the results.

The tool graphs the LFT values of every simulation case for every layer in order to understand the influence of the depth on LFT results. Then, if the influence is negligible, it averages theses values. Otherwise, the tool find the depth with the maximum LFT values and select it.

Next, the tool also graphs the LFT values of every simulation case for each initial phase in order to understand its influence on LFT results. Then, if the influence is negligible, it averages theses values. Otherwise, the tool find the initial phase with the maximum LFT values and select it.

In other analysis, it fits to a quadratic function (Equation (3.36)) all LFT values depending on river flow and tidal amplitude from the simulation cases. Next, it graphs the response surfaces. Then, the LFT values of the lower variable forcing are averaged obtaining the response curve to the main forcing. On the contrary, if the two forcings are significant no task are conducted.

Finally, it integrates the resulting area under the curve for each grid cell in order to build a rectangle with the same area and, thereby, providing a unique LFT value as the height of this rectangle. In the case that forcing is not averaged, it integrates the resulting volume under the surface for each grid cell in order to build a prism with the same volume and, thereby, providing a unique LFT value as the height of this prism.

4.4.8 Determining the stratification patterns in estuaries

The determination of the stratification patterns in estuaries provides the location of the mixed, partially mixed/stratified and stratified areas in the estuary. This determination will focus on calculate water levels, current speeds and densities with the hydrodynamic model to estimate the Richardson layer number (Ri_L) and determine the most probable stratification type.

Figure 4.11 shows the schematic view of the determination of the stratification patterns in estuaries. Note that light grey box represent the used tool (Delt3D-FLOW) and the dark grey box is the developed tool (STRATIFICA). STRATIFICA was programmed in MATLAB.

STRATIFICA

Firstly, the tool extracts the information about water levels, current speeds and densities from Delt3D-FLOW outputs on each M model scenario. Next, Ri_L is calculated by the equation 3.39 on each time step at grid cell level. If the grid cell displays a $Ri_L > 20$ is classified as stratified, for values between $20 > Ri_L > 2$ is classified as partially mixed/stratified and for values of Ri_L below 2 is classified as vertically mixed.

Secondly, the time duration and the percentage of time that a grid cell spend as mixed, partially mixed/stratified and stratified for every M model scenario is computed. From these results, three probability maps for every stratification type are determined multiplying each M map by the occurrence probability of the M model scenario. Finally, the tool classifies every grid cell into a stratification type according to the occurrence probability. If the probability of any stratification type surpasses 0.3333 then this grid cell is finally zoned with that stratification type.

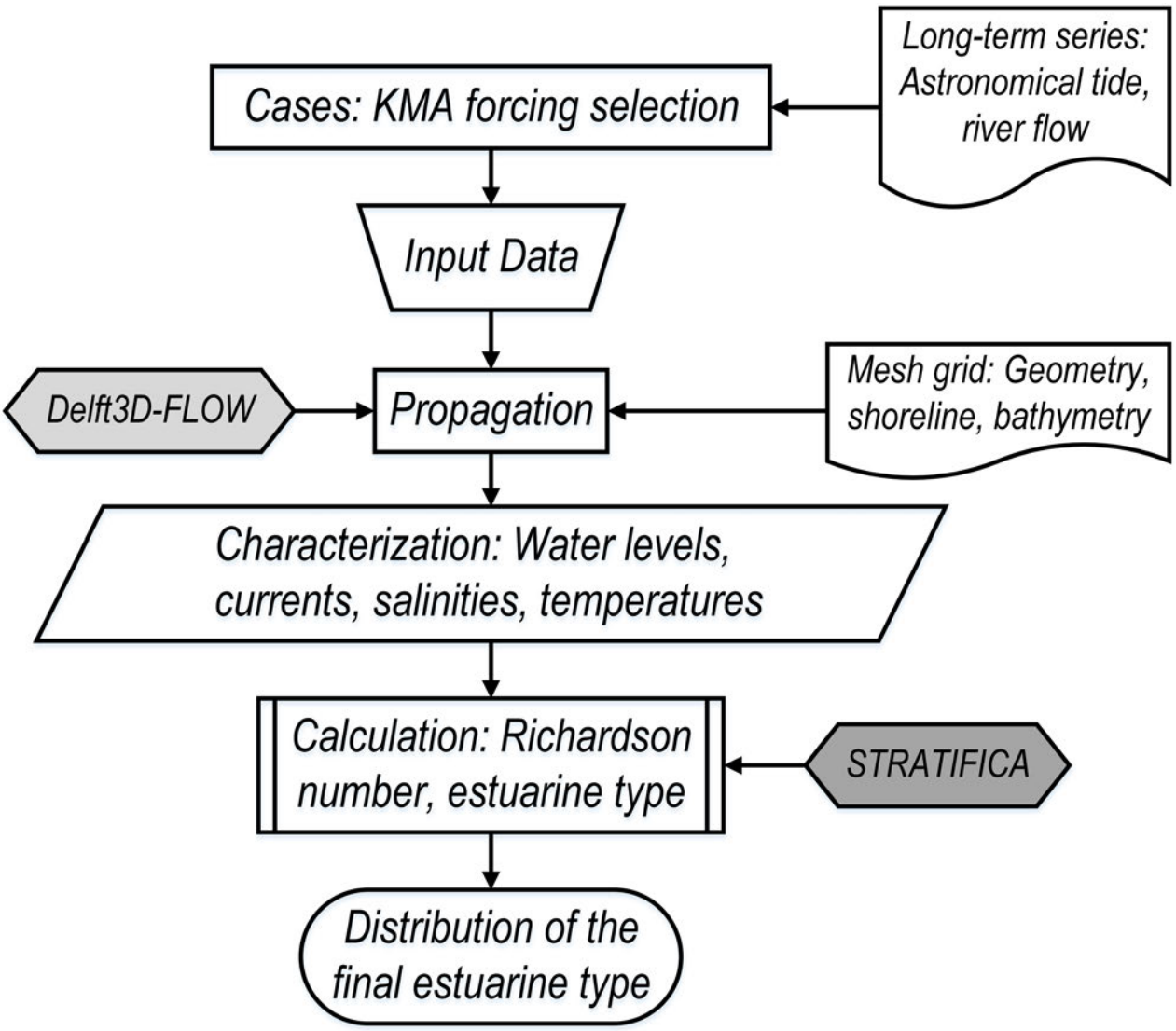

Figure 4.11: Schematic view of the determination the stratification patterns in estuaries. Light grey and dark grey boxes represent the used and developed tools respectively.

4.4.9 Assessing the admissibility of Mixing Zones

The assessment of the admissibility of Mixing Zones estimates the estuarine vulnerability in a spatio-temporal framework analysis and provides the acceptability criteria of the size of MZs and location of discharges. It is based on a holistic approach which considers, simultaneously, the physical processes involved in dispersion and diffusion mechanisms, the ecological features of the receiving water body and the social aspects related with the water body uses.

Figure 4.12 shows the schematic view of the assessment of the admissibility of Mixing Zones. Note that dark grey boxes represent the developed tools (CAPA-GIS and ADMITE). Both tools were developed and implemented on ArcGIS 10.1. Additionally, it is worthy to mention that all parameter calculations are carried out on the study area through the same mesh grid employed with the hydrodynamic and transport models. All results are integrated at grid cell level to estimate spatially the vulnerability and admissibility on the whole domain using 'shapefiles' of ArcGIS 10.1.

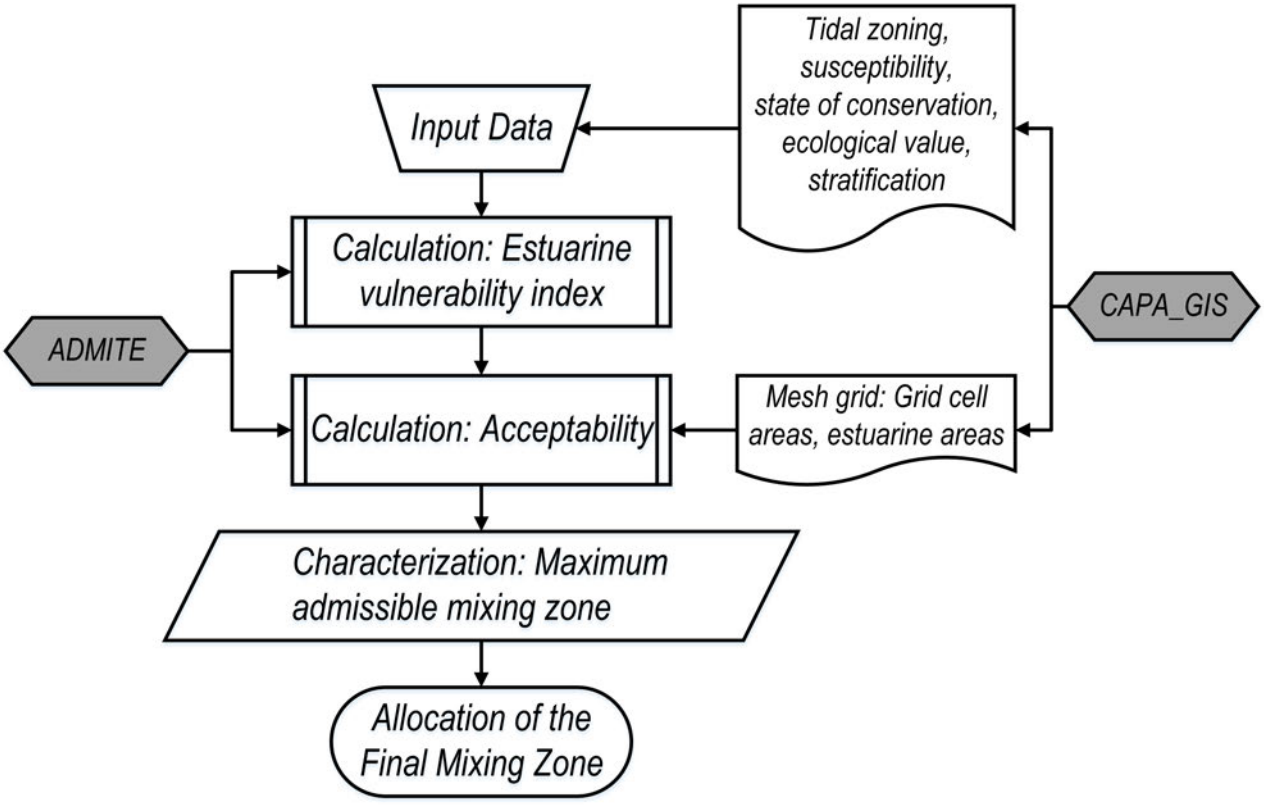

Figure 4.12: Schematic view of the assessment of the admissibility of Mixing Zones. Dark grey boxes represent the developed tools respectively.

CAPA-GIS

Estuarine Vulnerability is referred to characteristics of an estuarine ecosystem that describes its potential to be harmed. As it was mentioned in Chapter 3, the estuarine vulnerability index (EVI) is presented as a combination of four parameters: tidal zoning (TZ), susceptibility (SU), state of conservation (SC) composed by naturalness (NA) and ecological value (EV), and stratification (ST). This tool generates GIS layers ("shapefiles") of all these parameters using the information of Table 3.6 and GIS tools.

TZ allocates the intertidal and subtidal zones in the estuary according to the value of tidal amplitude that is not exceeded during the 95% of the time ($A95$) and the depth of each grid cell (H) using selection tools in GIS.

NA is defined computing buffer areas around each HP using buffer tools in GIS. Buffer distance of a HP is shown in equation (3.38).

EV is defined by recognizing local, regional, national and international protected areas such as bathing waters, drinking waters, sensitive areas or shellfishing areas. CAPA-GIS displays all of these land use maps in the same framework and, after, it uses GIS selection tools to integrate them in one map.

SU is defined by the distribution of the final LFT. CAPA-GIS converts the information given by the mathematical tool FINAL-LFT to a GIS layer ('shapefile').

ST is defined by the stratification type according to the occurrence probability. CAPA-GIS converts the information given by the mathematical tool STRATIFICA to a GIS layer ("shapefile").

ADMITE

This tool calculates the EVI by means of the equation (3.41). This equation was coded in the "field calculator" GIS tool to obtain EVI values at every grid cell and a GIS layer ("shapefile").

Next, it determines the acceptability (AC*) depending on the EVI value of every grid cell. If the discharge point is located in a grid cell with EVI equals one is non-acceptable. Otherwise, we compute the value of AC* multiplying the EVI by the percentage of estuarine area cover per cell (Equation (3.42).

After, the tool computes the maximum allowable corrected MZ size (MAS*) by dividing the maximum admissible percentage of estuarine area that a MZ can cover in the "worst case of dilution" (AA-MAS and MAC-MAS) with a correction factor (α, Equation (3.44)) which depends on the estuarine average EVI (Equation (3.43)).

Finally, the tool evaluates the final admissibility (AD*) as the sum of all the AC* values covered by AA-MZ and MAC-MZ obtained in the calculations of the "real case of dilution" (Equation (3.45)).

4.5 Conclusions

Depending on the characteristics of the receiving environment and the relevance of the discharge, the sophistication of the models and the cost of the project will vary according to the decisions made during the expert system decision. A series of standard models were selected in this thesis based on the review of the state of the art for the calculation along the several Steps of the developed methodology. We use ***Delft3D-FLOW*** for simulation of hydrodynamics, ***VISJET*** for simulation of near-field (primary dilution) and ***D-Water Quality*** for simulation of far-field (secondary dilution).

Additionally, we programmed a series of self-developed mathematical tools for integrating, transferring, communicating and plotting the required and obtained information along the overall methodology. These mathematical tools were coded using two programming languages: MATLAB and PYTHON and a GIS software: ArcGIS 10.1. MATLAB software was used for calculations of any type. PYTHON software was employed to run dynamically models and to modify and format ASCII files. ArcGIS was used to integrate all the results in a geodatabase and calculate spatial operations such as buffers.

These self-developed mathematical tools were:

- Hydrodynamic calibration: Composed by the used tool (Delft3D-FLOW) and the developed tools (EXTRACTOR, GENERA and CALIBRA).
- Offline passive initial dilution: Composed by the used tool (VISJET) and the developed tools (ENVDATA, LANZA-VISJET and PAINT-JET).

- Offline passive coupling (intermediate-field): Composed by the developed tools (DILUTION, ACOPLA and VERTIDO).
- Far-field calibration: Composed by the used tool (D-Water Quality) and the developed tools (GENERA2, CALIBRA2).
- Selecting hydrodynamic forcings (model scenarios): Composed by the developed tools (KMA-FORZA and OPTIMIZA).
- Delimitating the AA-MZ and MAC-MZ: Composed by the developed tools (RECONSTRUCT, SAMPLEA, PROB-MZ and DELIMITA-MZ).
- Estimating the local flushing time: Composed by the used tool (Delt3D-FLOW) and the developed tools (RENOVA and FINAL-LFT).
- Determining the stratification patterns in estuaries: Composed by the used tool (Delt3D-FLOW) and the developed tool (STRATIFICA).
- Assessing the admissibility of Mixing Zones: Composed by the developed tools (CAPA-GIS and ADMITE).

The public interest requires doing today those things that men of intelligence and good will would wish, five or ten years hence, had been done.

Edmund Burke

5

Results: Application to Suances Estuary

This chapter presents the application to Suances Estuary of the proposed methodology for allocating mixing zones of industrial discharges. This estuary, located on the coast of the Cantabrian Sea, might represent a valuable opportunity in terms of the applicability of the method to a hypothetical real case that requires a quick and efficient management due to the high degree of industrial pollution.

While the information available, from the industrial discharges and environmental quality, is not as extensive and detailed as desirable. It is enough to satisfactorily establish some cases of analysis and validation of the results generated by the overall methodology.

It should be underlined that the application walks through each Step of the methodology in order to facilitate its understanding. We analyze the transport of two toxicants: chloroform or trichloromethane ($CHCl_3$) and lead (Pb).

5.1 Step 1. Preliminary characterization

The preliminary characterization of the effluents and the study area was a primary and essential task in the methodological approach. The main aspects of this characterization were shown in figure 3.3.

Next, we characterized two examples of wastewater discharges, named Industrial Discharge 1 (ID1) and Industrial Discharge 2 (ID2), to illustrate the application of the proposed methodology to the Suances Estuary (henceforth SE, figure 5.1).

5.1.1 Toxicant discharges

In this study, we selected two theoretical discharges based on two real toxicant loads discharged into the Suances Estuary. The information of the two real toxicant loads was specified in a public permit to release wastewaters called Integrated Environmental Authorization (IEA). Taking into account the "combined ap-

Figure 5.1: Orthophoto of the Suances Estuary and zoom of the outer part of the estuary. Source: Google Earth and http://es.wikipedia.org/wiki/Ría_de_San_Martín_de_la_Arena.

proach", IEA aimed to protect the environment as a whole in order to prevent the transfer of pollution from one medium to another. Thus, IEA specified ELVs on all environmental matrices (air, water, soil, ...).

The location of ID1 and ID2 is shown in figure 5.2. The mean depth in the receiving water was 2.87 m and the angle with the shoreline 163º for ID1 meanwhile the mean depth was 6.28 m and the angle 212º for ID2.

ID1 was theoretically discharging chloroform or trichloromethane ($CHCl_3$) and ID2 lead (Pb) in a constant and continuous way. According to IEAs, ID1 was permitted to release 0.02 mg/l with a effluent flow of 0.83801 m^3/s while for ID2 was authorized to 1 mg/l with an effluent flow of 0.00472 m^3/s. It is important to mention that salinity and temperature were considered equal for both discharges, being 0.5 psu and 15.2 ºC respectively.

Moreover, two theoretical single-port configurations were designed for both industries. ID1 was a single-port with a pipe diameter of 0.1 m and discharging at 1 m above the bottom. In the case of ID2, the single-port had a pipe diameter of 0.85 m and discharged at 1 m above the bottom as well.

Finally, we had filled the summary sheet for ID1 and ID2 in figures 5.3 and 5.4 respectively.

5.1.2 Study area

The Suances Estuary (-4.0237/43.4007 ED50) is a shallow mesotidal estuary located in the northern Spanish coast between the municipalities of Santander, Polanco, Miengo, Santillana del Mar and Torrelavega (Figure 5.1). It is approximately 7.5 km long; with a 150 m mean width and a surface area of 339.7 ha where intertidal flats occupy 76%. Land reclamation has reduced the original estuarine area by 30% (Jiménez *et al.* 2012). Furthermore, 50% of the estuary is bordered by dikes (over 13000 m), which dramatically altered its naturalness and flow conditions (Romero *et al.* 2008).

In figure 5.2, the bathymetry of the study area obtained from the available nautical charts of the Spanish coast in the database BACO (González *et al.* 2007) is shown. The shallowest depth is 3.2 m (above the mean sea level) corresponding to the tidal flats located along the Suances Estuary. The depth of the main channel varies between 1 m to 8 m. At the adjacent coastal sea, the deepest depth within the study area is 43 m (below the mean sea level) near the northwest corner.

The main freshwater input to the system comes from two similar rivers draining relatively small basins, the Saja and the Besaya, which occupy a catchment area of 966.67 km^2 with a perimeter of 166.27 km. These river basins converge in the town of Torrelavega (56000 inhabitants). After the confluence, a small river stretch (1890 m) flows up to an industrial weir which limits the end of the tidal influence into the river basin, i.e., the head of the SE (Figure 5.2).

During the last century, major industrial activities modified the basin river hydrology extracting water prior the estuary (2.25 m^3/s) and discharging wastewater into the estuary (1.25 m^3/s). Furthermore, it is worth pointing out that the Alsa-Torina reservoir discharges about 10 millions of cubic meters to balance out the industrial withdrawals during summer and drought periods (Bárcena *et al.* 2012a).

On one hand, the time series of river flow coming from Saja and Besaya rivers was obtained from "Estudio de Recursos Hídricos de las Cuencas de la Vertiente Norte de Cantabria Periodo 1970-2010", conducted by IH Cantabria for the Government of Cantabria (Figure 5.6a). This work was based on a lumped hydrological model developed for the assessment of the surface water resource in scarcely gauged basins by García *et al.* (2008). The point of calculation (point 17) was located at the industrial weir (Figure 5.2). The location of that point and its watershed is displayed in figure 5.5.

On the other hand, we selected the AG95.1 model developed by Andersen (1994). This database works

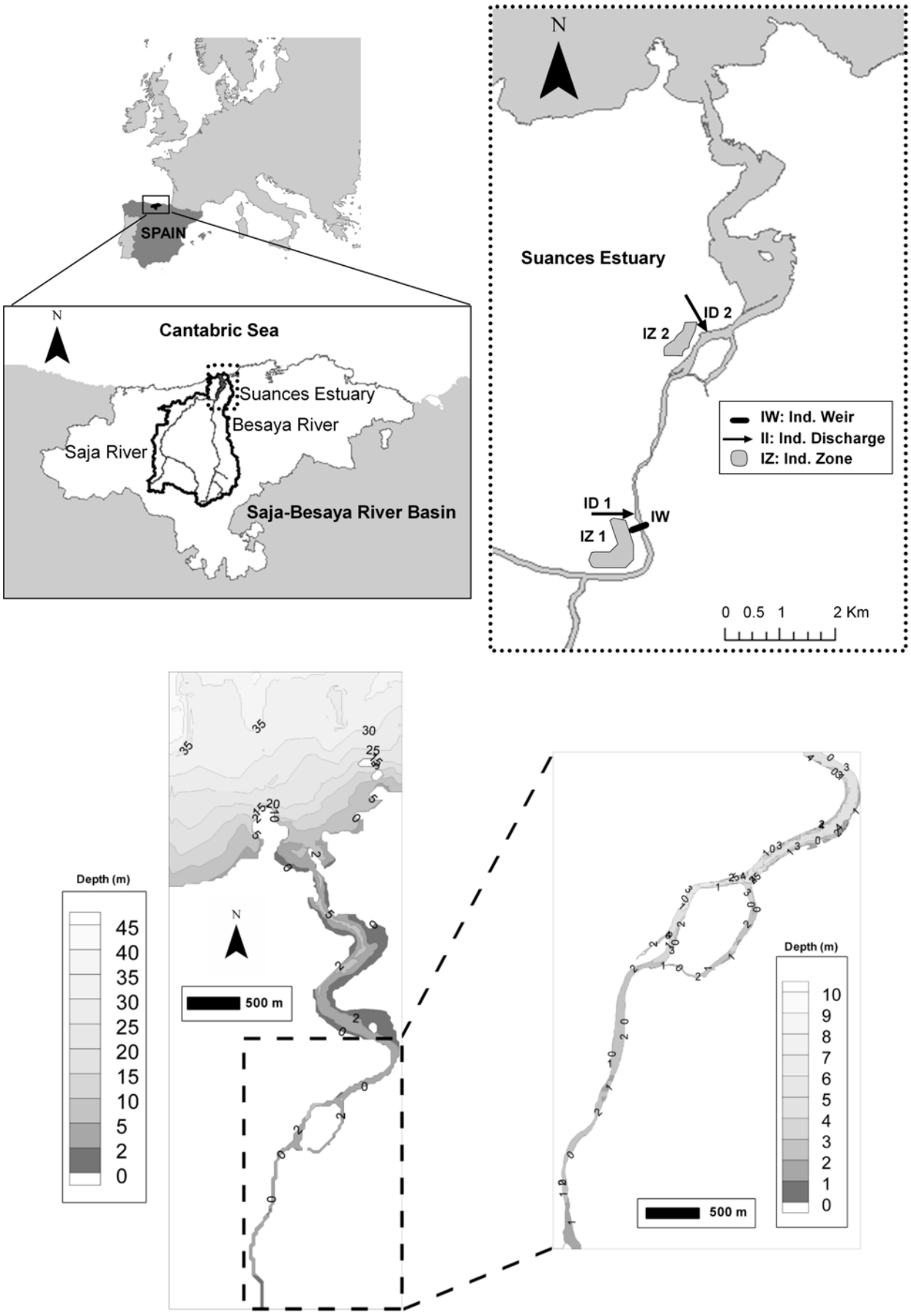

Figure 5.2: Location, bathymetry, river basin and selected discharges (ID1 and ID2) at Suances Estuary.

SUMMARY SHEET OF TOXICANT DISCHARGES

NAME	Industrial Discharge 1
CODE	ID1

Location

UMTX (ED50)	415030.5	Site name	Hinojedo
UTMY (ED50)	4802252.0	Holder	Theoretical Factory 1

Toxicant load

Flow	0.83801	m^3/s	Salinity	0.05	psu
			Temperature	15.2	ºC

Pollutant	Concentration (mg/l)	AA-EQS (mg/l)	MAC-EQS (mg/l)
Trichloromethane ($CHCl_3$)	0.02	2.50E-03	Not applicable

Discharge mechanism

Pipe diameter	0.85	m	Mean depth in the receiving water	2.87	m
Angle with shoreline	163	º	Discharge depth (from bottom)	1.00	m

Figure 5.3: Summary sheet to characterize ID1 in the Suances Estuary.

SUMMARY SHEET OF TOXICANT DISCHARGES

NAME	Industrial Discharge 2
CODE	ID2

Location

UMTX (ED50)	416217.0	Site name	Hinojedo
UTMY (ED50)	4805564.4	Holder	Theoretical Factory 2

Toxicant load

Flow	0.00472	m^3/s	Salinity	0.05	psu
			Temperature	15.2	ºC

Pollutant	Concentration (mg/l)	AA-EQS (mg/l)	MAC-EQS (mg/l)
Lead (Pb)	1.00	1.30E-03	1.40E-02

Discharge mechanism

Pipe diameter	0.10	m	Mean depth in the receiving water	6.28	m
Angle with shoreline	212	º	Discharge depth (from bottom)	1.00	m

Figure 5.4: Summary sheet to characterize ID2 in the Suances Estuary.

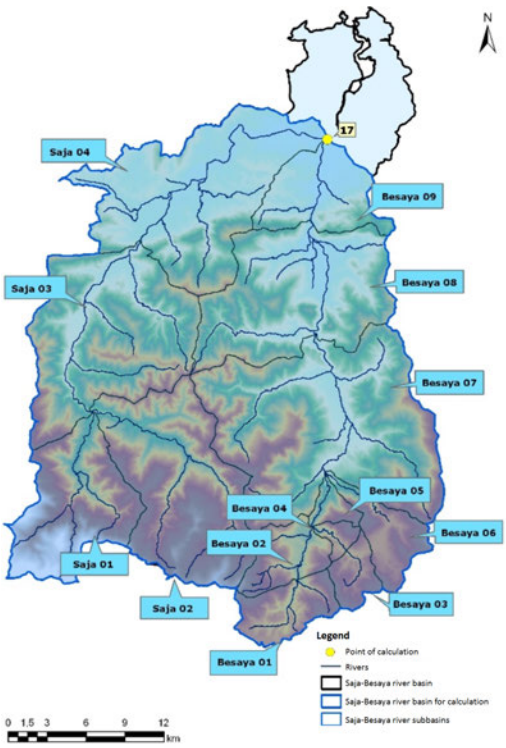

Figure 5.5: Location of the point of calculation of Saja-Besaya river flows and its river basin.

with thirteen tidal harmonics (M2, S2, K2, L2, N2, T2, MU2, NU2, 2N2, K1, O1, P1 and Q1) and points equidistant mesh $0.5^o \times 0.5^o$. Based on this model, the astronomical tidal level in the study area was obtained from 1970 to 2010 (Figure 5.6b). From the astronomical tide series, we calculated the "astronomic tidal range period" as the difference between the minimum and the maximum value of the astronomical tide series for 24 h in order to calculate the "daily tidal range series" (Figure 5.6c).

The freshwater inflow, in natural conditions, varied from about 1 to 600 m^3/s, with annual mean flows in the range of 7-24 m^3/s (García *et al.* 2008) (Figure 5.7a). The relatively small surface area, short length and steep led to a rapid hydrological response to rainfall between 15.91 and 20.76 hours and, consequently, a high variability in the river flow.

SE presented a semi-diurnal tidal signal with typical spring-neap cycle of about a fortnight. Tidal ranges varying between about 5 m during the extreme spring situation and 0.7 m when the extreme neap occurs (Figure 5.7b). Due to its characteristics, the estuary presented a high variability in the tide and different spatial behaviours (Bárcena *et al.* 2012b).

Regarding protected areas, SE only presented areas of recreational uses related to bath waters and beaches (Figure 5.8).

Finally, the summary sheet of SE with the above information is displayed in figure 5.9.

5.2 Step 2. Significance of discharge

Step 2 was designed to detect those discharges that had not significant impact on the estuarine waters (Figure 3.7).

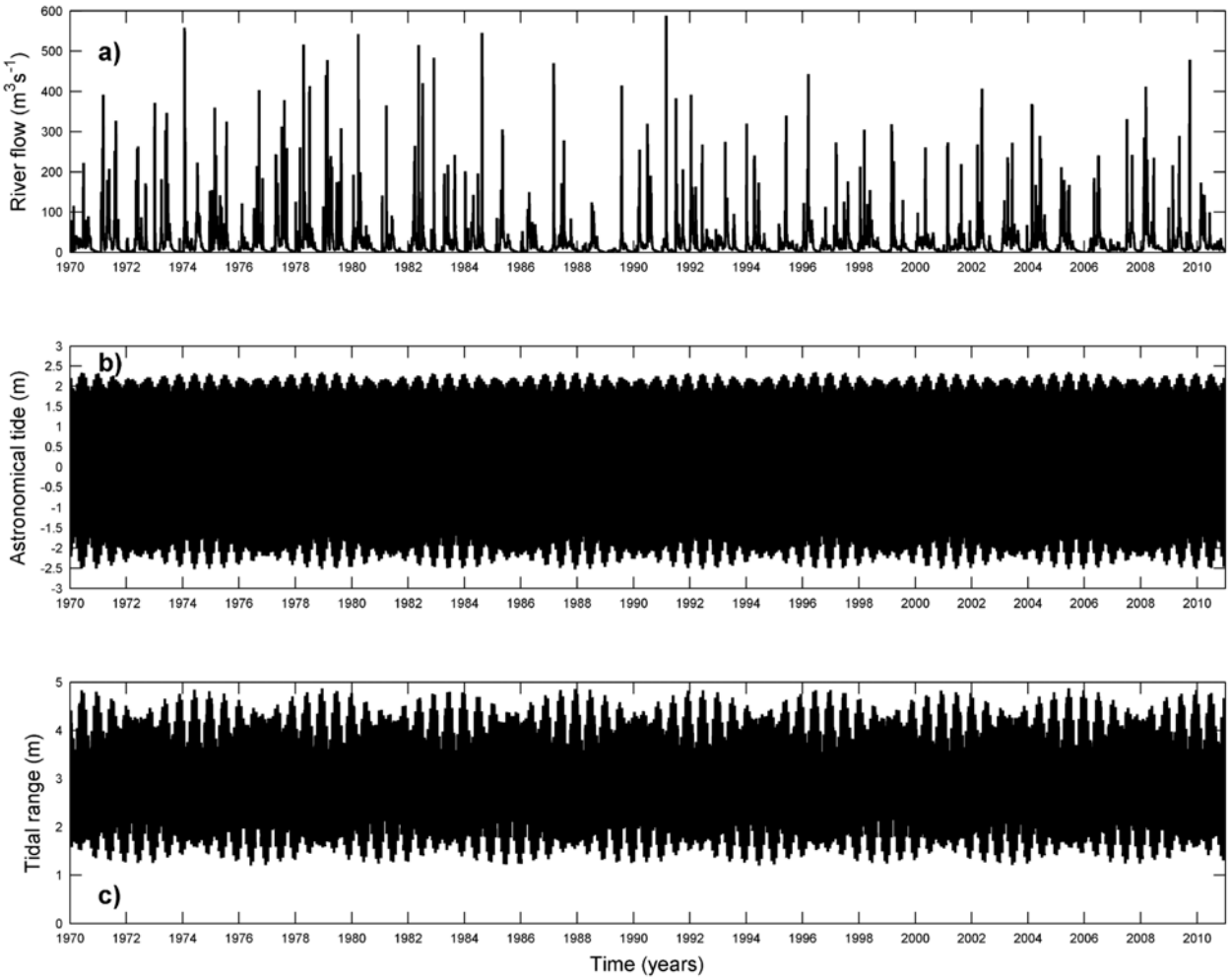

Figure 5.6: 40-years of forcing time series from 1970 to 2010. River flow (a), astronomical tidal wave (b) and astronomical tidal range (c) at Suances Estuary.

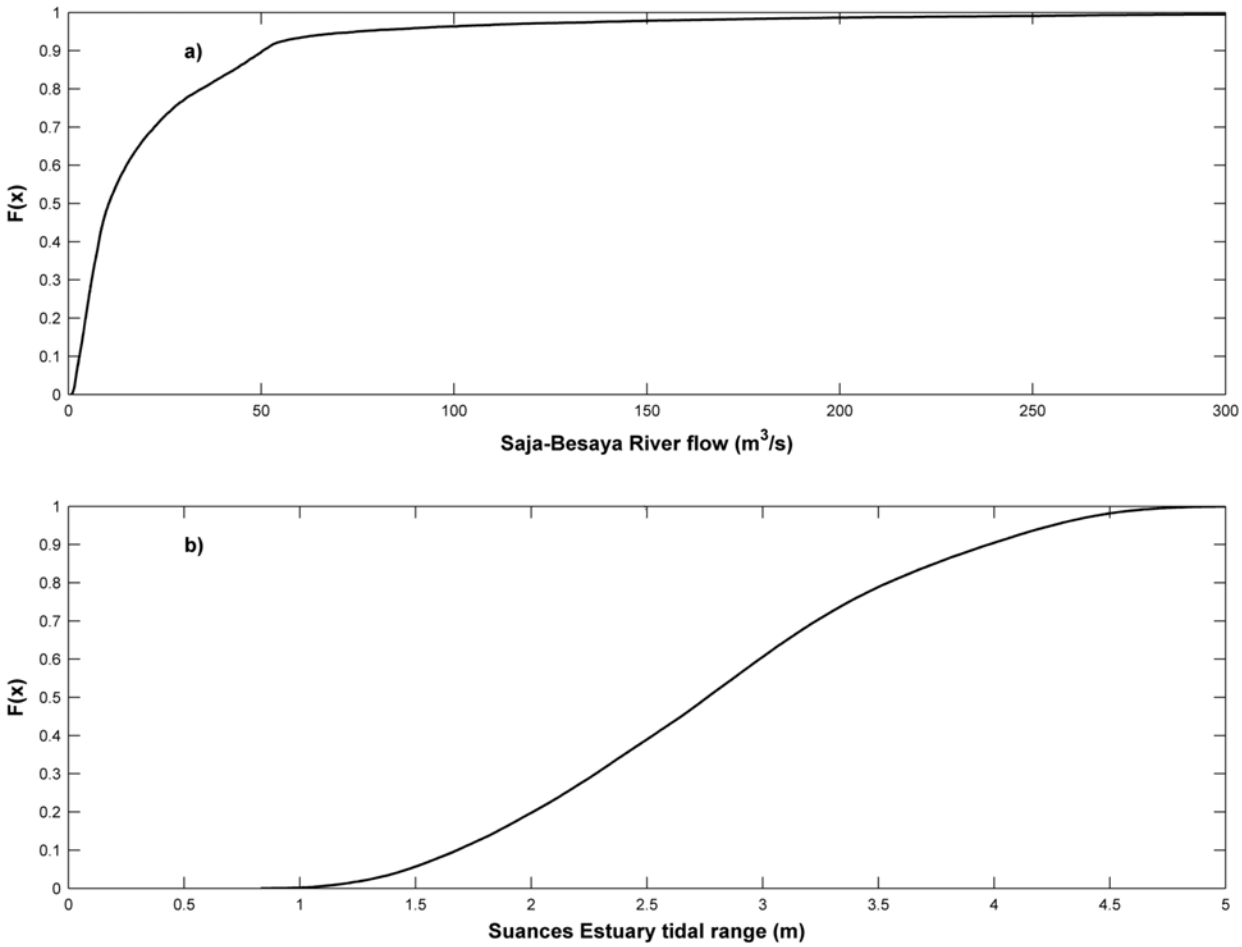

Figure 5.7: Empirical cumulative distribution function of river flow (a) and tidal range (b) at Suances Estuary.

Figure 5.8: Location of protected areas (beaches) at Suances Estuary.

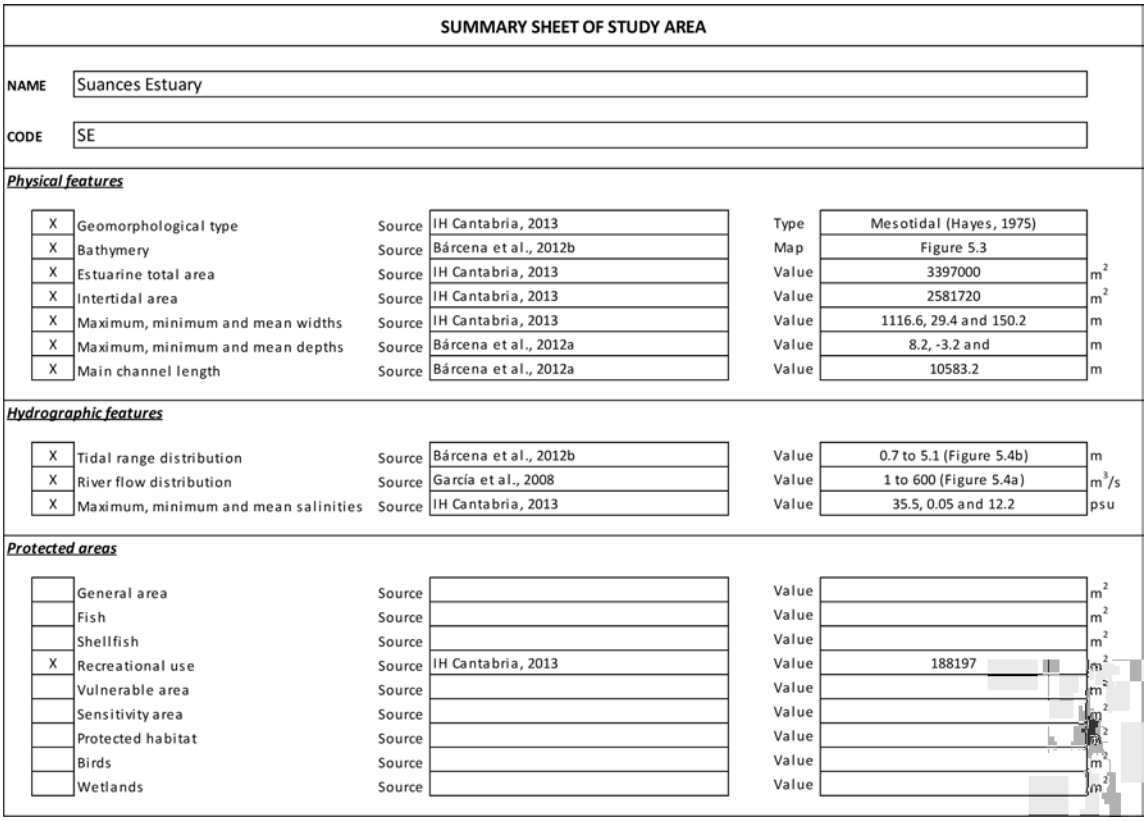

SUMMARY SHEET OF STUDY AREA

NAME: Suances Estuary

CODE: SE

Physical features

X	Geomorphological type	Source	IH Cantabria, 2013	Type	Mesotidal (Hayes, 1975)		
X	Bathymery	Source	Bárcena et al., 2012b	Map	Figure 5.3		
X	Estuarine total area	Source	IH Cantabria, 2013	Value	3397000	m^2	
X	Intertidal area	Source	IH Cantabria, 2013	Value	2581720	m^2	
X	Maximum, minimum and mean widths	Source	IH Cantabria, 2013	Value	1116.6, 29.4 and 150.2	m	
X	Maximum, minimum and mean depths	Source	Bárcena et al., 2012a	Value	8.2, -3.2 and	m	
X	Main channel length	Source	Bárcena et al., 2012a	Value	10583.2	m	

Hydrographic features

X	Tidal range distribution	Source	Bárcena et al., 2012b	Value	0.7 to 5.1 (Figure 5.4b)	m
X	River flow distribution	Source	García et al., 2008	Value	1 to 600 (Figure 5.4a)	m^3/s
X	Maximum, minimum and mean salinities	Source	IH Cantabria, 2013	Value	35.5, 0.05 and 12.2	psu

Protected areas

	General area	Source		Value		m^2
	Fish	Source		Value		m^2
	Shellfish	Source		Value		m^2
X	Recreational use	Source	IH Cantabria, 2013	Value	188197	m^2
	Vulnerable area	Source		Value		m^2
	Sensitivity area	Source		Value		m^2
	Protected habitat	Source		Value		m^2
	Birds	Source		Value		m^2
	Wetlands	Source		Value		m^2

Figure 5.9: Summary sheet to characterize the information about Suances Estuary.

5.2.1 Potential Risk

This subsection identified discharges with the potential to exceed the thresholds set in the EQS Directive (EC 2008a, EU 2013), i.e, the AA-EQS and the MAC-EQS, in three substeps.

1. ID1 and ID2 contain a toxicant specified in the EQS Directive: Trichloromethane ($CHCl_3$) and Lead (Pb) respectively. Thus, there are a potential risk of exceeding the EQS.

2. For ID1, $[X_{med}]_{ID1}$=0.02 mg/l and AA-EQS$_{CHCl3}$=$2.5{\cdot}10^{-3}$ mg/l $\Rightarrow$ $[X_{med}]_{ID1}$>AA-EQS$_{CHCl3}$. In the case of ID2, $[X_{med}]_{ID2}$=1.0 mg/l and AA-EQS$_{Pb}$=$1.3{\cdot}10^{-3}$ mg/l $\Rightarrow$ $[X_{med}]_{ID2}$>AA-EQS$_{Pb}$. Thus, there are an evidence of exceeding the EQS.

3. For ID1, $[X_{max}]_{ID1}$=0.02 mg/l and MAC-EQS$_{CHCl3}$=Not applicable $\Rightarrow$ Not applicable. in the case of ID2,

4. $[X_{max}]_{ID2}$=1.0 mg/l and MAC-EQS$_{Pb}$=$1.4{\cdot}10^{-2}$ mg/l $\Rightarrow$ $[X_{max}]_{ID2}$>MAC-EQS$_{Pb}$. Thus, there was an evidence of exceeding the EQS.

Both discharges were moved to the next substep in the decision tree to determine its significance.

5.2.2 Initial Screening

First, we calculated the river flow not exceeded during 10% of the time (Q10) from the river flow distribution (Figure 5.7a) being $Q10 = 3.6314 m^3/s$.

Second, we calculated the PC by applying the equation (3.1).

$$PC_{ID1} = \frac{[X_{med}]_{ID1} Q_{ID1}}{(Q_{river} + Q_{ID1})} = \frac{0.02 \cdot 0.83801}{(3.6314 + 0.83801)} = 0.003765 \tag{5.1}$$

$$PC_{ID2} = \frac{[X_{med}]_{ID2} Q_{ID2}}{(Q_{river} + Q_{ID2})} = \frac{1.0 \cdot 0.00472}{(3.6314 + 0.00472)} = 0.001298 \tag{5.2}$$

Third, the RI of the PC as a percentage of the AA-EQS was estimated by means of the equation (3.2).

$$RI_{ID1} = \frac{PC_{ID1}}{AA - EQS_{CHCl3}} \cdot 100\% = \frac{0.003765}{2.5 \cdot 10^{-3}} \cdot 100\% = 150.60 \tag{5.3}$$

$$RI_{ID2} = \frac{PC_{ID2}}{AA - EQS_{Pb}} \cdot 100\% = \frac{0.001298}{1.3 \cdot 10^{-3}} \cdot 100\% = 99.84 \tag{5.4}$$

Finally, RI was checked with the proposed allowable increase (PAI) given in table 3.2. The PAI for this river flow was 4 so **RI$_{ID1}$=150.60$\gg$PAI=4** and **RI$_{ID2}$=99.85$\gg$PAI=4**. Therefore, both toxicant discharges were classified as significant so they have been moved to Step 3.

5.3 Step 3. Simplified calculation (Worst case of dilution)

In the simplified calculation, toxicants were considered conservative tracers in the primary and secondary dilution and hydrodynamic forcings were established from a precautionary approach so the achieved dilution was minimum.

Step 3 is composed by 6 subsections as illustrated in figure 3.8.

5.3.1 Additional information

The information was related to measurements (field data) necessary to conduct the setup of numerical models. We collected information from two sources: one field campaign (CHN 1998) and the water quality network of the coast of Cantabria called "Red de Control de Calidad Litoral en Cantabria" (IHCantabria 2012). Figure 5.10 shows the location of the field data for both sources.

Field campaign (CHN 1998)

The available information came from the results of the field campaign of hydrological, biological, meteorological and oceanographic parameters in the estuary of Suances made by the "Confederación Hidrográfica del Norte" in the context of the study of sanitation in the low basin of the Saja-Besaya. The campaign took place in the last two weeks of January and the first week of February 1998 and it was focused on gathering information on the hydrodynamic behavior of the estuary.

The observed data included (see figure 5.10):

- Measurements of tidal water levels at two points (TG1 and TG2) every five minutes with a pressure tidal gauge (AANDERAA WLR-5).
- Measurements of instantaneous flows, temperatures and salinities in the Saja-Besaya River section (FG1), not influenced by the tide, every two hours with an electromagnetic flow meter (FLOWMATE

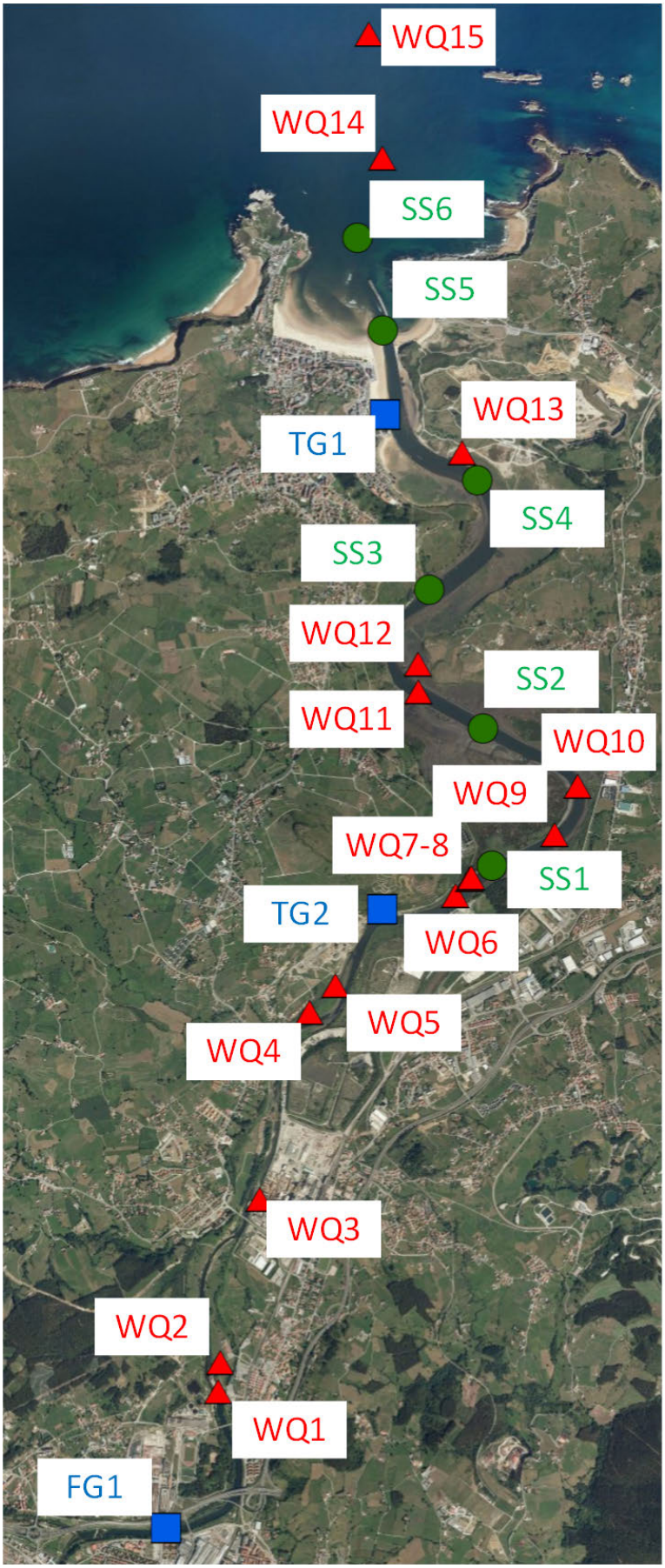

Figure 5.10: Location of the additional information for Step 3. Sources: CHN (1998) and IHCantabria (2012).

model 2000) and a limnimetric scale.

- Vertical profiles of instantaneous current speeds and directions located at six points (SS1 to SS6) measured with a portable current meter (BRAYSTORE 0008 MK3) on neap tide situations between the 24th and 25th of January 1998 and on spring tide situations between the 28th and 29th of January 1998. For both spring and neap tidal conditions, the measurements include high, ebb, low and flood tide.

- Vertical profiles of salinities and temperatures located at six points (SS1 to SS6) measured with a CTD device on neap tide situations between the 24th and 25th of January 1998 and on spring tide situations between the 28th and 29th of January 1998. For both spring and neap tidal conditions, the measurements include high, ebb, low and flood tide.

"Red de Control de Calidad Litoral en Cantabria" (IHCantabria 2012)

In the "Red de Calidad del Litoral de Cantabria", seasonal field campaigns of water, sediment and biota in the estuaries and coast of Cantabria were made. In SE and its adjacent coast, the network has 13 sampling stations (WQ1 to WQ13) located within the SE and 2 more (WQ14 and WQ15) in the coast as displayed in figure 5.10.

The selected data included measurements of salinities and temperatures since 2006 to 2013. As an example, figures 5.11, 5.12 and 5.13 present the evolution of the temperature and salinity at WQ3, WQ9 and WQ15 respectively. WQ3 was located in the inner part of the estuary, WQ9 was in the middle of the estuary and WQ15 was in the adjacent coast (Figure 5.10).

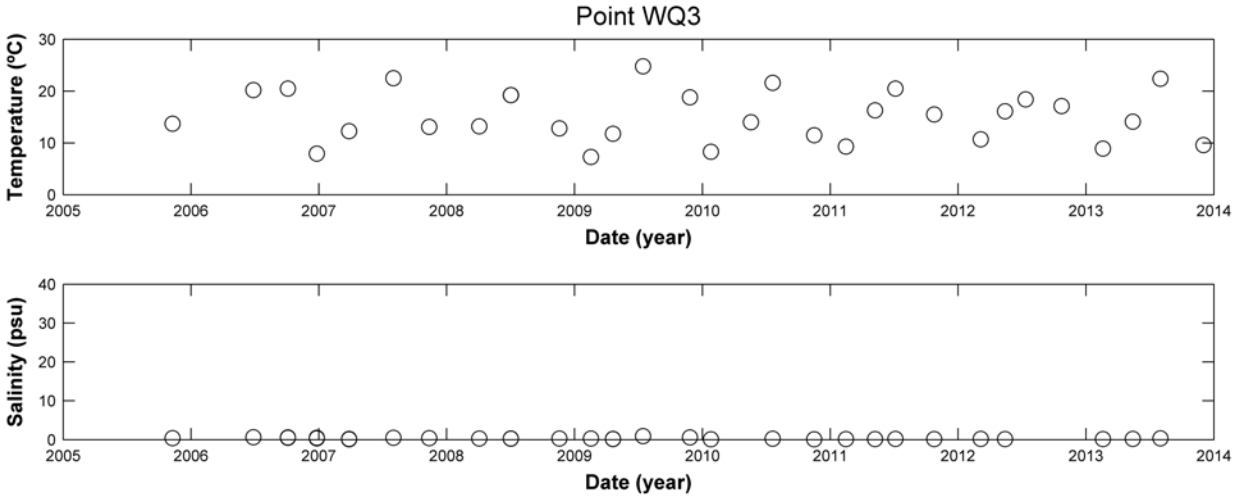

Figure 5.11: Measurements of temperature and salinity at WQ3 (inner estuary) from "Red de Calidad del Litoral de Cantabria".

5.3.2 Hydrodynamics

For modeling water levels, currents and salinities generated by tidal action and river inflows, the numerical integration of the equations of momentum, continuity and transport was performed using numerical methods that need to generate a grid that covers the area of interest and containing the depths at each point. These magnitudes were generated by applying Delft3D-FLOW to the study area (see Chapter 4).

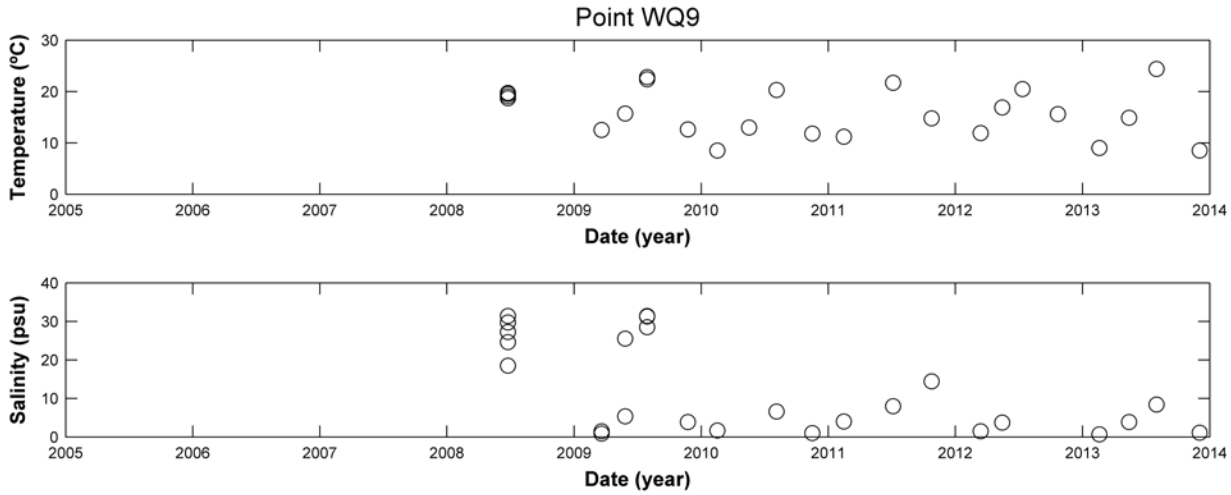

Figure 5.12: Measurements of temperature and salinity at WQ9 (middle estuary) from "Red de Calidad del Litoral de Cantabria".

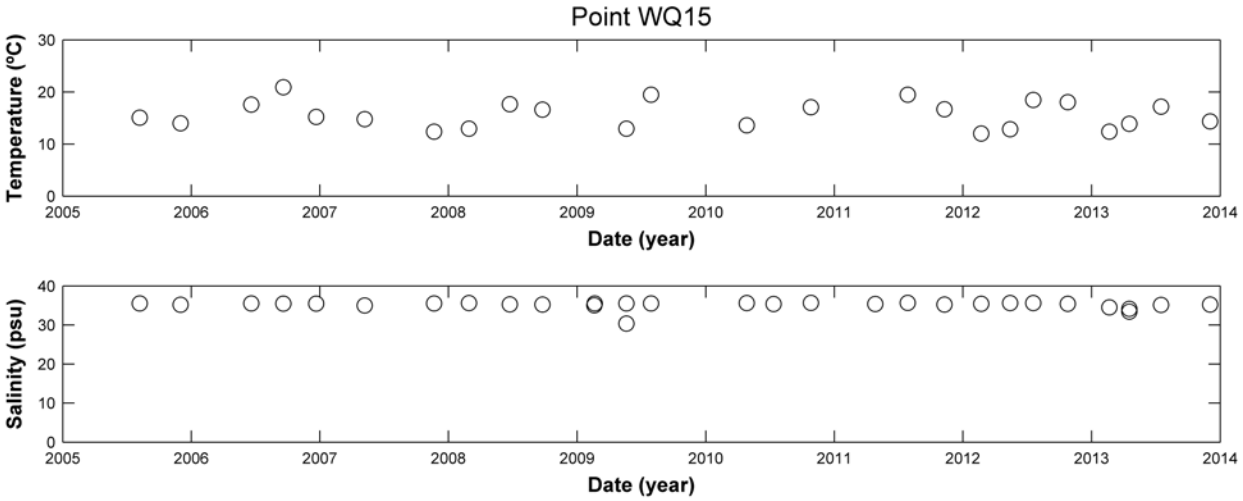

Figure 5.13: Measurements of temperature and salinity at WQ15 (adjacent coast) from "Red de Calidad del Litoral de Cantabria".

5.3.2.1 Model setup

Model setup was required to define the model domain discretization, to provide boundary and initial conditions and, finally, to carry on the model calibration/validation in order to select the best configuration of model parameters (Figure 3.9).

Model domain discretization

The three-dimensional grid, covering SE and its adjacent coastal zone, was represented horizontally using a curvilinear meshgrid (Figure 5.14). This meshgrid consisted in 93×800 grid cells in M and N directions respectively. The spatial resolution was between 47 and 235 m in the adjacent coastal zone and between 4.3 and 30 m in the estuary. Regarding the vertical discretization, the meshgrid was composed by 10 vertical σ-layers equally spaced along the water column. The vertical discretization in σ-coordinates had the same number of layers in deep water than in shallow water and allowed a good adaptation to the free surface and bathymetry.

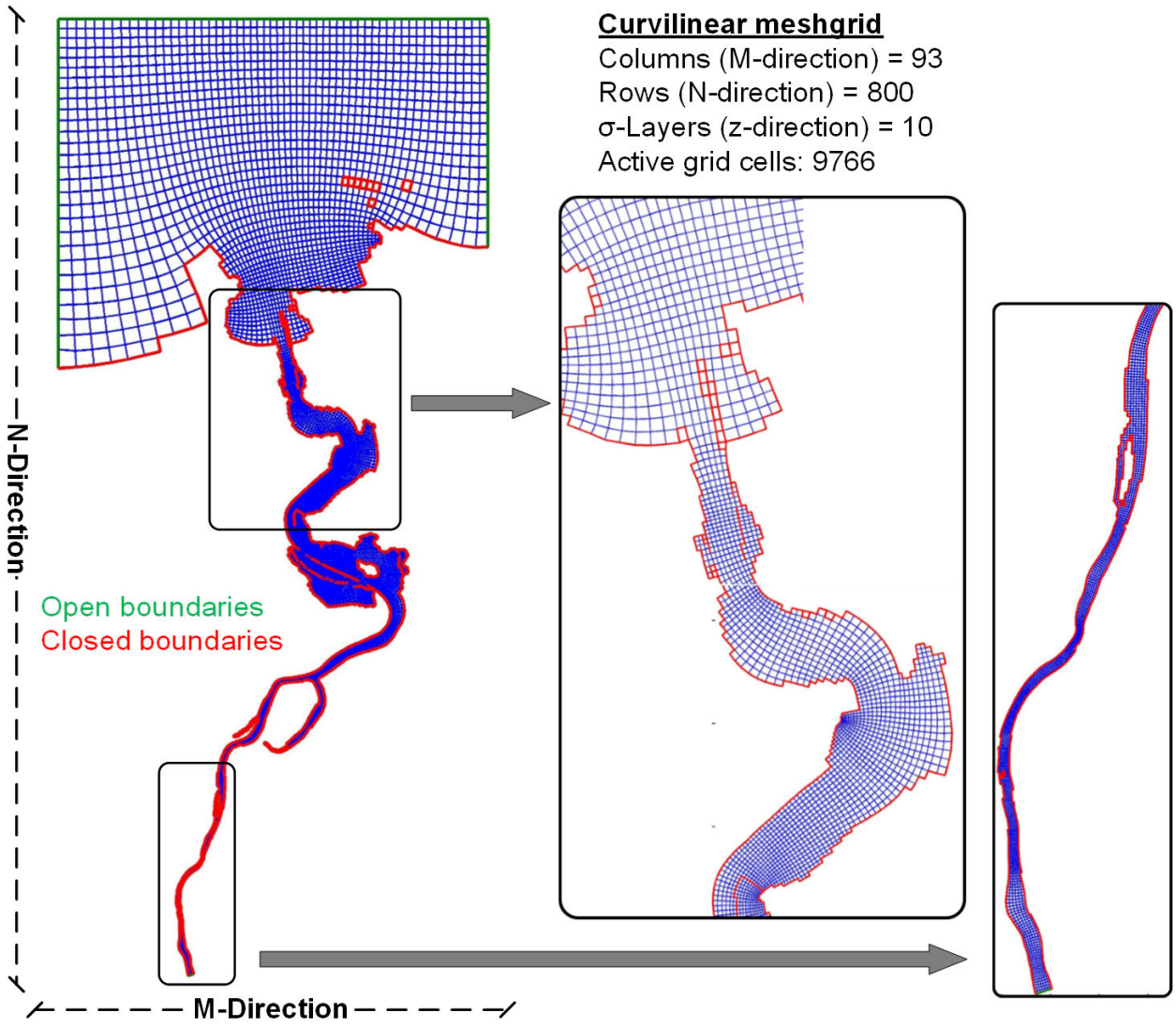

Figure 5.14: Meshgrid for numerical simulations and detail of the interior of Suances estuary.

Next, we assigned water depths for every grid cell by means of the estuarine bathymetry (Figure 5.2). In figure 5.15, the used bathymetry for numerical simulations is shown with a zoom of the outer and inner areas of the

SE. Note in figure 5.15 that the high resolution of the meshgrid and bathymetry allowed the full definition of dykes bordering the main channel (red ellipse).

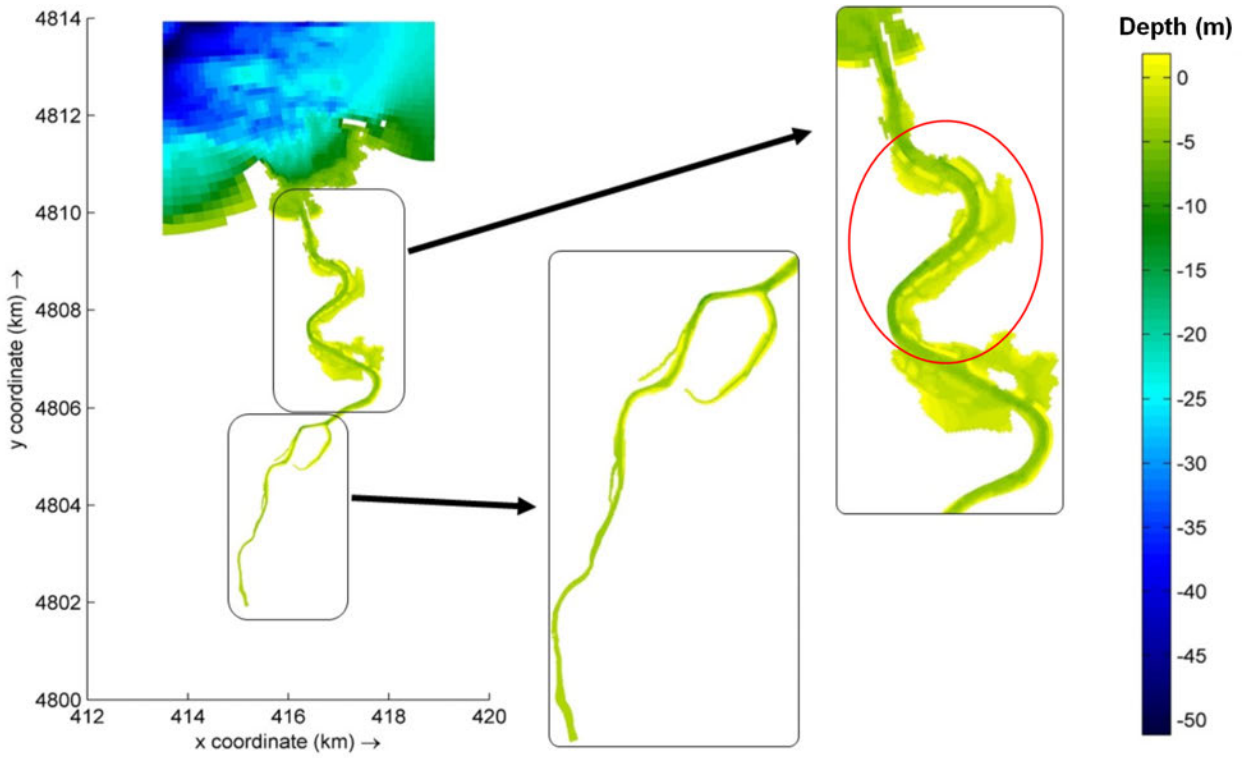

Figure 5.15: Bathymetry attached to the meshgrid with a zoom of the outer and inner areas of Suances Estuary.

Boundary and initial conditions

As boundary and initial conditions were used those shown in figure 5.16.

Open and closed boundary conditions

CBs were defined by the known shoreline, the bathymetry, and the free water surface, where the flow through the boundary was set to zero. The vertical diffusive flux through the free surface and bed were also set to zero except for the heat flux through the free surface. The influence of the lateral shear stresses along the lateral boundaries was neglected (free-slip condition).

Regarding OBs, we defined four boundaries (one upper, one lower and two lateral):

- The upper sea boundary condition, used to calibrate tidal wave propagation, was generated by the Grenoble database (Andersen 1994). Temperature and salinity were modeled by imposing a three-dimensional profile with the measurements of the sampling station SS6. Due to the vertical and temporal variation of salinity were not significant in SS6 during the calibration period, we established that the boundary was vertically and temporally constant being the average of all the measurements, i.e., 35.6623 psu. In the case of sea temperature, the temporal variation was significant and the vertical was insignificant. Thus, the sea temperature was established as a time series of a constant profile of temperature. Figure 5.17 shows the water levels (a) and sea temperatures (b) imposed during the calibration process.
- The lower river boundary condition was generated by imposing a flow condition with the available measurements for the Saja-Besaya River flow during the calibration and validation period (CHN 1998). Temperature and salinity were modeled by imposing a three-dimensional profile with the measurements

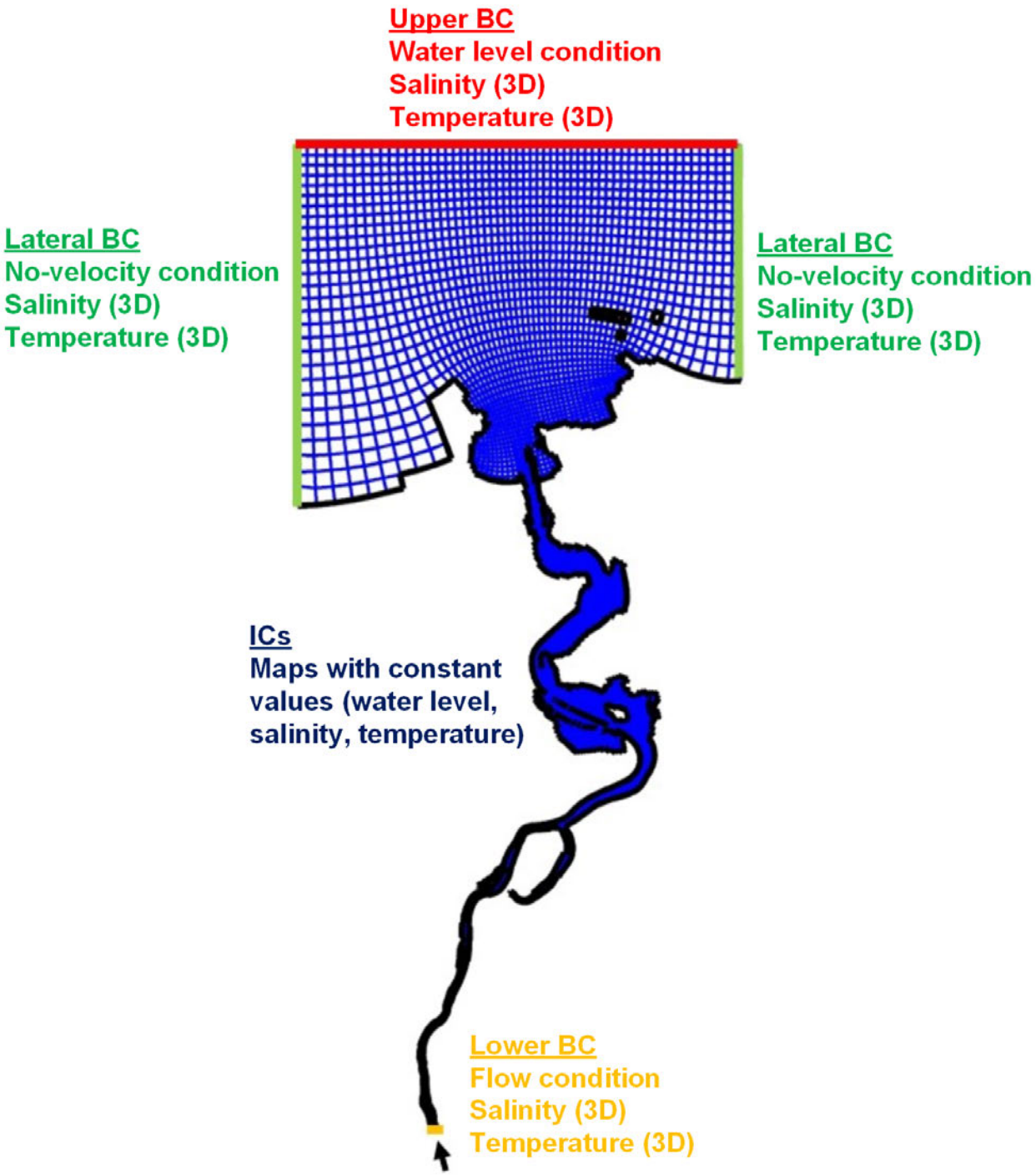

Figure 5.16: Schematic view of the boundary and initial conditions imposed during hydrodynamic simulations.

of the field campaign (CHN 1998). Due to the vertical and temporal variation of salinity was not significant in these data, we established that the boundary was vertically and temporally constant being the average of all the measurements, i.e, 0.286 psu. In the case of river temperature, the temporal variation was significant and the vertical was insignificant. Thus, the sea temperature was established as a time series of a constant profile of temperature. Figure 5.17 shows the river flows (c) and river temperatures (d) imposed during the calibration process.

- The lateral sea boundary conditions were modeled by imposing a condition of zero velocity and the same values of the upper boundary in the case of salinity and temperature.

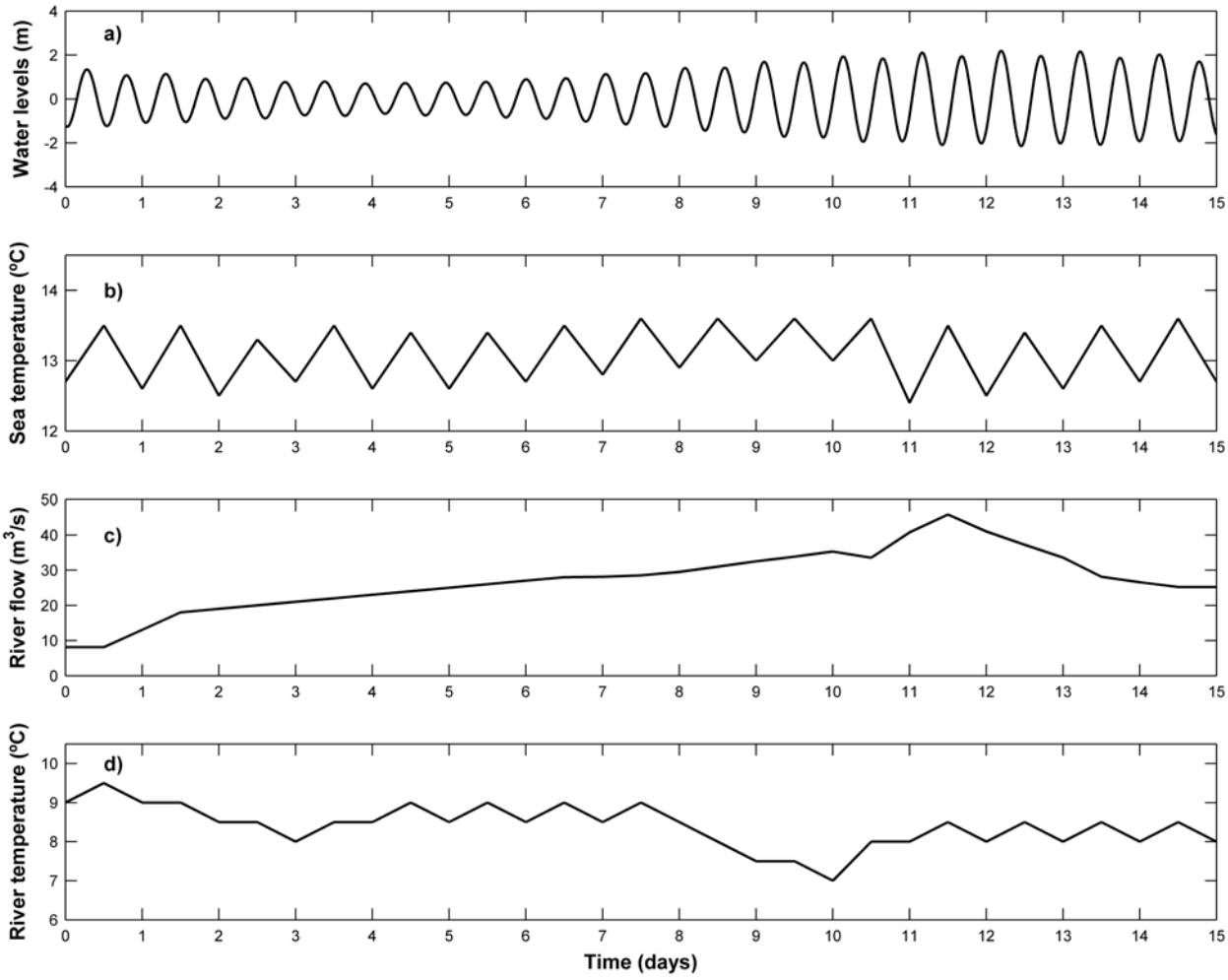

Figure 5.17: Boundary conditions imposed during the calibration period. Astronomical tidal elevations (a), sea temperatures (b), river flows (c) and river temperatures (d).

Initial conditions

To perform the simulation of this calibration period, ICs were maps with constant values (Figure 5.16). We specified a water level of 1.2248 m, a temperature of 11 °C and a salinity of 29 psu throughout every grid cell of the meshgrid to start the simulations.

Model calibration

Model calibration was focused on adjust the physical and numerical parameters used by the hydrodynamic model Delft3D-FLOW in order to ensure reliability. To carry on this calibration, we used the data of the field campaign (CHN 1998) in the period 18/01/1998 to 02/02/1998.

Water depth (m)	n1	n2
H≤-2.5	0.032	0.042
-2.5≤H<-2.0	0.028	0.042
-2.0≤H<-1.5	0.023	0.038
-1.5≤H<-1.0	0.020	0.034
-1.0≤H<-0.5	0.019	0.030
-0.5≤H<0.0	0.019	0.027
0.0≤H<0.5	0.024	0.024
0.5≤H<1.0	0.026	0.022
1.0≤H<3.0	0.025	0.020
3.0≤H<10.0	0.023	0.018
H≥10.0	0.022	0.015

Table 5.1: Manning coefficient (n) as a function of water depth (H). n1 and n2 correspond to the proposals of Dias *et al.* (2009) and Iglesias & Carballo (2010) respectively.

Physical parameters

Physical parameters were the eddy viscosity and diffusivity (horizontal and vertical) and the boundary stresses (bottom, lateral and surface).

- *Horizontal eddy viscosity* (μ_H): The value of this coefficient depends on the grid cell dimensions and it was estimated from equation (3.3) as a map with values varying spatially. In equation (3.3), u_{ch} was 1 m/s due to the dynamics of the estuary at the mouth. Additionally, k was ranged between 0.05 and 0.15 and increased in steps of 0.05.
- *Horizontal eddy diffusivity* (D_H): D_H was calculated with the equation (3.4) where σ_t was 0.7.
- *Vertical eddy viscosity* (μ_V): Three turbulence closure models were used during the calibration. Firstly, a constant value where μ_V was ranged between 10^{-2} and 10^{-6} m^2/s and increased in steps of 10^{-1}, Secondly, the algebraic model AEM was employed and, thirdly, the $k-\varepsilon$ model.
- *Vertical eddy diffusivity* (D_V): D_V was calculated with the equation (3.5) where σ_t was 0.7.
- *Bottom stresses*: The influence of water depth on bottom stresses was directly introduced into the calculations by the Manning coefficient (n). This coefficient was introduced as a constant value or spatially varying. This spatial variation depended on the depth of grid cells and followed the suggestions made by Dias *et al.* (2009) and Iglesias & Carballo (2010). Table 5.1 presents the Manning values proposed by these authors.
- *Lateral stresses*: Lateral stresses were neglected (free-slip condition).

Numerical parameters

Numerical parameters were numerical schemes, timestep, numerical filters and wetting and drying processes.

- *Numerical scheme:* The numerical solution of the equations was carried out by the Cyclic method included in Delft3D-FLOW. In this scheme, the advection terms were integrated implicitly in the stage of the ADI-method in which the free surface gradient is at the old time level. The upwind discretization was used in the stage in which both the horizontal advection and vertical viscosity term are integrated implicitly.
- *Timestep:* To ensure model stability and accuracy, CFL and Pe were used (Equations (3.8) and (3.9)). The timestep was $\Delta t = 0.1$ min.

Physical parameters	**Suggestions**	**Value ranges**
Horizontal eddy viscosity	Equation (3.3)	k=0.05:0.05:0.15
Horizontal eddy diffusivity	Equation (3.4)	σ_t=0.7
Vertical eddy viscosity	Best fitting	Constant=10^{-2}:10^{-1}:10^{-6} m^2/s, AEM, $k-\varepsilon$
Vertical eddy diffusivity	Equation (3.5)	σ_t=0.7
Bottom stresses	Manning	n=0.015:0.05:0.035, Table 5.1
Lateral stresses	Free-slip condition	No roughness
Numerical parameters	**Suggestions**	**Value ranges**
Numerical scheme	Second order accuracy	Cyclic
Timestep	Equations (3.8) and (3.9)	Δt=0.1 min
Numerical filters	Activated	Vertical artificial mixing
Wetting and drying	Activated	Threshold depth$\leq$0.1 m

Table 5.2: Overall picture of calibration parameters of the hydrodynamic model used during the calibration at Suances Estuary.

- *Numerical filters:* We activated the vertical filter because SE may display significant stratification.
- *Wetting and drying processes:* Since there are tidal flats in SE, the effects of the moving boundary on the water exchange must be taken into account by means of a threshold depth. This depth was specified at 0.1 m. Moreover, wetting and drying were checked on the sides and in the center of the grid cells.

Simulation-calibration cases

Simulation-calibration cases were all the different model simulations performed by means of combinations of M physical parameters and N numerical parameters. Table 5.2 synthesizes the calibration parameters, suggests the best option for estuarine modeling and gives the selected value or values of each parameter.

As it can be seen from table 5.2, in the case of physical parameters, there were 3 cases of horizontal eddy viscosity, 1 case of horizontal eddy diffusivity, 7 cases of vertical eddy viscosity, 1 case of vertical eddy diffusivity, 7 cases of bottom stresses and 1 case of lateral stresses. Regarding numerical parameters, there were 1 case of numerical scheme, 1 case of timestep, 1 case of numerical filters and 1 case of wetting and drying.

The combination of all of this cases resulted in 147 simulation-calibration cases. Finally, this cases were simulated in Delft3D-FLOW.

Final configuration

The final configuration of the model was the combination of values of model parameters that best match the results obtained by the model and the data measured in the study area.

Error measurements

For every simulation-calibration case, we compared the values of the model data and the field campaign (CHN 1998) in the period 18/01/1998 to 02/02/1998. The calibration was conducted by comparing the water level at two points (TG1 and TG2), the velocity at six points (SS1 to SS6) and three depths (surface=layer1, middle=layer5 and bottom=layer10) and, lastly, the salinity at the same points and depths used for velocity (see figure 5.10).

First, BIAS was calculated by means of equation (3.10). Second, the error between both series using CE, displayed in equation (3.11), was calculated.

Optimal calibration case

Physical parameters	**Calibrated values**
Horizontal eddy viscosity	k=0.10
Horizontal eddy diffusivity	σ_t=0.7
Vertical eddy viscosity	$k-\varepsilon$
Vertical eddy diffusivity	σ_t=0.7
Bottom stresses	Iglesias & Carballo (2010)
Lateral stresses	Free-slip condition
Numerical parameters	**Calibrated values**
Numerical scheme	Cyclic
Timestep	$\Delta t = 0.1$ min
Numerical filters	Vertical artificial mixing
Wetting and drying	Threshold depth$\leq$0.1 m

Table 5.3: Optimal calibration parameters of the hydrodynamic model for Suances Estuary.

In this study, the optimal calibration was the combination of parameters shown in table 5.3 because this case was simultaneously displaying the minimum BIAS and the maximum CE.

Therefore, this combination of model parameters was used along the rest of the methodology for conducting hydrodynamic simulations. Moreover, table 5.4 resumes the value of the depth-averaged errors (mean of surface, middle and bottom layers) at all the considered locations (TG1, TG2 and SS1 to SS6).

As it can be seen from table 5.4, the calibrated model displayed an acceptable level of performance in all the stations and variables. Water levels were reproduced excellently while velocities and salinities were between poorly and conveniently.

Figure 5.18 presents the comparison between the observed data at TG1 and TG2 and the model results. Very good agreement was obtained between the model-predicted water levels and the observed data at both stations. The numerical model also reproduced the features of the tidal signal (e.g., phase, amplitude, spring-neap variation of tidal range).

Figures 5.19, 5.20 and 5.21 show the comparison of the predicted and observed velocity components (u-eastward direction and v-northward direction) for the sampling event at SS1, SS3, and SS5 and two depths (surface=layer1 and bottom=layer10), respectively. As shown in all the figures, the model had a good fit for the velocity components in both layers. Overall, these comparisons confirmed that the hydrodynamic model reproduced water movements satisfactorily throughout the estuary.

In the same way as with the velocities, figures 5.22, 5.23 and 5.24 display the comparison of the predicted and observed salinities for the sampling event at SS1, SS3, and SS5 and two depths (surface=layer1 and bottom=layer10), respectively. Again, the model reproduced fairly reliably the variation of salinity experienced by the estuary in both layers during the calibration period. Overall, these comparisons confirmed that the hydrodynamic model reproduced water transport satisfactorily throughout the estuary.

As an example, figures 5.25 and 5.26 present the spatial distribution of velocities for surface and bottom layers in an instant of maximum velocities during ebb and flood tide respectively. These figures illustrated that the velocity in the surface layer was higher than the velocity in the bottom layer. Similarly, it was noteworthy that the maximum velocities of ebb tide found in the results were greater than the maximum velocities of flood tide. This fact was directly agreeing with the theories concerning the dynamic of estuaries influenced by river flow.

Finally, figures 5.27 and 5.28 display, as an example, the spatial distribution of salinities for surface and bottom layers in an instant of maximum velocities during ebb and flood tide respectively. These figures illustrated that the concentration of salinity in the bottom layer was higher than the concentration in the

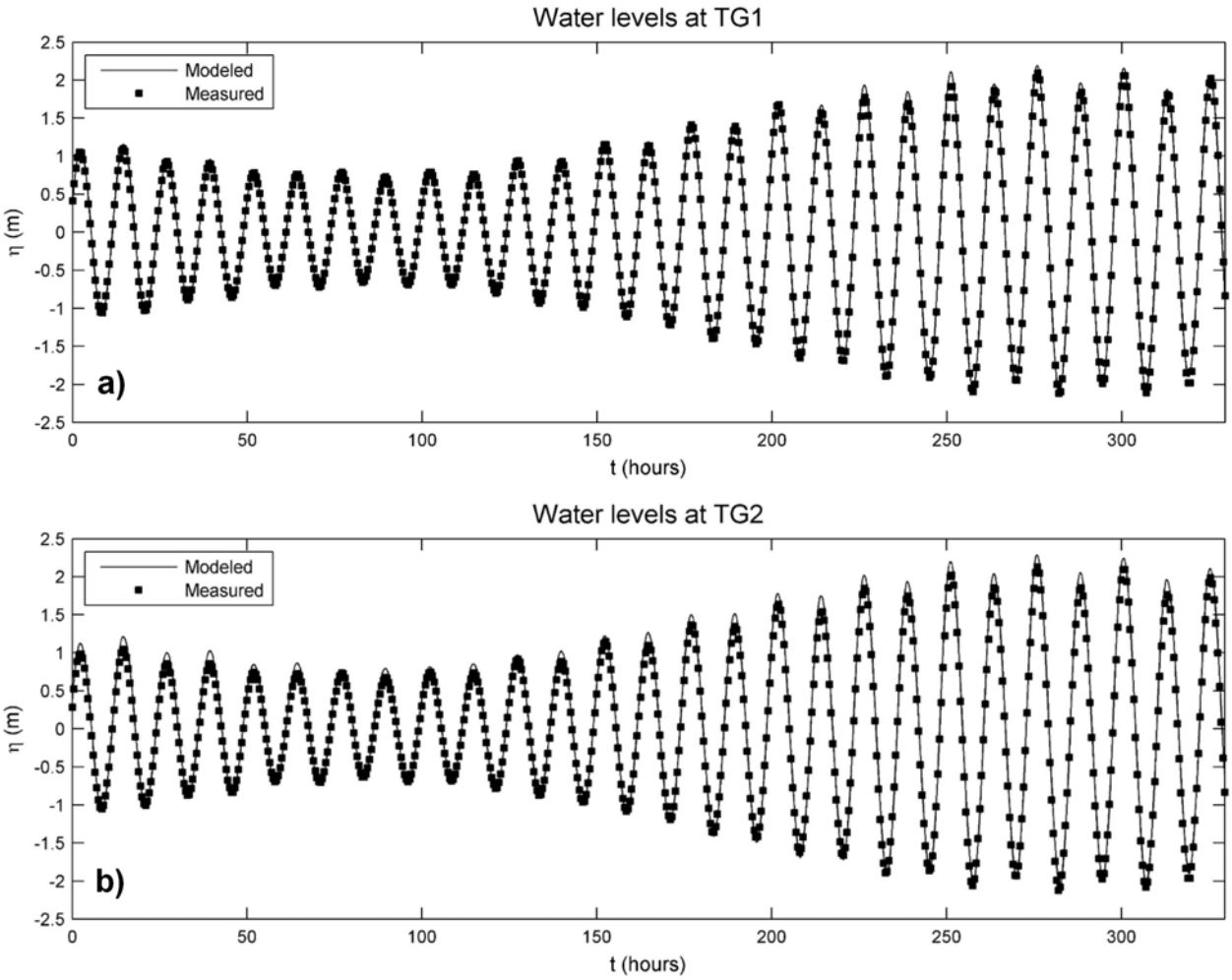

Figure 5.18: Comparison between the measured and modeled water levels at the tidal gauges TG1 (a) and TG2 (b).

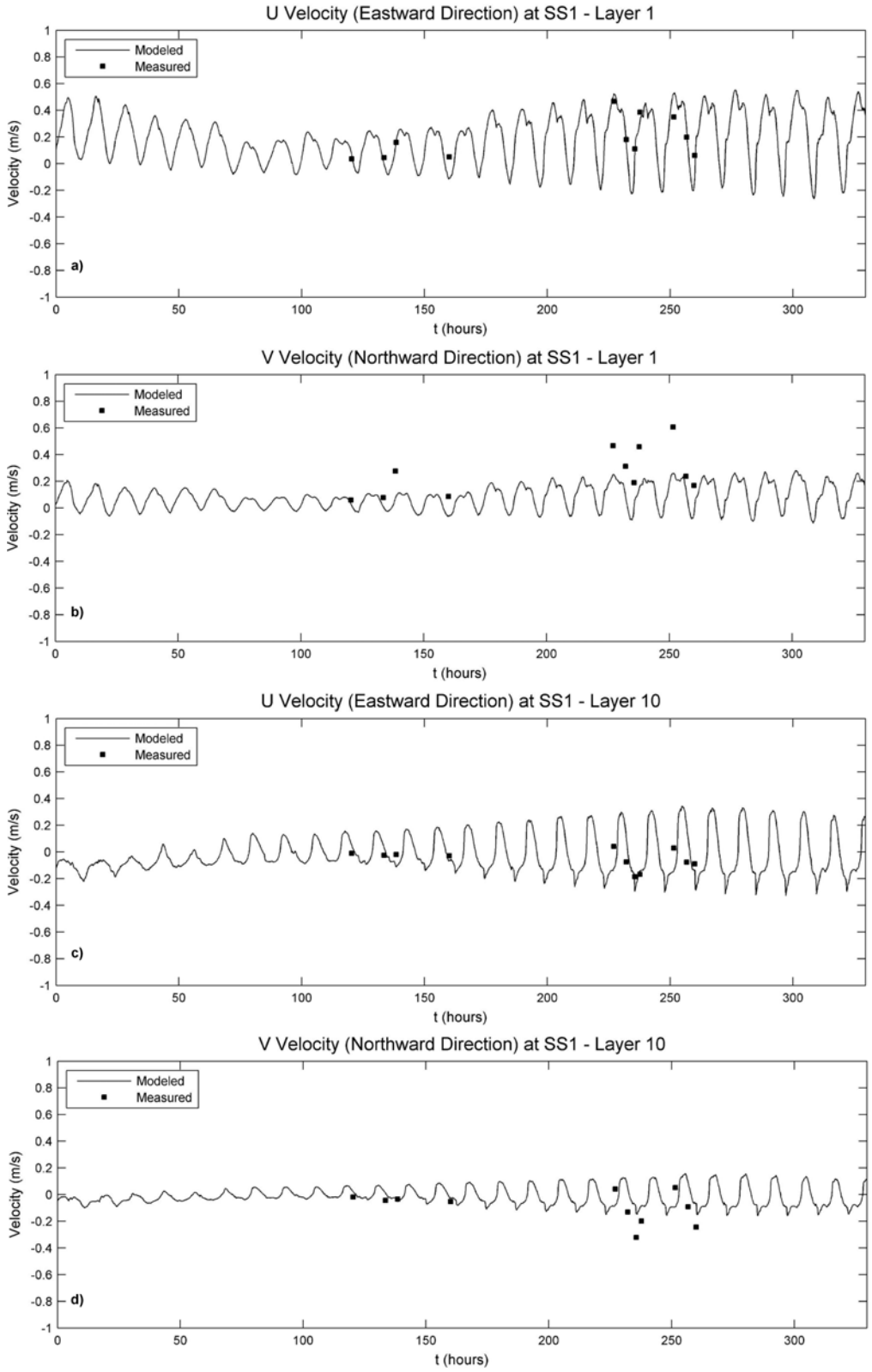

Figure 5.19: Comparison between the measured and modeled velocity components at the survey station SS1. U-velocity of surface layer (a), V-velocity of surface layer (b), U-velocity of bottom layer (c) and V-velocity of bottom layer (d).

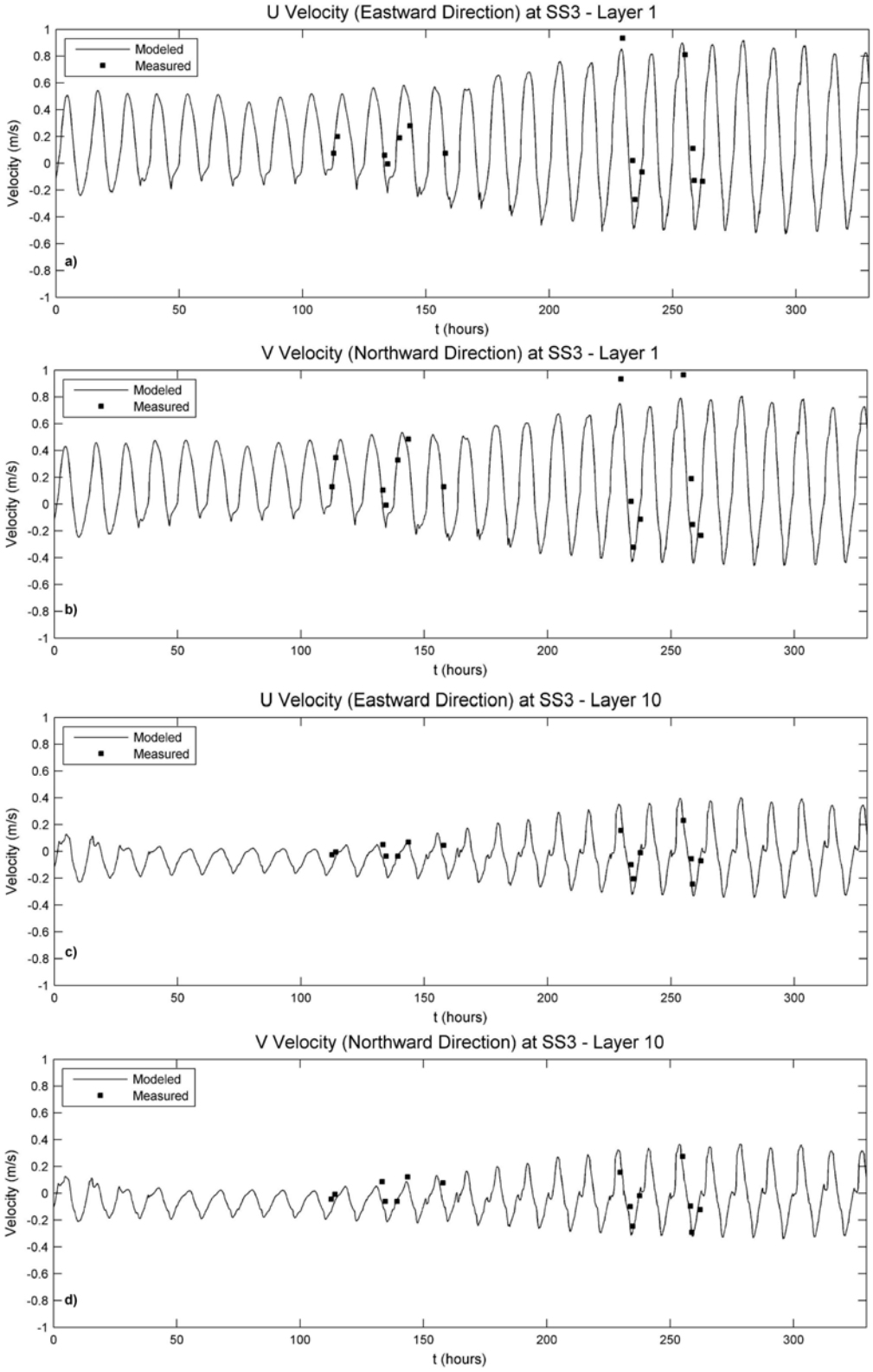

Figure 5.20: Comparison between the measured and modeled velocity components at the survey station SS3. U-velocity of surface layer (a), V-velocity of surface layer (b), U-velocity of bottom layer (c) and V-velocity of bottom layer (d).

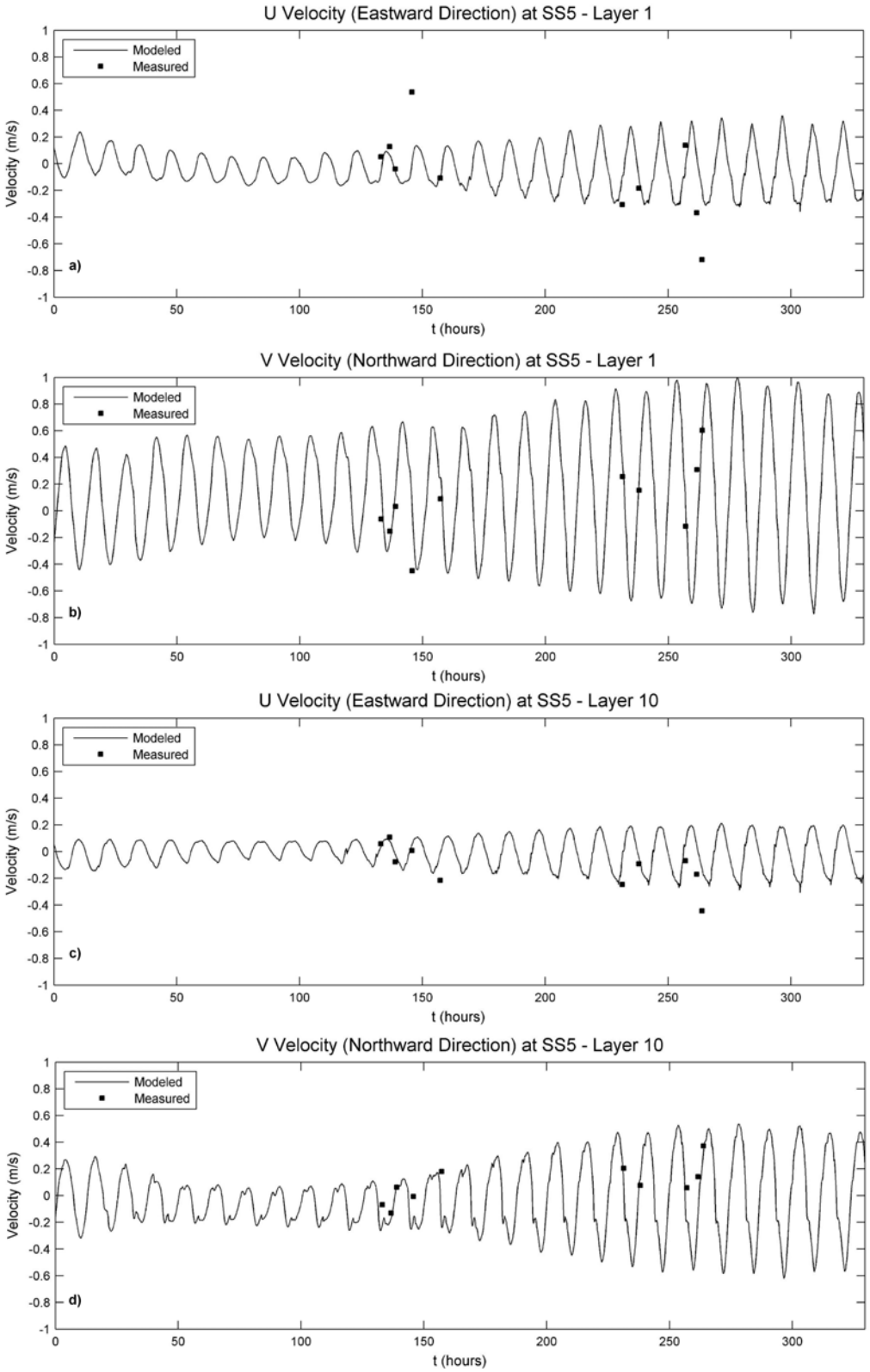

Figure 5.21: Comparison between the measured and modeled velocity components at the survey station SS5. U-velocity of surface layer (a), V-velocity of surface layer (b), U-velocity of bottom layer (c) and V-velocity of bottom layer (d).

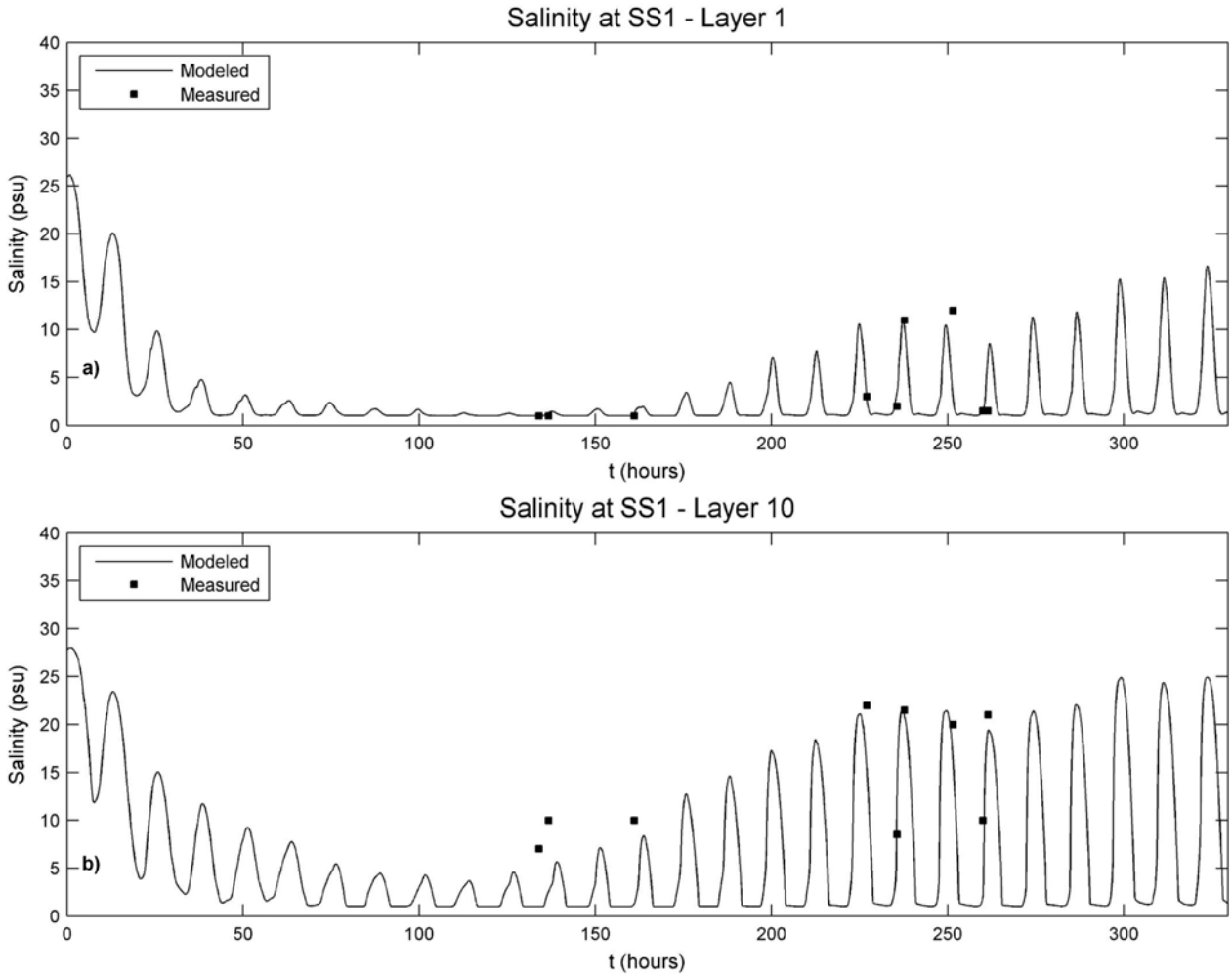

Figure 5.22: Comparison between the measured and modeled salinity at the survey station SS1. Surface layer (a) and bottom layer (b).

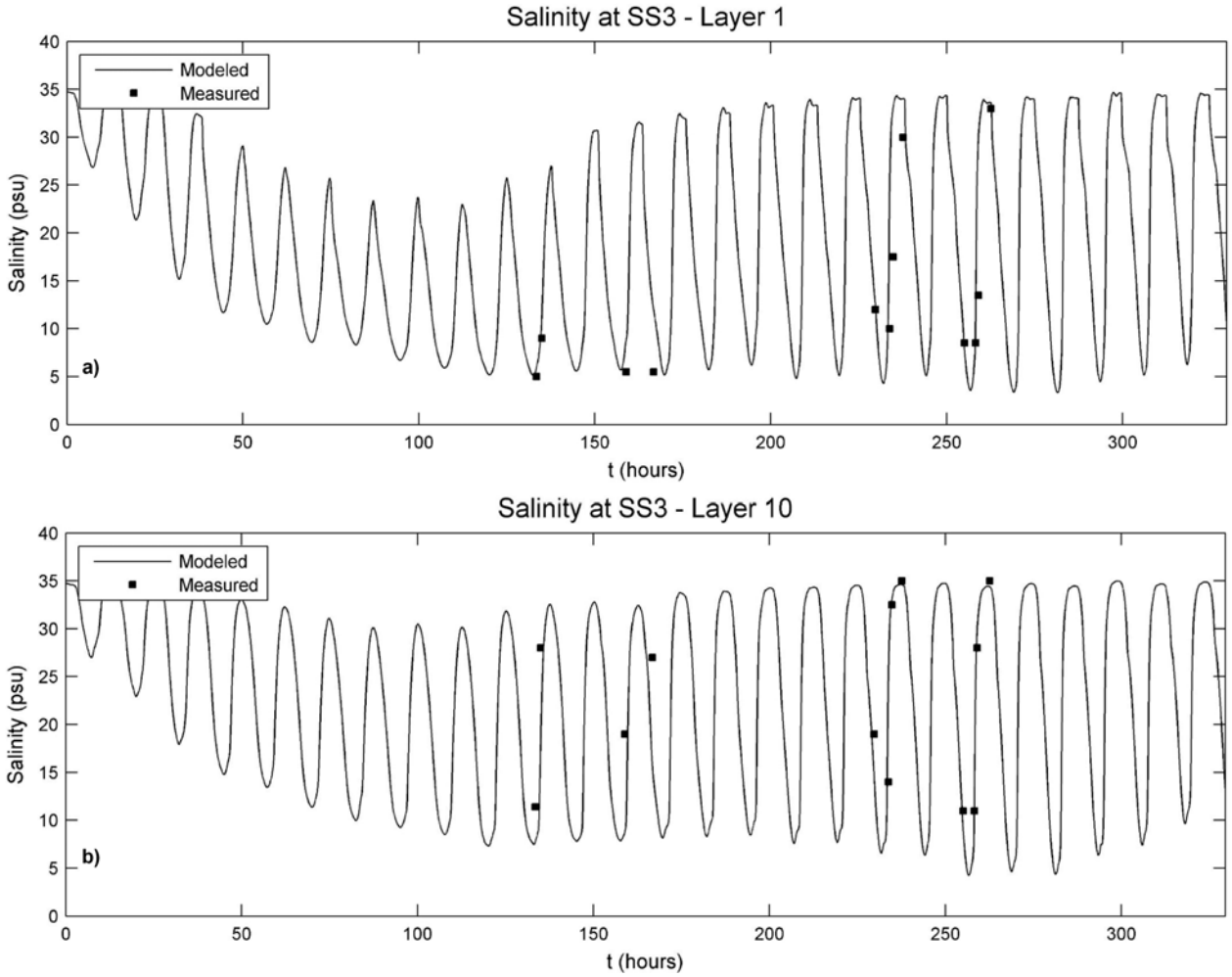

Figure 5.23: Comparison between the measured and modeled salinity at the survey station SS3. Surface layer (a) and bottom layer (b).

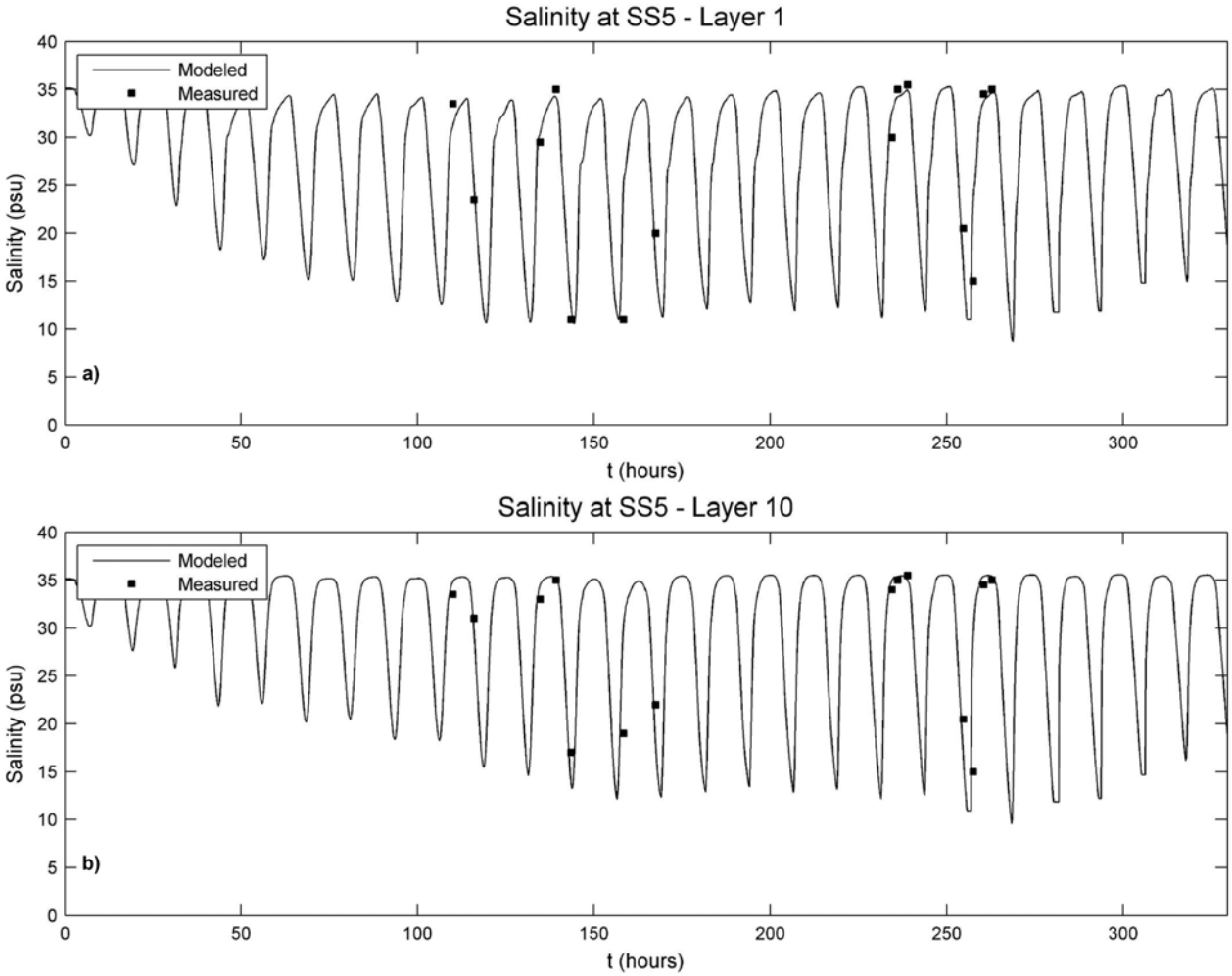

Figure 5.24: Comparison between the measured and modeled salinity at the survey station SS5. Surface layer (a) and bottom layer (b).

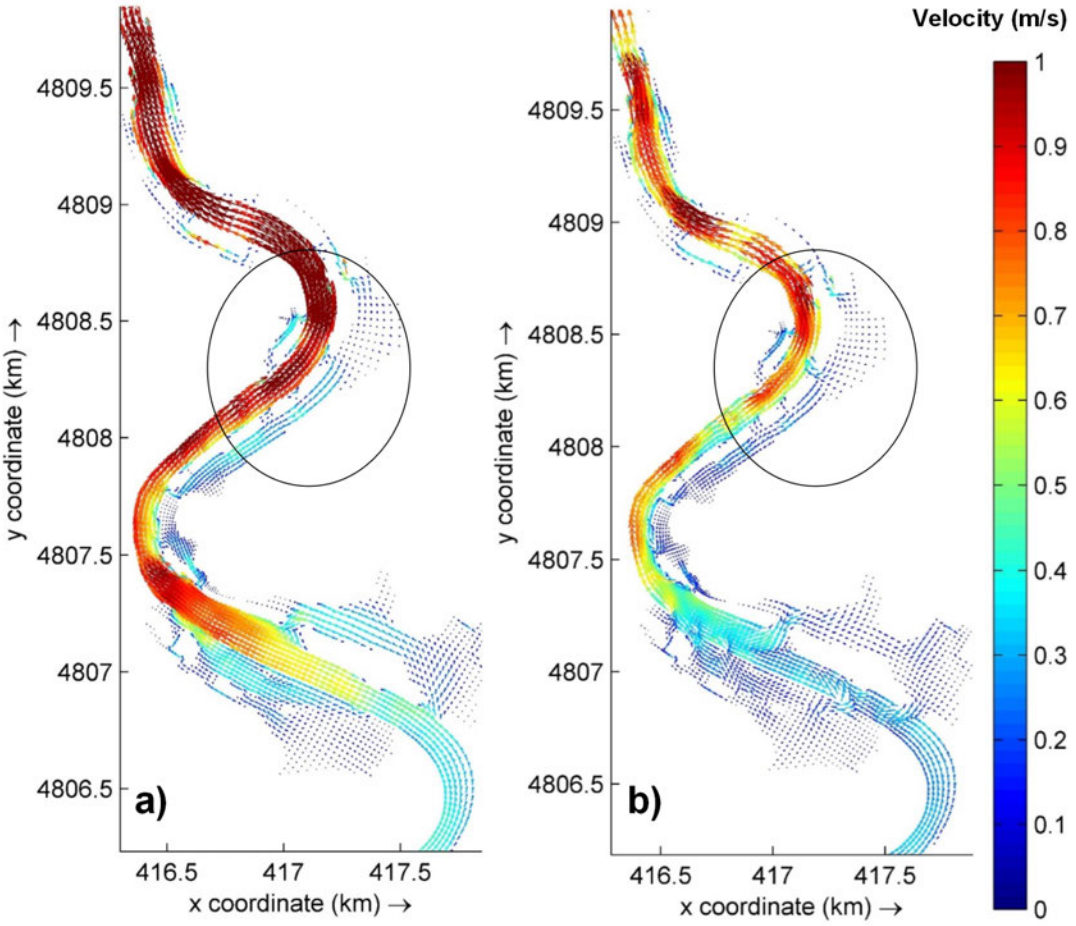

Figure 5.25: Map of the spatial distribution of velocities in an instant of ebb tide during the calibration period. Surface layer (a) and bottom layer (b).

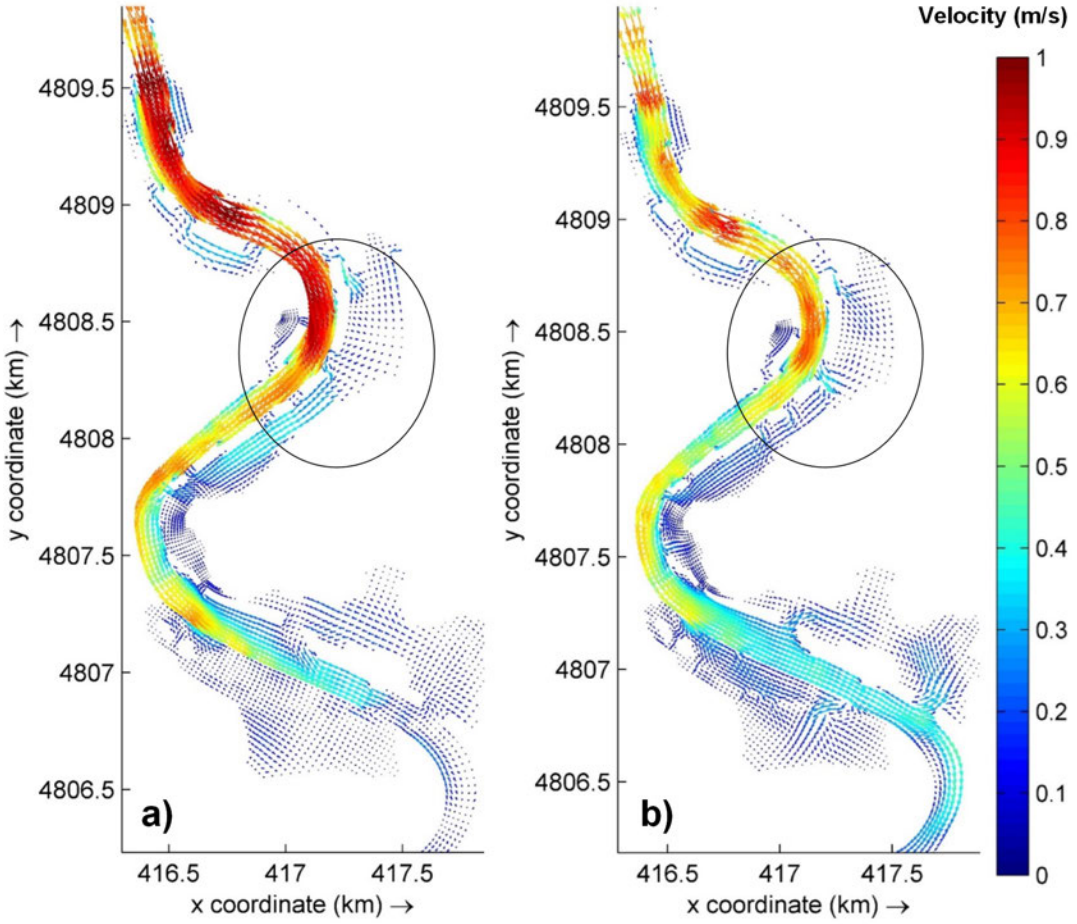

Figure 5.26: Map of the spatial distribution of velocities in an instant of flood tide during the calibration period. Surface layer (a) and bottom layer (b).

Variable	Station	Depth	BIAS	CE	Performance
Water level	TG1	-	0.015 m	0.994	Acceptable (excellent)
	TG2	-	0.077 m	0.987	Acceptable (excellent)
U Velocity	SS1	Depth-averaged	-0.024 m/s	0.368	Acceptable (poor)
	SS2	Depth-averaged	0.096 m/s	0.226	Acceptable (poor)
	SS3	Depth-averaged	-0.058 m/s	0.566	Acceptable (convenient)
	SS4	Depth-averaged	0.027 m/s	0.034	Acceptable (poor)
	SS5	Depth-averaged	0.093 m/s	0.125	Acceptable (poor)
	SS6	Depth-averaged	0.042 m/s	0.066	Acceptable (poor)
V Velocity	SS1	Depth-averaged	-0.073 m/s	0.099	Acceptable (poor)
	SS2	Depth-averaged	-0.073 m/s	0.166	Acceptable (poor)
	SS3	Depth-averaged	-0.073 m/s	0.614	Acceptable (convenient)
	SS4	Depth-averaged	-0.043 m/s	0.282	Acceptable (poor)
	SS5	Depth-averaged	-0.061 m/s	0.502	Acceptable (convenient)
	SS6	Depth-averaged	0.045 m/s	0.350	Acceptable (poor)
Salinity	SS1	Depth-averaged	-1.269 psu	0.392	Acceptable (poor)
	SS2	Depth-averaged	-2.432 psu	0.338	Acceptable (poor)
	SS3	Depth-averaged	1.148 psu	0.476	Acceptable (poor)
	SS4	Depth-averaged	2.577 psu	0.525	Acceptable (convenient)
	SS5	Depth-averaged	1.382 psu	0.642	Acceptable (convenient)
	SS6	Depth-averaged	0.154 psu	0.686	Acceptable (convenient)

Table 5.4: Depth-averaged errors of the optimal calibration case at Suances Estuary.

surface layer. This fact was related to the salt water entering from the open sea (upper boundary) was denser than the fresh water entering from the open river (lower boundary).

5.3.2.2 Hydrodynamic worst case modeling

Once the hydrodynamic and transport (salinity and temperature) model was set up, the hydrodynamic model (Delft3D-FLOW) was used to predict the flow and dispersion data that were used to run the transport models in the near- and far-field regions.

Following the methodology and considering the ecdf of the astronomical tide and river flow (see figure 5.7), the "worst case of dilution" assumed fixed conditions of the main forcing:

- Tidal amplitude was the forcing value that was not exceeded during the 10% of the time $\Rightarrow A10 = 0.9246$ m.
- River flow was the forcing value that was not exceeded during the 10% of the time, taking into account the average of 7 consecutive days $\Rightarrow 7Q10 = 3.6314$ m^3/s.

Boundary and initial conditions

As boundary and initial conditions were used those shown in figure 5.16.

Open and closed boundary conditions

CBs were the same as specified for the calibration process. Regarding OBs, we defined four boundaries (one upper, one lower and two lateral):

- The upper sea boundary condition was an astronomic tide forced by a M2 component with an amplitude

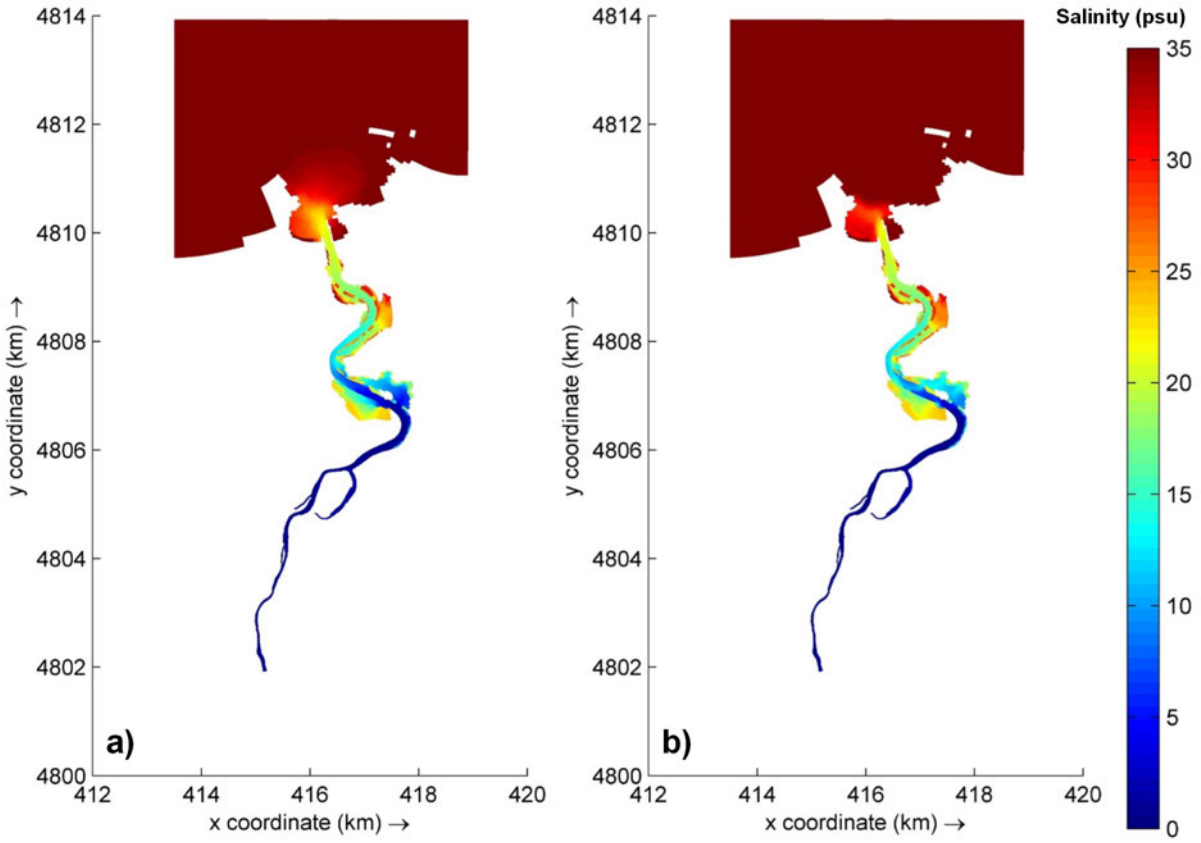

Figure 5.27: Map of the spatial distribution of salinities in an instant of ebb tide during the calibration period. Surface layer (a) and bottom layer (b).

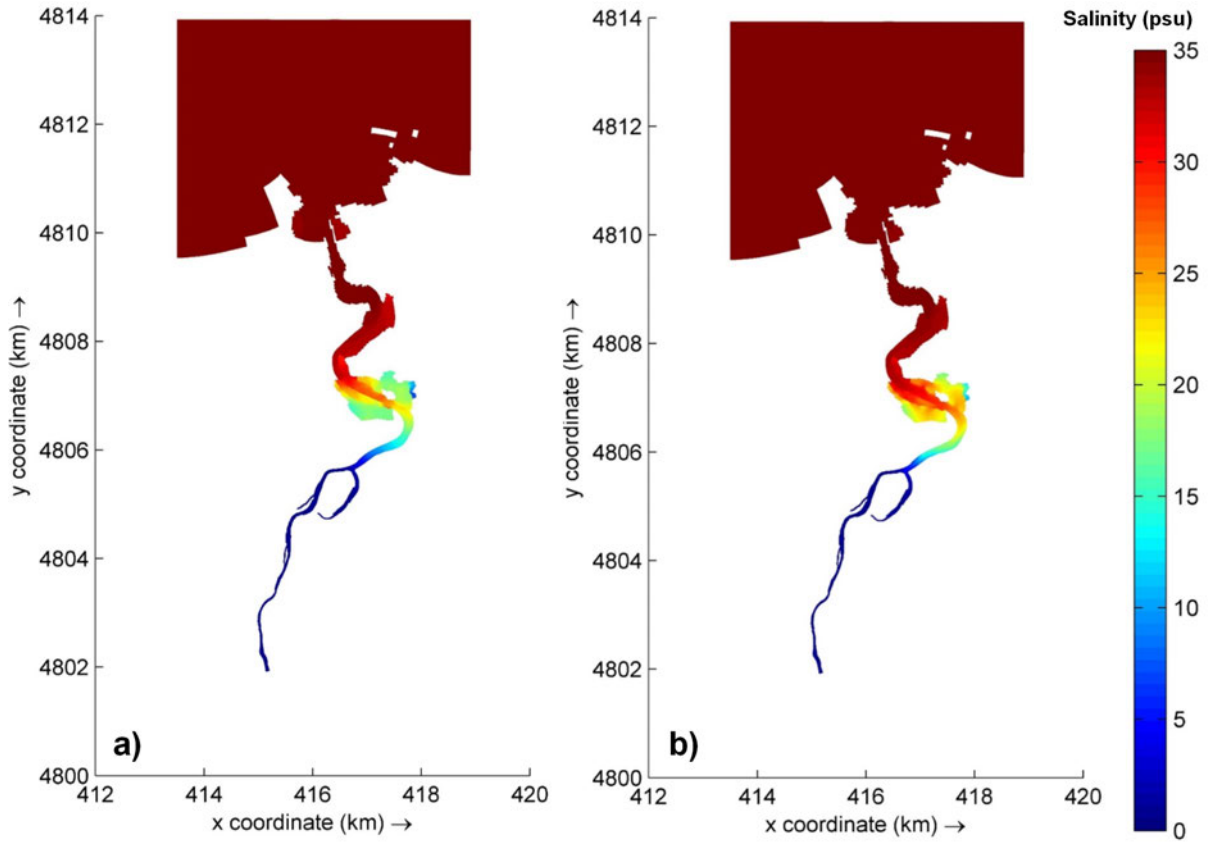

Figure 5.28: Map of the spatial distribution of salinities in an instant of flood tide during the calibration period. Surface layer (a) and bottom layer (b).

Industrial discharge	Q_{eff} (m^3/s)	ϕ (m)	d_{eff} (m)	S_{eff} (psu)	$T_{eff})$ (^oC)	ρ_{eff} (kg/m^3)
ID1	0.83801	0.85	1	0.05	15.2	999.11
ID2	0.00472	0.10	1	0.05	15.2	999.11

Table 5.5: Independent variables of each discharge mechanism for ID1 and ID2.

of A10. Due to the vertical and temporal variation of salinity and temperature were not significant in WQ15 along the years, we established that the boundary was vertically and temporally constant being the average of all the measurements, i.e., 35.27 psu and 15.96 ^{o}C.

- The lower river boundary condition was the 7Q10 river flow. Due to the vertical and temporal variation of salinity and temperature were not significant in WQ1 along the years, we established that the boundary was vertically and temporally constant being the average of all the measurements, i.e., 0.238 psu and 15 ^{o}C.
- The lateral sea boundary conditions were modeled by imposing a condition of zero velocity. Salinity and temperature were specified with the same values of the upper boundary.

Initial conditions

To perform the simulation of the simplified calculation, ICs were maps with constant values (Figure 5.16). We specified a water level of 0 m, a temperature of 15.5 ^{o}C and a salinity of 29 psu throughout every grid cell of the meshgrid to start the simulations.

Simulation

This model scenario was simulated until reach a "quasi-stationary" response so the effect of the initial conditions was avoided in the numerical simulation. Regarding the timescales of the "quasi-stationary" response, we selected two control points located at both discharge points. i.e., ID1 and ID2 (see figure 5.2). We assumed that the initial dilution can be estimated when the "quasi-stationary" response is reached around the industrial discharges.

Figures 5.29 and 5.30 illustrate the evolution of water levels (a), velocities (b), salinities (c) and temperatures (d) at ID1 and ID2 respectively. Note that the "quasi-stationary" response was highlighted in a grey dashed-line and the recorded period of hydrodynamic results between red lines.

According to both figures, the longest timescale of "quasi-stationary" response for hydrodynamics corresponded to salinity and temperature for ID2 and was 216 hours (9 days). Once it was reached this situation at ID1 and ID2, we recorded hourly one day of hydrodynamic model results (24 data) in every grid cell of the meshgrid between the hours 240 to 264 (see red lines in figures 5.29 and 5.30).

5.3.3 Primary or initial dilution (Near-field)

The buoyant jet behavior depends on Q_{eff}, ϕ, d_{eff}, ρ_{eff}, ρ_{env}, H and u_{env}. The first four variables are attached to the discharge mechanism, they were independent for every discharge (ID1 and ID2). Table 5.5 presents the values of these four variables for ID1 and ID2.

The remaining variables were related to the environmental conditions, they were dependent of the hydrodynamic changes and the single-port location. The primary dilution computations were conducted for every significant discharge (ID1 and ID2), employing the numerical model JETLAG and taking into account:

- All substances were considered conservative tracers.

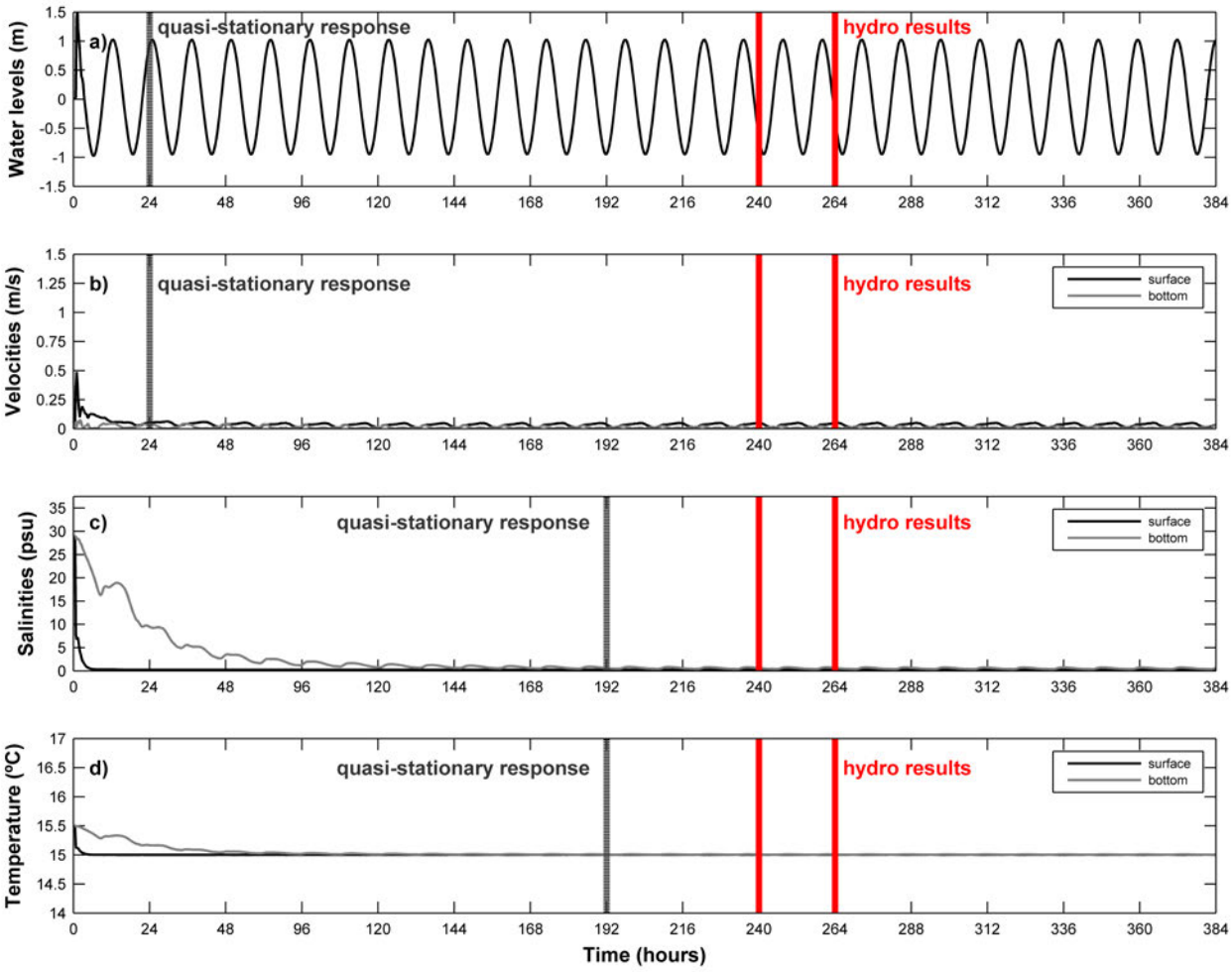

Figure 5.29: Evolution of water levels (a), velocities (b), salinities (c) at surface and bottom and temperatures (d) at surface and bottom in the discharge point ID1. Furthermore, timescales of the "quasi-stationary" response for each variable are highlighted in a grey dashed-line and the period for recording the hydrodynamics results between red lines.

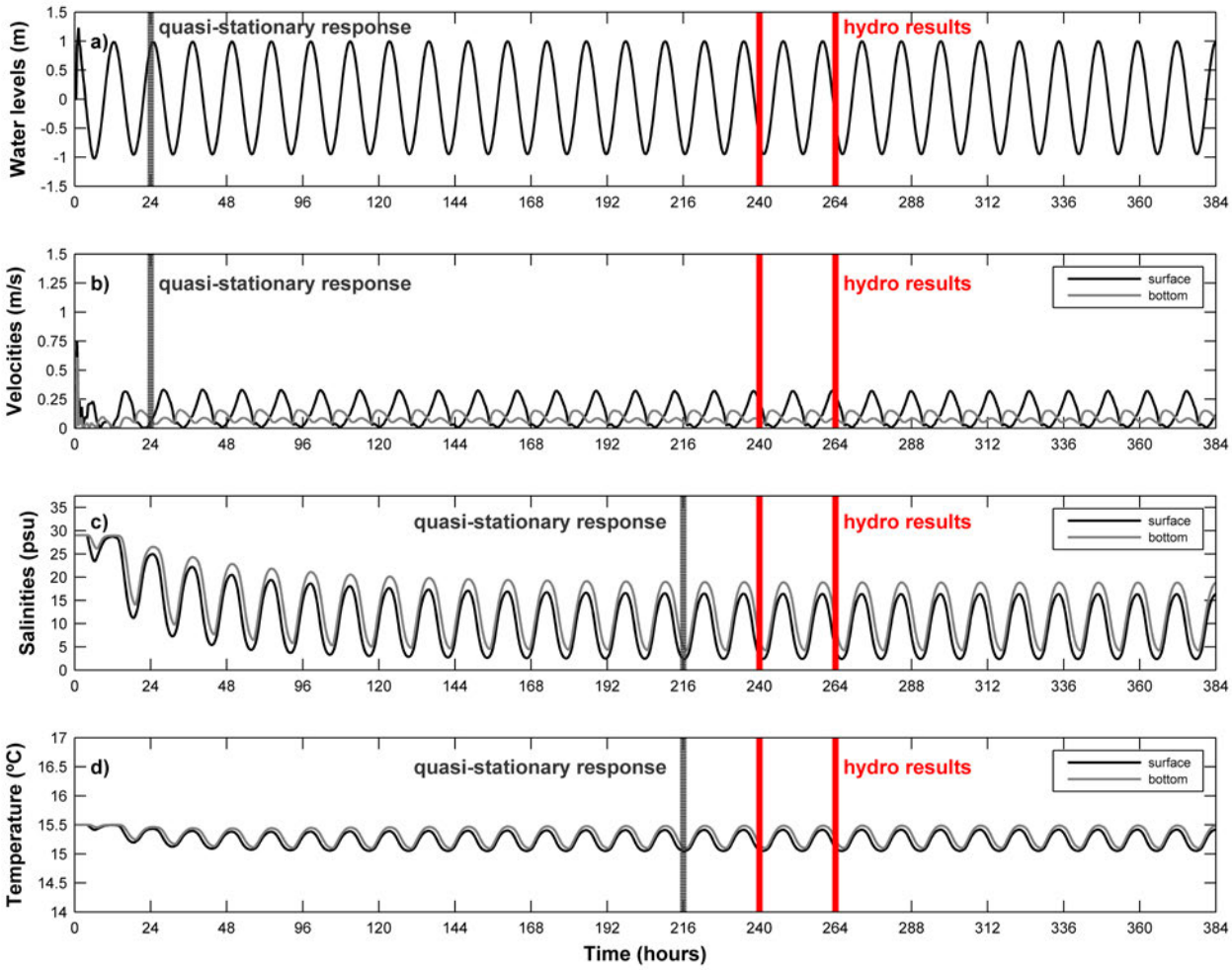

Figure 5.30: Evolution of water levels (a), velocities (b), salinities (c) at surface and bottom and temperatures (d) at surface and bottom in the discharge point ID2. Furthermore, timescales of the "quasi-stationary" response for each variable are highlighted in a grey dashed-line and the period for recording the hydrodynamics results between red lines.

- Environmental variables (H, ρ_{env} and u_{env}) were hourly extracted at each single-port location from Delft3D-FLOW results.
- We assumed an offline linkage where these results were specified as boundary condition for the initial dilution model.

Once all the required data were gathered, we ran the "worst case of dilution" with JETLAG for the significant discharges ID1 and ID2.

Figure 5.31 and 5.32 show the total water depth (a), the magnitude of the environmental velocity (b), the direction of the environmental velocity (c) and the environmental density (d) for the surface layer (blue line) and bottom layer (green line) at the point of discharge during the "worst case of dilution". Moreover, both figures display the initial dilution (e) of the effluent (black line) and the effluent concentration (f) after the initial dilution (black line). Finally, figure 5.31f displays the AA-EQS (magenta line) of chloroform ($CHCl_3$) and figure 5.32f the AA-EQS (magenta line) and MAC-EQS (red line) of lead (Pb).

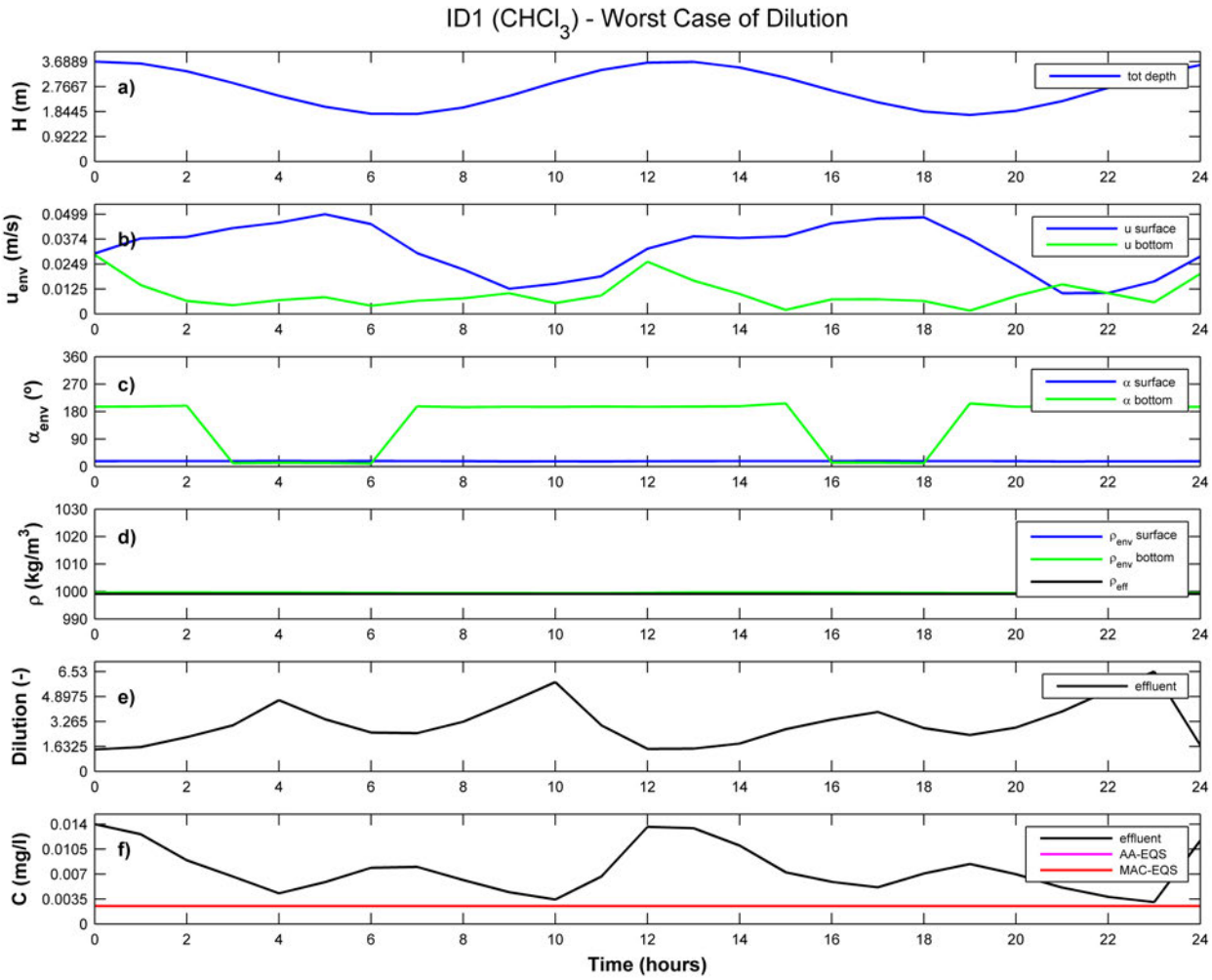

Figure 5.31: Evolution of the total water depth (a), the magnitude of the environmental velocity (b), the direction of the environmental velocity (c) and the environmental density (d) for the surface layer (blue line) and bottom layer (green line), the initial dilution (e) of the effluent (black line) and the effluent concentration (f) after the initial dilution (black line) at ID1 during the "worst case of dilution". Note it is also shown the AA-EQS (magenta line) of chloroform (f).

As it is shown in figure 5.31 and 5.32, ID1 dilution was oscillating between 1.63 and 6.53 and ID2 dilution between 109.11 and 27.27 due to the changes in the total depth, the environmental velocity and the environ-

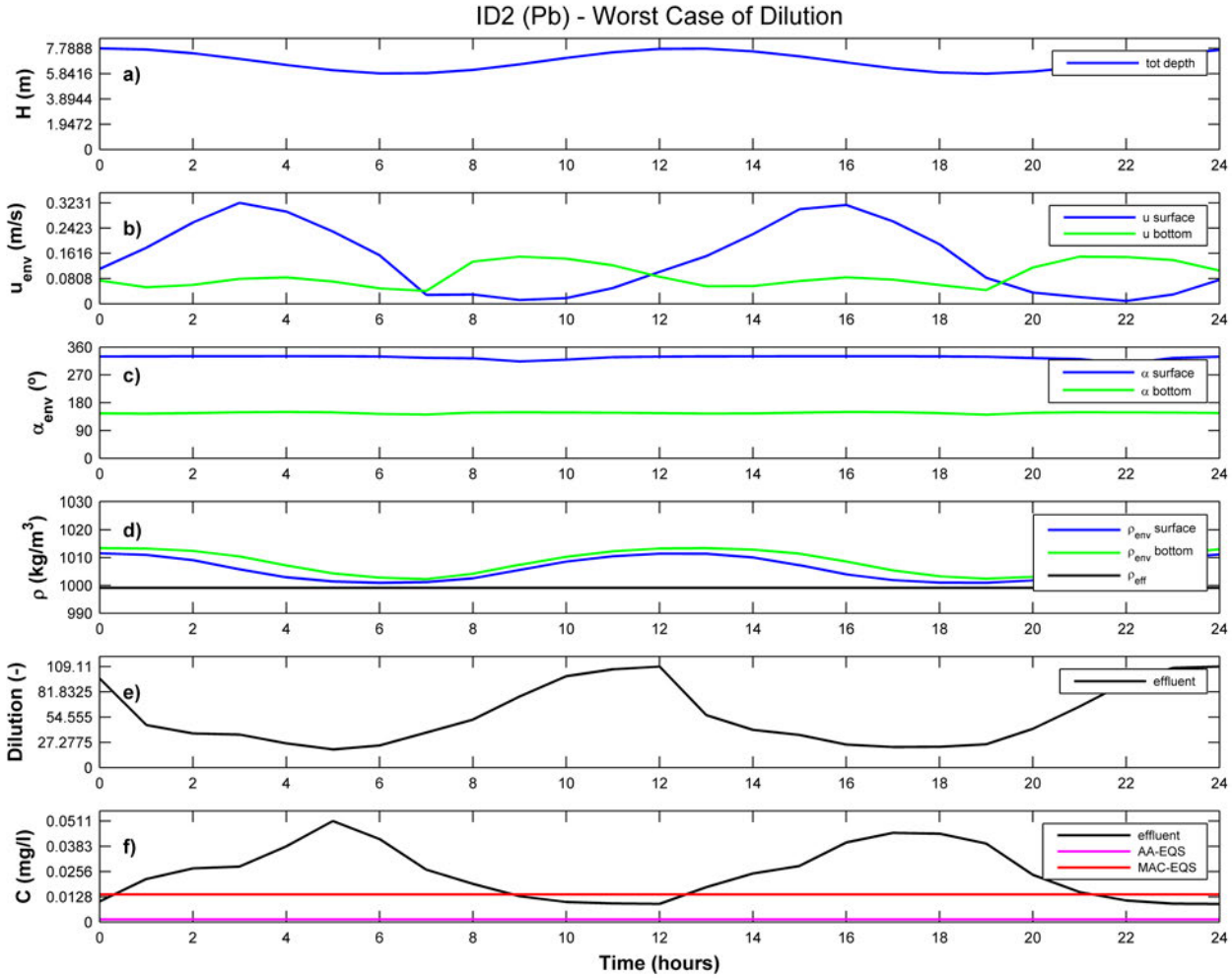

Figure 5.32: Evolution of the total water depth (a), the magnitude of the environmental velocity (b), the direction of the environmental velocity (c) and the environmental density (d) for the surface layer (blue line) and bottom layer (green line), the initial dilution (e) of the effluent (black line) and the effluent concentration (f) after the initial dilution (black line) at ID2 during the "worst case of dilution". Note it was also shown the AA-EQS (magenta line) and MAC-EQS (red line) of chloroform (f).

mental density. Regarding ID1 concentration, the AA-EQS was surpassed all the time in the "worst case of dilution". In the case of ID2 concentration, the AA-EQS was surpassed all the time in the "worst case of dilution" and the MAC-EQS was surpassed most of the time.

As an example of the trajectory described by ID1 and ID2 in the near-field region, figure 5.33 and 5.34 present one snapshot of the buoyant jet (ID1 and ID2) calculated in the "worst case of dilution" for the hour 5 (see figure 5.31 and 5.32). In both figures, the evolution of the 3D buoyant jet are shown on a 3D view (a), plan view (b) and side view (c). Moreover, the single-port pipe is represented with a black line (side and plan views) and the free surface with a blue line (side view) or a blue rectangle (3D and plan views).

As it can be seen in figure 5.33, the ID1 jet was fully mixed in the water column due to the lack of water depth and the magnitude of the effluent flow. It is also bent towards the river flow direction due to its closeness. On the other hand, figure 5.34 shows that the ID2 jet was trapped in the water column due to lack of momentum (low flow of the effluent) and buoyancy (density gradient between effluent and ambient water). It was also bent to the river flow direction because of the direction of the environmental velocity.

5.3.4 Coupling primary and secondary dilution (Intermediate-field)

In this methodology, the following coupling between both models was conducted:

- We assumed a passive coupling where the source-induced flow did not change the flow characteristics of the far-field, beyond the near-field or intermediate-field region. Thus, specific values of flow rates and toxicant concentration values of the discharge were determined by JETLAG.
- We generated an offline linkage. The JETLAG output was specified as source condition for the D-Water Quality in a subsequent simulation.
- We introduced hourly both the flow and the diluted concentration values of the ID1 and ID2 at the predicted grid cell and layers.
- We considered that the discharge flow on each layer is the ratio between the total flow and the number of layers covered by the intermediate-field ($Q_{layer} = Q_{total}/n^{o}{}_{layers}$).

Once all the required information was collected, we applied the describe method to the significant discharges ID1 and ID2 for the "worst case of dilution".

Figure 5.35 and 5.36 present the percentage of time that ID1 and ID2 was in different horizontal grid cells (left panel) and vertical layers (right panel) predicted by JETLAG during the coupling process. In these locations, we introduced ID1 and ID2 as a source term of flow and diluted concentration.

As it is shown in figure 5.35, ID1 coupling was located in several horizontal grids downstream of the discharge point due to the closeness to the river and the momentum of ID1. In the vertical direction, ID1 was coupled most of the time between layers 5 and 9, i.e., between 1 and 3.25 m of depth. The rest of the time ID1 was fully mixed in the water column as it was shown in figure 5.31. As it can be seen in figure 5.36, ID2 was always in the grid cell where was located the industrial pipe due to the buoyancy and the relative small discharged flow. Regarding vertical distribution, ID2 was most of the time between layers 5 and 7, i.e., between 3 and 5.5 m of depth indicating that ID2 plume was trapped (see figure 5.32).

5.3.5 Secondary or ambient dilution (Far-field)

Finally, in this subsection, the required tasks to conduct the simulation of the significant discharges with D-Water Quality were described.

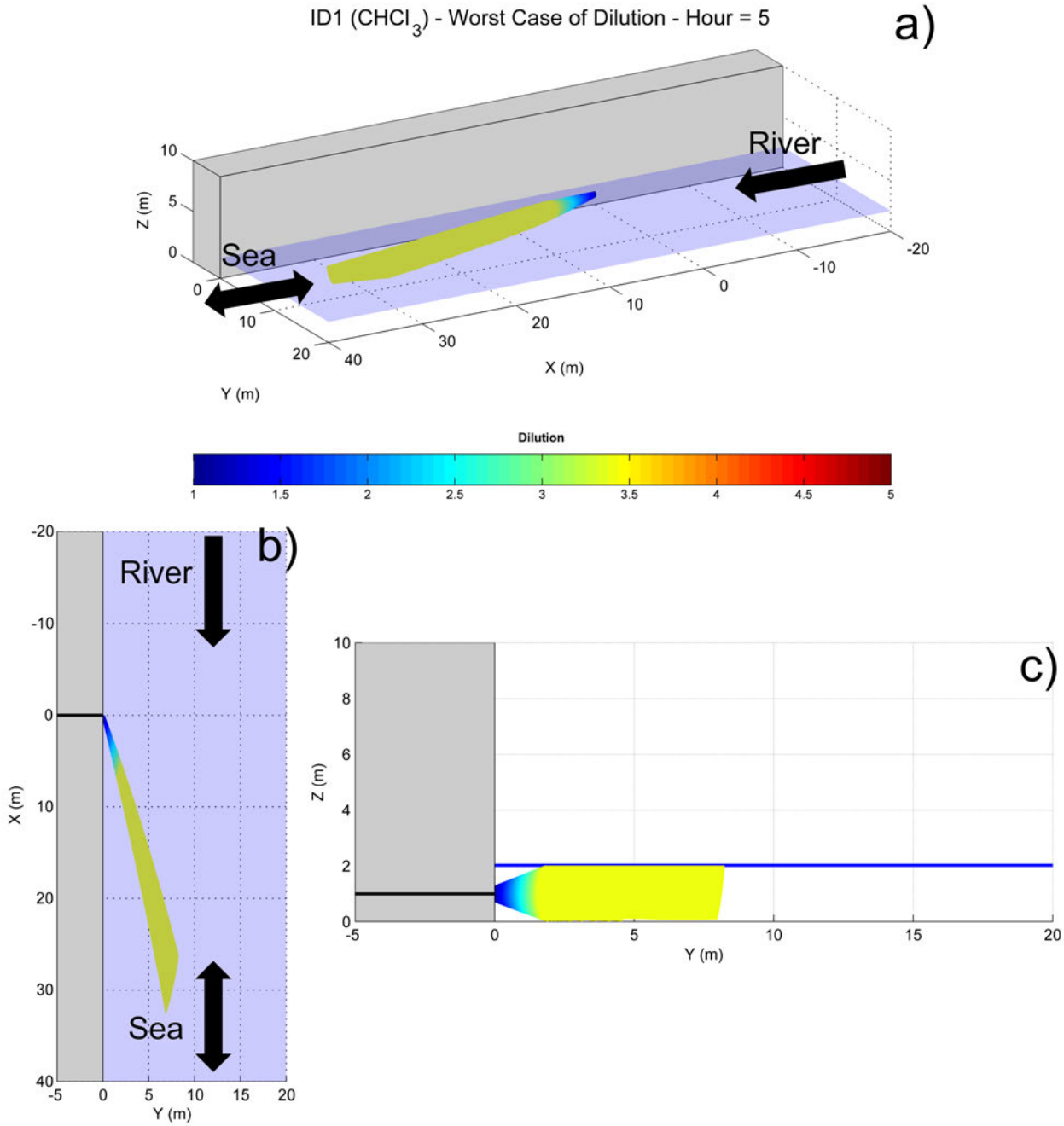

Figure 5.33: 3D buoyant jet of ID1 for the hour 5 in the simplified calculation. 3D view (a), plan view (b) and side view (c). The single-port pipe is represented with a black line (side and plan views) and the free surface with a blue line (side view) or a blue rectangle (3D and plan views).

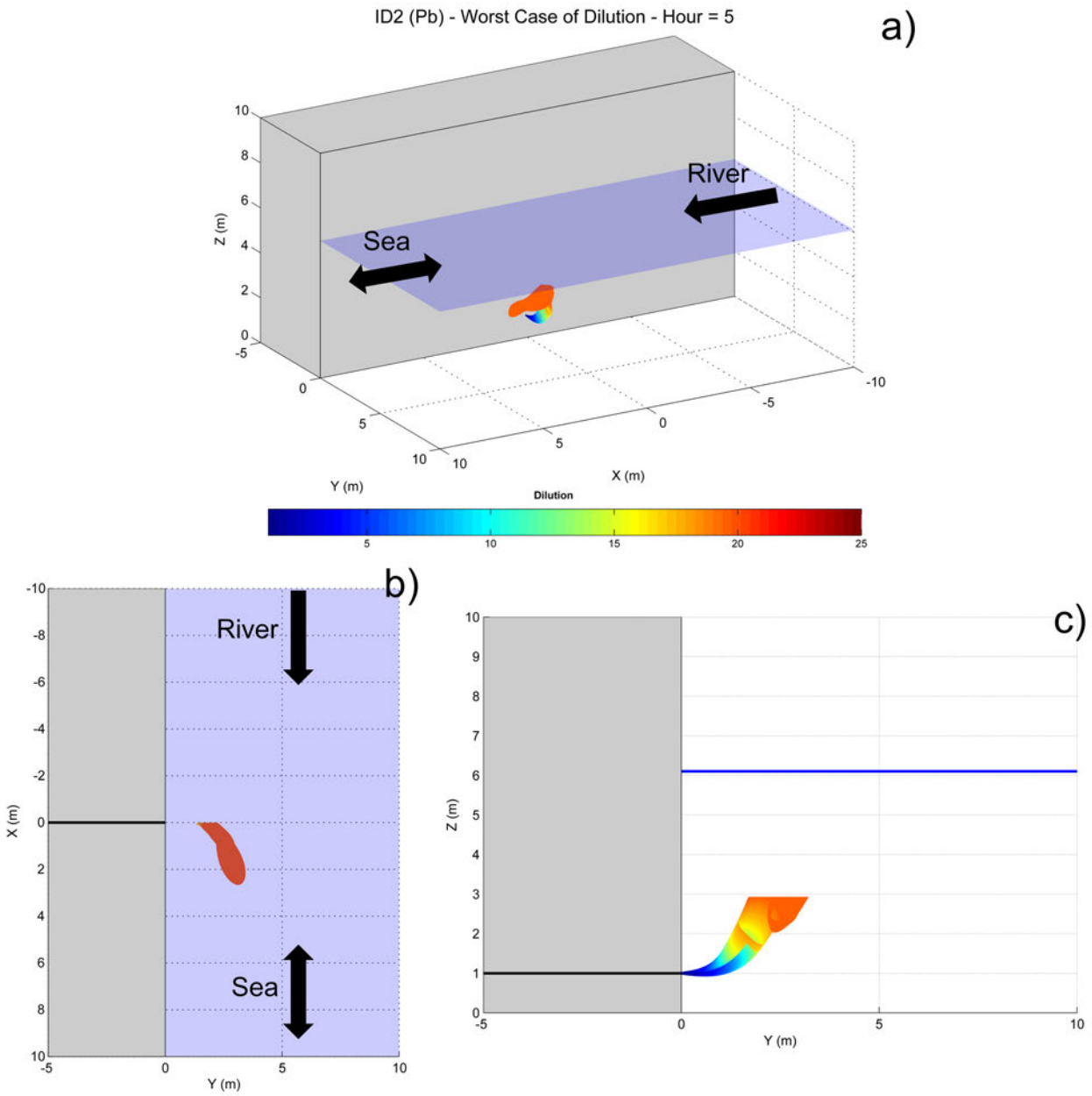

Figure 5.34: 3D buoyant jet of ID2 for the hour 5 in the simplified calculation. 3D view (a), plan view (b) and side view (c). The single-port pipe was represented with a black line (side and plan views) and the free surface with a blue line (side view) or a blue rectangle (3D and plan views).

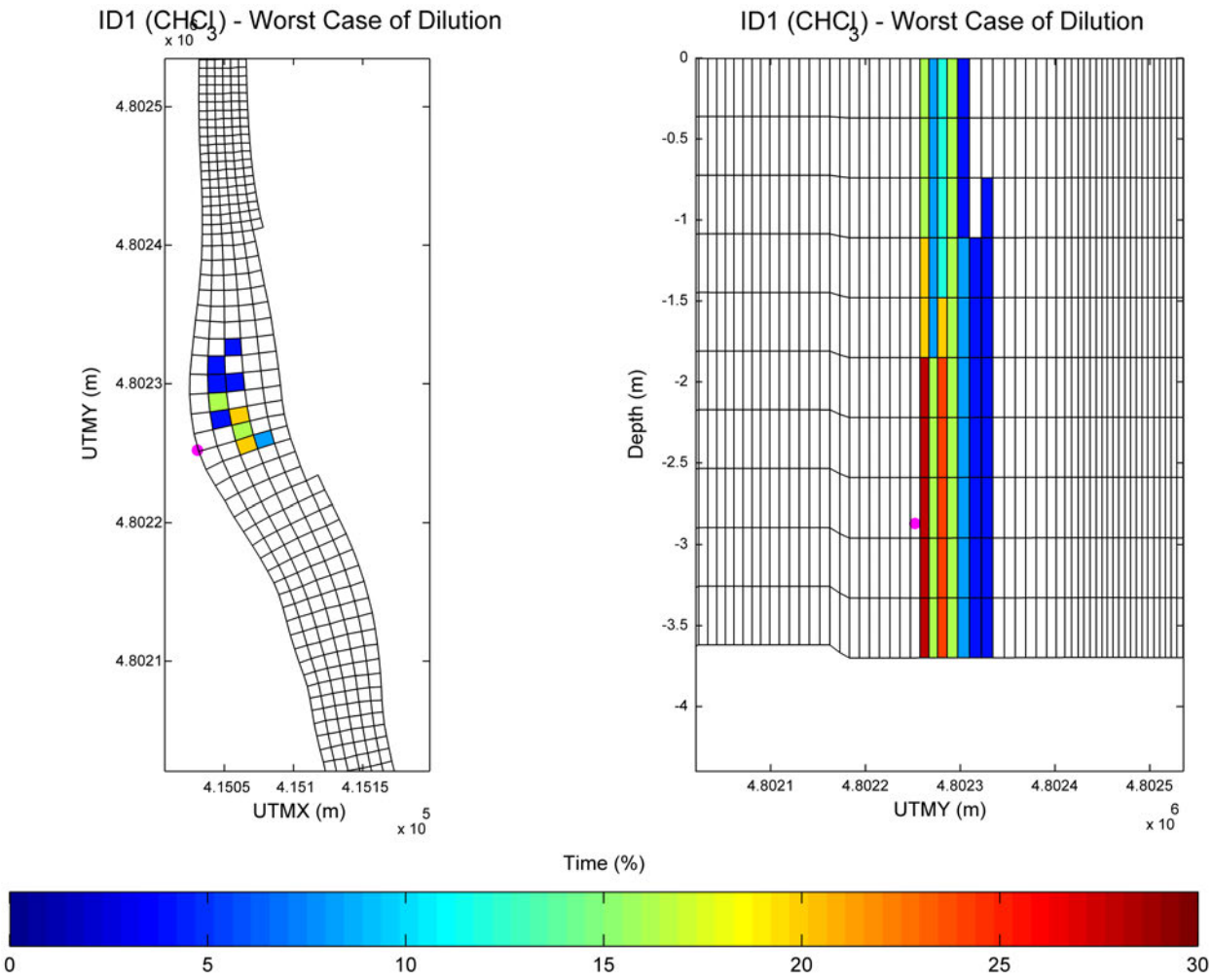

Figure 5.35: Schematic view of the time distribution of horizontal grid cells (left panel) and the vertical layers (right panel) covered by ID1 during the coupling between the primary and secondary dilution in the simplified calculation.

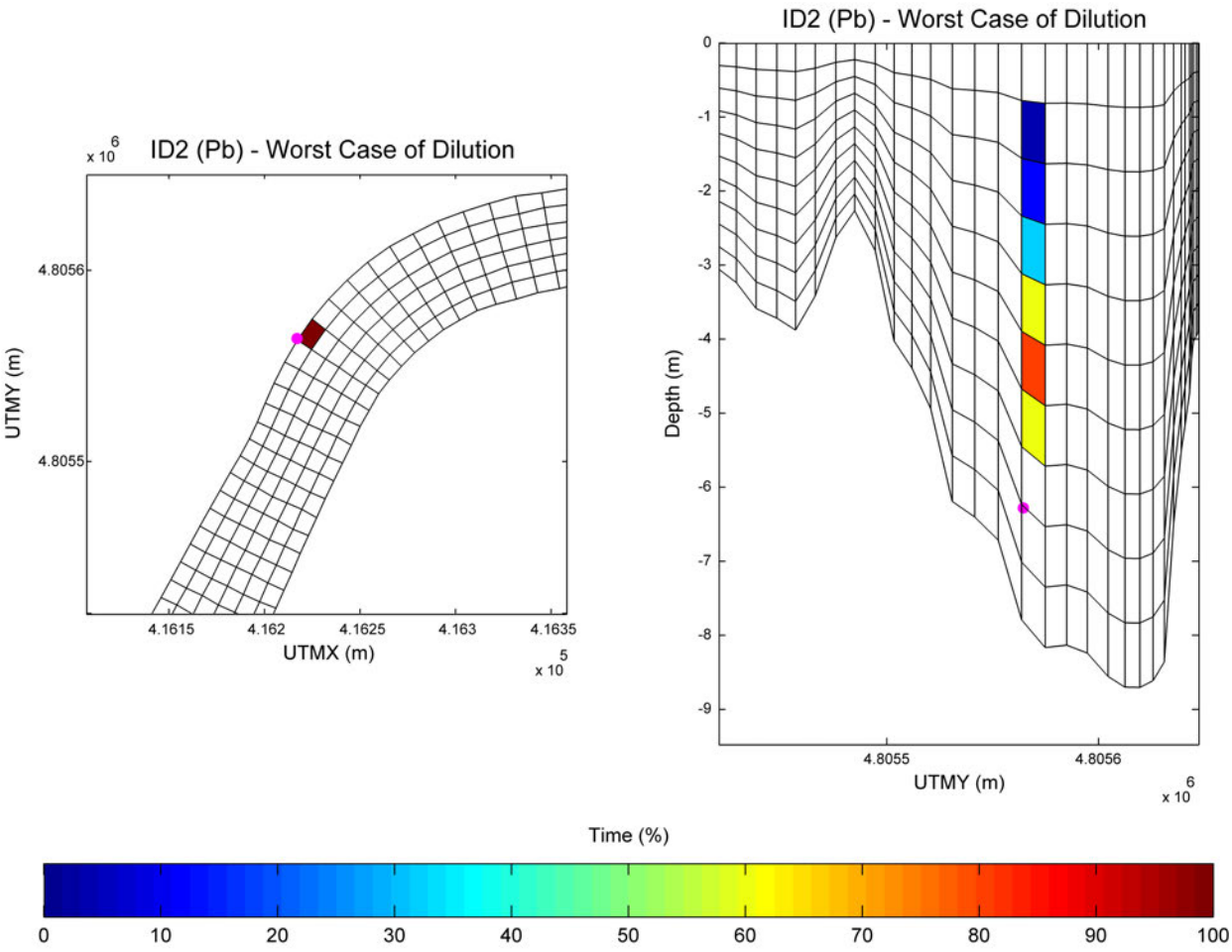

Figure 5.36: Schematic view of the time distribution of horizontal grid cells (left panel) and the vertical layers (right panel) covered by ID2 during the coupling between the primary and secondary dilution in the simplified calculation.

5.3.5.1 Model setup

The same way as for the hydrodynamic model (Figure 3.9), the first task for modeling the advection and dispersion of toxicants was setting up the transport model for conservative tracers.

Model domain discretization

The model domain discretization was the same used for the hydrodynamic model setup, i.e., the transport model grid had the same number of nodes (grid cells) and layers. No horizontal and/or vertical aggregation was used.

Boundary and initial conditions

As boundary and initial conditions were used those shown in figure 5.16 during the hydrodynamic calibration process. Moreover, OBs and IC for the conservative tracers were set to zero.

Model calibration

Due to the toxicants were considered conservative in Step 3, the physical parameters calibrated in the hydrodynamic model were the same for the transport model and, consequently, calibration was not necessary to conduct.

Physical parameters

Physical parameters were the horizontal and vertical eddy diffusivity when all substances were considered conservative tracers.

Numerical parameters

In the case of far-field models, it should be underlined that the finite volume method (FVM) was the best computational method to solve the "advection-diffusion-reaction" equation because it is mass-conserving by definition.

- *Numerical scheme:* We selected implicit upwind scheme with an iterative solver (Scheme 15 of D-Water Quality). This scheme was implicit in the vertical and horizontal directions so it was computationally efficient and there were no stability criteria for transport. The method was an iterative solver: it took a guess for the concentration vector (if available, this guess was the concentration of the previous time-step), and subsequently the method checked if this guess was correct or not.
- *Timestep:* To ensure the transport model stability and accuracy, the Peclet number was used (Equation (3.9)). The timestep was higher than in hydrodynamics due to the selection of an implicit scheme being $\Delta t = 1$ min.
- *Numerical filters:* We activated two filters for no dispersion over tidal flats and open boundaries. We also activated an iterative filter in order to remove the negative values.

Simulation-calibration cases

Simulation-calibration cases were all the different model simulations performed by means of N combinations of physical parameters and M combinations of numerical parameters in order to find the best combination of model parameters. Table 5.6 synthesizes the calibration parameters, suggests the best option for estuarine modeling and gives the optimal value ranges of each parameter.

As it can be seen from table 5.6, there were a less range of possibilities to combine model parameters than in a hydrodynamic model when the latter is previously calibrated. In the case of physical parameters, there

Physical parameters	**Suggestions**	**Value ranges**
All parameters	Same hydrodynamic model	Hydrodynamic calibration
Numerical parameters	**Suggestions**	**Value ranges**
Numerical scheme	Implicit Upwind with an iterative solver	Scheme 15
Timestep	Equation (3.9)	$\Delta t = 1$ min.
Numerical filters	Activated Activated Activated	No dispersion over tidal flats No dispersion over OB No negative values

Table 5.6: Overall picture of far-field model calibration parameters for conservative approach.

Physical parameters	**Calibrated Value**
All parameters	Hydrodynamic calibration
Numerical parameters	**Calibrated Value**
Numerical scheme	Scheme 15
Timestep	$\Delta t = 1$ min.
Numerical filters	No dispersion over tidal flats No dispersion over OB No negative values

Table 5.7: Optimal calibration parameters of the far-field model for Suances Estuary in the conservative approach.

was 1 case coming from the hydrodynamic calibration. Regarding numerical parameters, there were 1 case of numerical scheme, 1 case of timestep and 1 case of numerical filters.

The combination of all of this cases resulted in 1 simulation-calibration case. This was why calibration was not required. Therefore, the optimal calibration was the combination of parameters shown in table 5.7.

5.3.5.2 Transport worst case modeling

In order to run the transport of the "worst case of dilution" with D-Water Quality, the previous simulation of the hydrodynamic model and the initial dilution data from the coupling approach were used.

Boundary and initial conditions

CBs were set to zero. The vertical diffusive flux through the free surface and bed was also set to zero. OBs were set to zero for the four boundaries (one upper, one lower and two lateral). Finally, IC was a map with a constant value specified at zero for every toxicant.

Simulation

This model scenario was simulated for ID1 and ID2 until reach a "quasi-stationary" response for transport, i.e., transport variables display a modulated signal because of tides and river discharges and their magnitude were not varying with the tidal period (Figure 3.16). Once it was reached this situation, we recorded hourly one day (24 data) of transport model results (Figure 3.16).

The "quasi-stationary" response depended on the location, concentration and flow of the point discharge, the location of the considered grid cell respect to the point discharge and the magnitude of the river and tides. Therefore, in order to find the maximum timescale of the "quasi-stationary" response for transport, we conducted a sensitivity analysis with four different locations across the model domain (WQ3, SS1, SS3 and SS5; see figure 5.10).

Figure 5.37 and 5.38 display the initialization, the "quasi-stationary" response and the far-field model results

for the concentration evolution of ID1 and ID2 in the surface layer (black line) and the bottom layer (grey line) at WQ3 (a), SS1 (b), SS3 (c) and SS5 (d) respectively.

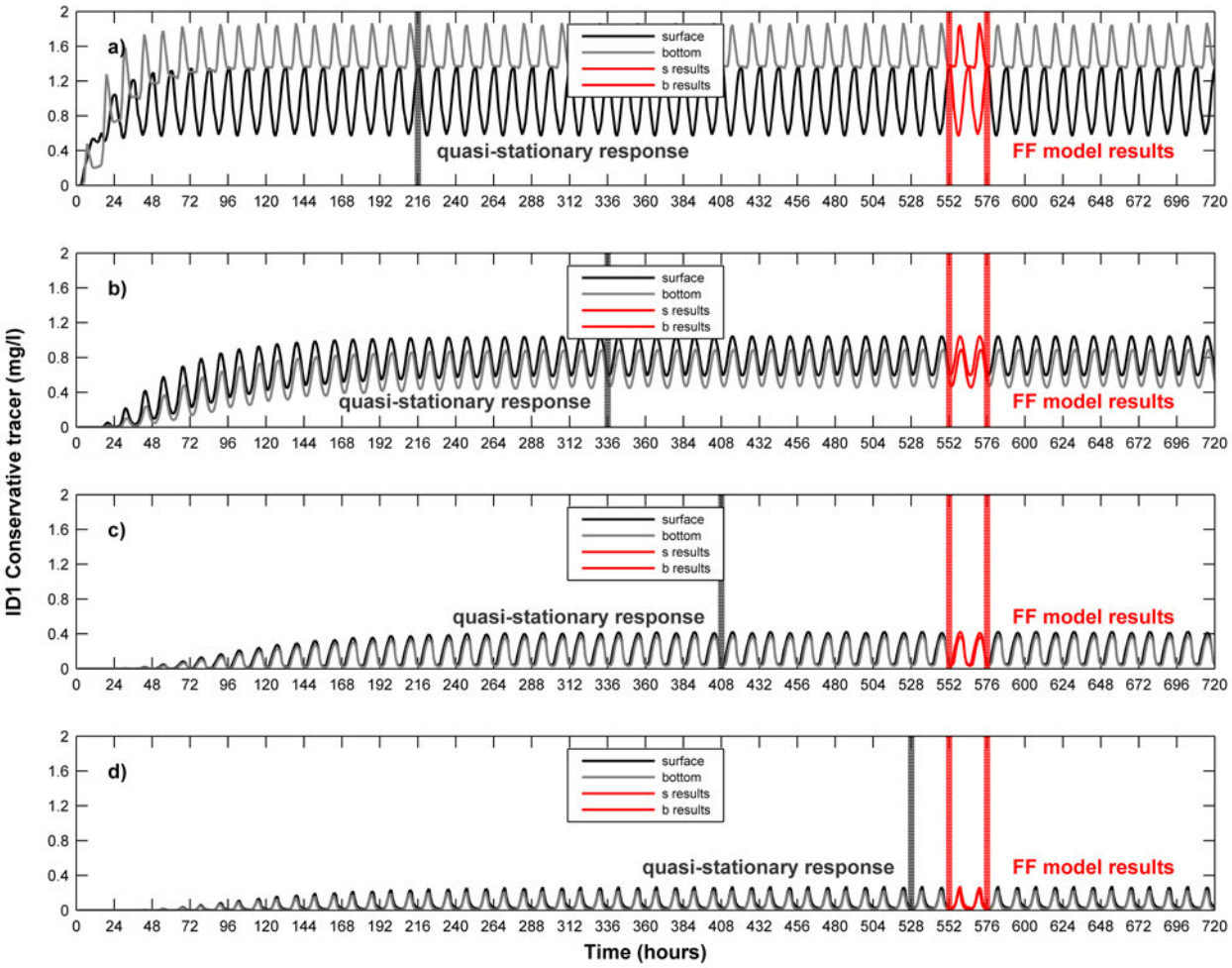

Figure 5.37: Evolution of ID1 concentration at the surface layer (black line) and the bottom layer (grey line), timescale of the "quasi-stationary" response and recorded period (red line) for the transport of the "worst case of dilution" at WQ3 (a), SS1 (b), SS3 (c) and SS5 (d).

According to both figures, the longest timescale of "quasi-stationary" response for trasnport was found at SS5 (d) for ID1 and ID2 being 528 hours (22 days).

Once it is reached this situation at ID1 and ID2, we recorded hourly one day of far-field model results (24 data) in every grid cell of the meshgrid between the hours 552 to 576 (see red lines in figures 5.37 and 5.38). At each time step (hour) and grid cell, it should be underlined that the recorded concentration is always the maximum concentration of the 10 vertical layers.

5.3.5.3 **Delimitation of mixing zones**

After model simulations, two MZs were determined: the AA-MZ and MAC-MZ (see figure 3.18). The effects of the maximum concentration of toxicant evolution were determined by the equation (3.12) for the AA-MZ and the equation (3.13) for the MAC-MZ (Figure 3.18).

Next, the delimitated AA-MZ and MAC-MZ of the "worst case of dilution" for ID1 (a-b) and ID2 (c-d) are shown in figure 5.39. Note that the chloroform (ID1) has not applicable MAC-EQS value so in this figure the MAC-MZ is only an example of the extent of the MAC-MZ considering as threshold the AA-EQS.

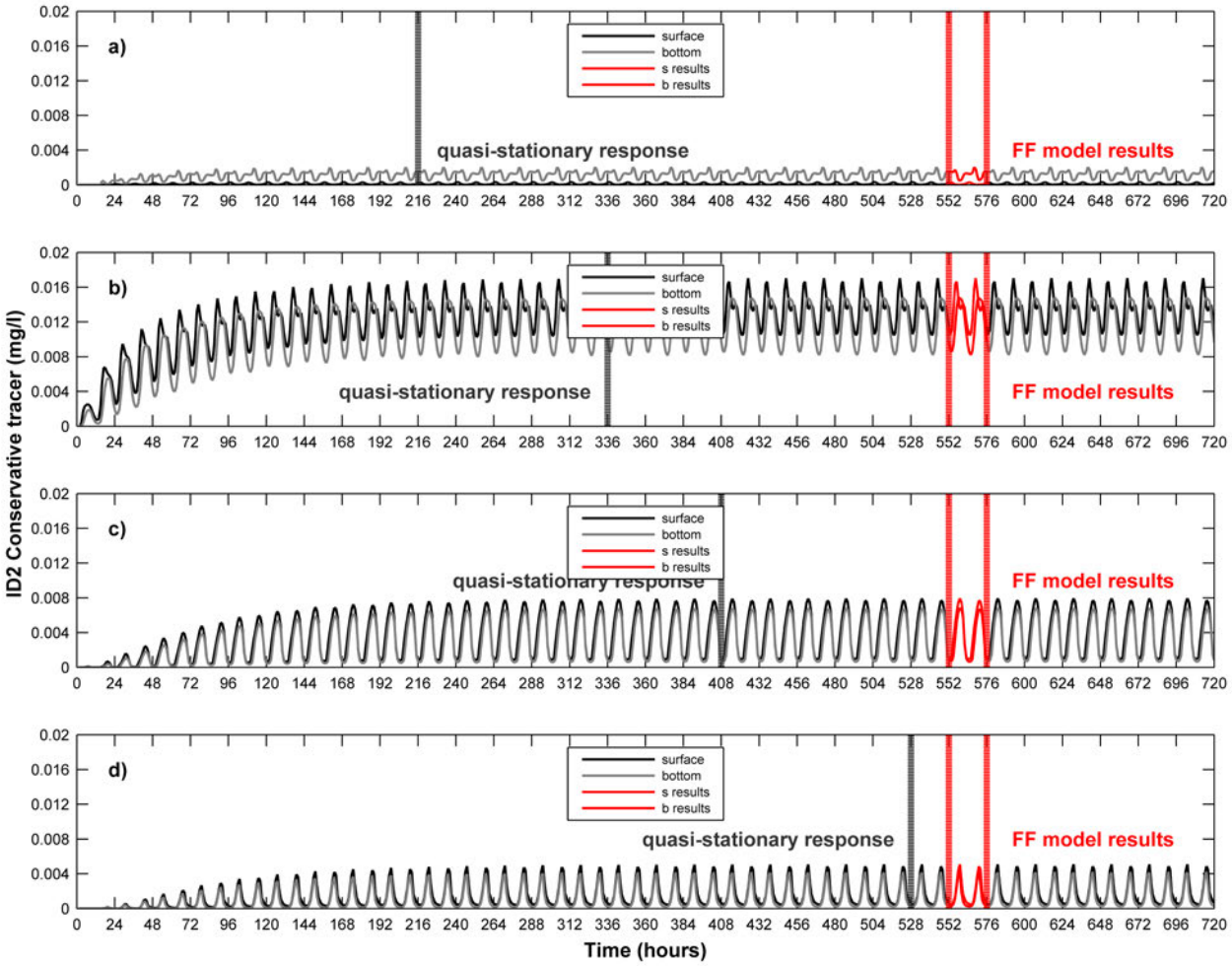

Figure 5.38: Evolution of ID1 concentration at the surface layer (black line) and the bottom layer (grey line), timescale of the "quasi-stationary" response and recorded period (red line) for the transport of the "worst case of dilution" at WQ3 (a), SS1 (b), SS3 (c) and SS5 (d).

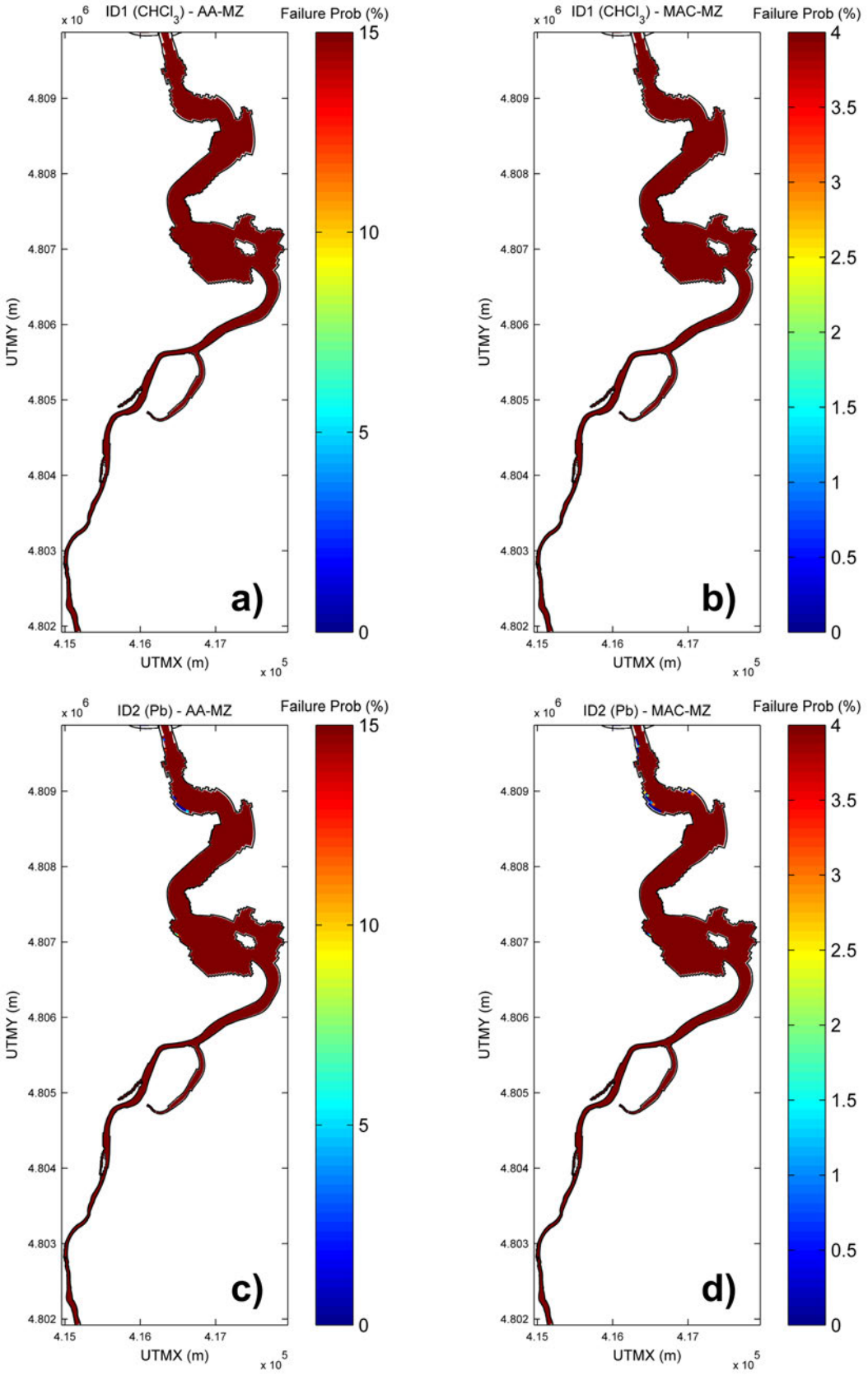

Figure 5.39: Delimitated Mixing Zones in the "worst case of dilution". AA-MZ of ID1 (a), MAC-MZ of ID1 (b), AA-MZ of ID2 (c) and MAC-MZ of ID2 (d).

Name Toxicant	AA-MZ m^2 AA-MAS	AA-AD	MAC-MZ m^2	MAC-AD MAC-MAS
ID1 ($CHCl_3$)	2557527.73	100.0>10	-	-
ID2 (Pb)	2533228.37	99.05>10	2510515.97	98.16>3

Table 5.8: Extent of the delimitated Mixing Zones (AA-MZ and MAC-MZ) and final admissibility (AA-AD and MAC-AD) in the simplified calculation for ID1 and ID2.

5.3.6 Admissibility (Acceptability/Extent)

In order to define de admissibility of ID1 and ID2 MZs, we evaluated the acceptability (AC), the maximum allowable MZ size (MAS) and the final admissibility (AD).

5.3.6.1 Acceptability (AC)

Intertidal zones were defined as the grid cells where the depth of the water column (H) were below the value of tidal amplitude that was not exceeded during the 95% of the time ($A95$). In SE, this value was $A95 = 2.138$ m and the depth of the water column at ID1 and ID2 was $H_{ID1} = 2.87$ m and $H_{ID2} = 6.28$ m respectively. Both discharges were in subtidal zones so both were acceptable.

Next, the value of AC as the percentage of estuarine area cover per cell was computed by equation (3.14) using GIS techniques (Figure 5.40). Regarding $A_{estuary}$, we defined two boundaries for the SE (the inner and outer). The inner boundary was an industrial weir which limits the end of the tidal influence into the river basin. The outer limit of the estuary has been established based on the breakwaters that channel the entrance to the estuary (Figure 5.40). Taking into account these limits and the meshgrid resolution, $A_{estuary}$ was 2557527.73 m^2.

5.3.6.2 Maximum allowable MZ size (MAS)

In the simplified calculation, the maximum allowable MZ size (MAS) had been defined by expert criteria. MAS did not exceed 10% and 3% of water body extent overall for the AA-MZ and the MAC-MZ respectively (Figure 3.19).

5.3.6.3 Final admissibility (AD)

Lastly, we evaluated the final admissibility of the MZs (AD) as the sum of all the AC values covered by AA-MZ and MAC-MZ by means of equation (3.17). Table 5.8 summarizes the covered area by MZs and the AA-AD and MAC-AD for ID1 and ID2.

Both industrial discharges presented a final admissibility AA-AD and MAC-AD bigger than AA-MAS (10%) and MAC-MAS (3%). Thereby, the extents of the AA-MZ or MAC-MZ were inadmissible for ID1 and ID2, and, consequently, both discharges were classified as large significant moving to the Step 4 of the decision tree in order to continue with the allocation procedure (Figure 3.2).

5.4 Step 4. Intermediate calculation (Dry case of dilution)

Once large significant discharges had been detected (figure 3.2), we started to apply the Step 4 of the decision tree. The proposed intermediate calculation was based on the spatial and temporal variations of the forcing

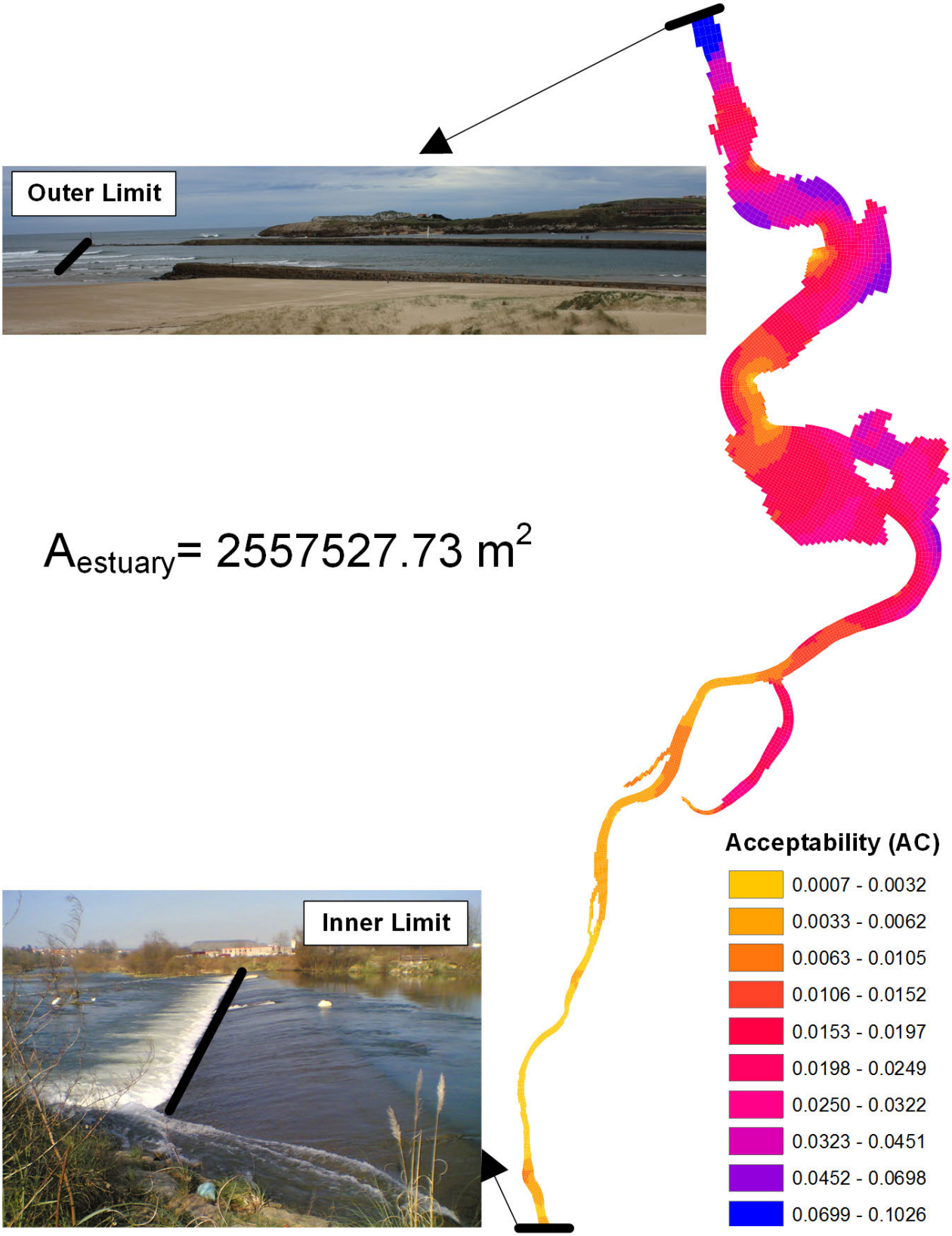

Figure 5.40: Outer and inner limits considered at Suances Estuary, value of $A_{estuary}$ and acceptability (AC) of the grid cells in the meshgrid.

(tide an rivers) during one year. These variations led to significant modifications of the hydrodynamics quantities and, consequently, big differences in the concentration evolution of the toxicants in all regions (near-intermediate- and far-field) were expected.

Step 4 is composed by 6 subsections as illustrated in figure 3.20.

5.4.1 Hydrodynamics

Spatial and temporal evolution of any substance or organism present in the water column in the estuarine environment is subject to know the velocity field at every point of the interest area.

5.4.1.1 Model setup

In the "dry case of dilution", model setup was the same as in the "worst case of dilution" so it was not necessary to conduct additional tasks.

5.4.1.2 Forcing selection

The proposed intermediate calculation was based on the continuous simulation of the driest year considering the 40-year time series of river flow at SE (Figure 5.6a). In order to select this driest year, the mean annual water volume ($MAWV$) was computed for each i-year by equation (3.16).

Figure 5.41 displays the ecdf of $MAWV$ for the 40-year time series. This graph typifies every year as a function of the $MAWV$ in very dry years (0-15%), dry years (15-35%), mean years (35-65%), wet years (65-85%) and very wet years (85-100%).

Next, the minimum value of $MAWV$ was identified as the year 1989. Finally, the time series of river flow and its its associated tidal elevations for this driest year (1989) were extracted from the 40-years time series and used as forcings of the model scenario in the "dry case of dilution". Figure 5.42 shows the time series of river flow (a) and tidal elevations (b) of the year 1989.

5.4.1.3 Hydrodynamic dry case modeling

The hydrodynamic model predicted the surface elevation, current velocity, temperature and salinity fields across the model grid during one year of simulation.

As it was underlined, we ran the model starting several days before the time of interest. According to figures 5.29 and 5.30, the timescale of "quasi-stationary" response was 216 hours (9 days).

Therefore, in the intermediate calculation, we carried on the hydrodynamic simulation assuming 9+365 days of river flow and tidal elevation as forcings. Thus, the first 9 days of model simulations were not taken into account. Once the model stabilization was reached and the influence of initial conditions was avoided, we hourly recorded 365 days of hydrodynamic model results during the year 1989.

5.4.2 Primary or initial dilution (Near-field)

As it was mentioned in Step 3, the buoyant jet behavior depends on Q_{eff}, ϕ, d_{eff}, ρ_{eff}, ρ_{env}, H and u_{env}. The first four variables were attached to the discharge mechanism. Table 5.5 presented the values of these four variables for ID1 and ID2. The remaining variables were related to the environmental conditions. The

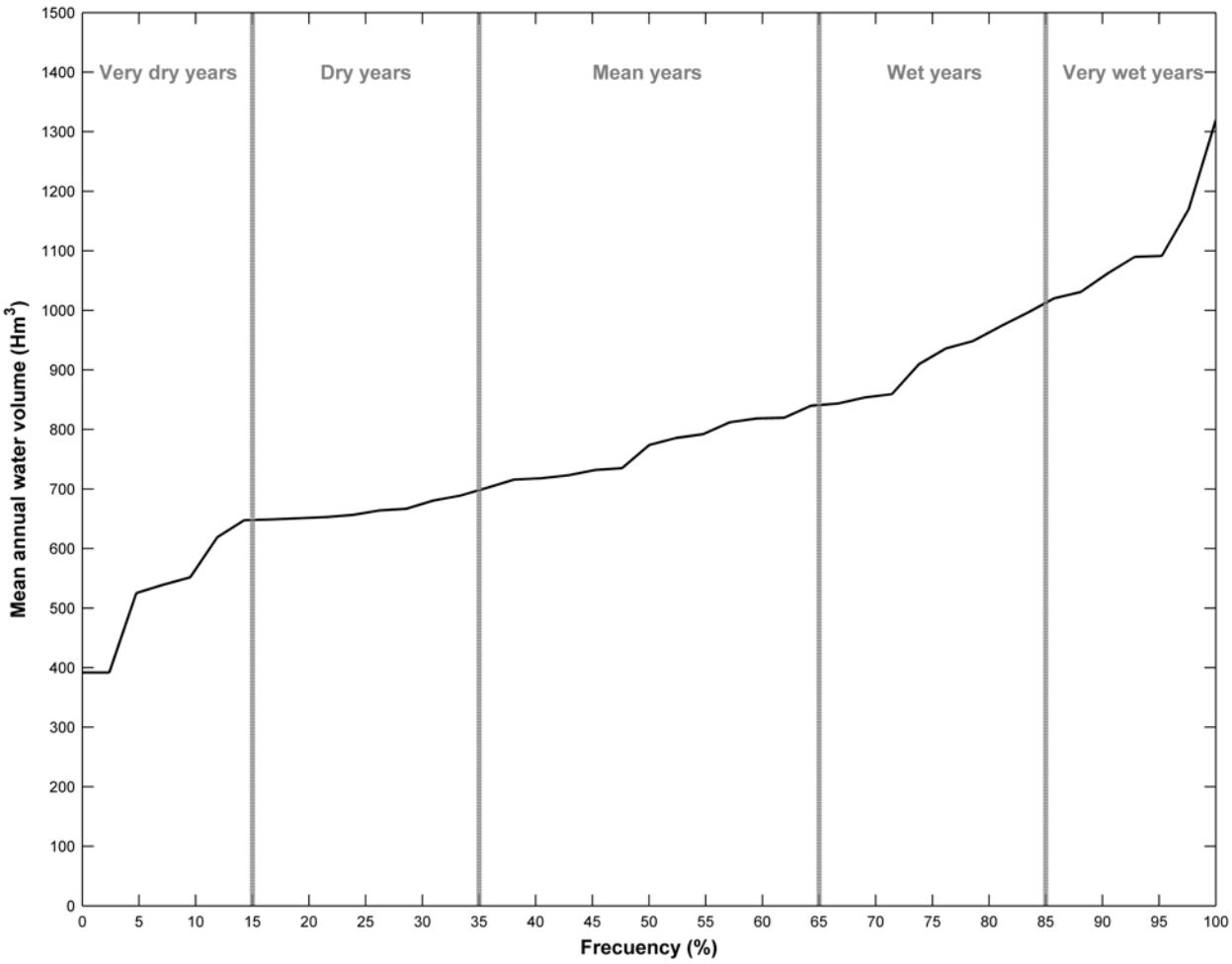

Figure 5.41: Empirical cumulative distribution function of $MAWV$ for the 40-year time series of Saja-Besaya river flow.

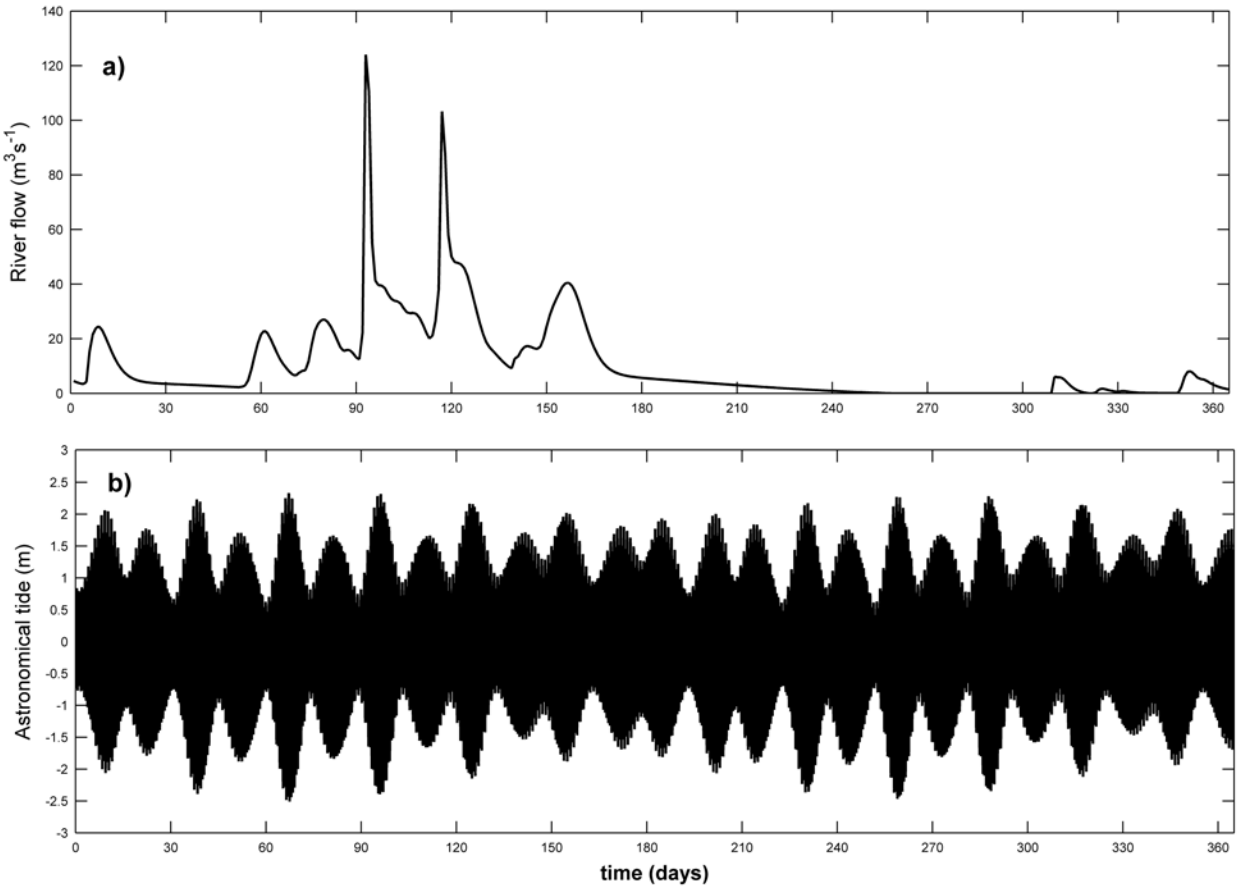

Figure 5.42: Driest year of forcing time series (1989 year). River flow (a) and astronomical tidal wave (b) at Suances Estuary.

primary dilution computations were conducted for every large significant discharge (ID1 and ID2), using the numerical model JETLAG and the same assumptions as in the simplified calculation.

Once all the required data were gathered, we ran the "dry case of dilution" with JETLAG for the significant discharges ID1 and ID2.

Figure 5.43 and 5.44 show the total water depth (a), the magnitude of the environmental velocity (b), the direction of the environmental velocity (c) and the environmental density (d) for the surface layer (blue line) and bottom layer (green line) at the point of discharge during the "dry case of dilution". Moreover, figure 5.31 and 5.44 display the initial dilution (e) of the effluent (black line) and the effluent concentration (f) after the initial dilution (black line). Finally, figure 5.43f also display the AA-EQS (magenta line) and MAQ-EQS (red line) of chloroform ($CHCl_3$) and 5.44f the AA-EQS (magenta line) and MAC-EQS (red line) of lead (Pb).

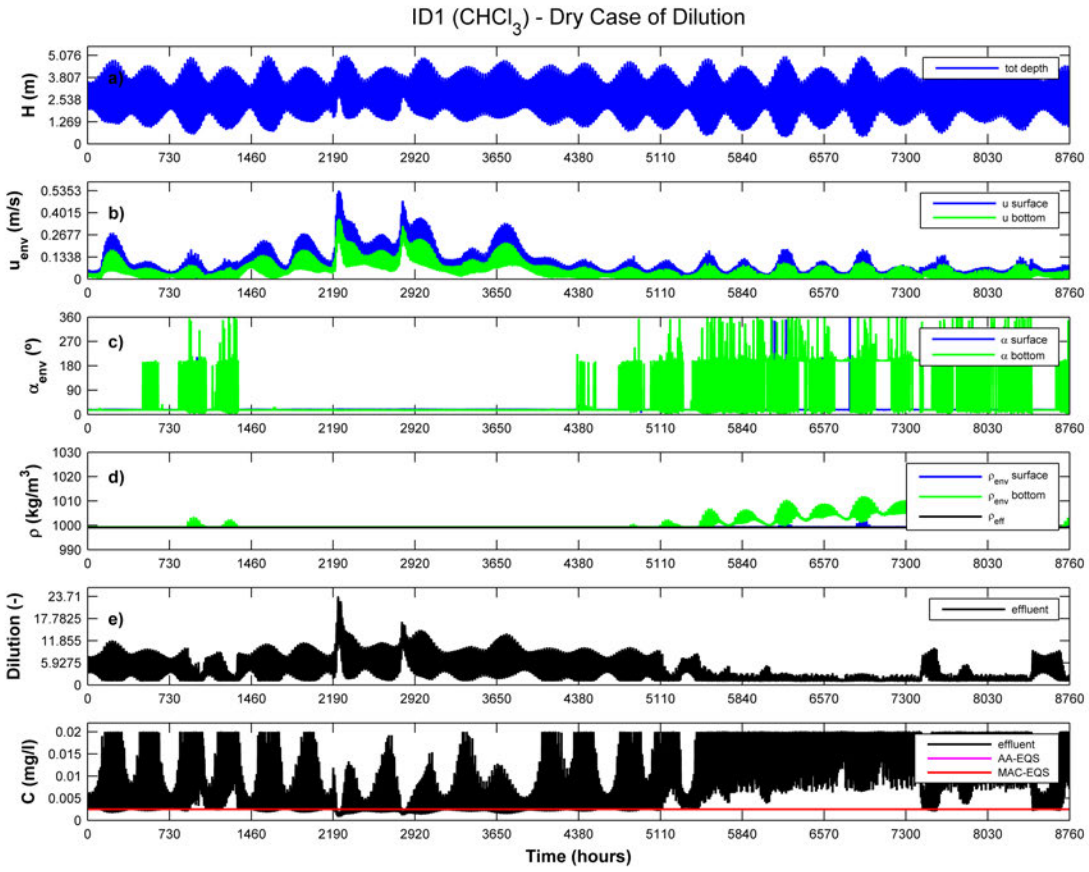

Figure 5.43: Evolution of the total water depth (a), the magnitude of the environmental velocity (b), the direction of the environmental velocity (c) and the environmental density (d) for the surface layer (blue line) and bottom layer (green line), the initial dilution (e) of the effluent (black line) and the effluent concentration (f) after the initial dilution (black line) at ID1 during the "dry case of dilution". Note it is also shown the AA-EQS (magenta line) and MAC-EQS (red line) of chloroform (f).

As it is shown in figure 5.43, ID1 dilution was oscillating between 23.71 and 1 and ID2 dilution between 3356.78 and 4.13due to the changes in the total depth, the environmental velocity and the environmental density. ID1 and ID2 dilution was directly proportional to the river flow time series (see figure 5.42a). Regarding ID1 concentration, the AA-EQS was surpassed most of the time in the "dry case of dilution". In the case of ID2 concentration, the AA-EQS and the MAC-EQS were surpassed most of the time in the "dry case of dilution".

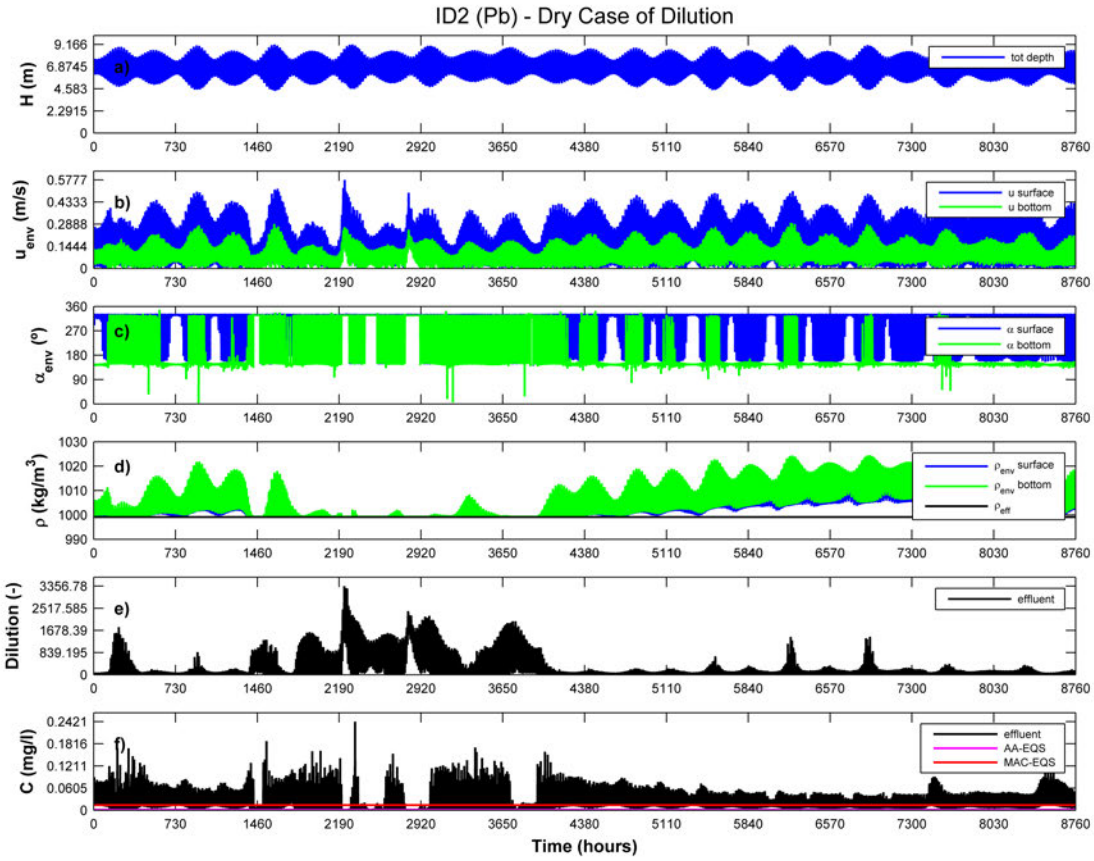

Figure 5.44: Evolution of the total water depth (a), the magnitude of the environmental velocity (b), the direction of the environmental velocity (c) and the environmental density (d) for the surface layer (blue line) and bottom layer (green line), the initial dilution (e) of the effluent (black line) and the effluent concentration (f) after the initial dilution (black line) at ID2 during the "dry case of dilution". Note it is also shown the AA-EQS (magenta line) and MAC-EQS (red line) of chloroform (f).

As an example of the trajectory described by ID1 and ID2 in the near-field region, figures 5.45 and 5.46 present one snapshot of the buoyant jet (ID1 and ID2) calculated in the "dry case of dilution" for the hour 3661 (see figures 5.43 and 5.44) respectively. In both figures, the evolution of the 3D buoyant jet are shown on a 3D view (a), plan view (b) and side view (c). Moreover, the single-port pipe is represented with a black line (side and plan views) and the free surface with a blue line (side view) or a blue rectangle (3D and plan views).

As it can be seen in figure 5.45, the ID1 jet was fully mixed in the water column due to the lack of water depth and the magnitude of the effluent flow. It is also bent towards the river flow direction due to its closeness. In the case of ID2, figure 5.46 shows that the ID2 jet rose until collide with the free surface due to buoyancy (density gradient between effluent and ambient water). It was also bent to the river flow direction because of the direction of the environmental velocity.

5.4.3 Coupling primary and secondary dilution (Intermediate-field)

Once all the required information was collected, we applied the describe method to the large significant discharges ID1 and ID2 for the "dry case of dilution".

Figures 5.47 and 5.48 present the percentage of time that ID1 and ID2 are in different horizontal grid cells (left panel) and vertical layers (right panel) predicted by JETLAG during the coupling process. In these locations, we introduced ID1 and ID2 as a source term of flow and diluted concentration.

As it is shown in figure 5.47, ID1 coupling was located in several horizontal grids downstream of the discharge point due to the closeness to the river and the momentum of ID1. In the vertical direction, ID1 was fully mixed in the water column most of the time. The rest of the time ID1 was mainly coupled between layers 5 and 9, i.e., between 1 and 3.25 m of depth. As it can be seen in figure 5.48, ID2 was almost always in the grid cell where was located the industrial pipe due to the buoyancy and the relative small discharged flow. Regarding vertical distribution, ID2 was most of the time between layers 4 and 8, i.e., between 2.5 and 6.5 m of depth indicating that ID2 plume was trapped. Moreover, figure 5.48 showed that the plume rose until free surface in the rest of situations.

5.4.4 Secondary or ambient dilution (Far-field): Conservative approach

Finally, in this subsection, the required tasks to conduct the simulation of the significant discharges with D-Water Quality were described.

5.4.4.1 Model setup

In the conservative approach, model setup was the same as in the Step 3 so it is not necessary to conduct additional tasks for calibrating the far-field model.

5.4.4.2 Transport dry case modeling

In order to run the transport of the "dry case of dilution" with D-Water Quality, the previous simulation of Delft3D-FLOW and the initial dilution data from the coupling approach were used. Anew, the time required for stabilizing the model results and the influence of initial conditions on these results were two issues difficult to handle. In order to accomplish these issues, we performed one "presimulation" to obtain the adequate initial condition of toxicant concentration and other "simulation" to record the concentration evolution along 1989.

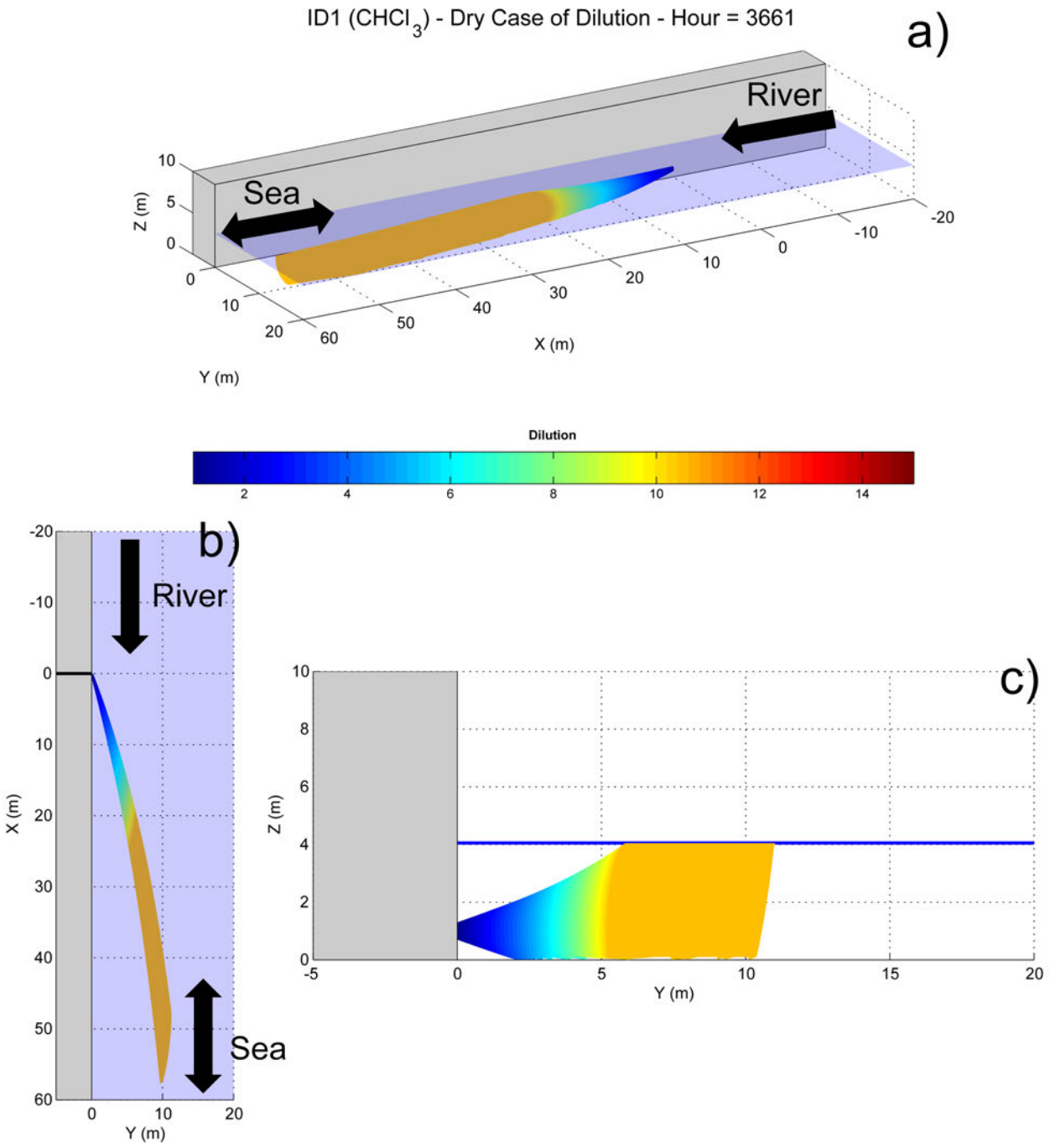

Figure 5.45: 3D buoyant jet of ID1 for the hour 3661 in the intermediate calculation. 3D view (a), plan view (b) and side view (c). The single-port pipe is represented with a black line (side and plan views) and the free surface with a blue line (side view) or a blue rectangle (3D and plan views).

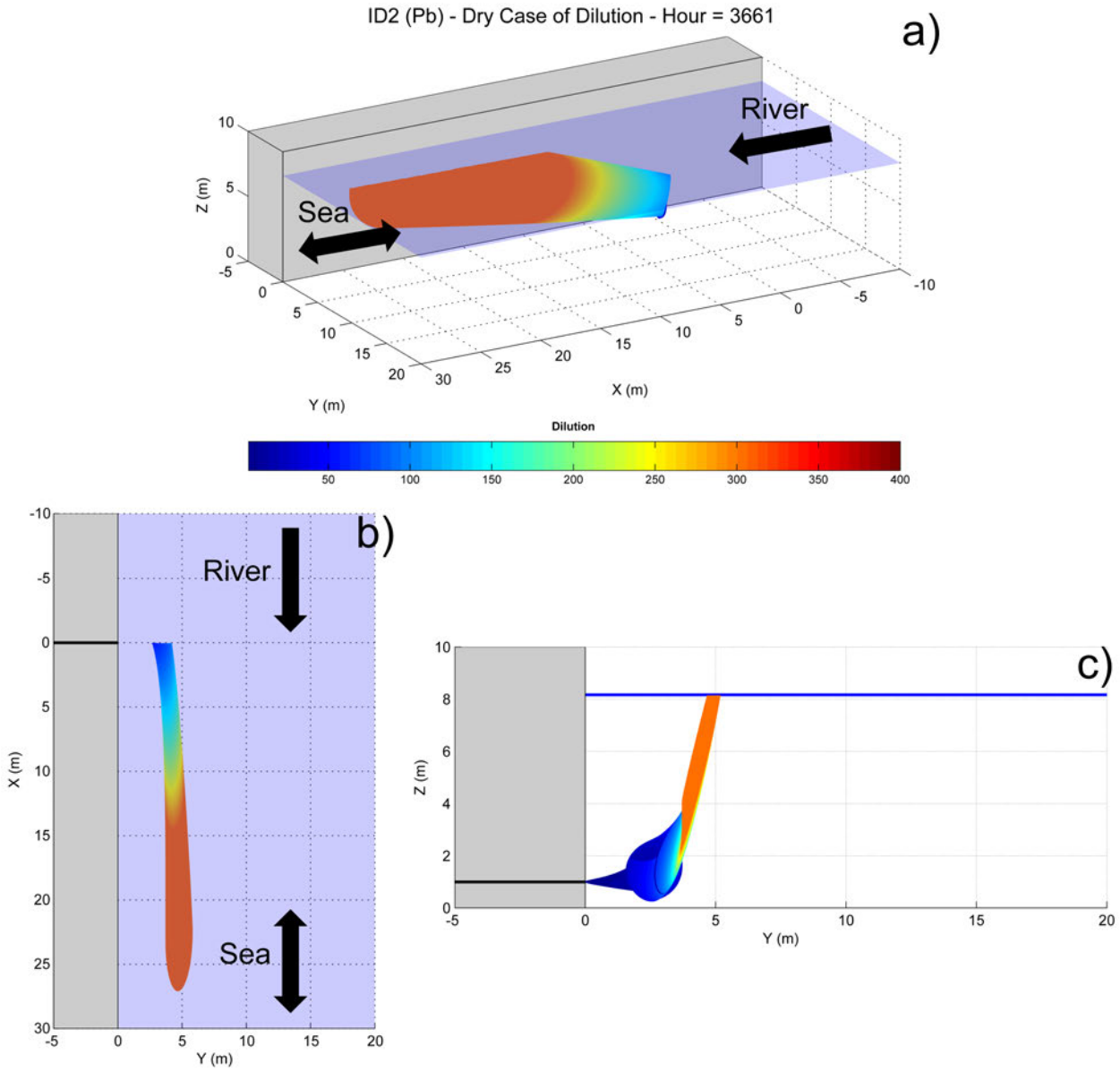

Figure 5.46: 3D buoyant jet of ID2 for the hour 3661 in the intermediate calculation. 3D view (a), plan view (b) and side view (c). The single-port pipe is represented with a black line (side and plan views) and the free surface with a blue line (side view) or a blue rectangle (3D and plan views).

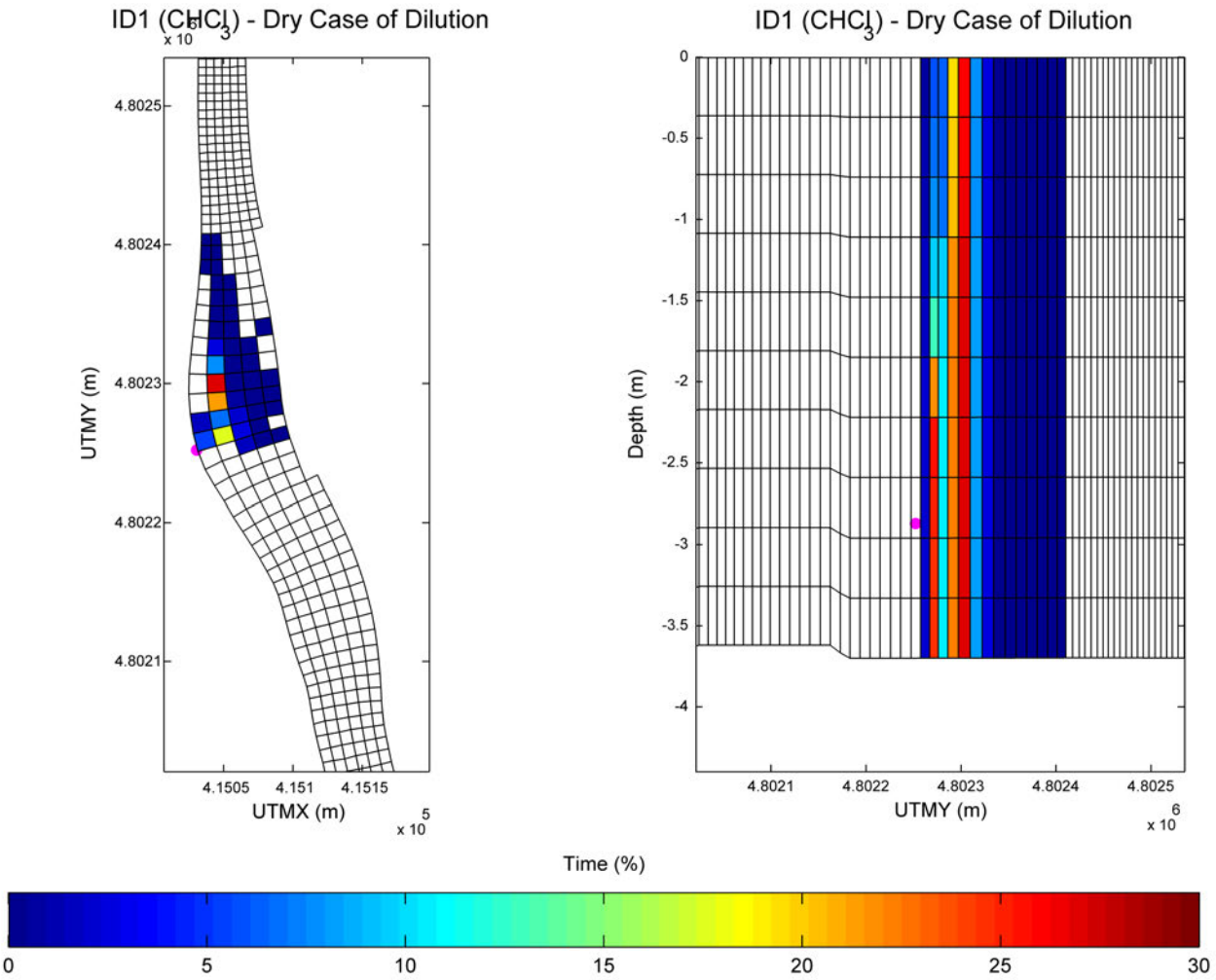

Figure 5.47: Schematic view of the time distribution of horizontal grid cells (left panel) and the vertical layers (right panel) covered by ID1 during the coupling between the primary and secondary dilution in the intermediate calculation.

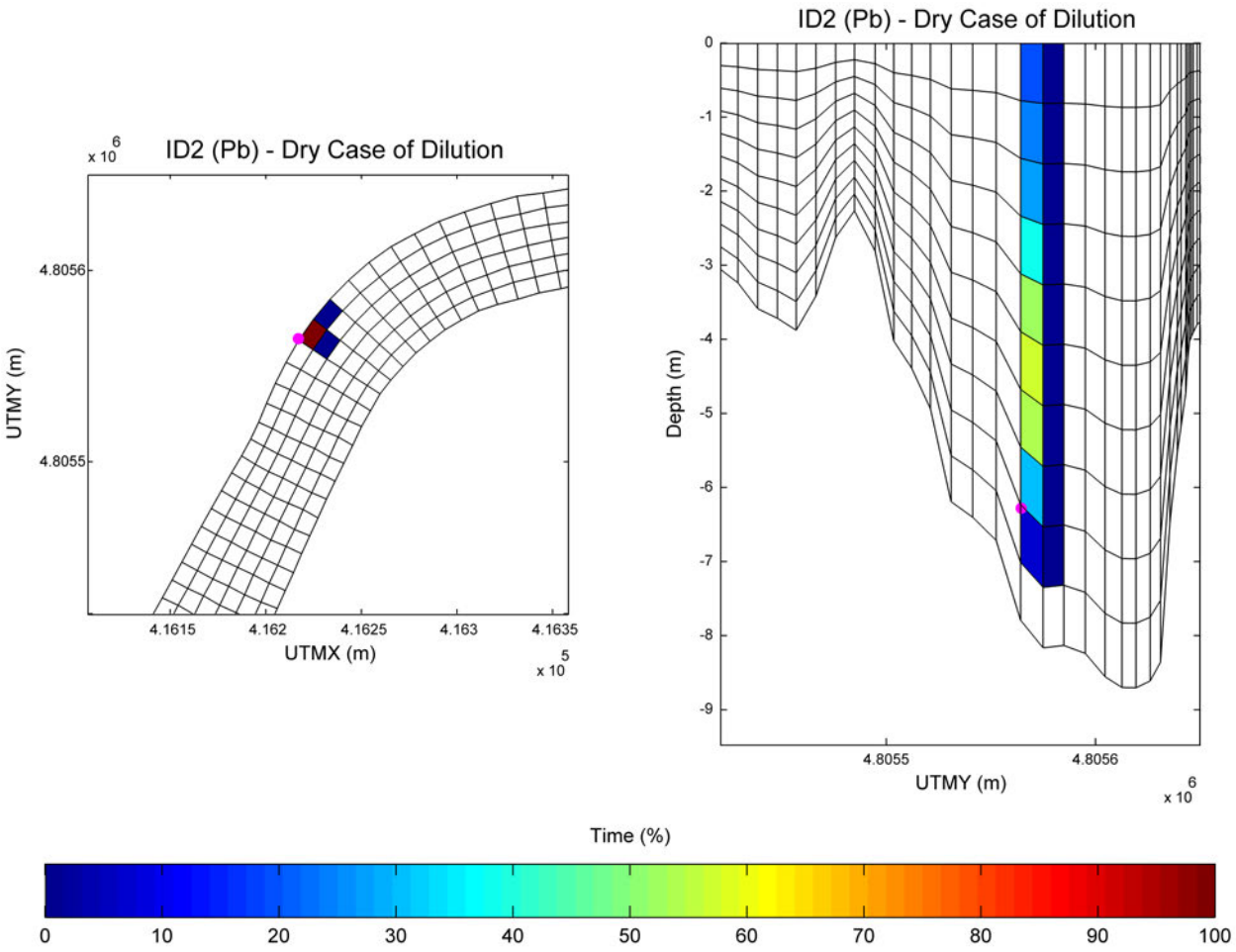

Figure 5.48: Schematic view of the time distribution of horizontal grid cells (left panel) and the vertical layers (right panel) covered by ID2 during the coupling between the primary and secondary dilution in the intermediate calculation.

"Presimulation"

The maximum timescale of the "quasi-stationary" response for transport was the timescale of the "worst case of dilution" being 528 hours (22 days). Thus, this timescale indicates the minimum duration of any far-field "presimulation" to ensure that initial conditions are trustable.

CBs, OBs and ICs were the same defined in the "worst case of dilution".

The "presimulation" was carried out using a constant river flow of the first day of 1989 and its associated tide during 24 hours (see figure 5.49). Next, we ran D-Water Quality for ID1 and ID2 with Delft3D-FLOW results of the first day in a continuous loop during 30 days.

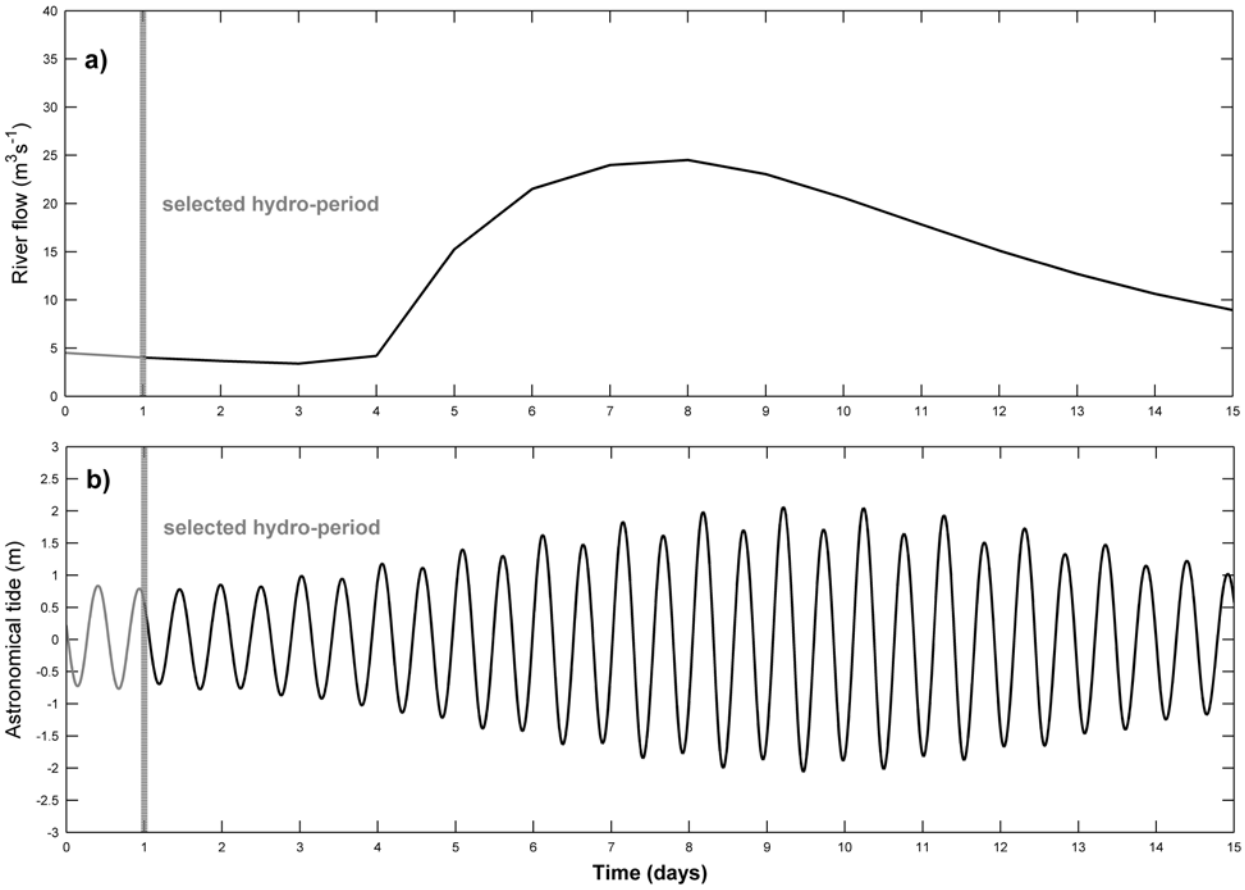

Figure 5.49: Forcing of the first 360 hours of the year 1989 (driest year) and selected hydro-period for the transport of the "presimulation" in the "dry case of dilution".

Once it was reached the "quasi-stationary" response, we recorded the map of toxicant concentration (conservative tracer) that corresponds to the first hour of 1989, i.e, the initial condition for the simulation of the "dry case of dilution" with ID1 and ID2 (see figures 5.50 and 5.51 respectively).

Figures 5.50 and 5.51 display the map of the spatial distribution of chloroform and lead at the surface (a) and bottom (b) used as the initial condition for the "simulation" during the 1989 year respectively.

"Simulation"

CBs and OBs were the same defined in the "presimulation". Meanwhile, IC was a map with the initial toxicant concentration for each discharge (see figures 5.50 and 5.51) obtained in the "presimulation".

We ran the model scenario during the year 1989 and hourly recorded 365 days of transport model results, i.e.,

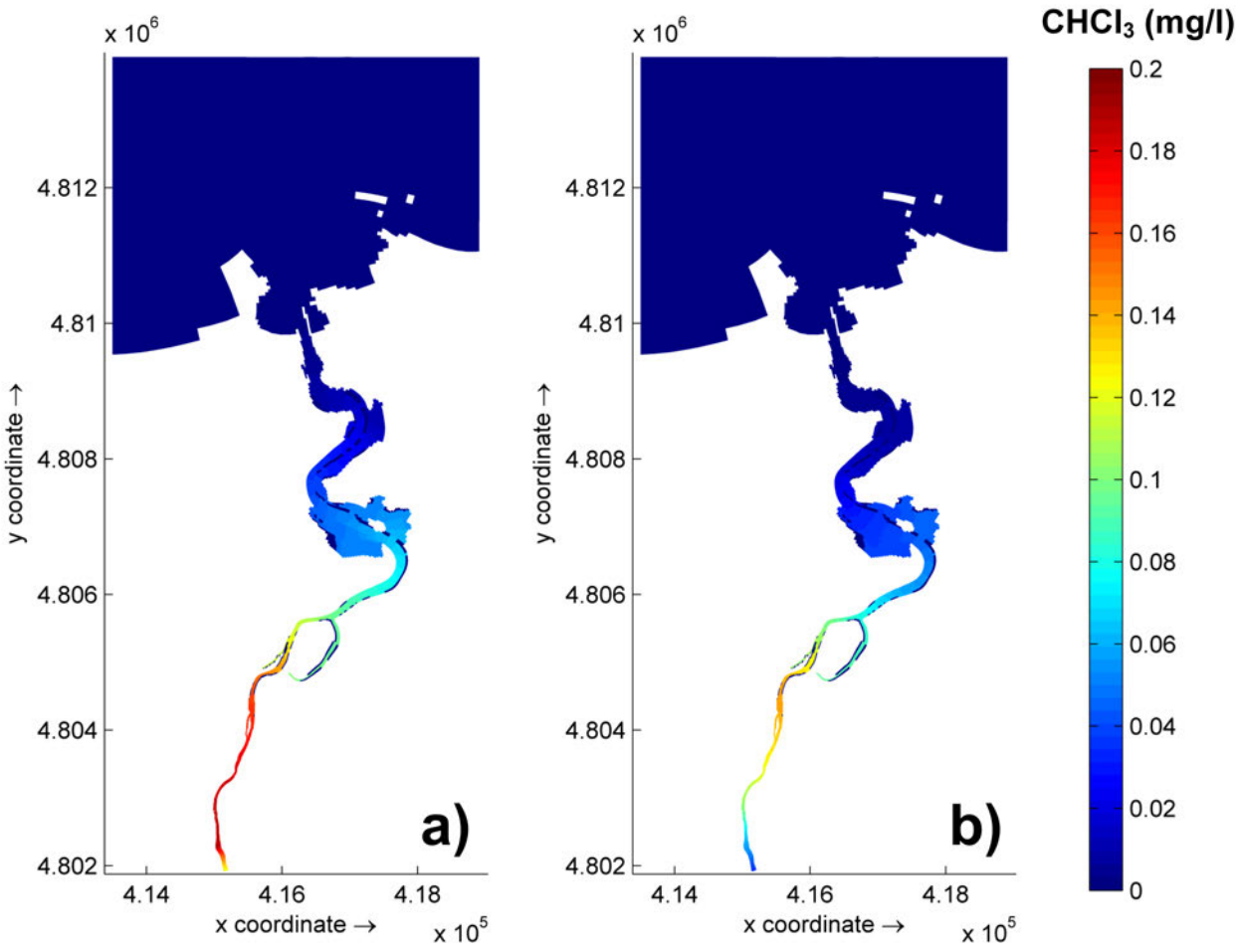

Figure 5.50: Map of the spatial distribution of chloroform used as the initial condition for the "simulation" during the 1989 year ("dry case of dilution" of ID1). Surface layer (a) and bottom layer (b).

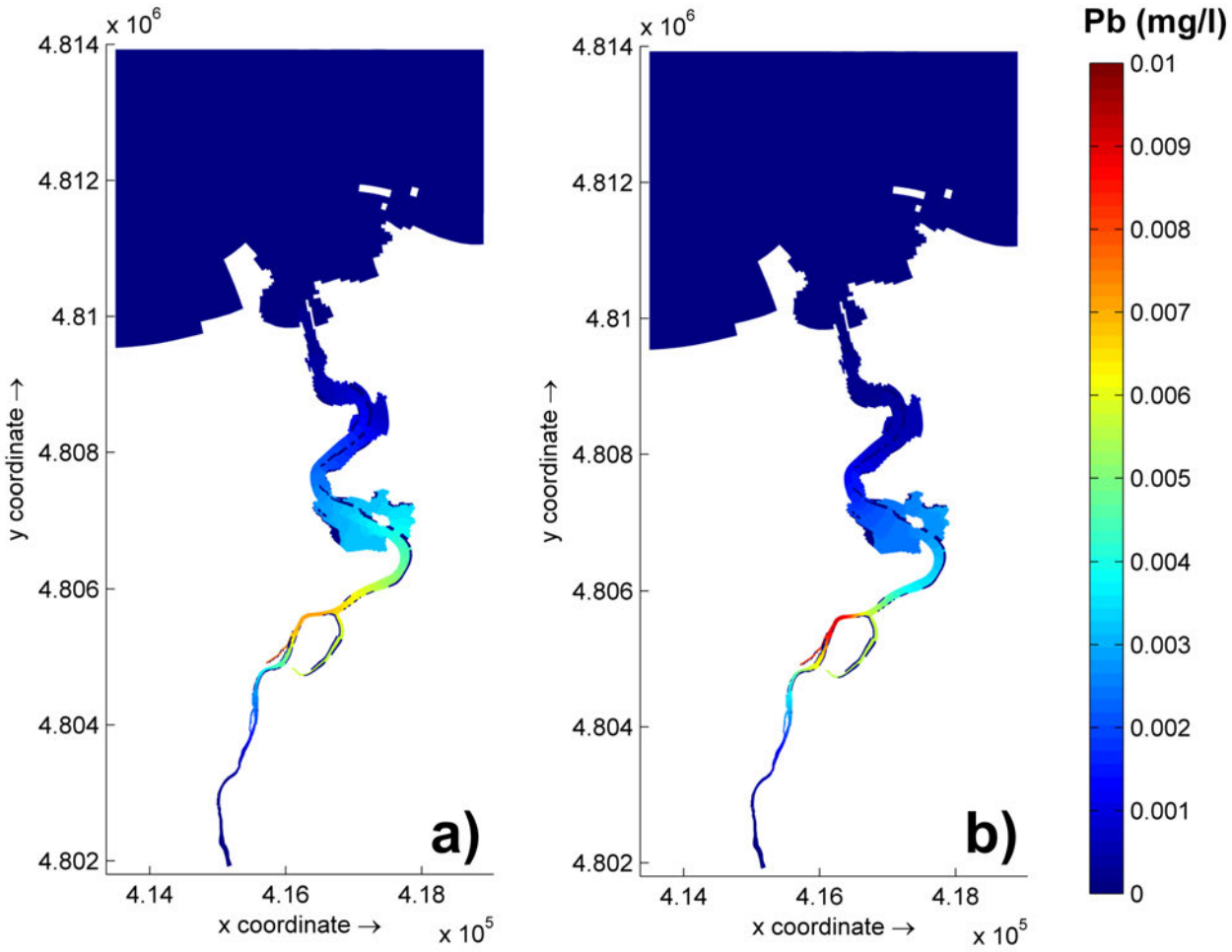

Figure 5.51: Map of the spatial distribution of lead used as the initial condition for the "simulation" during the 1989 year ("dry case of dilution" of ID2). Surface layer (a) and bottom layer (b).

the evolution of the toxicant concentration for ID1 (chloroform) and ID2 (lead) at SE.

Figure 5.52 and 5.53 display the far-field model results for the concentration evolution of ID1 and ID2 in the surface layer (black line) and the bottom layer (grey line) at WQ3 (a), SS1 (b), SS3 (c) and SS5 (d) respectively.

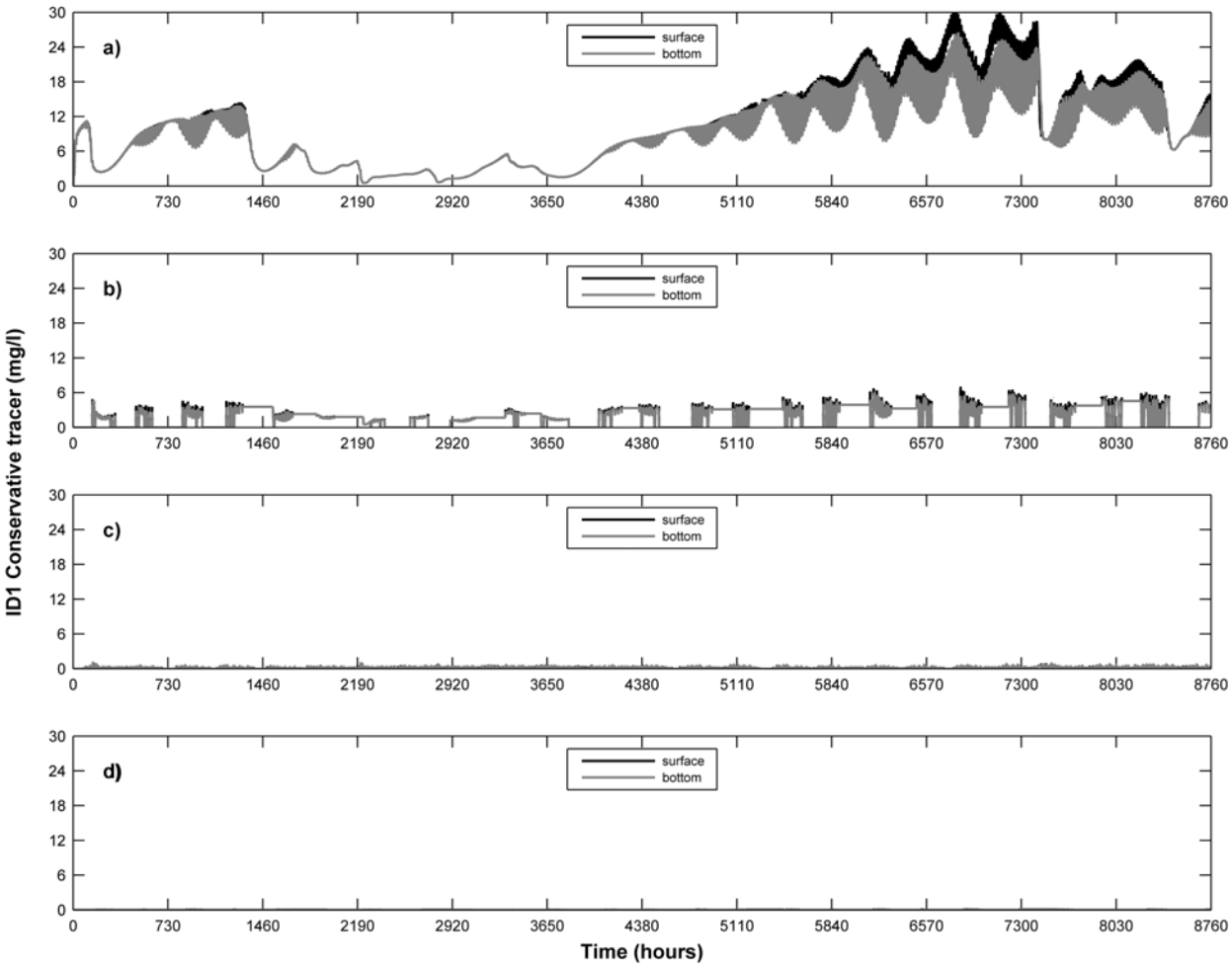

Figure 5.52: Evolution of ID1 concentration at the surface layer (black line) and the bottom layer (grey line) for the transport of the "dry case of dilution" at WQ3 (a), SS1 (b), SS3 (c) and SS5 (d).

5.4.4.3 Delimitation of mixing zones

Unlike the simplified calculation where one model scenario was only run under fixed conditions, in the intermediated calculation we ran one year (1989) under real conditions. After model simulations, we determined the AA-MZ and MAC-MZ by applying the developed method in Chapter 3 (Figure 3.24).

Specification of the annual number of samples

In this method, we followed the Spanish proposal (SPAIN 2014) and specified that the annual number of samples is 12 (one per month). Regarding the sampling period, each sample was measured at any time during every month (random sampling).

Determination of the optimal number of surveys

In this second tier, we firstly generated 10000 random samplings (10000×12 data) from model results along

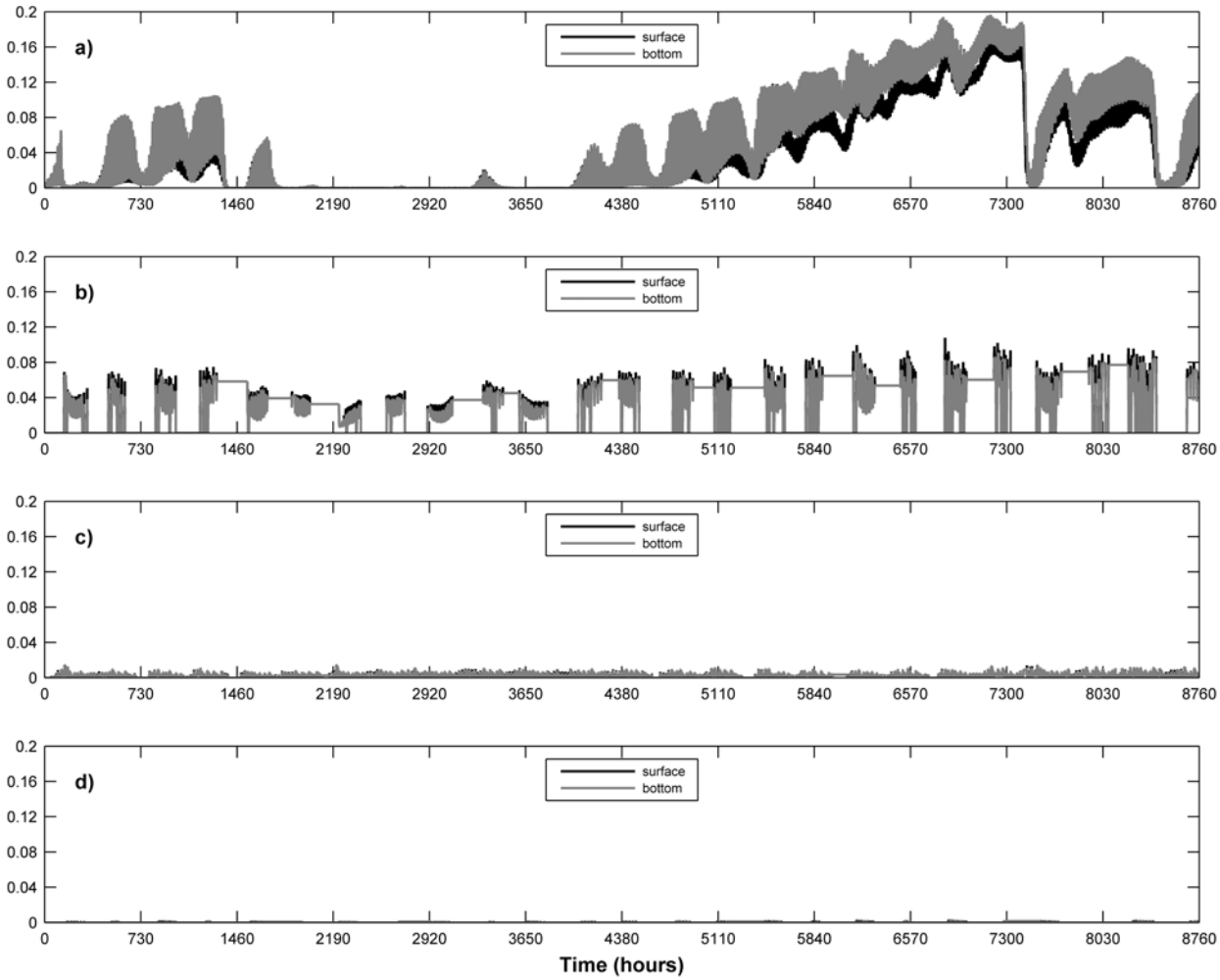

Figure 5.53: Evolution of ID2 concentration at the surface layer (black line) and the bottom layer (grey line) for the transport of the "dry case of dilution" at WQ3 (a), SS1 (b), SS3 (c) and SS5 (d).

the model domain with special attention to the area of the point discharge. These random samplings were performed following the statements made in the first tier.

Next, we evaluated the compliance of EQSs for the 10000 samplings in every control point. For every sampling, AA-EQS requirement was met if the average of the 12 data was below the AA-EQS meanwhile MAC-EQS requirement was met when all data were below the MAC-EQS. After these calculations, we determined the probability of failure for both EQSs in every control point for ID1 and ID2. In order to find the optimal number of surveys, we iteratively averaged the results of the surveys starting with 1 until 10000.

Finally, we plotted the mean probability of failure versus the number of surveys in order to find the optimal number of surveys (k), this was for the MAC-EQS in the case of ID2. Figure 5.54 illustrates, for ID2, the evolution of the mean probability of MAC-failure with the increase of the number of surveys for the MAC-EQS at ID2 (black solid line), WQ3 (light grey solid line), SS1 (black dotted line), SS3 (light grey dotted line) and SS5 (dark grey line) during the "dry case of dilution".

Considering figure 5.54, the optimal number of surveys was the minimum value that ensures the independence on the MAC-failure probability for ID2, i.e, **1000 surveys approximately**.

Final delimitation of MZs

In the intermediate calculation, we obtained 1000-surveys of 12 data that have an occurrence probability equals 1/1000. Therefore, the delimitation of MZs has to take into account the failure probability of the 1000-surveys.

Chronic effects of each toxicant in every grid cell were computed using the equation (3.17) for 1000-surveys. Next, if $CEF{*}^{k}_{i,j} > 1$ then $CEF{*}^{k}_{i,j} = 1$. On the contrary, if $CEF{*}^{k}_{i,j} \leq 1$ then $CEF{*}^{k}_{i,j} = 0$. Finally, the CEF* associated to the 1000-surveys was computed by the equation (3.18).

Acute effects of each toxicant in every grid cell were computed by the fraction of data in adverse conditions using the equation (3.19) for 1000-surveys. Next, if $AEF{*}^{k}_{i,j} > 0$ then $CEF{*}^{k}_{i,j} = 1$. On the contrary, if $AEF{*}^{k}_{i,j} \leq 0$ then $AEF{*}^{k}_{i,j} = 0$. Finally, the AEF* associated to the 1000-surveys was computed by the equation (3.20).

Anew, two MZs were determined (see figure 3.26): the AA-MZ indicates where chronic effects ($CEF{*}_{i,j} > 15$) meanwhile the MAC-MZ indicates the acute effects ($AEF{*}_{i,j} > 4$).

Next, the delimitated AA-MZ and MAC-MZ of the "dry case of dilution" for ID1 (a-b) and ID2 (c-d) are shown in figure 5.55. As it was mentioned in the "worst case of dilution", the chloroform (ID1) has not applicable MAC-EQS value so in this figure the MAC-MZ was only an example of the extent of the MAC-MZ considering as threshold the same value of the AA-EQS.

5.4.5 Admissibility (Acceptability/Extent)

In the "dry case of dilution", we used the same three-tiered method proposed for the "worst case of dilution". In this method, firstly, we evaluated the acceptability (AC), secondly, the maximum allowable MZ size (MAS) and, thirdly, the final admissibility (AD).

Table 5.9 summarizes the covered area by MZs and the AA-AD and MAC-AD taking into account a AA-Failure of 15% and a MAC-Failure of 4% for ID1 and ID2.

As it can be seen in table 5.9, there were not allocatable MZs. This is why we did not plot an abacus as the example shown in figure 3.27. Both industrial discharges presented a final admissibility AA-AD and MAC-AD bigger than AA-MAS (10%) and MAC-MAS (3%). Thereby, the extents of the AA-MZ or MAC-MZ were inadmissible for ID1 and ID2, and, consequently, both discharges were classified as very large

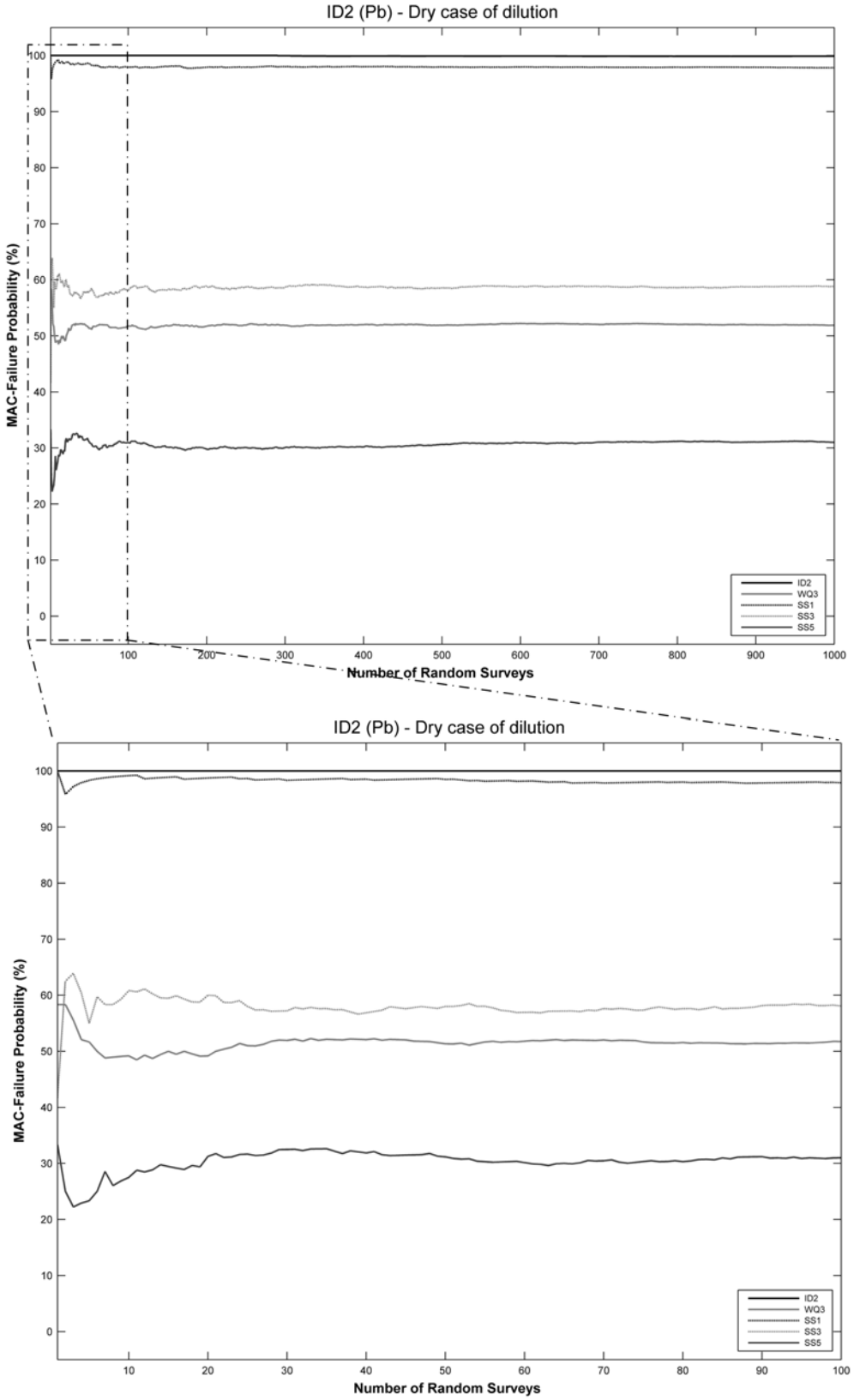

Figure 5.54: Example of the evolution of the mean probability of failure with the increase of the number of surveys for the AA-EQS (black line) and the MAC-EQS (grey line) in one grid cells during a “dry case of dilution”.

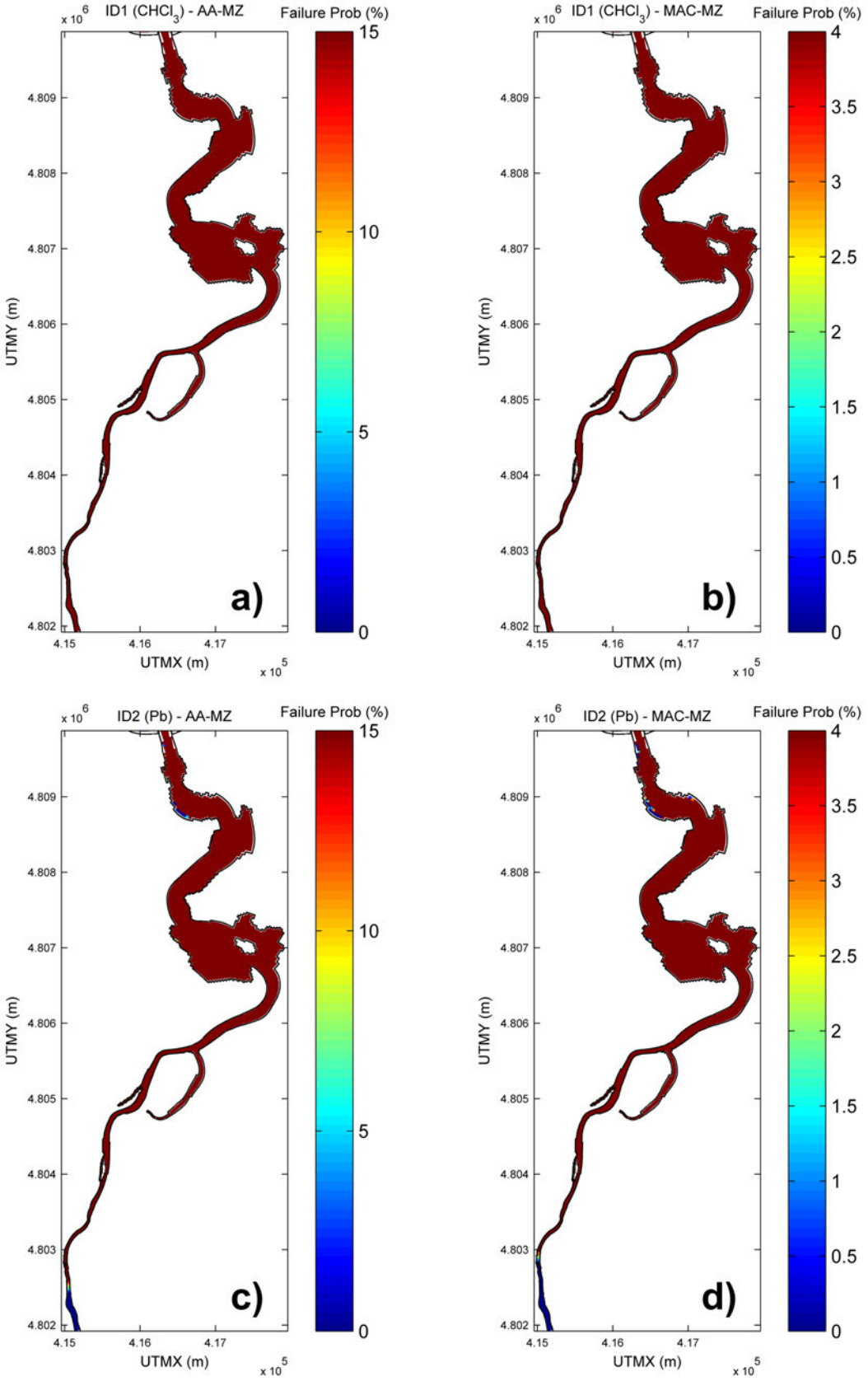

Figure 5.55: Delimitated Mixing Zones in the "dry case of dilution". AA-MZ of ID1 (a), MAC-MZ of ID1 (b), AA-MZ of ID2 (c) and MAC-MZ of ID2 (d).

Name Toxicant	AA-MZ m^2 AA-MAS	AA-AD	MAC-MZ m^2	MAC-AD MAC-MAS
ID1 ($CHCl_3$)	2557527.73	100.0>10	-	-
ID2 (Pb)	2491395.12	97.41>10	2452000.71	95.87>3

Table 5.9: Extent of the delimitated mixing zones (AA-MZ and MAC-MZ) and final admissibility (AA-AD and MAC-AD) in the intermediate calculation for ID1 and ID2.

significant moving to the Step 5 of the decision tree in order to continue with the allocation procedure (Figure 3.2).

5.5 Step 5. Detailed calculation (Real case of dilution)

Once very large significant discharges has been detected, we started to apply the Step 5 of the decision tree. The proposed detailed calculation was based on the spatial and temporal variations of the forcing (tide an rivers) throughout the 40-years time series. These new variations led to new significant modifications of the hydrodynamics quantities and, consequently, big differences in the concentration evolution of the toxicants in all regions were anew expected. Furthermore, physical and chemical dilution were the responsible mechanisms for the toxicant decay in the far-field so toxicant were considered non-conservative tracers in this region. As a consequence, significant variations on the concentration evolution of toxicants were additionally expected.

Step 5 was composed by 6 subsections as illustrated in figure 3.28.

5.5.1 Hydrodynamics

Spatial and temporal evolution of any substance present in the water column in the estuarine environment was subject to know the velocity field at every point of the interest area.

5.5.1.1 Model setup

In the “real case of dilution”, model setup was the same as in the “worst case of dilution” so it was not necessary to conduct additional tasks.

5.5.1.2 Forcing selection/classification

In this subsection, the proposed methodology had been applied to select scenarios of real hydrodynamic forcings at SE.

Methodology to select scenarios of river and tide

The methodology has been divided into several steps: Obtainment of the hydrodynamic forcing data, rearrangement of the input data for clustering, application of the proposed clustering approach, and sensitivity analyses for the forcing and modeling. An explanatory sketch of the methodology was shown in figure 3.30 and was applied in detail in the following paragraphs.

Hydrodynamic forcing data

Hydrodynamic forcing data were the time series of river flow (Q, figure 5.6a) and astronomical tidal level (A, figure 5.6b). From the astronomical tide series, we calculated the “astronomic tidal range period” as the

difference between the minimum and the maximum value of the astronomical tide series for 24 h in order to calculate the "daily tidal range series" (TR, figure 5.6c).

Data rearrangement for clustering

In order to select representative short-time series (clusters) from the 40 years record of Q and A in the SE, we firstly determined the number of days of the clusters. This length is attached to the timescales governing the Q and A signal (Figure 5.6).

SE presented a semi-diurnal tidal signal with typical spring-neap cycle of about 15 days. Additionally, the Saja-Besaya river basin was located in the northern Spanish coast where Cantabric Sea determined the climate (Figure 5.2). Therefore, the river flow signal did not present longer dry or wet periods. In addition, the dP of the Saja-Besaya river basin is 15.32 days taking into account the 40 years of daily flow series at the head of the SE.

Both forcings, Q and A, present timescales in the range of a fortnight in the SE, therefore the forcing scenarios should present a time length of 15 days as well. We rearranged the long-term series of Q and A in sequences of 15 days in order to build the matrix (database) used for clustering. In the case of Q, the first row of the matrix was composed by the 15 first data (days) of the time series, the second row was defined from the day 2 until the day 16 and so on until the end of the time series. In the case of A, the 15-minutal astronomical tide series was used to extract the daily tidal range series (Figure 5.6c). This transformation allowed having the same number of elements for clustering both forcings.

After all these rearrangements, the database was composed by two matrixes of 14610×15 elements (Q and TR). The clustering approach was conducted separately because Q and A are independent and random events.

Sensitivity analyses for explaining the forcing variability

Following the proposed methodological steps (shown in figure 3.30), we conducted a sensitivity analysis for both forcings, increasing the number of clusters to be classified by the KMA, in order to reconstruct the "synthetic series" (time series from sequential clusters) and compare them with the "real series" (time series from databases). Figure 5.56 shows the error of each comparison using the CE formulation. In this figure, the black line corresponds to the tidal range (TR) and the black line with squared markers to the river flow (Q).

Regarding the TR, the minimum number of clusters for explaining the forcing variability M_{mf} was 4 (CE$_f$=0.6149) and the optimal number of clusters M_{of} was 12 (CE$_f$=0.8164). Each cluster was composed by 15 days, so the 40-years variability of the astronomical tide could be explained conveniently (good) with only 60 days (0.1643 years) and excellently with 180 days (0.4931 years). For the Q, the M_{mf} was 7 (CE$_f$=0.6138) and the M_{of} was 35 (CE$_f$=0.8075). In this case, the 40-years variability of the river flow could be explained conveniently (good) with only 105 days (0.2876 years) and excellently with 525 days (1.4383 years).

Sensitivity analyses for running numerical models

The initial database and the M clusters were the same classified in the previous section. In addition, we used the formulation given by Bárcena *et al.* (2012a) to determine the water levels (WL) with the "synthetic" and "real series" at TG1, TG2 and WQ2. This formulation provided hourly WL based on the daily river flows (Q) and the daily astronomical tidal amplitude ($TR/2$):

$$WL = aQ^2 + b(TR/2)^2 + cQ(TR/2) + d(TR/2) + eQ + f \tag{5.5}$$

where a to f were the fitting coefficients determined by means of a method based on Least Squares. The coefficients of the fitting functions ($a - f$) and the regression coefficients (R^2) at TG1, TG2 and WQ2 are displayed in table 5.10.

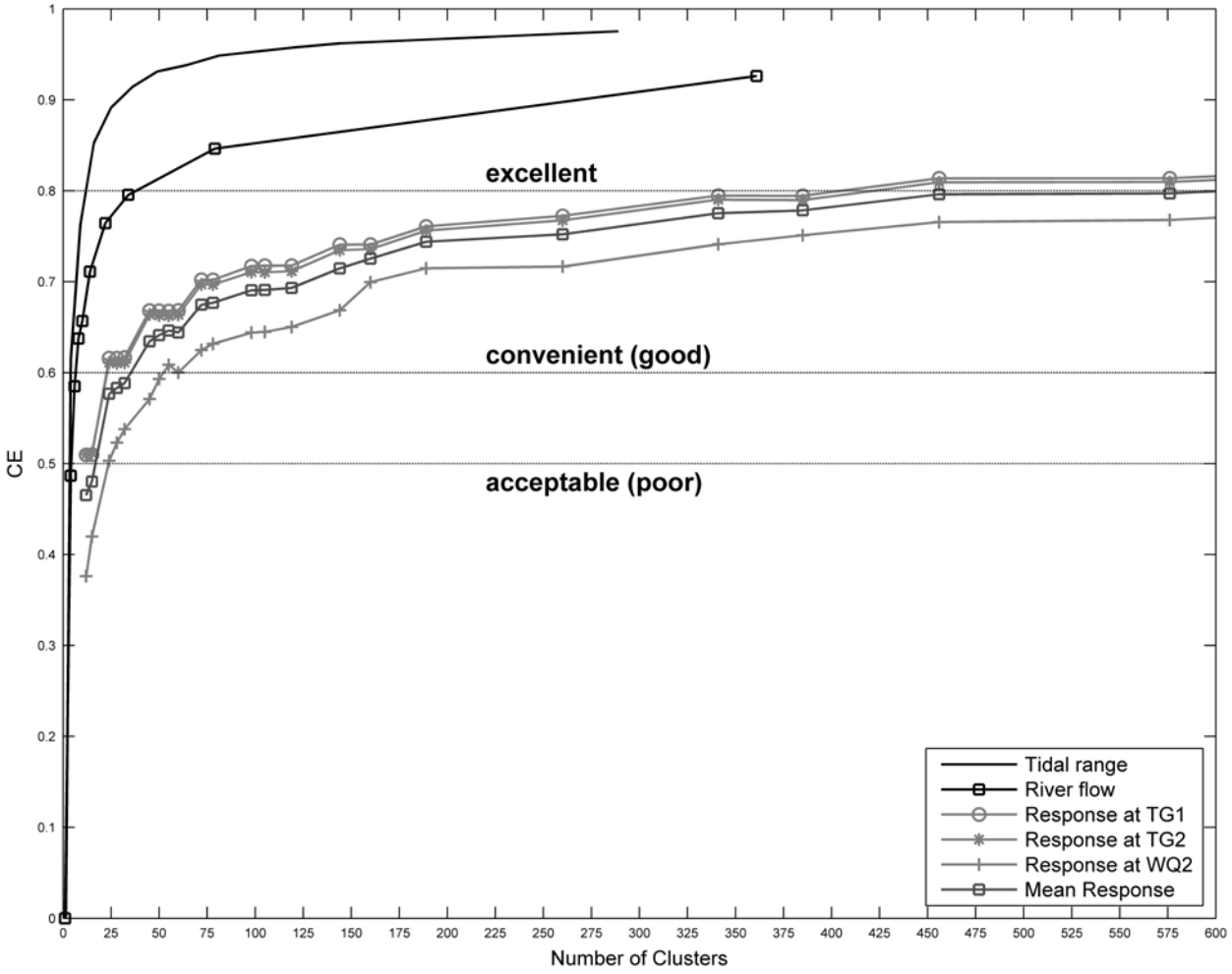

Figure 5.56: Sensitivity analyses for explaining the forcing variability (tidal range and river flow) and for running numerical models (Response at TG1, TG2 and WQ2 and Mean Response). The black line corresponds to the tidal range, the black line with squared markers to the river flow, the light grey line with round markers to TG1 (lower estuary), the light grey line with asterisk markers to TG2 (middle estuary), the light grey line with crossed markers to WQ2 (upper estuary) and the dark grey line with squared markers to the mean response of all the locations.

Hour	a	b	c	d	e	f	R^2
TG1							
1	-3.164E-02	5.299E-04	4.313E-07	9.368E-01	-2.695E-02	-9.099E-05	0.9898
2	-2.460E-02	4.634E-04	9.358E-07	5.835E-01	-1.686E-02	-3.821E-05	0.9905
3	-1.485E-02	4.007E-04	1.333E-06	8.402E-02	8.954E-03	1.004E-04	0.9959
4	5.859E-02	4.243E-04	1.696E-06	-5.858E-01	1.145E-01	2.114E-04	0.9571
5	1.314E-01	-5.555E-04	4.062E-06	-1.105E+00	1.904E-01	5.550E-04	0.9548
6	1.442E-01	-8.194E-04	4.125E-06	-1.291E+00	1.817E-01	9.099E-04	0.9901
7	1.201E-01	-1.108E-03	4.196E-06	-1.102E+00	9.829E-02	1.002E-03	0.9924
8	5.681E-02	-5.727E-04	3.060E-06	-6.275E-01	2.252E-02	5.053E-04	0.9904
9	1.639E-02	3.711E-04	9.036E-07	-8.854E-02	-1.003E-02	7.399E-05	0.9922
10	3.862E-03	6.749E-04	-2.166E-07	4.224E-01	-2.266E-02	5.084E-05	0.9906
11	-1.289E-02	7.567E-04	-5.494E-07	8.229E-01	-2.163E-02	3.756E-05	0.9898
12	-2.992E-02	6.642E-04	-1.320E-07	1.026E+00	-2.389E-02	-7.554E-05	0.9896
TG2							
1	-3.353E-02	1.572E-03	1.876E-06	9.570E-01	-2.591E-02	-4.260E-04	0.9901
2	-2.521E-02	1.567E-03	2.439E-06	6.311E-01	-1.852E-02	-2.674E-04	0.9926
3	-3.411E-02	1.792E-03	2.428E-06	1.861E-01	4.904E-03	-1.517E-05	0.9981
4	2.102E-02	1.986E-03	2.606E-06	-4.280E-01	1.094E-01	2.126E-04	0.9911
5	7.474E-02	1.408E-03	4.428E-06	-9.400E-01	2.053E-01	5.235E-04	0.9688
6	7.419E-02	1.388E-03	4.271E-06	-1.175E+00	2.137E-01	9.359E-04	0.9910
7	1.261E-01	1.027E-03	4.225E-06	-1.218E+00	1.799E-01	1.282E-03	0.9967
8	9.093E-02	-9.176E-06	5.802E-06	-7.434E-01	3.251E-02	1.150E-03	0.9952
9	2.684E-02	1.352E-03	2.425E-06	-1.735E-01	-3.372E-02	3.903E-04	0.9946
10	1.540E-03	2.158E-03	2.538E-07	3.351E-01	-3.797E-02	-8.491E-05	0.9937
11	-1.501E-03	2.068E-03	1.413E-07	7.215E-01	-1.167E-02	-2.096E-04	0.9900
12	-2.656E-02	1.758E-03	1.107E-06	9.888E-01	-1.411E-02	-4.268E-04	0.9894
WQ2							
1	-4.707E-03	6.891E-03	1.291E-06	9.499E-01	-1.967E-02	-1.147E-03	0.9949
2	1.473E-03	7.262E-03	8.179E-07	6.670E-01	-1.984E-02	-8.205E-04	0.9975
3	-2.419E-02	8.260E-03	-1.056E-06	2.707E-01	-4.288E-03	-3.552E-04	0.9995
4	-5.337E-02	9.944E-03	-4.583E-06	-1.916E-01	4.997E-02	1.438E-04	0.9996
5	-3.085E-02	1.148E-02	-7.416E-06	-7.168E-01	1.751E-01	4.171E-04	0.9956
6	-9.446E-02	1.339E-02	-1.185E-05	-9.381E-01	1.998E-01	7.866E-04	0.9965
7	-6.501E-02	1.440E-02	-1.471E-05	-1.089E+00	2.149E-01	1.093E-03	0.9964
8	2.730E-02	1.326E-02	-1.332E-05	-9.552E-01	1.371E-01	1.365E-03	0.9955
9	9.862E-03	1.021E-02	-7.051E-06	-3.049E-01	-3.482E-02	9.893E-04	0.9966
10	4.040E-03	8.227E-03	-1.891E-06	2.594E-01	-4.891E-02	-1.443E-04	0.9994
11	1.629E-02	7.570E-03	-3.942E-07	6.429E-01	-3.992E-03	-8.139E-04	0.9969
12	2.697E-03	6.956E-03	1.066E-06	9.337E-01	-5.889E-04	-1.193E-03	0.9942

Table 5.10: Coefficients of the forcing functions to calculate water levels (a, b, c, d, e and f) and the regression coefficients (R^2) at TG1, TG2 and WQ2.

Forcing CE	NClusters Tide	NClusters River
0.5	3	4
0.52	3	5
0.57	4	6
0.6	4	7
0.63	4	8
0.64	5	9
0.65	5	10
0.67	5	11
0.68	5	12
0.69	6	12
0.7	6	13
0.71	7	14
0.72	7	15
0.73	7	17
0.74	8	18
0.75	8	20
0.76	9	21
0.78	10	26
0.79	11	31
0.8	11	35
0.81	12	38
0.82	12	48
0.83	14	59
0.84	15	71
0.85	16	83
0.86	18	92
0.87	21	106
0.88	23	136
0.89	26	192
0.9	29	225

Table 5.11: Number of tidal and river clusters necessary to reach a determined model efficiency (CE) according to the sensitivity analysis for explaining the forcing variability at Suances Estuary. Each row represents every iterative step conducted during the sensitivity analysis for running numerical models.

Following the methodology (shown in figure 3.30), we carried out a sensitivity analysis increasing the number of clusters of Q and TR according to an increase of 0.01 on their CE_f values (starting at CE_f=0.5). The number of clusters used in every iterative KMA classification are displayed in table 5.11. When CE_r at TG1, TG2 and WQ2 is higher than 0.6, the M_{mm} is reached. The iterative procedure finishes when the average of CE_r at TG1, TG2 and WQ2 is higher than 0.8, being the M_{om}.

Figure 5.56 also shows the CE of the response (water levels) at TG1, TG2 and WQ2 for every iterative step (see table 5.11). In the figure 5.56, the light grey line with round markers corresponded to TG1 (lower estuary), the light grey line with asterisk markers to TG2 (middle estuary), the light grey line with crossed markers to WQ2 (upper estuary) and the dark grey line with squared markers to the mean response of all the locations.

Regarding WL, the minimum number of clusters for running numerical models was attached to the worst response, this was WQ2, equals 5×11=55 groups (CE_r=0.6149) and the optimal number of clusters M_{om} was the average of all the locations, giving a number of clusters equals 12×48=576 (CE_r=0.8164). Therefore, the

numerical modeling of hydrodynamic and transport processes might be ran conveniently (good) with only 825 days (2.2602 years) and excellently with 8640 days (23.6712 years) according to the sensitivity analysis of the predictand, i.e, the quality indicator of the clustering.

Finally, we show the M_{mm} of TR, WL and Q in figures 5.57, 5.58 and 5.59 respectively. Meanwhile, the M_{om} of TR, WL and Q are displayed in figures 5.60, 5.61 and 5.62 respectively. In all these figures, the title of every subplot was displaying the frequency (f) of the cluster in percentage (%). Furthermore, the subplots were sorted in descending order, starting in the top-left corner to the right.

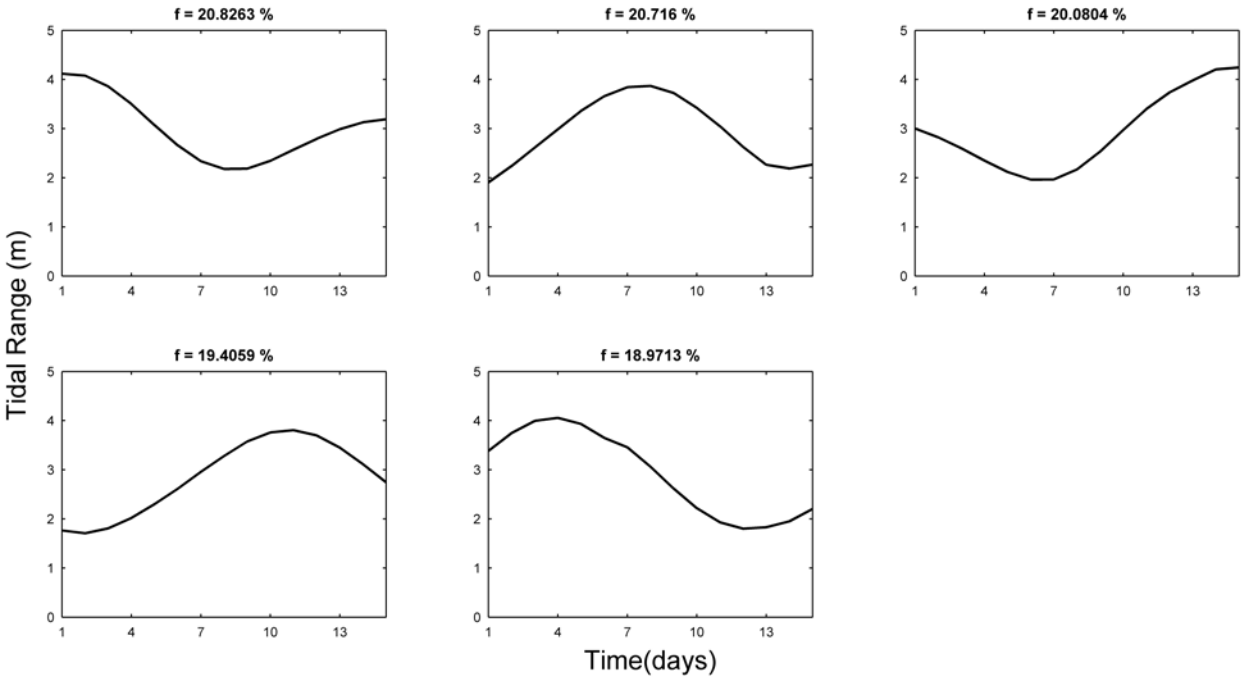

Figure 5.57: Minimum number of final classified clusters M_{mm} for tidal range at Suances Estuary where f is the frequency of the cluster in percentage (%).

In terms of TR clustering (Figures 5.57, 5.58, 5.60 and 5.61), the proposed KMA classified the tidal signal quite reasonably. This KMA differentiated between groups starting at neap, spring, or medium tide periods. It also differentiated the 15 days of the TR and WL magnitudes with groups showing lower or higher values and the tidal evolution with groups beginning with an increase and ending with a decrease or vice versa. In addition, the frequency of every group was quite similar, in the case of 5 groups (M_{mm}, figures 5.57 and 5.58,) the values were ranging between 18.9 and 20.8% while for 12 groups (M_{om}, figures 5.60 and 5.61) between 6.9 and 10.3%. These frequencies were indicative about the continuous and deterministic modulation of the tidal signal between neap and spring tides.

In terms of Q clustering (Figures 5.59 and 5.62), the proposed KMA also classified the river flow signal quite reasonably. This KMA differentiated between dry periods, quasi-steady periods and flood events. It also differentiated the peak of floods events with groups showing lower or higher values and the locations of these peaks along the 15 days with groups displaying peaks in any day. Unlike the tide, the frequency of each group was very dissimilar, in the case of 11 groups (M_{mm}, figure 5.59) the values were ranging between 64.9 and 0.7% while for 48 groups (M_{om}, figure 5.62) between 41.4 and 0.01%. The highest values of frequency corresponded to dry periods, the medium values to quasi-steady periods and the lower values to flood events. These differences on the frequencies were indicative about the high variability on the river flow signal, especially on the flood events. From figures 5.59 and 5.62, we could say that the higher the number of clusters, the better was characterized the different shapes of the flood events.

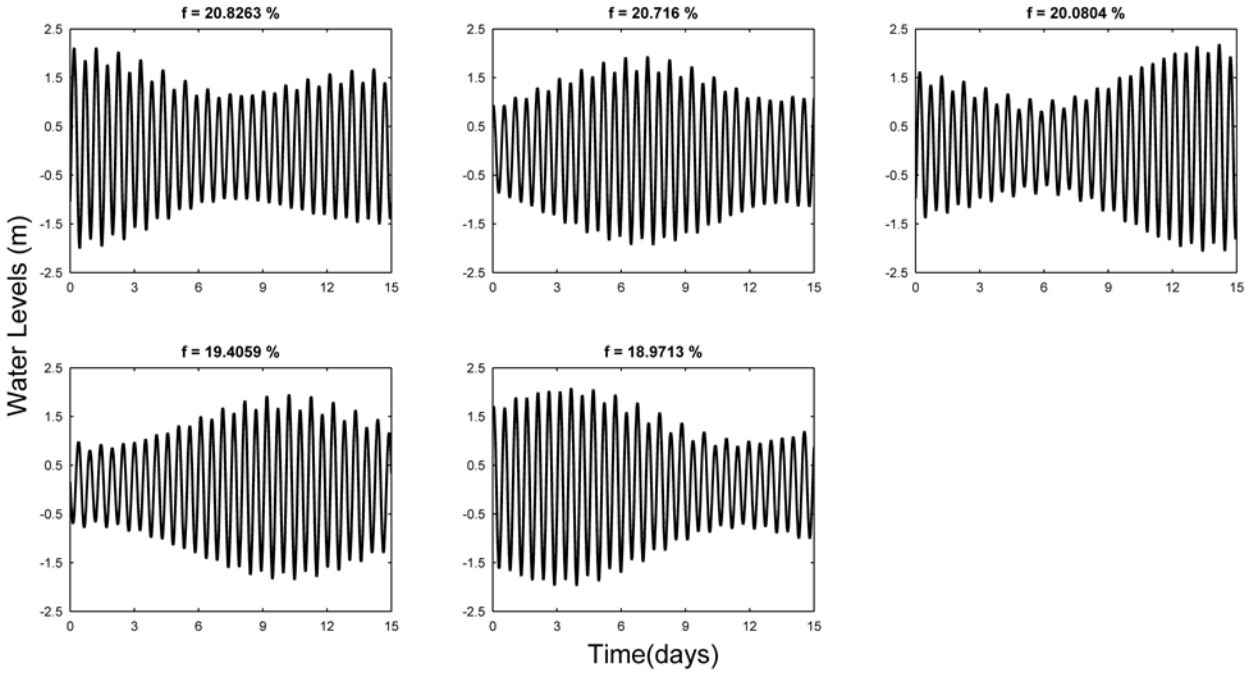

Figure 5.58: Minimum number of final classified clusters M_{mm} for water levels at Suances Estuary attached to tidal range where f is the frequency of the cluster in percentage (%).

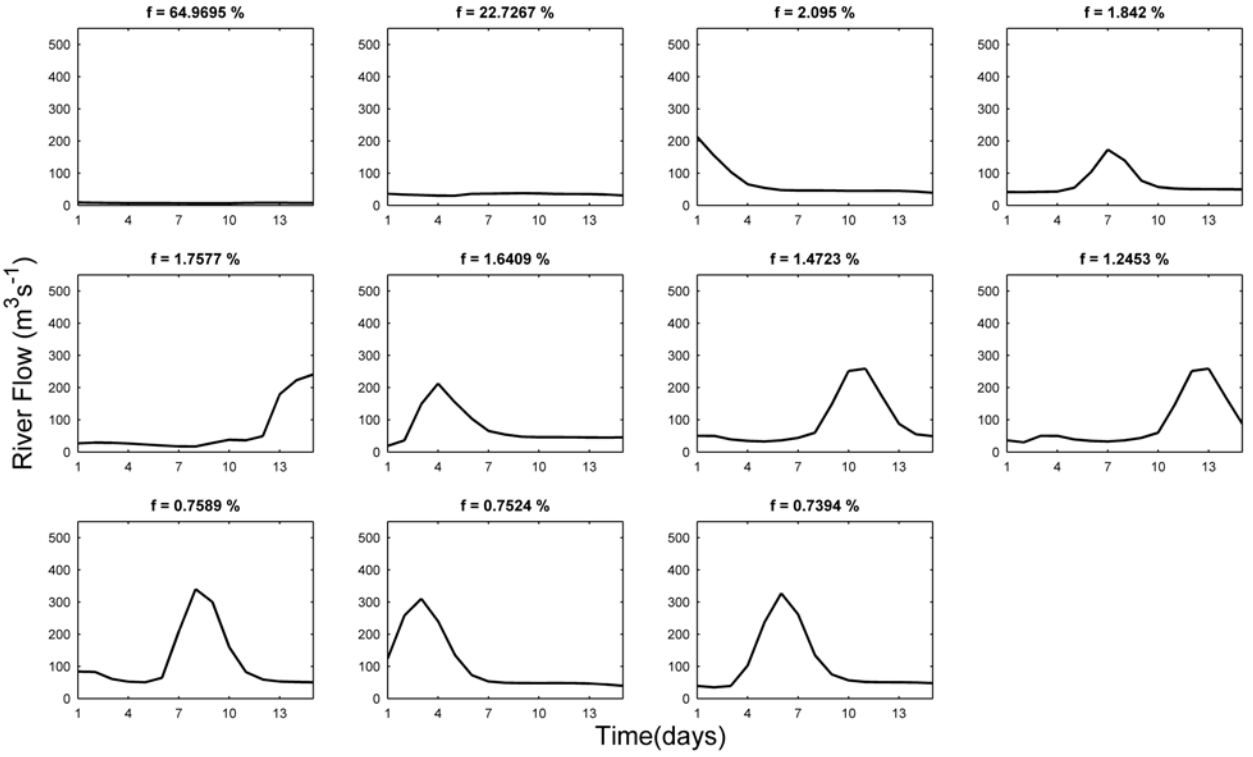

Figure 5.59: Minimum number of final classified clusters M_{mm} for river flow at Suances Estuary where f is the frequency of the cluster in percentage (%).

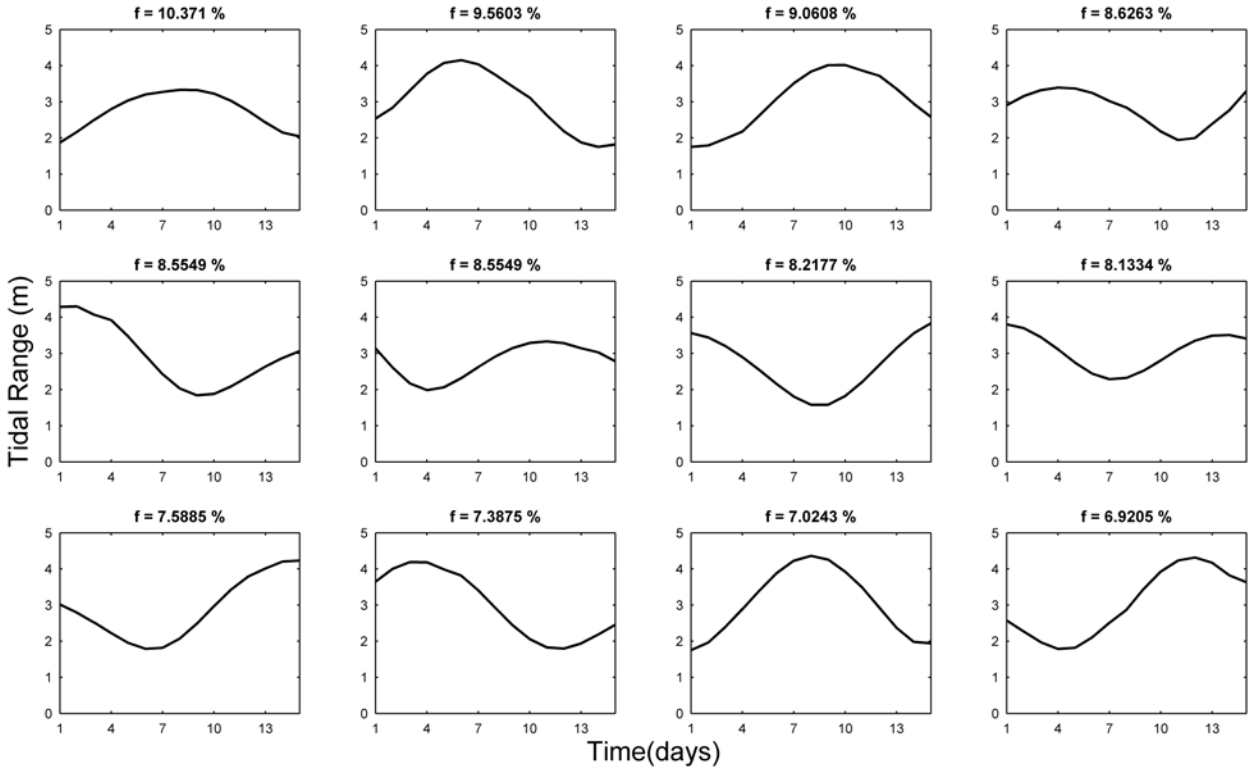

Figure 5.60: Optimal number of final classified clusters M_{om} for tidal range at Suances Estuary where f is the frequency of the cluster in percentage (%).

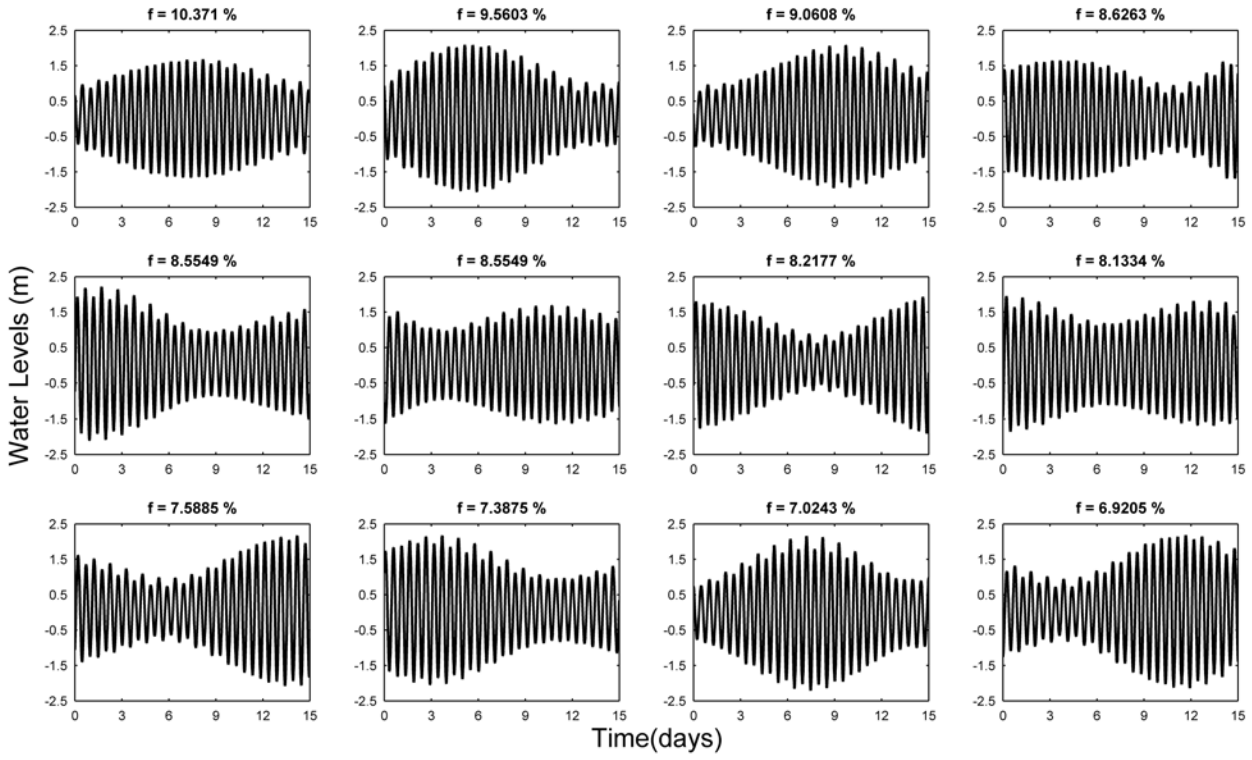

Figure 5.61: Optimal number of final classified clusters M_{om} for water levels at Suances Estuary where f is the frequency of the cluster in percentage (%).

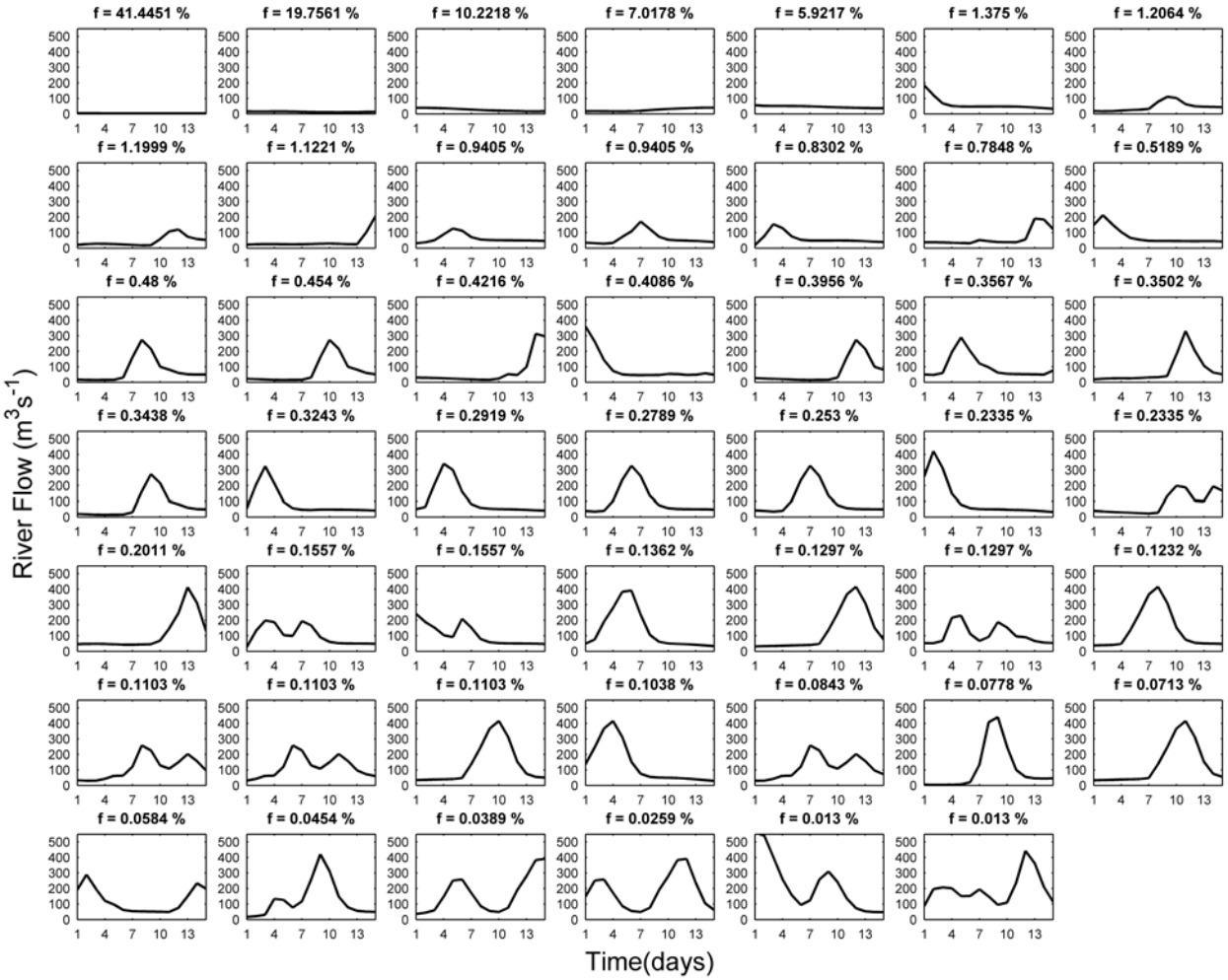

Figure 5.62: Optimal number of final classified clusters M_{om} for river flow at Suances Estuary where f is the frequency of the cluster in percentage (%).

NClusters Model	Time Years	40 years %	Forcing CE	Response CE
55	2.2602	5.6505	0.67	0.6463
60	2.4657	6.1642	0.68	0.6441
72	2.9589	7.3972	0.69	0.6747
78	**3.2054**	**8.0135**	**0.7**	**0.6768**
98	4.0274	10.0685	0.71	0.6906
105	4.3151	10.7877	0.72	0.6909
119	4.8904	12.2260	0.73	0.6932
144	5.9178	14.7945	0.74	0.7147
160	6.5753	16.4382	0.75	0.7254
189	7.7671	19.4177	0.76	0.7439
260	10.6849	26.7122	0.78	0.7521
341	14.0137	35.0342	0.79	0.7753
385	15.8219	39.5547	0.8	0.7784
456	18.7397	46.8492	0.81	0.7961
576	23.6712	59.1780	0.82	0.7971

Table 5.12: Number of model clusters, time duration, percentage over 40 years, CE of the forcing, CE of the mean response for every iterative step (row) conducted during the sensitivity analysis for running numerical models.

Final selection of classified clusters

The proposed methodology provided a minimum (M_{mm}=5×11=55) and optimal (M_{om}=12×48=576) number of simulations necessary to take into account the variability of the hydrodynamic forcings on estuaries driven by the river and the tide. Consequently, the final number (M) of model scenarios must be in a window spanning from 55 to 576 groups.

At first, it should be selected M_{om}, however, these number of model scenarios were equivalent to a continuous simulation of 8640 days (23.6712 years), i.e., more than half of the 40 years of time series (59.17 %). Because of this, the optimal number of simulations would be unaffordable due to computational constraints (time and size). At least, it must be selected M_{mm} to ensure valid results. From a computational cost point of view, these number of model scenarios were equivalent to a continuous simulation of 825 days (2.2602 years), i. e., only 5.65 % of the 40 years of time series. However, model results would be less accurate.

Bearing in mind these issues, the final number of model scenarios (M) should be determined by a trade off between the number of clusters, the accuracy of model results and the computational costs of these simulations (see also table 5.11 and figure 5.56). In order to complete this task, we analyzed in table 5.12 the evolution of the expected CE_r (column - Response CE) with the time simulation (column - Time Years). Furthermore, it is important to point that the known data when performing the classification by KMA were always the forcing time series. Thus, the final number of clusters must ensure that the CE_f>0.7 and the time duration must be less than 10 % of the 40-years time series of river an tide.

As it is showed in table 5.12 (bolded row), we selected 6(tides)×13(rivers)=78 model scenarios corresponding to CE_f=0.7 and CE_r=0.6768 as the final number of clusters (M). The time duration of the 78 model scenarios was 3.2054 years (8.0135 % of 40 years).

Lastly, the M of TR, WL and Q are displayed in figures 5.63, 5.64 and 5.65 respectively. In all these figures, the title of every subplot was displaying the frequency (f) of the cluster in percentage (%). Furthermore, the subplots were sorted in descending order, starting in the top-left corner to the right.

Finally, tables 5.13 and 5.14 synthesize the information of every model scenario presenting the name, number of tide and river cluster, frequency of tide and river cluster and final frequency for the model scenarios from 1

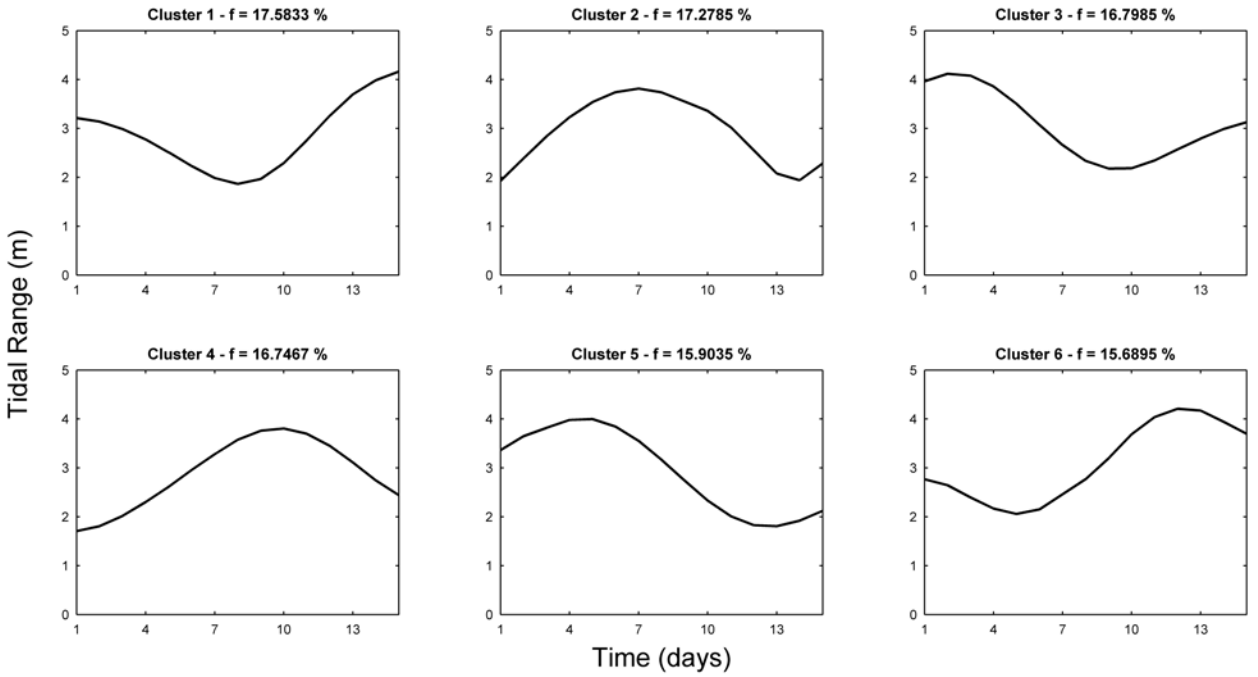

Figure 5.63: Final classified clusters M for tidal range at Suances Estuary where f is the frequency of the cluster in percentage ($\%$).

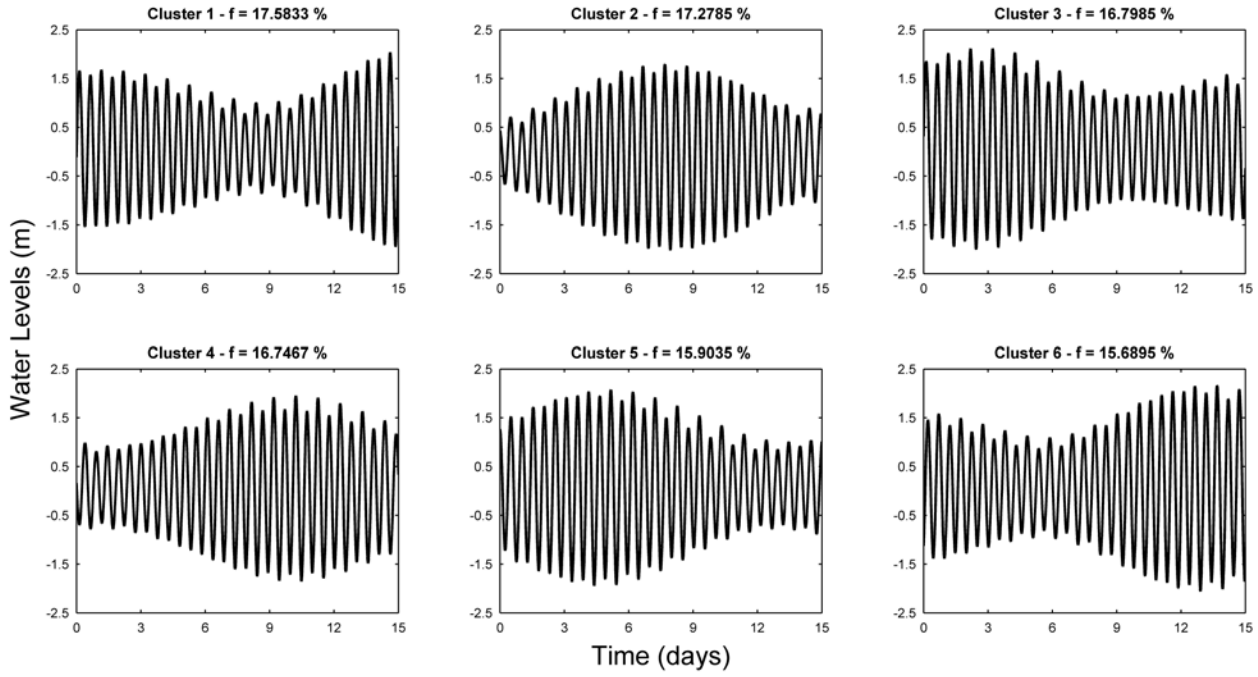

Figure 5.64: Final classified clusters M for water levels at Suances Estuary where f is the frequency of the cluster in percentage ($\%$).

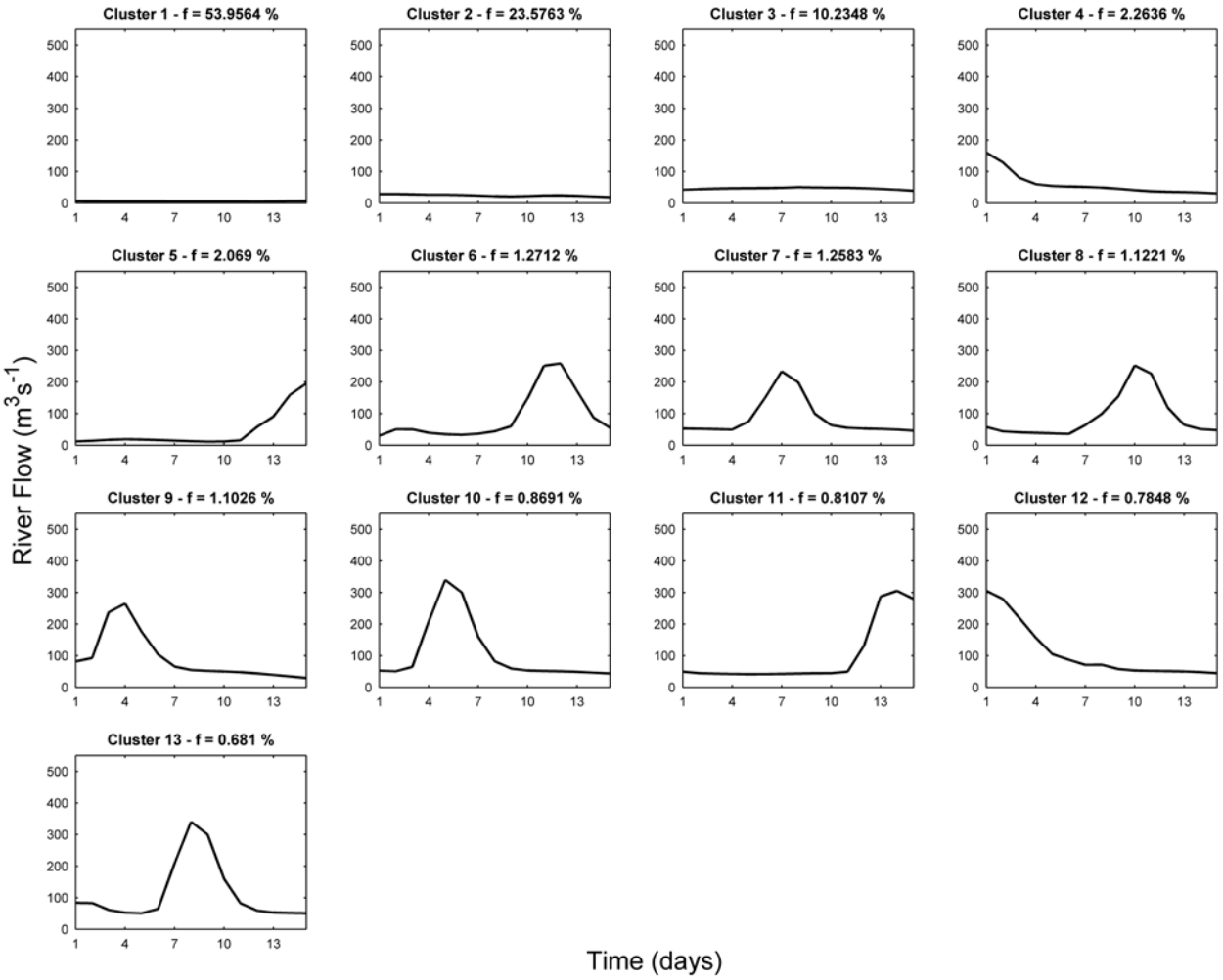

Figure 5.65: Final classified clusters M for river flow at Suances Estuary where f is the frequency of the cluster in percentage (%).

to 39 and from 40 to 78 respectively.

5.5.1.3 Hydrodynamic real case modeling

The hydrodynamic model predicted the surface elevation, current velocity, temperature and salinity fields across the model grid in the 78 model scenarios selected by the KMA.

As it was underlined, we ran the model starting several days before the time of interest. This timescale was 216 hours (9 days).

The 78 model scenarios assume $9 + 15$ days of river flow and tidal elevation as forcings. Thus, the first 9 days of model simulations were not taken into account. Once the model stabilization was reached and the influence of initial conditions was avoided, we recorded hourly 15 days of hydrodynamic model results for every model scenario.

5.5.2 Primary or initial dilution (Near-field)

Once all the required data were gathered, we ran the "real case of dilution" with JETLAG for the very large significant discharges ID1 and ID2 (78 model scenarios of 15 days with a hourly timestep) considering the same assumption made by the simplified or intermediation calculation.

Due to the many number of cases, as an example of the initial dilution, we illustrate the JETLAG results of cases 23 (see figure 5.66 and the bolded row in table 5.13) and 54 (see figure 5.66 and the bolded row in table 5.14) for ID1 and ID2 in the next paragraphs.

Figures 5.67, 5.68, 5.69 and 5.70 show the total water depth (a), the magnitude of the environmental velocity (b), the direction of the environmental velocity (c) and the environmental density (d) for the surface layer (blue line) and bottom layer (green line) at the point of discharge during the "real case 23 and 54 of dilution" for ID1 and ID2 respectively. Moreover, these figures display the initial dilution (e) of the effluent (black line) and the effluent concentration (f) after the initial dilution (black line). Finally, figures 5.67f and 5.68f also display the AA-EQS (magenta line) of chloroform ($CHCl_3$) meanwhile figures 5.69f and 5.70f the AA-EQS (magenta line) and MAC-EQS (red line) of lead (Pb).

As it was shown in figures 5.67 and 5.68, ID1 dilution was oscillating between 47.89 and 2.69 for the case 23 and between 11.92 and 1.00 for the case 54. In the case of ID2, ID2 dilution was oscillating between 6625.84 and 53.13 for the case 23 and between 1739.63 and 2.82 for the case 54 (see figures 5.69 and 5.70). As in the the "worst and dry case of dilution" of initial dilution, these oscillations were related to the changes in the environmental variables. ID1 and ID2 dilution was directly proportional to the river flow time series (see figure 5.66).

Regarding ID1 concentration, the AA-EQS was not surpassed during the peak flow in the "real case 23 of dilution" meanwhile the rest of the time the AA-EQS was approximately surpassed during the 40% of the time. In the case 54, ID1 concentration was almost of the time above the AA-EQS because of the magnitude of the river flow was smaller than in the case 23. For the ID2 concentration, the AA-EQS and MAC-EQS were not surpassed during the peak flow in the "real case 23 of dilution" meanwhile the rest of the time the AA-EQS was approximately surpassed during the 30% of the time while the MAC-EQS was almost not surpassed. In the case 54, ID2 concentration was almost of the time above the AA-EQS and MAC-EQS because of the magnitude of the river flow was smaller than in the case 23.

As an example of the trajectory described by ID1 and ID2 in the near-field region, figures 5.71, 5.72, 5.73 and 5.74 present two snapshots of the buoyant jet (ID1 and ID2) calculated in the "real cases 23 and 54 of dilution" for the hour 96 respectively (see figures 5.67, 5.68, 5.69 and 5.70). In these figures, the evolution

Model Scenario	Tide Cluster	River Cluster	Tide Freq (%)	River Freq %	Final Freq %
Case 1	1	1	17.5833	53.9564	9.4873
Case 2	1	2	17.5833	23.5763	4.1455
Case 3	1	3	17.5833	10.2348	1.7996
Case 4	1	4	17.5833	2.2636	0.3980
Case 5	1	5	17.5833	2.0690	0.3638
Case 6	1	6	17.5833	1.2712	0.2235
Case 7	1	7	17.5833	1.2583	0.2212
Case 8	1	8	17.5833	1.1221	0.1973
Case 9	1	9	17.5833	1.1026	0.1938
Case 10	1	10	17.5833	0.8691	0.1528
Case 11	1	11	17.5833	0.8107	0.1425
Case 12	1	12	17.5833	0.7848	0.1380
Case 13	1	13	17.5833	0.6810	0.1197
Case 14	2	1	17.2785	53.9564	9.3228
Case 15	2	2	17.2785	23.5763	4.0736
Case 16	2	3	17.2785	10.2348	1.7684
Case 17	2	4	17.2785	2.2636	0.3911
Case 18	2	5	17.2785	2.0690	0.3575
Case 19	2	6	17.2785	1.2712	0.2196
Case 20	2	7	17.2785	1.2583	0.2174
Case 21	2	8	17.2785	1.1221	0.1938
Case 22	2	9	17.2785	1.1026	0.1904
Case 23	**2**	**10**	**17.2785**	**0.8691**	**0.1501**
Case 24	2	11	17.2785	0.8107	0.1401
Case 25	2	12	17.2785	0.7848	0.1356
Case 26	2	13	17.2785	0.6810	0.1176
Case 27	3	1	16.7985	53.9564	9.0638
Case 28	3	2	16.7985	23.5763	3.9604
Case 29	3	3	16.7985	10.2348	1.7192
Case 30	3	4	16.7985	2.2636	0.3802
Case 31	3	5	16.7985	2.0690	0.3475
Case 32	3	6	16.7985	1.2712	0.2135
Case 33	3	7	16.7985	1.2583	0.2113
Case 34	3	8	16.7985	1.1221	0.1885
Case 35	3	9	16.7985	1.1026	0.1851
Case 36	3	10	16.7985	0.8691	0.1459
Case 37	3	11	16.7985	0.8107	0.1361
Case 38	3	12	16.7985	0.7848	0.1318
Case 39	3	13	16.7985	0.6810	0.1143

Table 5.13: Name, number of cluster of tide and river, frequency of tide and river clusters and final frequency for every of the final selected model scenarios M at Suances Estuary. Each row is displaying the configuration of each model scenario. Part 1.

Model Scenario	Tide Cluster	River Cluster	Tide Freq (%)	River Freq %	Final Freq %
Case 40	4	1	16.7467	53.9564	9.0359
Case 41	4	2	16.7467	23.5763	3.9482
Case 42	4	3	16.7467	10.2348	1.7139
Case 43	4	4	16.7467	2.2636	0.3791
Case 44	4	5	16.7467	2.0690	0.3465
Case 45	4	6	16.7467	1.2712	0.2128
Case 46	4	7	16.7467	1.2583	0.2106
Case 47	4	8	16.7467	1.1221	0.1879
Case 48	4	9	16.7467	1.1026	0.1845
Case 49	4	10	16.7467	0.8691	0.1455
Case 50	4	11	16.7467	0.8107	0.1357
Case 51	4	12	16.7467	0.7848	0.1314
Case 52	4	13	16.7467	0.6810	0.1140
Case 53	5	1	15.9035	53.9564	8.5809
Case 54	**5**	**2**	**15.9035**	**23.5763**	**3.7494**
Case 55	5	3	15.9035	10.2348	1.6277
Case 56	5	4	15.9035	2.2636	0.3599
Case 57	5	5	15.9035	2.0690	0.3291
Case 58	5	6	15.9035	1.2712	0.2021
Case 59	5	7	15.9035	1.2583	0.2001
Case 60	5	8	15.9035	1.1221	0.1784
Case 61	5	9	15.9035	1.1026	0.1753
Case 62	5	10	15.9035	0.8691	0.1382
Case 63	5	11	15.9035	0.8107	0.1289
Case 64	5	12	15.9035	0.7848	0.1248
Case 65	5	13	15.9035	0.6810	0.1082
Case 66	6	1	15.6895	53.9564	8.4654
Case 67	6	2	15.6895	23.5763	3.6990
Case 68	6	3	15.6895	10.2348	1.6057
Case 69	6	4	15.6895	2.2636	0.3551
Case 70	6	5	15.6895	2.0690	0.3246
Case 71	6	6	15.6895	1.2712	0.1994
Case 72	6	7	15.6895	1.2583	0.1973
Case 73	6	8	15.6895	1.1221	0.1761
Case 74	6	9	15.6895	1.1026	0.1729
Case 75	6	10	15.6895	0.8691	0.1363
Case 76	6	11	15.6895	0.8107	0.1271
Case 77	6	12	15.6895	0.7848	0.1231
Case 78	6	13	15.6895	0.6810	0.1068

Table 5.14: Name, number of cluster of tide and river, frequency of tide and river clusters and final frequency for every of the final selected model scenarios M at Suances Estuary. Each row is displaying the configuration of each model scenario. Part 2.

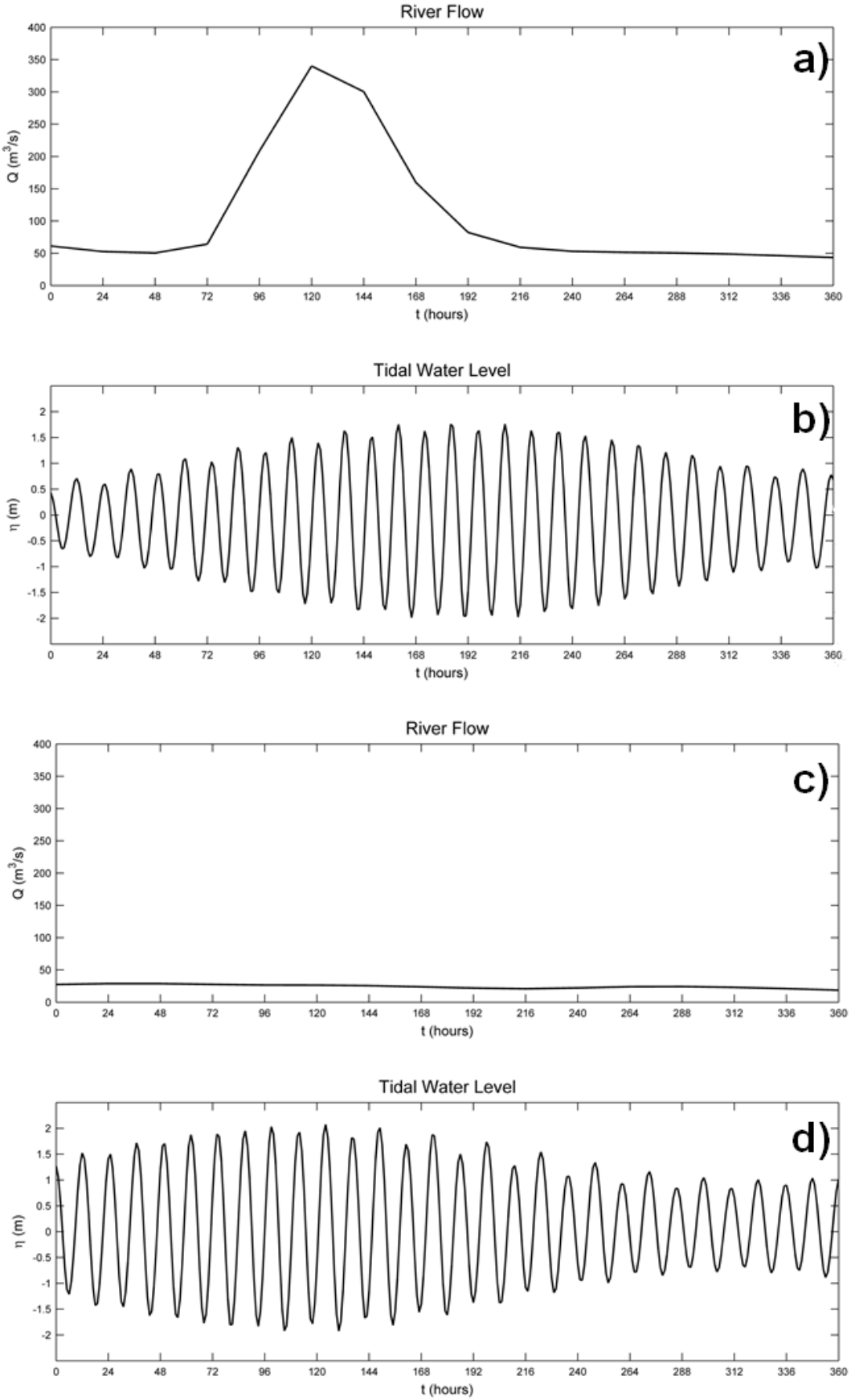

Figure 5.66: 15-days time series of forcings: a) river flows of case 23, b) water levels of case 23, c) river flows of case 54 and d) water levels of case 54.

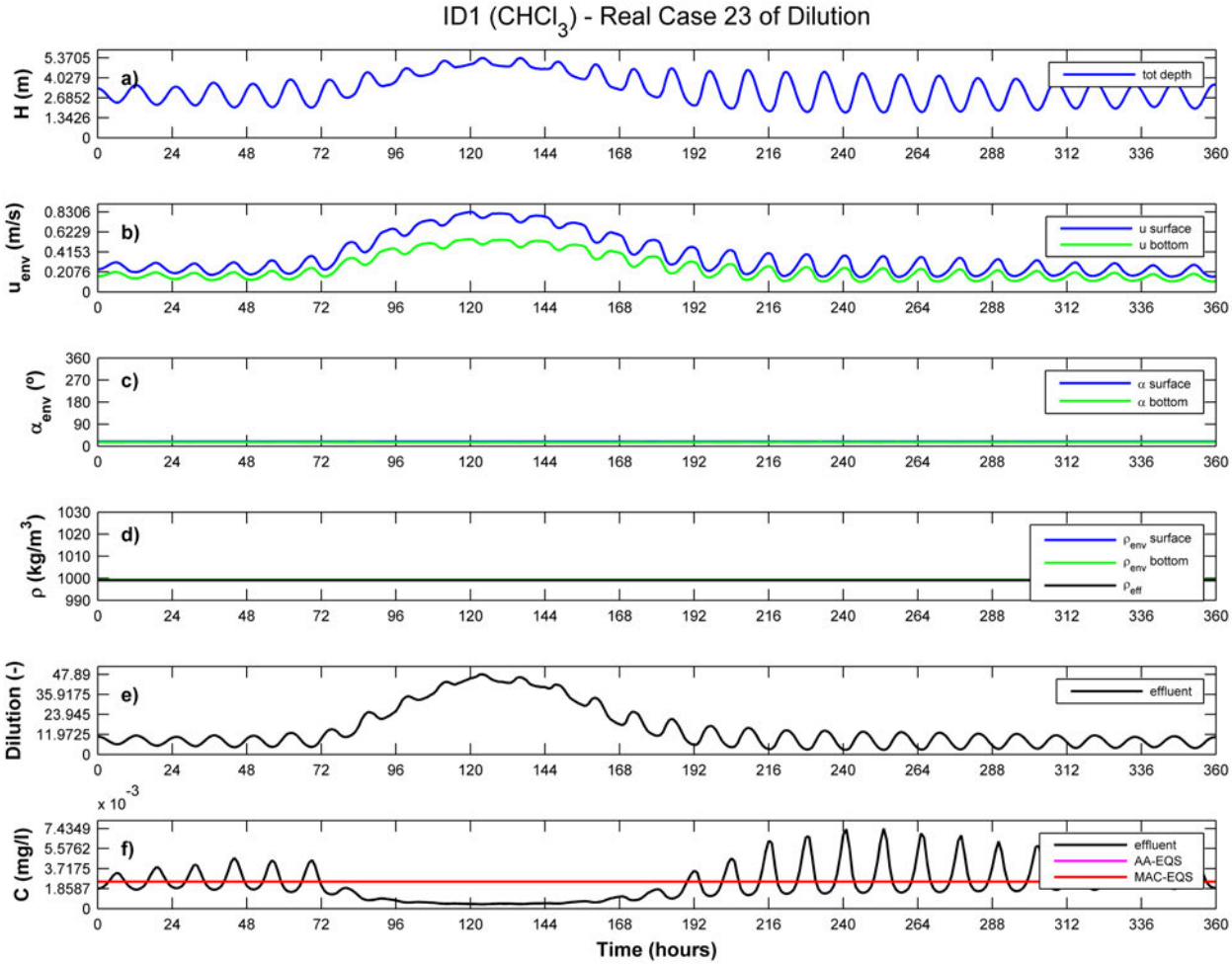

Figure 5.67: Evolution of the total water depth (a), the magnitude of the environmental velocity (b), the direction of the environmental velocity (c) and the environmental density (d) for the surface layer (blue line) and bottom layer (green line), the initial dilution (e) of the effluent (black line) and the effluent concentration (f) after the initial dilution (black line) at ID1 during the "real case 23 of dilution". Note it is also shown the AA-EQS (magenta line) of chloroform (f).

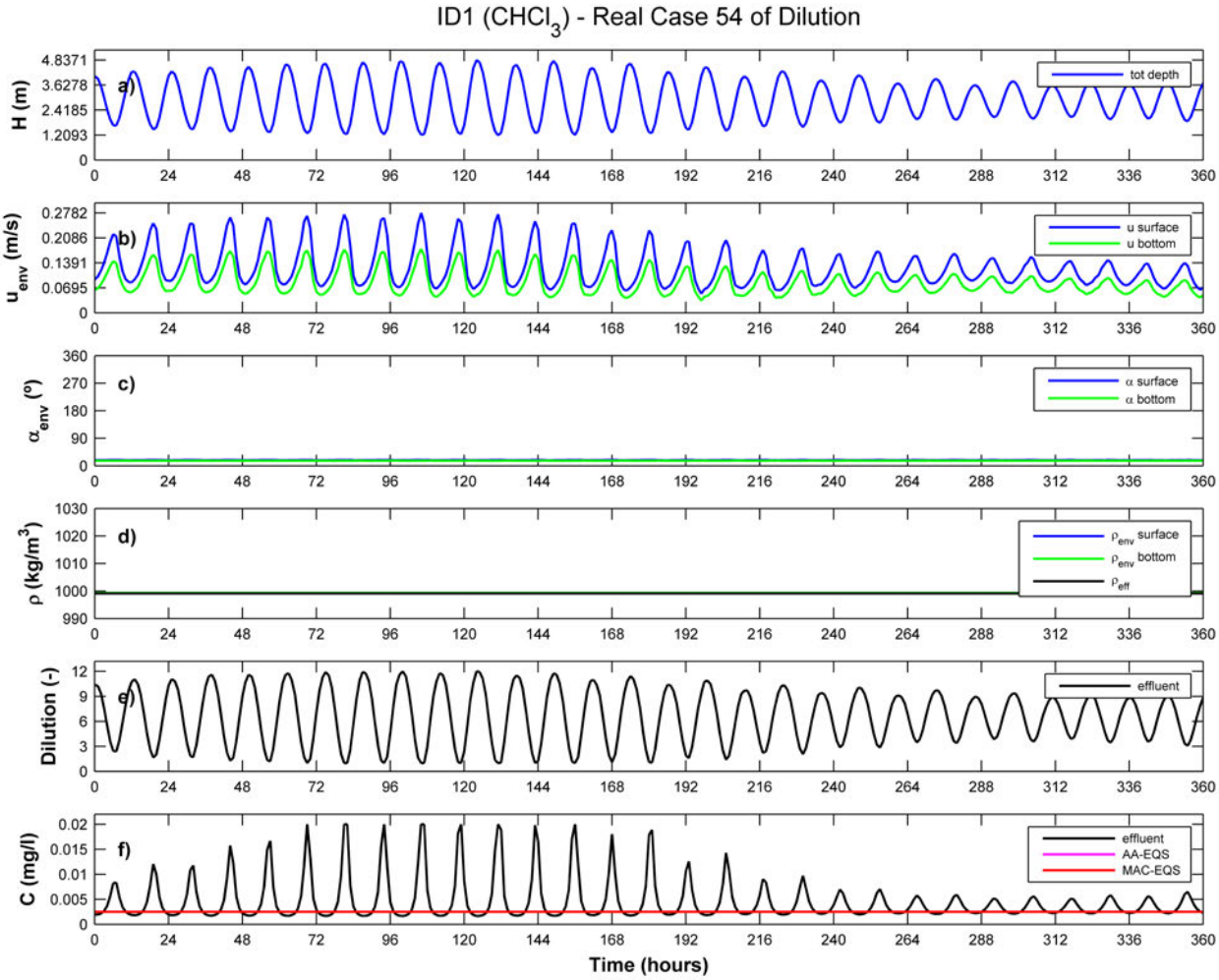

Figure 5.68: Evolution of the total water depth (a), the magnitude of the environmental velocity (b), the direction of the environmental velocity (c) and the environmental density (d) for the surface layer (blue line) and bottom layer (green line), the initial dilution (e) of the effluent (black line) and the effluent concentration (f) after the initial dilution (black line) at ID1 during the "real case 54 of dilution". Note it is also shown the AA-EQS (magenta line) and MAC-EQS (red line) of chloroform (f).

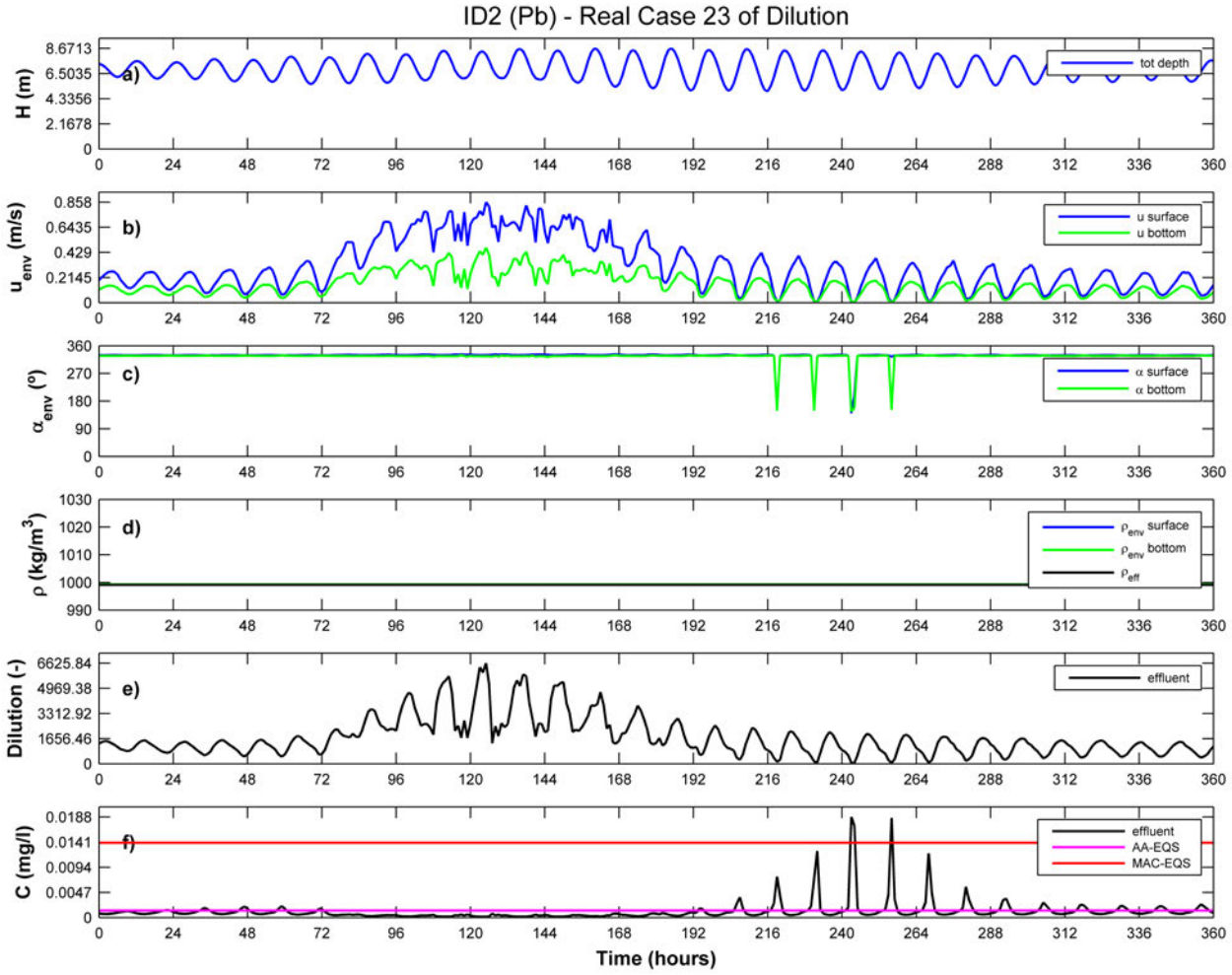

Figure 5.69: Evolution of the total water depth (a), the magnitude of the environmental velocity (b), the direction of the environmental velocity (c) and the environmental density (d) for the surface layer (blue line) and bottom layer (green line), the initial dilution (e) of the effluent (black line) and the effluent concentration (f) after the initial dilution (black line) at ID2 during the "real case 23 of dilution". Note it is also shown the AA-EQS (magenta line) and MAC-EQS (red line) of lead (f).

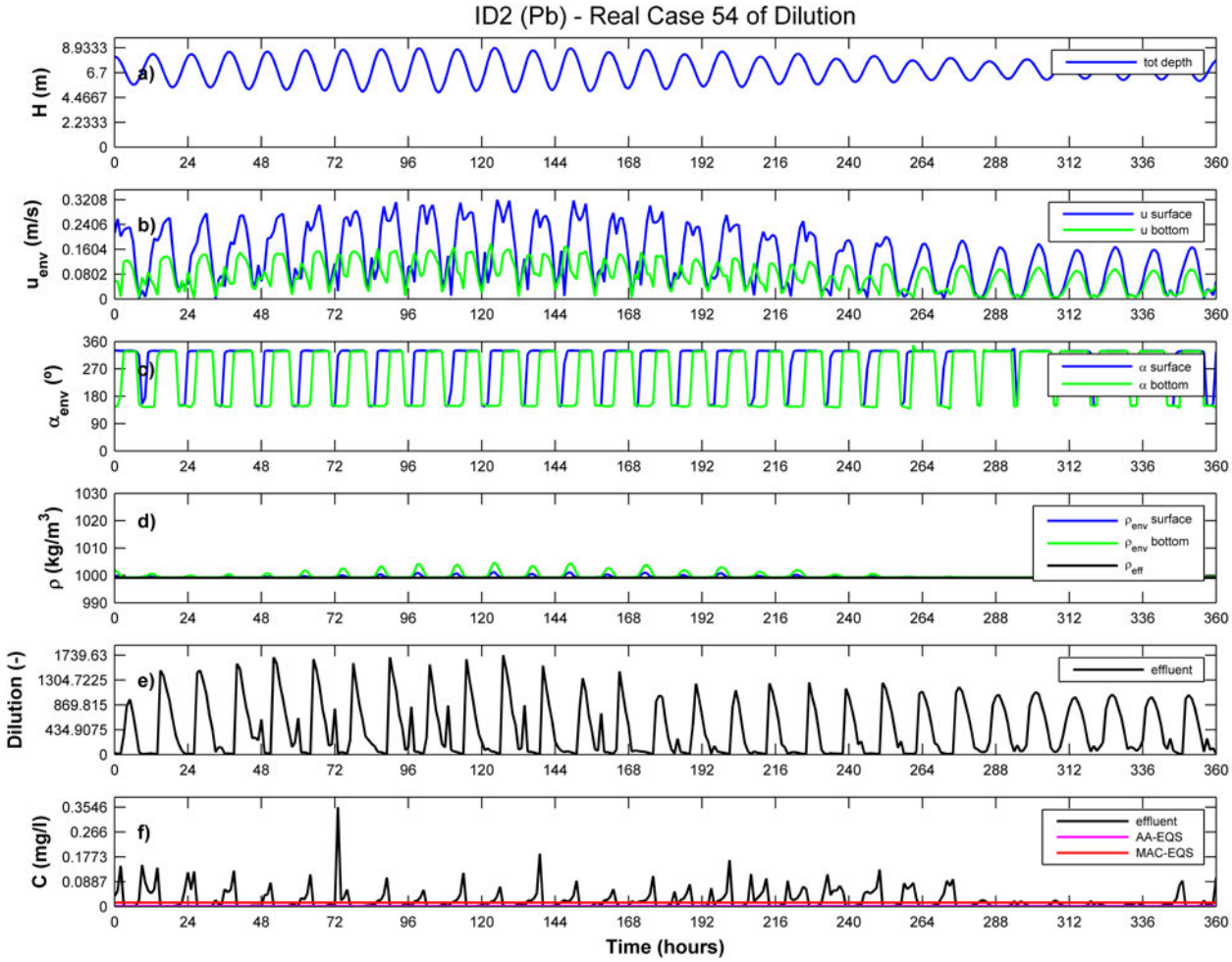

Figure 5.70: Evolution of the total water depth (a), the magnitude of the environmental velocity (b), the direction of the environmental velocity (c) and the environmental density (d) for the surface layer (blue line) and bottom layer (green line), the initial dilution (e) of the effluent (black line) and the effluent concentration (f) after the initial dilution (black line) at ID2 during the "real case 54 of dilution". Note it is also shown the AA-EQS (magenta line) and MAC-EQS (red line) of lead (f).

of the 3D buoyant jet is shown on a 3D view (a), plan view (b) and side view (c). Moreover, the single-port pipe is represented with a black line (side and plan views) and the free surface with a blue line (side view) or a blue rectangle (3D and plan views).

As it can be seen in figures 5.71 and 5.72, the ID1 jet was fully mixed in the water column due to the lack of water depth and the magnitude of the effluent flow. It is also bent towards the river flow direction due to its closeness. The distance and dilution experimented by the buoyant jet was directly attached to the magnitude of the river flow. Thus, the buoyant jet of case 23 presented a higher distance (≈250 m) and dilution (25) than in the case 54 (≈40 m and 5).

Regarding ID2, in figure 5.73 the ID2 jet rose until collide with the free surface due to buoyancy and it was also bent towards the river flow direction due to the environmental velocity. In figure 5.74, the ID2 jet was trapped in the middle of the water column due to lack of momentum (low flow of the effluent) and the low magnitude of the environmental velocity.

5.5.3 Coupling primary and secondary dilution (Intermediate-field)

Once all the required information was collected, we applied the described method to the very large significant discharges ID1 and ID2 for the "real case of dilution" (78 model scenarios of 15 days with a hourly timestep).

Due to the many number of cases, as an example of the intermediate-field, we illustrate again the coupling results of cases 23 (see figure 5.66 and the bolded row in table 5.13) and 54 (see figure 5.66 and the bolded row in table 5.14) for ID1 and ID2 in the next paragraphs.

Figures 5.75, 5.76, 5.77 and 5.78 present the percentage of time that ID1 and ID2 was in different horizontal grid cells (left panel) and vertical layers (right panel) predicted by JETLAG during the coupling process of the "real cases 23 and 54 of dilution" respectively. In these locations, we introduced ID1 and ID2 as a source term of flow and diluted concentration.

As it is shown in figures 5.75 and 5.76, ID1 coupling was located in several horizontal grids downstream of the discharge point due to the closeness to the river and the momentum of ID1. In the vertical direction, ID1 was fully mixed in the water column most of the time. The rest of the time ID1 was mainly coupled between layers 5 and 9, i.e., between 1 and 3.25 m of depth. As it can be seen in figures 5.77 and 5.78, ID2 was almost always in the grid cell where was located the industrial pipe due to the buoyancy and the relative small discharged flow. Regarding vertical distribution, ID2 was most of the time between layers 4 and 8, i.e., between 2.5 and 6.5 m of depth indicating that ID2 plume was trapped. Moreover, these figures showed that the plume rose until free surface in the rest of situations.

5.5.4 Secondary or ambient dilution (Far-field): Non-Conservative approach

Finally, the required tasks to conduct the simulation of the significant discharges with D-Water Quality were described. The transport model for non-conservative substances followed the conceptual model (processes and interactions) described in figure 3.34.

5.5.4.1 Additional information

The information was related to the measurements (field data) and the specific coefficients of chloroform (ID1) and lead (ID2) necessary to conduct the far-field model setup. We collected information from two sources: two field campaigns (CMA 2006-2007, IHCantabria 2008a) and the water quality network of the coast of Cantabria called "Red de Control de Calidad Litoral en Cantabria" (IHCantabria 2012).

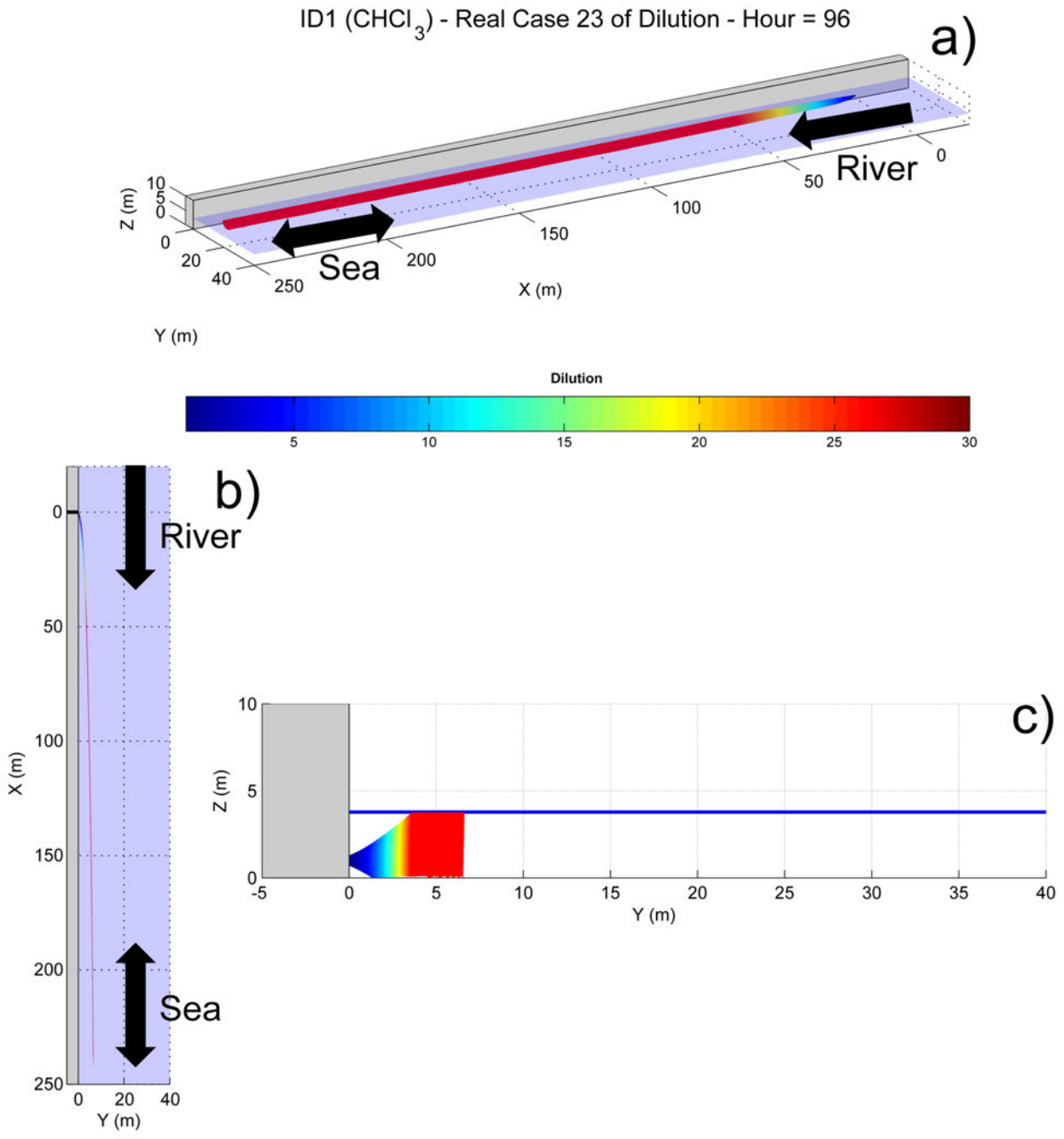

Figure 5.71: 3D buoyant jet of ID1 for the hour 96 in the detailed calculation (case 23). 3D view (a), plan view (b) and side view (c). The single-port pipe is represented with a black line (side and plan views) and the free surface with a blue line (side view) or a blue rectangle (3D and plan views).

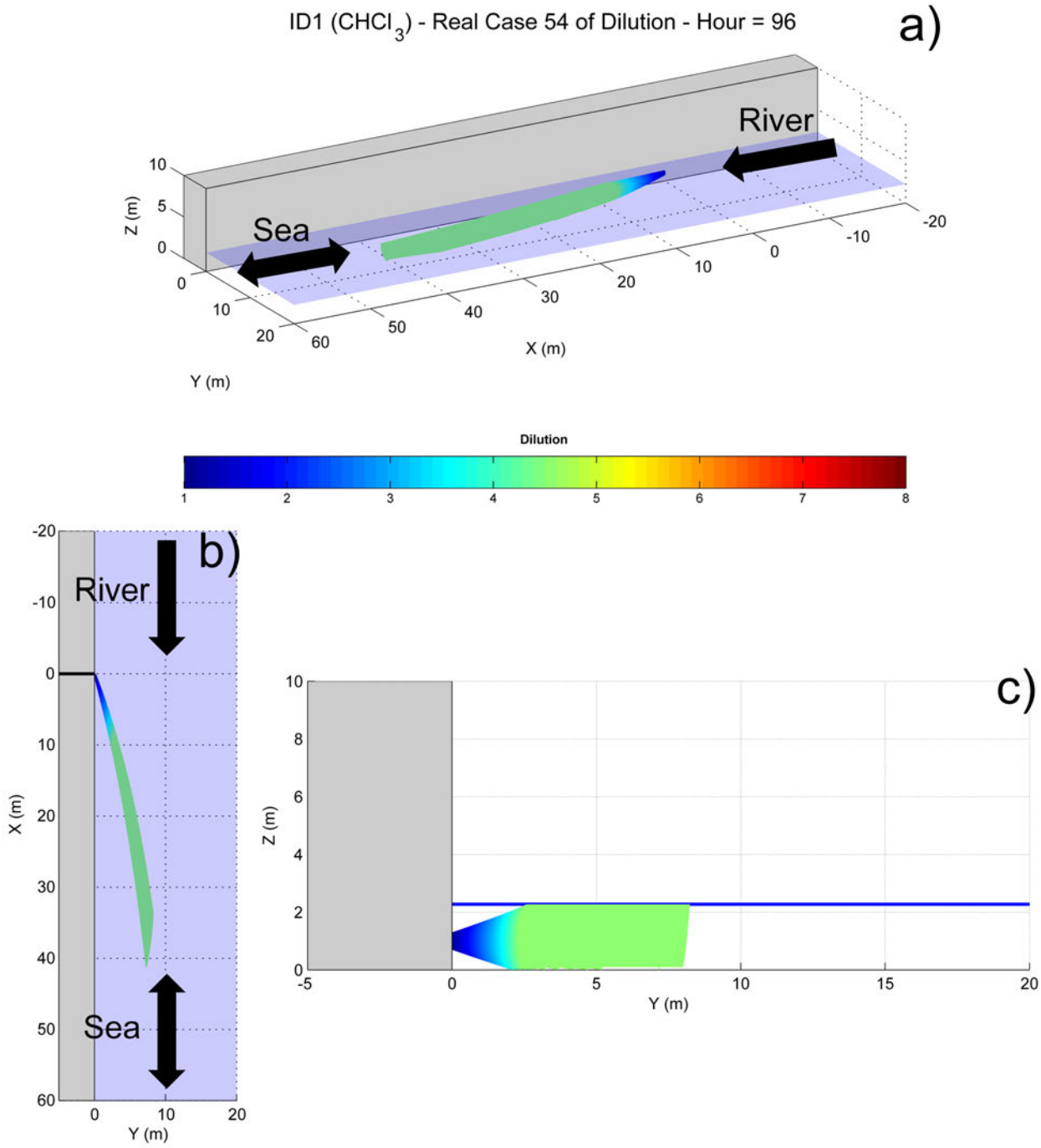

Figure 5.72: 3D buoyant jet of ID1 for the hour 96 in the detailed calculation (case 54). 3D view (a), plan view (b) and side view (c). The single-port pipe is represented with a black line (side and plan views) and the free surface with a blue line (side view) or a blue rectangle (3D and plan views).

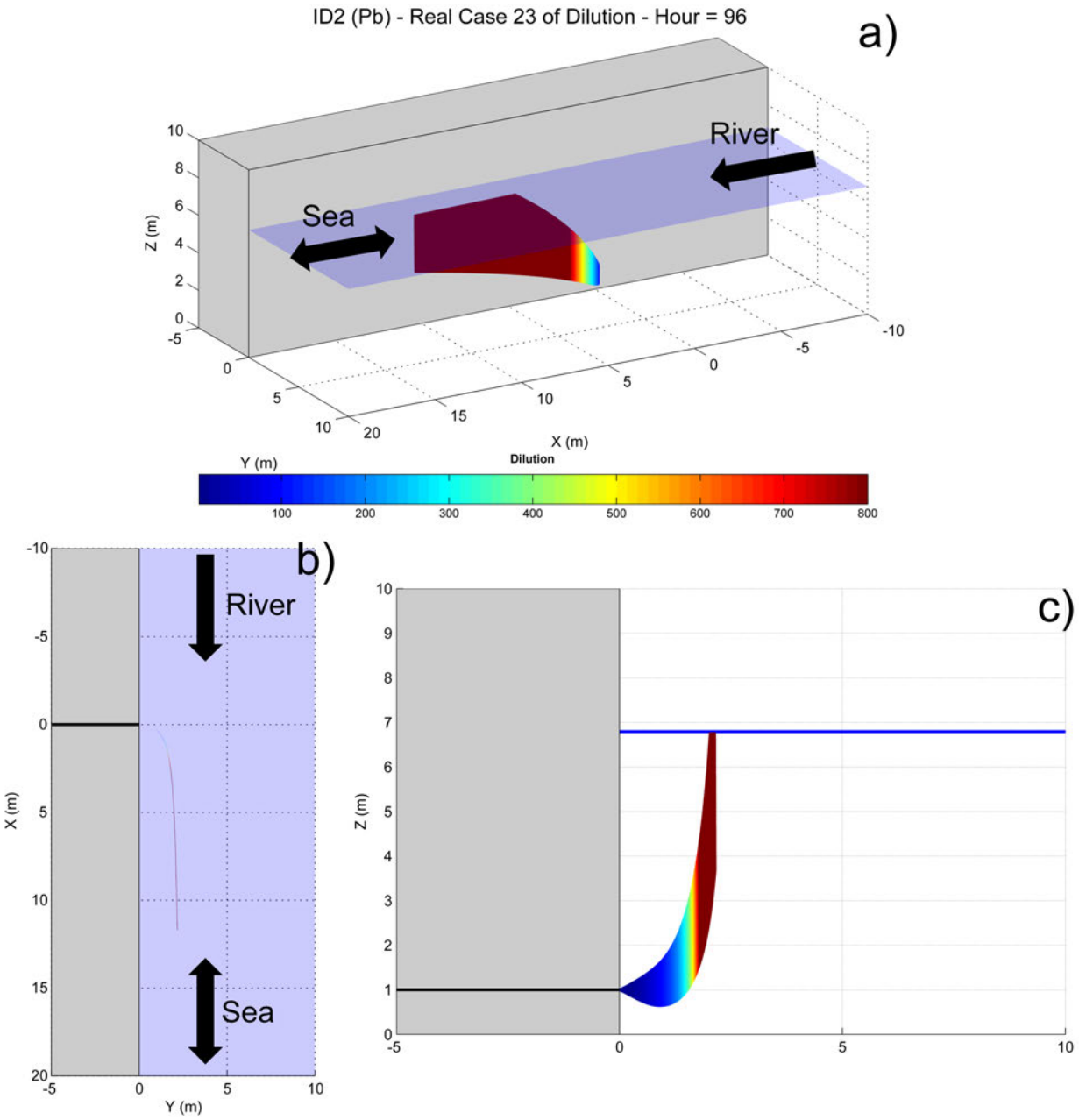

Figure 5.73: 3D buoyant jet of ID2 for the hour 96 in the detailed calculation (case 23). 3D view (a), plan view (b) and side view (c). The single-port pipe is represented with a black line (side and plan views) and the free surface with a blue line (side view) or a blue rectangle (3D and plan views).

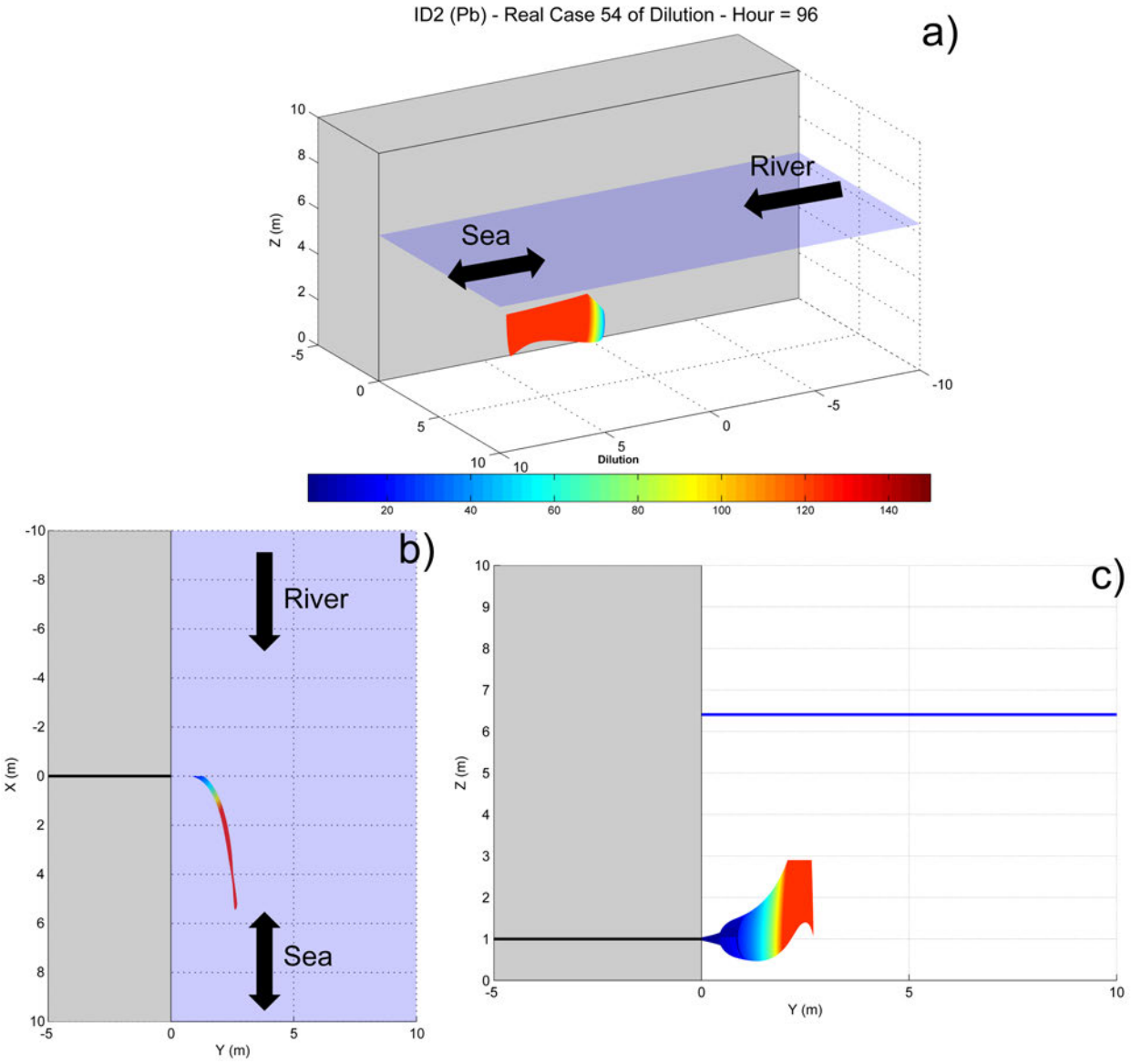

Figure 5.74: 3D buoyant jet of ID2 for the hour 96 in the detailed calculation (case 54). 3D view (a), plan view (b) and side view (c). The single-port pipe is represented with a black line (side and plan views) and the free surface with a blue line (side view) or a blue rectangle (3D and plan views).

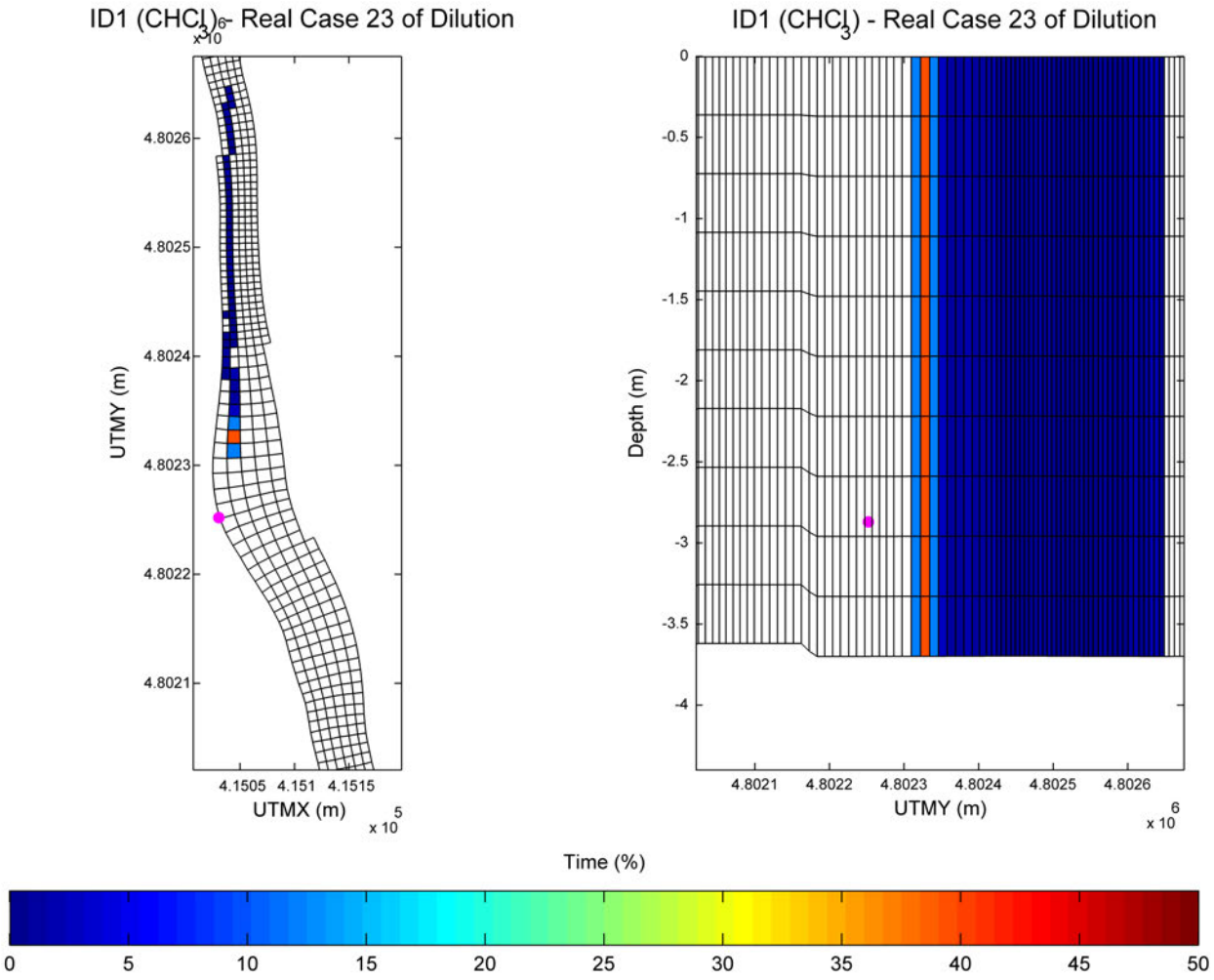

Figure 5.75: Schematic view of the time distribution of horizontal grid cells (left panel) and the vertical layers (right panel) covered by ID1 during the coupling between the primary and secondary dilution in the detailed calculation (case 23).

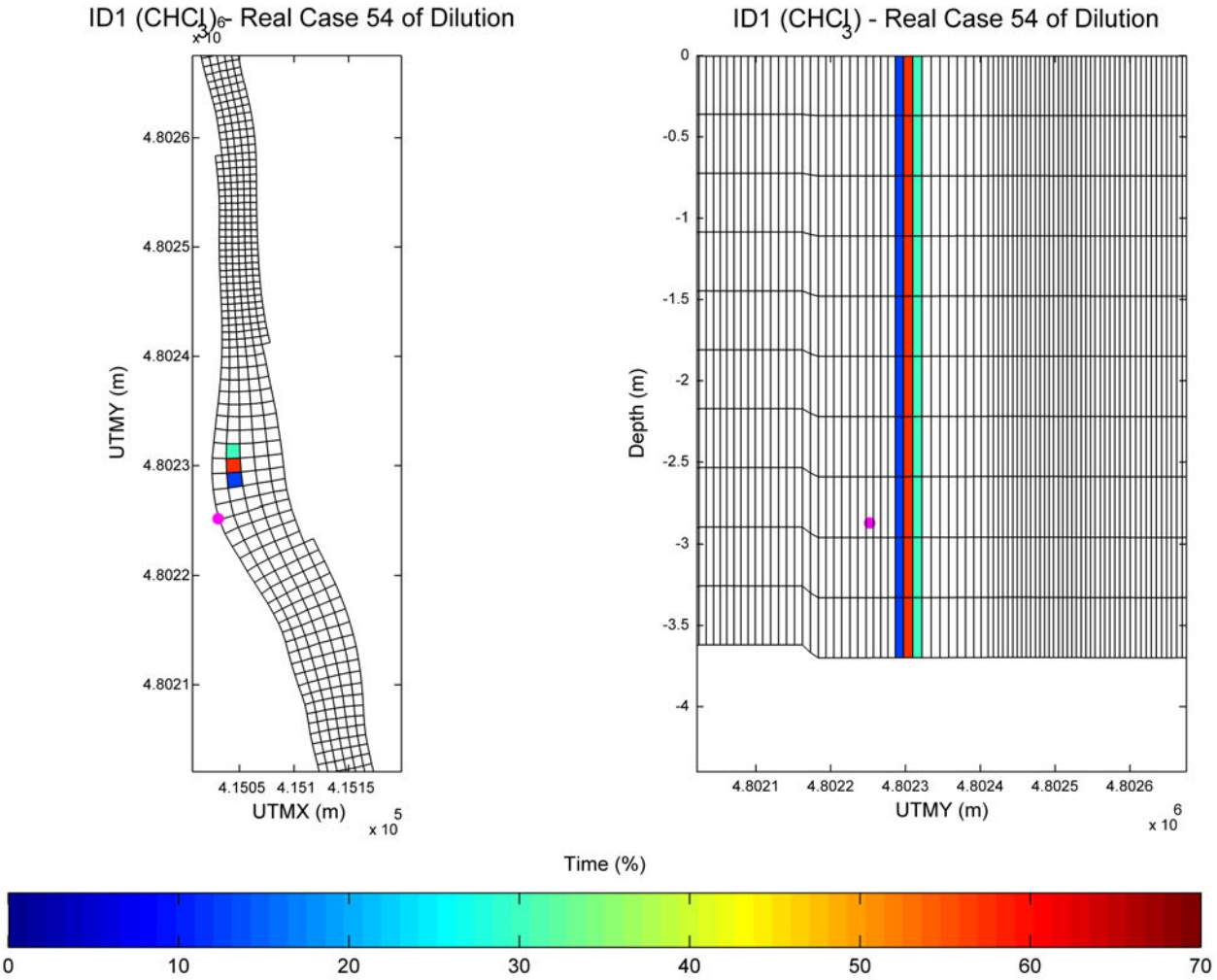

Figure 5.76: Schematic view of the time distribution of horizontal grid cells (left panel) and the vertical layers (right panel) covered by ID1 during the coupling between the primary and secondary dilution in the detailed calculation (case 54).

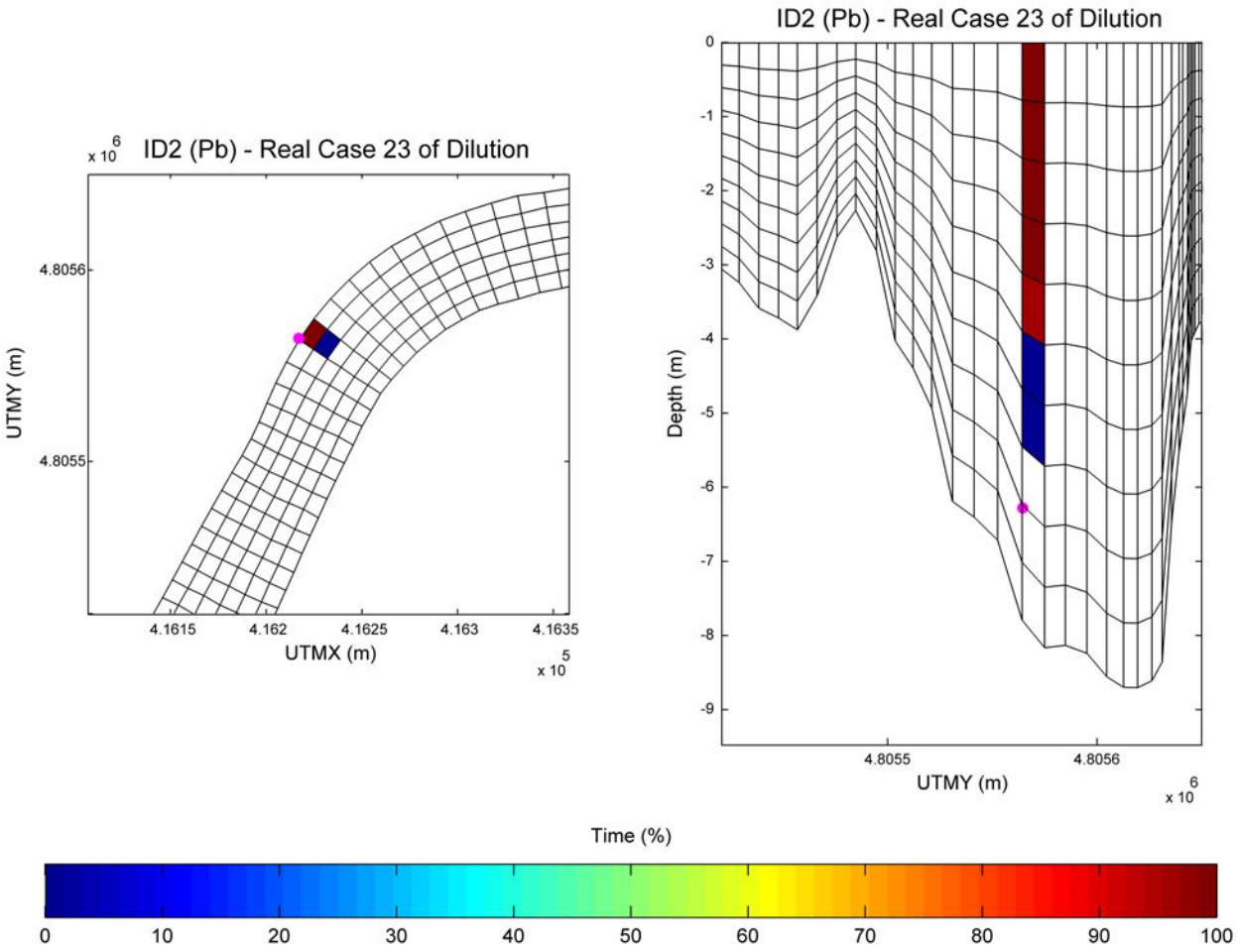

Figure 5.77: Schematic view of the time distribution of horizontal grid cells (left panel) and the vertical layers (right panel) covered by ID2 during the coupling between the primary and secondary dilution in the detailed calculation (case 23).

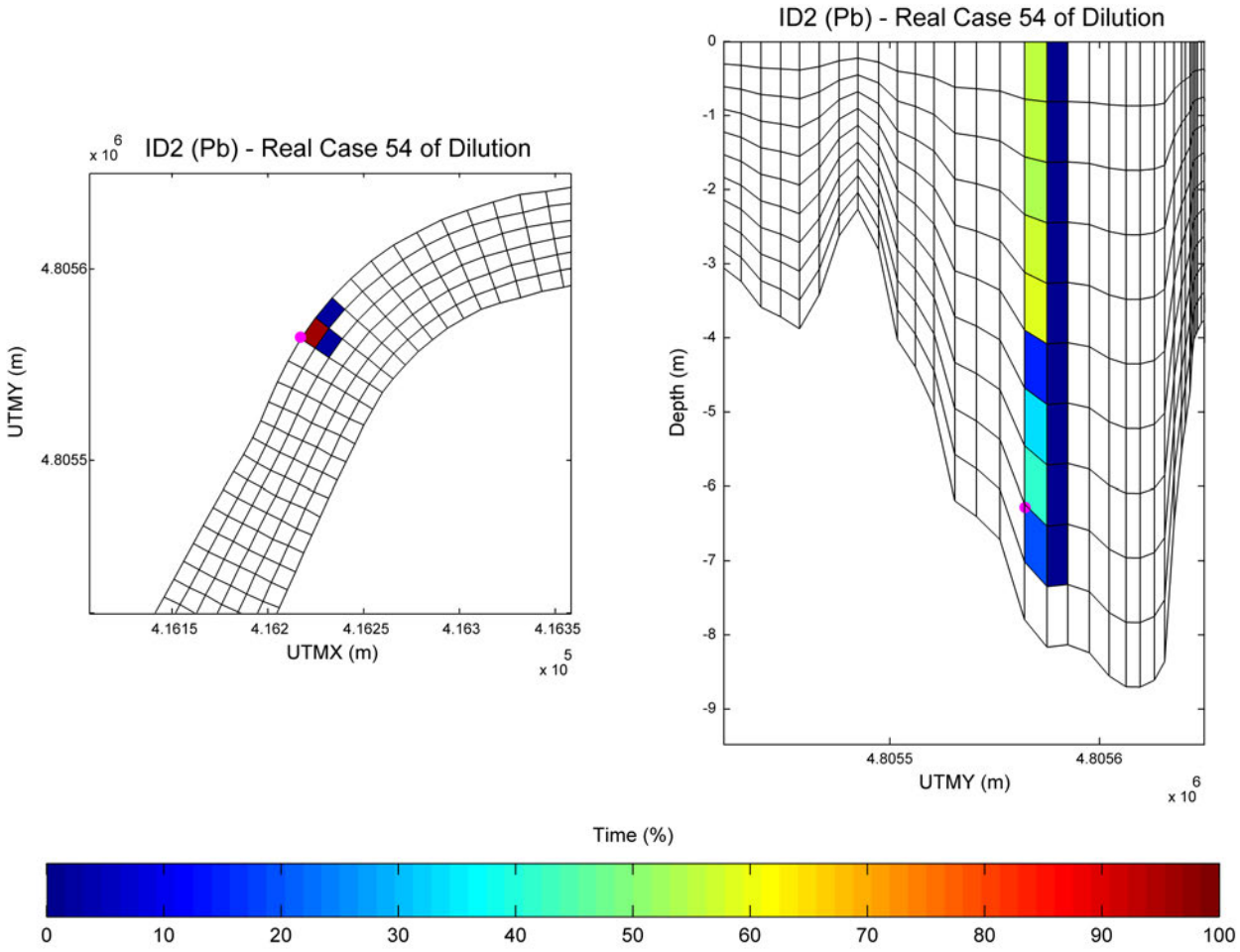

Figure 5.78: Schematic view of the time distribution of horizontal grid cells (left panel) and the vertical layers (right panel) covered by ID2 during the coupling between the primary and secondary dilution in the detailed calculation (case 54).

Date	Pb at WQ3	Pb at WQ6	$CHCl_3$ at WQ3	$CHCl_3$ at WQ6
23/06/2008	0.0050	0.0400	0.0004	0.0002
29/08/2008	-	0.0050	-	0.0003
12/11/2008	-	0.0010	-	0.0003

Table 5.15: Date and concentrations of the measurements conducted during the field campaign (IHCantabria 2008a).

Field campaigns (CMA 2006-2007, IHCantabria 2008a)

The field campaign (CMA 2006-2007) was conducted by the "Consejería de Medio Ambiente del Gobierno de Cantabria" in the context of the works of inspection of discharges from land to sea in Cantabria. The campaign took place during 2006 and 2007 and it was focused on collecting measurements of the contained toxicants at the end-of-pipe in the industrial discharges of Cantabria. In this thesis, we utilized the available measures of chloroform and particulate organic carbon concentration for ID1, and lead and suspended solid concentration for ID2.

The other field campaign (IHCantabria 2008a) was performed by the "IH Cantabria" in the preliminary analysis for the detection of priority substances in the coastal waters of Cantabria. The campaign took place at three dates: 23/06/2008, 29/08/2008 and 12/11/2008 and two locations WQ3 and WQ6 (see figure 5.10). Next, table 5.15 synthesizes all the available measures of $CHCl_3$ and Pb in the SE (mg/l).

"Red de Control de Calidad Litoral en Cantabria" (IHCantabria 2012)

As it was aforementioned, seasonal field campaigns of water, sediment and biota in the estuaries and coast of Cantabria were made in the "Red de Calidad del Litoral de Cantabria". The selected data included measurements of suspended solids (SS) and the weight fraction of the total organic carbon in the suspended solids (f_{OC}) since 2006 to 2013. As an example, figure 5.79 presents the evolution of the suspended solids and f_{OC} at WQ9.

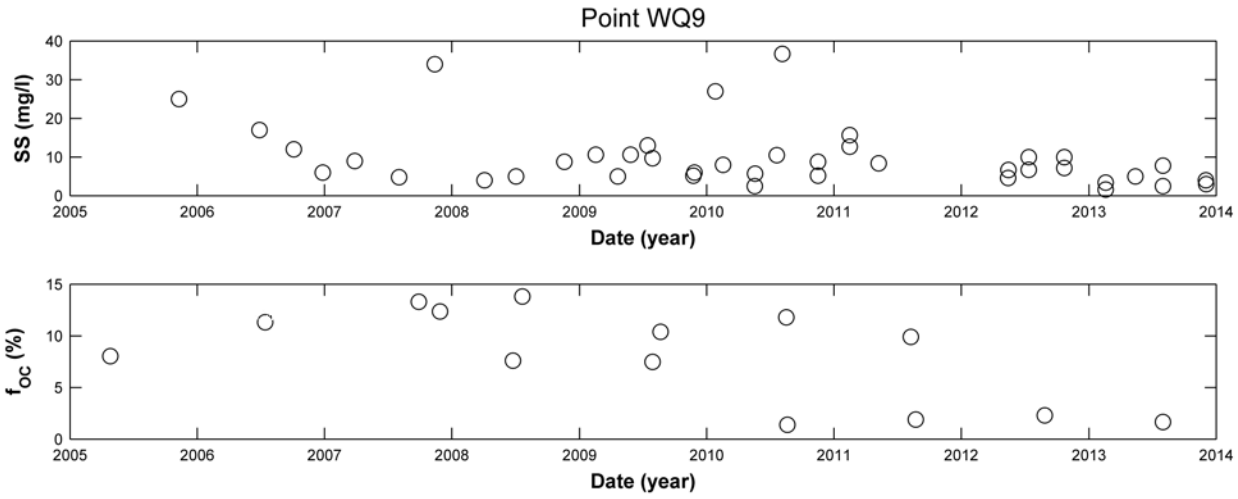

Figure 5.79: Measurements of suspended solids and f_{OC} at WQ9 (middle estuary) from "Red de Calidad del Litoral de Cantabria".

5.5.4.2 Model setup

In the non-conservative approach, model setup was different as in the Step 3 and 4 so it was necessary to conduct additional tasks for calibrating the far-field model. First of all, we ran Delft3D-FLOW in the period 01/06/2008 to 01/12/2008 (6 months) using the calibrated parameters and the river flows and water levels of this period as forcings (see figure 5.82).

Model domain discretization

The model domain discretization was the same that it was used for the hydrodynamic and transport (conservative) model setup, i.e., the transport (no conservative) model grid had the same number of nodes (grid cells) and layers. No horizontal and/or vertical aggregation was used.

Boundary and initial conditions

As boundary and initial conditions were used those shown in figure 5.80.

Open and closed boundary conditions

CBs were defined by the known shoreline where the flow through the boundary was set to zero. The vertical diffusive flux of toxicant through the free surface and bed was set with the specific processes acting on them, i.e. volatilization ($CHCl_3$) and sedimentation ($CHCl_3$ and Pb). OBs of $CHCl_3$ and Pb were set to zero, i.e., we assumed that toxicants outside the model domain were negligible.

At this point, it is worthy to recall that SS (inorganic) were attached to simulations of Pb while f_{OC} to $CHCl_3$. Regarding f_{OC} values, the model used the concentration of particulate organic carbon (POC) so we assumed that POC=$SS \times f_{OC}$ (mg/l).

We defined four OBs of SS and POC (one upper, one lower and two lateral):

- In the upper sea boundary condition, SS and POC (f_{OC}) were modeled by imposing a three-dimensional profile with the measurements of WQ15. Due to the vertical and temporal variation of both were not significant at WQ15 during the calibration period, we established that the boundary was vertically and temporally constant being the average of all the measurements, i.e., 7.989 and 0.7787 (9.74%) mg/l respectively.
- The lateral sea boundary conditions were modeled by imposing the same values of the upper boundary for all the variables.
- The lower river boundary condition was generated by regressing to a power-law (equation (5.6)) the relation between suspended solids concentration and river flow according to Dingman (2009).

$$SS(Q) = a_S \cdot Q^{b_S} \tag{5.6}$$

where SS is suspended solids concentration, and a_S and b_S are river-specific empirical values determined by logarithmic regression analysis. Generally, the exponent in such relations is almost always >1. In a comparative study of 59 drainage basins, Syvitski *et al.* (2000) found that a_s is inversely related to long-term average discharge and b_s is correlated with average air temperature and topographic relief.

Following the equation (5.6), we fitted to a power-law the river flow time series with the available measurements of "Red de Control de Calidad Litoral en Cantabria" (IHCantabria 2012) at WQ1. Figure 5.81 displays the obtained correlation in a log-log plot. The power-law was $SS = 0.0269 \cdot Q^{1.5773}$ and the regression coefficient (R^2) was 0.8997.

SS and POC (f_{OC}) were modeled by imposing a three-dimensional profile using the river flow series for the calibration period and the power-law relation between Q and SS. Due to the temporal variation

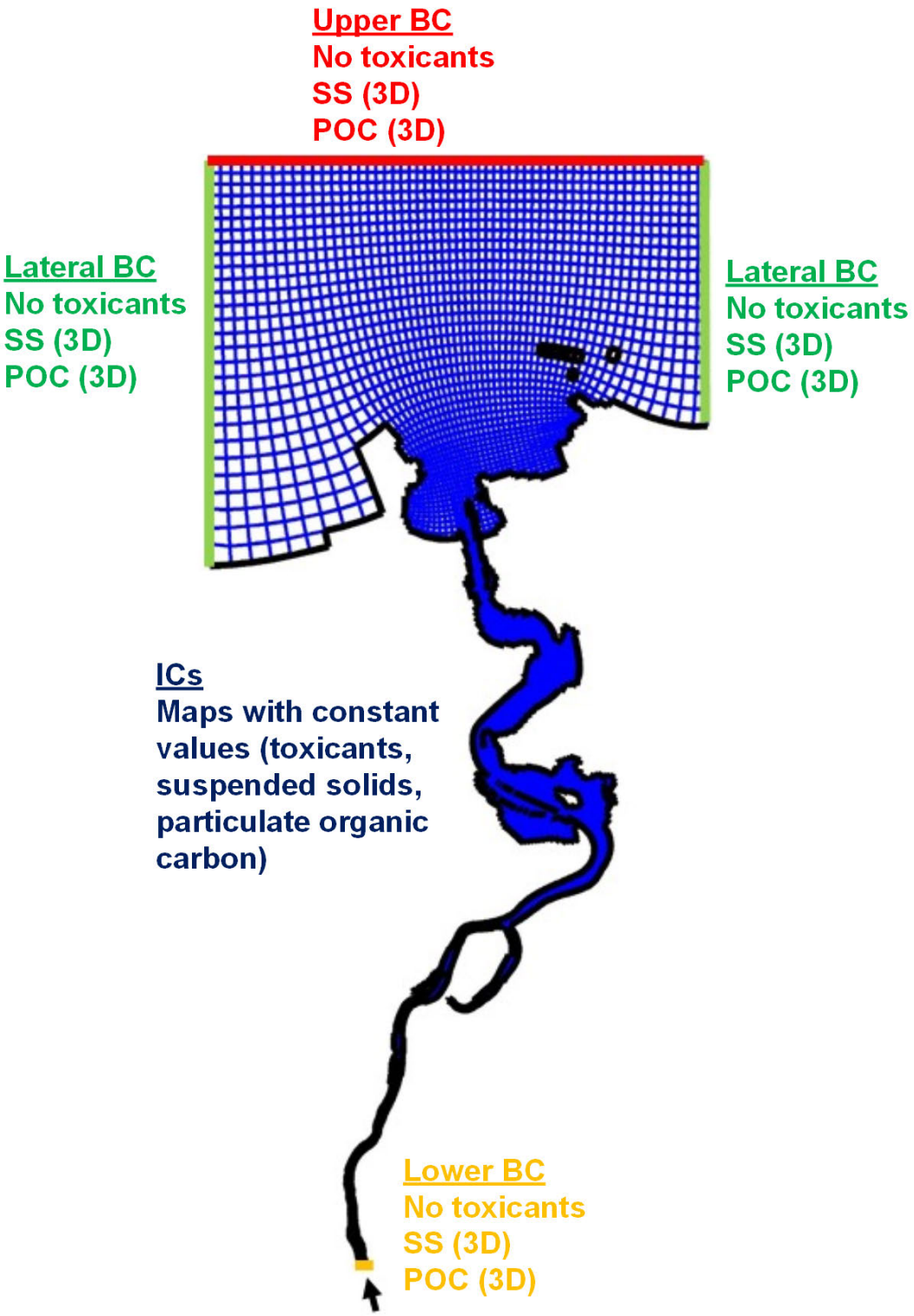

Figure 5.80: Schematic view of the boundary and initial conditions imposed during non-conservative transport simulations.

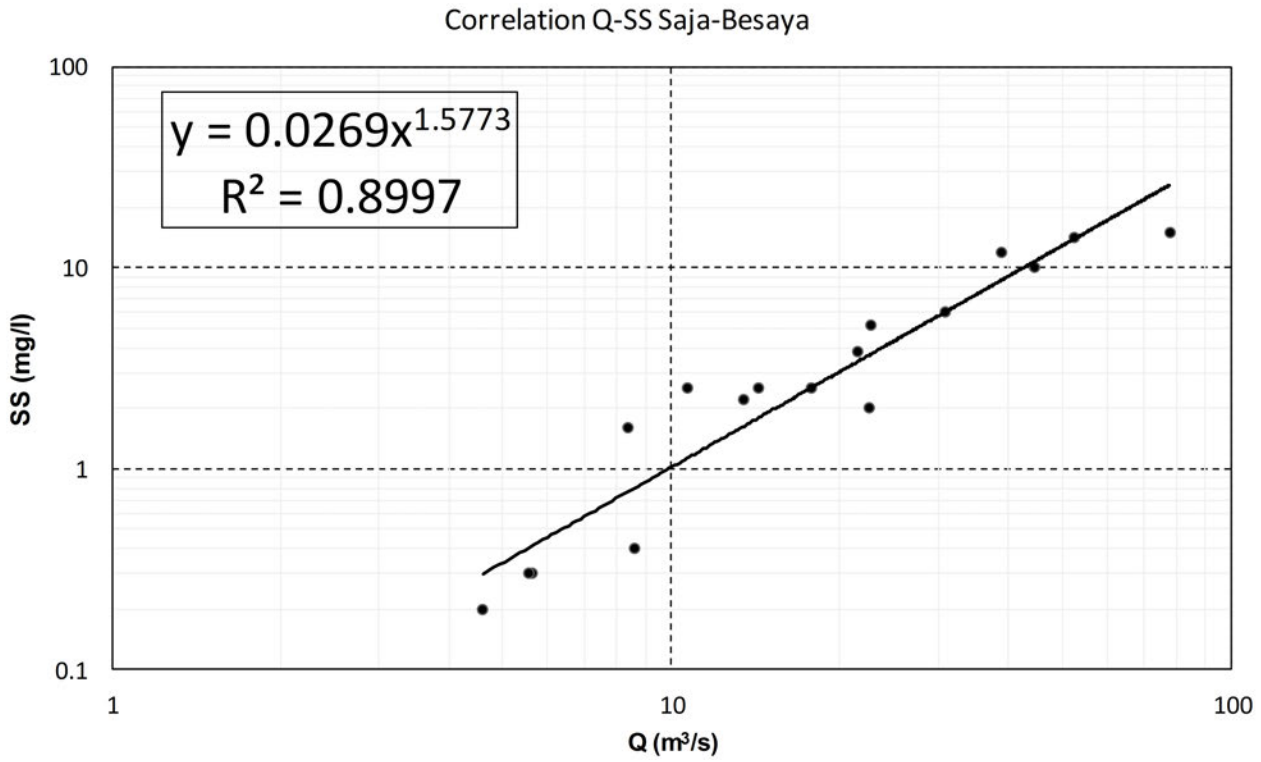

Figure 5.81: Logarithmic regression analysis between suspended solids concentration and river flow at WQ1 in the Suances Estuary.

was significant and the vertical was insignificant, both variables were established as a daily time series of a constant profile of SS and POC (f_{OC}). Figure 5.82 shows the water levels (a), river flows (b), river concentration of SS (c) and river concentration of POC (d) imposed during the calibration process.

Initial conditions

Due to the field of non-conservative tracer in the study area is unknown, the initialization of the transport model sets to zero during the model calibration. As a consequence, the timescale of the "quasi-stationary" response of the "worst case of dilution" should be considered in order to ensure that initial conditions are not influencing the model results. This time was 528 hours (22 days).

ICs were maps with constant values (Figure 5.80). We specified a concentration of 0 mg/l for both toxicants, a concentration of 8.886 mg/l for suspended solids (used in Pb model) and a concentration of 0.8662 (9.74%) mg/l for the POC (used in $CHCl_3$ model) throughout every grid cell of the meshgrid. SS and POC values were the average of all the available measures in SE during the calibration period.

Model calibration

Model calibration was focused on adjust the physical, physicochemical (lead and chloroform) and numerical parameters used by the far-field model D-Water Quality. To carry on this calibration, we used the data of the field campaign (IHCantabria 2008a) in the period 01/06/2008 to 01/12/2008 (6 months).

Physical parameters

Physical parameters were calibrated in Step 3. They were the same for the transport model of non-conservative substances and, consequently, calibration was not necessary to conduct for them.

Physicochemical parameters for lead (Pb)

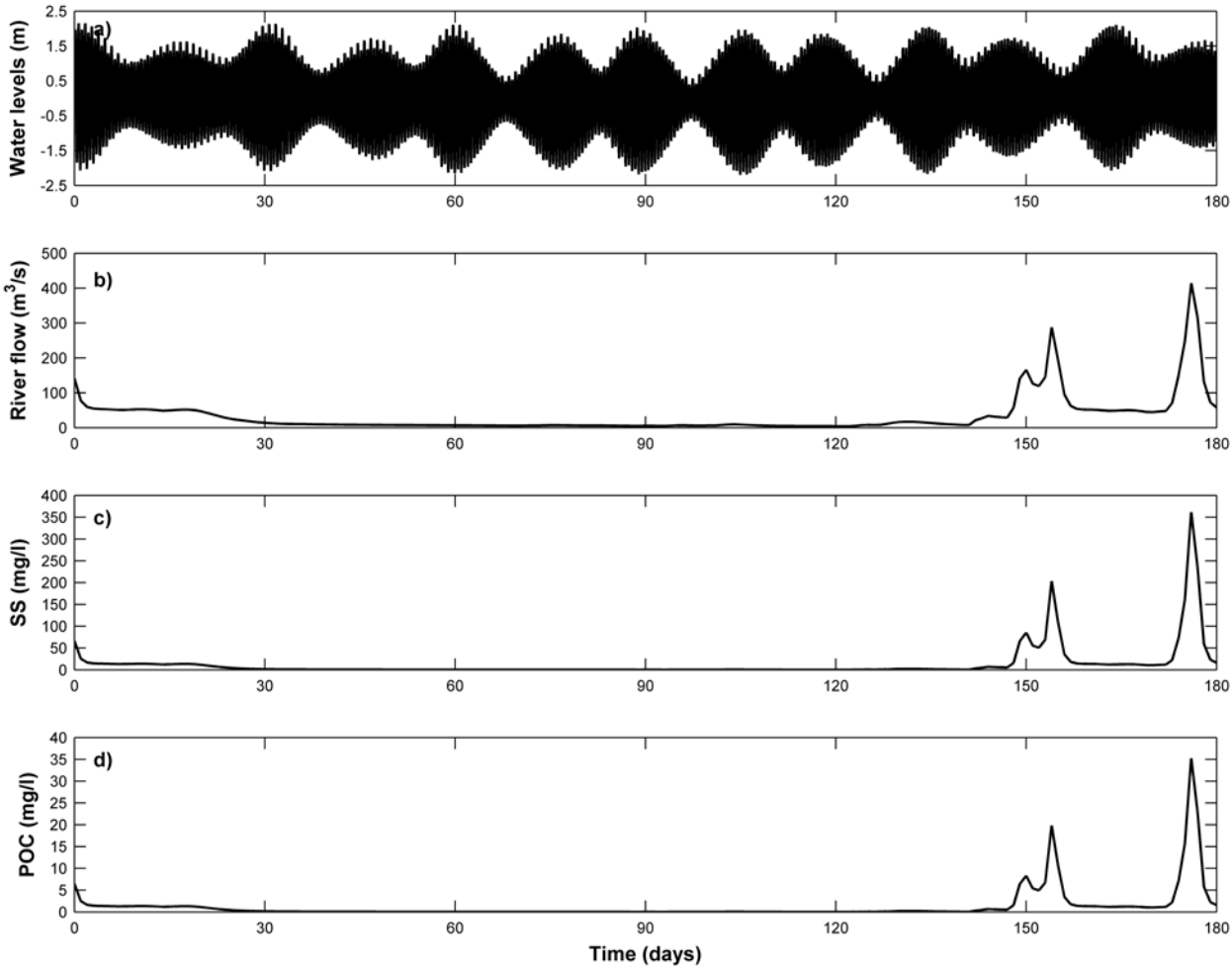

Figure 5.82: Open boundary conditions imposed during the calibration period of the far-field model (non-conservative approach). Water levels (a), river flows (b), river concentrations of suspended solids (c) and river concentrations of particulate organic carbon (d).

The total bottom shear stress was extracted from hydrodynamic model results at every time step. The sedimentation velocity of inorganic matter and the critical shear stress for sedimentation were collected from Sámano *et al.* (2014) being 31.968 m/day and 0.0635 N/m^2, respectively. The partition coefficient was 398 m^3/kg given by Gómez (2010). Finally, the half-time of non-equilibrium adsorption and desorption was 0 days because we assumed that both processes were controlled by an instantaneous equilibrium.

Physicochemical parameters for chloroform ($CHCl_3$)

The total bottom shear stress and the ambient water temperature were extracted from hydrodynamic model results at every time step. We assumed that the sedimentation velocity of organic matter and the critical shear stress for sedimentation were the same employed with inorganic matter so they were 31.968 m/day and 0.0635 N/m^2, respectively (Sámano *et al.* 2014).

In the case of the partition coefficient (l/kg), it was estimated from equation (3.27) as follows:

$$K_p = \frac{2 \cdot f_{OC} \cdot K_{ow}}{1 + \frac{(SS \cdot f_{OC} \cdot K_{ow})}{1.4}} = \frac{2 \cdot 0.0974 \cdot 95}{1 + \frac{(8.886 \cdot 10^{-6} \cdot 0.0974 \cdot 95)}{1.4}} = 18.52 \tag{5.7}$$

where K_{ow} was extracted from Gómez (2010) and, SS and f_{OC} were the same values used as ICs.

The liquid phase transfer coefficient was calculated by the equation (3.31) and the gas phase transfer coefficient by the equation (3.32) at every time step in all the grid cells. In these equations, $D_{liq_{O2}}$, M_{O2}, M_{OMP} and M_{water} were collected from Gómez (2010) being 0.000181 m^2/day, 32 Da, 119.38 Da and 18 Da.

Finally, the Henry's constant, the temperature coefficient loss and the constant rate of overall degradation were extracted from Gómez (2010) being 3536.24 Pa/m^3/mole, 1.07 and 0.008184 day^{-1}, respectively. Regarding the constant rate of overall degradation, it was calculated as the sum of three processes: hydrolysis, photolysis and biodegradation ($K_{pho} = 1.026 \cdot 10^{-6}$ day^{-1}, $K_{hyd} = 0.00433$ day^{-1} and $K_{bio} = 0.00385$ day^{-1}) by means of equation (3.33).

Numerical parameters

Numerical parameters were the same utilized in Step 3 and 4.

Simulation-calibration cases

Simulation-calibration cases were all the different model simulations performed by means of N combinations of physical parameters, M combinations of physicochemical parameters and L combinations of numerical parameters. Table 5.16 synthesizes the calibration parameters, suggests the best option for estuarine modeling and gives the optimal value ranges of each parameter.

As it can be seen from table 5.16, hydrodynamic and transport (conservative) model were previously calibrated so the model calibration of transport (non-conservative) was related to the specification of physicochemical parameters for lead (ID2) and chloroform (ID1). In the case of physicochemical parameters, there was 9 cases coming from the combination of different temperature coefficient loss. Regarding numerical parameters, there were 1 case. The combination of all of this cases resulted in 9 simulation-calibration cases.

Final configuration

Model calibration was focused on adjusting concentrations of Pb and $CHCl_3$ in order to simulate adequately transport of non-conservative tracers. Due to the scarcity of toxicant data (Table 5.15), instead of determining error measurements, a qualitative calibration of both toxicants was carried on. According to model results, the final configuration of the model was the combination of all mentioned parameters in table 5.17.

Lastly, figures 5.83 and 5.84 present the comparison between the observed data at WQ3 (upper panel) and WQ6 (lower panel) and the model results of lead and chloroform, respectively. Good agreement was obtained

Physical parameters	**Suggestions**	**Value ranges**
All parameters	Same hydrodynamic model	Hydrodynamic calibration
Physicochemical parameters (Pb)	**Suggestions**	**Value ranges**
Sedimentation velocity of SS	Sámano *et al.* (2014)	31.968 m/day
Total bottom shear stress	Imported from hydrodynamics	-
Critical shear stress for sedimentation	Sámano *et al.* (2014)	0.0635 N/m^2
Partition coefficient	Gómez (2010)	398 m^3/kg
Half-time of adsorption and desorption	Instantaneous equilibrium	Zero
Physicochemical parameters ($CHCl_3$)	**Suggestions**	**Value ranges**
Sedimentation velocity of POC	Sámano *et al.* (2014)	31.968 m/day
Total bottom shear stress	Imported from hydrodynamics	-
Critical shear stress for sedimentation	Sámano *et al.* (2014)	0.0635 N/m^2
Partition coefficient	Eq. (3.27) + Gómez (2010)	18.52 l/kg
Liquid phase transfer coefficient	Eq. (3.31) + Gómez (2010) + Hydro	Map field
Gas phase transfer coefficient	Eq. (3.32) + Gómez (2010) + Hydro	Map field
Henry's constant	Gómez (2010)	3536.24 Pa/m^3/mole
Constant rate of overall degradation	Gómez (2010)	0.008184 day^{-1}
Ambient water temperature	Imported from hydrodynamics	-
Temperature coefficient loss	Gómez (2010)	1.01:0.01:1.10
Numerical parameters	**Suggestions**	**Value ranges**
All parameters	Same conservative model	Conservative calibration

Table 5.16: Overall picture of far-field model calibration parameters for non-conservative approach.

Physical parameters	**Calibrated Value**
All parameters	Hydrodynamic calibration
Physicochemical parameters (Lead)	**Calibrated Value**
Sedimentation velocity of SS	31.968 m/day
Total bottom shear stress	Imported from hydrodynamics
Critical shear stress for sedimentation	0.0635 N/m^2
Partition coefficient	398 m^3/kg
Half-time of adsorption and desorption	Zero
Physicochemical parameters (CHCl3)	**Calibrated Value**
Sedimentation velocity of POC	31.968 m/day
Total bottom shear stress	Imported from hydrodynamics
Critical shear stress for sedimentation	0.0635 N/m^2
Partition coefficient	18.52 l/kg
Liquid phase transfer coefficient	Map field (spatial and temporal)
Gas phase transfer coefficient	Map field (spatial and temporal)
Henry's constant	3536.24 Pa/m^3/mole
Constant rate of overall degradation	0.008184 day^{-1}
Ambient water temperature	Imported from hydrodynamics
Temperature coefficient loss	1.07
Numerical parameters	**Calibrated Value**
All parameters	Conservative calibration

Table 5.17: Optimal calibration parameters of the far-field model of Pb and $CHCl_3$ for SE in the non-conservative approach.

between the model-predicted concentrations and the observed data at both stations and toxicants.

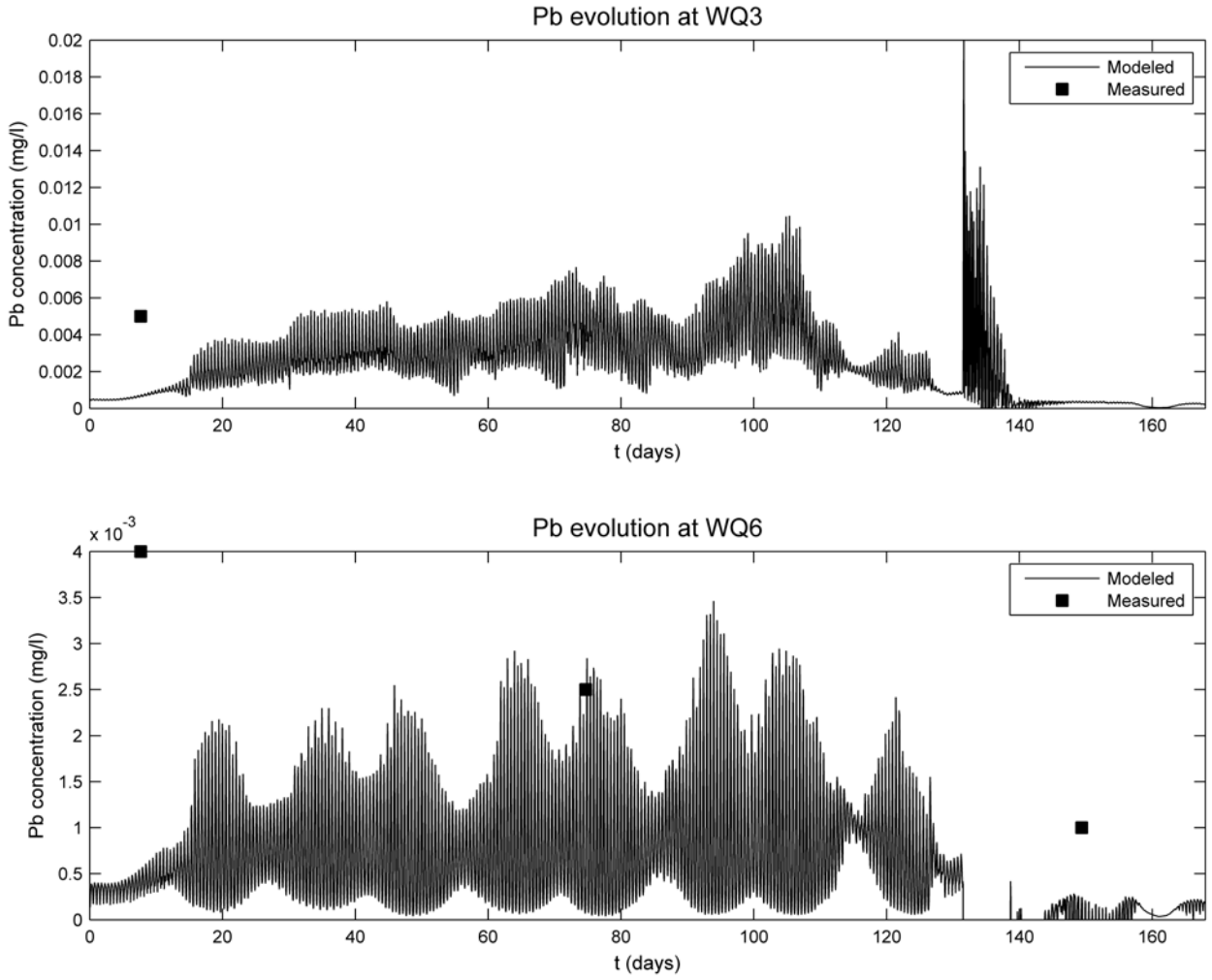

Figure 5.83: Comparison between the measured and modeled concentrations of lead at the sampling points WQ3 (upper panel) and WQ6 (lower panel).

5.5.4.3 **Transport real case modeling**

Anew, the time required for stabilizing the model results and the influence of initial conditions on these results were two issues difficult to handle. In order to accomplish these issues, we performed 78 "presimulations" to obtain the adequate initial condition of toxicant concentration for every model scenario and other 78 "simulations" to record the concentration evolution along the 15 days of every model scenario.

"Presimulations"

The maximum timescale of the "quasi-stationary" response for transport was the timescale of the "worst case of dilution" being 528 hours (22 days).

As boundary and initial conditions were used those shown in figure 5.80. CBs were the same defined in the model setup. OBs of toxicants were set to zero. We also defined four OBs of SS and POC (one upper, one lower and two lateral):

- In the upper sea boundary condition, SS and POC (f_{OC}) were again modeled by imposing a three-

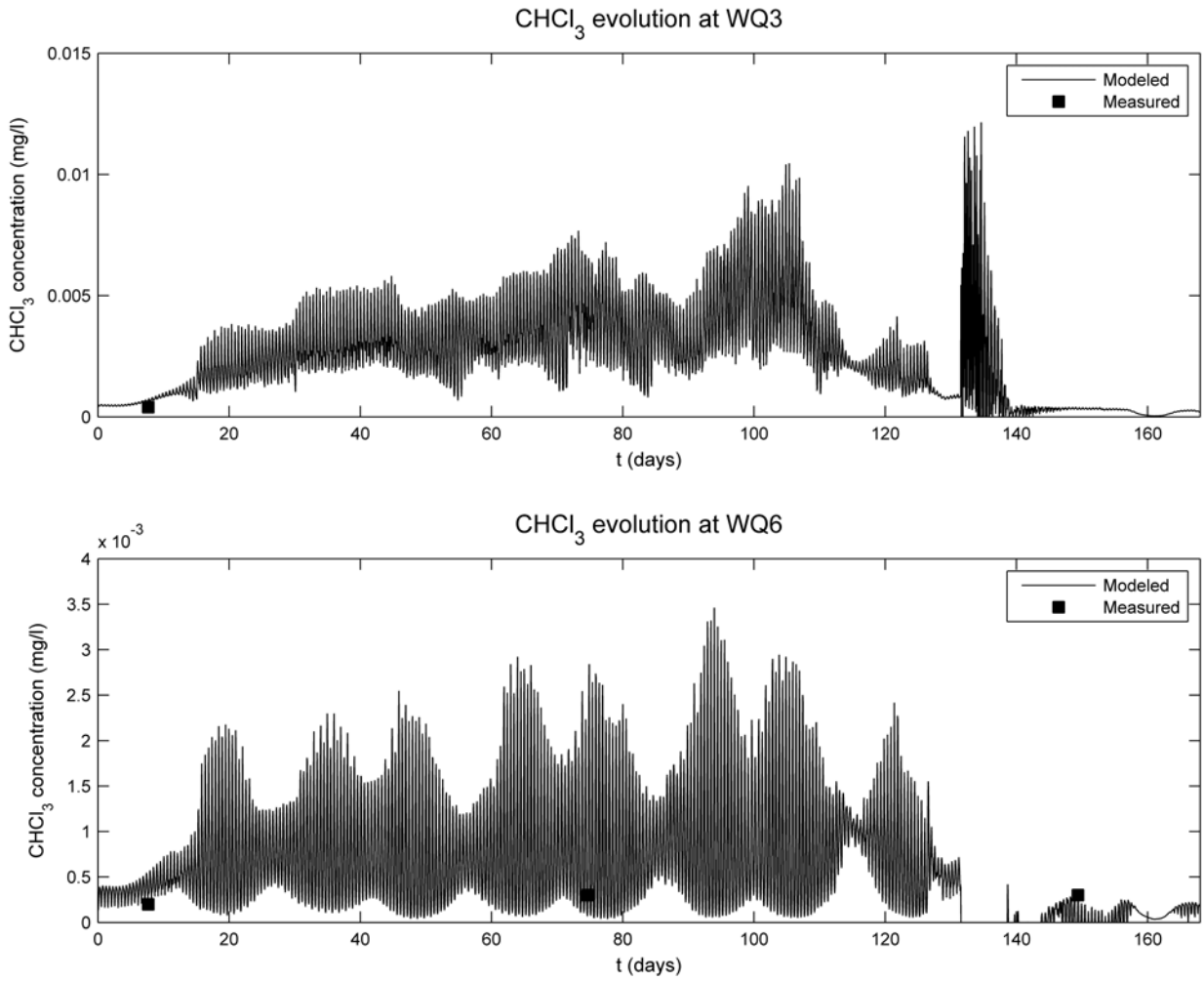

Figure 5.84: Comparison between the measured and modeled concentrations of chloroform at the sampling points WQ3 (upper panel) and WQ6 (lower panel).

dimensional profile with the measurements of WQ15. Due to the vertical and temporal variation of both were not significant at WQ15 during all the time, we established that the boundary was vertically and temporally constant being the average of all the measurements at any time, i.e., 8.978 and 0.6105 (6.80%) mg/l respectively.

- The lateral sea boundary conditions were modeled by imposing the same values of the upper boundary for all the variables.
- The lower river boundary condition was generated by the power-law $SS = 0.0269 \cdot Q^{1.5773}$. Thus, SS and POC (f_{OC}) were modeled by imposing a three-dimensional profile using the river flow series for every model scenario and the power-law relation. Due to the temporal variation was significant and the vertical was insignificant, both variables were established as a daily time series of a constant profile of SS and POC (f_{OC}). As a example of this boundary, figures 5.85 and 5.86 present the water levels (a), river flows (b), river concentration of SS (c) and river concentration of POC (d) imposed during the real cases 23 and 54, respectively.

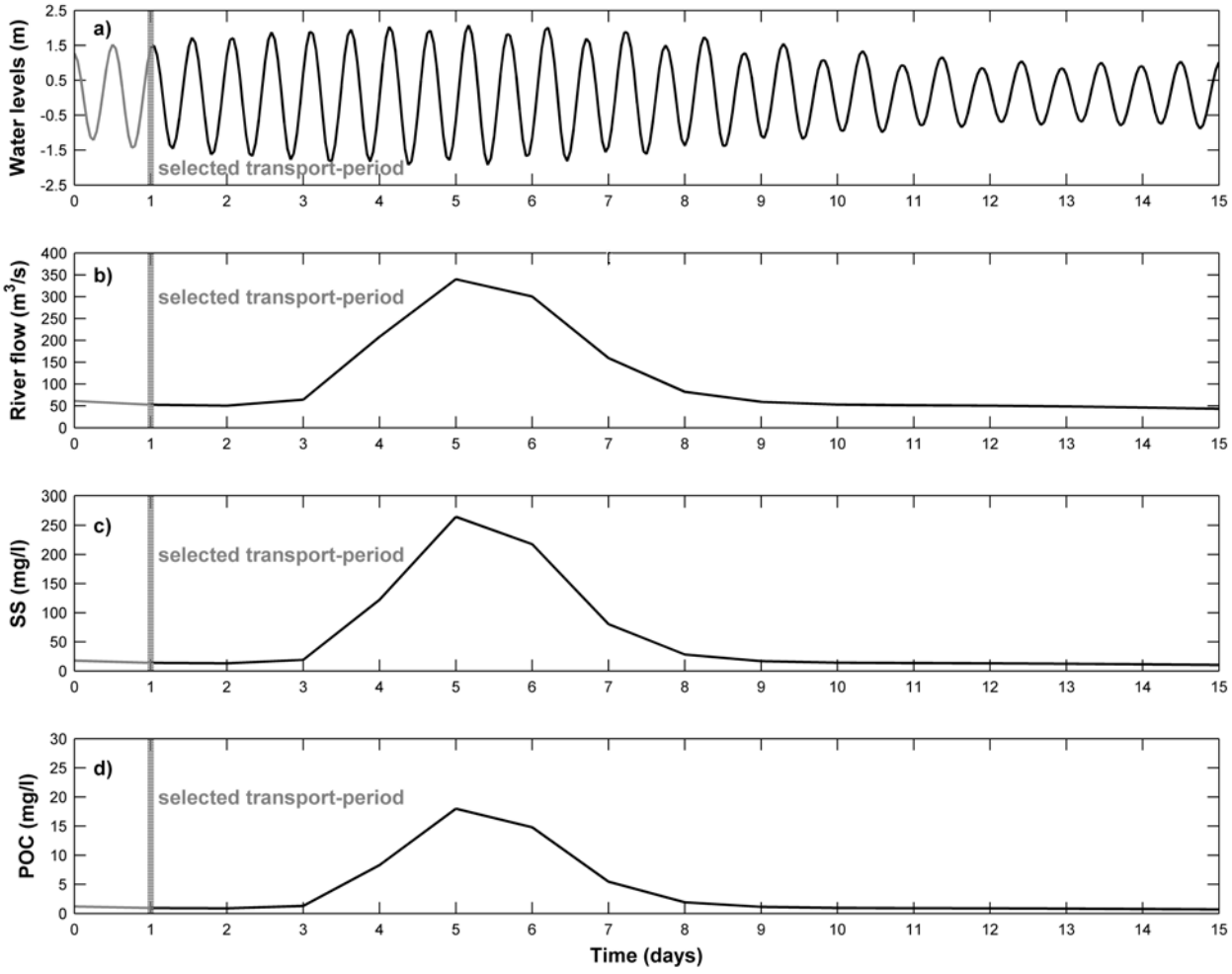

Figure 5.85: Open boundary conditions imposed during the "presimulation" (grey line) and "simulation" (black line) of the real case 23. Water levels (a), river flows (b), river concentrations of suspended solids (c) and river concentrations of particulate organic carbon (d).

ICs were maps with constant values (Figure 5.80). We specified a concentration of 0 mg/l for both toxicants, a concentration of 11.013 mg/l for SS (used in Pb model) and a concentration of 0.7489 (6.80%) mg/l for POC (used in $CHCl_3$ model) throughout every grid cell of the meshgrid to start the simulations. SS and POC values were the average of all the available measures in SE.

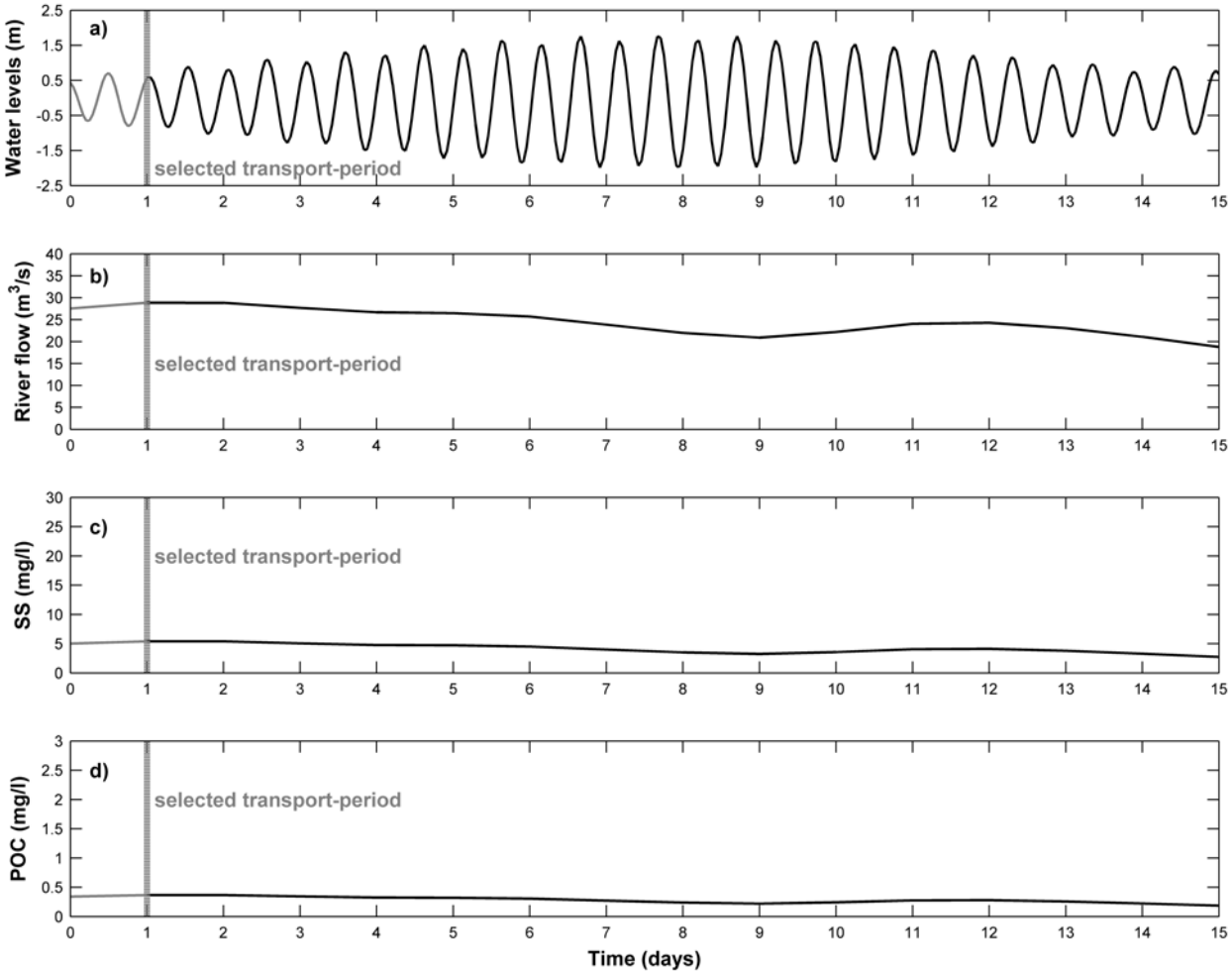

Figure 5.86: Open boundary conditions imposed during the "presimulation" (grey line) and "simulation" (black line) of the real case 54. Water levels (a), river flows (b), river concentrations of suspended solids (c) and river concentrations of particulate organic carbon (d).

The 78 "presimulations" were carried out using a constant river flow of the first day of every model scenario and its associated tide during 24 hours (see figures 5.85 and 5.86). Next, we ran D-Water Quality for ID1 and ID2 with the Delft3D-FLOW results of the first day in a continuous loop during 30 days in every model scenario.

Once it was reached the "quasi-stationary" response for transport, we recorded the map of toxicant concentration that corresponds to the first hour of the 78 model scenarios, i.e, the 78 initial conditions. Due to the many number of cases, as an example of the initial conditions, we illustrate the final map of case 23 (see figure 5.66 and the bolded row in table 5.13) and 54 (see figure 5.66 and the bolded row in table 5.14) for ID1 and ID2 in the next paragraphs.

Figures 5.87, 5.88, 5.89 and 5.90 display the map of the spatial distribution of toxicants and suspended solids at the surface (a-c) and bottom (b-d) layers used as the initial condition for the "simulation" of the "real case 23 and 54 of dilution" of ID1 and ID2, respectively.

"Simulations"

CBs and OBs were the same defined in the "presimulations". Meanwhile, ICs were two maps of concentrations obtained in the 78 "presimulations". In the case of ID1, these two maps with 10 layers were $CHCl_3$ and POC (see figures 5.87 and 5.88). In the case of ID2, these two maps with 10 layers were Pb and SS (see figures 5.89 and 5.90).

We ran the 78 model scenarios and hourly recorded 15 days of transport model results. Due to the many number of cases, as an example of the "simulations", we illustrated the far-field model results for the concentration evolution of four grid cells located across the model domain in the case 23 (see figure 5.66 and the bolded row in table 5.13) and 54 (see figure 5.66 and the bolded row in table 5.14) for ID1 and ID2 in the next paragraphs.

Figure 5.91, 5.92, 5.93 and 5.94 display the far-field model results for the concentration evolution of chloroform (ID1) and lead (ID2) in the surface layer (black line) and the bottom layer (grey line) at WQ3 (a), SS1 (b), SS3 (c) and SS5 (d) in the "real case 23 and 54 of dilution", respectively.

5.5.4.4 Delimitation of mixing zones

Unlike the simplified calculation where one model scenario was only run under fixed conditions or the intermediate calculation where one model scenario was ran during one year under real conditions. In the detailed calculation, we ran M model scenarios under real conditions with an occurrence probability. After model simulations, we determined the AA-MZ and MAC-MZ by applying the developed method in Chapter 3 (Figure 3.37).

Validation of the reconstructed series

The first tier was validate the ability of the 78 model scenarios to adequately reconstruct "real series". This validation was conducted in several steps.

Firstly, we carried on the continuous simulation of toxicants taking into account the "real series" of river flow and tidal elevations from 01/06/2008 to 01/12/2008 (period of the non-conservative model calibration). As it is shown in figure 5.82, this period was chosen because it encompassed every type of tidal groups and combined dry and wet periods of river flows, i.e, this period was a good descriptor of the environmental forcing variability. Regarding the stability of model results and the influence of initial conditions, we conducted again one "presimulation" under "quasi-fixed hydrodynamic conditions" using a constant river flow of the first day and its associated tide during 24 hours in a continuous loop during 30 days. Next, we recorded the concentration field of the first time step that corresponded to the first hour and, finally, we ran all the simulation

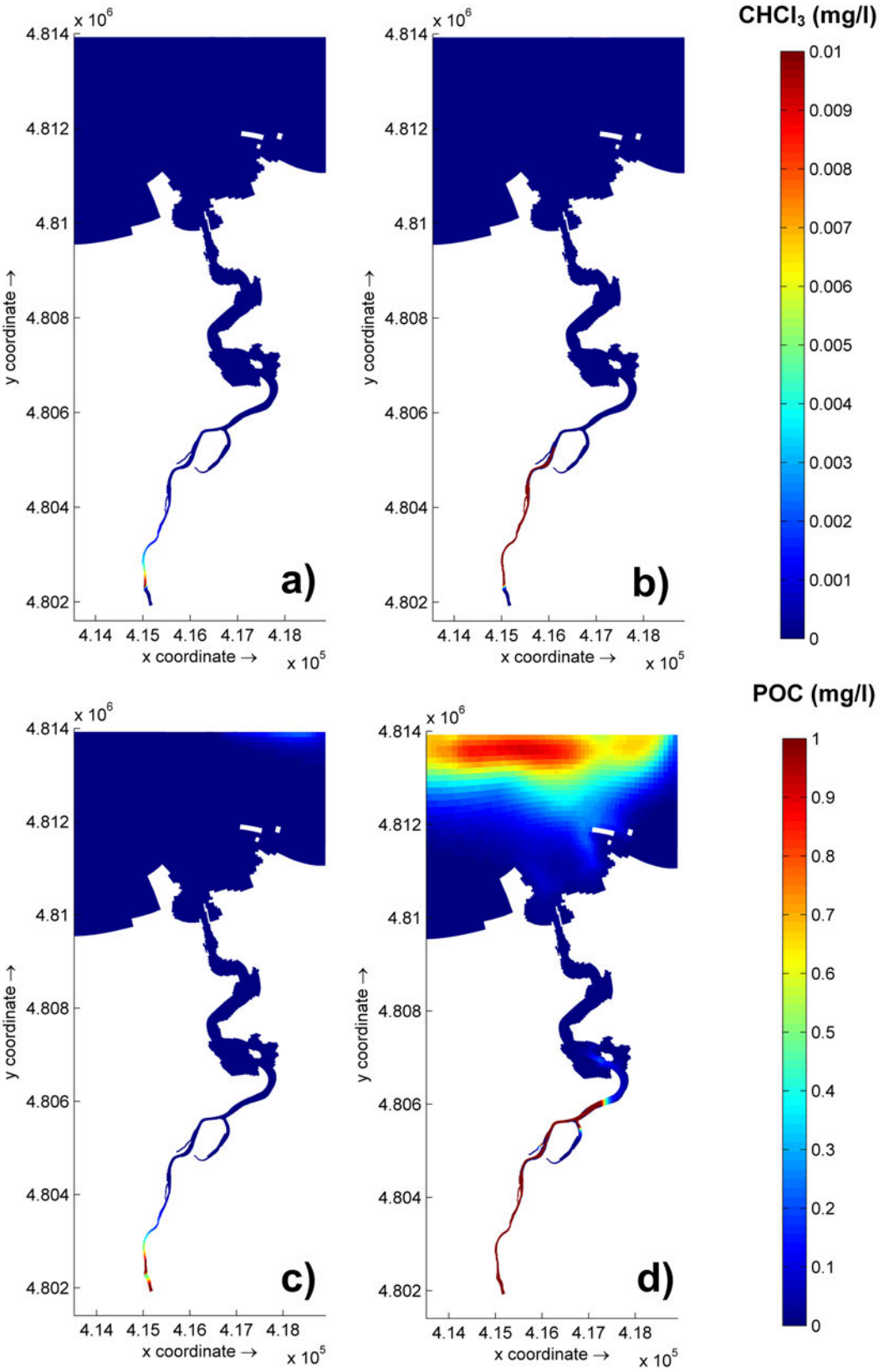

Figure 5.87: Map of the spatial distribution of chloroform and particulate organic carbon used as the initial conditions for the "simulation" of the "real case 23 of dilution" for ID1. $CHCl_3$ surface layer (a), $CHCl_3$ bottom layer (b), POC surface layer (c) and POC bottom layer (d).

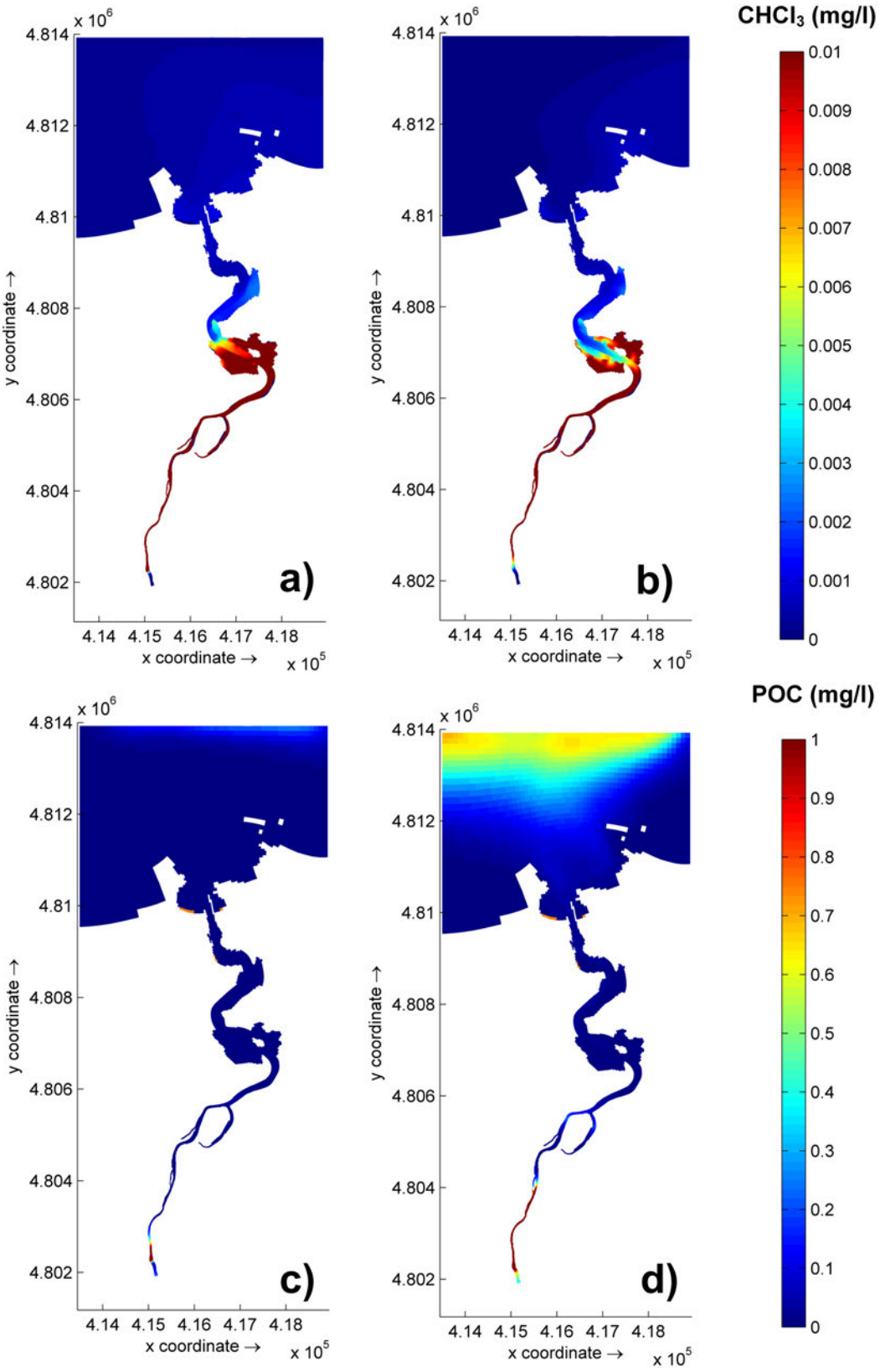

Figure 5.88: Map of the spatial distribution of chloroform and particulate organic carbon used as the initial conditions for the "simulation" of the "real case 54 of dilution" for ID1. $CHCl_3$ surface layer (a), $CHCl_3$ bottom layer (b), POC surface layer (c) and POC bottom layer (d).

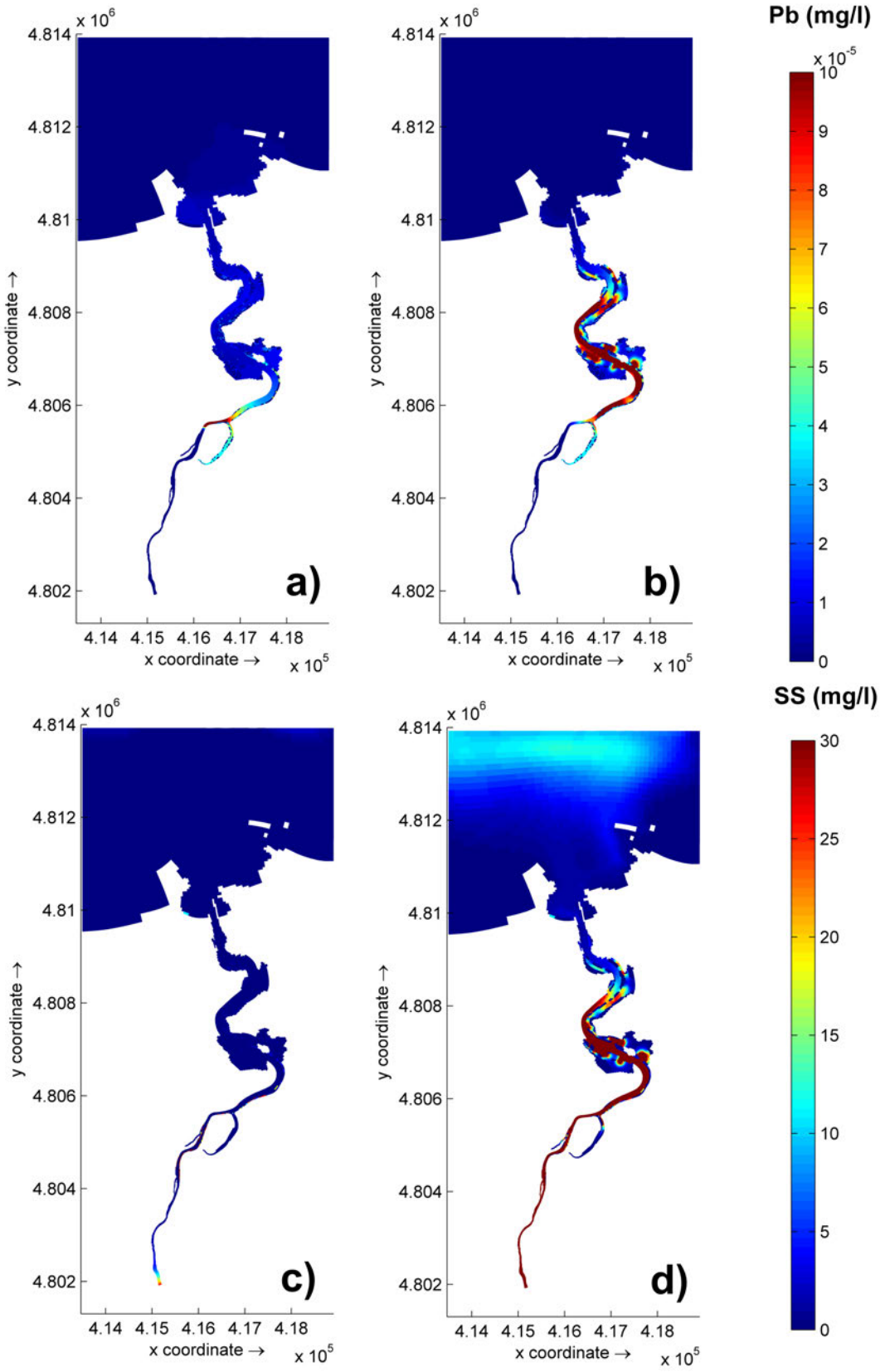

Figure 5.89: Map of the spatial distribution of lead and suspended solids used as the initial condition for the "simulation" of the "real case 23 of dilution" for ID2. Pb surface layer (a), Pb bottom layer (b), SS surface layer (c) and SS bottom layer (d).

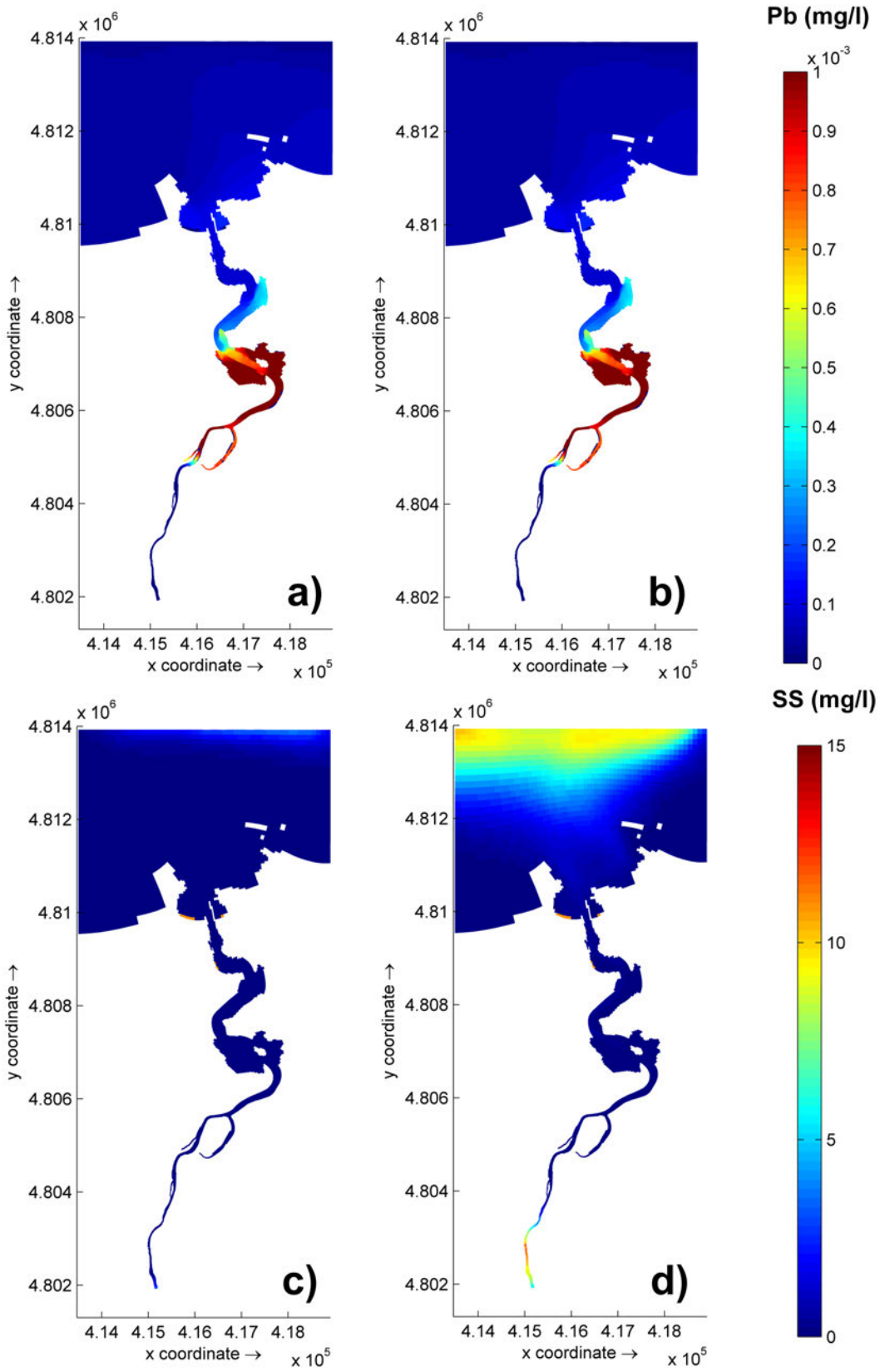

Figure 5.90: Map of the spatial distribution of lead and suspended solids used as the initial condition for the "simulation" of the "real case 54 of dilution" for ID2. Pb surface layer (a), Pb bottom layer (b), SS surface layer (c) and SS bottom layer (d).

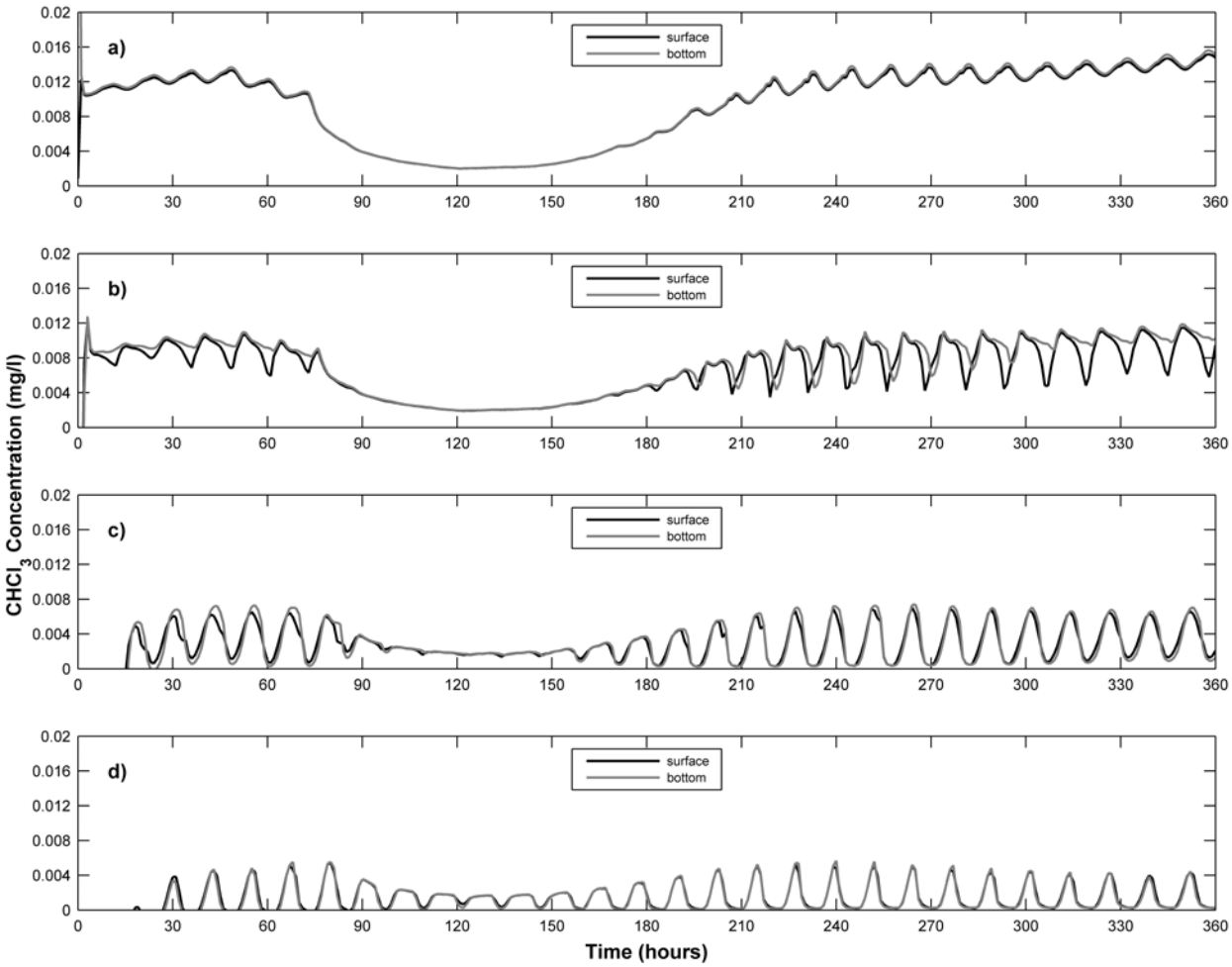

Figure 5.91: Evolution of chloroform concentration (ID1) at the surface layer (black line) and the bottom layer (grey line) for the transport of the "real case 23 of dilution" at WQ3 (a), SS1 (b), SS3 (c) and SS5 (d).

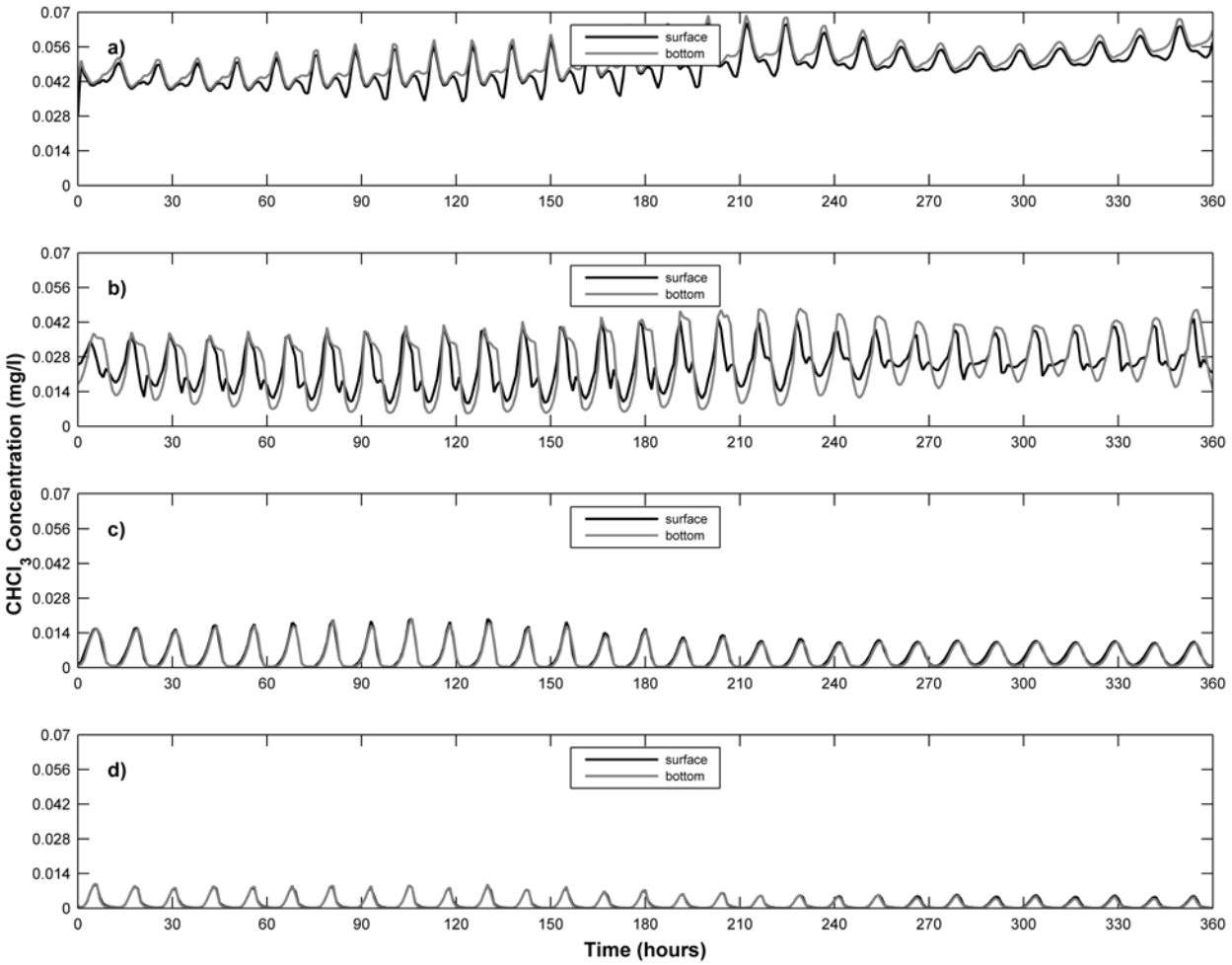

Figure 5.92: Evolution of chloroform concentration (ID1) at the surface layer (black line) and the bottom layer (grey line) for the transport of the "real case 54 of dilution" at WQ3 (a), SS1 (b), SS3 (c) and SS5 (d).

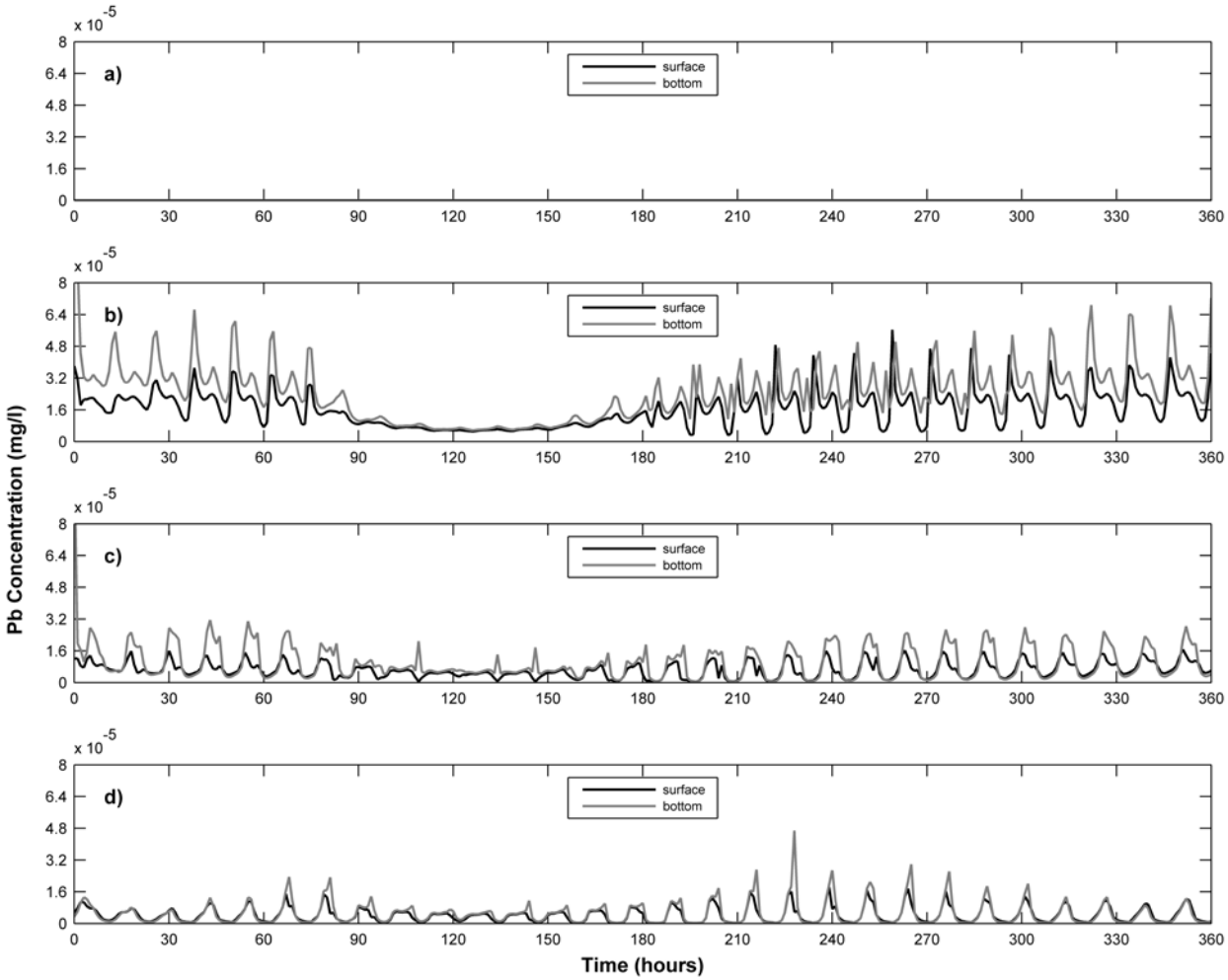

Figure 5.93: Evolution of lead concentration (ID2) at the surface layer (black line) and the bottom layer (grey line) for the transport of the "real case 23 of dilution" at WQ3 (a), SS1 (b), SS3 (c) and SS5 (d).

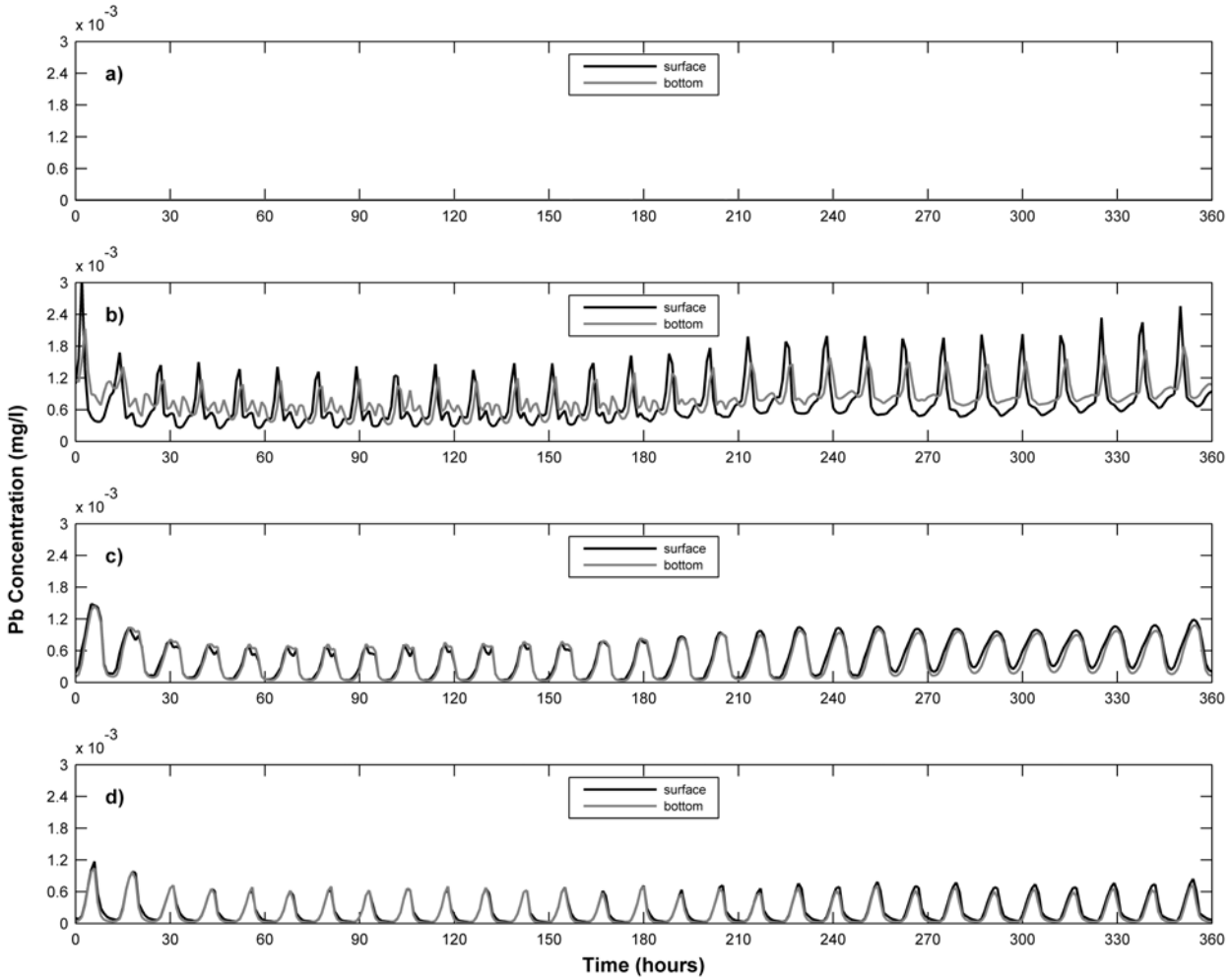

Figure 5.94: Evolution of lead concentration (ID2) at the surface layer (black line) and the bottom layer (grey line) for the transport of the "real case 54 of dilution" at WQ3 (a), SS1 (b), SS3 (c) and SS5 (d).

Station	Depth	Model-Cluster Mean (mg/l)	Model-Cluster MAC-duration (%)	BIAS (mg/l)	CE (-)
ID1	Surface	0.0889-0.1081	96.11-95.56	-0.0192	0.7263 Acceptable (convenient)
	Middle	0.1098-0.1541	96.67-96.67	-0.0443	0.5742 Acceptable
	Bottom	0.1009-0.1573	96.67-96.67	-0.0564	0.5008 Acceptable (convenient)
WQ3	Surface	0.0998-0.1210	98.33-98.33	-0.0212	0.7382 Acceptable (convenient)
	Middle	0.1194-0.1651	98.33-98.33	-0.0457	0.5983 Acceptable
	Bottom	0.1103-0.1678	98.33-98.33	-0.0575	0.5288 Acceptable
SS1	Surface	0.0444-0.0591	98.33-99.44	-0.0147	0.6637 Acceptable (convenient)
	Middle	0.0471-0.0645	98.33-99.44	-0.0175	0.6208 Acceptable (convenient)
	Bottom	0.0446-0.0592	98.33-99.44	-0.0146	0.6353 Acceptable (convenient)
SS3	Surface	0.0259-0.0290	97.78-99.44	-0.0031	0.8096 Acceptable (excellent)
	Middle	0.0254-0.0276	97.78-99.44	-0.0022	0.7828 Acceptable (convenient)
	Bottom	0.0237-0.0255	97.78-99.44	-0.0018	0.7571 Acceptable (convenient)
SS5	Surface	0.0164-0.0189	95.00-98.33	-0.0025	0.7934 Acceptable (convenient)
	Middle	0.0166-0.0186	95.00-98.33	-0.0019	0.8165 Acceptable (excellent)
	Bottom	0.0159-0.0175	95.00-98.33	-0.0016	0.8143 Acceptable (excellent)

Table 5.18: Measurements errors of the validation period (01/06/2008 to 01/12/2008) for ID1 at three depths of ID1, WQ3, SS1, SS3 and SS5.

with the initial conditions obtained in the "presimulation" and recording, hourly, 6 months of transport model results for ID1 and ID2.

Secondly, we searched on the 78 model scenarios the cases that best fitted each segment of the "real series" from 01/06/2008 to 01/12/2008.

Thirdly, we reconstructed the 10-layer evolution of toxicant concentration ($CHCl_3$ and Pb) from the selected model scenarios.

Finally, we compared the "real series" (model) versus the "synthetic series" (cluster) in order to validate the obtained results with "synthetic series" for a daily time resolution at three depths (surface=layer1, medium=layer5, and bottom=layer10). For this substep, CE, BIAS, the model and cluster mean concentration and the time exceeding the MAC-EQS of the model and cluster were used as error measurements.

Figures 5.95 and 5.96 illustrate, as an example, the evolution of chloroform concentration (ID1) and lead concentration (ID2) of the "real series" (model) in black color and the "synthetic series" (cluster) in grey color during the validation period at the point of doscharge (ID1 or ID2) and SS5. In both figures, the panels (a,b and c) corresponds to the surface, medium and bottom layers at the point of discharge, respectively. Meantime, the panels (d, c, and e) corresponds to the surface, medium and bottom layers at SS5, respectively.

In figure 5.96, the panels (a,b and c) corresponded to the surface, medium and bottom layers at ID2, respectively. Meantime, the panels (d, c, and e) corresponded to the surface, medium and bottom layers at SS5, respectively.

Table 5.18 summarizes the error measurements for ID1 in three depths at ID1, WQ3, SS1, SS3 and SS5. Along the estuary, model and cluster mean concentration were very similar. The mean of the "synthetic series" was always higher than the mean of the "real series". Consequently, a negative BIAS was obtained ranging between -0.0016 and -0.0575. Regarding the time exceeding the MAC-EQS in the case of $CHCl_3$, we considered that the AA-EQS was the MAC-EQS since this toxicant has not application to the MAC-EQS. The obtained values were the same or slightly different in all the stations indicating that both series might be interchangeable. Finally, the "synthetic series" displayed an acceptable level of performance in all the stations. ID1, SS1 and SS3 were reproduced conveniently, SS5 excellently and WQ3 was acceptable.

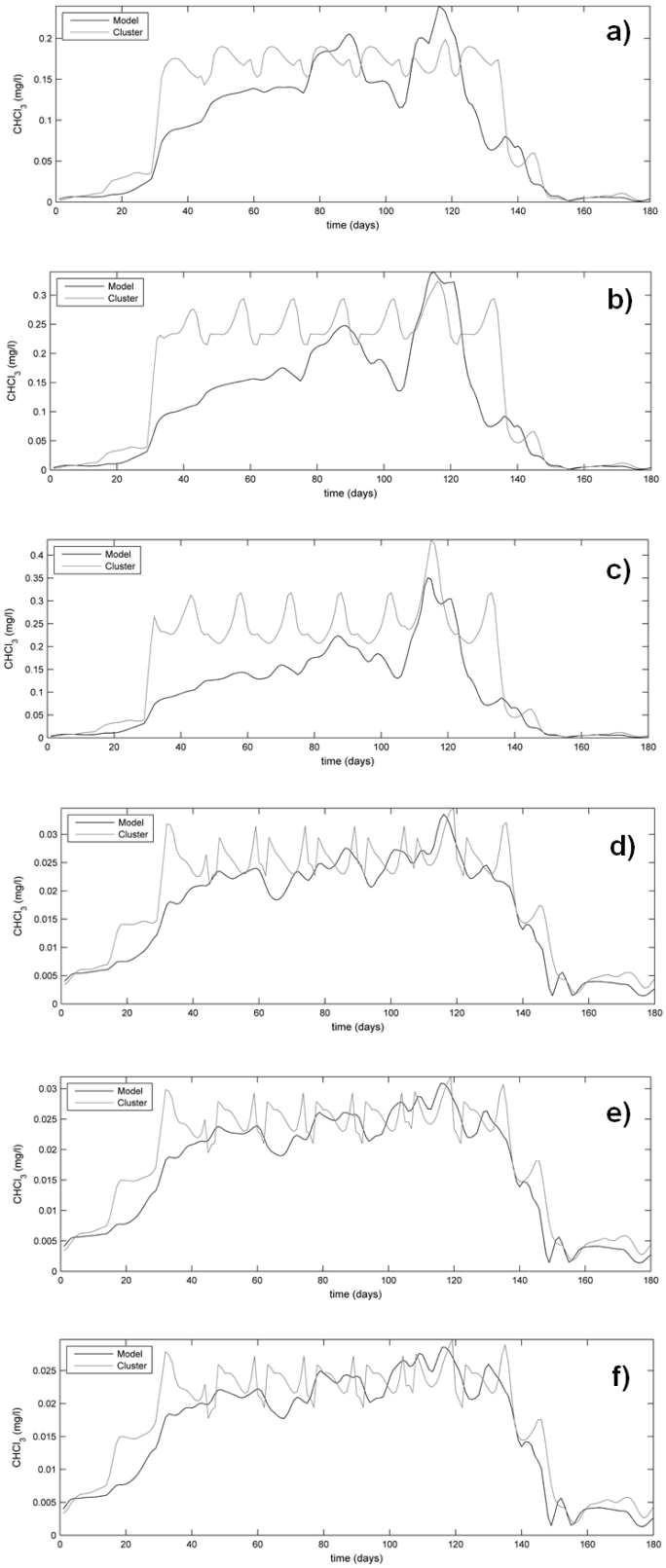

Figure 5.95: Evolution of chloroform concentration (ID1) of the model "real series" (black lines) and the cluster "synthetic series" (grey lines) for the transport of the validation period (01/06/2008 to 01/12/2008) at ID1 (surface (a), medium (b) and bottom (c) layers) and at SS5 (surface (d), medium (e) and bottom (f) layers).

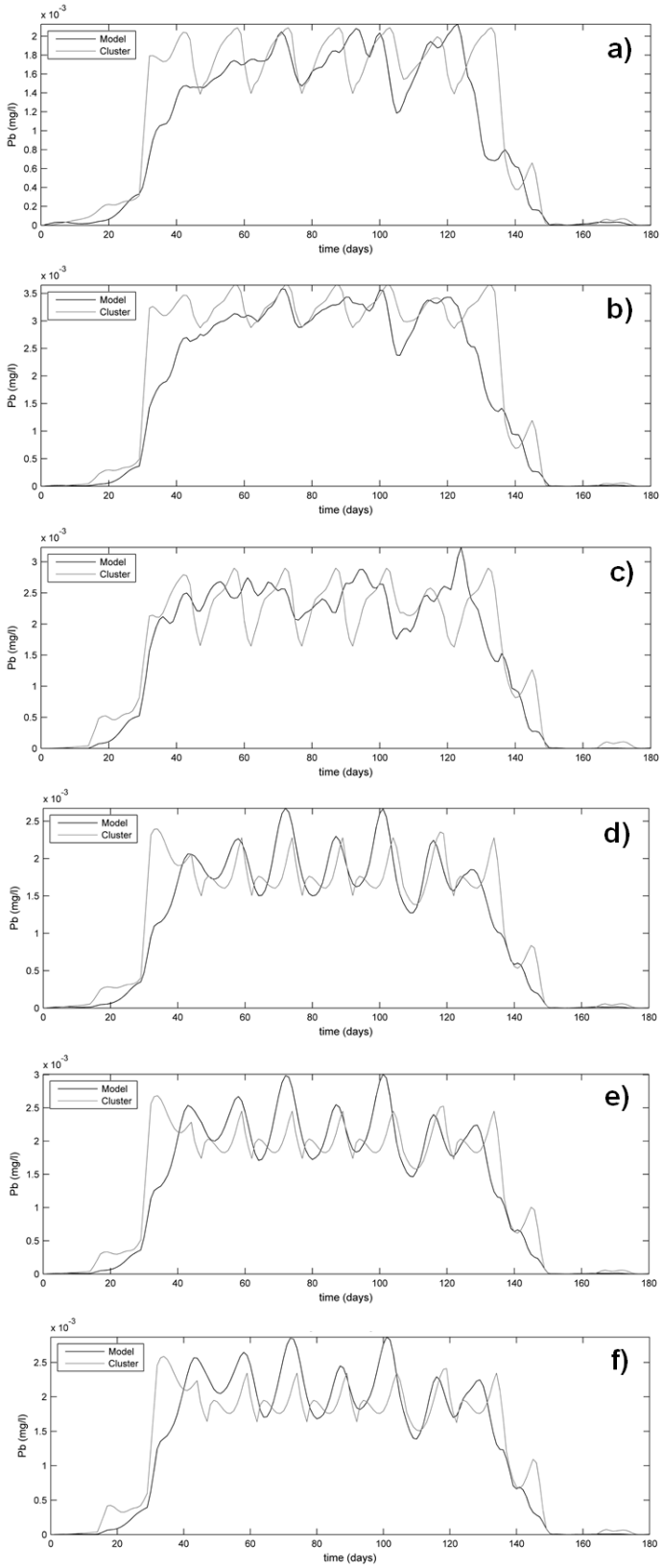

Figure 5.96: Evolution of lead concentration (ID2) of the model "real series" (black lines) and the cluster "synthetic series" (grey lines) for the transport of the validation period (01/06/2008 to 01/12/2008) at ID2 (surface (a), medium (b) and bottom (c) layers) and at SS5 (surface (d), medium (e) and bottom (f) layers).

Station	Depth	Model-Cluster Mean (mg/l)	Model-Cluster MAC-duration (%)	BIAS (mg/l)	CE (-)
ID2	Surface	0.0010-0.0011	0.0-0.0	-2.99e-04	0.7423 Acceptable (convenient)
	Middle	0.0017-0.0020	0.0-0.0	-5.64e-04	0.7969 Acceptable (convenient)
	Bottom	0.0014-0.0015	0.0-0.0	-5.55e-05	0.7648 Acceptable (convenient)
WQ3	Surface	0.0008-0.0008	0.0-0.0	-9.20e-05	0.2363 Acceptable (poor)
	Middle	0.0008-0.0009	0.0-0.0	-1.86e-04	0.2033 Acceptable (poor)
	Bottom	0.0010-0.0011	0.0-0.0	-2.97e-04	0.2402 Acceptable (poor)
SS1	Surface	0.0020-0.0021	0.0-0.0	-1.08e-04	0.6792 Acceptable (convenient)
	Middle	0.0021-0.0021	0.0-0.0	-3.02e-05	0.6070 Acceptable (convenient)
	Bottom	0.0021-0.0021	0.0-0.0	-8.85e-06	0.5730 Acceptable
SS3	Surface	0.0012-0.0012	0.0-0.0	-1.35e-04	0.5498 Acceptable
	Middle	0.0012-0.0012	0.0-0.0	-1.18e-04	0.5981 Acceptable
	Bottom	0.0012-0.0013	0.0-0.0	-1.15e-04	0.5845 Acceptable
SS5	Surface	0.0011-0.0011	0.0-0.0	8.54e-05	0.4352 Acceptable (poor)
	Middle	0.0013-0.0013	0.0-0.0	6.97e-05	0.5280 Acceptable
	Bottom	0.0013-0.0013	0.0-0.0	5.84e-05	0.6034 Acceptable (convenient)

Table 5.19: Measurements errors of the validation period (01/06/2008 to 01/12/2008) for ID2 at three depths of ID2, WQ3, SS1, SS3 and SS5.

Table 5.19 synthetizes the error measurements for ID2 in three depths at ID2, WQ3, SS1, SS3 and SS5. Along the estuary, model and cluster mean concentration were very similar. The mean of the "synthetic series" was always higher than the mean of the "real series" except at SS5. Consequently, a negative BIAS was obtained ranging between -8.85e-06 and -5.64e-04 except at SS5 where a positive BIAS between 5.84e-05 and 8.54e-05 was determined. Regarding the time exceeding the MAC-EQS in the case of Pb, the obtained values for both series were zero in all the stations indicating that there were not excursions above the MAC-EQS during the validation period. Finally, the "synthetic series" displayed an acceptable level of performance in all the stations. ID2 and SS1 were reproduced conveniently, WQ3 poorly, and SS3 and SS5 were acceptable.

The error measurements displayed on tables 5.18 and 5.19 during the validation period show that results were fairly accurate and reasonable. Thereby, we can generate any "real series" ("syntethic series") of toxicant concentration ($CHCl_3$ and Pb) based on a sequence of the 78 model results that best fitted the "real series".

Selection and generation of l-years

According to the criteria, we decided to reconstruct for both discharges, firstly, 40-years of time series based on the forcing series and, secondly, 100-statistical years using Monte Carlo. In both reconstructions, the values of the reconstructed evolution of toxicant concentration was the maximum concentration of the 10 layers at each time step (hour).

In the first reconstruction, we used the 40-years of forcing variability to search on the 78 model scenarios the cases that best fit each segment of the 40-years and reconstructed the evolution of toxicant concentration from the selected model scenarios every year. In the second reconstruction, we generated 100-statistical years by Monte Carlo techniques based on the probability of the 78 model scenarios.

Random sampling

In the Step 4, the optimal number of surveys was determined as 1000×12 data. Now, the random sampling was calculated for the 1000-surveys with the two criteria: every 40-years of time series (real forcings) and every 100-statistical years (Monte Carlo).

Final delimitation of MZs

In the intermediate calculation, we obtain 1000-surveys of 12 data that have an occurrence probability equals 1/1000 for one year. Besides this 1000-surveys, in the detailed calculation, we also generate 40-years or 100-statistical years of evolution of toxicant concentration. Therefore, the delimitation of MZs had to compute the probabilities of the 1000-surveys for every year.

Chronic effects of each toxicant in every grid cell were computed using the equation (3.17) for every 40-years or 100-statistical years taking into account 1000-surveys. Next, if $CEF**_{i,j}^{k} > 1$ then $CEF**_{i,j}^{k} = 1$. On the contrary, if $CEF**_{i,j}^{k} \leq 1$ then $CEF*_{i,j}^{k} = 0$. Then, the CEF** associated to all the 1000-surveys was computed by the equation (3.18) for every 40-years or 100-statistical years. Finally, we obtain an array of 40-CEF** or 100-CEF** values in every grid cell of the mesh grid, i.e., the AA-failure probability. From this array, the ecdf of CEF** in every grid cell was calculated for both reconstructions.

Acute effects of each toxicant in every grid cell were computed by the fraction of data in adverse conditions using the equation (3.19) for every 40-years or 100-statistical years considering 1000-surveys. Next, if $AEF*_{i,j}^{k} > 0$ then $CEF*_{i,j}^{k} = 1$. On the contrary, if $AEF*_{i,j}^{k} \leq 0$ then $AEF*_{i,j}^{k} = 0$. Then, the AEF** associated to all the 1000-surveys was computed by the equation (3.20) for every 40-years or 100-statistical years. Finally, we obtain an array of 40-AEF** or 100-AEF** values in every grid cell of the mesh grid, i.e., the MAC-failure probability. From this array, the ecdf of AEF** in every grid cell was calculated for both reconstructions.

As an example, figures 5.97 and 5.98 illustrate the ecdf of CEF** and AEF**, respectively, in the case of ID2 at ID2 (black line), WQ3 (red line), SS1 (blue line), SS3 (green line) and SS5 (magenta line). These figures show the occurrence probability based on 40-years (a) and 100-years (b) of having a specific failure probability for 1000-surveys.

Anew, two MZs were determined (see figure 3.40): the AA-MZ where the percentile of the ecdf of $CEF**_{i,j}$ is bigger than 5 or the 5^{th} percentile of the ecdf of $CEF**_{i,j}$ is bigger than 15, and the MAC-MZ where the percentile of the ecdf of $AEF**_{i,j}$ is bigger than 5 or the 5^{th} percentile of the ecdf of $AEF*_{i,j}$ is bigger than 4.

Finally, the delimitated AA-MZ and MAC-MZ of the "real case of dilution" for ID1 in the 40-years case (a-b) and the 100-statistical years case (c-d) are shown in figure 5.99, respectively. As it was mentioned in the "worst and dry case of dilution", the chloroform (ID1) has not applicable MAC-EQS value so in this figure the MAC-MZ was only an example of the extent of the MAC-MZ considering as threshold the same value of the AA-EQS. Meantime, the delimitated AA-MZ and MAC-MZ of the "real case of dilution" for ID2 in the 40-years case (a-b) and the 100-statistical years case (c-d) are shown in figure 5.100, respectively.

5.5.5 Admissibility (Acceptability/Extent)

From the concept of vulnerability and the percentage of estuarine area covered by MZs, we define and determine the admissibility of MZs in a four-tiered method (Figure 3.41):

1. Estuarine Vulnerability Index (EVI) was calculated by means of several parameters (TZ, SU, SC and ST)

2. Acceptability (AC*) was estimated by multiplying EVI values with the percentage of estuarine area cover per grid cell (AC of the Step 3 and 4).

3. Maximum allowable size (MAS*) was computed by dividing the maximum admissible percentage of estuarine area that a MZ can cover (expert criteria) with a correction factor (α) which depended on the average EVI of the estuary.

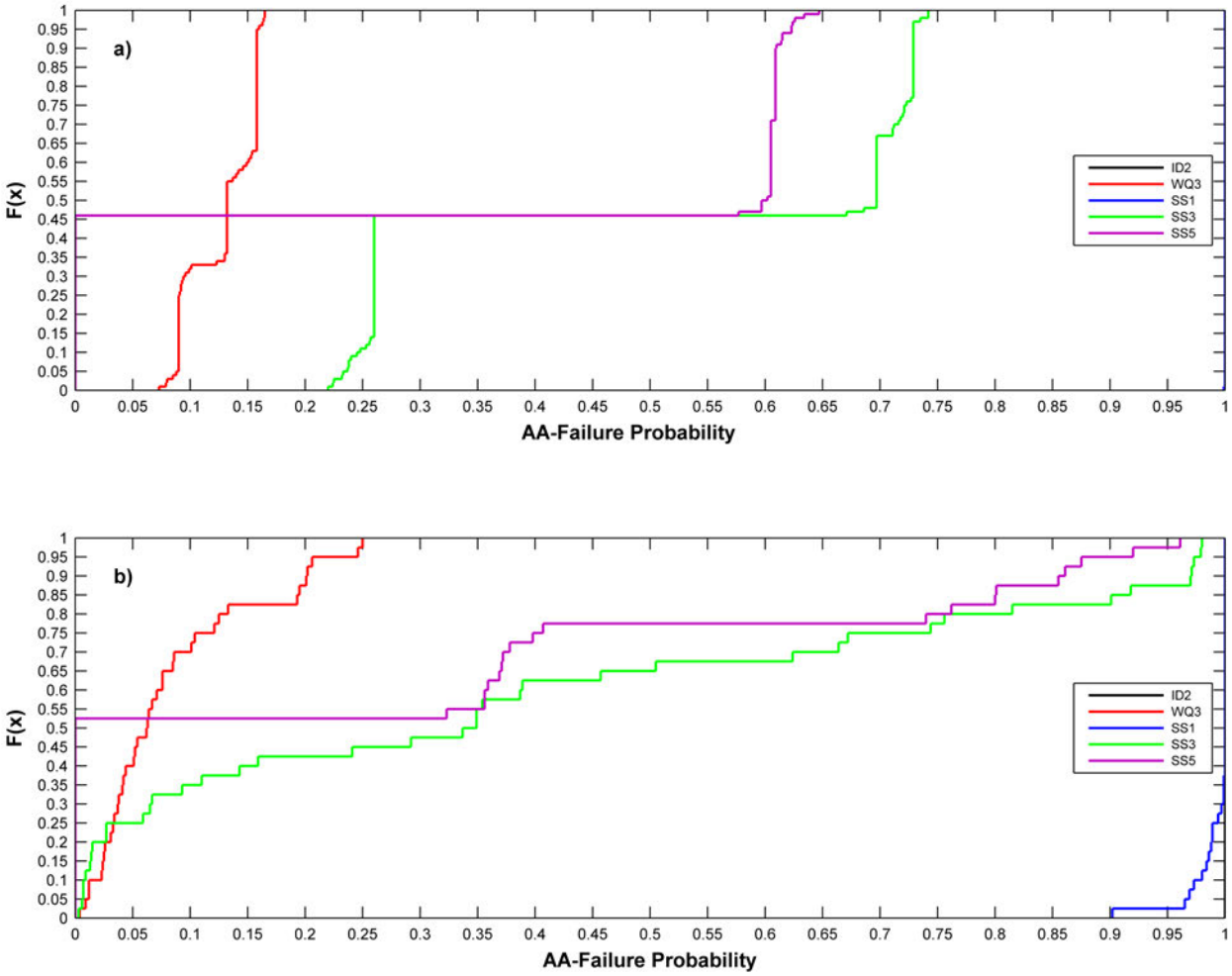

Figure 5.97: Empirical cumulative distribution function of CEF** in the case of ID2 for the 40-years (a) and the 100-years (b) at ID2 (black line), WQ3 (red line), SS1 (blue line), SS3 (green line) and SS5 (magenta line).

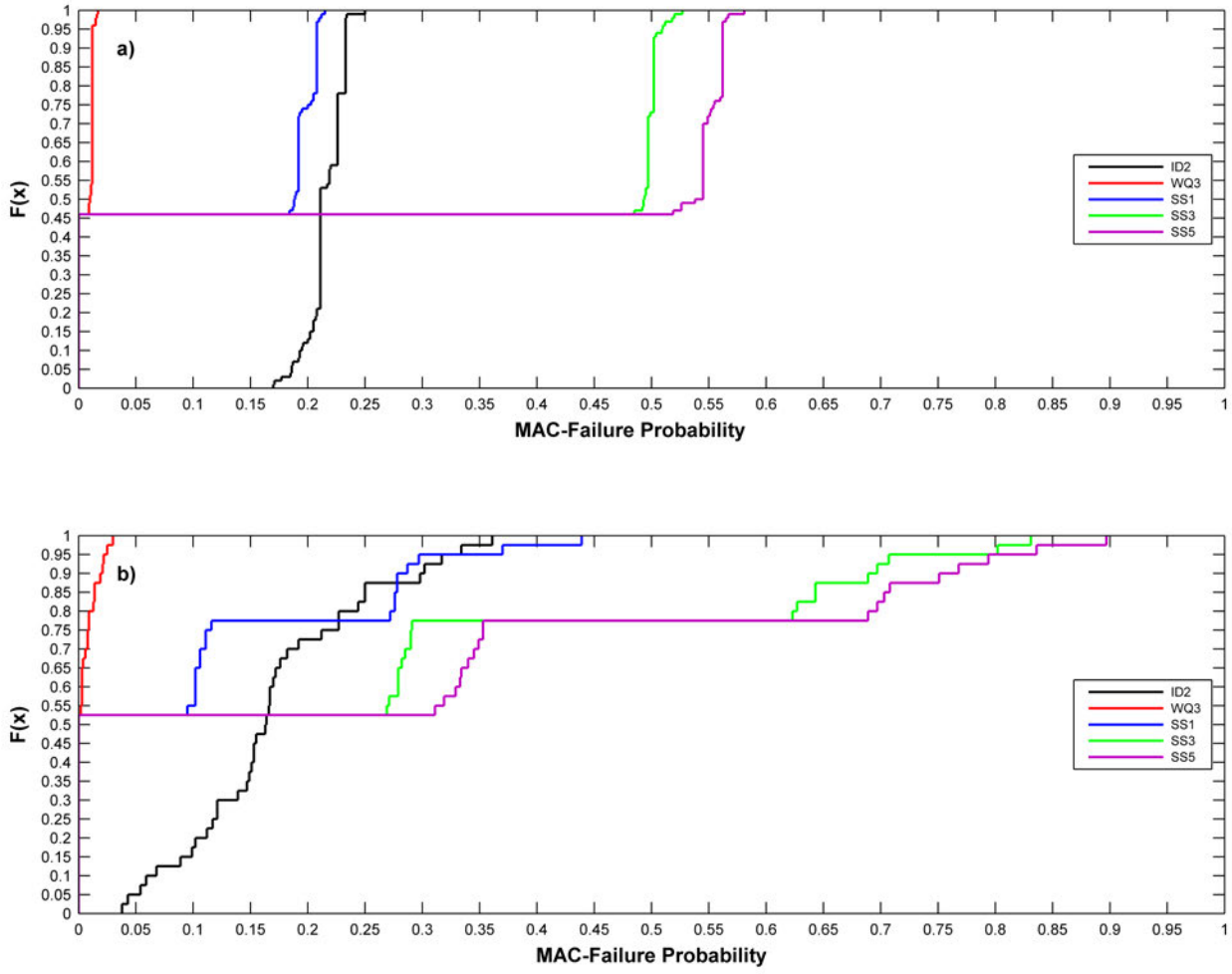

Figure 5.98: Empirical cumulative distribution function of AEF** in the case of ID2 for the 40-years (a) and the 100-years (b) at ID2 (black line), WQ3 (red line), SS1 (blue line), SS3 (green line) and SS5 (magenta line).

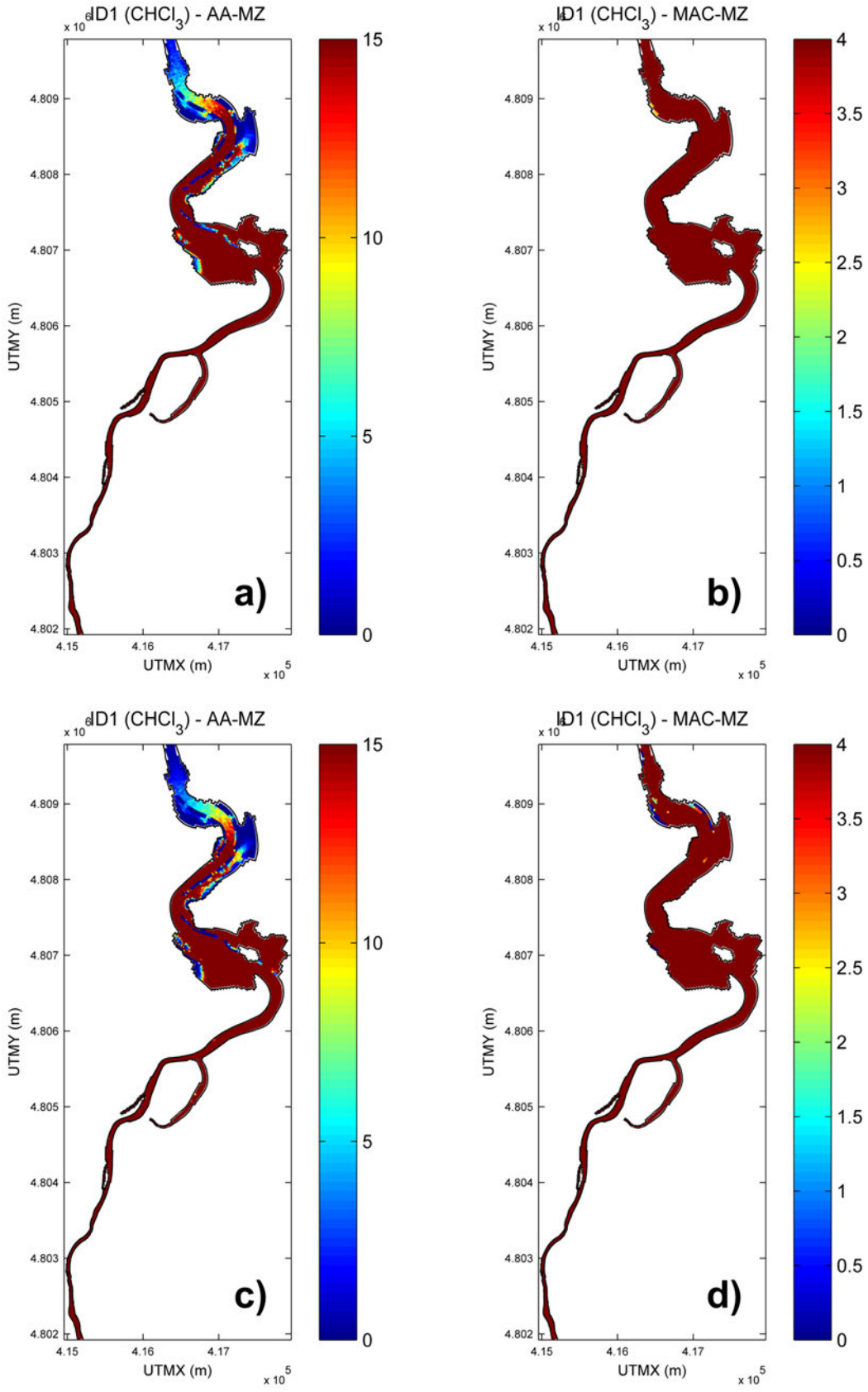

Figure 5.99: Delimitated Mixing Zones in the "real case of dilution" for ID1. AA-MZ of 40-years (a), MAC-MZ of 40-years (b), AA-MZ of 100-statistical years (c) and MAC-MZ of 100-statistical years (d).

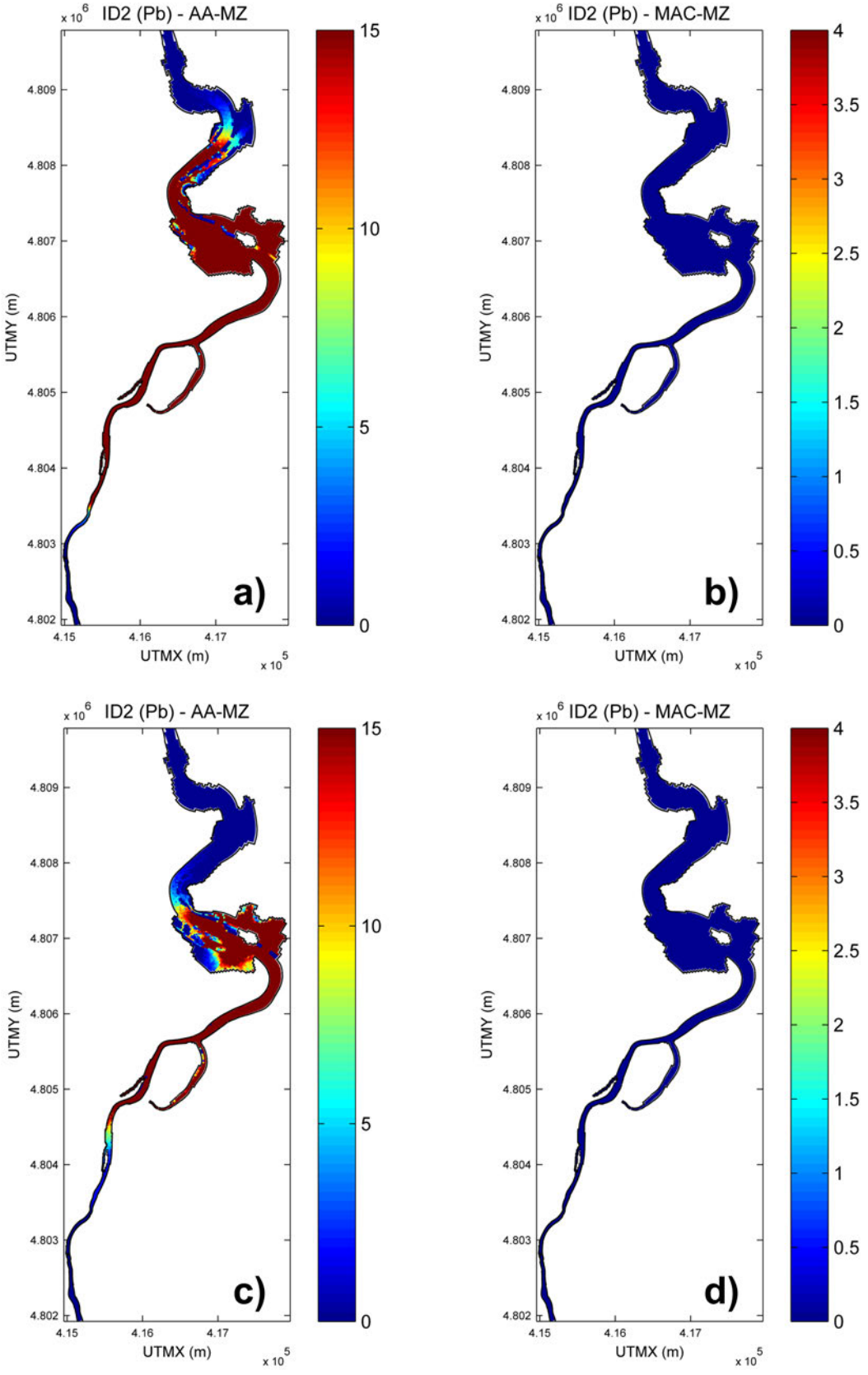

Figure 5.100: Delimitated Mixing Zones in the "real case of dilution" for ID2. AA-MZ of 40-years (a), MAC-MZ of 40-years (b), AA-MZ of 100-statistical years (c) and MAC-MZ of 100-statistical years (d).

4. Admissibility of the delimitated MZ (AD*) was determined by comparing the sum of all AC* covered by the delimitated MZ with the MAS*.

Additionally, it is worthy to mention that all parameter calculations are carried out on the study area through the same mesh grid used by the numerical models and integrated at grid cell level. Next subsections presented the application to the Suances Estuary of the proposal in order to allocate mixing zones in the Step 5.

5.5.5.1 **Tidal zoning (TZ)**

TZ was the location of the intertidal and subtidal zones according to the percentile 95^{th} of the tidal amplitude ($A95$) and the depth of every grid cell (H). From ecdf of tidal amplitude, we obtained that $A95$ was 2.13844 m (see figure 5.7).

Figure 5.101 shows the distribution of TZ in the SE. In this figure, subtidal zones are coloured in green and intertidal zones in red.

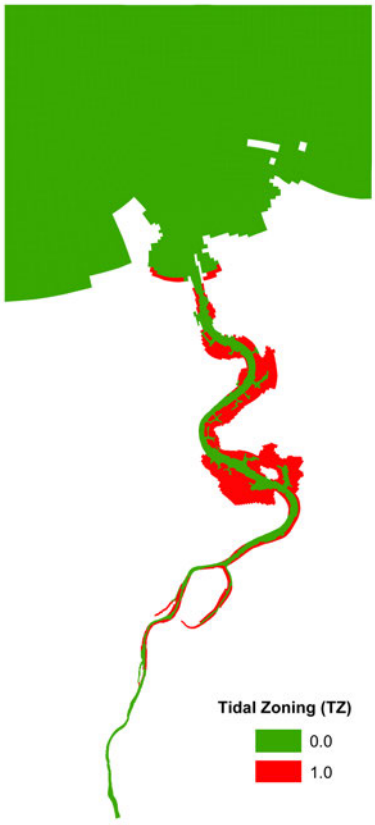

Figure 5.101: Tidal zoning (TZ) of the grid cells at Suances Estuary. Subtidal zones are coloured in green and intertidal zones in red.

5.5.5.2 **Susceptibility (SU)**

Susceptibility was related to the flushing capacity, and it was estimated by means of numerical models. We suggested a methodological approach based on the use of computational tools for the calculation of flushing time (FT) divided into four tiers: Hydrodynamic forcing analysis, FT calculation, FT sensitivity analysis and Final FT (see figure 3.42).

Hydrodynamic forcing analyses

In order to understand the magnitude and the occurrence of these forcing, we utilized the ecdf of the river flow series and the astronomical tidal range series (see figure 5.7).

From these curves and based on the breaking points of each ecdf curve, we selected 5 river flows equal to percentiles $Q0 = 0.725, Q10 = 3.492, Q50 = 12.061, Q90 = 51.634, Q100 = 561.170$ m^3/s, 1 tidal ranges equal to percentile $A50 = 1.468$ m and, finally, 4 tidal phases corresponding to 4 tidal situations equal to $ebb = 0, low = -1.468, flood = 0, high = 1.468$ m.

Regarding the astronomical tide, we only selected one case because its influence on the flushing time results was not very significant. As pointed by Bárcena *et al.* (2012b), the differences experimented by the FT due to the tidal amplitude were negligible for almost any river flow in SE. Therefore, the effect of tidal amplitude on FT in SE became significant during a ten percent of the time when river flow was lower than 5 m^3/s. Summarizing, we integrated the forcing variability in $5 \times 1 \times 4 = 20$ scenarios.

Flushing time calculation

Among all the existing methods in the literature, the proposed methodology by Jouon *et al.* (2006) was selected to compute water renewal. This method generated two local parameters for the 10 layers of the mesh grid at every grid cell, the "flushing lag" (FL) relating to the time required for water coming from outside the control volume to reach the mesh in significant quantity, and the "local flushing time" (LFT) which defined the time span required, after the FL, for water from inside the control volume (grid cell) to occupy approximately 37% $(1/e \approx 0.367)$ of the grid cell's volume.

After 20 model simulations and 10 layers, we obtained $20 \times 10 = 200$ maps with the distribution of LFT in SE.

Flushing time sensitivity analyses

The third tier consisted on performing a multi-sensitivity analysis of the LFT results to tailor the influence of the depth (10 layers), the initial simulation time (4 tidal phases) and the freshwater discharges (5 river flows).

To analyze the trend described by the LFT because of the depth, all the results were plotted and analyzed. As an example, figure 5.102 illustrates the distribution of LFT in the scenario with $Q10$ and ebb tide at the surface (a) and the bottom (b) layers. Moreover, figure 5.102 displays the distribution of LFT in the scenario with $Q90$ and low tide at the surface (c) and the bottom (d) layers, respectively.

As it can be seen in figure 5.102, the influence of depth on the LFT values was larger at low river flows while it was almost independent at high river flows. In the case of low flows (figures 5.102a and 5.102b), LFT values in the inner part were slightly smaller at the surface due to fresh water discharges while, in the middle and outer parts, LFT values were slightly smaller at the bottom due to the salt water coming from sea. In the case of high flows (figures 5.102c and 5.102d), LFT values were very similar because the combined action of the river and tide flushed away instantaneously the water column.

Nevertheless the small differences experimented by the LFT due to depth, the variability of LFT with the depth was not significant in all the scenarios. Thus, we averaged the 10-layer values of LFT on every grid cell for each model scenario. Consequently, we reduced the dimensionality from 200 maps to 20 maps of LFT.

Later, the initial simulation time for each grid cell were graphed and compared to understand this influence. As an example, figure 5.103 illustrates the distribution of LFT in the depth-averaged scenario with $Q0$ starting at $high$ tide (a), ebb tide (b), low tide (c) and $flood$ tide (d).

As it can be seen in figure 5.103, even when the river flow is almost nil, the variability of LFT with the tidal phase was not significant. This trend was similar in all the scenarios so we again averaged the 4-phase values

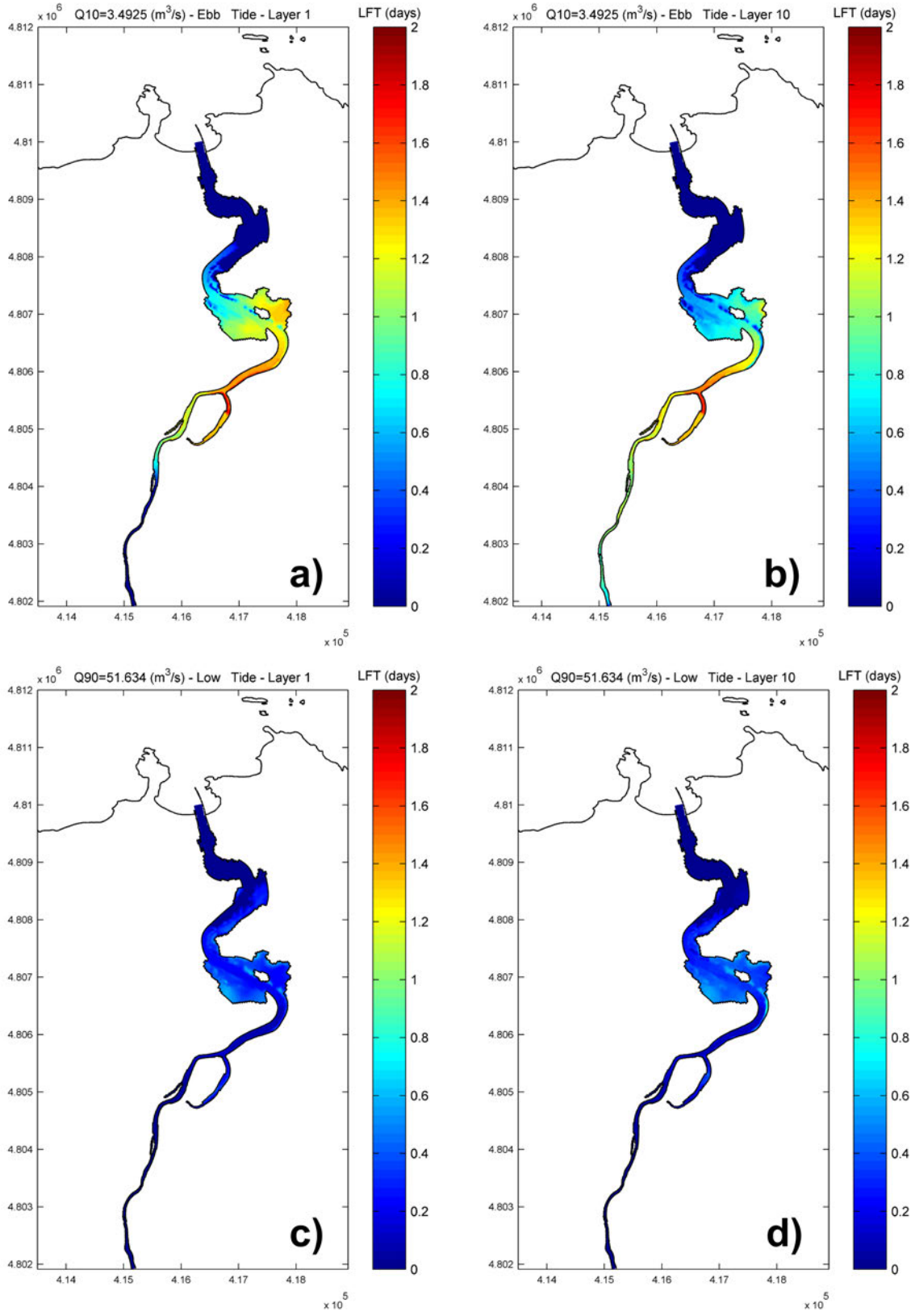

Figure 5.102: Distribution of the local flushing time in the scenarios with $Q10$ and ebb tide at the surface layer (a) and the bottom layer (b) and with $Q90$ and low tide at the surface layer (c) and the bottom layer (d) in the SE.

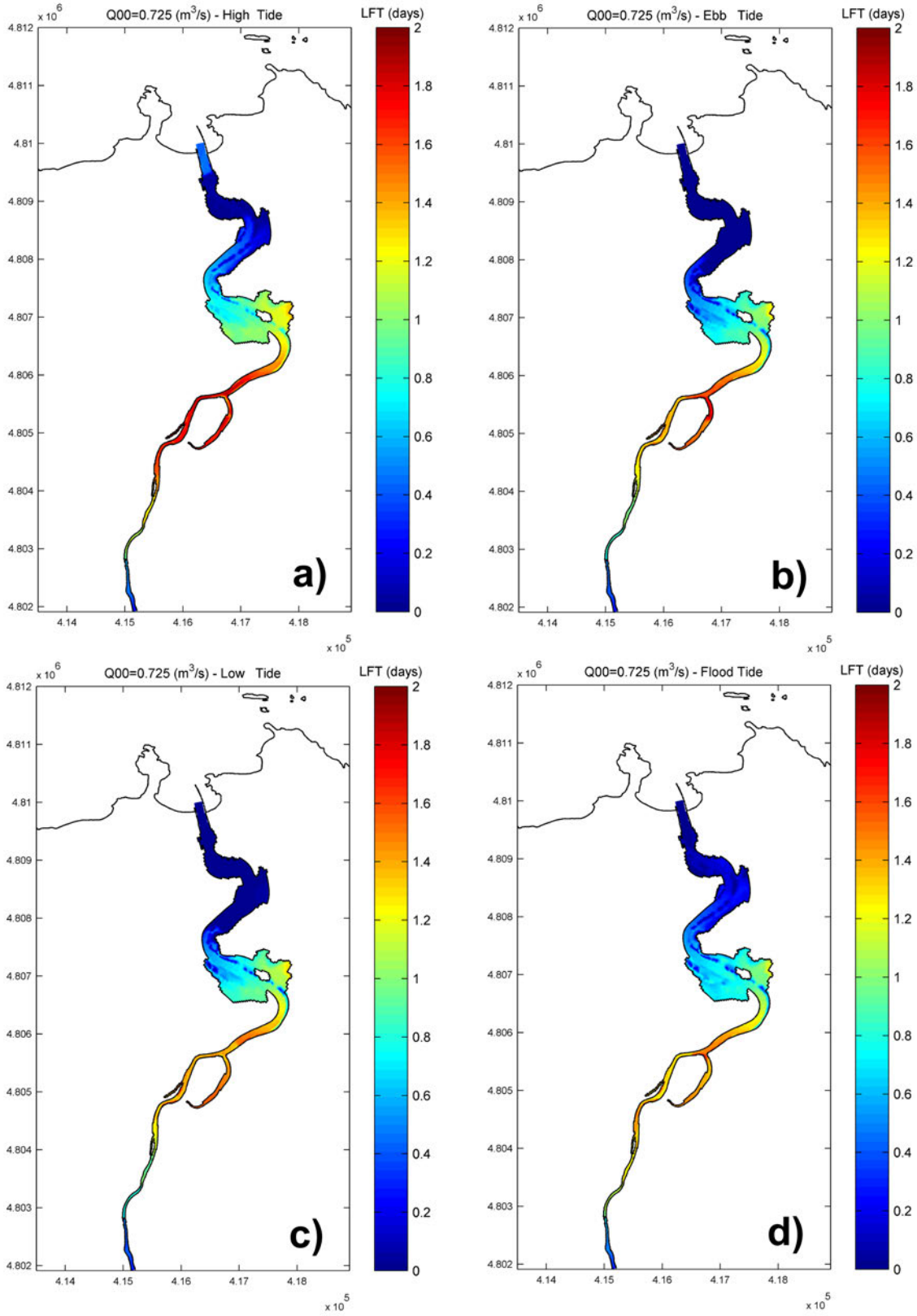

Figure 5.103: Distribution of the local flushing time in the depth-averaged scenario with $Q0$ starting at $high$ tide (a), ebb tide (b), low tide (c) and $flood$ tide (d) in the Suances Estuary.

of LFT on every grid cell for each model scenario. Now, we reduced the dimensionality from 20 maps to 5 maps of LFT describing the variability of the water renewal as a function of the river flow. As an example, figure 5.104 displays the distribution of LFT in the phase- and depth-averaged scenarios with $Q0$ (a), $Q10$ (b), $Q50$ (c) and $Q90$ (d) illustrating the influence of river flow on the LFT values. From this figure we can say that the higher the river flow was, the smaller the LFT was.

Final Flushing time

Once LFT maps were only related to the main forcing (river flow) in the SE, we integrated the resulting area under the curve for every grid cell in order to build a rectangle with the same area and, thereby, the height of this rectangle provided the final LFT as a unique value. Figure 5.105 presents the evolution of LFT as a function of river flow percentiles at WQ3, SS1, SS3 and SS5. Furthermore, this figure showed the final LFT at every grid cell as the height of the rectangle.

For instance, WQ3 (a) was located at the inner part of the estuary and, consequently, the LFT was decreasing when increasing the river flow. Thus, the influence of the river flow was very significant at this point. In the case of SS1 (b), the LFT was again decreasing when increasing the river flow, although the influence of river flow was slightly minor. Finally, SS3 (c) and SS5 (d) were the less influenced by the river due to the proximity to the estuarine mouth. Both points were almost independent of the magnitude of the river flow so they were primary controlled by the tide.

Regarding the final LFT values, SS1 (b) was the highest with 0.7972 days (19.1328 hours) because it was a less energetic point due to the distances from the forcings (river at the head and tide at the mouth). SS5 (d) was the lowest with 0.1259 days (3.0216 hours) because of the independence to the river and the proximity to the mouth. In the case of WQ3 (a), the final LFT was 0.3492 days (8.3808 hours) and it was weighed by the influence of the river flow: low flows displayed high values while high flows displayed low values. Finally, the final LFT at SS3 (c) was 0.2671 days (6.4104 hours), this value was higher than SS5 because of the distance to the estuarine mouth was also bigger.

After calculating the final LFT in every grid cell, figure 5.106a shows the final distribution of LFT. This calculation allowed us preserving the influence of the higher variable forcing by weighing the occurrence probability of this forcing in the final value. Additionally, the influence of other forcing such as tidal amplitude, tidal phase and depth was averaged and integrated in the final LFT.

Lastly, the final LFT map was translated into susceptibility terms by the expression: $SU_(i) = \frac{0.8 \cdot LFT_i}{LFT_{max}}$. In this way, we normalized LFT by means of the maximum LFT in the SE, this was 0.9494 days (22.7856 hours). The higher the LFT was in a grid cell, the more vulnerable was this grid cell. Figure 5.106b shows the distribution of SU in the SE according to the final LFT. In this figure, low SU was coloured in blue (0.0-0.3, less vulnerable), medium SU in green (0.3-0.5, vulnerable), high SU in yellow (0.5-0.6, more vulnerable), very high SU in orange (0.6-0.7, much more vulnerable) and highest SU in red (0.7-0.8, most vulnerable).

5.5.5.3 State of conservation (SC)

SC was determined as a combination of naturalness (NA) and ecological value (EV) by means of GIS techniques.

Naturalness (NA)

We defined an alteration by hydromorphological pressures (HP), computing buffer areas around every HP using buffer tools in GIS. Every buffer distance of a HP was calculated by means of the equation (3.38).

In the SE, we took into account 28 hydrodynamic alterations: 1 bridge and 27 dykes. The bridge was considered discontinuous (k_{HP}=0.5) and the critical value CV was 50 m. The dykes were considered continuous

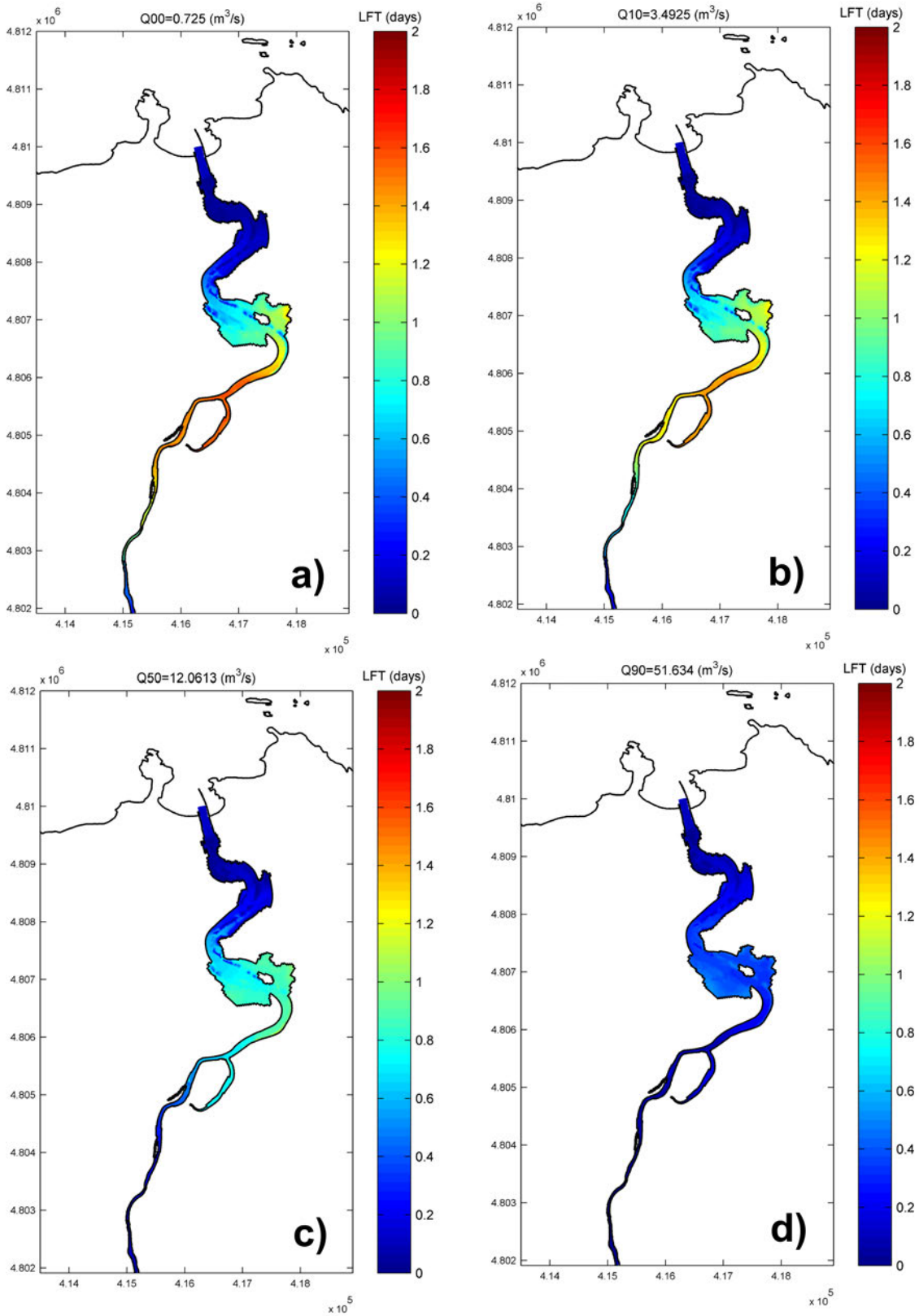

Figure 5.104: Distribution of the local flushing time in the phase- and depth-averaged scenarios with $Q0$ (a), $Q10$ (b), $Q50$ (c) and $Q90$ (d) in the Suances Estuary.

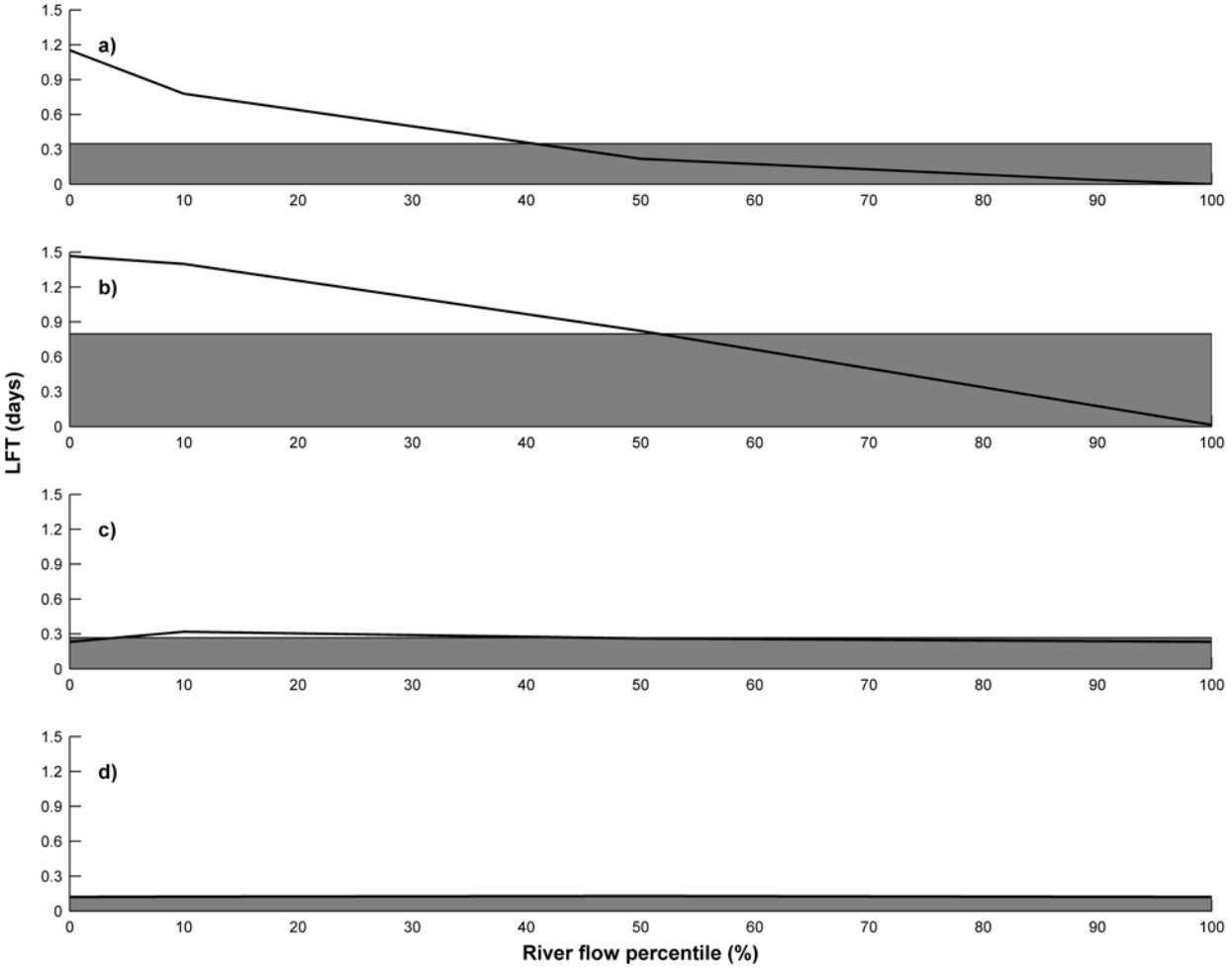

Figure 5.105: Evolution of the local flushing time as a function of river flow percentiles and final local flushing time at WQ3 (a), SS1 (b), SS3 (c) and SS5 (d) in the Suances Estuary.

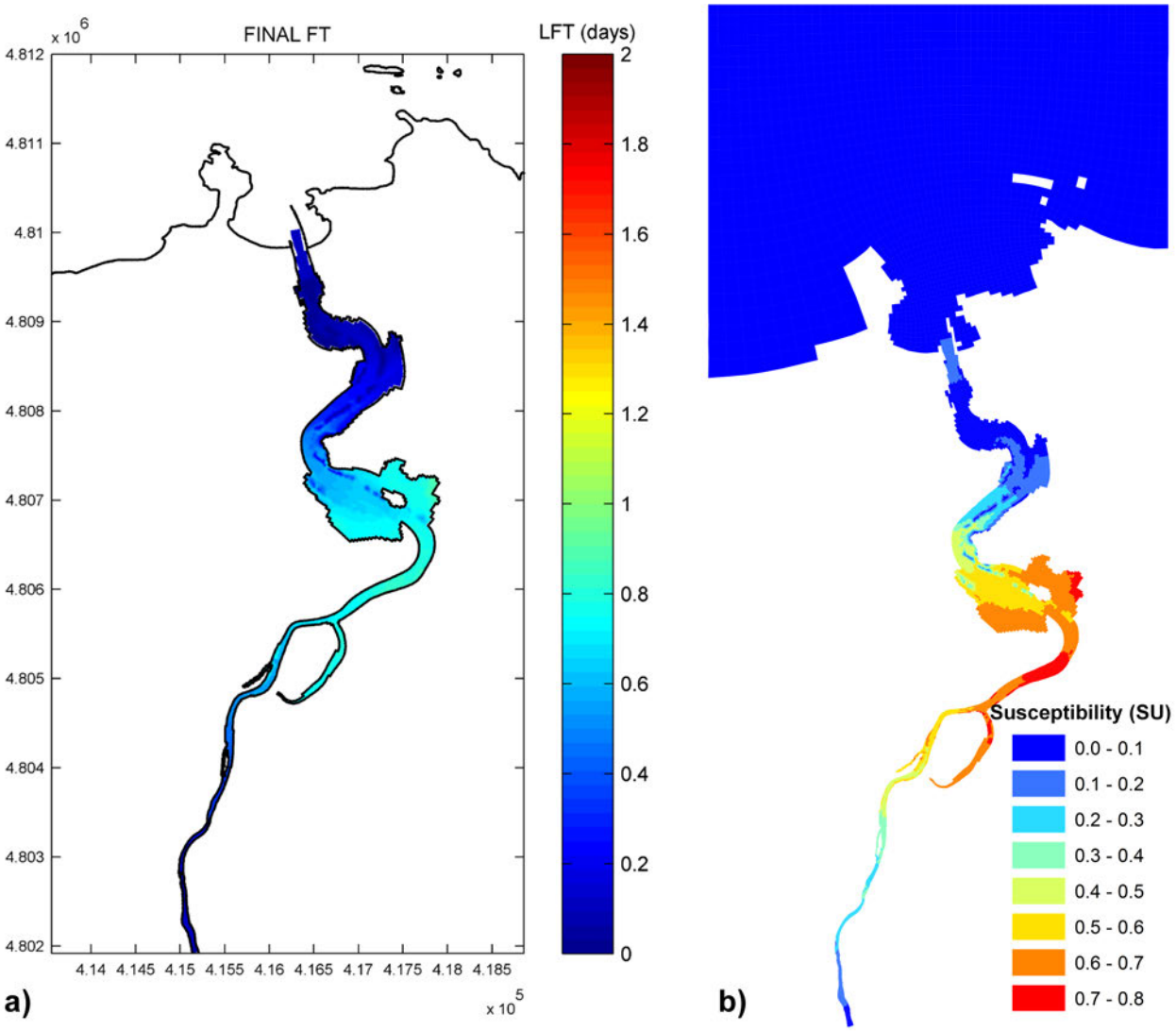

Figure 5.106: Panel a): Distribution of the final local flushing time taking into account the influence of the depth (10 layers), the tidal magnitude (1 tidal amplitude), the initial simulation time (4 tidal phases) and the freshwater discharges (5 river flows) at Suances Estuary. Panel b): Susceptibility (SU) of the grid cells at Suances Estuary.. Low SU in blue color (0.0-0.3, less vulnerable), medium SU in green color (0.3-0.5, vulnerable), high SU in yellow color (0.5-0.6, more vulnerable), very high SU in orange color (0.6-0.7, much more vulnerable) and highest SU in red color (0.7-0.8, most vulnerable).

(k_{HP}=1) and the critical value CV was 100 m. Moreover, we took into account 9 morphological alterations: all of them were margin protections with $k_{HP} = 1$ and CV=100 m. Lastly, it was worthy to underline that land reclamation was not considered because they were outside the mesh grid.

Finally, buffer areas of all identified HP were superimposed and considered altered areas presenting low naturalness as shown in figure 5.107a. The altered or modified areas are weighed with 0 and coloured in yellow (low naturalness and vulnerability) meanwhile non-altered or non-modified areas have a 0.8 and coloured in grey (high naturalness and vulnerability).

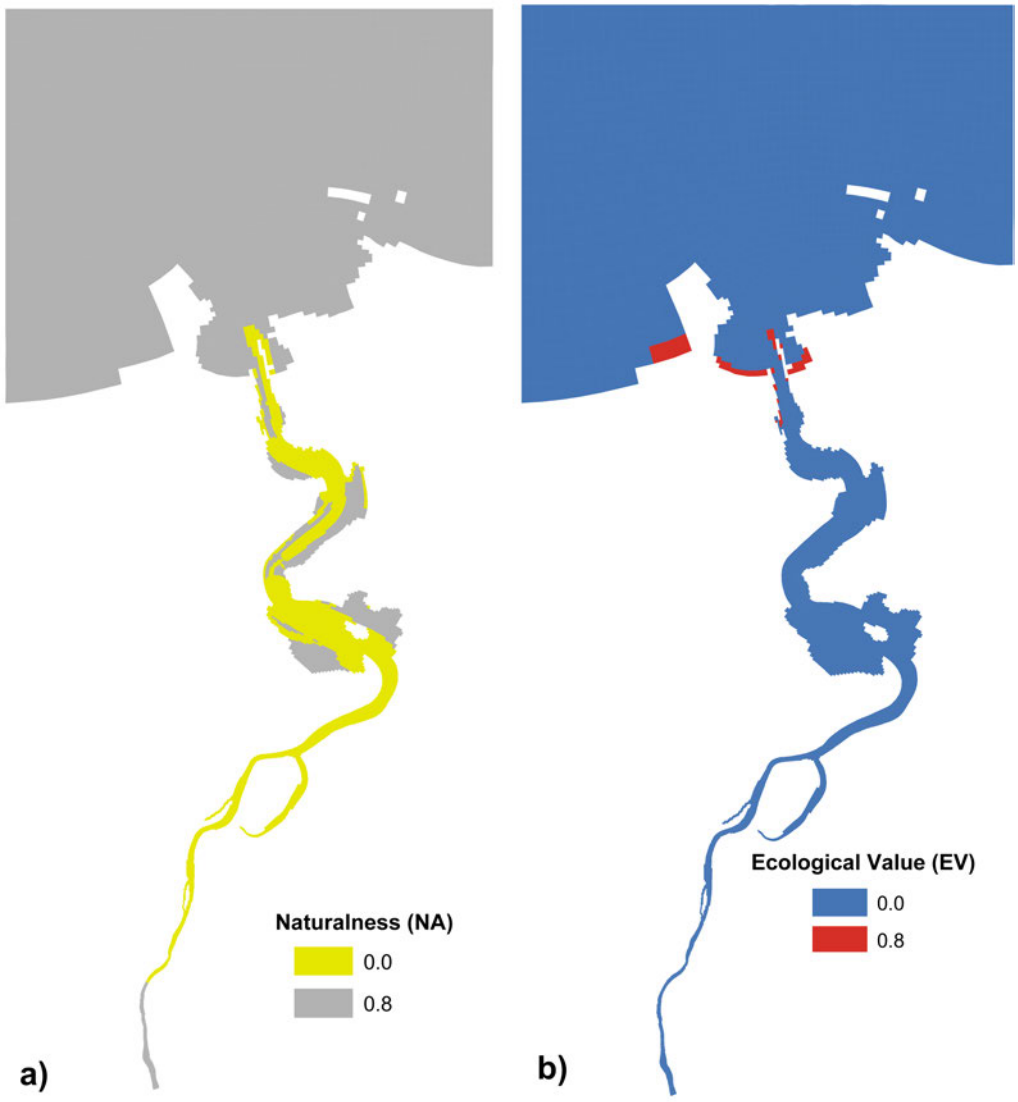

Figure 5.107: Panel a): Naturalness (NA) of the grid cells at Suances Estuary. Low NA in yellow color (0, non-vulnerable) and high NA in grey color (0.8, vulnerable). Panel b): Ecological value (EV) of the grid cells at Suances Estuary. Low EV in blue color (0, non-vulnerable) and high EV in red color (0.8, vulnerable)

Ecological Value (EV)

This parameter was quantified using the indicator Ecological singular elements (ESE). ESE were defined by recognizing regional, national and international protected areas (see table 3.1) in the mesh grid by means of location tools in GIS.

In the case of SE, protected areas were only presented areas of recreational uses related to bath waters and beaches (see figure 5.8). The protected areas are weighed with 0.8 and coloured in red (high ecological value

and vulnerability) meanwhile non-protected areas have a 0 and coloured in blue (low ecological value and vulnerability). Figure 5.107b shows the distribution of EV in the SE according to the ESE.

5.5.5.4 Stratification (ST)

In this subsection, we located the mixed, partially mixed/stratified and stratified areas in the Suances Estuary. The proposed methodology was divided into three tiers: Selection and modeling of hydrodynamic scenarios, Calculation of the Richardson number and Final zoning of stratification (Figure 3.45).

Selection and modeling of hydrodynamic scenarios

We used the same 78 model scenarios previously selected with the clustering approach. Thereby, this classification and the hydrodynamic results from the detailed calculation were used to compute the Richardson number at grid cell level in the SE.

Calculation of Richardson number

Secondly, the stability characteristics of the estuary were analyzed by the classical Richardson layer number Ri_L given by the equation (3.39). From the results of the hydrodynamic model, we hourly quantified the Ri_L for the 78 model scenarios for every grid cell. Next, we hourly classified the stratification type according to the criterion given by Dyer & New (1986).

Due to the many number of cases, as an example of the hourly estuarine type, we illustrate the final map of case 23 (see figure 5.66 and the bolded row in table 5.13) and 54 (see figure 5.66 and the bolded row in table 5.14) for the hours 96 and 248 in the next paragraphs.

Figures 5.108 and 5.109 display the distribution of the stratification type (fully mixed in blue, partially mixed/stratified in yellow and stratified in green) for the hours 96 (a) and 248 (b) in the "real case 23 and 54 of dilution", respectively.

In the real case 23, the hour 96 (a) is showing an instant with very high flow (approx. 200 m^3/s) and flood tide meanwhile the hour 248 (b) is with high flow (approx. 55 m^3/s) and ebb tide. As it is shown in figure 5.108a, the estuary was almost fully mixed except in the mouth due to the high flow mixed and flushed away all the estuarine water. Moreover, the estuarine mouth was partially mixed because the confluence between fresh water (river) and salt water (sea) was located at this area. In figure 5.108b, the head was fully mixed due to the action of the fresh water discharge while the mouth was also fully mixed because of the tidal action. Finally, in the middle section, the estuary was partially mixed and stratified, anew, due to the confluence between river and sea.

Regarding the real case 54, the hour 96 (a) is showing an instant with moderate flow (approx. 25 m^3/s) and flood tide (almost low tide) meanwhile the hour 248 (b) is with moderate flow (approx. 25 m^3/s) and high tide. As it is shown in figure 5.109a, the estuary was almost fully mixed due to the river flow at the head and mixing processes at the mouth and middle sections (depth of water column was smaller). Additionally, the intertidal areas connected to the main channel were partially mixed because of the salinity differences at both zones. In figure 5.108b, the head was fully mixed due to the action of the fresh water discharge while the mouth was partially stratified because of the the salinity differences between the bottom (sea water) and surface (brackish water) at high tide (maximum depth of water column). Finally, in the middle section, the estuary was mostly stratified, anew, due to the confluence between river and sea and the high tide situation (fresh water was sliding above salt water).

Final zoning of stratification

In this tier, we firstly calculated the percentage of time that every grid cell was in every stratification state for

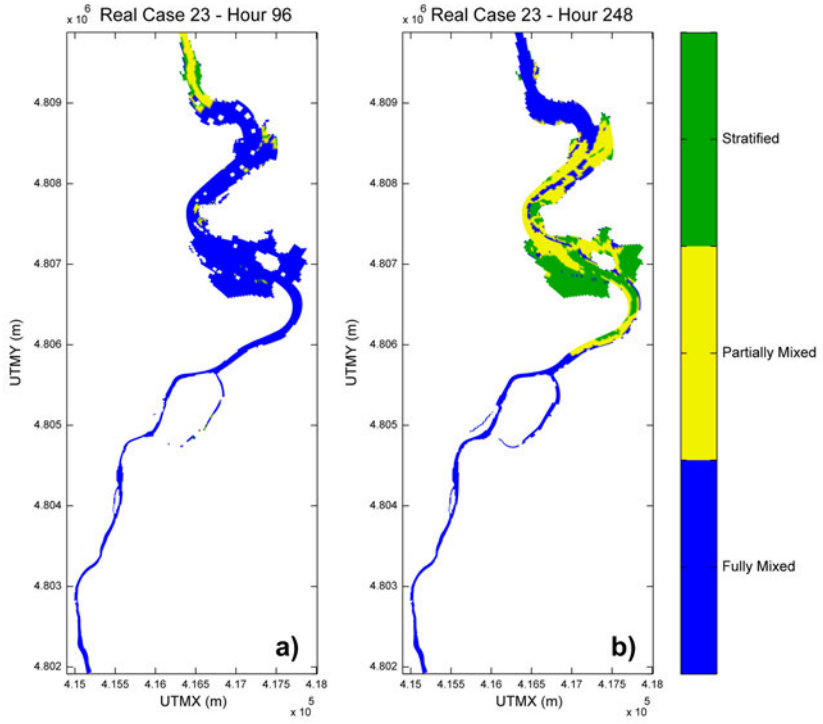

Figure 5.108: Distribution of the stratification type for the transport of the "real case 23 of dilution". Hour 96 (a) and hour 248 (b).

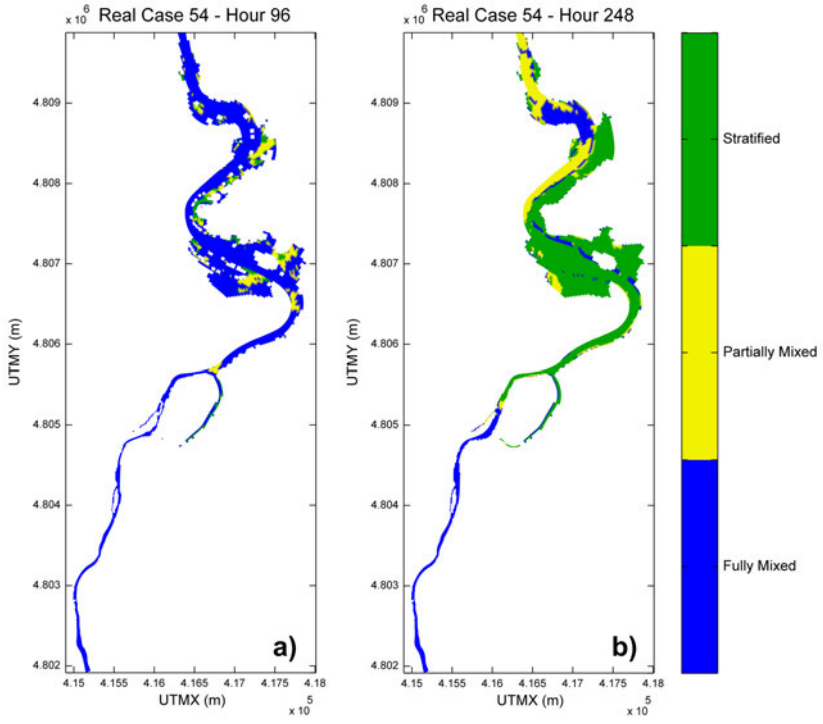

Figure 5.109: Distribution of the stratification type for the transport of the "real case 54 of dilution". Hour 96 (a) and hour 248 (b).

every model scenario (360 hours). As an example of the obtained 78 maps, figures 5.110 and 5.111 illustrate the distribution of the occurrence probability for every estuarine type in the "real case 23 and 54 of dilution", respectively.

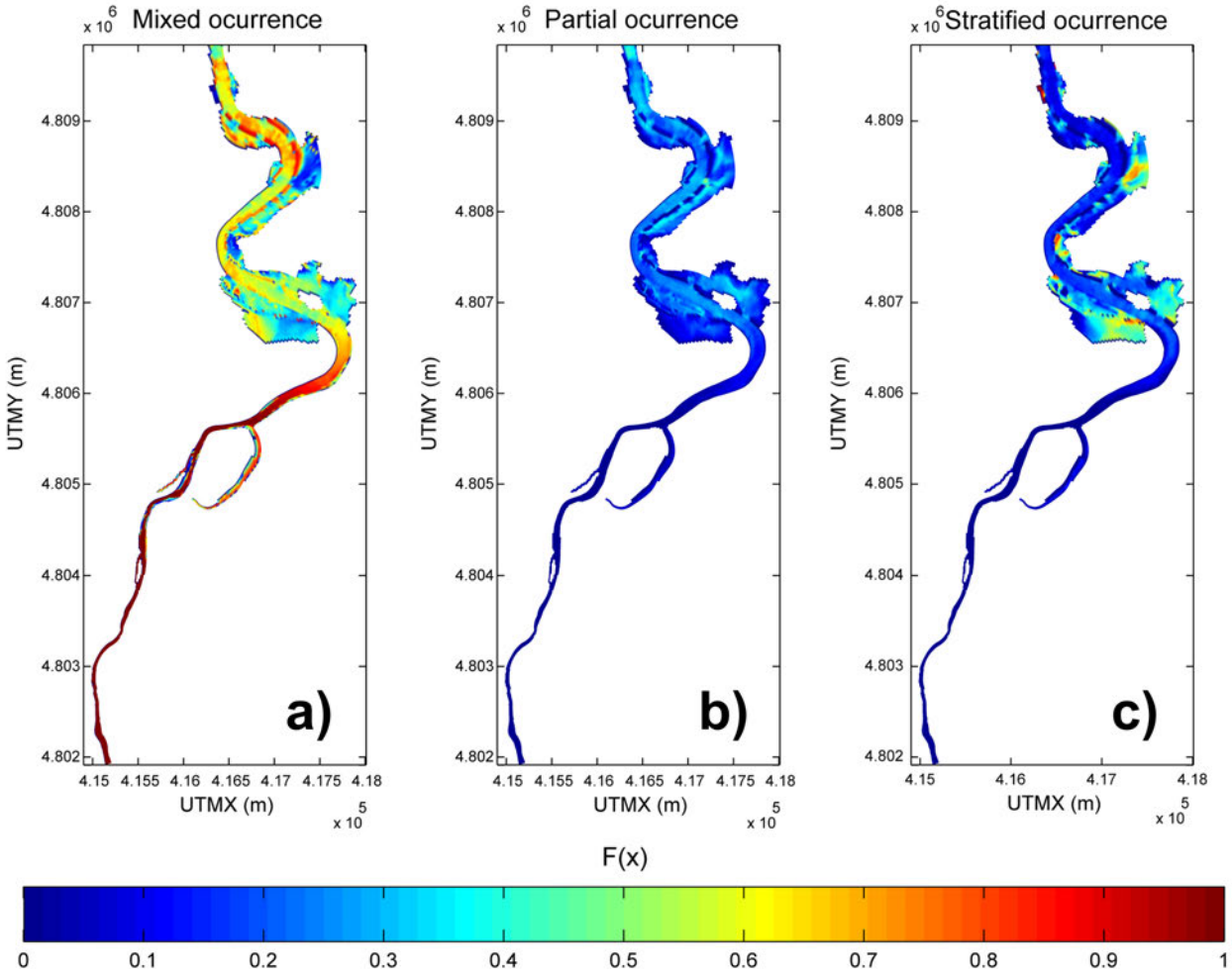

Figure 5.110: Distribution of the occurrence probability for every stratification type in the "real case 23 of dilution". Mixed (a), partially mixed/stratified (b) and stratified (c).

Figure 5.110 shows that SE was mixed most of the time during the "real case 23 of dilution" due to the flow pulse dulcified the estuary. In the "real case 54 of dilution", the moderate river flow (approx. 25 m^3/s) is almost constant leading to a different pattern of stratification types (figure 5.111). At the head, the estuary was mixed because of the river action (fresh water) while the estuary was also mixed at the mouth due to the tidal action (sea water) instead of river. Furthermore, the middle section of the estuary was partially mixed or stratified because of the combination of both forcings and the salinity differences experimented by the water column.

It was aforementioned that the 78 model scenarios have an occurrence probability, i.e., the product of the probability of the river flow period and the tidal period (see tables 5.13 and 5.14). From the 78×3 probability maps, we computed three probability maps for every stratification type multiplying every map (78×3) by the occurrence probability of the 78 model scenario (as shown in figure 5.112).

Last, we integrated all the information in a unique map showing the most probable estuarine type at grid cell level (Figure 5.113a). This map classified every grid cell into a stratification type when the probability of any type surpassed 33.33% of the time. Therefore, this grid cell was finally zoned with that stratification type.

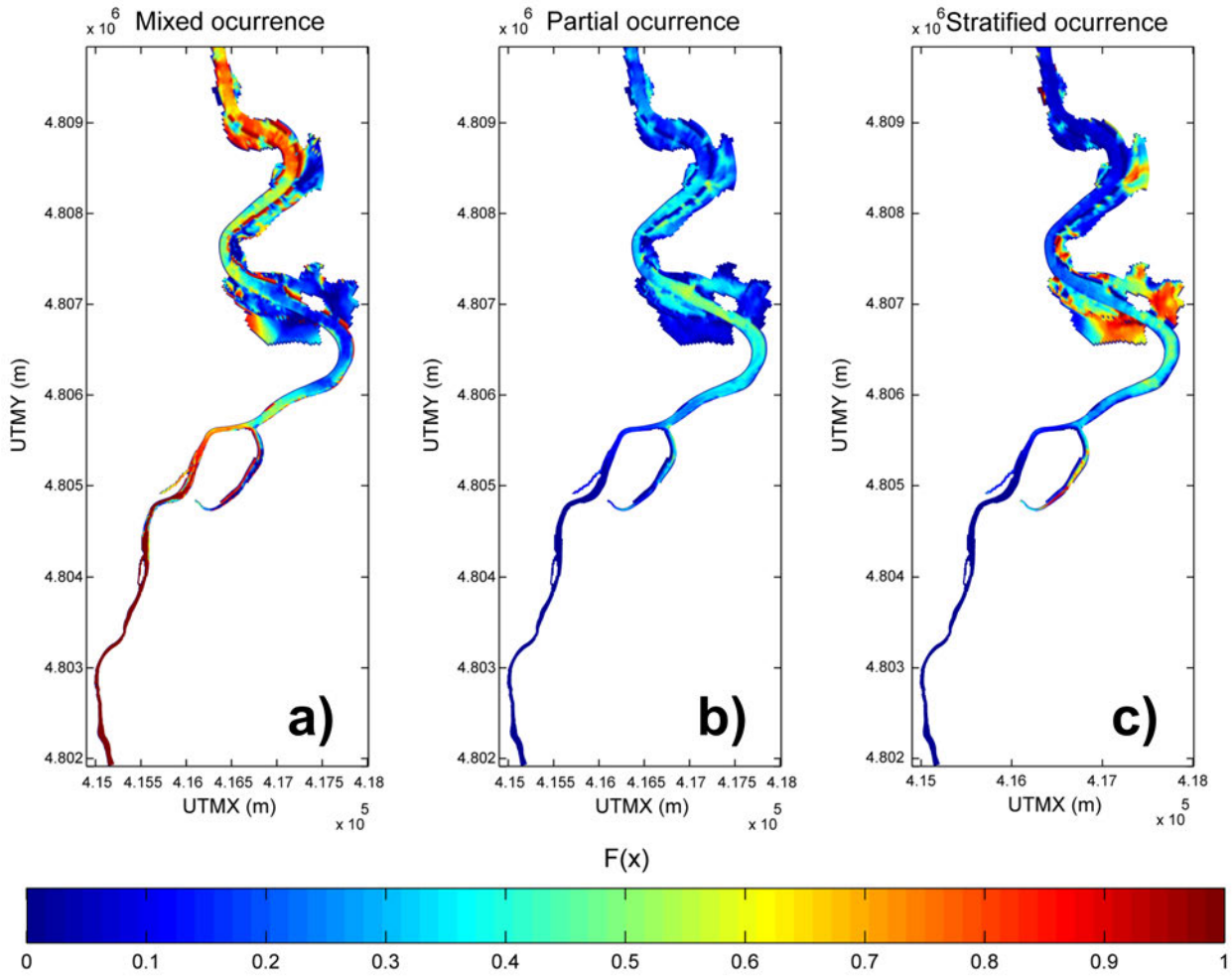

Figure 5.111: Distribution of the occurrence probability for every stratification type in the "real case 54 of dilution". Mixed (a), partially mixed/stratified (b) and stratified (c).

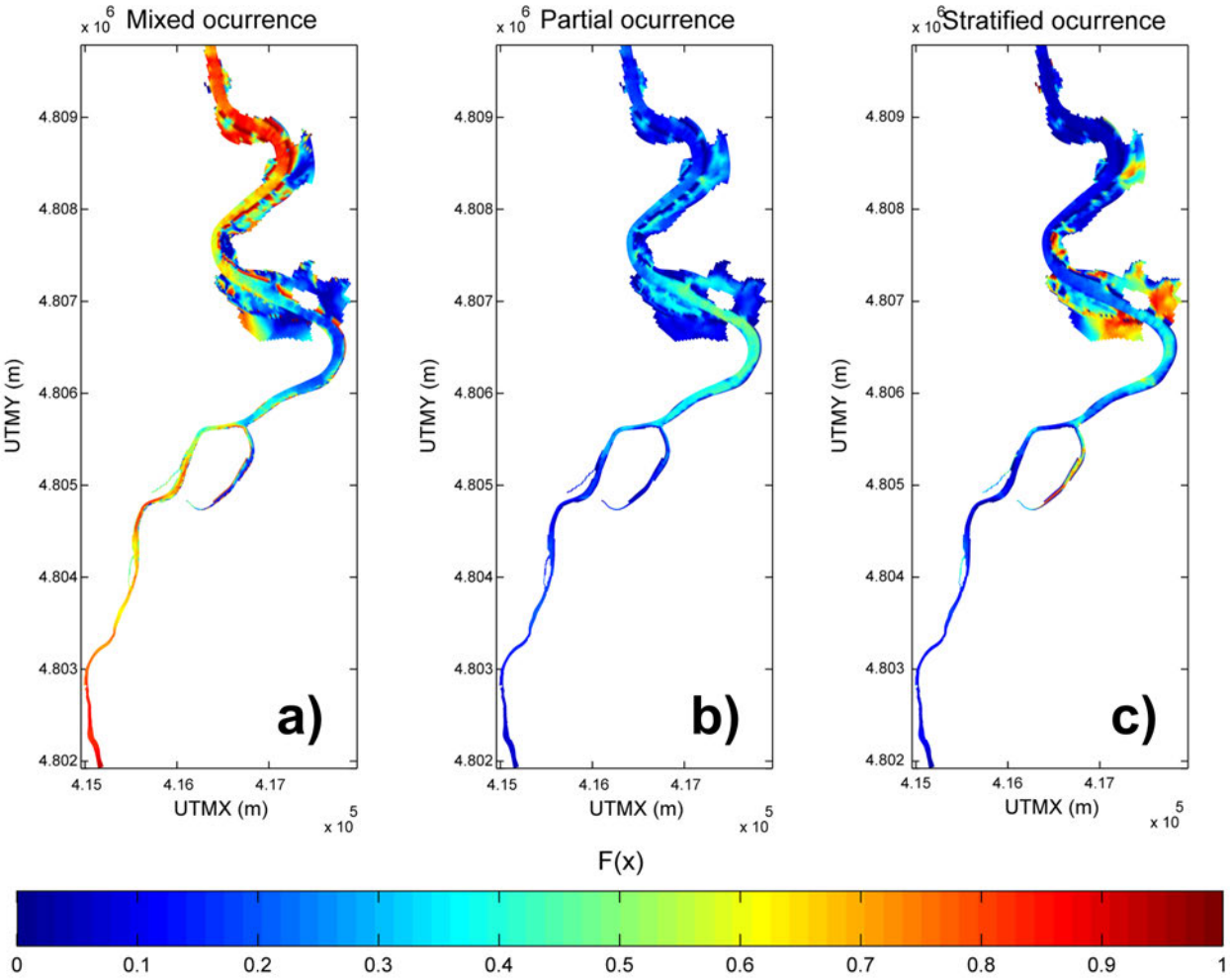

Figure 5.112: Distribution of the occurrence probability of every stratification type at Suances Estuary. Mixed (a), partially mixed/stratified (b) and stratified (c).

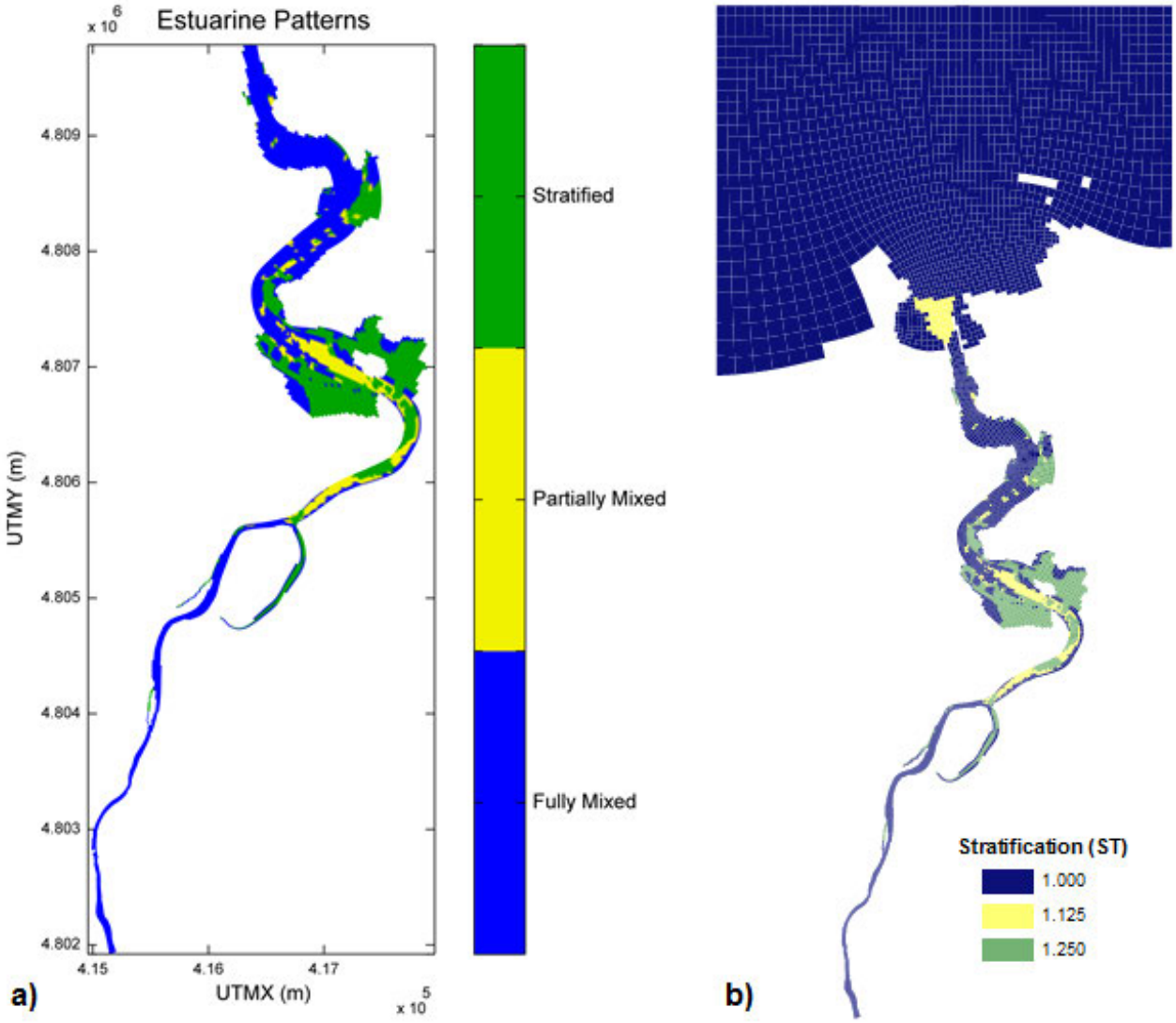

Figure 5.113: Panel a): Distribution of the most probable stratification type at Suances Estuary. Panel b): Stratification (ST) of the grid cells at Suances Estuary. Vertical mixed (1.000 in blue, less vulnerable), partially mixed/stratified (1.125 in yellow, vulnerable) and stratified (1.250 in green, most vulnerable).

Figure 5.112) shows the occurrence probability of every estuarine type and figure 5.113a displays the most probable estuarine type. According to both figures, SE was fully mixed in the inner part because of the river action (fresh water) filled the water column. At the outer part, the estuary was also mixed due to the tidal action (sea water) generated the enough turbulence for mixing the water column. Furthermore, the middle section of the estuary was partially mixed at the main channel or stratified at intertidal areas because of the combination of both forcings, the depth gradient between the main channel and the intertidal areas and the salinity differences experimented by the water column.

ST can be understood as a correction factor inside the methodology. In this way, figure 5.113b presents areas classified as vertical mixed (1.000 in blue, less vulnerable), areas classified as partially mixed/stratified (1.125 in yellow, vulnerable) and areas classified as stratified (1.250 in green, most vulnerable).

5.5.5.5 **Estuarine Vulnerability Index (EVI)**

Once all parameters were calculated, the first tier was the integration of this information by means of the so called "Estuarine Vulnerability Index" (EVI) (see figure 3.41).

We assigned the coefficient values according to the metrics established in table 3.6 and quantified the value of EVI at grid cell with the equation (3.41). EVI ranged between zero and one. Zero was referred to the estuarine areas less vulnerable to receive wastewater discharges meanwhile the areas with one were the most vulnerable. Figure 5.114a presents the spatial distribution of the EVI in the SE. In this figure, low EVI are coloured in green (0.0-0.4, less vulnerable), medium EVI in yellow (0.4-0.6, vulnerable), high EVI in orange (0.6-0.9, more vulnerable), and highest EVI in red (0.9-1.0, most vulnerable).

5.5.5.6 **Acceptability (AC*)**

Next tier was determining the acceptability (AC*) of the estuary by means of the equation (3.42). This equation multiplied the EVI value with the AC value calculated in the "worst case of dilution" (Figure 5.40). EVI worked as a multiplicative weighing factor in the calculation of AC* as a function of estuarine vulnerability at grid cell level. EVI_i could be seen as a correcting factor of the real area of a grid cell depending on its vulnerability. Figure **??**b presents the spatial distribution of the AC* in the SE.

5.5.5.7 **Maximum allowable MZ size (MAS*)**

The third tier was computing the maximum allowable corrected MZ size (MAS*) by dividing the AA-MAS and MAC-MAS (10% and 3% of water body extent) with a correction factor (α) which depends on the average EVI of the grid cells covered by the estuary (see figure 3.41). Equation (3.43) displays the value of MAS* meanwhile equation (3.44) the formulation for α.

In SE, $\overline{EVI}_{estuary}$ was 0.615 and could be seen as a correcting factor of the MAS depending on the estuarine vulnerability (Figure 3.46). Therefore, $\alpha = \frac{1}{1-\overline{EVI}_{estuary}} = \frac{1}{1-0.615} = 2.597$. α works as a divisive weighing factor in the calculation of MAS*.

Finally, the values of both MAS* were: $AA - MAS^* = \frac{AA-MAS}{\alpha} = \frac{10}{2.597} = 3.85$ and $MAC - MAS^* = \frac{AA-MAS}{\alpha} = \frac{3}{2.597} = 1.15$. Due to the vulnerability of the estuary against wastewater discharges, the maximum allowable MZ sizes in the "real case of dilution" were 3.85 and 1.15 for the AA-MAS* and MAC-MAS*, respectively.

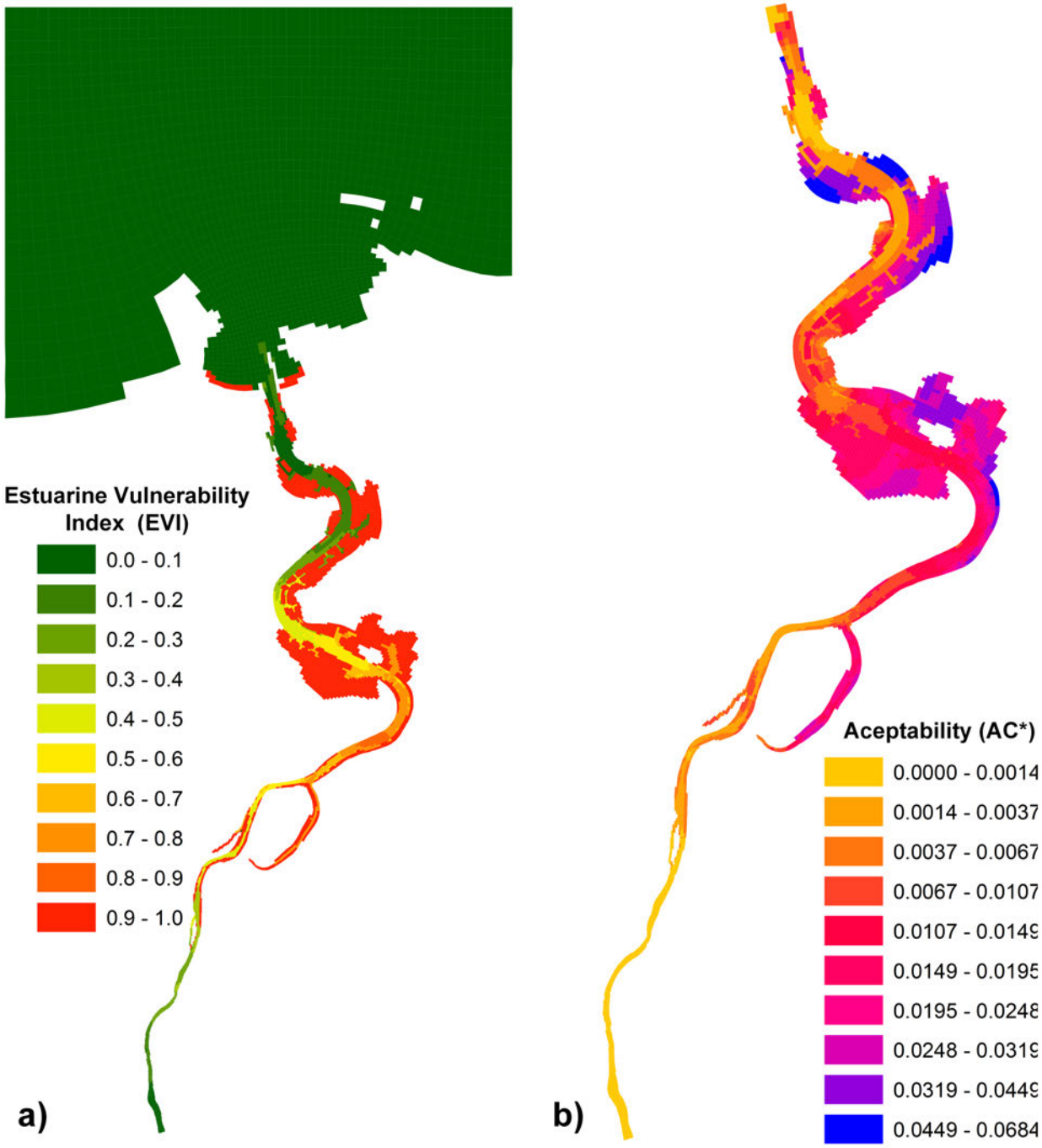

Figure 5.114: Panel a): Estuarine Vulnerability Index (EVI) of the grid cells at Suances Estuary. Low EVI in green color (0.0-0.4, less vulnerable), medium EVI in yellow color (0.4-0.6, vulnerable), high EVI in orange color (0.6-0.9, more vulnerable), and highest EVI in red color (0.9-1.0, most vulnerable). Panel b): Acceptability (AC*) of the grid cells for the detailed calculation at Suances Estuary.

Number Years	Name Toxicant	AA-MZ m^2	AA-AD* AA-MAS*	MAC-MZ m^2	MAC-AD* MAC-MAS*
40	ID1 ($CHCl_3$)	1771132.96	51.13>3.85	-	-
100	ID1 ($CHCl_3$)	1631267.25	47.32>3.85	-	-
40	ID2 (Pb)	1519284.18	47.38>3.85	115.01	0.0024<1.15
100	ID2 (Pb)	933457.88	29.74>3.85	115.01	0.0024<1.15

Table 5.20: Extent of the delimitated Mixing Zones (AA-MZ and MAC-MZ) and final admissibility (AA-AD* and MAC-AD*) in the detailed calculation for ID1 and ID2.

Name Toxicant	Case 0 C (mg/l)	Case 1 C (mg/l)	Case 2 C (mg/l)
ID1 ($CHCl_3$)	0.02	0.02/50=0.0004	0.02/100=0.0002
ID2 (Pb)	1.00	1.00/5=0.2	1/10=0.1

Table 5.21: Reduced toxicant concentration in the reevaluation of ID1 and ID2 for delimitating MZs.

5.5.5.8 Final admissibility (AD*)

Once both MZs were delimited, in the fourth tier, we evaluated the AD* as the sum of all the AC* values covered by AA-MZ and MAC-MZ (Equation (3.45)). The difference between the admissibility of the "real case of dilution" and the "worst and dry cases of dilution" was the inclusion of EVI into the calculations of AC* and MAS*. In the first reconstruction, we used the 40-years of forcing variability while, in the second reconstruction, we generated 100-statistical years by Monte Carlo techniques. Table 5.20 summarizes the covered area by MZs and the AA-AD and MAC-AD considering the 5^{th} percentile of the ecdf of the AA-Failure was 15% and the 5^{th} percentile of the ecdf of the MAC-Failure was 4%.

As it can be seen in table 5.20, there were not allocatable MZs for the AA-EQS. Both industrial discharges presented a final admissibility AA-AD* bigger than AA-MAS* (3.85%). Regarding the MAC-EQS, ID2 presented an allocatable MZ because the final admissibility MAC-AD* was smaller than MAC-MAS* (1.15%). In this case, all the MAC-MZ below the 4% of the MAC-Failure were allocatable because they were also below the MAC-MAS* (1.15%).

Thereby, the extents of the AA-MZ were inadmissible for ID1 and ID2, and, consequently, both discharges were classified as inadmissible finalizing the allocation procedure (Figure 3.2).

5.5.6 Reevaluation of inadmissible discharges

After the detailed calculation, ID1 and ID2 were still classified as inadmissible so the decision tree recommended to restart with the methodology at Step 1 in order to continue with the allocation procedure until reach an admissible MZ. The way to modify MZs was changing the location of the point discharge, reducing the toxicant load (flow or concentration) and/or both.

As an example of this reevaluation, we decided to reduce the concentration of ID1 and ID2 by different factors as pointed in table 5.21. Note that case 0 is referred to the discharges without any reduction, i.e., the study case along the explanation of the stepped methodology.

5.5.6.1 Reduction case 1

Delimitation of mixing zones

Number Years	Name Toxicant	AA-MZ m^2	AA-AD* AA-MAS*	MAC-MZ m^2	MAC-AD* MAC-MAS*
40	ID1 ($CHCl_3$)	1595842.23	47.13>3.85	-	-
100	ID1 ($CHCl_3$)	741056.16	19.62>3.85	-	-
40	ID2 (Pb)	1385980.74	44.45>3.85	115.01	0.0024<1.15
100	ID2 (Pb)	735870.42	23.11>3.85	0.00	0.00<1.15

Table 5.22: Extent of the delimitated Mixing Zones (AA-MZ and MAC-MZ) and final admissibility (AA-AD* and MAC-AD*) in the detailed calculation for ID1 and ID2.

After model simulations, we determined the AA-MZ and MAC-MZ by applying the developed method in the detailed calculation (Step 5) for the "reduction case 1". The same way as in the case 0, we made two reconstructions: 40-years of forcing variability and 100-statistical years.

The delimitated AA-MZ and MAC-MZ of the "reduction case 1" for ID1 in the 40-years case (a-b) and the 100-statistical years case (c-d) are shown in figure 5.115, respectively. As it was mentioned several times, the chloroform (ID1) has not applicable MAC-EQS value so in this figure the MAC-MZ was only an example of the extent of the MAC-MZ. Meantime, the delimitated AA-MZ and MAC-MZ of the "reduction case 1" for ID2 in the 40-years case (a-b) and the 100-statistical years case (c-d) are shown in figure 5.116, respectively.

Final admissibility (AD*)

Once both MZs were delimited, we evaluated the AD* (Equation (3.45)). Table 5.22 summarizes the covered area by MZs and the AA-AD and MAC-AD considering the 5^{th} percentile of the ecdf of the AA-Failure was 15% and the 5^{th} percentile of the ecdf of the MAC-Failure was 4%.

As it can be seen in table 5.22, there were not allocatable MZs for the AA-EQS. Both industrial discharges presented a final admissibility AA-AD* bigger than AA-MAS* (3.85%). Regarding the MAC-EQS, ID2 presented an allocatable MZ because the final admissibility MAC-AD* was smaller than MAC-MAS* (1.15%). Unlike the "case 0" for the 100-years reconstruction, the delimitated MAC-MZ in the "reduction case 1" started at 2% of the MAC-Failure due to that reduction in the concentration so all the MAC-MZ below the 2% of the MAC-Failure were allocatable because they were also below the MAC-MAS* (1.15%).

Thereby, the extents of the AA-MZ were again inadmissible for ID1 and ID2 in the "reduction case 1", and, consequently, both discharges were classified as inadmissible.

5.5.6.2 Reduction case 2

In this section, the delimitation and final admissibility for ID1 and ID2 was illustrated taking into account the toxicant load (flow or concentration) of the "reduction case 2"

Delimitation of mixing zones

After model simulations, we determined the AA-MZ and MAC-MZ by applying the developed method in the detailed calculation (Step 5) for the "reduction case 2" in the same way as in the case 0 and "reduction case 1".

Next, the delimitated AA-MZ and MAC-MZ of the "reduction case 2" for ID1 in the 40-years case (a-b) and the 100-statistical years case (c-d) aree shown in figure 5.117, respectively. Meantime, the delimitated AA-MZ and MAC-MZ of the "reduction case 2" for ID2 in the 40-years case (a-b) and the 100-statistical years case (c-d) are displayed in figure 5.118, respectively.

Final admissibility (AD*)

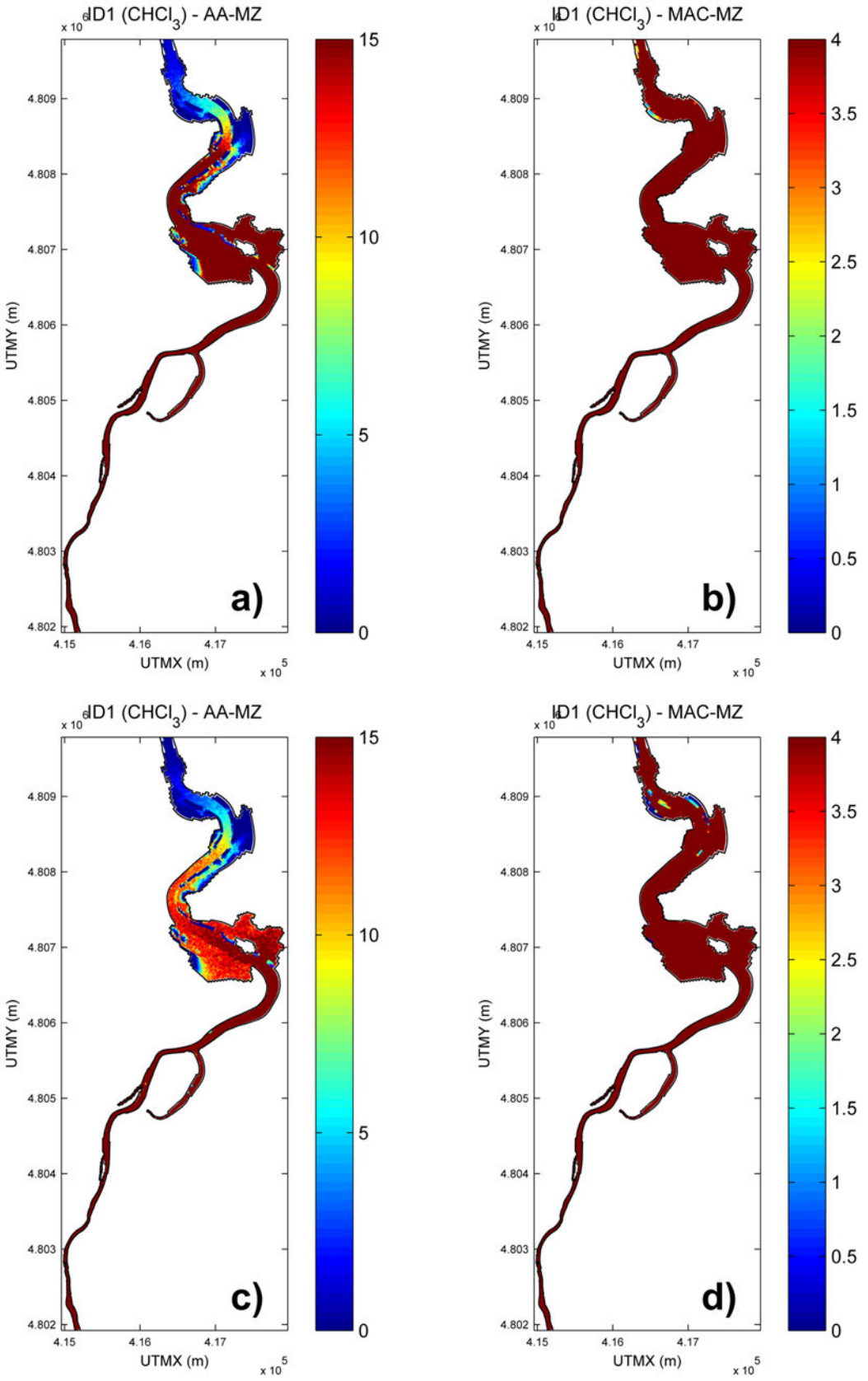

Figure 5.115: Delimitated Mixing Zones in the "reduction case 1" for ID1. AA-MZ of 40-years (a), MAC-MZ of 40-years (b), AA-MZ of 100-statistical years (c) and MAC-MZ of 100-statistical years (d).

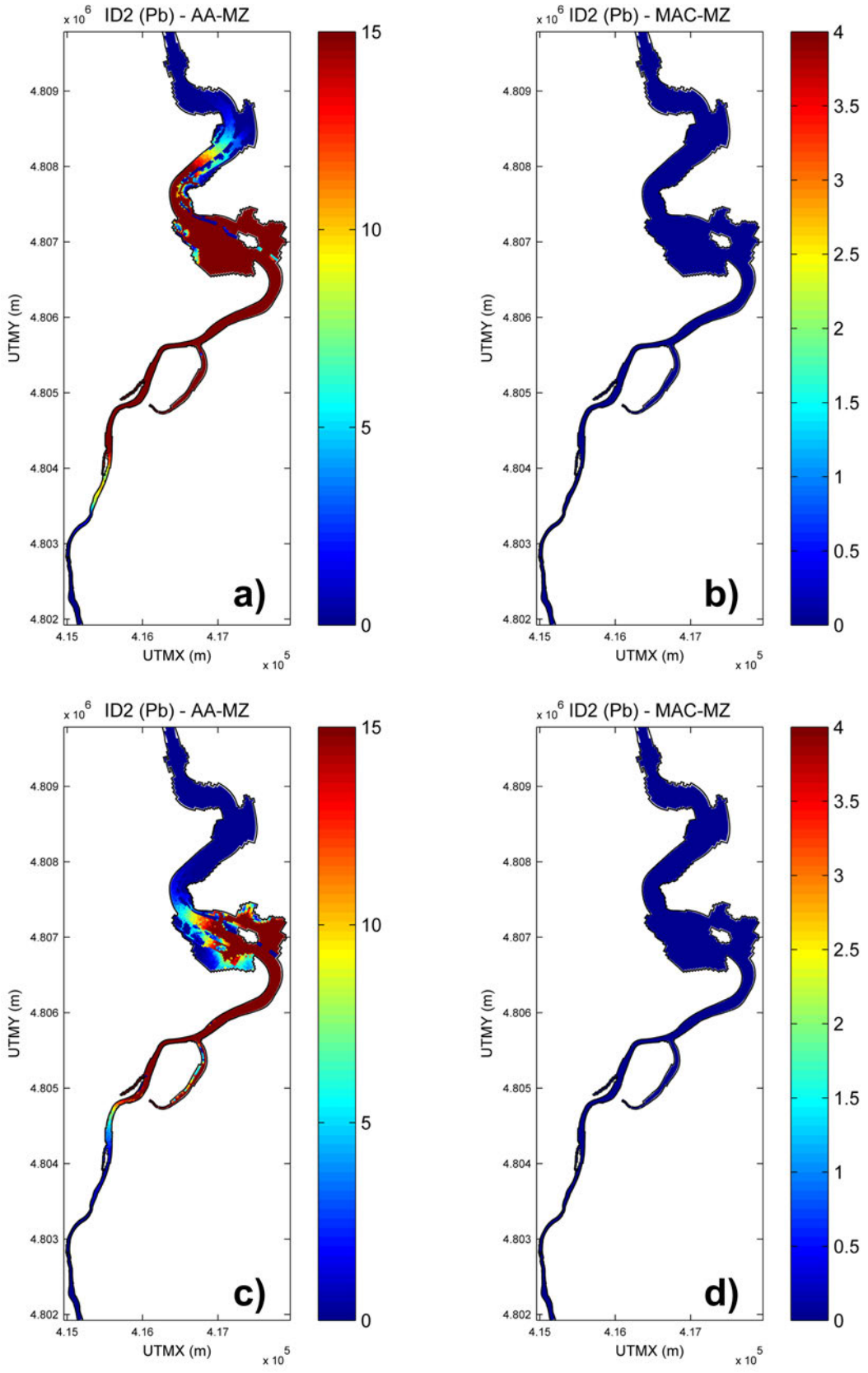

Figure 5.116: Delimitated Mixing Zones in the "reduction case 1" for ID2. AA-MZ of 40-years (a), MAC-MZ of 40-years (b), AA-MZ of 100-statistical years (c) and MAC-MZ of 100-statistical years (d).

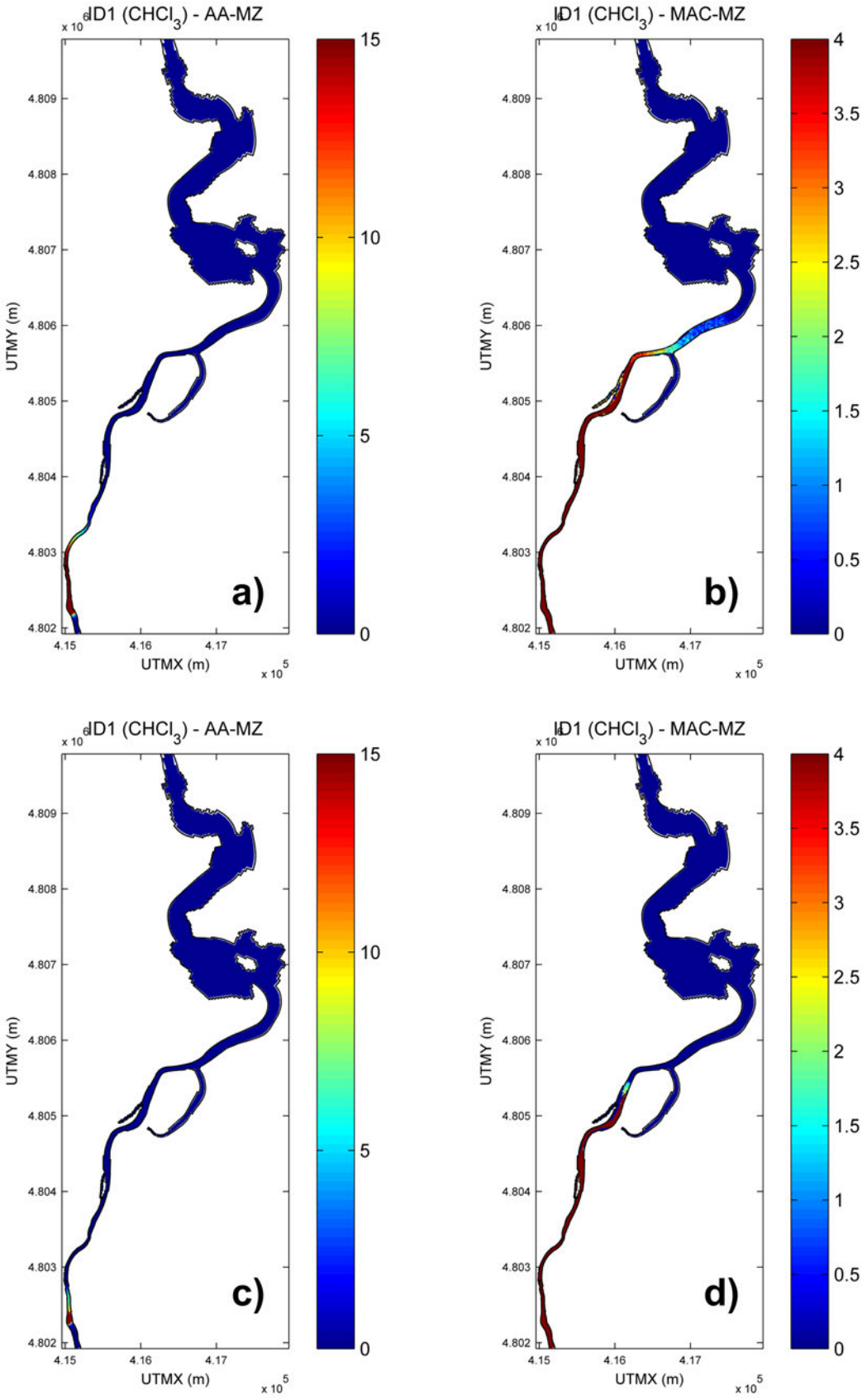

Figure 5.117: Delimitated Mixing Zones in the "reduction case 2" for ID1. AA-MZ of 40-years (a), MAC-MZ of 40-years (b), AA-MZ of 100-statistical years (c) and MAC-MZ of 100-statistical years (d).

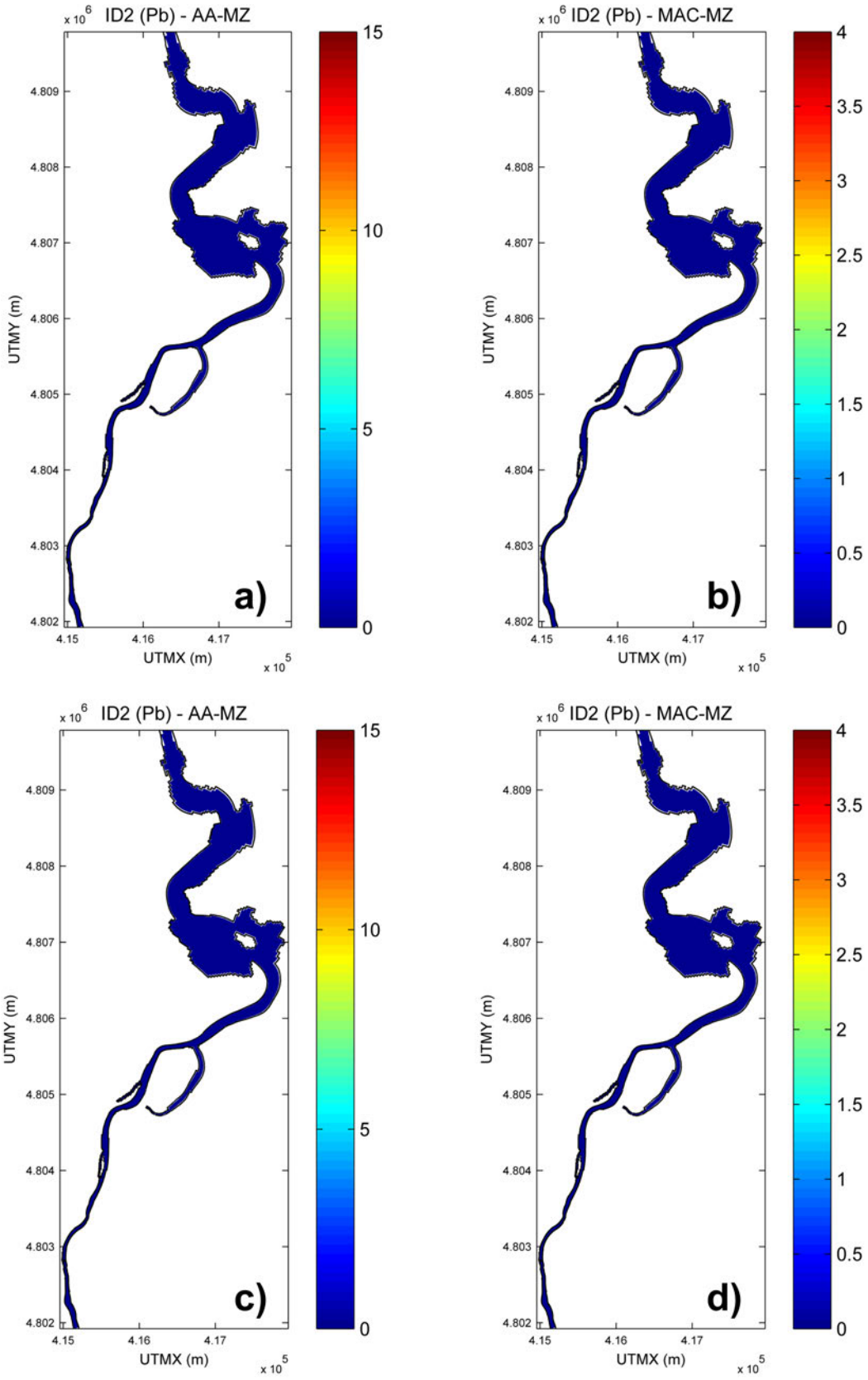

Figure 5.118: Delimitated Mixing Zones in the "reduction case 2" for ID2. AA-MZ of 40-years (a), MAC-MZ of 40-years (b), AA-MZ of 100-statistical years (c) and MAC-MZ of 100-statistical years (d).

Number Years	Name Toxicant	AA-MZ m^2	AA-AD* AA-MAS*	MAC-MZ m^2	MAC-AD* MAC-MAS*
40	ID1 ($CHCl_3$)	38420.27	0.174<3.85	-	-
100	ID1 ($CHCl_3$)	7302.25	0.027<3.85	-	-
40	ID2 (Pb)	0.00	0.00<3.85	0.00	0.00<1.15
100	ID2 (Pb)	0.00	0.00<3.85	0.00	0.00<1.15

Table 5.23: Extent of the delimitated Mixing Zones (AA-MZ and MAC-MZ) and final admissibility (AA-AD* and MAC-AD*) in the detailed calculation for ID1 and ID2.

Once both MZs were delimited, we evaluated the AD* (Equation (3.45)). Table 5.23 resumes the covered area and the AD of the AA-MZ and MAC MZ taking into account the 5^{th} percentile of the ecdf of the AA-Failure was 15% and the 5^{th} percentile of the ecdf of the MAC-Failure was 4%.

As it can be seen in table 5.23, ID2 did not presented MZs (0 m^2) in the "reduction case 2".

Regarding ID1, there were allocatable MZs for the AA-EQS. Both reconstructions presented a final admissibility AA-AD* smaller than AA-MAS* (3.85%). Therefore, figure 5.119 displays the evolution of the AA-AD* with the 5^{th} percentile of the ecdf of the AA-failure probability for the 40-years reconstruction (solid grey line) and the 100-years reconstruction (solid black line). As it can be seen in this figure, all the AA-MZ below the 15% of the AA-Failure were allocatable because they were also below the MAC-MAS* (3.85%). Within this allocatable AA-MZ, the final allocation should be discussed and agreed between the stakeholder and the competent authority due to the economical, social and ecological implications of any allocation.

Thereby, the extents of MZs were admissible for ID1 and ID2 in the "reduction case 2", and, consequently, both discharges were classified as admissible (very large significant). Finally, figure 5.120 shows the final allocation of the AA-MZ of ID1 for the 40-years reconstruction (a) and the 100-years reconstruction (b) at Suances Estuary considering an AA-Failure ($\%$) between 0.0-1.0 (light yellow color), 1.0-2.0 (dark yellow color), 2.0-5.0 (light orange color), 5.0-10.0 (dark orange color), 10.0-15.0 (light red color) and 15.0-100.0 (dark red color). It should be noted that the mixing zones are smaller in the case of 100 years because this reconstruction includes greater variability of hydrodynamic forcings.

5.6 Conclusions

The proposed stepped methodology was applied to the Suances Estuary taking into account two theoretical discharges and passing through all the proposed Steps in order to illustrate it. Following, the main conclusions of each Step are summarized.

Step 1. Preliminary characterization

Three summary sheets were elaborated in order to gather the preliminary characterization of the two industrial dicharges (ID1 and ID2) and the study area (Suances Estuary).

Step 2. Significance of discharge

Both discharges were classified as significant discharges.

Step 3. Simplified calculation (Worst case of dilution)

- The measurements (field data) necessary to conduct the model setup of hydrodynamic and conservative transport model were collected.

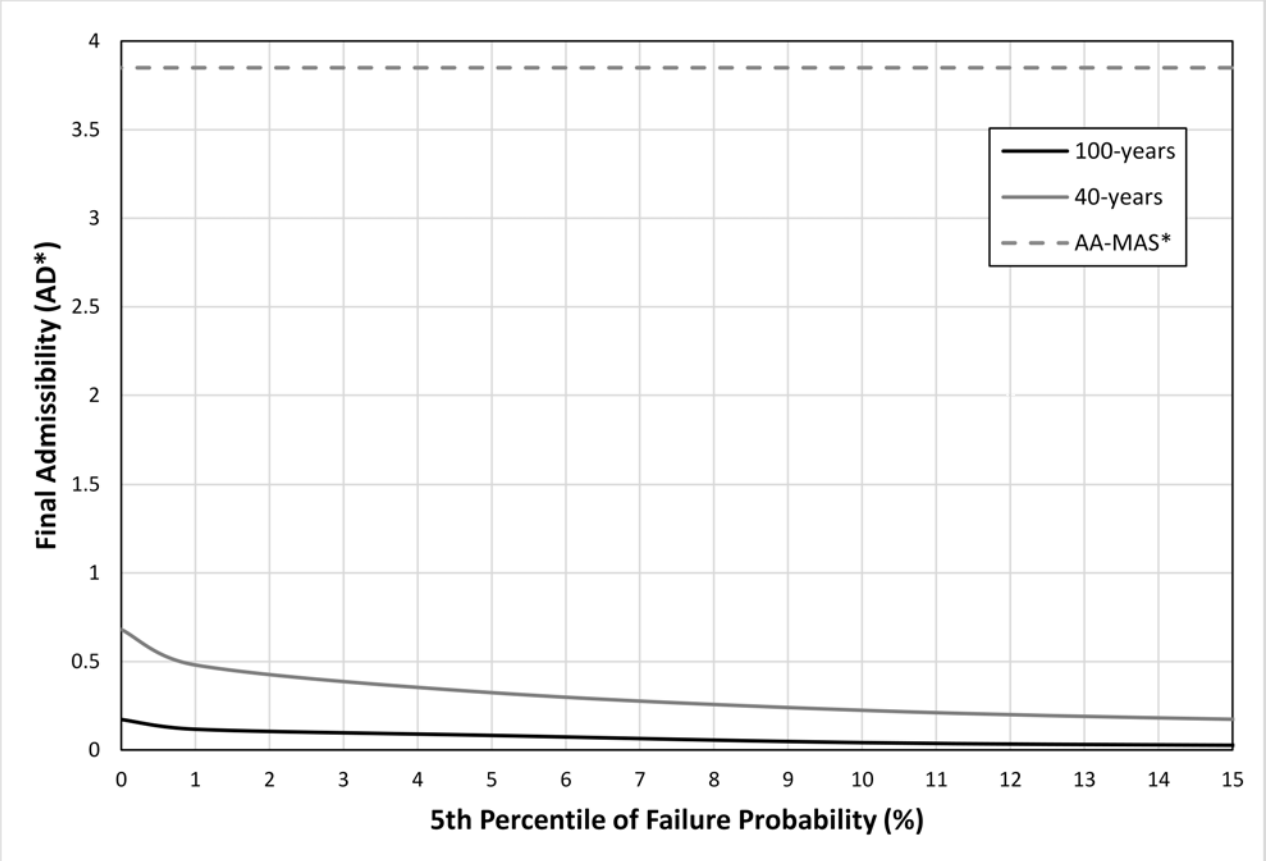

Figure 5.119: Abacus of ID1 presenting the evolution of the AA-AD* of the AA-MZ for the 40-years reconstruction (solid grey line) and the 100-years reconstruction (solid black line) in the detailed calculation. The value of the AA-MAS* in SE is the dashed grey line.

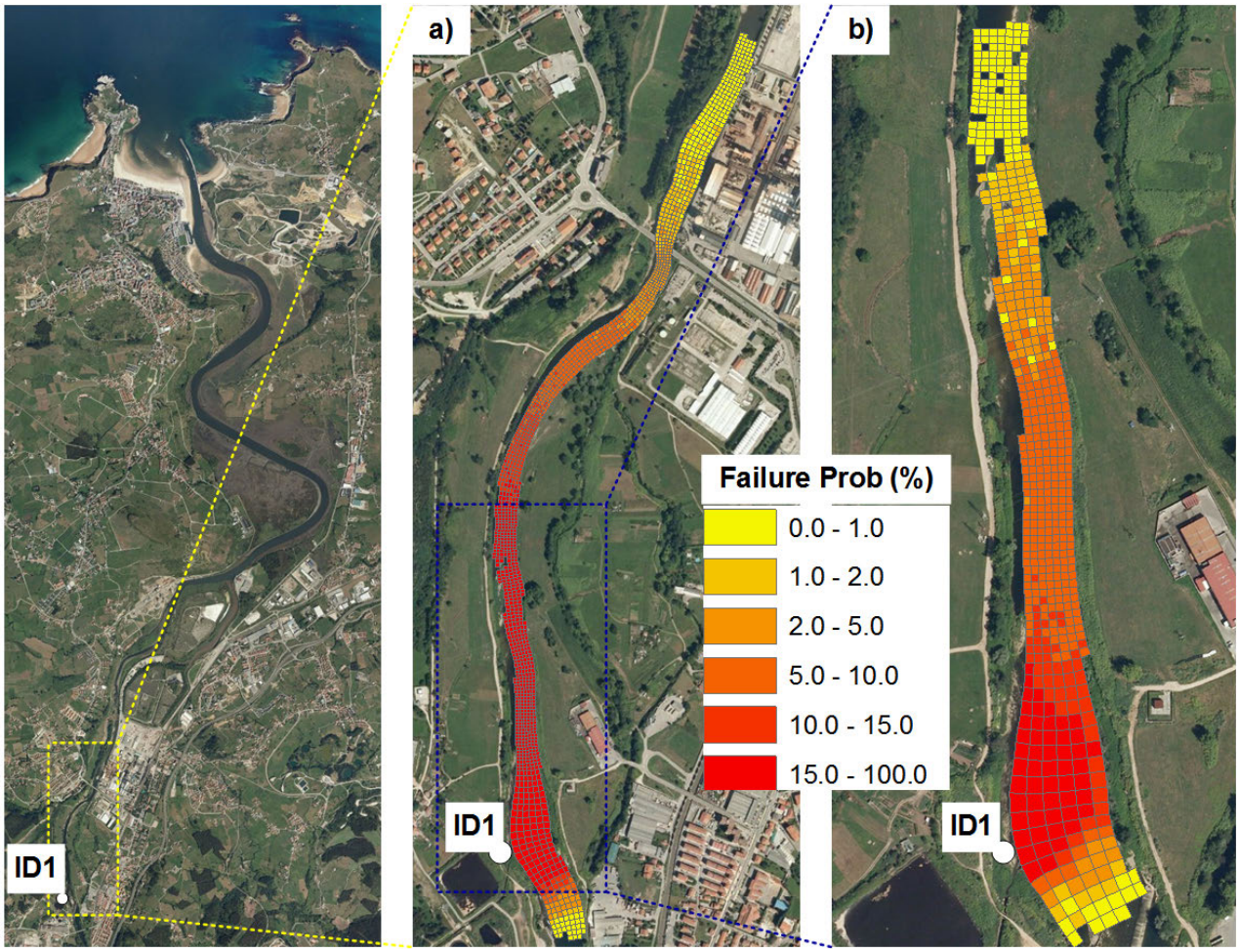

Figure 5.120: Final allocatable AA-MZ in the "reduction case 2" for ID1. AA-MZ of 40-years (a) and AA-MZ of 100-years (b).

- A three-dimensional grid, covering SE and its adjacent coastal zone, was represented horizontally using a curvilinear meshgrid (93×800 grid cells) and vertically using 10-σ layers.
- The model was calibrated displaying an acceptable level of performance in all the stations and variables.
- The "worst case of dilution" was proposed assuming fixed conditions of the forcing: tidal amplitude was $A10 = 0.9246$ m and river flow was $7Q10 = 3.6314$ m^3/s.
- The longest timescale of "quasi-stationary" response for hydrodynamic modeling corresponded to salinity and temperature and was 216 hours (9 days).
- ID1 dilution was oscillating between 6.53 and 1.63 meanwhile ID1 concentration surpassed all the time the AA-EQS. At ID2, the dilution was oscillating between 109.11 and 27.27 meanwhile ID2 concentration surpassed all the time the AA-EQS and most of the time the MAC-EQS.
- ID1 coupling was located in several horizontal grids downstream of the discharge point. In the vertical direction, ID1 was coupled most of the time between layers 5 and 9 (1 and 3.25 m). The rest of the time ID1 was fully mixed in the water column. For ID2, the coupling was always in the grid cell where was located the industrial pipe. Regarding vertical distribution, ID2 was most of the time between layers 5 and 7 (3 and 5.5 m) indicating that ID2 plume was trapped.
- The longest timescale of "quasi-stationary" response for transport modeling was 528 hours (22 days).
- The extent of the delimitated Mixing Zones was: AA-MZ(ID1)=2557527 m^2, MAC-MZ(ID1)=- m^2, AA-MZ(ID2)=2533228 m^2 and MAC-MZ(ID2)=2510515 m^2. Moreover, the final admissibility was: AA-AD(ID1)=100.0, MAC-AD(ID1)=-, AA-AD(ID2)=99.05 y MAC-AD(ID2)=98.16.
- Both industrial discharges presented a final admissibility AA-AD and MAC-AD bigger than AA-MAS (10%) and MAC-MAS (3%). Thereby, both discharges were classified as large significant.

Step 4. Intermediate calculation (Dry case of dilution)

- The driest year was identified as the year 1989.
- ID1 dilution was oscillating between 23.71 and 1 meanwhile ID1 concentration surpassed most of the time the AA-EQS. ID2 dilution was oscillating between 3356.78 and 4.13 meanwhile ID2 concentration surpassed most of the time the AA-EQS and the MAC-EQS.
- ID1 coupling was located in several horizontal grids downstream of the discharge. In the vertical direction, ID1 was fully mixed in the water column most of the time. The rest of the time ID1 was mainly coupled between layers 5 and 9 (1 and 3.25 m). In the case of ID2, the discharge was almost always in the grid cell where was located the industrial pipe. Regarding vertical distribution, ID2 was most of the time between layers 4 and 8 (2.5 and 6.5 m) indicating that ID2 plume was trapped and the plume rose until free surface in the rest of situations.
- The "presimulation" was carried out using a constant river flow of the first day of 1989 and its associated tide during 24 hours to obtain the adequate initial condition. and other "simulation" to record the concentration evolution along the dry year were conducted. The "simulation" ran the model scenario during the year 1989 and hourly recorded 365 days of transport model results.
- The optimal number of surveys was 1000 surveys approximately.

- The extent of the delimitated Mixing Zones was: AA-MZ(ID1)=2557527 m^2, MAC-MZ(ID1)=- m^2, AA-MZ(ID2)=2491395 m^2 and MAC-MZ(ID2)=2452000 m^2. Moreover, the final admissibility was: AA-AD(ID1)=100.0, MAC-AD(ID1)=-, AA-AD(ID2)=97.41 y MAC-AD(ID2)=95.87.

- Both industrial discharges presented a final admissibility AA-AD and MAC-AD bigger than AA-MAS (10%) and MAC-MAS (3%). Thereby, both discharges were classified as very large significant.

Step 5. Detailed calculation (Real case of dilution)

- The "real case of dilution" was selected taking into account the spatial and temporal variations of the forcing (tide an rivers) during 40-years (1970-2010) in the Suances Estuary.

- The timescales that govern river flow signal was correlated with the mean duration of flood events whilst spring and neap cycles for astronomical tides. Both forcings present timescales in the range of a fortnight in the SE, therefore the forcing scenarios presented a time length of 15 days.

- Based on K-means clustering, the minimum and optimal number of simulations was M_{mm}=5×11=55 and M_{om}=12×48=576. From this range, the final number of clusters (M) was 6(tides)×13(rivers)=78 model scenarios corresponding to a time duration of 3.2054 years (8.0135 % of 40 years). These 78 model scenarios assumed $9 + 15$ days of river flow and tidal elevation as forcings.

- The initial dilution at ID1 and ID2 was computed for 78 scenarios being directly proportional to the time series of river flow. The ID1 and ID2 concentration did not exceed the AA-EQS during flood events whereas for other situations, the concentration presented a very broad range of variability surpassing the AA-EQS sometimes. Additionally, it is noted that the MAC-EQS for ID2 was usually exceeded less than the AA-EQS.

- The coupling was carried out again for 78 scenarios. ID1 coupling was located on several horizontal cells downstream of the discharge point. In the vertical direction, ID1 was fully mixed in the water column most of the time whilst the rest of the time ID1 was mainly coupled between layers 5 and 9 (1 and 3.25 m). For ID2, the coupling was almost always in the grid cell where was located the industrial pipe. Regarding vertical distribution, ID2 was most of the time between layers 4 and 8 (2.5 and 6.5 m) indicating that ID2 plume was trapped whilst the plume rose until free surface in the rest of situations.

- The additional required information for setting up the non-conservative model was collected. This model was calibrated displaying an acceptable level of performance in all the stations for lead and chloroform.

- The "presimulations" were carried out using a constant river flow and its associated tide during 24 hours for the 78 scenarios to obtain the adequate initial conditions. and other "simulation" to record the concentration evolution along the dry year were conducted. The "simulation" ran the 78 model scenarios and hourly recorded 365 days of transport model results.

- The error measurements displayed for ID1 and ID2 during the validation period shown that any "real series" of toxicant concentration ($CHCl_3$ and Pb) can be generated based on a sequence of the 78 model results that best fitted the "real series" ("syntethic series").

- Two reconstructions were made: one of 40-years (time series) and other of 100-statistical years (Monte Carlo).

- Tidal zoning (TZ) was segregated using $A95 = 2.13844$ m.

- Susceptibility (SU) was determined by the proposed method where the local flushing time was calculated in 20 scenarios. The maximum LFT in the SE was 0.9494 days (22.7856 hours).
- Naturalness (NA) was defined by 28 hydrodynamic alterations: 1 bridge and 27 dykes.
- Ecological Value (EV) was defined by areas of recreational uses related to bath waters and beaches.
- Stratification (ST) was computed by the proposed method using the 78 model scenarios. Suances Estuary was fully mixed most of the time at the inner part because of the river action (fresh water) filled the water column. At the outer part, the estuary was also mixed due to the tidal action (sea water) generated the enough turbulence for mixing the water column. Furthermore, the middle section of the estuary was partially mixed at the main channel or stratified at intertidal areas because of the combination of both forcings, the depth gradient between the main channel and the intertidal areas and the salinity differences experimented by the water column.
- The "Estuarine Vulnerability Index" (EVI)was determined in Suances Estuary being its average 0.615. Due to the vulnerability, the maximum allowable MZ sizes in the "real case of dilution" were 3.85 and 1.15 for the AA-MAS* and MAC-MAS*.
- The extent of the delimitated Mixing Zones was: AA-MZ(ID1-40)=1771132 m^2, AA-MZ(ID1-100)=1631267 m^2, MAC-MZ(ID1-40)=- m^2, MAC-MZ(ID1-100)=- m^2, AA-MZ(ID2-40)=1519284 m^2, AA-MZ(ID2-100)=933457 m^2, MAC-MZ(ID2-40)=115 m^2 and MAC-MZ(ID2-100)=115 m^2. Moreover, the final admissibility was: AA-AD*(ID1-40)=51.13, AA-AD*(ID1-100)=47.32,MAC-AD*(ID1-40)=-,MAC-AD*(ID1-100)=-, AA-AD*(ID2-40)=47.38, AA-AD*(ID2-100)=29.74,MAC-AD(ID2-40)*=0.0024 and MAC-AD(ID2-100)*=0.0024.
- Both industrial discharges presented a final admissibility AA-AD* than AA-MAS* (3.85%) for the two reconstructions. Thereby, both discharges were classified as inadmissible.
- Two reductions of the concentration for ID1 (factors of 50 and 100) and ID2 (factors of 5 and 10) factors were performed to find admissible Mixing Zones in the two reconstructions. In the case of ID1, a reduction by a factor of 100 generated an admissible MZ for both reconstructions. In the case of ID2, a reduction by a factor of 10 did not generate MZs for both reconstructions.

Be very careful about the beginning.
Then, be very careful about the end.
Then, be very careful about the middle.

Robert Fripp

6

Conclusions and future research topics

6.1 Conclusions

In the introductory chapter, the main motivations and features required for regulating and modelling industrial wastewater discharges were stated. According to these statements, the aim of the present study was to provide a stepped methodology with a group of selected and/or developed numerical tools in order to establish where a mixing zone is required and determines its size and acceptability with an appropriate level of detail for each single-port industrial discharge located in a estuary according to its significance. This proposal may be adopted by Member States and/or Industries when setting Mixing Zones under Directive 2008/105/EC (EC 2008a) and Directive 2013/39/EU (EU 2013).

The state of the art review served to highlight which of the desired characteristics were already addressed in literature and which ones presented a lack in their development. The literature review showed mainly two different features as key aspects for the development of a methodology to allocate mixing zones in estuaries: (1) the mixing, transport and reaction of wastewaters in estuaries and (2) the existing methodological approaches for allocation Mixing Zones.

The term Mixing Zone, which is used in the EQS Directives, does not have a direct relationship with the classification in near-, intermediate- or far-field. Therefore, the admissible iso-concentration map may be found in any of these regions depending on the outflow characteristics, the rate of advection and the rate of mixing. For that reason a zonal modeling approach is necessary. This approach considers the application of zone models in regions with distinct hydrodynamic properties. Nowadays, it seems reasonable to deal with the allocation of Mixing Zones using a integrated numerical model where several transport models for each mixing region are feeded by a hydrodynamic model.

Regarding these numerical models, in the past decades, significant progress has been made in numerical model development, data collection and computer software and hardware. These developments have helped mathematical models to become reliable tools for environmental management and engineering applications within all the mixing regions (near-, intermediate- and far-field).

As a general rule, methodological approaches to allocate MZs in any aquatic system are based on two ambient

water quality criteria: the acute criterion of maximum concentration and the chronic toxicity criterion of average concentration. According to these values, two types of MZs may be established, corresponding to the two-number aquatic life criteria. Finally, more stringent limits are applied on a case-by-case basis if necessary to protect receiving water quality. Despite all the proposed methodologies are good tools to start addressing the associated risks to the discharge of wastewaters, metrics, formulations and calculations displayed on them are generally too oriented towards other aquatic systems, specially riverine discharges. In regard to estuarine discharges, the allocation of MZs is somewhat ambiguous because it lacks a detailed explanation of the tasks required to carry out such work. This leads to confusion and indecision among dischargers and enforcement agencies, this is why universally adaptable guidelines are necessary to initiate understanding and progress.

Besides the proposed method should be the most general as possible based on a stepped methodology with a group of selected and/or developed numerical tools, a case-by-case approach is essential to wise use of natural resources of estuaries, because each MZ should be tailored to the physical, chemical, and biological characteristics of the estuary and its particular community of organisms. Additionally, the method has to take into account the complex geometry, the natural variability and the different hydrometeorological conditions of estuaries and to determine the size and acceptability with an appropriate level of detail for each single-port industrial discharge located in a estuary according to its significance.

Lastly, it is relevant to mention that in tidal water bodies and estuaries, the acceptability of MZs is not establish in all countries. Other countries have established the acceptability with boundaries based on distance from the point discharge or allowing mixing within a fraction of the receiving water area.

Thereby, the allocation of mixing zones in estuaries needs a methodology taking into account the spatial and temporal variability of the hydrodynamic and transport processes, the vulnerability of the receiving waters and the water, and land uses. Following, general conclusions are presented for chapters 3, 4 and 5 of the thesis.

6.1.1 Overall methodology

The proposed stepped methodology provided a tailored solution with an appropriate level of detail in the form of schematic flow diagrams. The general rule was that the costs of the MZs allocation procedure will rise with the level of sophistication. Simpler procedures require less data and expertise, but they also tend to be less accurate. At each Step the aim was to identify those discharges that do not give cause for concern, and also to highlight discharges that require action to reduce the size of the MZ. The philosophy of the decision tree was to increase the resource uses when the order of the discharge increases.

The methodology promoted a uniform and soundly-based framework for such determinations to provide solutions which are: *Efficient* because resources were used only when necessary and then were commensurate with the environmental concerns being addressed; *Robust* for leading to sound reproducible decisions contributing to sustainable use of the estuarine environment; and *Flexible* to meet the needs of Europe's estuarine environments.

Figures 6.1 and 6.2 highlight, in the proposed methodology, the contributions made by this thesis in order to step forward the identified gaps (red color).

In the Step 1, two summary sheets were elaborated in order to gather the preliminary characterization of the effluent(s) and the study area.

In the Step 2, a method to detect those discharges that have not significant impact on the estuarine waters was implemented based on simple formulations. In these discharges, there was not need to evaluate the MZs in order to prevent detailed and expensive studies in discharges that are insignificance.

In the Step 3, a simplified calculation was proposed and based on the physical dilution and hydrodynamics

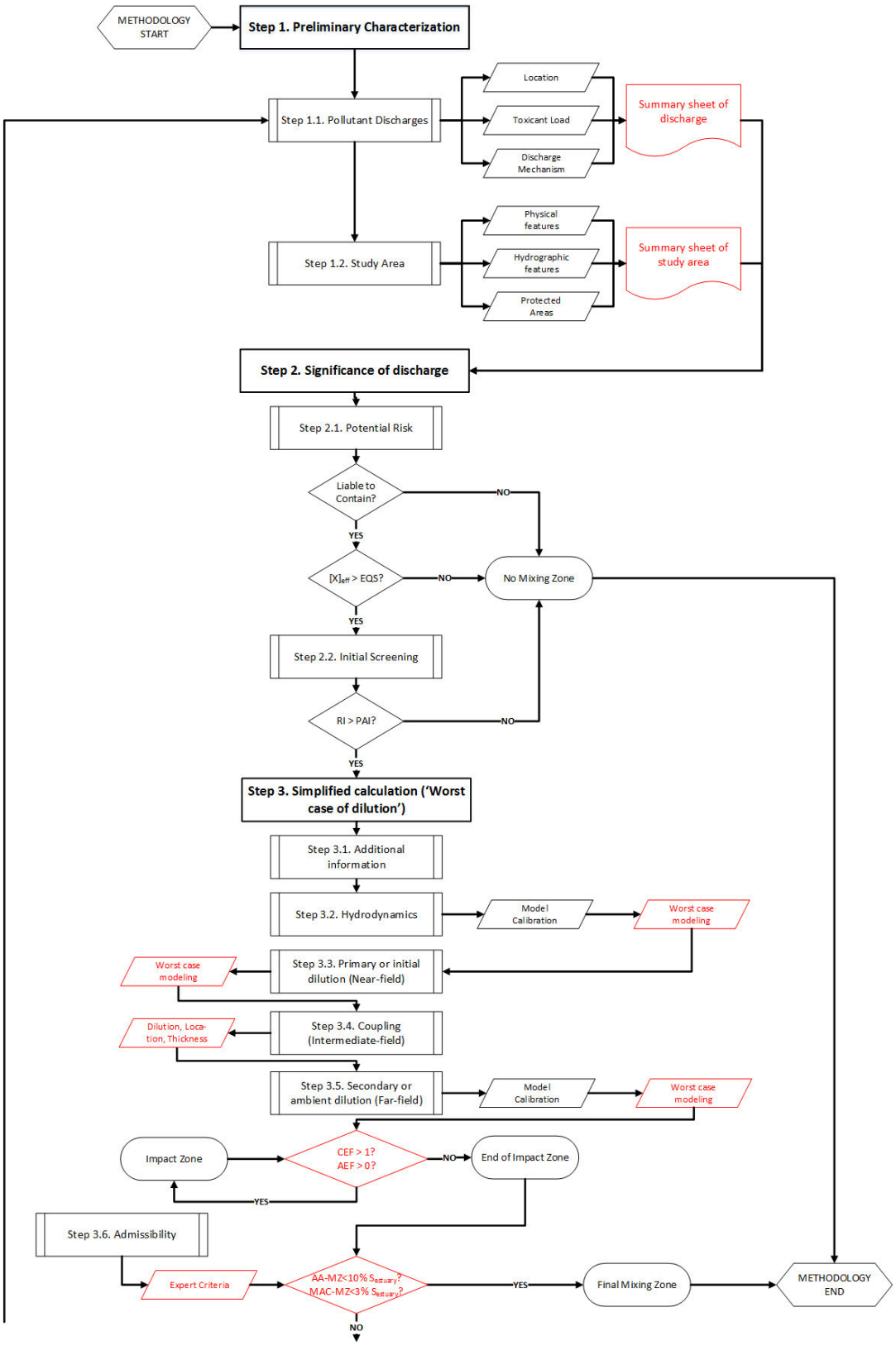

Figure 6.1: Full view of the proposed methodology where identified gaps are highlighted in red color. Part 1

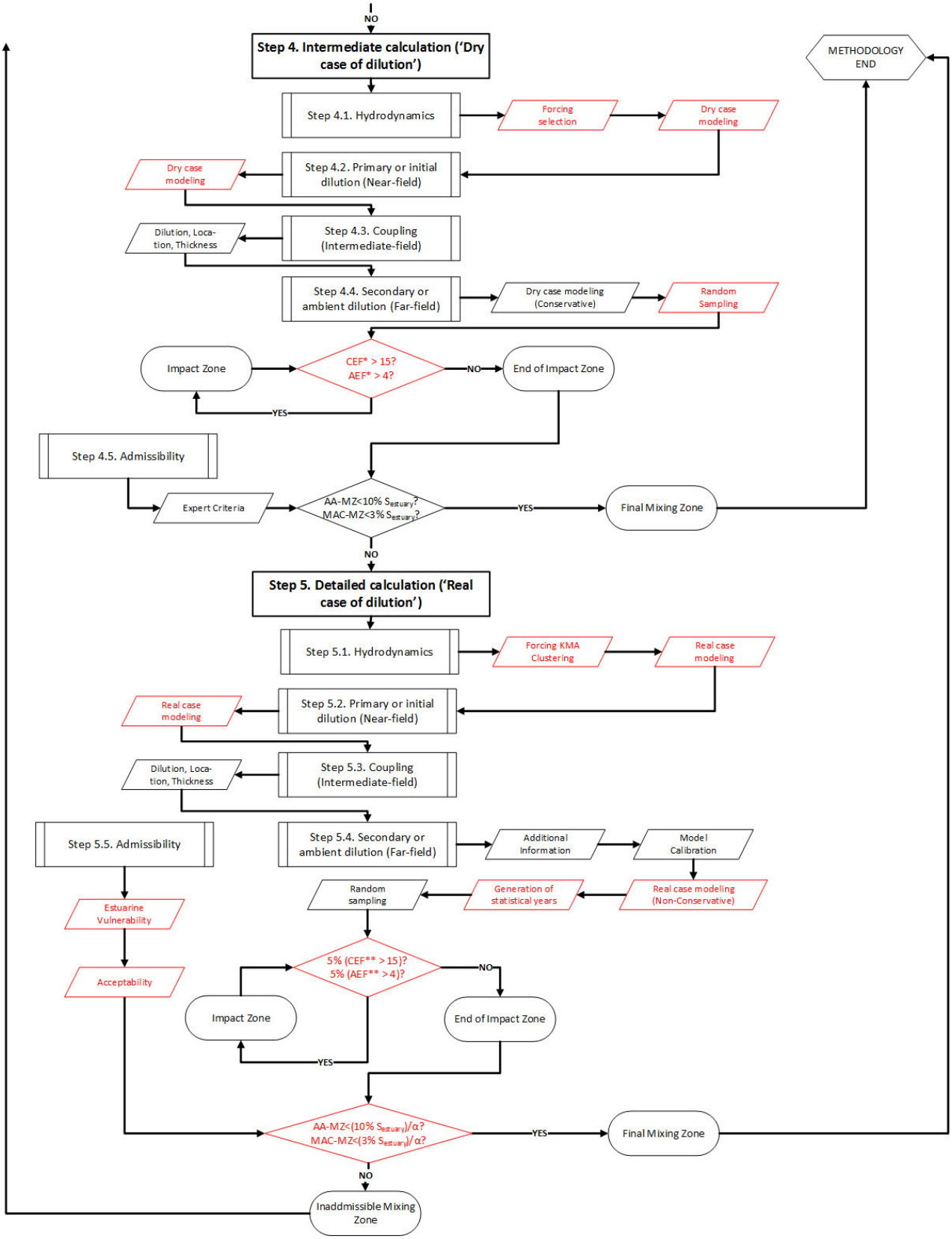

Figure 6.2: Full view of the proposed methodology where identified gaps are highlighted in red color. Part 2

forcings from a precautionary approach:

- The requirements for setting up the model were described and defined. These include the definition of the grid and bathymetry according to the study area, the prescription of boundary and initial conditions and the calibration and validation of the hydrodynamic model by the combination of physical and numerical parameters.
- The "worst case of dilution" was proposed assuming fixed conditions of the forcing: Tidal amplitude was constant and equal to the A10 and river flow was constant and equal to the 7Q10.
- An offline linkage was assumed where the output for hydrodynamic model is the input for the entire time of interest in the near-field model.
- An offline coupling was anew assumed where the source-induced flow, though considerably important for near-field mixing, does not change the flow characteristics of the far-field. The determined variables were the diluted concentration, the length, the width, the thickness and the trapped height of the buoyant jet.
- Because integral jet models did not take into account the interaction with boundaries, an algorithm was developed to specify the end of near-field when the jet-plume touches any boundary (free surface, stratified layer or lateral boundaries, i.e., walls).
- The requirements for setting up the conservative model were described and defined. The use of a 3D far-field model, involving the solution of the transport equation dividing the study area into square or curvilinear grids was suggested.
- The AA-MZ was defined as an area within the model domain where the time-averaged modeled concentrations are exceeding the AA-EQS. The minimum allowed MAC-MZ was defined as an area, within the model domain, where the modeled concentrations are not exceeding the MAC-EQS.
- The admissibility criteria were specified by expert criteria reading the AA-MZ does not exceed 10% of water body extent overall and the MAC-MZ does not exceed 3%.

In the Step 4, a intermediate calculation was proposed and based on the continuous simulation of one year where:

- The "dry case of dilution" was proposed assuming the driest year of the long-term time series of river flow and its associated tidal elevations.
- One "presimulation" to obtain the adequate initial condition of toxicant concentration and other "simulation" to record the concentration evolution along the dry year were proposed.
- To achieve this delimitation, a method was suggested involving three tiers: specification of the annual number of samples, determination of the optimal number of surveys and final delimitation of MZs.
- In this Step was assumed that aquatic life was sufficiently protected if the AA-EQS for chronic toxicity was maintained during at least 85% of the AA-Failure probability and the MAC-EQS for acute toxicity is maintained during at least 96% of the MAC-Failure probability.

In the Step 5, a detailed calculation was proposed and based on the analysis of the spatial and temporal variations of the forcing (tide an rivers) throughout a long-term series and considering the toxicants as non-conservative in the far-field:

- A methodology able to select the most relevant hydrodynamic scenarios in an estuary to perform high-resolution numerical modeling of short-term periods, taking into account the time evolution and the occurrence probability of the forcings in order to obtain realistic responses of the estuarine mean behavior, was developed. This methodology was divided into several steps: Obtainment of the hydrodynamic forcing data, Rearrangement of the input data for clustering, Application of the proposed clustering approach and Sensitivity analyses for the forcing and modeling.

- The conceptual model (processes and interactions) that, at least, the transport model for non-conservative substances must include, was described.

- Model setup for the transport model was explained by defining the model domain discretization, providing boundary and initial conditions and calibrating and validating the model by the combination of physical, physicochemical and numerical parameters.

- To achieve this delimitation, a method was suggested involving four tiers: Validation of the reconstructed series, Selection and generation of l-years, Random sampling and Final delimitation of MZs.

- In this Step was assumed that aquatic life was sufficiently protected if the AA-EQS for chronic toxicity was maintained during at least 85% of the 5^{th} percentile of AA-Failure probability and the MAC-EQS for acute toxicity is maintained during at least 96% of the 5^{th} percentile of MAC-Failure probability.

- In order to establish the admissibility criteria, a methodology was developed and based on a holistic approach, which considers simultaneously the physical processes involved in dispersion and diffusion mechanisms, the ecological features of the receiving water body and the social aspects related with the water body uses. The admissibility of MZs was determined in a four-tiered method: Estuarine Vulnerability Index (EVI), Acceptability (AC*), Maximum allowable size (MAS*) and Admissibility of the delimitated MZ (AD*).

- A methodological approach was developed, based on the use of computational tools for the calculation of flushing time (FT) and divided into four tiers: Hydrodynamic forcing analysis, FT calculation, FT sensitivity analysis and Final FT.

- A method for locating the mixed, partially mixed/stratified and stratified areas in the estuary was also developed, based on the use of hydrodynamic models and mathematical tools for the calculation of the stratification and divided into three steps: Selection and modeling of hydrodynamic scenarios, Calculation of the Richardson number and Final zoning of stratification.

6.1.2 Numerical tools

A series of standard models were selected in this thesis based on the review of the state of the art for the calculation along the several Steps of the developed methodology. We use ***Delft3D-FLOW*** for simulation of hydrodynamics, ***VISJET*** for simulation of near-field (primary dilution) and ***D-Water Quality*** for simulation of far-field (secondary dilution).

Additionally, we programmed a series of self-developed mathematical tools for integrating, transferring, communicating and plotting the required and obtained information along the overall methodology. These mathematical tools were coded using two programming languages: MATLAB and PYTHON and a GIS software: ArcGIS 10.1. MATLAB software was used for calculations of any type. PYTHON software was employed to run dynamically models and to modify and format ASCII files. ArcGIS was used to integrate all the results in a geodatabase and calculate spatial operations such as buffers. These self-developed mathematical tools were:

- Hydrodynamic calibration: Composed by the used tool (Delft3D-FLOW) and the developed tools (EXTRACTOR, GENERA and CALIBRA).
- Offline passive initial dilution: Composed by the used tool (VISJET) and the developed tools (ENVDATA, LANZA-VISJET and PAINT-JET).
- Offline passive coupling (intermediate-field): Composed by the developed tools (DILUTION, ACOPLA and VERTIDO).
- Far-field calibration: Composed by the used tool (D-Water Quality) and the developed tools (GENERA2, CALIBRA2).
- Selecting hydrodynamic forcings (model scenarios): Composed by the developed tools (KMA-FORZA and OPTIMIZA).
- Delimitating the AA-MZ and MAC-MZ: Composed by the developed tools (RECONSTRUCT, SAMPLEA, PROB-MZ and DELIMITA-MZ).
- Estimating the local flushing time: Composed by the used tool (Delt3D-FLOW) and the developed tools (RENOVA and FINAL-LFT).
- Determining the stratification patterns in estuaries: Composed by the used tool (Delt3D-FLOW) and the developed tool (STRATIFICA).
- Assessing the admissibility of Mixing Zones: Composed by the developed tools (CAPA-GIS and ADMITE).

6.1.3 **Results: Application to Suances Estuary**

The proposed stepped methodology was applied to the Suances Estuary taking into account two theoretical discharges and passing through all the proposed Steps in order to illustrate it. Following, the main conclusions are summarized:

- A three-dimensional grid, covering SE and its adjacent coastal zone, was represented horizontally using a curvilinear meshgrid (93×800 grid cells) and vertically using 10-σ layers.
- The hydrodynamic model and transport model (conservative and non-conservative approach) were calibrated displaying an acceptable level of performance in all the stations and variables.
- The longest timescale of "quasi-stationary" response for hydrodynamic modeling corresponded to salinity and temperature and was 216 hours (9 days). Meantime, The longest timescale of "quasi-stationary" response for transport modeling was 528 hours (22 days).
- The driest year was identified as the year 1989.
- The optimal number of surveys was 1000 surveys approximately.
- The timescales that govern river flow signal was correlated with the mean duration of flood events whilst spring and neap cycles for astronomical tides. Both forcings present timescales in the range of a fortnight in the Suances Estuary, therefore the forcing scenarios were classified with a time length of 15 days.

- Based on K-means clustering, the minimum and optimal number of simulations was M_{mm}=5×11=55 and M_{om}=12×48=576. From this range, the final number of clusters (M) was 6(tides)×13(rivers)=78 model scenarios corresponding to a time duration of 3.2054 years (8.0135 $\%$ of 40 years). These 78 model scenarios assumed $9 + 15$ days of river flow and tidal elevation as forcings.

- The initial dilution at ID1 and ID2 in all the calculations was directly proportional to the time series of river flow. The ID1 and ID2 concentration were minimum during flood events whereas for other situations, the concentration presented a very broad range of variability.

- The end of the near-field for ID1 was located on several horizontal cells downstream of the discharge point. In the vertical direction, ID1 was fully mixed in the water column most of the time whilst the rest of the time ID1 was mainly coupled between layers 5 and 9 (1 and 3.25 m). For ID2, the end of the near-field was almost always in the grid cell where was located the industrial pipe. Regarding vertical distribution, ID2 was most of the time between layers 4 and 8 (2.5 and 6.5 m) indicating that ID2 plume was trapped whilst the plume rose until free surface in the rest of situations.

- The error measurements displayed for ID1 and ID2 during the validation period shown that any "real series" of toxicant concentration ($CHCl_3$ and Pb) can be generated based on a sequence combining, every 15 days, the model result (78 scenarios) that best fitted the "real series" ("syntethic series").

- Two reconstructions were made: one of 40-years (time series) and other of 100-statistical years (Monte Carlo).

- The local flushing time was calculated in 20 scenarios. The maximum local flushing time in Suances Estuary was 0.9494 days (22.7856 hours).

- Suances Estuary was fully mixed most of the time at the inner part because of the river action (fresh water) filled the water column. At the outer part, the estuary was also mixed due to the tidal action (sea water) generated the enough turbulence for mixing the water column. Furthermore, the middle section of the estuary was partially mixed at the main channel or stratified at intertidal areas because of the combination of both forcings, the depth gradient between the main channel and the intertidal areas and the salinity differences experimented by the water column.

- The "Estuarine Vulnerability Index" (EVI)was determined in Suances Estuary being its average equal to 0.615. Due to the vulnerability, the maximum allowable MZ sizes in the "real case of dilution" were 3.85 and 1.15 for the AA-MAS* and MAC-MAS*.

- According to the obtained results for 40 and 100 years, the delimitated mixing zones are smaller in the case of 100 years because this reconstruction considers greater variability of the hydrodynamic forcings.

6.2 Future research topics

Considering the multiple aspects covered by the allocation of Mixing Zones from industrial discharges, future research must consider diverse knowledge fields. Following, the main aspects requiring further investigation are summarized.

Different type of discharges might be established considering ***other discharge mechanisms*** (surface discharges or channels) and ***other toxicant loads*** (variable flow and concentration). Therefore, numerical tools need to be developed for modeling other discharge configurations which may be suitable in some cases, such as direct surface discharge, over-spill in a cliff, or channels. Experimental data are necessary to calibrate, test and validate these tools.

Further investigations should be orientated to implement the proposed methodology on more complex problems taking into account ***other hydrodynamic forcings***, for instance, wind velocity and direction, sea and swell components of the sea states, storm surge level, inverse barometer or even the spatial variability of the estuarine forcings when these forcings become significant. However, one of the prerequisites to implement the method is that the river flow and tide are considered independent and random events. If inverse barometer, wind and/or waves are introduced, a preliminary study of the correlation between the wind, waves and river flow must be done because the joint probability, in this case, it is not the product of the single probabilities of each forcing. This fact could lead to an excessive number of clusters in order to explain the forcing variability or running numerical models. In these cases, the clustering approach should be done combining all the correlated variables in the same matrix.

Regarding initial dilution processes and modeling, available models (integral jet models) were developed for deep water discharges and modelers are not always confident in applying to shallow water applications. In this field, the ***inclusion of background concentration*** in near-field model could help to improve the accuracy of integral jet models at first.

On the other hand, lately promising ***CFD models*** like FLUENT, Open-FOAM or Flow3D have been presented and applied in relatively simple cases or in regions of limited extent, such as the region of initial mixing. These CFD models might deal with all the mixing regions. However, the high demand of computational resources of this models causes that they do not appear feasible for present-day engineering practice in all mixing regions. Nonetheless, CFD models might be helpful for the analysis of special cases, where either experiments are too difficult or too expensive and integral models do not apply.

Moreover, the combination of experimental data of buoyant jets from lab studies (PIV-LIF techniques) with an adequate calibration of a CFD model could be a powerful tool to improve the results of initial dilution and the definition of the intermediate-field to couple with far-field models. This tool might be also able to extend the experimental results with other environmental conditions in order to cover a wide range of variability. Finally, CFD model results could be use to construct abacus with the influence of key parameters on the initial dilution, the location, the width and the thickness of the near-field for industrial discharges. Next, all this information might be included in a expert system to predict the behaviour of any discharge in the near-field.

Other coupling approaches might be developed. For instance, if flow quantities from either region are dynamically important, an active coupling is desirable. In this approach, momentum conservation principles have to be considered in addition to fluid and substance mass conservation. Combined with this active coupling, a dynamic (online or realtime) linkage might be developed as well. In this type of model execution, the near- and far-field models exchange data after every time-step, thus, the zone models run in parallel. As a consequence, a much higher degree of accuracy can be attained in this fashion.

Partitioning coefficients were adopted from chemical databases. However, this coefficients are highly influenced by the pH, the salinity, the specific form of the toxicant and the chemical composition of the two phases (water and sediment). Thus, a correct definition of partitioning coefficients should be done by means of experimental data in a laboratory on a case-by-case basis.

In the proposed methodology, the used ***conceptual model*** considered the minimum number of processes for modeling non-conservative substances and ensuring reliable results in the water column. Additional studies might include sediment-water interactions such as diffusion, resuspension and sedimentation and specific sediment processes such as burial and consolidation. Furthermore, other ***bio-processes*** might be also include in order to determine the influence of biotic factors such as the bio-film (a film generated by microalgae and bacteria at the water-sediment interface) on the spatial and temporal distribution of toxicant concentrations in the water and sediment.

The proposal for estimating water renewal based on the ***local flushing time*** assumed fixed conditions of the forcing. New studies could be done in order to develop a method based on real forcing conditions. For

instance, the method could has into account the estimation of the local flushing time at hourly frequency, this is, starting every hour during the real conditions in order to obtain the spatial and temporal distribution of the local flushing time.

The use of the ***Estuarine Vulnerability Index*** (EVI) in the admissibility criteria considered the average value of the estuary to determine the maximum allowable MZ size (MAS). This method could be further developed, taking into account the average value of EVI covered by the MZ, in order to delimitate the MZ with a more flexible criterium. However, this approach should be carefully handle because the MAS would be variable and specific for each discharge.

Uncertainty is an inevitable source of noise in water quality management and will weaken the adequacy of decisions. Uncertainty is derived from imperfect information, natural variability, and knowledge-based inconsistency. To make better decisions, it is desirable to reduce uncertainty. Uncertainty includes quantitative uncertainty and non-quantitative uncertainty, which is also called qualitative uncertainty. Qualitative uncertainty originates from human subjective and biased beliefs. A systematic process of qualitative uncertainty analysis might be developed for assisting complete uncertainty analysis, in which a qualitative network could then be built with qualitative relationship and quantifiable functions. To limit biased information, a checklist might be helpful to construct the qualitative network. The checklist could help one to ponder arbitrary assumptions that have often been taken for granted and may yield an incomplete or inappropriate decision analysis. The checklist also might enable decision makers to gain insight on the uncertainty level of the system at early steps as a convenient tool to review the adequacy of a allocation procedure. Following the instruction of the checklist, an appropriate algorithm in a form of probability, possibility, or belief may then be assigned for the network. Consequently, the risk or evidence of the success of outcomes will be obtained. The incorporation of the systematic consideration of qualitative uncertainty into water quality management is expected to refine the decision-making process.

The method was focused on individual discharges but it could be applied to ***multiple discharges*** when two effluents are discharging the same toxicant/s. However, the way to overcome the numerous issues that arise when dealing with multiple discharges, regarding the admissibility criteria, were not tackle in the methodology. In industrialized areas, numerous individual discharges may mean that mixing zones can overlap or may need a further assessment to determine whether the cumulative effect can be regarded as acceptable when occur non-intersecting mixing zones. The initial focus will be the consideration of discrete point source discharges but in certain urban catchments there may be numerous very minor point sources that also demand consideration collectively. Accordingly, the basis for determining the acceptability of the combined discharges should take into account the range of case-specific factors like the total maximum daily load assimilated by the estuary, the possible non-linearity, the existence of thresholds, the correlation between discharges or the possibility of synergistic or antagonistic effects.

This thesis explained how to model heavy metals and organic micropollutants. This was illustrated by modeling lead and chloroform at Suances Estuary. Further studies in this estuary might included ***other heavy metals*** such as mercury, chromium, zinc or arsenic and ***other organic micropollutants*** such as PAHs, PCBs, dioxins or furans.

Finally, the developed or improved methodology might be ***implemented in other estuaries*** with the aim to validate and reproduce it. In this way, we will be able to ensure the adequacy of the method for allocating mixing zones in all kind os situations.

6.3 Contributions of the thesis

In this section, all the contributions made by this thesis were grouped in 4 categories: papers, conferences, workshops and R+D+i projects. Next, we enumerate the contributions in every category.

6.3.1 Papers

1. **Bárcena, J.F.**, García, A., García, J., Álvarez, C., and Revilla, J.A., 2012a. Surface analysis of free surface and velocity to changes in river flow and tidal amplitude on a shallow mesotidal estuary: An application in Suances Estuary (Northern Spain). Journal of Hydrology 420-421, 301-318.

2. **Bárcena, J.F.**, García, A., Gómez, A.G., Álvarez, C., Juanes, J.A., and Revilla, J.A., 2012b. Spatial and temporal flushing time approach in estuaries influenced by river and tide. An application in Suances Estuary (Northern Spain). Estuarine, Coastal and Shelf Science 112, 40-51.

3. Sámano, M.L., **Bárcena, J.F.**, García, A., Gómez, A.G., Álvarez, C., and Revilla, J.A., 2012. Flushing time as a descriptor for heavily modified water bodies classification and management: Application to Huelva Harbour. Journal of Environmental Management 107, 37-44.

4. López, I., Álvarez, C., Gil, J.L., García, A., **Bárcena, J.F.**, Revilla, J.A., 2013. A method for the source apportionment in bathing waters through the modeling of waste water discharges: Development of an indicator and application to an urban beach in Santander (Northern Spain). Ecological Indicators 24, 334-343.

5. Gómez, A.G., **Bárcena, J.F.**, Juanes, J.A., Ondiviela, B., and Sámano, M.L., 2014. Transport time scales as physical descriptors to characterize heavily modified water bodies near ports in coastal zones. Journal of Environmental Management 136, 76-84.

6. **Bárcena, J.F.**, Camus, P., García, A., and Álvarez, C., 2015. Selecting model scenarios of real hydrodynamic forcings on mesotidal and macrotidal estuaries influenced by river discharges using K-means clustering. Environmental Modeling and Software 68, 70-82.

7. **Bárcena, J.F.**, García-Alba, J., García, A., and Álvarez, C., 2015. Analysis of the stratification patterns in mesotidal and macrotidal estuaries influenced by river discharges using a 3D hydrodynamic model and K-means clustering. Estuarine, Coastal and Shelf Science (under review).

8. **Bárcena, J.F.**, Gómez, A.G., García, A., Álvarez, C., and Juanes, J.A., 2015. Estuarine vulnerability index: quantifying the vulnerability of mesotidal and macrotidal estuaries influenced by river discharges against point-source wastewaters. Ecological Indicators (in preparation).

6.3.2 Conferences

1. Estuarine and Coastal Sciences Association 47 Symposium. **Javier F. Bárcena**, Andrés García, Aina García, César Álvarez, José A. Juanes, José A. Revilla, 2010. Influence of river flow and tide on water renewal in a narrow and shallow estuary. An application to the Suances Estuary (North of Spain). Oral communication.

2. 9th International Symposium on Ecohydraulics. **Javier F. Bárcena**, Andrés García, César Álvarez, José A. Juanes, 2012. First-Order assessment to delimitate environmental risk zones due to wastewater discharges on estuaries. Oral communication.

3. XVII Congreso de la Asociación Española de Limnología. **Javier F. Bárcena**, Aina G. Gómez, Andrés García, César Álvarez, José A. Juanes, 2014. Estuarine Vulnerability Index: Quantifying the acceptability of mixing zones generated by point discharges. An application to Suances estuary (N Spain). Oral communication.

6.3.3 Workshops

1. Participant in the 2^{nd} CIS Mixing Zones Workshop (JRC Centre Ispra, Italy, 2010)

6.3.4 R+D+i Projects

Competitive

1. VERTITOX: Desarrollo de procedimientos para el control operativo integrado de vertidos al medio litoral (urbano e industrial), mediante el uso de biomarcadores, bioensayos e indicadores del estado ecológico (018/RN08/02.1), 2008-2010.
2. QEST: Estudio de los aspectos clave para la determinación de caudales ecológicos en estuarios (CTM2009-10620), 2010-2012.
3. PORTONOVO: Water quality in harbours (2009-1/119), 2010-2012.
4. VULMA: Establecimiento de criterios para la valoración de la vulnerabilidad de las masas de agua sometidas a vertidos urbanos e industriales (CTM2009-11206), 2010-2012.
5. VERTIZE: Análisis de aspectos claves de la dispersión de vertidos industriales para la delimitación de zonas de mezcla ambiental de estuarios (CTM2012-32538), 2013-2015.

Non-Competitive

1. Aplicación de la ROM 5.1. "Calidad de aguas litorales en áreas portuarias" en el Puerto de Santa Cruz de Tenerife, 2010-2011.
2. Impacto del nuevo canal de Bocachica en la renovación de agua, salinidad y turbidez de la bahía de Cartagena de Indias, Colombia, 2013.
3. Asistencia técnica para la aplicación de modelos matemáticos para sustitución de la existente EDAR Vuelta Ostrera, 2014-2015.

Bibliography

ABDELRHMAN, M.A. (2005). Simplified modeling of flushing and residence times in 42 embayments in new england, usa, with special attention to greenwich bay, rhode island. *Estuarine, Coastal and Shelf Science*, **62**, 339–351. 157

AKAR, P.J. & JIRKA, G.H. (1994). Buoyant spreading processes in pollutant transport and mixing. part i: Lateral spreading in strong ambient current. *Journal of Hydraulic Research*, **32**, 815–831. 49

AKAR, P.J. & JIRKA, G.H. (1995). Buoyant spreading processes in pollutant transport and mixing. part ii: upstream spreading in weak ambient current. *Journal of Hydraulic Research*, **33**, 87–100. 49

ALBER, M. & SHELDON, J.E. (1999). Use of a date-specific method to examine variability in the flushing times of georgia estuaries. *Estuarine, Coastal and Shelf Science*, **49**, 469–482. 157

ALBERTSON, M.L., DAI, Y.B., JENSEN, R.A. & ROUSE, H. (1950). Diffusion of submerged jets. *Transport ASCE*, **115**, 639–644. 42

ALLEY, E.R. (2007). *Water Quality Control Handbook, Second Edition*. McGraw-Hill. 1, 4, 7, 2, 5, 8, 70

AMBROSE, R.B. & WOOL, T.A. (1988). Wasp7 stream transport-model theory and user's guide. supplement to water quality analysis simulation program (wasp) user documentation. Tech. rep., U.S. Environmental Protection Agency. 64

AMBROSE, R.B., WOOL, T.A., CONNOLLY, J.P. & SCHANZ, R.W. (1988). Wasp4, a hydrodynamic and water quality model—model theory, user's manual, and programmer's guide. Tech. rep., U.S. Environmental Protection Agency. 64

ANDERSEN, O.B. (1994). Ocean tides in the northern north-atlantic and adjacent seas from ers-1 altimetry. *Journal of Geophysical Research*, **99**, 22557–22573. 45, 70, 75, 134, 205, 217

ANZECC & ARMCANZ (2000). Australian and new zealand guidelines for fresh and marine water quality: Volume 2 – aquatic ecosystems – rationale and background information. Tech. rep., Australian and New Zealand Environmental and Conservation Council. 8, 9, 81

API (1998). Mixing zone modeling and dilution analysis for water-quality-based npdes permit limits. Tech. rep., American Petroleum Institute. 72, 73

ASCIONE-KENOV, I., GARCIA, A.C. & NEVES, R. (2012). Residence time of water mondego estuary (portugal). *Estuarine, Coastal and Shelf Science*, **106**, 13–22. 19, 92

AUS (2008). Water act 2007. 7, 8, 70

BACHMETEV, B.A. (1932). *Hydraulics of Open Channels*. McGraw-Hill. 38

BAI, Y., WANG, Z. & SHEN, H. (2003). Three-dimensional modeling of sediment transport and the effects of dredging in the haihe estuary. *Estuarine, Coastal and Shelf Science*, **56**, 175–186. 19, 92

BALLEGOOYEN, R.V., TALJAARD, S., NIEKERK, L.V. & HUIZINGA, P. (2004). Using 3d modeling to predict physico-chemical responses to variation in river inflow in smaller, stratified estuaries typical of south africa. *Journal of Hydraulic Research*, **42**, 563–577. 181

BANAS, N.S. & HICKEY, B.M. (2005). Mapping exchange and residence time in a model of willapa bay, washington, a branching, macrotidal estuary. *Journal of Geophysical Research*, **110**. 35

BÁRCENA, J.F. (2009). *Procedimiento de cálculo para delimitar zonas de afección de vertidos industriales en estuarios de aguas someras (in Spanish)*. Master thesis, Universidad de Cantabria. 4, 5

BÁRCENA, J.F., GARCÍA, A., GARCÍA-ALBA, J., ÁLVAREZ, C. & REVILLA, J.A. (2012a). Surface analysis of free surface and velocity to changes in river flow and tidal amplitude on a shallow mesotidal estuary: An application in suances estuary (nothern spain). *Journal of Hydrology*, **420–421**, 301–318. 67, 108, 205, 271

BÁRCENA, J.F., GARCÍA, A., GÓMEZ, A.G., ÁLVAREZ, C., JUANES, J.A. & REVILLA, J.A. (2012b). Spatial and temporal flushing time approach in estuaries influenced by river and tide. an application in suances estuary (northern spain). *Estuarine, Coastal and Shelf Science*, **112**, 40–51. 19, 59, 140, 35, 92, 158, 208, 329

BAUMGARTNER, D.J., FRICK, W.E., & ROBERTS, P.J.W. (1994). Dilution models for effluent discharges, 3rd edition. Tech. rep., U.S. Environmental Protection Agency. 46

BCMOE (2013). Guidance for the derivation and application of water quality objectives in british columbia. Tech. rep., British Columbia Ministry of Environment. 78

BLENINGER, T. (2006). *Coupled 3D hydrodynamic models for submarine outfalls: Environmental hydraulic design and control of multiport diffusers*. Doctoral thesis, Universitat Fridericiana zu Karlsruhe. xxix, xxx, 11, 13, 35, 45, 49, 52, 66, 68

BLENINGER, T. & JIRKA, G.H. (2004). Near- and far-field model coupling methodology for wastewater discharges. In *Proceedings of the 4th international symposium on environmental hydraulics and the 14th Congress of Asia and Pacific division*, 447–453, Taylor and Francis. 31, 52, 111

BLUMBERG, A.F. & MELLOR, G.L. (1987). *Description of a three-dimensional coastal ocean circulation model, Three-Dimensional Coastal ocean Models*. American Geophysical Union. 39

BOLIN, B. & RODHE, H. (1973). A note on the concepts of age distribution and transit time innatural reservoirs. *Tellus*, **25**, 58–62. 35, 160

BOWDEN, K.F. (1978). Mixing processes in estuaries. estuarine transport processes. *Baruch Library in Marine Science*, **7**, 11–36. 62, 163

BÁRCENA, J.F., GARCÍA, A., ÁLVAREZ, C. & JUANES, J.A. (2012). First-order assessment to delimitate environmental risk zones due to wastewater discharges on estuaries. In *9th International Symposium on Ecohydraulics 2012 Proceedings*, Helmut Mader and Julia Kraml. 57, 154

BROOKS, N.H. (1960). Diffusion of sewage effluent in an ocean current. In *Proceedings of the First Conference on Waste Disposal in the Marine Environment*, 246–267, Pergamon Press. 53

BROWN, M.M., MULLIGAN, R.P. & MILLER, R.L. (2014). Modeling the transport of freshwater and dissolved organic carbon in the neuse river estuary, nc, {USA} following hurricane irene (2011). *Estuarine, Coastal and Shelf Science*, **139**, 148–158. 181

CAMERON, W.M. & PRITCHARD, D.W. (1963). *The Sea. Estuaries*, vol. 2. John Wiley and Sons. 61, 22, 23, 162

CAMUS, P., COFIÑO, A.S., MENDEZ, F.J. & MEDINA, R. (2011a). Multivariate wave climate using self-organizing maps. *Journal of Atmospheric and Oceanic Technology*, **28**, 1154–1568. 136

CAMUS, P., MENDEZ, F.J., MEDINA, R. & COFIÑO, A.S. (2011b). Analysis of clustering and selection algorithms for the study of multivariate wave climate. *Coastal Engineering*, **58**, 453–462. xix, 135, 136

CANALE, R.P. & VOGEL, A.H. (1974). Effects of temperature on phytoplankton growth. *Journal of the Sanitary Engineering Division*, **100**, 231–241. 62

CANU, D.M., SOLIDORO, C., UMGIESSER, G., CUCCO, A. & FERRARIN, C. (2012). Assessing confinement in coastal lagoons. *Marine Pollution Bulletin*, **64**, 2391–2398. 134

CARRER, S., COFFARO, G., BOCCI, M. & BARBANTI, A. (2005). Modeling partitioning and distribution of micropollutants in the lagoon of venice: a first step towards a comprehensive ecotoxicological model. *Ecological Modeling*, **184**, 83–101. 144

CASTANEDO, S. (2000). *Desarrollo de un Modelo Hidrodinámico Tridimensional para el Estudio de la Propagación de Ondas Largas en Estuarios y Zonas Someras (in Spanish)*. Doctoral thesis, Universidad de Cantabria. xviii, 39, 104, 105

CCME (1999). Canadian environmental quality guidelines. 7, 8, 70, 76

CCME (2003). Guidance on the site-specific application of water quality guidelines in canada: Procedures for deriving numerical water quality objectives. Tech. rep., Canadian Council of Ministers of the Environment. 76, 77

CEDERWALL, K. (1968). Hydraulics of marine wasterwater disposal. Tech. rep., Chalmers Institute of Technology, Sweden. 43

CEDEX & IHCANTABRIA (2008). Desarrollo de una metodología para la evaluación del estado de las aguas superficiales del entorno de afección de los saneamientos litorales. aplicación a los saneamientos litorales de la confederación hidrográfica del norte (in spanish). Tech. rep., Centro de Estudios y Experimentación de Obras Públicas and Instituto de Hidráulica Ambiental de la Universidad de Cantabria. 87

CHAINHO, P., CHAVES, M., COSTA, I. & DAUER, J.L.D.M. (2008). Use of multimetric indices to classify estuaries with different hydromorphological characteristics and different levels of human pressures. *Marine Pollution Bulletin*, **56**, 1128–1137. 3, 2

CHAPRA, S.C. (1997). *Surface Water Quality Modeling*. McGraw-Hill. xviii, 57, 58, 61, 62, 63, 64, 144

CHAPRA, S.C. & RECKHOW, K.H. (1983). *Engineering Approaches for Lake Management, Vol. 2: Mechanistic modeling*. Butterworth Publishers. 62

CHAWLA, A., JAY, D.A., BAPTISTA, A.M., WILKIN, M. & SEATON, C. (2008). Seasonal variability and estuary-shelf interactions in circulation dynamics of a river-dominated estuary. *Estuaries and Coasts*, **31,**, 269–288. 19, 92

CHEN, C., LIU, H. & BEARDSLEY, R.C. (2003). An unstructured grid, finite-volume, three-dimensional, primitive equations ocean model: Application to coastal ocean and estuaries. *Journal of Atmospheric and Oceanic Technology*, **20**, 159–186. 39, 64

CHEN, C.W. (1970). Concept and utilities of ecological models. *Journal of the Sanitary Engineering Division*, **96**, 1085–1086. 62

CHEN, G.Q. & LEE, J.H.W. (2002). Advected turbulent line thermal driven by concentration difference. *Communications in Nonlinear Science and Numerical Simulation*, **7**, 175–195. 43

CHEN, X. (2007). A laterally averaged two-dimensional trajectory model for estimating transport time scales in the alafia river estuary, florida. *Estuarine, Coastal and Shelf Science*, **75**, 358–370. 19, 92

CHENG, R.T., CASULLI, V. & GARTNER, J.W. (1993). Tidal, residual, intertidal mudflat (trim) model and its applications to san francisco bay, california. *Estuarine, Coastal and Shelf Science*, **36**, 235–280. 106

CHEUNG, S.K.B., LEUNG, D.Y.L., WANG, W.P., LEE, J.H.W. & CHEUNG, V. (2000). Visjet - a computer ocean outfall modeling system. In *CGI 2000: The 18th Computer Graphics International 'Humans and Nature'*, 75–80, Université de Genève. 46, 176

CHEUNG, V. & LEE, J.H.W. (1996). Discussion of improved prediction of bending plumes. *Journal of Hydraulic Research*, **34**, 260–262. 180

CHN (1998). Trabajos complementarios al estudio de alternativas e informe de impacto ambiental del saneamiento del saja-besaya (in spanish). Tech. rep., Confederación Hidrográfica del Norte. xxi, 73, 75, 212, 213, 217, 219, 221

CHOI, K.W. & LEE, J.H. (2004). Numerical determination of flushing time for stratified water bodies. *Journal of Marine Systems*, **50**, 263–281. 157

CHOI, K.W. & LEE, J.H.W. (2007). Distributed entrainment sink approach for modeling mixing and transport in the intermediate field. *Journal of Hydraulic Engineering*, **133**, 804–815. 13, 15, 47, 53

CHU, P.C.K., LEE, J.H.W. & CHU, V.H. (1999). Spreading of turbulent round jet in coflow. *Journal of Hydraulic Engineering*, **125**, 193–204. 46

CMA (2006-2007). Inspección de vertidos desde tierra al litoral de cantabria (in spanish). Tech. rep., Consejería de Medio Ambiente del Gobierno de Cantabria. 124, 290, 299

COFIÑO, A.S., GUTIERREZ, J.M., JAKUBIAK, B. & MELONEK, M. (2003). Implementation of data mining techniques for meteorological applications. *Realizing Teracomputing*, 215–240. 135

COMMINS, M.L., DEAS, M.L., SMITH, D.W., SOGUTLUGIL, I.E., TANAKA, S. & VAUGHN, J. (2010). Evaluation of a mixing zone policy for human health related constituents. Tech. rep., Merrit Smith Consulting. 73

COURANT, R., FRIEDRICHS, K.O. & LEWY, H. (1928). Uber die partiellen differenzgleichungen der mathematischen physik. *Mathematische Annalen*, **100**, 32–74. 68

CSANADY, G.T. (1965). The buoyant motion within a hot gas plume in a horizontal wind. *Journal of Fluid Mechanics*, **22**, 225–239. 43

CUCCO, A., UMGIESSER, G., FERRARIN, C., PERILLI, A., CANU, D.M. & SOLIDORO, C. (2009). Eulerian and lagrangian transport time scales of a tidal active coastal basin. *Ecological Modeling*, **220**, 913–922. 134

CUSHMAN-ROISIN, B. (2013). *Environmental Fluid Mechanics*. John Wiley and Sons. 1, 10, 11, 41

DALRYMPLE, R.W., ZAITLIN, B.A. & BOYD, R. (1992). Estuarine facies models: conceptual basis and stratigraphic implications: Perspective. *Journal of Sedimentary Petrology*, **62**, 1130–1146. 22

DAVIES, A.M., JONES, J.E. & XING, J. (1997). Review of recent developments in tidal hydrodynamic modeling. i: Spectral models. *Journal of Hydraulic Enginnering*, **123**, 278–292. 39

DAY, J.H. (1981). *Estuarine Ecology with particular reference to southern Africa*. Cambridge University Press. 22

DCIWM (2000). Prioritering van bronnen en de immissietoets (in dutch). Tech. rep., Dutch Commission for Integrated Water Management). 86

DEC (2006). Implementation guidance: 2006 mixing zone regulation revisions. Tech. rep., Department of Environmental Conservation of the State of Alaska. 72

DEFANT, A. (1958). *Ebb and Flow—the Tides of Earth, Air, and Water*. University of Michigan Press. 32

DEHP (2012). Technical guideline - wastewater release to queensland waters. Tech. rep., Department of Environmental and Heritage Protection. 82

DEININGER, R.A. (1965). Water quality mangaement-the planning of economically optimal control systems. In *Proceedings of the First Annual Meeting of the American Water Resources Association*, American Water Resources Association. 62

DELEERSNIJDER, E., WANG, J. & MOOERS, C.N.K. (1998). A two-compartment model for understanding the simulated three-dimensional circulation in prince william sound, alaska. *Continental Shelf Research*, **18**, 279–287. 160

DELFTHYDRAULICS (2001). Delft3d user interface, capabilities and applications. Tech. rep., RIZA Institute for Inland Water Management and Waste Water Treatment. 39

DELOS, C.G., RICHARDSON, W.L., DEPINTO, J.V., AMBROSE, R.B., RODGERS, P.W., RYGWELSKI, K., JOHN, J.P., SHAUGHNESSY, W.J., FAHA, T.A. & CHRISTIE, W.N. (1984). Technical guidance manual for performing waste load allocations, book ii: Streams and rivers. Tech. rep., U.S. Environmental Protection Agency. 60

DELTARES (2014a). D-water quality: Processes library description-detailed description of processes. technical reference manual. version: 5.01.33319. Tech. rep., Deltares. 186, 187

DELTARES (2014b). D-water quality: Sediment water interaction. user manual. version: 3.0.19949. Tech. rep., Deltares. 186

DELTARES (2014c). D-water quality: Versatile water quality modeling in 1d, 2d or 3d systems including physical, (bio)chemical and biological processes. user manual. version: 4.99.33647. Tech. rep., Deltares. 64, 183, 184, 186, 187

DELTARES (2014d). Delft3d-flow: Simulation of multi-dimensional hydrodynamic flows and transport phenomena, including sediments. user manual. version 3.15.33641. Tech. rep., Deltares. 38, 172, 174, 175, 176, 185

DIAS, J.M. & LOPES, J.F. (2006). Implementation and assessment of hydrodynamic, salt and heat transport models: the case of ria de aveiro lagoon (portugal). *Environmental Modeling and Software*, **21**, 1–15. 106, 189

DIAS, J.M., SOUSA, M.C., BERTIN, X., FORTUNATO, A.B. & OLIVEIRA, A. (2009). Numerical modeling of the impact of the anca˜o inlet relocation (ria formosa, portugal). *Environmental Modeling and Software*, **24**, 711–725. xxx, 106, 220

DIMOU, N. & ADAMS, E. (1993). Random-walk particle tracking models for well-mixed estuaries and coastal waters. *Estuarine, Coastal and Shelf Science*, **37**, 99–110. 52

DINGMAN, S.L. (2009). *Fluvial hydraulics*. Oxford: Oxford University Press. 300

DITORO, D.M. (1969). Line source distribution in two dimensions: Applications to water quality. *Water Resources Research*, **8**, 1541–1546. 62

DITORO, D.M. (1985). A particle interaction model of reversible organic chemical sorption. *Chemosphere*, **14**, 1503–1538. 49, 144

DITORO, D.M., FITZPATRICK, J.J. & THOMANN, R.V. (1983). Water quality analysis simulation program (wasp) and model verification program (mvp) - documentation. Tech. rep., U.S. Environmental Protection Agency. 64

DONEKER, R.L. & JIRKA, G.H. (1990). Expert system for hydrodynamic mixing zone analysis of conventional and toxic submerged single port discharges (cormix1). Tech. rep., U.S. Environmental Protection Agency. 46

DPIPWE (1997). State policy on water quality management 1997. Tech. rep., Department of Primary Industries, Parks, Water and Environment. 82, 83

DREWRY, J.J., NEWHAM, L.T.H. & CROKE, B.F.W. (2009). Suspended sediment, nitrogen and phosphorus concentrations and exports during storm-events to the tuross estuary, australia. *Journal of Environmental Management*, **90**, 879–887. 108

DYER, K.R. & NEW, A.L. (1986). *Estuarine Variability. Intermittency in Estuarine Mixing*. Academic Press. 62, 63, 147, 163, 164, 337

EC (2000). Directive 2000/60/ec of the european parliament and of the council of 23 october 2000 establishing a framework for community action in the field of water policy. 7, 9, 8, 10, 22, 25, 70, 84, 85, 117, 119, 120

EC (2008a). Directive 2008/105/ec of the european parliament and of the council of 16 december 2008 on environmental quality standards in the field of water policy, amending and subsequently repealing council directives 82/176/eec, 83/513/eec, 84/156/eec, 84/491/eec, 86/280/eec and amending directive 2000/60/ec of the european parliament and of the council. 7, 9, 18, 19, 26, 39, 72, 8, 10, 17, 24, 25, 70, 84, 85, 87, 91, 92, 93, 99, 117, 120, 128, 143, 155, 211, 357

EC (2008b). Directive 2008/1/ec of the european parliament and of the council of 15 january 2008 concerning integrated pollution prevention and control. 7, 9, 8, 10, 70, 84, 85, 86, 120

EC (2008c). Directive 96/61/ec of 24 september 1996 concerning integrated pollution prevention and control. 84, 85

EC (2010). Technical guidelines for the identification of mixing zones pursuant to art. 4(4) of the directive 2008/105/ec. Tech. rep., European Commission. xxix, xxx, 18, 26, 13, 17, 84, 86, 101

EDWARDS, A.M.C. & WINN, P.S.J. (2006). The humber estuary, eastern england: Strategic planning of flood defences and habitats. *Marine Pollution Bulletin*, **53**, 165–174. 19, 92

ELLIOT, M. & MCLUSKY, D.S. (2002). The need for definitions in understanding estuaries. *Estuarine, Coastal and Shelf Science*, **55**, 815–827. 21

EPA (2003). State environmental protection policy (waters of victoria). Tech. rep., EPA Victoria. 83

EPA (2010). Guidance for the determination and assessment of mixing zones. Tech. rep., EPA Victoria. 83

EU (2010). Directive 2010/75/eu of the european parliament and of the council of 24 november 2010 on industrial emissions (integrated pollution prevention and control). 84, 85

EU (2013). Directive 2013/39/eu of the european parliament and of the council of 12 august 2013 amending directives 2000/60/ec and 2008/105/ec as regards priority substances in the field of water policy. 7, 9, 18, 19, 22, 26, 34, 39, 72, 8, 10, 24, 25, 70, 84, 85, 91, 92, 93, 96, 99, 117, 119, 120, 128, 143, 155, 211, 357

FAYYAD, U., PIATETSKY-SHAPIRO, G. & SMYTH, P. (1996). From data mining to knowledge discovery in databases. *AI Magazine*, **17**, 37–53. 135

FERZIGER, J.H. & PERIĆ, M. (2002). *Computational methods for fluid dynamics. 3rd rev. ed.*. Springer. 35

FETTEROLF, C.M. (1973). Mixing zone concepts. In *Biological Methods for the Assessment of Water Quality*, 31–45, American Society for Testing and Materials. 70

FISCHER, H.B., LIST, E.J., KOH, R.C.Y., IMBERGER, J. & BROOKS, N.H. (1979). *Mixing in inland and coastal waters*. Academic Press. 10, 11, 12, 33, 43, 55, 57, 105

FOSTER, N.M., HUDSON, M.D., BRAY, S. & NICHOLLS, R.J. (2013). Intertidal mudflat and saltmarsh conservation and sustainable use in the uk: a review. *Journal of Environmental Management*, **126**, 96–104. 3, 2

FRICK, W.E. (1984). Non-empirical closure of the plume equations. *Atmospheric Environment*, **18**, 653–662. 46, 180

FRICK, W.E., ROBERTS, P.J.W., DAVIS, L.R., KEYES, J., BAUMGARTNER, D.J. & GEORGE, K.P. (2001). Dilution models for effluent discharges, 4th edition, (visual plumes). Tech. rep., U.S. Environmental Protection Agency. 45, 46

FRICK, W.E., KHANGAONKAR, T., SIGLEO, A.C. & YANG, Z. (2007). Estuarine-ocean exchange in a north pacific estuary: Comparison of steady state and dynamic models. *Estuarine, Coastal and Shelf Science*, **74**, 1–11. 19, 92

GALVÁN, C. (2014). *Clasificación de estuarios a diferentes escalas espaciales mediante la integración de modelos físicos y biológicos (in Spanish)*. Doctoral thesis, Universidad de Cantabria. 135

GALVÁN, C., JUANES, J.A. & PUENTE, A. (2010). Ecological classification of european transitional waters in the north-east atlantic eco-region. *Estuarine, Coastal and Shelf Science*, **87**, 442–450. 157

GARCÍA, A. (2004). *Desarrollo de un Modelo Tridimensional para la Determinación del Transporte de Suastancias en Estuarios y Zonas Someras (in Spanish)*. Doctoral thesis, Universidad de Cantabria. 104

GARCÍA, A., SAINZ, A., REVILLA, J.A., ÁLVAREZ, C., JUANES, J.A. & PUENTE, A. (2008). Surface water resources assessment in scarcely gauged basins in the north of spain. *Journal of Hydrology*, **356**, 312–326. 45, 70, 108, 134, 205, 208

GARCÍA, A., JUANES, J.A., ÁLVAREZ, C., REVILLA, J.A. & MEDINA, R. (2010a). Assessment of the response of a shallow macrotidal estuary to changes in hydrological and wastewater inputs through numerical modeling. *Ecological Modeling*, **221**, 1194–1208. 19, 92

GARCÍA, A., SÁMANO, M.L., JUANES, J.A., MEDINA, R., REVILLA, J.A. & ÁLVAREZ, C. (2010b). Assessment of the effects of a port expansion on algae appearance in a costal bay through mathematical modeling. application to san lorenzo bay (north spain). *Ecological Modeling*, **221**, 1413–1426. 134

GARCÍA-ALBA, J. (2011). *Estudio de Chorros Turbulentos con Modelos CFD: Aplicación al Diseño de Emisarios Submarinos (in Spanish)*. Doctoral thesis, Universidad de Cantabria. xviii, 37, 42, 44, 45

GARCÍA-ALBA, J., ÁLVAREZ, C., GARCÍA, A., REVILLA, J.A. & JUANES, J.A. (2009). 3d modeling of a thermal and brine discharge through a submarine outfall. In *33rd IAHR Biennial Congress 18*, ASCE, American Society of Civil Engineers. 49

GARCÍA-ALBA, J., ÁLVAREZ, C., GARCÍA, A., REVILLA, J.A. & JUANES, J.A. (2010). Study of a thermal brine discharge using a 3d model. In *Environmental Hydraulics*, CRC Press/Balkema. 49

GARCÍA-ALBA, J., GÓMEZ, A.G., TINOCO, R.O., SÁMANO, M.L., GARCÍA, A. & JUANES, J.A. (2014). A 3-d model to analyze environmental effects of dredging operations – application to the port of marin, spain. *Advances in Geosciences*, **39**, 95–99. 64, 108, 172

GASPERI, J., GARNAUD, S., ROCHER, V. & MOILLERON, R. (2008). Priority pollutants in wastewater and combined sewer overflow. *Science of The Total Environment*, **407**, 263–272. 9, 10

GILL, A.E. (1982). *Atmosphere - Ocean Dynamics*. Academic Press. 31

GILS, J.V., HEERINGEN, K.J.V., SCHWANENBERG, D., GOEDE, E., ZIJL, F., TWIGT, D., ICKE, J., PENAILILLO, R., MEIJER, K., GROOT, S. & POSTMA, L. (2008). Development of a pearl river delta water quality model. Tech. rep., WL | Delft Hydraulics. 181

GIUPPONI, C., EISELT, B. & GHETTI, P.F. (1999). A multicriteria approach for mapping risks of agricultural pollution for water resources: The venice lagoon watershed case study. *Journal of Environmental Management*, **56**, 259–269. 13, 15

GÓMEZ, A.G. (2010). *Desarrollo de un Procedimiento Metodológico para la Estimación del Riesgo Ambiental debido a Emisiones Contaminantes en Zonas Litorales (in Spanish)*. Doctoral thesis, Universidad de Cantabria. 11, 13, 48, 61, 125, 143, 162, 304, 305

GÓMEZ, A.G., BÁRCENA, J.F., JUANES, J.A., ONDIVIELA, B. & SÁMANO, M.L. (2014a). Transport time scales as physical descriptors to characterize heavily modified water bodies near ports in coastal zones. *Journal of Environmental Management*, **136**, 76–84. 35, 134

GÓMEZ, A.G., GARCÍA-ALBA, J., PUENTE, A. & JUANES, J.A. (2014b). Environmental risk assessment of dredging processes – application to marin harbour (nw spain). *Advances in Geosciences*, **39**, 101–106. 34, 57, 61, 117, 130, 155, 162

GÓMEZ, J.I., HERNÁNDEZ, O. & IGLESIAS, S. (2004). The sea and its contaminants. *Journal of Maritime Research*, **1**, 85–93. 3, 2

GONZÁLEZ, M., MEDINA, R., GONZÁLEZ-ONDINA, J., OSORIO, A.F., MÉNDEZ, F.J. & GARCÍA, E. (2007). An integrated coastal modeling system for analyzing beach processes and beach restoration projects, smc. *Computers and Geosciences*, **33**, 916–931. 67, 205

GRIFOLL, M., JORDÀ, G. & ESPINO, M. (2014). Surface water renewal and mixing mechanisms in a semi-enclosed microtidal domain. the barcelona harbour case. *Journal of Sea Research*, **90**, 54–63. 134, 135

GUÉRIT, I., BOCQUENÉ, G., JAMES, A., THYBAUD, E. & MINIER, C. (2008). Environmental risk assessment: A critical approach of the european tgd in an in situ application. *Ecotoxicology and Environmental Safety*, **71**, 291–300. 13

HAIDVOGEL, D.B., ARANGO, H., BUDGELL, W.P., CORNUELLE, B.D., CURCHITSER, E., LORENZO, E.D., FENNEL, K., GEYER, W.R., HERMANN, A.J., LANEROLLE, L., LEVIN, J., MCWILLIAMS, J.C., MILLER, A.J., MOORE, A.M., POWELL, T.M., SHCHEPETKIN, A.F., SHERWOOD, C.R., SIGNELL, R.P., WARNER, J.C. & WILKIN, J. (2008). Ocean forecasting in terrain-following coordinates: Formulation and skill assessment of the regional ocean modeling system. *Journal of Computational Physics*, **227**, 3595–3624. 40

HALPERN, B.S., MCLEOD, K.L., ROSENBERG, A.A. & CROWDER, L.B. (2008). Managing for cumulative impacts in ecosystem-based management through ocean zoning. *Ocean Coastal Management*, **51**, 203–211. 2

HAMRICK, J.M. (1992). A three - dimensional environmental fluid dynamics computer code: Theoretical and computational aspects. Tech. rep., The College of William and Mary, Virginia Institute of Marine Science. 39

HANSEN, D.V. & RATTRAY, M. (1966). New dimensions in estuary classification. *Limnology and Oceanography*, **11**, 319–326. 22

HANSLER, G.M. & FIKSLIN, T.J. (1995). Implementation policies and procedures: Phase i tmdls for toxic pollutants in the delaware river estuary. Tech. rep., Delaware River Basin Commission. 29, 74, 109

HANSLER, G.M., FIKSLIN, T.J., TSAI, J., SUK, N. & WILCOX, D. (1998). Wasteload allocations for volatile organics and toxicity: Phase i tmdls for toxic pollutants in the delaware river estuary. Tech. rep., Delaware River Basin Commission. 29, 74, 109

HARCOURT-BALDWIN, J.L. & DIEDERICKS, G.P.J. (2006). Numerical modeling and analysis of temperature controlled density currents in tomales bay, california. *Estuarine, Coastal and Shelf Science*, **66**, 417–428. 134

HASTIE, T., TIBSHIRANI, R. & FRIEDMAN, J. (2001). *The Elements of Statistical Learning*. Hastie. 136, 137

HAYES, M.O. (1975). Morphology of sand accumulation in estuaries: an introduction to the symposium. *Estuarine Research*, **2**, 3–22. 22

HERVOUET, J. & BATES, P. (2000). The telemac modeling system. *Hydrological Processes*, **14**, Special issue. 39

HIPSEY, M.R., ROMERO, J.R., ANTENUCCI, J.P. & IMBERGER, J. (2007). The computational aquatic ecosystem dynamics model (caedym): a versatile water quality model for coupling with hydrodynamic drivers. In *Proceedings of the 7th International Conference on Hydroinformatics, Vol 1.*, 526–533, Research Publisher Services. 64

HODGES, B.R. (2000). Numerical techniques in cwr-elcom. Tech. rep., Centre for Water Research, University of Western Australia. 39

HODGSON, E. (2003). *A Textbook of Modern Toxicology*. John Wiley and Sons. 57

HUANG, W. (2007). Hydrodynamic modeling of flushing time in a small estuary of north bay, florida, usa. *Estuarine, Coastal and Shelf Science*, **74**, 722–731. 157

HUITT, W. (1992). Problem solving and decision making: Consideration of individual differences using the myers-briggs type indicator. *Journal of Psychological Type*, **24**, 33–44. 93

IGLESIAS, G. & CARBALLO, R. (2010). Effects of high winds on the circulation of the using a mixed open boundary condition: the ría de muros, spain. *Environmental Modeling and Software*, **25**, 455–466. xxx, 77, 106, 134, 172, 189, 220, 222

IHCANTABRIA (2008a). Análisis preliminares para la detección de sustancias prioritarias en aguas litorales de cantabria (in spanish). Tech. rep., Gobierno de Cantabria. xxix, xxx, 124, 125, 290, 299, 302

IHCANTABRIA (2008b). Trabajos de asesoramiento para el diseño ambiental de la conducción de vertido de la central térmica de ciclo combinado del puerto del musel (asturias) (in spanish). Tech. rep., NOEGA Ingenieros, S.L. 177

IHCANTABRIA (2010). Asistencia técnica para el estudio de los efectos de los vertidos de los emisarios de mogán, la aldea y salinetas (gran canaria) (in spanish). Tech. rep., Dirección General De Aguas del Gobierno de Canarias. 177

IHCANTABRIA (2012). Red de control de calidad litoral en cantabria. informe técnico final (in spanish). Tech. rep., Gobierno de Cantabria. xxi, 73, 124, 125, 212, 213, 214, 290, 299, 300

IHCANTABRIA (2014a). Caracterización del vertido térmico procedente del sistema de refrigeración del centro botín (in spanish). Tech. rep., Bovis Lend Lease. 177

IHCANTABRIA (2014b). Servicio técnico para la realización de un estudio ambiental del vertido conjunto de aguas residuales urbanas e industriales a través del emisario submarino de xagó (in spanish). Tech. rep., Junta de Saneamiento del Principado de Asturias. 181

JACOBSEN, F. & RASMUSSEN, E.B. (1997). Mike 3 mt: A 3-dimensional mud transport model. Tech. rep., Danish Hydraulic Institute. 39, 64

JI, Z.G. (2007). *Hydrodynamics and Water Quality: Modeling Rivers, Lakes, and Estuaries*. John Wiley and Sons. 29, 30, 33, 55, 59

JI, Z.G., HAMRICK, J.H. & PAGENKOPF, J. (2002). Sediment and metals modeling in shallow river. *Journal of Environmetal Engineering*, **128**, 105–119. xviii, 62

JIMÉNEZ, M., CASTANEDO, S., MEDINA, R. & CAMUS, P. (2012). A methodology for the classification of estuary restoration areas: A management tool. *Ocean and Coastal Management*, **69**, 231–242. 67, 205

JIMÉNEZ, M., CASTANEDO, S., ZHOU, Z., COCO, G., MEDINA, R. & RODRIGUEZ-ITURBE, I. (2014). Scaling properties of tidal networks. *Water Resources*, **50**, 4585–4602. 172

JIRKA, G.H. (1999). Five asymptotic regimes of a round buoyant jet in stratified crossflow. In *28th IAHR Biennial Congress*, IAHR, International Association for Hydro-Environment Engineering and Research. 47

JIRKA, G.H. (2004). Integral model for turbulent buoyant jets in unbounded stratified flows. part 1:the single round jet. *Environmental Fluid Mechanics*, **4**, 1–56. 31, 45, 46, 111

JIRKA, G.H. (2006). Integral model for turbulent buoyant jets in unbounded stratified flows, part 2:plane jet dynamics resulting from multiport diffuser jets. *Environmental Fluid Mechanics*, **6**, 43–100. 46, 49

JIRKA, G.H. & AKAR, P.J. (1991). Hydrodynamic classification of submerged single-port discharges. *Journal of Hydraulic Engineering*, **117**, 1095–1111. xviii, 50

JIRKA, G.H., ABRAHAM, G. & HARLEMAN, D.R.F. (1975). An assesment of techniques for hydrothermal prediction. Tech. rep., M.I.T. Parsons Laboratory for Water Resources and Hydrodynamics. 43

JIRKA, G.H., DONEKER, R.L. & HINTON, S.W. (1996). User´s manual for cormix: A hydrodynamic mixing zone model and decision support system for pollutant discharges into surface waters. Tech. rep., DeFrees Hydraulics Laboratory, Cornell University. xviii, 46, 47, 48, 54

JIRKA, G.H., BLENINGER, T., BURROWS, R. & LARSEN, T. (2004). Environmental quality standards in the ec-water framework directive: Consequences for water pollution control for point sources. *European Water Management Online*, **1**. 8, 31, 9, 111

JOUON, A., DOUILLET, P., OUILLON, S. & FRAUNIÉ, P. (2006). Calculations of hydrodynamic time parameters in a semi-opened coastal zone using a 3d hydrodynamic model. *Continental Shelf Research*, **26**, 1395–1415. 59, 140, 134, 157, 158, 329

KASHEKIPOUR, S.M., LIN, B., HARRIS, E. & FALCONER, R.A. (2001). Hydro-environmental modeling for bathing water compliance of an estuarine basin. *Water Research*, **36**, 1854–1868. 19, 92

KAUFMAN, J.T. & ADAMS, E.E. (1981). Coupled near and far field thermal plume analysis using finite element techniques. Tech. rep., M.I.T. Parsons Laboratory for Water Resources and Hydrodynamics. 15, 47

KEFFER, J.F. & BAINES, W.D. (1963). The round turbulent jet in a cross wind. *Journal of Fluid Mechanics*, **15**, 481–496. 42

KIKKERT, G.A. (2006). *Bouoyant jets with two and three-dimensional trajectories*. Doctoral thesis, University of Canterbury. xviii, 42, 43, 44, 45

KIM, Y.D., SEO, I.W., KANG, S.W. & OH, B.C. (2002). Jet integral-particle tracking hybrid model for single buoyant jets. *Journal of Hydraulic Engineering*, **128**, 753–760. 31, 52, 111

KJERFVE, B. & MAGILL, K.E. (1989). Geographic and hydrodynamic characteristics of shallow coastal lagoons. *Marine Geology*, **88**, 187–199. 22

KLEISSEN, F.M. (2012). Emissie-immissietoets voor oppervlaktewateren (in dutch). Tech. rep., Deltares. 86, 87

KNUDSEN, M. (1988). *Buoyant horizontal jets in an ambient flow*. Doctoral thesis, University of Canterbury. 43

KOLMOGOROV, A.N. (1942). Equations of turbulent motion in incompressible fluid. *Izvestiya Akademii Nauk Azerbaidzhanskoi SSR. Seriya Fiziko-Tekhnicheskikh*, **1**, 56–58. 38

KONTERMAN, I., SCHEREN, P., LEUVEN, R., RAGAS, A., LUBBERDING, H., NIEBEEK, G. & STORTELDER, P. (2003). Environmental quality objective approach to effluent standards definition: A useful approach within the developing countries context? Tech. rep., Ministry of Transport, Public Works and Water Management. 86

KRENKEL, P. & NOVOTNY, V. (1980). *Water quality management*. Academic Press. 24, 25

KRISHNA-PRASAD, M.B., LONG, W., ZHANG, X., WOOD, R.J. & MURTUGUDDE, R. (2011). Predicting dissolved oxygen in the chesapeake bay: applications and implications. *Aquatic Sciences*, **73**, 437–451. 108

KUNDU, P.K. & COHEN, I.M. (1990). *Fluid Mechanics*. Elsevier Science. 41, 42

LAUNDER, B.E. & SPALDING, D.B. (1972). *Lectures in Mathematical Models of Turbulence*. Academic Press. 38

LAW, A.W.K., LEE, C.C. & QI, Y. (2002). Cfd modeling of a multi-port diffuser in an oblique current. In *MWWD 2002: Marine Waste Water Discharges*, International Association for Hydro-Environment Engineering and Research and International Water Association. 49

LDEQ (2010). Pemitting guidance document for implementing louisiana surface water quality standards. Tech. rep., Louisiana Department of Environmental Quality. 29, 74, 109

LEE, J.H.W. & CHEUNG, V. (1986). Inclined plane buoyant jet in stratified fluid. *Journal of Hydraulic Engineering*, **112**, 580–589. 47

LEE, J.H.W. & CHEUNG, V. (1990). Generalized lagrangian model for buoyant jets in current. *Journal of Environmental Engineering*, **116**, 1085–1105. 45, 46, 47, 177, 180, 181

LEE, J.H.W., CHEUNG, V. & CHEUNG, W.P.W.S.K.B. (2000). Lagrangian modeling and visualization of rosette outfall plumes. In *Proceedings of the Hydroinformatics 2000*, University of Iowa. 46, 47

LEE, J.W.W. & CHU, V.H. (2003). *Turbulent Jets and Plumes - a Lagrangian Approach*. Kluwer Academic Publishers. xx, 46, 47, 177, 178, 181, 182

LESSER, G.R., ROELVINK, J.A., KESTER, J.A.T.M.V. & STELLING, G.S. (2004). Development and validation of a three-dimensional morphological model. *Coastal Engineering*, **51**, 883–915. 172

LEVENSPIEL, O. (1972). *Chemical reaction engineering*. John Wiley and Sons. 157

LEWIS, W.K. & WHITMAN, W.G. (1924). Principles of gas absorption. *Industrial and Engineering Chemistry*, **16**, 1215–1220. 50, 145

LINDEBOOM, H.J. (2002). *The Coastal Zone: An Ecosystem Under Pressure. In Oceans 2020: Science,Trends and the Challenge of Sustainability*. Island Press. 2

LIU, W.C., HSU, M.H. & KUO, A.Y. (2002). Modeling of hydrodynamics and cohesive sediment transport in tanshui river estuarine system, taiwan. *Marine Pollution Bulletin*, **44**, 1076–1088. 19, 92

LOTZE, H.K., LENIHAN, H.S., BOURQUE, B.J., BRADBURY, R.H., COOKE, R.G., KAY, M.C., KIDWELL, S.M., KIRBY, M.X., PETERSON, C.H. & JACKSON, J.B.C. (2006). Depletion, degradation, and recovery potential of estuaries and coastal seas. *Science*, **312**, 1806–1809. 2

LUCAS, L.V., THOMPSON, J.K. & BROWN, L.R. (2009). Why are diverse relationships observed between phytoplankton biomass and transport time? *Limnology and Oceanography*, **54**, 381–390. 35

LUETTICH, R.A. & WESTERINK, J.J. (2004). Formulation and numerical implementation of the 2d/3d adcirc finite element model version 44.x. Tech. rep., University of North Carolina and University of Notre Dame. 40

MACKAY, D. & YEUN, A.T.K. (1983). Mass transfer coefficients correlations for volatilization of organic solutes from water. *Environmental Science and Technology*, **17**, 211–233. 145

MADERICH, V., HELING, R., BEZHENAR, R., BROVCHENKO, I., JENNER, H., KOSHEBUTSKYY, V., KUSCHAN, A. & TERLETSKA, K. (2008). Development and application of 3d numerical model threetox to the prediction of cooling water transport and mixing in the inland and coastal waters. *Hydrological Process*, **22**, 1000–1013. 53

MAU, J.C., WANG, D.P., ULLMAN, D.S. & CODIGA, D.L. (2007). Charactering long island sound outflows from hf radar using self-organizing maps. *Estuarine, Coastal and Shelf Science*, **7**, 155–165. 135

MCINTYRE, N.R. & WHEATHER, H.S. (2004). A tool risk-based management of surface water quality. *Environmental Modeling and Software*, **19**, 1131–1140. 13

MCINTYRE, N.R., WAGENER, T., WHEATER, H.S. & YU, Z.S. (2003). Uncertainty and risk in water quality modeling and management. *Journal of Hydroinformatics*, **5**, 259–274. 13

MCLUSKY, D.S. & ELLIOTT, M. (2007). Transitional waters: A new approach, semantics or just muddying the waters? *Estuarine, Coastal and Shelf Science*, **71**, 359–363. 22

MDDEP (2007). Calculation and interpretation of effluent discharge objectives for contaminants in the aquatic environment. Tech. rep., Ministère du Développement durable, de l'Evironnement et des Parcs du Quebec. xviii, 79, 80

MILLENNIUM-ECOSYSTEM-ASSESSMENT (2005). *Ecosystems and Human Well-being: Current State and Trends. Coastal systems*. Island Press. 3, 2

MILLS, W.B., DEAN, J.D., PORCELLA, D.B., GHERINI, S.A., HUDSON, R.J.M., FRICK, W.E., RUPP, G.L. & BOWIE, G.L. (1982). Water quality assessment: A screening procedure for toxic and conventional pollutants, part 1. Tech. rep., U.S. Environmental Protection Agency. 60, 145

MIRANDA, R., BRAUNSCHWEIG, F., LEITAO, P., NEVES, R., MARTINS, F. & SANTOS, A. (2000). *MOHID 2000 - A coastal integrated object oriented model*. Hydraulic Engineering Software VIII, WIT Press. 39, 64

MOEE (1994a). Deriving receiving-water based, point-source effluent requirements for ontario waters. Tech. rep., Ontario Ministry of Environment and Energy. 78

MOEE (1994b). Water management policies guidelines: Provincial water quality objectives of the ministry of environment and energy. Tech. rep., Ontario Ministry of Environment and Energy. 8, 9, 78

MOLL, A. & RADACH, G. (2003). Review of three-dimensional ecological modeling related to the north sea shelf system. part 1: models and their results. *Progress in Oceanography*, **57**, 175–217. 13

MONSEN, N.E., CLOERN, J.E., LUCAS, L.V. & MONISMITH, S.G. (2002). A comment on the use of flushing time, residence time, and age as transport time scales. *Limnology and Oceanography*, **47**, 1545–1553. 34, 35, 157

MONSEN, N.E., CLOERN, J.E. & BURAU, J.R. (2007). Effects of flow diversions on water and habitat quality: examples from california's highly manipulated sacramento–san joaquin delta. *San Francisco Estuary and Watershed Science*, **5**. 35

MORIASI, D.N., ARNOLD, J.G., LIEW, M.W.V., BINGNER, R.L., HARMEL, R.D. & VEITH, T.L. (2007). Model evaluation guidelines for systematic quantification of accuracy in watershed simulations. *Transactions of the ASABE*, **50**, 885–900. 108

MORTON, B.R., TAYLOR, G.I. & TURNER, J.S. (1956). Turbulent gravitational convection from maintained and instantaneous sources. *Proceedings of the Royal Society of London*, **A234**, 1–23. 42, 46

NASH, J. & SUTCLIFFE, J. (1970). River flow forecasting through conceptual models part i – a discussion of principles. *Journal of Hydrology*, **10**, 282–290. 29, 108, 141

O'CONNOR, D.J. (1985). Modeling frameworks, toxic substances notes. Tech. rep., Manhattan College Summer Institute in Water Pollution Control. 145

O'CONNOR, D.J. (1988). Models of sorptive toxic substances in freshwater systems. i: Basic equations. *Journal of Environmental Engineering*, **114**, 507–532. 62

ONDIVIELA, B., SÁMANO, M., JUANES, J.A., GÓMEZ, A.G. & REVILLA, J.A. (2007). ¿cómo deberían ser consideradas las zonas de servicio portuario en el desarrollo de los planes de demarcación de la dma? In *V Congreso Nacional de la Ingeniería Civil*, Colegio de Ingenieros de Caminos, Canales y Puertos. 17

ONDIVIELA, B., RECIO, M. & JUANES, J.A. (2015). A management approach for the ecological integrity of ne atlantic estuaries. *Ecological Indicators*, **52**, 105–115. 3, 2

PALMA, E.D. & MATANO, R.P. (1998). On the implementation of passive open boundary conditions for a general circulation model: the barotropic mode. *Journal of Geophysical Research*, **103**, 1319–1341. 68

PALMA, E.D. & MATANO, R.P. (2000). On the implementation of passive open boundary conditions for a general circulation model: the three-dimensional case. *Journal of Geophysical Research*, **105**, 8605–8628. 68

PAPANICOLAU, P. & LIST, E.J. (1988). Investigations of round vertical turbulent bouyant jets. *Journal od Fluid Meachanics*, **195**, 341–391. 42

PAWLOWICZ, R., BEARDSLEY, B. & LENTZ, S. (2002). Classical tidal harmonic analysis including error estimates in matlab using t-tide. *Computers and Geosciences*, **28**, 929–937. 45, 134

PEÑAS, F.J., BARQUÍN, J., SNELDER, T.H., BOOKER, D.J. & ÁLVAREZ, C. (2014). The influence of methodological procedures on hydrological classification performance. *Hydrology and Earth System Sciences Discussions*, **11**, 945–985. 46, 138

PERILLO, G.M.E. (1995). Chapter 2 definitions and geomorphologic classifications of estuaries. *Geomorphology and Sedimentology of Estuaries*, **53**, 17–47. 22

PHILLIPS, N.A. (1957). A co-ordinate system having some special advantages for numerical forecasting. *Journal of Meteorology*, **14**, 184–185. 66

PRANDTL, L. (1945). Über ein neues formelsystem für die ausgebildete turbulenz. *Nachrichten von der Akademie der Wissenschaften in Gottingen*, 6–19, mathematisch-Physikalische Klasse. 38

PRITCHARD, D.W. (1952). Salinity distribution and circulation in the chesapeake bay estuarine system. *Journal of Marine Research*, **11**, 106–123. 61, 22, 23, 162

PRITCHARD, D.W. (1960). Lectures on estuarine oceanography. *Journal of Hopkins University*, 1–154. 22

PUN, L.K. (1998). *Hybrid models for jets and plumes in a flowing ambient fluid*. Doctoral thesis, The Hong Kong University of Science and Technology. 45

RAGAS, A.M.J. (2000). *Uncertainty in Environmental Quality Standards*. Doctoral thesis, University of Nijmegen. 8, 9

RAGAS, A.M.J., HAMS, J.L.M. & LEUVEN, R.S.E.W. (1997). Selecting water quality models for discharge permitting. *European Water Pollution Control*, **7**, 59–67. 7, 8, 9, 10

RAVELLE, C., LOUCKS, D.P. & LYNN, W.R. (1967). A management modelfor water quality control. *Journal of Water Pollution Control Federation*, **39**, 1164–1183. 62

RECIO, M., ONDIVIELA, B., PUENTE, A., GALVÁN, C., GÓMEZ, A.G. & JUANES, J.A. (2013). Response of estuarine vegetation indicators compared to hydromorphological stressors. *Estuar. Coasts,*, **36**, 997–1005. 2

RICHTER, B.D., BAUMGARTNER, J.V., POWELL, J. & BRAUN, D.P. (1996). A method for assessing hydrologic alteration within ecosystems. *Conservation Biology*, **10**, 1163–1174. 46, 138

RICHTER, B.D., BAUMGARTNER, J.V., WIGINGTON, R. & BRAUN, D.P. (1997). How much water does river need? *Freshwater Biology*, **37**, 231–249. 46, 138

RICHTER, B.D., BAUMGARTNER, J.V., BRAUN, D.P. & POWELL, J. (1998). A spatial assessment of hydrologic alteration within a river network. *Regulated Rivers: Research and Management*, **14**, 329–340. 46, 138

RIZA (2001). Water pollution control in the netherlands: Policy and practice. Tech. rep., Delft Hydraulics. 86

ROBERTS, P.J.W. (1979). Line plume and ocean outfall dispersion. *Journal of Hidraulics Division*, **105**, 313–331. 41, 47

ROBERTS, P.J.W. (1999a). Modeling mamala bay outfall plumes. i: Near field. *Journal of Hydraulic Engineering*, **125**, 564–573. 13

ROBERTS, P.J.W. (1999b). Modeling mamala bay outfall plumes. ii: Far field. *Journal of Hydraulic Engineering*, **125**, 574–583. 13

RODI, W. (1984). Turbulence models and their application in hydraulics, state-of-the-art paper article sur l'etat de connaissance. In *Fundamentals of Division II: Experimental and Mathematical Fluid Dynamics*, IAHR, International Association for Hydro-Environment Engineering and Research. 174

RODI, W. (1993). *Turbulence models and their application in hydraulics: a state-of-the-art review*. Balkema. 36

ROMERO, M., ANDRÉS, A., ALONSO, R., VIGURI, J. & RINCÓN, J.M. (2008). Sintering behaviour of ceramic bodies from contaminated marine sediments. *Ceramics International*, **34**, 1917–1924. 67, 205

ROOSE, P. & BRINKMAN, U.A.T. (2005). Monitoring microcontaminants in the marine environment: principles, programmes and progress. *Trends in Analytical Chemistry*, **24**, 897–926. 3, 2

ROUSE, H., YIH, C.S. & HUMPHREYS, H.W. (1952). Gravity convection from boundary source. *Tellus*, **4**, 201–210. 43

RUZA, J., BORDAS, M.A., ESPINOSA, G. & PUIG, A. (2007). Manual para la gestión de vertidos. autorización de vertido. (in spanish). Tech. rep., Ministerio Medio Ambiente. 13, 15

SÁMANO, M.L., BÁRCENA, J.F., GARCÍA, A., GÓMEZ, A.G., ÁLVAREZ, C. & REVILLA, J.A. (2012). Flushing time as a descriptor for heavily modified water bodies classification and management: Application to the huelva harbour. *Journal of Environmental Management*, **107**, 37–44. 19, 35, 92, 157

SÁMANO, M.L., GARCÍA, A., REVILLA, J.A. & ÁLVAREZ, C. (2014). Modeling heavy metal concentration distributions in estuarine waters: an application to suances estuary (northern spain). *Environmental Earth Sciences*, **72**, 2931–2945. 125, 304, 305

SANCHEZ-ARCILLA, A., RODRIGUEZ, A. & MESTRES, M. (1998). A three-dimensional simulation of pollutant dispersion for the near- and far-field in coastal waters. *Journal of Marine and Environemtnal Engineering*, **4**, 217–243. 10, 11, 47

SAOUTER, E., PITTINGER, C. & FEIJTEL, T. (2001). Aquatic environmental impact of detergents: From simple to more sophisticated models. *Ecotoxicology and Environmental Safety*, **50**, 153–159. 11, 13

SCHNOOR, J.L. (1996). *Environmental Modeling: Fate and Transport of Pollutants in Water, Air, and Soil*. John Wiley and Sons. 60

SCHWARZENBACH, R.P., GSCHWEND, P.M. & IMBODEN, D.M. (1993). *Environmental organic chemistry*. John Wiley and Sons. 145

SCHWARZENBACH, R.P., ESCHER, I.B., FENNER, K., HOFSTETTER, T.B., JOHNSON, C.A., VONGUNTEN, U. & WEHRLI, B. (2006). The challenge of micropollutants in aquatic systems. *Science*, **313**, 1072–1077. xvii, 3, 4, 2, 5, 25

SCORER, R.S. (1959). The behaviour of chimney plumes. *International Journal of Air Pollution*, **1**, 198–220. 42

SEPA (1998). Initial dilution and mixing zones for discharges from coastal and estuarine outfalls, policy no. 28, version 1. Tech. rep., Scottish Environmental Protection Agency. 8, 9

SEVAT, E. & DEZETTER, A. (1991). Selection of calibration objective functions in the context of rainfall-runoff modeling in a sudanese savannah area. *Hydrological Sciences Journal*, **36**, 307–330. 108

SEVERINSEN, M., ANDERSEN, M.B., CHEN, F. & NYHOLM, N. (1996). A regional chemical fate and exposure model suitable for denmark and its coastal sea. *Chemosphere*, **32**, 2159–2175. 13

SHELDON, J.E. & ALBER, M. (2002). A comparison of residence time calculations using simple compartment models of the altamaha river estuary, georgia. *Estuaries*, **25**, 1304–1317. 35

SHELDON, J.E. & ALBER, M. (2006). The calculation of estuarine turnover times using freshwater fraction and tidal prism models: a critical evaluation. *Estuaries and Coasts*, **29**, 133–146. 34

SHEN, J. & HAAS, L. (2004). Calculating age and residence time in the tidal york river using three-dimensional model experiments. *Estuarine, Coastal and Shelf Science*, **61**, 449–461. 160

SHI, J.Z. & ZHANG, H.L. (2011). Note on a 2dh finite element model of tidal flow of the north passage of the partially-mixed changjiang river estuary, china. *Journal of Hydro-environment Research*, **5**, 49–62. 107

SINGH, V.P. & WOOLHISER, D.A. (2002). Mathematical modeling of watershed hydrology. *Journal of Hydrologic Engineering*, **7**, 270–292. 45, 134

SNAREY, M., TERRETT, K.N., WILLET, P. & WILTON, D.J. (1997). Comparison of algorithms for dissimilarity-based compound selection. *Journal of Molecular Graphics and Modeling*, **15**, 372–385. 136

SNELDER, T.H. & BOOKER, D. (2013). Intertidal mudflat and saltmarsh conservation and sustainable use in the uk: a review. *River Research and Applications*, **7**, 822–838. 46, 138

SØBALLE, D.M. & BACHMANN, R.W. (1984). Influence of reservoir transit on riverine algal transport and abundance. *Canadian Journal of Fisheries and Aquatic Sciences*, **41**, 1803–1813. 35

SOMMERFELD, A. (1949). *Partial Differential Equations in Physics*. Academic Press. 69

SOULSBY, C. & TETZLAFF, D. (2008). Towards simple approaches for mean residence time estimation in ungauged basins using tracers and soil distributions. *Journal of Hydrology*, **363**, 60–74. 157

SOUSA, M.C., VAZ, N., ALVAREZ, I., GOMEZ-GESTEIRA, M. & DIAS, J.M. (2014). Influence of the minho river plume on the rias baixas (nw of the iberian peninsula). *Journal of Marine Systems*, **139**, 248–260. 134

SPAIN (2011). Real decreto 60/2011, de 21 de enero, sobre las normas de calidad ambiental en el ámbito de la política de aguas. 87

SPAIN (2014). Proyecto de real decreto por el que se establecen los criterios de seguimiento y evaluación del estado de las aguas superficiales y las normas de calidad ambiental. 40, 97, 117, 128, 265

STAMOU, A.I. & NIKIFORAKIS, I.K. (2013). Integrated modeling of single port, steady-state thermal discharges in unstratified coastal waters. *Environmental Fluid Mechanics*, **13**, 309–336. 53

STREETER, H.W. & PHELPS, E.B. (1925). A study of the pollution and natural purification of the ohio river, iii. factors concerning the phenomena of oxidation and reaeration. Tech. rep., U. S. Public Health Service. 62

SUH, S.W. (2001). A hybrid near-field/far-field thermal discharge model for coastal areas. *Marine Pollution Bulletin*, **43**, 225–233. 52

SUH, S.W. (2006). A hybrid approach to particle tracking and eulerian–lagrangian models in the simulation of coastal dispersion. *Environmental Modeling and Software*, **21**, 234–242. 52

SWRCB (2000). Policy for implementation of toxics standards for inland surface waters, enclosed bays, and estuaries of california. Tech. rep., State Water Resources Control Board (California Environmental Protection Agency). 73

SYVITSKI, J.P., MOREHEAD, M.D., BAHR, D.B. & MULDER, T. (2000). Estimating fluvial sediment transport: The rating parameters. *Water Resources Research*, **36**, 2747–2760. 300

TAKEOKA, H. (1984). Fundamental concepts of exchange and transport time scales in a coastal sea. *Continental Shelf Research*, **3**, 311–326. 35, 157, 160

TANG, H., PAIK, J., SOTIROPOULOS, F. & KHARAONGAKAR, T. (2008). Three-dimensional numerical modeling of initial mixing of thermal discharges at real life configurations. *Journal of Hydraulic Engineering*, **134**, 1210–1224. 49

TAYLOR, G.I. (1954). The dispersion of matter in turbulent flow through a pipe. *Proceedings of the Royal Society of London*, **A223**, 446–468. 55

TETRATECH (2000). Ocean circulation and plume dispersion modeling review, with emphasis on orange county sanitation district's offshore outfall and wastewater plume. Tech. rep., Orange County Sanitation District, USA. 39

THOMANN, R.V. & DITORO, D.M. (1983). Phisico chemical model of toxic substances in the great lakes. *Journal of Great Lakes Research*, **9**, 474–496. 62

THOMANN, R.V. & MUELLER, J.A. (1987). *Principles of Surface Water Quality Modeling and Control*. Harper and Row. 60, 61, 64, 144

THOMANN, R.V. & SOBEL, M.J. (1964). Estuarine water quality management and forecasting. *Journal of the Sanitary Engineering Division*, **90**, 9–36. 62

TNRCC (2003). Implementation of the texas natural resource conservation commission standards via permitting. publication rg-194. Tech. rep., Texas Natural Resource Conservation Commission. 75

UITTENBOGAARD, R.E., VAN KESTER, J.A.T.M. & STELLING, G.S. (1992). Tmplementation of three turbulence models in 3d-trisula for rectangular grids. Tech. rep., Delft Hydraulics. 38

UKEA (2011a). H1 annex d - basic surface water discharges. Tech. rep., U.K. Environment Agency. 85

UKEA (2011b). H1 annex e – surface water discharges (complex). Tech. rep., U.K. Environment Agency. 85

UKEA (2011c). H1 environmental risk assessment - horizontal guidance: Overview document. Tech. rep., U.K. Environment Agency. 4, 2, 85

UNESCO (1981). Background papers and supporting data on the international equation of state. Tech. rep., UNESCO. 31, 174

USA (1948). Federal water pollution control act. 70

USA (1972). Clean water act. 7, 8, 70

USA (1977). Clean water act. 7, 8, 70

USA (1985). Water quality act. 7, 8, 70

USAQUÉN, O.L., GÓMEZ, A.G., GARCÍA, A., ÁLVAREZ, C. & REVILLA, J.A. (2012). Methodology to assess sustainable management of water resources in coastal lagoons with agricultural uses: An application to the albufera lagoon of valencia (eastern spain). *Ecological Indicators*, **13**, 129–143. 108

USEPA (1991). Technical support document for water quality-based toxics control. Tech. rep., U.S. Environmental Protection Agency. xvii, 8, 11, 29, 9, 13, 14, 71, 74, 75, 109

USEPA (1992). Technical guidance manual for performing waste load allocations, book iii: Estuaries. Tech. rep., U.S. Environmental Protection Agency. 72

USEPA (1994). Water quality standards handbook: Second edition. Tech. rep., U.S. Environmental Protection Agency. 8, 9, 71

USEPA (1995). Allocated impact zones for areas of non-compliance. Tech. rep., U.S. Environmental Protection Agency. 71

USEPA (1996). Npdes permit writer's manual. Tech. rep., U.S. Environmental Protection Agency. 4, 8, 2, 9, 72

USEPA (2010). Npdes permit writer's manual. Tech. rep., U.S. Environmental Protection Agency. 4, 2, 72

VALLE-LEVINSON, A. (2008). Density-driven exchange flow in terms of the kelvin and ekman numbers. *Journal of Geophysical Research: Oceans*, **113**. 22

VALLE-LEVINSON, A. (2010). *Contemporary Issues in Estuarine Physics*. Cambridge: Cambridge University Press. xvii, 2, 23, 33

VIJITH, V. & SHETYE, S.R. (2012). A stratification prediciton diagram from characteristics of geometry, tides and runoff for estuaries with a prominent channel. *Estuarine, Coastal and Shelf Science*, **98**, 101–107. 19, 92

WAGNER, R.W., STACEY, M., BROWN, L.R. & DETTINGER, M. (2011). Statistical models of temperature in the sacramento–san joaquin delta under climate-change scenarios and ecological implications. *Estuaries and Coasts*, **34**, 544–556. 108

WALLACE, R.B. & WRIGHT, S.J. (1984). Spreading layer of a two-dimensional buoyant jet. *Journal of Hydraulic Engineering*, **110**, 813–828. 47

WARNER, J.C., GEYER, W.R. & LERCZAK, J.A. (2005). Numerical modeling of an estuary: A comprehensive skill assessment. *Journal of Geophysical Research*, **110**, C05001. 19, 92

WDOE (2003). Water quality program permit writer's manual. Tech. rep., Whasington State Deparment of Ecology. 75

WESTMAN, W.E. (1985). *Ecology, impact assessment and enviornmental planning*. John Wiley and Sons. 13, 15

WHO (2003). *Health Risks of Persistent Organic Pollutants from Long-range Transboundary Air Pollution*. Pergamon Press. 4, 5, 27

WHO (2007). *Health Risks of Heavy Metals from Long-range Transboundary Air Pollution*. Pergamon Press. 27

WILLIAMS, R.N., DESOUZAJR, P.A. & JONES, E.M. (2014). Analysing coastal ocean model outputs using competitive-learning pattern recognition techniques. *Environmental Modeling and Software*, **57**, 165–176. 135

WOLANSKI, E. (2007). *Estuarine ecohydrology*. Elsevier. 22

XU, J., LEE, J.H.W., YIN, K., L, H. & HARRISON, P.J. (2011). Environmental response to sewage treatment strategies: Hong kong's experience in long term water quality monitoring. *Marine Pollution Bulletin*, **62**, 2275–2287. 177

YUAN, D., LIN, B. & FALCONER, R.A. (2006). A modeling study of residence time in a macro-tidal estuary. *Estuarine, Coastal and Shelf Science*, **71**, 401–411. 13, 15

ZHANG, X.Y. & ADAMS, E.E. (1999). Prediction of near field plume characteristics using far field circulation model. *Journal of Hydraulic Engineering*, **125**, 233–241. 31, 52, 111

ZHOU, Z., OLABARRIETA, M., STEFANON, L., D'ALPAOS, A., CARNIELLO, L. & COCO, G. (2014). A comparative study of physical and numerical modeling of tidal network ontogeny. *Journal of Geophysical Research: Earth Surface*, **119**, 892–912. 172

ZIMMERMAN, J.T.F. (1978). Mixing and flushing of tidal embayments in the westerndutch wadden sea. part i: Distribution of salinity and calculation of mixing time scales. *Netherlands Journal of Sea Research*, **10**, 149–191. 35, 157

Declaration

I herewith declare that I have produced this work without the prohibited assistance of third parties and without making use of aids other than those specified; notions taken over directly or indirectly from other sources have been identified as such. This work has not previously been presented in identical or similar form to any examination board.

The dissertation work was conducted from 2010 and 2015 under the supervision of Dr. Andrés García and Dr. César Álvarez at the Universidad de Cantabria.

This dissertation was finished writing in Santander on August 2015

This page is intentionally left blank